

24th INTERNATIONAL MULTIDISCIPLINARY SCIENTIFIC GEOCONFERENCE - SGEM 2024

01 – 07 July 2024 - Albena, Bulgaria

CONFERENCE PROCEEDINGS OF SELECTED PAPERS in

SCIENCE AND TECHNOLOGIES IN GEOLOGY, EXPLORATION AND MINING

ISSUE 1.1

DISCLAIMER

The **International Multidisciplinary Scientific GeoConference SGEM (Survey, Geology, Ecology, and Management)** serves as a global platform for pioneering research and scientific dialogue across the diverse fields of geosciences. It is dedicated to advancing interdisciplinary solutions for the most pressing environmental challenges of our time — **Global Warming, Climate Change, CO_2 Reduction, Biodiversity Conservation, and the Development of Green Technologies**. By fostering a collaborative exchange of knowledge and **aligning its objectives** with the **United Nations Sustainable Development Goals (SDGs), SGEM aims to inspire scientific excellence and drive sustainable practices toward a greener, more resilient future for our planet.**

Authors are responsible for the content and accuracy of the written papers. Opinions expressed are not meant to represent or reflect the position of the SGEM International Scientific Committee members.

No part of this book may be reproduced or transmitted in any form or by any means, electronic or mechanical, for any purpose, without the express written permission of the SGEM International Scientific Committee on Earth and Planetary Sciences.

Copyright © SGEM WORLD SCIENCE (SWS) Scholarly Society 2024
Haidingergasse 1, C / 1113, Vienna 1030, Austria
Published by STEF92 Technology
Total print: 5000

E-mail: **sgem@sgem.org** | URL: **www.sgem.org**

ISBN 978-619-7603-67-5

ISSN 1314-2704

DOI: 10.5593/sgem2024/1.1

FOREWORD

Dear Readers,

It is our honor to present the **24th volume of the SGEM GeoConference 2024 Conference Proceedings**, a six-issue series showcasing pioneering research across the diverse fields of Earth and Planetary Sciences. This year's collection highlights the multidisciplinary nature of **geosciences, encompassing topics such as geology, hydrogeology, engineering geology, mineral processing, exploration and mining, geophysics, and oil and gas exploration**. Together, these interconnected disciplines play a pivotal role in addressing some of today's most pressing global challenges.

In the face of climate change and resource scarcity, the research in these proceedings aligns closely with the United Nations Sustainable Development Goals (SDGs), particularly in areas such as **clean water and sanitation (SDG 6), affordable and clean energy (SDG 7)**, **sustainable cities and communities (SDG 11), responsible consumption and production (SDG 12), and climate action (SDG 13)**. These issues contribute significantly toward a more sustainable and resilient future by offering innovative solutions and actionable insights.

A distinctive feature of the proceedings is their embodiment of the multidisciplinary spirit of modern geosciences. They reflect the **collaborative efforts of researchers and practitioners from various fields to address complex, real-world problems**. From advanced geostatistical methods in mineral exploration to state-of-the-art seismic risk assessments, the research demonstrates the evolving role of geosciences in meeting societal needs.

Each paper included in these collections of papers has undergone a rigorous **peer review process**. This thorough **evaluation by subject-matter experts** ensures the highest standards of **scientific integrity, originality, and relevance**. Such a commitment to quality underlines our dedication to promoting credible, impactful research that drives innovation and informs policy-making.

This first issue focuses on Geology, exploring topics such as the genesis of critical mineral deposits, the environmental impacts of mining, and innovative approaches to geotourism. These studies contribute to the **sustainable management and responsible stewardship of Earth's geological resources**.

The subsequent issue delves deeper into specialized areas:

- **Hydrogeology and Engineering Geology**, addressing sustainable water resource management and geotechnical resilience.
- **Exploration and Mining**, showcasing advancements in extraction technologies and mineral discovery.
- **Applied Geophysics**, highlighting its applications in **disaster risk reduction** and planetary exploration.
- Mineral Processing and Oil and Gas Exploration, focusing on the **efficient and sustainable utilization of Earth's energy resources**.

In this era of rapid environmental and societal transformation, these proceedings serve as a vital resource for advancing collective understanding and action. We extend our sincere gratitude to the authors, reviewers, and conference organizers for their invaluable contributions. **Together, we continue to push the boundaries of scientific knowledge to tackle the urgent challenges facing humanity**.

We invite you to explore the rich and diverse research presented in these issues and join us in advancing innovation and sustainability in geosciences.

Sincerely yours,

Prof. Dr. hab. oec. Baiba Rivza
Editor-in-Chief of XXIV SGEM GeoConference Proceedings
Member of the Presidium of the Latvian Academy of Sciences, LATVIA
President of the Latvian Academy of Agricultural and Forestry Sciences
Vice-chair of the Latvian Council of Higher education
President of Latvian universities professors' association
Expert from the European Academy of Sciences Academic Advisory Board (EASAC)

Prof. DSc. Oleksandr Trofymchuk
Editor-in-Chief of XXIV SGEM GeoConference Proceedings
National Academy of Sciences of Ukraine, UKRAINE

CONFERENCE PROCEEDINGS CONTENTS

GEOLOGY

1. ABOUT THE NEW PORPHYRY COPPER MINERALIZATION OBJECT IN THE EASTERN BALKHASH REGION (KAZAKHSTAN), Daulet Muratkhanov, Kanat Bulegenov, Gulimshat Shakirova, Assoc. Prof. Dr. Maxat Kembayev 3

2. ANALYSIS OF THE MINERAL RESOURCE OF KAZAKHSTAN, Assoc. Prof. M.A. Mizernaya, Assoc. Prof. T.A. Oitseva, Assoc. Prof. O. N. Kuzmina, PhD st. T.M. Aitkazyyev, PhD Z.I. Chernenko 11

3. ABOUT THE GENETIC TYPES OF COPPER DEPOSITS IN KAZAKHSTAN AND THE PROSPECTS FOR IDENTIFICATION OF NEW ECONOMIC COPPER OBJECTS, Daulet Muratkhanov, Yerkhozha Mamanov, Bulegenov Kanat.....19

4. ASSESSING THE AGRICULTURAL CONSEQUENCES OF LANDFILL KELMEND-ASSOCIATED HEAVY METAL CONTAMINATION IN RAHOVË VILLAGE, PhD(c). Elida Lecaj, PhD(c). Bahri Sinani, PhD(c). Adelina Haskaj, PhD(c). Berat Sinani, PhD(c). Majlinda Ramada.....27

5. CRITICAL ELEMENTS IN SEQUENTIAL LEACHED PHASES FROM DEEP-SEA POLYMETALLIC NODULES AND SEDIMENTS, Assoc. Prof. Dr. Atanas Hikov, Assoc. Prof. Dr. Zlatka Milakovska, Assoc. Prof. Dr. Valentina Lyubomirova**,** Dr. Nadezhda Lihareva 37

6. DESIGNING GEOEDUCATIONAL TOOLS FOR GEOTOURISM NEEDS – A CASE STUDY OF THE OUTER FLYSCH CARPATHIANS, Zbigniew Jan Ziarek.....45

7. EVALUATING FLOOD RISKS AND VULNERABILITIES IN CARAORMAN, DANUBE DELTA: INSIGHTS FROM HYDRAULIC MODELLING, Dr. Banescu Alexandry, Simionov Matei, Phd Ress. Livanov Oliver, Pindic Paula, Phd Ress. Balaican Dragos 53

8. ENVIRONMENTAL STATISTICAL ANALYSIS OF THE BASINS OF THE MINING DISTRICT OF PONCE ENRÍQUEZ (ECUADOR), Daniel Garcés, Yolanda Sanchez-Palencia, Samantha Jimenez, Juan Llamas 61

9. GEOLOGICAL STRUCTURE AND MINERALOGICAL COMPOSITION OF THE KARA-AYAK RARE METAL ORE OCCURRENCE (EAST KAZAKHSTAN), PhD Tatyana Oitseva 71

10. GEOSTATISTICAL DISTRIBUTION OF LEAD AND ZINC METALS IN ARTANA 1 LANDFILL: MINERALOGICAL CHARACTERIZATION OF THE LANDFILL OBTAINED FROM RESIDUES FROM THE LEAD-ZINC FLOTATION PROCESS, MSc. Berat Sinani, Phd. Cand, MSc. Fisnk Frangu, MSc. Ramiz Krasniqi, MSc. Besnik Shala, MSc. Bahri Sinani, Phd. Cand, MSc. Vehbi Berisha, Prof. Dr. Ivan Boev, Prof. Dr. Arianit A. Reka, Prof. Dr. Blazo Boev.....79

11. HOLOCENE LACUSTRINE SEDIMENTATION PATTERNS ON LORI PLATEAU (SOUTH CAUCASUS), Assoc. Prof. Dr. Grigory Fedorov, Dr. Dmitry Sadokov, Vsevolod Rudakov, Assoc. Prof. Dr. Irina Fedorova, Larisa Ghazaryan.....91

12. MINERAL COMPOSITIONS OF SOME ROCK-FORMING MINERALS IN THE LOW-GRADE SEDIMENTARY AND MAFIC ROCKS, EASTERN CIRCUM-RHODOPE BELT, BULGARIA, Prof. DSc. Nikolay Bonev 99

13. THE PARTICLE SIZE OF THE BOTTOM SEDIMENTS IN SOME CANALS OF THE FLUVIAL-MARINE DANUBE DELTA, Phd Ress. Livanov Oliver, Dr. Banescu Alexandru, Burada Adrian, Pindic Paula, Anore Ciprian, ...105

14. VOLCANOTECTONIC STRUCTURES AND LINEAMENT PRELIMINARY IDENTIFICATION RESULTING FROM THE APPLICATION OF REMOTE SENSING AND GIS IN BOLNISI ORE DISTRICT, GEORGIA, PhD Ress. Irakli Avkopashvili.....113

HYDROGEOLOGY, ENGINEERING GEOLOGY AND GEOTECHNICS

15. ANALYSIS OF ENGINEERING PROTECTION EFFECTIVENESS OF THE KYIV-PECHERSK LAVRA TERRITORY BASED ON LONG-TERM HYDROGEOLOGICAL MONITORING, CSc. Iryna Cherevko, CSc. Tetiana Kril, CSc. Dmitri Bugai, Prof. DSc. Stella Shekhunova.....123

16. COMPLEX ENGINEERING DESIGN OF COASTAL PROTECTION, Assoc. Prof. Dr. Miroslav Todorov, Eng. Mihail Todorov.....131

17. DETERMINATION OF WATERLOGGING ZONES AND THEIR FACTORS USING NON-DESTRUCTIVE MONITORING METHODS AT HISTORICAL AND ARCHITECTURAL MONUMENTS, CSc. Iryna Cherevko, CSc. Tetiana Kril, CSc. Dmytro Bezrodnyi, CSc. Serhii Popov.....143

18. FEATURES OF STUDYING THE MATERIAL COMPOSITION OF POLYMETALLIC ORE FOR ITS COMPLEX USE, Expert ecologist, PhD Natalia Tyushkova, Research Associate Tatiana Losina 151

19. HISTORICAL FLOODS OF THE LOWER DANUBE BASIN RIVERS DURING THE LAST MILLENNIUM, Carmen-Andreea Bădăluță, Ionel Popa, Gheorghe Bădăluță, Anișoara Filip 161

20. INSTABILITY CHARACTERIZATION OF THE GEOLOGICAL FORMATION "AREIAS E ARGILAS DE TAVEIRO" IN THE CONDEIXA AND COIMBRA AREAS (CENTRAL-WESTERN PORTUGAL), Msc. Beatriz Neto, Assist. Prof. Dr. Pedro Santarém Andrade, Assist. Prof. Dr. António Neves Trota 169

21. INVESTIGATION OF SEAWATER INTRUSION IN SHABLA-KRAPETS REGION, NE BULGARIA, Ing. Marin Ivanov, Assoc. Prof. Evelina Damyanova ..177

22. ROCK FALL STUDY IN DIFFERENT AREAS OF SOUTHWEST ANGOLA, Assist. Prof. Dr. Pedro Santarém Andrade, MSc. Elsa Kaúla 185

23. THE VAL RONCAGLIA LANDSLIDE (NORTHERN ITALY): FROM CONCEPTUAL TO NUMERICAL MODELLING, Assoc. Prof. Dr. Paola Gattinoni, Dr. Angelo Molteni 193

EXPLORATION AND MINING

24. ANALYSIS OF LABORATORY METHODS USED FOR THE DETERMINATION OF THE MINIMUM IGNITION ENERGY IN THE CASE OF AIR/FUEL DUST MIXTURES, Sc. Res. III PhD Eng. Catalin Mihai POPA, Sc. Res. I PhD Eng. Emilian GHICIOI, Sc. Res. I PhD Eng. Florin Adrian PĂUN, Sc. Res. III PhD Eng. Dan Sorin GABOR 203

25. ASSESSMENT AND PROSPECTS FOR DEVELOPMENT OF COAL RESOURCE POTENTIAL OF THE NORTH-EAST ARCTIC ZONE OF THE REPUBLIC OF SAKHA (YAKUTIA), Evgenii Khoiutanov**,** Dr. Natalia Batugina**,** Vladislav Fedorov**,** Yurii Andreev 211

26. BLASTING DEMOLITION CHALLENGES OF A TALL COOLING TOWER AND CHIMNEY, PhD. Eng. Ress. Robert Laszlo, PhD. Eng. Ress. Ciprian Jitea, PhD. Eng. Ress. Bogdan Garaliu, PhD. Eng. Bogdan Aurelian Nicola, Eng. Levente Miklos 219

27. BLASTING TECHNOLOGY FOR NEUTRALIZING IMPROVISED EXPLOSIVE DEVICES, Ph.D Eng. Emilian Ghicioi, Ph.D eng. Dan Gabor, Ph.D. Ress. Ing. Mirela Radu, Anca Tazlauanu 227

28. CFD SIMULATION OF CARBON MONOXIDE CIRCULATION DYNAMICS IN A VENTILATION INSTALLATIONS TUBING, PhD. Eng. Ion Gherghe**,** PhD. Eng. Florin Rădoi**,** PhD. Eng. Emeric Chiuzan**,** PhD. Eng. Nicolae Ianc 235

29. COMPUTERISED RISK ASSESSMENT FOR STORAGE OF PYROTECHNIC ARTICLES, PhD. Eng. Cristian Rădeanu, Eng. Miron Claudia, PhD. Eng. Vasilescu Gabriel, PhD. Ress. Eng. Pintilie Dan, PhD. Eng. Popescu Claudius 243

30. DEVELOPING THE PRACTICAL SKILLS OF RESCUERS FOR INTERVENTIONS IN HIGH TEMPERATURE AREAS, Phd. Eng. Daniel Pupăzan, Phd. Eng. Andrei Lucian Gireadă, Phd. Eng. George Artur Găman, Phd. Eng. Cosmin Ilie, Phd. Eng. Cristian Nicolescu 253

31. DEVELOPMENT OF THE INFRASTRUCTURE FOR VALIDATING THEORETICAL METHODS THROUGH COMPUTER SIMULATION AND MODELING OF BLASTING AND SAFETY PARAMETERS OF CIVIL EXPLOSIVES, PhD Ress. Ciprian Jitea, PhD. Daniela Rus, PhD. Edward Gheorghiosu, PhD Ress. Johannes Fabian Bauer2 PhD Ress. Mateiu Ciprian.....261

32. DYNAMIC BEHAVIOR OF METHANE IN CONFINED SPACES BY CFD SIMULATION, Vlad Lăutaru, Alexandru Simion, Laurențiu Munteanu.....269

33. EVALUATION OF COMPUTER SIMULATION AND MODELING METHODS FOR BLASTING PROCESSES IN SURFACE MINES, PhD.Eng.-Ress. Bogdan Garaliu-Buşoi, PhD.Eng. Gabriel Vasilescu, PhD.Eng.-Ress. Claudius Popescu, PhD.Eng.-Ress. Claudia-Raluca Ilici, PhD.Eng.-Ress. Adina Păsculescu 277

34. EVALUATION OF THE WEAR OF THE CARRYING ROLLERS OF BELT CONVEYORS, Assoc. Prof. M.Sc. Lubomir Ambrisko, PhD., M.Sc. Dusan Kubala, PhD., M.Sc. Lucia Cabanikova, M.Sc. Marek Ondov 287

35. GENESIS OF THE ERVA Pb–Zn DEPOSIT KAYSERI (YAHYALI): MINERALOGY AND TRACE ELEMENT GEOCHEMISTRY, Ozge Ozer Atakoglu, Prof. Dr. Mustafa Gurhan Yalcin 295

36. HEALTH AND SAFETY OF WORKERS IN THE MINING INDUSTRY FOLLOWING THE IMPLEMENTATION OF ARTIFICIAL INTELLIGENCE, PhD Andrada Denisa Matei, PhD Ligia Ioana Tuhut, PhD Marius Simion Morar, PhD Cioara Cristian Raul, PhD Florin Manea 303

37. IDENTIFICATION OF AREAS PRONE TO SEISMIC ACTIVITY OCCURRENCE USING 3D FEM NUMERICAL SIMULATIONS, Dr. Krzysztof Fuławka, Assoc. Prof. Dr. Piotr Mertuszka, Dr. Lech Solecki, Dr. Marcin Szumny, MSc. Roman Kołodziej 311

38. INTERVENTION AND RESCUE IN CONFINED SPACES IN CASE OF POTENTIALLY EXPLOSIVE AREAS CAUSED BY THE PRESENCE OF HYDROGEN, PhD. Eng. Andrei Lucian Gireadă**,** PhD. Eng. Daniel Pupăzan**,** PhD. Eng. Artur George Găman**,** PhD. Eng. Cristian Nicolescu**,** PhD. Eng. Cosmin Ilie.....321

39. JUST IN BLAST- VR TRAINING, Julia Piestrzynska 329

40. MULTICRITERIA ANALYSIS OF THE AGGREGATE PRODUCTION BY-PRODUCT PURPOSES, Marek Ondov, MSc., Prof. Marian Sofranko, Jan Chovan, MSc., Marek Szucs, MSc., Lukas Hlavaty, MSc. 337

41. NOISE EVALUATION FOR THE DUMPER DRIVERS IN MINING ACTIVITIES: A CASE STUDY, Alfaro Degan Guido, Antonucci Andrea, Coltrinari Gianluca, Innocenzi Sara, Lippiello Dario 345

42. RESEARCH ON THE BEHAVIOR OF METAL CONSTRUCTIONS UNDER THE ACTION OF EXPLOSIONS, Eng. Stefan Ilici, PhD. Eng. Ress Robert Laszlo, Prof. Florea Dinu, PhD. Eng. Edward Gheorghiosu, PhD. Eng. Ress. Bogdan Simon.....355

43. RISK ASSESSMENT AT DEMOLITION ACTIVITY OF INDUSTRIAL / CIVIL OBJECTIVES WITH THE EXPLOSIVES FOR CIVIL USES, Eng. Claudia Miron, PhD.Eng. Cristian Rădeanu, Eng. Stefan Ilici, PhD. Ec.-Ress. Dan Pintilie, PhD.Eng.-Ress. Ciprian Mateiu.....365

44. ROMANIAN COAL AND ENERGY HYBRIDIZATION, D Dr. Cristian Tomescu, Dr. Cornel Boanta, Dr. Emeric Chiuzan, Assoc. Prof. Dr. Sorina Stanila.....375

45. SIMULATIONS CARRIED OUT AT THE LEVEL OF THE TÂRGU OCNA SALT MINE FOR REVERSAL VENTILATION, Doru Cioclea, Adrian Matei, Nicolae Ianc, Răzvan Drăgoescu, Alexandru Cămărășescu.....383

46. THE CONTINUATION OF THE EXTRACTION OF USEFUL MINERAL SUBSTANCES IN THE CURRENT GEOPOLITICAL CONTEXT, PhD Eng. Adrian Matei, PhD Eng. Doru Cioclea, PhD Eng. Răzvan Drăgoescu, PhD Eng. Alexandru Cămărășescu 391

47. TRANSPORT CAPACITY OF MINING HOISTING EQUIPMENT - CALCULATION BASED ON SIMULATION, Assoc. prof. Janka Saderova, M.Sc., PhD., Prof. Andrea Rosova, M.Sc., PhD., Patricia Muchova, M.Sc., Marek Ondov, M.Sc.....399

48. WIND BARRIERS AS A POSSIBLE SOLUTION TO PM10 EMISSIONS IN INDUSTRIAL PLANTS, PhD, Eng. Stefano Carbone, Dr. V. De Brito 407

MINERAL PROCESSING

49. ALUMINIUM SMELTER ANODE WASTE BOND INDEX DETERMINATION, Assoc. Prof. Dr. Surracco Marco, Prof. Tilocca Maria Caterina.....417

50. IMPROVEMENT OF MECHANICAL PROPERTIES OF AUSTEMPERED DUCTILE IRON (ADI) BY MAGNETIC FIELD, Assoc. Prof. Ing. Peter Futas, PhD., Prof. Ing. Alena Pribulova, PhD., Assoc. Prof. Ing. Jozef Petrik, PhD., Ing. Peter Peter Blasko, PhD., Dr hab. Inz. Marcin Brzezinski 425

51. FLOTATION AND MAGNETIC SEPARATION PROCESSES FOR A MINERAL OF WOLLASTONITE, Assoc. Prof. Dr. Surracco Marco**,** Prof. Tilocca Maria Caterina 433

52. RECOVERY OF LITHIUM AND DESALTED WATER FROM OILFIELD BRINE, Dr. Ewa Knapik, Dr. Grzegorz Rotko.....441

53. USE OF REGRESSION ANALYSIS AND SIMULATION TO OPTIMIZE THE COMPOSITION OF THE CAST IRON CHARGE, Assoc. Prof. Ing. Peter Futas, PhD., Prof. Ing. Alena Pribulová, PhD., Assoc. Prof. Ing. Jozef Petrik, PhD., Ing. Peter Peter Blasko, PhD., Assoc. Prof. Ing. Mária Mihaliková, PhD. 449

APPLIED AND ENVIRONMENTAL GEOPHYSICS

54. ASSESSMENT OF THE QUALITY FACTOR OF LITHOSPHERE FOR THE LENA DELTA (LAPTEV SEA REGION), Dr. Artem A. Krylov, Dr. Sergey A. Kovachev 459

55. ASSESSMENT OF GEOPHYSICAL DATASET IN THE CENTRAL SEGMENT OF THE SOUTHERN CARPATHIANS ROMANIA, Dr. Natalia-Silvia Asimopolos, Dr. Laurentiu Asimopolos, Asist. Prof. Adrian-Aristide Asimopoos 467

56. DETERMINATION OF DEPTH PARAMETERS OF SUBSURFACE VOIDS USING GRAVIMETRIC AND GLOBAL NAVIGATION SATELITTE SYSTEMS MEASUREMENTS, PhD Eng. Severina Djorova, Eng. Maria Nikolova.....475

57. DETERMINISTIC EARTHQUAKE SCENARIO FOR THE CITY OF SOFIA, Prof. Dr. Dimcho Solakov, Assoc. Prof. Dr. Stela Simeonova, Assoc. Prof. Dr. Plamena Raykova 483

58. GEOPHYSICAL EXPLORATION IN ARGEMELA DISTRICT, FUNDÃO, PORTUGAL – VLF RESULTS, MSc Ricardo Ribeiro, Assoc. Prof. Rui Moura, MSc Ana Carvalho, Assoc. Prof. Alexandre Lima, Assoc. Prof. Charles Gumiaux 491

59. PRELIMINARY ESTIMATION OF ELECTRICAL PROPERTIES OF THE LUNAR NEAR SURFACE FROM THE CHINESE YUTU-2 LUNAR PENETRATING RADAR (LPR), Assoc. Prof. Rui Moura, Assoc. Prof. Lucía Arévalo Lomas, Assoc. Prof. Fernando Almeida 499

60. RECEIVER FUNCTIONS APPLICATION FOR STUDYING THE DEEP STRUCTURE OF THE LENA DELTA REGION, Mikhail Novikov, Dr. Artem Krylov, Dr. Konstantin Roginskiy.....507

61. SEISMIC RISK ASSESMENT FOR TRANSBOUNDARY AREA OF ROMANIA AND REPUBLIC OF MOLDOVA UNGHENI – UNGHENI-PRUT, Prof. Dr. hab. Vasile Alcaz, Assoc. Prof. Dr. Igor Nicoara, Assoc. Prof. Dr. Alina-Mihaela Precul, Evgheni Isicico, Lecturer Ioana Olteanu.....515

62. PROBABILISTIC EARTHQUAKE SCENARIOS FOR THE CITY OF VARNA, Prof. Dimcho Solakov, Assoc. Prof. Stela Simeonova, Assoc. Prof. Plamena Raykova.....523

OIL AND GAS EXPLORATION

63. ANALYSIS AND ASSESSMENT OF SECURITY REQUIREMENTS FOR USE OF HYDROGEN AS A FUEL IN THE TRANSPORT SYSTEM, Danut Grecea, Gabriela Pupazan, Adriana Andris, Alexandru Beldiman, Aurelian Nicola.....533

64. APPLICATION OF CULTURE SUPERNATANTS CONTAINING SURFACTANTS TO ENHANCE OIL RECOVERY, Dr. Liliya Biktasheva, Nikita Ezhkin, Zlata Osmorskaya, Alexander Gordeev, Assoc. Prof. Dr. Polina Kuryntseva.....541

65. ASSESSING THE IGNITION SOURCES GENERATED BY THE MECHANICAL EQUIPMENT IN THE CONTEXT OF HYDROGEN EXPLOSIVE ATMOSPHERES, Sc. Res. I PhD Eng. Adrian Marius Jurca, Sc. Res. I PhD Eng. Florin Adrian Păun, Sc. Res. III PhD Eng. Mihai Cătălin Popa, Sc.Res.PhD Eng.Mirela Radu.....549

66. DETERMINATION OF EXPLOSION PARAMETERS FOR AIR-GASOLINE MIXTURES, PhD Chem. Eng. Irina Nălboc, Ph.D Chem. Maria Prodan, Ph.D Chem. Andrei Szolloşi-Moţa, Ph.D Phys. Sonia Suvar.....557

67. DEVELOPMENT OF A COMBINED SPUD BIT FOR DRILLING TECHNOLOGICAL WELLS IN KAZAKHSTAN, Prof. Dr. Boranbay Ratov, Prof. Dr. Boris Fedorov, Assoc. Prof. Dr. Volodymyr Khomenko, Assoc. Prof. Dr. Aidar Kuttybayev, Assoc. Prof. Manshuk Sarbopeyeva.....565

68. DEVELOPMENT OF METHODOLOGY FOR OPTIMAL CYCLIC INJECTION TECHNIQUES BASED ON MATHEMATICAL MODELING, Idrisov Kamil M., Shipaeva Maria S., Ziniukov Rustam A., Sudakov Vladislav A.....575

69. DETERMINATION OF EXPLOSION CHARACTERISTICS FOR COMBUSTIBLE POWDERS (STARCH – MAGNESIUM), Ph.D Chem. Maria Prodan, Ph.D Chem. Eng. Irina Nălboc, Ph.D Chem. Andrei Szolloşi-Moţa, Ph.D Phys. Sonia Suvar.....583

70. HYDROGEOCHEMICAL CHARACTERIZATION OF CARBONATE OIL DEPOSITS: INSIGHTS INTO IONIC COMPOSITION, FRACTURING AND CONNECTIVITY, Maria Shipaeva, Kamilya Talipova, Nil Fakhriev, Vladislav Sudakov 591

71. IDENTIFICATION OF INPUT-OUTPUT PARAMETERS OF THE COMMAND AND CONTROL SYSTEM FOR TESTING FLAMEPROOF PROTECTED ELECTRIC MOTORS USED IN HYDROGEN ATMOSPHERE, PhD.eng. Marcel Daniel Rad, PhD.eng. Mihai Magyari, PhD.eng. Dragos Fotau, Eng. Attila Sorin Zsido, Eng. Constantin Valentin Sirbu 599

72. IMPEDANCE SPECTROSCOPY ANALYSIS OF INTRINSIC SAFETY CIRCUITS, Sc. Res. I Ph.D Eng. Marius DARIE, Sc. Res. I Ph.D Eng. Sorin BURIAN, Sc. Res. I Ph.D Eng. Tiberiu CSASZAR, Sc. Res. I Ph.D Eng. Cosmin COLDA, Assoc. Profesor. Ph.D Chem. Clementina MOLDOVAN.....607

73. INVESTIGATION OF THE PROCESS OF INTRODUCING THE CENTRALIZER SLATS INTO THE WALLS OF THE TRUNK WHEN DRILLING INCLINED WELLS, Prof. Dr. Akshyryn Zholbassarova, Prof. Dr. Danabek Saduakassov, Prof. Dr. Aliya Togasheva, Prof. Dr. Maxat Tabylganov, Prof. Dr. Aigul Gusmanova.....615

74. METHODOLOGY FOR OPTIMIZING DRILL BIT PERFORMANCE, Assoc. Prof. Dr. Oleksandr Pashchenko, Prof. Dr. Boranbay Ratov, Assoc. Prof. Dr. Volodymyr Khomenko1 Assoc. Prof. Aigul Gusmanova, Assoc. Prof. Elmira Omirzakova 623

75. PHYSICAL EXPERIMENTS REGARDING THE LINEAR PROPAGATION OF HYDROGEN EXPLOSIONS IN ENCLOSED SPACES, Phd. Ress. Eng. Gheorghe Daniel Florea, Phd. Eng. Nicolae Ioan Vlasin, Phd. Ress. Eng. Adrian Bogdan Simon-Marinica, Phd. Ress. Eng. Cristian Raul Cioara, Eng. Laurentiu Munteanu 633

76. PRACTICAL ASPECTS OF IMPROPER INSTALLATION AND MAINTENANCE OF EQUIPMENT INTENDED TO BE USED IN POTENTIALLY EXPLOSIVE AREAS AND RECOMMENDED MEASURES, Sc. Res. I Ph.D Eng. Tiberiu Csaszar, Sc. Res. I Ph.D Eng. Cosmin Colda, Sc. Res. III Ph.D Eng. Danut Grecea, Sc. Res. III Ph.D Eng. Gabriela Pupăzan, Eng. Alexandru Beldiman.....643

77. PREVENTING PIPE STICKING IN OIL AND GAS WELLS USING AN IMPROVED TORQUE AND DRAG MODEL, ALONG WITH ANALYTICAL AND MACHINE LEARNING METHODS, Assistant Professor, PhD, Dr. Aizada B. Sharaouva, Machine Learning Engineer, Bs of Computer Science, Myrzanov Beket Senior lecturer, Dinara N. Delikesheva 651

78. SPECIFIC ASPECTS REGARDING THE TESTING OF FLAMEPROOF ENCLOSURE EQUIPMENT INTENDED FOR USE IN HAZARDOUS AREAS ENDANGERED BY THE PRESENCE OF HYDROGEN, Sc.res. I PhD Eng. Lucian Moldovan, Sc.res. I PhD Eng. Adrian Jurca, Sc.res. I PhD Eng. Mihai Magyari, Sc.res. III PhD Eng. Marcel Rad, Sc.res. assist. Eng. Valentin Sîrbu.....659

79. THE PARTICULARITIES OF ELECTRICAL EQUIPMENT WITH TYPE OF PROTECTION FLAMEPROOF ENCLOSURE USED IN POTENTIALLY EXPLOSIVE ATMOSPHERES GENERATED BY HYDROGEN, PhD. Eng. Dragoş Fotău, PhD. Eng. Lucian Moldovan, Eng. Râsnoveanu Sorin, Eng. Sîrbu Valentin, PhD. Eng. Diana Sălăşan 669

80. USING MACHINE LEARNING TECHNIQUES TO FORECAST CUTTINGS REMOVAL IN HOLE CLEANING, Senior lecturer, Dinara N. Delikesheva, Assistant Professor, PhD, Dr. Aizada B. Sharaouva 677

SECTION GEOLOGY

ABOUT THE NEW PORPHYRY COPPER MINERALIZATION OBJECT IN THE EASTERN BALKHASH REGION (KAZAKHSTAN)

Daulet Muratkhanov[1]

Kanat Bulegenov[1]

Gulimshat Shakirova[1]

Assoc. Prof. Dr. Maxat Kembayev[1]

[1] Satbayev University, Almaty, **Republic of Kazakhstan**

ABSTRACT

In Kazakhstan, the main porphyry copper deposits are located in the Northern Balkhash region. The Konyrat, Aktogay, Aidarly, and Borly copper-porphyry deposits have been explored and exploited in this area. The main reserves of the country's copper raw materials are associated with these deposits. The Eastern Balkhash region is part of the North Balkhash ore zone. Previous studies on the Eastern Balkhash region focused on the Aktogay region and did not pay due attention to the southern part of the East Balkhash region, despite the fact that this region borders the Aktogay ore field and has prerequisites for the discovery of new ore sites. The geological structure of the area includes devonian and carboniferous terrigenous-effusive formations which are broken through by granitoid intrusions. Hydrothermal changes are widespread in the host rock and intrusive massifs. We have conducted cosmogeological studies and compiled a cosmogeological scheme of the territory with the allocation of ore-controlling annular and linear structures, the spread of areal bodies of intrusive rocks and metasomatic changes. According to the data of geological and cosmogeological studies, promising areas have been identified, within which geological and geophysical prospecting works have been carried out. According to the data of geophysical work, local anomalies have been identified for drilling mapping and prospecting wells. As a result of geological, geophysical, drilling, mineralogical and petrographic studies in the buried intrusion of granitoids, a new promising sulfide copper-molybdenum mineralization was revealed.

Keywords: Prediction of ore deposits, blind intrusion of granitoids, porphyry copper deposits, sulfide ores, Kazakhstan

INTRODUCTION

Mineral resources are the basis of the economy of Kazakhstan and in the foreseeable future they will not lose their role [1], [2], [3]. Every year, the problem of raw materials supply for the country's existing mining and metallurgical complex becomes more and more urgent [4], [5], [6]. Kazakhstan occupies one of the leading places in the world in terms of reserves of copper ores [4].

The prospects for identifying new industrial copper deposits in Kazakhstan are still significant [7], [8], [9], [10], [11]. Today, the copper industry of the republic is provided

https://doi.org/10.5593/sgem2024/1.1/s01.01

with a raw material base [12]. The problem is the presence of a significant part of inactive reserves (poor porphyry copper ores). Large copper-porphyry deposits include Konyrat Aktogay, Aidarly, Zhaman-Aybat, Bozshakol, Koksai, Kaskyrmys, Nurkazgan (Samarskoye) [13], [14], [15]. Of the total number of about 70 deposits, there are 30 copper ore deposits, the rest belong to complex, copper-containing ones. In recent years, the shortage of mineral raw materials, including copper, has increased in Kazakhstan. The copper reserves of the developed deposits are at the final stage. There is a certain problem with the discovery of new deposits [16], [17]. This is mainly due to the lack of development of methods for searching for "blind deposits" in areas covered by sedimentary complexes [18], [19].

The Eastern Balkhash region of Kazakhstan (Figure 1) was not considered perspective for searching for copper ore deposits. Nevertheless, in the adjacency of this region, there are porphyry copper object - Aktogai, Aidarly, etc. Our scientific study based on creating new theoretical base and analysing satellite images showed that in the previous considered unpromising area, it is possible to predict areas for searching new deposits, [20]. This paper presents the geological structure features of a new porphyry copper occurrence.

MATERIALS AND METHODS

Firstly, we analysed data from satellite images to clarify the structure of the territory buried by the sedimentary cover and to organise prospecting work. The initial remote sensing data for the work were archived from Landsat ETM+ and Aster satellite surveys, as well as digital terrain models – SRTM (2000y) and AsterGDEM (2011y) data. After interpreting satellite images, the geological structure scheme was drawn.

Field geophysical work was carried out on magnetic anomalies. Mapping and prospecting wells were drilled on geophysical anomalies, which corresponds with a buried intrusive body of granitoids. Mineralogical studies were carried out on samples from borehole cores to study sulfide copper-molybdenum mineralisation in hydrothermally altered granitoids.

RESULTS

By interpreting satellite images of the area, we have created a structural map of the area. Ring, linear and areal structures were highlighted on this map.

More than 900 linear structures have been identified, among which about 640 have received geological interpretation. Such structures include discontinuous faults, geological boundaries and stratification elements of lithified stratified complexes.

Discontinuous disturbances in the Arganata section have predominantly a north-westerly and sublatitudinal strike (Figure 2).

The main discontinuous violation is a right-lateral displacement located at the north-eastern boundary of the area. It has a north-easterly strike, and it is not possible to determine the amplitude of the displacement, due to the widespread development of modern sediments and the relief located near the site.

Sublatitudinal discontinuities associated with the main structure are classified as discontinuous disturbances of the second order. The amplitudes of right-hand displacement in such structures reach 860 m. Other discontinuous faults have a predominantly north-easterly strike.

Ring structures with a radius from 0.13 to 48 km are mapped on the Arganata site and in its immediate vicinity. It should be noted at once that the site is located in the central part of a magmatogenic telescoped ring structure of the second order with a radius of 48 km. The annular structures with smaller radii are "embedded" in this ring structure. The presence of such a complex of annular structures usually indicates the multi-tiered position of intermediate magmatic foci.

The data of geophysical studies allowed us to outline the contour of the hidden intrusive massif, which was studied by drilling operations.

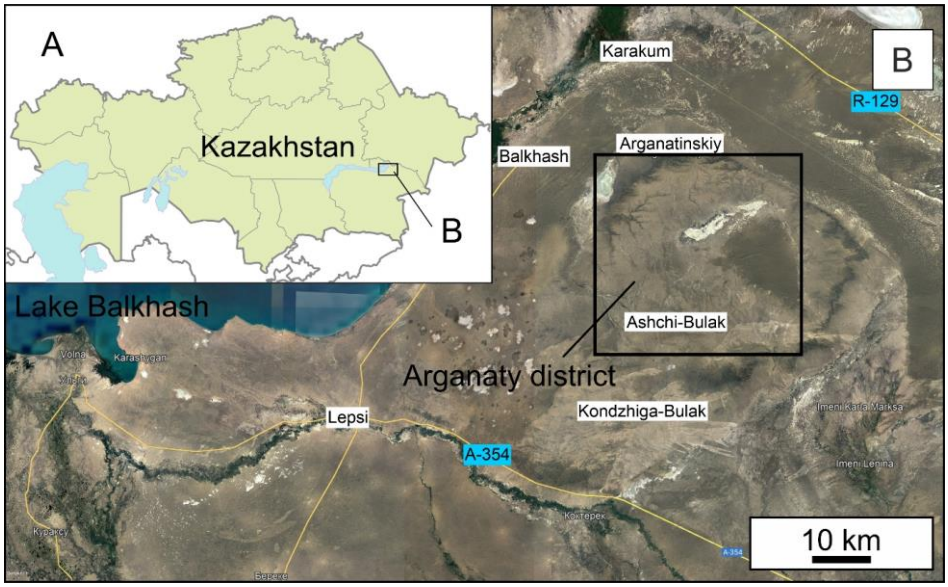


Figure 1. A - Location of the Eastern Balkhash region on Kazakhstan map; B – Borders of the Arganaty district

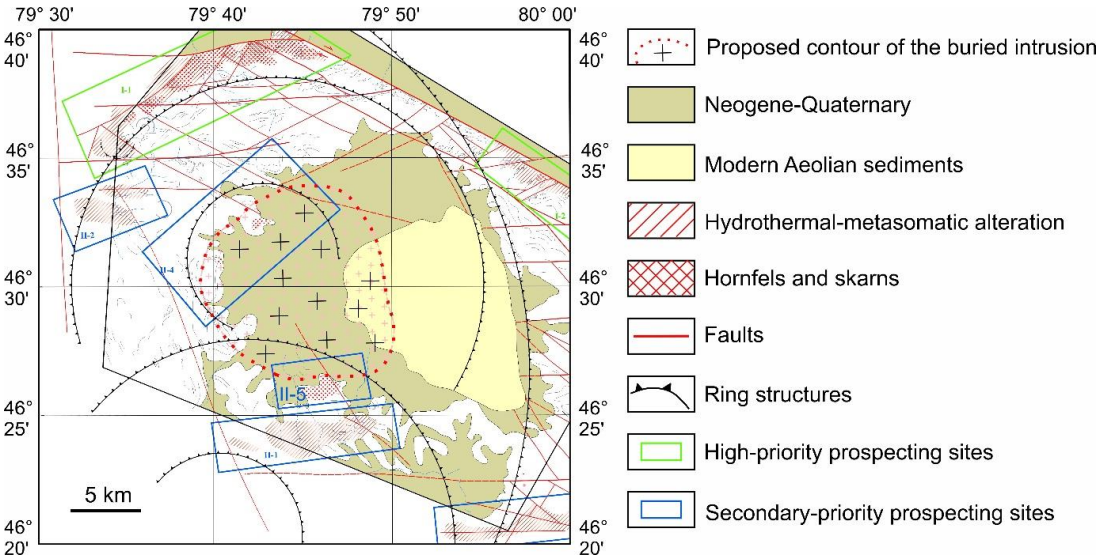


Figure 2. Geological structure map of the Arganaty district.

Petrographic examination of core samples showed that its composition refers to porphyritic biotite granite, light, silicified and metasomatized to varying degrees (Figure 3). Albitization is observed here in comparison with the well-known Aktogay porphyry-

https://doi.org/10.5593/sgem2024/1.1/s01.01

copper deposit, where potassium feldspathization is widespread. Sulfide mineralization of ore is associated with silicification. Molybdenum mineralization is associated with late vein quartz and overlaps with silicified and variably metasomatized light porphyritic granodiorites (Figure 4).

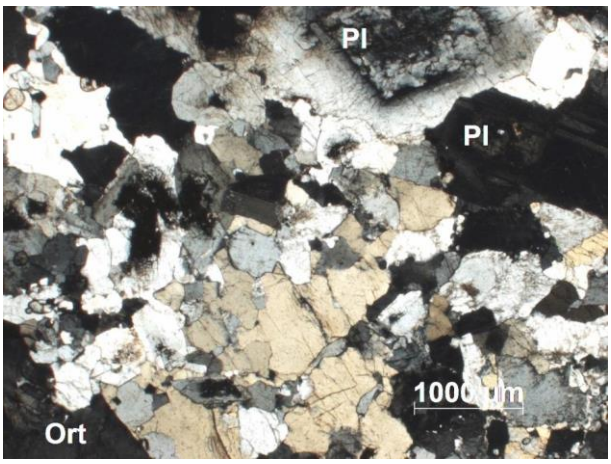


Figure 3 – Porphyritic biotite granite: phenocrystals of orthoclase (Ort), zonal albitized andesine (Pl)

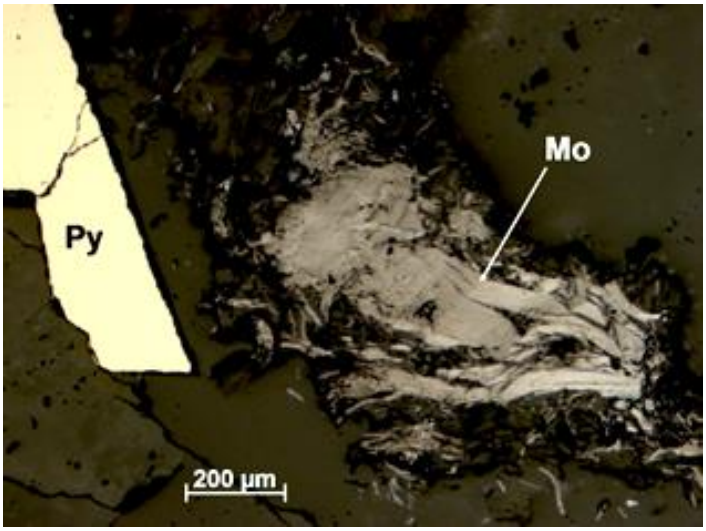


Figure 4. The molybdenum aggregate (Mo) and pyrite (Py)

DISCUSSION

Comparing the new site with the known deposits of the Aktogay ore field (Aktogai, Aidarly), it can be noted that there are similarities in the geological structure of the deposits of both groups. In the Arganaty region, as well as in the Aktogai region, there is a blind intrusion of granitoids, linear and annular structures, and discontinuous disturbances are widespread [11]. The rocks have undergone hydrothermal changes. Ore mineralization is associated with intrusions by porphyritic granodiorites having an annular structure. Taking into account the similarity with the Aktogay ore field, it can be assumed that there may be a porphyry-type copper-molybdenum object on our area.

CONCLUSION

Predecessor researchers gave a negative view on the fertility of the Arganaty region, but current achievements in geology made it possible to get a new view on the data and get a different interpretation. We have identified the new perspective site, the prospects of which have been confirmed by field research, drilling operations and laboratory analyses of core material.

Considering the resemblance with the Aktogai ore district, it can be assumed that mineralization in the Arganaty district is associated with intrusive magmatism [10], [15]. Its signs (a single stock, magmatic ring structures, and areas of thermal impact on the host rocks) are found within this region. In addition to the porphyritic granitoids of Arganaty massif, there may also be earlier phase granodiorite massifs in the adjacent region to Arganatinsky district, which may be covered by sedimentary rocks of cenozoic age and may be a source massif for copper-molybdenum mineralisation. It is expected Copper-molybdenum porphyry object in this region. Also gold, lead, tungsten, and tin ores are expected in this area. It is recommended to conduct prospecting in this region by applying ground geophysical works, drilling mapping, and prospecting wells.

ACKNOWLEDGEMENTS

This research has been funded by the Science Committee of the Ministry of Science and Higher Education of the Republic of Kazakhstan of AP14870909.

REFERENCES

[1] Baibatsha, A., Arshamov, Y., Bekbotayeva, A., Baratov, R. Geology of the main industrial types of copper ore deposits in Kazakhstan, International Multidisciplinary Scientific GeoConference Surveying Geology and Mining Ecology Management, SGEM 2017, Bulgary, vol. 17/issue 1.1, pp 231-238, 2017.

[2] Baibatsha, A., Omarova, G., Dyussembayeva, K., Kassenova, A. Kokkiya - a promising for Kazakhstan gold-metasomatic type of deposit, International Multidisciplinary Scientific GeoConference Surveying Geology and Mining Ecology Management, SGEM 2016, Bulgary, pp. 289-296, 2016.

[3] Baibatsha, A.B., Bekbotayeva, A.A., Bekbotayev, A.T. Ore minerals of Carboniferous copper sediment-hosted Zhezkazgan deposit (Central Kazakhstan), International Multidisciplinary Scientific GeoConference Surveying Geology and Mining Ecology Management, SGEM 2015, pp 329-335, 2015.

[4] Baibatsha, A.B., Bekbotayev, A.T., Bekbotayeva, A.A. Ore-bearing strata lithology of the Zhezkazgan copper sandstones deposit. International Multidisciplinary Scientific GeoConference Surveying Geology and Mining Ecology Management, SGEM, 2013, vol. 1, pp 135-140.

[5] Duczmal-Czernikiewicz, A., Baibatsha, A., Bekbotayeva, A., Omarova, G., Baisalova, A. Ore minerals and metal distribution in tailings of sediment-hosted stratiform copper deposits from poland and kazakhstan. Minerals, vol. 11/issue 7, 752, 2021.

[6] Baibatsha, A.B., Muszyński, A., Shaiyakhmet, T.K., Shakirova, G.S. 3d modeling for estimation of engineering-geological conditions of operating mineral deposits, News

https://doi.org/10.5593/sgem2024/1.1/s01.01

of the National Academy of Sciences of the Republic of Kazakhstan, Series of Geology and Technical Sciences, Kazakhstan, vol. 4/issue 442, pp 19-27, 2020.

[7] Baibatsha, A., Dussembayeva, K., Bekbotayeva, A., Abdullayeva, M.T. Tails of enrichment factories as the technogenic mineral resources, International Multidisciplinary Scientific GeoConference Surveying Geology and Mining Ecology Management, SGEM 2018, Bulgary, vol 18/issue 1.1, pp. 519-526, 2018.

[8] Baibatsha, A., Dyussembayeva, K., Bekbotayeva, A. Study of tails enrichment factory Zhezkazgan as a technogenic ore deposits, International Multidisciplinary Scientific GeoConference Surveying Geology and Mining Ecology Management, SGEM 2016, Bulgary, vol. 1, pp. 579-586, 2016.

[9] Baibatsha, A.B., Bekbotayeva, A.A., Mamanov, E. Detection of deep ore-controlling structure using remote sensing, International Multidisciplinary Scientific GeoConference Surveying Geology and Mining Ecology Management, SGEM 2015, Bulgary, 2015, pp. 113-118.

[10] Baibatsha, A.B., Peng, S., Satibekova, S.B. Estimation of the physical-mechanical properties of the rocks on the degree of coal metamorphism, News of the National Academy of Sciences of the Republic of Kazakhstan, Series of Geology and Technical Sciences, Kazakhstan, 2019, vol. 1, pp 187-194.

[11] Baibatsha, A.B. Paleovalleys mapping using remote sensing, International Archives of the Photogrammetry, Remote Sensing and Spatial Information Sciences – ISPRS, Archives, vol. 40/issue 5, pp. 83-86, 2014.

[12] Omarova, G., Baibatsha, A., Abdykirova, G.Z. Flotation enrichment of enrichment factory tailings for use as technogenic ore, International Multidisciplinary Scientific GeoConference Surveying Geology and Mining Ecology Management, SGEM 2019, Bulgary, vol. 19/issue 1.1, pp. 195-202, 2019.

[13] Baibatsha, A.B., Mamanov, E.Z. Geology and geodynamics of Karsakpay-Ulytau geosuture zone and its prospects for minerals, News of the National Academy of Sciences of the Republic of Kazakhstan, Series of Geology and Technical Sciences, Kazakhstan, vol. 1, number 421, pp. 46-62, 2017.

[14] Baibatsha, A. Relationship of paleozoides and mineral deposits of Kazakhstan with the paleozoic superplume, International Multidisciplinary Scientific GeoConference Surveying Geology and Mining Ecology Management, SGEM 2017, Bulgary, vol. 17/issue 11, pp. 479-486, 2017.

[15] Antonenko, A. A., Zhukov, N. M., Pavlova, Z. N., Goikolova, T. V. The Varvarinskoye Complex Copper–Gold Deposit in Northern Kazakhstan: Mineral Types and Ore Composition, Geology of Ore Deposits, Russia, vol. 62/issue 4, pp 314-331, 2020.

[16] Baibatsha, A., Omarova, G., Shakirova, G. Innovative technologies of mineral resources predictioin on covered territories, International Multidisciplinary Scientific GeoConference Surveying Geology and Mining Ecology Management, SGEM, 2019, vol. 19/issue 1.1, pp 271-278, 2019.

[17] Baibatsha, A., Mamanov, Y., Bekbotayev, A. Allocation of perspective ores on the areas Shu-Ile belt on the materials remote sensing, International Multidisciplinary

Scientific GeoConference Surveying Geology and Mining Ecology Management, SGEM, 2016, vol. 1, pp 35-42.

[18] Kembayev, M., Muratkhanov, D., Rais, S. On the plume-tectonic nature of the geological structure of the Shu-Ile region of Kazakhstan, International Multidisciplinary Scientific GeoConference: SGEM 2023, vol. 23/issue 1.1, pp 93-99, 2023.

[19] Antonenko, A.A., Zhukov, N.M., Gerzen, L.Y., Goikolova, T.V. Features of mineral and element composition of poor ores of deposits Aktogay and Bozshakol, News of the National Academy of Sciences of the Republic of Kazakhstan, Series of Geology and Technical Sciences, Kazakhstan, 2016, vol. 4, number 418, pp. 18–27.

[20] Muratkhanov, D., Kembayev, M., Sayat, R. A new approach to the forecast of porphyry copper deposits on the buried territories of Kazakhstan, International Multidisciplinary Scientific GeoConference: SGEM 2023, vol. 23/issue 1.1, pp 3-9, 2023.

https://doi.org/10.5593/sgem2024/1.1/s01.01

ANALYSIS OF THE MINERAL RESOURCE OF KAZAKHSTAN

Assoc. Prof. M.A. Mizernaya[1]
Assoc. Prof. T.A. Oitseva[1]
Assoc. Prof. O. N. Kuzmina[1]
PhD st. T.M. Aitkazyyev[1]
PhD Z.I. Chernenko[1]

[1] D. Serikbaev East Kazakhstan State Technical University, Ust-Kamenogorsk, **Republic of Kazakhstan**

ABSTRACT

The objective of this study is to conduct an in-depth analysis of the mineral resource base in Kazakhstan, specifically focusing on copper, zinc, lead, and gold, with the aim of identifying key determinants crucial for ensuring its sustainable development. The mineral resource sector serves as a cornerstone of Kazakhstan's economy and industrial landscape. This article seeks to elucidate the critical parameters defining its current state, placing particular emphasis on the presence and quality of mineral deposits. Furthermore, it encompasses a comprehensive examination of the technological advancements in both extraction and processing methodologies, as well as the efficient utilization of natural resources within the contemporary economic milieu of the country.

The research methodology employed entails a rigorous scrutiny of data pertaining to reserves and extraction rates of the primary metal groups, which hold strategic significance within Kazakhstan's resource agenda. Notably, this analysis is conducted against the backdrop of a concerning trend marked by declining reserves across virtually all categories of raw materials. Additionally, the study delves into the intricacies of industrial production diversification.

The findings underscore that mining enterprises predominantly export more than 80% of their output to foreign markets in the form of competitively priced raw materials, driven by factors such as accelerated investment returns, reduced capital outlays, and sustained demand. However, a notable and consistent uptrend is observed in Kazakhstan's economic reliance on imported finished metal products.

Of particular concern is the disproportionately high proportion of foreign investors wielding significant decision-making authority within Kazakhstan's mining enterprises, exceeding a third of the total investor base. Such a pronounced foreign presence poses a substantial risk to the domestic raw materials industry, necessitating urgent reforms in the procedures governing rights allocation for geological exploration and access to geological data.

Furthermore, the study highlights the pressing need to address issues such as outdated equipment and technologies prevalent in certain industry enterprises, as well as the inadequate adaptation of transportation-logistics and energy systems to effectively cater to the requirements of the mining sector.

In summary, the comprehensive analysis of the mineral resource industry's current status has revealed a myriad of challenges that must be diligently addressed to foster its sustainable development trajectory.

Keywords: raw materials, “critical metals” , Kazakhstan, mineral resource, economic stability

https://doi.org/10.5593/sgem2024/1.1/s01.02

INTRODUCTION

Kazakhstan occupies one of the leading places in the world in terms of resource availability; we occupy the 6th position in the ranking of countries. Thus, in terms of reserves of chromium, molybdenum, uranium, lead, zinc and silver, Kazakhstan is among the top five; in terms of reserves of copper, oil and gold - in the top 15 countries. In addition, on a global scale, our country has huge deposits of coal, bauxite, molybdenum, and iron ore (figure 2.1).

According to the data of the National Statistical Committee of the Republic of Kazakhstan [1-2], in 2022, the share of the mining industry in the domestic regional product (DRP) of Kazakhstan was about 10.3%. This figure indicates the high economic importance of this industry for the country's standard of living. The mining industry is also economically important in resource-rich countries such as Australia, China, Russia, etc., where its share in GDP is in the range of 10-18% [3].

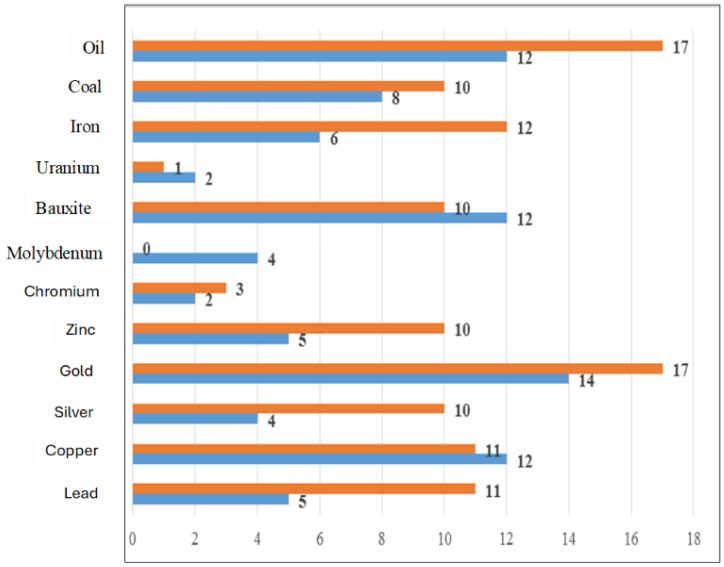


Figure 1. Range of mineral resources (blue- reserves; orange-production) of Kazakhstan in 2022 year

As can be seen in figure 1, Kazakhstan occupies a leading position not only in reserves, but also in the export of mineral raw materials. However, most of the products are shipped abroad in the form of products of low stages of production (crude oil, concentrates). This situation is ineffective from the point of view of the long-term perspective.

1 Discussion of problems of the mineral resources industry of Kazakhstan

One of the biggest risks of the development of the country's mining complex is the global depletion of natural resources. In the last decade, in the context of ever-increasing production at the developed fields and a very small volume and low final efficiency of geological exploration, the trends of non-replenishment of recoverable reserves, reduction of production rates and deterioration of the quality of raw materials have been constantly increasing. The reserves of Pb, Zn, Cr, Ag decreased by almost 15%. A slight increase in the reserves of Fe, Mn, Pb, Zn, Au was obtained due to revaluation and additional study of the developed objects on the flanks and deep horizons. The ores of the deposits explored in recent years are often characterized by poor quality and cannot be equivalent to the depleted reserves.

Mining enterprises engaged in the extraction and processing of non-ferrous metals face serious problems now. Most of the deposits are provided with previously explored reserves for no more than 10-15 years. The situation is not saved yet by the poor ores copper-porphyry deposits involved in the exploitation, the processing of which is carried out using modern high-performance and efficient mining and processing schemes [4].

A tense situation has developed with the use of the mineral resource base of precious metals. Currently, 97% of the explored gold reserves are at the disposal of subsoil users, and only 53% of them are involved in exploitation. This is due to the exhaustion of a significant part of the explored reserves of easily enriched oxidized ores, the insufficient introduction of acceptable technologies for the beneficiation of refractory ores of gold ore deposits and the low quality of reserves of leading minerals in complex gold-bearing deposits of pyrite-polymetallic and copper-porphyry geological and industrial types.

First, it is necessary to realize the natural potential of the subsoil to replenish and develop the mineral resource base of Kazakhstan by increasing scientific and technological provision and organizing geological exploration [5-6].

The second, no less significant problem of the mining complex is the weak diversification of industrial production. The industry's enterprises export more than 80% of their products to foreign markets in the form of products of the first and second stages, due to faster return on investment, lower capital costs and stable demand. There is a risk of growing economic dependence of the Republic of Kazakhstan on the supply of finished higher value-added metal products, the volume of which is growing from year to year. The share of foreign investors with the pre-emptive right to make management decisions in the fields of Kazakhstan is 1/3 of the total number of investors. Such a large share is a high risk for the domestic raw materials industry, creating such negative factors as: structural unemployment through competition with an enterprise with foreign investments, a high degree of dependence on foreign investors, repatriation of profits, deterioration of the environmental situation, strengthening of monopolistic trends in the markets, conflict of interests of the recipient country and foreign investors, facilitating the movement of resources abroad, deepening of social differentiation.

It is necessary to intensify the processes of diversification of production, especially in the copper, lead-zinc, aluminum, magnesium and gold processing industries; to develop special economic and industrial zones, with the subsequent transition to the following clusters: "Metallurgy and metalworking" in Karaganda, "Precious metals and jewelry production" in Astana, "Production and processing of rare and rare earth metals" in East Kazakhstan region; to build mini-factories based on the clusters being created.

The industry faces a problem of limited access to geological information for potential investors; long deadlines and a complex procedure for approving project documents for geological exploration; inconsistency of the current system of assessment and accounting of mineral reserves with international standards.

This requires reforming legislation in the field of subsoil use and, above all, in geological exploration. The procedure for granting rights to geological exploration and geological information needs to be liberalized. It is necessary to develop the market of geological exploration services by creating a favorable investment climate in the country, state regulation and legislative framework in the field of subsoil use. The system of assessment and accounting of mineral reserves of the Republic of Kazakhstan should be brought into line with international standards.

https://doi.org/10.5593/sgem2024/1.1/s01.02

Outdated machinery, equipment and technologies at individual enterprises of the industry do not meet the modern requirements of ecology, economics and integrated use of mineral raw materials, making it uncompetitive [7-9].
Poor adaptation of the transport, logistics and energy system to the needs of the industry. The transport component in the cost of production of mining enterprises reaches 30-40% or more. The low capacity of border crossing points of railway stations negatively affects the competitiveness of manufactured and exported products, making it difficult to sell them to foreign markets.
The high dependence of the industry on the energy infrastructure and the level of electricity tariffs affects the cost of production. Enterprises need a long-term and transparent tariff policy.
It is necessary to take measures to further development of the railway transport infrastructure, especially in East Kazakhstan, Kyzylorda, Akmola, Kostanay, Pavlodar and Karaganda regions; we need to revise transportation tariffs for industry products; to create alternative border crossing points for rail transport.

2. Analysis of the distribution of the main mineral deposits by region of Kazakhstan

In general, in the context of macro–regions, the deposits are distributed as follows: Northern Kazakhstan – 110 deposits of solid minerals; Southern Kazakhstan - 118 deposits of solid minerals; Central–Eastern Kazakhstan - deposits of solid minerals; Western Kazakhstan – 46 deposits of solid minerals.
North Kazakhstan region is represented by deposits of tin, titanium, phosphorite, lead and polymetals. South Kazakhstan, which includes Turkestan, Kyzylorda, Almaty and Zhambyl regions, has deposits of uranium, gold, phosphorite, manganese, copper, lead, vanadium and polymetals [10-12].
Many types of minerals have been identified and studied to varying degrees in this macro-region. 286 deposits have been explored (110 of them are solid minerals). Among them are 34 - metal, 2 - nonmetals, 217 -construction and technological raw materials and 33 - groundwater, of which 6 are mineral ones. The territory of the region is a part of the North Kazakhstan uranium-ore, diamond-bearing and tin-rare metal province. It revealed significant reserves of mineral raw materials, which make up the balance of the Republic of Kazakhstan: tin - 65%, zirconium - 36.6%, uranium - 19%, titanium - 5%, tungsten - 1.1%. The prospects for expanding the mineral resource base are very significant, especially in the south-west of the macro-region. There are a number of significant deposits and ore occurrences of gold, silver, technical and jewelry diamonds, tin, titanium, non-ferrous and rare metals, brown coals.
In Akmola region, exploration and production is carried out at deposits of gold, uranium, quartzite, iron, manganese and coal. The deposits of Kostanay region are represented by the presence of deposits of bauxite, molybdenum, rare earth elements, iron, asbestos, polymetals, gold and brown coals.
South Kazakhstan. It includes Turkestan, Zhambyl, Kyzylorda and Almaty regions.
This macro-region contains deposits of uranium, gold, phosphorites, manganese, copper, lead, vanadium and polymetals. In addition, mineral resources for the production of building materials (limestone, gypsum, quartz sands, refractory ceramic and bentonite clays, mineral paints, ornamental stones). Significant reserves of non-ferrous and rare earth metals (vanadium - 66%, uranium - 14.7%, zinc - 16.4%, lead - 11.1%) [13] (figures 2).

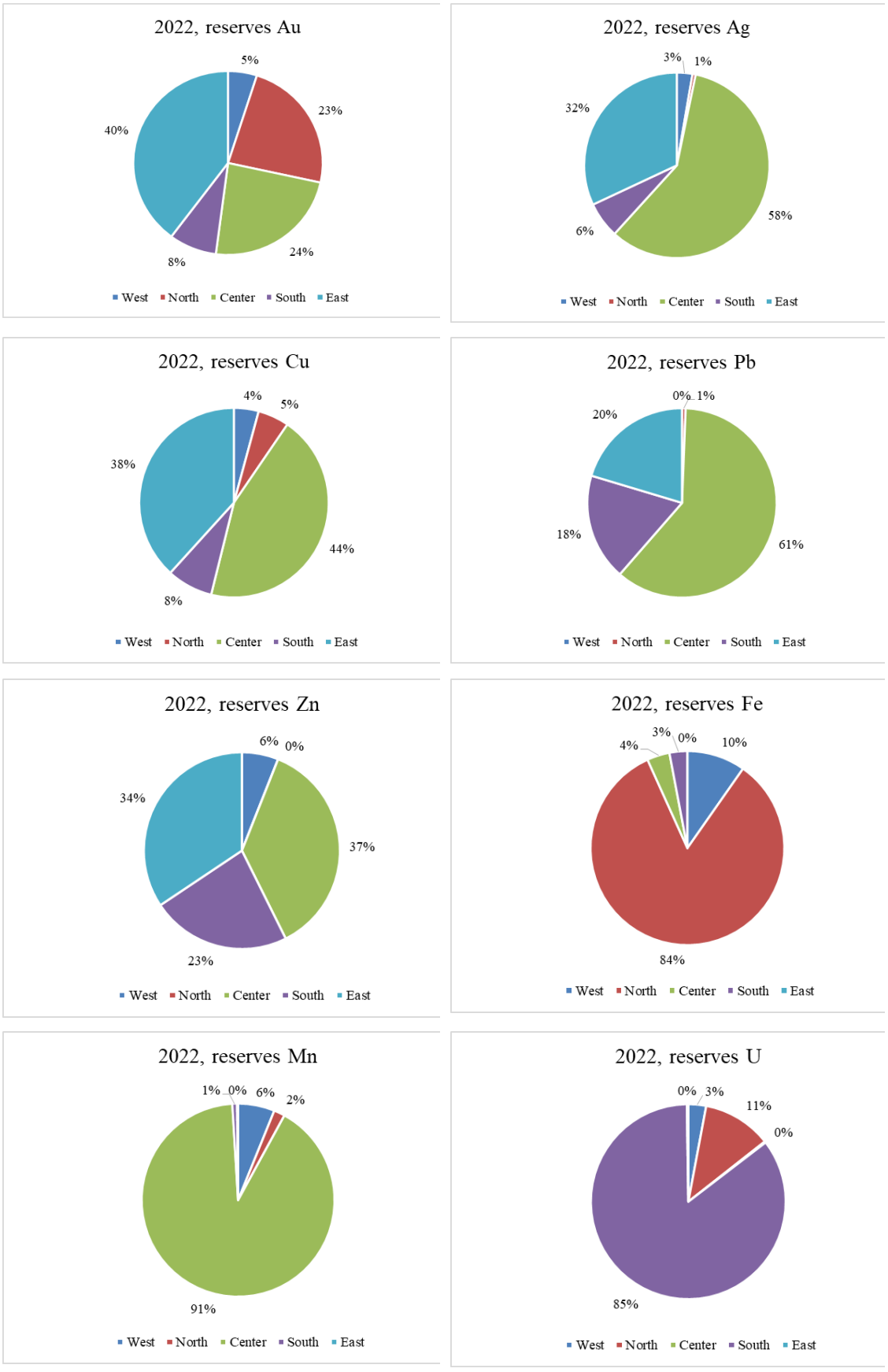


Figure 2. State of reserves by macroregion of Kazakhstan, 2022

https://doi.org/10.5593/sgem2024/1.1/s01.02

Of the 118 fields in operation by subsoil users, production is carried out at 43 fields, exploration is carried out at 45, and production together with exploration activities is carried out at 30 fields. In Kyzylorda region, exploration and production are carried out on deposits of gold, uranium, vanadium and lead. The deposits of Almaty region are represented by the presence of deposits of manganese, polymetals and gold. Turkestan region is represented by the presence of deposits of uranium, gold and phosphorites. In Zhambyl region, exploration and production are carried out at deposits of gold, phosphorites, titanium, barite, ferrous, non-ferrous, rare earth and rare metals.

Central Kazakhstan macro-region (Karaganda and Pavlodar regions) has deposits of copper, methane, gold, phosphorite, manganese, iron, cobalt, and polymetals. There are 268 solid mineral deposits on its territory, including deposits of copper, gold, phosphorites, manganese, iron, cobalt, and polymetals. Production is carried out at 94 fields, exploration at 112, and production together with exploration activities - at 61 fields. In Karaganda region, exploration and production are carried out at deposits of copper, manganese, coal, barite, gold, polymetals, iron. The deposits of Pavlodar region are represented by the presence of deposits of coal, copper, cobalt, and gold.

In East Kazakhstan macro-region (East Kazakhstan, Abaн regions), exploration and production are carried out at deposits of gold, copper, polymetals, nickel. As of January 1, 2023, there are only 718 subsoil use objects in East Kazakhstan: 252 contracts, 299 licenses for exploration of solid minerals, 7 licenses for extraction of solid minerals, 43 licenses for production of widespread mineral deposits, 10 licenses for geological survey of subsoil, 4 licenses for individual income tax, 61 licenses for artisanal mining, 42 permits for widespread mineral deposits.

In relation to the total reserves of the Republic of Kazakhstan, a significant proportion of metals with balance reserves is concentrated on the territory of East Kazakhstan (East Kazakhstan region and Abay region): copper - 38.15%, lead - 21.1%, zinc - 36.38%, gold - 32.6%, silver - 32.06%, nickel - 9%, cobalt - 6%, titanium - 10.6%, zirconium - 29%, coal - 3%[14].

On the territory of West Kazakhstan macro-region (West Kazakhstan, Atyrau, Mangistau and Aktobe regions) there are 46 solid mineral deposits, including chromite, copper, gold, rare earth elements, manganese, borate, bitumen, kaolin and titanium. Production is carried out at 21 fields, exploration -at 14, and production together with exploration activities - at 10 fields. In Aktobe region, exploration and production are carried out on deposits of gold, manganese, kaolin, chromite, copper, and titanium. The deposits of Mangystau region are represented by rare earth elements and bitumen. In West Kazakhstan region, exploration and production is carried out at kaolin and borate deposits.

Thus, the main reserves of solid minerals are concentrated in Northern, Central and East macro-regions, where the bulk of the existing contracts for exploration and production are implemented [15].

CONCLUSIONS

An analysis of the distribution of solid minerals on the territory of Kazakhstan showed that the main deposits of metal ores, rare earth elements are concentrated in Kostanay, Akmola, Pavlodar and East Kazakhstan regions. South Kazakhstan is mainly represented

by gold, phosphorus, and non-ferrous metals. Western Kazakhstan is represented by deposits of manganese, titanium, and borates.

Reserves of certain types of solid minerals - gold, copper, lead, zinc - by region are as follows: gold - East Kazakhstan region (36%), Akmola region (21%), Karaganda region (11%); 82% of copper reserves are concentrated in the eastern and central regions of the country; more than three thousand lead-zinc deposits are concentrated in Central, East and Southern Kazakhstan.

ACKNOWLEDGEMENT

This research has been funded by the Science Committee of the Ministry of Science and Higher Education of the Republic of Kazakhstan (Grant No. AP19676805)

REFERENCES

[1] Shcherba G.N., Bespaev X.A. et al. The Great Altai (Metallogeny), Book. 2. Alma-Ata: RIOVAKRK, 400 p., 2000.

[2] www.stat.gov.kz.

[3] https://www.gold.org/goldhub/data/gold-trading-volumes.

[4] Issayeva L., Togizov K., Duczmal-Czernikiewicz A., Kurmangazhina M., Muratkhanov D. Ore-controlling factors as the basis for singling out the prospective areas within the Syrymbet rare-metal deposit, Northern Kazakhstan, Mining of Mineral Deposits, vol. 16. pp 14-21,2022.

[5] https://www.barrick.com/English/investors.

[6] Rafailovich M.S. Geology of Central Asian gold: ore evolution, metasomatic formations, explosive breccia. Monograph, Almaty, p. 423, 2013. (in Russian)

[7] https://www.statista.com/statistics/1295667/kazakhstan-mine-production-of-gold

[8] Mizernaya, M.A, Aitbayeva, S. S., Mizerny, A. I., Dyachkov, B. A., Miroshnikova A. P. Geochemical characteristics and metalogeny of Herzin granitoid complexes (Eastern Kazakhstan) Naukovyi Visnyk Natsionalnoho Hirnychoho Universytetu, Ukraine, vol. 1, pp. 5-10, 2020.

[9] Nikitchenko I.I. Minerals of Kazakhstan: Explanatory note to the Map of mineral resources of Kazakhstan on a scale of 1:1000000. – Kokshetau, 2002. – 188 p. (in Russian).

[10] Mizernaya, M.A., Miroshnikova, A.P., Pyatkova, A.P., Akilbaeva, A.T.

The main geological-industrial types of gold deposits in East Kazakhstan Naukovyi Visnyk Natsionalnoho Hirnychoho Universytetu, 5, pp. 5–10, 2019.

[11] Geology of mineral deposits: A. B. Baybatsha. - Almaty: KazNTU, 2008. - 368 p. (in Russian)

[12] Shcherba G.N., Djachkov B.A. et al. The Great Altai (Geology and Metallogeny). Book 1. Geological structure. Alma-Ata: Gylym, p. 229, 1998. (in Russian)

https://doi.org/10.5593/sgem2024/1.1/s01.02

[13] Rare earth metals. World ranking of countries. – URL: https://nedradv.ru/nedradv/ru/msr?obj=ca79a46078f5785d6a24f2c3830d59b6 (in Russian)

[14] Reference books on industrial raw materials (deposits of gold, copper, lead, zinc, rare metals), 2015 – 2017 y. (in Russian).

[15] Rare earth elements are strategic metals of the future. – URL: //https://www.rough-polished.com/ru/analytics/127226.html (in Russian)

ABOUT THE GENETIC TYPES OF COPPER DEPOSITS IN KAZAKHSTAN AND THE PROSPECTS FOR IDENTIFICATION OF NEW ECONOMIC COPPER OBJECTS

Daulet Muratkhanov[1]

Yerkhozha Mamanov[1]

Bulegenov Kanat[1]

[1] Satbayev University, Almaty, **Republic of Kazakhstan**

ABSTRACT

Kazakhstan is on leading position in the world in terms of reserves and mining of copper ores. There are 30 deposits with approved reservest. Nowadays, the copper industry of the Rrepublic is provided with a raw material base. Among them, the Zhezkazgan deposit remains unique in terms of reserves and a set of components. The main geological and industrial types of copper deposits (in terms of mining) are deposits of copper sandstones (58%), copper pyrite (17.1%), copper porphyry (8.2%), scarn (4.2%), etc. In the total balance of reserves, ores such as copper sandstones account for 28%, copper porphyry – 42%. Deposits of copper sandstones Zhezkazgan, Itauyz, Zhamanaybat, etc. are located in Central Kazakhstan, copper-porphyry – in Central (Bozshchakol, Konyrat, etc.) and Southern (Koksai, Aktogay, Aidarly) Kazakhstan. Among the copper-pyrite deposits are distinguished: named after 50 years of October, Priorskoye, etc. – in Mugalzhar; Akbastau, Kosmurun – in Chingiz. Of the copper-skarn deposits, the Sayak group is known, and Shatyrkul is known from quartz-sulfide (vein copper) deposits. In addition to the listed leading types, copper-nickel deposits (Maksut, etc.), copper-zeolite deposits of the manto type (Temirlik), etc. are known in Kazakhstan. The depletion of reserves of previously discovered deposits raises the question of the discovery of new natural sources that lie deep. A new theoretical framework is proposed for the prediction of copper deposits, based on the provisions of the plume-tectonic concept, taking into account metallogenic analysis.

Keywords: Prediction of ore deposits, copper deposits, sulfide ores, plume tectonics, porphyry copper deposits.

INTRODUCTION

Kazakhstan occupies one of the leading places in the world in terms of reserves of copper ores. Kazakhstan's proven copper reserves are estimated at 37 million tons (or 5.5 % of global reserves) [1], [2], [3], [4]. According to this indicator, the Republic ranks 4th in the world after Chile, Indonesia and the USA [5], [6], [7]. More than 90 copper deposits have been explored on the territory of the Republic of Kazakhstan. The Dzhezkazgan deposit of copper sandstones, the Aktogay and Aidarly copper-porphyry deposits are among the largest [8], [9], [10], [11].

https://doi.org/10.5593/sgem2024/1.1/s01.03

The balance sheet approved 30 deposits. Among them, Zhezkazgan is unique in terms of reserves and a set of minerals. The large deposits include Konyrat, Zhaman-Aybat, Bozshakol, Koksai, Kaskyrmys, Nurkazgan (Samarskoye). Of the total number of about 70 deposits, there are 30 copper ore deposits, the rest belong to complex, copper-containing ones. Deposits of copper sandstones Zhezkazgan, Zhaman-Aybat, Saryoba, Itauz, etc. They are located in Central Kazakhstan, copper porphyry - in Central (Konyrat, Bozshakol, Borly, Nurkazgan, Kyzyltu, etc.) and Southern (Koksai, Aktogay, Aidarly, Kaskyrmys, Vostok I-IV) Kazakhstan. Among the copper-pyrite deposits, the following are distinguished: 50 years of October, Priorskoye, Avangard, Arilshinskoye, etc. in Mugolzhary; Akbastau, Kosmurun in Shyngys. Of the copper-skarn deposits, the most famous are the Sayak and Karatas deposits. quartz-sulfide (copper core) Shatyrkul, Jaisan. In addition to the listed leading types, copper-nickel deposits (Maksut, Koytas, Kamkor), copper-zeolite deposits of the manto type (Temirlik), etc. are known in Kazakhstan [12], [13], [14]. The prospects for identifying new industrial copper deposits in Kazakhstan are still significant. Today, the copper industry of the republic has been provided with a raw material base for 30 years. The problem is the discovery of new deposits, which requires a new interpretation of the geology and tectonics of Kazakhstan to explain the patterns of placement of copper deposits in Kazakhstan to predict new deposits [15], [16].

MATERIALS AND METHODS

In the light of new evidence and their modern generalizations, the views of previous researchers on scientific developments in the geology of Kazakhstan need a new interpretation. An attempt to correlate the tectonic structure of Kazakhstan with the main structural elements of the planet according to plate tectonics was not successful. The mechanical transfer of plate-tectonic elements obvious on a planetary scale has not been confirmed in practice and has confused the geotectonics and geodynamics of the country's territory [17].

A fundamentally new geodynamic model of the development and formation of the geological structure of the territory of Kazakhstan developed on the basis of plume tectonics explains the features of localization of active sedimentation zones, magmatic complexes, metamorphism of geological objects, ophiolite zones and olistostromes, localization of productive and promising metallogenic zones and areas with large and unique mineral deposits [18].

RESULTS

Kazakhstan's copper deposits are grouped into the following industrial and genetic types.

Bozshakol Lower Cambrian industrial genetic type. This type is confined to the Bozshakol Cambro-Ordovician island-arc system formed on the Lower Cambrian oceanic crust, represented by cushion aphyric basalts with jasperoids and hyaloclastites of the Or-Dabai (Maikain) formation.

Konyrat-Aktogay industrial genetic type. Copper-porphyry deposits associated with porphyry intrusions of the Balkhash early-middle carboniferous and Koldar (Topar) early permian magmatic complexes have been identified in this type [19]. These include the practically exhausted Konyrat deposit, the explored large deposits of Aktogai,

Aidarly, Koksai and a number of smaller deposits and manifestations: Borly, Kenkuduk, Kaskyrkazgan, Auzbaki, etc.

Zhezkazgan industrial genetic type. This type includes the upper red-colored molasse with deposits of copper sandstones associated with it. In terms of ore quality and industrial significance, the deposits of the complex are in the first place among copper deposits in the republic, including about 30% of its total reserves. The unique Zhezkazgan field under development is of the greatest industrial importance [3], [4], [8]. The fields of the Northern Group (Saryoba, Itauz, Kypshakpai) and Zhamanaybat are prepared for development. In the Teniz depression, this complex includes small non-industrial deposits Kepen, Kyzyloba, Borisovskoye, Vladimirovskoye, etc., localized in sandstones of the middle-upper carboniferous, and Kopkazgan, Aksu, Ushkarasu, Altynkazgan, Kiymin group, etc., confined to rocks of the Lower Permian. In the southern part of the Shu-Sarysui depression, mineralization was cut by a number of deep wells in the Tastinsky, Nizhneshusky uplifts and in the Iirkuduk ledge.

Samara industrial genetic type. It is confined to the outer part of the central region of the northern and northeastern branches of the Devonian belt, in which volcanites of the middle-main composition of the Lower Devonian are distributed, interspersed with volcanomictic sedimentary rocks and broken through by granitoids of the tonalite series of the Early-Middle Devonian Karamendinsky and sub-alkaline granitoids of the Middle Devonian Kokkuduktobinsky, Karasorsky and Kainarsky intrusive complexes, which are associated with the mineralization of gold-copper- porphyry type. The Nurkazgan (Samarskoye) field has been explored and put into operation.

The Nizhne-Ili industrial genetic type. The considered one is confined to the inner part of the central region of the Devonian belt, composed mainly of acidic subalkaline volcanites of the Lower-Middle Devonian and their erupting intrusions of the Middle-Late Devonian. The complex is most pronounced in the southwestern branch of the Devonian belt, where it is represented by the deposits of the Nizhneili (Kaskyrmys, Vostok I-V, Semizkol) and Saryshagan (Saryshagan, Kokbuzau) groups. The mineralization of the molybdenum-copper-porphyry complex. The predominantly acidic composition of the rocks containing porphyry systems caused a low copper content in the ores, which does not exceed 0.5%.

Mugalzhar metallogenic type. This type is confined to the Greenstone zone of Mugalzhar and is represented by Middle Devonian igneous rocks and other associated zinc-copper pyrite deposits and ore occurrences [15]. The volcanoes of the complex are divided into four formations: Aktogai, Mugalzhar, Kurkudyk and Milyashinsky. The first three of them are lava strata of oceanic crust formed in an oceanic rift. The lower Aktogay formation is composed of a series of parallel steeply falling dikes of diabases, between which the gently lying pillow lavas of the main composition are sandwiched.

The Rudny Altai metallogenic type. It is developed within the Rudny altai structural and formation metallogenic zone, separated in the southwest from the East Kalba (Kalba-Narym) Irtysh crushing zone, in the northeast from the structures of the Beloubinsk-Sarymsakta zone by discontinuous faults that extend from the south-west to the Northeastern crushing zone. Mineralization is associated with the terrigenous-basalt-rhyolite formation formed in the conditions of the island-arc system, laid down on the Caledonian sialic base.

https://doi.org/10.5593/sgem2024/1.1/s01.03

The Maykain metallogenic type. The tin under consideration is confined to the Ordovician encymatic island arc of the Maikain metallogenic zone, which arose on the Cambrian oceanic crust, composed of pillow soda basalts, spilites, jaspers, quartzites, siliceous siltstones, limestones, sandstones of the Kosgombai formation. Volcanites predominate in the composition of the rocks. Sedimentary rocks are of subordinate importance, their number increases slightly towards the top of the section.

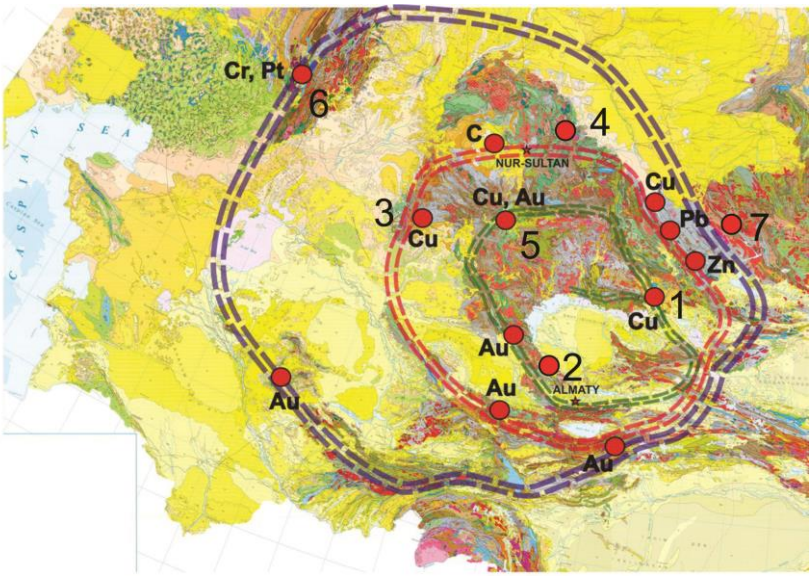


Figure 1 - The location of metallogenic zones of copper deposits (according to A.B. Baybatsha, 2017 with additions and changes by the authors). The numbers indicate the deposits: 1 – Aktogai, 2 – Nizhne-Ili, 3 – Zhezkazgan, 4 – Bozshakol, 5 – Samar, 6 – deposits of the Mugalzhar type, 7 – deposits of the Rudny Altai type.

DISCUSSION

According to modern tectonic zoning [14], the following ring structures are distinguished on the territory of Kazakhstan: the inner (its contour is green), the middle (red) and the outer ring (purple) (Figure 1). Large deposits and ore belts of Kazakhstan are associated with the ring structures. The Shu-Ili ore belt with gold (Akbakai, Beskempir) and rare metal (Karakamys, Shakshagaily) deposits and copper deposits of *Konyrat-Aktogay* and *Nizhne-Ili* types are confined to the first inner ring [20]. The Kurumsak uranium-molybdenum-vanadium, Karsakpai iron ore, Zharma tantalum-niobium-rare earth and *Zhezkazgan* lead-zinc-copper complex, and *Maykain* copper-lead-zinc metallogenic zones and copper deposits of the *Samara type* are confined to the second ring. The outer ring structure controls the copper-nickel (with accompanying platinum) and chromite mineralization of the Mugalzhar type and copper-polymetallic deposits of the Rudnoaltai metallogenic type, the Bakyrshyk gold mineralization and the rare metal mineralization of the Kalba ore zone [7].

CONCLUSION

It follows from this that there is a pattern of copper deposits being confined to ring structures associated with plume tectonics. Predictive studies of sites and ore-

controlling structures promising for copper ores should be based on a new theoretical basis and using space sensing data. In light of this, the following can be considered the main objectives of the research:

- forecast of new promising copper sites, description of their geological structure and geodynamics with identification of signs of potential localization of minerals;

- identification of ore-controlling zones with characteristic geodynamic features, geological structures, magmatic manifestations and signs of mineralization;

- scientific description of geological features, characteristics and signs of promising sites;

- investigation of the geological nature of promising areas identified on a new theoretical basis based on plume tectonics and localization of promising sites for prospecting on them according to cosmic and geological data;

- It should be taken into account during planning prospecting operations the regularity of the occurrence of ore belts to regional ring structures.

ACKNOWLEDGEMENTS

This research has been funded by the Science Committee of the Ministry of Science and Higher Education of the Republic of Kazakhstan of AP14870909.

REFERENCES

[1] Baibatsha, A., Arshamov, Y., Bekbotayeva, A., Baratov, R. Geology of the main industrial types of copper ore deposits in Kazakhstan, International Multidisciplinary Scientific GeoConference Surveying Geology and Mining Ecology Management, SGEM 2017, Bulgary, vol. 17/issue 1.1, pp 231-238, 2017.

[2] Baibatsha, A., Omarova, G., Dyussembayeva, K., Kassenova, A. Kokkiya - a promising for Kazakhstan gold-metasomatic type of deposit, International Multidisciplinary Scientific GeoConference Surveying Geology and Mining Ecology Management, SGEM 2016, Bulgary, pp. 289-296, 2016.

[3] Baibatsha, A.B., Bekbotayeva, A.A., Bekbotayev, A.T. Ore minerals of Carboniferous copper sediment-hosted Zhezkazgan deposit (Central Kazakhstan), International Multidisciplinary Scientific GeoConference Surveying Geology and Mining Ecology Management, SGEM 2015, pp 329-335, 2015.

[4] Baibatsha, A.B., Bekbotayev, A.T., Bekbotayeva, A.A. Ore-bearing strata lithology of the Zhezkazgan copper sandstones deposit. International Multidisciplinary Scientific GeoConference Surveying Geology and Mining Ecology Management, SGEM, 2013, vol. 1, pp 135-140.

[5] Duczmal-Czernikiewicz, A., Baibatsha, A., Bekbotayeva, A., Omarova, G., Baisalova, A. Ore minerals and metal distribution in tailings of sediment-hosted stratiform copper deposits from poland and kazakhstan. Minerals, vol. 11/issue 7, 752, 2021.

[6] Baibatsha, A.B., Muszyński, A., Shaiyakhmet, T.K., Shakirova, G.S. 3d modeling for estimation of engineering-geological conditions of operating mineral deposits, News

https://doi.org/10.5593/sgem2024/1.1/s01.03

of the National Academy of Sciences of the Republic of Kazakhstan, Series of Geology and Technical Sciences, Kazakhstan, vol. 4/issue 442, pp 19-27, 2020.

[7] Baibatsha, A., Dussembayeva, K., Bekbotayeva, A., Abdullayeva, M.T. Tails of enrichment factories as the technogenic mineral resources, International Multidisciplinary Scientific GeoConference Surveying Geology and Mining Ecology Management, SGEM 2018, Bulgary, vol 18/issue 1.1, pp. 519-526, 2018.

[8] Baibatsha, A., Dyussembayeva, K., Bekbotayeva, A. Study of tails enrichment factory Zhezkazgan as a technogenic ore deposits, International Multidisciplinary Scientific GeoConference Surveying Geology and Mining Ecology Management, SGEM 2016, Bulgary, vol. 1, pp. 579-586, 2016.

[9] Baibatsha, A.B., Bekbotayeva, A.A., Mamanov, E. Detection of deep ore-controlling structure using remote sensing, International Multidisciplinary Scientific GeoConference Surveying Geology and Mining Ecology Management, SGEM 2015, Bulgary, 2015, pp. 113-118.

[10] Baibatsha, A.B., Peng, S., Satibekova, S.B. Estimation of the physical-mechanical properties of the rocks on the degree of coal metamorphism, News of the National Academy of Sciences of the Republic of Kazakhstan, Series of Geology and Technical Sciences, Kazakhstan, 2019, vol. 1, pp 187-194.

[11] Baibatsha, A.B. Paleovalleys mapping using remote sensing, International Archives of the Photogrammetry, Remote Sensing and Spatial Information Sciences – ISPRS, Archives, vol. 40/issue 5, pp. 83-86, 2014.

[12] Omarova, G., Baibatsha, A., Abdykirova, G.Z. Flotation enrichment of enrichment factory tailings for use as technogenic ore, International Multidisciplinary Scientific GeoConference Surveying Geology and Mining Ecology Management, SGEM 2019, Bulgary, vol. 19/issue 1.1, pp. 195-202, 2019.

[13] Baibatsha, A.B., Mamanov, E.Z. Geology and geodynamics of Karsakpay-Ulytau geosuture zone and its prospects for minerals, News of the National Academy of Sciences of the Republic of Kazakhstan, Series of Geology and Technical Sciences, Kazakhstan, vol. 1, number 421, pp. 46-62, 2017.

[14] Baibatsha, A. Relationship of paleozoides and mineral deposits of Kazakhstan with the paleozoic superplume, International Multidisciplinary Scientific GeoConference Surveying Geology and Mining Ecology Management, SGEM 2017, Bulgary, vol. 17/issue 11, pp. 479-486, 2017.

[15] Antonenko, A. A., Zhukov, N. M., Pavlova, Z. N., Goikolova, T. V. The Varvarinskoye Complex Copper–Gold Deposit in Northern Kazakhstan: Mineral Types and Ore Composition, Geology of Ore Deposits, Russia, vol. 62/issue 4, pp 314-331, 2020.

[16] Baibatsha, A., Omarova, G., Shakirova, G. Innovative technologies of mineral resources predictioin on covered territories, International Multidisciplinary Scientific GeoConference Surveying Geology and Mining Ecology Management, SGEM, 2019, vol. 19/issue 1.1, pp 271-278, 2019.

[17] Baibatsha, A., Mamanov, Y., Bekbotayev, A. Allocation of perspective ores on the areas Shu-Ile belt on the materials remote sensing, International Multidisciplinary

Scientific GeoConference Surveying Geology and Mining Ecology Management, SGEM, 2016, vol. 1, pp 35-42.

[18] Kembayev, M., Muratkhanov, D., Rais, S. On the plume-tectonic nature of the geological structure of the Shu-Ile region of Kazakhstan, International Multidisciplinary Scientific GeoConference: SGEM 2023, vol. 23/issue 1.1, pp 93-99, 2023.

[19] Antonenko, A.A., Zhukov, N.M., Gerzen, L.Y., Goikolova, T.V. Features of mineral and element composition of poor ores of deposits Aktogay and Bozshakol, News of the National Academy of Sciences of the Republic of Kazakhstan, Series of Geology and Technical Sciences, Kazakhstan, 2016, vol. 4, number 418, pp. 18–27.

[20] Muratkhanov, D., Kembayev, M., Sayat, R. A new approach to the forecast of porphyry copper deposits on the buried territories of Kazakhstan, International Multidisciplinary Scientific GeoConference: SGEM 2023, vol. 23/issue 1.1, pp 3-9, 2023.

https://doi.org/10.5593/sgem2024/1.1/s01.03

ASSESSING THE AGRICULTURAL CONSEQUENCES OF LANDFILL KELMEND-ASSOCIATED HEAVY METAL CONTAMINATION IN RAHOVË VILLAGE

PhD(c). Elida Lecaj[1]
PhD(c). Bahri Sinani[3]
PhD(c). Adelina Haskaj[1]
PhD(c). Berat Sinani[2]
PhD(c). Majlinda Ramadani[1]
PhD(c). Blerta Retkoceri[4]
[1]Alma Mater Europaea Campus College "REZONANCA", **Prishtinë, Kosovo**
[2]University of Mitrovica, Faculty of Geo-Science, **Mitrovicë, Kosovo**
[3]Mitrovica Municipality, **Mitrovicë, Kosovo**
[4]University for Business and Technology UBT, **Prishtine Kosovo**

ABSTRACT

Soil contamination near waste dumps is a complex problem, landfills are major contributors to environmental pollution, causing continuous degradation of land surfaces and significant environmental consequences. The challenge in question is to combat soil degradation and heavy metal pollution by implementing targeted soil protection measures and policies. Soil pollution disrupts the delicate balance of nutrients within the soil.

This study focuses on assessing the impact of heavy metals by collecting soil samples in 5 different locations at a depth of 50 cm around a landfill and subsequently determining the concentration of heavy metals in the soil. The analysis involved the use of the NITON XL3t. XRF Analyzer device for measuring heavy metal concentrations, while pH levels in the soil samples were determined using a pH meter WTW 3310. Results from the soil sample analysis reveal that the concentrations of most heavy metals exceeded both national and international maximum allowable values.

The majority of metals analyzed exhibited median values higher than those found in European soil. To better understand the metal concentrations in soil, basic statistical methods, Pearson correlation, and cluster analysis were employed.

Ongoing environmental monitoring around landfills is crucial to alleviate adverse effects on human populations and the environment. To address these causes of land pollution, it is important to implement sustainable waste management policies and practices and to develop general awareness of the importance of environmental stewardship in the district where we live.

Keywords: Landfill, Heavy metal, soil, Niton XRF, Kosovo

INTRODUCTION

Soil pollution is one of the major concerns among the threats to land resources in Europe and globally. Economic and industrial activities worldwide have increasingly degraded

https://doi.org/10.5593/sgem2024/1.1/s01.04

the environment, and these degradations are also present in our country. Maintaining a clean environment is a persistent and troubling challenge, as is waste management, which is influenced by numerous factors.

Kosovo is known for its underground wealth, where in addition to mineral extraction, the management of mining waste resulting from mineral processing is of great importance. This waste management contributes to economic development and causes environmental pollution, such as air, water, and soil contamination, affecting not only Mitrovica but also surrounding areas [1]. The sites where this waste material is collected are called landfills. Among the many landfills in Kosovo is the Kelmendi landfill near Mitrovica, established in 1975 for the collection of industrial waste. High concentrations of heavy metals in these landfills have toxic effects on the environment, plants, and humans [5,6,7].

The purpose of this research was to determine the pollution levels of heavy metals in and around the Kelmendi landfill in Mitrovica. Seventeen heavy metals were analyzed using X-ray fluorescence (XRF) to assess the impact of activities at the Kelmendi landfill. Statistical analysis was used to calculate Pearson correlation and hierarchical clusters among different metals and locations.

Pollution factor (CF), pollution load index (PLI), and geo accumulation index (Igeo) were calculated to evaluate the level of soil pollution with heavy metals [4].

Some authors report high levels of heavy metals near these pollution sources, often exceeding the allowable values for soils [2,3]. Therefore, this paper aims to determine and monitor the levels of heavy metals in this area and to examine the influence of pH values, where soil pH (also known as soil reaction) is an indicator of soil acidity or alkalinity.

MATERIAL AND METHODS

Study Area

The study area encompasses agricultural lands and residential areas near the Kelmendi landfill. The use and exploitation of ores from the Trepça mine, along with their processing in the flotation of the first tunnel, has led to the disposal of industrial waste in the Kelmendi landfill. This landfill covers an area of 2-3 km² and is situated between two hills in the northeastern part of Mitrovica. On the western side, there is a stream that carries pollutants into the Ibër River. The landfill has a storage capacity of 8.2 million m³ over an area of 18.4 ha, with materials transported from the flotation facility to the landfill via a pipeline conveyor [3].

Soil sampling

The entire process of taking soil samples at the Kelmendi landfill was conducted across various locations covering the entire landfill area. The samples were collected following all norms and standards required for testing, using appropriate sampling tools. A total of five samples were taken at a depth of 50 cm. The collected soil samples were stored in well-labeled plastic bags and sent to the laboratory [8,9].

In the laboratory, the samples were air-dried, ground, and sieved using a 63 μm mesh to obtain a fine powder [10]. These samples were then analyzed using a Niton XLP Portable XRF Analyzer. The pH value was measured at the sampling site, and the exact sampling points were recorded using a handheld GPS "GARMIN CS 64. The concentrations of seventeen metals (K, Ca, Ti, V, Cr, Mn, Fe, Ni, Cu, Zn, As, Rb, Sr, Y, Zr, Th, and Nb)

were analyzed at five different locations. The locations are described in Table 1. The study area with sampling locations are shown in Figure 1.

Table 1. Sampling locations

Samples				
Nr.	Village	X	Y	Z
S_1	Rahove	4752675	7490161	655
S_2	Kelmend	4752366	7489899	612
S_3	Kelmend	4752169	7489615	594
S_4	Lisice	4751890	7490266	632
S_5	Lisice	4751967	7490583	655

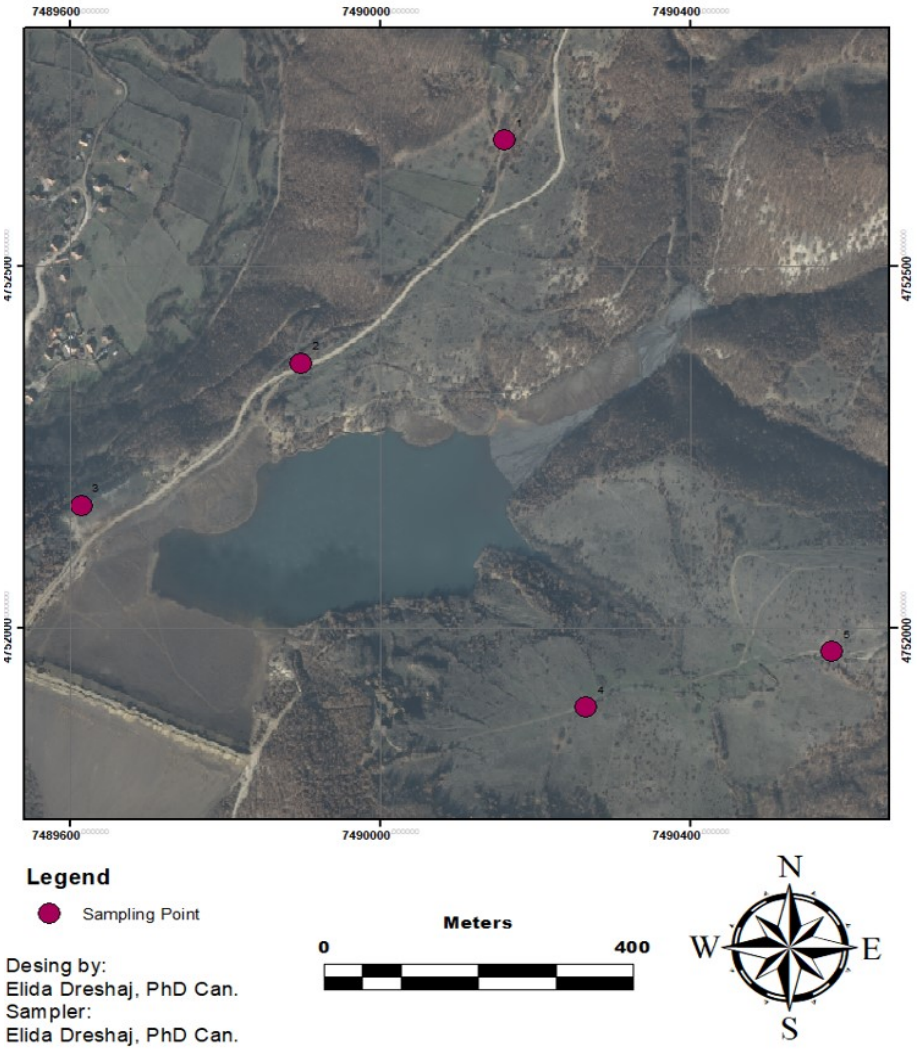


Figure 1. Study area with sampling sites (ArcGIS 10.7)

https://doi.org/10.5593/sgem2024/1.1/s01.04

Statistical Analysis

PAST 4.11 software was used for statistical analysis, including the calculation of minimum, maximum, mean, median, standard deviation, skewness, and kurtosis, as well as for cluster analysis.

Contamination Level Analysis for PTEs

Soil pollution by potentially toxic elements (PTEs) of the study area was assessed through various contamination assessment indices, namely the contamination factor (CF) and the pollution index (PLI) [15].

Contamination Factor

CF is defined as the ratio of metal content in the sample to the background value of the same metal, we used the formulas:

$$CF = C\ (metal)\ Sample/C\ (metal)\ background\ value$$

where C (metal) Sample: the concentration of the specific metal in the sample being tested and where C (metal) Background value: The natural or baseline concentration of the same metal in an uncontaminated reference sample or area.

Pollution Load Index (PLI)

The Pollution Load Index (PLI) is an estimation method first proposed by [15]. It has been widely used for detecting pollution levels.

If the pollution load index (PLI) is less than 1 it indicates optimal soil quality, and if a PLI equal to 1 proves that only basic levels of pollutants are present, while a PLI greater than 1 indicates ending the degradation of the quality of the area [11].

The pollution load index (PLI) equation is given by the following:

$$PLI = n\sqrt{}\ (CF_1 \times CF_2 \times CF_3 \times \ldots \times CF_n)$$

Where CF_i is the contamination factor for the i^{th} metal and n is the number of metals studied.

Geoaccumulation index (Igeo)

To evaluate the contamination impact of heavy metals in the soil, the geoaccumulation index (Igeo) was used to calculate the metal concentrations above background and presented in a classification system based on the intensity of heavy metal pollution in the soil.

$$Igeo = \frac{log2Cn}{1.5\ Bn}$$

Where: C_n is the measured concentration of the element in mg/kg, B_n is the average geochemical concentration of the corresponding metal in European stream soil in mg/kg [6,7,11,12,13]
The factor 1.5 is used to account for possible variations in the background values due to lithological variations

Müller [4] proposed the following classification system to interpret the Igeo values:
Igeo > 5 - extremely contaminated, 4 < Igeo ≤ 5 - strongly to extremely contaminated, 3 < Igeo ≤ 4 - strongly contaminated, 2 < Igeo ≤ 3 - moderately to strongly contaminated, 1 < Igeo ≤2 - moderately contaminated, 0 < Igeo ≤ 1 - uncontaminated to moderately contaminated, Igeo ≤ 0- uncontaminated [4].

RESULTS AND DISCUSSIONS

XRF results for the analyzed samples show the presence of trace elements. The presence of heavy metals in the analyzed samples, considering these values that represent the degree of pollution. From the data obtained from going out into the field and taking samples and the results obtained from laboratory analyses, we see that the area is quite contaminated.

Table 2. Contamination factor (CF) of the metals in the soil samples.

	Samples 1	Samples 2	Samples 3	Samples 4	Samples 5	Mean
K	0.24	0.66	1.51	0.62	0.67	0.74
Ca	19.09	10.44	2.14	6.04	6.01	8.74
Ti	18.39	23.68	32.54	23.42	29.19	25.44
V	1.03	1.50	1.88	1.60	2.08	1.62
Cr	0.28	0.71	0.77	0.40	0.23	0.48
Mn	0.21	8.30	20.77	1.41	0.51	6.24
Fe	0.45	2.50	5.09	1.34	1.41	2.16
Ni	0.91	2.33	1.12	0.32	0.21	0.98
Cu	ND	0.49	0.84	0.57	0.06	0.39
Zn	0.22	2.35	2.25	3.99	0.25	1.81
As	0.85	8.43	24.53	1.83	ND	7.13
Rb	0.49	0.67	1.42	0.69	0.98	0.85
Sr	4.85	4.17	0.96	5.71	8.20	4.78
Y	0.35	0.56	0.93	1.04	0.47	0.67
Zr	1.27	1.11	1.25	1.16	2.03	1.36
Th	2.90	2.90	2.30	2.90	4.40	3.08
Nb	0.55	0.53	1.06	0.44	0.80	0.68

From Table 2 which shows the Contamination Factor (CF) for metals that we analyzed in five soil samples, together with their average values showed: high contamination: Ca and Ti show significantly higher values of CF compared to metals of others, with average values of 8.74 and 25.44, respectively. Moderate contamination showed Mn, As and Sr where they also show significant values of CF, with average values of 6.24, 7.13 and 4.78 respectively.

Low contamination indicated metals such as K, Cr, Fe, Ni, Cu and Y have relatively lower CF values, with an average of less than 3.0, indicating lower levels of contamination.

Variation between samples: Some metals, such as Mn, show significant variation between samples (ranging from 0.21 to 20.77), suggesting uneven distribution of contamination, while other metals showed low values [8,14].

https://doi.org/10.5593/sgem2024/1.1/s01.04

Table 3. Basic statistical characteristics of the soil PTE concentrations in the study area.

	K	Ca	Ti	V	Cr	Mn	Fe	Ni	Cu	Zn	As	Rb	Sr	Y	Zr	Th	Nb	pH
N	5.0	5.0	5.0	5.0	5.0	5.0	5.0	5.0	5.0	5.0	5.0	5.0	5.0	5.0	5.0	5.0	5.0	5.0
Min	3776.0	5341.0	2575.0	41.0	34.0	127.0	11278.0	16.0	0.0	67.0	0.0	48.7	96.4	17.5	222.0	23.0	8.8	6.6
Max	24164.0	47729.0	4556.0	83.0	116.0	12461.0	127349.0	175.0	117.0	1196.0	981.0	141.7	820.0	52.1	405.0	44.0	21.2	8.7
Sum	59209.0	109308.0	17811.0	323.0	359.0	18721.0	269700.0	367.0	274.0	2716.0	1425.0	424.9	2389.4	167.8	1361.0	154.0	67.5	37.2
Mean	11841.8	21861.6	3562.2	64.6	71.8	3744.2	53940.0	73.4	54.8	543.2	285.0	85.0	477.9	33.6	272.2	30.8	13.5	7.4
Std. error	3341.5	7253.2	344.8	7.2	16.8	2353.8	20068.5	28.5	22.1	213.9	183.9	16.2	117.3	6.7	33.7	3.5	2.3	0.4
Stand. dev	7471.9	16218.7	771.0	16.0	37.6	5263.3	44874.6	63.6	49.4	478.3	411.2	36.2	262.2	15.0	75.3	7.8	5.1	0.8
Median	10605.0	15108.0	3315.0	64.0	60.0	847.0	35126.0	68.0	68.0	674.0	73.0	69.4	485.0	28.1	249.0	29.0	11.0	7.5
25 percntil	6850.0	10188.0	2927.0	50.5	38.0	216.5	22373.0	20.0	4.5	71.0	17.0	58.0	256.7	20.5	227.0	26.0	9.7	6.7
75 percntil	17452.0	36912.0	4321.0	79.0	111.5	8720.5	94914.0	129.5	98.5	950.0	659.0	119.8	695.5	49.4	329.0	36.5	18.6	8.1
Skewness	1.3	1.2	0.1	-0.6	0.4	1.6	1.4	1.2	0.0	0.3	1.7	1.1	-0.3	0.4	2.1	1.6	1.0	1.0
Kurtosis	3.0	1.5	-0.9	0.3	-2.9	2.0	2.1	1.4	-2.0	-1.3	2.8	0.9	1.2	-2.5	4.5	3.4	-0.1	1.1
Geom. mean	10061.9	17212.9	3494.4	62.8	63.9	1153.6	40238.7	52.1	0.0	309.8	0.0	79.4	390.9	30.9	265.3	30.1	12.8	7.4
Coeff. var	63.1	74.2	21.6	24.8	52.3	140.6	83.2	86.7	90.2	88.1	144.3	42.6	54.9	44.8	27.7	25.4	37.6	11.2

The table 3 provided contains statistical analysis for various elements and the pH value. Fe, Ca and K have high mean values, indicating their prevalence. The pH values are relatively stable, with a low standard deviation. Mn and Ni exhibit high coefficients of variation, suggesting significant variability in their concentrations. Fe has the highest concentration range (Min: 11278, Max: 127349). Cu and As often show minimal or no concentrations, with zero at their minimum.

Table 4. Pearson correlation coefficients between metal concentrations in soil

	K	Ca	Ti	V	Cr	Mn	Fe	Ni	Cu	Zn	As	Rb	Sr	Y	Zr	Th	Nb
K		0.09	0.04	0.25	0.17	0.03	0.01	0.86	0.10	0.60	0.03	0.01	0.22	0.28	0.92	0.52	0.09
Ca	-0.82		0.04	0.04	0.49	0.33	0.20	0.74	0.19	0.41	0.35	0.09	0.76	0.16	0.75	0.99	0.31
Ti	0.89	-0.89		0.04	0.49	0.21	0.11	0.84	0.35	0.89	0.23	0.01	0.66	0.48	0.52	0.90	0.06
V	0.64	-0.89	0.90		0.84	0.60	0.41	0.61	0.60	0.88	0.63	0.13	0.82	0.56	0.28	0.47	0.26
Cr	0.72	-0.42	0.42	0.13		0.05	0.06	0.16	0.07	0.40	0.06	0.40	0.07	0.44	0.29	0.18	0.56
Mn	0.92	-0.55	0.67	0.32	0.89		0.00	0.47	0.10	0.65	0.00	0.11	0.05	0.43	0.58	0.25	0.17
Fe	0.97	-0.69	0.79	0.49	0.86	0.98		0.57	0.08	0.61	0.00	0.06	0.11	0.37	0.72	0.37	0.13
Ni	0.11	0.20	-0.13	-0.31	0.73	0.43	0.35		0.63	0.84	0.52	0.87	0.37	0.78	0.32	0.43	0.88
Cu	0.81	-0.70	0.53	0.32	0.85	0.81	0.83	0.29		0.12	0.10	0.28	0.15	0.06	0.34	0.20	0.57
Zn	0.32	-0.48	0.09	0.09	0.50	0.28	0.31	0.12	0.78		0.66	0.90	0.59	0.05	0.26	0.37	0.67
As	0.92	-0.54	0.66	0.30	0.86	1.00	0.97	0.39	0.80	0.27		0.11	0.04	0.42	0.56	0.23	0.16
Rb	0.95	-0.82	0.96	0.76	0.49	0.79	0.87	-0.10	0.60	0.08	0.79		0.42	0.44	0.70	0.83	0.02
Sr	-0.67	0.19	-0.27	0.14	-0.84	-0.88	-0.79	-0.52	-0.74	-0.32	-0.90	-0.47		0.49	0.21	0.03	0.46
Y	0.61	-0.73	0.42	0.36	0.45	0.46	0.52	-0.17	0.86	0.88	0.48	0.46	-0.41		0.51	0.40	0.81
Zr	-0.06	-0.20	0.38	0.60	-0.60	-0.34	-0.22	-0.57	-0.55	-0.63	-0.35	0.24	0.68	-0.40		0.03	0.56
Th	-0.39	-0.01	0.08	0.43	-0.71	-0.63	-0.51	-0.46	-0.69	-0.52	-0.66	-0.13	0.90	-0.49	0.90		0.93
Nb	0.82	-0.58	0.86	0.62	0.35	0.73	0.76	-0.09	0.34	-0.26	0.73	0.93	-0.44	0.15	0.35	-0.05	

The Pearson correlation coefficient table from the data shows: Strong positive correlations show K and Nb as well as Fe and Mn show a very strong positive correlation. While strong negative correlations indicate Ca and Sr, V and Ca, K and Fe shows no significant correlation, K and As shows a very weak correlation. Th has strong positive correlations with Sr (r=0.90) and Nb (r=0.93), Mn has a perfect correlation with As (r=1.00). Elements such as Mn, Fe and As show high correlations, indicating that they often change together [4,9,10].

Table 5 Geoaccumulation index values of heavy metal parameters.

	Igeo Value 1	Igeo Value 2	Igeo Value 3	Igeo Value 4	Igeo Value 5	Igeo Class
K	-2.67	-1.18	0.01	-1.27	-1.16	0
Ca	3.67	2.80	0.51	2.01	2.00	4
Ti	3.62	3.98	4.44	3.96	4.28	5
V	-0.55	0.00	0.32	0.09	0.47	0
Cr	-2.42	-1.07	-0.96	-1.91	-2.73	0
Mn	-2.83	2.47	3.79	-0.09	-1.56	4
Fe	-1.73	0.74	1.76	-0.16	-0.09	1
Ni	-0.73	0.64	-0.42	-2.23	-2.81	0
Cu	ND	-1.63	-0.84	-1.39	-4.54	0
Zn	-2.75	0.65	0.58	1.41	-2.58	2
As	-0.82	2.49	4.03	0.28	ND	5
Rb	-1.62	-1.16	-0.08	-1.11	-0.62	0
Sr	1.69	1.48	-0.64	1.93	2.45	3
Y	-2.10	-1.42	-0.69	-0.53	-1.67	0
Zr	-0.25	-0.43	-0.27	-0.37	0.43	0
Th	0.95	0.95	0.62	0.95	1.55	2
Nb	-1.45	-1.51	-0.50	-1.77	-0.91	0

https://doi.org/10.5593/sgem2024/1.1/s01.04

K, V, Cr, Ni, Cu, Rb, Y, Th, as well as Nb are considered practically uncontaminated while Fe uncontaminated to average with only one contaminated value, Th, Zn are moderately contaminated, Ca Very e contaminated to extremely, Ti appears highly contaminated, Mn also appears severely contaminated, with one practically uncontaminated value and two moderately contaminated values, while Sr is moderately to highly contaminated, with one practically uncontaminated value.

CONCLUSION

From this study, which was analyzed using XRF results, the Contamination Factor (CF) analysis shows the presence of trace elements and contamination with heavy metals, indicating general high levels of contamination in the analyzed area. The pollution factor (CF) highlights the essential contribution to overall pollution, warranting special attention in environmental management strategies. Elements such as Ca and Ti show high contamination, while metals such as Mn, As, and Sr show moderate contamination. Fe, Ca, and K also have high concentrations, with stable pH values. Geochemical analyses, particularly the Geoaccumulation Index (Igeo), highlight significant contamination. K, V, Cr, Ni, Cu, Rb, Y, Th, and Nb from the analysis are practically uncontaminated, while Fe is uncontaminated to moderately contaminated. Th and Zn are moderately contaminated, while Ca, Ti, Mn, and Sr are highly contaminated. Correlation analysis reveals strong positive relationships between certain elements, while others show negative or weak correlations. Specific elements are categorized from virtually uncontaminated to heavily contaminated based on contamination levels.

REFERENCES

[1] Edon Maliqi, Edmond Haziri, Gani Maliqi, & Abdurrahman Kuleta. (2015). (PDF) Developing of Digital Terrain Model in Civil 3D for calculating the volumes for the Kelmend Landfill. https://doi.org/DOI: 10.13140/RG.2.1.4844.5606

[2] Maxhuni, A., Lazo, P., Kane, S., Qarri, F., Marku, E., & Harmens, H. (2016). First survey of atmospheric heavy metal deposition in Kosovo using moss biomonitoring. Environmental Science and Pollution Research, 23(1), 744–755. https://doi.org/10.1007/S11356-015-5257-1

[3] Kadriu, S., Sadiku, M., Kelmendi, M., Mulliqi, I., Aliu, M., & Hyseni, A. (2019). Scale of pollutions with heavy metals in water and sediment of River Ibër from landfill in Kelmend, Kosovo. Mining Science, Vol. 26, 147–155.https://doi.org/10.5277/MSC192610

[4] G. Muller, Index of geo–accumulation in sediments of the Rhine River. Geo Journal 2. 1969, 108–118.

[5] Fernandes- Ugalde, O., Scarpa, S., & Orgiazzi, A. (2022). LUKAS 2018 soil Module. https://esdac.jrc.ec.europa.eu/public_path/shared_folder/dataset/75-LUCAS-SOIL-2018/JRC_Report_2018-LUCAS_Soil_Final.pdf

[6] EU. (2006). EU Soil policy - Environment - European Commission. https://ec.europa.eu/environment/soil/soil_policy_en.htm

[7] FAO. (2015). World reference base for soil resources 2014.https://www.fao.org/3/i3794en/I3794en.pdf

[8] Tóth, G., Hermann, T., Da Silva, M. R., & Montanarella, L. (2016). Heavy metals in

agricultural soils of the European Union with implications for food safety. Environment International, 88, 299–309. https://doi.org/10.1016/j.envint.2015.12.017

[9] Abdolkarim Chehregani Rad, & Behrouz E. Malayeri. (2007). (PDF) Removal of Heavy Metals by Native Accumulator Plants. International Journal of Agriculture and Biology 9(3):462-465. https://www.researchgate.net/publication/234075893_Removal_of_Heavy_Metals_by_Native_Accumulator_Plants

[10] Ahmad, W., Alharthy, R. D., Zubair, M., Ahmed, M., Hameed, A., & Rafique, S. (2021). Toxic and heavy metals contamination assessment in soil and water to evaluate human health risk. Scientific Reports 2021 11:1, 11(1), 1–12. https://doi.org/10.1038/s41598-021-94616-4

[11] Alina Kabata-Pendias, A. B. M. (2007). Soils. Trace Elements from Soil to Human, 9–38. https://doi.org/10.1007/978-3-540-32714-1_3

[12] Kabata-Pendias, A., & Mukherjee, A. B. (2007). Trace elements from soil to human. Trace Elements from Soil to Human, 1–550. https://doi.org/10.1007/978-3-540-32714-1/COVER

[13] Prasad, S., Saluja, R., Joshi, V., & Garg, J. K. (2020). Heavy metal pollution in surface water of the Upper Ganga River, India: human health risk assessment. Environmental Monitoring and Assessment, 192(11). https://doi.org/10.1007/S10661-020-08701-8

[14] Udhezim administrativ, 2018. (n.d.). Republika e Kosovës · PDF file 2019-03-21 · imovine na kojima se nalaze supstance opasne po životnu sredinu. 5. Lokacije koje su sumljive kao zagađene u smislu ovog Administrativnog

[15] Tomlinson, D.L., Wilson, J.G., Harris, C.R. *et al.* Problems in the assessment of heavy-metal levels in estuaries and the formation of a pollution index. *Helgolander Meeresunters* **33**, 566–575 (1980). https://doi.org/10.1007/BF02414780

https://doi.org/10.5593/sgem2024/1.1/s01.04

CRITICAL ELEMENTS IN SEQUENTIAL LEACHED PHASES FROM DEEP-SEA POLYMETALLIC NODULES AND SEDIMENTS

Assoc. Prof. Dr. Atanas Hikov[1]

Assoc. Prof. Dr. Zlatka Milakovska[1]

Assoc. Prof. Dr. Valentina Lyubomirova[2]

Dr. Nadezhda Lihareva[1]

[1] Geological Institute, Bulgarian Academy of Sciences, **Bulgaria**
[2] Faculty of Chemistry and Pharmacy, "St. Kliment Ochridski" University, **Bulgaria**

ABSTRACT

The deep-sea metalliferous sediments and Fe-Mn polymetallic nodules formed in modern environment at the deep-sea ocean floor (> 4000 m depth) were evaluated as promising new raw materials, especially for critical elements as Li, Co, Cu, Mn, Ni, and rare earth elements (REE). We use a selective sequential leaching procedure to study the distribution of main and trace elements in sequential leached phases from deep-sea polymetallic nodules and sediments from the eastern part of the Clarion-Clipperton fractures zone, NE Pacific. Results show extraction of Mn in the leach 2 in both nodules and sediments. Cobalt, Ni, Cu, Zn have similar behavior because these elements are preferentially incorporated into MnO_2 phases. The extraction of Fe, K, P and most of trace elements is different for leach 2, 3 and residual fraction for nodules and sediments. Partially extraction of Fe in leach 2 and the extraction of P from sediments in leach 2 attests to the presence of FeOOH and authigenic fine-grained phosphate component (apatite) which are intergrown with the Mn oxyhydroxides. The second group of elements (Al, Fe, Ti, K, Rb, V, Zr, Nb, Mo, Sb, W, Ba, U) represents a detrital (illite, kaolinite, chlorite, andesine, zircon, rutile) and authigenic (barite) composition and has higher content in the residual fraction in sediments. Part of these elements (Zr, Nb, Mo, U) as well as Sc, Y and REE have strong positive correlation with phosphorous and form the third group of elements which is bound in the authigenic apatite. The results will reveal the main factors that control the trace element concentration in both polymetallic nodules and sediments and help future extraction of these raw materials.

Keywords: sequential leaching, critical elements, polymetallic nodules, deep-sea sediments

INTRODUCTION

The fast growth of the world economy and development of new emerging technologies has led to a growing demand for rare and trace elements, some of them defined as critical raw materials. The deep-sea Fe-Mn polymetallic nodules and crusts and metalliferous sediments formed in modern environment at the deep-sea ocean floor (> 4000 m depth) were evaluated as promising new raw materials, especially for high-tech elements as Li, Co, Cu, Mn, Ni, and rare earth elements (REE) *[5]*. That is why the Clarion-Clipperton Zone (CCZ) in the NE Pacific is the area of greatest economic interest for nodules and sediments extraction *[14]*.

https://doi.org/10.5593/sgem2024/1.1/s01.05

In the present study, we use a selective sequential leaching procedure applied by Koschinsky and Halbach (1995) that allows us to separate the major mineral phases of the polymetallic nodules and sediments and their associated elements with special attention on the trace elements. Our aim is to reveal the main factors that control the trace element concentration in both polymetallic nodules and sediments from the Interoceanmetal (IOM) exploration area located in the eastern part of the Clarion-Clipperton Zone, NE Pacific.

GEOLOGICAL SETTING AND SAMPLING

The studied area covers 630 km^2 of the seafloor in the eastern part of the Clarion-Clipperton fractures Zone (CCZ), NE Pacific between $11^0$06'–$11^0$26'N latitude and $119^0$25'–$119^0$42'W longitude at depth varying from 4,300 to 4,500 m (Fig. 1). Box-core samples were collected during the 2019 Interoceanmetal cruise. The explored stations were distributed among various geomorphological types of the bottom relief, represented mostly by undulating hilly plains, intersected by longitudinal ridges oriented in the meridional direction, and sub-parallel volcanic massifs *[2]*. All stations sampled are located below the critical carbonate compensation depth. The nodules (between 1 and 10 cm in diameter) were observed on the top of and partly buried in the seabed sediments. Their main mineral phases are fine-grained, amorphous or poorly crystalline (10°A manganate (todorokite), quartz, muscovite, vernadite). Detrital and authigenic minerals are chlorite, Na-K micas, apatite, barite *[6]*. Based on morphology, size, surface texture, growth environment, and Mn/Fe ratio the nodules are classified as diagenetic, hydrogenetic and mixed hydrogenetic-diagenetic genetic types *[4, 9]*.

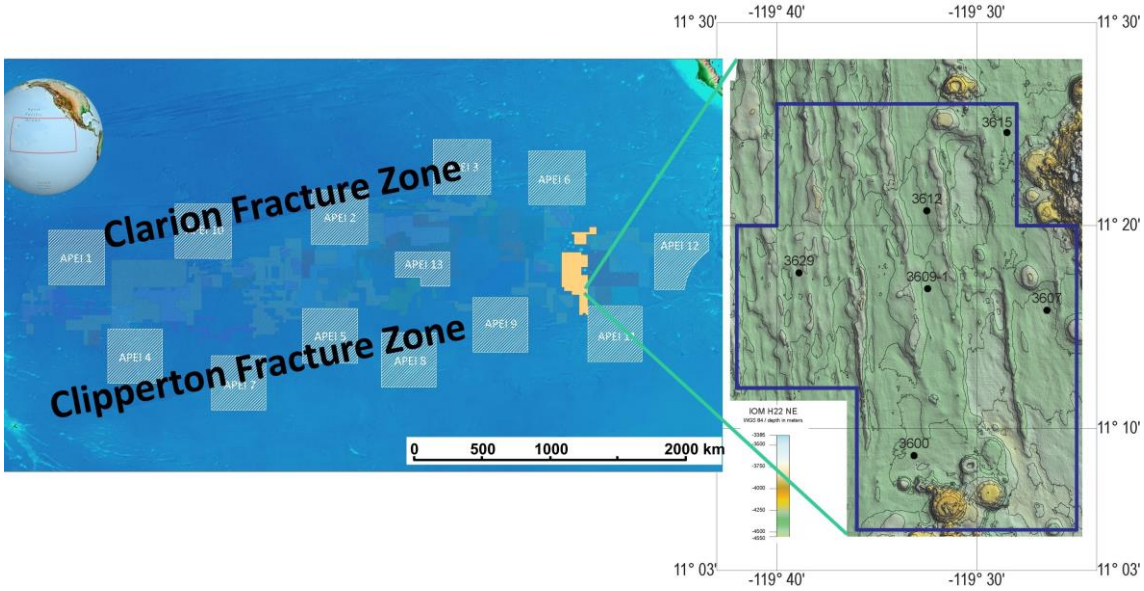


Fig. 1. Geomorphological map of the seafloor and location of the sampling area in the Interoceanmetal exploration area (yellow) in the eastern part of the Clarion-Clipperton fractures Zone

The sediment composition at all stations is dominated by light brown siliceous silty clays with irregular dark patches along the entire core down to 45-cm in depth. The top

7–12 cm layer comprises semiliquid, predominantly dark brown-coloured, siliceous silty clay, denoted as geochemically active layer (GAL), the medium for polymetallic nodule formation. The redox potential (Eh) value of the GAL ranges from +462 mV to +545 mV (average +494 mV) and indicates a tendency to decrease with depth. The active reaction (pH) of the environment is mostly neutral for all sediments, changing weakly from 7.01 to 7.52, averaging 7.36. The mineral composition according to the XRD data is uniform in quality and quantity. An amorphous phase (84–88%) predominates, representing biogenic opal, authigenic Fe-Mn (hydr)oxides and clay minerals. This phase composition defines the sediments as clayey siliceous ooze. The crystalline phases illite, kaolinite, chlorite, quartz, andesine represent a detrital component, as halite, cristobalite and barite are of authigenic origin. Illite, illite/smectite, chlorite/vermiculite and kaolinite, and quartz admixture were detected in all fractions < 2 μm *[7]*.

Two nodules and one sediment sample were selected for the leaching procedure. The first nodule (3600N) from sample station 3600 is diagenetic and contains 32.95 wt % Mn, 5.44 wt % Fe, 0,16 wt % Co, 1,70 wt % Ni and 1,50 wt % Cu while the second nodule (3607N) from sample station 3607 is hydrogenetic with 22.62 wt % Mn, 8.26 wt % Fe, 0,30 wt % Co, 0,58 wt % Ni and 1,07 wt % Cu *[6]*. The sediment sample (3600/3-5) is from depth interval 3 to 5 cm and contains 0.70 wt % Mn, 4.36 wt % Fe, 65 ppm Co, 191 ppm Ni and 379 ppm Cu *[7]*.

METHODS

The bulk samples were separated into four fractions of different mobility and bonding forms *[8]*: (1) Easily leachable fraction (extracted by acetic acid/Na acetate buffer, pH 5) for exchangeable adsorbed cations and Ca carbonates; (2) Easily reducible fraction (extracted by hydroxylamine hydrochloride buffer, pH 2) for Mn oxides; (3) Moderately reducible fraction (extracted by oxalic acid/ammonia oxalate buffer, pH 3.5) for amorphous Fe oxyhydroxides; (4) Residual fraction (total digestion with HF, HCI, HNO_3) for crystalline detrital phases (oxides, silica, aluminosilicates). Organic components are negligible in both nodules and sediments.

The chemical analyses of the leached fractions were carried out at the Faculty of Chemistry and Pharmacy, Sofia University using ICP-MS (Perkin-Elmer SCIEX Elan DRC-e) with a cross-flow nebulizer, following the analytical techniques of *[11]*. The concentrations of 69 elements were determined. Standard solutions were prepared from ICP-MS multi-element calibration standard solution-2 (Ultra Scientific) and ICP-MS Multielement Standard B (High Purity Standards).

RESULTS

The results are presented by relative element distribution in the leaches of the studied samples (Fig. 2). Leaching step 1 for exchangeable adsorbed cations and Ca carbonates shows low concentrations for most of the elements, especially for Mn and Fe, because of the lack of Ca carbonates below the critical carbonate compensation depth. The proportion of P is < 1 % in nodules and 3 % in sediments. The highest extraction in leach 1 show Sr (40–45 % in nodules and 24 % in sediments), Y (10.6–13.7 % in nodules and 23.3 % in sediments), K (10.5–12.8 % in nodules and 7.5 % in sediments), Tl (8.7–13 % in nodules and 5.1 % in sediments), U (9.6–15.5 % in nodules and 19.8 % in sediments) and Cu (2.3–3.4 % in nodules and 26.7 % in sediments).

https://doi.org/10.5593/sgem2024/1.1/s01.05

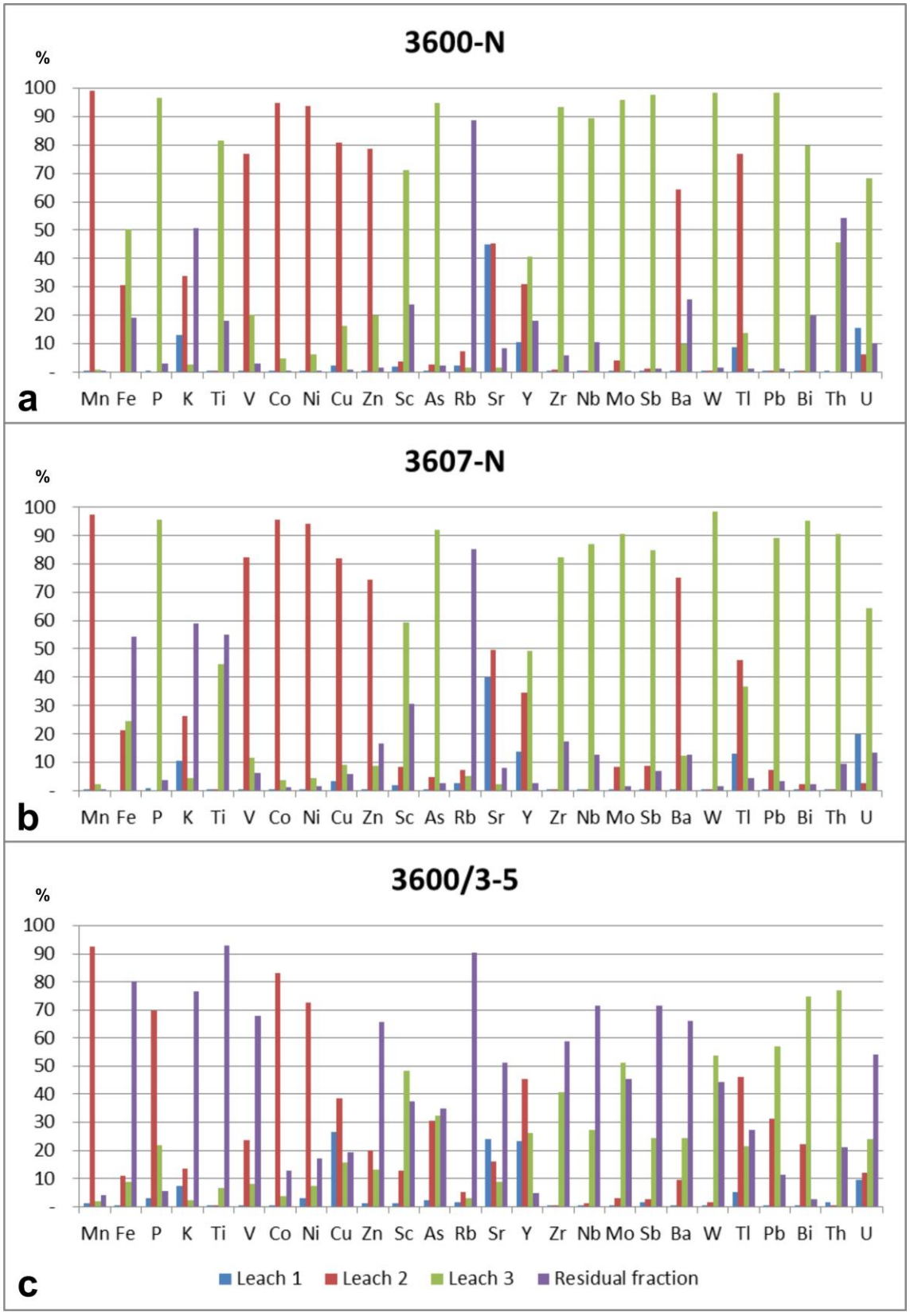


Fig. 2. Relative distribution of Mn, Fe, P, K and trace elements in the leaches of two nodule samples: *a)* 3600-N and *b)* 3607-N and one sediment sample: *c)* 3600/3-5 from the IOM exploration area in the eastern part of the CCZ, NE Pacific

The leach 2 is characterized with complete leaching of Mn in the nodules (97–99 %) and sediments (93 %). Cobalt and Ni have very similar distribution while V, Cu, Zn and Ba are leached significantly in nodules (65–82 %) and weaker in sediments (9–38 %). Iron and K are leached 22–34 % in nodules and 11–13.6 % in sediments. Phosphorous is not leached from nodules but it is leached significantly from sediments (69.6 %). Strontium, Y and Tl show similar proportion in different samples while As, Pb and Bi are leached only in sediments between 20 and 30 %.

The characteristic features of leach 3 are a significant extraction for Fe – 50.33 % in nodule 3600-N (24.57 % in nodule 3607-N and 8.63 % in sediments (3600/3-5)) and mostly complete extraction of P in nodules (95–96 %) while in sediments the extraction is only 22 %. High extraction in all samples is registered for Bi (75–95 %) while As, Zr, Nb, Mo, Sb, W, Pb and U are significant extracted in nodules (64–98 %) and weaker in sediments (24–54 %). Some elements like Ti, Sc, Y have similar distribution but lower extraction in leach 3 in all samples.

The residual fraction is poor of Mn and P (3–6 %) while the content of Fe and K increase from 19 % (3600-N) to 80 % (sediments) and from 51 % (3600-N) to 76.6 % (sediments) respectively. Only Rb has high extraction in all samples (85–90 %). Some elements like Ti, V, Zn, Zr, Nb, Mo, Sb, W, Ba, U have low extraction in nodules (0.2–25 %) and high extraction in sediments (44–93 %). Cobalt, Ni, Cu, As, Tl have similar distribution but lower extraction (13–35 %) in residual fraction in all samples.

The calculated correlations show varied element relations. Manganese has strong positive correlation (0.7–1) in the leaches with Mg, P, V, Co, Ni, Cu, Zn, Se, Cd, Te, La and moderate (0.5–0.7) with Sr and Eu. Iron has strong positive correlation with Ge and moderate with B, Ti and Cs. Phosphorous has strong positive correlation with Sc, V, Mn, Co, Ni, Cu, Zn, As, Y, Zr, Nb, Mo, all REE, Pb, Bi, U and moderate correlation with Cs, Ta, Hg and W. Titanium has strong to moderate positive correlation with Al, K, Sc, Fe, Rb, Zr, Nb, Mo, In, Sb, Cs, Hf, Ta, Pb, U. Most of the REE have strong positive correlation with P, Be, Y, Zr, Nb, Mo, Pb, Bi, U.

DISCUSSION

The metal ions and complexes from seawater and sediment pore fluids are sorbed onto the two major host phases, MnO_2 with a negatively charged surface and FeOOH with a positively charged surface. The 7-Å and 10-Å disordered phyllomanganates that compose the diagenetic nodules incorporate metal ions such as Ni^{2+}, Cu^{2+} and Li^{+} to balance negative charge deficits in their crystal lattice *[4, 5]*. On the other hand, negatively charged complexes of V, Pb, U and REE are attracted by the slightly positively charged FeOOH *[5]*.

Our results show extraction differences between polymetallic nodules and sediments. Only Mn is completely extracted in leach 2 in all studied samples. High extraction in leach 2 is registered for Co, Ni, Cu and Zn which is due to the sorption of these elements onto MnO_2 phases *[4, 5]*. Iron is preferentially extracted in leach 3 for the diagenetic nodule 3600-N (30 % is in leach 2) and prevails in the residual fraction for the hydrogenetic nodule 3707-N and sediments. This feature can be explained by the different origin of the nodules and by the high amount of detrital sediment material in nodule 3607-N. Partially extraction of Fe in leach 2 attests to that part of Fe is in the form of FeOOH intergrown with the Mn oxide in the vernadite *[8]*. The main Mn

https://doi.org/10.5593/sgem2024/1.1/s01.05

mineral phase (todorokite) contains small quantities of potassium *[6]* which explain partially extraction of K in leach 2. Phosphorous is mostly completely extracted from nodules in leach 3, while from sediments it is extracted in leach 2. Koschinsky and Halbach (1995) explain the highest extraction of P in leach 3 with strong association of phosphate to the Fe phase. The extraction of P from sediments in leach 2 and the positive correlation of Mn and P can be a result of an authigenic fine-grained phosphate component (apatite) which is intergrown with the Mn oxyhydroxides.

High extraction of Fe, K, Ti, Rb, V, Zn, Zr, Nb, Mo, Sb, W, Ba, U is registered in the sediment residual fraction. This is connected with detrital mineral phases as illite, kaolinite, chlorite, andesine, zircon, rutile and authigenic barite *[10]* as well as the influence of volcanic activity and/or hydrothermal processes *[15]*. Part of these elements (Zr, Nb, Mo, Sb, W and U) has high extraction in leach 3 for nodules which can be explained with their inclusion in authigenic apatite in nodules *[10, 12]*.

The correlations found between major and trace elements reflect the mineral composition of the studied nodules and sediments. The first group of elements includes Mn, Co, Ni, Cu, Zn, partly Fe and P. These elements are preferentially incorporated into MnO_2 phases *[5]*. The second group of elements (Al, Fe, Ti, K, Rb) represents a detrital clay (illite, kaolinite, chlorite) and volcanic (andesine) mineral composition *[7, 10]* and has higher content in the residual fraction. The third group of elements (P, Sc, Y, Zr, Nb, REE, U, etc.) is bound in the authigenic apatite *[10, 12]*. The carriers of these elements in deep-sea nodules and sediments include Fe-Mn oxyhydroxides, phosphate components and clay minerals *[1, 3, 5, 13]*. Our results show that the main important carrier is the phosphate component but the other two carriers cannot be excluded.

CONCLUSION

The selective leaching of deep-sea polymetallic nodules and sediments from the eastern part of the Clarion-Clipperton fractures zone, NE Pacific, show extraction of Mn in the leach 2 in both nodules and sediments. Cobalt, Ni, Cu, Zn have similar behavior because these elements are preferentially incorporated into MnO_2 phases. The extraction of Fe, K, P and most of trace elements is different for leach 2, 3 and residual fraction for nodules and sediments. Partially extraction of Fe in leach 2 and the extraction of P from sediments in leach 2 attests to the presence of FeOOH and authigenic fine-grained phosphate component (apatite) which are intergrown with the Mn oxyhydroxides. The second group of elements (Al, Fe, Ti, K, Rb, V, Zr, Nb, Mo, Sb, W, Ba, U) represents a detrital (illite, kaolinite, chlorite, andesine, zircon, rutile) and authigenic (barite) composition and has higher content in the residual fraction in sediments. Part of these elements (Zr, Nb, Mo, U) as well as Sc, Y and REE have strong positive correlation with phosphorous and form the third group of elements which is bound in the authigenic apatite. The results will reveal the main factors that control the trace element concentration in both polymetallic nodules and sediments and help future extraction of these raw materials.

ACKNOWLEDGEMENTS

The study was supported by Bulgarian National Science Fund grant KP-06-N34/6.

REFERENCES

[1] Abbott A., Löhr S., Trethewy M., Are clay minerals the primary control on the oceanic Rare Earth Element budget?, Frontiers in Marine Science, vol. 6, 504, pp 83–101, 2019. https://doi.org/10.3389/fmars.2019.00504.

[2] Baláž P., Results of the first phase of the deep-sea polymetallic nodules geological survey in the Interoceanmetal Joint Organization licence area (2001–2016), Mineralia Slovaca, vol. 53, pp 3–36, 2021. Web ISSN 1338-3523, ISSN 0369-2086.

[3] Dubinin A., Geochemistry of Rare Earth Elements in the ocean, Lithology and Mineral Resources, vol. 39, pp 289–307, 2004.; https://doi.org/10.1023/B:LIMI.0000033816.14825.a2.

[4] Halbach P., Scherhag C., Hebisch U., Marchig V., Geochemical and mineralogical control of different genetic types of deep-sea nodules from the Pacific Ocean, Mineralium Deposita, vol. 16, pp 59–84, 1981.

[5] Hein J., Koschinsky A., Kuhn T., Deep-ocean polymetallic nodules as a resource for critical materials, Nature Reviews Earth & Environment, vol. 1, pp 158–169, 2020. https://doi.org/10.1038/s43017-020-0027-0.

[6] Hikov A., Stefanova E., Stoyanova V., Milakovska Z., Abramowski T., Chavdarova S., Stavrev M., Peytcheva I., Genetic types and REE composition of polymetallic nodules from the eastern part of the Clarion–Clipperton Fractures zone, NE Pacific, In: Christie, A. (Ed.), Proceedings of the 16th SGA Biennial Meeting, New Zeeland, 28-31 March 2022, 1, pp 129–132, 2022a.

[7] Hikov A., Milakovska Z., Stoyanova V., Stefanova E., Abramowski T., Chavdarova S., Stavrev M., REE and trace elements distribution in the deep-sea sediments from the Interoceanmetal (IOM) polymetallic nodule exploration area in the Clarion-Clipperton fractures zone, NE Pacific, Comptes rendus de l'Académie bulgare des Sciences, vol. 75/ issue 7, pp 1018–1027, 2022b.; https://doi.org/10.7546/CRABS.2022.07.10.

[8] Koschinsky A., Halbach P., Sequential leaching of marine ferromanganese precipitates: Genetic implications, Geochimica et Cosmochimica Acta, vol.59/ issue 24, pp 5113–5132, 1995.; https://doi.org/10.1016/0016-7037(95)00358-4.

[9] Kotlinski R., Stoyanova V., Nodule coverage, morphology and distribution in the Eastern CCZ, In: ISA, Technical Study No 6: Prospector's Guide for Polymetallic Nodule Deposits in the Clarion-Clipperton Fracture Zone, pp 34–42, 2012.

[10] Li Y.H., Schoonmaker J. E., Chemical composition and mineralogy of marine sediments, Treatise on Geochemistry 2nd Edition, vol. 9, pp 1–35, 2014.; http://dx.doi.org/10.1016/B978-0-08-095975-7.00701-4.

[11] Lyubomirova V., Mihaylova V., Djingova R., Chemical characterization of Bulgarian bottled mineral waters, Journal of Food Composition and Analysis, vol. 93, 103595, pp 1–12, 2020.; https://doi.org/10.1016/j.jfca.2020.103595.

[12] Menendez A., James R., Lichtschlag A., Connelly D., Peel K., Controls on the chemical composition of ferromanganese nodules in the Clarion-Clipperton Fracture Zone, eastern equatorial Pacific, Marine Geology, vol. 409, pp 1–14, 2019.; https://doi.org/10.1016/j.margeo.2018.12.004.

https://doi.org/10.5593/sgem2024/1.1/s01.05

[13] Ren J., Liu Y., Wang F., He G., Deng X., Wei Z., Yao H., Mechanism and influencing factors of REY enrichment in deep-sea sediments, Minerals, vol. 11, 196, pp 1–16, 2021.; https://doi.org/10.3390/min11020196.

[14] Stoyanova V., Hikov A., Stefanova E., Milakovska Z., Abramowski T., Peytcheva I., Chavdarova S., Stavrev M., Deep-sea polymetallic nodules as opportunity for future supply with critical raw materials, Review of Bulgarian Geological Society, vol. 82/issue 3, pp 153–155, 2021.; https://doi.org/10.52215/rev.bgs.2021.82.3.153.

[15] Zawadzki D., Maciag J., Abramowski T., McCartney K., Fractionation Trends and Variability of Rare Earth Elements and Selected Critical Metals in Pelagic Sediment from Abyssal Basin of NE Pacific (Clarion-Clipperton Fracture Zone), Minerals, vol. 10, 320, pp 1–38, 2020.; https://doi.org/10.3390/min10040320.

DESIGNING GEOEDUCATIONAL TOOLS FOR GEOTOURISM NEEDS – A CASE STUDY OF THE OUTER FLYSCH CARPATHIANS

Zbigniew Jan Ziarek[1]

[1]AGH University of Krakow, Faculty of Geology, Geophysics and Environmental Protection, **Poland**

ABSTRACT

A geoeducational tools are innovative solutions used to popularize knowledge in the field of Earth Sciences and the promotion of geotourism. These methods enhance the appreciation of geodiversity, raising awareness about cognitive and aesthetic values. By adopting this approach, there is a commitment to geoheritage protection for future generations. The efficacy of geoeducational instruments relates on a knowledge of geological processes and their outcomes, coupled with adept geointerpretation. During the geointerpretative phase it is important to maintain correctness and reliable explanation of the most significant elements, while ensuring a comprehensible transfer of knowledge. The primary beneficiaries are geotourists and tourists interested in the genesis of inanimate natural objects. The purpose of the presented geoeducational tools is a simplified visualization of the key stages of the basin-tectonic history of the Carpathian Flysch Belt, starting from the processes of sediments deposition (Outer Carpathian flysch), to the formation processes of regional tectonic units (Outer Carpathian nappes) during the Alpine orogenesis. The designed tools are based on the concept of process geology, in which: (a) based on the factual description of the outcome (rock or geological structure), (b) the geological process is interpreted, and as a result, (c) a general model of environmental conditions consistent with the observations and interpretation is constructed – "from detail to general". The presented models aim to visualize geological processes and exhibit their results in a clear and comprehensible way. In the process of modeling it is crucial to maintain a level of realism that allows for the creation of the most naturalistic depiction of the environment and the circumstances under which the analyzed process and its results could occur. The implementation of the projects allowed to determine the main attributes of the geoeducational tools: repeatability of the experiments, their clarity, expressiveness, spectacularity, and realism. Thanks to them, the recipient is able to learn and understand processes related to the deposition of clastic sediments that predominantly build the Flysch Carpathians and then formation of their nappes (accretionary prisms) as a result of orogenic fold-and-thrust movements. The finished products (films) may arouse the interest of museums and be applied to exhibitions.

Keywords: geoeducation, geotourism, geoheritage, process geology, Outer Carpathian flysch

https://doi.org/10.5593/sgem2024/1.1/s01.06

INTRODUCTION

The aim of the project was to create educational tools in the form of geoeducational films with geointerpretational content considering selected sedimentological and tectonic issues of the geological history of the Outer Carpathian arc. The inspiration for conducting the series of modelling was the author's field observations made during student field trips in the outcrops of the Carpathian flysch, as well as the reactivation of the sedimentological laboratory at the Faculty of Geology, Geophysics and Environmental Protection of the AGH University of Krakow [1], and literary studies on the Carpathian tectonics [2, 3]. The geoeducational tool project is based on the idea of geoeducation, which involves promoting geological knowledge through exploring natural geological features and/or processes responsible for their formation, recognized as touristically attractive. [4–9] The tools were intended to present and explain the nature of sedimentary processes responsible for the formation of sediment gravity flows, known as turbidites – representing one of the types of flysch formations that build the Outer Carpathians (known as Flysch Carpathians) [7–14], as well as the tectonic development of continental accretionary prisms, such as the so-called Carpathian nappes [7, 9, 11, 12].

MATERIALS AND METHODS

Since the author's intention was to create two films, appropriate analogue models had to be designed. The first film was intended to illustrate the mechanism of a sediment gravity flow and the formation of its product (turbidite) [7–14] while the second aimed to simulate the process of tectonic deformation resulting from horizontal compression of the Earth's crust [2, 3, 9, 11, 12]. It became necessary to design two separate tools. The first tool was to imitate the environment of sedimentary processes and the erosional-depositional system of a submarine fan [15], as well as turbulent suspension flow and deposition of normally graded turbidites [8–14]. The second was to simulate lateral pressures in the Earth's crust, continuous and discontinuous tectonic deformations, the formation of thrust surfaces, and ultimately the formation of an accretionary prism symbolizing the Carpathian nappe [2, 3, 7, 9, 11, 12]. To achieve these, assumptions the following tools were constructed: an aquarium for sedimentological modelling and a sandbox model for tectonic modelling.

The components of the aquarium for sedimentological modelling included:

a) a water-filled aquarium as the sedimentary basin (100 cm x 40 cm x 40 cm);
b) a matte plexiglass continental slope;
c) sand as an alternative to filling the bottom;
d) a plastic tube with a funnel as a point source of supply.

The elements of the sandbox model included:

a) a wooden frame with windows providing a longitudinal cross-section view of the deformed sediment model;
b) a winch mechanism ensuring progressive relative movement of the Earth's crust;
c) sandpaper providing friction and serving as a movable substrate for deposited sand formations;
d) multicoloured sand representing rock layers.

TABLES, GRAPHS & FIGURES

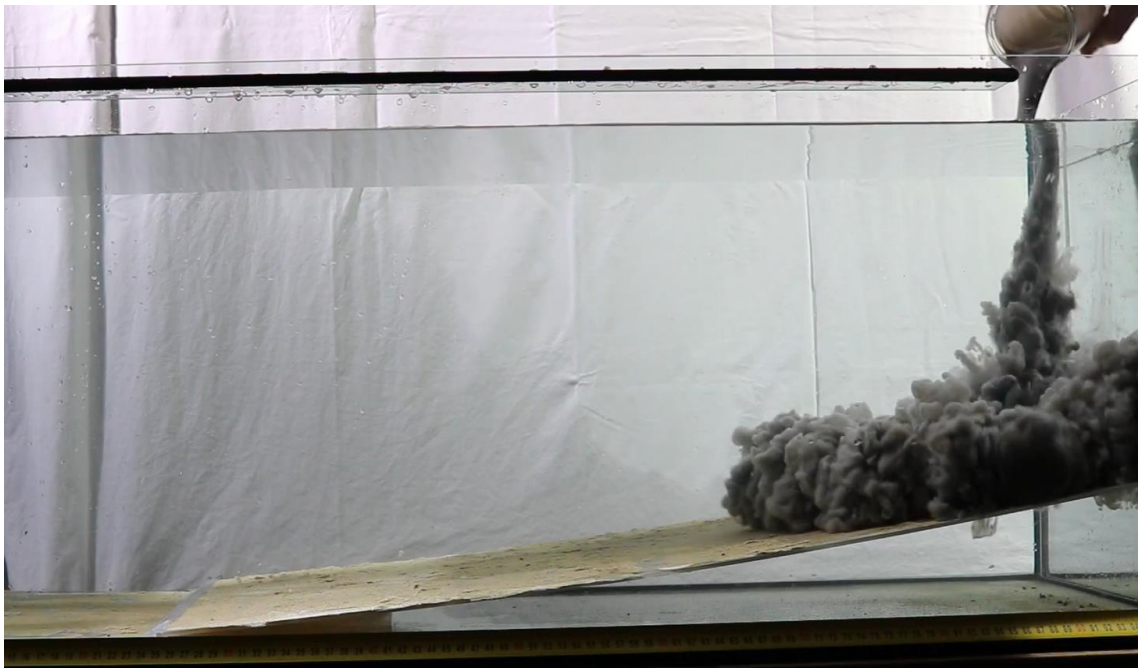


Fig. 1. Turbidity current (suspension of water and clay with a volume concentration ca. 23%) – initial attempts at unchannelized modeling on an artificial plexiglass slope (photo by Z. Ziarek, 2023).



Fig. 2. Turbidity current – captured from three cameras (photo by K. Kulik, 2023).

https://doi.org/10.5593/sgem2024/1.1/s01.06

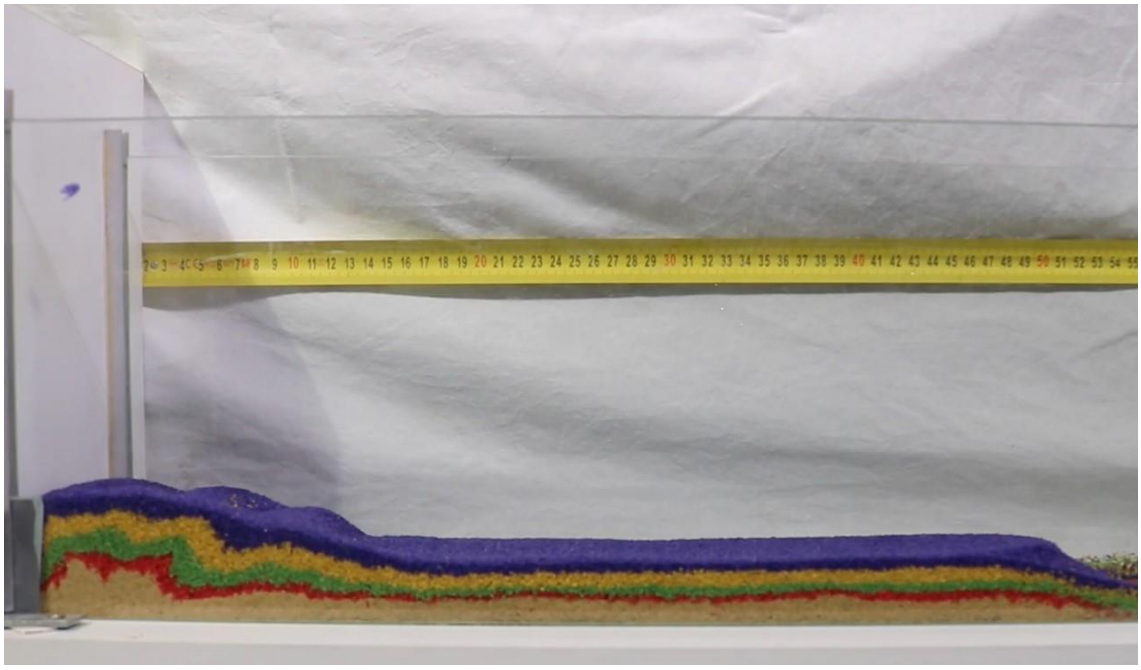


Fig. 3. First unsuccessful attempts to deform sand layers (did not result in the formation of a detachment surface and thus the formation of a nappe model) (photo by Z. Ziarek, 2023).

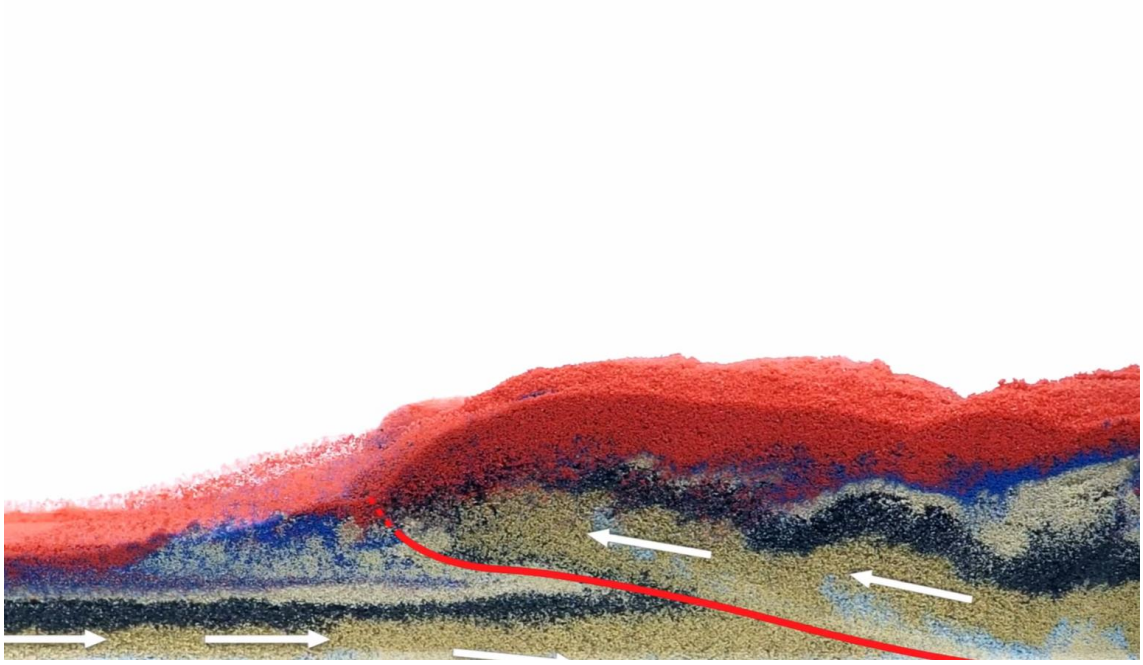


Fig. 4. Nappe model with delineated detachment surface (photo by K. Kulik, 2023).

RESULTS

The initial attempts of turbidity currents modelling were conducted using a continental slope model in the form of a matte plexiglass plate (Fig. 1). However, this did not produce the expected naturalistic deposition environment model. To increase the realism of the tool, a naturalistic filling of the bottom was applied, made of sand in two colours, symbolizing sigmoidal bedding on the continental slope. The turbidity current was channelized by a central channel model. The turbulent suspension of sand and clay with a volume concentration ca. 23% propagated in the form of submarine fan, depositing sediment that approximately corresponded to experimental turbidites (Fig. 2) [8–14].

Modelling tectonic compressional movements of the Earth's crust was more demanding. To achieve the effect of deformed rock layers shearing and the formation of a detachment surface, it was necessary to select an appropriate set of rheological parameters for individual layers of coloured sand (originally symbolizing horizontal bedding) (Fig. 3). The individual layers were composed of material with different fractions, while others were stiffened with a binder obtained by evaporating water from sugar dissolved in it, which was soaked into these layers. The prepared layers were nestled between slides within a structure crafted from boards, angles, and slides, resting atop sandpaper that extended through a gap in a sidewall, winding onto a reel. As the sandpaper was wound, the layers were pushed against the rear wall of the sandbox, which served as a backstop, and underwent continuous deformation. As the winding continued, they also underwent discontinuous deformations as the continuity was disrupted and a detachment zone was formed. These sheared layers constituted an experimental model of the Carpathian nappes (Fig. 4) [2, 3, 7, 9, 11, 12].

DISCUSSION

The designed tools are based on the concept of process geology, in which:

a) based on the factual description of the outcome (litho-sedimentological characteristics of the rock or description of the geological structure);
b) the geological process, i.e., matching physical mechanisms, is interpreted;
c) a general model of environmental conditions consistent with the observations collected at the beginning and with subsequent interpretation is constructed – "from detail to general".

This methodology prevents the mixing of facts with interpretation and ensures the most realistic and natural portrayal of reality [8, 12, 13]. Only such a representation of reality can achieve the intended goal of explaining to the recipient the processes occurring throughout the Carpathian basin-tectonic history.

Previous attempts to create analogous tools did not consistently synthesize the two most important issues in the development of the Outer Carpathians geological history: the process of Carpathian flysch deposition and the tectonic processes of its nappes formation. They also lacked a properly developed explanatory package – the so-called geointerpretation, necessary in geoeducation [8].

Flysch deposits, predominantly turbidites, accumulated in the Carpathian basins, including the Silesian sub-Basin. They were involved in the Neogene geotectonic reorganisation of the Alpine Tethys. As a result of this orogeny, the flysch series underwent: folding, detaching from the parent basin substrate, overlapping in the form of regionally sized tectonic units (so-called Carpathian nappes), and together were

https://doi.org/10.5593/sgem2024/1.1/s01.06

tectonically and gravitationally transported to the foreland of Carpathians, forming a continental accretionary prism of the Carpathian orogen [2, 3, 7, 9, 11, 12].
Outer Carpathian flysch can be defined broadly [7, 9–14] as:

a) a set of deep-water sediments formed by terrigenous material (source area – Carpathian cordilleras), primarily deposited by sediment gravity flows (in genetical approach);
b) sedimentary series built by alternating sandstone and shale beds, sometimes accompanied by coarser-grained conglomerates (in lithological approach);
c) series of sedimentary rocks formed in the pre- and early orogenic stage of Carpathian sedimentary basins development (in geotectonical approach).

CONCLUSIONS

Working on the construction and implementation of geoeducational tools allowed to determine the most important attributes, which include: clarity of the experiment, expressiveness, spectacularity, theatricality, realism, and repeatability. Thanks to these attributes, the recipient is able to learn and understand processes related to the deposition of clastic sediments that predominantly build the Flysch Carpathians, turbidity currents as the examples of sediment gravity flows, and the model of deep-sea fan, the configuration of natural sedimentary basin, and the formation of nappes (accretionary prisms) as a result of orogenic fold-and-thrust movements. From the second model the recipient is able to learn and understand reasons for tectonic deformations in the Earth's crust, their role in shaping mountain ranges, and their influence on the geological structure of Carpathian arc, built by a series of nappes (accretionary prisms).
It was observed that:

a) developing geoeducational tools demand a higher level of expertise from the creator than what is eventually communicated to the audience;
b) iterative refinement of the tools involve multiple trial-and-error cycles to achieve desired outcomes;
c) the final presentation requires visually appealing design;
d) the level of geointerpretation of the presented processes should match the audience defined at the beginning;
e) geointerpretation levels can be adjusted smoothly based on audience type;
f) the finished products may attract interest from museum units for use in exhibitions.

An introduction and broader application of geoeducational tools in geotourism and geoeducation could contribute to increasing awareness of the necessity to protect natural geodiversity for future generations. This could be achieved by enhancing the appreciation of geodiversity by the recipients of these tools (geotourists) and raising awareness about cognitive and aesthetic values of geosites. Analogue models in a simple and accessible way provide the audience with an understanding of the environment and the conditions under which rock formations and geological structures are created, enhancing the attractiveness of the geosites.

ACKNOWLEDGEMENTS

The author extends his gratitude to Supervisors – Ms. Ewa Welc and Mr. Piotr Strzeboński for their invaluable comments, suggestions, and substantive support in the fields of geotourism and sedimentology. Special thanks go to Mr. Marek Wendorff for engaging discussions, advice, and assistance with English translations. The author also expresses appreciation to the Supervisors of the Student Scientific Association "Azymut" – Mr. Jerzy Zasadni, Mr. Andrzej Świąder, and Mr. Piotr Strzelecki – for their care and assistance in obtaining the necessary financial resources for the creation and operation of the students sedimentological laboratory. Furthermore, the author acknowledges the following individuals for their personal support of the project idea and development: Mr. Wojciech Mastej, Mr. Tomasz Bartuś, Mr. Piotr Siwek, Mr. Stanisław Godyń, Mr. Konstanty Kulik, as well as Ms. Monika Pilarz and Mrs. Renata Stadnik. Special thanks are extended to Mr. Piotr Strzeboński for invaluable ideas and substantive assistance during laboratory work, and to colleagues – Radosław Szczęch, Jakub Andrzejak, Mikołaj Pawlak, Jan Szydłowski, Marcel Mroczka, Karol Herok, Adam Garbarczyk, Michał Majewski, Nicolas Sołek, and Dominik Polak – for their logistical support. The work was conducted with the support and under the scientific supervision of Ms. Ewa Welc and Mr. Piotr Strzeboński as part of the activities of the Student Scientific Associations of the Faculty of Geology, Geophysics, and Environmental Protection of the AGH University of Krakow – the "Geotourism" and the "Azymut".

REFERENCES

[1] Bukowski K., Mastej W.& Kępiński J., Badania laboratoryjne nad sedymentacją osadów mułowo-solnych w zależności od warunków przepływu i charakteru materiału sedymentacyjnego — Laboratory studies on deposition of salty-mud sediments controlled by flow regime and sediment characteristic, Technika Poszukiwań Geologicznych. Geosynoptyka i Geotermia, Poland, vol. 4–5, pp. 69–76, 2007.

[2] Strzelecki P. J., Jaworska K., Kozłowska M., Szczypka M. & Szewczyk M., Ewolucja strukturalna pasma fałdowo-nasuwczego w świetle modelowania analogowego. Konferencja Geotematyczna GAUS, Poland, 2017.

[3] Rauch, M., Powstawanie utworów chaotycznych związanych z nasunięciami, w świetle wyników modelowania analogowego. Nafta-Gaz, Poland, vol. 9, pp. 661–664, 2015.

[4] Słomka T.& Kicińska-Świderska A., Geoturystyka – podstawowe pojęcia., Geoturystyka, Poland, vol. 1, issue 1, pp. 5–7, 2004.

[5] Welc E. & Miśkiewicz K., Geoturystyka i geoedukacja w rezerwacie przyrody nieożywionej „Prządki" im. prof. Henryka Świdzińskiego., Geotourism/Geoturystyka, Poland, vol. 1–2, issue 56–57, pp. 11–42, 2019.

[6] Migoń P., Geoturystyka, Wydawnictwo Naukowe PWN SA, Poland, 2012.

https://doi.org/10.5593/sgem2024/1.1/s01.06

[7] Strzeboński P., Residual rocky forms in the landscape of the Outer Carpathians (Silesian Beskid Mts, Poland) – geotourist and sedimentological case study, Geotourism/Geoturystyka, Poland, vol. 18 (1–2), issue 64–65, pp. 3–22, 2021.

https://doi.org/10.7494/geotour.2021.1-2(64-65).3

[8] Ziarek Z., Projektowanie narzędzia geoedukacyjnego dla potrzeb geoturystyki – studium przypadku sedymentologicznego modelowania prądu zawiesinowego in 64. Barbórkowa Konferencja Studenckich Kół Naukowych AGH – Materiały Konferencyjne, Poland, pp.76–77, 2023.

https://www.researchgate.net/publication/376312074_Designing_a_geoeducational_tool_for_geotourism_needs_-_a_case_study_of_sedimentological_modeling_of_turbidity_current_-_Projektowanie_narzedzia_geoedukacyjnego_dla_potrzeb_geoturystyki_-_studium_przyp

[9] Unrug R. (red.),. Przewodnik po zachodnich Karpatach fliszowych, Wydawnictwa Geologiczne, Poland, p. 260, 1969.

[10] Gradziński R., Kostecka A., Radomski A. & Unrug R., Zarys Sedymentologii, Wydawnictwa Geologiczne, Poland, p. 628, 1986.

[11] Ślączka A. & Kaminski M.A., A Guidebook to Excursions in the Polish Flysch Carpathians. Field Trips for Geoscientists. Special Publication No. 6. Grzybowski Foundation, Poland, 1998.

[12] Strzeboński P., Contrasting styles of siliciclastic flysch sedimentation in the Upper Cretaceous of the Silesian Unit, Outer Western Carpathians: sedimentology and genetic implications, Annales Societatis Geologorum Poloniae, Poland, vol. 92, issue 2, pp. 159–180, 2022.

[13] Shanmugam, G., Mass transport, gravity flows, and bottom currents: Downslope and along slope processes and deposits, Elsevier, ISBN: 9780128225769, UK, p. 608, 2021.

[14] Talling P.J., Masson D.G., Sumner E.J. & Malgesini G., 2012. Subaqueous sediment density flows: depositional processes and deposit types, Sedimentology, UK, vol. 59, issue 7, pp. 1937–2003, 2012.

[15] Reading H.G. & Richards M., Turbidite systems in deep-water basin margins classified by grain size and feeder system, AAPG Bulletin, UK, vol. 78, issue 5, pp. 792–822, 1994.

EVALUATING FLOOD RISKS AND VULNERABILITIES IN CARAORMAN, DANUBE DELTA: INSIGHTS FROM HYDRAULIC MODELLING

Dr. Banescu Alexandru [1]
Simionov Matei[1]
Phd Ress. Livanov Oliver [1,2]
Pindic Paula[1]
Phd Ress. Balaican Dragos[1]

[1] Danube Delta National Institute for Research and Development of Tulcea, **Romania**
[2] University of Bucharest, Doctoral School of Geology, **Romania**

ABSTRACT

Rural areas and infrastructure in the Danube Delta are affected by natural disasters, and the frequency and severity of hydrological phenomena are increasing due to climate change. The rural areas of the Danube Delta experience significant flooding due to the high levels of the Danube, often resulting from quantitatively significant precipitation. The protection dyke system related to the Danube River is most often affected by floods that sometimes lead to the failure of the dykes. Dyke failure is noted by the appearance of one or more breaches in the body of the dyke that may extend along the dammed part, in most cases due to the diving of the banks. Floods that occur on the Danube are usually very long-lasting, resulting in impressive flows that can persist for weeks or even months. In this paper, the flooded areas of the Caraorman locality in the Danube Delta will be analyzed using two specialized programs. Two methods of flood risk analysis will be used for the development of flood maps: the static method and the dynamic method. The entire analysis process is based on the Digital Terrain Model for the Danube Delta, a tool with which we will perform hydraulic modelling in highly accurate conditions. The results will be expressed as flood maps that will indicate the water depth in different areas of Caraorman, the flood limit and its intensity depending on the simulated inundation level. At the same time, the results obtained in this paper can be useful to decision-makers, local authorities and implicitly to the population of the area of the affected locality. Therefore, this paper uses several categories of data sets such as hydrological data on water flows and water levels on the Danube, and also topo-bathymetric data represented by cross sections along the Danube bed and adjacent channels. Nevertheless, to perform hydraulic modeling we will also use the roughness coefficient from Manning's formula. Climate change is an important challenge that needs to be prioritized and addressed as best as possible. Among the most significant consequences of climate change, river flash floods are events that usually cause significant damage. Finally, this research renders an important framework both for the local authorities of the Danube Delta and for the population living in that area.

Keywords: Flash floods, hydraulic modelling, Danube Delta, simulation, flood scenarios

INTRODUCTION

The estimation of flood risk in the areas of the Danube Delta can be achieved through hydraulic modeling, which allows flood-prone areas to be simulated in specialized

https://doi.org/10.5593/sgem2024/1.1/s01.08

programs. The 1D and 2D models are now increasingly used on a large scale to determine flooded areas due to the recent development of hydraulic modeling software. Additionally, there are tools that have been developed recently for hydraulic modeling, such as specialized programs like Delf 3D, Mike, HEC-RAS, as well as Geographic Information Systems (GIS) that display the 1D or 2D representation of simulated hydraulic parameters. In hydraulic modeling, one of the most important elements is the bathymetry of the channel or river, along with the topography of the banks and floodplain, which influence the entire modeling process, particularly the obtained results [1], [2].

In the Danube Delta, the floodplain presents areas with negative altitudes and this can lead to errors in the hydraulic modeling process, with considerable differences in delineating the flooded area. In risk assessment, the effects of these potential errors in the modeling process underscore the optimization of field-collected data and their quality. Nowadays, the use of digital terrain models in hydraulic modeling processes and even GIS analysis is contingent upon their availability, and the resolution of these models makes a difference in generating results [3].

In all cases, the quality of the digital terrain model, referring to its precision and accuracy, is determined by the process through which the data have been collected and processed. Typically, field-collected data can be centralized in a topographic survey or using photogrammetry and remote sensing tools. Digital models obtained through global positioning system (GPS) mechanisms or conventional scanning methods are very precise and are useful and easily implemented in limited areas. The quality of the information obtained ultimately depends closely on the accuracy of the surveying equipment and, of course, on the density and distribution of collected points [4].

At the same time, digital surface models can be displayed in various manners. One approach is to combine data points into nodes, which involves a Triangulated Irregular Network known as TIN. Another approach is through regular tessellation, represented by a terrain model at a larger scale [5]. This regular mode is not recommended for hydraulic analysis of rivers or channels as it may present many pronounced terrain changes in the model. For hydraulic modeling, the most commonly used models are TINs because they provide a much larger representation of river geometry, allowing for considerable adjustment of the density of all network elements to a variation volume of data [6], [7].

In general, TIN models can be modified by inserting additional data, such as digital points indicating maximum elevations, depressions, and areas where the slope is interrupted. This allows for a precise depiction of floodplain properties, such as riverbanks or alluvial perimeters, as well as hydraulic structures such as dikes and dams that impact the river's hydraulic behavior. In all cases, the resolution of the networks is an important element in hydraulic modeling because it defines both the geometry of the smallest feature represented in the Digital Terrain Model and the time period over which the calculation is performed [8], [9].

Until recently, research and studies concerning Digital Terrain Models and hydraulic modeling have taken into account the impact of spatial resolution on flood hydraulic models based on raster and finite element models [10]. Therefore, the main objective of our research is to assess flood risks and vulnerabilities in the Caraorman locality within the Danube Delta Biosphere Reserve. The research objective will be achieved using hydraulic modeling and specialized GIS techniques. The obtained results will consist of flood maps displaying potentially flooded areas in the Caraorman village in case the local protection dike fails during a strong rush of water.

1. STUDY AREA AND DATA

1.1. STUDY AREA

The Danube Delta is one of the wildest wetland areas in Europe and the only delta in the world declared a biosphere reserve, serving as a true natural museum of biodiversity. Formed at the confluence of the Danube River with the Black Sea, the Danube Delta is renowned for its diversity of plant species and for being the largest and most compact reed area in the world [11]. In many of the fishing villages in the Danube Delta (such as Caraorman, Salceni, Mila 23, or Ceatalchioi), there is a huge collapse risk of the protection dikes when Danube water levels are high. The Caraorman locality is situated in the Danube Delta Biosphere Reserve, the best-preserved reservation among the European deltas [12]. The settlement is part of Crisan commune, Tulcea County, Dobrogea, Romania, as depicted in Figure 1.

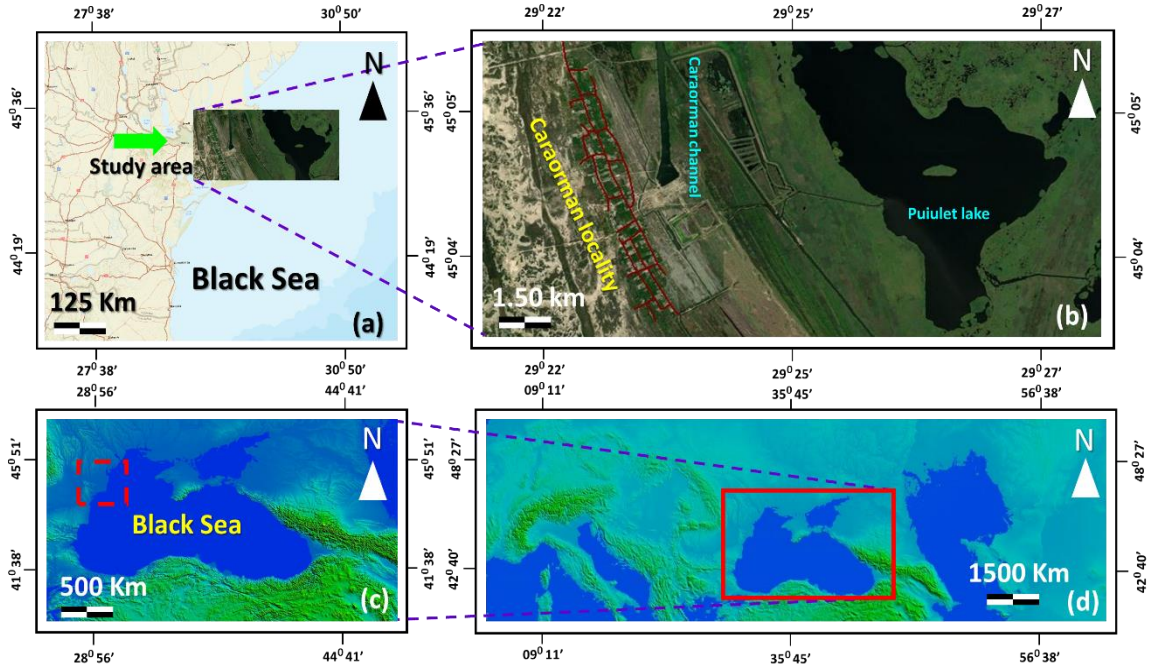


Figure 1. The geographical location of the Caraorman locality considered in this study. (a) the study area superimposed on the topographic map; (b) the locations of the Caraorman locality superimposed on the satellite map; (c) and (d) the study area superimposed on the digital terrain model

The locality of Caraorman is situated on the maritime sandbar with the same name, located between the localities of Sfântu Gheorghe to the south and Sulina to the north, approximately 12 km from the Crișan commune. In terms of layout, the locality stretches over a length of approximately 3.5 km and a width of approximately 500 meters. In the eastern part, the locality of Caraorman borders the Crișan - Caraorman canal. Due to the strong current of the Danube and the positioning of the canal, its mouth is constantly silted up, and dredging works are carried out approximately every 3 years to remove the sediment.

In the summer of 2010, significant floods occurred in the Danube Delta due to high water levels on the Danube. Numerous localities were affected by flooding, and many dikes gave way under the force of the floodwaters. As a result, significant damages were

https://doi.org/10.5593/sgem2024/1.1/s01.08

recorded, households were destroyed, and infrastructure collapsed simultaneously. The discharge recorded in the summer of 2010 reached the value of 16,600 m^3/s [13]. In the present study, a flow hydrograph was created and validated with the historical discharge value, which will be used in hydraulic modeling to obtain flood scenarios for the locality of Caraorman.

1.2. DATA

For flood risk analysis, 2 specialized programs were used in this work: HEC-RAS and Global Mapper. To obtain flood scenarios we need to insert relevant hydrological data into the HEC-RAS, a hydraulic modeling software. Using the static method, digital flood maps are obtained with the Global Mapper software which includes the digital model of the terrain as the base map.

The use of hydrological data in hydraulic modeling is important because they are used to calibrate the hydraulic model. The reference year for the selection of the flow hydrograph was set to 2010. Table 1 shows the maximum water levels in 2010 in compliance with the Black Sea 75 (BS 75) and the Sulina Black Sea (BSS) reference levels next to the localities distributed along the Sulina branch. For the flood risk analysis, the water level near the Caraorman village (specifically from Crișan commune, a locality north of Caraorman) was taken into account. Crișan commune is located north of Caraorman village and has daily hydrometric records.

Table 1. Maximum water levels in 2010 (in meters) reported to the Black Sea 75 (BS75) and the Black Sea Sulina (BSS) levels on the Sulina branch

Locality	Maximum Water Level (Meters BS75)	Maximum Water Level (Meters BSS)	Locality	Maximum Water Level (Meters BS75)	Maximum Water Level (Meters BSS)
Partizani	4.32	4.54	Gorgova	3.11	3.33
Ilganii de Sus	4.32	4.54	Mila 23	2.70	2.92
Vulturu	3.61	3.83	**Crișan**	**2.50**	**2.72**
Maliuc	3.43	3.65	Sulina	1.24	1.46

After the boundary conditions are met, the modeling process is validated. The boundary conditions involve inserting the flow hydrograph upstream and the normal depth downstream, which is 0.03 for finalizing the process. For the static method, the same hydrological data is used, but the basis map for analysis is the digital terrain model for the Caraorman locality. Surface flooding is conducted in stages, using flood levels (increments of 0.20 meters).

The scenario for the dynamic modeling method involves flooding the locality in the event of a breach in the protective dike with an opening of 10 meters which remains active for 2 days at maximum Danube levels (flooding scenarios from 1.70 meters to 2.72 meters reported to the Sulina Black Sea levels). The scenario for the static method is determined by overlaying water level information onto the digital terrain model. This method is unfavourable, as this scenario is the most disastrous, characterized by the prolonged maintenance of the breach in the protective dike for a much longer period (several days).

2. RESULTS AND DISCUSSIONS

In the case of the dynamic hydraulic modeling method, the processing is carried out using the HEC-RAS software where the riverbank lines, the centerline of channels, cross-sectional profiles capturing terrain relief information, the 2D flow area, and the location of the breach in the protective dike (the most compacted and degraded location in the protective dike) are defined. Manning's roughness coefficient was input into the program between the interval 0.025-0.30. The geometric 2D grid was set at 30 x 30 m in the x and y direction.

The indicators for the flood risk assessed zone in the evaluated area have been derived from the Digital Terrain Model and the Digital Model of the minor bed obtained through LIDAR measurements and topo bathymetric surveys. The topo bathymetric measurements involved the creation of cross-sectional profiles on the Sulina branch and the Crișan-Caraorman channel using multifascicle and multibeam equipment.

Thus, for the upstream area, the flow hydrograph was established and validated with a maximum discharge of 16,600 m^3/s. Figure 2 presents the flood maps obtained through hydraulic modeling for the Caraorman locality using the HEC-RAS hydraulic model.

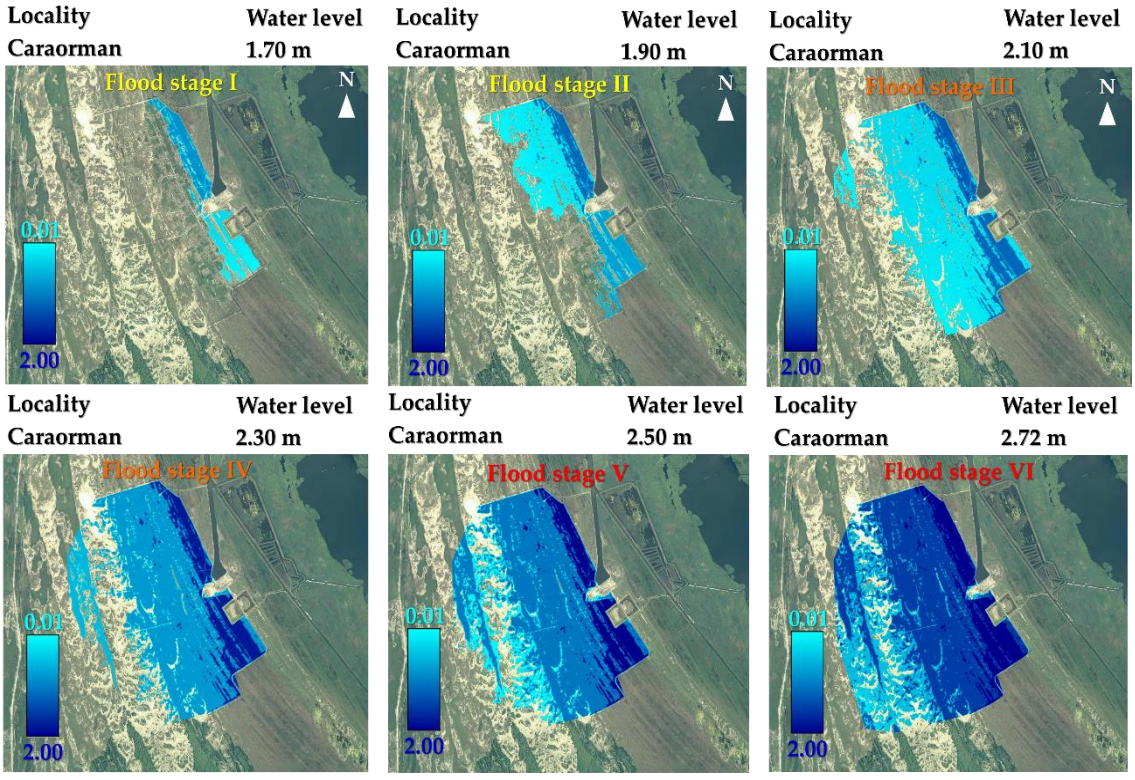


Figure 2. Flood scenarios maps for Caraorman locality, corresponding to the situation from July 2010, by using the 1D/2D HEC-RAS model, at high - resolution DTM

The 2D flow area for the Caraorman locality and adjacent areas was obtained after the running of the hydraulic modeling program. The dynamic hydraulic modeling method took into account the flooding scenario that may occur in the event of a breakthrough in the protective dike at maximum Danube levels, with a 48-hour interval during which the 10-meter-wide breach remains open.

https://doi.org/10.5593/sgem2024/1.1/s01.08

In the case of the static method, processing was carried out using the Global Mapper software. The static method involved importing the digital terrain model into the program and aligning it with the appropriate reference system, followed by delineating the flood calculation areas. Simulation is conducted by applying flood increments of 20 centimetres. This information is then overlaid onto the Digital Terrain Model. Figure 3 presents the digital maps of potentially flooded areas obtained by using the static method.

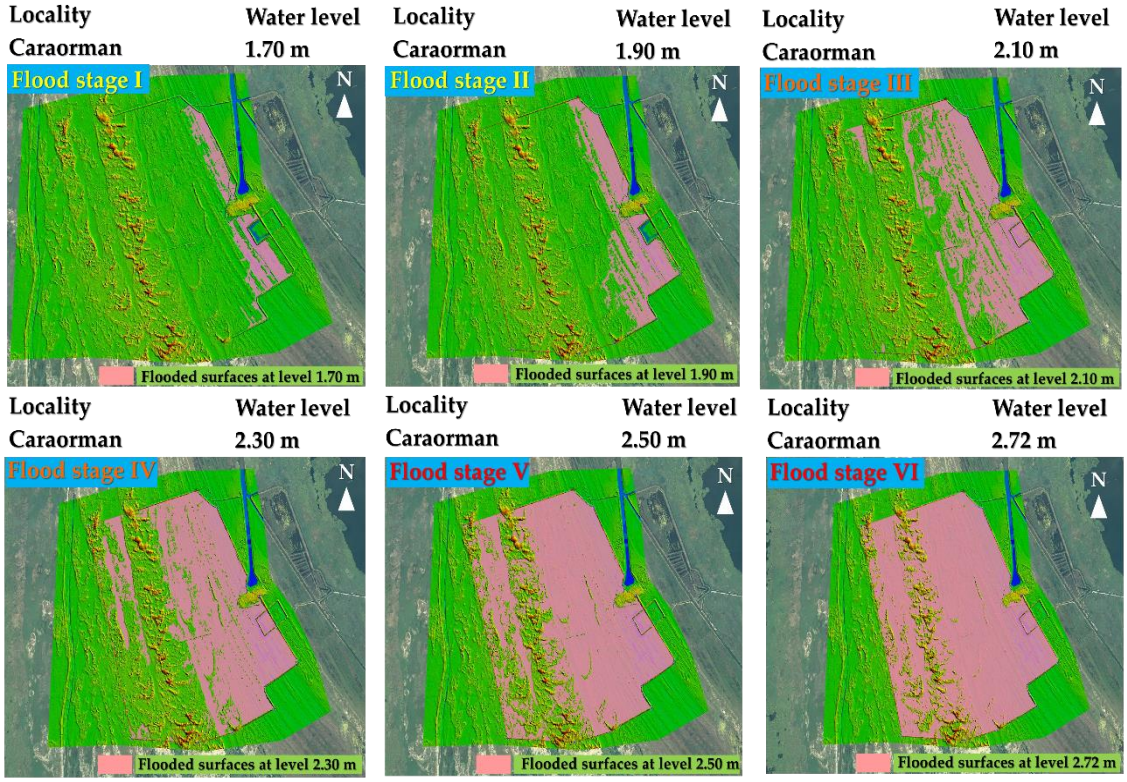


Figure 3. The representations of digital maps with flooded areas for Caraorman locality by using static method, at high DTM

After running the program, digital flood maps are obtained for the Caraorman locality. The static method takes into account the scenario where the breach remains in the protective dike for a much longer period (more than 48 hours) at maximum Danube levels (the most unfavourable case). For both methods, multiple flood levels were established, ranging from the lowest to the highest flood level - which is 2.72 meters reported to the Sulina Black Sea Level.

In the end, 6 flood scenarios were obtained for each method, resulting in a total of 12 flood maps for the Caraorman locality. Table 2 presents the flooded areas corresponding to each method separately and the percentages of flooding for the Caraorman locality. Analyzing the obtained results, we can observe that there are no significant differences regarding the flooded areas.

Table 2. The flooded areas of the Caraorman locality

Caraorman locality		Dynamic Method		Static Method	
	Water Level (m)	Floodable Surfaces (km^2)	Flooded Areas (%)	Floodable Surfaces (km^2)	Flooded Areas (%)
Flood stage I	1.70	0.96	9.31%	0.81	7.81%
Flood stage II	1.90	2.10	20.35%	1.74	16.83%
Flood stage III	2.10	4.43	42.93%	3.51	34.01%
Flood stage IV	2.30	5.75	55.72%	5.37	52.05%
Flood stage V	2.50	7.22	69.97%	7.44	72.13%
Flood stage VI	2.72	8.51	82.47%	8.68	84.14%

For the first stage of flooding, the inundation percentage is higher when applying the dynamic hydraulic modeling method, resulting in a flooded area of 0.96 km^2 compared to 0.81 km^2 when using the static method. For the second stage of flooding, the flooded area extends to 2.10 km^2 when applying the dynamic method and 1.74 km^2 when applying the static method, with a difference of 0.36 km^2. For the third stage, the flooded area using the dynamic method is 4.43 km^2 and 3.51 km^2 for the static method, resulting in a difference of 0.92 km^2. For the fourth stage, the difference between the flooded areas is much smaller (0.38 km^2). The same trend can be observed for the other two stages of flooding, with differences of 0.22 km^2 for the fifth stage and 0.17 km^2 for the sixth stage.

CONCLUSIONS

Using the HEC-RAS software, which performs hydraulic modeling in the context of climate change, and not only, and with the assistance of the Global Mapper program, which performs GIS analysis, a scenario simulation was carried out in the event of a breach in the protective dike for 48 hours and a longer period, at high Danube water levels. The hydraulic modeling delimited the flooded areas of the Caraorman locality.

The results presented in this study were obtained using data from the Digital Terrain Model for the Caraorman locality, as well as data regarding the upstream flow hydrograph and the water levels near the locality.

The results showed that in the event of a breach in the protective dike, the Caraorman locality is flooded differently when applying the two flood risk analysis methods. The major difference occurred at the third and fourth stages of flooding, where the flooded area was much larger when using the dynamic hydraulic modeling method. As the Danube level rises, the flooded area in the locality also increases when applying the dynamic method, from a minimum of 9.31% flooded area to 82.47% at the maximum extent level of 2.72 meters reported to the Sulina Black Sea level.

The accuracy of the obtained results is attributed to the high-precision data provided by the Digital Terrain Model. The Digital Model served as the informational basis through which flood simulations were made possible for both the dynamic and static methods. These flood maps serve as initial considerations for decision-making planning in the context of a potential disaster that could endanger human lives.

https://doi.org/10.5593/sgem2024/1.1/s01.08

REFERENCES

[1] Grimaldi S., Petroselli A., Arcangeletti E., Nardi F., Flood mapping in ungauged basins using fully continuous hydrologic-hydraulic modeling. J. Hydrol. pp. 39-47, 2013

[2] Negrei C., Craciun A., Tudor M., Contributions to Analysis of Flows of Environmental Information on the Danube Delta Biosphere Reserve. Journal of Environmental Protection and Ecology, 19(2), pp. 849-858, 2018

[3] Banescu A., Georgescu L. P., Rusu E., Iticescu, C., Use of GIS technology to support the navigation on the Danube River. In International Conference on Traffic and Transport Engineering ICTTE, Belgrade, Serbia, pp. 160-168, 2018

[4] Arseni M., Rosu A., Iticescu C., Georgescu L.P., Development of flood risk and hazard maps for the lower course of the Siret River, Romania. Sustainability, 12, 2020

[5] Banescu A., Simionov M., Livanov O., Pindic P., Tudor M., Analysis of the flood risk in the Patlageanca area near Ceatal Ismail from the Danube Delta. International Multidisciplinary Scientific GeoConference: SGEM, 23(3.1), pp. 19-26, 2023

[6] Balaican D., Teubner K., Tudor I.M., Nichersu I., Burada A., Trifanov C., ... & Georgescu, P.L., Water Energy Food Nexus in Urbanizing Wetlands: Challenges and Solutions Explored through Choremes and Focus Maps. Water, 16(7), 922, 2024

[7] Livanov O., Banescu A., Simionov M., Pindic P., Tudor M., The limestones from the walls of several dobrogean fortresses and their possible extraction area. International Multidisciplinary Scientific GeoConf.: SGEM, 23(1.1), pp. 173-180, 2023

[8] Crăciun A., Costache R., Bărbulescu A., Pal S.C., Costache I., Dumitriu C.Ș., Modern techniques for flood susceptibility estimation across the deltaic region (Danube Delta) from the black sea's Romanian sector. Journal of Marine Science and Engineering, 10(8), 1149, 2022

[9] Balaican D., Nichersu I., Nichersu I. I., Pierce A., Wilhelmi O., Laborgne P., Bratfanof, E., Creating knowledge about food-water-energy nexus at a local scale: A participatory approach in Tulcea, Romania. Environmental Science & Policy, 141, pp. 23-32, 2023

[10] Niculescu S., Lardeux C., Hanganu J., Mercier G., David L., Change detection in floodable areas of the Danube delta using radar images. Nat. Hazards, 78, pp. 1899-1916, 2015

[11] Covaliov S., Doroftei M., Chirilă S.D., Hanganu, J., Stufărișurile din Delta Dunării. Editura Centrul de Informare tehnologică Delta Dunării, 186 pp., 2023

[12] Chirilă S.D., Doroftei M., Vassilev K., Covaliov S., Phytocoenology, distribution and habitat preferences of the species Aldrovanda vesiculosa (Droseraceae) in Romania. Botanica Serbica, 2024

[13] Banescu A., Arseni M., Georgescu L.P., Rusu E., Iticescu, C., Evaluation of different simulation methods for analyzing flood scenarios in the Danube Delta. Applied Sciences, 10(23), 8327, 2020

ENVIRONMENTAL STATISTICAL ANALYSIS OF THE BASINS OF THE MINING DISTRICT OF PONCE ENRÍQUEZ (ECUADOR)

Daniel Garcés[1,2]
Yolanda Sanchez-Palencia[2]
Samantha Jimenez[1]
Juan Llamas[2]

[1]Facultad de Ingeniería en Ciencias de la Tierra, Escuela Superior Politécnica del Litoral, **Ecuador**
[2]E.T.S. Ingenieros de Minas y Energía, Universidad Politécnica de Madrid, **España**

ABSTRACT

Camilo Ponce Enriquez is in the southwest coastal zone of Ecuador, and it is surrounded by 4 river basins (Gala, Tenguel, Siete and Pagua) with an area of 1,780 km^2. Mining has been the main economic activity since 1980 and is classified as Artisanal and Small-Scale Mining Activity. However, since 2000s there is evidence of contamination by heavy metals in water and sediments due to irregular mining practices and inefficiency environmental's regulations. Despite the evidence, there are not enough scientific studies, and few reports are published about chemistry and contamination. The study goal is to analyze 333 river sediments samples taken from the four river basins, using geostatistical and geochemical methods, to determinate possible correlations and associations between contaminant elements. Samples were analyzed for 35 elements (Ag, Al, As, Au, Ba, Bi, Ca, Cd, Co, Cr, Cu, Fe, Ga, Hg, K, La, Li, Mg, Mn, Mo, Na, Nb, Ni, Pb, Sb, Sc, Sr, Te, Ti, Tl, V, W, Y, Zn, Zr). The elements results were studied using univariate statistical methods, Spearman's Ordinal Correlation, factor analysis using PCA, and cluster analysis using Ward's method. The results evidence nine elements (Co, Cr, Cu, Fe, Mg, Ni, Sc, Ti and V) with significant correlations ($r \geq 0.5$). The strongest correlation is V-Fe (0.91), followed by V-Ti, Ni-Co and Ni-Cr and Sc-Co ($r \geq 0.8$). The correlation in the V, Fe, Ni, Cr elements are related with orthomagmatic deposits. Also, V and Ti are related to titanium and iron oxides mainly in mafic deposits, which could be associated with the Pallatanga Fm. The factor analysis identified five groups of elements that are comparable to the Goldschmidt classification, where the groups are related with arsenopyrite, oxy-hydroxides, mafic and porphyry deposits. The cluster analysis revealed four groups, where the spatial distribution matched with the contamination level areas in the Siete, Tenguel and Gala River basins. The results provide an environmental baseline against which the impacts of anthropogenic activities (including mining) may be assessed. A basis for the formulation of sediment quality criteria and for the identification of natural geochemical hazards is also provided.

Keywords: Cluster analysis, heavy metals, geostatistical analysis, geochemistry.

INTRODUCTION

In Camilo Ponce Enríquez, mining has been generating economic activity since 1980 (Sandoval, 2001). Mining concessions occupy 77.62% of the territory and are carried out in an Artisanal and Small-scale Manner (ASM) [1]. However, inadequate and irregular

https://doi.org/10.5593/sgem2024/1.1/s01.09

mining practices, and inefficiency in environmental regulations have caused adverse environmental impacts in the area, mainly due to the discharge of potentially toxic elements into the rivers. In the 1990s, the Mining Development and Environmental Control Project (PRODEMINCA in spanish) conducted studies in this area and reported water and sediment contamination with heavy metals and metalloids in the Siete and Tenguel river basins. The main contaminant was As, followed by high concentrations of Hg, Cu, Cd, and Pb [2]. After 2000, some researchers reported similar information [3], [4], [5], [6]. This study aims to analyze samples from four river basins (Gala, Tenguel, Siete, and Pagua) present in the mining area of Ponce Enríquez using geostatistical and geochemical methods to determine possible correlations and associations between the analyzed elements.

Geographically, the canton of Camilo Ponce Enríquez is in the southwestern coastal zone of Ecuador. Hydrographically, it includes the Gala, Tenguel, Siete, and Pagua river basins, covering an area of approximately 1,780 km² (Fig. 1).

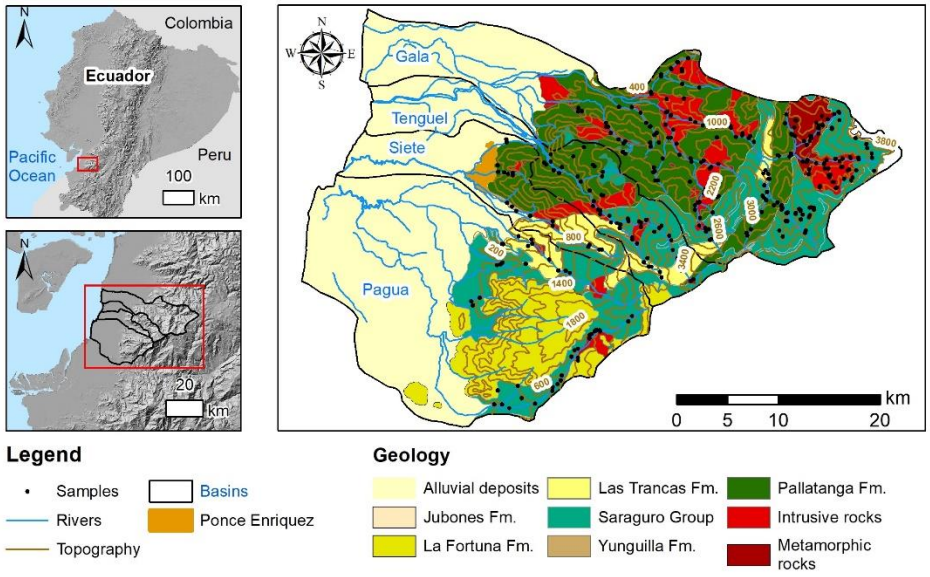


Fig. 1.- Location of the study area, showing the geology and the samples distribution.

The geology of the study area comprises alluvial deposits and the main geological units of Pallatanga, Yunguilla, Saraguro, Las Trancas, La fortuna, Jubones and intrusive and methamorphic rocks [7], [8]. The alluvial deposits are located on the western flank of the study area, which includes an alluvial terrace at the foothills of the river basins. The Pallatanga Fm. (Cretaceous) consists of tholeiitic basalts, and blue-green hyaloclastites. It is also characterized by a propylitic mineral association that includes epidote, chlorite, and quartz, with some traces of titanite, illite, and prehnite. The Yunguilla Fm. (upper Cretaceous-Maastrichtian) is a turbidite sequence and consists of sandstones, shales, and siltstones, quartz-feldspathic sandstones, and quartz arenites. The Saraguro Group (Late Eocene) mainly encompasses welded ash-flow tuffs of dacitic to rhyolitic composition, andesitic lavas, reworked volcanic material, and sedimentary rocks. There are also scarce intercalations of turbiditic sandstones and shales. Most of the outcrops of the Saraguro Group are not uniformly subdivided, but four tuff formations are recognized in the area:

Las Trancas Fm., Jubones Fm., La Fortuna Fm., La Paz Fm., and Portovelo Unit. In the study area, Las Trancas and La Fortuna formations outcrop from the Saraguro Group. Las Trancas Fm. (Oligocene) overlies the Pallatanga Formation and consists of andesitic to dacitic ignimbrites, conglomerates, argillites, muscovite, and quartz-rich sandstones. La Fortuna Fm. (Miocene) is composed of aphyric ignimbrites and contains scattered crystals of plagioclase, biotite, and quartz.

MATERIALS AND METHODS

In this study, 333 sediment samples collected from the alluvial river's plains in the four basins were used. These samples were from to the environmental monitoring project carried out between 1996 and 1998 in mining areas of southern Ecuador, where a total of 4,850 samples were collected [2]. The samples were sieved to 177 µm, then dried at 40 ^{o}C and pulverized with a ceramic mortar. They were then quartered and reduced to 65 g subsamples for multi-element instrumental analysis. The elements (Ag, Al, As, Au, Ba, Bi, Ca, Cd, Co, Cr, Cu, Fe, Ga, Hg, K, La, Li, Mg, Mn, Mo, Na, Nb, Ni, Pb, Sb, Sc, Sr, Te, Ti, Tl, V, W, Y, Zn, and Zr) were analyzed by inductively coupled plasma emission spectrometry (ICP-ES). The elements Au, As, Hg, and Sb were determined by atomic absorption spectrophotometry (AAS) [9].

The elements content of the samples was studied through univariate statistical analysis to describe the data, followed by multivariate analysis using Spearman's Ordinal Correlation to highlight the relationships between the elements. Then, Factor Analysis was performed using a factorization based on the principal component method, with Pearson correlation, and setting the varimax rotation method to observe possible associations. Later, to identify groupings among the elements, a cluster analysis was performed using Ward's statistical method with unstandardized Euclidean distance, to evaluate the distance between groups by minimizing the sum of squares of residuals between them. The groupings were performed by observations and by variables to highlight spatial relationships. The spatial analysis and segmentation of the data according to the studied river basins were conducted using ArcMap version 10.8.2 software, while the statistical analysis was carried out using STATGRAPHICS version 16.

RESULTS

Table I presents the statistical analysis of the data, including the mean, standard deviation, coefficient of variation, minimum, median, maximum, standardized skewness, and standardized kurtosis. Elements with a very low coefficient of variation (< 50%), such as W, Tl, Al, and Fe, were identified. Conversely, elements such as Hg, Cd, As, Cu, Sb, and Pb exhibit very high coefficients of variation, ranging between 400% and 604%. Additionally, both As and Fe values surpass the maximum detection equipment limit, with others like Cu and Sb also nearing the limit. Despite this, the elements with the highest values are As, Cu, Ti, Mn, and Pb, indicating a significant disparity between the median and maximum values, accompanied by considerable standard deviations.

The multivariate method of Ordinal Spearman Correlation was applied to the 35 variables, resulting in 9 elements (Co, Cr, Cu, Fe, Mg, Ni, Sc, Ti, and V) with significant correlations ($r \geq 0.5$) and a significance level below 0.05 (Table II). The strongest

https://doi.org/10.5593/sgem2024/1.1/s01.09

correlations (r≥ 0.9) are V-Fe, followed by high correlations (r≥ 0.8) Ni-Co, Ni-Cr, Sc-Co and V-Ti. The remaining correlations are considered medium (0.8≥ r≥ 0.5).

Table I.- Descriptive statistics: mean (Me), standard deviation (SD), coefficient of variation (CV), minimum (Min), median (Med), maximum (Max), standardized skewness (SE), and standardized kurtosis (CE). Values in mg/kg, unless otherwise indicated.

	Me	SD	CV	Min	Med	Max	SE	CE
Ag	0.93	1.81	193.42%	0.66	0.66	19.00	57.86	237.40
Al(%)	2.86	1.00	34.88%	0.37	2.76	5.88	3.67	0.75
As	224.13	1213.54	541.44%	2.66	17.4	10000.00*	53.13	194.16
Au	0.32	1.20	371.50%	0.00	0.016	9.95	43.76	139.48
Ba	128.50	86.19	67.08%	3.60	110	594.00	13.38	20.55
Bi	6.12	9.82	160.45%	4.00	4	105.00	53.14	206.12
Ca(%)	0.51	0.41	81.94%	0.08	0.42	4.20	41.92	162.88
Cd	1.49	8.22	550.79%	0.46	0.46	103.00	84.62	504.30
Co	23.13	38.27	165.46%	1.73	14	462.04	62.44	320.40
Cr	64.51	66.34	102.85%	2.46	39	433.00	14.91	16.73
Cu	154.43	672.83	435.68%	3.00	40	9012.00	69.89	387.78
Fe(%)	5.02	2.26	45.00%	0.75	4.38	10.00*	4.29	-1.92
Ga	4.53	3.11	68.74%	1.33	4	14.00	5.61	-0.42
Hg	0.35	2.12	603.47%	0.03	0.056	33.84	99.84	741.31
K(%)	0.10	0.06	65.69%	0.01	0.09	0.52	16.67	30.98
La	9.17	6.24	68.06%	0.66	8	39.00	9.45	10.96
Li	12.68	6.90	54.39%	0.80	11	44.00	12.06	12.62
Mg(%)	0.90	0.53	59.07%	0.04	0.85	4.02	11.63	19.27
Mn	789.18	414.43	52.51%	164.00	679	2846.50	12.00	13.92
Mo	1.87	1.44	77.23%	0.70	1.833	8.00	10.83	8.46
Na(%)	0.02	0.01	62.74%	0.01	0.02	0.14	29.18	110.09
Nb	2.40	2.62	109.46%	0.66	1	18.00	18.97	30.15
Ni	33.62	48.33	143.77%	2.20	17	393.06	26.62	63.79
Pb	33.22	137.74	414.63%	2.66	15	1832.00	76.55	426.29
Sb	6.34	27.50	433.77%	1.26	1.26	306.60	60.12	264.24
Sc	7.97	6.75	84.68%	3.33	6	36.00	13.51	9.93
Sr	23.08	13.15	56.98%	0.66	22	102.00	8.71	17.51
Te	7.67	6.46	84.28%	6.66	6.66	77.00	57.19	239.08
Ti	836.87	730.75	87.32%	66.00	600	3800.00	10.69	7.36
Tl	6.79	1.42	20.96%	6.66	6.66	25.00	89.24	544.72
V	122.29	78.65	64.32%	9.00	95	382.00	6.30	-0.13
W	13.44	1.19	8.86%	13.33	13.33	29.00	82.58	469.81
Y	6.62	3.50	52.86%	1.00	6	27.00	15.30	24.21
Zn	99.89	115.70	115.82%	3.33	75	1023.50	40.02	120.86
Zr	2.26	2.73	120.91%	0.66	0.66	16.50	16.54	20.03

*Asterisk indicates values upper detection limit.

Regarding the factor analysis, the ideal number of factors to represent 75% of the samples according to the eigenvalues is 10. However, an extensive number of factors do not allow a proper analysis of variable behavior. Therefore, 5 factors were used, which explained 60.2% of the variance.

Table II.- Spearman's Ordinal Correlation, values < 0.8 highlighted in bold.

	Co	Cr	Cu	Fe	Mg	Ni	Sc	Ti
Cr	0.75							
Cu	0.69	0.68						
Fe	0.69	0.71	0.72					
Mg	0.76	0.70	0.59	0.52				
Ni	**0.85**	**0.83**	0.72	0.58	0.71			
Sc	**0.82**	0.72	0.55	0.60	0.65	0.74		
Ti	0.55	0.70	0.64	0.64	0.56	0.54	0.53	
V	0.59	0.76	0.69	**0.91**	0.49	0.53	0.55	**0.80**

Table III presents the factorial analysis of 25 elements with coefficients above 0.5, categorized into five factorial groups named F1 to F5. The other elements have factorial coefficients bellow 0.5. Factor 1 includes elements with high coefficients: Ag, As, Bi, Te, Cu, and Au (above 0.8), followed by elements with medium coefficients: Pb, Zn, and Cd (between 0.7 and 0.8); and finally, elements with low coefficients: Co and Sb (between 0.6 and 0.5). Factor 2 includes elements with high coefficients such as Sc and Ti, followed by medium coefficients for Zr, Al, Y, and V; and low coefficients for Fe, Cr, Mn, Mg, and Ni. Factor 3 groups fewer elements, with Ca having a high coefficient, and Ni, Mg, and Sb having low coefficients. Factor 4 shows weak relationships, including Mo and W (coefficients 0.45 and 0.40, respectively), while Factor 5 did not show significant values.

The cluster analysis classified the elements into four groups. The results are compared with the mining activity areas (Fig. 2), where the fourth group may represent high pollution sample

Table III.- Factor analysis of elements, values above 0.5 are in bold.

	F1	F2	F3	F4	F5
Ag	**0.95**	-0.09	0.17	0.00	0.00
Al	-0.16	**0.74**	0.05	-0.13	0.23
As	**0.93**	-0.08	0.24	-0.03	-0.01
Au	**0.81**	-0.01	0.39	-0.06	-0.08
Bi	**0.91**	0.02	-0.13	0.19	-0.06
Ca	0.14	0.17	**0.83**	-0.24	0.02
Cd	**0.71**	-0.07	0.19	-0.06	0.05
Co	**0.66**	0.37	0.03	0.12	-0.10
Cr	-0.03	**0.69**	0.44	0.25	-0.17
Cu	**0.87**	0.04	0.00	0.08	-0.06
Fe	0.33	**0.69**	-0.07	0.30	-0.36
Mg	0.08	**0.53**	**0.63**	0.25	-0.02
Mn	0.00	**0.67**	0.21	-0.06	0.33
Mo	0.01	0.03	-0.08	0.45	0.02
Ni	0.09	**0.50**	**0.66**	0.17	-0.13
Pb	**0.79**	0.02	-0.12	0.07	0.03
Sb	**0.63**	-0.11	**0.58**	-0.17	-0.02
Sc	0.06	**0.89**	0.21	0.07	-0.02
Te	**0.89**	-0.02	-0.11	0.13	-0.07
Ti	-0.05	**0.81**	0.13	0.09	-0.29
V	0.09	**0.70**	-0.07	0.25	-0.49
W	-0.06	-0.04	0.10	0.40	0.09
Y	0.02	**0.72**	-0.04	-0.19	0.25
Zn	**0.79**	0.13	0.05	0.00	0.19
Zr	0.01	**0.78**	0.19	-0.04	-0.05

https://doi.org/10.5593/sgem2024/1.1/s01.09

DISCUSSION

As shown in Table 1, there are anomalous concentrations of heavy metals such as As, Fe, Cu, and Sb, with maximum values exceeding the detection limits. Some of these values correspond to samples located near mineral deposits and are linked to Factors 1 and 2.

The Spearman correlation index between Fe and V (r = 0.9) is possibly related to orthomagmatic deposits, where V^{3+} can substitute for Fe^{3+} during magmatic crystallization in mafic and ultramafic igneous rocks, which could be associated with the Pallatanga Fm. The V is considered a redox-sensitive element with three oxidation states: V^{3+}, V^{4+}, and V^{5+}. The first two ions are immobile under reducing conditions, while the third is immobile under oxidizing conditions [10]. The correlation between Ni and Cr (r = 0.83) is typically associated with orthomagmatic deposits. Similarly, the correlation between V and Ti (r = 0.8) relates to titanium and iron oxides associated with mafic deposits, which could also be linked to the Pallatanga Formation and the Saraguro Group.

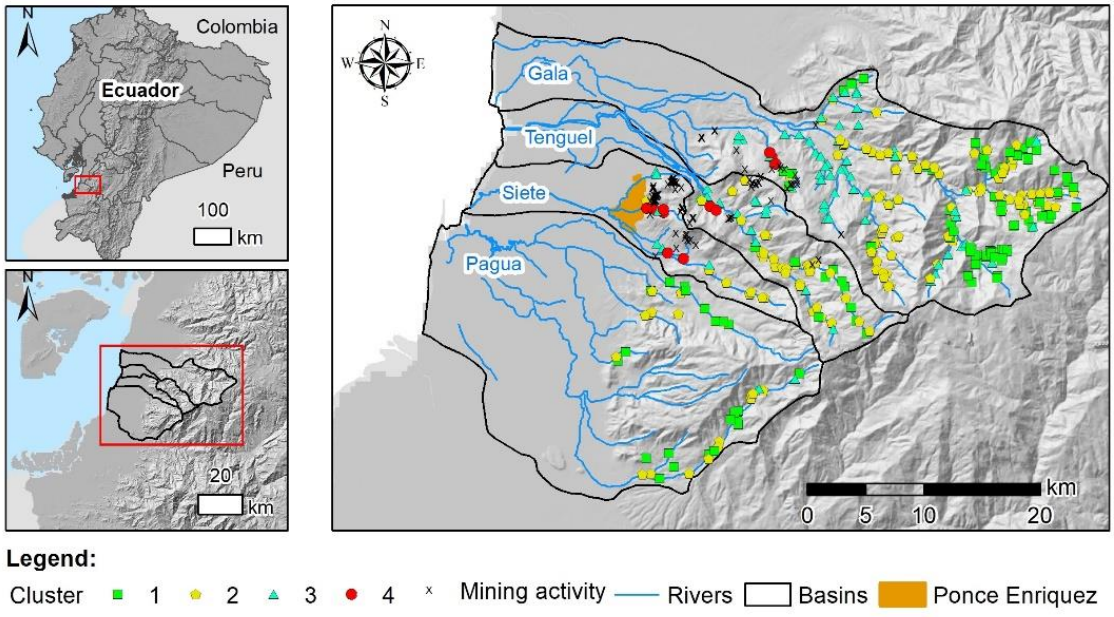


Fig. 2.- Cluster Analysis using Ward's statistical method with unstandardized Euclidean distance

A correlation of the factorial groups with the elements from the Goldschmidt table was performed (Fig. 3). Factor 1 mostly groups chalcophile elements (Cu, Ag, Zn, Cd, Pb, As, Sb, Bi, Te) and some siderophile elements (Co, Au). Factor 2 includes lithophile (Sc, Ti, V, Y, Zr, Nb, Al) and siderophile (Mn, Fe) elements, and a lithophile/siderophile element (Cr). Factor 3 is characterized by lithophiles (Mg, Ca) and a siderophile element (Ni). The elements W and Mo in Factor 4 are siderophile elements.

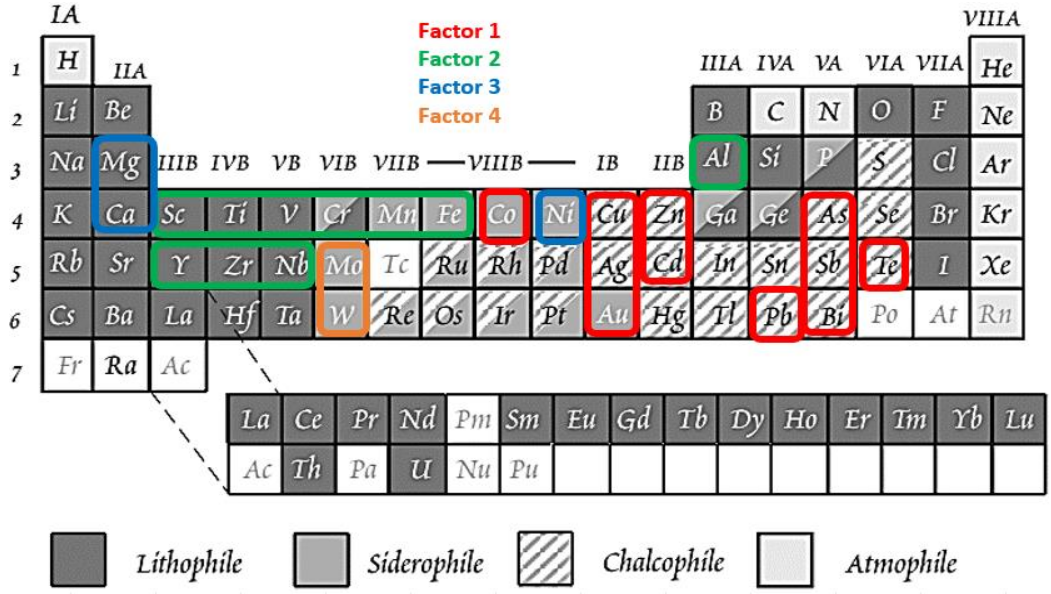


Fig. 3.- Grouping of factors with respect to Goldschmidt's classification [11].

Using the factor analysis, the elements grouped in Factor 1 can be found in the Ponce Enríquez mining district in minerals associated with hydrothermal processes where Au, Ag, Cu, As, Pb, and Cu are present as arsenopyrites in Pallatanga Fm. [12], [13]; also, it was identified that epidotes in porphyry deposits are characterized by the content of As and Sb [8]. Factor 2 elements like Fe, Ti and Mn are usually found together forming oxy-hydroxides such as goethite, hematite and titanite, minerals that mainly form due to hydrothermal and meteoric alteration processes, also associated with the Pallatanga Fm. Factor 3 are also related to mafic deposits and hydrothermal alteration minerals such as chlorite and calcite; or related with pyroxenes, commonly observed in metamorphic and igneous rocks. The correlated elements in Factor 4 are Mo and W, classified as siderophile, where Mo is usually associated with propylitic alteration, normally developed as an outer halo of many Cu-Au-Mo porphyry deposits [8].

Overall, the mineralogy of the Pallatanga Fm. is strongly related to the elements described in the factorial analyses, due to its basaltic lavas with Cu-Au-Mo porphyry deposits and minerals such as pyrrhotite (Fe), pyrite (Fe), galena (Pb), hematite (Fe), sphalerite (Zn), chalcopyrite (Cu, Fe), magnetite (Fe), molybdenite (Mo), and calcite (Ca), among others. Additionally, it presents hydrothermal propylitic alterations with minerals like epidote (Ca, Fe, Al), chlorite (Mg, Fe), illite (Fe, Mg, Al), titanite (Ti, Ca), prehnite (Ca, Al), and quartz. The Saraguro Group is also related to the elements in the factorial analyses. La Fortuna Fm. is composed of crystals of plagioclase (Na, Ca, Si, Al) and biotite (K, Mg, Fe, Al), while Las Trancas Fm. contains minerals like muscovite (K, Al) and quartz.

Regarding the cluster analysis, the order of the cluster groups (from 1 to 4) may be related to the samples level pollution, where cluster 1 got the lowest pollution, while cluster 4 was the most polluted. The spatial distribution showed a coincidence between Cluster 4 and areas reported with possible contamination from mining activities [2], [3], [4], [12], [13]. Cluster 4 included 11 samples with the highest concentrations of heavy metals like As, Au, Fe, Ag, Cd, Cu, Pb, Sb, Te, and Zn, while having the lowest concentrations of Ba.

https://doi.org/10.5593/sgem2024/1.1/s01.09

CONCLUSION

This study analysed 333 samples in the mining area of Ponce Enríquez using geostatistical and geochemical methods to determine possible correlations and associations between elements. Anomalous concentrations of As, Fe, Cu, and Sb were found, with maximum values exceeding detection limits.

The statistical results revealed correlations between V-Fe, Ni-Co, Ni-Cr, Sc-Co, and V-Ti, which are related to orthomagmatic deposits and could be associated with the Pallatanga Fm. and Saraguro Group. A correlation of the factorial groups with elements from the Goldschmidt table (classified lithophile, siderophile, and chalcophile elements) was carried out. Most Factor 1 elements were chalcophiles, while Factors 2 and 3 were lithophiles, and Factor 4 was siderophile. Factors 1 and 2 were associated with the Pallatanga Fm. and Saraguro Group due to their mineralogy and volcanic genesis, while Factor 3 was related to metamorphic and intrusive rocks. The cluster analysis spatial distribution showed a match between the order of the four cluster groups and the contamination level of the samples. Cluster 4 included 11 samples with the highest concentrations of As, Au, Fe, Ag, Cd, Cu, Pb, Sb, Te, and Zn. These samples' locations matched with polluted areas near mining activities in the basins.

The results provide an environmental baseline to assess the impacts of anthropogenic activities, including mining. They also offer a basis for formulating sediment quality criteria and identifying natural geochemical hazards. A future study to distinguish geogenic and anthropogenic pollution is recommended.

REFERENCES

[1] R. Estupiñan, P. Romero-Crespo, M. Garcia, D. Garces, and P. Valverde, “La minería en Ecuador. Pasado, presente y futuro,” *BOLETÍN GEOLÓGICO Y MINERO*, vol. 132, no. 4, pp. 533–549, Dec. 2021, doi: 10.21701/bolgeomin.132.4.010.

[2] UCP PRODEMINCA, *Monitoreo ambiental de las áreas mineras en el sur del Ecuador 1996 -1998*, I., vol. 59. Quito: SWEDISH ENVIRONMENTAL SYSTEMS, 1998.

[3] J. D. Appleton, T. M. Williams, H. Orbea, and M. Carrasco, “Fluvial Contamination Associated with Artisanal Gold Mining in the Ponce Enríquez, Portovelo-Zaruma and Nambija Areas, Ecuador,” *Water Air Soil Pollut*, vol. 131, no. 1/4, pp. 19–39, 2001, doi: 10.1023/A:1011965430757.

[4] G. T. Carling *et al.*, “Particulate and Dissolved Trace Element Concentrations in Three Southern Ecuador Rivers Impacted by Artisanal Gold Mining,” *Water Air Soil Pollut*, vol. 224, no. 2, p. 1415, Feb. 2013, doi: 10.1007/s11270-012-1415-y.

[5] K. Escobar-Segovia *et al.*, “Heavy metals in rivers affected by mining activities in Ecuador: Pollution and human health implications,” *WIT Transactions on Ecology and the Environment*, vol. 250, pp. 61–72, 2021, doi: 10.2495/WRM210061.

[6] K. Villamar-Marazita *et al.*, “Heavy Metal Pollution Assessment in Surface Water and Groundwater in the Ponce Enriquez Mining Area, Ecuador,” in *Proceedings of the LACCEI international Multi-conference for Engineering, Education and Technology*, Latin American and Caribbean Consortium of Engineering Institutions, 2023. doi: 10.18687/laccei2023.1.1.493.

[7] W. T. Pratt, J. Figueroa, and B. Flores, “Mapa Geológico de la Coordillera Occidental del Ecuador entre 3° - 4°S,” Quito, 1997.

[8] P. Fulignati *et al.*, “The propylitic alteration in the Ponce Enriquez Gold Mining district, Azuay province, Ecuador: genetic constraints from a mineral chemistry and fluid inclusions study,” *Front Earth Sci (Lausanne)*, vol. 11, p. 1255712, Sep. 2023, doi: 10.3389/feart.2023.1255712.

[9] T. M. Williams *et al.*, “Regional geochemical reconnaissance of the Cordillera Occidental of Ecuador: Economic and environmental applications,” *Applied Geochemistry*, vol. 15, no. 4, pp. 531–550, 2000, doi: 10.1016/S0883-2927(99)00059-1.

[10] J. L. Manrique-Carreño and G. A. Guamán-Jaramillo, “Estudio de prospección geoquímica en sedimentos de las microcuencas Chirimoyo y Guineo, Ecuador,” *Revista Boletín de Geología*, vol. 42, no. 1, pp. 39–55, Jan. 2020, doi: 10.18273/revbol.v42n1-2020002.

[11] W. White, *Geochemistry*. John Wiley & Sons, 2005.

[12] S. Jiménez-Oyola *et al.*, “Ecological and probabilistic human health risk assessment of heavy metal(loid)s in river sediments affected by mining activities in Ecuador,” *Environ Geochem Health*, vol. 43, no. 11, pp. 4459–4474, Nov. 2021, doi: 10.1007/s10653-021-00935-w.

[13] E. Peña-Carpio and J. M. Menéndez-Aguado, “Environmental study of gold mining tailings in the Ponce Enriquez mining area (Ecuador),” *DYNA (Colombia)*, vol. 83, no. 195, pp. 237–245, 2016, doi: 10.15446/dyna.v83n195.51745.

https://doi.org/10.5593/sgem2024/1.1/s01.09

GEOLOGICAL STRUCTURE AND MINERALOGICAL COMPOSITION OF THE KARA-AYAK RARE METAL ORE OCCURRENCE (EAST KAZAKHSTAN)

PhD Tatyana Oitseva[1,2]

[1] D. Serikbaev East Kazakhstan Technical University, **Kazakhstan**
[2] Geos LLP, **Kazakhstan**

ABSTRACT

In the development of high technologies, “lightweight” - rare metals - are of great importance. Almost all modern devices: from a player to an electric bus cannot do without them. These metals are used in mechanical and aircraft manufacturing, digital technologies, and medicine; the implementation of a green program without them is generally impossible. According to statistical forecasts, the need for rare metals will only grow every year. During the Soviet period, most of the rare metal deposits were mined; small ore occurrences were not considered due to low contents and reserves. Currently, the Republic of Kazakhstan has developed a Comprehensive Plan for expanding the resource base and introducing technologies for the integrated extraction of rare metals, modernizing existing production facilities, developing standards regulating the industry and lifting the secrecy regime for individual metals, as well as mining all known ore occurrences and a detailed study of mineralization points. The Kara-Ayak ore occurrence belongs to an unconventional type of rare metal mineralization (Sn, W, Ta, etc.), superimposed on more ancient tectonically prepared intrusions and dikes of the Kunush complex. In the Kalba-Narym zone, similar examples are the already explored and studied greisen-quartz vein deposit Cherdoyak (Sn, W), rare metal-pegmatite objects Medvedka, Tochka, Novo-Saryozek and others (Ta, Nb, Be, Li). The similarity of the geological structure of these objects emphasizes the prospects for assessing the Kara-Ayak ore occurrence.

Keywords: granites, Kunush complex, rare metals, tungsten, Eastern Kalba.

INTRODUCTION

The territory under consideration is part of the structure of Greater Altai and is directly located in the Kalba-Narym tectonic zone, the geological characteristics of which are discussed in many works [1-3]. The Kara-Ayak site is located in Eastern Kalba in the exocontact zone of the Kashemin granite massif (Fig. 1). It was first identified during a geological survey at a scale of 1:50,000 (B.A. Dyachkov et al., 1960, 1966) and which remained unappreciated. The type of mineral discovered is tungsten. In this area, in the upper reaches of the Kara-Ayak rivers and the Kalbinsky key, greisenized and silicified dikes of granodiorite-porphyries of the Kunush complex are exposed, containing quartz-muscovite greisens and quartz veins with tourmaline, fluorite, scheelite and arsenopyrite. The tungsten content in them, according to ore samples, reaches 0.1 and >1%. The source of ore-bearing solutions is probably the unexposed granite massifs of the Kalbinsky complex, by analogy with the Malo-Chernovinsky ore occurrence [4-6].

https://doi.org/10.5593/sgem2024/1.1/s01.10

In the study area, ore occurrences were also identified: Martyanovskoye, East Kalbinskoye, Kalbinskoye, Laibulakskoye, mineralization point No. 9, which also have rare metal mineralization.

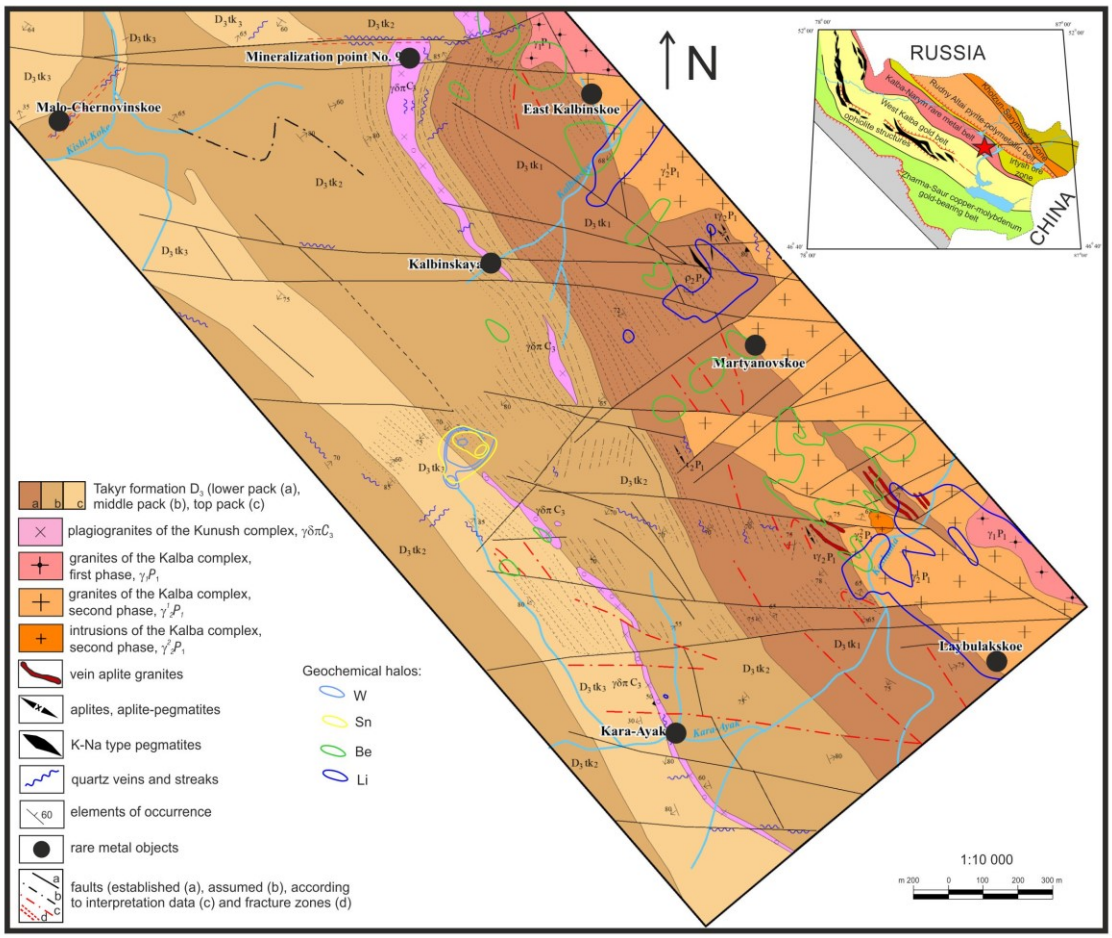


Fig. 1. Geological map of the Kara-Ayak ore occurences. Based on materials [4].

MATERIALS AND METHODS

The main method was a systematic analysis of geological and field documentation. Extensive materials of geological survey and prospecting and exploration works carried out in different years in the study area were used (Dyachkov B. A. et al., 1960, 1961, 1981, 2015; Ermolin V. T. et al., 1968; Navozov O.V. et al., 2009) [4-5, 7].

Samples were taken from ore-bearing rocks and greisens (more than 300 samples) for laboratory studies. Fragments of samples, the remains of the core were taken as a sample, the furrows of the ditches were re-tested. Analytical studies were carried out in the VERITAS laboratory of the D. Serikbaev East Kazakhstan Technical University and the laboratory "NPC "Plasma-analit" (Ust-Kamenogorsk). The complex of analytical works included spectral semi-quantitative analyses, physico-chemical, chemical and mineralogical determinations of the contents of useful and associated elements in samples of ores and host rocks. The chemical composition of minerals was analyzed on

an Agilent 7500cx ICP-MS mass spectrometer (Agilent Technologies) and an MC-46 Cameca microprobe, which determined 73 elements, on Jeol-100C scanning electron microscopes with a Kevex-Ray energy dispersive attachment and ISM-6390 LV from Jeol with the INCA Energy prefix from OXFORD, which also investigated fluid inclusions of ore and associated minerals, and also determined trace elements in them.

FEATURES OF THE GEOLOGICAL STRUCTURE

The Kara-Ayak ore occurrence belongs to an unconventional type of rare metal mineralization (Sn, W, Ta, etc.), superimposed on more ancient tectonically prepared intrusions and dikes of the Kunush complex. In the Kalba-Narym zone, examples are the already explored greisen-quartz vein deposit Cherdoyak (Sn, W), rare metal-pegmatite objects Medvedka, Tochka, Novo-Saryozek and others (Ta, Nb, Be, Li) [1, 3, 8, 9].

At the ore occurrence under consideration, the host sedimentary rocks are represented by sandstone-siltstone deposits of the Takyr Formation (D_3tk), subdivided into three members (Fig. 1). The lower member (D_3tk_1) is developed in the exocontact of the granite massif. It is composed predominantly of thin-layered carbonaceous-clayey siltstones with a subordinate amount of fine-grained sandstones up to 0.5 m thick. The ratio of siltstones and sandstones is more than 4:1. The middle member (D_3tk_2) is essentially sandstone and consists of coarse, uneven interbedding of fine-grained sandstones and siltstones. The ratio of sandstones and siltstones is 2:1. The upper member (D_3tk_3) is siltstone, consisting of carbonaceous-clayey siltstones with rare interlayers of fine-grained quartz-feldspathic sandstones (more than 5:1).

The formation is characterized by dark gray hornfelsed fine-grained quartz-feldspathic sandstones of irregular texture and silty-psammitic structure. The cement is clayey-calcareous, replaced by graphite, carbonate, sericite and chlorite. In terms of chemical composition (Table 1), they are close to arkosic quartz-feldspathic sandstones, which are characterized by a fairly high SiO2 value, low CaO and F contents. According to the results of bituminological analysis, the content of carbonates and organic matter in the sandstones is 9.47%.

Siltstones are carbonaceous-clayey hornfelsed, composed of uneven-grained quartz aggregate with an admixture of sericite and graphitized carbonaceous material. Their petrochemical composition is close to sandstones, from which they differ in a higher K2O value and a decrease in SiO2. Occasionally there are interlayers of pyroxene hornfels developed on calcareous sandstones. Their mineral composition: quartz, feldspar, monoclinic pyroxene, epidote-zoisite minerals, sphene, apatite, chlorite. Compared to sandstones, siltstones have 2.9 times more organic matter.

The ore-bearing bodies are three dike-like bodies of medium-to-coarse-grained sharply porphyritic biotite granodiorite porphyries, which occur in conformity with the structures of the host sequence [1, 2, 10, 11]. The strike of the bodies is NW 330-3400, length varies from 750 to 2800 m with thickness from 1 to 100 m, in swells up to 300 m; dikes fall to the southwest 50-550. The contacts of granodiorite porphyries with rocks of the Takyr Formation are sharp and clear. Similar large bodies of granodiorite-porphyry belong to the first generation of dikes of the Kunush complex; they cross gabbro-diabases of the Karabiryuk complex (C_{2-3}), are themselves cut by granitoids of the Kalba complex (P_1) and are reference formations for the entire Kalba-Narym zone.

https://doi.org/10.5593/sgem2024/1.1/s01.10

Table 1. Chemical compositions of rocks at the Kara-Ayak ore occurrence, weight. %

Oxides	Takyr series		Kunush complex									Modified rocks			
	2252	2253	843-15	845-15	1623	1635	1635-1	1644	2256	2258	Average (8)	1649-2	2249-1	2249-2	Average -3
	1	2	3	4	5	6	7	8	9	10	11	12	13	14	15
SiO_2	69,75	66,90	64,56	64,68	64,48	65,30	64,76	66,34	65,69	66,84	65,33	80,64	64,76	73,07	72,82
TiO_2	0,52	0,52	0,87	0,87	0,86	0,87	0,78	0,68	0,64	0,57	0,77	0,32	0,60	0,45	0,60
Al_2O_3	15,09	16,35	16,96	16,81	16,65	16,65	16,74	16,25	15,79	15,31	16,40	3,17	17,43	12,60	11,06
Fe_2O_3	1,03	1,59	1,72	0,69	1,47	1,15	1,89	1,89	1,52	1,38	1,46	6,49	1,50	1,01	3,00
FeO	2,44	2,23	3,66	4,86	3,91	4,23	4,16	3,52	3,30	3,23	3,73	2,87	1,22	1,93	2,01
MnO	0,08	0,05	0,07	0,09	0,08	0,07	0,06	0,06	0,08	0,08	0,07	0,01	0,05	0,05	0,03
MgO	1,02	1,17	1,95	1,95	1,71	1,54	1,05	1,10	1,12	0,82	1,40	0,41	1,02	0,82	0,75
CaO	1,35	0,78	2,49	2,49	2,26	2,26	2,49	2,06	2,41	2,34	2,35	0,56	1,06	0,43	0,68
Na_2O	3,75	3,64	3,07	3,12	3,12	3,02	3,01	2,81	3,31	3,31	3,10	0,43	0,75	0,44	0,54
K_2O	2,44	3,68	3,55	3,45	3,41	3,69	3,98	3,55	3,55	3,82	3,62	1,35	7,06	5,29	4,56
H_2O	0,02	0,03	0,22	0,19	0,50	0,18	0,19	0,21	0,03	0,04	0,19	0,43	0,09	0,09	0,20
F	0,03	0,04	0,056	0,056	0,048	0,056	0,072	0,048	0,04	0,05	0,05	0,056	0,25	0,26	0,18
Cl	0,07	0,07							0,07	<0,1			0,07	0,07	0,07
P_2O_5	0,14	0,15	0,08	0,07	0,09	0,08	0,23	0,15	0,24	0,25	0,15	0,07	0,21	0,09	0,12
SO_3	<0,1	<0,1							<0,1	<0,1	<0,1		<0,1	0,12	<0,1
CO_2	<0,1	0,08	0,11	<0,1	<0,1	<0,1	0,11	<0,1	<0,1	<0,1	<0,1	<0,1	0,08	<0,1	<0,1
n.n.n	1,51	2,18	1,20	0,79	2,02	1,16	1,26	1,64	1,45	1,24	1,23	3,66	3,35	2,50	3,17
Total	99,24	99,46	100,40	100,06	100,56	100,20	100,60	100,26	99,24	99,28	100,07	100,46	99,42	99,22	99,70
Note: 1 – fine-grained hornfelsed sandstone; 2 – carbonaceous-clayey siltstone; 3-11 – medium-to-coarse-grained irregularly porphyritic biotite granodiorites of the Kunush complex; 12-15 – muscovite-quartz greisens															

Microscopically, the structure of granodiorite porphyries is porphyritic or cryptic with a microhypidiomorphic granular groundmass. Phenocrysts are represented by grains of plagioclase, K-feldspar and accumulations of brown biotite. The groundmass consists of pelitized grains of plagioclase, quartz, microcline-perthite and fine-flaky biotite. In the burrows, the leading accessories include lamellar ilmenite (2-520 g/t), prismatic apatite (150-790 g/t), zircon (4-73 g/t). In isolated characters there are scheelite, cassiterite, fluorite, and tourmaline. The presence of sulfide minerals is characteristic: galena, chalcopyrite, arsenopyrite and pyrite (Fig. 2). The altered varieties contain increased contents of garnet (78.5 g/t) and fluorite (14.2 g/t).

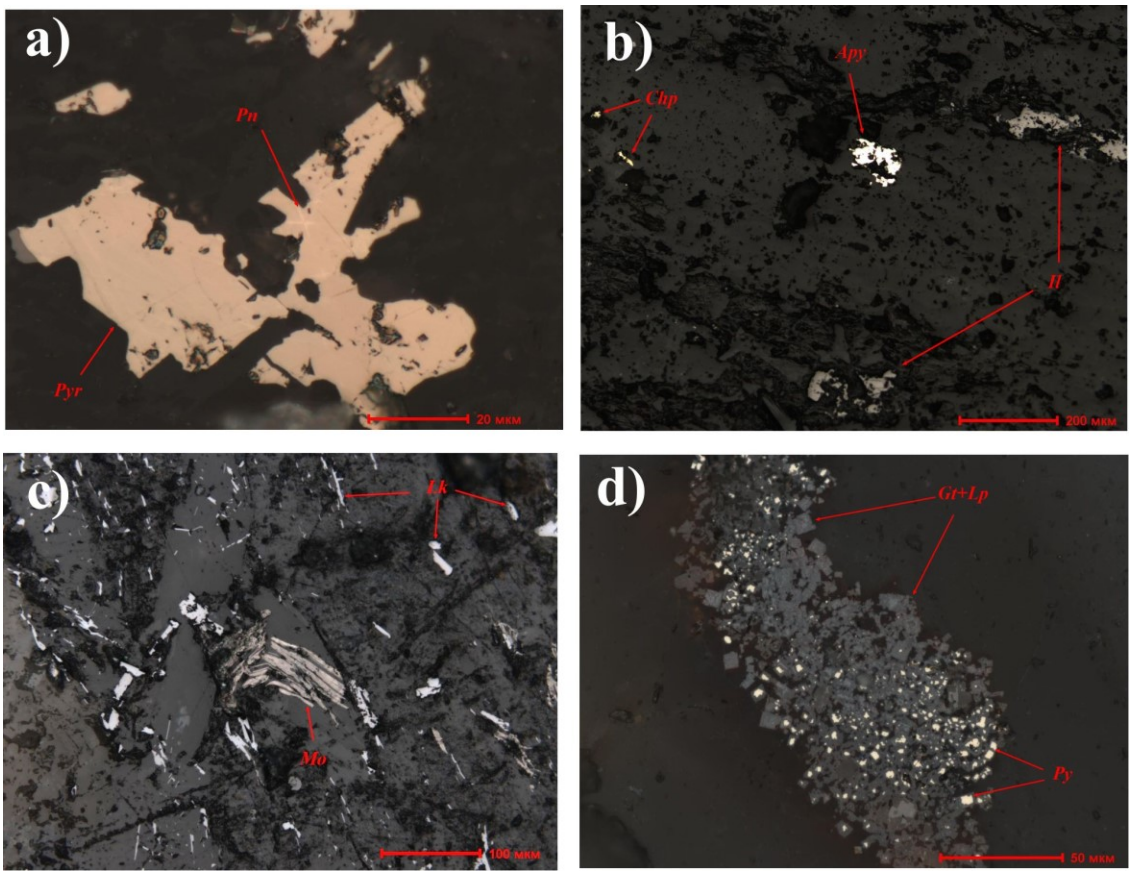


Fig. 2. Microinclusions of minerals in rocks of the Kara-Ayak ore occurences.

a - ксеноморфные зерна пирротина (Pyr) с игольчатыми, пламеневидными структурами распада, сложенными пентландитом (Pn); b - ксеноморфные зерна ильменита (Il). Единичные зерна халькопирита (Chp) и арсенопирита (Apy); c - скопления зерен лейкоксена (Lk) и чешуек молибденита (Mo) and d – извилистый прожилок, сложенный гидроокислами железа (Gt – гетит, Lp – лепидокрокит) с останцами пирита (Py)

/system translation: a - anhedral grains of pyrrhotite (Pyr) with acicular, flame-shaped structures of disintegration, composed of pentlandite (Pn); b - anhedral grains of ilmenite (Il). Single grains of chalcopyrite (Chp) and arsenopyrite (Apy); c - clusters of leucoxene (Lk) grains and molybdenite (Mo) flakes and d - a sinuous vein composed of iron hydroxides (Gt - goethite, Lp - lepidocrocite) with remnants of pyrite (Py)/

https://doi.org/10.5593/sgem2024/1.1/s01.10

The Kalba complex (P_1) is represented by medium-to-coarse-grained porphyritic biotite granites of first phase, medium-uniform grained biotite granites of second phase, fine-grained granites of an additional subphase and vein aplite granites, pegmatites, aplites and quartz veins. Structurally, the site is confined to the southwestern wing of the Mirolyubovskaya anticlinal fold of the second order, with a predominant dip of rocks to the southwest. Large northwestern faults control granodiorite porphyry dikes and linear contact of the granite massif; latitudinal and northeastern faults are also widely developed.

In a significant part of the study area, lithogeochemical routes were carried out, based on the results of which geochemical anomalies of the elements Li, Zr, Sr, Be were compiled, which are indicator elements of rare metal mineralization, including the supposed tungsten mineralization of the greisen-quartz vein type, characteristic of the study area. Single halos with contents of tungsten up to 0.6%, tin - 0.1%, beryllium - 0.03%, lithium - 0.008% have been established (Fig. 1). The areas are assessed as promising for tin, tungsten and possibly tantalum.

Minerals are represented by two types of ore formations: tin-tungsten mineralized zones (quartz veinlets in a granodiorite porphyry dike) and hydrothermal quartz-veined tin-tungsten zones (silicified and greisenized granodiorite porphyry, saturated with quartz veinlets with near-vein greisen).

DISCUSSION

The geological structure of the Kara-Ayak ore occurrence confirms the superimposed type of rare metal mineralization in association with dikes of the Kunush complex (favorable ore-bearing environment), and the source of rare metals is the rare metal-bearing granites of the Kalba complex. Analysis of large material from the Kalba-Narym zone shows that at a number of rare metal objects (Cherdoyak, Tochka, Medvedka, Novo-Saryozek, etc.), intrusions and dikes of the Kunush complex turned out to be a favorable physicochemical environment for the precipitation and concentration of rare elements under the influence of later rare metal-bearing granites of the Kalba complex [1, 7, 12-15]. From these positions, the Kara-Ayak ore occurrence is the most promising for further exploration. The reliability of the analytical data obtained in Soviet times is being questioned; it is possible that richer WO_3 contents may be discovered.

CONCLUSION

The Kara-Ayak site is located in Eastern Kalba in the exocontact zone of the Kashemin granite massif (Fig. 1). Refers to an unconventional type of rare metal mineralization (Sn, W, Ta, etc.), superimposed on more ancient tectonically prepared intrusions and dikes of the Kunush complex. At the ore occurrence under consideration, the host sedimentary rocks are represented by sandstone-siltstone deposits of the Takyr Formation (D3tk), subdivided into three members (lower, middle, upper members). The ore-bearing bodies are three dike-like bodies of medium-to-coarse-grained sharply porphyritic biotite granodiorite-porphyries of the Kunush complex, which lie in conformity with the structures of the host strata. Minerals are represented by two types of ore formations: tin-tungsten mineralized zones (quartz veinlets in a granodiorite porphyry dike) and hydrothermal quartz-veined tin-tungsten zones (silicified and greisenized granodiorite porphyry, saturated with quartz veinlets with near-vein

greisen). Due to the emerging need for rare metal raw materials, it is promising for further study and exploration.

ACKNOWLEDGEMENTS

This research has been funded by the Science Committee of the Ministry of Science and Higher Education of the Republic of Kazakhstan (Grant No. AP19676805).

Thanks are extended to Kuzmina O.N., Mizernaya M.A., Khromykh S.V., and Kotler P.D who contributed a lot to the joint geological research. Analysts from the VERITAS engineering laboratory and from the V.S. Sobolev Institute of Geology and Mineralogy (Novosibirsk) have performed good analytical work.

REFERENCES

[1] Dyachkov B.A. Genetic Types of Rare-Metal Deposits in the Kalba-Narym Belt. Ust`-Kamenogorsk, 2012, 129 p. (in Russian).

[2] Solodov N.A. On the assessment of rare-metal pegmatite manifestations of Kalba. Academy of Sciences of the USSR, Moscow, 1963, 17 p. (in Russian).

[3] Khromykh S. V., Vishnevskiy A. V., Kotler P.D., Antsiferova T. N., Semenova D., Kulikova A. V. The Kalba batholith dyke swarms (Eastern Kazakhstan): Mafic magmas effect on granite formation, Lithos, V. 426–427, 2022, 106801.

[4] Dyachkov B.A., Kazakevich I.V., Kisilev N. P., Kisilev L. V. Geological structure of sheet M-44-108-A (Report of the Mirolyubov geological survey party on the work of 1960. Funds MD "Vostkaznedra", pos. Irtyshsky, 1961, 280 p. (in Russian).

[5] Ermolin V.T., Ivanova K.N., Pushko E.P. et. al. Report on prospecting and revision-geochemical work of the Irtysh hydraulic fracturing site in 1966-67. EKSU funds, 1968, 260 p. (in Russian).

[6] Ponomareva, Y.V., Ponomareva, M.V., Sadchikov, A.V., Zhelayeva, N.V. A model of the tectonic development of Irtysh shar zone in terms of present day radioisotope data. Naukovyi Visnyk Natsionalnoho Hirnychoho Universytetu, 2021 (4), pp. 5–9.

[7] Kotler P., Khromykh S., Kruk N., Min Sun, Pengfei Li, Khubanov V., Semenova D., Vladimirov A. Granitoids of the Kalba batholith, Eastern Kazakhstan: U–Pb zircon age, petrogenesis and tectonic implications. Lithos, 2021, V. 388-389, 106056.

[8] Orazbekova G.B. Application of systems approach to prognostication of ore fields in local auriferous nidalstructures (On the example of vera-char-baladzhalnidal structure in west-kalbinsk gold-bearing area of East Kazakhstan). News of the National Academy of Sciences of the Republic of Kazakhstan, Series of Geology and Technical Sciences, 2018, 3 (429), pp. 208–217.

[9] Murzintsev N.G., Annikova I.Yu., Travin A.V., Vladimirov A.G., Dyachkov B.A., Maslov V.I., Oitseva T.A., Gavryushkina O.A. Thermochronology and mathematical modeling of the formation dynamics of rare-metal-granite deposits of the Altai collision system. Geodynamics & Tectonophysics, 2019, 60(2), pp. 375-404. (in Russian)

[10] Gavryushkina O.A., Sokolova E.N., Smirnov S.Z., Kruk N. N., Ponomarchuk A. V., Tomas V. G. Evolution of Rare-Metal Li–F Granite Melts in Sources of Ore-

https://doi.org/10.5593/sgem2024/1.1/s01.10

Magmatic Systems of Tigrinoe and Zabytoe Sn–W deposits (Central Sikhote-Alin, Primorye). Geol. Ore Deposits, 2023, 65, pp. 525–543.

[11] Levashova E. V., Skublov S. G., Oitseva T. A., Dyachkov B. A., Li X.-H., Li Q.-L., Shatova N. V., Shatov V. V. First Age and Geochemical Data on Zircon from Riebeckite Granites of the Verkhnee Espe Rare Earth–Rare Metal Deposit, East Kazakhstan. Geochemistry International, 2022, Vol. 60, No. 1, pp. 1–15.

[12] Fanka Alongkot, Tadthai Jaruphichaya. Petrology and geochemistry of Li-bearing pegmatites and related granitic rocks in southern Thailand: implications for petrogenesis and lithium potential in Thailand. Frontiers in Earth Science, 2023, V.11.

[13] Lopez-Moro F.J., Diez-Montes A., Timon Sanchez S.M., Llorens Gonzalez T., Sanchez Garcia T. Peraluminous Rare Metal Granites in Iberia: Geochemical, Mineralogical, Geothermobarometric and Petrogenetic Constraints. Preprints 2024, 2024010163.

[14] Yong T., Hong W., Hui Zh., Lv Z.-H. K-feldspar composition as an exploration tool for pegmatite-type rare metal deposits in Altay, NW China. Journal of Geochemical Exploration, 2018, 185, pp. 130–138.

[15] Wang H., Gao H., Zhang X.-Y., Yan Q., Xu Yi., Zhou K., Dong R., Li, P. Geology and geochronology of the super-large Bailongshan Li–Rb–(Be) rare-metal pegmatite deposit, West Kunlun orogenic belt, NW China. Lithos, 2020, 360-361, 105449.

GEOSTATISTICAL DISTRIBUTION OF LEAD AND ZINC METALS IN ARTANA 1 LANDFILL: MINERALOGICAL CHARACTERIZATION OF THE LANDFILL OBTAINED FROM RESIDUES FROM THE LEAD-ZINC FLOTATION PROCESS

MSc. Berat Sinani, Phd. Cand[1], MSc. Fisnk Frangu[2]
MSc. Ramiz Krasniqi[4], MSc. Besnik Shala[2]
MSc. Bahri Sinani, Phd. Cand[1], MSc. Vehbi Berisha[6]
Prof. Dr. Ivan Boev[3]
Prof. Dr. Arianit A. Reka[5]
Prof. Dr. Blazo Boev[3]
[1] Faculty of Geo-Science, University "Isa Boletini", Mitrovicë, **Republic of Kosova**
[2] Shoqëria Aksionare "Trepça" Sh.A. **Republic of Kosova**
[3] Faculty of Natural and Technical Sciences, University "Goce Delcev", Stip, **North Macedonia**
[4] Independent Commission for Mines and Minerals, **Republic of Kosova**
[5] Department of Chemistry, Faculty of Natural Sciences and Mathematics, University of Tetovo, **North Macedonia**
[6] Horn & Co. Analytics, **Republic of Kosova**

ABSTRACT

The surface area of the studied area in the Artana 1 landfill is about 24,000 m2. Presented here are samples taken from 11 boreholes with survey designations S-6, S-8, S-9, S-11, S-12, S-16, S-19, S-20, S-24, B /Y-2 (S-Y-2), Y-5 (S-Y-5). Drilling was carried out using the spiral survey method up to the base level of the soil. The works were carried out by the Trepça-Karova institutions within the project of recycling waste from the ore flotation of the Artana-Kishnica mines. Samples were taken at each meter, the survey number separately and by meter were counted and bagged and prepared for separation and reduction of samples by survey. The depth of soundings taken was as follows for sounding S-6 (10.5m); S-8 (10m); S-9 (9m); S-11 (12.5m); S-12 (9.6m); S-16 (15.5m); S-19 (13.5m); S-20 (10m); S-24 (9m); B/Y-2 (S-Y-2) (18m); Y-5 (S-Y-5) (12m).

The average value of lead, zinc based on the metric volume (titrimetric) analysis in these samples resulted in 4,463.60mg/kg Pb (~0.45%); 9,900.00mg/kg Zn (~0.99%); 1,263.64mg/kg PbO (~0.13%) and 1,600.00mg/kg ZnO (~0.16%), while based on X-ray diffraction (XRD) results, from the 11 samples analyzed so far (samples taken at Artana landfill 1), the analyzed samples contain the mineral Pyrite FeS2; Quartz mineral SiO2; the mineral Hydronijumjaros H7.95 Fe3 K0.35 O14.65 S2 as well as the gypsum mineral CaSO4x2H2O. Analyzing the sample with SEM-EDS on the surface, identifies the chemical elements O, Mg, Al, Si, S, K, Ca, Mn, Fe, Zn, As, while the analysis of the chemical composition at the point of a mineral also reveals the presence of the metal Pb.

The instruments used (besides the volumetric analysis for the quantitative determination of Pb, Zn and their oxides) for mineralogical and geochemical analysis, X-ray diffraction (XRD), as well as scanning electron microscopy (SEM-EDS).

Keywords: distribution, heavy metals, geostatistics, mineral, waste, landfill.

https://doi.org/10.5593/sgem2024/1.1/s01.11

INTRODUCTION

Along the Marec river, the flotation plant has been operating, which with its work has created landfills for waste from the flotation process. The old flotation is characterized by two landfills created from lead-zinc waste, which today are seen as an opportunity to enrich and extract chemical elements at a low but interesting concentration level [2].

These landfills, even after rehabilitation, are exposed to continuous erosion, thus causing significant regional pollution. Since so far some research and studies have been carried out about the chemical and mineralogical composition of these landfills, we as a working group have taken 11 samples from the laboratory of the Department of Flotation Mining in Kishnica and Artana, (duplicate samples, from the drilling carried out by the company Karmine Kardeniz Madencilik Ve Dis Ticaret A.S. in 2010 in the framework of the realized project of recycling waste from the flotation of ore from the Artana-Kishnica mines carried out by the "Trepça-Karova" institutions)[1] and we have done a diffraction analysis of the same X-rays determining the presence of the minerals that contain them, also in the laboratory of the Department of Flotation Mining Kishnica and Artana with the metric volume (titrimetric) analysis, a quantitative chemical analysis was done only for two chemical elements, lead, zinc and their oxides PbO and ZnO, determining the presence of these elements and their oxides in this landfill [2].

MATERIAL AND METHODS

The surface area of Artana 1 landfill is approximately 24,000.00m2, where the disposals described in this paper.

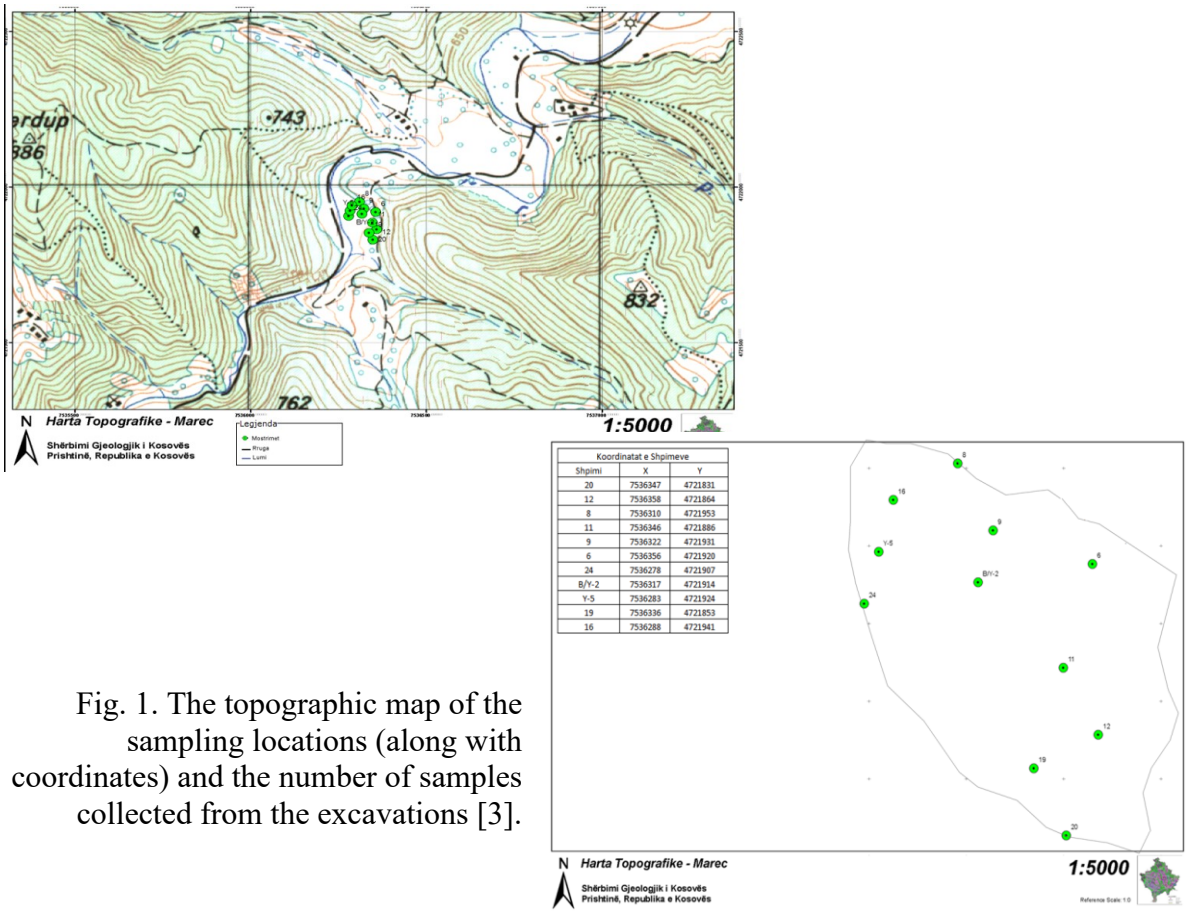


Fig. 1. The topographic map of the sampling locations (along with coordinates) and the number of samples collected from the excavations [3].

Referring to the study realized between Trepça and Karova [1] the total amount of waste in this landfill is estimated to be 233,000.00 m^3, based on the density of wet waste which has turned out to be 2.56 tons/m^3 and the amount of total waste is estimated to be around 600,000.00 tons. The analysis of the density of dry waste is estimated at 1.90 tons/m^3 and according to this the total amount of waste is estimated to be 443,000.00 tons.

According to the analyzes carried out with lithological surveys, it has been determined that there is an oxide zone in the area. The average thickness of the oxide layer was determined to be 1 m and the volume of the oxide area was calculated accordingly. In conclusion, the total volume of the oxide layer that exists in area is 11,500.00 m^3. The total amount of average oxide thickness in the model defined at 1m is estimated to be 11,500.00 m^3 [1]. From the horizontal cuttings of the survey in the studied area, the drilling of the surveys was introduced.

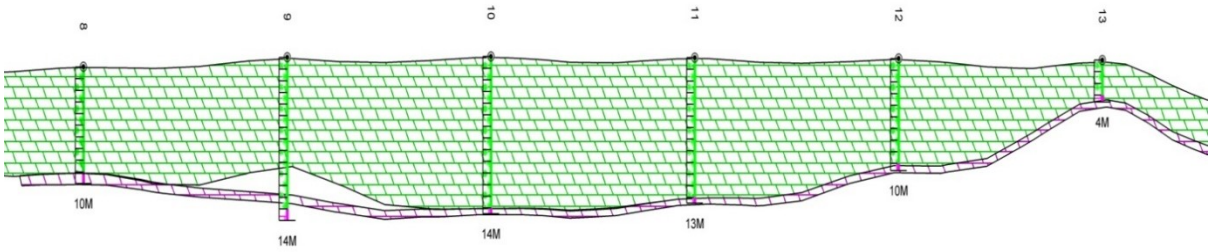


Fig. 2. One of the several horizontal cuts of the boreholes during the extraction of the surveys in the report carried out by Trepça-Karova[1].

The area of Artana includes the part of the territory of the Republic of Kosovo, between the coordinates 4716114, 4725406 of the northern latitude and 7530293, 7540539 of the eastern longitude. This part is mainly a mountainous area, with the mountains of Gollaku in the north and the mountains of Strazha and Zhegoc in the south [4].

The world-famous mine Trepca (also known as the Trepca Stari Trg or Stan Terg mine) has produced 2 Mt of lead and 1.5 Mt of zinc, 2,500.00 t of silver, 4,000.00 t of bismuth and 9.00 t of gold[4].

The ore deposit of Novobërda (Artana) has highlighted in particular the (relative) abundance of indium in this deposit (200 g/t In within the zinc concentrate). Furthermore, the high grade in the old Artana/Novobërda wastes, especially of gold, already identified by Trepca geologists (possibly up to 2.5 g/t Au) is confirmed. They represent a potential target whose order of magnitude could reach 21 Mt of ore containing hypothetically about 30 t Au and 300 t Ag[4].

From a metallogenic point of view, according to the definition of Neubauer (2002), Heinrich and Neubauer (2002) and Neubauer et al. (2005), Trepça is located, within the Alpine-Balkan-Carpathian-Dinarid belt (ABCD belt), in the Oligocene-Miocene belt, being told by these authors that this belt includes two very different branches: one (to the east) that cuts Cu-Au-Mo porphyry and epithermal Au mineralization (Rhodope belt) and the second (in the West) hosting epi-to mesothermal deposits of Pb-Zn veins (Ag-Au) and replacing carbonates such as Trepça. It stretches from Bosnia, through Serbia and North Macedonia, to Greece and southern Bulgaria. From the geotectonic point of view, Trepça is located within the "Vardar Area"[4].

https://doi.org/10.5593/sgem2024/1.1/s01.11

SOIL SAMPLING AND PREPARATION - INSTRUMENTATION

Since the collected samples contained a large amount of moisture, each survey sample was dried at a temperature of 60°C in a drying oven. Based on discussions with the Company official, the samples are pooled according to the survey lengths. After mixing to a certain extent the crushed and dispersed samples of the survey, they have been transformed into a homogeneous state. After macroscopic analysis, large and small pebbles were observed inside the samples. In order to distribute the sample and clay slurries, after mixing for one hour at a high speed in the mechanical mixing machine, the whole material was put into sieves with holes of -0.5 mm where the pebbles on this format were cleaned. The material in the size of -0.5 mm was brought to a homogeneous state after drying and after passing through the automatic sample separator representative samples were obtained for the previously defined objectives [6].

RESULTS AND THEIR DISCUSSION

During the X-ray analysis of these samples, a total of 7 different minerals were identified, highlighting here the 4 main minerals that make up this landfill with a participation of about 93%.

Based on the XRD analysis, performed on these 11 samples, it results that these samples contain the minerals quartz, pyrite, hydroniumjaros and gypsum mineral. Below in figure 3 is shown the XRPD spectrum of sample S-24.

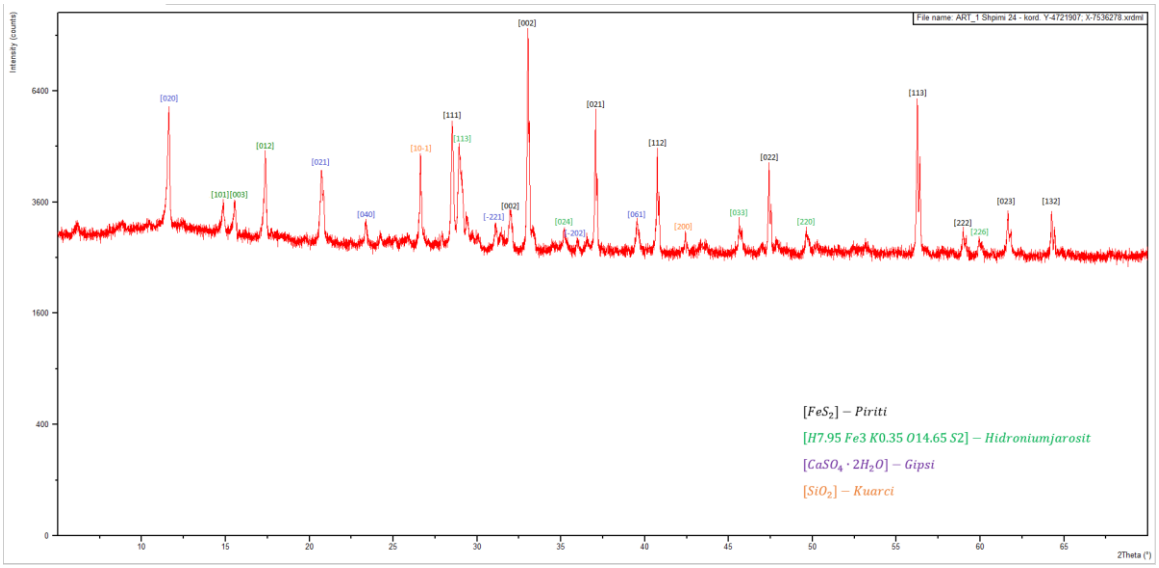


Fig. 3. Diffraction spectrum for sample S-24 (description of minerals identified based on peaks identified with Miller indices)

The identified minerals contain these crystallographic parameters:

a. Quartz as one of the most widespread minerals that form the rocks of the Earth's crust and one of the main minerals of most igneous rocks has been identified with a hexagonal crystal system with a calculated density of 2.65g/cm3 and a unit cell volume of 113.05x106 pm3 [7].

b. Pyrite as a fairly widespread mineral with a cubic crystal system with a calculated density of 5.01g/cm3 and a unit cell volume of 159.13x106 pm3 [8].

c. Hydroniumjaros mineral with hexagonal crystal system with calculated density of 3.05g/cm3 and unit cell volume of 797.33x106 pm3 [9].

d. Gypsum mineral with a monoclinic crystal system with a calculated density of 2.31g/cm3 and a unit cell volume of 495.15x106 pm3 [10].

During the analysis by X-ray diffraction, of the 11 samples, the mineral pyrite as a sulphide mineral results with a mass participation of 36.41%. If we refer to an earlier study about this landfill, Mineralogical and Geochemical Characterization of Mine in the Landfill of Artana, Kosovo, the authors, referring to the semiquantitative analysis with XRD, extract the pyrite mineral with a mass participation of 37.38% and the quartz mineral with 16.93%, similar to the data presented in the table from the results obtained by X-ray diffraction, in this paper.

Table 1. Minerals identified by x-ray diffraction, expressed as a percentage

	Samples / %											
Minerals	S-6	S-8	S-9	S-11	S-12	S-16	S-19	S-20	S-24	S-Y-2	S-Y-5	Average
SiO_2	50.1	11	18.4	51.3	10.5	12.1	10.2	14.8	11.2	10.3	13.6	9.41
FeS_2	12.7	29.7	81.6	14.8	30.8	39.8	33.8	35.7	41.2	38.5	41.9	36.41
$H_{7.95}\ Fe_3\ K_{0.35}\ O_{14.65}\ S_2$ *Hydronijumjarosit*	0.0	27.4	0.0	31.5	18.7	28.5	25.6	34.0	37.6	30.1	21.22	21.22
$H_4\ Ca_1\ O_6\ S_1$ *- Gips*	0.0	31.9	0.0	0.0	27.2	29.4	27.5	23.9	13.6	13.6	14.4	16.5
$N_{6.02}\ H_{22.4}\ C_{12}\ O_6$	24.8	0.0	0.0	25.8	0.0	0.0	0.0	0.0	0.0	0.0	0.0	4.6
$Fe_{16}\ C_{192}\ H_{112}\ N_{192}$	8.0	0.0	0.0	8.1	0.0	0.0	0.0	0.0	0.0	0.0	0.0	1.46
Ge4 In6 Y11 – Yttrium Germanium Indium	4.4	0.0	0.0	0.0	0.0	0.0	0.0	0.0	0.0	0.0	0.0	0.4

When analyzing the samples with SEM-EDS, through the detector used to measure the energy of the emitted photons in the X-ray electromagnetic spectrum, the main type of signals that are detected are back (back) electrons (BSE) and secondary electrons (SE), which generate a grayscale image of the sample at very high magnifications. The observation of the S-16 sample, with the SEM-EDS electron microscope, while analyzing the sample on its surface, extracted Fe metal with a mass participation of 16.69%, while zinc with 1.13% and calcium with 4.63%, as part of group of sulphide minerals, pyrite, galena and gypsum mineral in this case.

https://doi.org/10.5593/sgem2024/1.1/s01.11

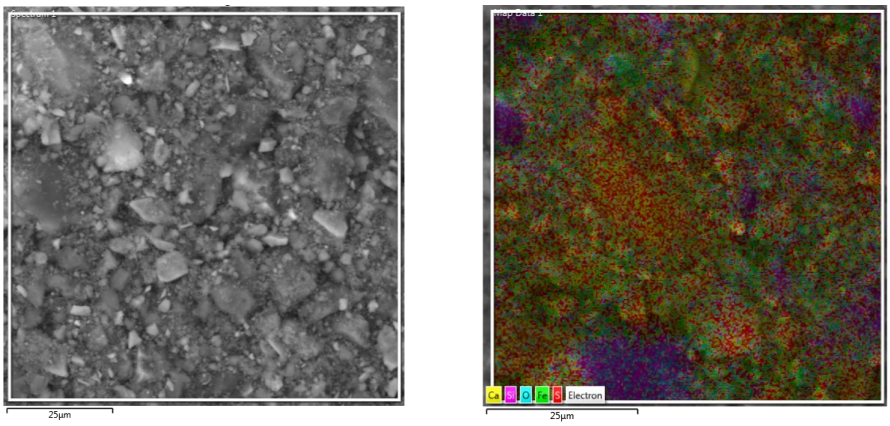


Fig. 4. Image taken with the BSE detector for sample S-16 as well as the map of the extent (distribution) of chemical elements on the surface of this sample.

Table 2. Quantitative chemical composition expressed in mass participation for the S-16 sample on its surface with the EDS detector.

Statistics/%	O	Mg	Al	Si	S	K	Ca	Mn	Fe	Zn	As
Max	50.45	0.35	2.39	5.17	17.03	0.71	4.63	0.87	16.69	1.13	0.57
Min	50.45	0.35	2.39	5.17	17.03	0.71	4.63	0.87	16.69	1.13	0.57
Average	50.45	0.35	2.39	5.17	17.03	0.71	4.63	0.87	16.69	1.13	0.57
St. Deviation	0.00	0.00	0.00	0.00	0.00	0.00	0.00	0.00	0.00	0.00	0.00

The EDX analysis identifies the presence of galena mineral as another mineral of the sulphide group, from the point of view of qualitative analysis. While the quantitative analysis of this mineral present in the sample (and that the presence of Pb in this deposit from the volumetric analysis results in a mass participation of about 0.45%) results in a mass participation of 19.91%.

Table 3. Quantitative chemical composition expressed in mass participation for sample S-16 in galena mineral, spot analysis with EDS detector.

Statistics/%	O	Al	Si	S	K	Ca	Mn	Fe	Zn	As	Pb
Max	41.52	1.76	3.18	13.37	0.42	2.64	0.53	15.58	0.56	0.54	19.91
Min	41.52	1.76	3.18	13.37	0.42	2.64	0.53	15.58	0.56	0.54	19.91
Average	41.52	1.76	3.18	13.37	0.42	2.64	0.53	15.58	0.56	0.54	19.91
Standard Deviation	0.00	0.00	0.00	0.00	0.00	0.00	0.00	0.00	0.00	0.00	0.00

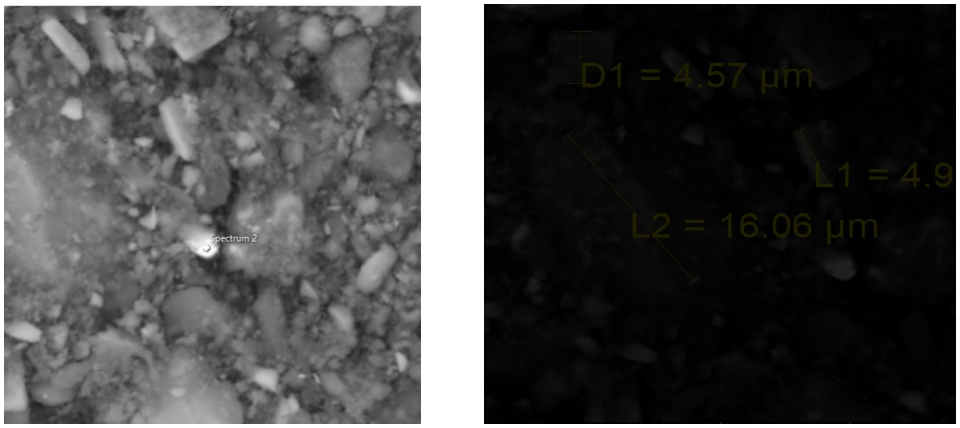


Fig. 5. Image taken with the BSE detector for sample S-16, spot analysis (spectrum 2), identification of the mineral galena.

There are a lot of number of statistical and geostatistical methods for their analysis[5]. Further, the statistical and geostatistical analysis for the elements Pb and Zn also for their oxides are shown in the table below.

Table 4. Statistical descriptive for Pb, Zn and PbO in ppm and %

	Pb [%]	*Pb [ppm]*	*PbO [%]*	*PbO [ppm]*	*% Zn*	*Zn [ppm]*	*ZnO [%]*	*ZnO [ppm]*
Mean	0.45	4463.64	0.13	1263.64	0.99	9900.00	0.16	1600.00
Median	0.39	3900.00	0.12	1200.00	0.92	9200.00	0.18	1800.00
Mode	0.39	3900.00	0.12	1200.00	0.86	8600.00	0.18	1800.00
Standard Deviation	0.31	3061.13	0.06	550.04	0.23	2313.01	0.07	744.31
Sample Variance	0.09	9370545.45	0.00	302545.45	0.05	5350000.00	0.01	554000.00
Skewness	1.41	1.41	0.80	0.80	0.63	0.63	-0.04	-0.04
Range	0.95	9500.00	0.19	1900.00	0.77	7700.00	0.23	2300.00
Minimum	0.14	1400.00	0.05	500.00	0.66	6600.00	0.05	500.00
Maximum	1.09	10900.00	0.24	2400.00	1.43	14300.00	0.28	2800.00
Sum	4.91	49100.00	1.39	13900.00	10.89	108900.00	1.76	17600.00
Count	11	11	11	11	11	11	11	11

In the table presented above, we have seen the general statistics for all the parameters taken into consideration, from the total of 11 analyzed samples, we have presented the parameters of the minimum, maximum, average value, sum, standard deviation as well as many parameters through which we see distribution of general data. But, to talk more about the relationship between these parameters, we will also present the correlation analysis or the correlation between these parameters.

https://doi.org/10.5593/sgem2024/1.1/s01.11

While in the following we will present each parameter in histograms as follows:

Range	*Frequency*
2000	1
4000	6
6000	2
8000	0
10000	1
More	1

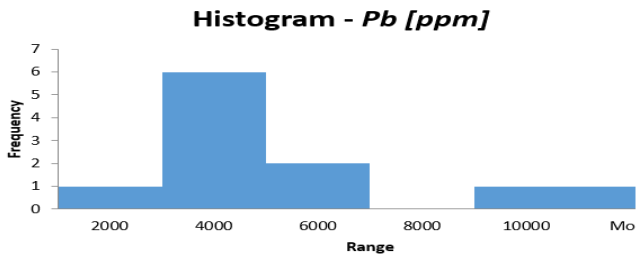


Fig. 6. Histogram of distribution of Pb [ppm]

From the histogram presented above we see the distribution of Pb for the 11 samples taken in the study, from this we see that the concentration of Pb to the greatest extent is at the values of 4000ppm, here we have the largest distribution of 6 samples.

Range	*Frequency*
500	1
1000	3
1500	4
2000	2
2500	1
More	0

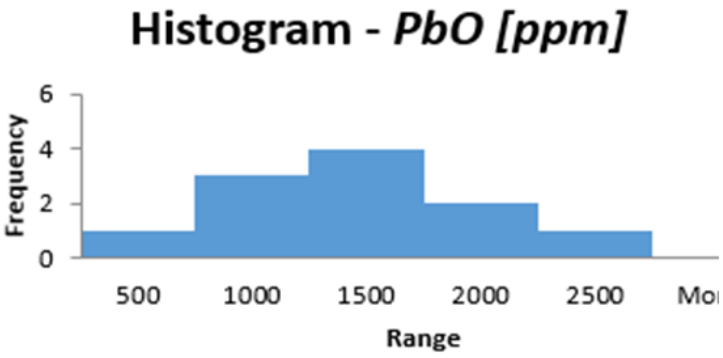


Fig. 7. Histogram of distribution of PbO [ppm]

From the histogram presented above we see the distribution of PbO for the 11 samples taken in the study, from this we see that the concentration of PbO to the greatest extent is at the values of 1500ppm, here we have the largest distribution of 4 samples and 1000 where we have the distribution of three samples.

Range	*Frequency*
6000	0
8000	2
10000	4
12000	2
14000	2
More	1

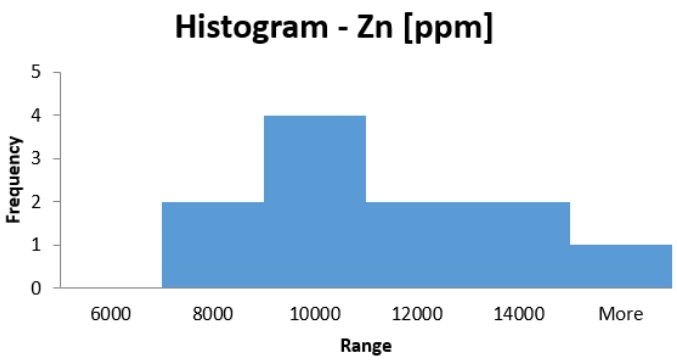


Fig. 8. Histogram of distribution of Zn [ppm]

From the histogram presented above we see the distribution of Zn for the 11 samples taken in the study, from this we see that the concentration of Zn to the greatest extent is at the values of 8000 to 1400ppm, here we have the largest distribution of the 10 samples.

Range	*Frequency*
500	1
1000	2
1500	2
2000	3
2500	2
More	1

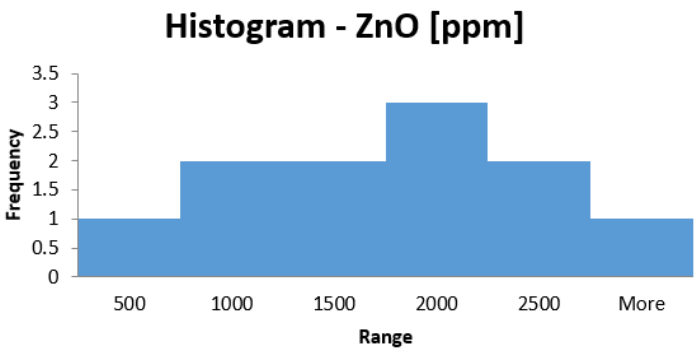


Fig. 9. Histogram of distribution of ZnO [ppm]

From the histogram presented above we see the distribution of Zn for the 11 samples taken in the study, from this we see that the concentration of Zn to the greatest extent is at the values of 2000 to 2500ppm, here we have the largest distribution of the 3 samples, while the distribution the most frequent is that of 1000 to 2000 and 2500, where we have 6 samples distributed in these values.

In the following we will present the geo-spatial distribution of Pb, PbO, Zn and ZnO.

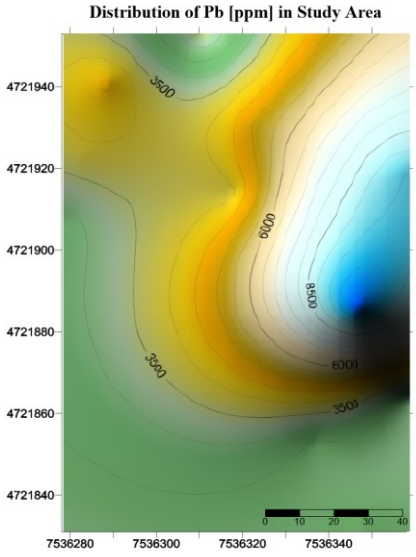


Fig. 10a. Distribution of Pb[ppm]

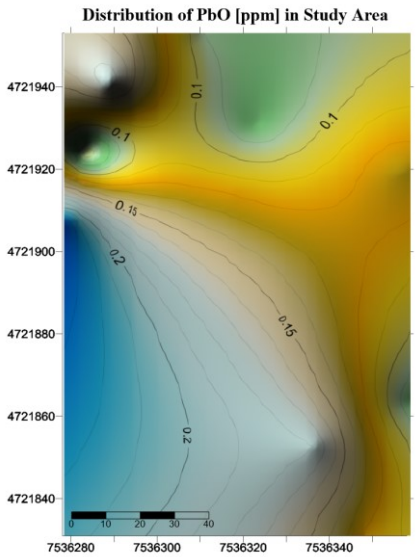


Fig. 10b. Distribution of PbO [ppm]

From the figure presented above, we have the spatial distribution of Pb. Fig. 10a, we see that the greatest distribution or concentration of Pb is in the east part of the landfill, but we have an even higher representation in the South-Eastern part, while the western part is poorer with the presence of Pb, while PbO is more distributed in the North-Western part, while the South-Western part is seen with a smaller concentration.

https://doi.org/10.5593/sgem2024/1.1/s01.11

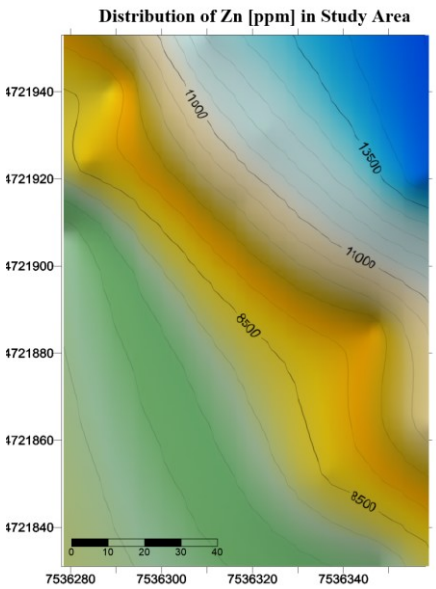


Fig. 11a. Distribution of Zn [ppm]

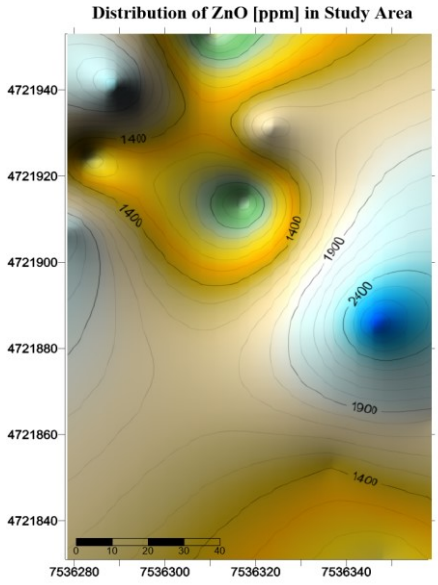


Fig. 11b. Distribution of ZnO [ppm]

From the figure presented above we can see that we have an almost symmetrical distribution of Zn throughout the landfill, but the most prominent part is the NW-SE, where we have a distribution from the beginning to the end of the landfill, while the distribution of ZnO is characterized by distribution in the North-West part and in the central part towards the East.

CONCLUSION

Based on the data estimated that this landfill contains about 443,000.00 tons of mineral waste (after Pb and Zn flotation process), dry amount after moisture removal, and with a density value of 1.9 g/cm^3 (kg/ton).

Referring to the Lead data presented in this paper from volumetric analysis where the concentration of pure Pb metal turns out to be 4,463.60mg/kg (4.463kg/ton ~0.45%), the amount of pure lead in this landfill is 1976 tons Pb, while referring to the amount of zinc from the metric volume analysis with a concentration of 9,900.00 mg/kg Zn (9.9kg/ton ~0.99%), the amount of pure zinc in this landfill is approximately 4,382.73 tons of Zn.

If we refer to sample S-16 in the diffraction analysis, we see that the quartz mineral in this sample is only 12.1%. Referring to the same sample that was analyzed quantitatively with SEM-EDS, the mass participation of Si is 5.17%, and based on stoichiometric calculations, in sample S-16, with 12.1% participation of quartz, it results that the participation of silicon is 5.65% and oxygen is 6.44%.

REFERENCES

[1] Trepça-Karova, Raporti Final i Riciklimit te mbetjeve nga flotimi i xehes se minierave Artane-Kishnice ne flotacionin e Kishnices. (2010): 1-86.

[2] Berat Sinani, Blazo Boev, Arianit Reka, Ivan Boev, Musaj Paçarizi, Epir Qeriqi. (2023). Geo-Statistical analysis of distribution of As, Fe, Mn, Cu and Zn in Artana mine tailing from flotating proces. www.sgem.org, section of geoinformaitcs: 171-178.

[3] Sinani, B., Qeriqi, E., Sahiti, F., Shala, I., Musa, I., Geological sampling wiht GSKSOFT 1.0, International Multidisciplinary Scientific GeoConference Surveying Geology and Mining Ecology Management, SGEM 2018, 18(2.2), pp. 203–210

[4] French scientific cooperation 2007-2008 on the Trepča lead-zinc-silver mine and the gold potential of Novo Brdo/Artana tailings (Kosovo) Final Report BRGM/RP-57204-FR October. (2009): 1-102.

[5] Sinani, B., Peci, N., Elezaj, Z., Sinani, B., Statistical analysis of distribution of Ag, Au, Pb and ZN in Trepca mine, International Multidisciplinary Scientific GeoConference Surveying Geology and Mining Ecology Management, SGEM, 2018, 18(1.1), pp. 497–503

[6] Karmine Kardeniz Madencilik Ve Dis Ticaret A.S. lidhur me përdorueshmërinë e mbetjeve të Pb-Zn nga impianti. (2010): 1-20.

[7] Hazen, R.M., Finger, L.W., Hemley, R.J., Mao, H.K., Solid State Communications, 72. (1989): 507-511.

[8] Elliott, N., Journal of Chemical Physics, 33. (1960): 903-905.

[9] Peterson, R.C; Basciano, L.C., American Mineralogist, 92. (2007): 1464-1473.

[10] Semmingsen, D.; D.; Pedersen, B.F., Acta Crystallographica B (24, 1968 – 38,1982), 38, 1074-1077, (1982)

https://doi.org/10.5593/sgem2024/1.1/s01.11

HOLOCENE LACUSTRINE SEDIMENTATION PATTERNS ON LORI PLATEAU (SOUTH CAUCASUS)

Assoc. Prof. Dr. Grigory Fedorov[1]

Dr. Dmitry Sadokov[2]

Vsevolod Rudakov[1]

Assoc. Prof. Dr. Irina Fedorova[1]

Larisa Ghazaryan[1]

[1] A. Takhtajan Institute of Botany, National Academy of Sciences of the Republic of Armenia, **Armenia**
[2] Shenzhen MSU-BIT University, **China**

ABSTRACT

This study provides a characterization of the Holocene sedimentary processes in Lake Urasar (Lori plateau, Armenia). Lake Urasar is less than 0.1 sq. km with 8.5 m max. depth. 2 m -long sediment core was retrieved by using peat corer in the deepest part of the lake during summer 2023. Obtained core was a subject for detailed lithological description and XRF-scanning. Three lithological units are identified in the sediment sequence reflecting different sedimentation patterns. Unit I (200 – 164 cm) characterized by frequent changes in the chemical elements concentrations and reflects sensitivity to the regional climate changes, which had been expressed as shifts in the eolian input rate, and surface soil fixation. Decrease of Fe and Ti values with less pronounced regular oscillations can be seen upcore in the Unit II (163 – 62 cm), which might be a clue for a decreased mineragenic input (for example, in the course of forest expansion and / or montane-steppe soil formation). Geochemical characteristics of the muddy uppermost deposits of Unit III reflect repeated disturbance and mixing.

Keywords: lacustrine sedimentation, Holocene, Lori Plateau, South Caucasus, Lake Urasar

INTRODUCTION

Alpine lakes are known to respond rapidly on anthropogenic and environmental forcing and, thus, allow to trace both local and global changes [1 and references therein]. It is known that in recent decades, mountain lacustrine ecosystems have undergone rapid, negative and, probably, irreversible changes [1 and references therein].

Past climatic and environmental changes, especially warmings may serve as an analogue to better evaluate the ecosystem response on short-term climate fluctuations and temperature rises of up to several degrees within a few decades. Lake sediments are known as very informative archive of paleoclimate and paleoenvironmental information.

Recently, significant progress has been made in the study of the Holocene vegetation and climate history using paleobotanical data from small lakes in the Armenian Highlands and peat bogs near Lake Sevan [2, 3]. Likewise, in the recent years new data

https://doi.org/10.5593/sgem2024/1.1/s01.13

on several high-mountain lakes (i.e. lakes Akna, Umroi and Kari) morphometry, hydrochemistry and sedimentation history has been obtained [4].

A comprehensive palaeolandscape study by [5] performed on a fen belonging to the lake Arpi watershed brings up an insight into Holocene climatic oscillations recorded even in a shallow peat. It gives evidence for the high significance of the lakes of western Armenia for the interregional palaeoclimatic reconstructions, due to their geographical positions as plateau sites.

However, collected data about recent environmental history up to now in Armenia and in South Caucasus in general by far not enough to understand past and current ecosystem responses on climate forcings.

We present some of the very first results obtained within the framework of a project aimed at researching lakes in Armenia. The first results of a study of sediment core from Lake Urasar, located on the Lori Plateau (fig. 1), are presented. Lake Urasar is one of the typical Lori lake with less than 0.1 sq. km area and with 8.5 m max. depth. The Lake elevation above sea level is 1561 m.

The Lori lakes were listed in the State Program on Conservation and Management of the Protected Areas of Armenia (2014-2020) as requiring special status of protection [6], though the Strategy have not been updated after the expiration date. The lakes are included into the Emerald Network List in frames of the Bern Convention, as an Area of Specific Conservation Interest (ASCI). Moreover, the Lori plateau is designated as one of 14 Freshwater Key Biodiversity Areas (FKBAs) of Armenia [7] and as an Important Bird Area (IBA) (No. AM007) [8].

MATERIALS AND METHODS

The lake sediment coring was performed during summer 2023 from the anchored inflatable raft, using the Russian peat corer (1 m in the sampling part length, 7 cm in diameter). One 2.7 m-long (according to field measurements) sediment core Urasar-1 with duplicate was retrieved from central part of Lake Urasar with water depth 7.4 m. Coring location is shown on Figure 1.
A lithological description was performed on site. Later core was a subject for XRF-scanning in the laboratory of the Institute of Geology and Mineralogy of the University of Cologne using an ITRAX core scanner (Cox Analytical Systems, Sweden) equipped with a Cr-tube and a Si-drift detector in combination with a multi-channel analyser.
Both core duplicates were scanned. Based on a detailed comparison of the duplicate scan results, a composite core was constructed. This made it possible to combine two duplicates into a single sequence and correct field core depths.

Elements Fe, Ti and indices Mn/Fe and Inc/Coh were employed to trace the palaeoenvironmental changes along the sediment sequence. Fe and Ti are widely used for unravelling the activity of physical weathering on the watershed, and for detecting periods of enhanced accumulation of mineragenic matter in lake [9]. Mn/Fe index responds to transitions in redox conditions [10], changes in bottom oxygenation regime [11] and in some cases to water level shifts [12]. Inc/Coh (stands for incoherent/coherent scattering ratio) is suggested for use as a qualitative measure of the organic content in wet sediments [13]. These proxies were chosen due to their direct

representation of the most significant driving forces responsible for the sedimentation, namely, allochtonous mineragenic input, redox conditions, organic matter content.

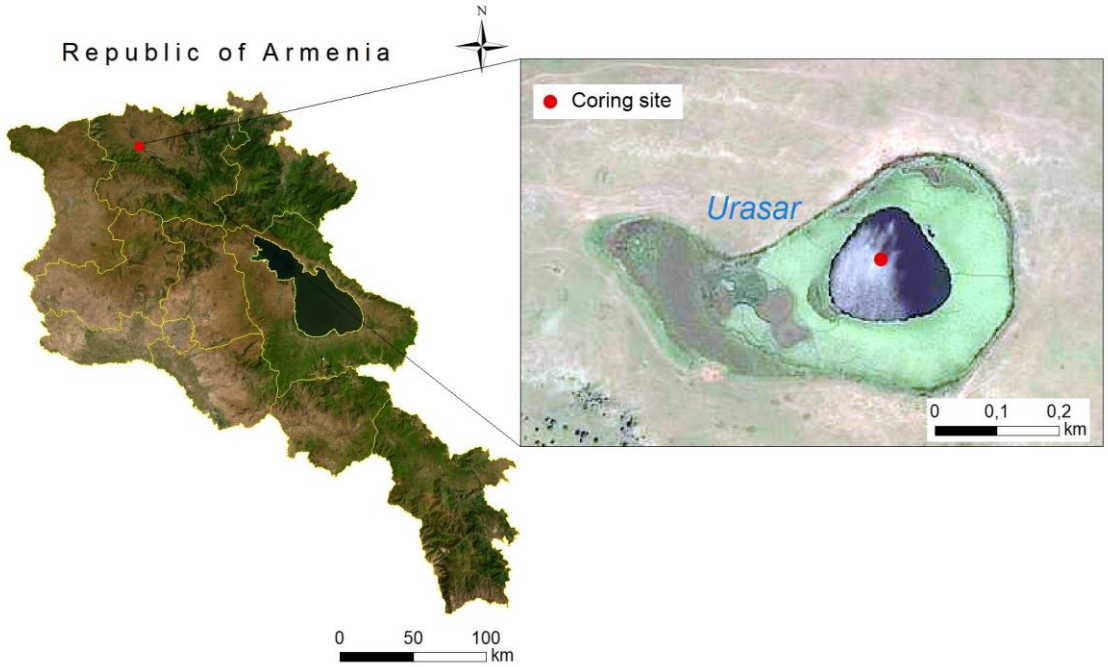


Figure 1. Location of Lake Urasar.

RESULTS

Sediment core Urasar-1 consist almost entirely homogeneous black organic gyttja but low most 10 cm represented by peat. Developed core composite ended up with total core length is only 200 cm (fig. 2). Significant deference with original field measurement likely due to cumulative error of every single coring run.

Three units with significant variations of geochemical patterns were outlined according to the XRF results (fig. 2).

Unit I (200 – 164 cm) was distinguished mainly due to the notable oscillations of Fe and Ti within a relatively short interval. The elements' abundance change synchronously, with the most explicit peaks at depths 198-192 cm, 178-173 cm, and a distinct fall at depth 172-169 cm.

Unit II (163 – 62 cm) is characterized by a very low-magnitude oscillations of Inc/Coh and Mn/Fe, and their overall unpronounced trend, with only slight graph bending of the former, at depth 160-142 cm.

Unit III (61 – 0 cm) is prominent for the notable rise in the Mn/Fe values.

https://doi.org/10.5593/sgem2024/1.1/s01.13

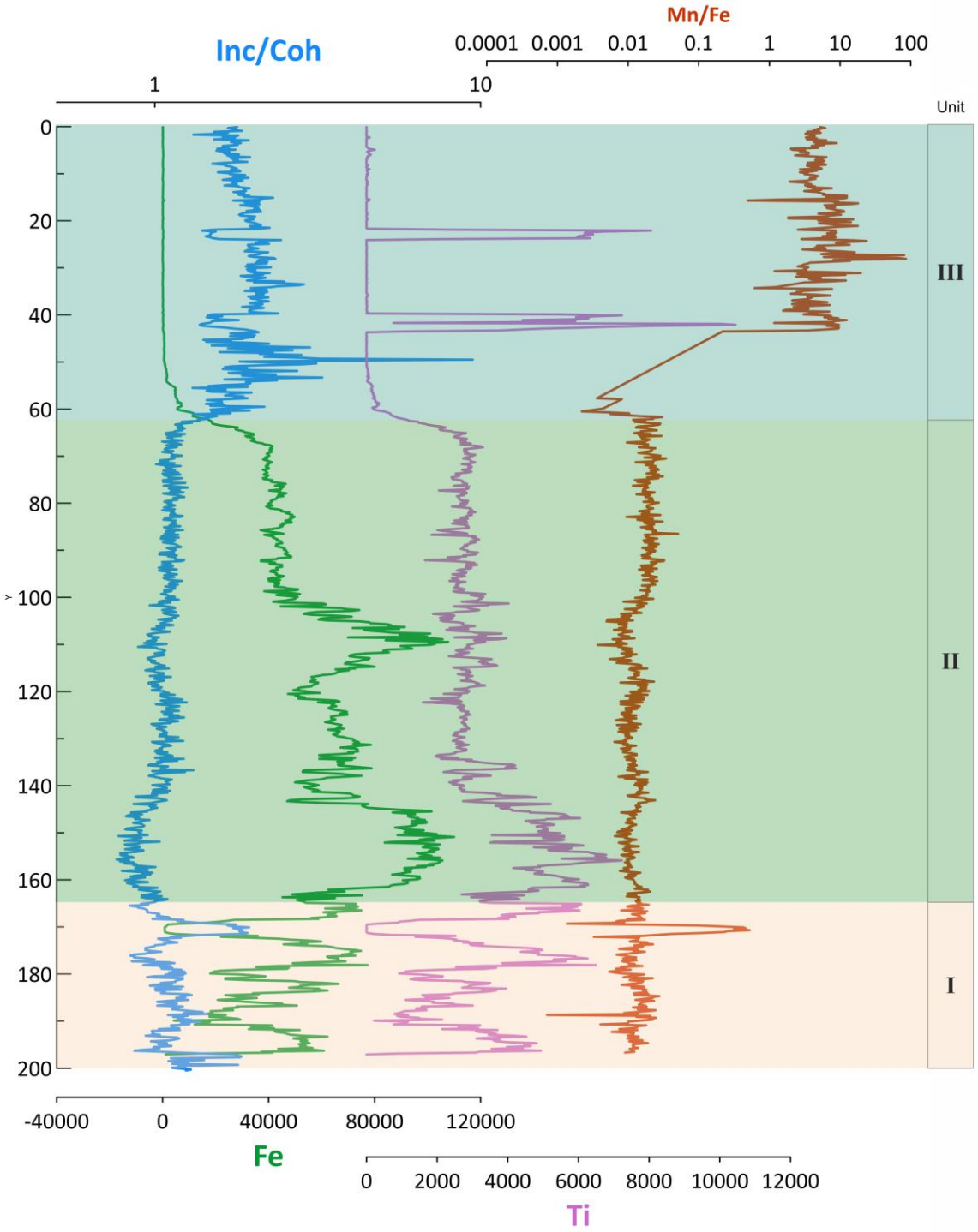


Figure 2. Core Urasar-1 XRF- scanning results.

DISCUSSION

Obtained results allow us to reconstruct environmental conditions during sedimentation of each detected sediment unit.

Unit I

Magnitude of the Fe and Ti oscillations reveals unstable conditions of surface flow that reached the lake. Since Fe largely follows the Ti upcore trend, Mn/Fe and Inc/Coh do not reflect any specific patterns, it can be concluded that no significant palaeohydrological changes occurred during the deposition of the unit I sediments. As Ti and Fe are integral elements of the eolian quartz and other well-weathered minerals, it can be assumed that unit I reflects sensitivity to the regional climate changes, which had been expressed as shifts in the eolian input rate, and surface soil fixation (by vegetation).

The only prominent event can be seen at depth 172-169 cm, which was presumably related to the palaeohydrological dynamics. Here, lake bottom oxygenation improved significantly (as derived from Mn/Fe increase), and organic sedimentation prevailed over the mineragenic input (see mutual proportion of Inc/Coh, Ti and Fe plots). It is suggested that the lake became shallow and overgrown at this interval.

Unit II

Fe and Ti content is distributed more evenly than in Unit I. For both of the elements' graphs, a rise is revealed at depth 160-142 cm, altogether with Inc/Coh representing a mineral sedimentation stage that occurred presumably under cool dry conditions. Steady decrease of Fe and Ti values with less pronounced regular oscillations can be seen upcore, which might be a clue for a decreased mineragenic input (for example, in the course of forest expansion and / or montane-steppe soil formation).

A distinguished peak of Fe at depth 116-103 cm most likely corresponds to enhanced input of specific Fe-rich matter (dust, minerals). As no other signs were noticed in the complementary XRF data, this Fe peak was assumed most likely to be evident of the local turbidity on the lake bottom that caused enhanced oxygenation (for example, due to the karst water movements).

Unit III

The significant rise in the Mn/Fe values most likely indicate a steady water level drop. We assume that a hiatus may exist on the border between units II and III, according to the straightforward trend of Mn/Fe values rise. Still, supplementary dating should be carried out to check this hypothesis.

Fe and Ti content reaches its lowermost level of the whole observed sequence. Simultaneously, Inc/Coh increase supports the evidence of the sedimentation regime switch to the typical organic accumulation.

Geochemical characteristics of the Unit III does not provide any certain clues for the palaeoenvironmental dynamics. It is supposed that the muddy uppermost deposits have undergone repeated disturbance before they had been uncovered by coring, since several elemental peaks can be noticed over the general calm trend of the plots.

CONCLUSION

The studies of sediment core collected from one lake located on Lori Plateau (South Caucasus, Armenia) provide the basis for reconstructions of the Holocene climate and environmental dynamics.

Three detected sediment units with different geochemical characteristics reveal the relevant stages in environmental history. At the initial stage of the lake's existence, very unstable climatic and paleohydrological conditions were observed. This most likely corresponds to the conditions of the early Holocene. Subsequently, in the middle Holocene, there was a significant increase in humidity, an increase in lake level and favorable conditions for the development of vegetation in the catchment area. The last stage, probably corresponding to the late Holocene, is characterized by significant drying of the climate and a drop in lake level.

The results obtained are still preliminary but are an extremely important basis for further more detailed reconstructions. In the near future, the results of radiocarbon dating will be obtained, as well as the results of a number of micropaleontological analyses. Moreover, ongoing work on other lakes of the Lori Plateau and other regions of Armenia will allow the regional overview.

ACKNOWLEDGEMENTS

The work is supported by the Ministry of Education, Science, Culture and Sports of Armenia, Higher Education and Science Committee in the frame of research project "Impact of past and current trenchant climatic and environmental changes on Armenian Highland Lake ecosystems – IMPACT" (23IRF-1E02). The authors are sincerely grateful to Prof. M. Melles, Prof. B. Wagner, N. Mantke and J. Feller from the Institute of Geology and Mineralogy of the University of Cologne for the opportunity to perform XRF - scanning of the core.

REFERENCES

[1] Szabó Z., Buczkó K., Haliuc A., Pál I., Korponai J. L., Begy R.-C., Veres D., Luoto T. P., Zsigmond A. R., Magyari E.K. Ecosystem shift of a mountain lake under climate and human pressure: A move out from the safe operating space, Science of the Total Environment, 743, 140584, 2020

[2] Leroyer C., Joannin S., Aoustin D., Ali A. A., Peyron O., Ollivier V., Tozalakyan P., Karakhanyan A., Fany J. Mid Holocene vegetation reconstruction from Vanevan peat (south eastern shore of Lake Sevan, Armenia), Quaternary International, 395, pp. 5-18, 2016 http://dx.doi.org/10.1016/j.quaint.2015.06.008

[3] Robles M., Peyron O., Brugiapaglia E., Ménot G., Dugerdil L., Ollivier V., Ansanay-Alex S., Develle A.-L., Tozalakyan P., Meliksetian K., Sahakyan K., Sahakyan L., Perello B., Badalyan R., Colombié C., Joannin S. Impact of climate changes on vegetation and human societies during the Holocene in the South Caucasus (Vanevan, Armenia): A multiproxy approach including pollen, NPPs and brGDGTs, Quaternary Science Reviews. Volume 277, 107297, 2022 https://doi.org/10.1016/j.quascirev.2021.107297.

[4] Sapelko T. V., Boynagryan V. R., Naumenko M. A., Sevastyanov D. V., Gabrielyan I. G., Piloyan A. S., Margaryan L. A., Aleksandrin M. Yu., Terekhov A. V. First Multy-Proxy Studies of High-Mountain Lakes in Armenia: Preliminary Results, Geography, Environment, Sustainability, Vol.12, No 4, pp. 272-284, 2019

[5] Joannin S., Ali A.A., Ollivier V., Roiron P., Peyron O., Chevaux S., Nahapetyan S., Tozalakyan P., Karakhanyan A., Chataigner C., Vegetation, fire and climate history of the Lesser Caucasus: a new Holocene record from Zarishat fen (Armenia), Journal of Quaternary Scicience, 29, pp. 70-82. 2014 https://doi.org/10.1002/jqs.2679

[6] Strategy of Specially Protected Areas of the Republic of Armenia, State Program for the Protection and Use of the Sphere (est. by RA Government decision N 1059-A, Sept. 25, 2014) (https://www.arlis.am/DocumentView.aspx?DocID=93166) [in Armenian]

[7] Freyhof J., Khorozyan I., Fayvush G. Freshwater Ecosystems and Biodiversity: Atlas of Freshwater Key Biodiversity Areas in Armenia. Yerevan. WWF-Armenia, p. 38, 2015.

[8] Important Bird Areas in Armenia. BirdLife International database. Available online at: http://datazone.birdlife.org/country/armenia (Accessed: 20.12.2021)

[9] Kylander M., Ampel L., Wohlfarth B., Veres D. High-resolution X-ray fluorescence core scanning analysis of Les Echets (France) sedimentary sequence: new insights from chemical proxies, Journal of Quaternary Science, 26, pp.109–117, 2011 doi:10.1002/jqs.1438

[10] Davies S. J., Lamb H. F., Roberts S. J. Micro-XRF core scanning in palaeolimnology: recent developments / Micro-XRF studies of sediment cores: applications of a non-destructive tool for the environmental sciences, Developments in palaeoenvironmental research. - I.W. Croudace, R.G. Rothwell. (Eds.), Vol. 17, pp. 189-226, 2015

[11] Melles M., Brigham-Grette J., Minyuk P. S., Nowaczyk N. R., Wennrich V., Andreev A. A., Coletti A., Cook T. L., Haltia-Hovi E., Kukkonen M., Lohzkin A. V., Rosén P., Tarasov P., Vogel H., Wagner B. 2.8 million years of Arctic climate change from Lake El'gygytgyn, NE Russia, Science, 337, pp. 315–320, 2012 doi:10.1126/science.1222135

[12] Naeher S., Gilli A., North R. P., Hamann Y., Schubert C. J. Tracing bottom water oxygenation with sedimentary Mn/Fe ratios in Lake Zurich, Switzerland, Chemical Geology, Vol. 352, No. 16, pp.125-133, 2013

[13] Burnett A., Soreghan M., Scholz C., Brown E. Tropical East African climate change and its relation to global climate: a record from Lake Tanganyika, tropical East Africa, over the past 90 + kyr, Palaeogeography Palaeoclimatology Palaeoecology, 303, 155167, 2011 doi:10.1016/j.palaeo.2010.02.011

MINERAL COMPOSITIONS OF SOME ROCK-FORMING MINERALS IN THE LOW-GRADE SEDIMENTARY AND MAFIC ROCKS, EASTERN CIRCUM-RHODOPE BELT, BULGARIA

Prof. DSc Nikolay Bonev[1]

[1]Sofia University St. Kliment Ohridski, **Bulgaria**

ABSTRACT

The eastern Circum-Rhodope belt (CRB) is a major unit that surrounds both the Serbo-Macedonian and the Rhodope zones in the Alpine orogen of the northern Aegean region. This belt contains Triassic-Jurassic metasedimentary successions and Middle Jurassic (176-165 Ma) supra-subduction zone Evros ophiolite. The latter has experienced ocean-floor hydrothermal metamorphism or very-low to low-grade metamorphism. We report on mineral compositions of rock-forming minerals in schist and mafic rocks from the eastern CRB. Our goal is to use the mineral compositions to assess the metamorphic conditions suffered by the rocks. The studied minerals include amphibole, garnet and mica. The electron probe microanalyzer was used to obtain the mineral chemistry recalculated into the mineral structural formula. The amphiboles in the mafic rocks have the compositions from magnesio-hornblende to edenite hornblende, which includes also actinolite-hornblende to actinolite and ferro-tschermakite in the greenschists. In the mica schist, the amphibole is magnesian-hastingsite, which is associated with almandine garnet, muscovite and biotite. The mineral assemblage studied, and its composition, reflects unequivocally greenschist facies metamorphic conditions experienced by the rocks. These conditions are further confirmed by the abundant chlorite and epidote observed in the metasedimentary and metamafic rocks. Thus, our study extends quantitively the metamorphic grade and conditions pertinent to the eastern CRB rocks.

Keywords: mineral chemistry, low-grade metamorphism, eastern Circum-Rhodope belt, Bulgaria

INTRODUCTION

The Circum-Rhodope belt (CRB) is a major tectonic unit that surrounds both the Rhodope and the Serbo-Macedonian zones of the Alpine orogen in the northern Aegean region (Fig. 1, inset). The biostratigraphically proven Triassic-Jurassic in age sedimentary successions have been initially used to recognise the Mesozoic age of the western CRB on the Chalkidiki Peninsula of northern Greece and its regionally extensive character across the Aegean Sea [1]. In the eastern CRB exposed in Thrace area and eastern Rhodope zone of southern Bulgaria and northern Greece biostratigraphic [e.g. 2], as well as radiometric [3 and references therein] age constraints have been used to infer Triassic and Jurassic depositional ages.

https://doi.org/10.5593/sgem2024/1.1/s01.14

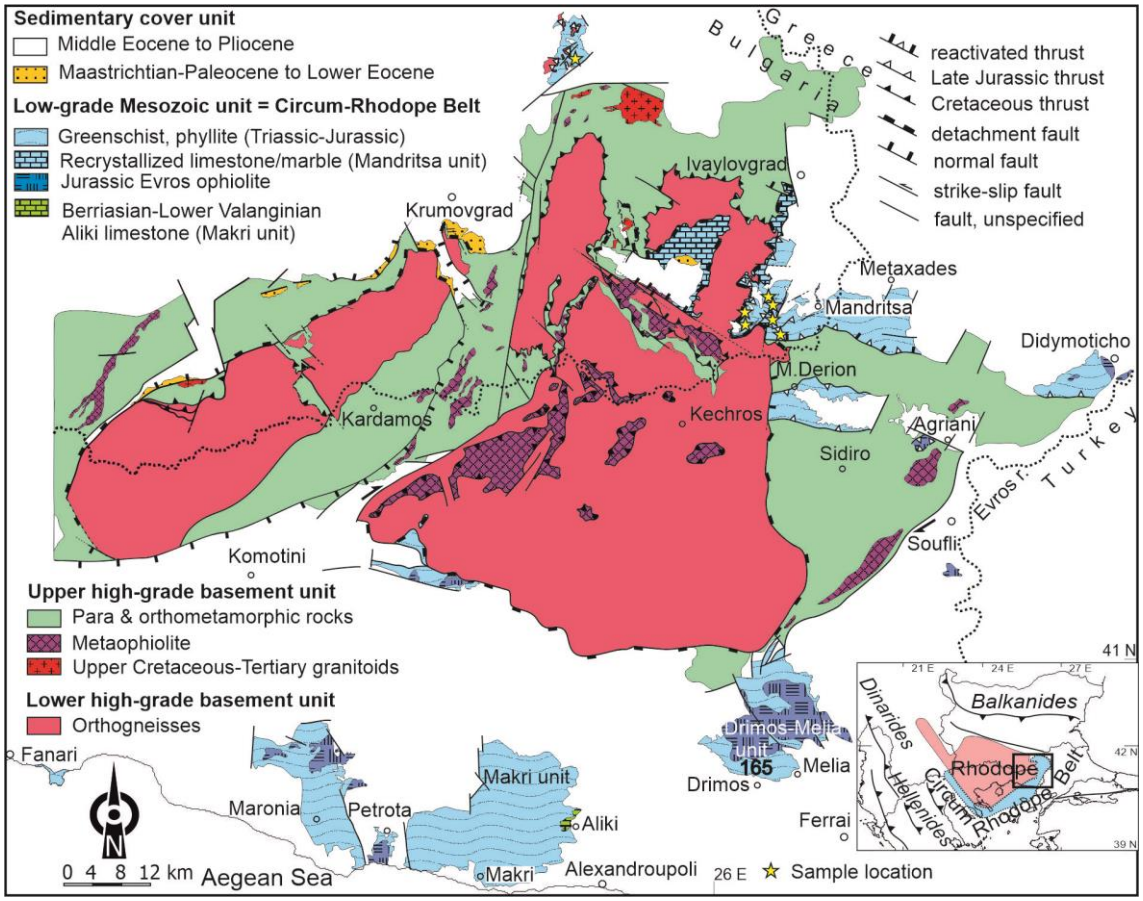


Figure 1. Synthetic geological map of the eastern Rhodope zone, showing the eastern CRB (adapted from [6]).

In the Bulgarian part of the eastern CRB, on the basis of the lithological similarity, the exposed sedimentary successions were correlated to the two main CRB units in Thrace area of northern Greece, namely Makri unit and Drimos-Melia unit [2] (see Fig. 1). An essential part of the eastern CRB represents the arc-related Evros ophiolite [4, 5, 6]. The eastern CRB has been shown to represent subduction-accretionary complex related to early Alpine tectonic evolution of an intra-oceanic arc system that gave birth to the Jurassic supra-subduction zone Evros ophiolite along the Eurasian plate margin [6].

The largest outcrop area of the eastern CRB in Bulgaria called the Mesozoic low-grade unit [6] or Mandritsa Group [2], and also Mandritsa unit [6], laterally continues in northeastern Greece. The second large and important area exposing the eastern CRB is the Kulidzhik nappe [7]. The metamorphic conditions in the eastern CRB rocks reached greenschist facies in the metasedimentary and metapyroclastic rocks decreasing to very low-grade ocean floor hydrothermal metamorphism in mafic lavas [2, 6, 8].

In this contribution, we provide new mineral chemistry of the low-grade sedimentary and mafic rocks, which forms part of the two main exposed above-mentioned areas of the eastern CRB in Bulgaria. The aim of this study is to identify the mineral compositions in some of the rock-forming minerals that will provide an important insight into the metamorphic grade and conditions suffered by the CRB rock successions.

MATERIALS AND METHODS

We used metamafic rock sample CRB 159 from the Kulidzhik nappe autochthon and metamafic sample CRB 47 from the Mandritsa unit, together with greenschist (metapyroclastic rock) samples CRB 47a, CRB 47b and CRB 37, also from the Mandritsa unit for obtaining the amphibole compositions. Only in the greenschist sample CRB 47b was analysed garnet. In the mica schist sample CRB 10 was analysed white mica, and micas and garnet were analysed in the mica schist sample CRB 29, both collected from the Mandritsa unit. A short petrographic summary of the studied samples is given in Table 1.

Table 1. Summary of the main petrographic features of the studied rock samples.

Sample	Rock type	Petrography	Reference	Location
CRB 159	metadolerite	massive, fine-grained consisting of amphibole, plagioclase, quartz, epidote, chlorite		Kulidzhik nappe
CRB10	psammitic schist	foliated, consisting of quartz, white mica, biotite, feldspar		Mandritsa unit
CRB29	garnet-bearing schist	foliated, consisting of quartz, white mica, garnet		Mandritsa unit
CRB37	greenschist	foliated, consisting of chlorite, amphibole, quartz	[6]	Mandritsa unit
CRB47	metadiorite	weakly foliated, medium-grained consisting of clinopyroxene, amphibole,	[6]	Mandritsa unit
CRB47	metadiorite	weakly foliated, medium-grained consisting of clinopyroxene, amphibole,	[6]	Mandritsa unit
CRB47a	garnet-bearing greenschist	foliated, consisting of chlorite, amphibole, quartz, garnet	[6]	Mandritsa unit
CRB47b	greenschist	foliated, consisting of chlorite, amphibole, quartz	[6]	Mandritsa unit

Electron microprobe mineral analyses were obtained by JEOL 8200 Superprobe instrument at the University of Lausanne (Switzerland). Operating conditions were 10 nA beam current at 15 kV accelerating voltage in 5μm spot-size analysis with 30s for peak and background counting, using natural standards and PAP correction. Selected chemical compositions and structural formula of the mineral phases analysed are listed in Table 2 and depicted in Fig. 2.

RESULTS

In the mafic rocks the amphiboles have a range of the compositions from magnesio-hornblende (metadolerite) to magnesio-hornblende and edenite hornblende (metadiorite) (Fig. 2). The amphiboles in the greenschists have also a range of the compositions from magnesio-hornblende and edenite hornblende, but in addition, the greenschists include

https://doi.org/10.5593/sgem2024/1.1/s01.14

also actinolite-hornblende to actinolite and ferro-tschermakite compositions. The amphibole in the garnet-bearing micaschist is magnesian-hastingsite. Unzoned garnet porphyroblasts have compositions mostly of almandine garnet ($Alm_{60.7-59.6}$ $Prp_{12.1-5.0}$ $Grs_{19.4-10.2}$) (Table 2). Psammitic schist sample contains both muscovite and biotite, whereas in the garnet-bearing schist the mica is biotite (Table 2).

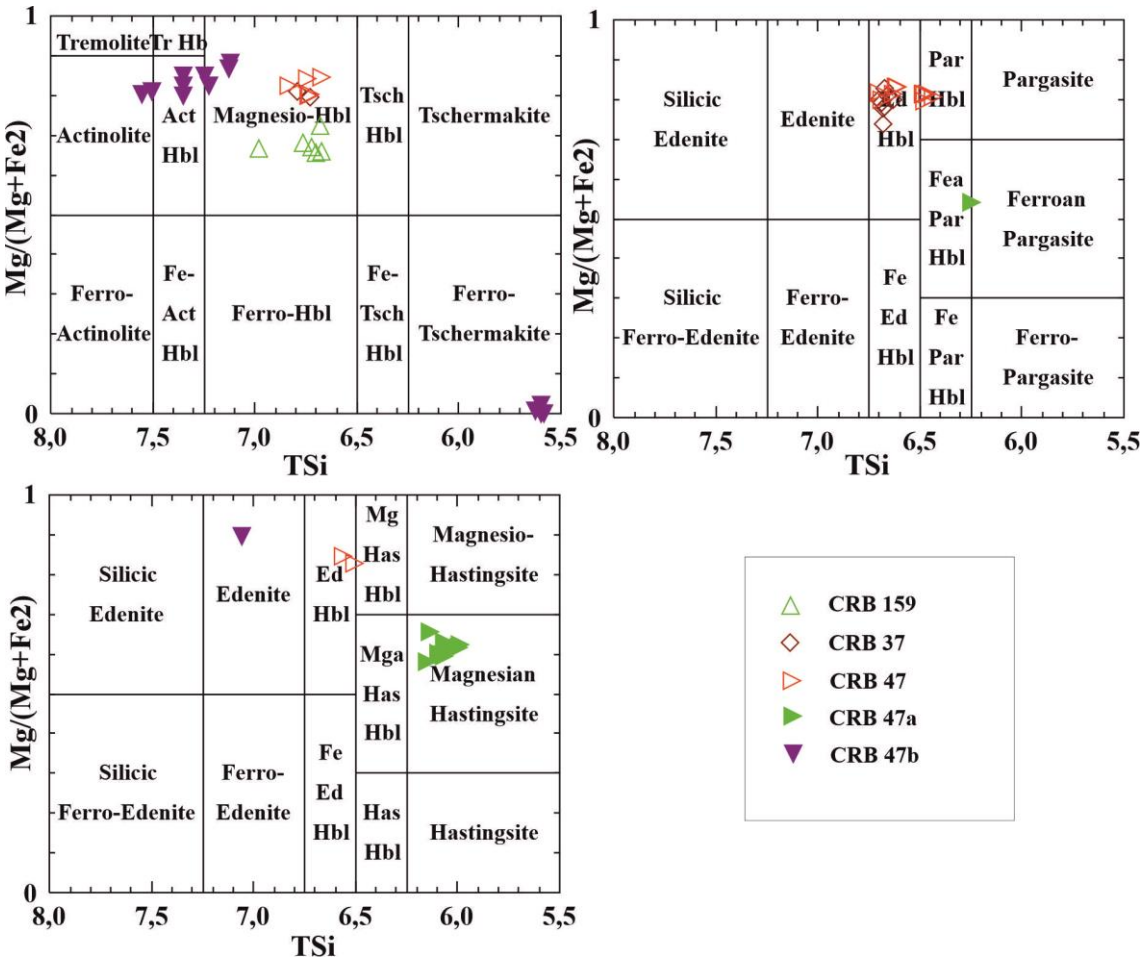


Figure 2. Amphibole compositions of the studied rock samples.

Table 2. Representative chemical analyses of the minerals in the studied rock samples Structural formula based on 22 and 24 oxygen atoms respectively for micas and garnets. Abbreviations: grt, garnet; ms, muscovite; bt, biotite.

Sample	CRB 29	CRB 47b	CRB 10	CRB 10	CRB 29
Mineral	grt	grt	ms	bt	bt
Rock type	grsch	grsch	grsch	grsch	grsch
SiO_2	37.20	36.72	44.43	34.86	30.40
TiO_2	0.10	0.11	0.41	1.98	0.12
Al_2O_3	20.79	20.49	32.17	16.73	22.25
Cr_2O_3	0.03	0.01	0.02	0.03	0.01
Fe_2O_3	1.90	2.61	-	-	-
FeO	27.04	26.21	3.91	19.13	23.65
MnO	4.06	4.53	0.06	0.14	0.32
MgO	1.26	2.99	1.27	10.53	9.49
CaO	8.73	6.15	0.03	0.18	0.06

Na_2O	-	-	0.88	0.20	0.01
K_2O	-	-	8.39	6.99	1.58
H_2O	-	-	4.30	3.79	3.70
Total	101.12	99.82	95.87	94.55	91.60
Si	2.961	2.946	6.194	5.519	4.932
Ti	0.006	0.007	0.043	0.236	0.015
Al ^{IV}	0.039	0.054	1.806	2.481	3.068
Al ^{VI}	1.911	1.883	3.478	0.641	1.186
Cr	0.002	0.001	0.002	0.003	0.001
Fe^{3+}	0.114	0.157	-	-	-
Fe^{2+}	1.800	1.759	0.456	2.533	3.208
Mn^{2+}	0.274	0.308	0.007	0.019	0.044
Mg	0.149	0.357	0.264	2.486	2.295
Ca	0.745	0.529	0.005	0.030	0.011
Na	-	-	0.236	0.060	0.004
K	-	-	1.492	1.412	0.326
OH	-	-	4.000	4.000	4.000
Py	5.025	12.103			
Alm	60.658	59.568			
Sp	9.219	10.426			
And	5.609	7.691			
Uv	0.104	0.039			
Gro	19.384	10.173			
xMg	0.077	0.169	0.366	0.495	0.417

DISCUSSION

In the sample CRB 47 (metadiorite) the magnesio-hornblende is primary in origin because the rock contains preserved clinopyroxene [6]. In the metadolerite sample CRB 159 the magnesio-hornblende also appears to be of primary, magmatic origin. In the greenschists, edenite hornblende in sample CRB 37 and magnesian-hastingsite CRB 47a resulted from the metamorphic process, whereas sample CRB 47b demonstrates a transition in the amphibole compositions from magnesio-hornblende to actinolite-hornblende and actinolite. Garnet and micas are unequivocally the result of the metamorphic process, which reached grade of the greenschist facies. Then, actinolite-chlorite-muscovite-biotite-garnet Barrovian zones of the greenschist facies metamorphism are recorded [9]. Therefore, the results support envisaged metamorphic grade, and they are consistent with the previously reported data on the metamorphism of the eastern CRB rocks.

CONCLUSION

Our study of the mineral compositions of some rock-forming minerals in the low-grade metasedimentary and metaigneous rocks of the eastern CRB revealed features characteristic for greenschist facies metamorphism. Particularly, metaigneous rocks preserve magmatic magnesio-hornblende, which amphibole composition passes to actinolite-hornblende and actinolite in the metapyroclastic rock represented by the greenschists. Therefore, the amphibole composition reflects the transition from primary

https://doi.org/10.5593/sgem2024/1.1/s01.14

composition to that resulting from experienced greenschist facies metamorphism. Almandine garnet is characteristic for greenschist facies metamorphism and higher metamorphic grade. Muscovite and biotite reflect metamorphic recrystallization of the sedimentary protoliths and can also occur in greenschist facies and higher metamorphic grade. In addition to the studied metamorphic assemblage amphibole-garnet-muscovite-biotite, the low-grade metasedimentary and metaigneous rocks contain chlorite, epidote and albite, and together with the presence of actinolite, collectively, all minerals are characteristic for greenschist facies metamorphism. Thus, we draw the following conclusion – the mineral assemblage studied confirms experienced greenschist facies metamorphism and further extends quantitatively the mineral compositions of the low-grade metasedimentary and metaigneous rocks of the eastern CRB. These rocks belong to actinolite-chlorite-muscovite-biotite-garnet zone of the greenschist facies metamorphism.

ACKNOWLEDGEMENTS

The support provided by National Science Fund (Bulgaria) (contract no. KP-06-N54/5) is greatly acknowledged.

REFERENCES

[1] Kauffmann G., Kockel F., Mollat H., Notes on the stratigraphic and paleogeographic position of the Svoula formation in the Innermost Zone of the Hellenides (Northern Greece). Bulletin de la Societe Géologique de France, vol. 18, pp 225-230, 1976.

[2] Boyanov I., Russeva M., Toprakcieva V., Dimitrova E., Lithostratigraphy of the Mesozoic rocks from the Eastern Rhodopes. Geologica Balcanica, vol. 20, pp 3-28, 1990.

[3] Meinhold G., Reischmann T., Kostopoulos D., Frei D., Larionov A.N., Mineral chemical and geochronological constraints on the age and provenance of the eastern Circum-Rhodope Belt low-grade metasedimentary rocks, NE Greece. Sedimentary Geology, vol. 229, pp 207-233, 2010. doi:10.1016/j.sedgeo.2010.06.007

[4] Magganas A.C., Constraints on the petrogenesis of Evros ophiolite extrusives, NE Greece. Lithos, vol. 65, pp 165-182, 2002.

[5] Magganas A., Sideris C., Kokkinakis A., Marginal basin-volcanic arc origin of metabasic rocks of the Circum-Rhodope Belt, Thrace, Greece. Mineralogy and Petrology, vol. 44, pp 235-252, 1991.

[6] Bonev N., Stampfli G., Petrology, geochemistry and geodynamic implications of Jurassic island arc magmatism as revealed by mafic volcanic rocks in the Mesozoic low-grade sequence, eastern Rhodope, Bulgaria. Lithos, vol. 100, 2008, pp 210-233. doi:10.1016/j.lithos.2007.06.019

[7] Boyanov I., Notes on the Kulidjik nappe. Bulletin of the Geological Institute of the Bulgarian Academy of Sciences, series Geotectonics, vol. 18, pp 159-1651969.

[8] Magganas A., Relict minerals of metavolcanics and metapyroclastic rocks from the Circum-Rhodope Belt in the area of Thrace, Greece. Geologica Rhodopica, vol. 2, pp 251-259, 1990.

[9] Bucher K., Frey M., Petrogenesis of Metamorphic Rocks. Springer-Verlag, Berlin Haidelberg, 1994, pp 318. ISBN 3-540-57567-7.

THE PARTICLE SIZE OF THE BOTTOM SEDIMENTS IN SOME CANALS OF THE FLUVIAL-MARINE DANUBE DELTA

Phd Ress. Livanov Oliver [1,2]
Dr. Banescu Alexandru[1]
Burada Adrian[1]
Pindic Paula [1]
Anore Ciprian[1]

[1] Danube Delta National Institute for Research and Development of Tulcea, **Romania**
[2] University of Bucharest, Doctoral School of Geology, **Romania**

ABSTRACT

In deltaic environments like the Danube Delta, sedimentary particles can range from clay and silt to sand and gravel. The proximity to the Black Sea introduces marine processes into the deltaic system that can be translated as a mixture of fine-grained sediments derived from the fluvial delta along with marine sediments from the Black Sea. This region is of particular importance for the ecology and hydrology of the Danube Delta due to the presence of sandy deposits that cause a major change in both natural and anthropogenic habitats. The emergence of artificial canals dug in sandy deposits had a huge impact on the deltaic ecosystems, as a better way of transportation but also a potential threat to the hydrological balance. Therefore the periodical dredging works became mandatory in maintaining waterway accessibility and supporting transportation. This work is intended to be a useful study for subsequent dredging works on the Danube Delta canals excavated on sandy material. The study involved the sampling of sediment from canals to assess its quality, determine dredging requirements, and manage dredged material effectively. An extensive sediment sampling program was established to collect samples from the bottom of several canals from the fluvial-marine Danube Delta (Cordon Litoral, Letea and Sidor Canals) at high and low water levels. At the Danube Delta National Institute laboratory, the sediment samples were subjected to particle size determinations. The main purpose of the particle size analysis was to quantify the fine fractions from the coarse ones. The results show that even though the material is expected to be predominantly sandy, significant percentages of finer material can be present as well. Following this study, three factors were identified to influence the particle size distribution, namely the variation of the water table during the year, anthropic activities and the additional supply of fine particles from the fluvial deposits. These considerations must be taken seriously into account especially in future dredging works, as these processes can significantly influence the depositional processes as dredging can resuspend fine sediments into the water column, increasing turbidity and altering its initial state.

Keywords: particle size, sediments, Danube Delta, canals, dredging

INTRODUCTION

The Danube Delta stands as a unique and complex natural system, where the interaction of natural processes, human activities, and cultural heritage creates a dynamic and intricate environment. The Danube River, one of Europe's major rivers, is a dominant hydrological force shaping the delta. Seasonal variations in river discharge, precipitation, and snowmelt influence water levels, sediment transport, and the overall

hydrological balance [2]. Sedimentation rates vary across different parts of the delta, influenced by factors such as canal morphology, vegetation, and human interventions.
The Danube Delta is a remarkable example of an alluvial plain that continues to form through an interplay of fluvial and marine processes. Depending on these processes, the Danube Delta is divided into the Fluvial Delta and the Fluvial-Marine Delta (Figure 1) [6]. The sediments in the Fluvial Delta are fine in terms of particle size (clay or silt, sometimes with sandy interlayers), while those in the Fluvial-Marine Delta are coarser (mainly sand).
In the present work, we studied the sedimentation processes that take place in the canals of the Fluvial-Marine Delta. Three anthropic-dug canals were chosen, from which bottom sediment samples were taken for particle size analysis. The Cordon Litoral Canal (CL) is the longest of the three, being located north of the Sfântu Gheorghe commune. The Letea Canal (L) is located west of the village of the same name, in the northern area of the Fluvio-Marine Delta. The Sidor Canal (S) comes in the extension of the latter, which suddenly changes its direction from SSE-NNW to SE-NW (Figure 1).

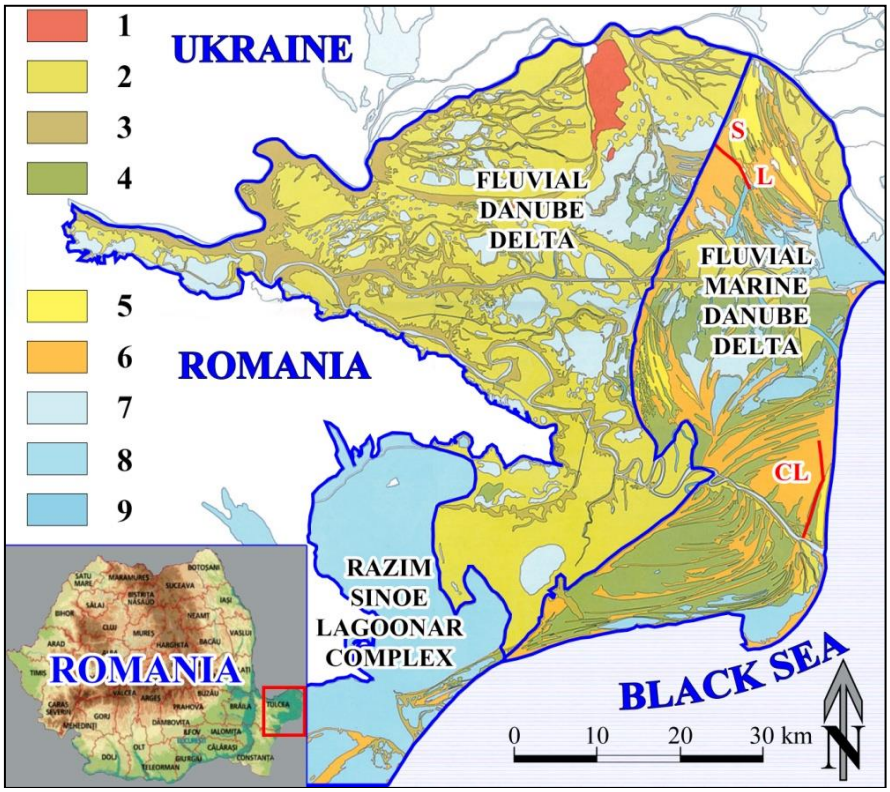


Figure 1. Location of the studied canals (CL - Cordon Litoral, L - Letea, S - Sidor) within the geomorphological map of the Danube Delta. Legend: 1. Remnants of the loessial plain, 2. Flat area of fluvial/lagoonary origin, 3. Fluvial and lacustrine levees, 4. Flat area of lagoonary/marine origin, 5. Coastal dunes, 6. Marine lagoonal sandbars, 7. Lacustrine-fluvial/lagoonary depressionary areas, water courses, 8. Lagoonary-marine depressionary areas, 9. Minor landforms: abandoned filled/open water course, cut meander of main branches. Adapted from [8]

The Cordon Litoral Canal was finalized in 1996 [5]. Letea and Sidor Canals located in the north of the Fluvial-Marine Delta, were dug in the 1970s with some rudimentary

tools by fishermen from the Letea area to connect the mentioned locality with Lake Merhei, at that time an important fish resource.

MATERIALS AND METHODS

Sampling was carried out in two stages, the first at high water levels (from 27th of March 2023 to 4th of April 2023) and another at low levels (from 23rd of October 2023 to 27th of October 2023). On the Letea and Sidor Canals, sediment samples were collected on three profiles (noted as P) while from the Cordon Litoral Canal, sediment samples were collected on four profiles. In the case of the last canal, on the third profile, there were issues regarding access, so in the autumn campaign (at low water levels), profile 3 (Cordon Litoral, Profile 3 - CLP3) was moved 260 m to the north (Cordon Litoral, Profile 3B - CLP3B). On each profile, substrate samples were taken from the middle of the channel and the two banks. The location of the substrate sampling points along with all the profiles are shown in Figure 2.

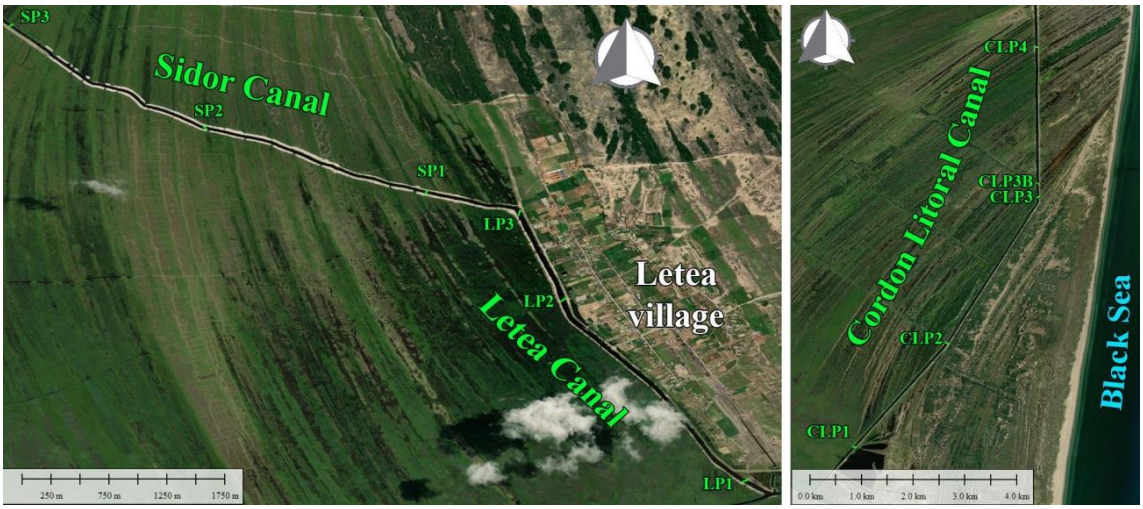


Figure 2. Location of the sampling profiles

Eijkelkamp hand auger set for heterogeneous soil was used for the sampling of the substrate. The maximum extracted substrate column was 20 cm, corresponding to the dimension of the drilling auger. The middle of the canals was sampled from a stationary motorboat from which the drilling rig was inserted into the water column to reach the substrate. An important aspect when sampling with the Eijkelkamp hand auger set is to select the appropriate auger head based on the soil type encountered. To penetrate the canal's water column, the auger head was linked to several one-meter connection rods. The maximum length of the rod assembly is 5 meters which proved to be sufficient for collecting substrate samples under optimal conditions. To sample from the banks, there was no need to use the rod assembly because the water was not deep, varying between 5 to 40 cm. All the samples were collected and labelled accordingly for later laboratory studies.

In the laboratory, sediment samples were oven-dried (Figure 3, left) to remove excess moisture. The sample will be subjected to dry sieving if it does show cohesion between the particles. If the sample shows even the smallest trace of cohesion, a dispersing agent (usually 0.2-0.4 g of lithium carbonate - Li_2CO_3) will be inserted into the aqueous solution of the sample. The dispersing agent is allowed to act on the sample for one day. After this period, the aqueous solution will be wet-sieved.

https://doi.org/10.5593/sgem2024/1.1/s01.17

The sieving was carried out using the Retsch AS200 Digit CA Vibratory Sieve Shaker, according to the requirements of [3]. Sieves with various mesh sizes ranging from 0.038 mm (38 μm) to 2 mm (2000 μm) were used. The sieves are mounted one above the other on the Retsch shaker in ascending order of mesh size. The dry or aqueous sample is poured into the top sieve which has the largest mesh diameter from the sieve assembly (Figure 3, right). The Retsch Shaker will generate vibrations and the particles will fall gravitationally according to their geometry through the sieve assembly until they are retained by the sieve with the mesh sizes corresponding to the particle diameters.



Figure 3. Laboratory analyses: **left**, placing the samples into the laboratory oven to remove moisture, **middle**, weighting the sample, **right**, pouring the weighed sample into the sieves assembly. Photos by Livanov O.

After the sieving is complete, the material on the site is weighed (Figure 3, center). In wet sieving, the remaining material is placed in the laboratory oven to remove the moisture and then weighed in the dry state. These data will be the basis for creating the granulometric curves and implicitly for obtaining the granulometric composition according to the particle sizes [3][9].
It should be specified that the goal of this study was to outline the concentration of fine particles (clay and silt) and the coarser ones (sand). Clay and silt were not differentiated, the nomenclature of "*fine particles*" being considered acceptable for this study.

RESULTS

Table 1 points out the results of the granulometric analysis for all the profiles corresponding to the three investigated canals. It is revealed that the coarse fraction is dominant and present in all analysed samples. The coarse fraction contains an important rate of fine and medium sand while the coarse sand and gravel fractions are insignificant. The percentage of coarse particles is important in dredging because it is more difficult to dig in sandy sediments [1][7]. The limit between coarse and fine particles was assessed at 0.063 mm (63 μm) according to [4]. The organic material composed of shell fragments or vegetation remnants present in the very coarse fraction is usually below 5%, falling within the allowed calculation error.

Table 1. Particle size analysis with emphasis on medium and fine sand particles. Legend: (1) fine particles (Ø<63 μm), (2) coarse particles (Ø>63 μm), (3) medium sand (200 to 630 μm), (4) fine sand (63 to 200 μm). *NOTE: For logistical reasons, profile 3 on the Cordon Litoral Canal was moved 260 m to the north at low water levels

			HIGH WATER LEVELS				LOW WATER LEVELS			
			(1) %	(2) %	(3) %	(4) %	(1) %	(2) %	(3) %	(4) %
Cordon Litoral Canal - CL	Profile 1 P1	NW Bank - CLP1NWB	3	97	7	88				
		Middle - CLP1MID	44	56	2	53	8	92	18	71
		SE Bank - CLP1SEB	3	97	6	90				
	Profile 2 P2	NW Bank - CLP2NWB	3	97	8	88				
		Middle - CLP2MID	10	90	41	48	~0.5	99	8	91
		SE Bank - CLP2SEB	1	99	11	86				
	Profile 3* P3	W Bank - CLP3WB	1	99	19	80	~0.5	99	12	86
		Middle - CLP3MID	1	99	11	88	~0	~100	10	89
		E Bank - CLP3EB	1	99	13	86	1	99	9	89
	Profile 4 P4	W Bank - CLP4WB	1	99	6	93				
		Middle - CLP4MID	1	99	6	93	3	97	9	83
		E Bank - CLP4EB	1	99	6	93				
Letea Canal - L	Profile 1 P1	NE Bank - LP1NEB	3	97	6	90				
		Middle - LP1MID	27	73	8	64	13	87	8	78
		SW Bank - LP1SWB	2	98	9	89				
	Profile 2 P2	E Bank - LP2EB	8	92	20	72				
		Middle - LP2MID	15	85	20	65	19	81	9	71
		W Bank - LP2WB	5	95	4	90				
	Profile 3 P3	E Bank - LP3EB	11	89	31	54				
		Middle - LP3MID	10	90	5	85	5	95	8	86
		W Bank - LP3WB	3	97	9	88				
Sidor Canal - S	Profile 1 P1	N Bank - SP1NB	2	98	30	63				
		Middle - SP1MID	~0.5	99	29	65	7	93	11	81
		S Bank - SP1SB	1	99	29	65				
	Profile 2 P2	N Bank - SP2NB	2	98	62	24				
		Middle - SP2MID	1	99	56	30	2	98	45	48
		S Bank - SP2SB	2	98	68	18				
	Profile 3 P3	NE Bank - SP3NEB	1	99	82	13				
		Middle - SP3MID	2	98	63	19	5	95	69	18
		SW Bank - SP3SWB	1	99	73	18				

The fine particles occasionally vary but are mostly very low in quantity, sometimes below 1%. There can be occasional seasonal variations due to the different supply of sediments that the canals transport when water levels are low or high. On each profile, samples were extracted from both banks and the middle of the canal. The banks are quite homogenous in terms of particle size and distribution because here the water velocity is almost zero. Precisely for this reason, banks were sampled only once, at high water levels, while the middle of canals were sampled twice at low and high water levels to capture the seasonal flux of bottom sediments. However, some banks were also sampled at low water levels as profile 3 on the Cordon Litoral Canal was moved a little further north due to unforeseen reasons. The laboratory tests concluded that there are no significant seasonal variations in the sediments of the banks proving that another sampling would have been redundant.

Further, we will summarize the particle size variation on each canal and most of the profiles. The samples analysed from the Cordon Litoral Canal, are predominantly coarse (especially fine sand) on the two banks and in the bottom sediments. Still, at high water levels, the bottom sediments may present variations on profile 1, where coarse particle

https://doi.org/10.5593/sgem2024/1.1/s01.17

concentration is only 56%. The explanation can be given by the fact that profile 1 is located near the sedimentary fluvial deposits of the southern branch of the Danube (Sfântu Gheorghe Branch), adding a supply of fine particles at high water levels. On the other hand, at low water levels, if not enriched with additional sedimentary material, the amount of coarse particles in the bottom sediments on profile 1 increases significantly to 92%.

There is also a minor variation in particle size on profile 2, where the bottom sediments contain 10% fine particles at high water levels. In our opinion, the influence of fluvial sedimentation is felt up to this point. On profiles 3 and 4, the percentage of fine particles from the bottom sediments is approx. 1% denoting that fluvial sediments no longer reach here. At low water levels, when there is practically no fluvial sediment input, the bottom sediments have a low percentage of fine particles (0-3%) and a high percentage of coarse particles (97-100%), the exception being on profile 1, mentioned above, where the fluvial influence is still slightly felt. The Letea Canal was dug on the sandy deposits specific to the fluvial-marine delta. As expected, the coarse fraction is in appreciable amount, even reaching values of 97-98% on the banks. As in the case of the Cordon Litoral Canal, there are differences between the bank and bottom sediments, namely that the amount of fine particles is higher in the middle of the canal. Moreover, the Letea Canal has a higher concentration of fine fraction compared to the other two studied canals, whether we refer to the banks or bottom sediments.

Regarding the higher concentrations of fine particles, we have identified two factors that may explain this fact. First of all, the southern part of the canal is bordered by marsh deposits which creates a noticeable input of fine sediments. The influence of marshy deposits is felt both at high and low waters, on the bottom sediments of profiles 1 and 2 (27% / 13% at high / low water levels on profile 1 and 15% / 19% on profile 2, respectively).

Another factor influencing the higher amount of fine particles is the proximity of the eastern bank to the Letea village. Due to human activities and the intensive use of boats, the sedimentary regime of the canal is strongly influenced. The presence of the Letea locality also influences the granulometric variation of the banks, a situation unprecedented in the case of the other two canals which have roughly the same composition on both banks. On the eastern bank of this canal which is shared with Letea village, higher concentrations of fine particles were determined compared to the western bank (profile 2: 8% on the eastern bank, compared to 5% for the western bank; profile 3: 11% on the eastern bank, compared to 3% for the western bank). On profile 1, which is close to the Letea village, low values were recorded on both banks (3% on the eastern bank and 2% on the western bank), which reinforces the idea that human activities can influence the sedimentary regime. The Letea Canal continues with the Sidor Canal until it flows into Lake Merhei. The latter canal is located on sandy deposits of fluvial-marine origin, but for the last 900 meters before discharging into the lake, it enters the fluvial delta on marshy deposits. Since this study was carried out for deposits specific to the fluvial-marine delta, this portion of the Sidor Canal was not sampled.

The granulometric analysis concluded that the coarse particle fraction is dominant with concentrations above 90%. Unlike the other two studied canals, the medium sand fraction at high water levels is much more present here, with values of approx. 30% on profile 1 and between 60-80% on the last profile (profile 3). At low water levels, the percentage is still high, ranging from 11 to 69%. The composition of the bottom sediments at high water levels does not differ from that of the banks (fine particles 1-

2%, coarse particles 98-99%), instead, it undergoes slight changes at low water levels (fine particles 2-7%, coarse particles 93-98%). Analyzing the results, it appears that the Sidor Canal is quite homogeneous in terms of particle size, with no significant variations either at high or low water levels.

DISCUSSIONS

Our analysis revealed unexpected variations in particle sizes, despite the canals being dug in what should theoretically be constant sandy deposits. This finding raises questions about the factors influencing sediment dynamics and canal morphology in these environments.

Variations in the water table can have distinct influences on the bottom sediments which can lead to changes in the deposition rates. Increased water levels may promote finer sediment deposition, particularly in low-lying areas within the channel. Conversely, during periods of low water levels, sediment erosion from the banks may be more prevalent as water levels recede, increasing coarser sediment accumulation.

Another determining factor is the anthropic influence. In deltaic environments, human activities can have significant impacts on the grain size distribution of bottom sediments. Intensive vessel traffic can contribute to sediment resuspension and erosion of canal bottoms potentially altering sediment composition within the canal.

The last factor is the additional supply of fine sediments from the fluvial deposits to nearby sandy deposits. The influx of fine sediments at high water levels can lead to increased sedimentation rates. Over time, this fact can cause accumulations of sediment layers, which can slightly modify the local geomorphology.

CONCLUSIONS

This analysis of the three studied canals regarding their sediment particle sizes will be the basis of their subsequent dredging. It is important to know the fluctuation between fine and coarse particles because during dredging the sandy material is lost more often than the fine material in the dredger bucket.

The granulometric analysis showed that coarse material (fine and medium sand) is present in appreciable quantities in the bottom sediments. Factors such as the water table variation, the antropic influence or the presence of nearby fluvial deposits may influence the sedimentation on these canals.

To mitigate the fall down of sandy sediments during dredging operations, it's essential to carefully plan and execute the dredging process while considering the factors mentioned above. This may involve selecting appropriate equipment, adjusting dredging techniques, and monitoring environmental conditions to minimize disturbances to the sediment and maintain navigational canals effectively. These considerations must be seriously taken into account, because a dredging operation can influence the hydrological regime and the ecology of the Danube Delta, already in a very fragile balance.

ACKNOWLEDGEMENT

The authors are expressing gratitude for the opportunity to conduct their work within the context of the project ”Cercetări privind evaluarea și analiza ritmului de colmatare a canalelor supuse intervențiilor inginerești de îmbunătățire a condițiilor hidrologice de pe teritoriul Rezervației Biosferei Delta Dunării”. This project was made possible through funding provided by Ministry of Research, Innovation and Digitalization.

REFERENCES

[1] Banescu A., Georgescu L.P., Rusu E., Iticescu C., Use of GIS technology to support the navigation on the Danube River. International Conference on Traffic and Transport Engineering ICTTE Belgrade, Serbia, pp. 160-168, 2018;

[2] Banescu A., Arseni M., Georgescu L.P., Rusu E., Iticescu C., Evaluation of different simulation methods for analyzing flood scenarios in the Danube Delta. Applied Sciences, 10(23), 8327, 2020;

[3] EN 933-1:2012, Tests for geometrical properties of aggregates - Part 1: Determination of particle size distribution - Sieving method. CEN, Brussels, Belgium, 18 pp., 2012;

[4] EN ISO 14688-1:2017, Geotechnical investigation and testing - Identification and classification of soil - Part 1: Identification and description. CEN, Brussels, Belgium, 23 pp., 2012;

[5] Gâștescu P., Driga B., Caracteristicile unităților morfohidrografice. In Gâștescu P., Știucă R. (eds), Delta Dunării. Rezervație a Biosferei. Editura Dobrogea, Constanța, Romania, pp. 138-161, 2006;

[6] Giosan L., Donnelly J.P., Vespremeanu E., Bhattacharya J.P., Olariu C., Buonaiuto F.S., River Delta Morphodynamics: Examples from the Danube Delta. River Deltas - Concepts, Models, and Examples, SEPM Special Publication No. 83, pp. 1-19, 2005;

[7] ICCPDC, Indicator de norme de deviz comasate pentru lucrări hidrotehnice portuare H_2. Institutul de proiectări transporturi, auto, navale și aeriene, Romania, 232 pp., 1981;

[8] Munteanu I., Curelariu G., Romanian Danube Delta Biosphere Reserve. Soil Map. NV Drukkerij Erasmus, Weteren, Belgium, 1 pp., 1995;

[9] Stroia F., Stănciucu M., Mecanica Rocilor. Lutite - rudite. Caiet de lucrări practice. Editura Universității din București, Romania, 179 pp., 1998.

VOLCANOTECTONIC STRUCTURES AND LINEAMENT PRELIMINARY IDENTIFICATION RESULTING FROM THE APPLICATION OF REMOTE SENSING AND GIS IN BOLNISI ORE DISTRICT, GEORGIA

PhD Ress. Irakli Avkopashvili[1]

[1] Ilia State University, Department of Earth Sciences, **Georgia**

ABSTRACT

The Bolnisi Ore District (Georgia), situated within the Tethyan-Eurasian metallogenic belt, embodies a multifaceted geological milieu marked by the intricate interplay of volcanic and tectonic processes, predominantly delineated by Late Cretaceous volcanic and sedimentary sequences entrenched between the Khrami and Loki Variscan crystalline massifs. Noteworthy for its rich mineral endowment, the Bolnisi Ore District harbors a plethora of ore deposits, with several operational mining sites situated within its bounds. This preliminary research aimed mainly by means of the remote sensing to investigate linear, curvilinear, arcuate, and circular features within the Bolnisi Ore District, Georgia, with the objective of enhancing exploration potential. Understanding the relationship between lineament intersections and caldera features is of particular interest due to their association with potential mineral occurrences. In this study, lineaments, curvilinear, arcuate, and circular features were delineated manually utilizing directional filters applied to satellite imagery. We obtained suitable satellite imagery along with high-resolution Digital Elevation Models (DEMs). Subsequently, GIS analysis was conducted, incorporating directional filters, geometric and atmospheric correction, and image enhancement techniques to enhance image quality and emphasize lineament features. To validate identified geological structures, a comparative analysis was performed utilizing geological maps, supplemented by partial field observations and a thorough review of existing literature about the study area. After incorporating the reliable geological structures from previous studies, we added the new preliminarily identified structures to the map. Additionally, the structures were cross-referenced with known volcanic features and geological interpretations to reinforce the findings.

Keywords: Volcanotectonics, Caldera, Lineaments, Bolnisi Ore District, Georgia

INTRODUCTION

The Caucasus is in a state of a continental collision between the Arabian and the Eurasian plates and having a very complicated history of geological development it represents a convenient natural polygon to study various tectonic, volcanogenic, and other geological phenomena [1]. The Bolnisi Ore District (BOD) situated in southeast Georgia, it is part of the Lesser Caucasus (Fig. 1) that is located in the north-eastern part

https://doi.org/10.5593/sgem2024/1.1/s01.18

of the Artvin-Bolnisi rigid massif [2]. From a tectonic and metallogenic point of view the district, situated within the Tethyan Eurasian metallogenic belt, embodies a multifaceted geological milieu marked by the intricate interplay of volcanic and tectonic processes, predominantly delineated by Late Cretaceous and Paleogene volcanic and sedimentary sequences entrenched between the Khrami, and Loki salients of Variscan intermountain massif. This massif represents a horst-like inlier of the pre-Alpine basement. Noteworthy for its rich mineral endowment, the BOD harbours a plethora of mineralized deposits, with several operational mines situated within its bounds (Madneuli, Sakdrisi and others. Fig. 3 and 4).

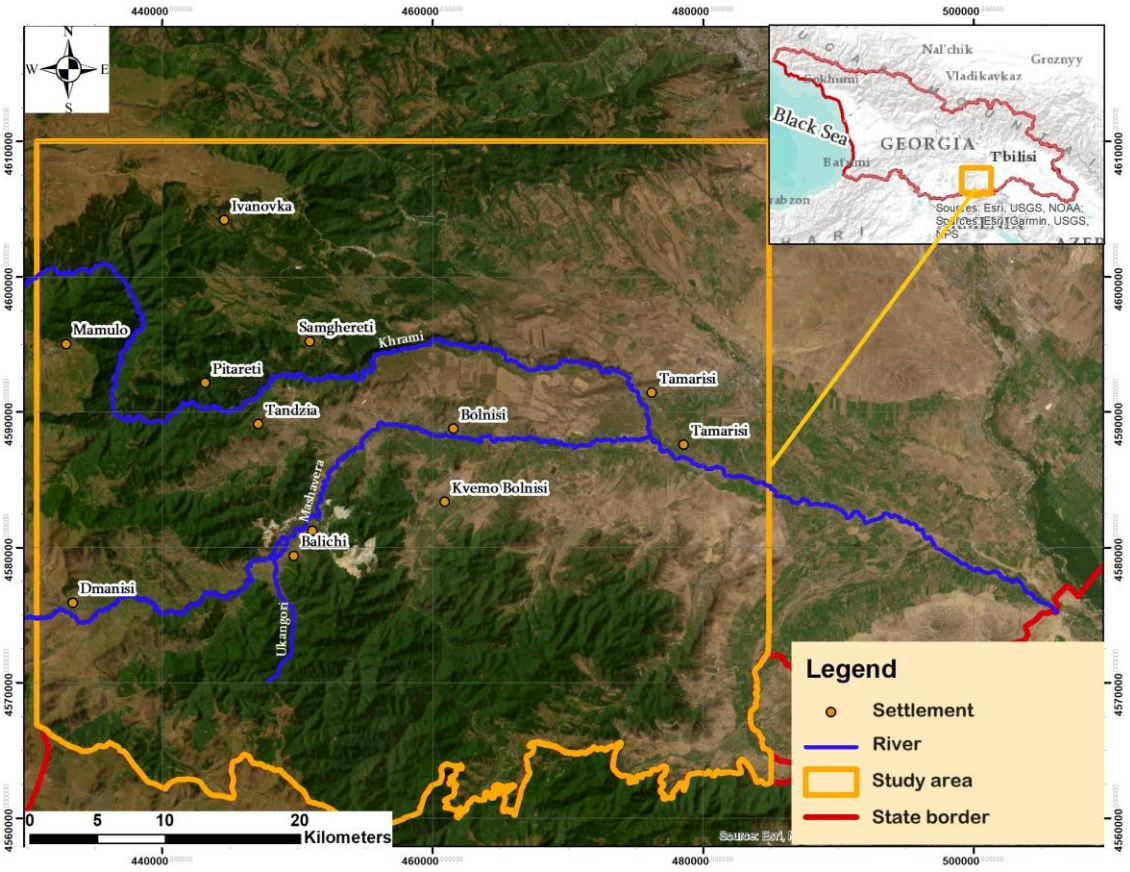


Fig. 1. Location of the study area.

The BOD, situated within Lesser Caucasus, which is intricately associated with the northeast-verging subduction of the Neothetys Oceanic crust along the Eurasian margin. Within this district, the Mashavera and Gasandami suites stand out as the primary stratigraphic units, hosting a diverse array of gold and base metal deposits the genesis of which is still debated [3, 4, 5, 6]. Ore deposits are developed in volcanic rocks mainly in rhyolites, rhyodacites, andesites and metasomatized tuffs.

Previous studies have shown the existence of volcanotectonic depressions and structures, as pointed out by several authors [5, 7]. Some authors indicate that most of the mineral deposits of the district are related to the various volcanogenic structures like calderas, domes, etc., Which are complicated by regional and local tectonics. All these geological phenomena concentrated within the relatively small and easily accessed area create favorable possibilities for scientific-educational purpose, the scientific discussions around this topic may help progress this field. To enhancing exploration potential and underline regions scientific and educational value we tried to study the BOD, and investigate and map the existing volcanotectonic structures to understand its geological history better. According to most authors, the study area is divided vertically into two structural units. The lower unit is represented by pre-Jurassic granitoid formations. In the upper structural layer, we find Meso-Cenozoic mostly Late Cretaceous (Cenomanian-Campanian) volcanic and volcanic-sedimentary rocks [8].

Particularly, the research aimed to investigate linear, curvilinear, arcuate, and circular features within the BOD, with the objective of reconstructing the tectonic, especially the volcanotectonic processes and enhancing exploration potential. For this purpose, we use remote sensing, (GIS), structural geological, and other methods.

Volcanotectonic field aims to provide a sufficient understanding of the internal processes in volcanoes, where the research is mostly related to active volcanoes and fossil and deeply eroded volcanoes [9]. Understanding the relationship between lineament intersections and circular features is of particular interest due to their association with potential mineral deposits. In a previous study, these cauldrons were assessed as post-ore formation, and some of these structures are ore-controlling and hence can be used as a lead indication in the course of exploration [5]. In this regard, it is important to consider the BOD's fossil volcanos and volcanotectonic structures, to re-examine them with modern research methods and means.

MATERIALS AND METHODS

Remote sensing and GIS play pivotal roles in mineral exploration and regional structural analysis. This research aimed to investigate linear, curvilinear, arcuate, and circular features within the BOD, with the objective of enhancing exploration potential and for understanding geological history.

In this study, lineaments, curvilinear, arcuate, and circular features were delineated manually utilizing directional filters applied to satellite imagery (Fig. 2). We obtained suitable satellite imagery along with high-resolution Digital Elevation Models (DEMs). A GIS integrates different types of geolocated data and can be used to analyze spatial positions, organize information into layers, and then visualize the data using maps and 3-D scenes [10].

Identification of structural lineaments, integral to establishing metallogenic belts and understanding their geologic history, is crucial for delineating trends of regional mineralization and identifying exploration targets [11].

https://doi.org/10.5593/sgem2024/1.1/s01.18

In this research, GIS analysis was conducted, incorporating directional filters, geometric correction, atmospheric correction, and image enhancement techniques to enhance image quality and emphasize lineament features. To validate these geological structures, a comparative analysis was performed utilizing geological maps, supplemented by partial field observations and a thorough review of other existing data about the study area. Additionally, identified calderas were cross-referenced with known volcanic features and geological interpretations to reinforce the findings.

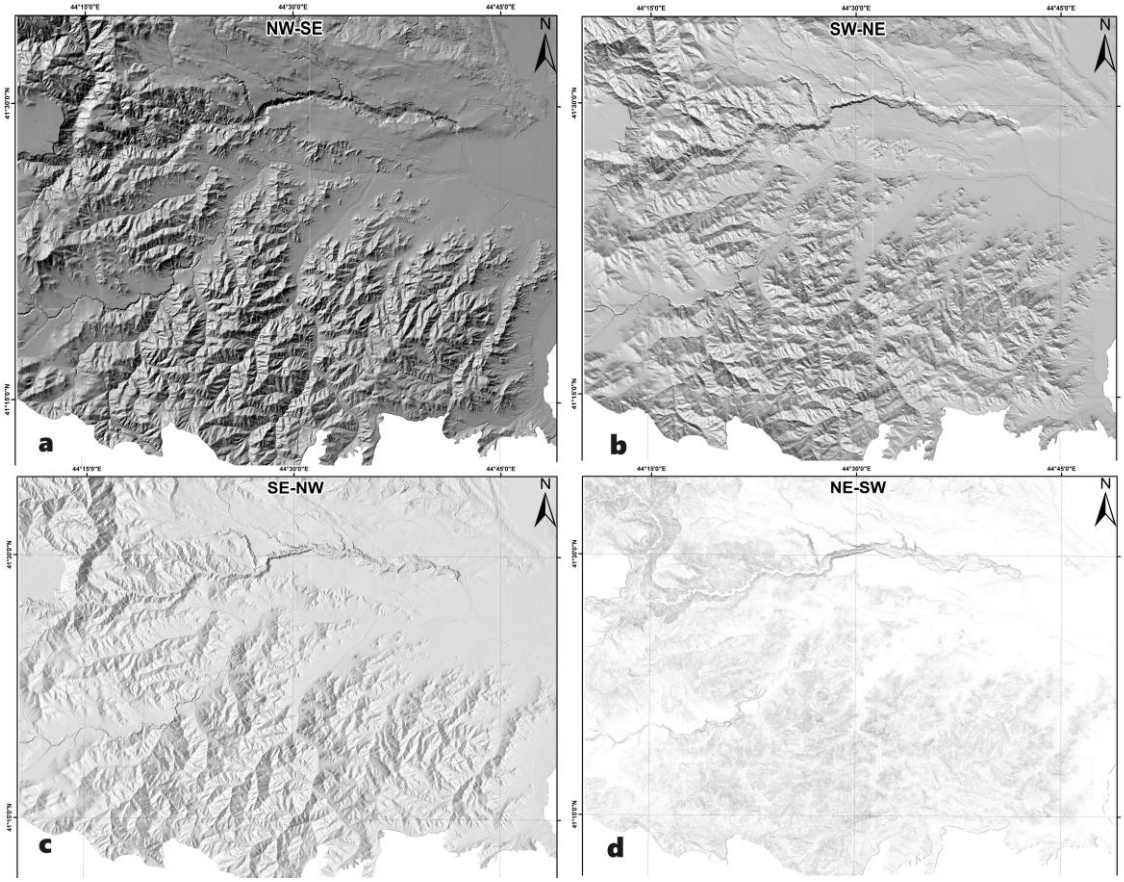


Fig. 2. Hillshade of study area with four directional filters applied: a) NW-SE. b) SW-NE. c) SE-NW. d) NE-SW.

RESULTS AND DISCUSSIONS

In our preliminary investigation of the BOD, we conducted a comprehensive review of available geological mapping data to identify key areas for further research. Utilizing remote sensing and GIS, we focused on mapping the main faults and lineaments within the region, results showed that they are predominantly oriented in the NW-SE direction. Analysis of lineament density revealed a correlation with the localization of ore deposits (Fig. 3). We manually delineated lineaments, curvilinear, arcuate, and circular features using directional filters applied to satellite imagery. High-resolution Digital Elevation Models (DEMs) were utilized alongside suitable satellite imagery. Subsequent GIS analysis involved directional filters, geometric and atmospheric correction, and image enhancement techniques to enhance image quality and highlight lineament features (Fig.

2). The fracture density map (Fig. 3) can help to identify fractures zones in the area of study (Fig. 1).

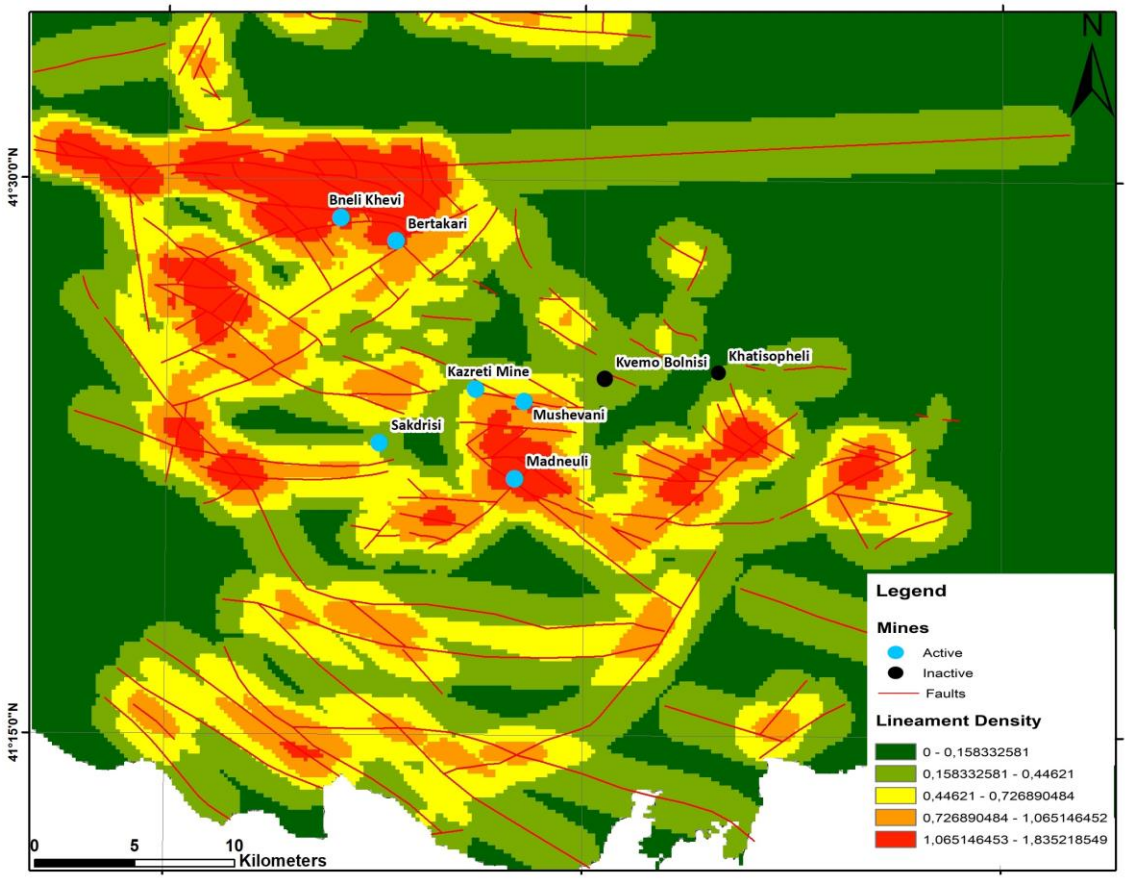


Fig. 3. The fracture density map can help to identify fractures zones in the area of study.

We compiled map from variouse geological maps [5, 14, 15], with main intrusive and extrusive rock bodies spanning from Paleozoic granitoids to Quaternary basalts. Our findings, illustrated in Figure 4, depict the spatial relationship between intrusive bodies, faults and circular structures. By using remote sensing and geological mapping data, we identified circular structures associated with volcanic processes, and volcanotectonic depressions. As this map represents the primary results, we excluded certain structures that need further validation through additional research.

Moreover, the late Cretaceous volcanic processes coupled with extensive erosion and vegetative cover present challenges in identifying circular structures [12, 13]. Therefore, our scheme includes only those circular structures with clear relief expression, ranging in diameter from 1500 m to 4500 m.

CONCLUSION

BOD has long and complicated geological development history with its tectonic location in collision zone between the Arabian and the Eurasian plates. The BOD

https://doi.org/10.5593/sgem2024/1.1/s01.18

(north-eastern part of the Artvin-Bolnisi rigid massif), was formed through Late Cretaceous magmatism driven by northeast-verging subduction of the Neothetys Ocean along the Eurasian margin. It hosts diverse types of gold and base metal deposits.

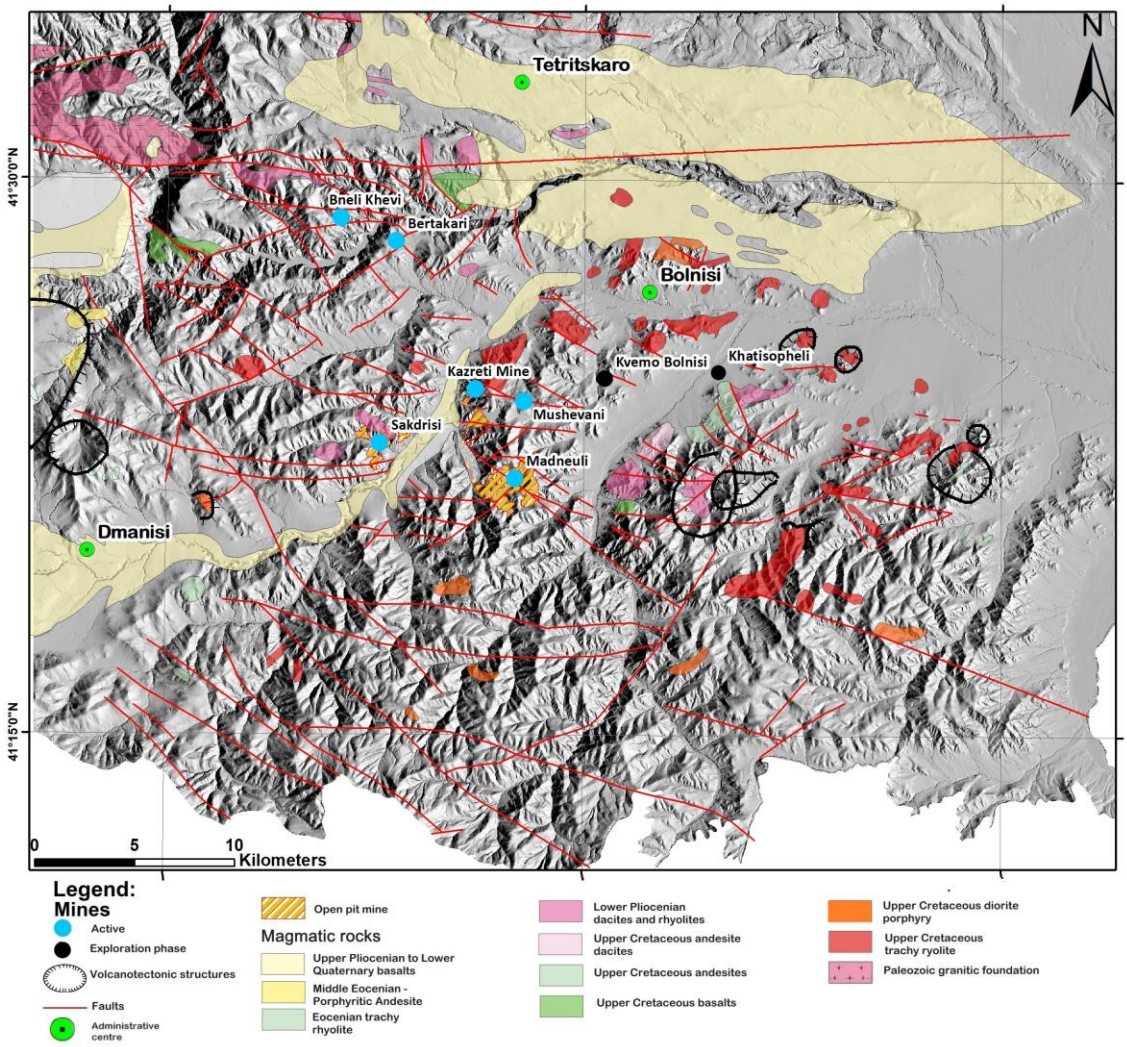


Fig. 4. Regional and local faults, volcanic circular structures and main intrusive and extrusive rock distribution in BOD. Magmatic rock formations, faults and volcanotectonic structurs were modified from various authors [5, 14, 15].

Previous studies have documented the presence of volcanotectonic depressions and calderas, highlighted by multiple authors. Structures with circular features, were assessed as post-ore formation, and some of these structures are ore-controlling [5-9]. They are intricately linked to the district's mineral deposits and are influenced by regional and local tectonics. Our preliminary investigation of the BOD aimed to map its volcanotectonic structures, contributing to a deeper understanding of its geological evolution and facilitating further advancements in this field.

We delineated intrusive and extrusive rock bodies spanning from Paleozoic granitoids to Quaternary basalts. By using remote sensing and geological mapping data, we

identified circular structures associated with volcanic processes, including calderas and volcanotectonic depressions. ranging in diameter from 1500 m to 4500 m.

ACKNOWLEDGEMENTS

This research has been supported by Shota Rustaveli National Science Foundation of Georgia (SRNSFG) (grant number PHDF-21-1718).

REFERENCES

[1] Magalashvili A., Javakhishvili Z., Elashvili M. (2013). Caucasus active tectonics – new challenges to study and new practical applications. 1st International Conference and Workshop Caucasus Active Tectonics and Magmatism – Hazards and Resources. 29 August-3 September, 2013, Tbilisi.

[2] Adamia Sh., Zakariadze G., Chkhotua T., Sadradze N., Tsereteli N., Chabukiani Al., Gventsadze Al. (2011). Geology of the Caucasus: A Review. Turkish J. Earth Sci. Vol. 20. pp.489-544. Doi: 10.3906/yer-1005-11.

[3] Gugushvili, V., Bukia, A., Goderdzishvili, N., Javakhadze, D., (2014) Bolnisi Ore District: geological development and structure, ore formation, economic potential and prospects based on data till April 2014. Caucasus Mineral Group, Georgia pp.15-20 (in Russian)

[4] Hässig, M., Moritz, R., Ulianov, A., Popkhadze, N., Galoyan, G., & Enukidze, O. (2020). Jurassic to Cenozoic Magmatic and Geodynamic Evolution of the Eastern Pontides and Caucasus Belts, and Their Relationship With the Eastern Black Sea Basin Opening. Tectonics, 39(10). https://doi.org/10.1029/2020TC006336

[5] Magalashvili, A. (2004). New economic geology factors of the Bolnisi mining district (Southern Georgia). Bulletin of Geological Institute of Georgian Academy of Sciences, New Ser. (119) 822-827 (in Russian).

[6] Little, C.,Magalashvili, A.,& Banks, D. (2007). Neotethyan Late Cretaceous volcanic arc hydrothermal vent fauna. Geology. v. 35; no. 9; p. 835–838; ttps://doi.org/10.1130/G23957A.1

[7] Zuliashvili, T., Apkhazava, M., (1985) Specialized study of paleovolcanic reconstruction, petrology of ore-bearing rocks, rock deposits, etc. / Darbazi-Abulmulk structure and exploration mapping for precious metals mineralization on a scale of 1:10,000. Caucasus Institute of Ore Deposits p.20 (in Russian).

[8] Gagnidze, M., Kvitsiani, A. (2020) Geology of Bolnisi Ore District, An overview of some issues. Mining Journal No. 1(43), (15-17) (in Georgian)

[9] Gudmundsson, A., Drymoni, K., Browning, J., Acocella, V., Amelung, F., Bonali, F. L., Elshaafi, A., Galindo, I., Geshi, N., Geyer, A., Heap, M. J., Karaoğlu, Ö., Kusumoto, S., Marti, J., Pinel, V., Tibaldi, A., Thordarson, T., & Walter, T. R. (2022). Volcanotectonics: the tectonics and physics of volcanoes and their eruption mechanics. Bulletin of Volcanology, 84(8). https://doi.org/10.1007/s00445-022-01582-4

https://doi.org/10.5593/sgem2024/1.1/s01.18

[10] Booysen, R., Gloaguen, R., Lorenz, S., Zimmermann, R., & Nex, P. A. M. (2021). Geological Remote Sensing. In Encyclopedia of Geology (Vol. 6, pp. 301–314). Elsevier. https://doi.org/10.1016/B978-0-12-409548-9.12127-x

[11] Sellepack, S., Goodell, P., Charest, A. (1996). A preliminary report on a disseminated gold prospect, Sausal, Chihuahua, México; in Grassroots Exploration in the Batopilas Region, Chi- huahua: Conf. Internac. de Mineriá, Chihuahua, p. 231-236

[12] Lezhava, Z., Asanidze, L., Tsikarishvili, K., Gaprindashvili, G., Chikhradze, N. 2019. About genesis of karst caldera of denudation-tectonic landform. Georgia, Caucasus. SGEM. 19 (1.1), 3-10. https://doi.org/10.5593/sgem2019/1.1/S01.001

[13] Hede, A. N. H., K. Koike, K. Kashiwaya, S. Sakurai, R. Yamada, and D. Singer (2017), How can satellite imagery be used for mineral exploration in thick vegetation areas?, Geochem. Geophys. Geosyst., 18,584–596, https://doi.org/10.1002/2016GC006501

[14] Gamkrelidze, M., Abutidze, O., Kordzadze, M., Gaprindashvili, M., Tedoradze, D., Kumladze, R., Gzirishvili, T., (2016) Tbilisi (K-38-XXI) geological mapping report (Part 2) Tbilisi, Georgia (in Georgian)

[15] Pruidze M., Khabelashvili A., (1985) – Report of the Bolnisi geological mapping survey scale 1:50,000 sheets K-38-89-A, and K-38-90-A, Funds of the “Georgian Geology“.

SECTION HYDROGEOLOGY,

ENGINEERING GEOLOGY AND GEOTECHNICS

ANALYSIS OF ENGINEERING PROTECTION EFFECTIVENESS OF THE KYIV-PECHERSK LAVRA TERRITORY BASED ON LONG-TERM HYDROGEOLOGICAL MONITORING

CSc. Iryna Cherevko[1]
CSc. Tetiana Kril[2]
CSc. Dmitri Bugai[2]
Prof. DSc. Stella Shekhunova[2]

[1]National Reserve "Kyiv-Pechersk Lavra", **Ukraine**
[2]Institute of Geological Sciences of the NAS of Ukraine, **Ukraine**

ABSTRACT

The extensive network of engineering protection of the territory of the Kyiv-Pechersk Lavra against the impact of hazardous processes (landslides, flooding) includes more than 5 km of retaining walls (brick, concrete, pile-based) and about 12 km of drainage networks (tunnel, gallery, and radial types). The effectiveness of the drainage adit systems (DAS) on the Upper Lavra and the radial drainage on the territory of the Guest Yard (Inn Courtyard) of the Lower Lavra was analyzed. The paper proposes an assessment of the efficiency of drainage adit systems according to such criteria as the specific flow rate q (m^3/day) and the specific removal of sediments v (m^3/year) into the tunnel, the efficiency is determined as poor (q=0.001...0.02, v=0.11...0.2), sufficient (q=0.021...0.1, v=0.017...0.1), or high (q=0.11...0.5, v=0.011...0.016). Patterns of groundwater supply, the lithological composition of the transported material, exogenous geological processes occurring in drainage areas, the amount of groundwater flow reaching the surface, and technical aspects of drainage system were analyzed. The results were obtained based on the analysis of the measured flow rates and data on sediment removal from 1980 to 1990. The efficiency of DAS-28 is assessed as sufficient and high. The effectiveness of radial drainage is measured as the flow rate of groundwater levels in monitoring boreholes and the reduction of moisture content in building structures. On the territory of Guest Yard, as a result of the work of radial drainage, the groundwater levels in monitoring boreholes dropped by 0.6-0.9 m, the moisture content of masonry walls reached the control level (4-6 %), periodic flooding with meltwater stopped. Monitoring observations for 2006-2023 were analyzed as well.

Keywords: Kyiv-Pechersk Lavra, architectural monuments, deformations and cracks, drainage systems, hydrogeological monitoring, specific discharge, specific removal, engineering protection.

INTRODUCTION

Kyiv-Pechersk Lavra is a unique historical, cultural and architectural heritage site underlain by varying geology and hydrogeology and affected by natural hydrogeological factors and significant human-induced activities [1-3].

The territory of the Lavra, with an area of 23 hectares, is divided by the edge of the Lavrsky Ravine into two almost equal parts – Upper and Lower Lavra, Fig. 1. The buildings of the Upper Lavra are based on loess rocks (up to 15 m), with elevation

https://doi.org/10.5593/sgem2024/1.1/s02.19

marks of 180-196 m. The structures of Lower Lavra are located on the slopes and within the soil layers of the Lavrsky Ravine, which has an angle of inclination of 23-26°, with a range of elevation marks from 170 to 118 m.

In Quaternary and Paleogene soils, aquifers with the possibility of overflow are common. In some areas of Lower Lavra, the formation of a temporary aquifer (temporary perched water) is observed, which is associated with seasonal changes, as well as human-induced accidents.

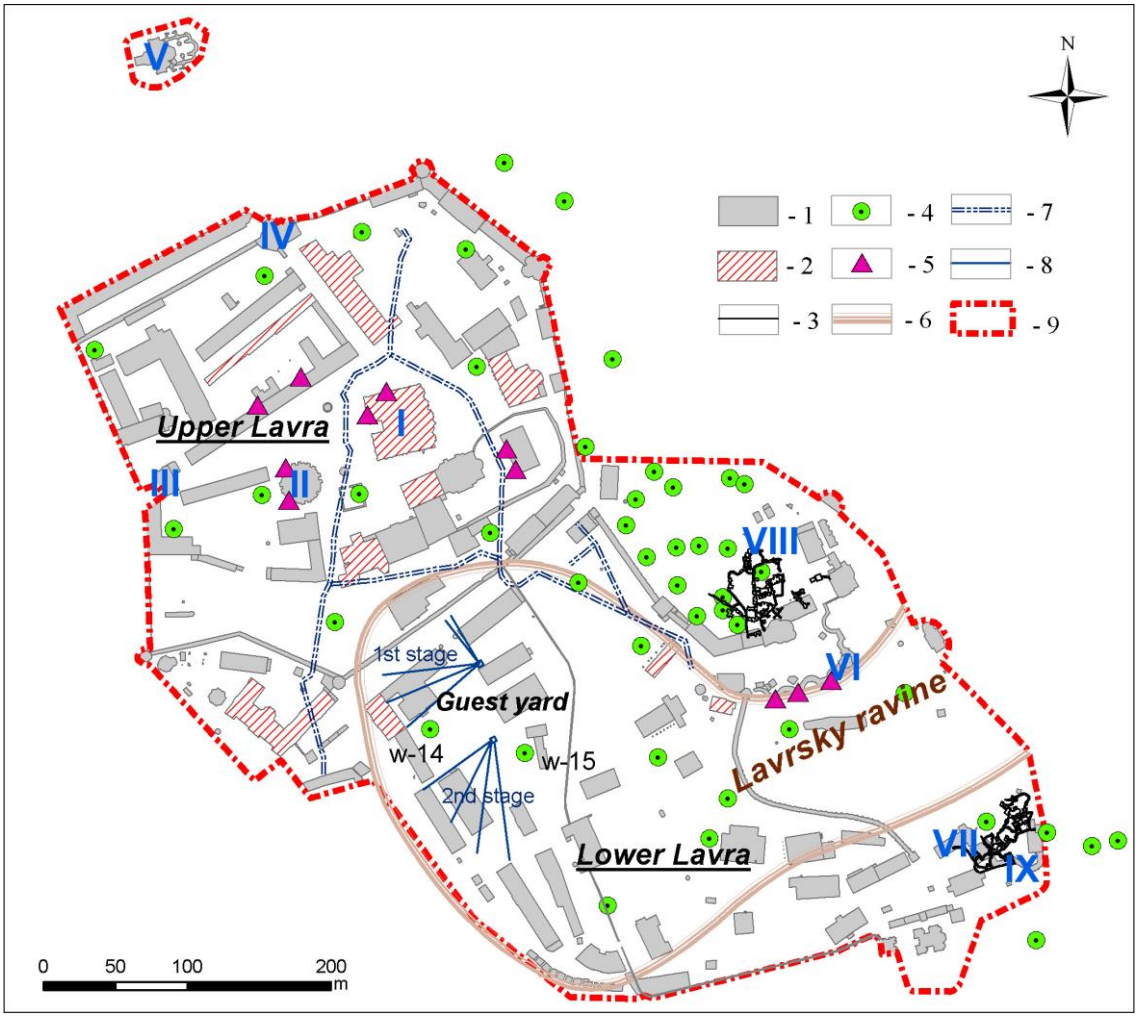


Fig. 1. Scheme of the Kyiv-Pechersk Lavra territory: 1 – historical buildings; 2 – buildings under deformation and cracks; 3 – caves; 4 – monitoring wells; 5 – geodetic benchmarks and marks; 6 – the edge of the Lavrsky Ravine; 7 – drainage adit system (DAS-28); 8 – radiation drainage (1st and 2nd stages); 9 – boundary of Lavra. Caption on main architectural monuments: I –Dormition Cathedral, 11 cent.; II – the Great Lavra Bell Tower, 18 cent.; III – Gate Church of the Trinity, 12-18 cent.; IV – All-Saints Church, 18 cent.; V – Church of the Saviour at Berestove, 12-19 cent.; VI – D. de Bosquet retaining wall, 18 cent.; VII –Church of the Conception of St. Anna, 17 cent.; VIII – Near Caves, 11 cent.; IX– Far Caves, 11 cent.

The unique buildings (landmarks) of Lavra suffer from flooding with groundwater and capillary rise of moisture, subsidence, landslides, suffusion processes, and sinkholes.

The heritage site is affected by strong foundation material damping, muddying of walls, deformation of structural elements, formation of cracks, etc [3, 4]. The hazardous effects are mostly derived from changes in local hydrogeological situation following abnormally severe meteorological effects, accidents on water supply networks, and excessive watering of vegetation in the gardens of Lavra.

From the 17th century, various types of engineering structures were erected to strengthen the slopes, and to drain underground and surface water on the territory of Lavra. Over time, individual buildings lost their protective functions or were not effective enough, they were re-equipped, and new ones were built.

At the end of the 19th century, water supply systems and sewage networks were built on this site, wear and tear to which creates accidents such as bursts of both cold and hot water networks in the soil layers of both the Upper and the Lower Lavra.

In order to improve and develop protective engineering measures, a system of hydrogeological monitoring of the site was launched in 1990. Currently, its system includes 48 monitoring wells, geodetic benchmarks, humidity and other sensors on buildings (see Fig. 1).

Therefore, the main purpose of this research was to analyze the effectiveness of the engineering protection of the Kyiv-Pechersk Lavra territory based on long-term hydrogeological monitoring.

MATERIALS AND METHODS

The scheme of engineering protection of the territory (scale 1:1000); the plan of the current state of the Reserve (scale 1:1000); data of engineering-geological surveys [5-8], geodetic plan (scale 1:500); data of engineering and geological investigations, historical and archaeological materials are used. The documentation used includes technical passports of drainages, data of monitoring observations on soil removal, and water flow rate.

To establish the efficiency of the drainage adits, we suggest using two main criteria – the specific flow rate (m^3/day) of the workings and the specific soil removal of (m^3/year) in the workings.

The maximum values of flow rates of 14 DASs on the territory of Lavra and the buffer hydrogeological zone are 0.5, the minimum values are 0.001 (m^3/day). According to long-term observations, the sediment removal in the drains varies from 0.001 to 0.2 m^3/year. Based on these indicators, three degrees of their effectiveness and the corresponding consequences for the soil are shown in Table 1.

The low specific flow rate of the production indicates the incorrect location of the excavation, its remoteness from water-bearing soils, and therefore the inefficiency of its functioning. A significant specific flow rate of the production is a sign of its correct location in the series or at the contact of aquifers.

Significant soil removal takes place in the areas of excavations passing through bulk soils of different lithological and mechanical composition.

Table 1. The efficiency of drainage systems according to indicators of specific flow and removal

https://doi.org/10.5593/sgem2024/1.1/s02.19

Efficiency	Specific flow rate, *cubic meter per day*	Specific removal *cubic meter per year*	Consequences
Low	0.001…0.02	0.11…0.2	The drains do not perform their function of draining groundwater and work only as collectors or storm drains. This leads to a significant weakening of the soil mass in the drainage adits zone due to suffusion and densification.
Sufficient	0.021…0.1	0.017…0.1	The operation of the drains does not negatively affect the condition of the soil mass, the moisture content of the protected structures is stable.
High	0.11…0.5	0.001…0.016	The maximum flow indicates a significant amount of groundwater entering the drainage adits, and therefore high efficiency of the drainage adits.

An important efficiency factor is the non-uniform flow of groundwater into the production, when out of several dozens of filters, a significant flow rate is characteristic of only one or two filters. This indicates the presence of directed water flows in the soil layer, and therefore the work of only a small part of the drainage is effective, and the other part works only as a collector.

Therefore, the uniformity of the inflow of groundwater into the drainage adits, the lithological composition of the removed or accumulated material, the absence of exogenous geological processes in the drainage areas throughout their functioning, the absence of groundwater exits to the surface, the technical condition of the drains, in addition to the selected indicators of drainage efficiency, should be assessed beforehand and indirectly – flow rate and removal.

For shallow radial drainage system, the efficiency indicators include a decrease in groundwater levels in monitoring boreholes, and a decrease in humidity indicators of building structures of architectural monuments.

RESULTS

To strengthen the buildings and to prevent the development of landslides on the slopes of Lavra retaining walls, ranging from low (2-4 m) to high (5-16 m) were constructed starting from the 17th century. Today there are more than 5 km of retaining walls (brick, concrete, and pile-based). In addition to maintaining the soil mass, the retaining walls retain groundwater, creating a barrage effect, which sometimes leads to the concentrated flooding of monuments, such as the Near Caves. In order to remove the support and drain groundwater, discharge holes were arranged in the walls, which made it possible to protect individual labyrinths of the Near Caves from flooding.

The efficiency of retaining walls in supporting soil and ensuring the long-term operation of structures requires the use of additional drainage measures.

At the beginning of the 19th century drainage systems were used to prevent the development of landslides caused by the overwetting of the soil mass by underground and surface (percolation) waters. Today, there are about 12 km of drainage tunnels and galleries, including rainwater drainage pipes and shallow drainages.

Deep-seated drainage tunnel system

DAS-28 tunnel was built in 1936-1938. The total length is 886.5 m (see Fig. 1). The channels are trapezoid in cross-section, made of reinforced concrete; there are altogether 15 wells. The average absolute marks of the trays are 156-161 m. The excavations are located in variegated (N_1sg) and brown clays (N_2čb), at a depth of 30 m.

To determine the efficiency of the drainage system DAS-28 operation, we analyzed the regime of flow rates (measured at certain network points) and specific discharges (calculated), as well as the volumes of salt and fine soil removal (according to the results of sediment removal) from 1980 to 1989. The total discharge of the DAS-28 according to observational data is 190-350 m^3/day, specific – 0.068-0.362 m^3/day, specific removal – 0.011-0.073 m^3/year. According to these indicators, DAS-28 has a sufficient and high degree of efficiency, respectively.

Figure 2 shows the regime of specific flow rate and specific sediments removal. An increase in flow rate after clearing and the onset of a stationary mode of water inflow into the drainage adits can be clearly observed, which contributes to the stabilization of the geodynamic conditions of the soil mass as a whole.

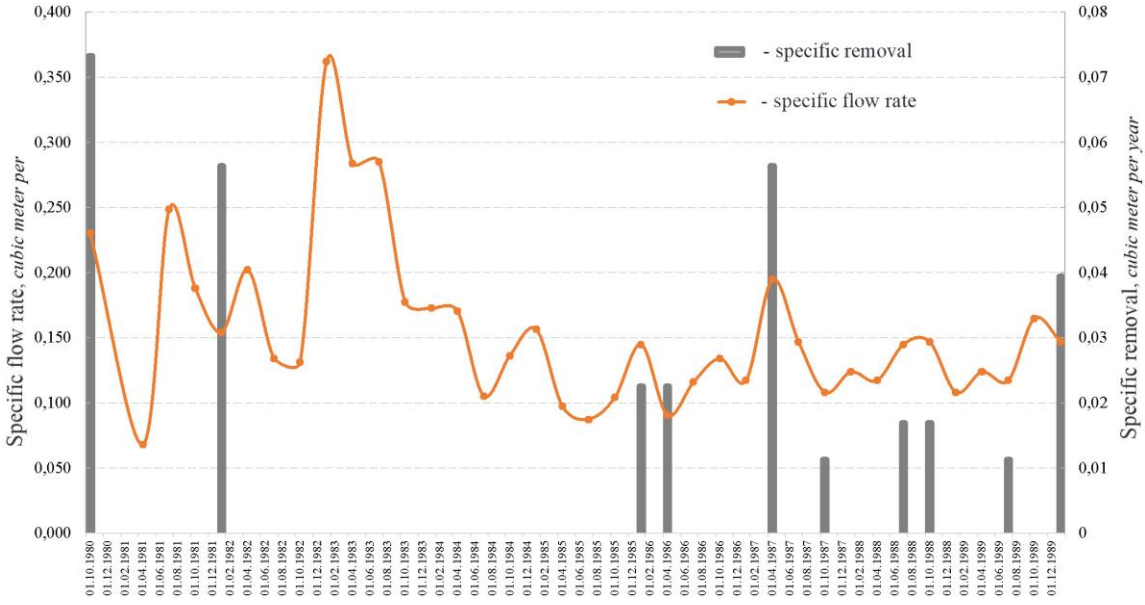


Fig. 2. Comparison of specific water flow and specific removal for DAS-28.

Radial shallow drainage.

On the territory of Lower Lavra within the boundaries of the Guest yard (see Fig. 1), drainage by non-destructive methods was used for the first time. In this area, the level of

https://doi.org/10.5593/sgem2024/1.1/s02.19

groundwater in deluvial deposits lies at a depth of 1.7 to 4.2 m and fluctuates over time, according to observations for 0.5–2.3 m. Fluctuating levels are associated with a low depth of the soil aquifer and the effect of atmospheric precipitation and human-induced leaks on the percolation depth. In 2014, in order to eliminate damping of the building foundations (buildings nos. 54, 55, 60, 56, 57, 98) and to reduce groundwater level, radial drainage system was arranged [9-12]. The first stage consists of five channels, with a total length of 277 m, equipped with filter columns 108 mm in diameter and a water receiving chamber 4×4×6 m. The channels are located at a depth of 4 – 6 m from the day surface.

Graphs of Fig. 3 clearly show the effective operation of the radial drainage of the first stage of the groundwater lowering project on the territory of Guest yard (drainage of building no. 68) – the groundwater level has dropped by 1 m in well 14, which is located at a distance of about 7 m from the drainage tunnel. Ascents of groundwater level in well 14, recorded by regime observations, caused by catastrophic accidents of the main heating network in February and April 2018, emergency leaks from local networks.

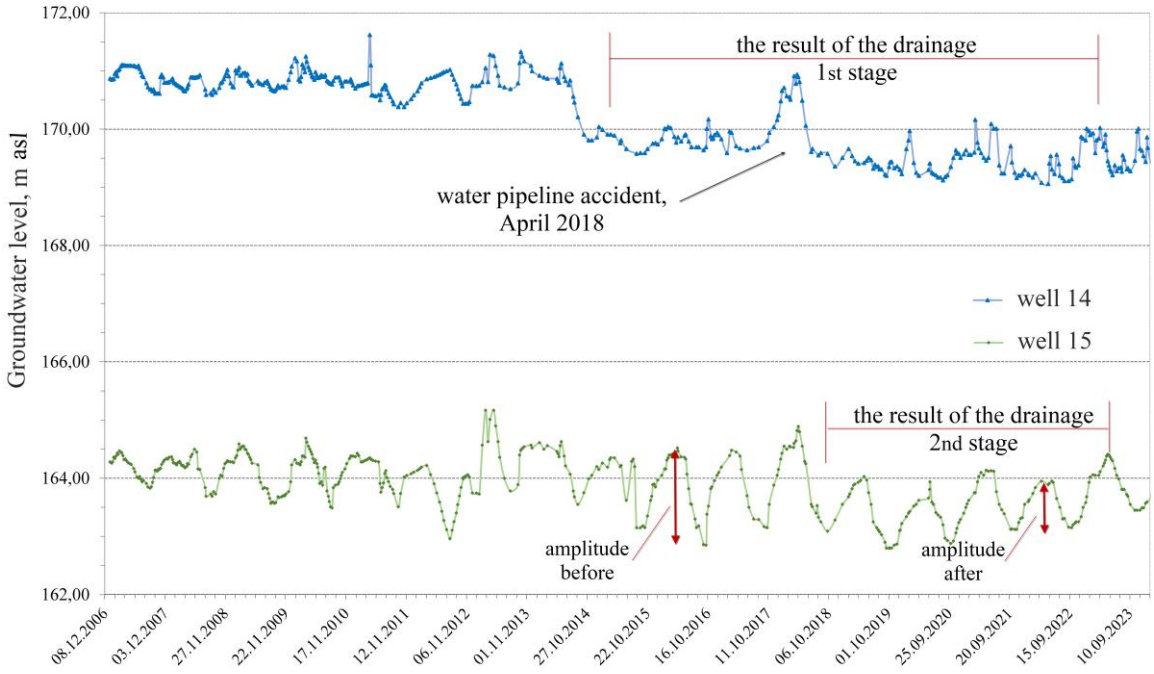


Fig. 3. Groundwater level reduction in observation wells near the radial drainage.

In contrast, the graph of the groundwater regime in 2012–2016 for well 15, located between buildings nos. 60 and 98, shows significant fluctuations depending on the season of the year and emergency leaks, which indicated the need for water lowering in the adjacent territory. This was confirmed by the progressing deformations of building no. 98.

In May-July 2018, the construction of the second stage of the radial drainage was completed (buildings nos. 56, 98). It consists of four channels with a total length of

275 m, equipped with filter columns 100 mm in diameter and a water receiving chamber 4×4×3 m. The channels are located at a depth of 2 – 6 m from the day surface.

Their implementation led to a general decrease in the groundwater level in well 14 by another 0.4–0.5 m, in well 15 (which did not fall into the zone of direct influence of the drainage) – to a general decrease in the groundwater level to 0.3-0,5 m and a decrease in the amplitude of oscillations. Thus, the first and second stages of radial drainage on the territory of the Lower Lavra Guest yard are classified as highly effective measures to protect areas and buildings from flooding.

DISCUSSION

High and sufficient effective operation of drainage systems according to the criteria proposed above varies due to the drawbacks and advantages of these systems and effect of extreme weather.

The disadvantage of deep-laying drainage systems is the slow ability to intercept huma-induced leaks and the slow response to the infiltration of atmospheric precipitation. Their undoubted advantage is the leading role in stabilizing the soil (since the drainage adits are usually located parallel to the slope, over time the water inflow to them acquires a stationary (permanent) regime, which ensures the stability of the soil mass).

CONCLUSIONS

The territory of Lavra is equipped with many types of engineering protection systems against engineering and geological hazards. It was established that the key factor in their development is changes in hydrogeological conditions due to abnormal meteorological conditions, accidents on water supply networks, etc.

The analysis of the data of long-term hydrogeological monitoring showed that the effectiveness of protective structures, such as drainage adits, must be evaluated according to the following indicators: specific flow rate, soil removal, uniformity of groundwater inflow into the excavations, absence of exogenous geological processes in the areas of the drainage adits, absence of groundwater exits to the surface, the technical condition of the drainage structures. Centripetal drainage shows its effectiveness in lowering groundwater levels in observation wells and improving the moisture regime of architectural monuments.

For the conditions of the plateau (Upper Lavra), deep-seated tunnel drainage systems are efficient. For the areas of slopes of streams and ravines (Lower Lavra), it is advisable and efficient to use shallow radial drainage systems with the appropriate location of the drains.

ACKNOWLEDGEMENTS

The authors acknowledge the funding received by the National Research Foundation of Ukraine from the state budget 2022.01/0209 “Complex research of the geoecological state of preservation of the historical and cultural heritage objects of the National Reserve "Kyiv-Pechersk Lavra" in the conditions of military operations” (NRFU Competition “Science for the Recovery of Ukraine in the War and Post-War Periods”).

https://doi.org/10.5593/sgem2024/1.1/s02.19

REFERENCES

[1] Kyiv: Saint-Sophia Cathedral and Related Monastic Buildings, Kyiv-Pechersk Lavra URL: https://whc.unesco.org/en/list/527/maps/

[2] Kril, T. & Cherevko, I. Identification on Unstable (Landslide Hazard) Areas on Lavra Far-Caves Hill. Fourth EAGE Workshop on Assessment of Landslide Hazards and impact on communities, Sep 2023, 2023, 1 – 5. https://doi.org/10.3997/2214-4609.2023500017

[3] Demchyshyn, MG, Kril, TV. (2019) Improvement of the Engineering Protection Systems of the Kyiv-Pechersk Lavra Reserve Territory, Nauka I Innovacii, 15(3), 37–51. https://doi.org/10.15407/scin15.03.037

[4] Kril T., Shekhunova S., Cherevko I. Identification of Potentially Unstable Areas by Engineering and Geological Processes Monitoring and Heritage Building Deformations. 17th International Conference Monitoring of Geological Processes and Ecological Condition of the Environment, Nov 2023, Volume 2023, p.1 – 5. DOI: https://doi.org/10.3997/2214-4609.2023520203

[5] Geological map of Ukrainian USSR of scale 1:50 000. Kyiv industrial area (1984). Explanatory note in 2 parts. Kolot Ye.I., Kuzyshyna L.P., Kutovoi V.Y., Lavryk V.F., Marakhovskaia Y.Y., Selyn Yu.Y., Solovytskyi V.N., Shestopalova E.V. Kyiv

[6] Golub V.P., Petrenko E.Yu., Polishchuk V.I. (2011) Technical report on engineering and geotechnical investigations on the site and examination of the technical condition of the object: "Varyaz Caves of the Holy Assumption Kyiv-Pecherska Lavra on St. Lavrska in the Pecherskyi district of Kyiv" (first stage). SE VCBK, 78 p

[7] Zhadan P.P., Martynenko M.B. (2012) Scientific and technical report on engineering and geological surveys to ensure engineering protection of the territory of Nizhnya Lavra (in the area of buildings No. 71-1, 51-52) on St. Lavrska, 15 in Kyiv. GEOLOG-BUD LLC, 54 p

[8] Arkhipenko A.O., Gavrusyeva S.S. Technical report on the results of engineering and geological surveys for the rehabilitation of the building of the building No. 57 (cells of the Guest House) of the Holy Dormition Kyiv-Pechersk Lavra in the Pechersk district of Kyiv. Comprehensive construction services LLC. 2006, 38 p.

[9] Radial drains to protect against flooding of territories and structures: SOU Housing and Housing 04.08-006:2010. Kyiv, Ministry of Housing, Commune and Agriculture of Ukraine, 2010. 75 p.

[10] Gorokhov V.A. Lunts L.B., Rastorguev O.S. Engineering improvement of urban areas. 1985, 389 p.

[11] Methodical recommendations for design and construction technology of walled and trenchless tubular drainage structures. Moscow. SOYUZDORNYI, 1989, 132 p.

[12] Torokhtii M.Yu. Regular observations of the debits of radial horizontal drainages on the territory of the Holy Dormition Kyiv-Pechersk Lavra Scientific and technical report. LLC "M-BUD". 2021, 33 p.

COMPLEX ENGINEERING DESIGN OF COASTAL PROTECTION

Assoc. Prof. Dr. Miroslav Todorov [1]

Eng. Mihail Todorov[2]

[1,2]Konstruktivno Proektirane EOOD, **Bulgaria**

ABSTRACT

In the face of an ever-evolving environment, a crucial challenge emerges concerning the dynamic interplay between the sea and the land. Amidst these complexities, a fundamental question arises: should human intervention seek to reshape the natural processes, or should it primarily focus on comprehensive understanding, aiming to maintain a semblance of equilibrium? These intricacies, along with several important technical considerations, underscore the imperative to safeguard coastal regions against the escalating impact of the sea. This study, in response to the urgent demands of the environment, examines a distinct section of the offshore expanse of the Black Sea, where the ceaseless advance of the sea erodes nearly 10 meters of land area annually.

The research embarks on a multidimensional exploration, encompassing an analysis of climatological data, meticulous observation of marine circulation patterns and litorial drift, geological investigations of the area, and a holistic assessment of potential scenarios—ranging from the optimistic to more conservative. Drawing on a robust foundation of studies conducted over the past quarter-century, coupled with insights obtained during the design process, the study establishes a projection extending to the 2100. Encompassing a coastal span of 11 kilometers, the quantitative parameters derived from these comprehensive studies lay the groundwork for the formulation of innovative solutions.

The project's design blueprint encompasses intricate coastal protection systems, including the construction of peninsulas, remote defense mechanisms, and anti-abrasion structures within the intertidal beach zone. Tailored to the distinctive sediment dynamics of this specific coastal stretch, the project is uniquely oriented towards fostering conducive conditions for the accumulation of beach formations and, crucially, a substantial reduction in direct maritime incursions. Illuminated by sophisticated predictive models, which underpin the complex design choices, the forecasts suggest a promising trajectory for the coming decade—a trajectory marked by commendable progress and a considerable curtailment of the sea's encroachment onto the land.

Keywords: Geological investigations; Geotechnical engineering; Coast Protection; Sustainable Design

INTRODUCTION

This analysis covered a part of the North East Black Sea coast of Bulgaria and the reasoning behind its development lies in the occurring processes of intense abrasion, which led to significant losses of agricultural land within the section under consideration. The area covers the coastline with a length of – 11000 m in the aquatory, with a dismemberment factor of 1.06 0.

https://doi.org/10.5593/sgem2024/1.1/s02.20

The coast has an east-northeast exposition. A vertical cliff coast prevails with a height of 6.0-19.0 m in the northern part to 6.0 m at Cape Shabla. The upper coast zone is made of loess and loess-shaped clays. Close to the middle sea level stratigraphic height are located shellfish limestones of the Karvuna formation. These materials are covered by the silty materials loess and loess-clays and thanks to this structural feature intensive abrasion takes 2-3 m per further intensified in the period January-March.

The complexity of the project and its design situations stems from the multitude of factors, both natural and anthropogenic contributing to the ever changing landscape.

DIRECTIONS OF RESEARCH

The main objective of this study was to create a sufficient set of data through which to design coastal protection facilities as the main focus is to be of the passive type. The research of the district began in March 2018 with systematic geodesic measurements of the coastline and the seabed in a 200-meter zone of the coastline. Given the geomorphology, this process took 3 months and within this period significant changes were registered in the thin beaches (Figure 1). These geodesic investigations were combined with the series of in-situ measurements and photogrammetry data collected for the past 50 . Also, within the framework of the geodetic surveys, data from archival maps, documents, planning permissions and materials of the zone were used.



Figure 1. General view of the beach with the coastal slope.

The second direction of the research scope was centered around marine water circulation and littoral drift. Based on data from the study of marine circulation, 12 scenarios were compiled and presented with different confidence intervals. The waves generated in the

deep sea undergo numerous changes as they move towards the coast. Most often, these changes are expressed as:

- Transformation, due to the reduction of the depth of the water in the shallow regions and refraction, which occur when the wave meets the seabed (which requires detailed photographing of the topography). Attention should also be paid here to the fact that at such small depths up to 3-4 m, the use of conventional geophysical methods is very difficult;
- Braking of the wave that occurs when the wave becomes too steep. Given the geometric features of the steep coast, the thin beaches and the wave height, the breaking wave can affect almost the entire lower half of the coastal cliffs;
- Interaction with or reflection from reefs, where present near the coast. By capturing the morphology of the seabed, it was found that the bottom can be represented by a wavy surface that implies the development of diffraction processes;
- Diffraction around capes or other natural barriers (in practice, on a wide scale this phenomenon is observed around the peaks of islands);
- Creep of the waves along the coasts.

According to the bathymetric studies, the isobath with a depth of 8 m is about 500-700 m away from the coastline, the isobath with a depth of 4 m is about 320 – 400 m inwards within the sea, and the isobath of 2.5 m is about 150 -180 m. This implies a slope of the seabed in the surf zone between 0.016 and 0.010, as in the area of the facilities around isobaths 2.0 m the slope is in the range 0.011 – 0.013.

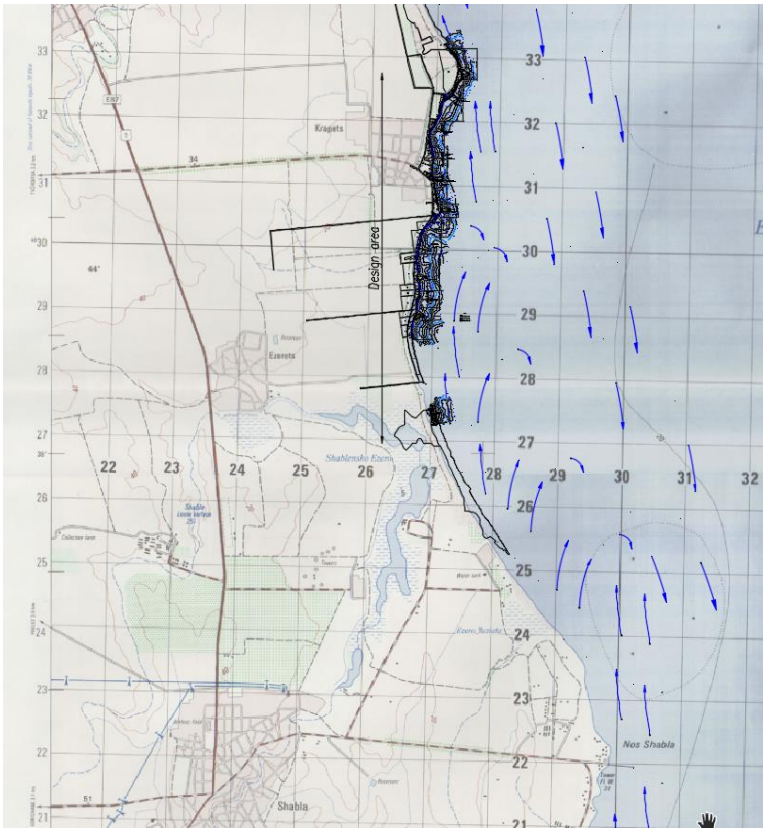


Figure 2. Schematic of shore energy circulations 0.

https://doi.org/10.5593/sgem2024/1.1/s02.20

The circulation of water masses in the coastal sea area is an extremely complex phenomenon, conditioned by a number of factors independent in nature and cause of occurrence - such as variability of water density in depth and plan, wind and wave impact, bottom relief and coastal outline, natural and induced phenomena of a random nature (Figure 2).

The results of a number of previous studies suggest that extreme climate processes will increase in frequency and impact, as a result of which the coastal erosion processes caused by the wave impact will accelerate. This will inevitably have an impact on the built coastal protection and port facilities.

As temperatures increases, ocean water warms, accelerating the melting of glaciers and ice caps, causing sea levels to rise, accelerating abrasion processes, furthermore one-directional winds intensify as a result of the changing climate, and leading to surface gravity waves (sea swell). In addition, warmer waters give rise to more powerful hurricanes that cause serious physical and economic damage. In the next Table 1 the expected rise in temperatures and water levels predicted with 2 scenarios up to the 2100 are shown. The data represents a summary sample from the previous 25- period, a review provided by the National Institute of Hydrology and Meteorology.

Table 1. Expected increase in temperature and sea level in the next 75 years.

		2025	2050	2075	2100
Average annual temperature increase (in degrees Celsius above the recorded 2000 temperature)					
Optimistic scenarios	° F	0.6	1.1	1.7	2.2
	° C	0.3	0.6	0.9	1.2
Pessimistic scenarios	° F	2.4	4.9	7.3	9.7
	° C	1.3	2.7	4.1	5.4
Sea level rise (meters above the recorded 2000 level)					
Optimistic scenarios	in	1.8	3.5	5.3	7.1
	cm	4.5	9	13.5	18
Pessimistic scenarios	in	11.3	22.6	34	45.3
	cm	28.8	57.5	86.3	115

Along with these studies the shore slope has been studied from the point of view of its stratigraphic structure and for the purpose of this study a system of boreholes have been executed in order to define the boundaries between the rock and the soil strata.

Based on a field studies, a drilling survey from February 2019 and a detailed survey of the area from Shabla Lake to Cape Posta (North of Krapetz village), a discovery of Neogene and Quaternary sediments is established. In the Shallow Water part, the materials of the Karvuna formation (kvN1s) are revealed. These are limestones - organogenic, shellfish and highly karstified in past periods. In the uppermost horizon of the stratigraphic cross section, above the limestones are deponed eolian and alluvial-diluvial silty-clayey materials.

Above them with a wide distribution lie loess and lossy clays (Quaternary-eQp2-3), which can be divided into two horizons.

As a result of the synthesis of this information and the general geomorphology of the area leads to the conclusion that the main source of the deterioration of the beaches in the area as well as the sediments is stemming from the development of abrasion and erosion processes in the coastal slope.

MATERIALS AND METHODS

Preliminary analysis of the geodesic information of the submerged and coastal slope studies, leads the authors of this project to investigate design options to optimize the engineering solution in terms of achieving the investment objectives:

Topography (analysis of bathymetric measurements) and geodesic measurements on land;

Studies on lithodynamics and marine circulation;

Technological solutions for protective construction works.

Reduction of the amount of bulk materials to be delivered from areas of greater distance. During the studies for the presence of rock materials, material sources with a distance of 80 to 90 km were found. These deposits have the available materials from the Ruse formation (rs K1ap -Valchi dol, Bojurovo) which can be utilized.

In order to ensure sufficient mitigation of the wave behind the protection facility, the height of the crown of the breakwater above the calm water level must be at least as high as the height of the design wave. The results of the conducted studies show 0, 0, that if the average maximum water level in a storm reaches the crown of the breakwater, half the wave height will pass over it. If the crown of the facility is located at a height equal to the height of the wave above the water level, about 15% of it passes through it. If the crown of the breakwater is located at a depth equal to the height of the wave, then about 85% of the wave will pass through the facility.

This process of passing the wave through the protective equipment and is defined by a wave passing coefficient: K_t

$$K_t = \frac{H_{m0,t}}{H_{m0,i}}$$

$H_{m0,t}$ is the height of the significant wave passed;
$H_{m0,i}$ is the height of the significant initial wave.
The limits within which the pass coefficient is logical to accept in the final limits of K_t = 0 (no transmission) and K_t = 1 (full pass i.e. no reduction in wave height).
In the present project, the upper edge of the breakwater of the bounces is foreseen at elevation +3.3 m. With swelling of the water level by 1.35 m, the freeboard is =2.0 m. For a ratio of =2.0/3.0 = 0.675, adopted $R_c \frac{R_c}{H_s}$ 0 according to a pass factor value of K_t= 0,1÷0,25. Other studies on this behavior, which are convenient to use for the purpose of comparative analyses, are presented in 0.
In this project, two methodologies have been used to evaluate the mass of the protection blocks 0, 0.

https://doi.org/10.5593/sgem2024/1.1/s02.20

$$m = \frac{3{,}16K_{fr}\rho_s H^3}{\left(\frac{\rho_s}{\rho_w}-1\right)^3\sqrt{1+cotg^3\varphi}}\sqrt{\frac{\bar{L}}{H}},$$ where:

K_{fr} - coefficient =0.008 for the protective tetrapods;
m - mass of the individual element of the protective layer of the breakwater, kg;
ρ_s - specific density of the material from which the elements are made, the specific case for the demonstration analysis was selected a specific density of 2400 kg/m^3;
ρ_w - volumetric weight of water (sea water = 1018 kg/m^3);
H – wave height; $cotg^3\varphi$=1.5 - slope;

$$m = \frac{3{,}16.0{,}008.2400.3^3}{\left(\frac{2400}{1018}-1\right)^3\sqrt{1+1.5^3}}\sqrt{\frac{80}{3}} = 1618 \text{ kg}$$

For comparison, other methods were used in this project to determine the weight of the rock blocks 0 and other studies examined by the Design Manual of Coastal Project Elements (2020).
In the basic design criteria, it is assumed that cladding blocks should be sized accordingly for durability during dimensional events, although in individual severe storms some destruction is allowed, as there is usually enough time between design events for damaged areas to be repaired. When analyzing the stability of the cores of the sea dikes, their behavior can be modelled as discretely interactive. Dependence by which the required unit size (weight) of the protective elements of breakwaters is to be determined 0, 0, 0.

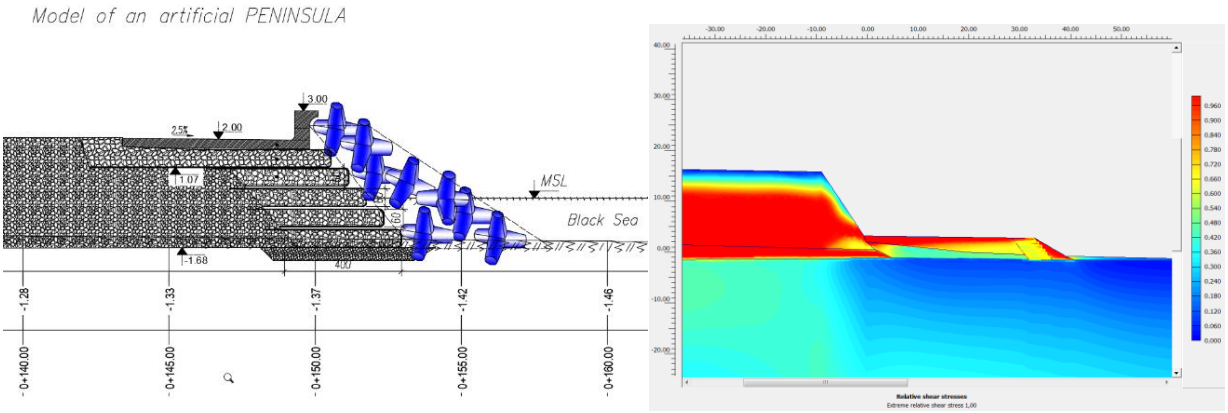


Figure 3. Model and Surfaces of Destruction at Ultimate Limit State Reach.

These analyses take into account the scale of the design situation, the available facilities and the impact of harmful processes on the built-up area. The computational geotechnical analyses were conducted using the software product PLAXIS 8.5, version 2D. Two main physical models of the software were used – Mohr-Coulomb 0 and Modified-Cam-Clay 0. Through the use of software modeled the behavior of artificial peninsulas and offshore breakwaters as with these models were conducted a series of analyses assessment of the ultimate and operational limit states. One of the computational models used is shown in Figure 3.
The construction of the protected peninsulas and offshore protection facilities is designed through a multilayer saturated structure which consists of the following elements:
Indoor unit 1 unsorted crushed stone material;

- ✓ The periphery of the fill capsulated in geogrid 2;

- ✓ Surface protection of concrete with wave breaker 3;
- ✓ System of gabions in the zone under direct wave attack.

DESIGN PARAMETERS- TABLES, GRAPHS & FIGURES

The application of all the methods described above gave us the opportunity to analyze the scenarios defined in the task and each step is verified by comparison between different and well known state-of-the-art evaluation methods. In solutions using variable parameters in the context of optimistic and pessimistic scenarios, the following results have been obtained for the waves generated in deep water. The data from these studies in general form are Table 2.

Table 2. Parameters of the excitement in the deep sea in the project area.

Case	Wind direction	Period of Storm occurrence [years]	Confidence in the system waves period [%]	Wave period [s]	Deep sea wave height [m]
Case 1	Northeast	50	1	10	13.65
Case 2	Northeast	50	13	10	8.17
Case 3	Northeast	1	5	7.7	5.13
Case 4	Northeast	1	13	7.7	4.23
Case 5	East	50	1	9.9	13.49
Case 6	East	50	13	9.9	8.07
Case 7	East	1	5	7.5	4.39
Case 8	East	1	13	7.5	3.62
Case 9	Southeast	50	1	7.5	8.30
Case 10	Southeast	50	13	7.5	5.00
Case 11	Southeast	1	5	7.0	3.90
Case 12	Southeast	1	13	7.0	3.22

Table 3. Bulk densities, porosity, water properties of the materials of eQ_{p3} (atypical loess)

	Specific density	Volume density	Dry density	Density in a water-saturated state	Porosity	Void ratio	Water content	Max water content	Degree of saturation
	r_s [G/cm^3]	r_n [g/cm^3]	r_d [g/cm^3]	r_r [g/cm3]	n	e	w_n [%]	w_r [%]	S_r
Lower characteristic value	2,69	1,70	1,41	1,88	0,43	0,77	19	28	0,60
Upper characteristic value	2,71	1,88	1,53	1,96	0,48	0,91	25	33	0,85

Presented at the Figure 4 0 dependence of triaxial tests confirms these conceptions, expressed by the relationship between the degrading modulus of deformations and

https://doi.org/10.5593/sgem2024/1.1/s02.20

dilatancy angle variations. In Figure 4 the different colored graphs illustrate the behavior of different test specimens of the same material.

Table 4. Shear strength parameters of materials from eQ_{p3} (atypical loess)

	Angle of internal friction	Cohesion
	degrees	kPa
Lower characteristic value	10,8	14
Upper characteristic value	15,2	19,9

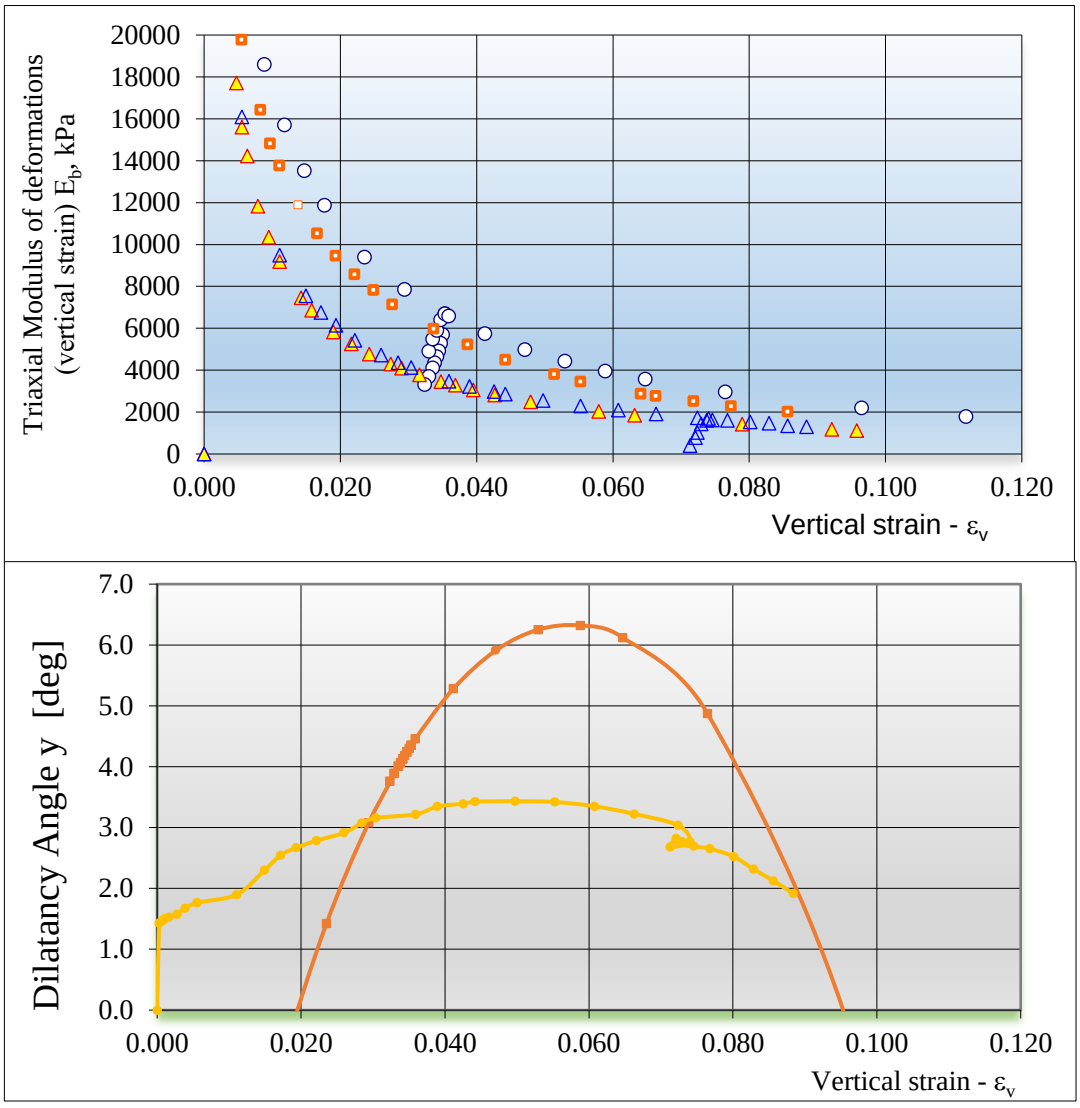


Figure 4. Degradation of Deformation modulus and Dilatancy angle curve.

On the other hand, using the relationships between the physical characteristic's porosity

n = e/(1+e),

for the solid phase we obtain the compaction coefficient

$$e_1 - e_2 = m_v \, \Delta\sigma_z (1 + e_i) \Rightarrow m_v = \frac{\Delta e}{\Delta\sigma_z (1 + e_i)}$$

and in a semilogarithmic representation of the compaction curve (q-deviatoric stress) the three deformation constants are conveniently determined:

$$C_c = \frac{\Delta e}{\Delta(log\ \sigma_z)},$$

$$C_{s(unloading)} = \frac{\Delta e}{\Delta(log\ \sigma_z)},$$

$$C_{\alpha(secondary\ consolidation\ -\ creep\ and\ other\ manifestations\ of\ rheological\ processes)} = \frac{\Delta e}{\Delta(log\ \sigma_z)},$$

how it is shown on the Figure 5.

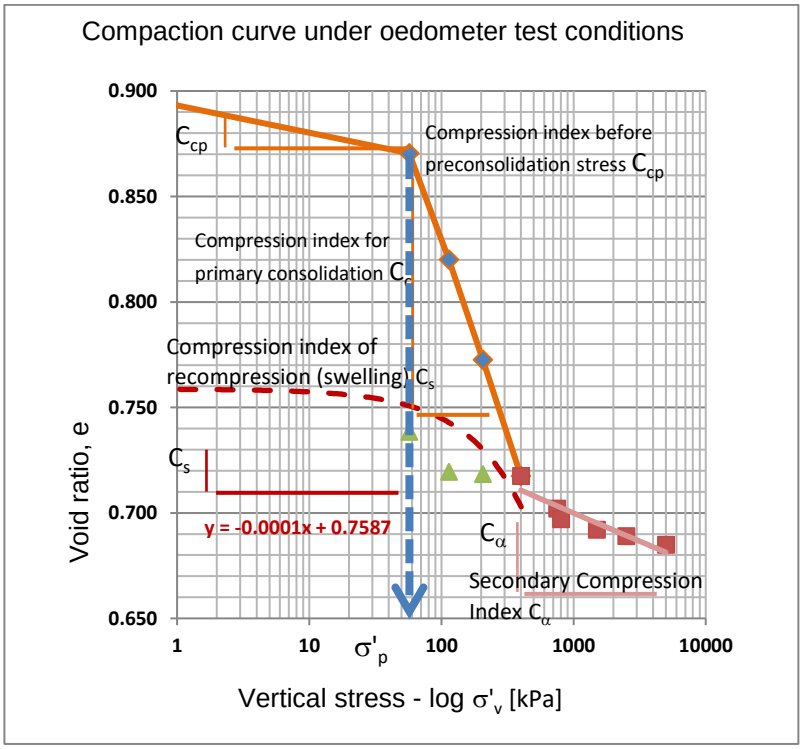


Figure 5. Compaction curve.

For the compression module, the dependence is defined. Using the compression dependence, the deformation in the overall behavior is conveniently presented: $E_{оед} = \frac{1}{m_v}$

$$s_m = C_{cp}\frac{H_0}{1+e_0}log\frac{\sigma'_p}{\sigma'_z} + C_c\frac{H_0}{1+e_0}log\frac{\sigma'_p + \Delta\sigma_z{}'}{\sigma'_p}$$

Table 5. Bulk densities, porosity, water properties of the soil materials of eQ_{p3} (atypical loess).

	Median	LCV	UCV
C_{cp}	0,0107	0,00961	0,01174
C_c	0,4167	0,37507	0,45841
C_s	0,0059	0,00532	0,0065
C_a	0,0347	0,03126	0,0382

https://doi.org/10.5593/sgem2024/1.1/s02.20

Used to allow us to conduct a series of laboratory triaxial tests by which in comparative terms to determine the variation of deformation parameters in order to reliably define the analytical models.

By means of selection of the above presented parameters described in this section, allows on one hand the formulation of a working model and on the other hand the investigation of the behavior of individual geotechnical structures and how are they influenced by abrasion made it possible to study multiple model situations.

DISCUSSION

The finalized design solution shown in Figure 6, shows not only the man-made structure for active protection of the coastal zone, but also the steep stratigraphic conditions and the intricate choice of the location of the protective facility, closely matching the natural bathygraphy. Here the components of the coastal dismemberment in combination with zone of active erosive material accumulation and the subsequent abrasion are the main reason behind the particular choice of sustainable coastal protection. This solution is by no means the only one implemented in both this project and in general and those other methods can be summarized by their activity or passivity in preserving the environment. The use of the reviewed methods for predicting the behavior of protective facilities has developed a series of design situations divided into two groups and including:

- Pile anchored anti-abrasion protection of the beach area (group 1);
- Sea dikes (group 1);
- Artificial peninsulas (group 2);
- And offshore breakwaters (group 2);

The first group of active facilities has the task to actively protect the coastal slope from direct wave attack, and the second group to create conditions for the development of abrasion-accumulative formation, which indirectly reduces direct influence wtih time.

Be dictated by the conditions of the environment in which the offshore zone is located. These factors and their study are synthesized into the following;

- Shallow water at depths of up to 5-6m at a distance of more than 200m from the coast;
- Structure of the geological formation Built calcareous rocks in the zone of mean sea level loess deposits over the rock mat. These conditions suggest an extremely strong influence of abrasion on the silty materials of loess and the processes of sea circulation are the main cause of the destruction of the coast. The main source of feeding of the beaches in the area are the sediments from the development of abrasion and erosion processes in the coastal zone;
- Due to the structure of alluvial and eolian materials, the intensively crumbling cliff, the sandy strips are narrow, in some places missing. The coastline, on the other hand, has relatively few river drainage zones.
- Another important aspect is the climatic conditions associated with the air circulation and the formation of relatively long periods with southeasterly winds that lead to our seabed are 1.3 m high. Here, one should follow in future periods the influence of swelling as one of the main factors for the coastal evolution.

- Last but not least, as a major factor in the degradation of the coast is the lack of sedimentary accumulation on the beaches. Studies of the considered coastal area found that the beaches are built solely from mollusks shells.

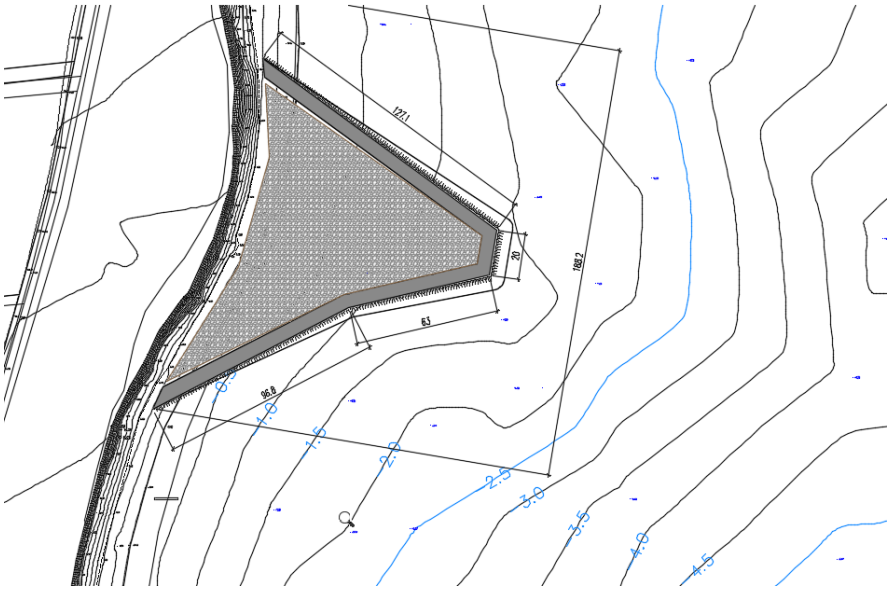


Figure 6. Desing of Artificial peninsula.

The study of the minimum zones with terrigenous mineral composition unequivocally proved that its origin is a product of the destruction of the coast. All these conditions of the considered design situation the common complex of the hydrosphere atmosphere and lithosphere interaction for the possibility to assess the reliability of the design decisions undertaken. The main objective of this project was to create conditions for passive protection of the coast through the construction of facilities that would retain materials as long as possible in the beach area. Along with the active constructions in future periods, observations were envisaged to prove the reliability of the implemented solutions.

CONCLUSION

As a result of the overall investigation, assessment and modelling of the coastal protection practices usually implemented, the problem of the ever-changing environmental conditions should be raised. The implementation of a sustainable monitoring system is crucial for the long term success and longevity of the project and will allow us to continue to collect data and enhance the capabilities of the design solution. All of the solutions discussed and proposed in the project were chosen with respect to the ever-evolving situation and the designers attempted to anticipate the changes that might come with time to allow for successful future usage and improvements.

ACKNOWLEDGEMENTS

The authors declare that the contents of this article has not been published previously. All the authors have contributed to the work described, read and approved the contents for publication in this journal. All the authors have been certified by their respective organizations for human subject research.

https://doi.org/10.5593/sgem2024/1.1/s02.20

REFERENCES

[1] Uhrin, Amy & Kershaw, Peter & Uhrin, Amy & Lusher, Amy. (2019). GESAMP 2019 Guidelines for the monitoring & assessment of plastic litter in the ocean Reports & Studies 99 (editors Kershaw, P.J., Turra, A. and Galgani, F.).

[2] Dimitrov, Dimitar & Hristova, Raina & Paychev, Veselin. (2018). Geological and geomorphological characteristics of miocene and quaternary marine sediments in coastal zone of the region "karantinata" in varna gulf. Conference with International Participation, "Geography, Regional Development and Education" 3-4 November, 2017, Department of Geography, Konstantin Preslavsky - University of Shumen, Bulgaria, ISSN: 2367-5721. 169-173.

[3] Mei, C. C. 1991. The Applied Dynamics of Ocean Surface Waves, World Scientific Pub. Co., Teaneck, NJ

[4] Cardone, V. J., Jensen, R. E., Resio, D. T., Swail, V. R., & Cox, A. T. (1996). Evaluation of contemporary ocean wave models in rare extreme events: The "Halloween Storm" of October 1991 and the "Storm of the Century" of March 1993. Journal of Atmospheric and Oceanic Technology, 13(1), 198-230.

[5] Takahashi, S, Tamimoto, Kand Shimosako,K(1990). Wave and block caisson covered with wave dissipation blocks. Report of Port and Harbour Institute, Yokosuka, Japan, Vol 30, №4,pp3-34;

[6] SP 38.13330.2010, Loads and actions on hydraulic engineering constructions

[7] Papadopoulos, D. (Dimitrios) (2013): Damage on rock slopes under wave attack. Version 1. 4TU. ResearchData. dataset. https://doi.org/10.4121/uuid:fe47c333-2965-4466-9f31-c2a4fac1709d

[8] van der Meer, Jentsje & Bruce, Tom. (2014). New Physical Insights and Design Formulas on Wave Overtopping at Sloping and Vertical Structures. Journal of Waterway, Port, Coastal, and Ocean Engineering. 140. 04014025. 10.1061/(ASCE)WW.1943-5460.0000221.

[9] Camfield, Fred E., Wave Forces on Wall, doi: 10.1061/(ASCE)0733-950X(1991)117:1(76)

[10] Wood, D.M. Soil Behaviour and Critical State Soil Mechanics; Cambridge University Press: Cambridge, UK, 2007.

[11] Roscoe, K. H. and Burland, J. B. (1968): "On the generalized stress-strain behavior of 'wet' clay," Engineering Plasticity, Cambridge Univ. Press, pp. 535-609.

[12] Hudson, R. Y. (1958). "Design of Quarry-Stone Cover Layers for Rubble-Mound Breakwaters; Hydraulic Laboratory Investigation" Research Report No. 2-2, U.S. Army Engineer Waterways Experiment Station, Vicksburg, MS.

[13] M.Todorov, "Cyclic Soils Properties", Seventh Iinternational Structural Engineering and Construction (ISEC-7), Hawaii, June 18—23, 2013, pp 85-90.

DETERMINATION OF WATERLOGGING ZONES AND THEIR FACTORS USING NON-DESTRUCTIVE MONITORING METHODS AT HISTORICAL AND ARCHITECTURAL MONUMENTS

CSc. Iryna Cherevko[1]
CSc. Tetiana Kril[2]
CSc. Dmytro Bezrodnyi[3]
CSc. Serhii Popov[3]

[1]National Reserve "Kyiv-Pechersk Lavra", **Ukraine**
[2]Institute of Geological Sciences of the NAS of Ukraine, **Ukraine**
[3]Taras Shevchenko Kyiv National University, **Ukraine**

ABSTRACT

The paper presents the results of determining waterlogging zones and their factors using non-destructive monitoring methods on the territory of the Kyiv-Pechersk Lavra Metropolitan's Garden. The research was carried out using the methods of electrotomography, natural electric field with the use of subsurface sounding radars. The results of electrotomography were interpreted using two- and three-dimensional models. The territory of the Upper Lavra Metropolitan's Garden is a combination of complex engineering and geological conditions and technogenic development, which creates conditions for the development of dangerous engineering and geological processes and emergency situations. In terms of danger, this area belongs to the unstable sites for the preservation of world heritage historical monuments. The last accident on the water supply networks occurred in October 2022. It caused sinkholes on the surface, increasing the groundwater levels, and significant destruction of the underground structure of historical importance – the Metropolitan's cellar. The existence of an anomalous cupola of leakage (soils of low resistance) observed in the western and central part of the area was established, which is probably the center of soil massif overwetting as a result of the heating network accident. The analysis of the adapted 3D model based on the results of non-destructive methods of the geological environment state monitoring allowed us to indirectly establish the places of unsatisfactory engineering networks (cold water supply) technical condition, where the waterlogging zone was recorded. The research has confirmed the presence of a man-made water inflow (leakages) from main water supply networks in the right part of all profiles, as a constant source and factor for waterlogging the soil foundations of architectural monuments – Monastery walls, Kushnyka tower, etc.

Keywords: Kyiv-Pechersk Lavra, emergency leaks, electrical tomography, natural electric field, architectural monuments, hydrogeological monitoring.

INTRODUCTION

Architectural objects of high historical significance and under the protection of UNESCO must be examined using special non-destructive methods. These include methods of electrical tomography (ET), natural electric field (NEF) with the use of

https://doi.org/10.5593/sgem2024/1.1/s02.21

subsurface sensing radars. They allow for diagnosing underground communications, local heterogeneities in soils, leaks from water supply networks, and groundwater levels, and conducting archaeological research.

We carry out systematic monitoring of historical monuments and other objects on the territory of the Kiev Pechersk Lavra [1-5]. One of the unstable sites for the preservation of historical and architectural heritage sites is the Metropolitan's Garden due to natural and man-made factors [5-8].

The Metropolitan's Garden is located on the territory of the Upper Lavra within the loess plateau. Absolute elevations are 182-189 m, the area is 0.6 hectares. The garden is surrounded by buildings No. 92, 31, 5, in the central part there is an underground structure No. 9 – the Metropolitan's cellar. Water supply networks (cold and hot) are laid at a depth of 1.5-2 m.

There are several known emergencies on water supply networks within the study area. The latest emergency on the territory of the Metropolitan's Garden of the National Reserve "Kyiv-Pechersk Lavra" was caused by a break in the main heating network, which was connected on October 27, 2022 [8]. A flow of pulp with a volume of about 300 m3 of hot water from the pipeline and waterlogged underground structure No. 9. As a result, sinkholes formed on the day surface (Fig. 1), and the underground structure was almost destroyed. Groundwater levels in observation wells located at a distance of 40-50 m from the place of the gust, on October 31, 2022, increased by 1-1.5 m.

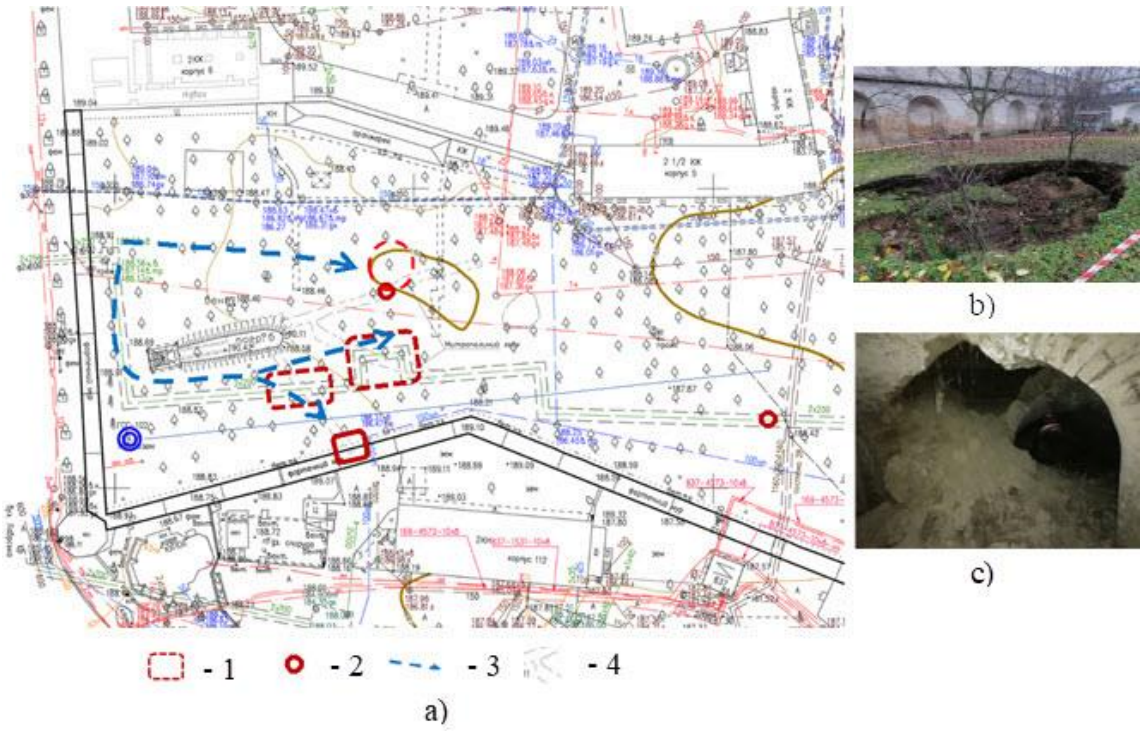


Fig. 1. The territory of the Metropolitan's Garden (a) and sinkholes on the surface (b) with the removal of pulp into an underground structure (c): 1 – sinkholes after the accident on October 27, 2022; 2 – sinkholes that appeared 2 months after the accident due to consolidation of waterlogged soils; 3 – direction of groundwater flow; 4 – contours of the underground structure.

Factors such as the lithological composition of soils, high levels of groundwater, and the density of engineering structures and communications in unsatisfactory technical conditions threaten the development of dangerous engineering-geological processes and damage to historical and cultural heritage sites.

Therefore, the main purpose of this research was to detailed determination of waterlogging zones and their factors using non-destructive monitoring methods (ET and NEF) on the territory of the Metropolitan's Garden. As well as determining the area and depth of water content of the soil mass and the presence/absence of siltation of existing underground cavities.

MATERIALS AND METHODS

Geophysical research was carried out in October 2023, almost a year after the accident [9]. Three geoelectric sections were obtained to a depth of up to 24 m, and a map of natural electric field potentials along ten profiles was created to identify areas of waterlogging. The authors of this research carried out their qualitative and quantitative interpretation, adapting to the technogenic conditions of the research area.

Qualitative interpretation of electrical tomography data is focused on determining the general patterns of the geological structure of the study area and assessing the probable zones of location of certain geological structures and anomalies.

Quantitative interpretation of the profiles consisted of determining the powers and resistivities of geoelectric horizons, automated selection of a theoretical electrical sounding curve that best coincides with the experimental (full-scale section) [10-12].

A qualitative and quantitative interpretation of the results of NEF survey was carried out. Based on the results of qualitative interpretation, anomalous zones were identified with an intensity that clearly exceeded the observational error and fluctuations in the normal background field. It was taken into account that in areas where filtration processes develop, negative anomalies of the natural field indicate areas of water inflow, and positive anomalies indicate areas of water discharge.

The results were adapted by overlaying (building a 3D model) a NEF map and three geoelectric profiles on a topobase with the main engineering networks and communications, as well as architectural monuments. The interpretation of the data, the establishment of the cause-and-effect relationship of the accident and the conditions for preserving the sights were carried out using data from long-term hydrogeological monitoring.

A detailed analysis of the resulting model made it possible to establish the spatial position of the existing waterlogging zones, taking into account the communications and other artificial structures present within the site.

RESULTS

Fig. 2 shows a 3D model construction of the geoelectric resistance of the Metropolitan's Garden soil massif based on data from three geoelectric profiles. A low-resistivity rock cupola (cupola of water leakage coloured by blue) has been established, which is observed in the western and central parts of the site. The cupola of leakage is most clearly visible on profile I in the area L 35-65, less contrastingly on profile II at L 40-80 and on profile III at L 35-75. On profiles II and III, it is distinguished by a wide strip of

https://doi.org/10.5593/sgem2024/1.1/s02.21

iso-ohms of reduced values of apparent resistivity ρ (8-12 Ohm·m), the relative vertical amplitude decreases in the northern direction from 4-5 m on profile I to 2 m on profile III.

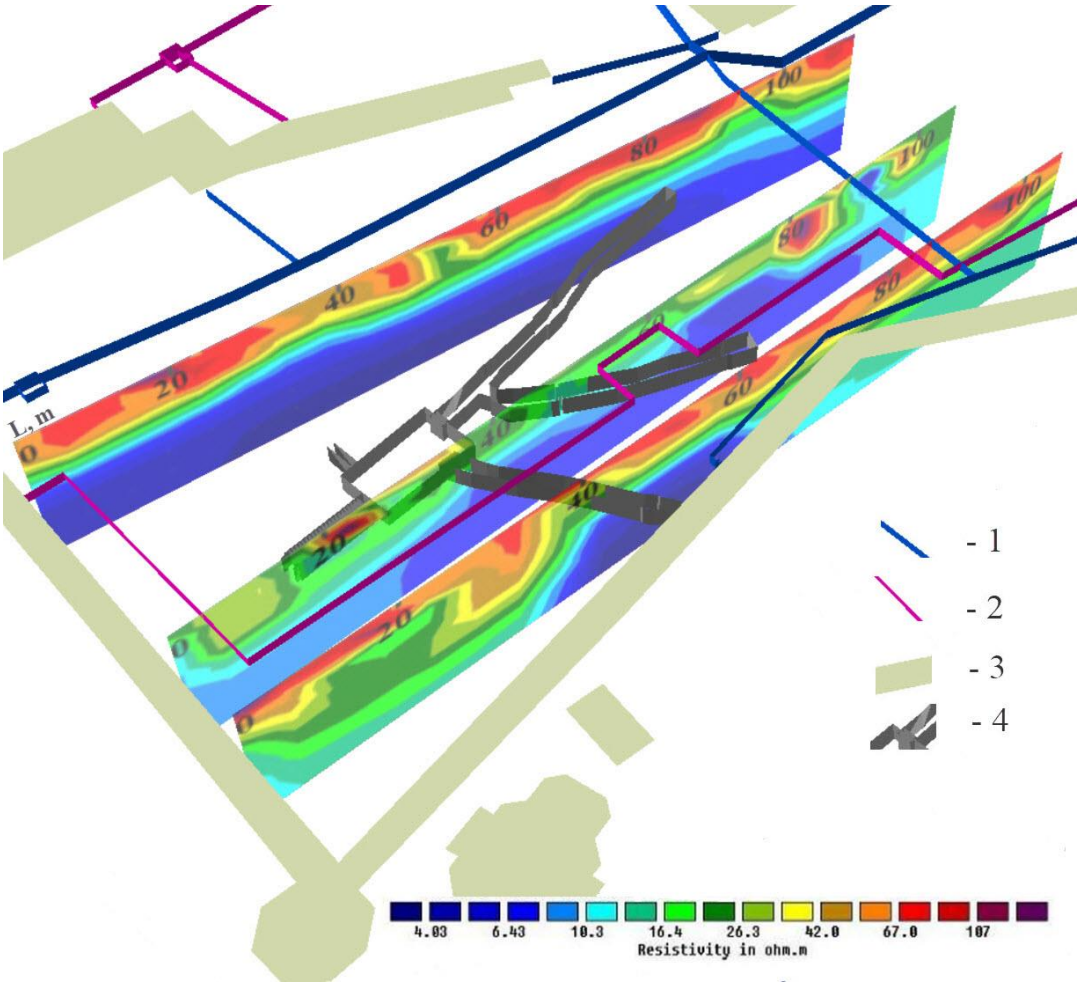


Fig. 2. 3D model of geoelectric resistance (Ohm·m) of the soil massif of the Metropolitan's Garden: 1 – cold water supply network; 2 – hot water supply networks; 3 – buildings and structures; 4 – underground structure.

The groundwater level within profile I, according to the results of the interpretation of data from the ET method (Fig. 2), ranges from 12-12.5 m in the west to 10-11 m in its eastern part. Most likely, groundwater spreads on both sides of the cupola of water leakage. In the upper part of profile II, areas of anomalously increased resistance are identified, confined to L 20-25 and L 82.5, the maximums exceeding 900 Ohm·m. This is probably explained by the formation of decompression zones caused by anthropogenic factors (archaeological excavations).

At L 92.5 of profile II, a significant minimum of apparent resistivity (8-10 Ohm·m) was recorded, which indicates the likely presence of a zone of significant waterlogging of the soil layer. This plan anomaly coincides with the associated anomaly of the natural field and the presence of a water supply network in this place. Based on the results of the interpretation of ET data, the groundwater level along the profile varies from 12 to 12.5 m in the west and from 11.5 to 13 m in the east.

The most stable in terms of the distribution of electrical properties is profile III, which is located in the north of the Metropolitan's Garden. Its section is low-resistivity, based on clays with an apparent resistivity of 9-12 Ohm·m. The first layer, represented by loess sandy loam with minor inclusions of construction waste, has a thickness of up to 3.5 m, which is probably due to the active economic development of the territory. Other layers are consistent in power and electrical resistance. Within L 50-55, an irregularly shaped high-resistivity anomaly was recorded, located at depths of 3-8 m, and is probably one of the branches of the Metropolitan's cellar. According to the results of interpretation of ET data, the surface of the groundwater level changes along the profile from 12 to 12.5 m.

Based on the results of field observations using the natural electric field method in the area of the Metropolitan's Garden, a map of its potentials (mV) was constructed, Fig. 3. Qualitative and simplified quantitative interpretation of research data was carried out. Based on the results of visual analysis and qualitative interpretation, it was established:

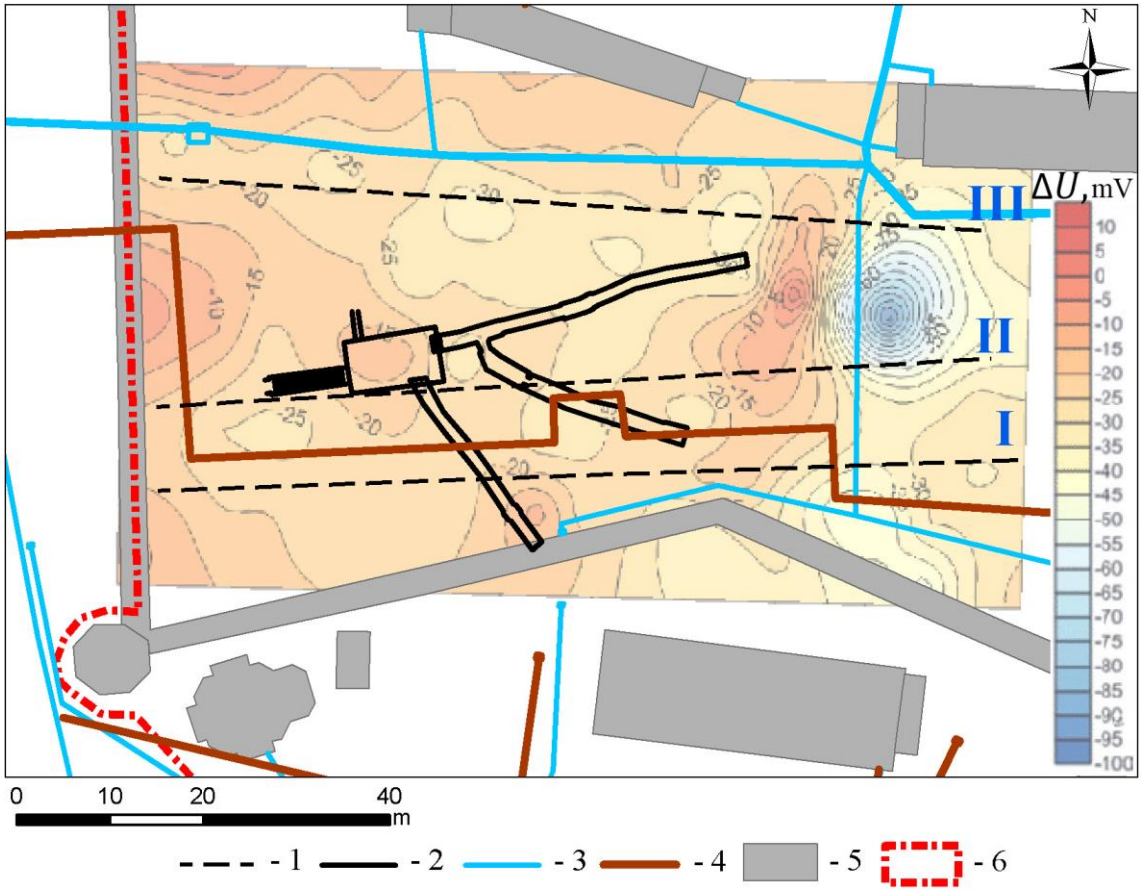


Fig. 3. Map of electrical potentials for the territory of the Metropolitan Garden: 1 – geoelectric profiles (see Fig. 2); 2 – contours of the underground structure; 3 – cold water supply; 4 – hot water supply; 5 – buildings; 6 – boundary of the Reserve.

- The area of the Metropolitan's cellar is a zone of development of quite noticeable filtration processes; the values of ΔU are negative over almost the entire area. Almost 90% of the site is inflow zones;

- zones of moderate filtration (water inflow), occupying about half the area of the surveyed site, are characterised by potentials ΔU of the natural field from -25 to -40

https://doi.org/10.5593/sgem2024/1.1/s02.21

mV. The anomalous zones have different directions (western, southern, eastern), among which the largest field gradients are represented by the southern and eastern ones, coinciding with the general direction of the slope of the day surface and the general direction of the slope of the groundwater table (direction of flow) according to long-term hydrogeological observations;

- the nature of the development of anomalies in the natural field allows us to assert that they are associated with man-made factors – leaks from networks, archaeological excavations, excavation work to eliminate the accident, watering a garden, etc.;

- quantitative interpretation, which was carried out according to the parameter q (the distance between the half-maxima of the anomalies) showed that the change in the depth of groundwater levels within the Metropolitan's Garden site varies from 8.5 to 11 m, which is inconsistent with the data of long-term hydrogeological regime observations. The maximum levels are recorded at a depth of 10.5 m. Apparently, the values obtained by the NEF method do not reflect the actual level of the groundwater table, but the limit of the capillary rise zone.

DISCUSSION

Since the field work by the ET and NEF methods was carried out after the hot summer of 2023 and dry September, the intensity of the detected anomalies may be even higher. Natural electric field methods are quite well correlated with the electrical profiling result, which gives basis for conducting seasonal monitoring measurements within the specified area and the adjacent territory. Assumptions regarding the interpretation of the q parameter as levels of capillary rise require additional monitoring investigations [13-14].

CONCLUSION

A detailed analysis, obtained by adapting the results of studies using the ET and NEF methods, of the 3D model of the geoelectric resistance of the soil mass of the Metropolitan's Garden made it possible to establish the spatial position of the existing areas of waterlogging, taking into account the communications and other artificial structures present within the site.

By analyzing the existing situation and field surveys of the territory, possible ways of spreading the flow of hot water in the soil massif after the accident on October 27, 2022 were established: spreading water through the insulating box of the heating network and reaching building no. 31, where it accumulated in front of the heat chamber; overfilling of the box and its destruction in 2 places; waterlogging and transition to a fluid state of the loess layer; flooding of an underground structure with pulp; further waterlogging of the soil mass and infiltration of water into the groundwater table.

The soil elements identified by the distribution of apparent resistance coincide with the geological section of the site determined during geotechnical surveys.

The ET method established the existence of an anomalous cupola (low-resistivity soils) observed in the western and central parts of the site, which is probably the cupola of water leakage (waterlogging of the soil mass) as a result of the accident of the hot Water supply network.

The dimensions of the spreading zone, according to the results of the interpretation of the research, are: length – 25-70 m, width – 25-45 m. They depend on the configuration of the underground structure (Metropolitan's cellar), along the flooded branches deepened to 5-8 m, further infiltration of the massif water took place.

Analysis of the adapted 3D model based on the results of non-destructive methods for monitoring the state of the geological environment made it possible to indirectly identify places of unsatisfactory technical condition of engineering networks (cold water supply), where a waterlogging zone with approximate dimensions of 5×5 m was recorded (see Fig. 2, profile II, L 90- 95).

Research has confirmed the presence of an influx of man-made water (leakage) from the main water supply networks on the right side of all profiles (L 0-10) as a constant source and factor for waterlogging the array of soil foundations of architectural monuments – Monastery walls, Kushnik tower, etc.

Geophysical research was carried out a year after the accident, which is probably why the initial zone of infiltration and spreading was somewhat smaller (in loess soils, filtration has an almost vertical direction), which is advisable to establish by mathematical modeling of filtration processes.

ACKNOWLEDGEMENTS

The authors acknowledge the funding received by the National Research Foundation of Ukraine from the state budget 2022.01/0209 "Complex research of the geoecological state of preservation of the historical and cultural heritage objects of the National Reserve "Kyiv-Pechersk Lavra" in the conditions of military operations" (NRFU Competition "Science for the Recovery of Ukraine in the War and Post-War Periods").

REFERENCES

[1] Kyiv: Saint-Sophia Cathedral and Related Monastic Buildings, Kyiv-Pechersk Lavra URL: https://whc.unesco.org/en/list/527/maps/.

[2] Petrenko, M.S. National Kyiv-Pechersk historical and cultural reserve. Guide. Kyiv: Mystetstvo, 1979, 262 p.

[3] Sitkaryova, O.V. Architecture of the Kyiv-Pechersk Lavra of the end of the 18th – 20th centuries, Kiyv: Golovkyivarkhitektura, NDITIAM, 2001, 336 p.

[4] Demchyshyn, MG, Kril, TV. Improvement of the Engineering Protection Systems of the Kyiv-Pechersk Lavra Reserve Territory, Nauka I Innovacii, 2019, 15(3), 37–51. https://doi.org/10.15407/scin15.03.037

[5] Arkhipenko O.A., Konyushin V.V. Works on the construction of a network of hydrogeological wells on the territory of the National Kyiv-Pechersk Historical and Cultural Reserve. LLC KB PRIDE, code 154/2-IG-TZ, Kyiv, 2018, 71 p.

[6] Kril, T. & Cherevko, I. Identification on Unstable (Landslide Hazard) Areas on Lavra Far-Caves Hill. Fourth EAGE Workshop on Assessment of Landslide Hazards and impact on communities, Sep 2023, 2023, 1 – 5. https://doi.org/10.3997/2214-4609.2023500017

[7] Kril T., Shekhunova S., Cherevko I. Identification of Potentially Unstable Areas by Engineering and Geological Processes Monitoring and Heritage Building Deformations.

https://doi.org/10.5593/sgem2024/1.1/s02.21

17th International Conference Monitoring of Geological Processes and Ecological Condition of the Environment, Nov 2023, Volume 2023, p.1 5. DOI: https://doi.org/10.3997/2214-4609.2023520203

[8] Complex research of the geoecological state of preservation of the historical and cultural heritage objects of the National Reserve "Kyiv-Pechersk Lavra" in the conditions of military operations. Bugai D.O. Scientific report. 2023, 125 p.

[9] Matsola O.I., Korbutyak O.M., Lopata O.V. Report on the provision of services in geological, geophysical and other types of scientific exploration "Special engineering and geophysical searches on the territory of the national reserve "Kyiv-Pechersk Lavra" within the boundaries of flooding zones, underground voids and the development of failure processes by the method of vertical electric sounding and natural electric field, area - 0.6 ha", Kyiv, 2023. 33 p.

[10] Mauriello P, Monna D, Patella D. 3D geoelectric tomography and archaeological applications. Geophysical Prospecting. Vol. 46, Issue 5, 1998, P. 543-570. https://doi.org/10.1046/j.1365-2478.1998.00102.x

[11] Bondar, K.M., Khomenko, R.V., Chernov, A.P., Kuksa, N.V. (2020). Results of the ground penetrating radar survey in the Church of St. Elias – Bohdan Khmelnytsky burial vault in Subotiv. Geophysical Journal, 42, 3, 175-194. https://doi.org/10.24028/gzh.0203-3100.v42i3.2020.204709

[12] Loke M.H. Time-lapse resistivity imaging inversion. 5th Meeting of the Environmental and Engineering Geophysical Society European Section Proceedings. Em1. 1999.

[13] La Vigna F. Review: Urban groundwater issues and resource management, and their roles in the resilience of cities. Hydrogeology Journal, 30, 2022. 1657–1683 https://doi.org/10.1007/s10040-022-02517-1

[14] Hayashi, T., Tokunaga, T., Aichi, M. & Shimada, J., Taniguchi, M. (2009) Effects of human activities and urbanization on groundwater environments: An example from the aquifer system of Tokyo and the surrounding area, Science of thr Total Environment, 407 (9) 3165–3172, https://doi.org/10.1016/j.scitotenv.2008.07.012

FEATURES OF STUDYING THE MATERIAL COMPOSITION OF POLYMETALLIC ORE FOR ITS COMPLEX USE

Expert ecologist, PhD Natalia Tyushkova[1]
Research Associate Tatiana Losina[2]
[1]International University of Professional Innovation, **Russia**
[2]Tula Scientific Research Geological Enterprise, **Russia**

ABSTRACT

The paper presents research on the development of enrichment of polymetallic ores of the Elan deposit. The heterogeneity of textures, structures and material composition of the ores of the Elan deposit make it a difficult object for technological research. The research was focused on the development of waste-free enrichment technology; progressive stadial, collective and collectively selective flotation schemes with full water circulation, ensuring environmental protection, using both currently manufactured by industry and promising (methyl isobutyl carbinol) reagents. The work was carried out using a number of modern accurate and precision physico-chemical research methods and well-known enrichment methods. Mathematical methods are widely used. Based on the identified features, a technology for the enrichment of all types of Elan deposit's ores has been developed and confirmed in experimental industrial conditions, providing the production of copper, lead, zinc, pyrite and fluorite concentrates with high extraction of the components of the same name and the integrated use of ore. The technological typification of ores was carried out and a method for classifying ore samples by technological properties for technological mapping of the deposit was developed. One of the methods of increasing the reliability of engineering and geological assessment of ore deposits in the subsurface is technological mapping of deposits. Reliability improvement is achieved mainly through a detailed study of all natural types and phases of ores extracted at the deposit; differentiated calculation of ore reserves by technological types; correction of recoverable value in the technical and economic assessment of proven reserves, taking into account different ore enrichment. The practical value of the work, expressed in the development of technology for the approval of stocks. The scientific value expressed in the development of a methodology for classifying ores based on multidimensional statistical analysis.

Keywords: development of complex technology, technological typification, polymetallic ores, multidimensional statistical analysis

INTRODUCTION

The complex of technological studies on the development of the technology for the enrichment of polymetallic ores of the Ulansky deposit associated with the expansion of the mineral and raw materials base was carried out by a team of researchers at different stages with the involvement of new methods and technologies. The heterogeneity of the textures, structures and material composition of the Ulan deposit makes it a

https://doi.org/10.5593/sgem2024/1.1/s02.22

complex object for technological research [1] [2].
The technological properties of complex ores from the zone of deposit oxidation are mainly influenced by: a solid association of lead minerals with iron hydroxides, manganese oxides, siliceous ferruginous formations, jarosite and clay-mica, aggregates; complex mineral composition; presence in the composition of carbonates of zinc-containing siderite. Technological properties of sulphide ores are determined by the following features of the material composition: uneven dissemination of ore minerals, which necessitates the gradual grinding of ore in preparation for flotation; small interdigitation of ore minerals, requiring re-grinding of coarse concentrates; high iron content in the crystalline lattice of sphalerite; close association of silver with sulphides, causing its inevitable distribution in all products of enrichment; the presence of two generations of chalcopyrite: 1- emulsion in the sphalerite, which causes loss of copper in zinc concentrate; 11- independent excretions and accumulations, which cause the concentration of copper in lead concentrate, its subsequent extraction in the metallurgical process; the presence of fluorite in the composition of lead-zinc ores on quartz-fluorite-sulphide cement;
The research was focused on the development of wasteless enrichment technology: progressive stadial collective and collective selective flotation schemes with full water rotation ensuring environmental protection, using promising reagents [3].

EXPERIMENTAL

1.Typification of ores of the Ulansky deposit by the method of sample recognition.

The formulation of the problem consisted in dividing the initial set of samples into relatively homogeneous groups by enrichment and building a classification rule based on the characteristics of the material composition. The classification rule at later stage will allow by ore characterization (in the unexplored common sample) to forecast the expected indicators of benefication and to use the results obtained with the technological mapping of the ores of this deposit.

The multidimensional classification of ores based on discriminant analysis for the technological mapping of polymetallic deposits becomes a complex task due to the multidimensionality of the output parameters of the enrichment process. Flotation of various samples in the laboratory is carried out according to the "stereotyped" technological scheme with obtaining. lead and zinc concentrates. The state vector at the output of flotation in the case under consideration is made up of ten factors. The task is to test the hypothesis of the belonging of the investigated samples to different technological types of ores according to the output parameters of the process. To solve the problem, a method of discriminant analysis has been adopted, which is carried out according to the following scheme: reduction of the multidimensional state vector to the one-dimensional one; the choice of the classification feature providing the best classification; the definition of the most significant factors affecting the classification; calculation of classification characteristics for the investigated ores and verification of the statistical hypothesis of their difference; construction of the classification scale. The calculations were carried out on an EC- computer. For this purpose, 35 small-volume samples-sulphide lead-zinc-silver ores-were selected and investigated, a technological assessment of 27 of which was carried out at this stage. The samples differ in lead content (from 0.36 to 3.19%); the content of zinc (from 0.39 to 8.66%), the ratio of lead content to zinc content. In connection with the contrast of the content of metals, in the first place,

the ore enrichment rates differed sharply. The following characteristics of the material composition of ores are accepted: lead and zinc content, the nature of the enclosing rocks, the content of oxidized forms of lead and zinc. The benefication indicators were characterized by the yield of concentrates, the content of useful components in them, and the extraction of metals into concentrates.

As a result of the research, cluster dendrograms were constructed, qualitative analysis of which allowed to produce a classification of ore samples. The decisive rule of the classification is obtained in the form of two equations of linear discriminant functions.
Based on the calculated values of the discriminant functions, the technological grade of ore was determined. The developed algorithm for ore typification is recommended for use in geological and technological mapping of deposits. According to the results of cluster analysis, all samples are divided into 7 groups. In each group there were ore close on enrichment. Using established classification rules, it is possible to predict the enrichment indices of any geological sample (with a certain degree of certainty) in which the lead content is known, the zinc content of the oxidized lead and the zinc content of the oxidized and use the results obtained in the technological mapping of the deposit [4].
Ulanskoye polymetallic deposit is represented by a single technological type of lead-zinc silver ores, among which are the following varieties:
- sulfide lead-zinc-silver ores;
- sulfide lead-zinc-silver ores with fluorite;
- sulfide lead-zinc-silver ore with copper;
-mixed lead-zinc-silver ores;
The reserves of the actual oxidized ores at the deposit are insignificant: they will be processed together with mixed in the first period of the factory's operation. Given the presence in the ore of various modifications of sphalerite, two technological varieties of ores are distinguished in products of the first 3 varieties: with high-iron sphalerite and low-iron sphalerite. As a result of studying the material composition and technological properties of ores, their technological typification was carried out (Table 1, Fig. 1)
The adopted methodology allowed to develop scientifically-based benefication technology for each ore, the results of the studies were used during the process of compiling conditions and approving ore reserves

2. Results and discussion

At the present stage, there are enough examples of work on technological mapping, but they concern rare metal ores or monometallic ores. The work on technological mapping of lead-zinc ores from the Zhairemsky deposit is known. But this work was carried out on the basis of studies of large-volume technological tests conducted over a long period (several years) by various institutions of the country.
When mapping based on the results of technological evaluation of small-volume samples of polymetallic ores, the task "Identification of technological types, varieties, varieties of ores" is posed. In the methodological aspect, the problem has two independent solutions. The first aspect: the number of experiments should be minimal, but sufficient, to obtain a reliable statistical homogeneous sample of the final enrichment indicators.
The task is not standard, as in the case of polymetallic ores, the results of enrichment are not uniquely determined, but are characterized by a number of indicators. The second aspect: the choice of a mathematical apparatus for the evaluation and classification of experimental data. Selection of the characteristics of the material composition of ores for classification. Such a choice should be justified in each specific case by data of

https://doi.org/10.5593/sgem2024/1.1/s02.22

mineralogical and chemical-analytical studies of ores. But in any case, the composition of the "input" factors-the characteristics of the ore, should include:the content of useful components in the ore, their ratio, as well as the content of elements and compounds characterizing the composition of host rocks, if it affects the technological properties of ores: carbonaceous, carbonaceous shales, chlorite-sericites.

Tab. 1. The results of technological typification of ores

Technological type	Technological ore grade	Quantity of ore, in% of total reserves	Useful components	Accompanying elements of practical interest with the integrated use	The scheme of enrichment	Commodity concentrates produced
Lead-zinc silver-bearing ores	Sulphide lead-zinc silver-bearing ores (Pb, Zn < 25%)	~70-75	Pb, Zn Ag	Cu, Au, Cd, S	The scheme of bulk flotation with the separation of bulk concentrate	Lead, zinc, pyrite
	Sulphide lead-zinc silver-bearing ores with fluorite (CaF_2 > 2%)	~20	Pb, Zn Ag	Cu, Au, Cd, S, F	The scheme of bulk flotation with the separation of bulk concentrate, added with a cycle of fluorite flotation	Lead, zinc, pyrite, fluorite
	Sulphide lead-zinc silver-bearing ores with copper (Cu > 0,3%)	~5,0	Pb, Zn Ag, Cu	Au, Cd, S	The scheme of bulk flotation with the separation of bulk concentrate, added with a cycle of separation of copper-lead concentrate	Lead, zinc, silver, copper
	Mixed lead-zinc silver-bearing ores (Pb, Zn >25%)	~1,0	Pb, Zn Ag	Cu, Au, Cd, S	The scheme of bulk flotation with the separation of bulk concentrate	Lead, zinc, pyrite

Experimental studies have established that the nature of the enclosing rocks in the ore of the Ulansky deposit has no effect on their technological properties. Therefore, as input

factors characterizing the material composition of ores, the following are accepted: the content of lead, zinc, iron in the ore; the ratio of lead to zinc content, as well as the content of oxidized lead and oxidized zinc in the ore.

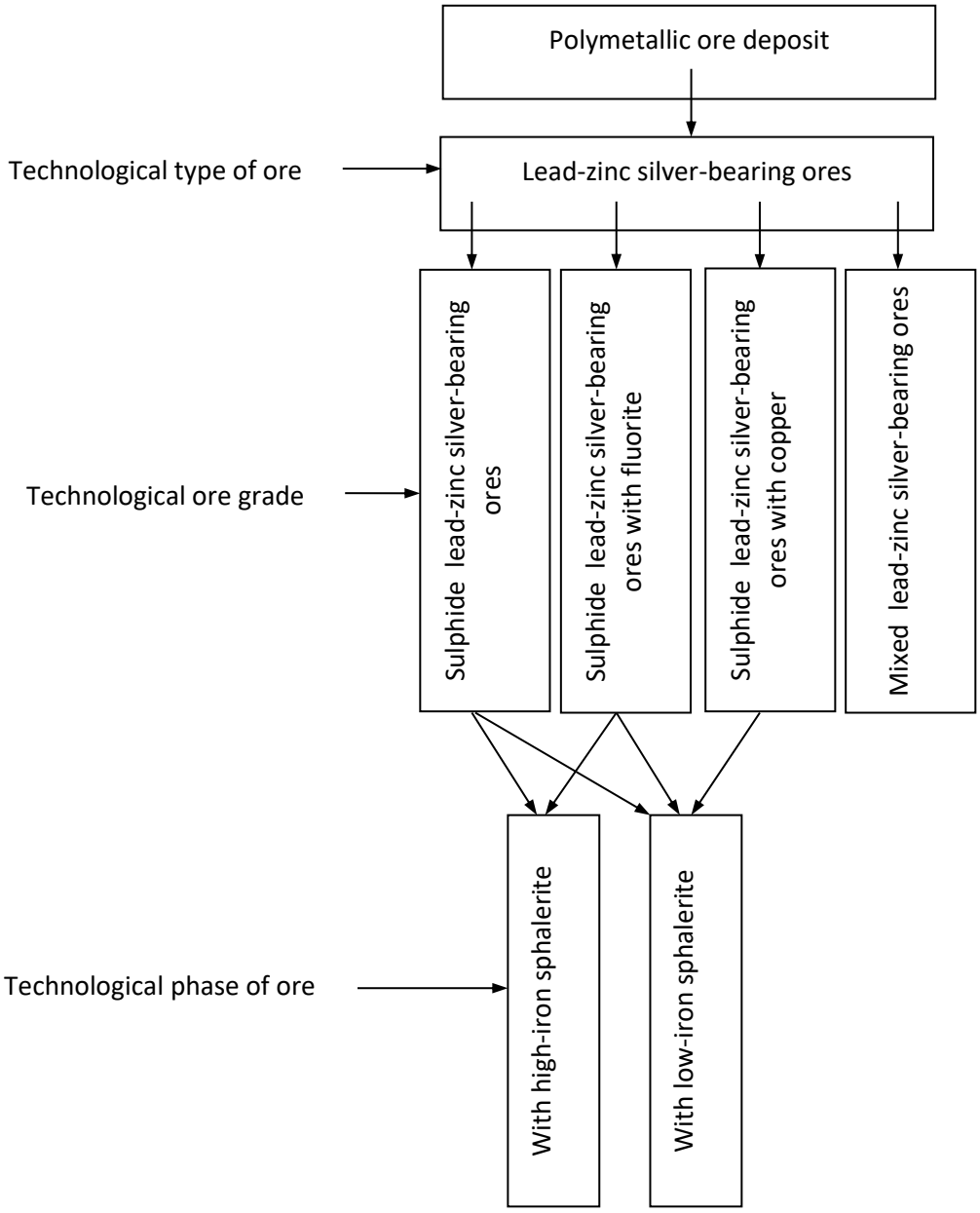


Fig 1. The scheme of technological typification of ores

3. Choosing an analog of the deposit

When carrying out technological studies of ores of various metals, a large amount of information on their material composition and technological properties is accumulated. Concentration and unification of this information, as well as the application of mathematical methods and computers for its processing, opens new opportunities in raising the level and effectiveness of analytical, mineralogical and technological research.

https://doi.org/10.5593/sgem2024/1.1/s02.22

This is achieved through the comparison of various data of the studied object with the available information, the definition of functionality between the characteristics being studied, as well as the detection of information about the study of objects, which ultimately leads to a reduction in terms and labor costs by finding the objects-the analogs. The solution of the tasks posed requires the creation of a data bank containing basic information about the technological sample (location and methods of selection, material composition, technological properties [5], [3].

At this stage of the work, a selection of the analogue deposit of the Ulansky deposit was carried out on the basis of analysis of the main country's lead-zinc deposits. The relative grindability of the compared ores is studied.

When the reserves of new deposits are handed over to the State Committee for Reserves of Russian Federation, the reference to the deposit-analog, whose ores are processed at operating enterprises must always be made. In this case, we had systematized data on the 20 main lead and zinc and polymetallic deposits of the country on the basis of which the analogue was selected.

At the same time the following was taken into account: the petrographic composition and structure of the host rocks, form of ore bodies and texture-structural features of ores, chemical composition and ratio of ore minerals. The study of the material composition was carried out by traditional methods of optical studies, as well as with the use of nuclear spectroscopy, thermographic and X-ray structural analysis.

Sample increments of ores differ in the composition of the surrounding rocks and textures, but in terms of the nature of the mineral associations, the chemical composition and internal structure of the ore minerals and texture-structural features they represent a single mineral type of ore.

The analysis showed that the ore of the Ulanskoye deposit can not be uniquely identified with the ores of some other deposit being processed at the operating enterprise. The following deposits are identified as relative analogues: Savinskoe-5, Altyn-Topkanskoye and Sadonskoe. Most of the signs closest to the Ulanskoye deposit is Savinskoe-5 deposit, located also in a single metallogenic province with Ulansky deposit. Further, according to the standard method developed by the Institute of Mechanobr, imitating an open cycle of drum-type grinding mills, the relative grindability of five samples of the Ulanskoye deposit was studied in comparison with samples from operating enterprises, where the ore of the selected deposits is processed.

4. Pilot-industrial tests of ore from the Ulanskoye Deposit

In Russia and developed capitalist countries, there are two varieties of flotation technology for the enrichment of lead-zinc ores: collectively selective schemes and direct selection. In Japan, 50% of polymetallic factories use collective-selective schemes [6], [7]. Both variants of technologies have been developed for the ores of the Ulansky deposit. After pilot-industrial tests, a collective flotation scheme was chosen, which is more environmentally friendly due to the use of water rotation (Fig.2).

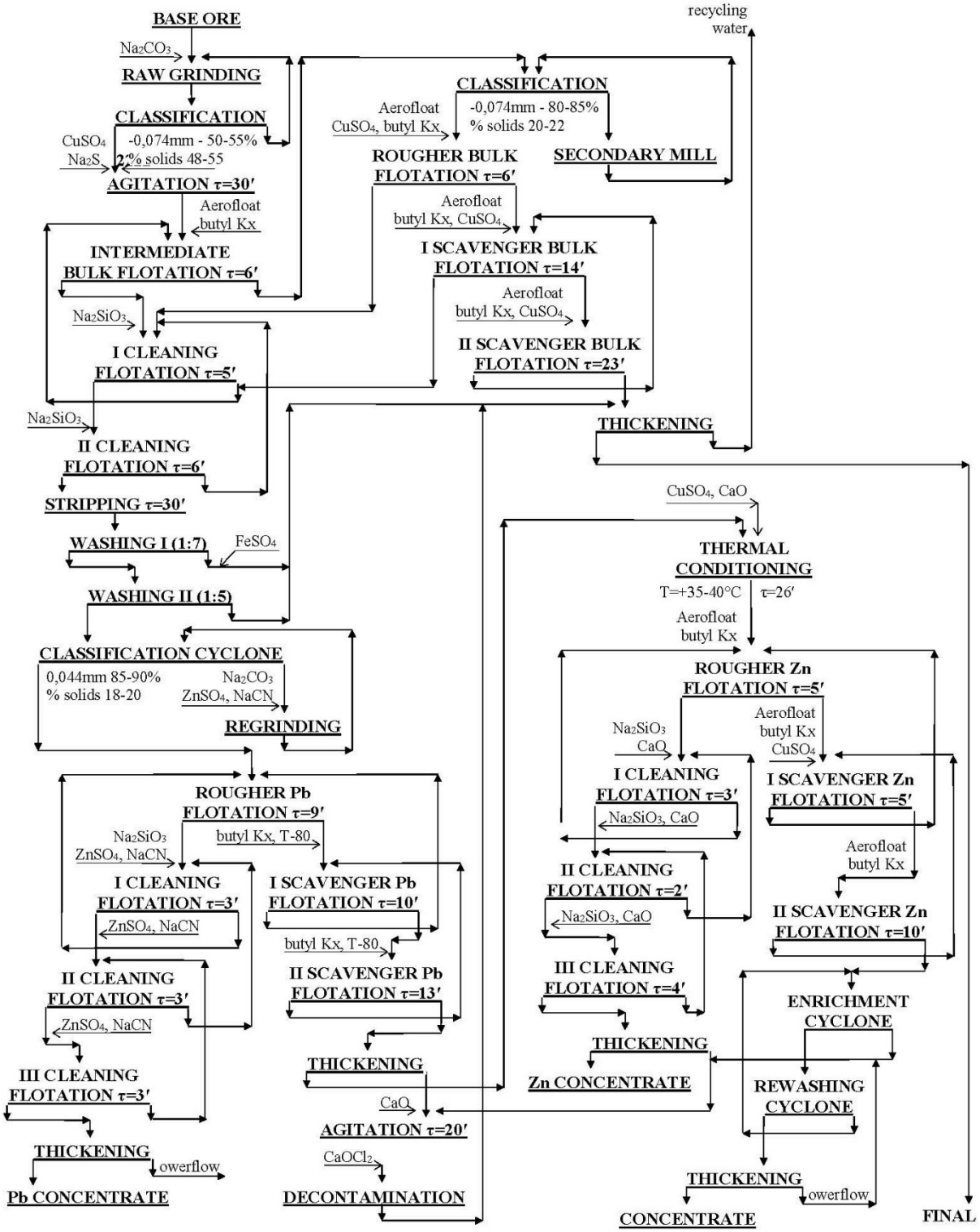


Fig.2. The scheme of beneficiation lead – when extracting lead from 88.4 to 95.7%; zinc - from samples of ores of medium horizons and from ores of the near-surface zone with extraction of zinc from 89.6 to 93.4%;
pyrite - with extraction of pyrite sulfur from 34.3 to 71.2%;
fluorite – when extracting fluorite 70;
Extraction of silver into lead and zinc concentrates was 80.0-94.5%. The cadmium of 80.5-89.5% was extracted in zinc concentrate.

https://doi.org/10.5593/sgem2024/1.1/s02.22

When carrying out laboratory studies of subsequent samples, the technological properties of ores were determined both by direct flotation experiments and by the method of comparative rapid assessment of minerals of the ore complex developed by TulNIIGP and IPCON RAS. As the results of these studies have shown, the investigated varieties of ores vary insignificantly in terms of the measured parameters, as well as in the extraction of metals in the collective concentrate during flotation. This allows us to conclude that the natural varieties of ores have sufficiently close technological properties and can be processed using a single technology. In addition, the expediency of two-stadial grinding of ore was established. In semi-industrial tests of ore, the optimal technological regimes of ore enrichment at the factory were tested on the basis of regression mathematical modeling of grinding and flotation processes.

During the development of the scheme, the registration of regulating factors and output indicators of the process was carried out. The statistical material for constructing a mathematical model is obtained. Mathematical modeling and optimization of enrichment were carried out in two stages [8], [9]. At the first stage, private models were developed, focused on the local optimization of individual processes: grinding, collective flotation - lead and zinc. At the second stage, the enrichment system was optimized as a whole. According to the data of technological studies conducted on samples representing the ores of the Ulanskoye Deposit, statistical characteristics of the main indicators of enrichment within a technologically homogeneous group were obtained. The recommended technology made it possible to obtain the following conditioned commodity concentrates from the studied ore samples:

lead – when extracting lead from 88.4 to 95.7%;

zinc - from samples of ores of medium horizons and from ores of the near-surface zone with extraction of zinc from 89.6 to 93.4%;

pyrite - with extraction of pyrite sulfur from 34.3 to 71.2%;

fluorite – when extracting fluorite 70;

Extraction of silver into lead and zinc concentrates was 80.0-94.5%. The cadmium of 80.5-89.5% was extracted in zinc concentrate.

CONCLUSION

1.To carry out technological mapping of the deposit, a classification of the investigated ore samples was carried out using methods of multidimensional statistical analysis.

2.Using the cluster analysis method, the studied set of samples representing the ores of the Ulan Deposit is divided into 7 technologically homogeneous groups characterized by" close " values of the main enrichment indicators.

3.Using the discriminant analysis method, a "decisive rule" is constructed that allows predicting its technological parameters (without conducting additional technological studies) on the basis of geological testing data on the characteristics of the material composition of the ore and using the obtained result in solving the problems of technological mapping. The main advantage of the methodology is the possibility of mapping polymetallic deposits on small geological samples, comparing the results of their enrichment according to the set of technological indicators.

4.The method is mainly used in ore deposits and includes investigation of mineral and chemical composition of ores, their textures and structures, physical and mechanical properties, spatial variability of ore quality, assessment of the enrichment of natural types and varieties, identification of dependence of enrichment indicators on ore quality parameters, development of industrial geological and technological classification with delineation of technological types and grades of ores and assessment of quality and enrichment for individual sites, blocks, horizons and etc.

5. The methodology was developed on the basis of research on the Ulanskoye Deposit, but this is the "algorithm" that will work for all other deposits. The main advantage of the methodology is the possibility of mapping polymetallic deposits on small geological samples, comparing the results of their enrichment according to the set of technological indicators.

REFERENCES

[1]. Tyushkova, N.I., Study on Intensification of baddeleyite concentrate deep cleaning by means of mechanical activation, Proceedings of XXIV International Mineral Processing Congress, China, 2008, vol. 2, pp 1696-1703.

[2]. Marasanova L.V., Losina T.K., Selivanov A.N., Multidimensional classification of ores based on discriminant analysis for technological mapping of polymetallic deposits, Theses of the reports of the scientific and technical conference. Collection of works on analysis, theory and practice of improving technological schemes, Russia, pp 39-40, 1983.

[3]. Tyushkova, N.I., Ecological and technological aspects of use of water recirculation at extraction of precious metals from quartzites, IFAC proceedings volumes (IFAC-papers online) 16th IFAC Symposium on automation in mining minerals and metal processing, MMM**,** USA, 2013, pp 464-469.

[4]. Marasanova, L.V., Losina, T.K., et al, An express evaluation of the flotation activity of small-volume ores for technological mapping of deposits, Abstracts of the scientific and technical Intensification of Enrichment Processes, Russia, p 20, 1986.

[5]. Selivanov A.N., Kalinichenko L.S., Filimonov N.V., Sychev M.N. et al., Establishment of a data bank on technological samples is a way to identify ores and improve the level of research, Abstracts of the scientific meeting Methods of technological research of the raw material of the world. Russia, Part 1, pp 8-9, 1988.

[6] Tyushkova, N.I., Marasanova, L.V., Gorenkov N.L., Research and developing of the technologies of oxidized pb-zn ores treatment, 26th international mineral processing congress, IMPC: innovative processing for sustainable growth –conference proceedings, India, 2012, pp 5551-5555.

[7]. L. V. Marasanova, T. K., Losina et al., Testing of recycled water supply in the enrichment of lead-zinc ore, Russia, Non-ferrous metals, vol. 9, pp 87-89, 1984.

[8]. Selivanov A.L., Marasanova L.V. et al., Optimization of technological regimes of enrichment of lead-zinc ore on the basis of mathematical models, Mining Journal, Russia, vol.4, pp 101-105, 1985.

https://doi.org/10.5593/sgem2024/1.1/s02.22

[9] Marasanova L.V, Tyushkova, N.I, Research and tests on improving the technology of enrichment of the copper–molybdenum ore, Mineral processing congress IMPC, Australia, 2010, pp 2449-2455.

HISTORICAL FLOODS OF THE LOWER DANUBE BASIN RIVERS DURING THE LAST MILLENNIUM

Carmen-Andreea Bădăluță[1]

Ionel Popa[2,3]

Gheorghe Bădăluță[1]

Anișoara Filip[1]

[1] Ștefan cel Mare University of Suceava, **Romania**
[2] National Institute for Research and Development in Forestry "Marin Drăcea", Câmpulung Moldovenesc, **Romania**
[3] Center for Mountain Economy – CE-MONT, Vatra Dornei, **Romania**

ABSTRACT

Most rivers in the temperate zone experience flooding due to snowmelt or heavy rainstorms. The lower Danube rivers has caused significant economic damages and in some cases even loss of human life. Understanding the relationship between the occurrence rate of Danube rivers flood events and climate change is crucial for flood risk management in Romania. Here we present a multiproxy and observational data set of floods from the lower Danube Basin Rivers over the last millennium. The results highlight that the lower Danube River floods can be divided into two periods: a period with low flood frequency between 1012 - 1490 AD and a period with high frequency of flooding in the years 1501 - 2014 AD. Floods of the Danube River occurred in the spring-summer period, but there are also some exceptions, such as when these events arise either in August-September or December-January. The number of floods increased considerably in the XX century (> 25 events/century) due to climate changes, which determined changes in precipitation regime and meteorological elements. In the last 50 years, the catastrophic floods of Romanian rivers were produced in 1970, 1972, 1975, 1984, 1985, 1988, 1991, 1996, 1998, 2005, 2008, 2010 and 2014. In conclusion, our floods reconstruction significantly contributes to the hydrometeorological events of the Central Eastern Europe database and can be used to improve flood risk management.

Keywords: floods, lower Danube Basin Rivers, last millennium, risk management

INTRODUCTION

The economic and social consequences of floods on the population living in flood-prone areas have increased in the past decades, magnifying the importance of studies in this direction. Analyzing recent and historical events, their patterns and the potentially influential factors are a significant part of understanding the needed management policies. They can provide information about the evolution, triggers and consequences of past and future extreme hydrological events. The middle of the 18th century marked the beginning of systematic meteorological and hydrological measurements. Therefore, most instrumental studies of flood events in Europe and Romania have a temporal extent of less than 150 years and are based on the official statistical data sets of water levels or

https://doi.org/10.5593/sgem2024/1.1/s02.23

constant archives of more or less detailed extreme climatic events. Given the high frequency of floods in the last decades, the significant events are studied intensely and have helped develop new analysis methods. Using SAR images of Bistret, Romania, the GIS techniques helped map the areas affected by the 2006 Danube River flood [1]. Jeneiová [2] analysed the floods in summer and winter in the Upper Danube River basin between 1961 and 2010 using circular statistics. The international effort towards the study of the floods in the Danube River basin has been materialized in a comprehensive regional cooperation of the countries the Danube river crosses regarding the flood regime of the Danube tributaries that includes a historical overview (from 1871 onwards), spatial and temporal analyses and practical management aspects [3]. Although in smaller numbers, studies about the historical floods covering more than 150 years have been conducted in Europe and Romania and have produced significant results. An important contribution was made in 2010 when Glaser et al. [4] evaluated the variability of the floods in Central and Southern Europe (including the Danube) in the last five centuries using documentary evidence. Country-scale analyses have been conducted in various European countries as follows. The floods on the Austrian section of the Danube during the 14th to 17th century were studied using a social approach by Rohr [5], who was interested in the human response to such critical climatic events. The documentary data between 1400 and 1800 in the Swedish territories helped develop a data set that allowed a variability analysis [6] of the flood occurrence pattern in the study area. The number of studies focusing on historical floods in Romania is relatively low. An instrumental dataset for Transylvania was produced in 2019, when Perșoiu & Perșoiu [7] reconstructed the record of flooding events during the last millennium, including the Medieval Warm Period (MWP) and the Little Ice Age (LIA), using historical and sedimentological data from the Somesul Mic River. The ice cover regime in the lower sections of the Danube River was evaluated for an extended time interval (1837 – 2016) in relation to the climate change process [8] and included in the long-term environmental history of the study area.

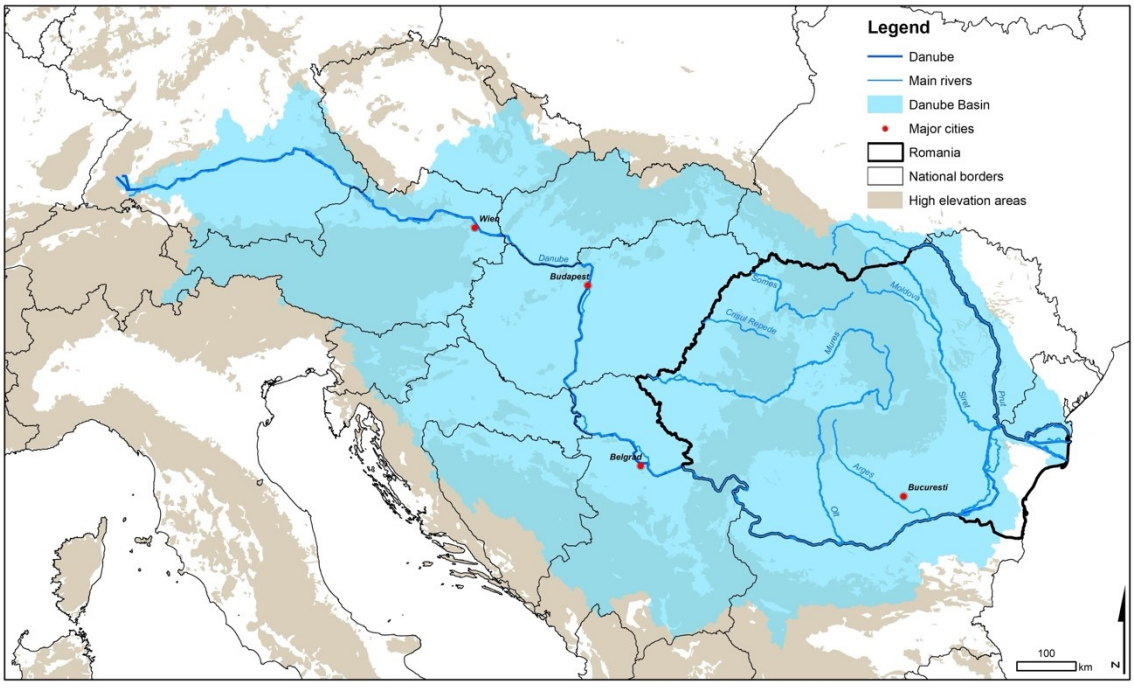


Figure 1. Major rivers of Romania and the Danube catchment mentioned in the text

The Danube River is one of Europe's most important hydrological elements, with a basin covering more than 800,000 km² of the continent. While the actual river crosses ten countries, the basin includes parts of nine other countries, making the research on flood events in the region a matter of international importance. The Lower Danube River Basin covers mainly the surface of Romania. The present study includes the lower section of the Danube River (Bazias – The Black Sea) and a series of its left-back tributaries: Siret, Mures, Somes, Crisul Repede, Prut, Olt, Bistrita, Moldova and Arges. The present study aims to complete the results of previous studies on historical floods by covering the Lower Danube River basin during the last millennium. The main objectives are to highlight the trend of the occurrence of floods from documentary evidences and identify the main factors of their occurrence, as well as the possibility of a synoptic reconstruction.

MATERIALS AND METHODS

Data. The present study is based on printed documents (chronicles, annals, travel notes, diaries) compiled in manuscripts dedicated to climate anomalies and natural disasters from the 20th and 21th centuries (Table 1). We extracted proxy data from the Carpathian regions to understand the drivers and variability of the present and past flood events.

Table 1. Sources of manuscripts used for floods database

Source	Year	Title of publication	Edited	Pages
Topor, N.	1964	Ani ploioși și secetoși	I.Meteorologic Bucuresti	304
Corfus	1975	Însemnări de demult	Junimea	347
Cernăvodeanu & Binder	1993	Cavalerii apocalipsului. Calamitatile naturale din trecutul Romaniei (pana la 1800)	Silex	255
Mustățea, A.	2005	Viituri excepționale pe teritoriul României	București	408
Teodoreanu, E.	2017	In căutarea timpului trecut. Schiță de climatologie istorică	Paidea	364
Boia, L.	2020	Scurtă istorie a dezastrelor naturale. Epidemii, cutremure si dereglări climtice	Humanitas	144

Occurrence rate estimation. To calculate the occurrence rate of the time-dependent floods events we used the following expression by Mudelsee [9] as

$$\lambda(t)=h^{-1}\sum_{n=1}^{m}K\left(\frac{t-T_n}{h}\right)$$

where h is the width of the kernel function (h = 50 years), m is the floods number that occurs, T_n is the time of the n^{th} flood event with the year unit and K is the Gaussian kernel function. The occurrence rate of the floods events was verified with the Cox and Levis statistical test [10].

RESULTS AND DISCUSSION

Long-term spatio-temporal variability of floods, based on 95% of documentary evidence, are presented below for the Eastern Carpathian region. The Dobrogea region was not included due to the absence of documentary data. The results of the observations from the documentary materials highlighted a total number of 236 floods in the period 1000 – 2000 AD (Table 2), of which 11 events were extracted from the work published by Nagavciuc et al., 2021 [11], and 17 events were extracted from hydrometric records. The main hydrographic basins affected by the floods were Siret, Prut, Bistrita, Moldova, Argeș, Olt, Crisul Repede, Mureș, Someș and Danube. To understand the occurrence trend of floods we split the periods into three: Medieval Warm Period (MWP, AD 900-

https://doi.org/10.5593/sgem2024/1.1/s02.23

1300), Little Ice Age (LIA, AD 1450–1850) and Modern Period (MP, 1850–present). The results indicate the lowest occurrence of floods during the MWP and an increase during the LIA and MP periods.

Table 2. Documentary evidence of floods events in Romania between AD 1000 – 2000

River	11th	12th	13th	14th	15th	16th	17th	18th	19th	20th	21th	Total
Siret								1	2	7	4	14
Prut								1	2	12	3	18
Bistrița						1			1	8	2	12
Moldova									1	4	4	9
Argeș									1	6	1	8
Olt						1	3	3	2	13	2	24
Crisul Repede						1	1	5	3	6	3	19
Mureș						4	6	7	8	8	2	35
Someș						1	6	6	2	15	3	33
Danube	3	2	6	2	3	1	1	3	10	22	9	64
Total amount	3	2	6	2	3	9	17	26	32	101	33	236

There is no clear picture of the MWP floods events of the lower tributary rivers of the Danube, but there is evidence of an increase in floods of the Danube River during the 13th century. There is clear evidence of more frequent floods events during the LIA, with the highest number of floods during the 19th century (32 events).

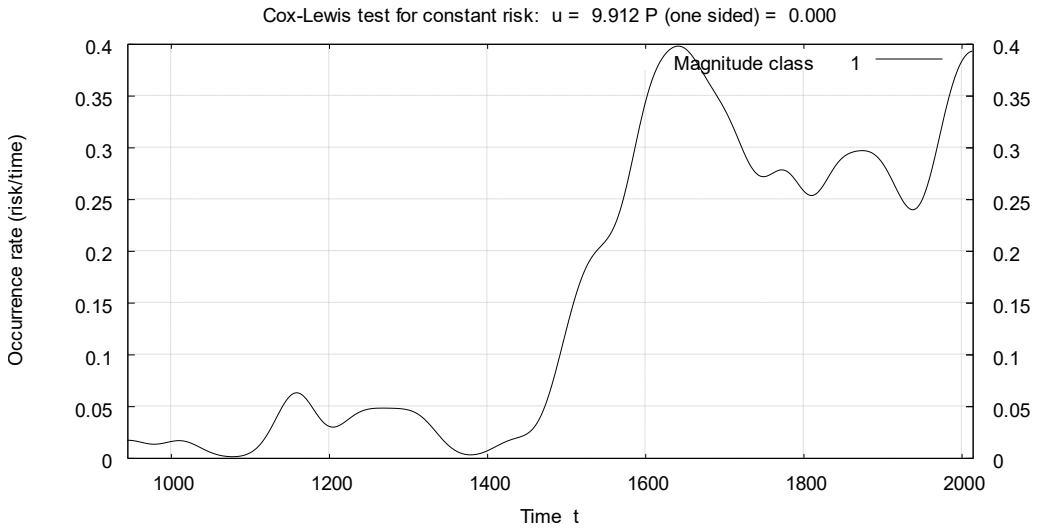


Figure 2. The long–term occurrence rate of flood events in Romania

The documents show that during the LIA the significantly severe floods (labeled by chroniclers as terrible floods) were recorded in the years 1492, 1501, 1504, 1508, 1578, 1593, 1618, 1636, 1654, 1668, 1670, 1730, 1771, 1774, 1783, 1805, 1816, 1831, 1837 and 1846. During the MWP we observed the highest frequency of floods (more than 150 events), with devastating floods occurring in 1897, 1910, 1924, 1970, 1975, 1998, 2005, 2006, 2008 and 2010. The image of the last period, AD 1850 - 2014, is of dramatic hydrology, which is highlighted by the fact that 63.5% of the events occurred during this period. The results coincide with the tendencies of floods events observed at the national level [7, 12, 13] and also for Europe [14,15, 6, 16]. The streamflow in Carpathians rivers depends on the complex interaction of the large-scale atmospheric circulation teleconnection patterns, such as Nord Atlantic Oscillation (NAO), El Niño-Southern

Oscillation (ENSO) [17] and East European–Western Russian pattern [18]. The river flow regime from the lower Danube basin is characterised by high flow during the spring and early summer and low flow during the autumn and winter. In our paper, more than 80% of floods are produced in the summer and spring, and only 15% are produced in the winter. Considering the wet hydrological regime during the MWP and dry during the LIA period [19], we notice that the data from the documentary records differ from those recorded in the natural archives. However, our data indicate changes in atmospheric circulation on a large scale, such as an increase in the frequency of floods during the LIA, which is associated with the negative phase of the NAO index. At the same time, Persoiu [7] associates the increase in flood events from eastern and western Europe from the 16th-17th centuries with increased humidity from the Atlantic Ocean during a predominantly negative NAO phase, but also with moisture advection and local summer storminess for the continental regions. Floods increased during the MP, reflecting the increasing temperature after 1850. The floods associated with the MP result from the rapid melting from the spring and heavy rains.

CONCLUSION

Here, we present the long-time occurrence rate of floods of the lower Danube basin rivers over the last millennium, based on documentary evidences and completed with instrumental data. The results indicate that the past floods variability is different in the three areas analysed: Moldova (Siret, Prut, Bistrita, Moldova rivers), Muntenia si Oltenia (Arges, Olt, Danube) and Transylvania (Mures, Crisul Repede, Somes). The lowest floods occurring during the MWP were identified only for the Danube river and were associated with wet summers. In contrast with MWP, LIA is characterised by a highly increasing occurrence rate of flood events related to a negative NAO phase. Also, our results show that during the LIA, the frequency of flood events is higher in the intra-Carpathian area (Transylvania) than in the extra-Carpathian area (Moldova and Muntenia). This contrast highlights the different moisture conditions of the two regions, with the former's atmosphere being supplied by the Western moist climatic influence and the latter relying on the moisture advection process and mainly summer storms. This study integrates the Lower Danube River basin in the European landscape of flood analysis. It highlights the importance of documentary evidences of such events, producing data that could be used to generate a millennial synoptic reconstruction for the study area.

ACKNOWLEDGEMENTS

C.-A.B. and I. P. were supported by a grant from the Ministry of Research Innovation and Digitization, CNCS/CCCDI–UEFISCDI, project number PN-III-P1-1.1-PD-2021-0744, within PNCDI III.

REFERENCES

[1] Gan, T. Y., Zunic, F., Kuo, C.-C., Strobl, T, Flood mapping of Danube River at Romania using single and multi-date ERS2-SAR images. International Journal of Applied Earth Observation and Geoinformation, 1999, 18, pp. 69–81, https://doi.org/10.1016/j.jag.2012.01.012

https://doi.org/10.5593/sgem2024/1.1/s02.23

[2] Jeneiová, K., Kohnová, S., Hall, J., Parajka, J. (2016). Variability of seasonal floods in the Upper Danube River basin. Journal of Hydrology and Hydromechanics, 64(4), 3, pp 57–366, https://doi.org/10.1515/johh-2016-0037

[3] Pekarova, P., Miklánek, P., Flood regime of rivers in the Danube River basin, 2019.

[4] Glaser, R., Riemann, D., Schönbein, J., Barriendos, M., Brázdil, R., Bertolin, C., Camuffo, D., Deutsch, M., Dobrovolný, P., van Engelen, A., Enzi, S., Halíčková, M., Koenig, S. J., Kotyza, O., Limanówka, D., Macková, J., Sghedoni, M., Martin, B., & Himmelsbach, I., The variability of European floods since AD 1500. Climatic Change, 2010, 101(1), 235–256. https://doi.org/10.1007/s10584-010-9816-7 .

[5] Rohr, C. The Danube Floods and their Human Response and Perception (14th to 17th C). History of Meteorology, 2005, 2, pp 71–86.

[6] Retsö, D., Documentary evidence of historical floods and extreme rainfall events in Sweden 1400-1800. Hydrology and Earth System Sciences, 2015, 19(3), pp 1307–1323, https://doi.org/10.5194/hess-19-1307-2015.

[7] Perșoiu, I., Perșoiu, A., Flood events in Transylvania during the Medieval Warm Period and the Little Ice Age. The Holocene, 2019, *29*(1), pp 85–96, https://doi.org/10.1177/0959683618804632.

[8] Ionita, M., Badaluta, C.-A., Scholz, P., Chelcea, S., Vanishing river ice cover in the lower part of the Danube basin – signs of a changing climate. Scientific Reports, 2018, *8*(1), 7948, https://doi.org/10.1038/s41598-018-26357-w.

[9] Mudelsee M., Börngen M., Tetzlaff G., Grünewald U., Extreme floods in central Europe over the past 500 years: Role of cyclone pathway "Zugstrasse Vb". Journal of Geophysical Research, 2005, 109: D23101, https://doi.org/10.1029/2004JD005034

[10] Cox, D. R., Lewis, P. A. W., The Statistical Analysis of Series of Events. Ann. Math. Statist., 1966, 6, pp 1852–1853, DOI: 10.1214/aoms/1177699183.

[11] Nagavciuc, V., Roibu, C-C., Mursa, A., Stirbu M-I.,Popa, I., Ionita M., The first tree-ring reconstrruction of streamflow variability over the last ∼250 years in the Lower Danube, Journal of Hydrology, 2023, Vol. 617, Part C, 129150, https://doi.org/10.1016/j.jhydrol.2023.129150 .

[12] Radoane M., Chiriloaei F., Sava T., Nechita C., Radoane N., Gaza O., Holocene fluvial history of Romanian Carpathian rivers, Quaternary International, 2019, pp 113-129, https://doi.org/10.1016/j.quaint.2018.11.014 .

[13] Chendeș, V. Bălteanu, D. Micu, D. Sima, M. Ion, B. Grigorescu, I., Perșu, M., Dragotă, C., A database design of major past flood events in Romania from national and international inventories. Aerul și Apa. Componente Ale Mediului, 2015, pp. 25-32, DOI: 10.17378/AWC2015_04

[14] Sheffer, N. A., Y. Enzel, G. Benito, T. Grodek, N. Poart, M. Lang, R. Naulet, and D. Cœur, Paleofloods and historical floods of the Arde'che River, France, Water Resour. Res., 2003, 39(12), 1376, doi:10.1029/2003WR002468.

[15] Benito, G., Castillo, O., Ballesteros-Cánovas, J. A., Machado, M., Barriendos, M. Enhanced flood hazard assessment beyond decadal climate cycles based on centennial historical data (Duero basin, Spain). Hydrology and Earth System Sciences, 2021, 25(12), pp 6107–6132, https://doi.org/10.5194/hess-25-6107-2021

[16] Elleder, L.: Historical changes in frequency of extreme floods in Prague, Hydrology Earth System Sciences, 2015, 19, pp 4307–4315, https://doi.org/10.5194/hess-19-4307-2015

[17] Rimbu, N., Dima, M., Stefan S., Impacts of the North Atlantic Oscillation and the El Niño–Southern Oscillation on Danube River flow variability, Geophysical Research Letters, 2004, 31, 23, https://doi.org/10.1029/2004GL020559

[18] Ionita, M., Interannual summer streamflow variability over Romania and its connection to large-scale atmospheric circulation. International Journal of Climatology, 2015, 35(14), pp 4186–4196, https://doi.org/10.1002/joc.4278

[19] Feurdean, A, Galka M, Kuske E et al., Last Millennium hydro-climate variability in Central–Eastern Europe (Northern Carpathians, Romania). The Holocene, 2015, 25, pp 1179–1192, https://doi.org/10.1177/09596836155801

https://doi.org/10.5593/sgem2024/1.1/s02.23

INSTABILITY CHARACTERIZATION OF THE GEOLOGICAL FORMATION "AREIAS E ARGILAS DE TAVEIRO" IN THE CONDEIXA AND COIMBRA AREAS (CENTRAL-WESTERN PORTUGAL).

Msc. Beatriz Neto [1]
Assist. Prof. Dr. Pedro Santarém Andrade [2]
Assist. Prof. Dr. António Neves Trota [3]

[1]AÇORGEO – Sociedade de Estudos Geotécnicos, Lda. Azores, **Portugal**
[2]University of Coimbra, CGEO - Geosciences Center, Department of Earth Sciences, **Portugal**
[3]University of Azores, CGEO - Geosciences Center, Department of Earth Sciences, **Portugal**

ABSTRACT

The work aims to characterize the slope instabilities present in the Taveiro Sand and Clay - Areias e Argilas de Taveiro - Formation, which occurs in the municipalities of Condeixa and Coimbra, in central-western Portugal. The Areias e Argilas de Taveiro Formation, of Upper Cretaceous – Campanian - age, is made up of successions of metric layers of red, and brownish or pinkish pelites, interbedded with coarse arkosic sandstones. It has as maximum thickness of about 170 m. A total of 27 slopes with stability problems were counted in both municipalities, 16 in Coimbra and 11 in Condeixa. Several information was collected, as morphometrics, the lithological type, the existence of vegetation, the presence of erosive processes, the probable age of occurrence and the type of instability movement. The characterized slopes correspond entirely to excavation slopes. They vary in length from 18 to 180 meters, in height from 1.5 to 7 meters, and in dip from 31° to near vertical. The type of instability found corresponds mainly to shallow landslides (48.4%), and with a significant number of rotational landslides (29.0%) and earth flows (12.9%). Regarding the possible consequences of instability, most of the situations related to instability movements can reach roads with permanent traffic (81.5% of the slopes).

Keywords: Slopes, Stability, Clay, Central Portugal

INTRODUCTION

The study area, with 27 slopes (Figure 1), is in the center-west of mainland Portugal, in the municipalities of Coimbra and Condeixa which border each other in a north-south direction. Coimbra corresponds to the capital of the district and the largest city in the central region, with a total area of around 319.41 km^2 and 140,816 residents. The municipality of Condeixa, also known as Condeixa-a-Nova (Condeixa) has an area of 138.7 km^2 and 16,735 inhabitants.

The study area belongs to the northern sector of the Lusitanian Basin, bordered to the south by the Nazaré Fault and to the northeast by the Porto-Tomar Fault. The Lusitanian Basin has sediments deposited during the Lower Jurassic and Upper Cretaceous.

https://doi.org/10.5593/sgem2024/1.1/s02.24

The geological and geomorphological context of the two studied municipalities, Condeixa and Coimbra, are very different, although some similarities can be observed, especially regarding the West of significant relief. Slope stability studies have been carried out in recent years by several authors, such as [1], [2] and [3].

The study area has a temperate Mediterranean climate, influenced by its proximity to the sea and its openness to humid westerly winds and openness to humid westerly winds, due to the presence of the wide opening of the Mondego River alluvial plain. According to the records between 1981 and 2001 of the Coimbra-Bencanta meteorological station, the months with the highest rainfall are, in descending order, December, November, October and January, with average values of 126.2 mm, 118.1 mm, 116.8 mm, and 107.8 mm, respectively, giving an annual average of 880.9 mm.

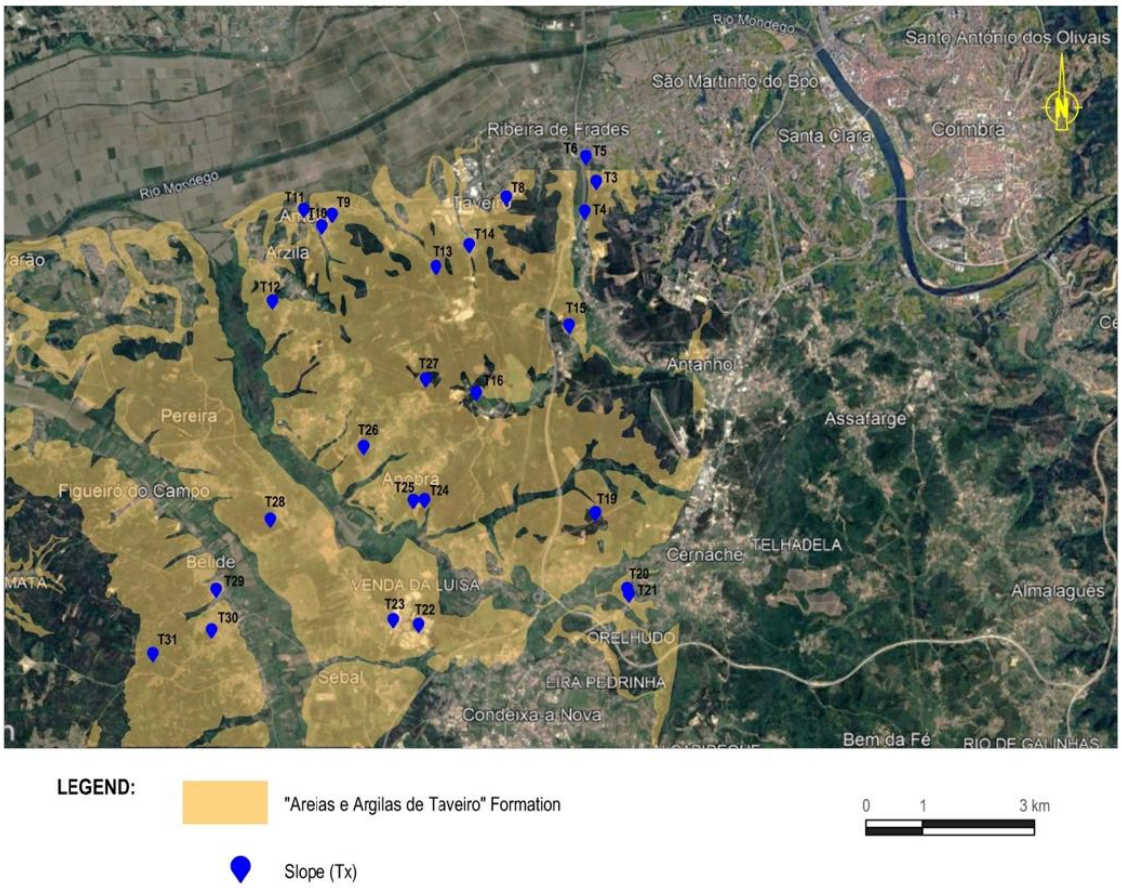


Figure 1 – Location of the studied slopes and cartographic representation of the "Areias e Argilas de Taveiro" Formation - Taveiro Sand and Clay Formation (TSC).

GEOLOGY

The geological unit studied in this work, the "Areias e Argilas de Taveiro" Formation - Taveiro Sand and Clay Formation (TSC) (Figure 1), according to [4], reaches a maximum thickness of 170 ± 10 m. The unit is characterized by successions of metric layers of red, brownish, or pink pelites, laminated and bioturbated. The pelites are interbedded, mainly with coarse sandstones, with pebbles and cobbles, submature to

immature, whitish to pinkish and with interlocking structures, at the base, these levels tend to be coarse. They are followed by kaoliniferous sands that rest discordantly on top of the previous one. It materializes the Middle to Upper Campanian, with the upper limit probably in the Maastrichtian. During the Lower Campanian, there were episodes of diapirism and reactivation of the structure of the Nazaré-Leiria-Pombal axis, which is considered an important diastrophic phase on the continental margin, resulting in the uplift of the southern block, with sedimentation occurring only in the northern sector of the Lusitanian Basin [5].

The Condeixa-Alfarelos aquifer is part of the TSC Formation. The productivity of the aquifer is generally low to very low, with an overall aquitard/aquiclude type behavior. There are some sandstone intercalations, but because they have a lenticular structure their importance is reduced. Recharge is affected by precipitation falling directly on the surfaces of permeable outcrops, considering an estimated recharge of 150 mm/year. The most permeable units of the TSC Formation have a higher piezometric level than the layers of the lower Cretaceous units.

METHODOLGY

The study area was first explored for identification, georeferentiation, and characterizations the slope instability movements (Figure 1). Morphometric, the probable age of occurrence, and the type of instability movement information's were collected.

Parameters evaluated in the slope study included: geometric data (length, height, strike and dip); characterization (lithology, vegetation, surface erosion and fractures, and water flow conditions on the slope); slope behavior: general stability, type of instability, stabilization works, activity (Table 1). To estimate the age of the instability movements and the slopes age construction (mainly the re-profiling), [6] was used, in particular the Street View and Historical Imagery. Some of the characterization parameters were adopted from [7]. The type of slope instability is defined according to [8] and [9]. Slope activity is determined according to [10]. A total of 27 slopes were considered for both municipalities, 16 of which in Coimbra municipality (59%) and 11 in Condeixa municipality (41%).

Table 1 - Parameters evaluated in the slope study.

Parameters	Description
Slope Geometric data	Length, Height, Direction, and Dip.
Characterization	Lithology, Vegetation, Surface erosion, and Water flow.
Slope behavior	Slope type, General stability, Instability type, Stabilization works, Activity.
Slope	Instability and Construction age

https://doi.org/10.5593/sgem2024/1.1/s02.24

RESULTS

The slope lengths vary between 18 and 180 m, whereas the instability zone varies between 2 and 50 m, height between 1.5 and 7.0 m, and dip between 31° and 88°.

The geological units, from top to bottom slope, includes: : vegetal soil, characterized by a thin, dark-colored surface layer of organic material, with a thickness varying between 6 and 18 cm; colluvial deposits, with a thickness varying between 10 cm and 2.3 m; and bottom unit includes sands and clays belonging to the TSC Formation, with a thickness range from 20 cm to 5.5 m., which correspond to the predominant soil on the studied slopes. The studied slopes of the TSC Formation range from clayey to sandy-silty soils, red, pink, gray and occasionally yellow, usually with clasts between 1 and 5 mm in size.

The presence of vegetation over the slopes, top and face slope areas, was assessed. It distinguished three types of vegetation cover: herbaceous cover, shrub cover, and tree cover. Statistically, all the slopes have an herbaceous cover (e.g. grasses, gorse, cyperus, fescue, bramble, heather, ferns), both on top and face slope, with an average height between 10 cm and 1 m, sometimes dense. The shrub cover (e.g. mock privet, acacia and gorse) is found on 5 slopes, mostly at the top of the slopes (60%), but also on the face slope (40%). The average height of the shrubs varies between 1.0 and 1.8 m and is generally scattered or insignificant. Tree cover (e.g. pine, eucalyptus and cork oak), with an average height of between 1 and 6.75 m, is found on 23 of the 27 evaluated slopes (85.2%). This vegetation cover occurs at the top of the slopes (60.9% - 14 slopes), on the slope face (4.3% - 1 slope) and on both (34.8% - 8 slopes). The depth of the roots in the top layers soils was also considered, ranging from 10 cm to 1.6 m.

Surface erosion on the slope face is evidenced by the presence of grooves and depends on the intensity of the erosive processes to which the slope is exposed (considering the number of grooves present, their opening and depth). The highest percentage of grooves was observed on the slopes in the municipality of Condeixa (nos. 22, 23, 25, 26, 27), with 71.4% (5 slopes), while erosion grooves occurred only on two slopes in the municipality of Coimbra (nos. 14 and 21), making a total of seven slopes with erosion processes.

The observed grooves had a minimum length of 25 cm and a maximum length of 6 m, a variable opening from 5 mm to 65 cm, and a depth from 3 cm to 50 cm. To define the density of the grooves, and following [11], a 1 m^2 frame was used as a scale to count the number of grooves in this interval; values between 2 and 5 grooves/m^2 were obtained, with a mean value of 4.14 furrows/m^2. Surface water flow, which is related to the presence of grooves in the slopes, is observed along the face of 13 slopes, representing 48.1% of the sites studied.

The slope characterization also includes the identification of traction cracks, especially in the clayey soils of the TSC unit. Minimum lengths of 10 cm and maximum lengths between 2 and 3 m were obtained, with aperture between 1 mm and 27 cm.

The characterized slopes correspond entirely to excavation slopes. The slopes were evaluated in terms of their general stability, considering the age of the movement, possibility of occurrence, intensity, and type of terrain, in particular rippability and strength. The studied slopes were classified according to [12] as having intermediate stability (40.7% - 11 slopes) and intermediate to poor stability (29.6% - 8 slopes). With

lower percentages, there were slopes with fair to good stability (7.4% - 2 slopes), and finally poor (14.8% - 4 slopes).

The instability type (Table 2) corresponds mostly to shallow landslides (48.4% - 15 movements), appearing associated with movements with a reduced thickness of unstable soil. Rotational landslides were also significant, with 9 movements (29%) observed, which had a spoon-shaped like failure surface. The flows correspond to 6,5% (4) of the recorded slope movements.

In terms of slope activity, according to [10], and during 2023, they are generally classified as inactive (77.8%), i.e. without activity in the last 12 months, but with signs of activity. It was found that there were 6 slopes with suspended activity (22.2%), corresponding to active instability in the last 12 months, but not active at present.

Table 2 - Type of instability and percentage values of slope movements.

Slope instability	Observed instability (%)
Shallow landslide (earth)	15 (48.4%)
Rotational landslide (earth)	9 (29.0%);
Flow (earth)	4 (12.9%)
Multiple	2 (6.5%)
Creep	1 (3.2%)

It was not possible to estimate the age of instability movement for all slopes, as movement occurred after the date of the last available satellite image (18.5% - 5 slopes). For slope n. 24, due to its location in a forest area, it was not possible to use the Google Street View functionality. The slopes where it was possible to define the age of the instability movements, corresponding to 77.8% (21 slopes), showed that the origin of the movements was between 2009 and 2023.

There are no stabilization measures in 40.7% (11 slopes) of the studied slopes. There are only three slopes with more extensive measures, namely slope 10, where there is a 70 cm high concrete wall. Slope n. 13 has a concrete retaining wall along the entire slope, 43 m long and 1.51 m high, with drains at the base and a drainage ditch between the retaining wall and the road. Slope n. 21, where there is a rockfill (about 5 m wide), wooden piles, drainage ditches at the top and on the face of the slope. The presence of drainage ditches at the toe of the slopes is observed in 11 slopes (40.7%). There are instabilities located on slopes in forest (25.9% - 7 slopes) and agricultural/pastoral areas (3.7% - 1 slope).

DISCUSSION

The analysis of slope characteristics, namely slope geometry and lithology, erosive processes, probable age of occurrence and type of instability movement allowed to establish probable causes for slope instability, external and internal.

The presence of vegetation provides information about favorable or unfavorable conditions regarding the stability of the slope. The existence of dense herbaceous

https://doi.org/10.5593/sgem2024/1.1/s02.24

vegetation, which occurs on all slopes, is an indicator of fertile soil with good drainage, and plays a protective role on slopes, reducing the action and direct impact of erosive processes on the slope face. Using [6], deforestation situations were observed between 2006 and 2020, corresponding to the definitive removal of the tree cover, which was present on more than half of the slopes considered (55.6%), and did not occur over the years on 12 slopes (44.4%).

The various studied parameters permitted to define the external causes of instability as surface erosion (92.6% - 25 slopes), water infiltration into the slope (77.8% - 21 slopes) and geometric characteristics, such as the slope's dip (77.8% - 21 slopes) and height (51.9% - 14 slopes). Also identified as likely external causes of slope failure were vibration (25.9% - 7 slopes), mainly from roadways and the constant passage of cars, and the increased weight of the slope due to the presence of overburden at the top (7.4% - 2 slopes), such as buildings and industrial landfills.

The internal causes of instability include clay lithology, which occurs on all the studied slopes (100% - 27 slopes), the decrease in soil strength (100% - 27 slopes) associated with erosion and water percolation. The increase in pore water pressure is also an internal cause of instability, present on 11 slopes (40.7%).

Regarding the possible consequences of instability, most instability situations affect communication routes (roads), with 22 occurrences (81.5% of the slopes). Situations of instability occur close to buildings, namely on two of the studied slopes.

CONCLUSIONS

Over the municipalities of Coimbra and Condeixa, 27 unstable slopes in the Taveiro Sand and Clay Formation were studied. The slope characterization allows the identification and study of various instability situations occurring on 27 slopes belonging to the Taveiro Sand and Clay Formation. It was registered the presence of shallow landslides (48.4% - 15 occurrences), rotational landslides (29.0% - 9 occurrences), and flows (6,5% - 4 occurrences). The major external probable causes of instability are surface erosion (92.6% - 25 slopes), water infiltration (77.8% - 21 slopes) and the slope's dip (77.8% - 21 slopes). The probable internal causes of instability are linked to the clayey lithology intrinsic characteristics, namely the decrease in soil strength, which was observed on all the slopes. Pore water pressure is also an important internal cause of instability, which is verified on 40.7% (11 slopes).

To obtain more detailed information about slope instability, a in situ geotechnical prospection campaign must be carried out. These campaigns might include mechanical borings, in situ test such as Standard Penetration Tests, and laboratory tests such as direct shear and triaxial tests. There is a particular interest in obtaining data on the terrain strength parameters such as the clays units.

When designing road slopes, namely for the Taveiro Sand and Clay Formation, the characteristics of the terrains, particularly the clayey units, must be well studied. Lower slope heights and lower dip angles than those currently existing should be adopted, since in saturated clay soils, strength decreases considerably and leads to slope instability. It is recommended that the clay cut slope’s dip of Taveiro Sand and Clay Formation does not exceed 15º.

ACKNOWLEDGEMENTS

The financial support of FCT-MEC through national funds and, when applicable, co-financed by the ERDF within the PT2020 partnership, through the research projects UID/Multi/00073/2020 of the Geosciences Centre and UID/Multi/00308/2020 is acknowledged.

REFERENCES

[1] Quinta-Ferreira, M., Andrade, P.S., Lemos, L., Saraiva, A., Cut slopes failures on the Triassic beds in Coimbra, Portugal. Bulletin of Engineering Geology and the Environment, vol. 72, pp 383–396, 2013. DOI: https://doi.org/10.1007/s10064-013-0483-6

[2] Quinta-Ferreira, M., Henriques, J., Sá, M., Quinta-Ferreira, M., Henriques, J., Sá, M.P., Study of the excavation slope to enlarge the Alcabideque reservoir, Condeixa-a-Nova. Comunicações Geológicas, 101/Especi III, pp 1151-1154, 2014. http://hdl.handle.net/10316/35244.

[3] Correia, A.A.S., Venda-Oliveira, P.J., Lemos, L.J.L., Strength assessment of chemically stabilised soft soils. Proceedings of the Institution of Civil Engineers: Geotechnical Engineering, vol. 172 / issue 3, pp 218-227, 2019. DOI: https://doi.org/10.1680/jgeen.17.00011

[4] Soares, A. F., Marques, J. F., Sequeira, A. J. D., Notícia Explicativa da Folha 19-D Coimbra-Lousã. Carta Geológica de Portugal, na escala de 1:50 000. Departamento de Geologia. Instituto Nacional de Engenharia, Tecnologia e Inovação, Lisboa, 2007. (in portuguese)

[5] Cunha, P., Reis, R., Cretaceous sedimentary and tectonic evolution of the northern sector of the Lusitanian Basin (Portugal). Cretaceous Research, vol. 16/, issues 2-3, pp 155-170, 1995. DOI: https://doi.org/10.1006/cres.1995.1013

[6] Google Earth Pro, Google Earth Pro 7.3.6.9345 (64-bit), 2022.

[7] Ko Ko, C., Flentje, P., Chowdhury, R., Landslide Qualitative Hazard and Risk Assessment Method and its Reliability. Bulletin of Engineering Geology and the Environment, vol. 63, pp 149-165, 2004. DOI: https://doi.org/10.1007/s10064-004-0231-z

[8] Dikau, R., Brunsden, D., Schrott, L., Ibsen, M., Landslide Recognition. Identification, Movement and Causes. John Wiley & Sons, Chichester, 1996, 272 p.

[9] Cruden, D. M., Varnes, D. J., Landslides. Investigation and Mitigation. Special Report 247. Ed. Keith Tuner e Robert Schuster. Transportation Research Board. National Research Council. National Academy Press, Washington D.C., 1996, 247 p.

[10] WP/WLI, Multilingual landslide glossary. Working Party on World Landslide Inventory - UNESCO. International Geotechnical Societies - IGS, Canadian Geotechnical Society, Richmond, British Columbia, 1993, 32 p.

[11] Sobotková, V., Dumbrovský, M., The new volumetric approach for field measurements of rill erosion. Eurasian Journal of Soil Science, vol. 4, issue 2, pp 94-99, 2015. DOI: https://doi.org/10.18393/ejss.10435

[12] IDOM, Ficha de Taludes – Subconcessão Baixo Alentejo. IP2 – Variante Nascente de Évora Lanço E – IP2 Évora (A6/IP7) / São Manços. APA – Avaliação de Impacte Ambiental n.°1202 – Anexos – Taludes, 2009. https://siaia.apambiente.pt/RECAPE2.aspx?ID=353 (in portuguese)

INVESTIGATION OF SEAWATER INTRUSION IN SHABLA-KRAPETS REGION, NE BULGARIA

Ing. Marin Ivanov[1]

Assoc. Prof. Evelina Damyanova[1]

[1] National Institute of Meteorology And Hydrology, BAS, **Bulgaria**

ABSTRACT

The present study aims to investigate the current conditions of saltwater intrusion in the Shabla - Krapets area, a long-known area of groundwater salinization. The main objectives of this investigation are (i) to find the interface (boundary) between fresh and salty (brackish) water and (ii) to study the seasonal dynamic of saltwater movement in the aquifer (intrusion). The results were obtained from July 2022 to the end of 2023. In the area of investigation (aquifer), there is a fresh groundwater layer which thins towards the sea. The interface between fresh and saltwater was found in 3 boreholes. The interface dynamics of seawater intrusion have been studied for one and a half years. The obtained results can be a reasonable basis for continuing and improving the monitoring of the seawater intrusion area and can be used as a base for groundwater modeling.

Keywords: groundwater, saltwater intrusion, electrical conductivity, NE Bulgaria

INTRODUCTION

The seawater intrusion problems are common with coastal aquifers all around the world and have been reported by many authors [9], [10], [12], [13]. Frequent extreme climatic events strongly impact saltwater intrusion processes in groundwater in coastal regions. More frequent torrential rains and droughts lead to decreased recharge and increased groundwater extraction. The coastal regions that depend only on groundwater are heavily affected by climate changes and human activities [8], [11], [12]. Most of the coastal areas have noticed rapid population growth during summer, increasing water demand for urban, agricultural, and industrial supply. Overexploitation of groundwater in combination with sea level rises will lead to a natural replacement of groundwater with saline water, increasing saltwater intrusion problems. Managing and controlling the delicate balance between fresh groundwater and seawater is a global challenge.

The first analytical solution describing the spatial location of the interface were made independently by Ghyben (1888) and Herzberg (1901).

Saltwater (or seawater) intrusion Shabla – Krapets area is situated in North-East Bulgaria, part of Dobrudja (Dobrudzha) region on the coast of the Black Sea (Fig.1a). The area of research is built up from Neogen karstified limestones - forming the Sarmatian aquifer, which recharge area is characterized by a decreasing the precipitation in recent decades. The aquifer has an average thickness of 80 m, covered by a layer of clay and loess with a 5 - 15 m thickness. The water-bearing formation has high hydraulic parameters. The area of interest is located in the “Shabla” seismic zone. There are no permanent rivers and

https://doi.org/10.5593/sgem2024/1.1/s02.25

surface runoff exists in this region. The aquifer is the main source of fresh water for all water needs of the local population (drinking water, agriculture, industry, etc.). The present study aims to investigate the current situation in the Shabla - Krapets area, which is a long-known area with saltwater intrusion problems, which have been documented along the coast of Bulgaria for more than 40 years [1-3], [11], [12]. The main objectives of this investigation are (i) to find the interface (boundary) between fresh and salty (brackish) water and (ii) to study the seasonal dynamic of saltwater movement in the aquifer. Generally, the studied area can be divided into the southern part of the Shabla subzone (agriculture) and the northern part of the Krapets subzone (urbanized and agriculture). A monitoring network consisting of 24 monitoring points (MP`s) was established for the research objectives (Fig.1b.), where monthly observations of groundwater levels, temperatures, and SEC (Specific Electrical Conductivity) profiles in boreholes were conducted. The main principles on which the network is based are to monitor in time (monthly) and space (areal and depth distribution) the background of the SEC, the interface, the mixing (transition) zone above the saltwater (brackish water).

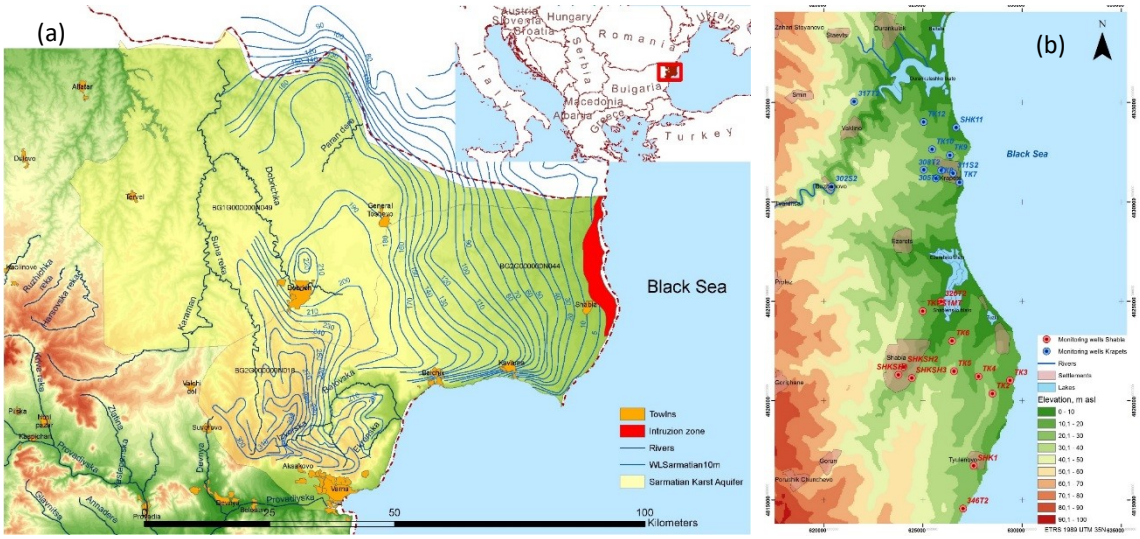


Fig. 1. Location of the study area (red colour)

MATERIALS AND METHODS

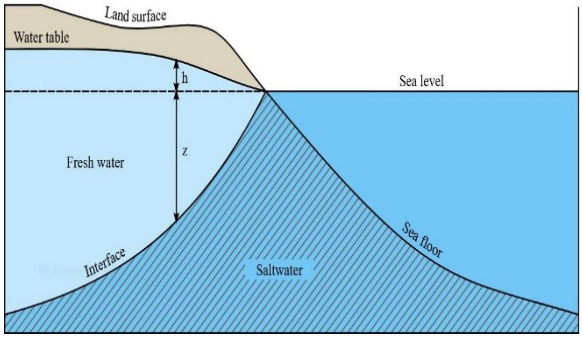
Initially, the main goal of this investigations was to find the interface between fresh and salt water, which was done in the first sampling campaign before the establishment of the monitoring network. Subsequently, the idea arose to monitor the dynamics of the interface and transition zone.

In order to evaluate the extent and depth of groundwater salinization and interface dynamic, this paper is based on the data of monthly profiling along the water column in existing monitoring points (boreholes and shaft wells), including groundwater levels and conductivity. Initially, the available archival materials for the area were reviewed. Based on information from previous studies [4], [5], [7], the potential area affected by intrusion was taken into account. All archive information for boreholes and well locations was collected in the GIS database, analyzed, and mapped. Based on data analysis and the first fieldwork campaign, a monitoring network for saltwater intrusion was created with appropriate boreholes. Monthly monitoring of SEC profiling was started. A sampling

campaign for water chemistry (Cl, SO_4, Na, and SEC) in different monitoring wells and depths was done to evaluate the relation between SEC and salinity [9]. Another field trip for precise elevation (altitude) geodetic measurements off all MP`s was conducted, and two water samples from the Black Sea for density were taken.

The created monitoring network consists of 25 wells, ten private boreholes, five public shaft wells, ten from the national monitoring groundwater network, seven boreholes, and three shaft wells. Based on recommendations and conclusions from past research [5], [6], where the Ghyben-Herzberg method was used and analysis of collected data, we assumed that the groundwater flow conditions can be taken as a steady state [10] and the same approach can be applied. The difference between the previous and the present studies is to verify the validity of the used approach by investigating the similarity between the calculated and observed interface depths.

The first analytical solution describing the spatial location of the interface were made independently by Ghyben (1888) and Herzberg (1901). Their analysis is based on the hydrostatic equilibrium between seawater and groundwater, resulting in the weight of fresh water (between the groundwater surface and the interface) being balanced by the weight of salt water (between the sea level and the interface) (Fig.2).



$z = \frac{\rho_f}{(\rho_s - \rho_f)} h$, where

ρ_s – density of freshwater, 1.000 g/cm^3 at 20 °C

ρ_f – density of sea water, about 1.025 g/cm^3

h – freshwater zone above sea level in meters

Fig. 2. Ghyben–Herzberg conceptual scheme

(Source: https://en.wikipedia.org/wiki/Saltwater_ intrusion)

RESULTS

The recharge rates and seasonal changes of groundwater levels are one of the main factors controlling the movement of saltwater intrusion. On Fig. 3 (a) are shown the industrial pumping wells with their average pumping rates in L/s, and in (b) and (c) are shown the MP`s in south and north subzones with average groundwater levels for 2023. The total pumping rate is 161 L/s, according to public information from the Black Sea Basin Directorate. Using the created hydrodynamic map and Darcy's law, with average transmissivity in Krapets subzone 845 m^2/d with a hydraulic gradient of 0.0007 and 2000 m^2/d and 0.001 In Shabla sub-zone, the average rate of flow drained across the intrusion zone is 59 L/s and 353 L/s respectively. The average thickness of the water column below sea level in the aquifer is 80.0 m. [2].

https://doi.org/10.5593/sgem2024/1.1/s02.25

The groundwater level changes during the study period in all MPs, near the coast and inland, have similar seasonal fluctuations, with the maximum amplitude reaching 30 to 45 cm and the minimum being 10 cm in 317T2 outside the intrusion zone. The water table fluctuations have no significant movement, so we assume that the system can be simplified as steady-state conditions, which gives us a reason to use the Ghyben-Herzberg approach. Due the small changes of groundwater levels the recharge rates are assumed as negligible – less than 1 %.

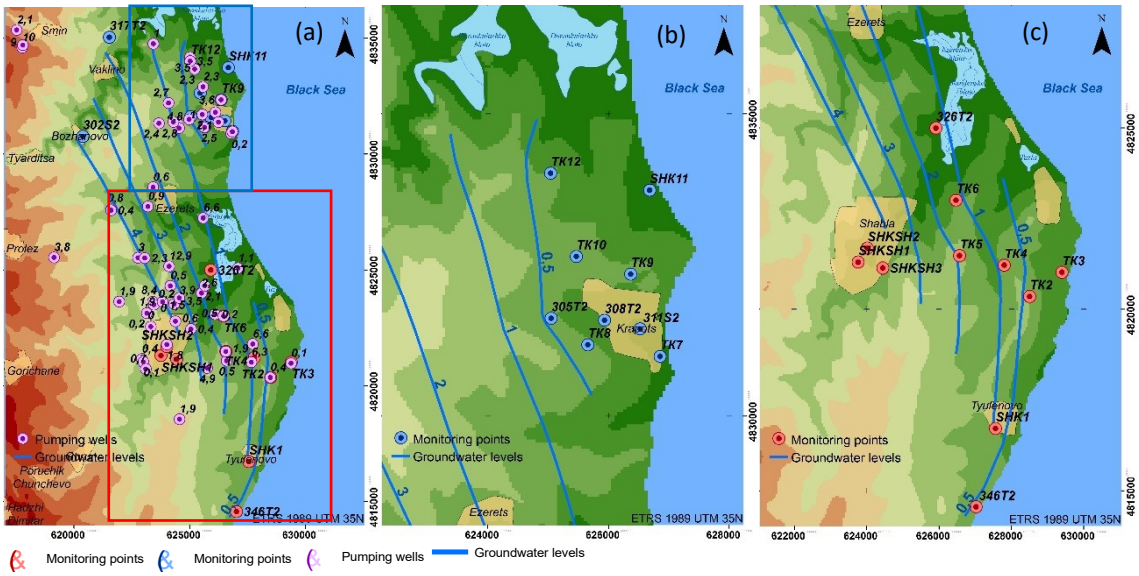


Fig. 3. (a) Purple is pumping wells; (b) north Krapets subzone; (c) south Shabla subzone.

The results from SEC profiles were obtained from July 2022 to the end of 2023. Water chemical studies show a good correlation between Cl, SO_4, and Na from one side and specific electrical conductivity (SEC) from the other side (Fig. 4). The determination coefficient is in the range from 0.983 for Cl to 0.994 for Na, where the main group are valid to SEC around 2500, and only one sample reach 7800 µ/cm [6].

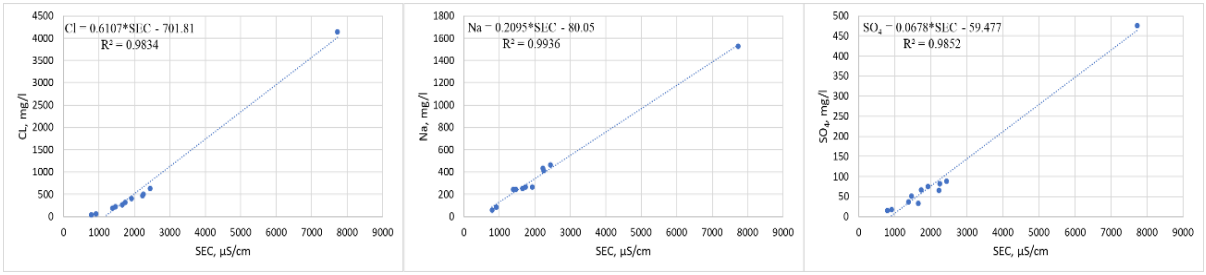


Fig. 4. Correlation between Cl, Na, SO_4, and SEC

During investigations we found that the top layer of groundwater is a freshwater (slightly affected by salinization – usable water) in entire area affected by salinization, which data should be used as a basis for further studies.

After the first field camping (during the establishment of the monitoring network), we found the interface in 2 boreholes (Table 1) where the SEC of the profile reached 20 000 µS/cm (Fig. 5). In TK4 where a significant increase of SEC profile was observed the transition zone (mixing or diffusion zone) has been found. We extrapolate data linearity (average from all available observations) to around 20 000 µS/cm, where the average

depth of interface – 40 m depth below sea level was found. The mean density of seawater samples taken offshore (north and south) in the intrusion zone is 1.0128 g/cm^3.

Based on the maximum aquifer depth of 100 [2], the area affected by saltwater intrusion was delineated using the Ghyben–Herzberg approach (Fig. 5), where the area of salinization reached 52 km^2 for 2023. Compared to previous studies, the average depth of the interface increased by 2 m from 1996 to 2023 in borehole 305T2 [2].

Table 1 Observed and estimated interface depth

Subzone	Number of MP	Distance from the Black Sea, m	The mean water level of groundwater above the Black Sea, m	Observed depth of mixing zone – z, m	Observed depth of interface – z, m	Estimated depth of interface – z, m	ρ s – density of seawater, g/cm^3
Krapets	TK7	60	0.05	4-6	5-7	6.2	1.0128
	305T2	1830	0.3	17-20	21-22	23.4	1.0128
Shabla	TK4	1710	0.51	28-34	Below 34	39.8	1.0128

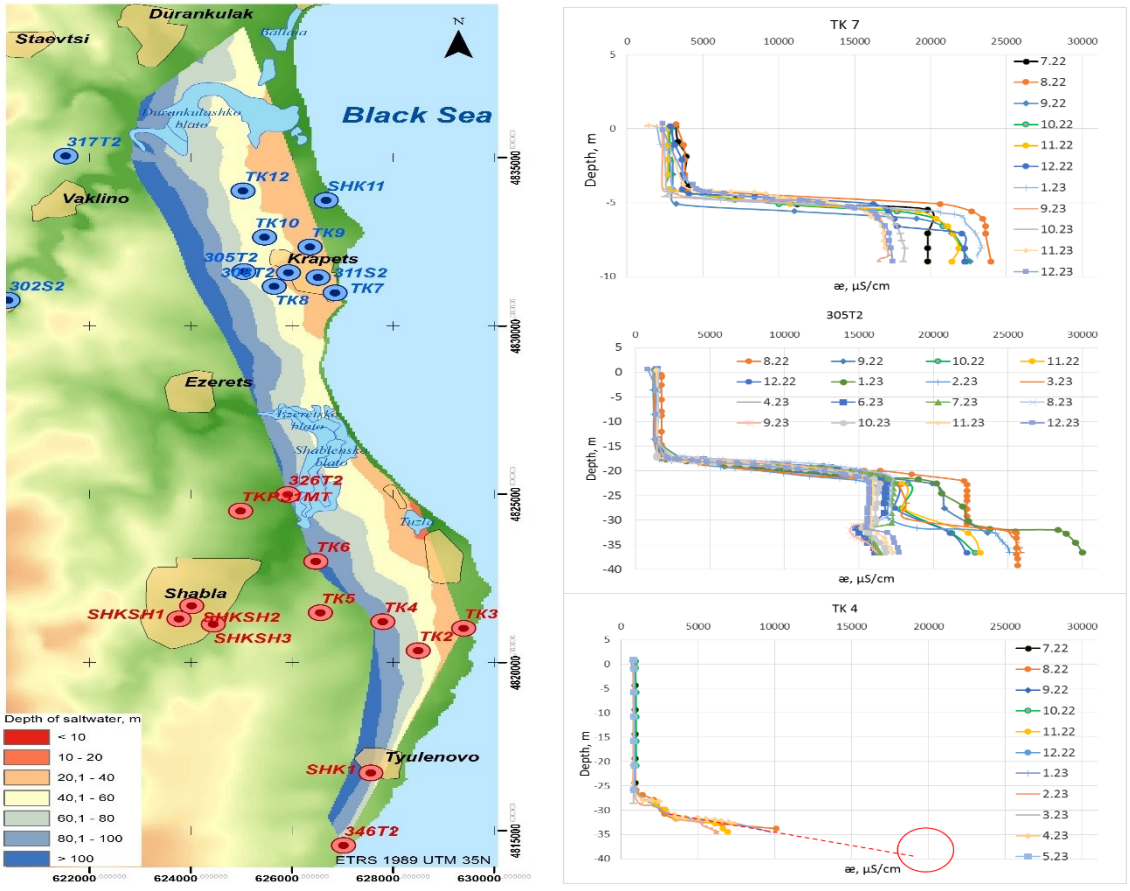


Fig. 5 Delineated intrusion zone (left) and MP profiles with observed Interface (right)

In the TK7, 305T2 boreholes where interface was found and in TK7 where transition zone of salinity water exists the groundwater changes during investigations vary from 0.45 m in 2022 to 0.13 m in 2023 shown on Fig. 5.

https://doi.org/10.5593/sgem2024/1.1/s02.25

To analyze the collected monthly data, we divide the obtained SEC profiles (Fig. 5) into two breakpoints to study the dynamics of the interface and the transition zone. The transition zone is assumed to be presented by the initial significant sharp changes of SEC, called the first breakpoint or the beginning of the transition zone (brackish water). The second breaking point presents the interface, beginning of profiles where SEC stays stable in depth. Above this point, SEC changes represent the upper usable freshwater layer. The second break point represents the interface, the beginning of the profiles, where the SEC remains stable at depth (Fig. 5).

In the following, the breaking points that were found are described in each monitoring borehole

The monitoring point TK7 is located 60 meters from the coast and presents the north Krapets subzone. The maximum variation in depth of the first breaking point is 1m with maximum SEC changes of 1600 μS/cm. In the second breaking point level changes are up to 1.60 m, with SEC to 8000 μS/cm. The amplitude of thickness of this transition zone is 3 m.

The observation borehole 305T2 is located 1830 m from the seashore in the northern part (Krapetz subzone). The maximum variation in the interface's depth in the first breaking point is 4.00 m, with SEC changes of 600 μS/cm. The depth of the second breaking point reaches 1,7 m, where SEC amplitude is again up to 8000 μS/cm. The overall depth of the transition zone is 5.30 m. In this borehole the third and fourth breaking points are observed in depth around 31 m below sea level. We took a water sample in depth and detected hydrogen sulphide in the sample by smelling.

TK4 is located in the southern part of the investigated area, 1710 m from the coast. The maximum amplitude of the first breaking point is up to 2.20 m where SEC deviate to 300 μS/cm. The second breaking point (interface) changes are not observed because the borehole is not deep enough. The transition zone here has to have a bigger thickness, from 28 to the assumed 40 m (extrapolated).

DISCUSSION

The water level changes during the investigation have amplitude of 45 cm, which does not significantly affect the interface location. This is probably because the period between high and low groundwater level changes is short enough not to significantly affect the interface's movement. The rates of recharge are predominantly stable, because of the negligible changes of water level compared to the thickness of the saturated zone (80 m).

The very good correlation between main salinization ions and SEC proves that the conductometric method can be used as one of the easiest and cheapest tools for seawater intrusion monitoring in the investigated area. The conductivity profiling in TK4 doesn`t reach the interface, because of not enough depth of the borehole, we use to extrapolate the data after first breaking point with linear trend till SEC reach around 20 000 μS/cm, as observed on other wells. After this assumption we found the average depth of around 40 m.

The calculated interface depth using the Ghyben-Herzberg approach was verified with the observed monthly average depths in three boreholes. The used method is suitable for monitoring the intrusion zone and proves the previous investigations [2].

Monitoring point TK7 is located 60 meters from the coast, where we expected to be affected by tides and storm waves in the Black Sea due to the very well karstified aquifer. The results shows that there is not significant changes of interface and transitions zone. This is probably due to the fact that the aquifer between the well and the sea is less permeable, due to the presence of the upper clay layer or poorly karstified limestones.

Above the first breakpoint, SEC changes represent the freshwater layer, which thinning towards the coast, where the main drivers of their changes should not be influenced by saltwater and are most likely influenced by natural or human activities in the inland aquifer. In general, the conductivity rises in the dry periods and decreases in the wet season.

CONCLUSION

Monthly observations of groundwater levels, temperatures, and SEC profiling along the water column were conducted in a long-known saltwater intrusion zone in the Shabla-Krapets region over a year and a half. Due to the small fluctuations in groundwater levels, compared to the average thickness of the saturated zone in the aquifer, the recharge rate changes are negligible and are less than 1%. An almost perfect correlation between main salinization ions and SEC was found with the lowest coefficient of determination 0.983. This proves that the method of SEC borehole profiling is one of the easiest and cheapest methods for saltwater intrusion monitoring. During investigations, a lot of data for SEC changes of the top freshwater layer was collected and should be used for further studies. The Ghyben–Herzberg approach was used to delineate the area and depth of the intrusion zone which reached 53 km^2. The results were calibrated from three observed boreholes (where the interface was found) and the differences between the calculated and measured depth of saline water are in the acceptable range from 2 to 3 m. The interface using breaking points represents the significant changes in SEC profile data used to study the dynamic of the interface and transition zone. The maximum deviation in the depth of the first breaking point represents the beginning of the transition zone reaching 4 m with maximum SEC changes of 1600 μS/cm. The interface or second breaking point in the observed boreholes has almost the same changes in depth from 1.6 to 1.7 m while the maximum specific conductivity variations reach the same values - 8000 μS/cm. The thickness of the transition zone is declining from inland to the sea. The interface in 305T2 situated 1830 m inland rose by 2 meters from 1996. The area of intrusion is naturally affected by seawater.

ACKNOWLEDGEMENTS

We greatly appreciate the support of the Ministry of Environment and Water of Bulgaria in sponsoring the investigation.

REFERENCES

[1] Danchev D., Damyanov At., Nikolov E., Velinov V., Andonova G. Hydrogeological study of groundwater in Bulgaria and compilation of a hydrogeological map for zoning according to water abundance in Southern Dobrudja and Ludogorie, Summary updated report, Contract – 764, Sofia, 1977. (Personal contact) In Bulgarian

https://doi.org/10.5593/sgem2024/1.1/s02.25

[2] Galabov M., Penchev P., Velikov B., Damyanov A., Development of measures to protect the aquifers near the Black Sea from pollution due to the seawater intrusion, Contract – 1130, 1989. (Personal contact) In Bulgarian

[3] Pentchev P., A general assessment of the seawater intrusion in the Sarmatian karst aquifer: Geology and Mineral Resources, 9-10, p, 19-23, 1996. (In Bulgarian)

[4] Pentchev P., Consultancy services in connection with the project: Integrated Management of Transboundary Groundwater between Bulgaria and Romania in Dobrudja/Dobrogea Area - Technical Assistance to ensure transboundary groundwater management using the WFD and Groundwater Directive, EuropeAid/122633/D/SER/BG), EPTISA Servicios de Ingenieria, S, A, 2007. (Personal Contract)

[5] Pentchev P., Velichkov V., Velichkova B. Carrying out exploratory monitoring to establish the sources of pressure in the event of a worsening in the state of the groundwater body in the Krapets - Shabla - Tyulenovo region of seawater intrusion, Contract - №370/09,05, Sofia, 2017 (Personal Contract) In Bulgarian

[6] Revelle R., Criteria for recognition of sea water in groundwaters, Trans, Amer, Geophysical Union, v. 22, pp 593-597, 1941.

[7] De Breuck W., Hydrogeology of Salt-Water Intrusion: Methods and Instruments, Verlag Heinz Heise GmbH & Co KG, Hannover, Germany, pp 223, 1991.

[8] Lanbo L., Saline water intrusion, Encyclopedia of Life Support Systems, Natural and Human Induced Hazards 2, 1 – 7, 2016.

[9] Hem J.D., Study and interpretation of the chemical characteristics of natural water: U. S. Geological Survey Water Supply Kaper 2254, 263, 1989.

[10] Essaid, H. I., USGS SHARP Model, in Seawater Intrusion in Coastal Aquifers: Concepts, Methods, and Practices, edited by J. Bear et al., pp. 213 – 246, Kluwer Acad., Norwell, Mass., 1999, DOI: 10.1007/978-1-4020-6682-5_9.

[11] Pulido Bosch, A., Machkova, M., Lopez-Chikano, M., Calvache, M.L., Dimitrov, D., Calaforra, J.M., Velikov, B. and Penchev, P., Hydrogeology of the Upper Aquifer, Dobrich Region (Northeastern Bulgaria), Hydrogeology Journal, Vol 5, No 2, p.75-85, 1997.

[12] Pulido-Bosch, A. (Principal contractor), Dimitrov, D., Machkova, M., Pentchev, P., Velikov, B., (Subcontractors), Ecological Problems of Karst Waters Caused by Overexploitation and Contamination (1994 -1996), Fixed Contribution Contract No. CIPA-CT93-0139 between the European Economic Community and the University of Granada, Spain, 1996.

[13] Cooper, H.H. A hypothesis concerning the dynamic balance of fresh water and salt water in a coastal aquifer. Journal of Geophysical Research 64: 461–467, 1959.

ROCK FALL STUDY IN DIFFERENT AREAS OF SOUTHWEST ANGOLA

Assist. Prof. Dr. Pedro Santarém Andrade[1]

MSc. Elsa Kaúla[2]

[1]University of Coimbra, CGEO - Geosciences Center, Department of Earth Sciences, **Portugal**
[2]Instituto Superior de Ciências de Educação da Huíla, Departamento dos Assuntos Científicos e Pós-graduação, **Angola**

ABSTRACT

In this work, a rock fall assessment was carried out in two distinct areas in southwest Angola. One is located next to Chapel of Nossa Senhora do Monte in the urban area of Lubango. The other area is located on the road between the city of Lubango and the tourist area of Tundavala. The rock mass of the first area belongs to the Tundavala Formation of the Chela Group and consists of quartzitic-sandstone with a sub-horizontal bedding attitude. The rock mass in the second area is composed of quartzitic-sandstone and red siliceous volcaniclastic rocks belonging to the Chela Group. Precipitation and anthropogenic action were defined as important causes for the occurrence of rock falls. Several slope sections were used to run rock fall analysis. The slope profiles and the origin, dimension and paths of the falling rocks were defined and studied using the Rocfall software of Rocscience packages. For each slope section different simulations were performed, assuming two different mass values for each seeder positions. It was observed that the characteristics associated with the coefficients of restitution and the friction angle of the materials that make up the slopes correspond to determining factors for the trajectory, speed, and bounces of the falling rock blocks. The existing rock fall can cause vehicular damage and cause human injury. Slope stabilization procedures are proposed based on the results of the rock fall assessment.

Keywords: Rock Fall, Slopes, Angola, Road

INTRODUCTION

The study considers two different areas in Lubango and its surroundings, Province of Huíla (SW Angola). One area is named Slope 1 and located near the Chapel of Nossa Senhora do Monte, which is situated in the Southwest part of the city of Lubango. The other area is designated as Slope 2 and is located along the road between Lubango and the tourist area of Tundavala and is of great patrimonial importance [1]. The quartz-sandstone presents outcrops in both the study areas, and the volcanoclastic rocks occur only in Slope 2. Each studied slope was divided into three sections. For Slope 1, the sections were named as S1, S2 and S3 (Figure 1) and for Slope 2 were designated as T1, T2 and T3 (Figure 2).

Climate is characterized by two main seasons in studied areas: the rainy season, which corresponds to a period of nine months, from mid-October to mid-April, and the dry

https://doi.org/10.5593/sgem2024/1.1/s02.26

season, which comprises the remaining months of the year. The heaviest rains generally occur between the beginning of January and the end of March, and the average total annual precipitation is around 800 mm. The distribution of the rainfall is quite variable, from year to year, sometimes with particularly rainy years, which contributes to the increase in slope instability. The considered areas are affected by slope stability problems, predominantly rock falls. The slope sections are characterized by rock fall trajectories that can reach or come close to roads or even pedestrian areas, such as the one situated next the Chapel of Nossa Senhora do Monte. The analysis of the slope sections with Rocfall software [2] was used for the study of the mass rock stability, contributing to an appropriate definition of mitigation measures.

GEOLOGY

The studied areas belong to the Marginal Mountain Range of Angola, which constitutes a morphological "step" that marks, especially in the western and southern half of the province of Huíla, the border between this and the province of Namibe. The studied slopes are constituted by rocks belonging to Chela Group formations, which are composed by various types of rocks, with prevalence of detrital sedimentary rocks and volcanoclastics. The Chela Group corresponds to a relatively undeformed Palaeoproterozoic supracrustal sequence, and generally presents a horizontal to sub-horizontal bedding and has a minimum thickness of 600 m. According to [3] the depositional age of the Chela Group in the Humpata Plateau is constrained at 1798.4 ± 10.6 Ma. The basement rocks of the Chela Group correspond to gneisses and migmatites, syntectonic foliated peraluminous granites, and late-tectonic metaluminous granites of the Chela and Gandarengos Mountains. Rb/Sr radiometric age of 2.1 ± 0.1 Ga was defined for the syntectonic granites, for the late-tectonic Chela granite was obtained a zircon U-Pb age of 1947 ± 5 Ma. This isotopic dating allowed establishing a maximum age for the Chela Group [4]. Chela Group comprises four formations, from the oldest to the most recent, respectively, designated as: Tundavala Formation; Humpata Formation; Bruco Formation and Cangalongue Formation.

The studied slope of Senhora do Monte (Slope 1) is composed of quartz-sandstone that belongs to the quartz-arenitic Senhora do Monte Member of the Tundavala Formation. The layers show an approximately horizontal orientation and overlie the granitic formation that outcrops in the city of Lubango. The rock formations are covered, in the upper part of the Slope 1, by debris deposits, of varied granulometry with coarser elements which correspond to quartzite, quartz-sandstone and greso-conglomeratic rocks that appear together with sandy material.

The quartz-sandstones of the Slope 1 have whitish, yellowish, brownish, or pinkish colors. Quartz is present as predominant mineral. The presence of feldspars and other mineralogical and lithological components is extremely reduced, being less than 5%. The quartz-sandstones show a granular texture, medium grain, and quartz cement, some of them have a reddish tint due to the quartz-hematitic cement. Quartz-sandstones show a textural and mineralogical maturity and present medium strength; it is observed an increase of strength with a greater presence of siliceous cement [5].

The local geology of the second study area (Slope 2) includes rocks belonging to the upper part of the Humpata Formation and to the bottom of the Bruco Formation, namely the member composed of red and siliceous volcanoclastic rocks and another member of sandstone, the latter can be seen at the top of the plateau area along the access road to

the Tundavala Cleft. Typical lithologies of the Humpata Formation can be observed on Slope 2, in which, in addition to whitish and yellowish quartz-sandstone layers, there are also layers of finer, pelitic lithology, intercalated with sills and veins of reddish volcaniclastic rocks or whitish siliceous and acidic veins. The quartz-sandstone are coarse and fine grained, sometimes compact or laminated and show medium strength. The pelitic rocks show a laminate internal structure.

METHODOLGY

For the accomplishment of the present work, it was carried out the identification of different locations, in the urban area of Lubango and its surroundings, where situations of unstability, namely falling rock blocks, can occur. This characterization was performed considering the location, lithology and dimension of the rock blocks.

In the present work, the software Rocfall belonging to [2] was used. For the instability situations study, the slope profiles and also the origin, dimension, velocity and paths of the falling rocks were defined. The slopes profiles allowed a perception of the terrain's topography; permitted to locate the geological formations and define the area where adjacent roads are situated. For each studied area, three slope sections were used on the Rocfall analysis. The possible rock fall trajectories on the slopes sections are obtained by considering different rock falls starting locations (seeders). It is necessary to define the parameters of the material that occurs on the slopes, which is decisive for the falling trajectory of the rock blocks. The ratio between the velocity before and after the impact of rock blocks on a given surface is expressed by the coefficient of restitution.

Rock surfaces less fractured show high values of restitution coefficients, while soils, gravel and weathered rock masses present low restitution coefficients. For the coefficient of normal restitution (Rn) and the coefficient of tangential restitution (Rt) values were considered those established by the Rocfall software, and by authors such as [6], [7], [8], [9] and [10]. For a better adjustment of Rn and Rt values, several back-analysis were carried out, considering the falling rock blocks present in the studied areas. The software Rocfall of [2] permits to determine the velocity and height of the bounces that occur along the trajectory of the rock blocks and its final location. Rocfall results can help planning stabilization or mitigation measures for falling rock material.

RESULTS

The Slope 1 is approximately 15 m high, 200 m long and with dip between 70ºS and 90º. There are 3 to 4 joint sets, one of them correspond to the stratification, with dip values between 6º and 13º, and the other sets show dip values greater than 60º.

For Slope 1 were considered 3 sections (S1, S2 and S3 (Figure 1)). The different sections show, approximately, an E-W direction, the perpendicular distance between Section 1 and 2, and between Section 2 and 3, are, respectively, 40.8 m and 43.8 m.

The values of the specific mass of the rock material were considered, according to results of laboratory tests of quartz-sandstones rocks that allowed defining the specific weights of 24.0 kN/m^3 and 25.0 kN/m^3, respectively, for the lower and highest strength quartz-sandstones. The joint spacing is, generally, between 6 and 20 cm, and also between 20 cm and 600 cm. The discontinuity surfaces associated with the stratification show a persistence between 1 and 3 m. Joints surfaces are generally classified as rough. Vegetation on face of Slope 1 is inexistent to scarce. The slope movements are

https://doi.org/10.5593/sgem2024/1.1/s02.26

predominantly rock falls and can cause human injury and sometimes damage infrastructures. Rock instability is conditioned, essentially, by the orientation of discontinuity and the steep dip slope and, caused, by rainfall occurring, essentially, from mid-October to mid-April.

Slope 2 presents a height varying from 3 to 7 m and a length of 100 m. The Slope 2 shows a variable dip between 40ºN and 80ºN, but more frequently between 50ºN and 55ºN. For Slope 2 were defined also 3 sections (T1, T2 and T3 (Figure 2)). The distances between T1 and T2, as well as between T2 and T3 are, respectively, 45.6 m and 46.9 m.

The instability processes on the Slope 2 are conditioned by the horizontal to sub-horizontal stratification, with a dip of approximately 10º, and by the existing jointing, with two more sets of vertical to subvertical discontinuities. The average specific weight of rock material is 24 kN/m^3. The slope movements are essentially rock falls, characterized by very/extremely rapid velocity. Instability is classified as active or suspended. The presence of vegetation is scarce to inexistent. The consequences of the instability affect the communication route between Lubango and Tundavala Cleft. The external causes of instability are the slope dip increase, water percolation, vibrations, surface erosion and the presence of livestock, while the internal causes correspond to lithology, increased water pressure and decreased soil resistance, and geological structures such as stratification, joints, veins.

The slope sections T1 and T2 of Slope 2 are characterized exclusively by the presence of quartz-sandstones with 3 sets of joints and with an orientation perpendicular to each other, the values of joint spacing vary between 3 to 30 cm, often being less than 10 cm. The lithology of the slope section T3 is comprised of quartz-sandstones with a variable grain dimension and yellowish and whitish colors located at the top and at the bottom of the section. It is visible a basic volcanic rock sill, which in slope section T3 is parallel to the stratification.

The parameter values used for the coefficient of normal restitution (Rn), coefficient of tangential restitution (Rt) and friction angle (ϕ^o) for the Slopes 1 and 2 materials are shown on Table 1.

A characterization of 48 and 59 rock fall blocks present, respectively, on the Slope 1 and Slope 2 areas, was carried out. The rock blocks are identified and located, and its lithology and dimension were defined. The rock blocks for Slope 1 were subdivided into seven volumetric classes (cm^3): <150, 150 – 500, 500 – 1000, 1000 – 2000, 2000 – 5000, 5000 – 15000 and > 15 000. For Slope 2 were considered five volumetric classes (cm^3): <150, 150 – 500, 500 – 1000, 1000 – 2000 and > 2000.

In the Slope 1 and 2, the rock blocks are composed by quartz-sandstone, however the volcaniclastic rocks are also present in Slope 2. For Slope 1, 41.9% and 25.6% of the rock blocks show, respectively, a dimension between 150 and 500 cm^3, and between 500 and 1000 cm^3. For Slope 2, the classes 150 – 500 cm^3 (42.3%) and 500 – 1000 cm^3 (25.0%) show similar percentage values to those found in Slope 1, but the class <150 cm^3 (19.2%) is more important than in Slope 1 (11.6%). The classes of greater dimension such as 5000 – 15 000 cm^3 and > 15 000 cm^3 are present in Slope 1, but inexistent in Slope 2.

Table 1 - Values used for the coefficient of normal restitution (Rn), coefficient of tangential restitution (Rt) and friction angle (ϕ^o).

Existing Material	Rn	Rt	ϕ^o
Slopes 1 & 2 – Quartz-Sandstone	0.52	0.92	35
Slope 1 – Soil	0.25	0.60	30
Slopes 1 & 2 – Concrete	0.48	0.53	41.6
Slopes 1 & 2 – Sand + Gravel	0.33	0.85	30
Slope 1 – Asphalt	0.40	0.90	6.3
Slope 2 – Volcanoclastic Rock	0.50	0.90	32
Slope 2 – Cobbled Road	0.35	0.85	32

For each Slope section were performed 4 distinct simulations, assuming two different mass values for each seeder positions, which are located at the highest level of the slope face and in an intermediate position. For the seeder points of the quartz-sandstones of Slope 1 and attending to rock fall dimension of 325 cm^3 and 10 000 cm^3, were considered weight values of, respectively, 7.96 N (0.812 kg) and 245.17 N (25 kg). For the seeder points of the rock materials of Slope 2, rock fall blocks dimension of 325 cm^3 and 750 cm^3 were considered, corresponding to weight values of, respectively, 7.80 N (0.795 kg) and 18.0 N (1.835 kg).

For the different sections of Slope 1, it was considered that the possible rock fall trajectories could injury people at a horizontal distance equal to or greater than 2 m from the slope toe. For the sections of Slope 2, it was assumed that the vehicles could be damaged, when the probable rock fall trajectories reach the road between Lubango and the Tundavala area.

According to results for Slope 1, the section S1 shows the most critical results to the seeders of values of, respectively, 7.96 N (0.812 kg) and 245.17 N (25 kg), located at highest level of the slope face, with 24% and 32%, of the rock fall paths reaching or surpassing the horizontal distance of 2 m from the slope toe. For the section S2 of Slope 1, the percentage values of the trajectories of rock blocks that can cause damage are, generally, higher than those found on section S1, verifying the value of 42% for the seeder located at an intermediate point and for the rock material with a weight of 245.17 N or mass of 25 kg. For the section S3 of Slope 1, the percentage values of falling rocks t.hat can reach or overcame the horizontal distance of 2 m from the slope toe are significantly higher than those found on the sections S1 and S2, with values between 56% (Figure 1) and 93%.

For the section T1 of Slope 2, the rock falls trajectories that reach the road between Lubango and the Tundavala area are inexistent or correspond to a small percentage value such as 3%. For the section T2 of Slope 2, the percentage values, of the rock fall paths that reach the road which connects Lubango to the Tundavala Cleft, are between 29% and 43%, and are clearly higher than those defined for section T1 of Slope 2. Section T3 of Slope 2 reveals the highest percentage values of the rock falls trajectories that reach the adjacent road of Slope 2, with values of 67% (Figure 2) and 59% for the s0elected seeder at the highest level of the slope face. For the seeder located at the intermediate point, the percentage values are 29% and 20%.

https://doi.org/10.5593/sgem2024/1.1/s02.26

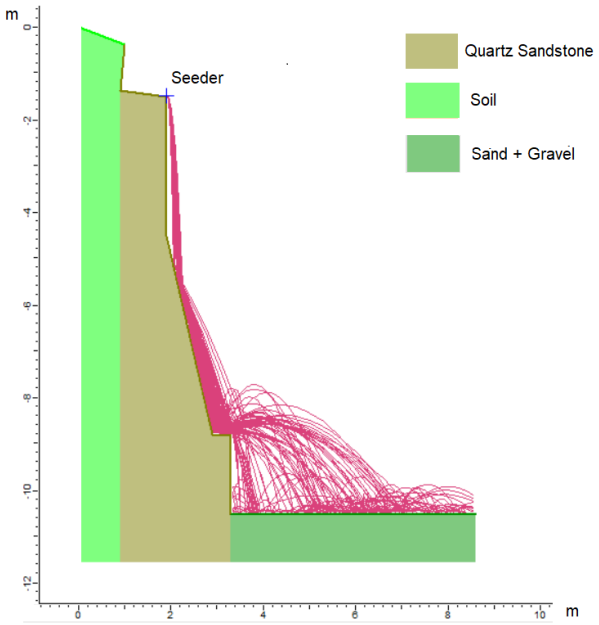


Figure 1 - Possible rock blocks fall trajectories on section S3 of Slope 1 for the selected seeder at the highest level of the slope face and with lower mass.

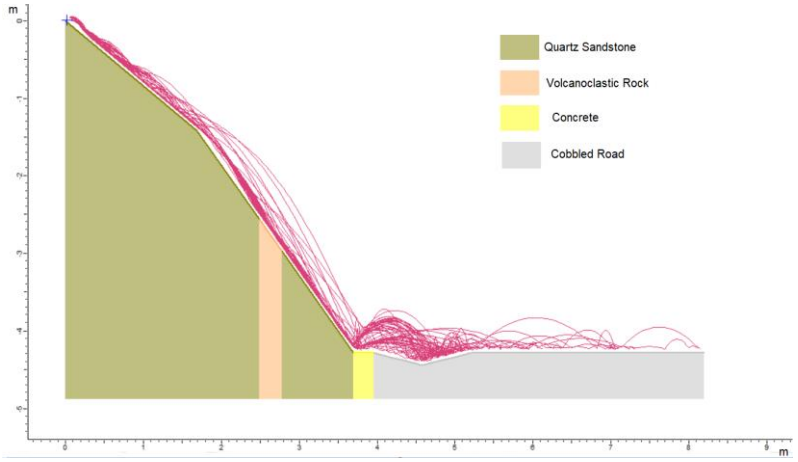


Figure 2 – Possible rock blocks fall trajectories on section T3 of Slope 2 for the selected seeder at the highest level of the slope face and with greater mass.

DISCUSSION

Using the Rocfall software, it was observed that the characteristics associated with the coefficients of restitution and the friction angle of the materials that make up the slopes correspond to determining factors for the trajectory, speed, and bounces of the falling rock blocks.

The Slopes 1 and 2 show a great number of blocks belonging, respectively, to the volumetric classes of 150 and 500 cm^3, and between 500 and 1000 cm^3. However, the class <150 cm^3 (19.2%) in Slope 2 is more important than in Slope 1 (11.6%), where the classes 5000 – 15 000 cm^3 and > 15 000 cm^3 are existent but absent in Slope 2. The

differences of the falling rock block dimension between Slope 1 and 2 can be explained by the greater joint spacing on the quartz-sandstones of Slope 1, comparatively to the joint spacing occurring on the quartz sandstone and volcanic rock outcrops of Slope 2.

The sections S2 and S3 of Slope 1 shows percentage values of the rock fall paths reaching or surpassing the horizontal distance of 2 m from the slope toe, superior to values found on the section S1. These results can be, partially, explained by the absence of a ditch nearby the bottom of sections 2 and 3 of Slope 1.

For the section T1 of Slope 2, the probability of the falling rocks reaching the road which connects Lubango and Tundavala Cleft is very small (3%) to inexistent, this can be explained by a lesser dip slope (50º), and by the presence, at bottom of section 1, of a layer of sand and gravel with a length of 1.1 m and a slightly wider roadside ditch (1.30 m). Sections T2 and T3 of Slope 2 show a face slope with a dip of 55º, and the layer of sand and gravel is, respectively, of 0.14 m and absent. The roadside ditches of the sections T2 and T3 have similar depth to the section T1, but present, respectively, a smaller width of 1.14 m and 1.25 m.

CONCLUSIONS

The present study provides information for the existing and potential rock falls, reducing hazards and defining stabilization measures of the studied slopes, to avoid losses associated with instability situations.

The section S3 of Slope 1 presents an intermediate segment with a dip of 76.8º that projects or bounces the falling rocks, increasing the percentage of the rock fall paths reaching or surpassing the horizontal distance of 2 m from the slope toe to values between 56% and 93%. The Section T3 of Slope 2 shows the greatest percentage values of the rock fall paths that reach the adjacent road of Slope 2, with values of 67% and 59%. Those values are associated to the seeder located at the highest level of the Slope 2, this starting position of the rock fall led to an increase in velocity and consequently to a longer length of the rock fall trajectories.

The values of restitution coefficient that have been considered in using the Rocfall software must consider the retro-analyses, according to the size and position of the rock blocks related to instability situations. The Slope 1 sections show a higher declivity and present rock fall trajectories that can cause destruction and human injury. The Slope 2 sections also present instability problems, which can lead to vehicle damage. Stabilization and remediation procedures were suggested to allow the protection of the area adjacent to Slope 1 and along the road of Slope 2. For Slope 1 was proposed the use of rock bolts and galvanized wire mesh. For Slope 2 was defined rock slope scaling or galvanized wire mesh. According to the results obtained with the Rocfall software, the causes of the slope movements and the proposed measures, it was also recommended to carry out periodic inspections of the studied slopes.

ACKNOWLEDGEMENTS

The financial support of FCT-MEC through national funds and, when applicable, co-financed by the ERDF within the PT2020 partnership, through the research projects UID/Multi/00073/2020 of the Geosciences Centre and UID/Multi/00308/2020 is acknowledged.

https://doi.org/10.5593/sgem2024/1.1/s02.26

REFERENCES

[1] Henriques, M. H., Tavares, A. O., Bala, A. L. M., The geological heritage of Tundavala (Angola): An integrated approach to its characterisation. J. African Earth Sci., vol. 88, pp 62 –71, 2013. DOI: https://doi.org/10.1016/j.jafrearsci.2013.09.003

[2] Rocscience, Rocfall, Statistical analysis of rockfalls. Rocscience LTD. Toronto, Ontario, Canada, 2020.

[3] McCourt, S., Armstrong, R.A., Jelsma, H., Mapeo, R.B.M., New U-Pb SHRIMP ages from the Lubango region, SW Angola: insights into the Palaeoproterozoic evolution of the Angolan Shield, southern Congo Craton, Africa. J. Geol. Soc., vol. 170, pp 353–363, 2013. DOI: https://doi.org/10.1144/jgs2012-059

[4] Pereira, E.; Tassinari, C. C. G., Rodrigues, J. F., Van-Dúnem, M. V., New data on the deposition age of the volcano-sedimentary Chela Group and its Eburnean basement implications to post-Eburnean crustal evolution of the SW of Angola. Comunicações Geológicas, 98, pp 29-40, 2011. http://hdl.handle.net/10400.9/2217

[5] Alberto, J.P., Avaliação dos Processos de lnstabilidade do Talude da Nossa Senhora do Monte, Lubango, Angola. Master's Thesis in Geoscience. University of Coimbra, 66p, 2010, 66 p. (in portuguese)

[6] Dorren, L.K.A., Seijmonsbergen, A.C., Comparison of three GIS-based models for predicting rockfall runout zones at a regional scale. Geomorphology, vol. 56 / issues 1-2, pp 49-64, 2003. DOI: https://doi.org/10.1016/S0169-555X(03)00045-X

[7] Massey, C.I., Hodgson, I., Petley, D.N., A rockfall simulation study for housing development in Gibraltar. Proceedings of the 10th IAEG International Congress, Nottingham, United Kingdom. The Geological Society of London, paper 337, pp 1-10, 2006.

[8] Andrade, P.S., Gonçalves, G., Quinta-Ferreira, M., Rock fall analysis on the city of Lubango, SW Angola. Eds. Lollino, G., et al. Engineering Geology for Society and Territory - Volume 2: Landslide Processes, Springer, pp 2027-2030, 2015. DOI: https://doi.org/10.1007/978-3-319-09057-3_360

[9] Mineo, S., Pappalardo G., Mangiameli M., Cappollo, S., Mussumeci, M., Rockfall analysis for preliminary hazard assessment of the cliff of Taormina Saracen Castle (Sicily). Sustain., vol. 10 / issue 2, 417, 2018. DOI: https://doi.org/10.3390/su10020417

[10] Sazid, M., Analysis of rockfall hazards along NH-15: a case study of Al-Hada road. International Journal of Geo-Engineering., vol. 10, 1, pp 1-13, 2019. DOI: https://doi.org/10.1186/s40703-019-0097-3

THE VAL RONCAGLIA LANDSLIDE (NORTHERN ITALY): FROM CONCEPTUAL TO NUMERICAL MODELLING

Assoc. Prof. Dr. Paola Gattinoni[1]
Dr. Angelo Molteni[2]

[1] Politecnico di Milano, **Italy**
[2] Politecnico di Milano, **Italy**

ABSTRACT

This paper focuses on the Deep Seated Gravitational Slope Deformation (DSGSD) affecting Val Roncaglia (Northern Italy). Based on the state of the art about DSGSD, the study area was characterized from geologic, tectonic, geomorphological, and hydrogeological points of view in order to reconstruct the conceptual model of the slope (geometry, geomaterials and their properties). Moreover, based on the available monitoring data, the landslide kinematics was pointed out together with its possible evolution and the related triggering factors. Then, the conceptual model of the landslide was implemented into a 2D numerical stress-strain model, which was calibrated based on monitoring data of displacement arising from inclinometric probes. Finally, the numerical model was employed to simulated the slope evolution for different geomechanical and hydrogeological conditions in order to find out the factors that affect stability the most. The results of the present study provide a comprehensive understanding of the causes and dynamics of the DSGSD affecting the Val Roncaglia slope and give insights useful for the general comprehension of this kind of large phenomena, therefore enanching a proper management of the related risks.

Keywords: DSGSD, Italy, landslide, slope monitoring, numerical modelling

INTRODUCTION

Italy is one of the European countries most affected by landslides, with an area corresponding to 7.3% of the national territory [1]. Among landslide phenomena, Deep Seated Gravitative Slope Deformations (DSGSDs) [2] play a key role; actually, in spite of their low number (they correspond to less than 0.3% of the total number of landslides in Italy), they cover quite wide territories, representing about 10% of the areas affected by landslides [1]. DSGSDs usually involve whole slopes characterized by high relief energy, with small displacements compared to the extent of the slope and sliding surfaces that are not always evident [3]. They are generally recognized for the presence of some typical morphostructures, such as the double ridges and counterslopes, with a typical bulge in the lower-middle part of the slope that often determines the activation of smaller landslides [4]. The applicative interest on these phenomena mainly arises from their effects, such as huge damage to structures and infrastructures both in surface and underground, the related degradation of the mechanical properties of geomaterials [5], as well as an eventual catastrophic evolution [6].

https://doi.org/10.5593/sgem2024/1.1/s02.27

The study of DSGSDs is difficult because of their high complexity, connected to the intrinsic spatial variability of the involved geological processes [7]. The approach is usually based on numerical modelling, enabling the simulation of the DSGSD in its various phases [5]: from the very early one (i.e., connected to glaciers retreat or erosion processes) to the post collapse condition, by assessing both displacements and deformation pattern [8], also considering the effects of groundwater on landslide evolution [9]. However, even if in recent decades numerical modelling, based on geological and geomorphological knowledge, has significantly improved the capability of mitigating the landslide risk, for slow and wide phenomena like DSGSDs monitoring still remain a key instrument for risk management. The aim of the present study is to join numerical modelling and monitoring data into the same framework, thus enabling a more comprehensive understanding of the phenomenon.

In the present paper the main features, causes, trigger events and possible predictive signs of the DSGSDs have been investigated, through the case study of the Val Roncaglia landslide (northern Italy). At this aim, geological, geomorphological and geomechanical information were collected and analysed, together with the available monitoring data. Based on them, the conceptual model of the landslide has been defined and then implemented into a numerical one and its results were analysed in order to identify different risk scenarios.

MATERIALS AND METHODS

The Val Roncaglia landslide is a large landslide belonging to a quite complex geomorphological setting, which can be classified as a DSGSD with active zones located at the foot of the slope (Figure 1).

From a geological point of view [10], the bedrock is mainly composed of micaschists, locally very fractured with mylonitic zones 15-30 m thick, covered by a layer of soil deposits having thickness of about 50 m (Figures 2 and 3). The tectonic setting of the area involves the presence of a large anticline fold associated to NE-SW trending faults.



Figure 1. Location map of the study area in Lombardy (northern Italy). The yellow line bounds the whole DSGSD area, whereas the red one identifies the active zone of the Val Roncaglia landslide.

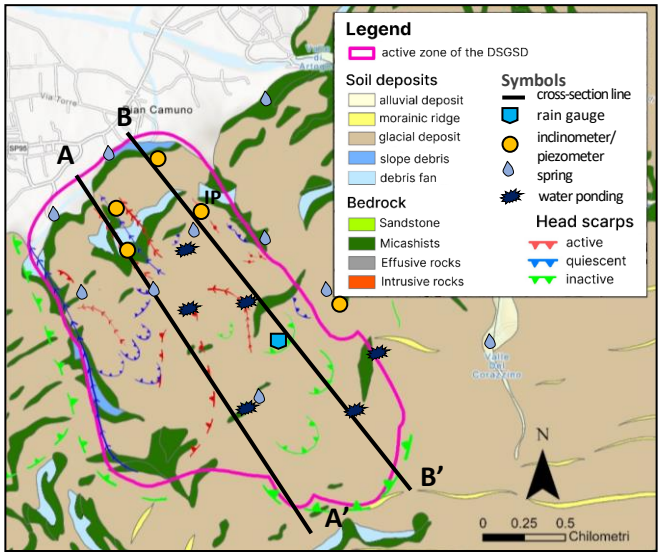


Figure 2. Geomorphological, geological and hydrogeological map of the Val Roncaglia landslide (based on data from [10], [11] and [12], modified from [13]).

As far as hydrogeology, the main aquifer is located in the alluvial deposits along the valley floor; this aquifer is supplied by local aquifers, mainly present within slope debris and fault zones, characterised by a good permeability, whereas the micaschists composing the bedrock usually exhibit quite low permeability, bringing about the outcropping of a number of springs (Figures 2 and 3).

From a geomorphological point of view, many active, quiescent and inactive head scarps are present all along the slope (Figures 2 and 3): the inactive ones are located at the highest altitude (from 800 to 1000 m a.s.l.), whereas active phenomena are mainly located at a lower altitude (between 400 and 700 m a.s.l.), and they are characterized by slow deformations with periodic reactivations; the most recent one occurred in 2010, after which a monitoring system has been installed, comprising inclinometric and piezometric probes that show displacement about 10 mm/year and water table changes lower than 1m [12]. By comparing displacements to rainfall data, no significant correlation can be detected, which is quite typical for DSGSD phenomena.

Afterwards, the conceptual model of the landslide has been implemented in a numerical 2D finite element code, able to describe the stress-strain behaviour of soil and rock in presence of water. The modelling domain is about 1 km long and it comprises the whole active zone of the slope (between 250 and 800 m a.s.l.); the mesh is composed by elements having size ranging between 20 and 100m.

The boundary and initial conditions are: null displacements (both vertical and horizontal) at the bottom of the modelling domain; null horizontal displacements along the vertical borders of the modelling domain; self-weight in the whole modelling domain; water table arising from monitoring data and springs.

For geomaterials an elastic-plastic model with the Mohr-Coulomb failure criterion has been used, by considering the parameters listed in Table 1. The mechanical parameters of geomaterials involved in the landslide kinematics have been calibrated based on the displacements supplied by the monitoring system, though a trial-and-error process.

Based on the calibrated model, in order to analyse the slope behaviour while failure is approaching, a strength reduction method was used and the corresponding safety factor

https://doi.org/10.5593/sgem2024/1.1/s02.27

has been assessed for each cross-section. Moreover, the hydrogeological susceptibility has been studied and the critical water table rise has been pointed out.

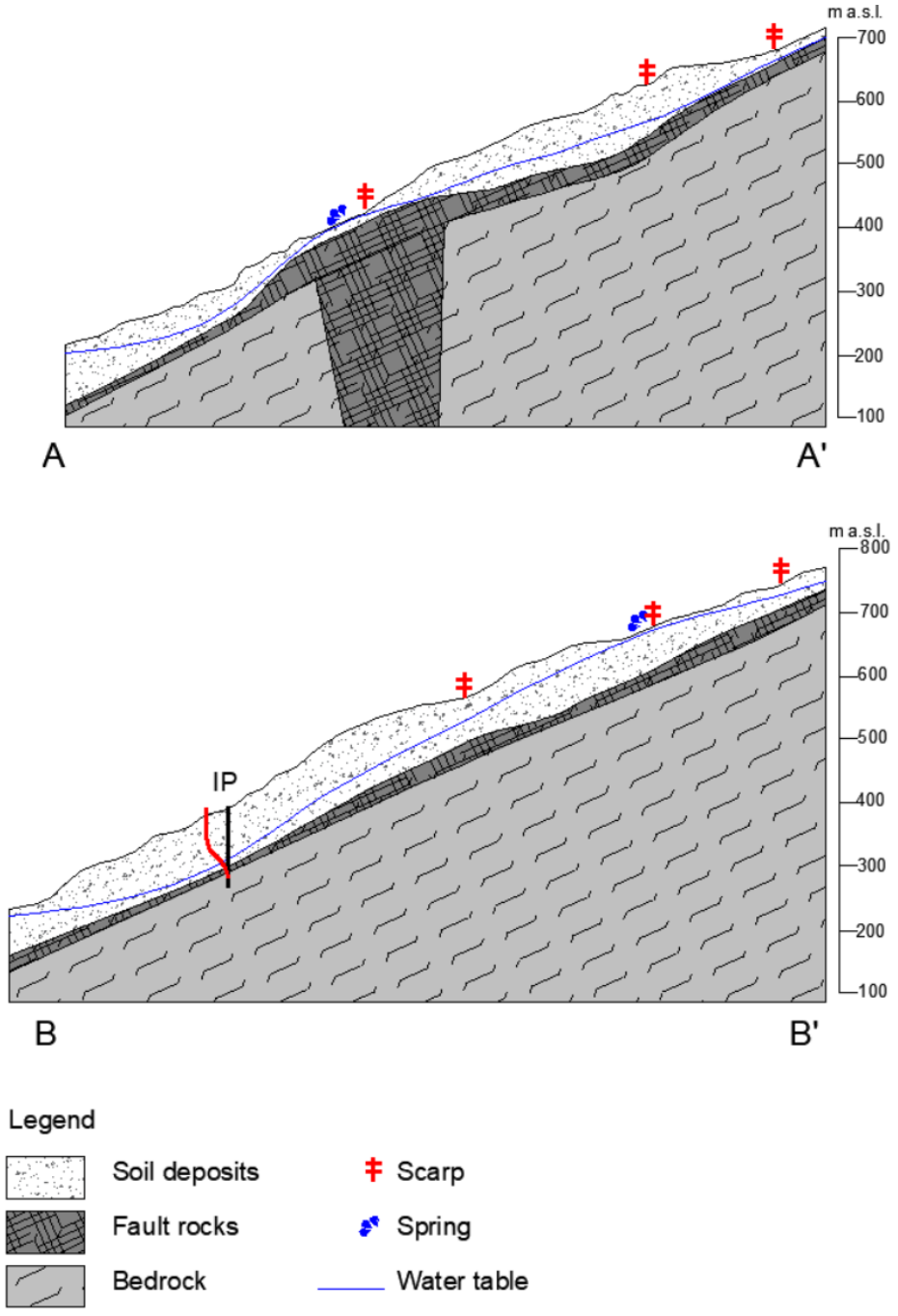
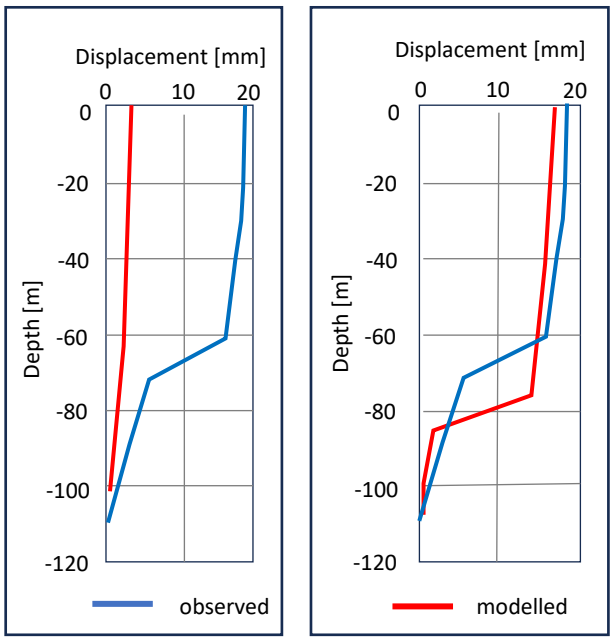


Figure 3. Geological cross-sections of the Val Roncaglia landslide (based on data from [10], [11] and [12]). See Figure 2 for the cross-section lines.

Table 1. Technical parameters used in the numerical model of the Val Roncaglia landslide (for the mechanical ones both initial and post-calibration values are shown).

Parameters	Michascist		Fault rocks		Slope debris	
	Intial	Calibr	Intial	Calibr	Intial	Calibr
Unit weight [kN/m^3]	24.5		19.5		19.5	
Young Modulus [GPa]	50	5	20	2	0.07	0.06
Friction angle [°]	30	30	30	30	35	25
Cohesion [MPa]	5	5	5	5	0.01	0.065
Permeability [m/s]	10^{-12}		10^{-4}		10^{-4}	



(a) (b)

Figure 4. Simulated versus observed displacements (data obtained from ARPA Lombardia, Protocol nr. arpa_mi.2022.0029708 of 25/02/2022) before (a) and after calibration (b) in point IP (see Figure 2 for location).

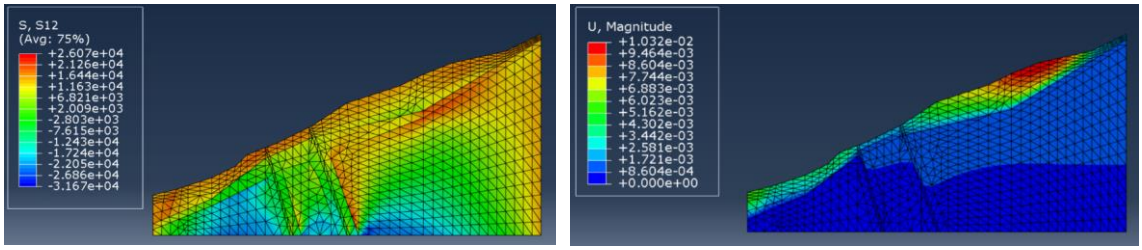
RESULTS

After calibration, the distributions of shear stresses and displacements allow to identify the slope kinematics, which mainly affects the shallow layer with multiple roto-translational sliding surfaces. Fault zones also involves the presence of local destressed areas; actually, faults are weakness layers enanching deformations, and therefore leading to possible degradation of the mechanical properties of geomaterials.

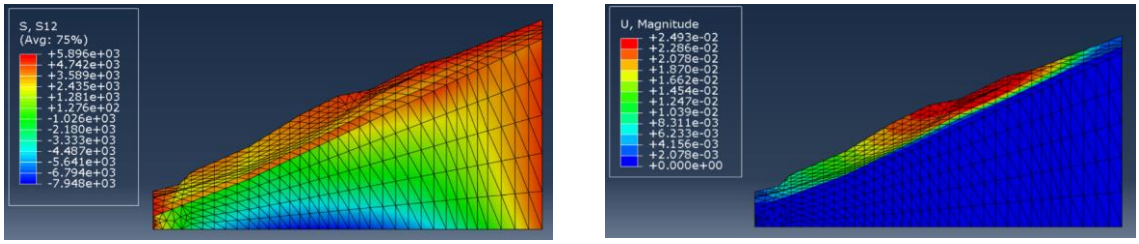
The safety factor obtained by applying the shear strength reduction method was equal to 1.5 for cross-sections A-A' and 1.3 for cross-section B-B'.

As far as the hydrogeological susceptibility, the modelling results pointed out that the critical rise of the water table able to trigger the slope failure is equal to about 30 m, corresponding to the historical maximum value recorded so far.

https://doi.org/10.5593/sgem2024/1.1/s02.27



(a)



(b)

Figure 5. Simulated shear stresses (S) and displacement (U) in: (a) cross-section A-A', (b) cross-section B-B'.

DISCUSSION

Generally speaking, numerical models aim at defining landslide evolution and assessing related hazards, but their reliability highly depends on the proper model calibration, which on its turn relies on the availability of data about past events usually described over some months or years by instrumental monitoring [14].

As far as the Val Roncaglia landslide, the available monitoring data allowed to calibrated the numerical model; however, a residual error is still present as regards the position of the failure surface (Figure 4), requiring an upgrade of the instrumental monitoring system.

In order to overcome the limitations arising from the quite short time length of instrumental monitoring data, changes occurring at the surface to vegetational cover could be considered. Actually, dendrogeomorphology can provides long-term base-line data on landslide activity, allowing to define a possible temporality of past events as well as to zone the affected areas [15]. At this aim, further studies are still ongoing in order to evaluate the opportunity of integrating dendrogeomorphological data into stress-strain numerical models [13].

CONCLUSION

The paper focused on the analysis of the DSGSD located in Val Roncaglia Northern Italy), which was first characterized from geomorphological, lithological, geological and hydrogeological point of views, in order to define the conceptual model of the

landslide, subsequently implemented in a finite element numerical model, which was calibrated based on the available monitoring data and then allowed to analyse the stress-strain behaviour of the slope under different conditions; in particular, geotechnical and hydrogeological triggering factors were considered in order to study the evolution of the slope dynamics; in particular, fracture zones along faults can be further weakened during the evolution of the phenomenon and faults can be seen as the result of the destress process that triggered the DSGSD.

Results allowed to broaden knowledge about the extent and depth of the Val Roncaglia landslide. Moreover, insights on the triggering factors of the landslide was obtained, and early-warning signals were identified which could be useful for risk forecasting and management, as well as for updating the monitoring network. The study also emphasised that the presence of fractured rock layers (i.e., connected to regional extension faults), bringing about weakness surfaces, could play a key role in the preparedness to large mass movements. Finally, as far as the availability of long time series of monitoring data in wide forested areas (such as the typical situation od DSGSDs), the opportunity of exploiting dendrogeomorphological information for model calibration has been introduced and it will be investigated in subsequent studies.

REFERENCES

[1] ISPRA, Dissesto idrogeologico in Italia: pericolosità e indicatori di rischio (Landslides in Italy: hazard and risk indexes), Report 2015.

[2] Agliardi F., Crosta G., Zanchi A., Structural constraints on deep-seated slope deformation kinematics, Eng Geol 2001, 59, 83-102, DOI: 10.1016/S0013-7952(00)00066-1.

[3] Dramis F., Soriso-Valvo M., Deep-seated gravitational slope deformations, related landslides and tectonics, Engineering Geology, 38, pp 231‑243, 1994.

[4] Capitani M., Ribolini A., Federici P.R., Influence of deep-seated gravitational slope deformations on landslide distributions: A statistical approach, Geomorphology, 201, 127–134, 2013.

[5] Preisig G., Eberhardt E., Smityman M., Preh A., Bonzanigo L., Hydromechanical Rock Mass Fatigue in Deep.Seated Landslide Accompanying Seasonal Variations in Pore Pressure, Rock Mechanics and Rock Engineering, 49(6), 2016, DOI: 10.1007/s00603-016-0912-5.

[6] De Finis E., Gattinoni P., Marchi L., Scesi L., Anomalous Alpine fans: from the genesis to the present hazard, Landslides, vol. 15, p.683-694, 2018, doi: 10.1007/s10346-017-0894-8.

[7] Longoni L., Papini M., Brambilla D., Arosio D., Zanzi L., The role of the spatial scale and data accuracy on deep-seated gravitational slope deformation modeling: the Ronco landslide, Italy, Geomorphology, 2015.

[8] Apuani T., Rossi M., Masetti M., Applicazione di modelli reologici tempo dipendenti nell'evoluzione di deformazioni gravitative profonde. Giornale Di Geologia Applicata, 2, pp 99‑105, 2005.

[9] Gattinoni P., Scesi L.. Landslide Hydrogeological susceptibility of Maierato (Vibo Valencia, Southern Italy), Natural Hazard 66(2), 629-648, 2013.

https://doi.org/10.5593/sgem2024/1.1/s02.27

[10] Comune di Pian Camuno, Pianificazione e Governo del territorio: Componente geologica, idrologica e sismica (Landplanning: geological, hydrogeological and seismic components), 2008.

[11] Geoportale Regione Lombardia, 2023 (www.geoportale.regione.lombardia.it)

[12] ARPA Lombardia - Rete di monitoraggio di Roncaglia (Monitoring network of Val Roncaglia), 2021, https://www.arpalombardia.it/temi-ambientali/frane-e-dissesti/reti-di-controllo/aree-monitorate-da-cmg/roncaglia/

[13] Curioni S., Gattinoni P., Leonelli G., Integrating dendrogeomorphology into stress-strain numerical models: an opportunity to monitor slope dynamic, Geosciences 14, 129, 2024.

[14] Ozturk U., Tarakegn Y.A., Longoni L., Brambilla D., Papini M., Jense, J. A, Simplified early-warning system for imminent landslide prediction based on failure index fragility curves developed through numerical analysis, Geomatics, Natural Hazards and Risk 2016, 7(4), 1406–1425, DOI: 10.1080/19475705.2015.1058863.

[15] Alestalo J., Dendrochronological interpretation of geomorphic processes, International Journal of Geography, 1971, 105(1).

SECTION

EXPLORATION AND MINING

ANALYSIS OF LABORATORY METHODS USED FOR THE DETERMINATION OF THE MINIMUM IGNITION ENERGY IN THE CASE OF AIR/FUEL DUST MIXTURES

Sc. Res. III PhD Eng. Catalin Mihai POPA [1]
Sc. Res. I PhD Eng. Emilian GHICIOI [1]
Sc. Res. I PhD Eng. Florin Adrian PĂUN
Sc. Res. III PhD Eng. Dan Sorin GABOR[1]
[1] National Institute for Mine Safety and Protection to Explosion - NRDI INSEMEX, **Petroșani, România**

ABSTRACT

The continued development of human society, from the technical and economic point of view, has led to the need for the increasingly widespread use in the various existing industrial branches of chemical substances and compounds in the form of combustible dust and dust. The processing, handling and storage of these pulverized substances often leads to the emergence of complex explosive mixtures whose explosiveness characteristics cannot be assimilated with the data available in the literature.

In places where the probability of the occurrence of potentially explosive atmospheres generated by the mixture of combustible dust with air is high, it is necessary to ensure an acceptable level of protection, in accordance with the rules in force, materialized mainly by the use of protected technical equipment in the respective areas suitable.

The safety requirements of technical equipment that can be used in areas with combustible dust are established after knowing the type of combustible dust and its sensitivity to ignition, defined mainly by determining the minimum ignition energy of the combustible dust.

The paper presents two methods for determining the minimum ignition energy, with a description of the equipment used and the principles of operation. Also, the results obtained from laboratory tests to determine the minimum ignition energy in the case of a combustible powder (nystatin) are presented, using the two methods.

Keywords: combustible dusts, minimum ignition energy - MIE, potentially explosive atmosphere, explosion protection.

INTRODUCTION

The continued development of human society, from the technical and economic point of view, has led to the need for the increasingly widespread use in the various existing industrial branches of chemical substances and compounds in the form of combustible dust and dust. The processing, handling and storage of these pulverized substances often leads to the emergence of complex explosive mixtures whose explosiveness characteristics cannot be assimilated with the data available in the literature.

Furthermore, the increasing use of chemical substances and compounds in the form of combustible dust and dust in the activities carried out in various industrial branches has

https://doi.org/10.5593/sgem2024/1.1/s03.28

also increased the likelihood of the occurrence of potentially explosive air/dust mixtures.

A dust explosive atmosphere is defined as a mixture of air, in atmospheric conditions, with combustible substances in the form of dust, which, after ignition, allows self-sustaining propagation. [1]

Most often, if an explosive atmosphere of air/dust is present simultaneously with an effective source of ignition, explosions can occur, concretized by recording major material damage and even with the death of some people.

As is known, an explosion of combustible dust occurs only when the fuel dust in suspension mixed with air within the explosion limits of that dust interacts with an actual ignition source whose ignition energy is large enough to initiate the explosive mixture air/dust. The combustible dust explosion is governed by a pentagon of interacting factors: oxygen/air, fuel, containment, ignition and dust dispersion – figure 1. [2]



Figure 1 – Fuel dust ignition pentagon

The explosion of the dust/air mixture is based on a mechanism that can be explained by a chain reaction. Thus, in the first phase, the heat of the ignition source comes into contact with the dust suspended in the air. Heating of dust particles results in the release of gaseous chemicals (hydrogen, methane, Etan, etc.). In turn, these flammable gases, mixed with air, form a gas explosive atmosphere which, in contact with the existing ignition source, is initiated. This creates favorable conditions for heating neighboring dust particles, this time with a larger volume. This reaction is repeated until the entire volume in which the fuel dust is in suspension is engaged.

Therefore, the use of technical equipment in areas where explosive air/dust mixtures may be present in maximum safety conditions is possible only after identification of the type of dust present and the parameters that define its sensitivity to ignition with different sources of initiation [3],[4].

In practice, one of the most common sources of initiation of a potentially explosive atmosphere generated by the air/dust mixture is electrostatic discharge. Evaluation of the risk of ignition of the explosive atmosphere of air/dust by electrostatic discharge shall be carried out by comparing the value of the discharging energy with the minimum ignition energy of the present explosion atmosphere. Because of this, in the process of assessing the risk of ignition, the knowledge of the minimum energy of igniting the dust generating the explosive atmosphere is of particular importance.

The minimum ignition energy (MIE) of a potentially explosive atmosphere generated by the mixture of a combustible dust with air may be defined as the smallest electrical energy stored in a capacitor and which, at the time of its discharge, has the capacity to produce the igniting of the most flammable dust mixture in question under specific test conditions.

METHODS AND EQUIPMENTS USED TO DETERMINATE MINIMUM IGNITION ENERGY IN THE CASE OF AIR/FUEL DUST MIXTURES

The minimum ignition energy can be determined by using two distinct methods, which use different principles and devices namely: the estimate method, for the application of which the equipment KSEP-20 is used, and the qualitative method for which the application is used the equipment MIE-D 1.2 with modified Hartmann tube, which is manufactured in the Czech Republic by OZM Research. The two aforementioned methods, as well as the related equipment, are currently used to determine the minimum ignition energy of explosive air/dust mixtures in the testing laboratories belonging to NIRD INSEMEX Petrosani.

The principle of the estimate method

The estimated method for determining the minimum ignition energy is based on recording and interpreting the combustion time t_1 in relation to different t_v delays with values of 60 ms, 120 ms, respectively. The combustion time, respectively the delay times, can be defined from the pressure/time diagram shown in Figure 2. [5]

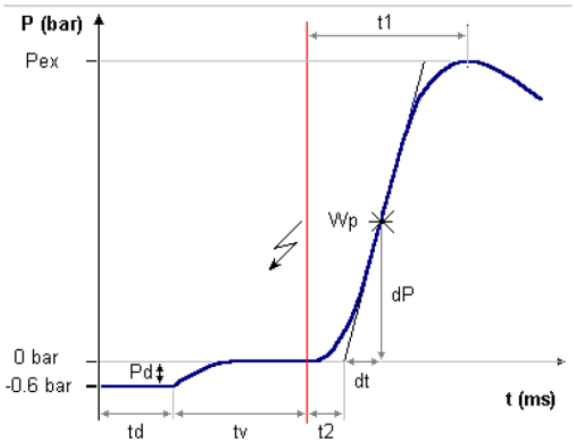


Figure 2 – Pressure/time-diagram of a fuel explosion

where:

P_{ex} - explosion overpressure; t_1 - duration of combustion; t_2 - induction time; P_d - expansion pressure of storage container; t_d - time-delay of the outlet valve; t_v - ignition delay time.

Therefore, two series of tests are carried out for the fuel dust analyses and the lowest value of the combustion time t1 is determined for the ignition delay time of 60 ms, respectively 120 ms. The lowest value of the combustion time t_1 for each series of tests shall be analyses, which shall be compared with the values in the four values ranges of combustions and delays, respectively, presented in table 1, resulting in the estimated value of minimum ignition energy.

https://doi.org/10.5593/sgem2024/1.1/s03.28

Table 1. The relationship between the correlated values of times t1 and MIE

Interval	t_1,60(ms)	t_1,120(ms)	MIE (mJ)
1	< 50	< 80	<10
2	50-60	80-95	10-100
3	61-80	96-120	101-1000
4	>80	>120	>1000

The application of this method can be achieved by using the test equipment KSEP-20l. This equipment is in the form of a spherical explosive vessel, made of stainless steel, with an internal volume of 20 liters, see figure 3.

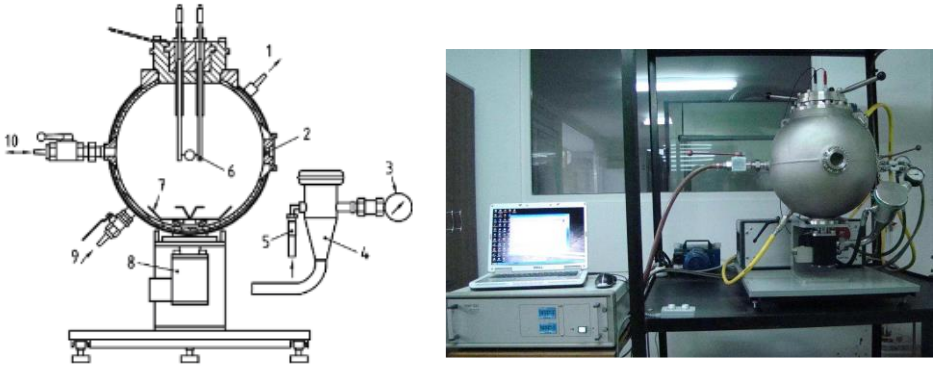


Figure 3 – The KSEP-20 test facility

KSEP-20 test equipment consists of: water outlet (1), pressure transducers (2), manometer (3), dust container (4), air intake opening (5), ignition source (6), spray nozzle (7), quick-acting valve (8), inlet for water (9), exhaust outlet (10).

For carrying out the test, the fuel dust is dispersed inside the sphere by means of special electrically and pneumatically driven devices. The ignition source consists of 2 electric ignitioners positioned in the center of the sphere. The variations of the explosion pressure inside the sphere are recorded with the help of two piezoelectric pressure converters located on the inner wall of the blast vessel. The data recorded by these piezoelectric transducers are collected and processed through a dedicated interface and software, resulting in the necessary graphs to determine the explosiveness parameters of the dust in question. [5]

The principle of the quantitative method

The quantitative method of determining the minimum ignition energy involves the completion of several stages, because in one stage the optimal concentration of dust and the minimum level of wrapping cannot be achieved. The steps to be undertaken are presented below: [6]

Step 1: For starters, a value of ignition energy is set which will safely lead to the ignition of the tested dust, whose concentration in the air is known. Decrease the percentage value of the spark energy in several steps (e.g. by 50%) at the given concentration of dust until the combustion air/dust mixture ceases to ignite at any of the 10 tests performed at a given energy.

Stage 2: The powder concentration is then changed (e.g. 200 mg, 400 mg, 600 mg, 800 mg, 1000 mg and 1200 mg), applying the lowest energy resulting from the completion of stage 1. At this stage there is the possibility of occurring a flame at a certain

concentration of dust. In this case, step 1 shall be resumed for the concentration in question.

Step 3: For this value of the spark energy and dust concentration resulting from the passage of the above steps, while changing the delay time (60 mc, 120 ms) the procedure will be repeated until the highest energy value (E_1) is determined at which no ignition occurs.

The minimum ignition energy, E_{min} (MIE), at which the fuel dust in the cloud can ignite is between the highest energy value, E_1, at which ignition does not occur during 10 consecutive tests, and the lowest energy amount, E_2, at which at least one ignition occurs during 10 successive tests.

$$E_1 < MIE < E_2 \quad (1)$$

Most of the time, however, especially for comparing the results obtained using different equipment, it is advisable to use only one value of the minimum ignition energy Es and not an energy range (E_1, E_2). In view of this, the E_s value can be determined using the probability of ignition as follows: we assume that the ignition energy E_2 has been tested at least equally distant dust concentrations, resulting that the E_s value can be estimated in the range E_1...E_2. The exponent of the equation (2), depending on the initial energy E_2, the number of concentrations of ignition dust (I[E_2]) is divided by the total number of dust concentrations (NI + I) [E_2].

$$E_s = 10^{\log E_2 \frac{I[E_2]\cdot(\log E_2 - \log E_2)}{(NI+I)\cdot[E_2]+1}} \quad (2)$$

The application of the quantitative method can be achieved by using a modern, highly complex equipment, MIE-D 1.2, manufactured in the Czech Republic, by OZM Research, equipment shown in figure 4.



Figure 4 – MIE-D 1.2 equipment

The following elements are included in the MIE-D 1.2 equipment: Hartmann glass tube (1), control panel (2), Sliding door equipped with a closed-position safety sensor (3), emergency stop button (4), high voltage switch (5), high voltage presence indicator (6), start button (7), function indicator (8), outlet for exhaust fumes (9).

The modified Hartmann tube included in the equipment MIE-D 1.2 is presented in the form of a glass explosive container with a volume of 1.2 liters (figure 5). The dust dispersion system at the base of the tube is mushroom-type around which the dust sample is freely dispersed. The dust stored at the base of the Hartmann tube is

https://doi.org/10.5593/sgem2024/1.1/s03.28

dispersed by a compressed air stream. The dust dispersed in the glass cylinder is then lit by an electric spark produced between two electrodes. [6]

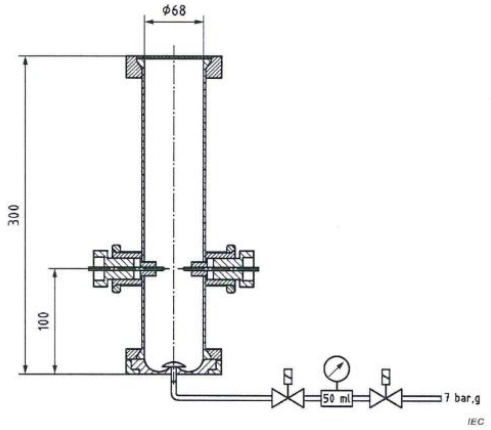


Figure 5 – Hartmann glass tube modified

DETERMINATION OF THE MINIMUM IGNITION ENERGY IN THE TEST LABORATORY FOR A COMBUSTIBLE POWDER USING THE TWO METHODS PRESENTED

Given the large number of powders used in the pharmaceutical industry for the manufacture of various medicines, a combustible powder that is included in the composition of antibiotics, namely atomized mycelium or nystatin, has been chosen. Laboratory tests were carried out on a sample of nystatin powder using the estimated method and, respectively, the quantitative method, in order to be able to determine the minimum ignition energy values in the two cases and to compare these values.

Thus, using the KSEP-20 equipment and applying the estimated method presented above, two series of tests were carried out on a sample of atomized mycelium powder, tests concretized by recording the combustion time t1. The results obtained in the two series of tests are presented in table 2.

Table 2. Combustion time values t_1

Nr. crt	Sample Identification		Concentration dust, (g/m^3)	Delay time t_v (ms)	Combustion time t_1 (ms)
1	Atomized Mycelium Powder - Nistatine	1 series at t_v=60ms	250	60	72
2			500	60	**64**
3			750	60	**64**
4		2 series at t_v=120ms	500	120	110
5			750	120	112
6			1000	120	**104**

By closely monitoring the t_1 combustion time values recorded in table 2, we note that for the t_v delay time of 60 ms (series 1 of tests), the lowest value of the combustion time t_1, for dust concentrations of 250 g/m^3, 500 g/m^3 and 750 g/ m^3, is 64 ms, and for the t_v delays time of 120 ms (series 2 of tests), the smallest value t_1 of the combustions time, for the dust concentrations of 500 g/m^3, 750 g/m^3 and 1000 g/m^3, is 104 ms.

By comparing the two values of the t_1 combustion time obtained – 64 ms, 104 ms, respectively – with the reference values presented in table 1, it can be concluded that the minimum ignition energy for atomized mycelium powder is part of a range between 101 mJ and 1000 mJ.

Interval	t_1,60(ms)	t_1,120(ms)	MIE (mJ)
3	61-80	96-120	101-1000

By applying the quantitative method and using the MIE-D 1.2 equipment, through the three stages presented in the description of the method, it resulted that E_1=100 mJ, and E_2=300 mJ and, consequently, the minimum MIE ignition energy for the dust in question has a value that falls within the following range:

$$100 \text{ mJ} < \text{MIE} < 300 \text{ mJ} \quad (3)$$

Going further, in order to be able to calculate the Es value, in table 3 are presented the values obtained from laboratory tests, in terms of the number of ignitions, respectively of non-inflammations in relation to the concentration of dust in the air, as well as the probability of ignition.

Table 3. Probability of ignition

	Concentrations [mg]						Probability of ignition	
	200	400	600	800	1000	1200	I	NI+I
E_2=300mJ	0	1	2	2	3	1	5	6
E_1=100mJ	0	0	0	0	0	0		

where: I represents ignition, and NI represents no ignition at 10 attempts carried out.

By entering the results obtained from laboratory tests into equation no. 2, we get the value of the energy E_s, which is 137 mJ.

DISCUSSION

For the determination of the minimum ignition energy value in the case of combustible dust that, in mixing with air, can form clouds of explosive dust, two distinct methods can be used as a principle and equipment used, namely: estimate method and quantitative method respectively.

By comparing and analyzing the results obtained from the application of the two methods in the testing laboratories belonging to NIRD INSEMEX Petrosani, we can conclude that the results achieved by applying the quantitative method are more accurate.

As regards the application of the estimation method, it can be used as a method for estimating the value of the minimum ignition and incineration energy within the four range values.

CONCLUSIONS

In areas where potentially explosive atmospheres generated by the combustion air/dust mixture may occur, an assessment of the risk of ignition of this explosion mixture shall be carried out. Following this risk assessment, if necessary, protective measures must be adopted and implemented to ensure an acceptable level of safety in conjunction with the

https://doi.org/10.5593/sgem2024/1.1/s03.28

rules in force, measures that can be materialized by the use of appropriate technical equipment for use in atmospheres with fuel dust.

Safety requirements for this technical equipment can be established, mainly, at the time when the type of combustible dust that generates the potentially explosive atmosphere and its sensitivity to ignition is known, materialized by determining the minimum ignition energy of that dust.

During this work are presented the principles of application and the equipment used for two methods of determination (estimative and quantitative) of the minimum ignition energy, which are used in the testing laboratories of NIRD INSEMEX Petroșani. The practical determination of the minimum ignition energy is also achieved by using the two methods for a fuel dust used in the pharmaceutical industry.

Considering the results obtained, it can be concluded that, in order to obtain the most accurate results of the minimum ignition energy value, the quantitative method will be used. This will also be useful to make it possible to repeat these tests in different testing laboratories in interlaboratory testing sessions.

ACKNOWLEDGMENTS

This work was carried out through the "Nucleu" program of the National Research, Development and Innovation Plan 2022-2027, supported by MCID, project no. PN EXH2 and IOSIN PCDIEX**.**

REFERENCES

[1] SR EN 60079-0 (2018) Explosive atmospheres - Part 0: Equipment - General requirements.
[2] Jurca A., Păun F.A., Părăian M., Gabor D.S., Lupu L, Study of influence factors of determination the explosive characteristics to the air / combustible dust mixtures, 18th International Multidisciplinary Scientific Geoconference (SGEM 2018), Mineral processing, Oil and Gas Exploration, Bulgaria, vol. 18, 2018, pp. 819-826;
[3] Directive 2014/34/EU - ATEX, (2014).
[4] Jurca A., Gabor D., Păun F.A., Vătavu N., Părăian M., Comparative study having in view the methods of determination the minimum ignition energy of the air/combustible dust mixtures, 19th International Multidisciplinary Scientific Geoconference (SGEM 2019), 28 June - 7 July, Albena Resort & Spa, Bulgaria, 2019.
[5] Jurca A., Ghicioi E., Părăian M., Burian S., Darie M., Sicoi S., Păun F., Implementation and carrying out of laboratory test stands required for conformity assessment of equipment intended for use in potentially explosive atmospheres generated by combustible dusts - IRECEEX, INSEMEX Petroșani, (Romanian) C 43/2005, 2005.
[6] SR EN ISO/IEC 80079-20-2:2016, (2016), Explosive atmospheres – Part 20-2: Material characteristics – Combustible dusts test methods.

ASSESSMENT AND PROSPECTS FOR DEVELOPMENT OF COAL RESOURCE POTENTIAL OF THE NORTH-EAST ARCTIC ZONE OF THE REPUBLIC OF SAKHA (YAKUTIA)

Evgenii Khoiutanov

Dr. Natalia Batugina

Vladislav Fedorov

Yurii Andreev

Chersky Institute of Mining of the North, Yakutsk, **Russian Federation**

ABSTRACT

The article analyzes the mineral and raw material base of coal deposits of the Arctic zone of the Republic of Sakha (Yakutia), all of them were explored in the Soviet time in the middle of 40-50 years. The paper presents a comparative characteristic of the geographic and economic, mining and geological and geotechnological conditions of coal deposits in the basins of north rivers Jana and Indigirka. The qualitative characteristics of the coals have been studied, which showed that from the point of view of consumers from the local better are the coals of the Krasnorechenskoe and Tikhonskoe deposits, and the worst brown coals of Uyandinskoe and Kularskoe fields, which have a very high humidity and ash content. The article assesses the possibility of using coal for generation of electric and thermal energy during development of ore and placer gold deposits in the Arctic zone of the Republic of Sakha (Yakutia). The unit cost of electricity generation is lowest when using coal as fuel, which can be extracted from the Kular deposit. Taking into account the lower quality of the coal fields of Kular deposit, it is possible for the subsoil user to consider the issue of extraction and delivery of better-quality coal from the previously developed Soginskoe deposit. The results give the opportunity of a fuller assessment of the potential, role and place of coal, especially local coal, for the generation of electrical and thermal energy for use by mining and processing companies, focused on the implementation of ore and placer deposits development projects in Arctic zone.

Keywords: raw material base, coal, quality, reserves, electricity generation, fuel

INTRODUCTION

The Arctic and Subarctic zones of the Republic of Sakha (Yakutia), hereinafter, RS (Ya), are the least explored and developed areas in the east of the northern polar zone of Russia; they accommodate 13 municipal districts, including 5 arctic districts, over a vast area greater than 1.6 million square kilometers.

This area features extreme natural and climatic conditions, underdeveloped industrial infrastructure, patchy human occupancy and very low level of land invasion. The settlement density is extremely low, moreover, the loss of population, started in the Soviet time, continues; this back-country also suffers from lack of transport facilities.

The distinctive features of the arctic regions in RS (Ya) are the high costs of construction of residential, production and infrastructure facilities, the high salaries and

https://doi.org/10.5593/sgem2024/1.1/s03.29

the heightened operating expenses. According to [1], the problem connected with the development of the Arctic, including RS (Ya), lies in the challenging actualization of the natural resource potential in these underdeveloped and sparsely populated regions.

Maintenance of majority of settlements in the polar zone of RS (Ya) has mostly a social trend [2]. These settlements have no industrial significance and are used generally as terminal points, including provision of rare plant facilities of the mining industry, as well and transportation of industrial products and operation personnel. These are the most remote arctic regions [3]. Production and facilities gravitate to the deposits of diamonds, gold and other minerals [4], and human resources are attracted by shifts.

In the Arctic Zone of RS (Ya) (AZ RS (Ya)), with a view to enhancing efficiency of operating and future mines at ore bodies, placers and manmade deposits, and for reducing risks and faulty operations, it is possible that power generation, alongside with imported diesel and coal, uses a local fuel [5]. In this case, a straight revaluation of the coal resource potential available in AZ RS (Ya) is required in conformity with the modern standards and criteria [6, 7]. The revaluation should include the existing experience and advanced achievements in the sphere of economically efficient and environmentally safe coal mining and combustion, as well as generation and distribution of electric and heat power [8].

This implies an expediency of a more detailed revision and assessment of different variants of supplying gold mines in AZ RS (Ya) with fuel and energy for the production needs. The relevance of such research increases even more as the cost of electric energy greatly defines the economic performance of mining companies.

MATERIALS AND METHODS

The methods and approaches used in the research included: the scientific analysis, comparison and generalization of experience gained by small mines in remote and inaccessible areas, inversion and metamorphoses of mineral resources in the arctic zone in the northeast of Russia, as well as the activated and updated database on mineral deposits in the region; the system analysis and the geoinformation methods of the spatial analysis, decision support, digital mapping, statistical processing and modeling of mineral deposits using mining and geological information systems.

The technical approach to the comparison of alternatives in coal supply and use included the comparative analysis of coal deposits for the assessment of usability of local coal in electric and heat power generation for the needs of production and heating during gold mining in the northeast of AZ RS (Ya). The main source of data were the geological exploration reports on the local coal deposits, and the data from the state balance sheet [9].

The scope of the comparative analysis embraced the geographical, geological and geotechnical characteristics and qualities of coals (moisture, ash content, volatile yield, heat value, sulfur content in mass%). The comparison involved local coals in the northeast of AZ RS (Ya) and imported coals.

The variants of purchase and shipping of coal were discussed as a case-study of the Deluvial ore field:

• variant 1: delivery of bituminous coal from the operating Dzhebariki-Khaya open pit (current delivery flow chart);

• variants 2–4: extraction and delivery of lignite from the Kularskoe, Uyandinskoe and Soginskoe deposits;

• variants 5 and 6: extraction and delivery of bituminous coal from the Krasnorechenskoe (Sogolokh site) and Tikhonskoe deposits;

• variant 7: import of diesel fuel to supply thermal power stations.

From the assessment, the variants of potential purchase (mining) and shipping of coal were selected. From the technical-and-economic evaluation and the subsequent comparison of the power generation cost per variants, the conclusion is drawn on expediency of using coal from the listed deposits in AZ RS (Ya).

RESULTS

The Verkhoyansk–Kolyma and Kolyma–Omolon metallogenic provinces in AZ RS (Ya) hold around 20 % of gold of Russia [10]. One of the most promising ore fields is the Deluvial ore field in the Verkhoyansk district in RS (Ya), 170 km southeastward of the Batagai settlement, on the middle-reach left bank of the river Adycha (right tribute of the Yana River). The ore field occurs within the boundaries of the Chenkelen Inya cluster of ore placers; the prospective gold reserves exceed 39 t. There are also small ore-bearing sites (Viyun, Lazo, Mastakh, Emelyanovo etc.), gold placers and numerous manmade deposits at former Kular mining and processing plant.

According to the state sheet balance of minerals of the Russian Federation, AZ RS (Ya) possesses 20 coal fields (14—bituminous coal; 6—lignite), with geological reserves of categories A+B+C1 of 433.2 Mt and category C2 of 199.3 Mt. The economic reserves of bituminous coal total: categories A+B+C1—398 Mt (91.9 % of overall reserves in the region), category C2—194 Mt (97.2 %), the non-economic reserves—24.8 Mt (49 %). The economic reserves of lignite are: categories A+B+C1—35231 Kt, category C2—5644 Kt; the noneconomic reserves of lignite are 25.9 Mt.

In the northeast of AZ RS (Ya), there are proven deposits of lignite (Kularskoe, Uyandinskoe, Soginskoe, Elikchanskoe) and bituminous coal (Krasnorechenskoe, Tikhonskoe). It often happens that at the proven deposits, equally promising coal fields occur to be explored and appraised.

The Kularskoe deposit of lignite lies in the east of the Omoloi coal region. Geotechnically, the deposit is suitable for mining by the open pit method. Lignite features a low quality: low rank, high ash content (33.9 % on the average), low heat value (4168 kcal/kg on the average). This circumstance became the reason for withdrawal of the deposit from mining process in the Soviet period.

The Uyandinskoe deposit of lignite occurs 80 km away of the Deputatski settlement and is connected with the latter by a winter snow road. Lignite is weakly metamorphized, and contains lenses and interbeds of ice or sand clay. Lignite has on the whole similar quality to the Kular coal and is a low-quality power-plant fuel. The average ash content per seams ranges from 18.5 to 27.0 %. The heat value is low, too. The Uyandinskoe deposit is explored best of all, and a part of it is suitable for mining by the open pit method.

An illustration of lignite extraction in the arctic regions can be the history of the Soginskoe deposit in the Lower Lena Coal Basin, 14 km away from the Tiksi

https://doi.org/10.5593/sgem2024/1.1/s03.29

settlement, in the valley of the river Sogo. Since 1943 to the mid-1960s, underground mining produced around 50–70 Kt of coal annually. The coal is lignite, low-ash (5.9 %), low-sulfur (0.56 %) and highly moist as at the Kularskoe and Uyandinskoe deposits. The coal was used as a power-plant fuel to supply the seaport and airport Tiksi, and a fish factory at the Bykov Cape.

The Krasnorechenskoe deposit of lignite in the middle-reach of the Indigirka River consists of two disjunct sites—Ugolny (18 km away from the river waterway along a straight line) and Sogolokh (1.5–4 km). From the viewpoint of open pit mining, shipment of coal to the river bank in the navigable time and supply of communities in the Indigirka River basin with coal, the most attractive site is Sogolokh. However, mining operations here bear potential environmental risks connected with the location of the site nearby the local natural area of preferential protection – Zashiversk nature reserve in the Abyi ulus (district). By the accounts of the Federal Service for the Oversight of Consumer Protection and Welfare of Russia (Rospotrebnadzor) in RS (Ya), in the neighborhood of the deposit, smallpox was widespread in 1812–1854. For this reason, before starting mining operations at the deposit, it is recommended to undertake special research on the risk of environmental contamination with pathogens of this disease.

The Tikhonskoe deposit of bituminous coal lies in the downstream basin of the Tikhon River which falls in the Indigirka River. There are no any roads in this area. Transport is only possible by deer and light-weight vehicles in winter and by floating across the Indigirka rapids in summer, which extremely complicates communication and supplies during geological exploration. The volume of the reserves suitable for open pit mining ensures coal production at the capacity of 80 Kt of coal annually for five years. On the whole, the Tikhonskoe deposit ensures coal production for a long time. Although coking, the coal from this deposit is only usable as a power generation feedstock from economic reasons, because of the remoteness and hardness of the deposit.

The summary cost analysis and the comparison of the variants of coal delivery from a deposit infrastructure is compiled in Table 1.

Table 1. Technical-and-economic calculations by variants of coal delivery from the Deluvial field

Variant	Coal cost at shipping place, thousand RUB/t (VAT excluded)	Cost of transportation and storage, thousand RUB/t (VAT excluded)	Coal cost in the area of consumption, thousand RUB/t	Power generation cost, RUB/(kW·h)
1	2.6	27.1	29.7	12.6
2	7.5	4.5	12.0	9.3
3	7.5	7.9	15.4	11.5
4	4.5	10.3	14.8	10.1
5	4.5	15.1	19.6	9.6
6	5.2	19.6	24.8	10.3
7	75.0 (free departure station price)	37.0	120.0	25.3

DISCUSSION

The analysis of coal resources in AZ RS (Ya) shows that the prime deposits are composed of coals of different ranks, from lignite to bituminous coal, with the widely ranged qualities. Exploration was carried mostly in the 1940–60s. The raw materials base of coal in the arctic regions was created in the conditions of the non-market economy, at the softer requirements imposed on the useful qualities of considered coals, as well as at the different level of cost, technology and technique. For these reasons, percentage of really economic reserves ('active', i.e. profitable and up to the modern standards) at the coal deposits in the Arctic is much lower than is accounted in the state balance sheet [11].

The resource potential of the deposits is underdeveloped even in terms of the proven reserves.

The analysis of the qualities of imported and local coal shipped from the deposits in the basins of the Yana and Indigirka Rivers shows that from the viewpoint of the useful qualities of the local coals, the best coal is bituminous coal from the Krasnorechenskoe and Tikhonskoe deposits, and the worst coal is lignite from the Kularskoe and Uyandinskoe deposits.

Table 2. Quality of imported and local coals in the basins of the Yana and Indigirka Rivers

Coal deposit, rank, grade	Average / limit moisture, mass%	Average / limit ash content, mass%	Volatile yield, %	Highest / lowest heat value, kcal/kg	Sulfur content, mass%
Imported					
Dzhebariki-Khaya, bituminous, long-flame	10.0/12.0	17.0/25.0	41.3	7500/5200	0.3
Nadezhdinskoe, bituminous, fat	8.0/10.0	19.0/21.0	35.0	8300/6100	0.4
Local					
Krasnorechenskoe, Sogolokh site, bituminous, long-flame and gas	–/16.0	18.0/23.0	42.0	7000/5286	0.8
Tikhonskoe, bituminous, fat and coking fat	10.0/–	13.6/–	–	7069/5200	0.6
Kularskoe, lignite, B	40.1/–	33.9/55.7	59.8	6359/3360	0.1
Uyandinskoe, lignite, B	50.0/55.1	23.8/27.0	57.9–63.6	6050/1930	0.3
Soginskoe, lignite, 2B	38.5/45.3	5.9/21.0	59.0	7932/6400	0.6

When diesel fuel is used in generation of electric and heat power, the cost of generation of 1 kW·h is 2.0–2.7 times higher than in case of coal, and is 25.3 RUB/(kW·h).

The power generation cost is the least when power generation is fueled by coal extracted from the Kularskoe deposit (9.3 RUB/(kW·h)). Considering the lowest qualities of coals from the Kularskoe and Uyandinskoe deposits, a subsoil user can take

https://doi.org/10.5593/sgem2024/1.1/s03.29

up mining and shipping of higher quality coal from the Soginskoe deposit as this coal has experience of effective combustion (boiler-houses at the Tiksi seaport and airport, and a fish factory at the Bykov Cape, etc). The difference in the cost of coals from the Kularskoe and Krasnorechenskoe deposits is minor, but in view of the risks connected with the development of the Krasnorechenskoe deposit, and with the more complex logistics, the use of the Krasnorechenskoe coal is problematic.

A conventional, comparatively affordable and finished approach to heat power generation in AZ RS (Ya) is supply of the Deluvial field infrastructure with the imported coals which have the quality up to the consumer requirements. On the other hand, this variant is 40% more expensive according to estimates.

The results, although inexhaustive in terms of fullness and accuracy, make it possible to revise the attitude to coal as one of the most accessible and profitable fuel-and-power resources in the subject area, and stimulate the further comparison of the considered coals with the more expensive sources of renewable [12] and nuclear energy [13].

CONCLUSION

The role of the coal resource potential in AZ RS (Ya) is yet low due to the complex market conditions and underdeveloped industrial and power-generating infrastructure, but it can grow with introduction of large rare earth, gold and tin deposits in commercial exploration and production.

The regional and federal budgets, and market participants appropriate hundreds million rubles to maintain the expensive procedure of before-schedule delivery of freights. Transportation cost in the area of consumption may reach 70–75 % in the total cost of fuel.

The proposed technical approach and the obtained results allow a more comprehensive evaluation of the resource potential and role of coal, mostly local coal, in generation of electric and heat power for the mining and processing plants aimed at development of ore deposits and placers in AZ RS (Ya).

The analysis of the economic and geography, mining and geological conditions and qualities of coal reserves occurring in neighborhood of ore deposits and gold placers in the northeast of AZ RS (Ya) shows that these coal reserves were explored and accounted in the Soviet era. It is required to revise the expedience and efficiency of extraction of these coal reserves using the modern criteria and with regard to the earlier formulated standards for the creation and sustainability of low-capacity coal mines in the subject area.

The Kularskoe and Uyandinskoe coals have very high moisture and ash contents. The effective use of these coals is possible after their preparation for combustion toward the higher heat value, including expensive deeper conversion. The Tikhonskoe deposit is more suitable for mining using the underground method. The proven coal reserves suitable for mining by the open pit method are extremely small. The risks of development of the Krasnorechenskoe deposit are connected with the environmental constraints. The use of the Soginskoe coal in power generation is 20 % more expensive as compared with the Kularskoe coal, but the quality of the Soginskoe coal and preparedness of the deposit for mining is much better. The simplest and practicable but

more expensive variant of fuel supply for electric power generation is the use of imported coal of the wanted quality.

Evaluation of prospects for local coal mining should take into account the trends of technological innovations in mining, pretreatment, processing and deeper conversion of the available and future grades of the solid fuel, and adaptability of these technologies to the actual mining conditions, with regard to natural properties of coal and to increasingly stringent environmental policies.

ACKNOWLEDGEMENTS

This work has been supported by the grants the Russian Science Foundation, RSF «Assessment of the Potential and Development of Scenarios for the Resource Saving Environmentally Development of Mineral Raw Materials of the Arctic Zone of North East of Russia» № 24-28-20376

REFERENCES

[1] Formation of strategic priorities for the study and integrated development of the Arctic territories of the Russian Federation, Ed.: A.I. Tatarkin, Ekaterinburg: Institute of Economics of the Ural Branch of the Russian Academy of Sciences, 2013, 374 p.

[2] Vasiliev V.V., Gritsevich A.V., Selin V.S., Historical tendencies and present organizational-economic challenges of the «northern delivery», Apatity: Publ. Kola Science Centre., Russia, 2009, 152 p.

[3] Huskey L. Resiliency in Remote Economies: External Challenges and Internal Economic Structure, Journal of Contemporary Issues in Business and Government, No. 1, pp 1-12, 2011.

[4] Fondahl G., Crate S., Filippova V. The Sakha Republic: Yakutia, in Arctic Social Indicators, ASI II Implementation, Denmark, 2014, pp 57-91.

[5] Energy Strategy of the Republic of Sakha (Yakutia) for the period up to 2030. Otv. red. N. A. Petrov. Yakutsk; Irkutsk, Yakutia Media Holding, 2010, 328 p.

[6] Batugina N. S., Gavrilov V. L., Barakaeva I. D., Tarskij N. D. The improvement of energy security in the transpolar regions of the Republic of Sakha (Yakutia) based on the development of local fuel and energy resources, Miner. resursy Rossii. Ekonomika i upravlenie, no. 6, pp 79—85, 2014.

[7] Tabachkova X., Prosekov S., Sokolinskaya N. Energy system structure in Russian Arctic: coal production forecast, International Journal of Energy Economics and Policy, no. 10 (3), pp 476—481, 2020. DOI: 10.32479/ijeep.9000.

[8] Stennikov V. A., Petrov N. A., Ivanova I. Yu., Dobrovolskaya T. V., Pavlov N. V. Problems and areas of heat supply development in the Sakha Republic (Yakutiya) in the medium term, Energet. politika, no. 1, pp 64—74, 2018.

[9] Asaul A. N., Asaul M. A., Levin Yu. A., Platonov A. M. Energy supply to isolated areas: attracting investment and developing regional economy, Ekonomika regiona, no. 3, pp 884—895, 2020. DOI: 10.17059/ekon.reg.2020–3-16.

[10] Coal base of Russia. Vol. 5. Book 2: Coal basins and deposits of Far East of Russia (Republic of Sakha, NorthEast, Sakhalin Island, Kamchatka Peninsula). Moscow, 1999.

https://doi.org/10.5593/sgem2024/1.1/s03.29

[11] Decree of the President of the Russian Federation “About Fundamentals of the state policy of the Russian Federation in the Arctic for the period up to 2035” no. 164 of March 5, 2020. Available at: http:// www.garant.ru/products/ipo/prime/doc/73606526/.

[12] Shakirov V. A., Tuguzova T. F., Muzychuk R. I. Problems of power supply in the public utility sector of the Arctic zone of the Republic of Sakha (Yakutia), Arktika: ekologiya i ekonomika. [Arctic: Ecology and Economy], no. 4 (40), pp 106—116, 2020. DOI: 10.25283/2223-4594-2020-4-106-116.

[13] Sarkisov A. A., Smolentsev D. O., Antipov S. V., Bilashenko V. P., Shvedov P. A. Economic Efficiency and Possibilities of Using Megawatt-class Nuclear Power Sources in the Arctic, Arktika: ekologiya i ekonomika. [Arctic: Ecology and Economy], no. 1 (29), pp 4—14, 2018. DOI: 10.25283/2223-4594-2018-1-4-14.

BLASTING DEMOLITION CHALLENGES OF A TALL COOLING TOWER AND CHIMNEY

PhD. Eng. Ress. Robert Laszlo [1]

PhD. Eng. Ress. Ciprian Jitea [2]

PhD. Eng. Ress. Bogdan Garaliu [3]

PhD. Eng. Bogdan Aurelian Nicola [4]

Eng. Levente Miklos [5]

[1,2,3] National Institute for Research and Development in Mine Safety and Protection to Explosion – INSEMEX Petroşani, **Romania**

[4] University of Petrosani, **Romania**

[5] Industrial Demolition Company, Dîmbau, **Romania**

ABSTRACT

The paper describes the practical solutions and safety conditions of realizing the demolition of an industrial chimney and a cooling tower located in a former thermal power plant, having in the very close vicinity several civil constructions. The chimney has a height of 208 m and consists of the outer tubular structure of reinforced concrete and as well as of the inner chimney made of refractory brick masonry. The cooling tower height was 108.0 m and the base diameter of 82.00 m. For chimney, the chosen solution of demolition was overturn in an intended direction and for the cooling tower was that of partial lateral collapse followed by a total crash of the tower on its position. Considering the location of civil constructions the challenge of the project was to find solutions to reduce the throwing distance of the concrete pieces under the action of the explosion, to mitigate vibrations through the collapse and sequential contact with the ground of the construction, to reduce the value of the overpressure of the air created due to the piston effect during the collapse the construction of the tower.

Keywords: demolition, explosives, blasting parameters, safety.

1. INTRODUCTION

In Eastern European countries there are numerous old industrial areas where, due to constraints from the point of view of environmental protection, there are activities of conserving or decommissioning some areas which will then be the object of the development of new projects. The thermal power plant, where the demolition of the two buildings that are the subject of this article, is an industrial type of property with a special purpose - combine production of electricity and thermal energy. Currently the activity is suspended, the constructions showing real signs of major degradation.

The paper describes the practical solutions and safety conditions of realizing the demolition of the industrial chimney and cooling tower located in a former thermal power plant (Figure 1), having in the very close vicinity several civil constructions. To establish the possible effects generated by the execution of the chimney demolition by

https://doi.org/10.5593/sgem2024/1.1/s03.30

blasting works, a risk assessment was made with reference to seismic wave, air shock wave, noise, dust, and the level of shock generated by the impact of constructions with the soil. The demolition works were successfully carried out and thanks to the technical solutions and the adopted protection and security measures, no relevant damage was recorded.

2. CONSTRUCTIONS DESCRIPTION

2.1. Cooling tower

The location of the cooling tower on the thermal power plant platform is shown in Figure 1 and 2. In the immediate vicinity of the cooling tower, in the area opposite the overturning direction, there are several private objectives, the most exposed being the following (Figure 2): 1 - to the north, north-east, 23.0 m from the boundary of the tower - private property land and house; 2 - to the north-west, west, 27.0 m from the boundary of the tower - private property land and house; 3 - to the west, 35.0 m from the boundary of the tower - private property land and house.

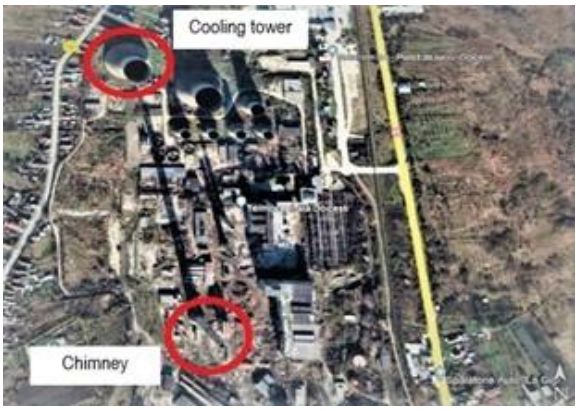


Figure 1. Objective location plan



Figure 2. Cooling tower and neighbouring objectives

The cooling tower is in the form of a hyperboloid of rotation made of reinforced concrete, by sliding with a variable section, having a height of 105.00 m, a diameter at the base of 82.00 m, respectively 49.00 m at the top. The tower structure consists of the following main component elements (Figure 3) [1]:

- **the inclined support columns** of the tower are made of reinforced concrete with a rectangular section, the main dimensions of which are 0.55 x 0.50 m. The tower rests on 36 pairs of "**V**" shaped inclined pillars with a height of 6 .0 m.
- **the ring belt** at the base of the tower is the main element of resistance and bearing capacity of the construction. The belt has a height of 1.5 m and a variable thickness with an average of 0.65 m.
- **the body of the tower** is the second resistance element of the construction. The hyperbolic mantle of the tower has a variable thickness per height, being between 0.70 m starting from + 7 m elevation and 0.25 m up to + 30 m elevation, further the thickness of the mantle remaining constant at 0.18 - 0.15 m to the ring belt at the top.



Figure 3. Cooling tower and Chimney structure

2.2 Industrial chimney

The chimney is 208 m high and consists of the external tubular structure made of reinforced concrete, having the radius at the bottom (elevation + 27 m) of 7.15 m, which remains constant throughout the height of the chimney, as well as the inner chimney from refractory brick masonry with a radius of 5.0 m . The thickness of the reinforced concrete wall is 50 cm, and the thickness of the masonry chimney wall is 15 cm.

The foundation of the concrete chimney is of the reinforced concrete screed type (Figure 3) with a diameter of 24.10 m and a thickness of 0.50 m. The walls of the chimney are supported in refractory masonry on a foundation with its own structure of concrete pillars and on brackets formed on the sliding wall and spoked wheel beams every 8.00 m. The related constructions - the flue gas channels, were made of solid brickwork and reinforced concrete, they were subsequently demolished by mechanical means. Between the reinforced concrete structural wall and the brick chimney wall, there is a free space used for the internal control of the structure and around the 27 m elevation is about 1.6 m [1].

3. CHIMNEY AND COOLING TOWER BLAST DEMOLITION

3.1 The cooling tower demolition process

From the point of view of demolition, hyperboloid cooling towers are one of the most interesting construction categories. When the thickness of the tower body is compared to that of an eggshell, the eggshell should be only 0.1 mm thick. Cooling towers feature a "shell" that is considerably thinner than that of an egg. Such structures withstand external shocks, as well as those caused by their own weight and temperature fluctuations, admirably. A greater unilateral action, on the other hand, can be fatal to the stability and integrity of such structures.

Damage to the buckling of the structure and its rotational polarization are the two main mechanisms known to "fail" structural integrity of hyperbolic cooling towers because of planned collapse. Taking into account the location of civil constructions in the close vicinity of the tower and in order to reduce the throwing distance of the concrete pieces under the action of the explosion, to mitigate vibrations through the collapse and sequential contact with the ground of the construction, to reduce the value of the

https://doi.org/10.5593/sgem2024/1.1/s03.30

overpressure of the air created due to the piston effect during the collapse the construction of the tower, the most appropriate demolition solution is that by polarization (rotation). Tower rotation using a so-called "heel and toe" effect is achieved by exploding charges placed on 2/3 of the tower body and/or support legs [2],[3].

As in the case of the cooling tower that is the subject of this paper, the slenderness index is lower than 2, which is why a combined variant of demolition is chosen - that of partial lateral collapse followed by a collapse of the tower itself. This will be achieved by blasting in a chosen direction at least half of the support legs and some portions of the ring belt, followed by a collapse of the tower on its own, facilitated by the cuts previously created in its body (Figure 4 and 5).

The non-detonated support pillars, the ones on the opposite side of the overturning direction, will function as a "hinge", allowing the creation of a beam energy, by collapsing the other half of the tower. This shear energy is indispensable, to induce a dynamic tension in the hyperboloid of the tower and to make it yield along the slits created in its body [2],[3].
In order to minimize the seismic wave and air overpressure due to the impact with the ground when the structure collapses, i.e. the creation of the torsional moment of the tower body in such a way as to allow the vertical escape of the air inside the structure as well as its unfolding into several pieces of smaller dimensions, with a reduced seismic effect upon their impact with the ground, it was decided to create a horizontal cut (which will allow the vertical descent of the tower over a shorter distance and which will favour the creation of the torsion moment) by blasting ½ of the perimeter of the body combined with vertical cuts with lengths of 6 - 7 m, executed between the ring belt and the horizontal cut as well as above it (Figure 4 and 5).

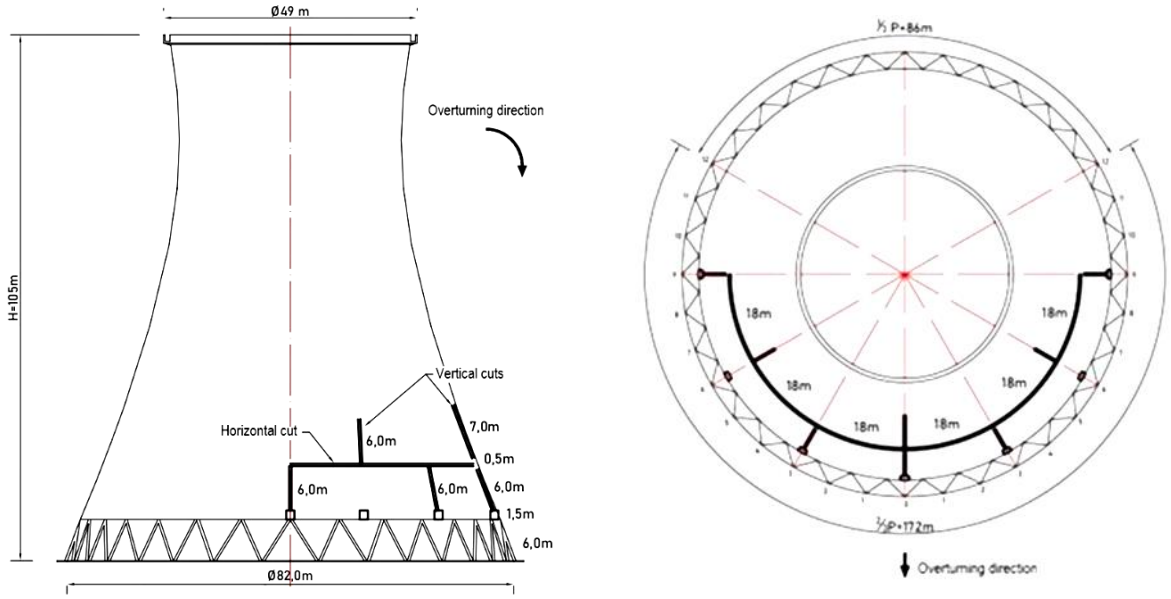


Figure 4. Cutting sections on the body of the cooling tower

Also, in the area from the direction of overturning, on 2/3 of the perimeter at the base of the tower, sections of cuttings will be executed by blasting in the ring belt as well as in the inclined columns that supporting the body of the tower.

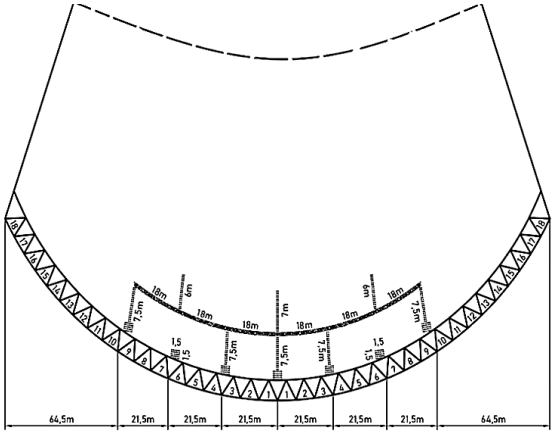


Figure 5. Type and location of break sections in the body of the cooling tower



Figure 6. Chimney cut location + 27 m

3.2 The chimney demolition process

For the demolition of the chimney, the overturning procedure was applied in a chosen direction. The existence at the elevation +27.0 m of the first visiting/working platform inside the chimney, determined the choice of the area at this elevation for the execution of the chimney overturning cut (Figure 6). This platform also allows access to the brickwork in the immediate vicinity of the chimney, at 250 - 300 m in the direction North, there are no objectives to be protected, its demolition was chosen in this direction.

To demolish the chimney structure, the following phases have been completed [2],[3], and [4].:

- creation by blasting works of two openings (windows) at the limits of the detachment cut, located at 2/3 of the outside perimeter, having a width of 1.0 m and a height of 1,2 m (Figure 7). The realization of the two openings also served to establish the way in which the reinforced concrete structure behaves under the action of explosive loads;
- realization of the detachment cut for which purpose will be drilled in the concrete wall, from outside the chimney, starting from the elevation +27 m, from bottom to top, 8 rows of holes placed in the square network (Figure 7), as follows:
  - ✓ row 1 of holes, starting from the elevation +27 m, on the opening of 1/4 of the outside perimeter of the reinforced concrete chimney (12.5 m), with a number of 34 holes. The holes will be arranged symmetrically on either side of the axis of the overturning direction;
  - ✓ row 2 and 3 of holes drilled above row 1 holes, on the opening of 1/2 of the outside perimeter of the reinforced concrete chimney (22.5 m), with a number of 66 holes. The holes will be arranged symmetrically on either side of the axis of the overturning direction;
  - ✓ rows 4,5.6,7 and 8 holes drilled above row 3 holes, on the opening of 2/3 of the inner perimeter of the reinforced concrete chimney (30 m), with a number of 5 rows x 84 holes per row. The holes will be arranged symmetrically on either side of the axis of the overturning direction;
  - ✓ creation of a break section in the masonry of the brick chimney. For this purpose, at the height + 28 m, five explosive charges will be fixed applied to the chimney wall, inserted into a metal or wooden case, one charge each placed in

https://doi.org/10.5593/sgem2024/1.1/s03.30

the overturning axis and in the two extremities of 2/3 of perimeter as well as one load placed laterally left - right of the overturning axis, in the middle of the distance between the other loads (Figure 8);

- ✓ decommissioning around the detachment cut of all additional elements such as metal stairs and lightning conductor.

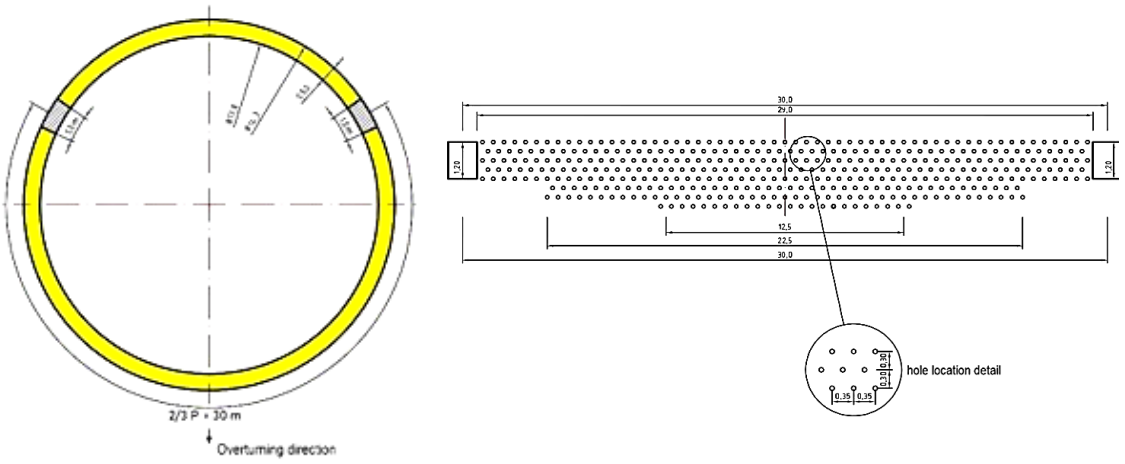


Figure 7. Realization of the detachment cut in the concrete wall

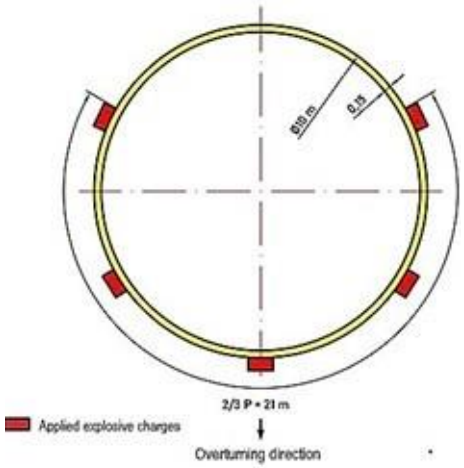


Figure 8. Applied charges on the brick masonry in the area of the detachment cut

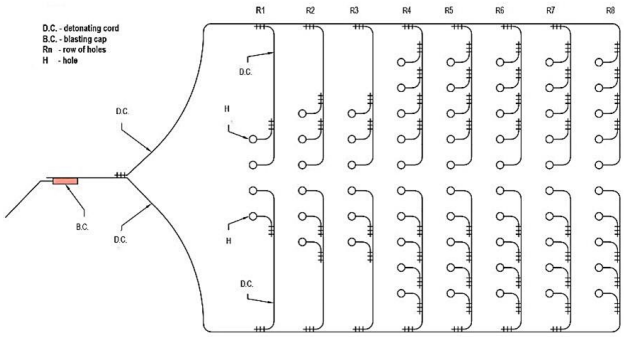


Figure 9. Chimney explosive charge initiation layout

To collapse the chimney construction in the expected direction, all the explosive charges from the concrete and brick chimneys were detonated instantly. Dynamite type explosive loads were placed in holes and the explosive charges in each hole were initiated with detonating cord. At the cut edge, the ends of these secondary lines were connected to a detonating cord main line together with that one coming from brick chimney area (Figure 9) [5].

3.3 Blasting parameters.

The total amount of explosive used to demolish the cooling tower and chimney constructions is as follows: Q_{Te} = 174 kg dynamite type for cooling tower and Q_{Te} = 91 kg dynamite type for chimney; Q_{Tdc} = 1850 lm detonating cord for cooling tower

and Q_{Tdc} = 800 lm detonating cord for chimney; N_d = 30 pcs of nonelectric elements for cooling tower and N_d = 10 pcs of nonelectric elements for chimney.

4. RISKS EVALUATION

The main outcomes from the risk evaluation specific for the performed work are presented bellow.

The impact of a collapsing structure on the ground may cause seismic effects, the magnitude of which is determined by the energy produced during impact. This energy is proportional to the mass of the building being demolished, the height of its center of gravity, and the properties of the ground on which it falls.

The risk assessment showed that at for the objective closest to the chimney (at a distance limit of 250 -300 m), the value of the velocity of seismic waves possible to be generated at the impact of a collapsing structure of the chimney on the ground, is 0.11 cm/s - value lower than 1.10 cm/s the one chosen as permissible. To reduce the impact with the ground, a damping bed was arranged in the direction of overturning the chimney.

At the evaluation of the level of vibrations induced in the ground upon the collapse of the cooling tower and referring to the closest civil targets and located at 25 m from the collapse area of the portions of the tower body, the calculated value of the velocity of seismic is 1.125 cm/s – value higher than 1.10 cm/s the one chosen as permissible. To reduce the level of vibrations during the demolition of the cooling tower, in the area opposite to the direction of overturning, between the cooling tower and its neighbouring constructions, on an area of 1/3 of the perimeter of the tower, a trench was dug on a depth of 2.0 m. To verify the level of vibration induced in the ground by the impact when the two demolished constructions, three seismometers equipment were placed at the closest civil buildings. The results of the measurements confirm that the seismic values induced by the collapse of the cooling tower and chimney are lower than the permissible ones of 1.10 cm/s.

The overpressure of the shock wave can generate a piston effect on the air, and which can be produced when the tower body descends vertically and to propagate outside the tower site at distances of 15-20 m, having high values. To prevent this effect, preparations were made to section the tower body with a combination of horizontal and vertical cuts. Also, between the construction of the cooling tower and the objectives to be protected, on 1/2 of the perimeter of the tower, in the area opposite the direction of overturning, a protective berm of earth / rubble resulting from the demolitions was set up, with a height of 6 – 7 m. In addition, a protection made of flexible wire mesh and geo-textile cloth was arranged in the area close to the fence of the properties neighbouring the tower. In the upper area of the built berm, a protective screen will be created made of cylindrical filters of plastic material, recovered from inside the tower cooling.

To reduce *dust pollution*, the surface on which the construction is to fall will be sprinkled with water, both before and immediately after the collapse of the construction.

Throwing of small material under the effect of the explosion, at the chimney demolition is diminished by the installation at the level of the detachment cut of means of protection with materials made of welded wire mesh with large mesh, flexible wire mesh with small mesh and an external protection of geo-textile cloth placed 0.5 m away

https://doi.org/10.5593/sgem2024/1.1/s03.30

from the construction. The external protection shall cover the area of the explosive charges, exceeding by at least 1.0 m the lower and upper part of the detachment cut. The arrangements made for the cooling tower demolition were described earlier.

5. CONCLUSIONS

A vast number of demolitions works using explosives and a high degree of complexity have demonstrated that the blasting approach is an appropriate option in terms of efficiency, quality, and security.

The novelty of the presented demolition work consisted in the solutions for preparing the structure for demolition, such as the use of a combination of horizontal and vertical cuts located at certain heights and having certain lengths, as well as in the solutions identified to minimize the effects of the demolition work - how would be the raising of an earth wave at the tower's limit, on the opposite side of the ramp and at a height equal to the supporting legs, digging a trench between the area behind the tower and the civil objectives to be protected, setting up a earth made bed to absorb the impact in the direction of toppling the tower. All these techniques are discussed in this paper, and based on the blasting concept and risk assessment, successfully was completed the demolition by blasting works of the cooling tower and chimney constructions.

ACKNOWLEDGEMENTS

This paper was developed within the Nucleu-Programme, carried out with the support of Romanian Ministry of Education and Research, project no. PN-23-32-01-03, project title: Development of monitoring methods in order to reduce the environmental impact of the use of explosive materials, pyrotechnic articles and the application of shooting technologies (in Romanian: Dezvoltarea metodelor de monitorizare în vederea reducerii impactului de mediu în urma utilizării materialelor explozive, articolelor pirotehnice și aplicării tehnologiilor de împușcare).

REFERENCES

[1] Miklos L. & all, 2022 - *Technical documentation for the demolition by blasting works combined with classical works - cooling tower and chimney from the premises of the former CTE Doicesti*, Industrial Demolition Company, Dambau, Romania.

[2] Laszlo R, Ghicioi E., Jitea C., Nicola A. & Miklos L., 2022 - *Technical and safety aspects for the demolition of a chimney with a height of 150 m in difficult location conditions*, Proceedings of the 11th EFEE World Conference on Explosives and Blasting, Maastricht, Netherlands.

[3] Yi L., Feng L., Xianglin G. & Xiaoqin L., 2014 - *Numerical research of a super-large cooling tower subjected to accidental loads*, Nuclear Engineering and Design, Volume 269, https://doi.org/10.1016/j.nucengdes.2013.08.028.

[4] Tat S., Zaporojan M.& Fisguss C.,1985 - *Explosives and blasting techniques applied in industry*, Petrosani, Romania.

[5] Jitea I.C., Lupu C., Șuvar M., Rus D., 2014 - *Procedure for metal cutting using explosives, with low environmental impact*, Environmental Engineering and Management Journal, Vol.13, No. 6, 1459-1462.

BLASTING TECHNOLOGY FOR NEUTRALIZING IMPROVISED EXPLOSIVE DEVICES

Ph.D Eng. Emilian Ghicioi[1]
Ph.D eng. Dan Gabor[1]
Ph.D. Ress. Ing. Mirela Radu[1]
Anca Tazlauanu[1]
[1]National Institute for Research and Development in Mine Safety and Protection to Explosion – INSEMEX**, Romania**

ABSTRACT

An attack with a "improvised" explosive device (IED) is when someone uses a bomb and/or destructive device to cause damage, render someone helpless, harass, or divert attention. Terrorists, criminals, vandals, suicide bombers, and rebels all utilize IEDs. IEDs can take many different shapes because they are improvised; they can be as simple as a pipe bomb or as complex as a sophisticated weapon that can inflict significant damage and casualties. IEDs can be transported or carried in a car; they can also be delivered in a package; they can be delivered by a person; or they can be hidden by the side of the road. In the course of 2023, INSEMEX perfected, patented, and tested the liquid-jet neutralization device of the improvised explosive devices DNJLDEI (prototype for an improvised bombs neutralization device, Patented Request ***CBI OSIM nr. a/00178/11.04.2023***), which has the potential to be a valuable tool for urban interventions against terrorist attack. In this paper was presented the liquid-jet neutralization device of the improvised explosive devices DNJLDEI (prototype for a neutralization device of improvised explosive bombs), which has the potential to be a valuable tool for urban interventions against the terrorist attack. Tests were carried out for the two improved variants of plastic containers, with measurements of the velocity of the projected liquid jet (water). The experimental test program of DNJLDEI included the final verification of functionality of new prototype of IED neutralization device, based on liquid-jet, the operational validation being performed upon a bomb briefcase, which was neutralised by accuracy destroying of detonator, without damages of explosive charge.

Keywords: improvised explosive device, safety, prototype for neutralization of IED

INTRODUCTION

An explosive weapon that is not conventional in nature and can be detonated in multiple ways is known as an improvised explosive device, or IED. Both citizens and troops are their objective. IEDs are becoming more and more significant in today's conflicts, and they will remain a component of the operational landscape for NATO military operations in the future [1]. IEDs have a severe negative impact on the local populace and are one of the primary causes of troop casualties [2,3]. The Alliance assists members and partners in building their own capabilities in an effort to lessen the

https://doi.org/10.5593/sgem2024/1.1/s03.31

hazards presented by IEDs, with a focus on creating counter-measure technology, doctrine, and education and training [4,5].

Depending on the function that their users want them to play, IEDs will vary. They could be intended to carry out deliberate attacks on people and vehicles, or they could be made to destroy infrastructure and result in a large-scale death toll. Their position, level of destruction, and method of "delivery" of the explosive device to the target all influence their role and intended impact [6]. Multiple configurations are always possible because the only thing limiting IED technology is the creativity of the person making or deploying the devices. However, one design limitation has to do with the attackers' inclination for close closeness to the victim. In certain situations, the attackers may decide to avoid discovery or cause themselves harm by staying far away from the equipment [7]. In the course of 2023, INSEMEX perfected, patented, and tested the liquid-jet neutralization device of the improvised explosive devices DNJLDEI (prototype for an improvised explosive device neutralization device), which has the potential to be a valuable tool for urban interventions against terrorist attack. These findings follow the results obtained in 2022 from the experimentation of a prototype de neutralization device for explosive devices DNDEI, which uses relatively small explosive remnants made of optimized metal and reusable water-receptacles. In this paper will be presented some of the features of the device and it's testing experimental program. The purpose of the DNJLDEI tests and experiments was to verify the workable capacity for urban area interventions. Tests were carried out for the two improved variants of plastic containers, presented in the previous paragraph, with measurements of the velocity of the projected liquid jet (water) [8-11].

MATERIALS AND METHODS

The ***n***eutralization ***d***evice with ***l***iquid ***j***et of ***i***mprovised ***e***xplosive ***d***evices (DNJLDEI) fig. 1, consists of an assembly consisting of a reinforced metal base (mortar), provided with a carrying handle, a base that has an adjustable frame, with perforated arms and fixing screws to various degrees of inclination (from horizontal to vertical working position), having a centrally positioned cylindrical plug (reinforced around the perimeter and at the bottom) for mounting the specially shaped plastic container (cylinder equipped with legs and fixing disc, fig. 2, with both flat closing surfaces or with one flat end and one hemispherical end, fig. 3), removable container, with a threaded cap, in which there is a volume of liquid, as well as a reduced charge of plastic explosive, moulded on the lower surface of the dry compartment intended for it, into which an electric detonating staple is inserted for initiation, connected to a detonator, operated by an operator from a safe distance.

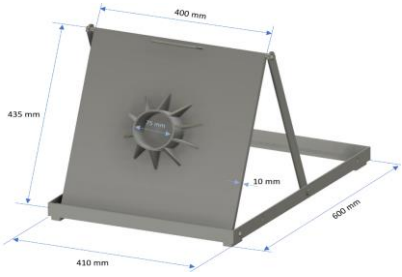


Fig.1 Device DNJLDEI



Fig.2 Cylindrical container with legs



Fig.3 Container with hemispherical end

RESULTS AND DISCUSSION

The testing and experimentation of the DNJLDEI was aimed at verifying the work capacity, which can be used in interventions in the urban area. Tests were carried out for the two improved versions of plastic containers, presented in the previous subsection, measuring the speed of the projected liquid jet (water). Also, a series of experimental tests were carried out with the DNJLDEI device to verify the ability of the water jet to penetrate a 0.4 mm thick steel plate, as well as to study how it affects an industrial explosive stick cartridge (RIOPERG, 250 g, diameter 32 mm, considered as explosive-target-part of DEI, fig.4). Reduced explosive charges were used, with a mass of 10 g and 20 g respectively (plastic explosive-SEMTEX), initiated by instant electric detonator, inserted in plastic containers (for the two types of containers with legs, cylindrical shape of approx. 450 ml, respectively with a hemispherical end-bottom of approx. 200 ml). A silicone wax was used to seal the lid thread and the filler plug of water containers.



Fig. 4 RIOPERG stick cartridge, considered as a target explosive-part of IED

The experimental program took place under controlled conditions, ensuring the safety of the research team and the operators (blasters), with the provision of landmarks and markers necessary to calibrate the distances traveled by the liquid jet, to measure the propulsion speed with the help of high-speed camera PHANTOM and image processing software, figs. 5-6.

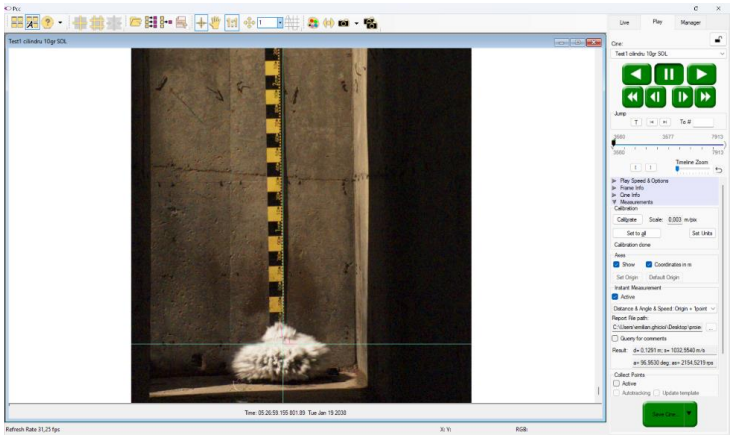


Fig. 5

DNJLDEI experiment results using the container of approx. 450ml water volume, cylindrical shape, in which an explosive charge of 10 g was placed. The maximum speed of the liquid jet Vmax=1080m/s (in the first 200mm of liquid ejection),

https://doi.org/10.5593/sgem2024/1.1/s03.31



Fig.6 Penetration of the steel plate with a thickness of 0.4 mm, placed at a distance of approx. 50mm, container of approx. 450ml, cylindrical shape, in which an explosive charge of 20g was placed, fragmentation and projection at a distance of more than 10m of the explosive stick cartridge (initial target, placed upon the steel sheet).

The last stage of experimental test program of DNJLDEI was called *the final functional and operational validation of the intervention module for DEI neutralization.*

For this scope it was built an improvised explosive device IED (fig. 7), consisting of a rectangular suitcase, equipped with an explosive stick cartridge, an electric cable connected to the headset jack of a mobile phone - as an electric detonator, which could be remotely operated/controlled via mobile phone radio waves.



Fig.7 Improvised explosive device DEI

Field positioning of the DNJLDEI neutralization device in the vicinity of the suitcase (fig. 8). It was considered that the suitcase was inspected non-invasively/x-rayed and the location of the detonator was identified (marked on the suitcase with X -DET), so the DNJLDEI was positioned so that the liquid jet acted directly on the detonator, in the present case being a mobile phone.



Fig.8 Field positioning of the DNJLDEI neutralization device in the vicinity of the suitcase (improvised bomb)

Presentation of the effects generated by the use of the LIQUID JET NEUTRALIZATION DEVICE OF IMPROVISED EXPLOSIVE BOMBS on the rectangular suitcase equipped with an explosive stick cartridge, electric cable connected to the headphone jack of a mobile phone – detonator, figs 9-12:



Fig.9 Perforating the DEI suitcase near the detonator



Fig.10 Non damage of the explosive stick cartridge in the IED suitcase



Fig.11 Projection of the mobile phone screen, part of detonator, at a distance of approx. 7.5 m

https://doi.org/10.5593/sgem2024/1.1/s03.31



Fig. 12 Projection by the liquid jet from DNJLDEI of the detonator-mobile phone - considered being a detonator of bomb at a distance of over 25m

The following is a sequence of representative frames of the use of the DNJLDEI, which allows direct observation of the effectiveness and precision with which the liquid jet expelled, destroyed and projected the IED detonator at a long distance and destroyed the electrical connection, without affecting some kind of explosive stick cartridge in the bomb suitcase, figure 13:

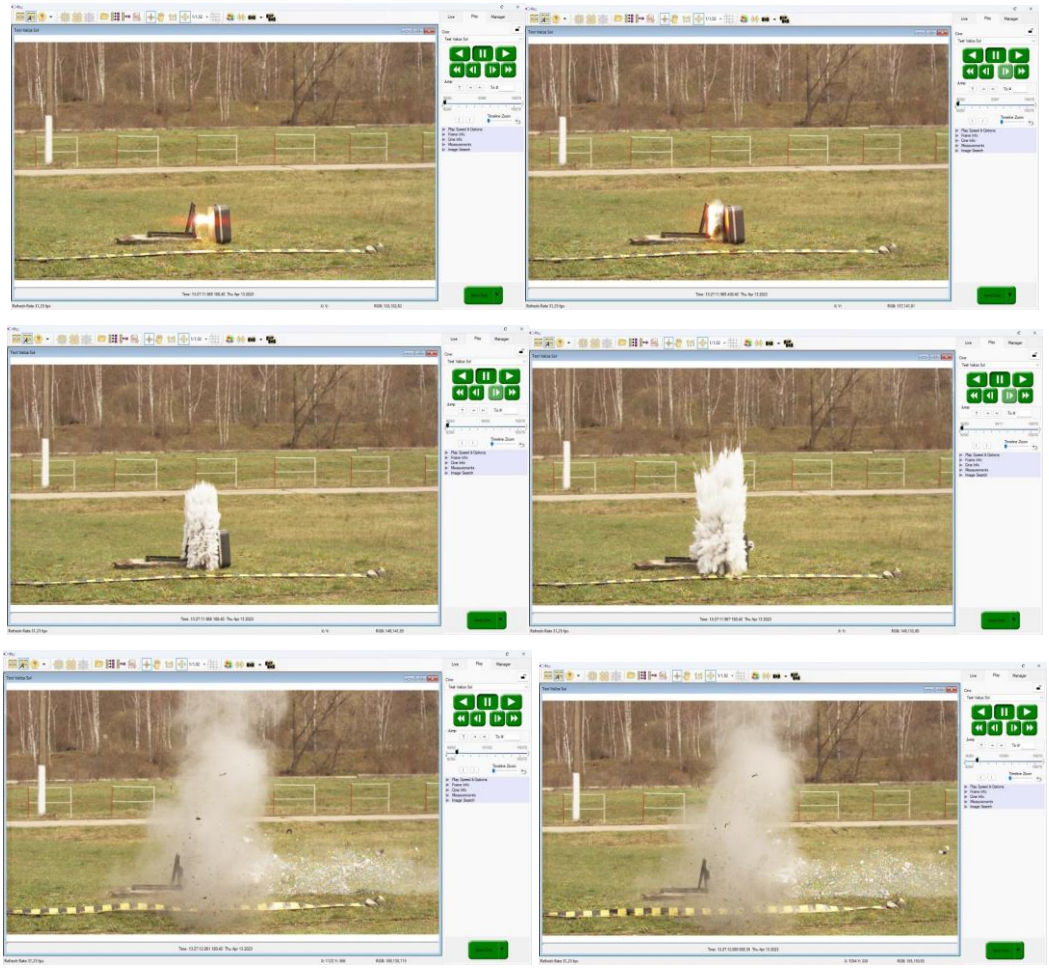


Fig. 13 Sequence of frames

As a result of the experiment carried out, it can be stated that the expulsion of the detonator from the target suitcase - IED (improvised explosive device), without affecting the explosive stick cartridge, validates: the functionality, effectiveness and selectivity of the DNJLDEI liquid jet neutralization device, its use being easy, and the operation is carried out in safe conditions.

CONCLUSION

In this paper was presented the liquid-jet neutralization device of the improvised explosive devices DNJLDEI (prototype for a neutralization device of improvised explosive bombs), which has the potential to be a valuable tool for urban interventions against the terrorist attack.

The device can be configured on site, depending on the way the target is presented (briefcase, backpack, package, etc.), being able to use reduced explosive charges (approx. 10-20g), with their placements in the dry place intended for containers of a special shape for the arrangement of the liquid (which can be: water, water with dissolved salt or another denser liquid), so as to obtain a more concentrated or more dispersed projected jet, at volumes different liquids, between 200ml and 600ml. The initiation is performed from a safe distance for the operator of the DNJLDEI device, after installation in the vicinity of the target.

The use of cylindrical containers (filled with liquid with a volume of approx. 450 ml), together with a reduced explosive load of 10 g of SEMTEX, allows obtaining a central liquid jet, perpendicular to the mortar, with a maximum liquid jet speed of 1080m /s (in the first 200mm of liquid ejection), and after passing 300mm, the jet has a speed of over 560m/s, with a limited deformation capacity, without penetrating the 0.4mm thick steel plate, located at a distance of approx. 50mm, and the explosive stick positioned on the sheet was fragmented and projected more than 10 m away (in the vertical plane). When using a 20g SEMTEX explosive charge, the sheet was perforated and the explosive stick was fragmented and projected over 10m away (vertically).

The last stage of experimental test program of DNJLDEI was final verification of functionality of new prototype of IED neutralization device, based on liquid-jet, the operational validation being performed upon bomb briefcase, which was neutralised by accuracy destroying of detonator, without damages of explosive charge.

ACKNOWLEDGEMENTS

This work was carried out through the Soluții 3 Project, with the support of the UEFISCDI project no 33 SOL/2021 - Complex simulator for the development, testing and validation of methods and means of response specific to intervention forces in the case of asymmetric threats and risks occurring in urban areas, the “Core program” of the National Research, Development and Innovation Plan 2022-2026, supported by MCID, project no. PN EXH2 INSEMEX and IOSIN- PCDIEX.

https://doi.org/10.5593/sgem2024/1.1/s03.31

REFERENCES

[1] Daniel C. G, Frances L. E., Improvised Explosive Devices, Crisis and Emergency Management, Routledge, 2014, pp. 120-124.

[2] Wilkinson A., Bevan J., Biddle I., Improvised Explosive Devices (IEDs): An Introduction, Conventional Ammunition in Surplus, Switzerland, 2008, pp. 136.

[3] Bradley, Graham and Thomas Ricks. 2004. 'Munitions Issue Dwarfs the Big Picture.' Washington Post. 29 October, p. A01.

[4] Beckett A. Pelletier P., Mamczak C., Multidisciplinary trauma team care in Kandahar, Afghanistan: current injury patterns and care practices, Injury, 2012, pp. 2072.

[5] Sławiński, G.; Świerczewski, M.; Malesa, P. Modelling and numerical analysis of explosion underneath the vehicle. J. KONES 2017, 24, 279–286.

[6] Jamroziak, K.; Bajkowski, M.; Bocian, M.; Polak, S.; Magier, M.; Kosobudzki, M.; Stepien, R. Ballistic Head Protection in the Light of Injury Criteria in the Case of the Wz.93 Combat Helmet. Appl. Sci. 2019, 9, 2702.

[7] Ramasamy, A.M.; Hill, A.M.; Clasper, J.C. Improvised explosive devices: Pathophysiology, injury profiles, and current medical management. J. R. Army Med. Corps 2009, 155, 265–272.

[8] Ghicioi, E., Patented Request CBI OSIM nr. a/00178/11.04.2023- DNJLDEI-INSEMEX, 2023.

[9] UEFISCDI project no 33 SOL/2021 - Complex simulator for the development, testing and validation of methods and means of response specific to intervention forces in the case of asymmetric threats and risks occurring in urban areas.

[10] Core Program Project - INSEMEX- EXH2 - Increasing the national expertise capacity of explosions, fires, equipment in explosion-proof construction, explosive materials, technological processes, the environment, as well as the development of solutions to improve the level of safety and health at work specific to industrial applications endangered by atmospheres explosives, generated by the presence of hydrogen, 2022-2026.

[11] PCDIEX – INSEMEX Explosives research / development and testing site, substances flammable / toxic, anti-explosive equipment and personnel training intervention for toxic / explosive environments – PCDIEx.

CFD SIMULATION OF CARBON MONOXIDE CIRCULATION DYNAMICS IN A VENTILATION INSTALLATIONS TUBING

PhD. Eng. Ion Gherghe

PhD. Eng. Florin Rădoi

PhD. Eng. Emeric Chiuzan

PhD. Eng. Nicolae Ianc

National Institute for Research and Development in Mine Safety and Protection to Explosion – INSEMEX Petrosani**, Romania**

ABSTRACT

Reducing the risk of occurrence of phenomena such as poisoning, as a result of the untimely penetration of a certain amount of toxic gases, inside a ventilation installation, is a priority, regarding the health and safety of workers, material assets and the negative influence on the environment, due to the possible problems caused by the occurrence of toxic atmospheres, formed by mixing air with toxic gases and vapors. In closed or semi-closed industrial and non-industrial buildings, effective ventilation is the primary measure to prevent toxic atmospheres. Knowing the behavior of toxic gases as well as their manner of dispersion is essential for preventing hazardous circumstances at the level of inadequately aired ventilation facilities, where toxic atmospheres might develop. For the study of the dynamics of carbon monoxide circulation inside the piping of an industrial ventilation installation under the influence of the air state parameters, the CFD technique was used with the help of the ANSYS MULTIPHISICS software package In order to carry out the simulation in a manner as close as possible to the experimental conditions, the topographic elevation of the ventilation installation was carried out within the experimental laboratory where the experiments were carried out in the laboratory, and the computer model was made The paper presents the CFD analysis regarding the influence of the state parameters on the dynamics of carbon dioxide flow inside the ventilation systems. Thus, the state parameters determined in the experimentation area and their introduction into CFD modeling are presented, respectively the establishment of the flow and dispersion model of carbon monoxide in ventilation ducts with high complexity, in the intake, transport and exhaust phases.

Keywords: CFD, dispersion, accumulation, exhaust, toxic gas, ventilation

INTRODUCTION

Specialized programs known as Computational Fluid Dynamics (CFD) techniques are utilized for simulating gas dispersion dynamics. The integrated tools within the CFD technique aim to replicate experimental tests using specific mathematical devices. Particularly in engineering, CFD has advanced to the point where "problems with complex geometries can be solved with simple physical models, and those with simple geometries can be solved with complex physical models" [1, 2]. To simulate the circulation dynamics and dispersion of carbon monoxide within the piping of a

https://doi.org/10.5593/sgem2024/1.1/s03.32

ventilation system, an "experimental system with variable structure for the study of complex industrial ventilation networks" was employed as a model. Ventilation systems, serving multiple enclosed spaces, are inherently complex. When variable concentrations of carbon monoxide unexpectedly occur in the suction area of the ventilation system, the flow pattern will be distinct, influenced by both the quantity of toxic gas and the parameters of the air state. Through CFD simulation, a virtual depiction of the intricate flow process is generated, highlighting areas within the piping with varying concentrations of carbon monoxide. The resulting insights can aid in determining preventive measures against toxic gas accumulation phenomena, and in identifying necessary measures to ensure worker safety.

CFD technique

For the study of toxic gas dispersion dynamics, the Computational Fluid Dynamics (CFD) technique was employed using the ANSYS MULTIPHISICS software package.
The ANSYS package enables parametric modeling and optimization of various problems, regardless of parameter type, finite element types used, analysis type, etc. It also allows the use of user-declared optimization algorithms. This package contains solvers dedicated to the analysis and resolution of various systems, including mechanical, thermal, and stability analysis for linear or nonlinear structural and thermal problems.
The software includes:
Structural and thermal solvers for structural and thermal problems, linear or nonlinear.
Entry-level thermal and structural analysis capabilities.
Fluid-structural and mechanical solvers for fluid dynamics, structural, and thermal analysis.
Multiphysics solvers for structural, thermal, electromagnetic (low and high frequency), and FLOTRAN analysis.
CFX or equivalent solver for fluid dynamics.
Solver for bidirectional fluid-structure interactions, involving multiphysics solvers and CFX-type solvers.
Fluent or equivalent solver for fluid dynamics.
Solver for NOx formation and combustion system consumption modeling.
Solver for drying and melting processes.
Magnetohydrodynamic module.
Multiphase flow module with particle distribution.
Solver for nonlinear solid, fluid, and gas dynamics, and their interactions (2D and 3D). [1, 2, 6, 10, 11]
ANSYS is widely used in industry and research for finite element analysis, aiming to simulate the response of multifysics

EXPERIMENTAL CONDITIONS

The experimental system with a variable structure for studying complex industrial ventilation networks consists of a centrifugal fan unit and a complex rectangular duct structure with dimensions of 300/400 mm. To ensure that the simulation closely reflects the experimental conditions, a topographic survey of the ventilation system in the experimental laboratory, where the experiments were conducted, was performed.

Additionally, a computerized model was created based on the laboratory setup. See figures 1-4. [3, 4, 8, 9]
In order to carry out the simulation in a manner as close as possible to the experimental conditions, the topographic elevation of the ventilation installation was carried out within the experimental laboratory, where the experiments were carried out in the laboratory, and the computer model was made, fig. 1-4. [5, 7, 8, 11]

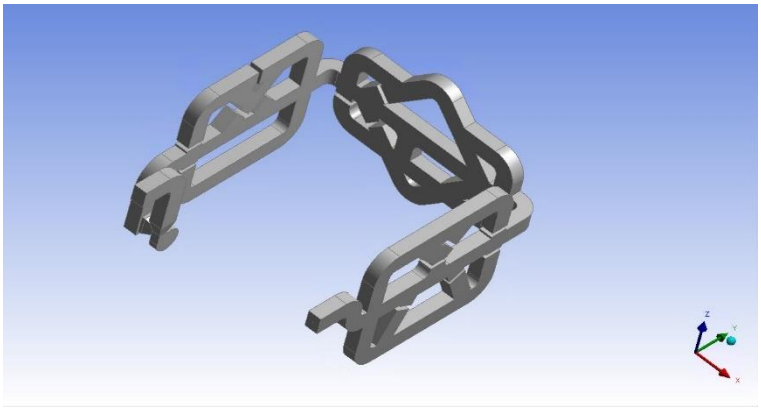


Fig. 1 Modeling of the ventilation system in a 3D environment

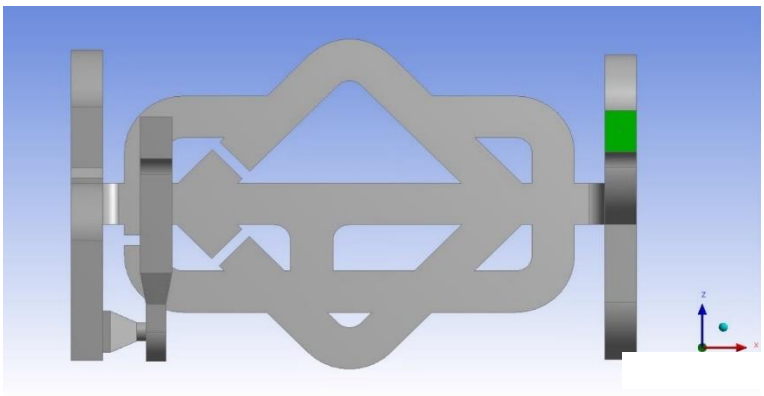


Fig. 2 Modeling of the ventilation system in a 2D environment with focus on the suction area

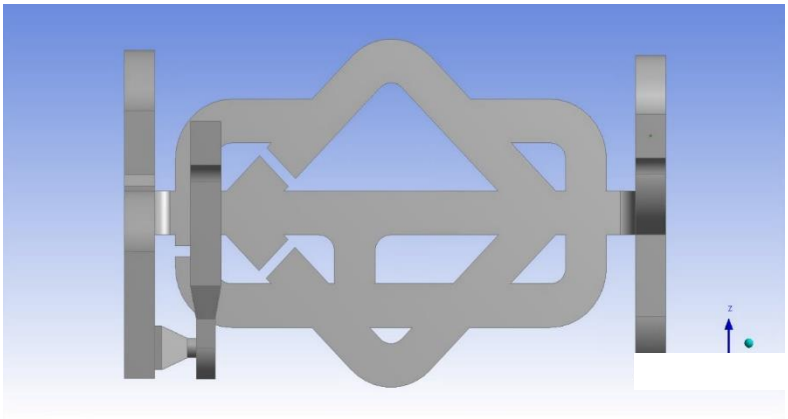


Fig. 3 Modeling of the ventilation system in a 2D environment with focus on the routing path.

https://doi.org/10.5593/sgem2024/1.1/s03.32

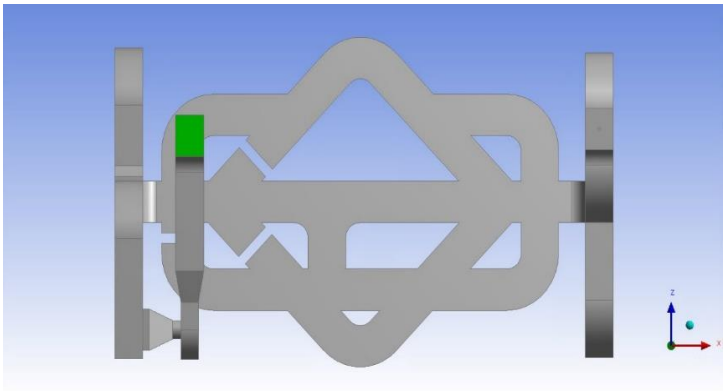


Fig. 4 Modeling the ventilation system in a 2D setup with focus on the exhaust area.

MODELING OF CARBON MONOXIDE DISPERSION INSIDE THE VENTILATION INSTALLATION

For modeling, the following aspects were established: The introduced carbon monoxide has a concentration of 9998 ppm; Gas introduction occurs at the level of the suction mouth; Carbon monoxide discharge is done through a hose with an inner diameter of 8 mm; The gas flow rate discharged into the ventilation duct is 25 l/min; The carbon monoxide dispersion phenomenon occurs at constant pressure; Atmospheric pressure, temperature, and humidity are typical for the experimental site; The simulation time is set at 5 minutes; The carbon monoxide concentration is 1000 ppm. Following the modeling of carbon monoxide dispersion inside the ventilation duct, the results of gas concentration in the right lateral chain, frontal area, left lateral chain, and evacuation area were obtained, as presented in Table 1.

Table no. 1 Carbon monoxide concentration results

Concentration modeling results CO/time									
Time (s)	CO (mol/mol)	Time (s)	CO (mol/mol)	Time (s)	CO (mol/mol)	Time (s)	CO (mol/mol)	Time (s)	CO (mol/mol)
0	0	60	0,000202732	120	0,00020287	180	0,000202903	240	0,000202921
0,04	2,52642E-13	60,04	0,000202731	120,04	0,000202869	180,04	0,000202902	240,04	0,00020292
0,08	1,00785E-10	60,08	0,00020273	120,08	0,000202868	180,08	0,000202902	240,08	0,00020292
0,12	2,27976E-10	60,12	0,00020273	120,12	0,000202868	180,12	0,000202901	240,12	0,00020292
0,16	1,01322E-09	60,16	0,000202729	120,16	0,000202868	180,16	0,000202901	240,16	0,00020292
0,2	2,8309E-09	60,2	0,000202729	120,2	0,000202868	180,2	0,000202902	240,2	0,00020292
0,24	9,15212E-09	60,24	0,000202729	120,24	0,000202868	180,24	0,000202902	240,24	0,000202921
0,28	3,86315E-08	60,28	0,00020273	120,28	0,000202868	180,28	0,000202903	240,28	0,000202922
0,32	1,33936E-07	60,32	0,00020273	120,32	0,000202869	180,32	0,000202904	240,32	0,000202922
…	……..	…..	……	…..	……..	…..	……..	…..	…….
59,52	0,000202725	119,52	0,000202868	179,52	0,000202903	239,52	0,000202922	299,52	0,000202931
59,56	0,000202726	119,56	0,000202869	179,56	0,000202904	239,56	0,000202923	299,56	0,000202932
59,6	0,000202727	119,6	0,00020287	179,6	0,000202905	239,6	0,000202924	299,6	0,000202933
59,64	0,000202729	119,64	0,000202871	179,64	0,000202906	239,64	0,000202925	299,64	0,000202934
59,68	0,00020273	119,68	0,000202872	179,68	0,000202907	239,68	0,000202925	299,68	0,000202934
59,72	0,000202731	119,72	0,000202873	179,72	0,000202907	239,72	0,000202926	299,72	0,000202934
59,76	0,000202732	119,76	0,000202873	179,76	0,000202907	239,76	0,000202925	299,76	0,000202934
59,8	0,000202732	119,8	0,000202873	179,8	0,000202907	239,8	0,000202925	299,8	0,000202933
59,84	0,000202733	119,84	0,000202873	179,84	0,000202906	239,84	0,000202924	299,84	0,000202932
59,88	0,000202733	119,88	0,000202872	179,88	0,000202906	239,88	0,000202924	299,88	0,000202931
59,92	0,000202733	119,92	0,000202872	179,92	0,000202905	239,92	0,000202923	299,92	0,00020293
59,96	0,000202732	119,96	0,000202871	179,96	0,000202904	239,96	0,000202922	299,96	0,000202929

For the dispersion of carbon monoxide inside the ventilation duct, the diagram showing the variation of carbon monoxide concentration was obtained, fig. 5.

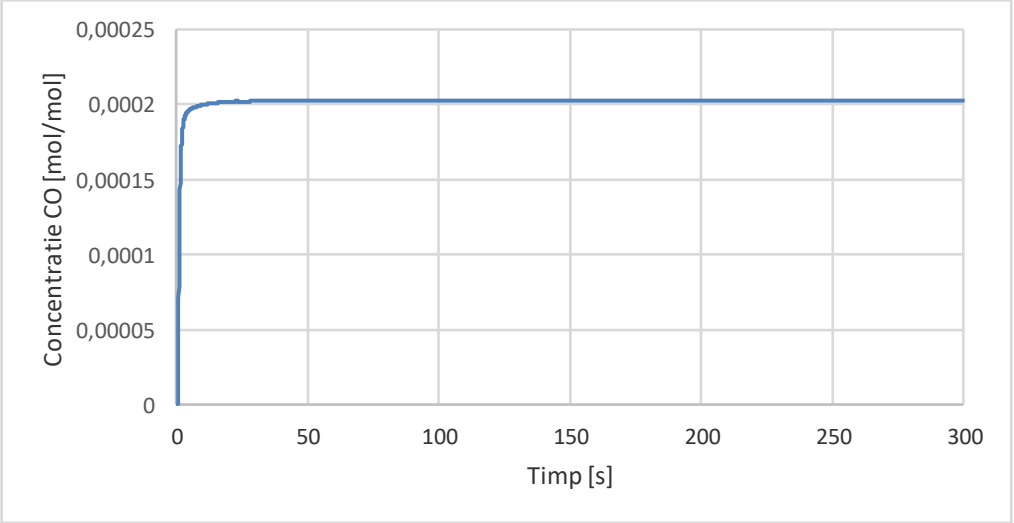


Fig. 5 The variation of carbon monoxide dispersion in the ventilation duct.

The result of computer modeling for a simulation time of 5 minutes is presented graphically in figures 6-9.

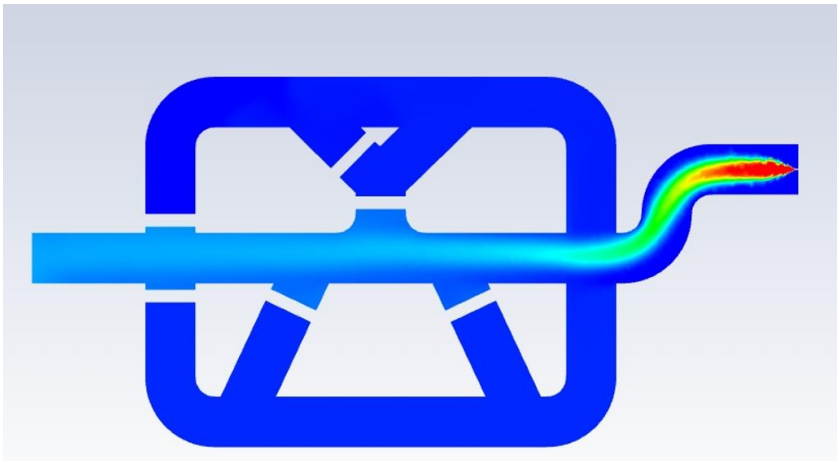


Fig. 6. The simulation of carbon monoxide dispersion in the right lateral chain ventilation duct.

https://doi.org/10.5593/sgem2024/1.1/s03.32

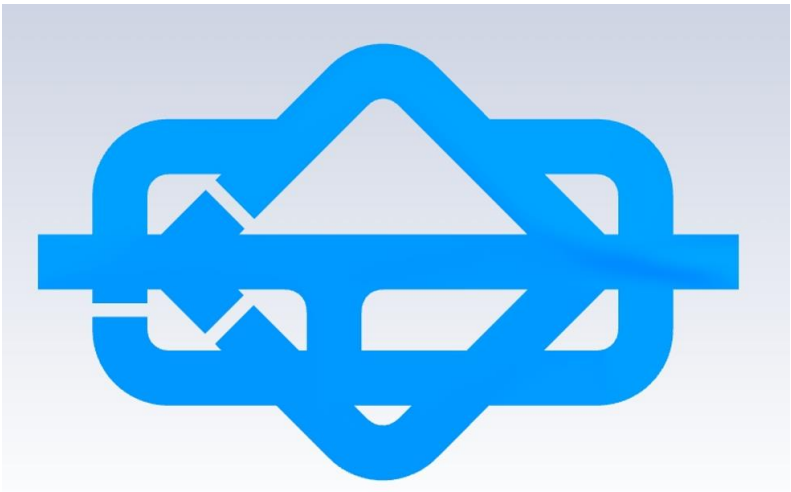


Fig. 7. The simulation of carbon monoxide dispersion in the ventilation duct, frontal area.

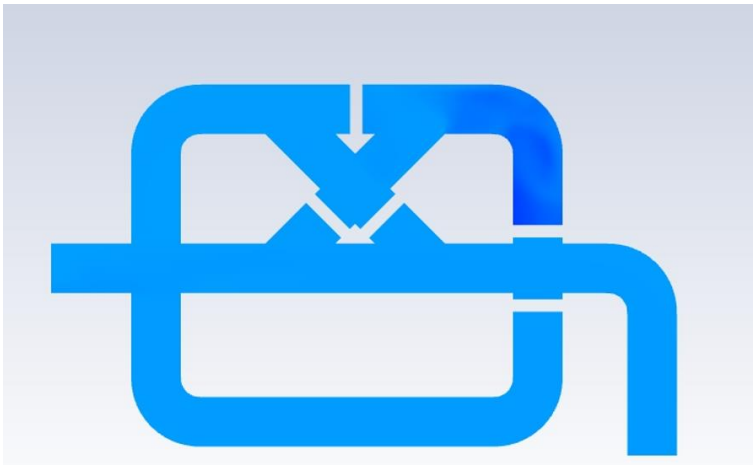


Fig. 8. Simulating the dispersion of carbon monoxide in the ventilation duct, left lateral chain.



Fig. 9. Simulating the dispersion of carbon monoxide in the ventilation duct, evacuation area.

DISCUTIONS

From the modeling regarding the variation of air state parameters inside industrial ventilation facilities using carbon monoxide (CO), the following conclusions can be drawn:

- The dispersion process at the level of the industrial ventilation facility's right lateral chain is characterized by a variable evolution. Thus, a variation in carbon monoxide concentrations was observed along the flow direction. Additionally, a preferential flow was noted in the median zone, while the upper and lower parts of the right lateral chain showed insignificant carbon monoxide concentrations.
- The dispersion process at the level of the industrial ventilation facility's frontal area is characterized by a variable evolution. It was observed that carbon monoxide concentrations vary across the entire structure of the frontal area. Furthermore, there is an equalization of carbon monoxide concentrations across all branches of the frontal area.
- The dispersion process at the level of the industrial ventilation facility's left lateral chain is characterized by a variable evolution. Carbon monoxide concentrations vary across the entire structure of the left lateral chain. Additionally, there is an equalization of carbon monoxide concentrations, at a high level, across all branches of the left lateral chain except for the upper anterior zone where the carbon monoxide concentration is insignificant.
- The dispersion process at the level of the industrial ventilation facility's evacuation area is characterized by a constant evolution. A uniform concentration of carbon monoxide was observed along the flow direction, at a high level.

CONCLUSIONS

This work has allowed for the following findings to be highlighted:

1. Inside a ventilation system, the air flow velocity must be sufficiently strong to entrain and direct toxic particles and gases such as carbon monoxide towards the intake mouth, while also ensuring their continuous transport towards the exhaust mouth.
2. Internationally, computational fluid dynamics (CFD) is used as a leading tool in research.
3. CFD technique using ANSYS MULTIPHISICS software was employed for studying the influence of air state parameters on toxic atmospheres.
4. The dispersion process of carbon monoxide exhibits variable behavior.
5. From the modeling regarding the variation of air state parameters inside industrial ventilation systems using carbon monoxide (CO), the concentration of carbon monoxide asymptotically tends towards the value of 205 ppm after 20 seconds of modeling.
6. The carbon monoxide dispersion process within the ventilation system was controlled in four zones:

- The right lateral chain of the industrial ventilation system, including the intake mouth.
- The frontal area of the industrial ventilation system.
- The left lateral chain of the industrial ventilation system.
- The exhaust area of the industrial ventilation system.

7. Modeling the variation of air state parameters inside industrial ventilation systems using carbon monoxide (CO) revealed a dispersion phenomenon oriented in the direction of gas flow. The flow of carbon monoxide is characterized by a constant vehicular motion at higher concentrations across all chains of the ventilation system.

8. The concentration of carbon monoxide is highest in the intake area, gradually decreasing through dilution as it moves away from the source, and becomes constant at the level of the ventilation system's chains, including the exhaust area.

ACKNOWLEDGEMENTS
This paper was developed within the Program PN EXH2 and IOSIN PCDIEX Program, carried out with the support of MCID.

BIBLIOGRAPHY

[1] H. Goodfellow, E. Tahti, Industrial Ventilation, Desing Guidebook, *Academic Press, 2001*.

[2] **Munier, L.**, Simulations experimentale et numerique des effets retardes d'une explosion en milieu clos et en presence de produits liquides, Universite de Provence – Aix Marseille I, Institut Universitaire des Systèmes Thermiques Industriels, *Thèse pour obtenir le grade de Docteur, 2011*.

[3] **Alexandru Cristea, et al**., Ventilation and air conditioning, I, *Technical Publishing House, Bucharest, 1968*.

[4] **Bancea O.,** Industrial ventilation systems, *Editura Politehnică, Timișoara,* 2009; pp14-19, pp 122-137.

[5] I. **Matei, R. Moraru, M. Samoilă, G. Băbuț,** Environmental engineering and underground ventilation, *Technical Publishing House, Bucharest, 2000*

[6] **W. A. Burgess, M. J. Ellenbecker, R. D. Treitman**, Ventilation for control of the work environment - second edition, *Copyright © 2004 John Wiley & Sons, Inc.*

http://healthf.kaums.ac.ir/UploadedFiles/jozveh/motalebi/ VENTILATIONFORCONTROLOFTHEWORKENVIRONMENT.pdf [Accessed 22 September 2016

[7] **D. Cioclea, C. Lupu, I. Gherghe,** Guid for sizing industrial ventilation installations, *Publishing House INSEMEX, 2013*

[8] **I. Gherghe, D. Cioclea,** Methodology for measuring air flow velocity in ducts, *INCD INSEMEX Petroșani, 2018*

[9] **N. Niculescu, Gh. Duță, P. Stoenescu, I. Colda**, Instalații de ventilare și climatizare, *E.D.P., București, 1982*

[10] **W.L. Le Roux,** Mine ventilation notes for beginners, *Published the mine ventilation society of South Africa – Printed by CTP Printers (Transvaal) Limited – 2nd Edition 1972*

[11] **J. H. J. Burrows, R. Hemp, F. H. Lancaster, J. H. Quilliam,** The ventilation of South African Gold Mines, *Printed by Cape& Transvaal Printers Ltd, Cape Town, 1974*

COMPUTERISED RISK ASSESSMENT FOR STORAGE OF PYROTECHNIC ARTICLES

PhD. Eng. Cristian Rădeanu[1]

Eng. Miron Claudia[1]

PhD. Eng. Vasilescu Gabriel[1]

PhD. Ress. Eng. Pintilie Dan[2]

PhD. Eng. Popescu Claudius[2]

[1] National Institute for Research and Development in Mine Safety and Protection to Explosion – INSEMEX Petrosani, **Romania**
[2] University of Petrosani, Doctoral School, **Romania**

ABSTRACT

Safety protection against detonation due to accidental initiation of stored fireworks is of particular interest for safety because such detonations endanger the life and health of workers as a result of the uncontrollable effects of deflagration and pressure, the presence of toxic reaction products and the consumption of oxygen in ambient air which workers must breathe. At the same time, it should be borne in mind that material losses caused by explosions can be particularly high.

The existence of the danger of accidental initiation / detonation of stored pyrotechnic articles determines imperatively the establishment of causes and possibilities that can generate the initiation / detonation of these pyrotechnic products for all components of the work system (work environment performer, work equipment and work load). In addition, the organisational aspects of explosion protection must be adapted to the technical problems specific to each workplace so that no weak points arise in explosion protection areas.

In accordance with the specifications in the technical documentation on the activity carried out at the level of an authorized pyrotechnic articles warehouse, the employer is responsible for the safety of the personnel employed. All persons involved must be informed of clearly defined procedures for operation and emergencies, and appropriate training must be provided for employees. It is also necessary that the work instructions and occupational health and safety, as well as the measures provided for in the internal regulations, be included in the specialized trainings, following the quality of the attributes, as well as the way of complying with them during the performance of specific activities and operations with pyrotechnic articles within each process stage, respectively transport, supply, reception and storage.

On the basis of the above, the scientific article will document the results of the computerised risk assessment (drawing of risk/overpressure curves and contour maps on the design of detonation fragments) generated by specific operations with fireworks in their storage.

Keywords: pyrotechnic articles, storage of pyrotechnic articles, safety and health at work, computerized risk assessment, deflagration and detonation effects.

1. INTRODUCTION

The existence of the danger of accidental initiation/detonation of stored pyrotechnic articles makes it imperative to establish the causes and possibilities that may generate the initiation/detonation of these pyrotechnic products for all components of the work system (work environment, work equipment and workload) existing at the legally authorised warehouse located on the site of the economic operator.

In accordance with the specifications in the technical documentation on the work carried out at the level of the authorised pyrotechnic article warehouse, the employer is responsible for the safety of the personnel employed. The responsibility for the safety of specific operations with pyrotechnic articles also lies with the employees during their involvement in the current actions carried out on the site of the authorised warehouse during the execution of operations with pyrotechnic articles at each stage of the process, i.e. transport, supply, reception and storage [1-3].

2. MATERIALS AND METHODS

2.1 The main risk scenarios that may lead to unwanted events resulting in fire and/or explosion due to the inadvertent/accidental initiation of pyrotechnic articles stored in an authorised warehouse

- Triggering of a pyrotechnic device (consisting of a pyrotechnic article, fast-burning fuse, electric igniter) during operations carried out for the preparation of firing tube rasters for bombs of various calibres, by mechanical actions of exposing the primer (consisting of the fast-burning fuse of the bombs and the electric igniter) carried out in the warehouse, through exposure to impact and friction stimuli as a result of inadequate work operations (accidental dropping of a work tool, i.e. inadequate handling of the raster with firing tubes (mortars) loaded with bombs of different calibres);

- Triggering of a pyrotechnic device (consisting of a pyrotechnic article, fast-burning fuse, electric igniter intended for the initiation of pyrotechnic articles) during the performance of operations carried out for the preparation of rasters with firing tubes for bombs, caused by the initiation of the primer (consisting of the fast-burning fuse of the bombs and the electric igniter) following the triggering of the electric igniter by a spark-type capacitive electrostatic discharge;

- Triggering of a pyrotechnic device (consisting of a pyrotechnic article, fast-burning fuse, electric igniter intended for the initiation of pyrotechnic articles) caused by initiation of the primer (triggering of the electric igniter when using mobile telephone means in its vicinity) by the electromagnetic effect generated by radio frequency waves;

- Triggering of an electrical source with ignition of the insulation of electrical equipment in the room;

- Exothermic reactions with chemical substances (concentrated acidic or basic substances) which may induce ignition of explosive materials such as pyrotechnic articles and other combustible materials;

- Improper use of open fire (smoking, welding/hot welding operations);

- Initiation of the pyrotechnic article/device by natural causes;

- ARSON effect (arson as an act of malice) [4 – 8].

2.2 Computerised explosion risk assessment specific to industrial sites for the storage of pyrotechnic articles

To solve the event scenarios, the specialised American software application IMESAFR v2 Bundle was used (see Fig. 1), which allows a probabilistic assessment of the risk situations generated by the detonation of explosive charges of different types, based on the results of the graphical-analytical quantification of the associated specific hazards, in order to determine the corresponding safety level or degree of insecurity [11].

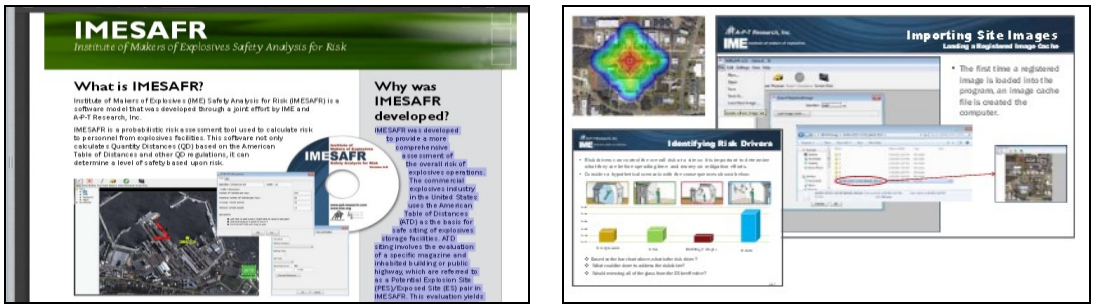


Fig. 1-Specialized software application type IMESAFR V2 Bundle

The use of the IMESAFR specialised software application is based on the QRA (Quantitative Risk Assessment) model for estimating the annual probability of fatality, property damage, as well as the resulting major and minor injuries, and involves going through the 6 logically ordered steps in the running architecture of the specialised software, respectively:

E1: Event scenario definition; Event and exposure analysis; It also includes user inputs describing the PES (Potential Explosion Site) scenario in relation to ES (Exposure Site), Net Explosive Quantities (NEW) existing; Explosion probability calculation Pe taking into account human exposure;

E2:-Dynamic wave overpressure. Calculate the value of pressure and major and minor fatality/trauma mechanisms based on the impact pulse;

E3:-Structural response of the exposed site. Calculates the magnitude of building collapse mechanisms and broken windows, fatality/bulk building damage accidents;

E4:-Debris (material resulting from the blast and the resulting fragment design). Calculate the magnitude of hazardous debris mechanisms, major and minor fatality/injury accidents;

E5:-Radiation and heat flow. Calculates the magnitude of the thermal fatality mechanism, only for event scenarios that are configured based on the use of explosive materials with Hazard Division 1.3 according to the Orange Book;

E6:-Determine and quantify the final results through analytical mechanisms of synergistic composition, aggregation and summation. Compose the total magnitude of all fatality mechanisms, calculate and resolve risk situations, and assess overall uncertainty.

The configuration of these accident scenarios is carried out by entering specific data and information, both for the hazardous structure type PES (intended for the temporary storage of pyrotechnic articles/pyrotechnic devices - authorised storage) and for the exposure structure type ES (intended for carrying out specific operations with pyrotechnic devices), in order to carry out a computerised assessment of the risk of accidental initiation/detonation of pyrotechnic articles/pyrotechnic devices and the specific effects generated [9 -11].

https://doi.org/10.5593/sgem2024/1.1/s03.33

2.3 Computer simulation of accident scenarios that may occur at an authorised warehouse site

For computer simulation of accident scenarios caused by accidental initiation/detonation of pyrotechnic articles/devices due to their exposure to a hazardous external stimulus: stray currents, electrostatic charge/electrical discharge, high temperature, mechanical shock, manifested in the pyrotechnic articles/devices test/unloading area, various quantities of explosive substances expressed in ETNT (trinitrotoluene equivalent) were used, located in different working areas at or near the authorized pyrotechnic articles warehouse in the loading/unloading ramp area, respectively on the car transport access route within the industrial site (see. Fig. 2).

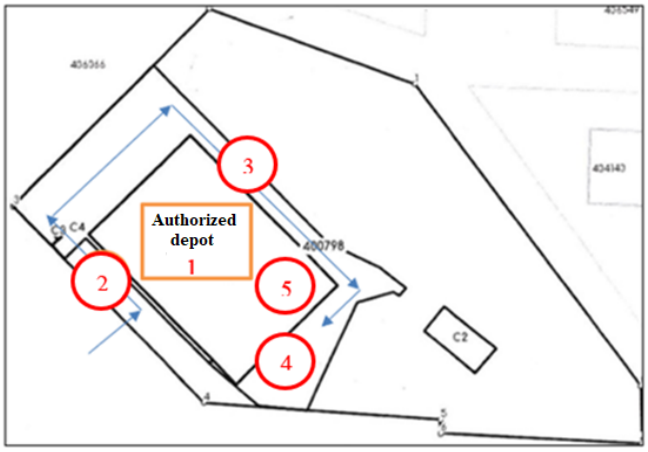


Fig. 2 - Sketch of the location of the authorised pyrotechnic articles depot with highlighting of vulnerable areas

1-Area of the point of unloading-receiving pyrotechnic articles from means of transport (TIR); 2-Area of the transport route with means of transport (utility vehicles) intended for the introduction of pyrotechnic articles into the warehouse or the marketing of the quantities stored; 3-Area of the ramp for the introduction/removal of pyrotechnic articles from the warehouse; 4-Area intended for pyrotechnic operations

Taking into account the plausible scenarios of accidental initiation/detonation of stored pyrotechnic articles mentioned above in section 2.1 of the paper, the following presents the main event scenarios that have been established at the level of specific activities and operations carried out on the site of the authorized warehouse, determining the safety distances for each case using the specialized software IMESAFER V2 of American origin, respectively:

a.-Accident scenario occurring in the storage area of pyrotechnic articles/ devices (40 kg ETNT) within the authorised warehouse located above ground;

b.-Accident scenario in the area of the point of unloading/receipt of pyrotechnic articles from TIR means of transport (2 kg ETNT);

c.-Accident scenario occurring on the predefined transport route to the area of test-unloading of pyrotechnic articles in the warehouse by means of a truck (0.5 kg ETNT);

d.-Accident scenario occurring in the area of the loading/unloading point for pyrotechnic articles in the warehouse (0.25 kg ETNT);

e.-Accident scenario in the area of the specific operations point for the preparation of pyrotechnic articles for fireworks (0.002 kg ETNT).

The following is the computer simulation of the scenario a) Accident scenario in the storage area of pyrotechnic articles/devices (40 kg ETNT) in the authorised warehouse located above ground (see Fig. 3).



Fig. 3-Situation plan of the site showing the assessed area (the space inside the authorised pyrotechnic articles depot)

Enter data and information specific to the hazardous structure type PES 1 (see Fig. 4)

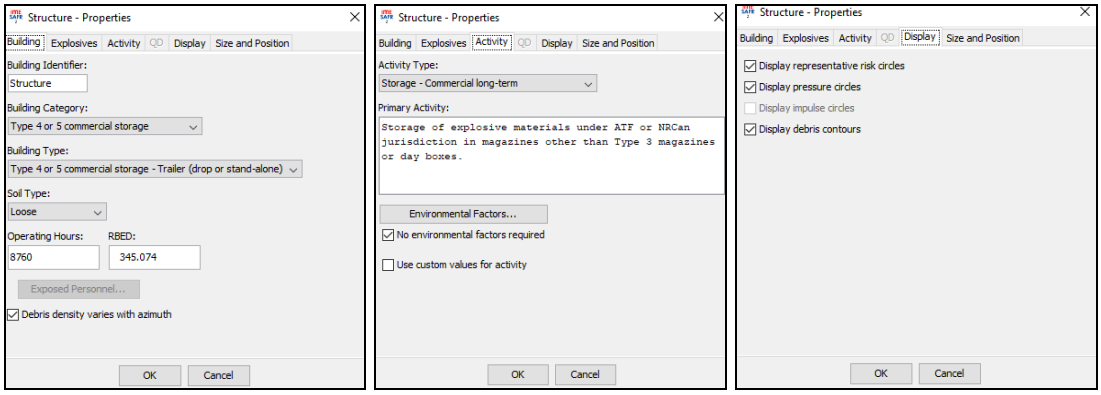


Fig. 4-File sheets with data and information on structure and dangerous substance

The following results are obtained with the specialised software (see Fig. 5 - 8)

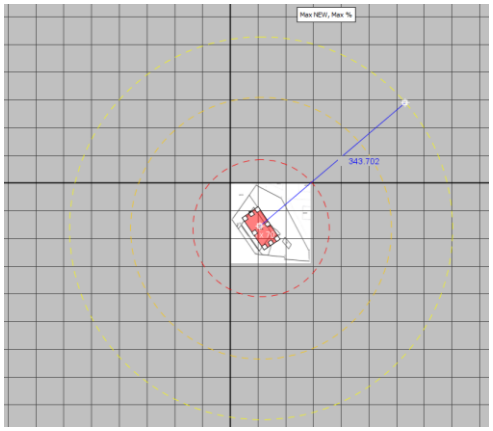


Fig.5- Highlighting the risk curve corresponding to 10^{-8} [deaths/year]

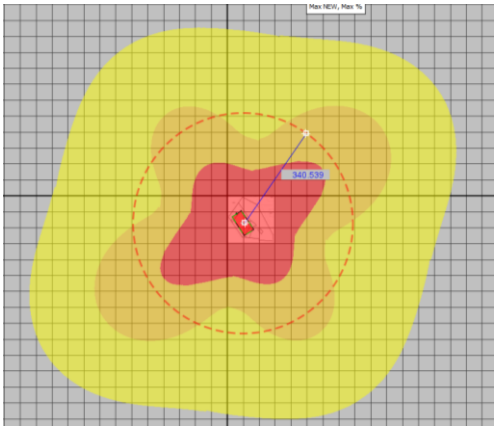


Fig 6- Risk-Based Evaluation Distance (RBED) curve highlighting based on distance evaluation (340.539 m)

https://doi.org/10.5593/sgem2024/1.1/s03.33

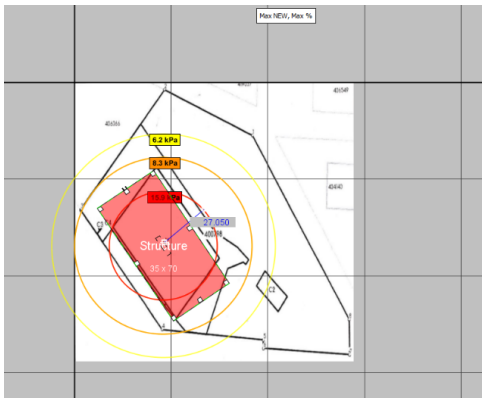


Fig.7 - Overpressure curve for 2.3 psi (15.9 kPa)

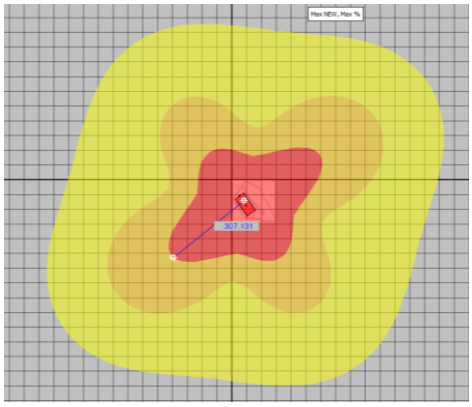


Fig. 8 - Contour map showing the lethal zone (red area) with a maximum distance from the epicentre of 307.131 m

3. RESULTS

The results of the computerised risk assessment of the accidental initiation/detonation of pyrotechnic articles intended for storage in the authorised warehouse are shown in Table 1:

Table 1 - Centralisation of risk assessment results

Scenario	Shaped hazard	Danger zone (area "circular" expressed by radius R)		
		Zone I Mortality (m)	**Zone II Irreversible injuries (m)**	**Zona III Reversible injuries (m)**
		Destruction buildings		
		Total and severe destruction of buildings	**Average building damage**	**Insignificant destruction Broken windows**
		Health damage		
		Very severe and severe trauma	**Medium trauma**	**Mild trauma**
I. Accident scenario occurring in the storage area of pyrotechnic articles/pyrotechnic devices (40 kg ETNT) within the authorized warehouse located above ground (PES 1)	Explosion overpressure	27,050 (15,9 kPa)	44,765 (8,3 kPa)	57,138 (6,2 kPa)
	Risk accident	128,555 (10^{-6} deaths/year)	233,755 (10^{-7} deaths/year)	343,702 (10^{-8} deaths/year)
	Projection of fragments resulting from the detonation of pyrotechnic articles/devices	307,131	516,472	739,158
II. Accident scenario occurring in the area of the point of unloading and receipt of pyrotechnic articles from means of transport type TIR (2 kg ETNT) (PES 2)	Explosion overpressure	9,918 (15,9 kPa)	16,372 (8,3 kPa)	20,172 (6,2 kPa)
	Risk accident	2,286 (10^{-6} deaths/year)	3,481 (10^{-7} deaths/year)	4,635 (10^{-8} deaths/year)
	Projection of fragments resulting from the detonation of pyrotechnic articles/devices	128,570	301,176	442,921

III. Accident scenario manifested on the predefined transport route to the pyrotechnic articles loading-uploading area in the warehouse with a van (0,5 kg ETNT). **(PES 3)**	Explosion overpressure	7,791 (15,9 kPa)	12,720 (8,3 kPa)	15,912 (6,2 kPa)
	Risk accident	2,286 (10^{-6} deaths/year)	2,477 (10^{-7} deaths/year)	3,739 (10^{-8} deaths/year)
	Projection of fragments resulting from the detonation of pyrotechnic articles/devices	3,627	93,055	290,844
IV. Accident scenario manifested in the area of the pyrotechnic articles loading/uploading point in the warehouse (0,25 kg ETNT). **(PES 4)**	Explosion overpressure	5,861 (15,9 kPa)	9,647 (8,3 kPa)	12,652 (6,2 kPa)
	Risk accident	1,091 (10^{-6} deaths/year)	1,724 (10^{-7} deaths/year)	2,876 (10^{-8} deaths/year)
	Projection of fragments resulting from the detonation of pyrotechnic articles/devices	3,166	3,423	5,406
V. Accident scenario occurring in the area of the point where specific operations are carried out for the preparation of pyrotechnic articles for fireworks (0,002 kg ETNT). **(PES 5)**	Explosion overpressure	1,264 (15,9 kPa)	2,074 (8,3 kPa)	2,620 (6,2 kPa)
	Risk * accident	0,347 (10^{-6} deaths/year)	0,489 (10^{-7} deaths/year)	0,646 (10^{-7} deaths/year)
	Projection of fragments resulting from the detonation of pyrotechnic articles/devices	0,129	0,364	0,840

* *Note: -$Pf_{acceptable}$=3.0x10-5 (for workers servicing PES structures)*
-$Pf_{acceptable}$=3.0x10-6 (for visitors)
-$Ef_{acceptable}$=3.0x10-4 (for workers serving PES-type facilities)
-$Ef_{acceptable}$=3,0x10-5 (for visitors)

DISSCUSIONS

The analysis of the 5 scenarios showed that the accidental initiation/detonation of pyrotechnic devices can result either in their ignition with a local burning effect or in specific explosion effects developed at different distances from the epicentre of the event, with the generation of flame, noise, smoke, gas, dynamic effects and projected particles/voltages.

4. CONCLUSIONS

Detonation protection due to accidental initiation is of particular safety concern because such detonations can endanger the life and health of workers, both as a result of the

uncontrollable effects of deflagration and dynamic pressure, and the presence of toxic reaction products in the working atmosphere of persons carrying out specific activities and operations with these types of products.

In accordance with the internal regulations and the specifications in the technical documentation of the authorised warehouse for pyrotechnic articles, the employer is responsible for the safety of the workers. The responsibility for ensuring the safety of specific operations also rests to the same extent with the employees throughout their involvement in the work process.

The risk assessment of the storage of pyrotechnic articles in the authorised pyrotechnic article / pyrotechnic device store as a result of accidental initiation / detonation of these types of products was carried out on the basis of the configuration of plausible risk scenarios taking into account the technical factors of their exposure to dangerous external stimuli (stray currents, electric discharge, high temperature, impact, friction, exposure to open flame).

In order to prevent and combat the risks of accidental initiation/detonation of pyrotechnic articles/devices identified and analysed at the level of the specific activities carried out in authorised warehouses, prevention and protection measures of a technical and organisational nature may be established with the aim of eliminating/reducing the effects produced in the event of undesirable events.

ACKNOWLEDGEMENTS

This work was developed within the Core Program, carried out with the support of the Romanian Ministry of Education and Research, project no. PN-19-21-02-02 “Development of the technical and methodological infrastructure for testing and evaluation of specific safety parameters of civil explosives and pyrotechnic articles”.

REFERENCES

[1] Law 126/1995 on the regime of explosive materials, as amended and supplemented;

[2] "Technical Norms - to Law 126/1995 as amended and supplemented;

[3] Law 319/2006 on health and safety at work;

[4] Ciprian Jitea, Attila Kovacs, Emilian Ghicioi, Edward Gheorghiosu, Florea Dinu ” *Research on the local effects of the detonation of improvised explosive devices on the steel building frames* ” International Multidisciplinary Scientific GeoConference : SGEM; Sofia, Vol. 23, Iss. 1.1, (2023). DOI:10.5593/sgem2023/l.l/s03.49

[5] Jitea C., Kovacs A., Vasilescu G., Gheorghiosu E., Rus D., Bordos S., *Prospective analysis of ambiental and weather effects on conform displaying of fireworks,* 8th International Conference On Manufacturing Science And Education (MSE 2017) - Book Series: MATEC Web of Conferences Volume: 121, Article Number: UNSP 11011, DOI: 10.1051/matecconf/ 201712111011, Published: 2017, WOS: 000435283800130;

[6] Darabont, D.-C., Moraru, R. I., Antonov, A. E., & Bejinariu, C. (2017). *Managing new and emerging risks in the context of ISO 45001 standard*. Quality-Access to Success, **18**, 11–14;

[7] S. Mannan, *Lees, Loss Prevention în the Process Industries. Hazard Identification, Assessment and Control*, Elsevier, Third Edition, Oxford, 2005;

[8] American Institute of Chemical Engineers AIChE. (2000). *Guidelines for Chemical Process Quantitative Risk Analysis*, 2nd Edition (Second Edition). New York;

[9] Aven, T. (2008). *Risk Analysis: Assessing Uncertainties Beyond Expected Values and Probabilities*. Wiley, Marea Britanie, 2008;

[10] Austrian Permanent Seveso Working Group, *Calculation of appropriate distances for the purposes of Land Use Planning, Emergency Planning and Domino Effects;*

[11] Ross, T., Tatom, J., & et al. (2015). IMESAFR Version 2.0, *Safety Assessment for Risk. Technical Manual.* A-P-T Research Inc, USA: Institute of Makers of Explosives

DEVELOPING THE PRACTICAL SKILLS OF RESCUERS FOR INTERVENTIONS IN HIGH TEMPERATURE AREAS

Phd. Eng. Daniel Pupăzan

Phd. Eng. Andrei Lucian Gireadă

Phd. Eng. George Artur Găman

Phd. Eng. Cosmin Ilie

Phd. Eng. Cristian Nicolescu

National Institute for Research and Development in Mine Safety and Protection to Explosion, **Romania**

ABSTRACT

In the case of dangerous incidents produced in industrial technological processes, where hydrogen is used, their mastery requires, in addition to a personnel servicing the facilities properly trained for such situations, the participation of professional staff for interventions in dangerous environments.

The activity of intervention and rescue in special conditions, in potentially explosive areas due to the appearance of hydrogen can be carried out exclusively by specialized personnel trained and authorized in this regard, personnel using individual breathing protection devices.

The critical factor for ensuring the success of an rescue intervention in aggressive toxic or chemical environments consists in the efficient and optimal training process for rescue personnel, in correlation with their testing in environments with high temperatures.

Intervention and rescue operations can be physically and psychologically challenging and require rescue personnel to operate in undesirable conditions, such as potentially toxic/flammable/explosive environments. Personnel involved in intervention and rescue operations may encounter contaminated air environments and are required to wear respiratory protective equipment in order to safely perform rescue operations.

Air temperature and humidity are likely to be high following fires and explosions. Therefore, members of the response and rescue teams face high temperature environments during rescue operations.

Keywords: intervention and rescue personnel, high temperature, breathing apparatus, training facility.

INTRODUCTION

The performer of direct and dangerous heavy work to save people and protect industrial objectives is the operative intervention and rescue personnel, who uses protective breathing apparatus. The success of the rescue operation primarily depends on how they will act, on them courage and trust in the insulating device that protects them.

Upon receiving the order to go into action, the morale of the rescuers is different, depending on each individual and the situation. If the damaged area is not extensive and

https://doi.org/10.5593/sgem2024/1.1/s03.34

there are no victims, the rescuers' morale is relatively high and they act calmly. However, if the situation in the area is not clear, the damage is extensive and there are victims, the rescuers are restless, nervous and an internal impulse predisposes them to haste and hasty actions [1].

Researching the damaged area is an operation of great responsibility, because the drawing up of the damage liquidation plan depends on it, and also on this occasion the survivors are searched for. Acting in conditions of large-scale damage is difficult because it takes place in unknown conditions, full of risks. The rescue teams are threatened by numerous dangers, the research is sometimes done in high temperature conditions, in a toxic environment. At this stage, the rescuers' tasks are multiple and difficult, because the intervention in this phase is full of unknowns. The unexpected can appear at any time, demanding increased efforts, concentration, devotion, physical resistance and a lot of courage from the rescuers.

EXPERIMENTAL

The air temperature is likely to be high following fires and explosions. Therefore, members of the response and rescue teams face high temperature environments during rescue operations, such as when entering burning buildings, when searching for survivors, when extinguishing fires, when building dikes and when restoring ventilation circuits affected by fires or explosions [2].

The Heat is generated normally as a result of metabolic processes taking place in the body of rescuers. As a result of muscle activity when there are performed working or training activities, there is released a considerable amount of heat.

The body temperature control is essential, and inability to maintain balance between cooling and overheating can lead to illness and even death. The temperature control is performed by an area of the brain known as the hypothalamus, which is responsive for the sensors in the body.

The heat exchange takes place through the skin, which can be described as a housing. The deepest tissues are into body cavities (chest, skull and abdomen), being known as central tissues. The hypothalamus regulates the temperature and is trying to keep the central tissue temperature in a narrow range. If their temperature gets too high, then there may occur due to high temperatures the induced illness or even death [3].

Factors to be considered for working in high temperatures of the rescue personnel:

- External factors: air temperature, relative humidity, temperature of surrounding objects (with radiant heat), skin temperature, air movement, type and amount of worn clothes, exposure time, load with work equipment, equipment weight, the type of breathing apparatus, confined spaces, availability of water for drinking or wetting skin;
- Human factors: age, degree of muscle activity, health state, physical work capacity, physical condition, the inherent ability to work in heat, experience, personality;
- Specific factors of health: dehydration, obesity, fever associated with diseases or vaccinations, vomiting and diarrhoea, diabetes, heart disease, medications, recent difficult exercises, history of disorders related to high temperature, disease, conditions which prevent sweat, work recently under high temperature.

Body temperature balancing is achieved by means of blood circulation and because the thermal conductivity of the tissues. This is done by thermal stability of relative thermoregulation process and is controlled by the nervous system at its different levels.

In the framework of accommodating body to the microclimate variations of the environment through thermoregulatory function, there is a zone in which thermal comfort or thermal neutrality is obtained by effortless thermoregulation [4].

The limits of thermal comfort vary with the effort which increases heat production, and clothing, which makes the possibility of removing it. On both sides of the thermal neutral zone, the body must fight the heat in the environment in order to be able to maintain normal temperature. Adjustment possibilities of the body in these circumstances are limited, but the body limits where it manages longer to keep warm blooded, correspond the upper or lower critical temperatures beyond which the body enters hyperthermia.

Heat accumulation of body represents the amount of heat produced by metabolism and heat received from the environment. The heat produced by the body has two parts: the first is related to metabolism at rest and the second one is variable in relation with muscular effort applied [5].

To maintain thermal balance under conditions of excessive heat microclimate, the body intervenes by reducing heat production and by favouring heat loss to the environment.

In a microclimate with an air temperature of 15 - 20^0C, under conditions of rest or performing light work, the body will give up metabolic heat in the proportion of 42% through radiation, 26% through convection and conductivity and 32% through evaporation. Under these conditions, but with physical effort, approx. 74% of metabolic heat is lost through radiation and evaporation. If the temperature of the environment is higher than that of the integuments, the body does not yield, but instead receives heat that is added to the metabolic one [6].

RESCUERS BEHAVIOUR IN ENVIRONMENTS WITH HIGH TEMPERATURE IN THE TRAINING FACILITY

To create environments with high temperatures within the INSEMEX Petroșani Training Ground Two were used electric heat generators. The equipment is used to create high-temperature environments within the training range in order to test the intervention and rescue personnel. Hot air generators are automatic and equipped with electronic devices to control the level of heat released.

The motor fan ensures a continuous flow of air inside the heat exchanger. Clean and warm air is released through the front exhaust. The hot air generators are equipped with wheels and can be transported easily. The combustion chambers of these heat generators are made of stainless steel, specially treated to withstand high temperatures.

The critical factor for ensuring the success of an rescue intervention in aggressive toxic or chemical environments consists in the efficient and optimal training process for rescue personnel, in correlation with their testing in environments with high temperatures.

In intervention operations rescue teams are traveling long distances transporting heavy loads, such as tools, rescue equipment, victims and stretchers.

https://doi.org/10.5593/sgem2024/1.1/s03.34

All the factors listed above, coupled with the rescuer's physical condition may contribute to its inability to cope with high temperatures environments. This can lead to heat stress, a condition that is life-threatening.

Preparing for emergencies, including procedures and training for rescue team members will optimize the probability of carrying out essential tasks and at the same time will prevent the development of diseases induced by high temperatures by those who perform this type of work.

To highlight changes in oxygen saturation in the blood and pulse, were carried out tests in the training facility for a team of four rescuers using breathing apparatus with open circuit based on air and positive pressure.

Testing was conducted in a training exercise, determining the two parameters, blood oxygen saturation and pulse, conducted for different activities depending on ambient temperature. Testing was conducted for three activities: tractions on ergometers, walking on the conveyor belt and traversing the polygon with closed spaces.

Determination of blood oxygen saturation was achieved by using oximeters. Oximetry is used for the management and proper dosage of amount of work performed in the training facility by rescuers.

The pulse determination was made using pulse telemetry system for measuring HRT-SYS. Pulse telemetry measurement system HRT-SYS is used to measure pulse of rescuers in the training facility and it allows continuous monitoring of progress for six people.

Measurements were conducted on blood oxygen saturation and pulse for every team member in part, beginning at 25^0C ambient temperature. Measurements were repeated in many stages of 5^0C temperature increase to a maximum of 50^0C.

Activity no. 1 - tractions on ergometers

In this activity, rescuers have conducted one session of tractions on ergometers, lifting a 15 kg weight, at 1,5 meters height, each session having 30 tractions for one threshold temperature in the training room (fig. 1).



Fig. 1 – Tractions on ergometers

For tractions on ergometers activity, blood oxygen saturation and pulse rate are shown in Table no.1.

Table no.1 – Determinations on ergometers tractions

No.	Environment temperature	Subject no.1		Subject no.2		Subject no.3		Subject no.4	
		Pulse	SpO_2	Pulse	SpO_2	Pulse	SpO_2	Pulse	SpO_2
1	25^0C	80	98	79	97	69	98	71	98
2	30^0C	102	96	89	95	82	96	82	98
3	35^0C	113	92	97	97	99	96	95	96
4	40^0C	123	93	110	94	112	95	110	95
5	45^0C	145	91	128	94	126	94	123	94
6	50^0C	155	92	149	93	151	92	145	94

Under activity. no 1 - tractions on ergometers was noticed that once with the temperature rise, rescuers pulse increases and blood oxygen saturation decreases (fig. 2).

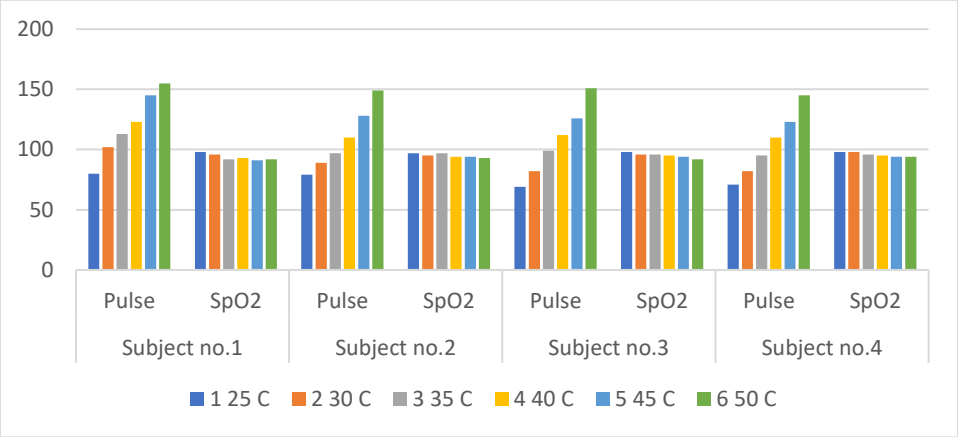


Fig. 2 – Changes in heart rate and SpO_2 on ergometers tractions

Activity no. 2 - walking on the conveyor belt

In this activity rescuers performed simulated walking on the conveyor belt with a speed of 6 km / h, for 3 minutes to one threshold temperature in the training room (fig. 3).



Fig. 3 – Walking on the conveyor belt

For walking on the conveyor belt, blood oxygen saturation and pulse rate are shown in Table no.2.

https://doi.org/10.5593/sgem2024/1.1/s03.34

Table no.2 – Determinations for walking on the conveyor belt

No.	Environment temperature	Subject no.1		Subject no.2		Subject no.3		Subject no.4	
		Pulse	SpO_2	Pulse	SpO_2	Pulse	SpO_2	Pulse	SpO_2
1	25^0C	80	97	79	97	69	98	71	98
2	30^0C	104	96	92	95	85	97	84	98
3	35^0C	112	94	99	96	99	96	98	96
4	40^0C	125	93	114	95	116	95	110	96
5	45^0C	146	91	126	94	128	94	125	94
6	50^0C	152	92	148	93	149	94	138	93

Under activity no 2 - walking on the conveyor belt, it was observed that once with the temperature rise, rescuers pulse increases and oxygen saturation in the blood decreases (fig. 4).

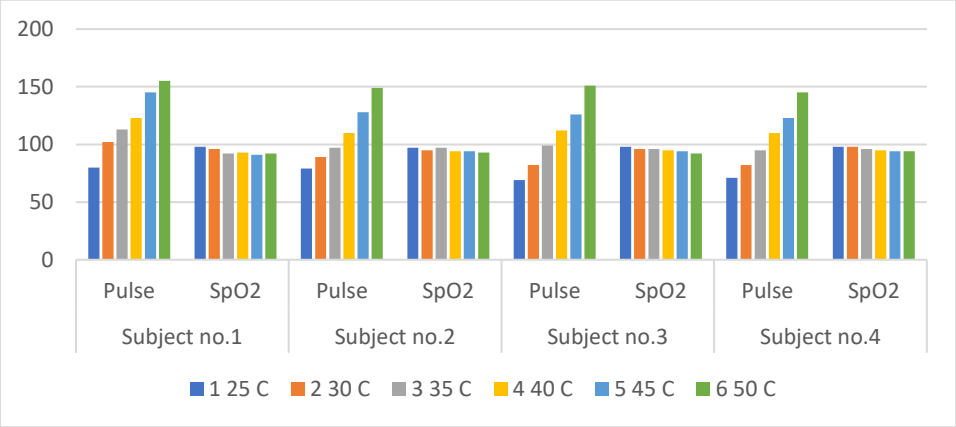


Fig. 4 – Changes in heart rate and SpO_2 at walking on the conveyor belt

Activity no. 3 – traversing the polygon with closed spaces

In this activity, the rescuers had to go through a part of the polygon with closed spaces for each temperature threshold in the training room (fig. 5).



Fig. 5 – Traversing the polygon with closed spaces

For traversing the polygon with closed spaces activity, blood oxygen saturation and pulse rate are shown in Table no.3.

Table no. 3 – Determination for traversing the polygon with closed spaces

No.	Environment temperature	Subject no.1		Subject no.2		Subject no.3		Subject no.4	
		Pulse	SpO_2	Pulse	SpO_2	Pulse	SpO_2	Pulse	SpO_2
1	25^0C	84	97	79	97	69	98	71	99
2	30^0C	105	96	92	95	85	97	88	98
3	35^0C	118	94	97	96	99	96	102	96
4	40^0C	125	93	114	94	114	95	120	96
5	45^0C	144	91	128	94	128	94	139	95
6	50^0C	149	92	146	93	147	95	142	94

Under activity no 3 - traversing the polygon with closed spaces, there has been noticed that once with temperature rise, the rescuers pulse increases and oxygen saturation in the blood decreases (fig. 6).

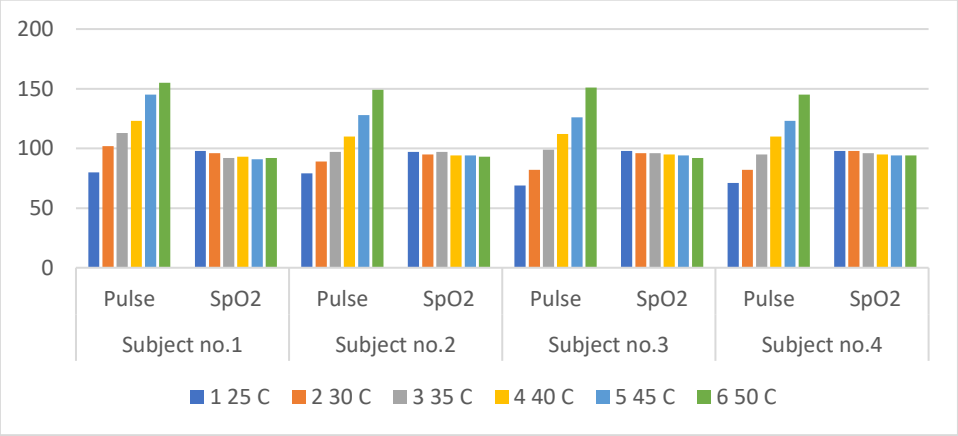


Fig. 6 – Changes in heart rate and SpO_2 for traversing the polygon with closed spaces

CONCLUSIONS

INSEMEX Petroşani has a training ground that is unique at the national level, being similar to those existing in countries with a tradition in the field and which includes training spaces where the practical exercises of the rescuers are carried out, and the installations, devices and operations performed during training, they are designed in such a way that they are close to the real conditions encountered in situations where various types of accidents occur.

The activity in hard conditions was developed for the prevention further underground or surface breakdowns which threat the personnel or property and because the toxic or hazardous gases concentrations, vapors or dust established by rules requires the use of protective respiratory apparatus.

The Heat is generated normally as a result of metabolic processes taking place in the body of rescuers. As a result of muscle activity when there are performed working or training activities, there is released a considerable amount of heat. The amount of heat generated is proportional to the intensity of work.

https://doi.org/10.5593/sgem2024/1.1/s03.34

To highlight changes in oxygen saturation in the blood and pulse, were carried out tests in the training facility for a team of four rescuers using breathing apparatus with open circuit based on air and positive pressure.

Within three activities: tractions on ergometers, walking on the conveyor belt and traversing the polygon with closed spaces was observed that as the temperature rises in the training room, the pulse of team members increases and oxygen saturation in the blood decreases.

The tests carried out in the Training Ground allowed the establishment of a link between the change in the physiological parameters of the intervention and rescue personnel and the environmental conditions (high temperature), which will allow the identification of temperature limit values up to which the rescuers can carry out their the activity in safe conditions.

ACKNOWLEDGEMENTS

This work was carried out through the "Nucleu" Program within the National Plan for Research, Development and Innovation 2023-2026, with the support of the Romanian Ministry of Research, Innovation and Digitalisation, project no. 23 32 01 02, title: Development of assessment, testing and intervention methods for explosive atmospheres generated by facilities for the production, storage, transport and use of hydrogen.

REFERENCES

[1] Buica G., Antonov A.E., Beiu C., Iorga I., Safety measures - tools for reducing the cost of working accidents in electrical installations, Environmental Engineering and Management Journal 11, 2012;

[2] Gaman G.A., Lupu C., Pupazan D., Procedures and Regulations of Intervention and Exploitation teams in toxic / explosive / flammable environments, INSEMEX Publishing House, 2009;

[3] Gaman G.A., Pupazan D., Ilie C., Development and implementation of an expert system for the management of crisis events in mining industry, Environmental Engineering and Management Journal, 2012;

[4] Pupazan D., Gaman G.A., Ilie C., Information system for simulation and assessment of rescuers interventions in toxic, explosive and flammable environments, Environmental Engineering and Management Journal, 2012;

[5] Ilie C., Research on issues related to the design of physical and psychosocial effort for optimizing the training process of intervention and rescue personnel in toxic / explosive / flammable environments, Nucleus Programme INSEMEX Petroşani, 2012;

[6] Nicolescu C.,Kovacs I., Ilie C., Training of intervention and rescue personnel in toxic / explosive / flammable environments, INSEMEX Publishing House, 2018.

DEVELOPMENT OF THE INFRASTRUCTURE FOR VALIDATING THEORETICAL METHODS THROUGH COMPUTER SIMULATION AND MODELING OF BLASTING AND SAFETY PARAMETERS OF CIVIL EXPLOSIVES

PhD Ress. Ciprian Jitea[1]

PhD. Daniela Rus[1]

PhD. Edward Gheorghiosu[1]

PhD Ress. Johannes Fabian Bauer[2]

PhD Ress. Mateiu Ciprian[3]

[1] National Institute for Research and Development in Mine Safety and Protection to Explosion – INSEMEX Petrosani, **Romania**

[2] University of Petrosani, **Romania**

[3] Institute for drilling and production engineering, Technical University Bergakademie Freiberg, Germany

ABSTRACT

This research paper explores the advancement of computer simulation techniques to improve the safety, efficiency, and environmental sustainability of civil explosives in various engineering applications. The study emphasizes the critical role that computer simulations play in modeling and optimizing blasting techniques, allowing for precise predictions of explosive behavior under diverse conditions. By simulating the detonation processes and their impacts, engineers can develop safer and more efficient blasting protocols, significantly reducing the risk of accidents and environmental damage. The paper delves into the use of sophisticated modeling tools, such as ANSYS Autodyn, to analyze the interaction between explosives and various materials, thereby improving the accuracy of simulations. The integration of real-time data and collaborative environments further enhances the utility of these simulations in real-world applications. A case study within the paper illustrates the comparative analysis of pentrite and hexogen explosives, demonstrating how varying conditions, such as the presence of water, affect detonation characteristics. The findings underscore the importance of selecting appropriate explosives based on environmental conditions to achieve optimal results while ensuring safety and compliance with regulatory standards. This research not only contributes to the theoretical understanding of explosive behavior but also provides practical insights for industries involved in mining, construction, and demolition. The use of computer simulations as a tool for validating theoretical methods in explosive engineering is presented as a key innovation, promising to enhance both operational safety and environmental stewardship in the use of civil explosives.

Keywords: computer simulation, civil explosives safety, blasting techniques, detonation modeling

https://doi.org/10.5593/sgem2024/1.1/s03.35

1. INTRODUCTION

The use of computer simulation in the realm of civil explosives is not merely a technological advancement but a critical enhancement in safety and operational efficiency. Computer simulations enable precise modeling of explosive behavior under various conditions, allowing engineers to predict and mitigate potential risks before actual deployment. This approach is vital as it provides a safer, cost-effective, and time-efficient method of testing and optimizing explosive use without the inherent risks of live testing. Moreover, simulations help in designing more effective blasting patterns, assessing the structural impact of blasts, and ensuring compliance with safety regulations. By leveraging these tools, industries can achieve more controlled and predictable blasting outcomes, minimizing environmental impact and enhancing worker safety.

Civil explosives are materials or chemical compounds that, when initiated, undergo rapid chemical decomposition resulting in the release of large volumes of gases and heat. This explosive energy is harnessed in various civil engineering tasks such as mining, quarrying, demolition, and construction. In mining, explosives are used to break rock for the extraction of minerals and ores. In construction, they are employed to clear space for infrastructure development like roads and tunnels. The efficiency of these tasks heavily depends on the quality and characteristics of the explosives used, which include parameters like velocity of detonation, stability, brisance (shattering effect), and strength. Accurately simulating these parameters allows for the optimization of explosive use, enhancing safety and efficiency across all applications. By understanding and controlling the energy released, experts can ensure minimal damage to surrounding structures and reduce unintended consequences, which is important in densely populated or environmentally sensitive areas.

Current Theoretical Methods:

The analysis and design of civil explosives rely on a variety of theoretical methods that encompass chemistry, physics, and engineering principles.

Key methods include:

- Thermodynamic models: these models calculate the energy output and gas production from chemical reactions of explosives, essential for understanding the explosion's potential power;
- Kinetic models: kinetic modeling focuses on the rate at which chemical reactions occur, which affects the speed and stability of the detonation process;
- Empirical formulas: widely used in the mining industry, empirical formulas such as the Konya and Walter formulas calculate the optimal amount of explosives and their placement based on rock properties and desired blast outcomes.
- Wave propagation theories: these theories analyze how shock waves generated by an explosion propagate through different media, affecting both the blasting site and surrounding structures.

- Structural response models: these models predict how different structures will respond to blast-induced vibrations, crucial for minimizing damage during demolition activities.

Despite the advancements in theoretical methods, several challenges and limitations persist, which can be addressed through enhanced computer simulations:

- Complexity of real-world conditions: traditional models often fail to capture the complex geological and environmental variables present at blasting sites, computer simulations can integrate these multifaceted data into more realistic models;
- Scale of interactions: the interaction between shock waves and rock formations involves phenomena at various scales, from microscopic cracks to large geological faults, current theoretical methods may not accurately predict these interactions across all scales;
- Data limitations: empirical and kinetic models rely heavily on historical data, which may not be available or may not cover the range of current applications, simulations can use synthetic datasets to extrapolate missing data and improve model robustness;
- Temporal and spatial resolution: high-resolution models are necessary to accurately simulate the rapid processes occurring during detonation, many existing theoretical models offer limited resolution, leading to less accurate predictions;
- Safety and cost constraints: conducting field tests to validate theoretical methods can be risky and expensive but computer simulations provide a safer and more cost-effective alternative by allowing for extensive testing in a virtual environment.

2. INFRASTRUCTURE DEVELOPMENT FOR SIMULATION

2.1 Hardware Requirements

To perform large-scale simulations of civil explosives, robust computational hardware is essential. The primary components required include: high-performance processors, Multi-core CPUs (Central Processing Units) with high clock speeds are essential for handling the complex calculations involved in explosive simulations. These processors must be capable of parallel processing to efficiently manage the simultaneous operations required by simulation software.[1]

Graphical Processing Units (GPUs): for simulations that involve visualizations and 3D modeling, powerful GPUs are indispensable, they accelerate the rendering process and are also used to handle computation-heavy tasks, particularly those involving finite element analysis and fluid dynamics.

High-Speed Memory and Storage: large RAM (Random Access Memory) capacities are required to quickly access data related to simulation scenarios, similarly, high-speed SSDs (Solid State Drives) are recommended for storing large datasets and simulation results, facilitating faster data retrieval and processing.

https://doi.org/10.5593/sgem2024/1.1/s03.35

Scalable Infrastructure: for larger simulations, the infrastructure must be scalable, often involving clustered computing or cloud-based solutions to handle the increased computational load.

2.2 Software and Tools

When it comes to software tools and simulation platforms, a variety of specialized applications are utilized in the modeling of explosives. ANSYS software, particularly ANSYS Autodyn, is a key player in this field.

ANSYS Autodyn: this software is specifically designed for simulating the non-linear dynamics of solids, fluids, gas, and their interaction, with the capabilities to handle complex material behaviours under extreme conditions such as high strain rates from explosions, Autodyn is ideally suited for simulating civil explosives, it supports a range of modeling approaches including finite element, smooth particle hydrodynamics (SPH), and Euler methods, which are critical for analyzing interactions in a blasting environment.

Integration with CAD Tools: ANSYS Autodyn integrates seamlessly with CAD (Computer-Aided Design) software, allowing engineers to import geometrical data directly into the simulation environment and this facilitates a smooth transition from design to analysis.

2.3. Integration of Data and Systems

Integrating various data systems is essential for the effective execution of simulations. This task involves ensuring that data formats across different platforms are compatible. Often, this requires using middleware or specialized software that can translate data into a format usable by simulation tools like Autodyn.

Real-Time Data Integration: In some cases, real-time data from sensors or monitoring systems (such as those used in mining operations) can be integrated into simulations to provide more accurate and timely results.

Collaborative Environments: simulations often require collaboration across different teams and disciplines, integrated systems allow for shared access to simulation results and data, enabling collaborative analysis and decision-making.

3. Case Study Example

This case study presents a simulation study of the explosive behaviors of pentrite and hexogen under varying conditions. Utilizing simulations, we examined the effects of explosive charge sizes and the presence of water on detonation characteristics. The case study leverages data from established references, to validate simulation outcomes and offers insights into the effective management and application of these materials in safety and engineering applications. Explosive materials such as pentrite and hexogen are critical to various applications ranging from military ordnance to civilian blasting operations. Understanding their behavior under different conditions is essential for safety and effectiveness [1].

The goal of this case study is to examine the detonation properties of pentrite and hexogen by comparing how they react to different charge sizes and environmental conditions in a controlled simulation setting. It focuses on analyzing aspects such as the explosives density, energy output, and the role of water in moderating their behaviour.

3.1. Simulation Setup

The simulations were conducted within a 500 x 500 mm domain See figure 1, with detailed meshing dimensions adjusted according to the explosive charge (ranging from 0.2 mm to 1 mm mesh size). See Figure 2, [2], [3].

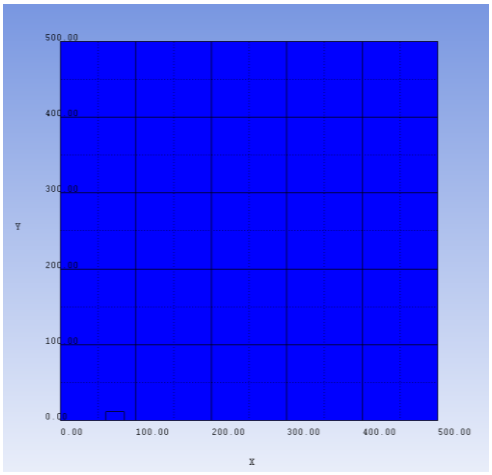


Figure 1. Domain 500 x 500 mm

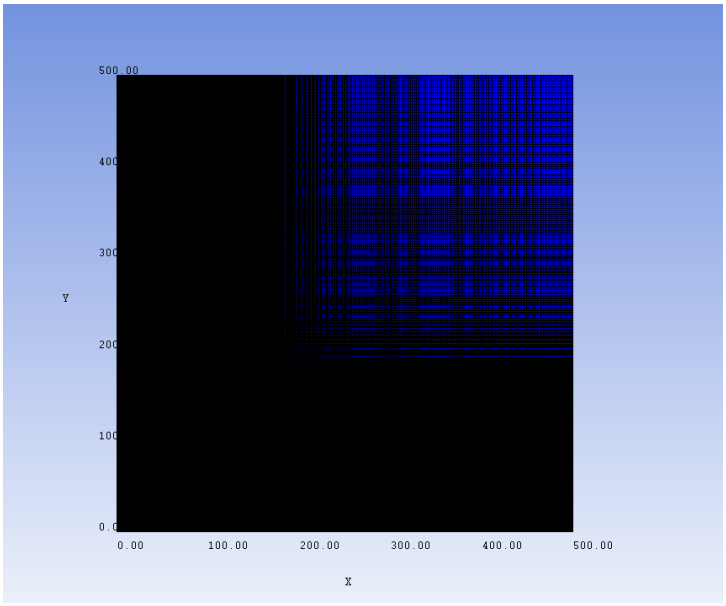


Figure 2. An example of the meshing setup used in the simulations.

3.2. Explosives parameters and testing conditions

We utilized parameters for pentrite and hexogen including density, equation of state , and gamma values, informed by explosive literature [4],[5].
The tests were conducted with a consistent charge of 5g for each explosive type, and were performed in both aquatic and dry environments. Simulations were carried out

https://doi.org/10.5593/sgem2024/1.1/s03.35

using Autodyn software, utilizing data on material properties and explosive behavior sourced from established explosive literature.

3.3. Results

Our results indicate that both explosives exhibit increased detonation velocities and energy output with larger charge sizes. Hexogen showed higher sensitivity to environmental changes than pentrite. Figure 3 illustrates the explosive behaviors under different testing conditions.

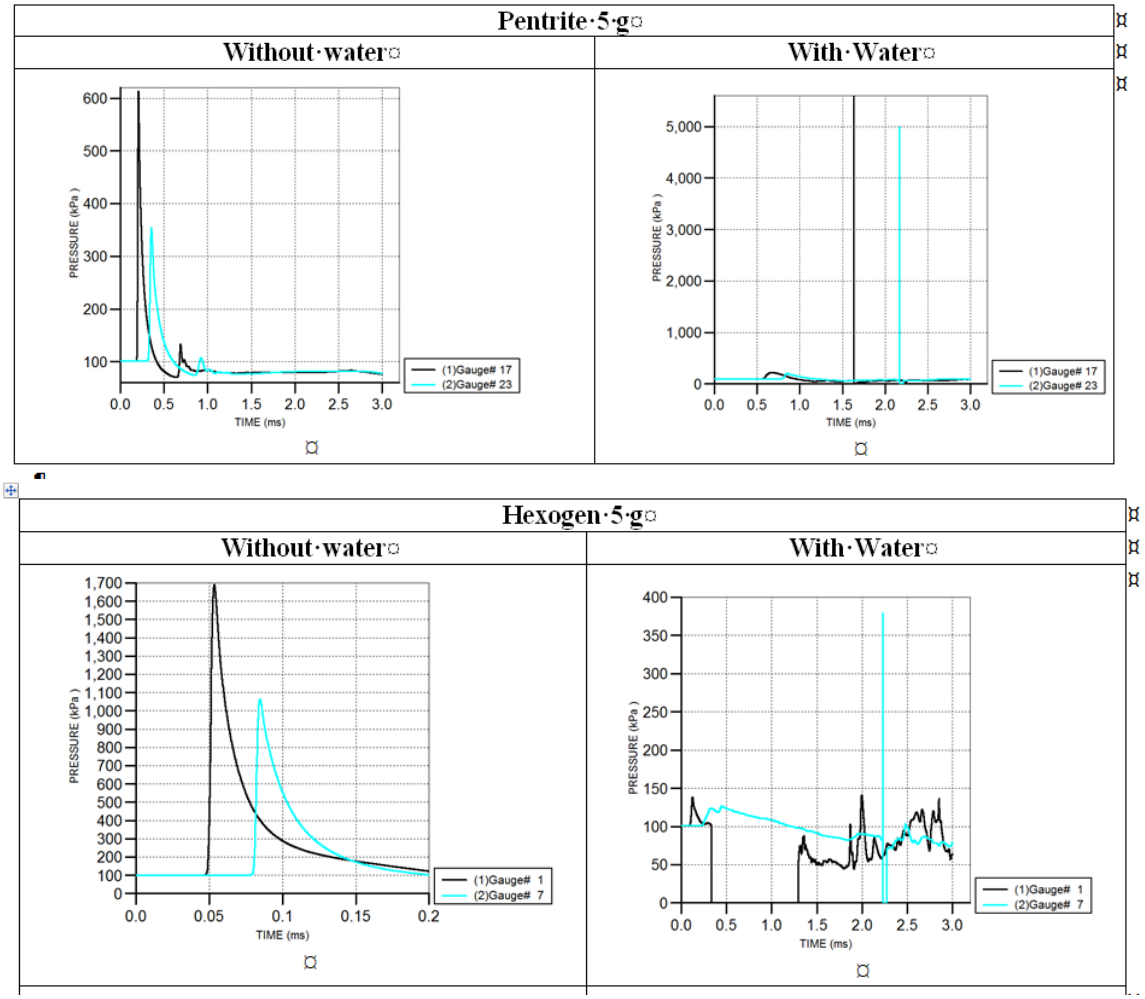


Figure 3. Comparisons between pentrite and hexogen under identical conditions

Comparisons between pentrite and hexogen under identical conditions revealed significant differences in pressure and energy distribution, highlighting hexogen's higher effectiveness in water-absent scenarios. See Figure 3 for a detailed comparative analysis [6].

Water presence generally reduced the peak pressure and energy output for both explosives, with more pronounced effects observed in hexogen. Figure 4 and 5 provides graphical data on the impact of water on detonation [7].

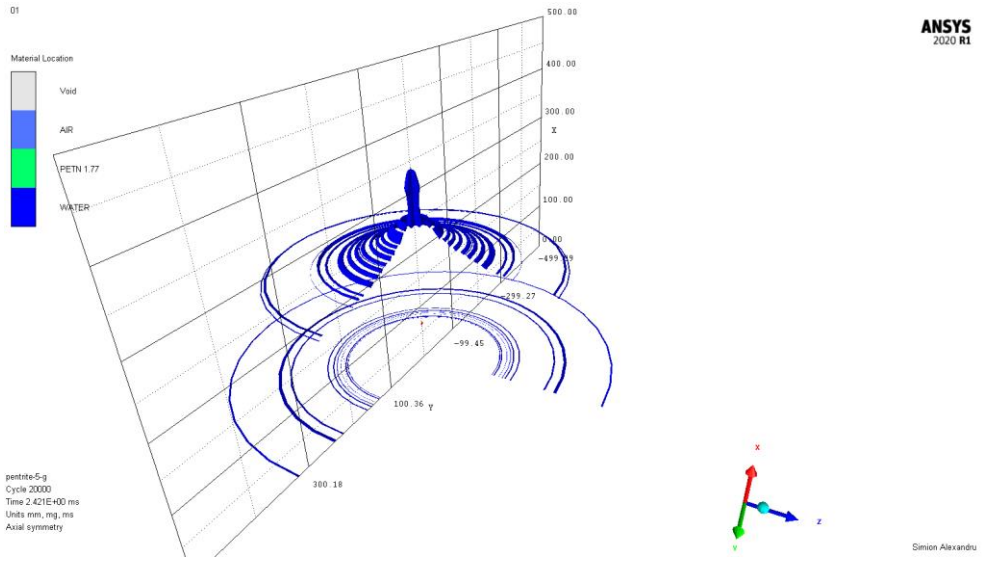


Figure 4. Pentrite 5 g with Water

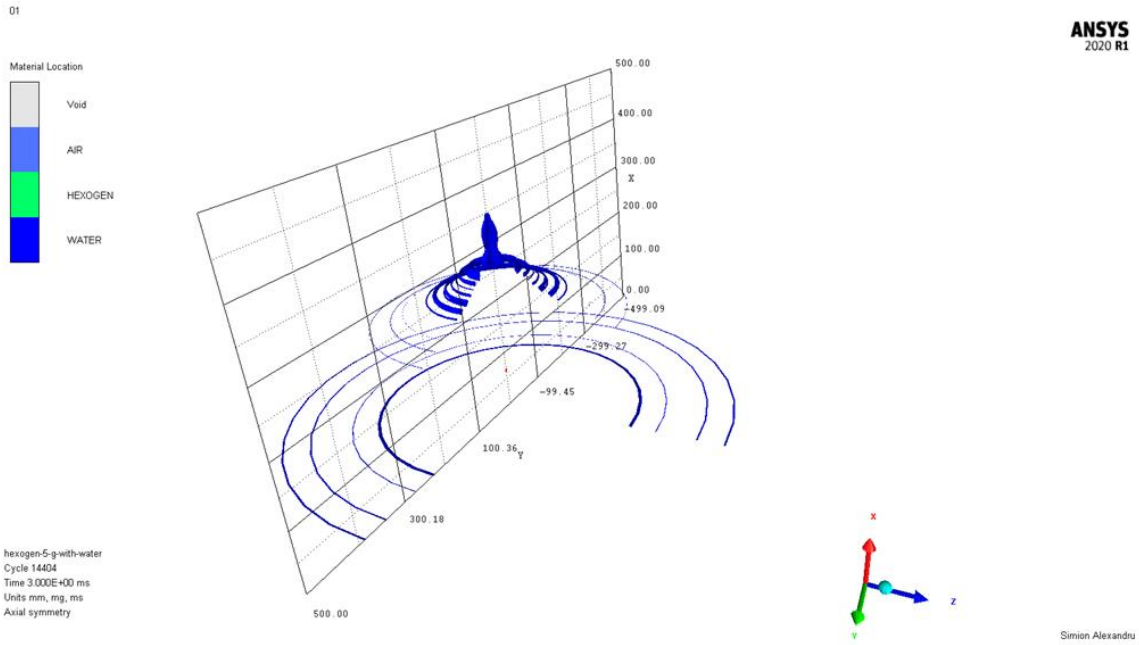


Figure 5. Hehogen 5 g with Water

3.4. Analysis of Results:

The data suggest that hexogen is more suitable for operations requiring high-energy output in dry conditions, whereas pentrite could be preferred in wet environments due to its less reactive nature.

Practical Implications, these findings could guide the application of these explosives in mining operations, demolition activities, and military applications, enhancing safety and efficiency.

https://doi.org/10.5593/sgem2024/1.1/s03.35

4. CONCLUSIONS

This study has thoroughly examined the detonation characteristics of pentrite and hexogen under varying conditions through computational simulations. Our findings indicate significant variations in the behavior of these explosives when subjected to different charge sizes and environmental conditions, particularly in the presence of water. Hexogen displayed higher sensitivity and a greater reaction to environmental changes compared to pentrite, showing increased detonation velocities and energy outputs with larger charge sizes. The presence of water generally reduced the peak pressures and energy outputs for both explosives, with more pronounced effects in hexogen.

These insights enhance our understanding of the practical applications of these explosives in fields such as mining, demolition, and military operations. They provide a foundation for optimizing the use of explosives, emphasizing the importance of selecting the appropriate material based on specific environmental conditions to ensure safety and efficiency.

REFERENCES

[1] Explosives regulations, Explosives regulations 2014: safety provisions: guidance on regulations. Mersey- side: Health and Safety Executive, HSE Books, 2014.
[2] Dinu F. et al., "Experimental blast tests on light non load bearing external walls," in Steel Constructions, Bucharest, Apr. 2022, pp. 125–132
[3] Shin J., Whittaker A. S., Cormie D., and Wilkinson W., "Numerical modeling of close-in detonations of high explosives," Engineering Structures, vol. 81, pp. 88–97, Dec. 2014, doi: 10.1016/j.eng- struct.2014.09.022.
[4] Ahn J. and Park D., "Prediction of Near-Field Wave Attenuation Due to a Spherical Blast Source," ROCK MECHANICS AND ROCK ENGINEERING, vol. 50, no. 11, pp. 3085–3099, Nov. 2017, doi: 10.1007/s00603-017-1274-3.
[5] Shin J. and Whittaker A., "Blast-Wave Clearing for Detonations of High Explosives," JOURNAL OF STRUCTURAL ENGINEERING, vol. 145, no. 7, Jul. 2019, doi: 10.1061/(ASCE)ST.1943-541X.0002327.
[6] Brode H. L., "Numerical solution of spherical blast waves," Journal of Applied Physics, vol. American In- stitute of Physics, 1955.
[7]Jitea Ilie-Ciprian; Vasilescu Gabriel; Laszlo Robert; Kovacs Attila; Rădeanu, Cristian "Verification of performance requirements and technical parameters of plastic explosives with civil and military use" International Multidisciplinary Scientific GeoConference : SGEM; Sofia, Vol. 19, Iss. 1.3, (2019).
DOI:10.5593/sgem2019/1.3/S03.092

DYNAMIC BEHAVIOR OF METHANE IN CONFINED SPACES BY CFD SIMULATION

Vlad Lăutaru[1]
Alexandru Simion[1]
Laurențiu Munteanu[1]
[1]INCD INSEMEX, **Romania**

ABSTRACT

Gases released because of accidents and events that cause the contamination of certain indoor spaces with methane have become more frequent recently. These gases endanger the lives of people who are inside the contaminated spaces, and there is a need for more and more in-depth research on the dynamic behavior of certain substances with a toxic effect, such as methane, once it begins to accumulate in a closed space, for to develop new detection systems and especially for its evacuation in the shortest possible time from the contaminated space. In this sense, in the paper we analyzed the dynamic behavior of the gas with a toxic and explosive effect, namely methane, through a CFD computer simulation, in a closed space, to analyze the mode and duration of the distribution of methane concentration. To perform the CFD simulation, the physical conditions of a closed space of 50 m2, and with a methane volume of 418.5 liters, were replicated, and the duration of the simulation was 93 minutes. Following the analysis, we developed a technical solution to prevent the spread of methane in closed spaces following an accident/event.

Keywrods: CFD simulation, Methane, Accidents

INTRODUCTION

Knowing how methane disperses in the air is very important for establishing certain preventive measures [1].The presence of noxes in industrial premises represents a major risk that is given priority attention. If there is an untimely occurrence or a significant release of methane gas in the enclosed space, then the risk of explosion is imminent and represents a fatal danger to the people in the enclosed space.[2]
The explosion phenomenon can occur if the three elements overlap in time and space: gases, mists, combustible dusts or powders, atmospheric oxygen, respectively the effective source of ignition. Methane gas, in addition to its explosive character, is in itself an asphyxiating gas that in closed premises can lead to a sharp decrease in the concentration of oxygen, but in the case of an explosion-type phenomenon, the dynamic effect is more important, an effect that also occurs in the case of explosions in semi-enclosed and open spaces.[3]
However the dispersion dynamics of explosive gases such as methane in closed enclosures has been less studied, but it can be analyzed mathematically with the help of fluid dynamics or through experiments [4]. The peculiarity of methane dispersion dynamics in the closed enclosure is generated by the appearance of non-uniform concentrations with large variations both in the horizontal and in the vertical plane. The results obtained from the detailed analysis can be used to establish the escape routes in case of an untimely release of methane in the closed industrial premises.

https://doi.org/10.5593/sgem2024/1.1/s03.36

MATERIALS AND METHODS

For the study of the dispersion dynamics of explosive, toxic and asphyxiating gases, the CFD technique was used with the help of the ANSYS MULTIPHISICS software package. ANSYS is a finite element analysis software package widely used in industry and research, with the aim of simulating the response of multiphysics analyses, offering the user the possibility to combine the effect of two or more physical phenomena (structural, thermal, electrical, magnetic, electromagnetic, electrostatic, fluid flow). The ANSYS package practically allows the parametric realization and then the optimization of any problem, regardless of the type of parameters, the types of finite elements used, the type of analysis, etc. and even the use of optimization algorithms declared by the user.
To establish the dynamics of accumulation - evacuation of explosive gases, dispersion - dilution modeling for CH4, CO and CO2, in a closed enclosure, was carried out using the CFD technique. To carry out the simulations in a manner as close as possible to the experimental conditions, the topographic survey of the location within the experimental laboratory where the experiments were carried out in the laboratory was carried out, and the computerized model was made.
To have conclusive data in order to carry out computer simulations, experiments were done in the INCD INSEMEX Petroșani laboratory, thus having real concentration values, which bring the computer simulation as close as possible to a real event.

EXPERIMENTS IN THE LABORATORY

The experiment regarding the establishment of the dynamics of the formation and dispersion of the explosive atmospheres, respectively of the exhaust, was carried out in the industrial ventilation laboratory within INCD INSEMEX Petroșani [6]. The experimental system used is composed of data acquisition equipment and a monitoring system consisting of 6 pulleys on which 6 ALTAIR type multigas detectors are attached, which can detect concentrations of O2, CO2, CO and CH4. The pulley system can configure a variable spatial layout in order to establish the speed of gas dispersion as well as the dynamics of the formation of explosive atmospheres. To ensure safety and health conditions at work at the experimental site, a complex ventilation system with variable structure is used to study the ventilation capacity of closed premises with the risk of forming potentially explosive/toxic/asphyxiating atmospheres.
In the experimental laboratory, the dynamics of explosive atmosphere formation using methane, CH4, was analyzed. The measuring devices used are MSA - ALTAIR type. The ground section of the experiment enclosure is 5.8x5.62m. The height of the enclosure is 3.65m. Consequently, the total volume of the experimental enclosure is 118.9754m3. Because other experimental systems are located in the premises, the free volume of the premises is 116 m3.
The "experimental system for the study of the dynamics of the formation of potentially explosive/toxic/asphyxiating atmospheres" was used to analyze the dynamics of explosive atmosphere formation.
The initial experimental conditions were as follows: Temperature: T = 29.9 °C; Atmospheric pressure: B = 9,440 daPa; Relative humidity: RH = 40.5%; Discharged gas flow rate: q = 4.5 l/min.
The system consists of a cylinder of compressed methane gas at a pressure of 200 bars at a concentration of 100% Vol., a pressure reducer, and a flowmeter with a float. The gas was introduced into the enclosure by means of a hose with an internal diameter of 8 mm. The gas flow velocity at the nozzle was 1.5 m/s. The discharge of methane gas inside the

enclosure was carried out by means of a support placed 0.25 m from the hearth on the eastern wall halfway up its base side. The hose was fixed in a horizontal position in the E-W direction.
The MSA – ALTAIR detection devices were positioned on the 6 pulleys at the ceiling level and the height at which the suction and detection area of the devices was positioned was 3.25 m from the hearth (fig.1).

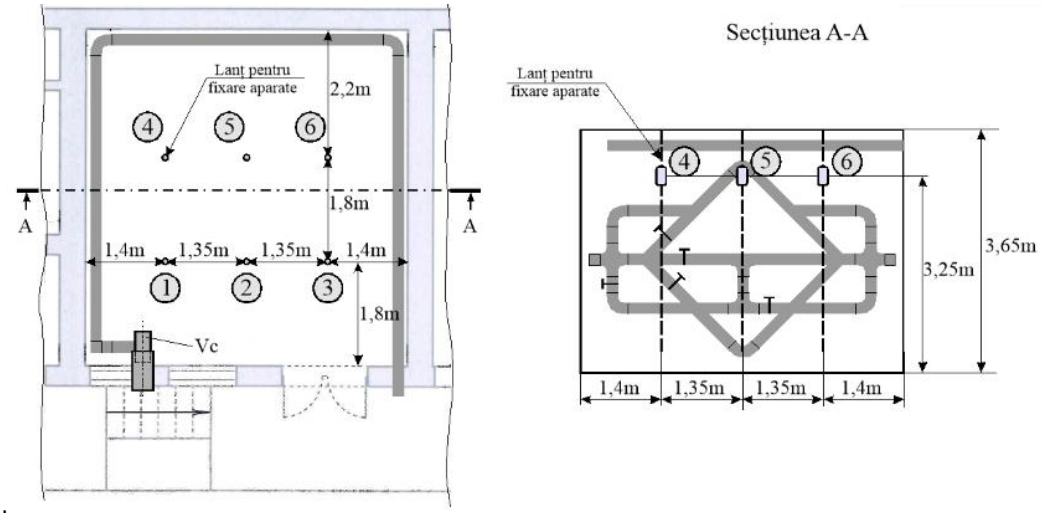


Fig.1 - Location of the detection system

THE DYNAMICS OF METHANE RELEASE

For experiments, as well as for ensuring safety and health conditions at work at the experiment site, respectively for the evacuation of gases from the premises, a complex ventilation system with variable structure was used to study the ventilation capacity of closed premises with the risk of potentially explosive atmospheres/ toxic/asphyxiating. This ventilation system consists of a 3-kW centrifugal fan-motor unit and a multifilar rectangular piping network with dimensions of 300/400 mm that controls the interior atmosphere. The rectangular piping network intended for air intake consists of short and long branches intended for the ventilation of premises where gases with low, medium or high specific gravity can be found.
For the analysis of the ventilation dynamics of the explosive atmosphere, the same "experimental system for the study of the dynamics of the formation of potentially explosive/toxic/asphyxiating atmospheres" was used.
The initial experimental conditions were like those identified for the methane accumulation stage in the closed enclosure.
The MSA – ALTAIR detectors were positioned on the 6 pulleys at the ceiling level and the height at which they were the same as for the methane accumulation stage in the closed enclosure.
The ventilation system of the premises was structured with the help of flow variators. The ventilation system as well as the flow variators were operated by the SCADA command and control system.

https://doi.org/10.5593/sgem2024/1.1/s03.36

CFD simulation of the accumulation dynamics – methane dilution

For the study of the dispersion dynamics of explosive, toxic and asphyxiating gases, the CFD technique was used with the help of the ANSYS MULTIPHISICS software package [7]. ANSYS is a finite element analysis software package widely used in industry and research, with the aim of simulating the response of multiphysics analyses, offering the user the possibility to combine the effect of two or more physical phenomena (structural, thermal, electrical, magnetic, electromagnetic, electrostatic, fluid flow). The ANSYS package practically allows the parametric realization and then the optimization of any problem, regardless of the type of parameters, the types of finite elements used, the type of analysis, etc. and even the use of optimization algorithms declared by the user. This package contains a series of solvers dedicated to the particularities of analyzing and solving the systems considered. In order to pre-process the analyzes and post-process their results, the ANSYS multiphysics package has: Pre-processor specific to fluid dynamics (CFX); Post-processor for using CFX and Fluent; Pre and post-processor specific to the interactions of solids, fluids and gases; Pre and post-processor specific to fluid dynamics, Fluent type or equivalent; Advanced discretization application, including methods: Cartesian, hexa, dominant-hexa, multi-zone, prismatic, shell meshing (quad and tri, patch-based and patch-independent), tetra (Delaunay, Octree), T-Grid ; And so on In order to simulate the dynamics of gas accumulation - dilution, the CFD technique uses the Navier - Stokes equations specific to the laminar flow of real fluids.[8]

To establish the dynamics of accumulation - evacuation of explosive gases, modeling of the dispersion - dilution of methane in a closed enclosure was carried out using the CFD technique. To carry out the simulations in a manner as close as possible to the experimental conditions, the topographic survey of the location within the experimental laboratory where the experiments were carried out in the laboratory was carried out, and the computer model was made (fig. 2).

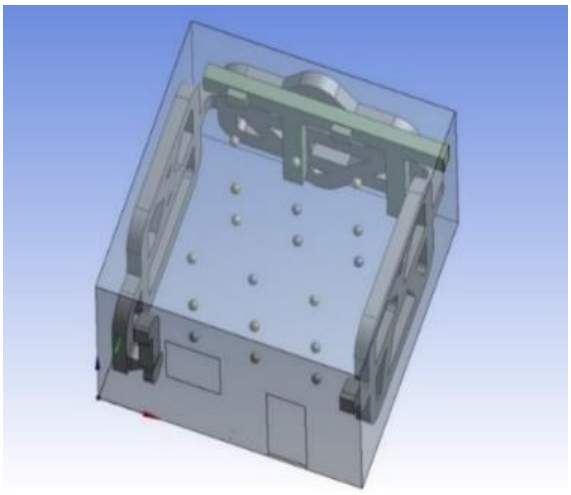


Fig.2 - Site modeling

RESULTS AND DISCUSSIONS

As a result of the experimentation, the following results were obtained shown in table 1:

Table 1 - At the level of the MSA ALTAIR

Date Altair 5X -1	COMB(1)	O2(2)		CO(3)	H2S(4)	CO2(6)	°C
	Peak	Min	Max	Peak	Peak	Peak	
8/6/2020 2:50:30 PM	0,7	20.8	20.8	0	0	0.03	30
8/6/2020 2:53:30 PM	0,7	20.8	20.8	0	0	0.03	30
8/6/2020 2:56 PM	0,6	20.8	20.8	0	0	0.03	31
8/6/2020 2:59:30 PM	0,45	20.8	20.8	0	0	0.03	31
8/6/2020 3:02:30 PM	0,3	20.8	20.8	0	0	0.03	31
8/6/2020 3:05:30 PM	0,25	20.8	20.8	0	0	0.03	31
8/6/2020 3:08:30 PM	0	20.8	20.8	0	0	0.03	31
8/6/2020 3:11:30 PM	0	20.8	20.8	0	0	0.03	31
8/6/2020 3:16:30 PM	0	20.8	20.8	0	0	0.03	31

*MSA ALTAIR – Explosive gas detection device

The duration of the experiment was 27 min. The volume of methane gas introduced into the premises was 418.5 liters or 0.4185 m3. The time allocated to the ventilation was 30 min. The dynamics of methane gas dispersion at the level of the closed enclosure is shown graphically in figure 3.

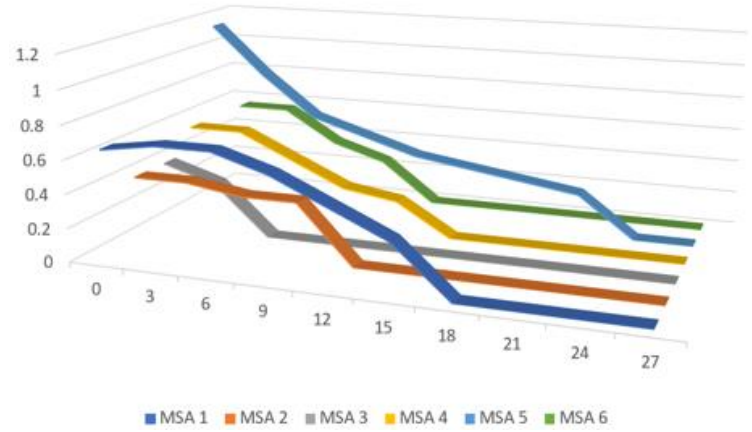


Fig.3-Dynamics of methane gas dilution and evacuation in the closed enclosure

https://doi.org/10.5593/sgem2024/1.1/s03.36

In order to carry out the dispersion modeling using the CFD technique, 3 sets of points presented in table 18 were established at the level of the modeled premises, located at 0.5m/1.5m/3m elevations from the hearth. The point sets are used to control the evolution of gas concentrations over the modeling period.

For the modeling of methane dispersion dynamics, the following aspects were established: The introduced methane gas has a concentration of 100% Vol.; The introduction of gas is carried out at the level of the eastern wall at 0.15 m from the hearth; The methane gas is discharged through a hose with an internal diameter of 8 mm; The gas flow inside the enclosure is 4.5 l/min; The phenomenon of methane dispersion was realized at constant pressure; Atmospheric pressure, temperature and humidity are those currently encountered at the place of experimentation; Simulation time set at 10 minutes; Following the modeling of the dispersion of methane inside the closed enclosure, the results of the gas concentration at the established control points were obtained, and for the dispersion of methane at the level of the plan of the measurement points located, diagrams of variation of the concentrations were obtained of gas, shown in figure 5.

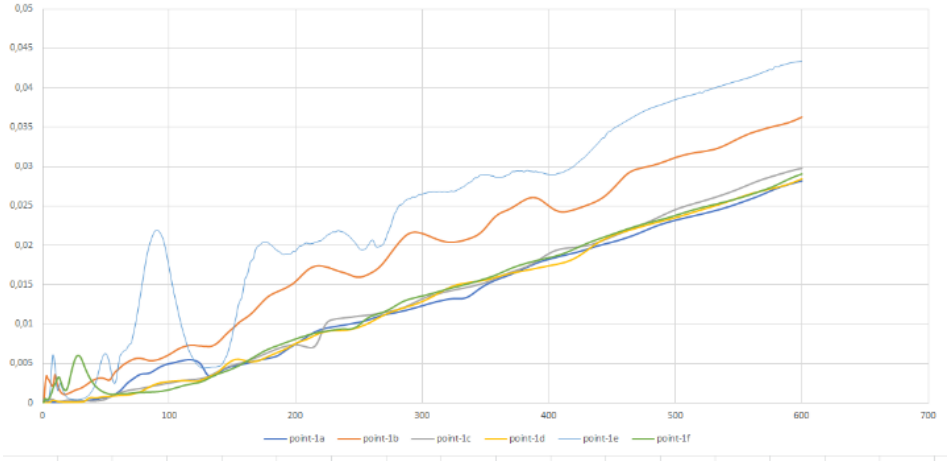


Fig.5 - Dynamics of methane dispersion at level 1

The result of the computer modeling for a simulation time of many minutes is shown graphically in figures 8÷11.



Fig.8 - Evolution of methane dispersion at 1 min. from the start



Fig.9 - Evolution of methane dispersion at 2 min. from the start

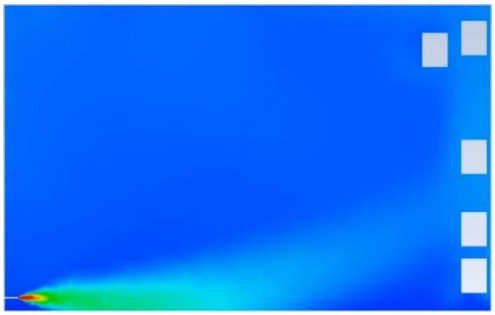


Fig.10 - Evolution of methane dispersion at 7 min. from the start

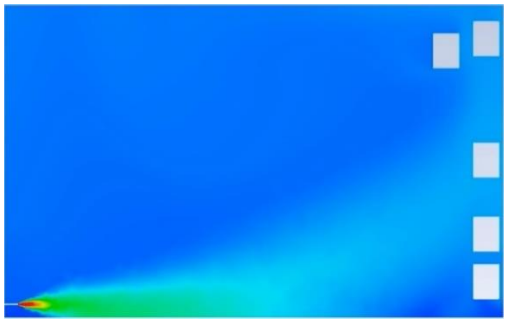


Fig.11 - Evolution of methane dispersion at 8 min. from the start

CONCLUSIONS

From experimenting with the dilution and evacuation of explosive gases from the closed area by using methane CH4, the following observations emerge:

• The process of diluting and exhausting the methane gas in the closed enclosure presented the ventilation period in which the gas is evacuated with the help of the ventilation system with variable structure.

• The dilution and evacuation process is characterized by a variable evolution both horizontally and vertically. This aspect is proven by the different values of the gas concentrations at the level of the detection devices, in the same time interval;

• The period of aeration and progressive dilution of the gas showed different evolutions depending on the position in the plan of the detection devices as follows: The period of aeration and progressive dilution of the gas was small at the level of the detection devices located in points 3 and 6, being 12 min .; The period of aeration and progressive dilution of the gas was average at the level of the detection devices located in points 1, 2 and 4, being 18, 21 and 21 min. respectively; The period of aeration and progressive dilution of the gas was long at the level of the detection device located at point 5, being 24 min.;

• The maximum concentration of the gas showed different evolutions depending on the position in the plan of the detection devices as follows: The maximum gas concentration of the gas was reduced at the level of the detection devices located in points 2 and 3, being 0.4 and 0.4% respectively vol.; The maximum gas concentration was average at the detection devices located in points 1, 4 and 6, being 0.7; 0.55, respectively 0.55 % Vol.; The maximum gas concentration of the gas was high at the level of the detection device located at point 5, being 1.15% Vol.;

• The gradient of dispersion and progressive dilution of the gas at the level of the closed enclosure, Gd, showed a variable evolution depending on the position in the plan of the detection devices as follows: The gradient of dispersion and progressive dilution of the gas at the level of the enclosure, Gd, showed reduced values at the level of the detection devices located in points 2 and 4 being 1.143 and 1.571 % Vol./h respectively; The gradient of dispersion and progressive dilution of the gas at the level of the premises, Gd, showed average values at the level of the detection device located at point 3, being 1.999 % Vol./h; The gradient of dispersion and progressive dilution of the gas at the level of the premises, Gd, presented a high value at the level of the detection device located at point 1, being 2.333 % Vol./h; The gradient of dispersion and progressive dilution of the gas at the level of the premises, Gd, showed a very high value at the level of the detection devices located in points 5 and 6, being 2.875 and 2.749 % Vol./h respectively;

https://doi.org/10.5593/sgem2024/1.1/s03.36

• Explosive gas – methane, accumulated in the closed enclosure, presented a medium and uneven dilution and evacuation phenomenon relative to the geometric shape of the enclosure. The average ventilation time in relation to the indications of the detection devices and the shape of the enclosure was over 15 min. which gives methane a moderate capacity for total evacuation from closed enclosures.
From the modeling regarding the dispersion of explosive gases in the closed enclosure using methane CH4, the following observations emerge:
• The methane gas dispersion process in the closed enclosure was controlled in 18 points evenly distributed on three distinct levels, namely: Lower Level 1 consisting of 6 control points located at an elevation of 0.5 m from the hearth; Medium level 2 consists of 6 control points located at a height of 1.5 m from the hearth; The 3rd upper level consists of 6 control points located at a height of 3 m from the hearth.
• The dispersion process at lower level 1 is characterized by a variable evolution. Thus, a variation of the specific gas concentrations for the turbulent flow was found at control points 1b and 1e. Also, at the level of points 1a, 1c, 1d and 1f, a relatively homogeneous variation specific to a laminar flow was found;
• The dispersion process at the upper 3rd level is characterized by a variable evolution. Thus, a variation of gas concentrations at the level of all control points was found, specific to a regime close to laminar flow.
• The gradient of dispersion and progressive dilution of the gas at the level of the closed enclosure, Gd, showed a variable evolution depending on the plan position of the control points as follows: The gradient of dispersion and progressive dilution of the gas, Gd, at the lower level 1 showed values between 1.691 and 2.603 % Vol./h;
• The gradient of dispersion and progressive dilution of the gas, Gd, at the middle level 2 presented values between 1.816 and 2.203 % Vol./h;
• The gradient of dispersion and progressive dilution of the gas, Gd, at the upper 3rd level presented values between 1.909 and 1.989 % Vol./h;
• The concentration of methane gas is maximum in the source area, gradually decreases by dilution as it moves away from the source and becomes variable and reduced in the ceiling accumulation area. If methane gas were continuously introduced for a longer period, the atmosphere in the premises would be displaced starting from the ceiling towards the hearth.

REFERENCES

[1] Leverson N., A new approach to sistem safety engineering, MIT Press, Cambridge, M.A., 2002
[2] Bessis J., La probabilité et l'évaluation des risques, Masson, 1984.
[3] Laprie, J.C., Guide de la sûreté de fonctionnement. Editions Cépaduès, 1995.
[4] Popa N., Pintilie D., Darsy A., Enache C., Tudor D., Vasilescu G., Optimizing the degree of integrated security for technical infrastructures intended for storage of explosives for civil use, Mining Revue 2023, Petroșani.
[5] Rasmussen B., Hazard identification on plant functional modeling, Reliability Engineering and System Safety, vol. 55, no. 2, pp. 77-84, 1997.
[6] Reason J, Richards A., A system approach to organisational error. Ergonomics, vol. 38, nr. 8/1995, p. 1708-1721
[7] Richards A., Whetton C., Blast vibration course measurement - assessment – control. Eltham Vic 3095: TERROCK Consulting Engineers, 2005.

EVALUATION OF COMPUTER SIMULATION AND MODELING METHODS FOR BLASTING PROCESSES IN SURFACE MINES

PhD.Eng.-Ress. Bogdan Garaliu-Buşoi[1]
PhD.Eng. Gabriel Vasilescu[1]
PhD.Eng.-Ress. Claudius Popescu[2]
PhD.Eng.-Ress. Claudia-Raluca Ilici[2]
PhD.Eng.-Ress. Adina Păsculescu[2]

[1]National Institute for Research and Development in Mine Safety and Protection to Explosion – INSEMEX Petrosani, **Romania**

[2]University of Petrosani, **Romania**

ABSTRACT

The evaluation of computer simulation and modeling methods of pull processes carried out in open pit mines is a broad and complex topic, which involves the analysis and comparison of different techniques and tools used to simulate and model pull processes in quarries and open pit mines.

The importance of computer simulation and modeling of recovery processes plays a crucial role in optimizing resource extraction, reducing costs, minimizing environmental impact, and ensuring worker safety. These technologies make it possible to predict the effects of different blasting strategies and choose the most effective approach.

Evaluating simulation and modeling methods involves comparing their accuracy, efficiency, and applicability under different operating conditions. This includes:

- Compare simulation results with observed data to gauge how close the simulations are to reality.
- The balance between detail and accuracy of the model and the need for it to be simple enough to be used effectively.
- Evaluate the resources required to run the simulations, including hardware costs and compute time.

Finally, the evaluation of simulation and modeling methods is also based on their applicability in real projects. Case studies and best practice examples highlight how these technologies have been used to solve specific problems in mining operations, such as optimizing explosion design, reducing induced vibration, improving rock fragmentation, and minimizing environmental impact.

Computer simulation and modeling of pull processes in open-pit mining operations are essential for optimizing mining operations. Evaluating and choosing the right method depends on several factors, including the type of mine, geological features, project objectives, and available resources.

Keywords: Simulation, Computer Modeling, Filming, Surface Mining, Optimization

INTRODUCTION

Blasting is a critical operation in surface mining that has a significant impact on the efficiency and safety of the mining process. It involves the use of explosives to break up rock formations, allowing for efficient mineral extraction. Optimizing blasting operations

https://doi.org/10.5593/sgem2024/1.1/s03.37

can lead to reduced operating costs, minimized environmental impact, and improved resource recovery. Given the complexity and variability of geological conditions, computer simulation and modelling have emerged as vital tools for predicting and improving explosion outcomes. These technologies allow for the analysis of numerous variables, including rock properties, types of explosives, and explosion design parameters, providing a detailed understanding of the effects of different blasting strategies.

Despite technological advances, the challenge remains to accurately simulate and model the pulling process in surface mining to optimize results. Traditional approaches often fail to predict the complex interactions between explosive energy and rock mechanics, leading to inefficient resource extraction and potential safety risks. This paper addresses the need for a comprehensive evaluation of current computer simulation and modeling methods to identify areas for improvement and integration into practical mining operations.

This paper aims to:

1. Evaluation of the accuracy and reliability of existing simulation tools and computer models used in surface mining blasting operations.

2. Identify the key factors influencing the effectiveness of these models in predicting explosion outcomes.

3. Explore the potential of integrating new computational techniques, such as machine learning and real-time data analysis, to improve the predictive capabilities of blasting patterns.

4. Propose recommendations to improve the design and implementation of the model in the real-world mining environment.

This paper will focus on evaluating current simulation methods and computer models specifically used for blasting in open-pit mines. The analysis will be limited to models simulating rock breakage and immediate explosion results (e.g. fragmentation, displacement, and vibration). In addition, the paper will only consider those technologies that have been widely adopted or that have demonstrated potential in academic research over the past decade. The ultimate goal is to provide actionable information that can be applied to modern mining operations to improve efficiency and safety.[1]

LITERATURE REVIEW

The literature on simulation and computer modeling of pull processes in surface mining is extensive, with several studies highlighting the evolution of these technologies. Early research focused mainly on empirical analysis of explosion results, which gradually shifted to more sophisticated numerical and computational models. For example, the because-Ram model, developed in the 1980s, was a pioneering effort in predicting rock fragmentation by integrating rock properties and explosion design parameters. More recent advances have seen the integration of 3D imaging and laser scanning technologies to capture pre-explosion rock formation features, improving the accuracy of models such as the Swebrec feature.
Studies also explored the use of finite element methods (FEMs) and discrete element methods (DEMs) to simulate the stress waves generated by explosions and the resulting rock rupture patterns.

The role of machine learning in blasting simulations has gained traction, with researchers applying these techniques to predict outcomes based on historical data. These models are able to identify complex patterns and relationships that traditional models might overlook, potentially providing predictions for optimal explosion patterns under different conditions.

Although considerable progress has been made in the simulation and modelling of blasting operations, several gaps remain in the literature. One significant area is the lack of integration between different types of models.

Another delay is in the real-time application of simulations. Most of the current models are used for planning and are based on pre-explosion static data. Dynamic modeling that incorporates changes that occur during the blasting process (such as unexpected changes in rock properties or explosive behavior) is still in its early stages. This limits operators' ability to make real-time adjustments that could optimize the results of the blasting job.

In addition, more empirical validation of simulation models is needed. Many models are tested under controlled conditions or in simulated environments, which may not accurately reflect the complex and unpredictable nature of real mining operations. This discrepancy raises questions about the practical applicability and reliability of simulation results in real-world scenarios.

This analysis highlights the importance of advancing simulation technologies not only to improve predictive accuracy, but also to bridge the gap between theoretical models and real-time practical applications in surface mining operations.

METHODOLOGIES

The paper uses a combination of industry-standard software and custom simulation tools to model recovery processes in surface mining. Key software includes [2]:

- BlastManager is a comprehensive software package for managing and processing data in explosion design, offering multiple functions tailored to the specific needs of engineers and project managers in the mining industry. Here are some of the key features and capabilities of the software:

- It allows the creation, modification and deletion of projects, providing the ability to manage detailed information about the client, careers and managers of the blasting work.

- It integrates a comprehensive database for clients, careers/sites, staff, and other relevant data, making it easy to organize and quickly access information.

- An intuitive and easy-to-use interface (GUI) that displays projects and their details in a tree structure, simplifying navigation and data management.

- The software provides advanced data import and export features, including the ability to import and export explosion databases in CSV format, as well as integration with other software via direct links.

- It includes options for data backup and security, ensuring the protection and integrity of the information you manage.

- It includes regression analysis functions to predict the impact of vibrations caused by explosions, which is critical for the safe planning of blasting work near sensitive areas.

- Compatible with various external tools and software, it facilitates an integrated and efficient workflow.

These features are designed to improve efficiency in explosion planning and execution, providing users with detailed control and clear visualization of explosion designs.

https://doi.org/10.5593/sgem2024/1.1/s03.37

• QuarryX facilitates the creation of detonation plans, the selection of explosive materials, and the calculation of detonation delays and sequence in several essential ways:

1. Detonation planning and design: Users can enter drill hole specifications and adjust their placement within the project. QuarryX allows for detailed planning of each well, including depth, angle, and diameter, providing a solid foundation for all subsequent explosive loading activities.

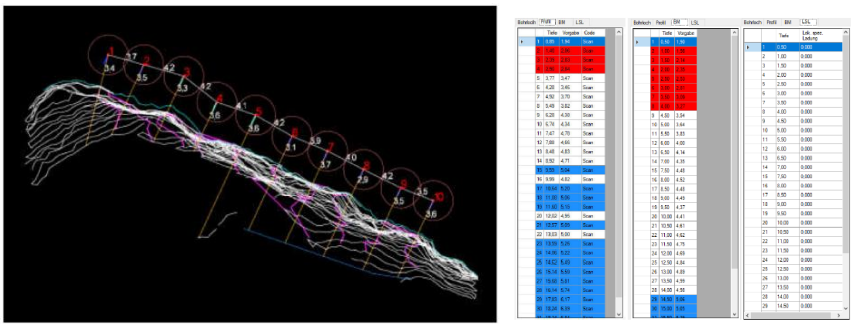


Figure 1. Position of holes on the 3D model

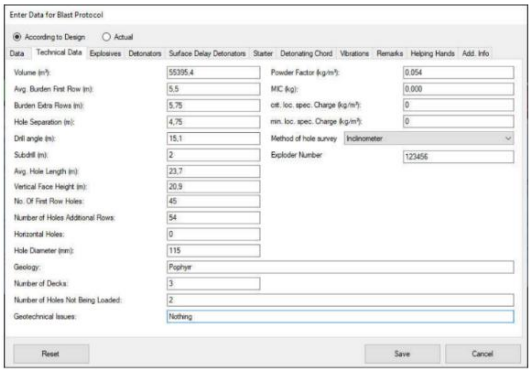


Figure 2. Blasting Hole Specifications

2. Explosives Selection and Management: The software includes a detailed database with different types of explosives and detonators, which can be selected according to the specific needs of each project. Users can configure the types of explosives and their quantities for each well, ensuring efficient use of resources and compliance with safety regulations.

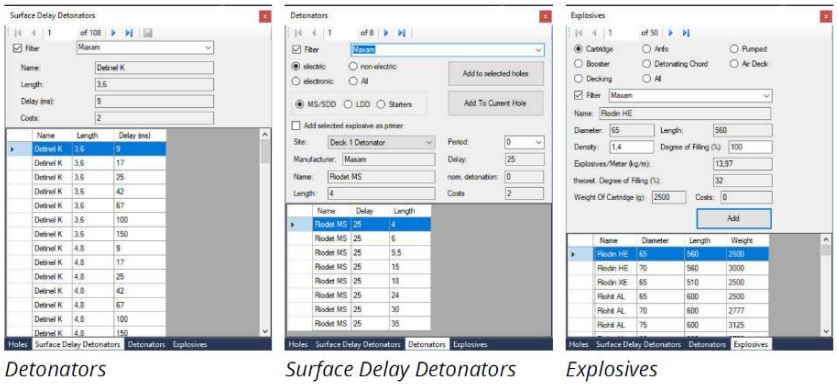


Figure 3. Database of explosive materials used in blasting

3. Calculation and Delay Planning: QuarryX provides advanced functionality for detonation sequence planning, including selecting and configuring delays between different sets of explosions. This makes it possible to optimize the detachment of rocks

and minimize induced vibrations, which are essential for the protection of adjacent structures and the environment.

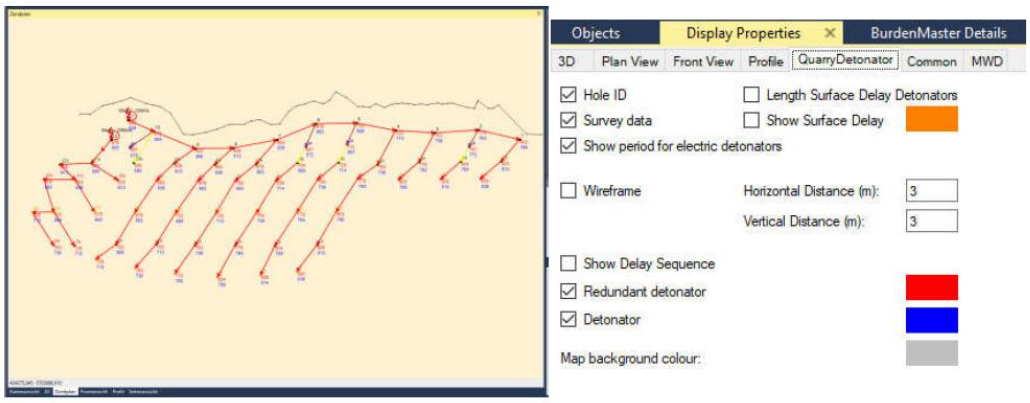


Figure 4. Blasting Pattern

4. 3D visualization and simulation: The software allows users to visualize and simulate detonation plans in an interactive 3D environment, providing a clear understanding of how planned detonations will affect the work environment. This includes assessing the distribution of explosives and their potential effects, as well as verifying the correctness of planned detonation sequences.

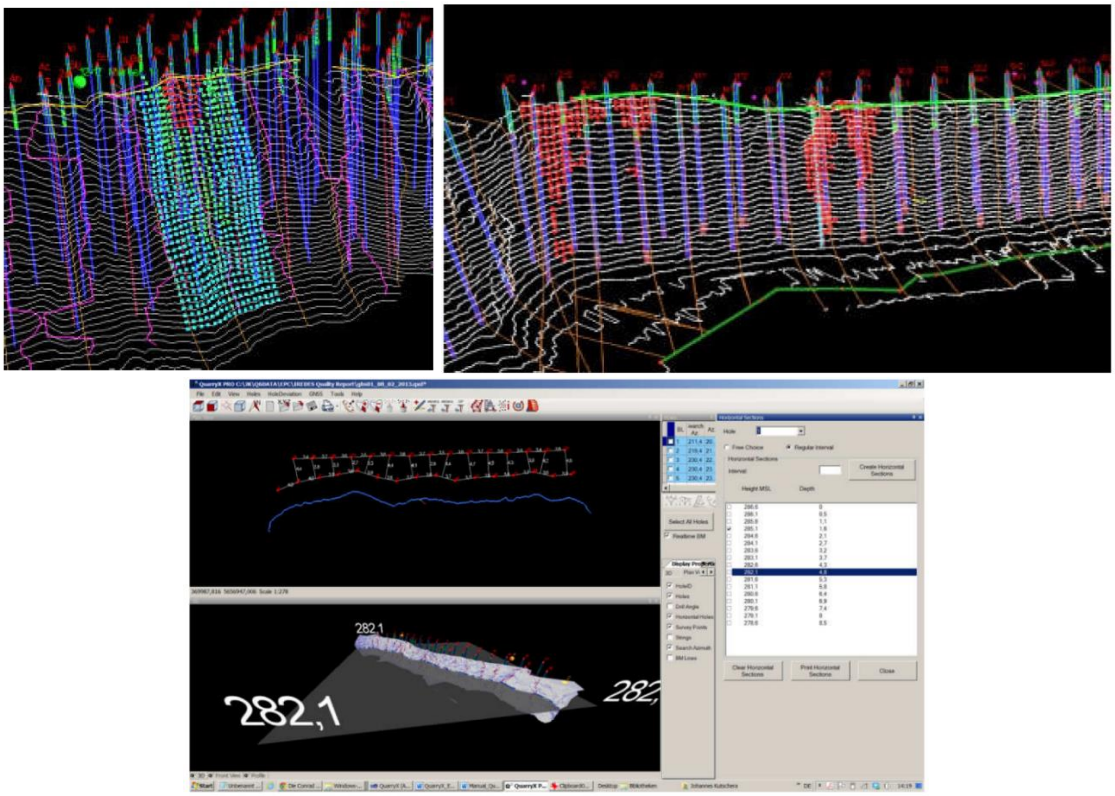


Figure 5. 3D simulation of the planned model

These features are integrated into an easy-to-use module that not only streamlines the explosion planning process, but also provides greater accuracy, reducing the risks associated with detonation operations.

https://doi.org/10.5593/sgem2024/1.1/s03.37

QuarryX software uses topographic and geological data in several essential ways to optimize detonations. QuarryX allows you to import topographic data in the form of XYZ, LAS, or other supported formats. This data is used to model the quarry surface in 3D, providing an accurate representation of the relief and other topographic features. This helps to accurately plan the locations of the drill holes and align them with the geological structure.
Using topographic data, the software is able to calculate the distances and heights needed to properly position the drills, avoiding overloading or underloading certain areas. It also analyzes the profile and cross-sections of the quarry to determine the most effective way to conduct the explosion.
Based on the 3D model, QuarryX is able to optimize the placement of explosives based on geological and topographical conditions. The software uses advanced algorithms to determine the ideal distribution of explosives, thereby minimizing the risk of excessive or insufficient rock fragmentation.
Using topographic and geological data, QuarryX is able to simulate different detonation scenarios to see their effects before actually implementing them. This includes predictions of vibration and rock dispersion, helping to prevent damage to nearby equipment or structures.

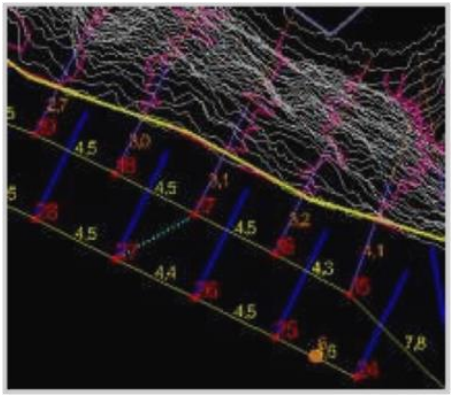


Figure 6. Simulation of the blasting scenario

By efficiently integrating and utilizing topographic and geological data, QuarryX ensures precise planning and optimal execution of blast work, helping to streamline the mining process and reduce associated costs.
QuarryX software processes the data generated by vibration, pressure, and other relevant measurement sensors in the following ways:

- allows the import of data from seismographs (vibration sensors) and other types of sensors that measure parameters relevant to detonations. This also includes managing the positions for the seismographs and the specific parameters of each measuring device.

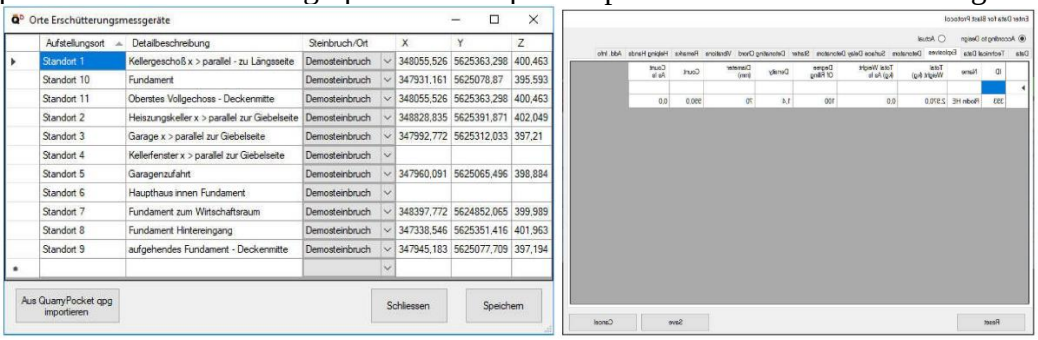


Figure 7. Database with the location of seismographs on site

- The software includes features for viewing and analyzing the vibration data collected. Users can input vibration measurement results directly into the software to assess the impact of detonations on the environment. It also allows data to be loaded directly from the log files of specified measuring devices, thus facilitating quick and efficient data integration into post-detonation assessments.

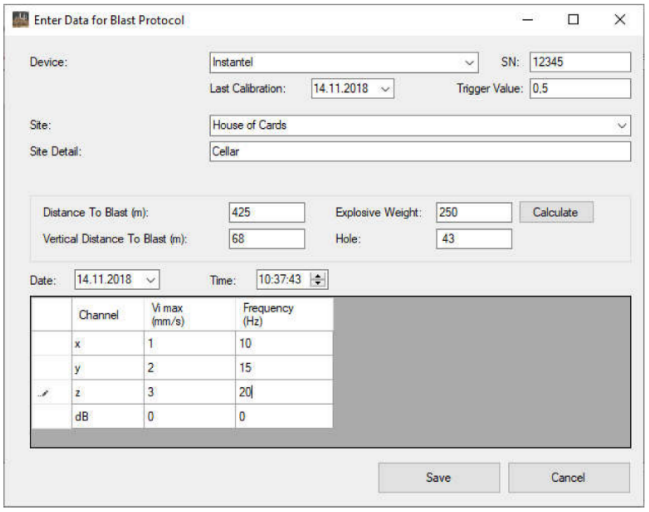


Figure 8. Input of data recorded by seismographs

- QuarryX enables the creation of detailed reports that include vibration and pressure data, providing complete documentation of each detonation. These reports can be used to demonstrate compliance with legal regulations and to ensure that detonations do not exceed the safety limits set for vibration and other impacts.
- By analyzing vibration and pressure data, QuarryX can help adjust detonation parameters to minimize impact on nearby structures and the environment. This includes adjusting the detonation sequence, the amount of explosive used, and the configuration of the wells. These capabilities highlight how QuarryX integrates and processes sensory data to improve the safety and efficiency of blasting operations.

DISCUSSION

The results of the simulations and modeling efforts in this paper provide compelling evidence that advanced computational techniques can significantly improve the accuracy and efficiency of pulling operations in surface mining. The integration of FEM and DEM allowed for a deeper understanding of the physics behind rock breaking, allowing for more accurate predictions of explosion outcomes. The application of machine learning further enhances this by using historical data to refine forecasts and dynamically adapt to changes in blasting conditions [3,4].

The successful application of advanced simulation and modeling techniques to tensile processes in surface mines reflects a significant technological leap forward. The findings highlight a paradigm shift from traditional, experience-based approaches to more predictive, data-driven methodologies. In a broader context, this transition aims not only to increase operational efficiency, but also to instill more science-based resource management. These technologies facilitate a deeper understanding of the interaction between explosives and rock formations, thus enabling more precise engineering decisions.

https://doi.org/10.5593/sgem2024/1.1/s03.37

In terms of broader goals, this paper contributes to sustainable mining practices. By optimizing recovery processes, we can minimize the waste of resources and reduce the environmental impact of mining operations. Accurate explosion simulations help achieve better fragmentation, reducing the need for secondary breakdowns, which in turn reduces energy consumption and wear and tear on the machine.
The comprehensive approach, which uses a combination of traditional simulation tools and modern data-driven models, illustrates the evolution of blasting simulations from purely empirical methods to more integrated predictive analytics. This change not only improves the accuracy of the models, but also supports a more holistic view of the blasting process, considering both the immediate physical effects and the subsequent operational impact.
In summary, while the results of this paper are promising and indicate a significant improvement in blasting operations, the transition to a fully predictive and optimized blasting process is complex and requires not only technological solutions but also organizational and cultural changes in the mining industry.

CONCLUSION

This work successfully demonstrated the effectiveness of integrating advanced computer simulation and modelling techniques into surface mining recovery processes.
Developing methods to incorporate real-time data into simulations could significantly increase the adaptability of blasting operations to changing conditions. Research into using sensors and IoT technology to feed real-time data into simulation models would be a promising direction.
Expanding datasets to include a wider range of geological conditions can improve model generalization. Studies should aim to apply these advanced simulations in different mining environments to validate their effectiveness in different rock types and mining conditions.
Further research should also be directed towards the development of models that can simultaneously predict the environmental impact of filming work, such as vibration, noise and dust dispersion. This would help create more environmentally friendly blasting practices.
It would be helpful to conduct a detailed economic analysis of the implementation of advanced simulation technologies in mining operations. Such studies would help justify investments in technology from a cost-benefit point of view and encourage wider adoption in industry.
Finally, there is a crucial need to develop effective training programs and implementation strategies to ensure that mining personnel can make appropriate use of these advanced technologies. Finding educational methods and tools that facilitate the integration of simulation technologies into day-to-day mining operations could have a significant impact on their success and acceptance.
By addressing these areas, future research can continue to increase the accuracy and effectiveness of blasting operations, paving the way for smarter, safer, and more sustainable mining practices.

REFERENCES

[1] Brown, L. (2021). Integration of machine learning with traditional blasting simulation. In Proceedings of the International Conference on Mining Innovation (pp. 204-210). Mining Innovation Press.

[2] Data Management and Processing for Shot Blasting Design – User Manual, Rev.G of 12.07.2018, Software Version: 2.4.8.36

[3] Wang, H., Zhang, Y., & Kumar, S. (2022). Real-Time Data Integration in Mining: Challenges and Solutions. Mining Operations Research, 45(4), 300-320.

[4]Tran, A., Lee, V. & Chou, P. (2019). Use of FEM/DEM in the prediction of rock breakage patterns. International Journal of Rock Mechanics and Mining Sciences, 66, 205-213.

https://doi.org/10.5593/sgem2024/1.1/s03.37

EVALUATION OF THE WEAR OF THE CARRYING ROLLERS OF BELT CONVEYORS

Assoc. Prof. M.Sc. Lubomir Ambrisko, PhD.[1]
M.Sc. Dusan Kubala, PhD.[1]
M.Sc. Lucia Cabanikova[1]
M.Sc. Marek Ondov[1]

[1]Technical University of Kosice, Faculty of Mining, Ecology, Process Control and Geotechnologies, **Slovakia**

ABSTRACT

The basic structural and functional element of a belt conveyor is the conveyor belt, which is supported by carrying rollers. Research in this area is important for increasing the service life of mining belt conveyor components. The rollers are subject to various forms of wear. Tribological interactions between the roller, the conveyor belt, and the particles of the transported material or impurities from the environment that enter the tribological system cause various forms of mechanical wear. Abrasion is the predominant type of wear for a given friction node. Abrasive wear causes tearing and cutting of the surface of the rollers. Moreover, they are also subject to chemical wear, namely corrosion of the damaged steel shells of the rollers. The combination of the individual types of wear led to damage that affected the thickness of the roller shell and its basic mechanical property, namely Vickers hardness. In this paper, non-destructive testing methods were applied, while the hardness was determined by the UCI (Ultrasonic Contact Impedance) method and the shell thickness was determined by the ultrasonic method.

Keywords: wear, belt conveyor, rollers, hardness

INTRODUCTION

Belt conveyors rank among the most frequently used conveyance systems that are used in various industries (mining, metallurgy, mechanical engineering, civil engineering, agriculture and power engineering). The advancement of their design is very fast, especially in terms of their performance, and they are applied in various types of operational conditions. The applications of belt conveyors cover a wide spectrum of industries, as well as the fields of service provision. In the mining industry, belt conveyors are used for the linear transport of mineral raw materials (coal, rock and other mineral raw materials) [1].

The structural elements of a belt conveyor (head pulley, tail pulley, take-up pulley, carrying rollers, conveyor belt, supplementary and protective devices) are carried by the carrying structure. The carrying structure of the belt conveyor carries all mechanical parts and forms the belt conveyor route. The carrying structure is comprised of the stands, longitudinal supports, roller sets and carrying rollers. Roller sets support the upper and lower parts of the conveyor belt. A roller set is comprised of a carrying support and carrying rollers. The individual parts of a roller are shown in Fig. 1.

https://doi.org/10.5593/sgem2024/1.1/s03.38

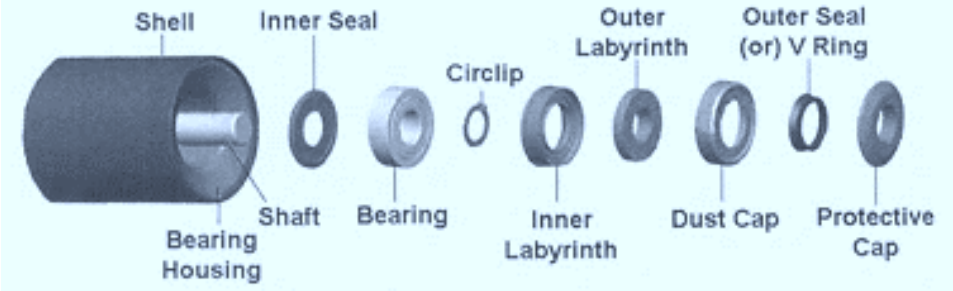


Fig. 1 Components of a roller [2]

The carrying support as a part of a roller set may be of various arrangements, depending on its function. The types of the carrying support are as follows [1]:

a) Upper support – supporting the upper rollers; depending on the number of rollers, it may be a one-roller, two-roller, three-roller or a multi-roller support;
b) Lower support – supporting the lower rollers; typically, it consists of a single roller, and in some cases, it may consist of two rollers.

Carrying rollers conduct and support the upper and the lower branches of the conveyor belt. They are embedded in carrying the roller sets and constitute the crucial part of the mechanical components of the belt conveyor. From the operational point of view, the rollers are expected to exhibit high reliability, minimum resistances to motion, as well as a long service life.

Wear, i.e. a process of the loss of material from the surface of one or both contact surfaces of solid objects, occurs during any type of their relative motion. This degradation process is defined as a permanent undesired change in the surface (changes in its size and shape and/or material changes in the surface areas) that is caused by interactions between the functional surface(s) and the material subjected to wear. It is manifested as a removal or displacement of particles from the surface that is worn as a result of mechanical effects. This process may also be accompanied by other effects (e.g. chemical, electrochemical, and electric) [3]. The wear primarily applies to solid objects. Analysis of friction and wear of solid objects should be based on a reduced tribological system which includes the primary friction object, the secondary friction object and the surrounding environment [4].

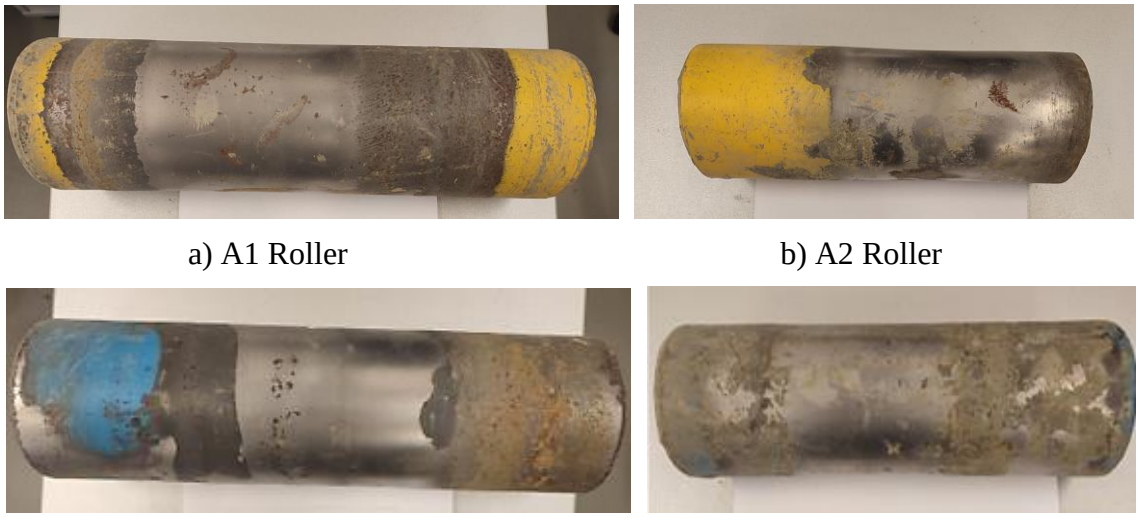
Wear may manifest itself in different forms, depending on the surface topography and the contact conditions in the environment. In general, it may be stated that there are two basic wear mechanisms – mechanical and chemical. Mechanical wear includes the processes that may cause adhesion, abrasion, erosion, cavitation, and fatigue. Chemical wear (triboxidation, tribocorrosion) is caused by the reactive components attacking the surface and by separating the products of the wearing process as a result of mechanical forces. If two surfaces contact each other, the actual contact area is significantly smaller as the surfaces, with a certain roughness, only contact each other on their protruding parts. The pressures in those areas are high and the material surface is subjected to deformation caused by the applied load; as a result, the size of the contact area increases. Changes in the surfaces of the friction pair is caused by deformation, an increased temperature and the chemical effects of the surrounding environment. The wearing process includes a set of adhesion, abrasion, and diffusion processes, as well as chemical processes [4].

Carrying rollers are exposed to strong wear due to a permanent contact with the conveyor belt and heavy transported materials [5]. This may lead to failures, such as non-coaxiality, wear of the shell, damage to the rollers, or structural deformation [6]. The rollers are usually exposed to harsh environments (dust, heat and moist), which may accelerate the degradation of components and increase the probability of failures [7].

As a result of the wear, the function of the rollers deteriorates; this may eventually lead to early decommissioning or a failure of the rollers. The purpose of this paper is to identify the wear of the smooth carrying rollers without the lining.

EXPERIMENTAL PART

The smooth carrying rollers (Fig. 2) were previously installed in belt conveyors used in a quarry to transport crushed aggregates as part of a picking roller. This specialised in-line troughing roller was furnished with a long roller and two shorter rollers (Fig. 3). The dimensions of the examined rollers are listed in Table 1. A1 and A2 Rollers were taken from a different conveyor than B1 and B2 Rollers. A1 and B1 were long horizontal rollers, while A2 and B2 were shorter inclined rollers.



a) A1 Roller b) A2 Roller

c) B1 Roller d) B2 Roller

Fig. 2 Carrying rollers subjected to the examination

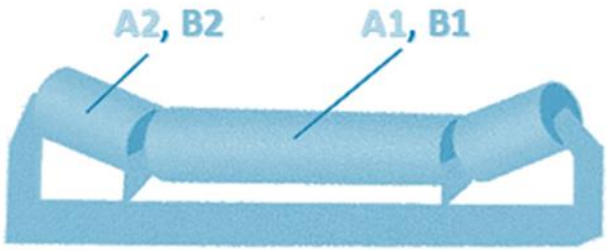


Fig. 3 Scheme of the placement of the examined rollers in the carrying roller set

https://doi.org/10.5593/sgem2024/1.1/s03.38

Tab. 1 Roller dimensions

Roller	A1	A2	B1	B2
Length [mm]	370	250	370	250
Diameter [mm]	108	87	107	88

PeakTech 5225 (Fig. 4), an ultrasonic coating and material thickness meter, was used to measure the thickness of the steel shells of the rollers. The device uses the speed of sound to measure the thickness of a majority of materials that conduct sound waves. They include, for example, metal, glass, plastic, ceramics and others. In addition to the high resolution (0.1 mm), the device also includes a self-calibration function. It has 2 sensors for different material thicknesses, facilitating measurements ranging from 1 mm to 300 mm at a sound frequency of 5 MHz [8].

For the purpose of measuring the thickness, the measurement area was treated by applying a bonding material (gel) to ensure the bonds between the sensor and the measured material.



Fig. 4 PeakTech 5225 meter



Fig. 1 MicroDur II hardness tester

Hardness of the belt conveyor rollers was identified using MicroDur II (Fig. 5). MicroDur II is a portable hardness tester that is used for non-destructive measurement of metal components [9]. Hardness is measured by applying the Ultrasonic Contact Impedance (UCI) method. The hardness testing process was carried out with the use of the Vickers diamond intender on a self-resonant probe. When pressed against the test probe, the impact frequency decreases depending on the surface hardness and the module of elasticity of the tested material and the contact surface. Based on the frequency characteristics of the material, the hardness of the surface may be identified [10]. MicroDur II hardness tester works without damaging the material. With regard to the small penetration depth of the diamond tip, this hardness test is also suitable for components with hardened surfaces.

RESULTS AND DISCUSSION

Wear of carrying rollers

In the analysis of wear of the carrying rollers, the friction process was divided into 3 stages: (i) interactions between the surfaces during the friction; (ii) changes occurring in the surface layer of the elements of the friction pair; and (iii) disruption of the surfaces – the steel shells.

The three stages above overlapped, while the interactions between the surfaces were changing throughout their relative motion. Surface disruption is the final stage of those effects; however, it does not necessarily have to be bound to the whole working surface

of the friction pair as the other parts are subject to physical and chemical changes. Wear was evaluated using primarily the parameters that directly determine the wear. Such parameters are identified either on the basis of the values obtained by the measurement of the undesired loss of material from its surface, or on the basis of the properties, condition and function of the worn components [11].
During their use, the carrying rollers of belt conveyors are subject to various forms of wear which affects their functionality.

Adhesive wear of the rollers

The friction and wear processes that run on the surface of the rollers caused the disruption of the surface layers and the degradation of the shell, which resulted in the deterioration of the functional properties of the carrying roller set. The manifestations of adhesive wear were accompanied by corrosion, while the damaged surfaces also exhibited the effects of abrasion by the separated products of wear (Fig. 6). Moreover, there were also visible signs of (gradual) combination of different types of wear.



a) B2 Roller b) B1 Roller c) A2 Roller

Fig. 6 Wear of the carrying rollers (1 – adhesive; 2 – abrasive; 3 – corrosive)

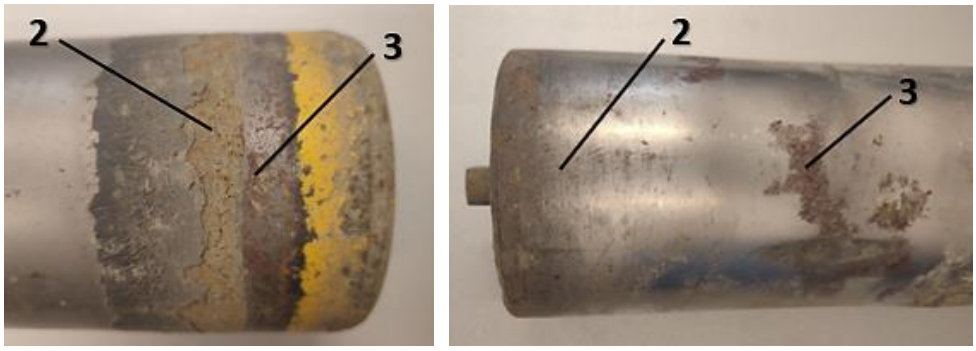
Adhesive wear is attributed to the fact that the contact surfaces are never smooth and they are never in contact across the entire surface, but on plenty of contact points. During the relative motion of the functional surfaces, those surfaces contacted each other, and their surface layers were disrupted. That led to the transfer of the material from one surface to another, while the individual particles were released and torn off. Seizing is an intensive form of adhesive effects, while a fine adhesive abrasion is a typical manifestation of damage [12], as was observed on B2, B1 and A2 (Fig. 6).

Abrasive wear of the rollers

Abrasive wear is one of the intensive processes of material degradation and is caused by the impact of hard, mostly mineral particles. In the process, particles of the material are separated and displaced [11]. Abrasive wear of the rollers is induced by the presence of hard particles (of the transported material as well as separated particles [13]) and/or particles from the surrounding environment formed between the rollers and the conveyor belt; it is a three-body abrasion caused by the tribological interactions between the objects.

Abrasive wear is characterised by disintegration of and damage to the functional surface of the roller that becomes worn due to the grooves and cuts (Fig. 6c and 7) made by the particles formed during the surface disintegration.

https://doi.org/10.5593/sgem2024/1.1/s03.38



a) A1 Roller b) A2 Roller

Fig. 7 Wear manifestations on the rollers (2 – abrasive, 3 – corrosive)

Abrasive wear may also develop from other types of wear (e.g. adhesive) that cause the formation of free particles. They are usually harder than the base material – either due to intensive plastic deformation, or due to oxidation by air oxygen [4]. The damaged surface of the steel shell is more susceptible to corrosive damage (Fig. 7). The rate of abrasive wear may be reduced by increasing the hardness of the rollers – the particles will not be pushed so deep into the surface and the grooves will be shallower.

Corrosive wear of the rollers

Corrosive wear occurs very frequently in practice, especially if friction pairs work in active environments. There are several mechanisms of environmental interactions: a) in friction without lubrication, the contact surfaces are attacked by oxygen from the air; b) in friction with lubrication, this type of wear may occur if the lubricant contains residual quantities of anti-seize additives that reduce the wear. The intensity of that process depends on materials of the friction pair and on their corrosion resistance [4]. All of the tested rollers exhibited corrosive wear (Fig. 6–8). A1, B1 and B2 Rollers exhibited more extensive wear, while A2 Roller exhibited less extensive corrosive damage.



a) A1 Roller b) B2 Roller

Fig. 8 Corrosive wear of the tested rollers

Thickness of the carrying rollers

The thicknesses of the carrying rollers of belt conveyors, which were measured using the PeakTech 5225 thickness meter, are listed in Table 2. The thickness of each roller was measured in 5 points evenly distributed across the surface of the steel shell. The

largest thicknesses were observed for B1 Roller, while the smallest ones were observed for A1 Roller. A2 and B2 Rollers exhibited comparable thicknesses.

Tab. 2 Measured thicknesses of the roller shells

Roller Thickness [mm]	A1	B1	A2	B2
1. Measurement	2.45	3.05	2.68	2.75
2. Measurement	2.37	2.90	2.72	2.80
3. Measurement	2.47	3.10	2.85	2.38
4. Measurement	2.65	2.84	2.52	2.68
5. Measurement	2.48	3.00	2.63	2.50
Mean	*2.48*	*2.98*	*2.68*	*2.62*

Vickers hardness of the carrying rollers

The measured values of Vickers hardness of the steel shells (Table 3) of the examined carrying rollers ranged, on average, from 115 to 154. Due to the development of the individual types of wear on the shell surfaces, their original material properties changed – in particular, their hardness. The highest hardness was observed for B1 Roller, while the lowest hardness was observed for A2 Roller.

Tab. 3 Vickers hardness (HV) values of the roller shells

Roller HV	A1	B1	A2	B2
1. Measurement	135	158	115	106
2. Measurement	109	149	112	133
3. Measurement	108	130	112	136
4. Measurement	125	126	112	146
5. Measurement	135	147	118	135
6. Measurement	138	168	94	129
7. Measurement	133	169	127	159
8. Measurement	113	165	95	127
9. Measurement	128	167	142	141
10. Measurement	133	164	126	142
Mean	*125.7*	*154.3*	*115.3*	*135.4*

CONCLUSION

Properly functioning carrying rollers are important parts of belt conveyors. During their use, they are subjected to various types of wear. The manifestations of their wear are determined by (i) the form of changes in the sizes and shapes of the surface areas of the rollers (deformation, hardening, softening, disintegration, displacement etc.); and (ii) the form of material changes of the surface areas of the rollers (absorption, diffusion, triboxidation, tribocorrosion etc.). The examined quantitative parameters, in particular the differences in the thicknesses of the rollers, the measured values of Vickers hardness, and the extent of the surface wear, indicated more extensive wear of the horizontal rollers, which are exposed to considerable loading as they are permanently in contact with the conveyor belt and heavy loads. In this regard, there are certain methods

https://doi.org/10.5593/sgem2024/1.1/s03.38

how to eliminate mechanical and chemical wear of those multiple components of belt conveyors. The methods that facilitate increasing the wear resistance of rollers also include reduction of the loading they are exposed to or the utilisation of harder shells.

ACKNOWLEDGEMENTS

This work was supported by the Slovak Research and Development Agency - contract No. SK-PL-23-0052 and from projects KEGA 013TUKE-4/2023 and VEGA 1/0728/24.

REFERENCES

[1] Grincova A., Andrejiova M., Marasova D., Measuring and comparative analysis of the interaction between the dynamic impact loading of the conveyor belt and the supporting system, Measurement, vol. 59, pp 184-191, 2015.

[2] Subba Rao D.V., The belt conveyor, A concise basic course, Boca Raton: CRC Press, Taylor & Francis Group, 2021, 168 p.

[3] Wear and wear resistant materials, [cit. 2023-12-10]. Available online: http://mtfdca.szm.com/subory/wear.pdf

[4] Tribological testing of materials, [cit. 2023-12-10]. Available online: https://www.engineering.sk/strojarstvo-extra/16293-tribologicke-skusky-materialov

[5] Alharbi F., Luo S., Zhang H., Shaukat K., Yang G., Wheeler C.A., Chen Z., A brief review of acoustic and vibration signal-based fault detection for belt conveyor idlers using machine learning models, Sensors, vol. 23/issue 4, pp 1-33, 2023.

[6] Dabek P., Krot P., Wodecki J., Zimroz P., Szrek, J., Zimroz, R., Measurement of idlers rotation speed in belt conveyors based on image data analysis for diagnostic purposes, Measurement, vol. 202, pp. 1-15, 2022.

[7] Morales A.S., Aqueveque P.E., Henriquez J.A., Saavedra, F., Wiechmann E.P., A technology review of idler condition based monitoring systems for critical overland conveyors in open-pit mining applications, Proceedings of the 2017 IEEE Industry Applications Society Annual Meeting, Cincinnati, OH, USA, 2017, 1-5, pp 1-8.

[8] PeakTech Ultrasonic Thickness Meter Manual 5225, [cit. 2024-01-10]. Available online: https://sk.manuals.plus/peaktech/5225-ultrasonic-thickness-meter-manual

[9] Mihalikova M., Ambrisko L., Pesek L., Videoextensometric measuring of deformation processes in automotive steel sheets at two strain rate levels, Kovove Materialy – Metallic Materials, vol. 49/issue 2, pp 137-141, 2011.

[10] Measuring instruments and systems, [cit. 2024-01-20]. Available online: https:// www.natis.cz/tvrdomery/prenosny-digitalni-tvrdomer-alphadur-ii/det/6/41/70/2/ 791/0

[11] Peťková V., et al., Tribotechnics in theory and practice (in Slovak), Košice: Vienala, Slovakia, 2012, 366 p.

[12] Helebrant F., Ziegler J., Marasova D., Technical diagnostics and reliability, I. Tribodiagnostics (in Czech), Ostrava: VŠB-TU, 2001, 178 p.

[13] Grincova A., Andrejiova M., Marasova D., Grendel P., Multicriterial assessment of the raw material transport, Acta Montanistica Slovaca, vol. 20/issue 1, pp 26-32, 2015.

GENESIS OF THE ERVA Pb–Zn DEPOSIT KAYSERI (YAHYALI): MINERALOGY AND TRACE ELEMENT GEOCHEMISTRY

Ozge Ozer Atakoglu[1]

Prof. Dr. Mustafa Gurhan Yalcin[1]

[1] University of Akdeniz, Department of Geological Engineering, **Türkiye**

ABSTRACT

As nonferrous metals, lead zinc is the most widely used ore after aluminum and copper. Considering the increasing demands in industry, it is understood that a sustainable mine supply is necessary to meet the Pb-Zn. In this context, the geochemical characteristics of the Erva lead zinc deposit in Yahyali (Kayseri) district were tried to be revealed. The study area, Yahyali district, is located in the Southeast of the Central Anatolia Region. The geological unit in which the Erva is located is the Yahyali Munzur Nappe, which tectonically overlies the Feke sequence. In this study, XRF (X Ray Fluorescence Spectrometry) and XRD (X-Ray Diffraction Analysis) geochemical analyzes were carried out in order to understand the lead zinc ore metal source. As a result of the XRF analysis, the average ZnO and PbO grade values (in %) were found as follows: 7.85 and 4.33. According to the XRD results, the mineral paragenesis that forms the ore is as follows: Galena, Cerussite, Smithsonite, Quartz, Gypsum, Hematite, Goethite, Anglesite, Kaolinite, Montmorillonite. Mineralization occurring in the region where geologically young formation aged rocks are present is not seen among large karst cavities. Instead, mineralization in the form of geological fillings is observed in the capillary cracks of the carbonates within the Yahyali Munzur Nappe.

Keywords: zinc–lead deposit, trace element geochemistry, ore deposit genesis, Kayseri

INTRODUCTION

Lead, which is in the carbon group in the periodic table, and zinc, which is a transition metal in the periodic table are elements that occur together in mineral deposit formation [1]. Both metals have low melting temperature properties are easy to shape, making them suitable using for industry, chemistry, etc. This situation ensures that it is in increasing demand across sectors. Considering the crystallization stages of magma, it is known that lead and zinc elements are most enriched in the hydrothermal (±pneumatolytic) phase and form mineral deposits [2].

The formation of magmatic mineral deposits mainly occurs in two stages: early and late. Zinc disseminates in the orthomagmatic phase, where the temperature is 1500-800˚C in the early magmatic phase, and enters the rock-forming minerals at the ppm level. During the differentiation of magma, zinc is concentrated in the gas and solution phase. Zinc can be easily dissolved and transported in magmatic solutions with a temperature of 600˚C. While the mobility of zinc is high in superficial environmental conditions, the mobility of lead is low. The reason for this is that while zinc can pass into solution as 2^{+} ions during the decomposition of sulphide minerals, lead is released in the environment when the galena mineral turns into anglesite mineral [2].

https://doi.org/10.5593/sgem2024/1.1/s03.39

Lead-zinc deposits are formed by sedimentary, volcano-sedimentary, karstic, hydrothermal sedimentary and lateral segregation processes. In addition, zinc (-lead) deposits with low formation temperatures, which have no visible relationship with magmatic rocks and are observed as strata-bound or stratiform within carbonate rocks, are also called Mississippi and Alpine types [2].

As non-ferrous metals, they are the most commonly used ores after lead, zinc, aluminum and copper. Lead, which has a bluish-white color when cut, is a very malleable metal with the advantages of being soft and heavy. Zinc, which is generally found in silvery-blue gray colors, has a relatively low melting temperature and is a corrosion-resistant alloy metal. Similar physical conditions, such as precipitation conditions, as well as chemical conditions, such as being found with similar related minerals, enable lead and zinc to coexist in nature. Lead-zinc deposits may exist in sulfide, oxide or mixed/complex (sulphide oxide) states. While galena, cerussite and anglesite are the main lead minerals; Sphalerite, smithsonite and zincite are the main zinc minerals. The minerals most commonly used as sources for lead-zinc are galena and sphalerite [2].

In recent years, the demand for lead zinc ore in industry has increased greatly. For example: lead acid batteries, radiation shielding, brass and bronze alloys, galvanizing, etc. Due to its increasing use in many industrial areas, the need for lead and zinc has also increased. Among the mentioned sectors, 80% of lead consumption is caused by lead-acid batteries, while 50% of zinc is consumed by the galvanizing industry. Considering the increasing demands in industry. it is understood that a sustainable mine supply is necessary to meet the demand for lead and zinc. Current reserves of some metals are insufficient for the increasing demands in industry. Studies on mineral deposits rich in precious metals are of great importance in order to meet increasing demands. It is important to discover new mining areas around the world in order to meet the increasing demands of lead-zinc mineral, which has many uses.

The source of mineralization has been reported through various geochemical analyzes in the Chahmileh Pb-Zn production in Iran. Varying geochemical features were revealed through liquid sealing, stable isotope analysis and lead isotope analysis. The confined sulfur ore minerals of the deposit are pyrite, galena, sphalerite and chalcopyrite. Non-sulphide ore minerals are arranged as follows: chalcocite, covellite, cerussite, hemimorphite, malachite, azurite, hematite, goethite. The gang minerals of the deposit are as follows: dolomite, quartz, calcite and barite. It is mineralized in the form of veins, showing silicification and dolomitization. Due to the textural, geological, mineralogical and fluid properties of the deposit, the Chahmileh Pb-Zn deposit is interpreted to be carbonate Mississippi Valley Type [3].

The formation processes, origin and mineralization of the Yuanbaoshan Pb-Zn deposit located in Southern China have been interpreted by various geochemical analyses. Using Rb-Sr isotope age, LA-ICP-MS analysis, S isotope analysis and C-O isotope analysis, the origin of the deposit, dissolved carbon and oxygen were interpreted as mainly the dissolution of sedimentary carbonate [4].

In the study conducted on the Huize and Maoping lead-zinc deposits in Southwest China, the relationships between fault fold structures and ore deposit localization were revealed [5].

The Erva Pb-Zn deposit, which was selected as the study area, is located within the borders of Yahyalı district in Kayseri province, Turkey. There are many Pb-Zn mineralizations within the borders of Yahyalı district. In this study, XRF (X Ray Fluorescence Spectrometry) and XRD (X Ray Diffraction Analysis) geochemical analyzes were carried out in order to understand the lead-zinc ore metal source of the Erva Pb-Zn deposit. As a result of the analysis, the ore metal source will be interpreted. The formation type of the lead-zinc deposit will be deduced.

GEOLOGICAL SETTING

The geological unit in which the Erva pit is located is the Yahyali-Munzur nappe, which tectonically overlies the Feke sequence. The Aladag nappe is at the bottom, and the units at the top are as follows: Late Devonian-aged Gumusali Formation (Dg), Carboniferous-aged Bademli Formation (Cb). Cevizli Formation consists of limestones with quartzite interlayers. The formation, which was deposited in a shallow shelf environment, consists of three members and is listed from bottom to top as follows: Girvenella limestone (Pcg), Quartzite member (Pck), Yellice member (Pcy). Unconformably overlying these formations are the Jurassic-Cretaceous Camlık Formation (JKç) and the Late Senonian Karabogurtlen Formation (Kka). While the Camlik Formation consists of carbonates; The Karabogurtlen Formation consists of block-containing clastics. Tectonically, it is overlain by the Aladag nappe, Domuzdag nappe and Ophiolite nappe, which belong to the Yahyali Munzur nappes. Tectonically, the lowest unit is the Gulbahar Nappe. The Gulbahar Nappe consists of the Huglu unit and the Turunc unit. Turunc unit consists of the Orhaniye Formation (TRKO) containing Triassic-Cretaceous aged cherty limestone. The Domuzdag nappe, which is located on the Gulbahar Nappe, consists of the Dutdere Formation containing Triassic-Jurassic aged neritic limestones. Finally, the Ophiolite nappe tectonically overlies the Gulbahar Nappe and the Domuzdag Nappe. In the study area, there are Urgup Formation (Tmu), Sarıca Volcanics (Tmusr) and Catakdere Tuff (Tplç) as Tertiary Cover Rocks and Volcanics. In addition, the youngest members of the region are Quaternary aged Alluvium (Qal) and Slope debris and debris parcel (Qym) [6] (Figure 1).

MATERIALS AND METHODS

X-Ray diffraction analysis (XRD), X-ray Fluorescence (XRF) and ore microscopy geochemical analyzes were applied to 30 samples collected from the study area.

XRD analyzes were carried out on dehumidified powder samples ground below 75 microns to determine the mineralogical composition, using the "Bruker D8 Advance" model X-ray powder diffraction (XRPD) device at the ITU Department of Geology XRD Laboratory. XRD peak results of samples E39 and E53 are given in Figure 2.

https://doi.org/10.5593/sgem2024/1.1/s03.39

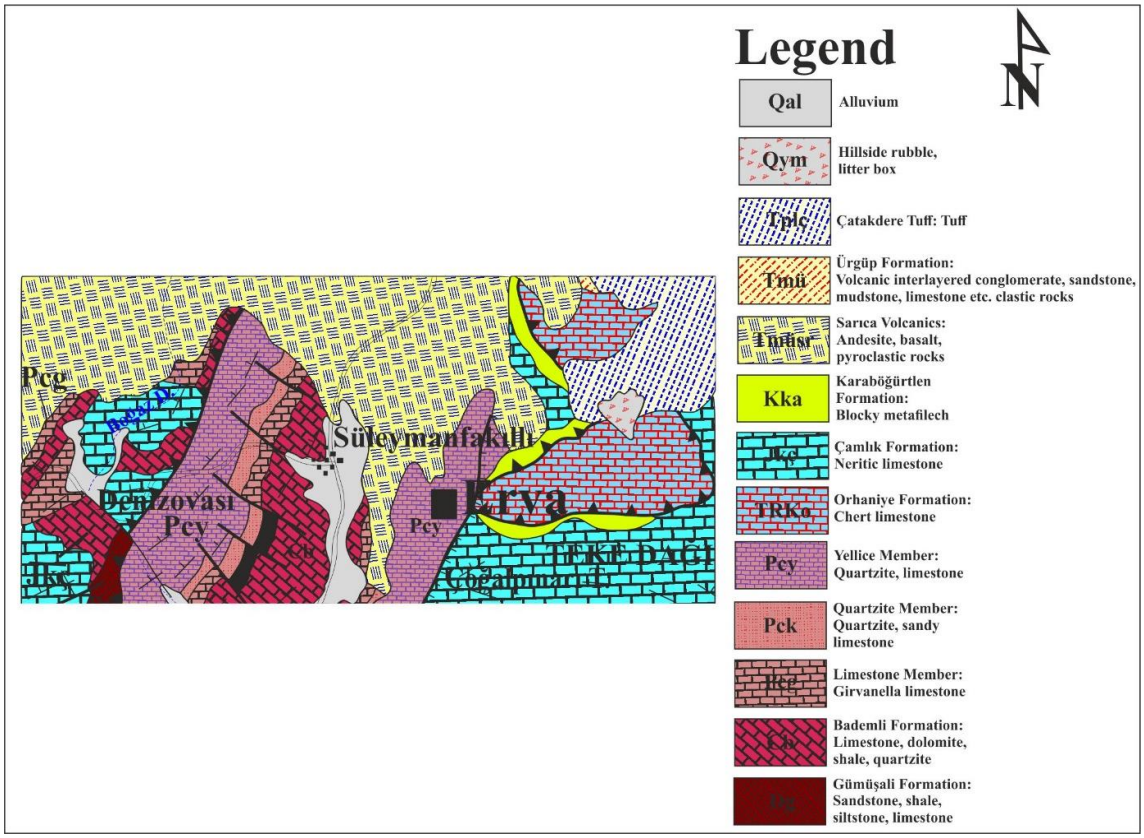


Figure 1. The Erva Pb-Zn deposit regional geology map (Modified from [6])

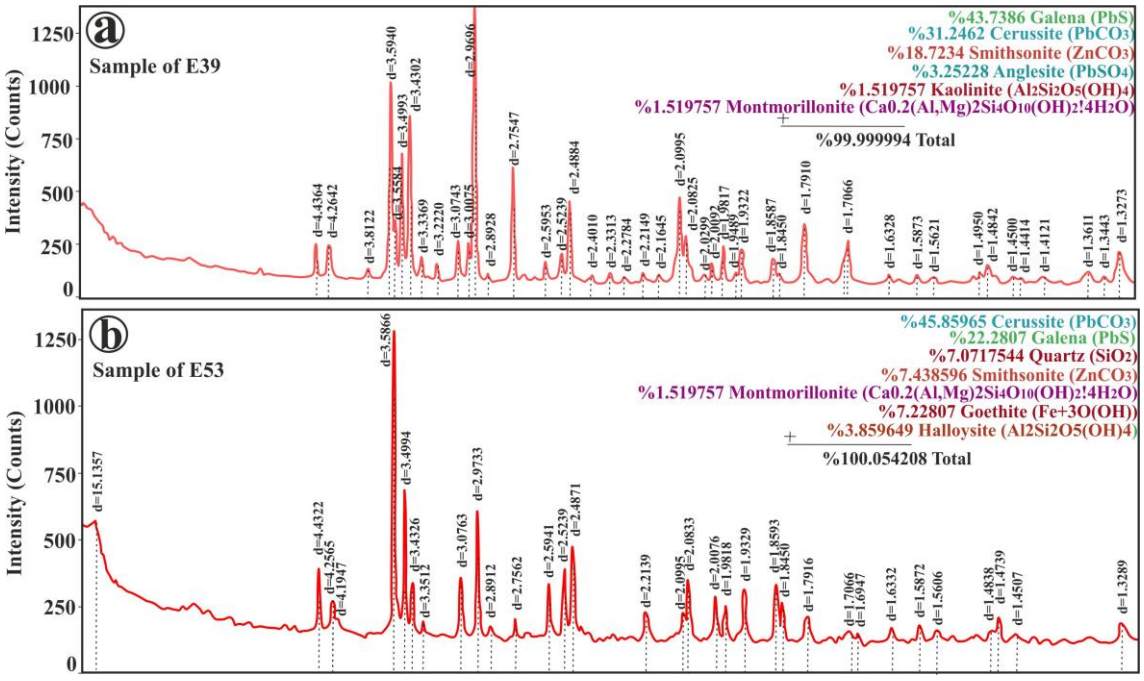


Figure 2. The XRD patterns of a the Erva Pb-Zn profile a) E39 b) E53

Rock and ore samples collected from the Erva mine were kept until they lost their water content. The samples that lost their moisture were ground to <75 microns. The ground

samples, to which 30 MPs pressure was applied, were turned into press-lozenges. The chemical contents of pressed-lozenge samples with smooth surfaces were revealed using the Rigaku (NEX-CG Applied Rigaku Technologies, Inc. Austin, TX, USA) X-Ray Fluorescence Spectrometry (XRF) device. Some important descriptive statistical results of chemical ingredients are given in Table 1.

Table 1. Descriptive statistical values of chemical analysis results of the Erva ore deposit

	Mean	Median	Mode	Std. Deviation	Variance	Range	Minimum	Maximum
Cl	0.020	0.019	0.000	0.019	0.000	0.109	0.000	0.109
Cr	0.016	0.013	0.0000[a]	0.012	0.000	0.054	0.000	0.054
Mn	0.025	0.002	0.000	0.043	0.002	0.170	0.000	0.170
Co	0.017	0.006	0.000	0.025	0.001	0.088	0.000	0.088
As	0.134	0.014	0.000	0.243	0.059	0.799	0.000	0.799
Sr	0.018	0.009	0.0037[a]	0.024	0.001	0.123	0.000	0.123
Ir	0.026	0.025	0.000	0.028	0.001	0.125	0.000	0.125
Pt	0.017	0.005	0.001	0.027	0.001	0.113	0.000	0.113
Hg	0.014	0.001	0.000	0.047	0.002	0.262	0.000	0.262
Bi	0.016	0.000	0.000	0.037	0.001	0.128	0.000	0.128
MgO	2.703	2.625	0.6160[a]	1.826	3.335	7.814	0.616	8.430
Al_2O_3	11.598	9.840	1.2700[a]	7.980	63.681	28.830	1.270	30.100
SiO_2	28.903	31.050	2.6200[a]	15.936	253.953	49.680	2.620	52.300
P_2O_5	0.012	0.000	0.000	0.046	0.002	0.246	0.000	0.246
SO_4	0.881	0.134	0.000	2.143	40.590	9.640	0.000	9.640
K_2O	0.813	0.523	0.1180[a]	0.773	0.597	3.062	0.118	3.180
CaO	17.854	1.990	10.620	26.409	697.432	75.754	0.546	76.300
TiO_2	0.412	0.357	0.0805[a]	0.261	0.068	0.838	0.081	0.918
Fe_2O_3	11.263	7.765	4.5900[a]	8.448	71.375	28.250	2.650	30.900
ZnO	7.850	7.255	0.0747[a]	8.703	75.750	41.225	0.075	41.300
PbO	4.337	0.697	0.0154[a]	8.899	79.191	35.785	0.015	35.800
Na	4.068	3.180	0.000	4.435	19.671	16.000	0.000	16.000
Zr	0.276	0.255	0.1550[a]	0.126	0.016	0.432	0.125	0.557
Eu	0.109	0.068	0.000	0.124	0.015	0.485	0.000	0.485
Tb	0.043	0.000	0.000	0.058	0.003	0.231	0.000	0.231
Yb	0.014	0.000	0.000	0.028	0.001	0.113	0.000	0.113
LOI	8.312	7.725	16.300	6.283	39.480	19.995	0.005	20.000

a. Multiple modes exist. The smallest value is shown.

https://doi.org/10.5593/sgem2024/1.1/s03.39

RESULTS

According to the XRD analysis performed on samples E39 and E53 collected from the Erva mine, the mineralogical compositions of the samples are listed as follows, together with their percentages: 43.7386% galena, 31.2462% cerussite, 18.7234% smithsonite, 3.25228% anglesite, 1.519757% kaolinite, 1.519757% montmorillonite; 45.85965% cerussite, 22.2807% galena, 7.0717544% quartz, 7.438596% smithsonite, 6.315789% montmorillonite, 7.22807% goethite, 3.859649% halloysite. According to these results, the main ore minerals of the deposit were determined to be galena, cerussite, smithsonite and anglesite. The gangue minerals of the deposit are listed as follows: kaolinite, montmorillonite, quartz, halloysite. As a result of the XRF analysis, the compositions that constitute the elemental composition of the bed together with their concentrations are listed as follows: 28.903% SiO_2 > 17.854% CaO > 11.598% Al_2O_3 > 11.263% Fe_2O_3 > 7.85% ZnO > 4.337% PbO > 4.068% Na > 2.703% MgO > 0.881% SO_4 > 0.813% K_2O > 0.412% TiO_2 > 0.276% Zr > 0.134% As > 0.109% Eu > 0.043% Tb > 0.026% Ir > 0.025% Mn > 0.02% Cl > 0.018% Sr > 0.017% Co > 0.017% Pt > % 0.016 Cr > 0.016% Bi > 0.014% Hg > 0.014% Yb > 0.012% P_2O_5.

DISCUSSION

It is the most common sulphide mineral compared to galena, sphalerite, pyrite and chalcopyrite in Pb-Zn deposits with intense superficial alteration [7]. In the study carried out in the carbonate wall rock Pb-Zn deposits in the Central and Eastern Taurus Mountains, primary ore-forming minerals were determined as: galena, sphalerite, chalcopyrite, pyrite, pyrargyrite, tetrahedrite and pyrrhotite. Secondary ore-forming minerals were observed as smithsonite, cerussite, anglesite, goethite, hematite, hydrozincite, hemimorphite and hematite [7].

Another study conducted in the Central Taurus Belt revealed that the sulphide ores found in the Bolkardagi region differ paragenetically compared to other deposits in the region [8]. Minerals with high formation temperatures in the paragenesis of the deposits were found as follows: arsenopyrite, bornite, fahlerz, pyrite, magnetite, molybdenite, skutterudite, meneghinite; Minerals with low formation temperatures were found as follows: barite, marcasite, native, silver, argentite, bravoyite, semseyite. Considering the high and low formation temperature, it is interpreted that the minerals in the paragenesis were formed in the mesothermal (200-300˚C) and epithermal (50-20˚C) phase from the beginning of the phase. High-temperature minerals started in the mesothermal phase, and as the temperature decreased, secondary minerals continued to form in the epithermal phase.

[9] commented that the Pb-Zn deposits in the Ulukisla-Nigde region are strata bound and epigenetic in character. It has been determined that the main minerals forming the deposit are pyrite, galena and sphalerite. Considering the high Sb and Ag concentrations and Zn/Pb ratios in the ore samples, the deposits were thought to be of hydrothermal origin.

[10] examined various Pb-Zn mineralization’s in the Yahyali-Demirkazik region. The ore minerals of the deposits were determined to be sphalerite, galena, smithsonite, anglesite and cerussite. As a result of the coexistence of minerals with high formation temperatures and the presence of Fe, Cu, Mn, Al, Mg, Ni, Ti, V, W, Co, Cd, Ir, Ge, Ag and Au elements, the mineralization was attributed to hydrothermal origin.

CONCLUSION

As a result of the analysis of the Erva lead-zinc deposit in Yahyali (Kayseri) district, the ore metal development source was interpreted. The formation type of the lead-zinc deposit was revealed. The origin of the fluids forming the ore, magma, magma crystallization stage and formation temperature are interpreted. The metallogenic origin of the fluids that play a role in the formation of the ore (granitic, marine carbonate, sedimentary organic matter, etc.) has been determined. In this study, XRF (X Ray Fluorescence Spectrometry) and XRD (X ray Diffraction Analysis) geochemical analyses were carried out to understand the lead-zinc ore metal source. As a result of the XRF analysis performed to understand the whole rock geochemistry of the lead-zinc deposit, the average ZnO and PbO (in %) grade values were found as follows: 7.85 and 4.33. Lead and zinc are often enriched together in ore deposits. The average values of the major oxides forming the Erva deposit are listed as follows: SiO_2 (28.90) > CaO (17.85) > Al_2O_3 (11.59) > Fe_2O_3 (11.26) > ZnO (7.85) > PbO (4.33) > Na (4.06) > MgO (2.70) > SO_4 (0.88) > K_2O (0.81) > TiO_2 (0.41) > P_2O_5 (0.01). In this enrichment stage, elements such as Mo, Au, Ag, Cd, Bi, Ge, Ga and As elements can also be found as byproducts. Trace elements found in significant concentrations in the Erva deposit are Zr and As, with average values of 0.27 and 0.13, respectively. According to the XRD results performed to understand the mineralogical compositions of the ore and host rocks in the Erva deposit, the mineral paragenesis that forms the ore is as follows: galena, cerussite, smithsonite, quartz, gypsum, goethite, anglesite, kaolinite, montmorillonite. Mineralization occurring in the region where geologically young formation-aged rocks are present is not seen among large karst cavities. Instead, mineralization in the form of geological fillings is observed in the capillary cracks of the carbonates in the Yahyali Munzur Nappe. Depending on the formation conditions, it is thought to show the characteristics of a hydrothermal sedimentary lead-zinc deposit. Hydrothermal sedimentary lead-zinc deposits are of hypogene and syngenetic origin. Since ore deposition takes place under reducing environmental conditions, the host rocks are generally black-coloured, fine detrital sediments or bituminous limestones. They are similar to volcano-sedimentary zinc deposits in terms of structure, texture, mineral paragenesis and ore location. However, volcanics are not found as wall rocks. Their formation is associated with magmatic or other hot solutions added to the environment during sedimentation. Zinc is a moderately mobile metal under atmospheric conditions. During the surface alteration of older zinc mineralization's or rocks containing high concentrations of zinc, under the influence of sulfuric acid, it was deposited as sulphide in reducing environments and as carbonate or oxide compounds in oxidizing environments. Lead-zinc mineralization's in the study area are generally deposited in strata-bold (between layers), karst cavities and sometimes at fault contacts. The host rocks are in the form of limestone-dolomitic limestone and/or dolomitic limestone-dolomitic limestone, and the interlayer mineralization's have a thickness between 1 m and 3 m. In karst mineralization's, the size of the void varies depending on the day. It is thought that the mineralization's are of hydrothermal origin.

ACKNOWLEDGEMENTS

The financial support for this research was provided by the Scientific Research Projects Coordination Unit (BAP, FDK-2023-6411) of Akdeniz University, Antalya/Turkey. The

https://doi.org/10.5593/sgem2024/1.1/s03.39

authors would like to thank the Scientific Research Projects Coordination Unit of Akdeniz University. This paper is a part of the PhD thesis of ATAKOGLU OZER O., the first author.

REFERENCES

[1] Ozer Atakoglu O., Yalcin M., Using multivariate statistical analyzes in geochemical data: Example of lead-zinc deposit, The 6th Mediterranean International Conference of Pure & Applied Mathematics and Related Areas (MICOPAM), 2023, pp 300-305.

[2] Gokce A., Ore Deposit. Cumhuriyet University, (1995).

[3] Mehrabi B., Chaghaneh N., Fazel E. T., Corfu F., Geology, fluid inclusions and C− O− S− Pb isotopic compositions of the Chahmileh Pb-Zn deposit, Central Iran: Implications for ore genesis. Geological Magazine, vol. 160/issue 11, pp 1953-1974, 2023.

[4] Yu L., Zou H., Li M., Pirajno F., Cao H., Xiao B., ... Hou M., Fingerprinting Pb-Zn mineralization events in the SW Yangtze Block, South China: A case from Yuanbaoshan deposit. Ore Geology Reviews, 105878, 2024.

[5] Pan P., Zhao C., Zhou W., Chang H., Numerical simulation of fault-fold structures-controlled ore formation: Case studies of the Huize and Maoping lead-zinc deposits in Northeastern Yunnan Province, southwest China. Ore Geology Reviews, 105906, 2024.

[6] Dalkilic H., Türkiye Geological Maps, 1: 100.000 scaled Kayseri-L35 Sheet. Publ General Directorate Min Res Exp, 124, 2009.

[7] Ozbek A. C., Alteration mineralogy and stable isotope properties of Pb-Zn ore formations with carbonate host rocks in the central and eastern Taurus Mountains. (Doctoral dissertation, Institute of Science), 2014.

[8] Temur, S., Genetic analysis of Zn-Pb deposits in Bolkardag (Ulukisla-Nigde) region features. Cukurova University M.M.F. Geological Eng. Plenty. Ahmet Acar Jeol. Sym. Papers. 191-198, 1991.

[9] Temur, S., Geochemical Investigation of Zn-Pb Deposits in Bolkardagi Region, TJK Bulletin, 35, 2, 101, 1992.

[10] Çopuroglu, I., Yahyali Kayseri-Demirkazik Nigde-Camardi region Zn-Pb mineralogy and genesis of its deposits. MTA journal 118, 35-46, 1996.

HEALTH AND SAFETY OF WORKERS IN THE MINING INDUSTRY FOLLOWING THE IMPLEMENTATION OF ARTIFICIAL INTELLIGENCE

Eng. Matei Andrada Denisa[1]
Eng. Ligia Ioana Tuhuț[1]
PhD. eng. Morar Marius Simion[1]
PhD. eng. Cioară Cristian Raul[1]
PhD. jr. Florin Manea[1]
[1]National Institute for Research and Development in Mine Safety and Protection to Explosion – INSEMEX Petroşani, **Romania**

ABSTRACT

Artificial intelligence (AI) is well known as a robust technique that can support and improve the quality of human life. In the mining industry, the applications of artificial intelligence have changed the sciences and technologies as well as the performance of the mining industry through machine learning, autonomous technologies that provide many economic benefits to the mining industry by reducing costs, efficiency and improving productivity. In principle, reducing the exposure of workers to hazardous conditions, continuous production and improved safety are the most beneficial factors of the implementation of artificial intelligence in the mining sector, coming to the aid of workers in this field.
In recent years, the adoption of artificial intelligence has changed the game in the mining industry by enabling more efficient exploration, taking automation to new levels, generating higher yields, improving safety and maximizing extraction, maintenance and operational performance.
This paper aims to highlight the multiple advantages that the implementation of artificial intelligence in the mining industry has for the health and safety of mining workers.

Keywords: artificial intelligence, mining industry, workers safety, health and safety, AI technology

INTRODUCTION

Mining companies have started using artificial intelligence to help them identify these mineral reserves. AI can help mining companies analyze large volumes of geological data, satellite images and historical records to identify potential mineral deposits. The use of artificial intelligence (AI) has changed the game in mining in recent years: it has enabled more efficient exploration, higher yields, improved safety and optimization of extraction, maintenance and operational performance.

The mining industry is the backbone of the global economy, providing the raw materials that drive development and innovation. However, traditional mining practices often face challenges that limit efficiency, safety and sustainability. These include geological uncertainties, hazardous working environments and high operational costs. Even as the demand for minerals and metals increases, these limitations have made it clear that innovative solutions are needed to propel the industry forward [2].

Safety is a primary concern in mining, and AI can play a significant role in improving it. AI-powered systems can monitor working conditions, predict equipment failures, and even detect safety hazards in real time.

https://doi.org/10.5593/sgem2024/1.1/s03.40

CURRENT APPLICATIONS OF ARTIFICIAL INTELLIGENCE AND AUTONOMOUS TECHNOLOGY IN THE MINING INDUSTRY FOR THE BENEFIT OF WORKER PROTECTION

The conditions and nature of mining allow that accidents at work can often be quite serious. However, risks and threats can be mitigated and reduced, and artificial intelligence appears to be an important way to do this. The use of AI in the mining industry can facilitate the identification, assessment and anticipation of potentially dangerous events and situations, thereby increasing employee safety and health [4].

Artificial intelligence is helping miners reduce their exposure to hazardous mining situations and by changing the industry from a people-oriented to a process-oriented industry. Autonomous AI-driven mining vehicles can reduce the risks associated with human operation in hazardous environments. The result is a safer working environment for miners [1].

One of the most significant applications of AI in mining is the use of autonomous vehicles, which can operate without human intervention in dangerous and remote environments. AI-powered trucks can traverse difficult terrain and detect obstacles, reducing the risk of accidents and improving safety. Autonomous vehicles can make working conditions safer in mining because they don't have to try to reach potentially dangerous areas of a site. Electric mining trucks are very useful for achieving productivity goals and will lead to advancements in suspension, transmission and independent operation [8].

One of the most important ways AI has improved mining health and safety is by combating driver drowsiness and fatigue. Drowsiness is one of the biggest causes of mining accidents, the main reason being that you often don't realize you're tired until it's too late. You can be fine one moment and then suddenly fall asleep the next. To prevent this from happening to miners, some mining quarries have already implemented the use of smart caps. These caps analyze the brain waves of mining vehicle drivers, alerting them as soon as their brain waves reveal that they are about to fall asleep. This technology eliminates costly and dangerous accidents caused by drowsiness [5].

Another significant yet indirect application of artificial intelligence lies in the real-time monitoring of machinery and data analysis through machine learning. Despite the presence of real-time monitoring sensors and data collection capabilities in modern mining technology, the collected data remains underutilized [6]. When machinery components approach failure, they exhibit various indicators such as vibrations, unusual sounds, or power loss. By employing machine learning algorithms, this data can be processed and comprehended in real-time, enabling the prediction of imminent machine failures and preemptively shutting down operations. This proactive approach not only mitigates repair costs associated with catastrophic breakdowns but also eliminates safety risks often associated with such incidents. In addition to monitoring mining equipment to detect equipment failures, sensors can also be used to monitor the environment for potential hazards. Geotechnical sensors and systems can monitor seismic activity and analyze seismic reports. This data can then be used to make more informed decisions about activities such as drilling and blasting. As with much data analysis, this task could be undertaken by humans, but AI is capable of analyzing more data, faster, and doing it in real time. This makes the application of AI in these scenarios an excellent prospect for further increasing the safety of mining [5].

The integration of AI in mining operations significantly enhances worker health management and accident prevention. For instance, Personal Protective Equipment, such as helmets, can now transmit alert signals to the control center, notifying miners of potential risks. Equipped with multiple sensors consolidated into a single module, these helmets continuously monitor ambient conditions (such as toxic gases, temperature, and humidity) as well as worker health metrics like heart rate and vibrations from excavation and blasting activities. The collected data is then transmitted to the control center via low-energy Bluetooth modules. Additionally, these helmets feature a panic button that immediately alerts the control unit in case of emergencies. One of the sensors employed in this system is the DHT11 (Digital Temperature Humidity Sensor), known for its high-performance capabilities in measuring temperature and humidity levels with an accuracy of ±5%. Another sensor, the MQ135, is sensitive to gases like ammonia, benzene, and hydrogen within a concentration range of 10 to 10,000 ppm. With an accuracy rate of 85%, it detects gas concentrations, crucial in environments like coal mines where high gas levels can lead to disorientation among miners. In case of such incidents, miners can activate the panic button on their headsets, expediting rescue operations. Furthermore, heart rate sensors are utilized to monitor abnormal conditions; heart rates below 60 or exceeding 100 are flagged as anomalies requiring immediate attention. Some mines have implemented machine learning algorithms, particularly convolutional neural networks, to train AI models in recognizing workers' gestures. These gestures, such as signaling 'OK,' 'NOT OK,' or 'EMERGENCY EVACUATION,' aid in communication and safety protocols. To streamline data transmission and facilitate timely interventions, it's suggested to implement an API for bidirectional data exchange between software applications. This allows for real-time monitoring of sensor data and prompt action to safeguard miners.

AI VISION FOR MINING SAFETY

Computer vision is an area of artificial intelligence (AI) that enables computers and systems to interpret and analyze visual data and derive meaningful information from digital images, video, and other visual input. Some of its typical real-world applications include: object detection, visual content processing (images, documents, videos), understanding and analysis, product search, image classification and search, and content moderation [7]. In this context, Computer Vision, also known as Vision AI, appears as a beacon of hope, heralding a new chapter in mining safety, harnessing cutting-edge artificial intelligence to strengthen safety measures. Vision AI transforms traditional safety protocols by seamlessly integrating real-time surveillance and automated hazard recognition capabilities with an emphasis on protecting workers and enhancing operational integrity [10].

In the mining industry safety remains paramount, Vision AI being created specifically for this industry, offers a lot of safety applications that through the capabilities of this artificial intelligence application cover a wide range of specialized applications, including:

- Secure Zone Monitoring: Automatically ensures the integrity of the secure zone and promptly informs authorities of any breach.
- Identifying danger areas: establishing and monitoring high-risk areas and improving safety procedures and protocols.

https://doi.org/10.5593/sgem2024/1.1/s03.40

- Air quality monitoring: Atmospheric conditions are monitored and alerts are issued for dangerous levels of gases or insufficient oxygen.
- Residence Time Control: refers to controlling the time workers spend in hazardous areas to meet safety and compliance rules.
- Optimizing human resources: ensuring a minimum and maximum number of safe employees in critical operational areas, preventing accidents caused by overcrowding or understaffing.
- Vehicle activity monitoring: monitoring vehicle movement to reduce collision risks and better manage traffic flow on the mining site.
- PPE compliance assessment: Ensure you are regularly using the safety equipment required to protect workers from potential injury.

AI Vision analyzes sensor data and video streams using advanced machine learning algorithms. Vision AI learns from mine operational models to adapt its monitoring and alerting mechanisms to site-specific requirements. By proactively detecting security protocol violations and impending threats, Vision AI helps mining companies adopt a proactive security approach. An aggressive stance allows for quick and preventive action, moving beyond reactive safety strategies and creating an environment of safety and caution in the mining industry.

MINING SECURITY APPLICATIONS OF VISION AI

1. Increased security by monitoring restricted areas

The purpose of Visionify Restricted Area Monitoring is to improve the security of mining operations. Using state-of-the-art AI technology, this system creates virtual boundaries around dangerous or prohibited areas on mining sites. When these boundaries are breached, it immediately notifies the surveillance team, enabling rapid reactions to possible security breaches. The main advantages consist in the prevention of accidents, reducing the probability of their occurrence by prompt alerting of unauthorized access, operational consistency by complying with strict operational standards, protecting the integrity of high security areas and last but not least the protection of the infrastructure that serves as a line of defense against attacks, protecting people important resources. Restricted area monitoring is essential for controlling access to demolition sites, machine tracks and hazardous material storage locations in mining. These places are continuously monitored to alert on violations. The device sends urgent alerts if a worker accidentally enters a blast zone, enabling rapid evacuation and operational continuity. This real-time monitoring technology is critical to maintaining safety standards in mining operations despite many obstacles.

2. Addressing risks with the identification of dangerous areas

The Hazard Zones application is an integral component of safety strategies in dynamic mining where safety hazards abound by identifying and delineating high-risk areas in mining environments. Using advanced AI, this tool highlights areas prone to specific hazards, such as those with frequent heavy machinery use or unstable ground conditions. It serves as a vital mechanism for alerting workers and management to these risks, significantly improving existing safety measures. For example, in sections of a mine characterized by heavy machinery activity or overhead crane operations, the

application promptly alerts workers entering these areas or flags any violations of safety protocols.

3. Monitoring atmospheric conditions in closed spaces

In mining, maintaining air quality is vital, especially in underground and confined areas. Vision AI's atmosphere monitoring app was designed to monitor these areas, where exposure to harmful gases and oxygen depletion are a serious threat. Due to operational activities and geological features, this tool is essential for identifying dangerous atmospheric changes. It issues quick alerts when it notices unstable weather conditions. In the mining environment, this rapid response mechanism is critical as it allows for rapid evacuation or other safety measures needed to respond to air quality threats. This tool provides immediate notifications and updates, helping to maintain the ongoing safety management that is critical to navigating the active and potentially hazardous environment of mining operations.

4. Rest time monitoring

One of the key features of Vision AI safety applications is monitoring the amount of time workers spend in hazardous areas of a mine. In high-risk areas, it is essential to enforce safety rules and ensure that employees do not exceed safe time limits. Dwell Time Monitoring is an essential tool for complying with safety protocols, as these restrictions have been carefully established based on risk assessments and compliance standards. To reduce the risk of accidents and health problems resulting from long-term exposure to high-risk environments, it is essential to manage the exposure of workers to these environments. Thus, this application balances safety and efficiency, creating a safer and more efficient mining environment.

5. Optimizing critical area manpower allocation — Monitoring minimum and maximum staffing levels

Applications such as Visionify Min and Max Workers Monitoring are crucial for managing workers in critical mining areas. This ensures that sensitive areas are adequately staffed and not overcrowded, which is essential for safety and efficiency. The Min Workers feature ensures that the workers needed for important tasks, such as operating heavy machinery, are available. However, the Max Workers feature reduces the risks of overcrowding, especially in small spaces.

Because workforce data is provided in real time, quick adjustments can be made to maintain established staffing levels. The app increases safety and prevents operational disruptions by consistently meeting these parameters, making it essential for well-regulated mining operations.

6. Monitoring compliance with personal protective equipment (PPE).

In the mining industry, AI vision-based PPE compliance monitoring is critical, as AI helps ensure that workers adhere to essential safety equipment protocols. It uses image recognition to regularly check the proper use of personal protective equipment such as helmets, gloves and goggles, quickly identifying and correcting any non-compliance.

The system significantly reduces the risk of workplace accidents through active monitoring and prompt intervention of discrepancies in PPE.

https://doi.org/10.5593/sgem2024/1.1/s03.40

7. Improving vehicle navigation through monitoring

Visionify's vehicle monitoring applications optimize vehicle routes and traffic flow to improve mine safety. The technology optimizes mining site traffic and plans safe paths using AI to understand real-time visual data. This includes hazard assessment, coordination of vehicle movements and accident prevention in high traffic areas.

Vehicle tracking uses real-time data to improve vehicle navigation techniques. The system predicts traffic patterns and tracks vehicle movements by generating comprehensive heat maps and providing mine-specific information. This proactive vehicle navigation strategy reduces vehicle hazards in mines and improves safety and efficiency.

ADVANTAGES AND DISADVANTAGES OF IMPLEMENTING ARTIFICIAL INTELLIGENCE IN THE MINING INDUSTRY

Advantages:

- Unsafe jobs, work and dangerous tasks done by robots instead of people;
- Increased efficiency of work and processes;
- Reduced labor cost and improved safety;
- No health, vision and dental costs, pension and other necessary car costs;
- Reduction of errors, mistakes and accidents resulting in reduction of operational costs;
- Quick solutions to problems;
- Reliable results from a small number of experiments;
- Reducing the number of expensive field and laboratory experiments and increasing the reliability of prediction and forecasting;
- 24/7 availability, resulting in increased productivity;
- Improved safety (roof loading an example) as robots performing dangerous work;
- Better guidance and control system for mine rescue and safety operations;
- The systems fill the gaps in labor availability and labor needs in the industry;
- The AI system has more situational awareness and can make better decisions in dangerous, accident and emergency situations;
- Increased speed of good decision;
- Simple and timely solutions to complex problems [3].

Disadvantages

- Loss of jobs;
- Complex human-machine interaction and psychological issues while working with machines, such as feelings of isolation and non-companion ship;
- Reliability of results, as still based on trial and error;
- Loss of control over intelligent machines;

- Misuse of technology such as autonomous weapons and explosives;
- Too much reliance on machines can lead to poor decision-making as technology has the potential to be misused;
- Security vulnerability (eg bugs, viruses, system hacking);
- Ethical implications and responsibilities for unsafe behavior;
- No employment for the communities where the mines are being developed [3].

CONCLUSIONS

AI has the potential to revolutionize the mining industry over the next decade if companies are willing to embrace the technology. Increased safety, increased efficiency, environmental sustainability and cost reduction are just some of the benefits that AI can provide. By investing in AI and addressing the associated challenges, mining companies can not only remain competitive, but also lead the way in shaping a more innovative, efficient and sustainable future for the industry [1].

Machine learning and autonomous technology have the potential to revolutionize the mining industry by reducing costs, improving productivity and efficiency of operations, and reducing the environmental footprint of mining through the use of intelligent systems. The mining industry is slow moving towards the implementation of these systems, especially in the field of autonomous cars [6].

However, to realize the full potential of these different mining technologies, more concerted efforts are needed. As more mining companies take the initiative to implement intelligent AI-based systems and autonomous technologies, more data will become available on the successes and failures of these attempts, their impact on jobs and the number of jobs , future skills and training requirements, the economic, societal and social impact of AI implementation. This will provide more robust data to analyze different impacts, to assess current issues and future trends and to provide a basis for a better understanding of the implications of AI implementations in the mining industry [3].

As we can see with many of the use cases for AI in mining, there is a shift that is making mining from being a people-oriented industry to being a more process-oriented industry. Artificial intelligence is being used to improve many processes and reduce human risks, making industry a safer place for workers in general [5].

As mining companies continue to embrace this technology, they can unlock new opportunities for growth, productivity and environmental stewardship. By harnessing the power of AI, the mining industry can move towards a safer, more efficient and sustainable future [9].

ACKNOWLEDGEMENTS

This work was carried out through “Core program” of the National Research, Development and Innovation Plan 2022-2027, supported by MCID and IOSIN - PCDIEX.

https://doi.org/10.5593/sgem2024/1.1/s03.40

REFERENCES

[1] Jack G - How AI Could Revolutionize the Mining Industry in the Next Decade - Pretoria, Gauteng, South Africa, 2023.

[2] https://www.identecsolutions.com/mining-safety

[3] Zeshan Hyder, Keng Siau, Fiona Nah - Artificial Intelligence, Machine Learning, and Autonomous Technologies in Mining Industry, Journal of Database Management (JDM), Volume 30, 2019.

[4] Assoc. Prof. Dr. Imran ASLAN1, Nour El Houda BENHARKAT2, Souad Bentaalla-Kaced – Cesser - The applications of artificial intelligence in occupational health and safety, 7TH International conference onemprical social sciences, economy, management and education researches, November 10 - 12, 2023 - Jakarta – Indonesia.

[5] https://www.axora.com/insights/how-ai-is-being-used-to-improve-health-and-safety-in-mining

[6] K. Lalitha, G. Ramya, M. Shunmugathammal - AI based Safety Helmet for Mining workers using IoT Technology and ARM Cortex-M, IEEE Sensors Journal, vol. 23, issue 18, pp. 21355-21362, September 2023.

[7] https://cleste.ro/modul-senzor-detector-gaz-mq-135.html

[8] https://miningdigital.com/articles/top-10-uses-of-artificial-intelligence-in-mining

[9] Glenn Stewart - AI in the Mining Industry**,** Manchester, England, United Kingdom, May 2023.

[10] https://medium.com/@hmurari/understanding-mining-safety-with-vision-ai-and-its-proactive-solutions-for-enhanced-workplace-4e818f06b331.

IDENTIFICATION OF AREAS PRONE TO SEISMIC ACTIVITY OCCURRENCE USING 3D FEM NUMERICAL SIMULATIONS

Dr. Krzysztof Fuławka[1]

Assoc. Prof. Dr. Piotr Mertuszka[1]

Dr. Lech Solecki[1]

Dr. Marcin Szumny[1]

MSc. Roman Kołodziej[2]

[1]KGHM CUPRUM Ltd. - Research and Development Centre, **Poland**
[2]KGHM Polska Miedź S.A.- Lubin Mine, **Poland**

ABSTRACT

The seismic hazard in Polish copper mines has remained continuously at a high level, generating a relatively large number of accidents and negatively affecting the continuity of the exploitation process. To minimize the threat, a number of preventive actions are taken to reduce the ability of the rock mass to accumulate stresses, which should ultimately result in a reduction in the number and energy of seismic phenomena. Unfortunately, as previous experience shows, the effectiveness of preventive measures is severely limited due to the lack of reliable information about zones of potential instability. This study presents the results of 3-dimensional numerical simulations developed in stages system, based on which attempts were made to locate zones prone to instability. The analysis was performed for a period of 10 months and the time between each stage was 1 month. For validation purposes, measurements of convergence of mining excavations were used. Then, the strength parameters of the rocks were reduced in accordance with the principles of the GSI scale so that the modelling results were as close as possible to measurements in in-situ conditions. Finally, on the basis of validated numerical models, stress concentration zones in the rock mass were determined and the calculation results were compared with the actual location of seismic phenomena in the analyzed area. Ultimately, the results of the research are the basis for stating that the use of numerical tools can significantly support the process of designing active rockburst preventive opeartions in deep underground mines.

Keywords: geomechanical hazard, mining-induced seismicity, active rockburst prevention

INTRODUCTION

The use of numerical simulations in solving geomechanical problems is a topic that has developed very rapidly in recent years [1-2]. Increasing computing power, as well as developing new three-dimensional algorithms and complex codes for dynamic simulations in discontinuous media have significantly contributed to increasing the efficiency and safety of mining in recent years [3]. A well-prepared and validated numerical model makes it possible to determine the safety margins of underground and surface mining infrastructure, determines the distribution of stresses [4-5], displacements

https://doi.org/10.5593/sgem2024/1.1/s03.41

[6], and analyse the effect of external impacts (water/seismicity etc.) on the stability of the object [7-9]. Additionally, advanced numerical simulations constitute the basis for understanding the complicated behaviour of the rock mass as a result of the progressing mining process, the emergence of dynamic impacts, or the use of additional excavation support. Nevertheless, the vast majority of analyses carried out so far for underground miners are performed on a small scale (the scale of several workings). Large-scale models enabling the simulation of stress distribution, displacements and stability indicators for the entire mining panel, i.e. with an area of several square kilometres, are not currently standard practice in geomechanics. This situation results from a number of aspects. Firstly, building a large-scale, non-linear numeric model in 3D requires significant computing power and is very time-consuming due to the complicated process of building and optimizing the model. Secondly, small-scale models are easy to validate based on in situ measurements, while large-scale models, due to the complexity of the rock mass, require validation using devices located in many places, which generates additional costs and is timeconsumed. Thirdly, the construction of large-scale models requires empirical observations based on which the lab-determined strength parameters of rocks will be appropriately reduced. As a result, numerical models for underground mining areas are prepared using significant simplifications and enable only comparative qualitative analysis. The use of such models to predict, for example, seismic activity and areas prone to instability occurrence, unfortunately, had a large margin of error, which ultimately determined the lack of interest on the part of mining operators. Moreover, reliable numerical simulations are an extremely complicated issue in the case of room-and-pillar mining systems (Figure 1). The significant pace of the front's advance combined with the variability of the pillar geometry determine the low usefulness of single-stage models. In such a system, appropriate tracking of changes in stresses and displacements as the front advances requires the preparation of a series of stage numerical models reflecting the mining situation.

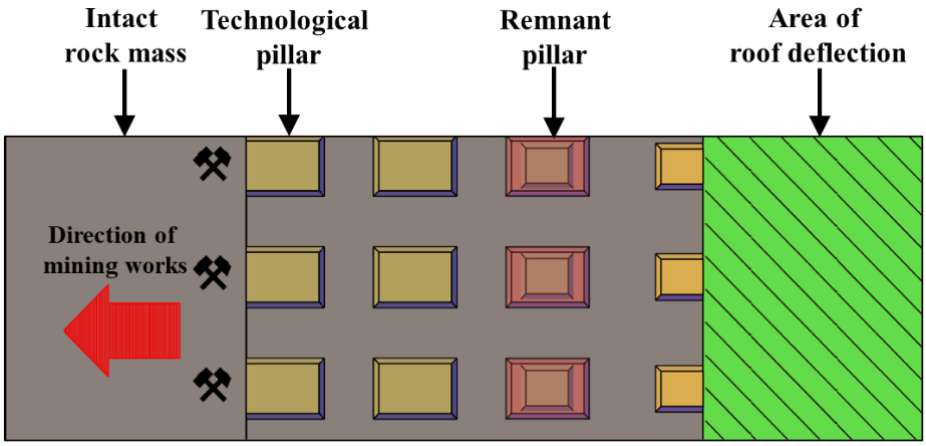


Figure 1. General scheme of room and pillar mining system with roof deflection.

This article attempts to develop and validate a large-scale 3D numerical model using the finite element method. The model was built based on the real geometry of the excavations, and data from rock strength laboratory tests. Then, the model parameters were validated based on underground convergence measurements. Finally, the results of the stability index were compared with the location of seismic shocks in the analysed section.

MATERIALS AND METHODS

Numerical simulations have been performed with the use of 3D FEM-based GTS NX software, which allows the solving of geotechnical problems including large-scale non-linear static and dynamic analyses of underground structures. Simulation has been performed in quasi-static conditions. It means that the model consists of 10 stages representing the progress of mining works (1-month time step). Each stage was calculated in non-linear static conditions. The geology of the model was prepared based on real data from four exploration drillings around the analysed mining panel. Geological profiles used for building of 3D model are presented in Figure 2.

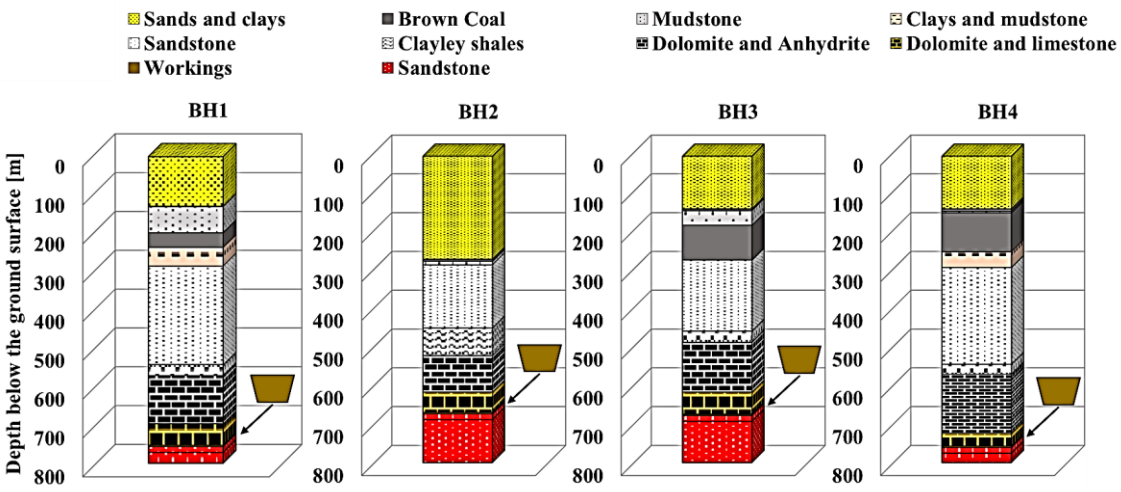


Figure 2. Geological profiles in the surroundings of the analyzed mining panel with a marked depth of excavation level.

The dimensions of the model were 1.5×1.5×1.0 km. To optimize the calculation time the model discretisation was carried out using the Hybrid-Mesh Algorithm, which enabled the achievement of an optimal combination of tetrahedral and hexahedral elements. A general view of the numerical model is presented in Figure 3.

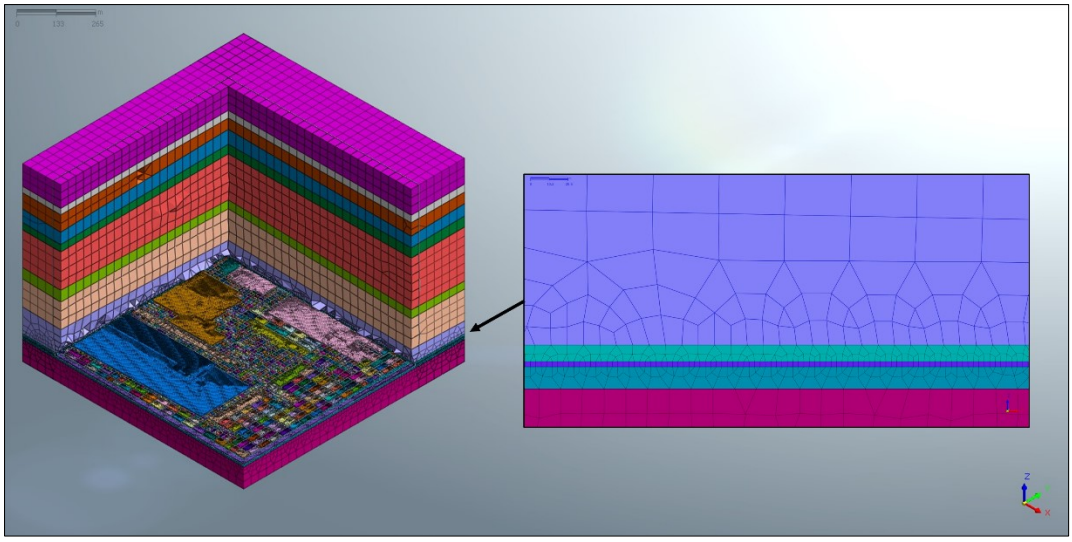


Figure 3. General scheme of room and pillar mining system with roof deflection.

https://doi.org/10.5593/sgem2024/1.1/s03.41

The strength properties of the rock were determined depending on the analysed structure. The backfilling area includes yielded pillars in a post-critical state and is partially filled with waste rock. To simulate such conditions, a backfilling area was described using Mohr-Coulomb model with strength properties similar to sands and clays. In turn, all regions consisting of intact rock mass, technological pillars, residual pillars and other rock layers were described with the use of the Generalized Hoek-Brown (GH-B) criterion. The Generalized Hoek-Brown approach is described in detail in reference [10]. To achieve a good correlation between numerical simulation results and in-situ measurements 3 scenarios of rock strength parameters were analysed. In each of the scenarios values representing the strength of intact rock were reduced with the GSI scale. The variable parameters in the numerical models are presented in Table 1.

Table 1. GSI parameters are used during the calculation of different scenarios.

Type of structure	Scenario I			Scenario II			Scenario III		
	GSI	*D*	m_i	*GSI*	*D*	m_i	*GSI*	*D*	m_i
Intact rock mass	95	0	12.36	90	0	12.36	80	0	12.36
Technological pillars	95	0	12.36	75	0.25	12.36	60	0.25	12.36
Residual pillars	95	0	12.36	60	0.5	12.36	40	0.50	12.36
Backfilling	*Sand (M-C criterion)*			*Sand (M-C criterion)*			*Sand (M-C criterion)*		

The parameter that was used to validate the numerical models was the convergence of workings recorded using a dozen or so convergometers installed in selected areas of the mining panel. In Figure 4 the location of each convergometers is presented.

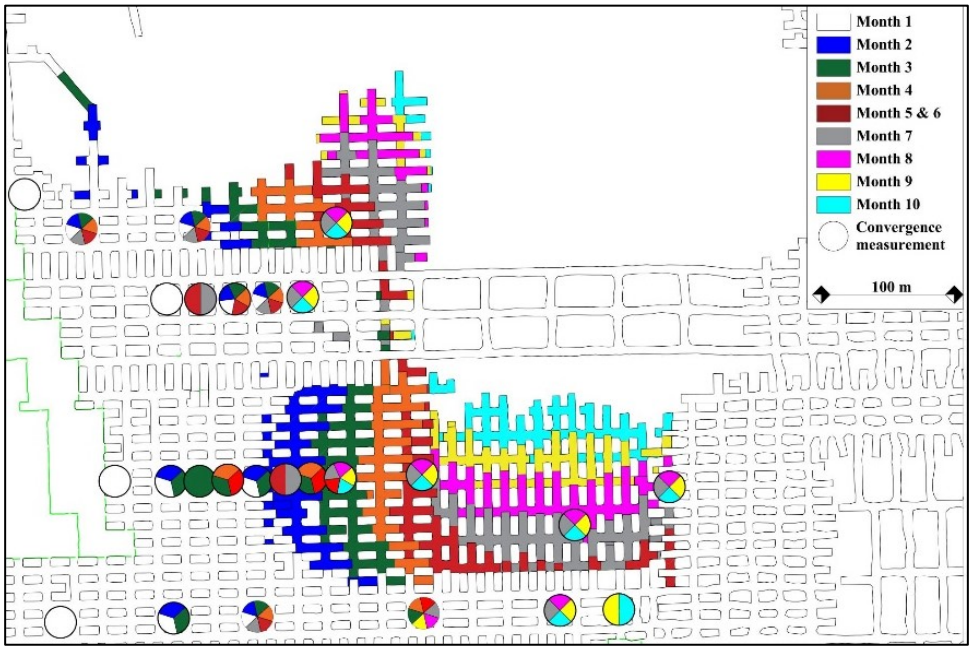


Figure 4. Convergence measurement in analysed mining panel.

The simulated convergence of workings H_{con} was defined as the difference in the height of workings (H_p) and the sum of the values of roof settlement (S_r) and floor uplift (S_f). Since the roof settlement has a negative direction in the model, the absolute value of this parameter was taken into account for the calculations.

$$H_{con} = H_p - (S_f + |S_r|) \quad (1)$$

RESULTS

From the point of view of a mining operator, the most intuitive indicator is the safety factor. Generating SF values <1 indicates a risk of instability. In turn, SF≥1 determines the stability of excavations. Figure 5 shows an isometric projection of the large-scale 3D numerical model.

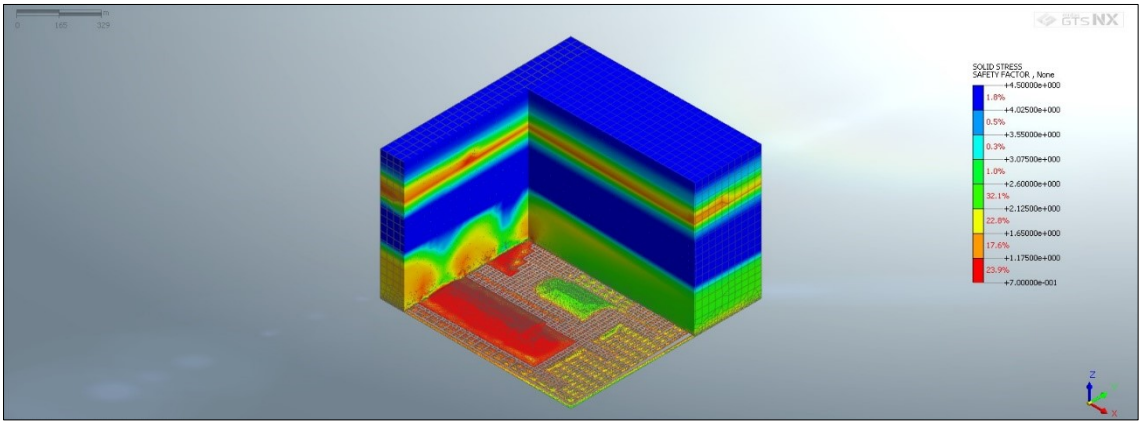


Figure 5. 3D results of large-scale numerical simulations of the analysed mining panel.

To ensure the reliability of the results, the analysis was carried out for a period of 10 months. A separate model was prepared for each month and excavation convergence measurements were made. Figure 6 shows the recorded (gray) and averaged (colored) convergence values in the analysed mining panel.

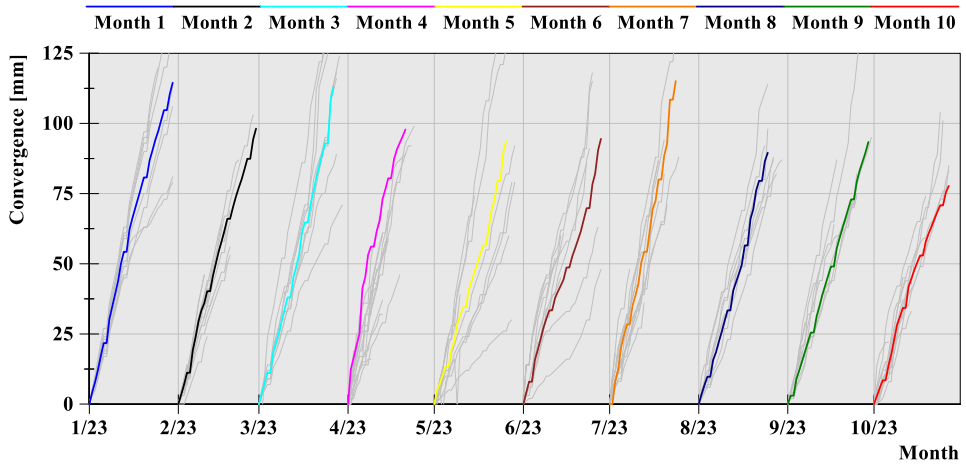


Figure 6. Results of 10-months long convergence measurement in analysed mining panel.

https://doi.org/10.5593/sgem2024/1.1/s03.41

After conducting a series of 30 numerical simulations (10 stages × 3 scenarios), the model's fit to the displacement values observed in in-situ conditions was assessed. As can be seen from Figure 7, a satisfactory fit of the model to underground measurements was achieved only in the case of scenario No. 3, where the strength parameters of the rocks were significantly reduced compared to the results obtained during intact rock mass strength tests (see Table 1). At the same time, scenarios in which the strength of the rocks was close to intact rock (scenario I) and in which moderate weakening of the pillars was assumed (scenario II) generated results that were significantly underestimated compared to the values recorded using convergometers.

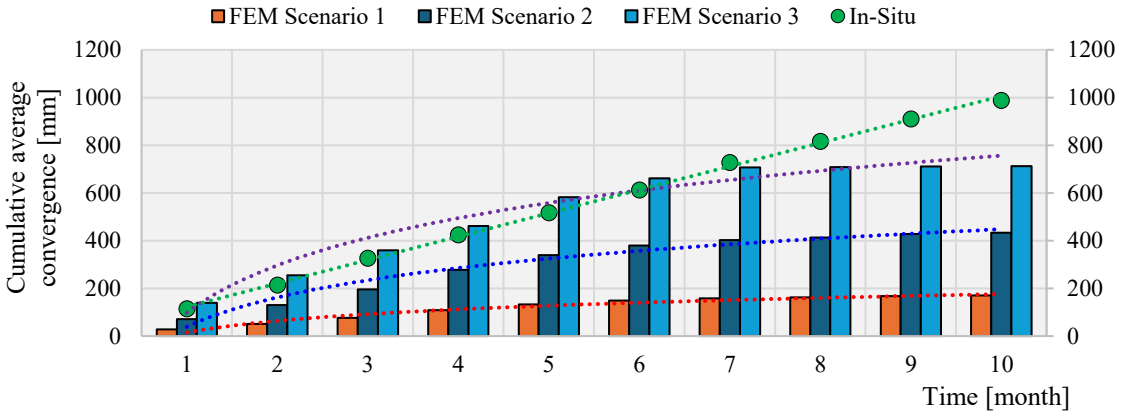


Figure 7. Simulation results vs. results of in-situ convergence measurement in analysed panel.

Finally, having a validated numerical model, the 3-dimensional distribution of stresses and safety factors was analysed. The calculation results were compared with the location of seismic events induced by mining activities in the analysed region. The evaluation results are shown in Figures 8-10.

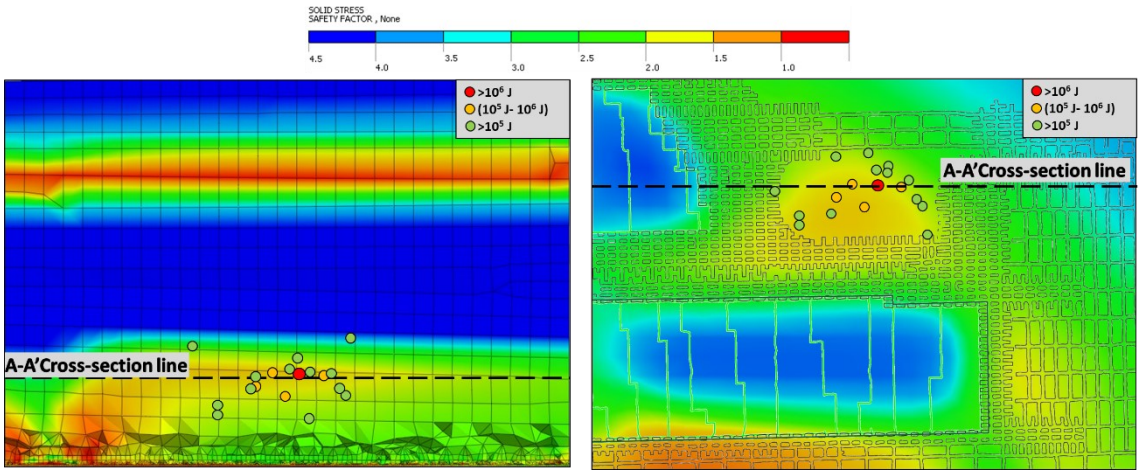


Figure 8. Horizontal cross-section representing safety factor distribution within analysed area (left), vertical A-A' cross-section representing safety factor distribution (right) – January.

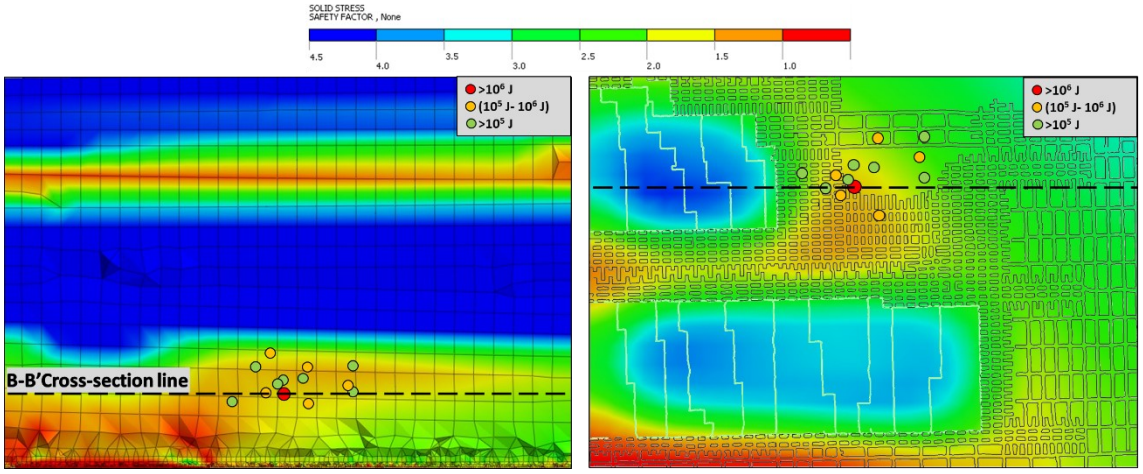


Figure 9. Horizontal cross-section representing safety factor distribution within analysed area (left), vertical B-B' cross-section representing safety factor distribution (right) – June.

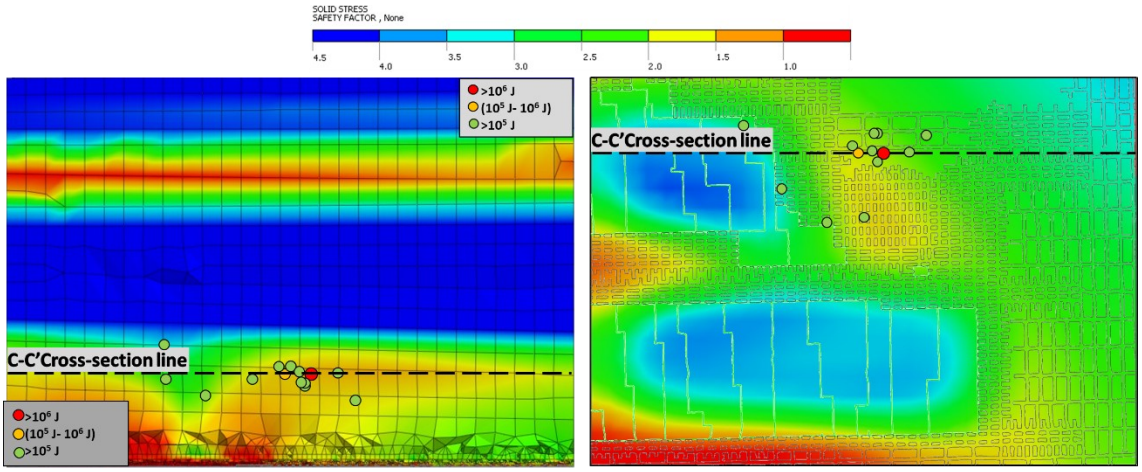


Figure 10. Horizontal cross-section representing safety factor distribution within the analysed area (left), vertical C-C' cross-section representing safety factor distribution (right) – October.

DISCUSSION

Based on detailed analysis, it was found that scenario III ensures the best convergence of results with on-site observations of displacement. Generally, the measurement curves almost overlap with the calculated trend within the first seven months. The characteristics of convergence recorded in real conditions are close to linear while, the simulation results indicate the logarithmic nature of roof and floor displacements. Some differences may be detected in the last three months of measurement due to the lack of convergometers located close to the mining front. This situation is most likely due to the limitations of the developed numerical models, which do not take into account the plasticization of the pillars over time. Still, even despite some differences correlation level is highly satisfying. Good model validation and data-driven reduction of strength parameters made it possible to identify areas prone to seismic activity occurrence using 3D FEM numerical simulations. As shown by the comparative analysis, the location of mining-induced seismic tremors coincides with the location of the zone of increased stress (reduced SF). Interestingly, the well-validated model correlates with seismic activity in both the

https://doi.org/10.5593/sgem2024/1.1/s03.41

horizontal and vertical planes. As a result, it is possible to determine potential zones of hypocentral mining tremors location. This information may be useful e.g. at the stage of designing active rock burst prevention in the form of destress blasting.

CONCLUSION

This study analyzed whether it is possible to use numerical methods based on 3D FEM to predict seismic activity in an underground mine. During the analysis, three scenarios for reducing rock strength parameters based on the GSI scale were analyzed. The displacement results within the model determined for each scenario were compared with the results of underground measurements. As it turned out, the approach based on data-driven model validation allows for a significant increase in the calculations accuracy and may be used for the purposes of mining-induced seismicity prediction. Of course, it should be noted that the proposed approach must be further developed in order to adapt the GHB criterion to the conditions prevailing in the analyzed area by empirically adjusting the strength parameters of the pillars in the computational model, but already at this stage, it can be stated that large-scale 3D modelling using FEM may be groundbreaking in the planning of large-scale exploitation at great depths.

ACKNOWLEDGEMENTS

This paper was prepared within the framework of the AGEMERA project “Agile Exploration and Geo-modelling for European Critical Raw materials”. The project received funding from the European Union’s Horizon Europe Research and Innovation Program under grant agreement No. 101058178.

REFERENCES

[1] Li L., Special Issue on Numerical Modeling in Civil and Mining Geotechnical Engineering, Processes, vol. 10, no. 8, Aug. 2022, p. 1571, https://doi.org/10.3390/pr10081571.

[2] Wang J., Apel D.B., Pu Y., Hall R., Wei C., Sepehri M., Numerical Modeling for Rockbursts: A State-of-the-Art Review, Journal of Rock Mechanics and Geotechnical Engineering, vol. 13, no. 2, 2021, pp. 457–478, https://doi.org/10.1016/j.jrmge.2020.09.011.

[3] Nikolić M., Roje-Bonacci T., Ibrahimbegović A., Overview of the Numerical Methods for the Modelling of Rock Mechanics Problems, Tehnicki Vjesnik - Technical Gazette, vol. 23, no. 2, 2016, https://doi.org/10.17559/TV-20140521084228.

[4] Dhawan K.R, Singh D.N., Gupta I.D., 2D and 3D Finite Element Analysis of Underground Openings in an Inhomogeneous Rock Mass, International Journal of Rock Mechanics and Mining Sciences, 39, no. 2, 2002, pp. 217–227, https://doi.org/10.1016/S1365-1609(02)00020-5.

[5] Alonso-Jiménez A., Arlandi-Rodríguez M., Lopez-Jimeno C., García-Berrocal A., Determination of the Stress State Prior to Excavation in an Underground Slate Mine Using Flat Jack and Numerical Methods, Journal of the Southern African Institute of Mining and Metallurgy, 122, no. 9, October 31, 2022, pp. 1–6, https://doi.org/10.17159/2411-9717/1916/2022.

[6] Marian D.-P., Onica I., Finite Element Modelling of the Stability of Underground Mining Excavations at Old Mines – Slănic Salt Mine, Mining Revue 27, no. 1, March 1, 2021, pp. 12–23, https://doi.org/10.2478/minrv-2021-0002.

[7] Aydan Ö., Ohta Y., Geniş M., Tokashiki N., Ohkubo K., Response and Stability of Underground Structures in Rock Mass during Earthquakes, *Rock Mechanics and Rock Engineering* 43, no. 6, 2010, pp. 857–75, https://doi.org/10.1007/s00603-010-0105-6.

[8] Li Y., Jin X., Lv Z., Luo W., Dong J., Effect of Earthquake on Stability of Subway Station and Ground Motions of Surrounding Rock Masses, Journal of Vibroengineering 18, no. 2, March 31, 2016, pp. 1060–1070, https://doi.org/10.21595/jve.2015.16109.

[9] Ma C., Zhou S., Chi J., Seismic Performance Analysis of Underground Structures Based on Random Field Model of Soil Mechanical Parameters, Earthquake Research Advances 2, no. 4, 2022, 100170, https://doi.org/10.1016/j.eqrea.2022.100170.

[10] Hoek E., Brown E.T., The Hoek–Brown Failure Criterion and GSI – 2018 Edition, Journal of Rock Mechanics and Geotechnical Engineering, 11, no. 3, 2019, pp. 445–463. https://doi.org/10.1016/j.jrmge.2018.08.001.

https://doi.org/10.5593/sgem2024/1.1/s03.41

INTERVENTION AND RESCUE IN CONFINED SPACES IN CASE OF POTENTIALLY EXPLOSIVE AREAS CAUSED BY THE PRESENCE OF HYDROGEN

PhD. Eng. Andrei Lucian Gireadă
PhD. Eng. Daniel Pupăzan
PhD. Eng. Artur George Găman
PhD. Eng. Cristian Nicolescu
PhD. Eng. Cosmin Ilie
National Institute for Research and Development in Mine Safety and Protection to Explosion, **Romania**

ABSTRACT

It is essential to adopt appropriate prevention measures to protect workers operating in confined spaces.

Working in confined spaces poses a risk factor for accidents or unwanted events with an impact on human health. Implementation of good practice rules in these situations is a mandatory preventive measure.

A confined space is any location not intended for regular work, has entry or exit restrictions, is under atmospheric pressure, has inadequate ventilation, a risk of drowning or suffocation, a contaminated atmosphere, or an oxygen deficiency.

Therefore, in the case of confined spaces, measures are necessary to protect workers from hostile atmospheres, from materials that may cover them, or other hazards that do not provide safety.

By implementing safety measures, the risk of accidents or unwanted events in confined spaces with potentially explosive atmospheres, cause by the presence of hydrogen, can be significantly reduced, and workers can be efficiently protected against the dangers associated with these work environments.

Keywords: confined space, explosive atmosphere, intervention and rescue personnel, hydrogen.

INTRODUCTION

Hydrogen is used as a raw material, fuel or for energy transport and storage and has many applications [1]. The ignition temperature of hydrogen is 560°C, very high temperatures being required to ignite a hydrogen-air mixture.

Hydrogen is considered the fuel of the future [2], due to the low impact on the environment through the lens of the carbon footprint. Hydrogen is a simple element, burning it does not generate carbon unlike fossil fuels. Producing hydrogen is not simple, there are many sources of hydrogen. By obtaining hydrogen there is an internationally accepted color code that defines the environmental impact:

https://doi.org/10.5593/sgem2024/1.1/s03.42

- black hydrogen is the most damaging to the environment [1,2]. It is obtained from the gasification of coal, in this process harmful carbon emissions are released which can have long-term impacts on the climate;

- gray hydrogen, is obtained from natural gas, most commonly from methane, through a process called methane steam reforming. Currently, it is the most common form of hydrogen production, where the greenhouse gases produced during the process are not captured [2]. Steam reforming involves the combination of hydrocarbons with steam to produce hydrogen and carbon dioxide. Hydrocarbons such as natural gas or bio-gas are exposed to high temperatures, forming hydrogen and CO2 [1];

- blue hydrogen is based on the conventional process of reforming methane with steam, but the carbon dioxide [2], obtained as a by-product, is captured and stored underground;

- turquoise hydrogen, is one of the newest colors [1], added to the hydrogen spectrum, it is produced through a process called methane pyrolysis. The principal resulting elements are solid hydrogen and carbon;

- green hydrogen is the only product with zero emissions of greenhouse gases. It is obtained using renewable energy sources such as solar, [1,2] wind and hydroelectric power. Large-scale production of green energy from hydrogen is usually accomplished by two main methods, water electrolysis and steam reforming. The resulting reaction produces only hydrogen and oxygen, which means that zero carbon dioxide is emitted in the process [1].

Working in confined spaces constitutes a risk factor generating accidents or unwanted events with an impact on human health [3,4]. Applying the rules of good practice in these situations constitutes a mandatory preventive measure [5,6].

A confined space is any place that is not intended for work in the current way, has entry or exit restrictions, is at atmospheric pressure, has inadequate ventilation, danger of drowning or suffocation, contaminated atmosphere or oxygen deficiency [7].

ACCESS AND WORK IN CONFINED SPACE

Access and work in the confined space is allowed only after meeting the security requirements resulting from the application of an access and work procedure in Security [3,4], specific to the confined space, are developed by the workplace leader (figure 1) [5].



Fig. 1 - Access and work in confined space

The procedure for accessing and working in confined spaces must include the following operations: the chronological designation of the operations required to be performed in the confined space as well as the selection of appropriate tools and tools [6], the identification of dangers, the nomination of specific protective measures, the establishment and procurement the specific protective means and equipment that must be used [7], drawing up the work permit, selecting, from the health point of view, the personnel involved, drawing up the specific safety work instructions in the confined space, the nomination of employees from the rescue teams and the protection and fire fighting; theoretical and practical training of personnel on how to access and escape in case of an accident [5,6], as well as on how to work, how to use protective means and equipment, fire fighting, rescue and first aid help, making, if necessary, the means of access and evacuation, identifying the possibilities of isolating the confined space and carrying out all possible isolation operations.

For any kind of intervention, revision and repair to installations, machines, equipment, tanks, cisterns, a FIRE-FREE WORK PERMIT must be drawn up.

Welding, cutting, gluing or other similar operations that present a fire hazard will require a FIRE WORK PERMIT.

The permit is a document issued by the head of work that must contain at least the following information: the precise identification of the enclosed space to be entered, the purpose of entry, the authorized period for entry [4], authorized persons entering, supervisor, head of work, known dangers , the space control methods, which are the acceptable entry conditions, the values of the initial and periodic tests, the emergency procedure that will be used, the communication methods used.

Other requirements for the document: to be completed before entry; it is signed by the supervisor, the foreman, as well as by the people entering, the document can be found with the supervisor upon entering the confined space.

Preliminary assessments of confined space entry: carrying out tests and measurements to allow entry, what is the minimum number of workers required and assigning responsibilities, whether the confined space was well ventilated or ventilated before people entered, the individual protective equipment of each person, what devices, tools, specific safety systems required for operations in confined space (figure 2), there are procedures and equipment for emergency situations.



Fig. 2 - Movement in confined space

https://doi.org/10.5593/sgem2024/1.1/s03.42

The operations of checking the atmosphere in confined spaces must initially be performed only by authorized persons.

For access and work without respiratory protection devices in a confined space, its atmosphere must correspond to the following parameters:

- the concentration of oxygen, in percentage by volume, must be between 19% and 22%;

- gazelle, toxic, noxious, corrosive or irritating vapors or powders or biological agents must be below the admissible exposure limit values set out in the regulations in force.

The warning signals emitted by the automatic equipment for detecting, measuring, signaling and monitoring the atmosphere of the enclosed space must be able to be perceived simultaneously by the supervisor and the workers in the enclosed space, respectively the equipment must be in good working order and periodically checked by the bodies of metrology, the use of equipment with an expired verification period and/or inadequate precision class being prohibited.

Equipment that is to be used in potentially explosive atmospheres must be certified for explosion protection.

The equipment must emit warning signals easily perceptible by the supervisor and by the workers working in the confined space, in the event of reaching the permissible limit values.

Before starting to wash confined spaces, they must be ventilated until the concentration of flammable gases in the air is reduced to below 20% of the lower explosion limit of their atmosphere.

It is prohibited to continue welding, polishing or any activity generating sparks in the enclosed space where explosive atmospheres may occur, at values of the concentrations of gases or vapors or mists or dusts higher than 20% of their lower explosion limit.

It is forbidden to turn off general and partial ventilation fans without the approval of the workplace manager.

POSSIBLE HAZARDS IN CONFINED SPACES (figure 3)

- danger of suffocation can be caused by a chemical working environment, the replacement of oxygen with other gases, the consumption of oxygen through bacterial fermentation or absorption by plants, soils and seeds, consumption by fire or following massive rusting, the effect is asphyxia, respiratory disorders, then of the brain, and even death;



Fig. 3 – Confined spaces

- the toxic danger for humans is given by the working atmosphere in a confined space which can be made up of gases, vapors, mist, powders, dust, fumes with toxic effects on humans;

- the danger of fire or explosion is due to the content of gases, vapors, mists or flammable powders that can ignite in a mixture with air by initiation by an ignition source;

- the danger of suffocation through inhalation or chest compression exists where the person is exposed to the danger due to the opening of hatches or the spraying of liquids or powdery materials;

- the danger of drowning / clogging exists where solid or granular materials (soil, sand, grains, other powdery materials) can flow freely and cover the body completely;

- danger of a mechanical nature manifests itself through the direct impact on the human body crushing, hitting, catching, sectioning, cutting, stabbing by moving mechanical elements and organs;

- thermal stress in the confined space manifests itself on the people entered, through uncomfortable temperatures or temperature variations. External temperatures that are too low or too high (over 40˚C or below -15˚C);

- other types of dangers, depending on the operations performed during the intervention in a confined space, there may be other dangers of a physical nature: noise, vibrations, falling objects, manipulation of materials, electricity, working with hazardous substances;

- the appearance of hydrogen in confined spaces can be caused by various processes and situations, including: chemical reactions - hydrogen can be produced in confined spaces as a result of electrolysis reactions or chemical reactions between various substances; biological reactions - some microorganisms can produce hydrogen in their metabolic processes, such as certain anaerobic bacteria can produce hydrogen in specific environmental conditions; physical reactions - some physical processes, such as the thermal decomposition of organic materials, can generate hydrogen in confined spaces; accidents or leaks - hydrogen can appear in confined spaces as a result of accidents or leaks, for example, when equipment or systems using hydrogen malfunction (figure 4).

https://doi.org/10.5593/sgem2024/1.1/s03.42



Fig. 4 – Gas monitoring

The training of people entering the confined space must contain: the risks of injury and the method of action in case of their manifestation; handling the technical equipment, tools and devices used; the appropriate behavior in the event of breakdowns or critical situations; use of individual protective or rescue equipment; use of the surveillance system and connection with the outside; procedures for specific emergency situations; first aid measures appropriate to the operations performed.

POTENTIALLY EXPLOSIVE ATMOSPHERE IN CONFINED SPACES (figure 5)

In situations where there is a risk of a potentially explosive atmosphere due to the accumulation of hydrogen in a confined space, intervention and rescue requires a specialized and careful approach: assessment of the situation is essential to assess and determine the level of danger. It is important to determine the source of the hydrogen and the amount accumulated, as well as whether there are any other flammable or hazardous substances present in the area.



Fig. 5 – A potentially explosive atmosphere

Ensuring safety Before entering the confined space, it is essential to ensure that all sources of ignition are removed and that the environment is suitable for the intervention. This may involve venting the space to remove hydrogen build-up and prevent the formation of an explosive atmosphere.

Personal protective equipment must be worn throughout the intervention to minimize the risk of exposure to hazardous substances or the risk of explosion. This may include protective suits, breathing masks and firefighting equipment.

Intervention and rescue, after all necessary security measures have been taken, can be carried out. It is important that the personnel involved are trained and follow the

intervention procedures in such situations. Depending on the circumstances, this may involve the evacuation of people from the affected area or the removal of the hydrogen source.

Continuous monitoring of the situation is essential throughout the intervention to ensure that the risk of explosion is minimized and that everyone involved is safe.

CONCLUSIONS

Whatever the cause of hydrogen in confined spaces, it is important to take appropriate measures to manage the situation and minimize the risk of accidents or fire/explosion. These measures may include ventilating the space to disperse hydrogen, isolating the source of hydrogen, using gas detection equipment to monitor hydrogen levels, and implementing appropriate safety procedures to prevent incidents.

In any situation where there is a potential for explosion due to hydrogen build-up, the primary priorities must be personnel safety and minimizing risk to all involved.

The decisive factor in ensuring the success of an intervention and rescue operation in aggressive toxic or chemical environments resides in the optimal design and efficiency of a training process for the rescue personnel, which includes intervention in confined spaces.

A confined space is any place that is not intended for work in the current manner. It has entry or exit restrictions, is at atmospheric pressure, has inadequate ventilation, and presents a danger of drowning or suffocation, contaminated atmosphere, or oxygen deficiency. For these reasons, in the case of enclosed spaces, measures are necessary to protect workers from the hostile atmosphere, the materials that may cover them, or other unsafe hazards.

In the process of intervention and rescue in confined spaces, aspects are dealt with: working in confined spaces, the access procedure / working in confined spaces, the obligations of workers, the supervisor's obligations, checking the atmosphere while working in a confined space; specific measures for working in a confined space.

Working in confined spaces constitutes a risk factor generating accidents or unwanted events, with an impact on human health. The application of good practice rules in these situations constitutes a mandatory preventive measure.

Intervention in confined spaces presents unique challenges and requires a careful and specialized approach, especially when the use of hydrogen or other flammable substances is involved.

Cooperation and communication between workers, local authorities and industrial security specialists is essential for effective emergency management. Clear and quick communication can make the difference in protecting lives and minimizing damage.

The approach to intervention in confined spaces must consider aspects such as: risk assessment, prevention, planning, protective equipment and monitoring, as well as effective cooperation and communication between all involved.

ACKNOWLEDGEMENTS

This work was carried out through the "Nucleu" Program within the National Plan for Research, Development and Innovation 2023-2026, with the support of the Romanian

https://doi.org/10.5593/sgem2024/1.1/s03.42

Ministry of Research, Innovation and Digitalisation, project no. 23 32 01 02, title: Development of assessment, testing and intervention methods for explosive atmospheres generated by facilities for the production, storage, transport and use of hydrogen.

REFERENCES

[1] Z. Zhou, C. Wen, X. Liu., Hydrogen as a Sustainable Fuel: Recent Advances in Hydrogen Production and Utilization, Applied Energy, 2021.

[2] Y. Zhang, Z. Shen, Y. Xu, Recent Advances in Hydrogen Production and Storage for Fuel Cell Applications, Energy & Fuels, 2020.

[3]. Kovacs, A. Gireada, A. Irimia, L. Munteanu, Assessment of psychosocial risks associated to intervention and rescue activity in toxic / flammable / explosive environments, MATEC Web of Conferences Volume 342 (2021) 9th edition of the International Multidisciplinary Symposium "UNIVERSITARIA SIMPRO 2021": Quality and Innovation in Education, Research and Industry – the Success Triangle for a Sustainable Economic, Social and Environmental Development" Petrosani, Romania, May 27-28, 2021 DOI: https://doi.org/10.1051/matecconf/202134201007.

[4]. I. Kovacs, A. Gireada, L. Toth, S. Simion, Stress and psychological resilience in intervention and rescue activities, 10th Edition of the International Symposium on Occupational Health and Safety – SESAM 2021.

[5]. A. Gireada, C. Ilie, A. Irimia, I. Kovacs, Research on rescuers' training process in toxic / explosive / flammable environments, 10th Edition of the International Symposium on Occupational Health and Safety – SESAM 2021.

[6]. A. Gireada, G. Găman, C. Nicolescu, C. Ilie, A. Irimia, I. Kovacs, Research on establishing the physical effort of rescuers according to the activity performed and type of respiration protection equipment, Revista Quality Vol. 20 – S1, Ianuarie 2019 Pag. 61-66.

[7]. N. Cristian, A. Gireada, C. Ilie, Advanced Methods of Practical Training of Intervention and Rescue Personnel in Toxic / Explosive / Flammable Environments, SESAM -International Symposium on Occupational Health and Safety Published online: 10 January 2024 DOI: https://doi.org/10.1051/matecconf/202438900061

JUST IN BLAST- VR TRAINING

Julia Piestrzyńska[1]
[1] AGH University of Krakow/Faculty of Civil Engineering and Resource Management/ Mining Engineering, **Poland**

ABSTRACT

"Just in blast - VR training" is a student project, the main idea of which was to create a VR (Virtual Reality) training in blasting technology. The footage was recorded on the site of the Holcim Dolomite Mine "Radkowice" in cooperation with SSE Poland in the summer of 2023, with 360-degree wide-angle cameras. The acquired material was then properly selected and edited for further activities, which ultimately led to the editing and creation of an application in VR extension. The whole project is aimed at popularizing issues in the fields of mining and geological sciences to a wider audience, in particular the field of Open Pit Mining. During the session presentation of the created application-training in 360 technology which tests the user's knowledge of blasting technology. It consists of elements covering the process of designing blasting works, the process of preparation, carrying out blasting works and detonation. In addition, the training also includes the stage of preparing blasting holes with drilling works. The paper will include an introduction and explanation of VR 360 technology and its impact on the effective and rapid absorption of information by the user. The process of recording the training with a 360 camera will be presented, followed by the process of assembling the application and a demonstration of the final product on a tablet.

Keywords: Mining engineering, blasting works, Virtual Technology, Open-pit mine

INTRODUCTION

Virtual reality (VR) is a three-dimensionally created reality that allows us to create objects, events, or interactions with the environment, which is additionally enclosed in a completely fictional world created from scratch or combines elements of the fictional and real world. On a daily basis, it is mainly associated with entertainment and the gaming industry, but as it turned out, it can also carry out many numerous benefits in heavy industry. In recent years, the technology has become increasingly popular in many industrial and scientific fields. As its capabilities and popularity grow, so does the number of industries that are choosing to use the technology to train employees remotely. The industries in which mainly this technology has been implemented so far are healthcare, construction, military and aviation [2], [3]. For some time now, mining has also joined the ranks of those fields that are implementing VR technology. In 2022 a Group of researchers from AGH University of Cracow created a 360 video and WebXR interactive environment considering mining technologies and characteristic points of mining cycle in open-pit minig [1]. Their work shows how immersive technology and virtual training are developing and how they can be provided for a wider audience.

Conducting training in virtual reality brings with it a number of numerous advantages such as: ensuring the safety of the trainee, the possibility of conducting training remotely (fully remotely), the possibility of repeating training multiple times and improving one's performance, reduced costs, greater involvement of the trainee and better assimilation of

knowledge. Increased safety during the conduct of training is mainly related to the fact that the trainee is not exposed in an open work environment, where there are numerous hazards [2] that the trainee is not yet aware of at this time. Such a person is usually in a room environment in the building or even in his own apartment, so we reduce the risk of a dangerous event such as an accident or injury during learning. What's more, it gives more comfort to the trainee and reduces the amount of stress, when suddenly "throwing" the future employee right into the work field and allows him to gradually get accustomed to the future workplace. VR technology, thanks to the support of various operating systems, also allows you to run training in this technology not only on glasses dedicated to this, but such training can be as well effectively conducted on a tablet, smartphone, laptop or desktop computer. This makes it possible to conduct such training at any time and in any place that is not part of the workplace or a rented room, which greatly facilitates the process of employee induction. Using virtual reality, training can actually be conducted an infinite number of times if we provide employees with continuous access to it. This results in the fact that not only will a given material be assimilated once before the start of work in the plant, or when obtaining qualifications, but it can be repeated many times and provides an opportunity to systematize knowledge on an ongoing basis. As a result, the efficiency of learning is significantly improved, and the trainee, thanks to the involvement of the senses: hearing, sight and touch, enters into almost full immersion, which contributes to better memorization of the assigned material. An important point is also that we significantly reduce the number of costs that need to be incurred to organize such training for a single employee, because by creating training in virtual reality we immediately have material that will be used by many people. Also, there is no need to dedicate an employee, or even several employees, specifically to conduct training and pay them extra, nor will there be any need to disturb or interfere with the standard work day of others due to the training of newly hired employees. In addition, as previously mentioned, renting a small room, or setting up such a space on the premises, or otherwise giving remote access to employees for such training, is sufficient to conduct such training.

There are many fields in the mining industry that have a high risk factor for hazards and dangerous incidents [2], and require lengthy and multi-level training due to the complexity and intricacy of such a field. One such field is the broadly defined blasting works, which is practiced very frequently in the mining industry, especially in open-pit mining. It consists of several stages that are necessary for blasting works on a mine to be conducted efficiently and safely, and these are: drilling works, design of blasting works, preparation of blasting works and execution of blasting works. Due to the great interest in VR technology and blasting works among students of Mining Engineering, the idea was born to create a comprehensive and detailed blasting training in virtual reality in cooperation with SSE POLAND SP. Z O.O. Such training had to include all the aforementioned elements of blasting works, and to combine elements of the real and fictional worlds, so that the trainee could feel as if they were on a real mining pit during a working day. The main part of the material necessary for the creation of the training was recorded at the mining plant of the Dolomite Mine "Radkowice" Holcim Poland, during a total of 6 days of intensive work of students from the Student's Scientific Research Group called SKALNIK AGH and employees of the company SSE POLSKA SP. Z O.O.

MATERIALS AND METHODS

In order to create the application (Fig. 1.), a scenario was first developed that included legally regulated aspects and good and bad practices in the field of drilling and blasting works. The scenario was based on knowledge gained during a visit to Holcim Poland's "Radkowice" Dolomite Mine and covered the design and execution of such works. The footage was then collected using 360° spherical cameras, Insta 360 One X2 and Insta 360 One R, over several days. Footage was collected both from a special small tripod attached to the mine worker's helmet to get a first-person view (Fig. 6.) and from two tripods and a drone. Next, the collected material had to be subjected to a selection process, during which the interesting parts and the best shots were cut out, colour corrected to reflect the natural terrain of the excavation field, and exported in the form of panoramas for further work in an appropriate program. The dedicated program for such photo export and processing is Insta360 Studio, while the dedicated program for creating virtual training and walkthroughs that was used in the project is 3Dvista Virtual Pro. It was with the help of this program that the entire training was created. Selected panoramas (Fig. 5.) and 360 videos were entered into it, the appropriate interface was created, all interactive events and questions were added, and additionally individual 3D models (Fig. 4.) of the excavation field walls on which, for example, blasting works were to be carried out. The training was created in such a way that during the course of the training, the participant, was able to learn about the basic theoretical issues (Fig. 2.) and the workplace, thanks to the info window function, and also to immediately corrected trainee if they choose the wrong answer, and in most cases, after choosing such a wrong answer, a new info window appears informing why the answer is wrong and brings the trainee closer to the issue in more detail. The scenes were connected by hotspots that allowed users to be redirected to further questions, videos or scenes. The basis of the scenes were 360-degree panoramas. Actions were assigned to the hotspots that triggered the training process and displayed a screen with the question, answers and relevant videos or photos. To each answer was assigned action that redirected the user further, allowing him or her to explore a given topic. After completing a given path, the user returned to the previous stage, where they could continue exploring or to move on. The transitions (Fig. 3.) between the different stages of the training are punctuated by a short video informing the user of the transition to the next part of the training. At the very end, the user gets a report in the form of points awarded to them, the time in which they completed the training, the number of questions completed, and additionally receives information on what level of knowledge they are at in relation to those in the employee hierarchy, whether they are at the level of an apprentice or perhaps at the level of a blasting engineer or above.

https://doi.org/10.5593/sgem2024/1.1/s03.43

FIGURES

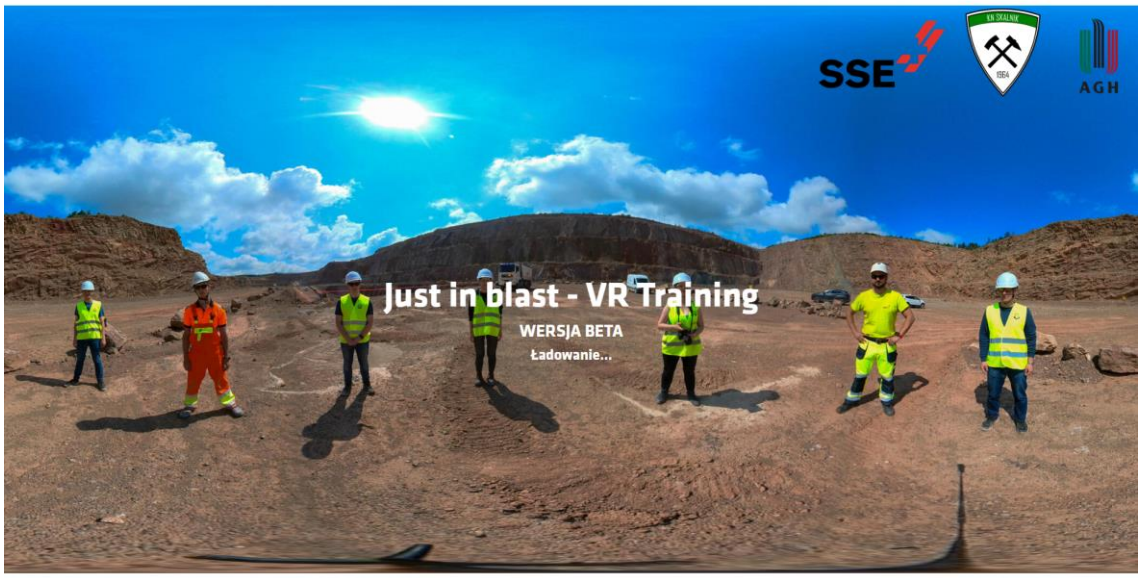


Figure 1. Training startup screen.

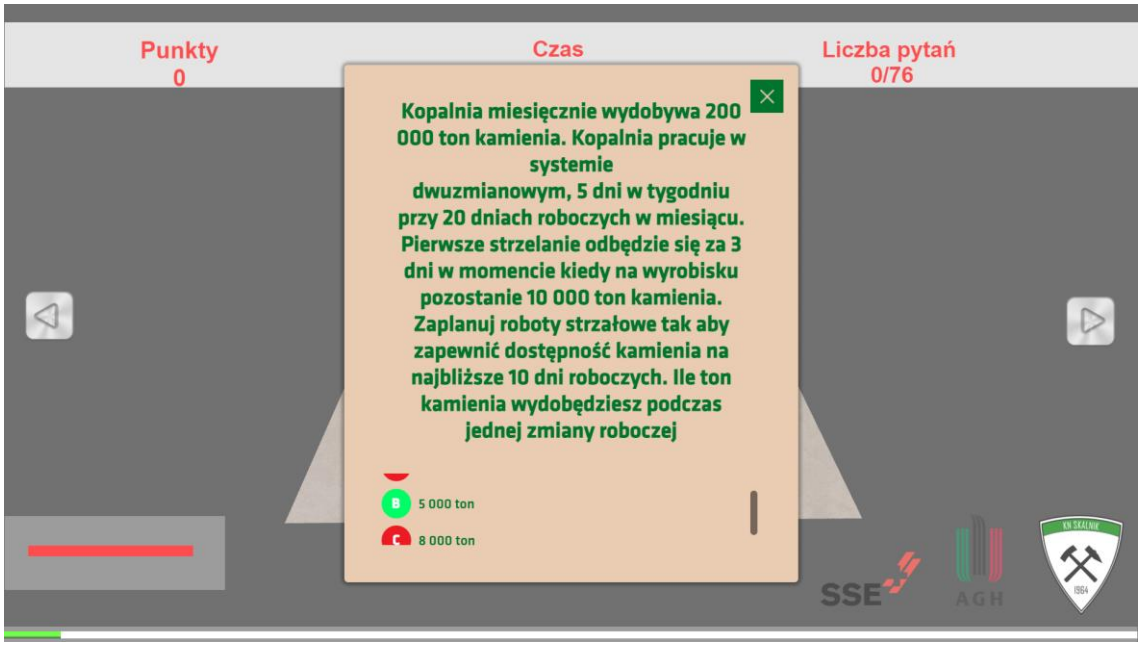


Figure 2. View of the screen with the opened question card and the answers highlighted.



Figure 3. An example of video transition between the stages of training.



Figure 4. A 360 view of the 3D model showing an example mine front on which the user is performing blasting works.

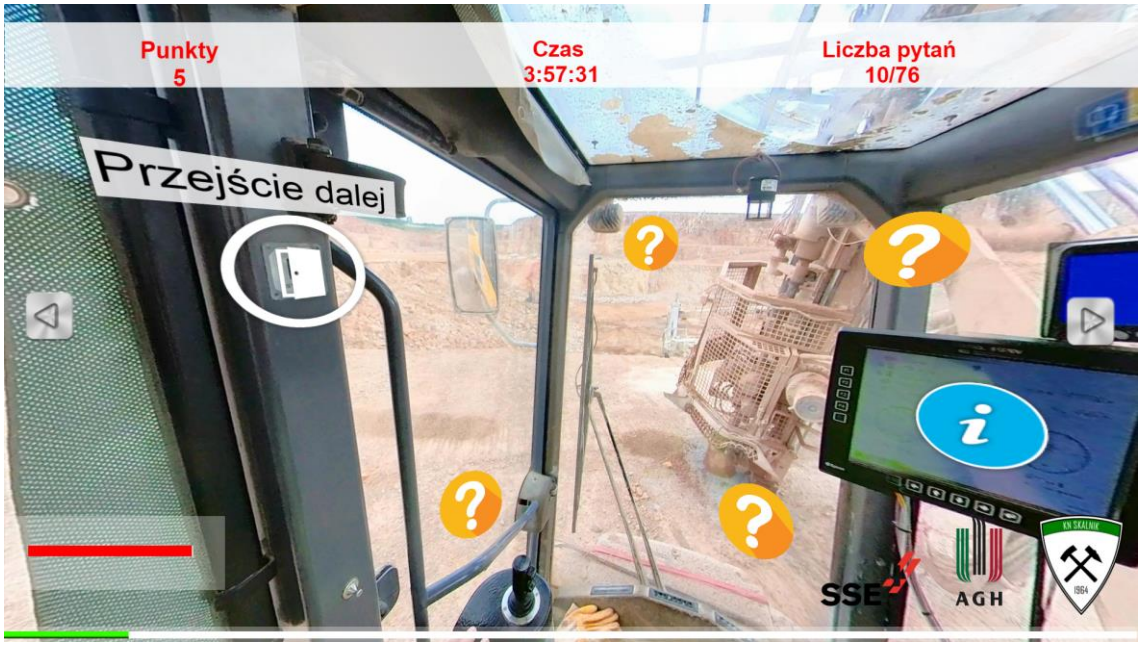


Figure 5. Sample panorama with question's hotspots and info windows.



Figure 6. The first-person view of a mine worker that allows the user to transfer to the real workplace.

RESULTS

The final result of the project is to obtain a fully substantive and interactive VR training in blasting technology, created by the students of the Scientific Research Group SKALNIK AGH, where I am in the position of vice-president, while during the implementation of the project I was as well one of the main designers and developers.

DISCUSSION

Blasting technology from the Mining industry has been chosen as the object for creating training in Virtual Reality, because it is a multi-step and very complicated issue, which in addition is fraught with high risk and requires specialized and structured knowledge to carry it out. Situating it in VR technology opens up a lot of new opportunities to train employees or students for future work in a safe and highly engaging way. With its many advantages and gaining popularity, this type of training can further serve to popularize and bring the rest of the mining industry closer to the public. Opening up to VR technology of the heavy industry gives room for innovation and improves the quality of work. This is an ever-evolving technology that will have more and more opportunities to offer in the future, and in order to keep up with the progressive world, open-pit mining should open up to it. In the future, there are plans to further develop training and virtual tours in other areas related to mining industry and safety. In addition, studies can be conducted showing how much better people trained using VR technology are prepared for the challenges awaiting them on the worksite compared to those trained using traditional methods.

CONCLUSION

The prepared training in Virtual Reality demonstrates innovative possibilities of presenting knowledge and issues from aspects of the mining industry that are characterized by high complexity and hazard risk. The creation of the virtual training was a huge challenge and took a great number of hours. The result is a virtual application with an enormous database of questions, a large amount of material to provide and a comprehensive introduction to issues in the field of blasting works. Participants are able to find their way around and navigate their own training progress in a very fast and intuitive way, despite using the technology for the first time. Thanks to numerous panoramas recorded in a mine carrying out blasting works on a regular basis, the trainees are able to feel as if they are at a real blasting site. Despite the short time since its inception, the training is beginning to resonate not only within AGH University and the mining industry, but is additionally beginning to attract the interest of non-miners. This proves how VR technology is gaining favour and popularity among the public, and that it can be used to innovatively modernize the way heavy industry works.

ACKNOWLEDGEMENTS

This work was supported by a grant “Just in blast – VR training” in cooperation with SSE POLAND SP. Z O.O. Special thanks to the authorities and employees of SSE POLAND SP. Z O.O., to Blasting Technique Department Manager/Blasting Engineer Łukasz Kordyzon of SSE POLAND SP. Z O.O., to the Kopalnia Dolomitu “Radkowice” Holcim Polska, to Michał Patyk from the Department of Mining Engineering and Work Safety, AGH University of Krakow, to Kinga Firmanty the leader of “Just in blast project” and president of the Student Research Group SKALNIK AGH.

REFERENCES

[1] ”Put your feet in open pit”-a Web XR Unity application for learning about the technological processes in the open pit mine, Pomykała R., Patyk M., Sikora M., Cybulski A., Boniecka J., Juszczak J., Klatka T., Kędzierski M., Igras – Cybulska M., IEEE

Conference on Virtual Reality and 3D User Interfaces Abstracts and Workshops (VRW), (2022).

[2] Use of virtual reality in underground roof fall hazard assessment and risk mitigation, Isleyen E., Duzgun H. S., International Journal of Mining Science and Technology (2019).

[3] Virtual Reality Models for Hazard Assessment and Risk Mitigation in Tunneling, E. Isleyen, S. Duzgun, P. Nelson, Tunnels and Underground Cities: Engineering and Innovation meet Archaeology, Architecture and Art (pp.4857-4863), (2020).

MULTICRITERIA ANALYSIS OF THE AGGREGATE PRODUCTION BY-PRODUCT PURPOSES

Marek Ondov, MSc.[1]
Prof. Marian Sofranko[1]
Jan Chovan, MSc.[1]
Marek Szucs, MSc.[1]
Lukas Hlavaty, MSc.[1]
[1] Technical University of Kosice, Faculty BERG, **Slovakia**

ABSTRACT

Aggregate is one of the essential components of artificial structures. Aggregate is obtained by mining, as is the case with mineral raw materials. The output of aggregate mining is, in addition to the main product, also a secondary one - sludge. Sludge is an integral part of the wet processing of the most minor aggregate fractions. The amount of sludge in quarries is increasing, while the task of sludge management is to find a purpose for it and thus utilize it. Sludge management methods must consider the most negligible possible burden on the environment and the use of mining areas. Sludge pressings may be a way to reuse waste material. The properties of sludge pressings indicate the possibilities of their inclusion in the processes of various branches of industry. The multicriteria analysis also focuses on the economic side of their potential purposes because their price as a commodity created from waste is low on the market. The goal is to find a variant that will benefit the potential customer but, at the same time, will not worsen the economic situation of the quarry that will supply the sludge pressings. Among the analysis criteria, logistic criteria must be included, considering the costs of the preparation, storage, handling, and transportation of sludge pressings.

Keywords: Multicriteria analysis, production of aggregates, waste, sludge pressings, costs

INTRODUCTION

Various by-products or waste are generated in addition to the main products during the extraction and production of aggregate. Due to their properties, these outputs from the aggregate production process usually have limited use. These by-products often become a problem and a burden for aggregate producers, necessitating the search for further utilization options. New approaches to handling mining by-products should minimize waste and increase the efficiency of the entire process or create added value.

Reverse logistics and waste management aim to find solutions for effectively handling by-products and waste in companies, thereby creating added value from these outputs of their production processes. The task of reverse logistics is to ensure the collection, sorting, disassembly, and processing of used products, components, by-products, excess inventory, and packaging materials. Its primary goal is to find new uses for these items or to recover their materials in a way that is both environmentally friendly and

economically efficient [1]. Reverse logistics is one of the growing areas of study within supply chain management. It is considered a crucial element of the circular economy, which embraces a restorative or regenerative approach to industrial economics [2].

Waste management encompasses a series of activities that deal with processing generated waste and its prevention and reduction. An integral part of effective waste management is the gradual reduction of waste produced and the recovery of high-quality secondary raw materials, ultimately leading to the conservation of primary resources and energy. Waste processing involves various measures to improve handling, storage, and reuse properties. Waste utilization focuses on recovering its value, which includes activities aimed at exploiting the waste's physical, chemical, or biological properties. The priority is material recovery over energy recovery, meaning the use of waste as a secondary raw material for the production of new products that can be reused [3]. Many companies have implemented and strengthened their waste management programs to achieve better resource efficiency and reduce costs for products intended for sale. Pressure from consumers, government intervention, or a combination of both has usually motivated these companies to introduce new initiatives. These initiatives can be divided into two main categories: traditional waste management and the circular economy concept. Reducing the amount of raw materials used in production helps to lower the costs of products intended for sale. Creating a circular economy, which involves transforming waste products into revenue sources, increases income by utilizing by-products that would otherwise be discarded. Both companies and governments have seen significant financial benefits from effective waste management strategies [4].

The research subject is sludge pressings as a by-product of mining in Slovak quarries. After the wet processing method, the tiniest fraction remains in a water-saturated state, typically ranging from 0 to 4 mm. Sludge management focuses on dewatering fine-grained waste products from the water suspension so they can be deposited in waste dumps and returning the maximum amount of used water into the processing cycle [5]. The sludge in the examined operation, containing fine dust particles, is further recycled to maximize water reuse in the production line. After dewatering, the sludge is pumped into a filter press, where the fine particles are compressed into pressings with a maximum moisture content of 20%. These sludge pressings fall into a prepared concrete box and can be quickly loaded with a wheel loader and deposited at a designated site. Between 2019 and 2023, the average amount of sludge, including a 29% water content in the sludge pressings, was 14,975 tons [6,7].

The sludge pressings in the examined quarry significantly occupy space and are becoming a limiting factor. The attitude towards them is shifting towards considering them as waste, which does not bring any benefits or advantages to the company. This article aims to highlight the potential uses of sludge pressings as a by-product and conduct a multicriteria analysis of possible uses through economically and logistically oriented criteria.

MATERIALS AND METHODS

Before conducting an economic assessment of sludge pressings, it is necessary to define their applications. Sludge pressings can be justified in various sectors of human activity because of their chemical and physical properties.

The first logical solution is their use at the place of origin. They can be utilized for reclamation in the quarry where they were produced or in another quarry. The most

significant advantage is their application in the same geological environment where they originated. However, quarry reclamation might not occur in the foreseeable future. This uncertain period leads to storage costs and increases spatial requirements in the quarry. Transportation costs and the low purchase price of sludge pressings burden distribution to other quarries.

Sludge pressings have potential applications in the construction industry, although not in concrete mixtures [8]. They can be used as substitutes for concrete mixtures, particularly in quarry operations, where geopolymer mixtures (Figure 1) can replace various types of concrete. Additionally, they could be used to produce artificial aggregate or lightweight concrete [9].



Figure 1 Geopolymer from andesite dust [9]

Using sludge pressings to produce other construction products, such as bricks or plasters, seems feasible [10], but further precise research is needed in this area.

The sealing potential of sludge pressings can be utilized in the case of watercourses, water structures, or water disasters. These properties are applicable in the modification of riverbanks or the construction of water dams. A specific area of interest is flood protection, where sludge pressings could serve as a suitable sandbag alternative. Sandbags are widely used in temporary flood protection systems [11, 12].

The sealing properties of sludge pressings can also be useful in constructing bottoms and slopes of non-hazardous waste landfills. Decree of the Ministry of Environment of the Slovak Republic No. 382/2018 Coll. considers sludge pressings as mineral sealing [13].

One of the alternative uses of sludge pressings is their utilization in forestry to create a foundational soil layer in tree nurseries. In 1994, an observation was made during the reclamation of a quarry operated by EUROVIA. Dried sludge pressings were spread over the areas above the mine tailings, and small saplings were planted in the strip bordering the forest. After some time, a faster growth of the saplings was observed compared to those in the traditional nursery. However, this phenomenon has yet to be further investigated [7].

A multicriteria analysis is applied to evaluate the potential uses of sludge pressings for economic evaluation. Multicriteria analysis is used when multiple dimensions and criteria are involved in the decision-making process. However, the concept of multicriteria

analysis encompasses a variety of methods and approaches. These methods can be divided into formal and simplified ones. Formal methods are based on numerous rules and mathematical relationships and require time and resources. Meanwhile, simplified methods were developed for quick application in multicriteria decision-making, often influenced by subjectivity [14].

Simple additive weighting methods are straightforward and utilize a weighted additive model, which is also typical for formal methods. This method concludes the analysis with overall scores as the weighted sum of individual performance assessments, showing the best option. The process's results are usually presented through performance tables [14]. Table 1 illustrates the procedure of a simple additive weighting method and its specification for the multicriteria analysis of sludge pressings utilization.

Table 1 Procedure of a simple additive weighting method [14]

Key step	**Specification**
Primary problem analysis	The ranking problem of sludge pressings using
Development of the options to be assessed	Reclamation of quarries (O1), Production of concrete and geopolymers (O2a), Production of other building products (O2b), Application in water sealing (O3), Application in waste landfills (O4), Application in forestry (O5)
Identification of criteria	As specified in the Results chapter
Construction of the performance profile of each option	Subjectively, according to the evaluator, based on information from various publications and their own experiences.
Scoring	Direct approach on a scale from 0 to 10
Weighting of criteria	Simple rating normalized to 0-1
Combination of scores and weights	Multiplication
Sensitivity analysis	Exchange of the highest and lowest weights
Presentation of the results	Performance table

RESULTS

The evaluation of various options for sludge pressings utilization and the determination of criteria weights were performed using an expert-based approach, introducing a higher degree of subjectivity into the applied multicriteria analysis method.

The criteria monitored in the method are as follows:

1. Transportation costs,
2. Product adjustment costs,
3. Storage costs,
4. Lost opportunity costs,
5. Readiness inventory of sludge pressings costs,
6. Revenue from value-added sludge pressings,
7. Revenue from sales,
8. Revenue from the elimination of other resources used.

Table 2 displays the results of the simple additive weighting method. The problem was addressed in terms of maximization.

Table 2 Performance table of the simple additive weighting method

		O1		O2				O3		O4		O5	
				a		b							
Criterion	**Weight**	**Score**	**W*S**	**Score**	**W*S**	**Score**	**W*S**	**Score**	**W*S**	**Score**	**W*S**	**Score**	**W*S**
Transportation costs	0.15	7	1.1	6	0.9	6	0.9	6	0.9	8	1.2	5	0.8
Product adjustment costs	0.15	6	0.9	6	0.9	5	0.8	5	0.8	8	1.2	4	0.6
Storage costs	0.1	2	0.2	4	0.4	4	0.4	5	0.5	5	0.5	4	0.4
Lost opportunity costs	0.06	9	0.5	4	0.2	3	0.2	4	0.2	8	0.5	5	0.3
Readiness inventory costs	0.11	6	0.7	1	0.1	1	0.1	2	0.2	7	0.8	2	0.2
Revenue from value-added	0.15	4	0.6	1	0.2	1	0.2	2	0.3	5	0.8	2	0.3
Revenue from sales	0.15	3	0.5	6	0.9	7	1.1	7	1.1	7	1.1	7	1.1
Revenue from the elimination of other resources used	0.13	5	0.7	5	0.7	5	0.7	5	0.7	5	0.7	5	0.7
Σ=	1	**Total:**	5.1	**Total:**	4.3	**Total:**	4.2	**Total:**	4.6	**Total:**	6.6	**Total:**	4.3
	Rank	**2.**		**5.**		**6.**		**3.**		**1.**		**4.**	

https://doi.org/10.5593/sgem2024/1.1/s03.44

According to the selected criteria and the expert approach to multicriteria decision-making, the ranking of options in terms of economic feasibility is as follows: Application in waste landfills, Reclamation of quarries, Application in water sealing, Application in forestry, Production of concrete and geopolymers, Production of other building products.

After calculating the result using the simple additive weighting method, a sensitivity analysis was conducted. During this analysis, each of the four highest weight values was successively replaced by the lowest, while the ranking of the individual options remained unchanged in each case.

DISCUSSION

Currently, among the proposed and analyzed options for using sludge pressings, alternatives for their use in waste management and the mining industry are the most promising. The decisive factor for applying sludge pressings in landfill sealing is their relatively low price compared to other suitable materials. Furthermore, minimal modification and additional costs for these pressings are required from the producer's perspective in the case of this option. This alternative also has a high potential for obtaining funding from external sources because waste management is an important topic, and suitable solutions are financially supported.

The option of quarry reclamation, especially the quarry where the sludge pressings are located, ranked second mainly due to minimal or absent transportation costs. For this option, using the company's product versus purchasing material for quarry reclamation weighed heavily. However, this option entails the need for sufficient storage space where the sludge pressings will have to wait until quarry reclamation occurs.

The alternative of using sludge pressings for water sealing, even in the case of water disasters, is unattractive primarily for authorities responsible for flood protection due to the classification and stance towards the by-product of mining activities. However, this usage places high demands on the sludge pressings, and their relatively costly modification is necessary to make them suitable for water sealing.

The options for use in construction and forestry were the worst in the multicriteria analysis. Further research is required in the cases of various construction products and tree planting. Currently, their use is not supported by anything. There is zero interest from the relevant parties, and we cannot speak of added value for the producer. Utilization in concrete production is currently challenging to realize, as evidenced by the research mentioned in the Materials and Methods chapter. Geopolymers were added to this category, where sludge pressings can be applied. In this case, however, further research is needed to confirm their suitability, as with the previous options. Also, geopolymers are less widespread so that any significant economic benefits may be expected only in the future.

CONCLUSION

This paper explored the economic aspects of utilizing sludge pressings. Sludge pressings are a by-product of mining activities, which assigns them a low market value. However, their production continues unabated, occupying more and more space in quarry plants. Therefore, finding ways to bring added value to the producer is necessary.

In this paper, potential uses in five areas of human activity were outlined and assessed using an expert approach based on economic criteria. The input data for the multicriteria analysis were significantly limited and mainly assessed subjectively because objective data for individual options are either limited or non-existent. Nevertheless, experts see potential, particularly in waste management and quarry reclamation.

To increase the multicriteria analysis's accuracy, researchers need to conduct more research focused on potential uses of sludge pressings, as such research was lacking in some cases. Regarding the analysis process, unifying the use of sludge pressings in concrete and geopolymers could have distorted the final ranking of these options if they had been defined separately. Changes in the stages of development of options, setting scores, and weights have the most significant potential to improve multicriteria analysis and reduce subjectivity. It is essential to ensure the precise formulation of options and avoid unification. Even with an expert approach to multicriteria analysis, providing experts with more precise information, especially regarding economic evaluations, is better. Obtaining these economic data is challenging, which is not the researchers' fault. The market for sludge pressings is limited and needs to be utilized by buyers from various sectors. Developing the market for sludge pressings is one of the main challenges in accurately determining the economic evaluation of various options.

ACKNOWLEDGEMENTS

The authors thank the representatives of EUROVIA for their cooperation.
This article was created through the implementation of the grant project VEGA 1/0588/21 Research and development of new methods based on the principles of modelling, logistics, and simulation in managing the interaction of raw material extraction processes and the establishment of mining blocks with regard to economic efficiency and safety of raw material extraction.

REFERENCES

[1] HUSÁKOVÁ, N., Reverse logistics–theoretical bases (in Slovak), Logistický monitor, Slovakia, 2012, pp. 1-9, ISSN 1336-5851, access by: https://www.logistickymonitor.sk/images/prispevky/husakova2-okt-2012.pdf.

[2] CRICELLI, L., GRECO, M., GRIMALDI, M., An investigation on the effect of inter-organizational collaboration on reverse logistics, International Journal of Production Economics, 2021, DOI: https://doi.org/10.1016/j.ijpe.2021.108216, ISSN 0925-5273.

[3] LIŠKA, R., The alternatives of waste minimization in a selected company (in Slovak), diploma thesis, Masarykova univerzita: Ekonomicko-správní fakulta, 2008, access by: https://is.muni.cz/th/acrn4/DP_final_Archive.pdf.

[4] ROMERO-HERNÁNDEZ, O., ROMERO, S., Maximizing the value of waste: From waste management to the circular economy, Thunderbird International Business Review, 2018, Vol. 60, pp. 757-764, DOI: https://doi.org/10.1002/tie.21968, ISSN 1520-6874.

[5] ZAŤKO, F., 2017 – 04 - Supplement to the plan for opening, preparation, and mining of the exclusive deposit Vrútky – Dubná Skala for the years 2015 – 2025 (in Slovak), 2017, Company internal documentation.

[6] SULOVEC, V., Mobile aggregate washing in the conditions of the company EUROVIA (in Slovak), Košice. Proceedings SZVK, Publisher: Slovenské združenie výrobcov kameniva, 2016, approved by Ministry of Culture of the Slovak Republic.

[7] Internal Documentation of EUROVIA Slovakia.

[8] VESELÝ, V., Current status and perspectives of using recycled aggregate in concrete (in Czech), Betón, 1/2021, Praha 2021, ISSN: 1213-3116.

[9] BREZÁNI, J. MOSEJ, J. SISOL, M., Utilization of andesite dust generated during aggregate production for the manufacture of geopolymers (in Slovak), SZVK journal for experts, Publisher: Slovenské združenie výrobcov kameniva, 2014, approved by Ministry of Culture of the Slovak Republic.

[10] MOSEJ, J., SISOL, M., DRÁBOVÁ, M., MICHALIKOVÁ, F., Possibilities of using fly ash from brown coal combustion in granulation boilers for the production of alkali-activated binders (in Slovak), Recyklace odpadů, Ostrava, VŠB-TU, pp. 187 - 191, 2012, ISBN 978-80-248-2888-6.

[11] ŘÍHA, J., Protective dikes on watercourses (in Czech), Grada Publishing a.s.,

223 p., 2010, ISBN: 8024735709.

[12] OGUNYOYE, F., VAN HEEREVELD, M., Temporary and demountable flood protection: interim guidance on use, Bristol: Environment Agency, 2002,
ISBN 1 857 05845 3.

[13] Decree of the Ministry of the Environment of the Slovak Republic

No. 382/2018 Coll. on Landfilling of Waste and Storage of Waste Mercury.

[14] DEAN, M., A practical guide to multi-criteria analysis, Bartlett School of Planning, University College London, 2022, DOI: 10.13140/RG.2.2.15007.02722.

NOISE EVALUATION FOR THE DUMPER DRIVERS IN MINING ACTIVITIES: A CASE STUDY

Alfaro Degan Guido[1]
Antonucci Andrea[1]
Coltrinari Gianluca[1]
Innocenzi Sara[1]
Lippiello Dario[1]
[1] Università degli Studi Roma Tre, **Italy**

ABSTRACT

Mining activities are carried out employing a variety of machineries and equipment; in many cases these can generate relevant health problems for workers. One of the biggest hazards for workers is noise, since prolonged exposure to a noise source could cause damage through long-term exposure. Various researchers pointed out that the damage that can be generated by exposure to noise is of various types with sometimes very serious consequences. Specially drivers of particular vehicles of the mining sector, such as dumper truck and excavator, are exposed to the risk of whole-body vibrations and at the same time noise generated by the engine truck. This problem is especially founded for Load-Haul-Dump (LHD) vehicles where the driver's seat is positioned near to the engine. The objective of this study is to assess how different work phases can affect the noise exposure of LHD drivers. A measurement campaign was carried out at a site if mining 100 km from Rome a mountain context. The measurements were carried out on dump truck drivers with the aim of assessing noise exposure. The measurements were carried out with a device to detect the sound signal. The measurements were repeated several times to be able to characterize the actual working cycle during all driving phases of the LHD vehicle. The signal after being acquired was processed with a specific instrument in order to determine the sound levels and frequency spectrum and the signal analysis was carried out in third-band octave frequencies. The results obtained in the measurement campaign carried out showed a significant influence of the different phases of vehicle use on the driver's noise exposure.

Keywords: noise, dumper, mining activities, human health, quarry

INTRODUCTION

In extractive industries, workers are exposed to a multitude of occupational risks. One of the most serious dangers is the potential for rockfalls, which can occur due to various factors and have devastating consequences, including immediate fatalities of the workers [1]. In addition to this significant risk, workers in extractive activities are constantly exposed to noise, vibrations, and dust [2],[3]. Specially, the operators most exposed to simultaneous levels of noise and vibrations are dump truck drivers and operators of other

https://doi.org/10.5593/sgem2024/1.1/s03.45

heavy earth-moving machinery. It has been found that their discomfort, calculated using the regression equation developed by Huang and Griffin, has a relevant role [4]. These hazardous working conditions extend beyond physical discomfort. High levels of noise exposure ($L_{Aeq8h} \geq 80$ dB) not only lead to progressive hearing loss but also increase the risk of accidents, making workplace safety a critical concern in such environments [5].

The limits for daily noise exposure are regulated by Italian Legislative Decree 81/08. This specific law defines specifically four maximum permissible levels of noise exposure in the workplace to ensure the safety and health of workers. These limits are crucial in preventing noise-induced hearing loss and other health effects associated with prolonged exposure to high noise levels. In mining activities, it is recognized that exposure to noise is significant risk. It is caused by various machines such as excavators, hammer drills, drilling machines, and the operation of loading and unloading by dump trucks, as well as by blasting in quarries. In all these operations, the noise levels persist throughout the entire work shift and pose a danger to quarry workers. The Director General of Mine Safety (DGMS) has stipulated that the noise level inside the cabin should be less than 85 dB. To ensure compliance with these regulations, studies were conducted to find ways to mitigate the noise inside the cabin and maintain it within the acceptable limits [6]. Various materials were analysed to understand their acoustic properties in order to reduce the noise exposure. Additionally, combinations of six different materials were examined. From these studies, an optimal material was proposed to improve sound pressure levels and enhance driver comfort [7]. Despite these advancements, the noise inside the cabin is usually associated with the engine. Passive absorbers are commonly used to address the noise problem, but they are not effective for the lowest frequencies. For this reason, an alternative approach is to use an active noise control (ANC) system to tackle this issue at low frequencies, where passive absorbers are less efficient. An active noise control system using loudspeakers mounted inside the cabin of a forklift truck was utilized, demonstrating that the noise level in the low-frequency region can be significantly reduced [8]. The health implications of constant exposure to noise for vehicle operators have been a point of concern. A study investigating the vulnerability of bus and truck drivers revealed that the pulse rate of truck drivers was correlated with the noise level inside their vehicle cabins, which ranged from 87.95 to 103.4 dB. Thus, the effects of noise inside the cabin are detrimental to drivers' health [9]. Similarly, monitoring noise levels inside the cabins of heavy earth-moving machines in a chromite mining complex showed significant differences from 85 dBA, varying with the time of monitoring and type of machine, with a high association between noise levels and the dozer ($p<0.01$) [10]. Exposure to Whole-Body-Vibration (WBV) is another occupational hazard in the mining industry. The literature shows significant variability in exposure values, attributed to the different approaches authors have adopted for data collection. Whole-Body-Vibration has a multifactorial and dynamic nature; therefore, a comprehensive assessment should include road conditions, operator and equipment conditions, and the type of activity performed [11,12]. The vertical z-axis emerged as the predominant axis of exposure, while the exposure along the x and y axes increased with truck size [13,14].

MATERIALS AND METHODS

The study was conducted through an experimental campaign at a limestone quarry in Carsoli, located 100 km from Rome. The study protocol involved measuring the noise

levels in the cabin of the dump trucks and comparing them between two different dump trucks used in the quarry: *Perlini DP 405 and Komatsu HD 405* model. Table 1 provides the specifications for both examined dump trucks, specifically the year of manufacture, empty weight, load capacity, and maximum speed during ascent and descent phases.

Table 1: Technical specifications of the dumpers

	Perlini DP 405	**Komatsu HD 405**
Year	2004	2021
Tare weight	35.00 ton	37.00 ton
Payload	45.00 ton	40.00 ton
Maximum downhill speed	22 km/h	25 km/h
Maximum uphill speed	10 km/h	10 km/h



Figure 1: Dumper Perlini DP 405 (left picture) and Dumper Komatsu HD 405 (right picture)

The purpose of this study was to determine which of the four operational phases produced the highest noise levels. Once the phase with the highest noise levels was identified, the study aimed to evaluate the difference between the noise levels recorded with the open car window and with closed the car window. The two participants at the measurement campaign, who also served as the drivers of the dump trucks, were instructed to perform their normal duties during the measurement period, maintaining their typical work cycle as follows: 1) loading material, 2) loaded haul, 3)unloading in plant, 4) empty haul. The evaluation route was approximately 250 meters long, from the material loading point to the material unloading point. The weather conditions of the measurement were sunny skies with a temperature of around 30 degrees Celsius; these conditions ensured that noise levels were captured under typical working conditions in the quarry. A Larson Davis *PRM900C* (Sensitivity: 0,04240 V/Pa) sound level meter was positioned inside the driver's cab both dump trucks to measure sound pressure levels during their work cycle. The sound level meter was carefully secured on the right side of the operator's seat, close to ear height as shown in the figure and connected to a Soundbook data acquisition system.

https://doi.org/10.5593/sgem2024/1.1/s03.45

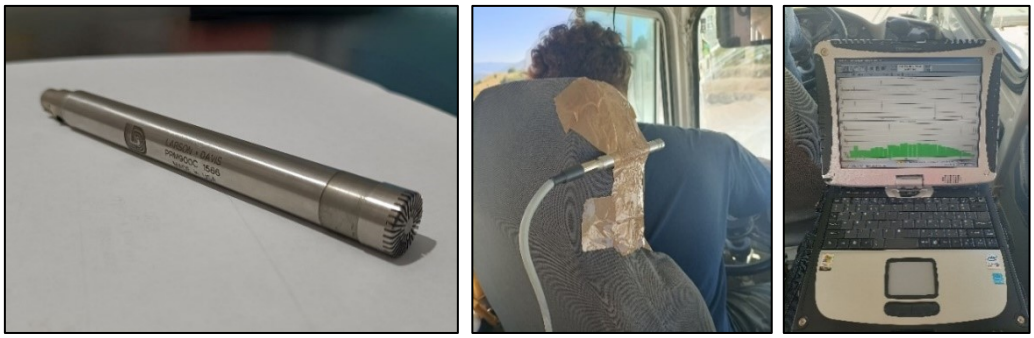
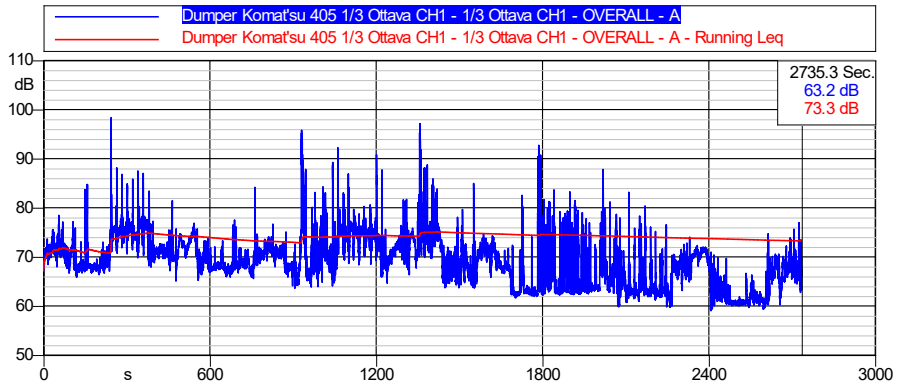


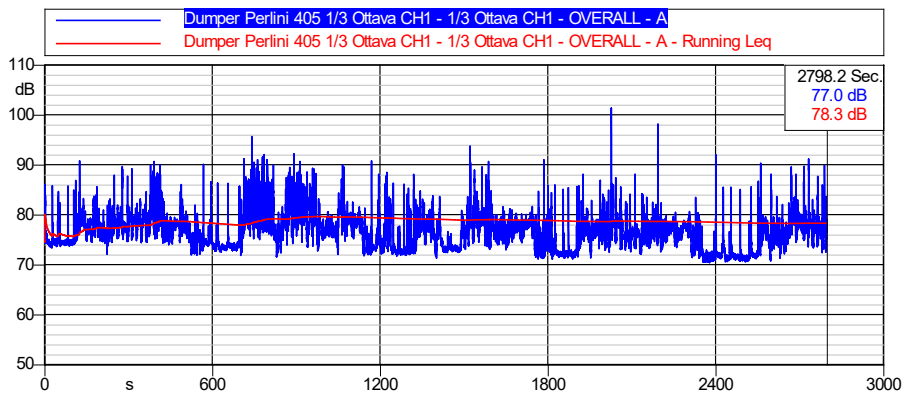
Figure 2: Larson Davison sound level meter and, Mounting the sound level meter on the seat, Soundbook

RESULTS

The graphs shown below were directly extracted from the Noise Vibration Work program, which allows for the analysis of the acquired signal. In particular, the time history graph and the frequency spectrum graph are reported. The time history graph shows how the noise levels change over time, providing a detailed view of the variations in the noise signal. The frequency spectrum graph displays the distribution of the noise signal across different frequencies, illustrating which frequencies are more prominent in the noise profile. Below are the two time history graphs for the two dump trucks for the entire 45-minute measurement period. The x-axis, representing time expressed in terms of seconds, while the y-axis represents the sound pressure level (dB) recorded at each time instant.

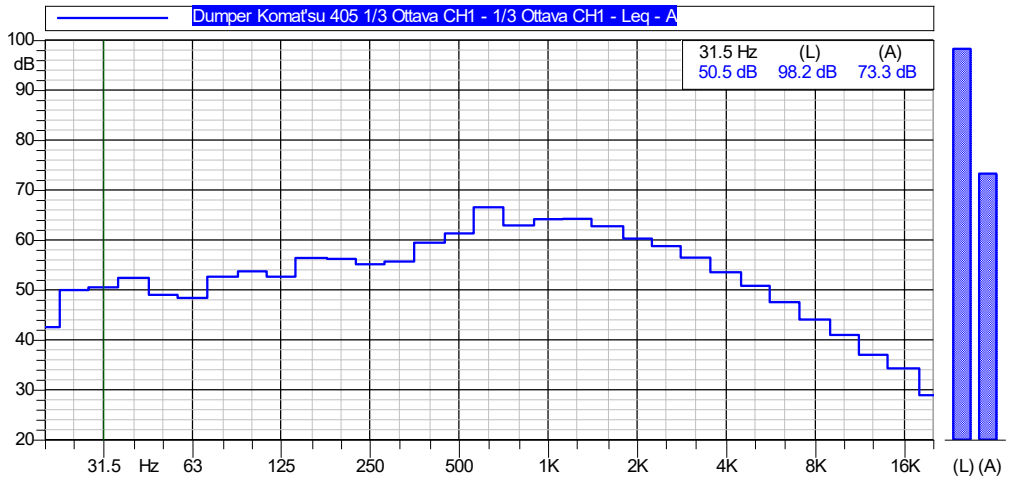


Graph 1: Time History of the entire measurement Dumper Komatsu HD 405

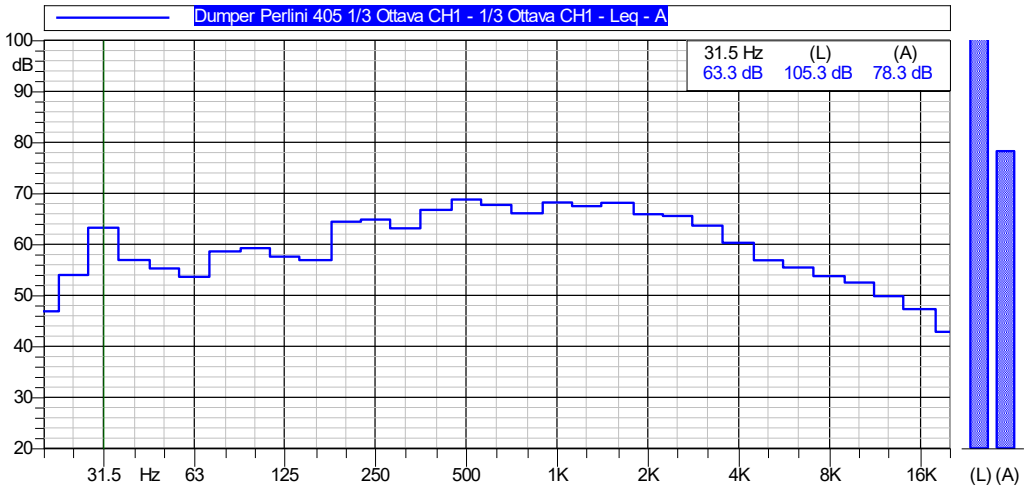


Graph 2: Time History of the entire measurement Dumper Perlini DP 405

Below are the frequency spectrum graphs of the two dump truck, illustrating the distribution of frequencies emitted during their operation. The x-axis shows the analysed acoustic frequencies, while the y-axis represents the noise intensity at each frequency (dB).



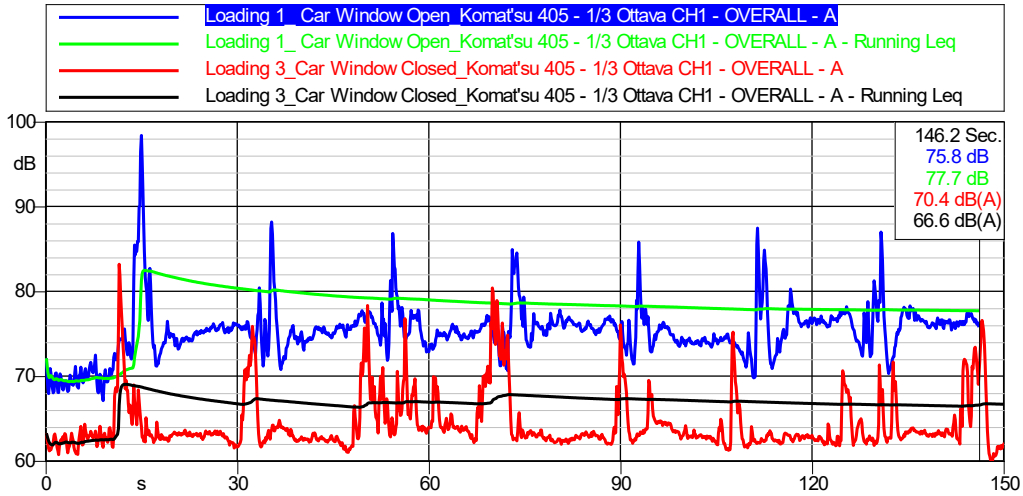
Graph 3: Frequency spectrum of the entire measurement Dumper Komatsu HD 405



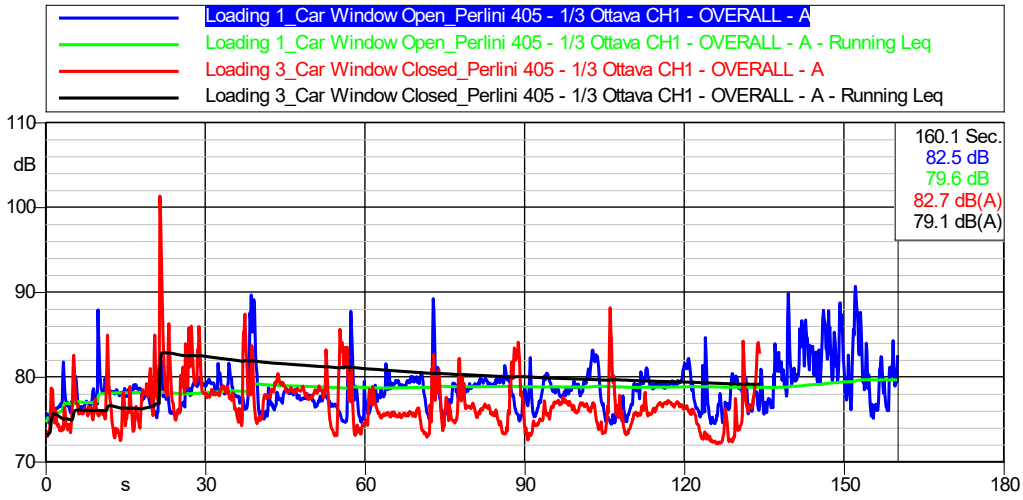
Graph 4: Frequency spectrum of the entire measurement Dumper Perlini DP 405

In Graph 5, the blue line represents the time history of the material loading phase for the Komatsu dump truck with the open car window and the green line shows the L_{eq} for the same condition. For the Komatsu dump truck with closed car window, the red line indicates the time history, and the black line shows the L_{eq}. Similarly, in Graph 6, the same information is presented for the Perlini dump truck using the same color scheme.

https://doi.org/10.5593/sgem2024/1.1/s03.45

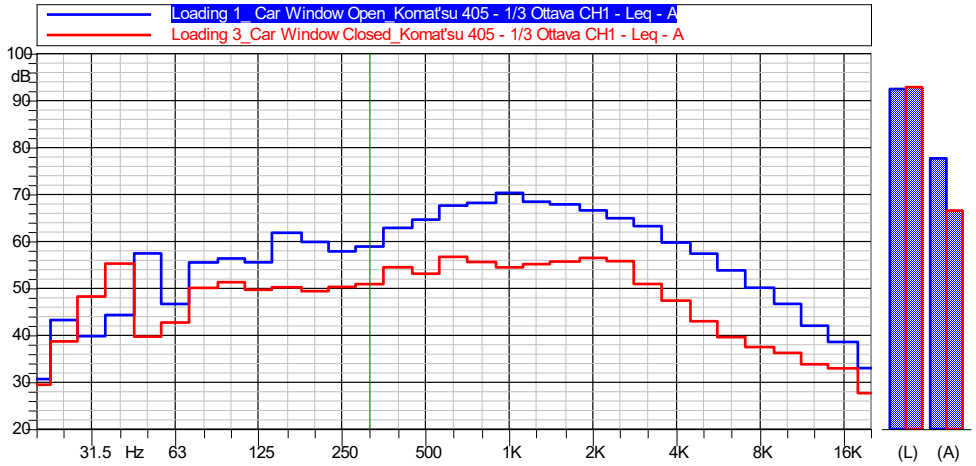


Graph 5: Time History and Leq of the loading phase Dumper Komatsu

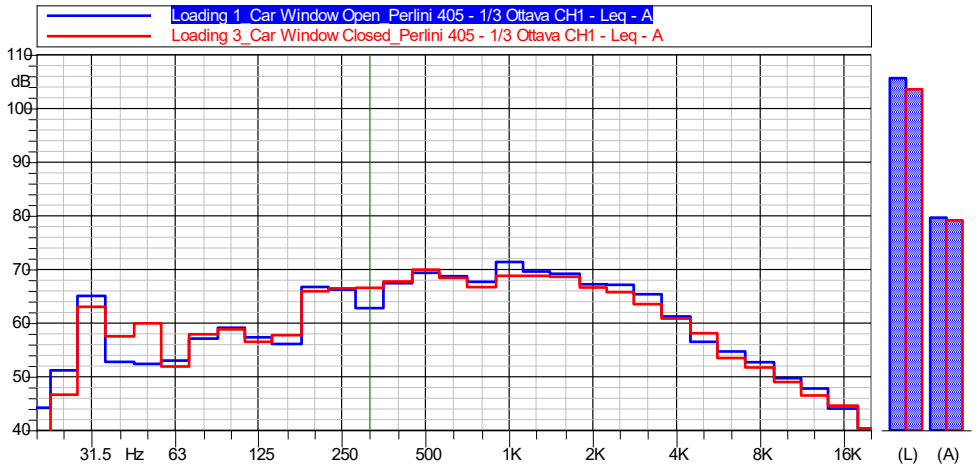


Graph 6: Time History and Leq of the loading phase Dumper Perlini

In graphs 7 and 8, the frequency spectrum for the two dump trucks are presented, first for the Komatsu and then for the Perlini. The spectra measured with the open car window are indicated in blue, while the spectra measured with closed car window are indicated in red.



Graph 7: Frequency spectrum of the loading phase Dumper Komatsu HD 405



Graph 8: Frequency spectrum of the loading phase Dumper Perlini

DISCUSSION

The time history graphs of the measurements on the two dump trucks point out that the L_{eq} parameter is higher by 5 dB for the Perlini dump truck, which is also the older model. Additionally, there is a relavant higher frequency contribution across all frequency bands. From the measurements conducted, it has been observed that there is a higher noise influence during the material loading phase from the excavator into the dump truck compared to the other three phases within the entire work cycle. For this reason, the loading phases were examined more closely, revealing a peak during the initial loading of material when the dump truck was completely empty, with subsequent peaks gradually decreasing as vehicle bed filled up. In order to obtain a detailed analysis, graphs of the time histories from measurements were compared between the open and closed operator side car windows. It is observed that on Komatsu dump truck, there is a significant reduction in recorded noise with closed car window, measuring 66.6 dB L_{eq} value compared to 77.7 dB with the open car window. However, this advantage is not observed for the Perlini dump truck, which shows 79.6 dB noise level with the open car window

https://doi.org/10.5593/sgem2024/1.1/s03.45

and 79.1 dB during the loading phase with closed car window. Alle the values are referred to the whole work cycle of the vehicles.

CONCLUSION

This study involved the experimental measurement of noise levels during the material loading phase for two types of dump trucks, Komatsu and Perlini, under different conditions (open car window and closed car window). The work was conducted with an experimental approach referred to context of a limestone quarry. The measurements were taken with both open and closed car windows to assess the impact on the driver of different noise levels. The noise levels were found to be significantly influenced by whether the car windows were open or closed, with higher noise levels associated with open car windows, as expected. It is important to note that having the open car window is strictly necessary to maintain a suitable microclimate within the operator's cabin. In order to prevent health risks for truck drivers, an important way could involve improving the soundproofing of the truck cabins. Enhancing the insulation could significantly reduce the noise levels experienced by the operators, thereby improving working conditions and potentially reducing noise-related health issues. This soundproofing should be addressed during the design phase and should involve the entire structure of the vehicle to be most effective. Additionally, it would be beneficial to conduct monitoring of noise levels to understand how they change over time with the same dump trucks. This would provide valuable insights into the long-term performance and effectiveness of any noise-reduction measures implemented.

REFERENCES

[1] Marchelli M., Coltrinari G., Alfaro Degan G., e Peila D., Towards a procedure to manage safety on construction sites of rockfall protective measures, Saf. Sci., vol. 168, p. 106307, 2023;

[2] Normatova M. e Pardayeva S., Reducing dust pollution in the production of mass explosions in quarries, E3S Web Conf., vol. 525, p. 01003, 2024;

[3] Saka M. B., e Hashim M. H. B. M., Critical assessment of the effectiveness of different dust control measures in a granite quarry, J. Public Health Policy, vol. 45, fasc. 2, pp. 212–233, 2024;

[4] Dhatrak S. V., Shah I. A., e Prajapati S. S., Determinants of discomfort from combined exposure to noise and vibration in dumper operators of mining industry in India, J. Occup. Environ. Hyg., vol. 21, fasc. 6, pp. 389–396, 2024;

[5] Picard M., Girard A., Simard M., Larocque R., Leroux T., e Turcotte F., Association of work-related accidents with noise exposure in the workplace and noise-induced hearing loss based on the experience of some 240,000 person-years of observation, Accid. Anal. Prev., vol. 40, fasc. 5, pp. 1644–1652, 2008;

[6] Jaikrishnamurthy M. E., Balu G., Anbumani A., Jayakumar S., e Basavaraju S., A Detailed Study on Various Sources of Cabin Noise and Vibration in Crawler Dozers and Methodology Followed to Reduce the Noise, Int. J. Sci. Res. Sci. Eng. Technol., pp. 487–495, 2023;

[7] Patil V. S., Bano, F., Kurahatti, R. V., Patil, A. Y., Raju, G. U., Afzal, A., Saleel, C. A., A study of sound pressure level (SPL) inside the truck cabin for new acoustic materials: An experimental and FEA approach, Alex. Eng. J., vol. 60, fasc. 6, pp. 5949–5976, 2021;

[8] Andren L., Johansson S., Winberg M., e Claesson I., Active noise control experiments in a fork-lift truck cabin, 11th International Congress on sound and Vibration, 2004;

[9] Mondal N. K., Dey M., e Datta J. K., Vulnerability of bus and truck drivers affected from vehicle engine noise, Int. J. Sustain. Built Environ., vol. 3, fasc. 2, pp. 199–206, 2014;

[10] Kerketta S. e Bagh S., Noise Levels inside the Cabin of Heavy Earth Moving Machineries: Its Significance and Association, Noise Vib. Worldw., vol. 42, fasc. 5, pp. 14–19, 2011;

[11] Ntsiful F. e Stemn E., Whole-Body Vibration in the Mining Industry: a Systematic Review of Assessment Methods, Min. Metall. Explor., vol. 40, fasc. 1, pp. 191–210, 2023;

[12] Chaudhary D. K., Palei S. K., Kumar V., e Karmakar N. C., Whole-body vibration exposure of heavy earthmoving machinery operators in surface coal mines: a comparative assessment of transport and non-transport earthmoving equipment operators, Int. J. Occup. Saf. Ergon., vol. 28, fasc. 1, pp. 174–183, 2022;

[13]Johnson P.W. Dennerlein J. Ramirez L. M. Arias C. e Rodriguez A.C., Assessment of continuous and impulsive whole body vibration exposures in heavy equipment mining vehicles, Proceedings 19th Triennial Congress of the IEA, vol.9, p.14, 2015;

[14] Erdem B., Dogan T., e Duran Z., Assessment of whole-body vibration exposure of mining truck drivers, J. South. Afr. Inst. Min. Metall., vol. 120, fasc. 9, 2020.

https://doi.org/10.5593/sgem2024/1.1/s03.45

RESEARCH ON THE BEHAVIOR OF METAL CONSTRUCTIONS UNDER THE ACTION OF EXPLOSIONS

Eng. Stefan Ilici [1]

PhD. Eng. Ress Robert Laszlo [2]

Prof. Florea Dinu [3,4]

PhD. Eng. Edward Gheorghiosu [5]

PhD. Eng. Ress. Bogdan Simon [6]

[1,2,5.6] National Institute for Research and Development in Mine Safety and Protection to Explosion – INSEMEX Petroşani, **Romania**

[3] Politehnica University, Department of Steel Structures, Timisoara, **Romania**

[4] Romanian Academy, Timisoara Branch, Timisoara, **Romania**

ABSTRACT

The explosions produced in industrial/chemical facilities, such as hazardous material storage facilities, are events with low probability but high destructive potential. When occurring in a densely populated area, such explosions can lead to extensive damage of nearby buildings or infrastructures, resulting in high economic costs and human injuries and fatalities. The explosions may be the result of an accident but may also be intentional. As the pressure released by the external explosions decreases exponentially with the distance to the target, increasing the stand-off distance is one of the most effective ways to mitigate the effects against structures. In addition, the local resistance of the facade elements must be increased to prevent or limit the spread of damage. Even though these issues are well known and understood, there are relatively few provisions in the current European practice. The destructive effect of the high velocity debris projected by the explosion should also require attention, as they can cause severe harm to people. The study presented in the paper investigates the capacity of light steel-based building facades to resist the effects of near field blasts. The experimental results showed the ultimate capacity of the wall panels is strongly dependent on the initial design conditions and panel-to-structure fastening solution.

Keywords: blast wave, robustness, external explosion, overpressure, steel frame.

1. INTRODUCTION

The explosions can cause significant damage to neighboring structures or infrastructure when they happen in a highly populated region, which can have a significant financial impact as well as cause casualties and fatalities ([1],[2],[3]). Intentionality or accident-related causes might both be responsible for the explosions. One unfortunate instance from the first category is the unintentional detonation of ammonium nitrate on August 4, 2020, at a warehouse in the port of Beirut. This explosion resulted in a massive explosion that left over 6500 people injured and over 200 people dead. In reference to the latter group, terrorism continues to be a major and serious issue in many nations even if its impact has decreased globally [4]. Enhancing the stand-off distance is a highly successful strategy to reduce the impacts on buildings, as the pressure generated

https://doi.org/10.5593/sgem2024/1.1/s03.46

by the external explosions diminishes exponentially with the target's distance. Moreover, to stop or restrict the spread of damage, the local resistance of the facade elements needs to be raised.

2. FULL-SCALE BLAST TEST

2.1. Description of test set-up

The panels were designed to withstand a specific wind pressure of qb = 0.5 kN/m^2. The liner trays of the wall system were mounted on a steel frame structure to accurately replicate the site conditions and interaction with the support structure. The structure consisted of two spans of 4.5 m each, two bays of 3.0 m each, and two stories of 2.5 m each (Fig. 1).



Figure 1. View of the experimental setup

2.1 Instrumentation and loading scenario

Pressure sensors (PS), acceleration sensors (AS), and high-speed cameras (HCam) were part of the equipment (see Fig. 2). A LiDAR device was also used to record the façade's original shape as well as its changed shape. Pressure sensors 1 and 2 (PS1 and PS2) were set up 1.5 m above the ground (that is, 10 cm from the wall face) and in the middle of the third panel.

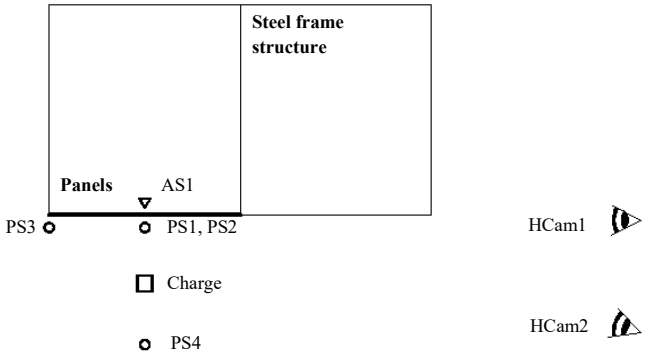


Figure 2. Plan view of the blast test set-up (not to scale).

The face of PS1 was against the wall, and the back of PS2 was against the wall. These two monitors were used to find out how much pressure the panel was under. It was 10 cm from the left end of the wall and 1.5 m above the ground where the PS3 was sitting. It was placed so that the back faced the wall and was used to measure the pressure that built up at the end of the panel. PS4 was put at the back of the charge, the same distance away from it as PS1 and PS2 sensors. This sensor was used to find out how much air

was coming into the field. Acceleration sensors (AS) were connected to the third panel in the middle, but on the back, across from pressure sensors PS1 and PS2. One high-speed camera was placed on the side of the structure (HCam1), 30 meters away from the charge, and the other was placed 15 meters away from the side of the structure at an angle (HCam2).

The blast loading scenario involved the employment of cylindrical charges placed at 1.5 meters from the midpoint of the left-hand side wall. The charges were positioned at a height of 1.5 meters from the ground, namely at the center of the third panel from the ground, as shown in Figure 2. The charge weights were incrementally raised until the wall panels experienced total failure, following the specified loading sequence: T1- two cartridges, total weight of 0.286 kg eTNT; T2- four cartridges, a total weight of 0.572kg eTNT; T3 - six cartridges, total weight of 0.858 kg eTNT; T4 - eight cartridges, total weight of 1.144 kg eTNT.

It is important to observe that the eTNT of the explosive, which is the measure of the explosive's weight relative to the weight of TNT required to generate an equivalent explosion effect at the same distance from the charge, was equal to one. To classify the explosion, i.e., near-field or far-field, the scaled distance, Z, was calculated [6].

According to the data shown in Table 1, the scaled distance Z ranges from 2.28 $m/kg^{1/3}$ for T1 to 1.43 $m/kg^{1/3}$ for T4. The higher charges are therefore in proximity to the near field range, especially when the scaled distance is less than 1 $m/kg^{1/3}$ ([7], [8]). The shock wave in near-field explosions is influenced by the products of afterburning and detonation [7]. The sensor that measured the incident pressure in test T4 sustained damage during testing, resulting in the recording of only incomplete data. Consequently, a second test was conducted with the same amount of charge (1.144 kg) but directed against a concrete wall. This test is referred to as R4. The experiment was carried out using the same equipment and blast conditions, including the charge height above the ground, distance from the wall, and position of pressure sensors. Please refer to Table 1 for further details.

Table 1. Description of the blast charges.

Test	Weight - W [kg]	Stand-of distance - R [m]	Scaled distance - Z [$m/kg^{1/3}$]
T1	0.286	1.5	2.28
T2	0.572	1.5	1.81
T3	0.858	1.5	1.58
T4	1.144	1.5	1.43
R4	1.144	1.5	1.43

3 FIELD TEST RESULTS

3.1. Experimental results

Figure 3a displays photos depicting the wall panels' failure following test T4, view with large deformations and distortions in the lower panels (left) and failure of end connection in the 3rd panel (right). The photographs reveal significant deformations, distortions, and the breakdown of the end connection in the third panel. The intricate distorted form of the wall was also recorded using a LiDAR system (Fig. 3b).

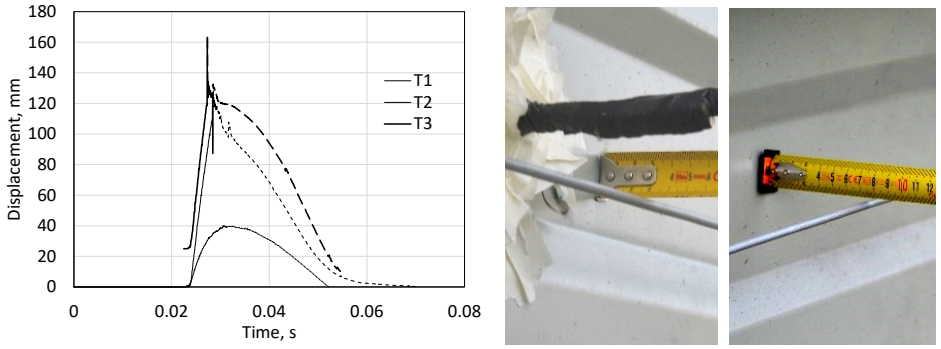
https://doi.org/10.5593/sgem2024/1.1/s03.46

The accelerometers were used to measure the instantaneous displacements of the panels. Using integral calculus, the velocity function was derived from the acceleration function, and then the displacement function was produced from the velocity (Fig. 4a). Furthermore, given the intricacies of calculus, only the maximum values are of significance. The highest residual deflections were determined manually after each test using a basic steel tape ruler (Fig. 4b).



a) b)

Figure 3. Failure of the panels after test T4



a) b)

Figure 4. Midspan out of plane deflection history, 3rd panel, tests T1, T2 and T3 (a), and maximum residual displacements in tests T2 and T3 (b).

The application of charge T1 resulted in little deformations in the wall panels, with the overall reaction being predominantly elastic (no noticeable permanent deflections) and a maximum temporary deflection of 40 mm. Charge T2 resulted in a peak temporary deflection of 128 mm and a peak permanent deflection of 25 mm. No apparent signs of plastic deformation were seen in the end fasteners. The application of T3 charge resulted in significant out-of-plane deflections, severe plastic deformations of the broad flange and webs, but only minor elongations of the holes at the end fasteners. The peak transient deflection was 163 mm, whereas the remaining deflection measured 80 mm. It is important to observe that the deflections in T3 encompass the 25 mm remaining deflection that was measured after T2. The T4 charge, which was the biggest, resulted in the total failure of the third panel. This was caused by the end fasteners being pulled through the material and the holes becoming excessively elongated. There is no relevant information on temporary deviations in this context. The 2nd and 4th panels exhibited significant deformation, but the end fasteners saw very minor impact.

3.2 Blast pressure

The highest blast pressure encountered by the panel that was under the most strain, the third panel from the ground, was measured using two sensors, P1 and P2. Sensor P4

detected the corresponding pressure of the blast (see Figure 2 for the placement of the sensors). The collected statistics were also compared with data acquired using a formula found in the literature. Therefore, the incident overpressure, Pso, was determined using analytical calculations utilizing the connection suggested as shown in equation (1):

$$P_{so} = \frac{0.975}{z} + \frac{1.455}{z^2} + \frac{5.85}{z^3} - 0.019 \quad for \quad 0.1 < P_{so} < 10 \; bar \tag{1}$$

where, Z is the scaled distance, in m/kg$^{1/3}$, and P_{so} is the overpressure, in bar.

The corresponding reflected overpressures, P_r, were calculated using reflected pressure coefficients c_r defined using eq. (2), for a surface perpendicular to the shock front, i.e., angle of incidence $\alpha = 0^o$, [20]:

$$c_r = \frac{P_r}{P_{so}} \tag{2}$$

The results shown in Table 2 provide a comparison between the analytical and experimental pressures for charges T1 to T4, as well as an additional charge R4. It is evident that the maximum pressure measured in each test closely matches the analytical value.

Table 2. Experimental vs analytical incident and reflected overpressures.

Test	Scaled distance, - Z [m/kg$^{1/3}$]	Incident overpressure, P_{so} [bar]		Reflected overpressure, P_r [bar]		
		Experimental	Analytic	Experimental		Analytic
T1	2.28	1.30	1.19	3.10		3.44
T2	1.81	2.30	1.96	6.17		6.46
T3	1.58	2.98	2.67	9.45		9.75
T4	1.43	-	3.16	11.19	11.88*	12.0
R4	1.43	3.19	3.16	12.58		12.0
* Average value between T4 and R4						

In Fig.5 it is displayed the recorded pressure data from test T4 and compared with the pressure data acquired from the concrete wall, R4. It is evident that the peak pressures are rather close, while the time histories differ, likely because of abnormalities in the geometry of the profiled liner trays. It should be noted that the experimental incident pressure at T4 was unavailable, only the reflected pressure was measured. Hence, the reference experimental value for the incident pressure is 3.19 bar (as recorded in R4). However, for the experimental reflected pressure, the reference value is the average of the pressures measured in T4 and R4, which is 11.88 bar.

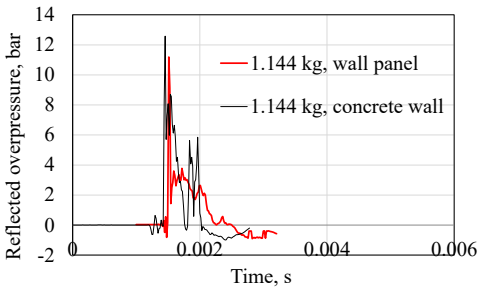


Figure 5. Reflected pressure history, tests T4 and R4.

The photographs captured during T4 using the high-speed camera (refer to Fig. 6a) depict the outward expansion of the detonation products originating from the detonation center. Additionally, the photos reveal significant temporary distortions of the panels, resulting in full separation of the overlapping webs of neighboring panels.

https://doi.org/10.5593/sgem2024/1.1/s03.46



a) b)

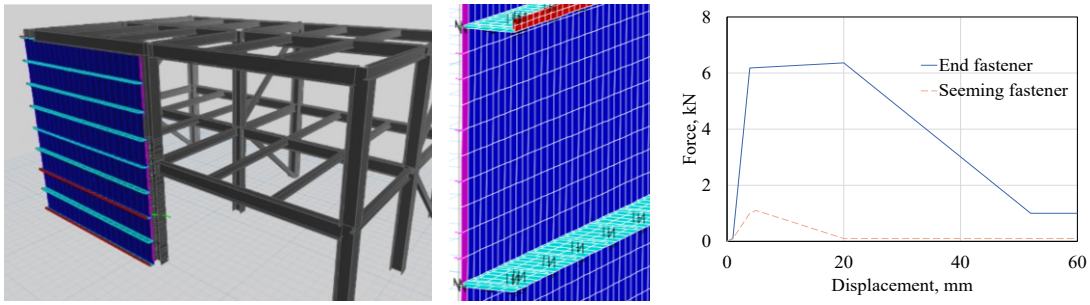
Figure 6. Views during blast for T4

In Fig. 6 a) it presented the blast development for T4 with expansion of the detonating products and large deformations in the panels. Figure 6b shows a snapshot with the shock waves, with the clear indication of the three wavefronts, namely the incident wave (1), the reflected wave from the ground (2), and the reflected wave from the wall (3). The contour pressures were obtained using the BOS (Background Oriented Schlieren) technique.

4 NUMERICAL MODELLING AND SIMULATIONS

4.1 Calibration of the numerical model

The numerical modeling was conducted utilizing the widely employed Etabs program [9], renowned for its capabilities in analyzing and designing multi-story structures, as well as its extensive functionalities for nonlinear time-history analysis. Fig.7a illustrates the inclusion of both the wall panels and the supporting steel frame structure in the computational model. By considering the primary steel frame structure, we can create more accurate models of panel boundary conditions, namely the in-plane stiffness of the perimeter steel frame. This stiffness directly impacts the development of catenary action in panels [5]. The wall panels were organized as individual continuous components and simulated using stratified nonlinear shell elements, as seen in Figure 7b. The steel material properties of the panels were determined using tensile testing on materials [5]. The fasteners at the end, which attach the panels to the supporting columns, were simulated using nonlinear link elements. The behavior of link elements was simulated by employing multilinear plastic force-displacement curves that were adjusted based on experimental data [5], as shown in Figure 7c. The webs of neighboring panels that overlapped were connected using nonlinear link elements.



a) b) c)

Figure 7. Full numerical model

To account for the impact of the rapid deformation rate, the connections' maximum resistance was adjusted by applying a Dynamic Increase Factor (DIF) of 1.1. It is important to acknowledge that while the rates of deformation caused by explosions are quite high, the ultimate resistance is less affected by the deformation rate compared to the yield strength. The experimental program's observations revealed that, beginning with test T3, the webs of neighboring panels started to separate due to the pullover failure of the fasteners that appeared to be holding them together (refer to Fig. 8). As observed in the high-speed camera HCam2 images, the webs of the 3rd panel entirely detached from the surrounding panels due to the highest blast pressure recorded in T4, as shown in Fig. 6a. Considering the observation, the numerical model was simplified by focusing just on the 3rd panel (Fig. 9), which saw the most exposure to the blast wave. Additionally, this decreases the computational intricacy of the explosion analysis. It should be noted that there were no modifications made to the panel end connectors, mesh size, and material qualities.

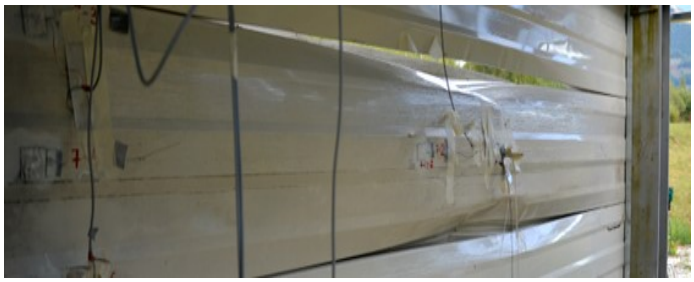


Figure 8. Separation of panel webs after T3 (view from inside)

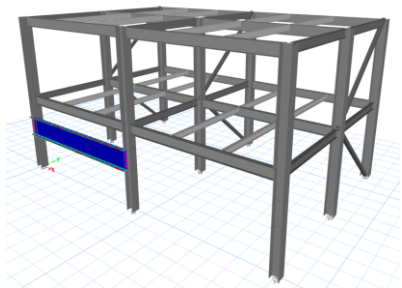


Figure 9. Simplified numerical model (3rd panel from the ground)

The blast pressure was calculated using test data obtained in the experimental program, as shown in Table 2. The pressure-time history only considered the positive phase and disregarded the negative phase (Fig.5), which is typically less significant than the positive phase. The pressures exerted across the panel span changed based on the angle of incidence, a. Given the brief duration of the blast, an analysis was conducted using a time step of 0.0001 sec. The numerical model was calibrated using the results obtained in test T3 and in test T4 after T3. The panel response was disregarded due to its quasi-elastic nature (T1) or the presence of small residual deformations (T2).

In the subsequent test T4, the numerical results once again confirm the panel's failure, with significant out of plane deflections and analysis being halted due to the end links giving way. Figure 10 displays the distorted shape of the panels, both from experimental and numerical tests T3 and T4. There may be slight variations in the deflected shapes, but these have minimal impact on the overall strength of the panel. The primary factor determining its capacity is the catenary response of the wide flange, with the two webs playing a lesser role.

https://doi.org/10.5593/sgem2024/1.1/s03.46

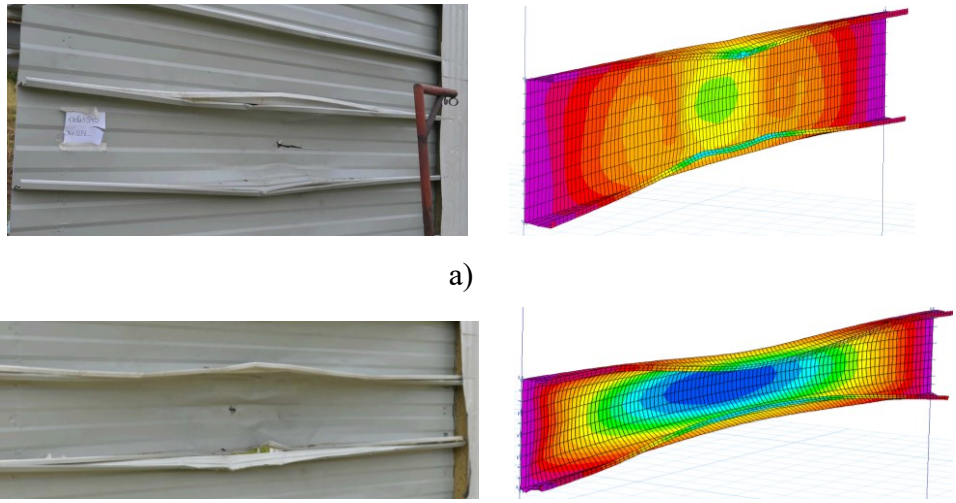


Figure 10. Deflected shapes, experimental vs numerical: a) test T3; b) test T4

CONCLUSIONS

When explosions happen close to a building's facades, there is a higher chance of causing severe damage or even complete collapse of the walls. This poses a serious threat to the safety of the people inside and the stability of the structure. Increasing the stand-off distance can significantly decrease the amount of damage caused. When the stand-off distance is small, the traditional design of light steel-based wall panels to withstand out of plane pressures becomes inefficient, as it relies solely on their ability to flex. With the enhanced ability of the panels and end connections to deform, the energy from explosions can be effectively dissipated through plastic deformation, resulting in a reduction of risks associated with accidental actions. The numerical simulations demonstrated excellent agreement with the test data, even when utilizing single panels rather than multiple panel assemblies. Additional research is currently underway, involving intricate numerical modeling, varying the placement of the explosive charge, and adjusting the intensity of pressure.

ACKNOWLEDGEMENTS

This work was carried out through the" Nucleu" Program within the National Plan for Research, Development, and Innovation 2022-2027, with the support of the Romanian Ministry of Research, Innovation and Digitalisation, project no. 23 32 02 03, title: "Development of monitoring methods to reduce environmental impact from the use of explosive materials, pyrotechnic articles, and application of blasting technologies".

REFERENCES

[1] Studzinski R. *et al*., *Blast Test and Failure Mechanisms of Soft-Core Sandwich Panels for Storage Halls* Applications, Materials, 14, 1, 2021.

[2] Dinu F. *et al.*, *Experimental blast tests on light non-load bearing external walls, Steel Constructions*, 125–132, 2022.

[3] Explosives regulations, *safety provisions: guidance on regulations. Merseyside: Health and Safety Executive*, HSE Books, 2014.

[4] Global terrorism index 2020, *Measuring the impact of terrorism*, Institute for Economics & Peace IEP, 2020.

[5] SAFE-WALL, *Safety of buildings walls and claddings against accidental explosions*, UEFISCDI, 2020.

[6] Cranz, C. *Lehrbuch der Ballistik, Springer-Verlag*, 1926.

[7] J. Shin, A. S. Whittaker, D. Cormie, W. Wilkinson, *Numerical modeling of close-in detonations of high explosives*, Engineering Structures, 81, 88–97, 2014.

[8] J.-K. Ahn and D. Park, Prediction of Near-Field Wave Attenuation Due to a Spherical Blast Source, Rock Mechanics and Rock Engineering, 50, **11**, 3085–3099, 2017.

[9] ETABS, Computers and Structures, Inc. - *Technical Knowledge Base*, 2020.

https://doi.org/10.5593/sgem2024/1.1/s03.46

RISK ASSESSMENT AT DEMOLITION ACTIVITY OF INDUSTRIAL / CIVIL OBJECTIVES WITH THE EXPLOSIVES FOR CIVIL USES

Eng. Claudia Miron[1]

PhD.Eng. Cristian Rădeanu[1]

Eng. Stefan Ilici[1]

PhD. Ec.-Ress. Dan Pintilie[2]

PhD.Eng.-Ress. Ciprian Mateiu[2]

[1]National Institute for Research and Development in Mine Safety and Protection to Explosion – INSEMEX Petrosani, **Romania**

[2]University of Petrosani, **Romania**

ABSTRACT

The paper presents a theoretical and practical approach to the concept of risk assessment specific for the demolition of the industrial civil objectives with the help of explosives in terms of ensuring security premises for the effects generated following the blasting demolition work of this type of constructions. Blasting realization of industrial civil objectives to be demolished involves a series of operations that generate health and safety risks to economic operator employees which are carrying out work and for people in neighborhoods and the environment. The primary goal of occupational risk assessment is to prevent the risk of injury and professional disease, and when it is not possible to eliminate these risks, it is necessary to reduce them to the amount of residual risk that must be controlled properly. Both in the occupational risk assessment process stage and subsequent implementation of occupational security, special attention should be directed to the possibility that the risk of injury and occupational disease shall not be moved from one area to another system work, namely technical and organizational solutions adopted to reduce or eliminate these risks do not create additional situations of their manifestations. The legislative framework obliges employers to take all measures to ensure that workers are not exposed to risks that could cause accidents or illnesses. In this paper only considered issues that can influence health and safety due to work company authorized to work with explosives and those that can be generated by other staff of ignorance, lack of coordination and communication.

Keywords: risk assessment, demolition activity, blasting operations, explosives for civil use, safety and health at work

INTRODUCTION

Blasting realization of industrial / civil objectives to be demolished involves a series of operations that generate health and safety risks to economic operator employees which are carrying out work and for people in neighborhoods and the environment. The primary goal of occupational risk assessment is to prevent the risk of injury and professional disease, and when it is not possible to eliminate these risks, it is necessary to reduce them to the amount of residual risk that must be controlled properly. Both in

https://doi.org/10.5593/sgem2024/1.1/s03.47

the occupational risk assessment process stage and subsequent implementation of occupational security, special attention should be directed to the possibility that the risk of injury and occupational disease shall not be moved from one area to another system work, namely technical and organizational solutions adopted to reduce or eliminate these risks do not create additional situations of their manifestations [1,2]

MATERIALS AND METHODS

Theoretical and practical issues on the quantification of specific risks at demolition activities of the industrial objectives / civil with explosives

The legislative framework obliges employers to take all measures to ensure that workers are not exposed to risks that could cause accidents or illnesses. The national methodological norms for applying Law 319 of 14 July 2006 on security and health at work regulates the mechanism by which the employer must do to eliminate or reduce these risks. When carrying out demolition with explosives, by specialized companies authorized for this purpose, combine the risk that can be identified on any construction site with those specific at work with explosives [3,4]. From the structural point of view, the main stages of occupational risk assessment are: Identify the hazards of accidents and occupational disease; Identifying people who may be exposed to these hazards; Estimation and assessment of occupational risks; Study of the potential to eliminate occupational hazards; Analysis the appropriateness and necessity of stopping additional measures to reduce (decrease) / control or eliminate risks. Occupational risk assessment methodology is based on two essential requirements in this area: The assessment procedure must include an analysis of all the dangers of accidents and occupational disease, whatever their mode of manifestation (obvious hazards or potential); Elimination, if possible, to all the dangers of accidents and occupational diseases identified in the evaluation process. Risk assessment represents an ongoing concern of the leaders working process from the design stage of the processes, continuing with the preparatory work, the demolition work effectively and monitor the effects on human health and safety, integrity of material goods and the environment.

Analysis and reduction of occupational risk of specific risks at demolition activities of the industrial objectives / civil with explosives

If the assessed risks which are located at the risk of unacceptable, is applying the procedure of analysis and reducing thereof by applying an appropriate preventive and protective measures of a technical and organizational, to prevent and combat the causes of production of undesirable events (accidents at work and occupational diseases) [5]. In this regard, it is used for "the Risk Analyzer" (whose matrix is shown in Figure 1), which was built based on scales related classes corresponding values of two parameters, the probability of occurrence of an event unwanted peak P and the seriousness of the consequences of predictability G. It shows further corresponding grid of the professional risk parameters (R) / occupational safety (S), and the scale of the risk attitude and risk matrix analyzer.

Grid for assessing the level of professional risk

Levels of Risk Professional / Occupational Safety	Professional risk estimation values R	Level of professional risk assessment	Appreciation of occupational safety level
1 / 7	1 ÷ 7	Minimal risk	Maximum security
2 / 6	8 ÷ 13	Very small risk	High security
3 / 5	14 ÷ 21	Low risk	High security
4 / 4	22 ÷ 29	Medium risk	Medium security
5 / 3	30 ÷ 35	High risk	Small security
6 / 2	36 ÷ 39	Very high risk	Security very small
7 / 1	40 ÷ 42	Maximum risk	Minimum security

Legenda:

	Represents the domain of acceptable risk
	Represents the domain of unacceptable risk

Scale of attitude towards the professional risk

Levels of Risk	Level of professional risk appreciation	Attitude to the professional risk
1	Minimal risk	No special action is taken
2	Very small risk	
3	Low risk	
4	Medium risk	It makes monitoring dangerous situations, control event risk factors additional corrective measures can be applied taking into account cost-effectiveness
5	High risk	Efforts will be made to reduce the level, but the costs of prevention should be carefully measured. Measures to reduce the risk level is implemented in strictly determined period of time. Where high risk is associated with serious consequences, should be set exactly the probability of manifestation of responsible risk factors, and measures will be taken to diminish them.
6	Very high risk	Activities can not continue until the risk is not reduced! Resources should be assigned to reduce the risk. On the occurrence of other risks in the labor action is taken immediately..
7	Maximum risk	Activities can not start until the risk level is not reduced! If it is not possible the immediately reducing of the level of risk, work in these circumstances IS PROHIBITED!

			CLASS OF PROBABILITY "P"					
			1 ↓	2 ↓	3 ↓	4 ↓	5 ↓	6 ↓
			Extremely rare	hardly ever	rare	LESS FREQUENT	FREQUENT	very frequently
Classes of severity "G"	CONSEQUENCES		P > 10 years	5 years < P < 10 years	2 years < P < 5 years	1 years < P < 2 years	1 month < P < 1 year	P < 1 month
7 →	MAXIMUM	DEATHS	21	29	35	39	41	42
6 →	VERY SERIOUS	DISABILITYGR. I	20	28	34	37	38	40
5 →	SERIOUS	DISABILITY GR. II	19	26	27	32	33	36
4 →	HIGH	DISABILITY GR. III	13	18	24	25	30	31
3 →	AVERAGE	ITM 45 – 180 DAYS	11	12	16	17	22	23
2 →	SMALL	ITM 3 – 45 DAYS	7	8	9	10	14	15
1 →	NEGLIGIBLE		1	2	3	4	5	6

Fig.1 - Matrix of the professional risk analyzer

https://doi.org/10.5593/sgem2024/1.1/s03.47

If following the risk assessment for Occupational Safety and Health identify a risk level located in the unacceptable it will highlight the risk index fiches, after which the full form of analysis and risk reduction and diagram will be constructed to reduce this level on prevention and protection measures that must be taken.

RESULTS

Identify specific risks to demolition work of the industrial / civil with explosives

The main risks arising from the execution of demolition of buildings using explosives can be grouped, as a source of production, in two categories: Risks arising from preparatory work; Risks of carrying out blasting

Specific risks preparatory work for construction demolition using explosives

When demolition using explosives is recommended to carry out an investigation on the possibilities of reducing the structural strength of the building blasting process with the aim of carrying out demolition using explosives at minimal cost. Preparatory work done in advance should provide for the construction phase of demolition sufficient stability for drilling work and preparation having safety into consideration of workers which carries out blasting holes, placement and protect cargo. Also, these works are necessary: reducing the time spent drilling works for placing the explosive charges in order to detachment constructive elements which lead to the demolition itself; the volume of exhaust restriction debris resulting from the blasting; achievement of technical conditions on the assurance of the drop and secure the blasting area; precise sizing of consumption of explosives required for demolition. The main risks arising from carrying out preparatory work are: the poor condition of access roads; unprotected electrical installation / damaged; obstacles present on escape routes; falls from heights; objects falling from height; lack of specific elements PSI; enclosed spaces / narrow unventilated; toxic and harmful environment; extreme heat or variable; inadequate lighting, etc. Concrete analysis and prior assessment risks outlined above, allows both the designer and contractor to establish practical measures to eliminate or reduce their level.

The specific risks to the execution of blasting for demolition of buildings using explosives

Making civil engineering demolition by blasting involves a series of operations that generate health and safety risks for the company's employees which carries out work and for people in neighborhoods. Explosive materials are hazardous materials (Class 1 A) always represents a potential risk to any operation preparation, experimentation, use, storage, transport or destruction. Site conditions when demolition by blasting raises additional problems to other jobs (a quarry) due to the following: presence on site to people who do not have adequate knowledge on the use of explosives and may be exposed to risks of accidents to the extent that the company that runs blasting does not take all appropriate measures to inform these, not apply effective measures to limit access in the area for works performing with explosives; sites in most cases are much closer to the inhabited than quarries; Another factor that raises special problems is storage in site conditions of explosive materials before the works themselves with explosives

The main risks arising from carrying out preparatory work are: Improper use of

explosives; The presence of current sources, open flames, lightning, electromagnetic field; Lack of opportunity to keep separate (in various storage facilities) of explosives and means of initiation; Falls from height; Falling objects from height; Correlation inappropriate or mismatch between the task of qualified human potential; Incorrect performance of the operation of loading and circuit realization of initiation; The occurrence of failures and their disposal; Throwing fragments unrocked material; Noise emitted after performing blasting operation; The effect of pressure in the shock wave front on constructive elements; The effect of seismic wave hazard the safety of other buildings in the area; Uncontrolled detonation, using the networks of initiation, the electric detonating caps low intensity in the presence of foreign current sources; Increasing air wave explosion effect at the use of, within the system of initiation of detonating cord, out of holes blasting; Network interruption or failure to initiate reliably of loads from holes the use of detonating cord with reduced linear load; The occurrence of partial misfire following the detection of errors mounting clunky when using non-electric elements; Accidental detonation of unexploded explosive remnants of debris during charging (manual or mechanical); Entry into illegal possession by unauthorized personnel, remnants of unexploded explosive material.

Concrete analysis and risk assessment prior to the above, allows both the designer and contractor to establish practical measures to eliminate or at least reduce their level.

Specific risk assessment at demolition activity of industrial / civil objectives with the help of explosives

Risk assessment of the safety and health of workers in demolition activities of the industrial / civil with explosives was made based on identifying and analyzing specific risks of the preparatory work and blasting, highlighted in the risk index cards (1), the results partial and general assessment is recorded in the form of professional risk analysis and mitigation (2) which includes the reduction of the level diagram based on preventive and protective measures that must be taken.

Risk index cards (1)

No. doc	Description of identified risk factor (concrete form of manifestation)	Workplace (subsystem)
1.	Specific risks preparatory work for controlled demolition of buildings using explosives.	Industrial objectives / civil subject to decommissioning.
2.	Specific risks when conducting the blasting for controlled demolition of buildings using explosives.	

Form of analysis and professional risk reduction (2)

SPECIFIC ANALYSIS AND RISK REDUCTION DEMOLITION ACTIVITIES OF THE INDUSTRIAL / CIVIL WITH EXPLOSIVES		
Workplace (subsystem): Construction within the industrial / civil subject to decommissioning		
A. Specific risks at preparatory work for controlled demolition of buildings using explosives		
Document no.1	**Risk: Medium**	**Level: 4**

Professional risk determined - Injury and / or illness to personnel conducting preparatory work for the controlled demolition of buildings using explosives	**P**	**G**	**Estimate of / risk assessment R**	
	5	3	22	Me

https://doi.org/10.5593/sgem2024/1.1/s03.47

Identification of potential risk factors: $R_{ig}(p_i,g_i)=(\sum r_iR_i)/\sum r_i \rightarrow R_{ig}(5,3)=22$ (In terms of value $|r_i|=|R_i|$, i=1...10)
- Poor condition of access roads: $R_1(p_1,g_1)\rightarrow R_1(5,5)=33$
- Unprotected electrical installation / damaged: $R_2(p_2,g_2)\rightarrow R_2(2,7)=29$
- Obstacles present on escape routes: $R_3(p_3,g_3)\rightarrow R_3(6,3)=23$
- Falls from height:$R_4(p_4,g_4)\rightarrow R_4(1,7)=21$
- Falling objects from height: $R_5(p_5,g_5)\rightarrow R_5(1,7)=21$
- Lack of specific elements PSI: $R_6(p_6,g_6)\rightarrow R_4(5,3)=22$
- Confined spaces / narrow unventilated: $R_7(p_7,g_7)\rightarrow R_5(5,3)=22$
- Environmental toxic and harmful: $R_8(p_8,g_8)\rightarrow R_8(5,3)=22$
- Extreme heat or variable: $R_9(p_9,g_9)\rightarrow R_9(4,2)=10$
- Lighting inappropriate: $R_{10}(p_{10},g_{10})\rightarrow R_{10}(4,2)=10$

Description of the risk factors identified (concrete form of manifestation):
- Damage stability and soundness of access roads
- Direct touch electrical installation
- Blocking escape routes staff
- The use of improvised devices or improper scaffolding
- Failure or lack of supervision, objects left at different height levels
- Remove items related to PSI
- Inadequate ventilation
- Presence of gases, vapor, dust and noise
- High temperatures in summer, respectively low in winter
- Limited and insufficient natural lighting

Causes:
- Making preparatory work for the controlled demolition of buildings within the industrial / civil subject decommissioning

Dysfunction- Favouring the phenomenon of injury and / or occupational diseases due to exposure to the risks identified

Technical and organizational measures:

Technical measures
- Choosing safe routes to go
- Checking and uncoupling electrical installations from the network
- Checking the quality of the air in the work environment
- Appropriate endowment with EIP and work
- Use of appropriate apparatus for the measurement of air quality in the work area

Organisational measures
- Appropriate training of staff
- Procedure for the operating mode
- Coordination and appropriate deployment of personnel at the workplace / workstations

References:
- Law 319/2006 on safety and health at work and rules for the application of its subsequent amendments
- Law 126/1995 republished and Technical Norms for applying them
- Approved technical documentation for demolition
- Instructions on SSM

Residual Risk identification:
- Nature and configuration of buildings subject to demolition using controlled explosives and the related working environment.

P	G	Estimate of / risk assessment R	
4	3	17	Mi

Residual risk:
- Execution of preparatory work for the controlled demolition of the building with explosives, in compliance with technical and organizational measures mentioned above

Actions:
Reducing the risk from the value of 22 (medium risk) to the value of 17 (low risk), by applying technical and organizational measures.

Diagram of professional risk reductionin carrying out preparatory work

Classes of severity "G"	Classes of probability "p"					
	1 ↓	2 ↓	3 ↓	4 ↓	5 ↓	6 ↓
7 →	21	29	35	39	41	42
6 →	20	28	34	37	38	40
5 →	19	26	27	32	33	36
4 →	13	18	24	25	30	31
3 →	11	12	16	← 17	← 22	23
2 →	7	8	9	10	14	15
1 →	1	2	3	4	5	6

B. Specific risks for conducting the blasting for controlled demolition of buildings using explosives

Document no. 2	Risk: High	Level: 5

Professional risk determined			Estimate of / risk

- Injury and / or illness of personnel that carry out controlled blasting for demolition of buildings using explosives	**P**	**G**	**assessment R**	
	6	4	31	M

Identification of potential risk: $R_{ig}(p_i,g_i)=(\sum r_iR_i)/\sum r_i \rightarrow R_{ig}(6,4)=31,5$ (In terms of value $|r_i|=|R_i|$, i=1...18)
- Improper use of explosives: $R_1(p_1,g_1)\rightarrow R_1(3,7)=35$
- The presence of current sources, open flames, lightning, electromagnetic field: $R_2(p_2,g_2)\rightarrow R_2(3,7)=35$
- Lack of possibility to keep separate (in various storage) explosives and the means of initiation: $R_3(p_3,g_3)\rightarrow R_3(2,7)=29$
- Falls from height: $R_4(p_4,g_4)\rightarrow R_4(2,7)=29$
- Falling objects from height: $R_5(p_5,g_5)\rightarrow R_5(2,7)=29$
- Inappropriate correlation or mismatch between the human potential and the qualified tasks: $R_6(p_6,g_6)\rightarrow R_6(3,6)=34$
- Incorrect performance of the operation of loading and circuit realization of initiation: $R_7(p_7,g_7)\rightarrow R_7(2,7)=29$
- The occurrence of failures and their disposal: $R_8(p_8,g_8)\rightarrow R_8(3,7)=35$
- Disposal of material fragments unrocked: $R_9(p_9,g_9)\rightarrow R_9(5,4)=30$
- Noise emitted from performing the operation of blasting: $R_{10}(p_{10},g_{10})\rightarrow R_{10}(5,3)=22$
- The effect of pressure in the shock wave front on the constructive elements: $R_{11}(p_{11},g_{11})\rightarrow R_{11}(2,7)=29$
- The effect of seismic wave safety hazard to other buildings in the area: $R_{12}(p_{12},g_{12})\rightarrow R_{12}(2,7)=29$
- Uncontrolled detonation, to the use of the networks of initiation, capes low intensity electric detonators in the presence of foreign current sources: $R_{13}(p_{13},g_{13})\rightarrow R_{13}(2,7)=29$
- Increasing air wave explosion effect to use in the network initiation of detonating cord, blasting out holes: $R_{14}(p_{14},g_{14})\rightarrow R_{14}(2,7)=29$
- Interruption or failure to initiate reliable network loads of holes to use detonating cord with reduced linear load: $R_{15}(p_{15},g_{15})\rightarrow R_{15}(2,7)=29$
- The occurrence of partial misfire detection cumbersome due to mounting errors when using non-electric items: $R_{16}(p_{16},g_{16})\rightarrow R_{16}(2,7)=29$
- Accidental detonation of unexploded explosive remnants of debris during charging (manual or mechanical): $R_{17}(p_{17},g_{17})\rightarrow R_{17}(5,3)=22$
- Entry illegal possession by unauthorized personnel remnants of unexploded explosive material: $R_{18}(p_{18},g_{18})\rightarrow R_{18}(5,3)=22$

Description of the identified risk factors (concrete form of expression):
- Lack of measures or ineffective measures to limit access to the area where the work with explosives is perform
- Distances close to inhabited area
- Storage of explosive materials in conditions of site before the works themselves with explosives is perform
- The lack of lightning protection and grounding ring for provisional storage spaces on site
- Improper placement of temporary storage areas on site
- The use of improvised devices or improper scaffolds
-Failure to ensure or lack of supervision allowed objects at different height levels
- Inadequate distribution of work tasks in relation to staff training and potential work
- Fatigue installed in different stages of loading and blasting making network as a result of under-sizing the number of staff
- Using unsafe working technologies with major negative impact on the environment
- Execution of additional operations required to liquidate misfire
- Inadequate control of the work area after blasting
- Gas, vapor, dust and noise
- High temperatures in summer, low during winter

Causes:
- Conducting controlled blasting for demolition of buildings of the the industrial / civil subject to decommissioning

Dysfunction:
- Promote phenomenon of injury and / or occupational diseases due to exposure to the risks identified

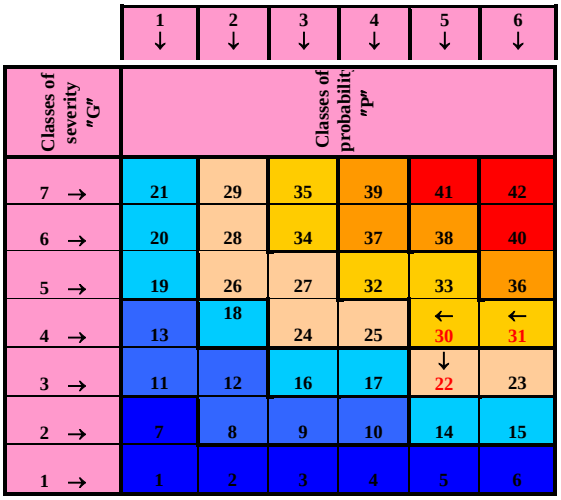
Technical and organizational measures:	**Referințe:**
Technical measures - Compliance with the technical documentation technology work approved demolition - Following instructions of SSM - Monitoring the effects due to blasting Organisational measures - Appropriate training of staff - Procedure for the operating mode - Coordination and appropriate deployment of personnel at the workplace / workstations	- Law 319/2006 on safety and health at work and rules for the application of its subsequent amendments - Law 126/1995 republished and Technical Norms for applying them - Approved technical documentation for demolition - Instructions on SSM

Residual Risk identification: - Nature and configuration of debris resulting from the explosive destruction of buildings	**P**	**G**	**Estimate of / risk assessment R**	
	5	3	22	Me

Residual risk:	**Actions:**
Controlled area after blasting.	Reducing the risk of the value 31 (high risk) to the value of 22 (medium risk) through technical and organizational measures.

https://doi.org/10.5593/sgem2024/1.1/s03.47

Diagram to reduce occupational risk when blasting



CONCLUSION

Blasting realization of industrial / civil objectives to be demolished involves a series of operations that generate health and safety risks to economic operator employees which are carrying out work and for people in neighborhoods and the environment.

The primary goal of occupational risk assessment when demolished of industrial / civil objectives with the help of explosives is to prevent and combat the causes that can cause accidents and / or occupational disease while carrying out preparatory operations and security of the effects generated by blasting execution of these types of construction.

For estimation and risk assessment when demolished of industrial / civil objectives with the help of explosives were developed, both graphic-analytical tools for quantifying the risk parameters represented by "professional risk analyzer" and "professional risk reduction diagram", as and "form of professional risk analysis and reduce."

The results of the risk assessment provide data and information pertinent to the state of health and safety at work to demolition specific activity of industrial / civil objectives with the help of explosives for improving and more dynamic fundamental process of policies to prevent and combat the causes that can cause accidents and / or occupational diseases.

ACKNOWLEDGEMENTS

This paper was developed within the Nucleu-Programme, carried out with the support of Romanian Ministry of Education and Research, project no. PN-23-32-01-03, project title: Development of monitoring methods in order to reduce the environmental impact of the use of explosive materials, pyrotechnic articles and the application of shooting technologies (in Romanian: Dezvoltarea metodelor de monitorizare în vederea reducerii impactului de mediu în urma utilizării materialelor explozive, articolelor pirotehnice și aplicării tehnologiilor de împușcare).

REFERENCES

[1] Law 126/1995 on the regime of explosive materials, as amended.

[2] "Technical Norms - to Law 126/1995 - on the possession, preparation, experimentation, destruction, transport and storage, handling and use of explosive materials in any other specific operations in the activities of holders, as well as the authorization of fireworks and pyrotechnicians", with subsequent amendments and additions.

[3] Law 319/2006 on health and safety at work.

[4] Dumitru F., „*Engineering of shooting, materials and working techniques*", ISBN: 978-973-87855-20/ 978-973-87855-1-9, Publisher Corvinu Deva, 2007.

[5] Dragos Vasilescu *Non-conventional methods for analysis and evaluation of occupational risks*, INSEMEX Publishing House, Petrosani, ISBN 978-973-88590-0-5, 2008.

https://doi.org/10.5593/sgem2024/1.1/s03.47

ROMANIAN COAL AND ENERGY HYBRIDIZATION

D Dr. Cristian Tomescu[1]
Dr. Cornel Boanta[1]
Dr. Emeric Chiuzan[1]
Assoc. Prof. Dr. Sorina Stanila[2]
[1]National Institute for Research and Development in Mine Safety and Protection to Explosion – INSEMEX, **Romania**
[2]University of Petrosani, **Romania**

ABSTRACT

The climate, energy, and health crises, alongside the conflict events in Eastern Europe, have generated new directions regarding the perspectives of global and national energy transition, by orienting it towards a decarbonized economy. The increased frequency of climate change-related weather events affects the availability of renewable energy sources (wind and solar) and energy supply security.

The abandonment of fossil fuel-based electricity and heat due to commitments and objectives established in the United Nations' 2030 Agenda for Sustainable Development, the 2015 Paris Agreement, and the adoption of policies aiming for climate neutrality, leads to both positive and negative consequences for the economy and population.

The Romanian energy transition will require the reform of the current energy model by combining different classical, traditional sources with renewable ones, resulting in a specific energy mix, i.e., an energy hybridization, and implicitly a Hybrid Energy System.

Currently, Romanian coal accounts for a maximum of 20% in electricity production, and Romania is rated as the fifth lignite consumer in Europe, given the increase in coal consumption worldwide in recent years, reaching record levels at the expense of the growing demand for clean energy sources.

This paper aims, on one hand, to analyze the current situation of Romanian thermal coal extraction in the context of decarbonization, and on the other hand, to explore the perspectives of modernizing the system with clean energies and implementing energy hybridization.

Keywords: coal, energy, renewable sources, energy transition, energy hybridization.

INTRODUCTION

Reforming the current Romanian energy system by transitioning to a climate-neutral energy system, through the application of complete decarbonization according to adopted programs, brings major changes to this sector with significant challenges, risks, and opportunities.

https://doi.org/10.5593/sgem2024/1.1/s03.48

In the European Union, there are directives related to hybrid energy, emphasizing the promotion of renewable energy sources with a Certification of Energy Origin System [1], to ensure transparency and credibility in the regional renewable energy market, identifying sources and options for clean energy suppliers.

At the European level, there are measures for the efficient implementation of renewable and hybrid energy projects with funding through the European Regional Development Fund and the European Union's Research and Innovation Fund [2]. Directive 2009/28/EC of the European Union, transposed into national legislation in Romania through Law No. 220/2008 on the promotion of energy production from renewable energy sources, outlines ways of processing and preliminary contribution to energy hybridization.

Solid fuel (coal)-based energy will become history in less than a decade, and natural gas and petroleum-based fuels will gradually decline in share. Focused on an accelerated transition to green energy at the European level, in the context of the war in Ukraine, European countries are still resorting to coal-based reserve capacities to enhance the security of electricity supply, and Romania is obliged by international agreements to reduce and close its energy capacities.

ABANDONING THERMAL POWER PLANTS

Romania has committed to eliminating coal from its national energy system by 2032. The total installed capacity of lignite and hard coal-based electricity that will be gradually phased out is 4,920 MW, with 3,780 MW set to be decommissioned by the end of 2025, as established by the Government Ordinance on decarbonizing the energy sector adopted in the summer of 2022 [3].

Data from the National Institute of Statistics for the entire year of 2023 indicates a decline in energy production from thermal power plants, with a total production of 18,005 million kWh, a decrease of 3,570.3 million kWh (-16.5%) compared to 2022 [4].

Coal is the fossil fuel with the highest carbon consumption, making its gradual elimination essential for limiting climate change, as outlined in the Paris Agreement on climate change. The International Energy Agency (IEA) estimates that fossil fuels (coal) are responsible for over 30% of the average global temperature increase above pre-industrial levels. European countries have made considerable efforts to reduce or eliminate the use of coal in electricity production due to environmental concerns, climate change, and public health [5].

In Romania, coal (lignite and brown coal) is primarily mined in Hunedoara (underground coal mines) and Gorj (surface mining quarries), accounting for approximately 90% of the entire coal mining and energy industry's workforce in the country, representing 11,220 jobs (2024), with 2,020 employees in the Jiu Valley of Hunedoara County. Coal is used for 14-18% of electricity production, although the installed and available capacity in the National Energy System (SEN) of coal-based units is 3,350 MW, with less than 1,000 MW used for average consumption.

The hard coal production of the Jiu Valley is used for generating electricity and heat in the Paroșeni thermal power plant in Hunedoara County, providing 1-2% of the country's energy production. Known hard coal resources in Romania are 232 million tons (85 million toe), with 83 million tons (30 million toe) exploitable within concessioned perimeters. With an average reserve consumption of 0.3 million toe/year, the supply of hard coal resources is secured for 104 years, but the feasibility of exploiting this primary energy resource depends on economic viability. The Oltenia Energy Complex provides 14-18% of the energy produced in thermal power units, with an annual production of 13.307 million tons (2023). Romania's lignite resources are estimated at 690 million tons (124 million toe), with 290 million tons (52 million toe) exploitable within concessioned perimeters. With an average resource consumption of 4.5 million toe/year, lignite resources are secured for over 30 years, assuming consumption remains constant and no other lignite deposits are developed [6].

According to the provisions of the National Recovery and Resilience Plan (PNRR), from 2022, 660 MW of lignite-based capacity has been permanently and irreversibly withdrawn from operation, specifically: Rovinari Energy Group 3 – 330 MW and Turceni Energy Group 7 – 330 MW [7].

The year 2025 marks a new stage, outlined in the PNRR, in terms of phasing out the total installed lignite and hard coal-based capacity by the permanent and irreversible shutdown of the following groups totaling 1,425 MW. The lignite exploitation quarries Alunu and Berbesti, which serve CET Govora, will permanently and irreversibly cease operation in 2025. On December 31, 2029, lignite extraction at the Rosiuta quarry will cease, and at the Rosia and Pinoasa quarries, activity will end on December 31, 2030. These quarries supply coal for the Rovinari 4, Rovinari 5, and Turceni 4 energy groups, which will provide technical reserves for the 2026-2030 period.

At CET Craiova 2, the restructuring program includes closing the two current 150 MW groups starting in 2025. These capacities will be replaced with a 295 MW cogeneration gas block, a project funded through the PNRR. The thermal power plant separated from the Oltenia Energy Complex and provides thermal energy for Craiova, occasionally producing electricity.

At Isalnita, block no. 8 will be closed starting in 2025, and block 7 starting in 2026. Each of these groups will be replaced with a 400 MW gas group with a combined cycle (CCGT) that can be adapted to run on hydrogen.

At Turceni, a 330 MW group, group 3, will be closed in 2025. This follows the commissioning of a 400 MW gas group in 2024.
The restructuring program also involves closing several coal exploitation quarries, as some groups will be converted to gas. Specifically, four out of the 11 quarries operated by the company will close. By the end of 2024, the Pesteana and Husnicioara quarries will close, and in 2027, the Lupoaia quarry will close.

The final closure of the remaining lignite and hard coal-based energy groups, totaling 1,140 MW, will be completed by December 31, 2030 [8].

https://doi.org/10.5593/sgem2024/1.1/s03.48

ENERGY TRANSITION

The Integrated National Energy and Climate Plan (PNIESC) is a requirement for EU member states under the Governance Regulation of the Energy Union. This plan involves developing 10-year policy strategies for energy and climate starting from the decade 2021-2030. Following the EU's accession to the Paris Agreement and the publication of the Energy Union Strategy, the Union has assumed a significant role in combating climate change through five main dimensions: energy security, decarbonization, energy efficiency, the internal energy market, and research, innovation, and competitiveness.

The coal sector will face increasingly severe obstacles and restrictions: rising prices of EU ETS certificates, exclusion of new coal units from the capacity market after 2025 (by limiting permitted emissions to 550g CO2/kWh), and increasingly stringent NOx emission limits. In the absence of abrupt new regulations contrary to EU policies, the high ETS price will facilitate the replacement of coal by natural gas in the electricity production mix.

National policies and action plans (within the decarbonization dimension) for reducing GHG emissions are essential for limiting the effects of climate change on the environment, economy, and society. To support green economic growth with a low carbon footprint, the EU has introduced ambitious climate and energy targets for 2030. Romania’s obligations as an EU member state include participating in the EU-ETS scheme for trading GHG emission certificates [9].

Cross-sectoral policies and measures include promoting investments in developing new low-carbon electricity generation capacities by 2030, given that 80% of existing thermal power groups have exceeded their normal lifespan, and the energy sector generates over 66% of GHG emissions. In this regard, the decarbonization plan proposed by CE Oltenia aims to replace and supplement (by 2030) 1,260 MW of coal-based power plants with 1,400 MW of natural gas power plants and 300 MW of renewable energy (solar panels).

Nuclear technologies can and will prove to be a clean decarbonization path for Romania. These will be complemented by renewable sources, with notable potential in offshore wind and the rapid development of prosumers, especially using photovoltaics, with Romania currently having over 110,000 active consumers.

The Recovery and Resilience Mechanism is the main pillar of the temporary financial instrument NextGenerationEU, established by the European Union to complement the Multiannual Financial Framework for 2021-2027. The mechanism has a total budget of 672.6 billion euros, consisting of up to 312.5 billion euros in grants and up to 360 billion euros in loans.

Access to the mechanism depends on the National Recovery and Resilience Plan developed by Romania, which considers the new climate targets assumed by the respective states through the Integrated National Energy and Climate Plans 2021-2030.

The funds to be allocated through the Recovery and Resilience Mechanism for Romania amount to approximately 29.2 billion euros. Of this total, 14.4 billion euros will be allocated as grants, and 14.935 billion euros as loans.

The National Recovery and Resilience Plan is built on six pillars: green transition, digital transformation, smart, sustainable and inclusive growth, social and territorial cohesion, health and economic, social, and institutional resilience, and policies for the next generation, children, and youth.

REFORMING THE CURRENT ENERGY MODEL. ENERGY HYBRIDIZATION

Green Transition Pillar includes several components, one of which is "Renewable Energy and Energy Efficiency." This component aims to implement high-efficiency cogeneration investments and will also include investments for the new energy industry in the Jiu Valley and Gorj. The initial negotiation budget for this component is 1.3 billion euros.

Component 6 – Energy within the National Recovery and Resilience Plan (PNRR) proposes 6 reforms and 6 main types of investments, with a total proposed budget of 1.62 billion euros. The reforms under Component 6 – Energy are as follows:
1. Reforming the electricity market by replacing coal in the energy mix and supporting a stimulating legislative and regulatory framework for private investments in renewable energy production.
2. Developing a favorable legislative and regulatory framework for future technologies, especially hydrogen and storage solutions.
3. Improving corporate governance of state-owned companies in the sector.
4. Reducing the energy intensity of the economy by developing a sustainable mechanism to stimulate energy efficiency in the industry.
5. Increasing competitiveness and decarbonizing the heating and cooling sector.
6. Decarbonizing the transport sector through investments in electric transport infrastructure and creating incentives for green transport.

The Just Transition Operational Program 2021-2027 is aimed at regenerating areas affected by the energy transition, considering their dependence on fossil fuels or high greenhouse gas emission industrial processes. The Just Transition Fund provides financial assistance at the European level for the gradual elimination of coal from the energy mix of countries dependent on this fuel. Thus, Priority 2 of the Just Transition Framework will finance investments in the development of technologies for green energy, including carbon capture and storage solutions, and investments in the creation of grid-connected photovoltaic parks. One solution is to fund these parks on land belonging to former mines or plants, thereby achieving integrated projects of decontamination/regeneration/reconversion. The allocation will be 2.239 billion euros, with an additional national co-financing of 301 million euros, according to the specific Regulation for the Just Transition Fund.

Romania has adopted the National Renewable Energy Action Plan for the period 2021-2030, with objectives such as: 30.7% of final energy consumption to come from renewable sources and increasing the installed capacity for wind, solar, and hydro energy to reach 17.8 GW by 2030. Hybrid energy in Romania is promoted through

https://doi.org/10.5593/sgem2024/1.1/s03.48

programs and initiatives like the Integrated National Energy and Climate Plan, the National Rural Development Program (PNDR), the Regional Operational Program (POR), and the Large Infrastructure Operational Program (POIM). There is noticeable interest in establishing a balanced energy mix in Romania, with plans for increasing the participation of renewable energy in hybrid energy production by 2050 [10, 11].

The combined use of two or more energy sources to obtain a mixed energy source leads to the idea/concept and application of hybrid energy. This involves the integration and simultaneous use of different technologies and energy sources to harness the advantages of each and achieve greater efficiency in the use of energy resources.

An already common example of the existence and application of a hybrid energy formula is the hybrid propulsion system in electric cars. In this system, the electric motor is powered by an electric battery in conjunction with an operational generator through an internal combustion engine (petrol, diesel) to charge the battery while the vehicle is in motion. Thus, the vehicle takes advantage of an electric motor's benefits (reduced greenhouse gas emissions, energy efficiency) along with the benefits of an internal combustion engine (extended autonomy, rapid refueling capability). Another common example of hybrid energy is using solar photovoltaic systems combined with wind turbines or diesel generators. Solar systems generate electricity during the day, with the surplus stored in batteries for use at night or during periods of high energy demand.

If battery levels drop or during periods of reduced solar energy production, wind turbines or diesel generators operate to supply the additional required electricity.

The advantages of using hybrid energy confirm that it can contribute to reducing greenhouse gas emissions, protecting the environment, and reducing dependence on traditional energy sources (fossil fuels) that generate polluting emissions. Similarly, hybrid energy helps diversify energy sources and increase the energy autonomy of a region or nation.

Energy hybridization refers to combining multiple energy sources and technologies to achieve a mixed system of production and/or use of energy. This involves the integration and synergy between renewable and traditional energy sources and using storage and energy management technologies [12].
Applications of energy hybridization include:

- Hybridization of energy sources: This involves combining multiple energy sources (solar, wind, hydroelectric, geothermal, and fossil fuel-based energy). By integrating and coordinating these sources, a more stable and consistent energy production can be achieved, reducing fluctuations and dependency on a single source.
- Hybridization of energy production technologies: Energy production technologies can also be combined to achieve synergistic benefits.
- Hybridization of energy storage technologies: Energy storage technologies (such as batteries, flywheels, thermal storage, or hydrogen storage) can be integrated to create specific hybrid multi-storage systems.

- Hybridization of energy applications: Hybridization can also be applied in various energy applications, such as transport, building power systems, or industrial infrastructure.

CONCLUSION

Coal-based energy decreased by 16% in 2023 compared to 2022 and will become history in less than a decade, while natural gas and oil-based fuels will gradually decline in share. Romania has committed to eliminating coal from the national energy system by 2032, through a Government Ordinance on decarbonizing the energy sector. The total installed capacity of lignite and hard coal-based electricity that will be gradually phased out is 4,920 MW, of which 3,780 MW by the end of 2025.Coal is used for 15-20% of electricity production, although the installed and available capacity in the National Energy System (SEN) of coal-based units is 3,350 MW, of which less than 1,000 MW are used for average consumption.

The restructuring program involves the phased closure of several coal mining units, with some of the operational energy groups being converted to gas by 2025, some of them with combined cycle gas turbines (CCGT) that can be adapted for hydrogen operation. The final closure of the remaining lignite and hard coal-based energy groups, totaling a capacity of 1,140 MW, will be completed by December 31, 2030.

Romania, alongside the EU, assumes an important role in combating climate change through the five main dimensions: energy security, decarbonization, energy efficiency, the internal energy market, and research, innovation, and competitiveness, according to the Energy Union Strategy.

Romania has adopted the National Renewable Energy Action Plan for the period 2021-2030, with objectives such as 30.7% of final energy consumption to be from renewable sources and increasing installed capacity for wind, solar, and hydro energy to reach 17.8 GW by 2030. Hybrid energy in Romania is promoted through programs and initiatives, such as the Integrated National Energy and Climate Plan, the National Rural Development Program (PNDR), the Regional Operational Program (POR), or the Large Infrastructure Operational Program (POIM).

The use of hybrid energy provides a number of advantages as it can contribute to reducing greenhouse gas emissions, protecting the environment, and reducing dependence on traditional energy sources (fossil fuels) that generate polluting emissions. Equally, hybrid energy contributes to diversifying energy sources and increasing the energy autonomy of an area, region, or nation.

ACKNOWLEDGEMENTS

This work was carried out through the NUCLEU Program within the National Research Development and Innovation Plan 2022-2027 (PN EXH_2), carried out with the support of MCID, project no. PN 23 32 02 03 - The superior valorization for energy purposes of coal deposits under the conditions imposed by environmental strategies (VSMET) end IOSIN PCDIEX.

https://doi.org/10.5593/sgem2024/1.1/s03.48

REFERENCES

[1] * * *, - REPowerEU, 2021

[2] * * *, - Hybrid Renewable Energy Converter for continuous and flexible power production. Un système hybride pour les énergies renouvelables, Seventh Framework Programme, CORDIS Résultats de la recherche de l'UE, 2020.

[3] http://www. gov.ro/ Emergency Ordinance/On some measures to decarbonise the energy sector – no.108 /30.06.2022/ Pdf (in Romanian)

[4] http://www.insse.ro/ Primary energy resources in the period 1.I-31.III.2024

[5] * * *, - https://www.energynomics.ro/iea

[6] C. Tomescu, D. Cioclea, M. Morar, S. Stanila, A. Camarasescu, 23th International Multidisciplinary Scientific Geoconference SGEM 2023, *Romanian Coal and the Energy Trilema,* (Albena-Bulgaria, 2023)

[7] https://mfe.gov.ro/pnrr/ National Recovery and Resilience Plan, Ministry of European Investments and Projects

[8] https://www.ceoltenia.ro/ Revised restructuring plan of the Oltenia Energy Complex 2021-2026 with a perspective to 2030 approved by the European Commission by Decision C (2022) 553 final of 26.01.2022

[9] C. Tomescu, I. Gherghe, F. Radoi, A. Matei, A.Camarasescu, 22nd International Multidisciplinary Scientific Geoconference SGEM 2022, *Exploration and Mining Romanian coal between decarbonization programs, exploitation closure and energy crisis,* (Albena, Bulgaria, 2022)

[10] * * *, - Romania's energy strategy, 2019-2030-2050, București, ME, 2019 (in Romanian)

[11] * * *, - Roadmap for the transition to a competitive low-carbon economy by 2050, (COM (2011) 112 final

[12] D.C., Momete, - The management of energy sources and resources of Romania: a challenge in the current geopolitical context, U.P.B. Sci. Bull., Series B, Vol. 68, No. 1, 2006.

SIMULATIONS CARRIED OUT AT THE LEVEL OF THE TÂRGU OCNA SALT MINE FOR REVERSAL VENTILATION

Doru Cioclea[1]
Adrian Matei[1]
Nicolae Ianc[1]
Răzvan Drăgoescu[1]
Alexandru Cămărășescu[1]
[1]National Institute for Research and Development in Mine Safety and Protection to Explosion – INSEMEX , **Romania**

ABSTRACT

On the territory of Romania, there are large salt deposits grouped on either side of the Carpathian mountains. Made up of over 300 large salt deposits covering an area of about 30,000 km2. The Trotuş mine within the Târgu Ocna Saltworks Branch was opened and put into operation in 1971, with the objective of dry salt exploitation, using the mining method with small chambers and abandoned square pillars, with a vaulted ceiling. Currently, Salina Trotuș has 14 horizons: 2 at the level of the Pilot mine and 12 at the level of the Trotuș mine. The paper presents a simulation on the ventilation network modeled and solved with the specialized program 3D CANVENT, which consists in the analysis of the possibility of reversing the general ventilation by using Gallery 401 and the Ocnița Well for the entry of fresh air.

Keywords: software, solving, ventilation, reverse, salt mine

INTRODUCTION

One of the greatest riches of Romania is represented by the salt deposits. Among these salt deposits is the one located in the Tg Ocna depression where the salt deposit approaches the surface, often coming to surface. The exploitation of salt in the Trotuș salt mine takes place on the horizons, descending, and the horizons are in withdrawal. The active mine has three connections with the surface through the following works: Coastal Gallery I 101; Coastal gallery "UNIREA" respectively the Air Well. The inclined planes expand as a new horizon opens, thus ensuring a permanent connection with the horizon in operation, serving both to ensure ventilation and for the movement of machinery and personnel. The ventilation shaft, at the surface of which the main ventilation stations are located, has a depth of 132 m.

THE VENTILATION NETWORK OF TROTUŞ SALT MINE

The general ventilation of the Tg.Ocna Salt mine is carried out in a suction system, by means of two main ventilation stations (motor-fan aggregate), located on the surface. One installation is equipped with a double suction centrifugal fan type V562-00 DA and the second main station is equipped with two axial fans type VOKD-1.5. Currently, Trotuș salt mine has 14 horizons: 2 at the level of the Pilot mine and 12 at the level of the Trotuș mine. Salt extraction is carried out at the XI and XII horizons (xxx, 2023 [20]).

https://doi.org/10.5593/sgem2024/1.1/s03.49

MODELING OF THE VENTILATION NETWORK

In order to ensure safety and health conditions at work when mining salt underground, it is necessary to ensure the distribution of the necessary flows at the level of each branch (Le Roux, 1990 [18]). In order to ensure optimal flows, specialized programs are used. In this sense, the 3D CANVENT program (Gherghe I., Rădoi F., 2020 [10]; CANMET [19]) is used to solve the complex ventilation network of the Trotuș salt mine, which can simulate the ventilation systems in operation, which include parameters such as: air flow rates and their distribution in the system, frictional pressure losses, fan performances, air energy requirements and operating costs both for each mine separately and for the entire network. Mainly for modeling and solving an ventilation network (Boantă, C. Rădoi, F. , 2017 [2]; Cioclea, D., 2007 [4]; Cioclea, D., 2011 [7]; Gherghe, I., 2004 [11]; Cioclea, D., 2008 [6]; Cioclea, D., 2009 [5], Gherghe, I., 2008 [13]), it is necessary to go through several successive steps. In order to know the real values of the aerodynamic parameters specific to mining works in the composition of the ventilation network related to the salt mine, flow-metric and depressiometric measurements are performed (Cioclea, D., 2006 [3]; Cioclea, D., 2013 [8]; Gherghe, I., 2006 [12]; Jurca, L. , 2008 [15]; Gherghe, I., Jurca, L., 2006 [14]). The value of the pressure loss, of the measured and corrected air flow, serves to establish the specific aerodynamic resistance of the respective section or branch (Băltărețu, R., Teodorescu, C., 1971 [1]; Cioclea, D., Lupu, C., Gherghe, I., 2013 [9]; Matei, I., Moraru, R., 2000 [16]; Patterson, A. M., 1992 [17]).

SIMULATION FOR REVERSAL VENTILATION USING GALLERY 401 AND OCNIȚA WELL FOR AIR INTAKE.

To determine the distribution of air flow throughout the ventilation system of the Trotuș Salt mine regarding the inversion of ventilation by using the 401 Coastal Gallery and Ocnița Well for the entry of fresh air, the base situation was used comparatively. In this sense, the 497 nodes, respectively 703 branches, were maintained. For this, at the level of the ventilation network related to the Trotuș Salt mine, the following were removed: the ventilation door located on Coastal Gallery 401, the closing system located on the surface at Ocnița Well, the register door located on Coastal Gallery 401 in the Pilot Mine area, the door with register located on the Pilot I Mine Access Gallery. The door with the register located on the Access Gallery in the Moldova Nouă Mine has been removed. The ventilation door located on Gallery 405 of the outline at Mine Moldova Nouă was removed. The ventilation door located on Gallery 406 of access to the Moldova Nouă Mine was removed. Removed the vent door located on Inclined Plan 502 access to the Horizon. A group of sluice-type ventilation doors has been placed on Coastal Gallery 101. An isolation dyke was placed on Gallery 405 of the outline at the Moldova Nouă Mine. An isolation pier was placed on Gallery 406 connecting to the Moldova Nouă Mine. At the level of the ventilation network related to the Trotuș Salt mine, under the conditions of inversion of the ventilation by using the Coastal Gallery 401 and the Ocnița Well for the entry of fresh air, the inversion of the direction of the air flow at the level of the branches as well as the decrease of the air flows was found, fig. no.1. The optimized ventilation network is shown in fig. no. 2 ; respectively the data presented in tables 1 (for nodes), 2 (for branches) and 3 (for fans). In fig. no. 3 (ventilation shaft fan) shows the characteristic curve related to the fan V 562 00 D.A., resulting from the solution of the ventilation network.

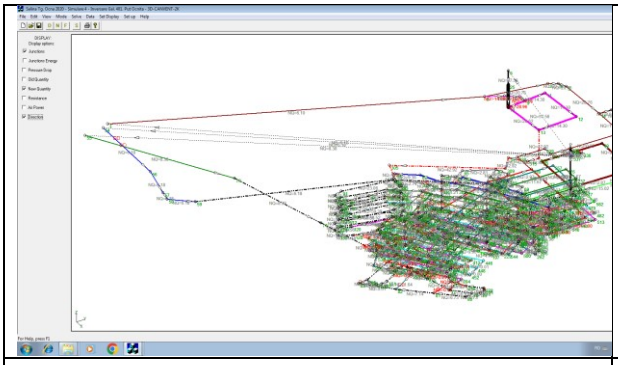


Fig. no.1. The simulated ventilation network

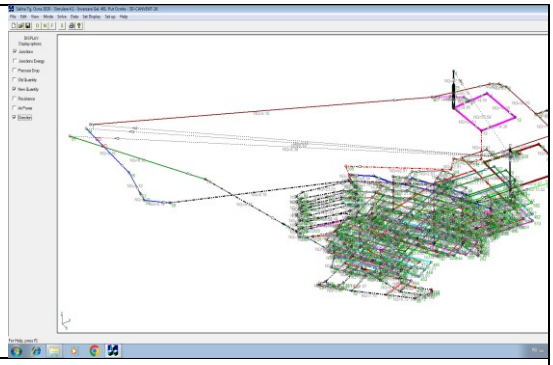


Fig. no. 2 The optimized ventilation network

Table no. 1 nodes

Junc.#:	Description:	Energy[NM/KG]:	Junc.#:	Description:	Energy[NM/KG]:
1	Galeria 401 cota 274	0.00	291	Gal. leg. Oriz. VI	-138.00
2	Galeria 401 cota 274	-33.86	292	Gal. leg. Oriz. VI	-139.60
3	Galeria legatura Mina Pilot	-36.72	293	Gal. dir. Oriz. VI	-139.60
4	Galeria legatura Mina Pilot	-37.16	294	Gal. dir. Oriz. VI	-139.60
5	Galeria legatura Mina Pilot	-37.59	295	Plan acces Oriz. VI	-139.61
6	Suprafata Ocnita	0.88	296	Gal. dir. Oriz. VI, suitor 206	-139.60
7	Gal leg Moldova Veche	-20.80	297	Gal. dir. Oriz. VI, Suitor 207	-139.60
8	Gal leg Moldova Veche	-10.61	298	Gal. dir. Oriz. VI	-139.60
9	Gal. Mina Moldova Veche	-4.24	299	Galerie dir. Oriz. VIII	-149.63
10	Salina Ocnita	-4.21	300	Gal. dir. Oriz. VI	-139.60
11	Mina Moldova Veche	-4.25	301	Suitor aerai 204	-204.64
12	Mina Moldova Veche	-4.28	302	Gal. acces Oriz. V	-130.33

Table no. 2 branches

Branch From:	To:	Description:	Sym-bol	Resistance [Ns²/M8]:	Quantity [m³/s]:	Pressure Drop [PA]:	Air Power [KW]:	Annual Cost [$]:
1	2	Galeria 401 cota 274		0.9108	6.10	33.86	0.21	904
2	3	Galeria 401 cota 274		0.0066	20.76	2.86	0.06	280
7	2	Gal leg Moldova Veche		0.0607	14.66	13.06	0.19	839
3	4	Galeria legatura Mina Pilot		0.0010	20.76	0.45	0.01	41
4	5	Galeria legatura Mina Pilot		0.0010	20.76	0.43	0.01	39
5	14	Gal 401		0.0061	20.76	2.61	0.05	238
6	25	Putul Ocnita		0.0012	57.58	4.14	0.24	1043
8	7	Gal leg Moldova Veche		0.0474	14.66	10.19	0.15	654
9	8	Gal leg Moldova Veche		0.0296	14.66	6.37	0.09	409
10	9	Mina Moldova Veche		0.0000	28.96	0.04	0.00	5
9	11	Mina Moldova Veche		0.0001	14.30	0.01	0.00	1
10	13	Mina Moldova Veche		0.0001	28.61	0.09	0.00	11
11	12	Mina Moldova Veche		0.0001	14.30	0.02	0.00	1
12	13	Mina Moldova Veche		0.0001	14.30	0.02	0.00	1
13	318	Mina Moldova Veche		0.0001	42.91	0.24	0.01	46

Table no. 3 fans

Fan Name:	Branch From:	To:	Pressure [Pa]:	Quantity [m³/s]:	Air Power [KW]:	Cost [$]:
fixed	221	232	700.00	32.49	22.74	99815
fixed	237	556	730.00	39.64	28.94	126752
V 3 - 52600 - D.A.	334	337	1732.94	80.28	139.13	609380
fixed	606	581	500.00	24.96	12.48	54671

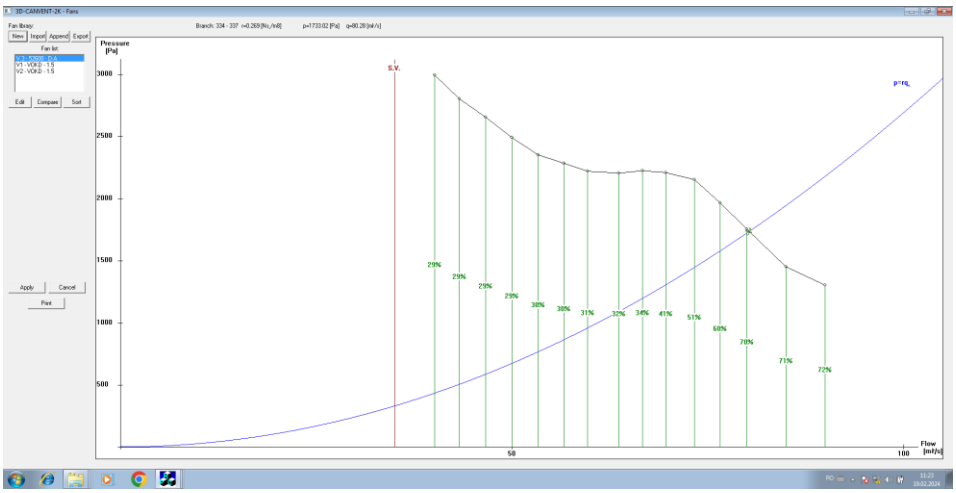


Fig. no. 3 Characteristic curve related to the fan V 562 00 D.A.

https://doi.org/10.5593/sgem2024/1.1/s03.49

The following solution of the ventilation network related to the Trotuș salt mine under the conditions of inversion of ventilation by using Coastal Gallery 401 and the Ocnița Well for the entry of fresh air, the following air flows were obtained, compared to the basic situation: On Coastal Gallery 101, of fresh air supply, was 6.18 m3/s compared to 68.64 m3/s, a value that represents an extremely large decrease in air flow by 90.9%. On the Galeria de Coastă Unirea, fresh air supply, it was 8.38 m3/s compared to 5.61 m3/s, a value that represents a large increase in air flow by 49.3%. On Coast Gallery 401, fresh air supply, it was 6.1 m3/s compared to 4.51 m3/s, a value that represents a moderate increase in air flow by 35.2%. On the Ocnița Well, fresh air inlet, it was 57.58 m3/s compared to 0.55 m3/s, a value that represents a fulminant increase in air flow by 10,369.1%. On the Mina Pilot II access gallery, fresh air intake, it was 8.84 m3/s compared to 0.07 m3/s, a value that represents a fulminant increase in air flow by 12,528.5%. On the Mine Pilot I Access Gallery, for exhaust air, it was 15.02 m3/s compared to 1.61 m3/s, a value that represents an extremely high increase in air flow by 832.9%. At the level of the Old Moldova Mine, the fresh air intake was 28.96 m3/s compared to 1.31 m3/s, a value that represents a fulminant increase in air flow by 2,110.6%. At the level of the Moldova Nouă Mine, fresh air intake was 4.47 m3/s compared to 0.62 m3/s, a value that represents an extremely high increase in air flow by 620.9%. On gallery 405 of the Moldova Nouă Mine, for exhausting the contaminated air, it was 0.05 m3/s compared to 3.96 m3/s, a value that represents a drastic decrease in air flow by 98.7%, the work is closed with an isolation dam. On the main transversal gallery at the Ventilation Shaft, horizon I Pilot Mine, for exhausting the poluted air, it was 78.23 m3/s compared to 79.33 m3/s, a value that represents an insignificant decrease in the air flow by 1 ,4%. At the level of the Ventilation Shaft, horizon I of the Pilot Mine, for exhausting the stale air, it was 78.23 m3/s compared to 79.33 m3/s, which represents an insignificant decrease in air flow by 1.4%. At the level of the main ventilation station VOKD 1.5 of shortcut with the surface, it was 1.67 m3/s compared to 1.63 m3/s, a value that represents an insignificant increase in air flow by 2.4%.

At the level of the air shortcut with the surface, it was 0.38 m3/s compared to 0.37 m3/s, a value that represents an insignificant increase in air flow by 2.7%. At the level of the main ventilation station V 562 D.A., it was 80.29 m3/s compared to 81.33 m3/s, a value that represents an insignificant decrease in air flow by 1.3%.

In the last column of table no. 17, the annual cost of air transportation is presented, compared to the basic situation, on each branch of the ventilation network, at an average price of 0.48 lei / kWh, as follows: On Galeria de Coastă 101, fresh air supply, was 4,254 lei compared to 2,331 lei, a value that represents a very large increase in cost by 82.5%. On the Galeria de Coastă Unirea, fresh air supply, it was 6,365 lei compared to 1,907 lei, a value that represents an extremely high increase in cost by 233.7%. On Galeria de Coastă 401, fresh air entrance, it was 1,240 lei compared to 785 lei, a value that represents a large increase in cost by 57.9%. On the Ocnița Well, for fresh air intake, it was 1,431 lei compared to 98 lei, a value that represents a fulminant increase in cost by 1,360.2%. On the contour gallery 405 of the Moldova Nouă Mine, for exhausting the contaminated air, it was 0 lei compared to 3,204 lei, a value that represents a total decrease in the cost, work closed with an isolation dam. On the main transversal gallery at the ventilation Shaft, horizon I Pilot Mine, for exhausting the contaminated air, it was 2,934 lei compared to 3,056 lei, a value that represents an insignificant decrease in cost by 3.9%. At the level of the ventilation Shaft, horizon I of the Pilot Mine, for exhausting the poluted air, it was 509,184 lei compared to 530,330

lei, a value that represents an insignificant decrease in the cost by 3.9%. At the level of the main ventilation station VOKD 1.5 of shortcut with the surface, it was 14,017 lei compared to 12,958 lei, a value that represents a reduced cost increase of 8.1% (branch 336-335). At the level of the shortcut ventilation shaft with the surface, it was 3,291 lei compared to 3,055 lei, a value that represents a reduced cost increase of 7.7%. At the level of the ventilation channel related to the main aeration station V 562 D.A., it was 140,360 lei compared to 145,754 lei, a value that represents an insignificant decrease in the cost by 3.7%. At the level of the main ventilation station V 562 D.A., it was 835,689 lei compared to 816,505 lei, a value that represents an insignificant increase in the cost by 2.3%.

DISCUSSIONS

The following solution of the ventilation network related to the Trotuș Salt mine in the conditions of inversion of ventilation by using the Galeria de Coastă and the Ocnița Well for the entry of fresh air, it was observed that the fan V - 56200 D.A., achieves a flow of 80.43% of the maximum flow that such a type of fan can achieve it. In this sense, at the level of the main ventilation station, a flow rate of 80.29 m3/s is circulated at a developed depression of 1,732.84 Pa and a total resistance of the ventilation network of 0.269 Ns2/m8. The following solution of the ventilation network related to the Trotuș Salt mine in the conditions of inversion of the ventilation by using the Galeria de Coastă and the Ocnița Well for the entry of fresh air, it was observed that the direction of circulation of the air currents was changed in the following areas: Old Moldova Mine; The access gallery to the Old Moldova Mine; 501 Plan; Horizon I; Little change in Horizon V; Significant change at Horizon VI level; Significant change at Horizon VII level; Significant change at Horizon VIII level; Little change in Horizon IX; Little change in Horizon XII. The air flow in the ventilation network was reduced by 1.2%. The gases from the exploitation area are not circulated on the routes of the mining works related to the sanatorium located at the level of the IX horizon. Also, the gases from the exploited spaces are circulated to the Car Transport Plan at Horizon II level. At the Sanatorium level, a total air flow of 5.97m3/s is circulated. As a result of the inversion of the ventilation by using the Coastal Gallery and the Ocnița Well for the entry of fresh air, an extremely large increase in the air flow at the level of the Ocnița Well was found, as well as a drastic decrease in the air flow at the level of the Coastal Gallery 101. On the Unirea and 405 Coastal Galleries a large increase in air flow was observed. A very high air flow rate of 42.92 m3/s is circulated at the level of the water outlet gallery, which enters the fresh air supply circuit at the level of horizon III. In the rest of the network, the distribution of air currents was similar to the basic situation. The costs required for the circulation of air flows at the level of the branches of the ventilation network presented a predominantly low to moderate variable evolution in relation to the costs resulting from the basic simulation. The variable evolution of the predominantly low to moderate costs in the context of a predominantly low to moderate variable evolution of the flows circulated at the level of the ventilation network can lead to an additional annual cost of 19,184 lei in absolute value.

CONCLUSIONS

To modeling and solve the ventilation network of Trotuș Saltmine, which presents an extremely high degree of complexity, the method of the iterative technique, namely that

https://doi.org/10.5593/sgem2024/1.1/s03.49

of successive approximations, was used, which is the basis of the program for solving the 3D-CANVENT ventilation networks. For the economic characterization of the ventilation process of Trotuș salt mine, an average energy price of 0.48 lei / kWh was taken into account. The ventilation network related to the Trotuș Salt Mine includes three old mines: the Ocnița Mine, the Old Moldova Mine and the New Moldova Mine. It also includes the Pilot Mine with two horizons, namely Horizon I and Horizon II. The central area of exploitation includes 12 horizons from Horizon I to Horizon XII. The active horizons are Horizon IX – Sanatorium, Horizon XI and Horizon XII. Salt mine has 2 main ventilation stations, namely: the main ventilation station V 562 D.A. - the main ventilation station VOKD 1.5 is active. The following solution of the ventilation network related to Trotuș Salt mine under the conditions of inversion of ventilation by using Coastal Gallery 401 and Ocnița Well for fresh air entry - simulation 4, the following were found: 497 nodes, respectively 703 branches, were used. For this, at the level of the ventilation network related to Trotuș Salt mine, 7 doors or groups of ventilation doors were removed, respectively the surface closure system of the Ocnița well. Also, a group of ventilation doors with airlocks and 2 isolation dams were placed. The air flow at the level of the main ventilation station V 562 D.A. was 80.29 m3/s compared to 81.33 m3/s, compared to the situation corresponding to the basic simulation, a value that represents an insignificant decrease in the air flow with 1.3%. The annual cost of circulating air at the level of the main ventilation station V 562 D.A. was 835,689 lei compared to 816,505 lei, compared to the base situation, a value that represents an insignificant increase in the cost by 2.3%. Following the simulation of the ventilation network related to the Trotuș Salt mine under the conditions of inversion of the ventilation by using the Galeria de Coastă and the Ocnița Well for the entry of fresh air, it was observed that the fan V - 56200 D.A. achieves a flow of 80.43% of the maximum flow that such a type of fan can achieve. At the level of the main ventilation station, a flow rate of 80.29 m3/s is circulated at a developed depression of 1,732.84 Pa and a total resistance of the ventilation network of 0.269 Ns2/m8. It was also observed that the direction of circulation of the air currents was changed in the following areas: Old Moldova Mine; The access gallery to the Old Moldova Mine; 501 Plan; Horizon I; Horizon V; Horizon VI; Horizon VII; Horizon VIII; Horizon IX; Horizon XII; The air flow in the ventilation network was reduced by 1.2%. At the level of the Sanatorium, a total air flow of 5.97m3/s is circulated. As a result of the inversion of the ventilation by using the Coastal Gallery and the Ocnița Well for the entry of fresh air, an extremely large increase in the air flow at the level of the Ocnița Well was found, as well as a drastic decrease in the air flow at the level of the Coastal Gallery 101. On the Unirea and 405 Coastal Galleries a large increase in air flow was observed. A very high air flow rate of 42.92 m3/s is circulated at the level of the water outlet gallery, which enters the fresh air supply circuit at the level of horizon III. The costs required for the circulation of air flows at the level of the branches of the ventilation network showed a mostly low to moderate variable evolution in relation to the costs resulting from the basic simulation. The variable evolution of the predominantly low to moderate costs in the context of a predominantly low to moderate variable evolution of the flows circulated at the level of the ventilation network can lead to an additional annual cost of 19,184 lei in absolute value.

ACKNOWLEDGEMENTS

This paper was developed within the Nucleu - Programme, carried out with the support of ANCSI, project no. PN-23-32-02-03

REFERNCES

[1.] Băltăreţu,R., Teodorescu, C., *Ventilation and labor protection in the mine,* Didactic and Pedagogical Publishing House, Bucharest 1971

[2.] Boantă, C., Rădoi, F., *Study regarding the optimization of the general ventilation of the Cacica mine.* INSEMEX 2017 study.

[3.] Cioclea, D., *Solving the ventilation network based on depressiometric measurements for the purpose of commissioning the new VOD 2.1 fan station from well no. 10 - Valea Arsului,* INSEMEX Study 2006.

[4.] Cioclea, D., *Solving the ventilation network after commissioning the new VOD 2.1 fan station,* INSEMEX Study 2007.

[5.] Cioclea, D., *Modeling, solving and simulating the ventilation network of the Uricani mine,* INSEMEX Study, 2009.

[6.] Cioclea, D., *Modeling, solving and simulating the ventilation network of the Paroşeni mine,* INSEMEX Study, 2008.

[7.] Cioclea, D., *Reducing the risk of explosion in coal mines through the computerized management of ventilation networks,* SECTORAL Plan 2010-2011.

[8.] Cioclea, D., Gherghe, I., *Updating the ventilation network of Salina Praid, in order to establish the air flows at the branch level,* INSEMEX Study 2013.

[9.] Cioclea,D., Gherghe, I., *Guide for sizing industrial ventilation installations, ISBN: 978-973-88753-4-0,* INSEMEX Publishing House, Petroşani, 2013.

[10.] Gherghe, I. Rădoi, F., *Modeling and solving the ventilation network of the Trotuş mine using the 3D CANVENT program,* INSEMEX 2020 Study.

[11.] Gherghe, I., *The rationalization of the ventilation networks of the mines in the Jiului Valley under the conditions of their restructuring as a result of the closure of some inactive areas,* INSEMEX Study 2004

[12.] Gherghe, I., *Modeling and simulation services of the ventilation network for E. M. Petrila,* Study INSEMEX 2006

[13.] Gherghe, I., *Modeling and optimization services of the mine ventilation network E. M. Lonea,* Study INSEMEX 2008

[14.] Gherghe, I., Jurca, L., *Cacica salt mine ventilation project,* INSEMEX Petroșani Study, 2006.

[15.] Jurca, L., *Establishing the distribution of air flows and modeling the ventilation network related to the Praid Salt mine in order to optimize the environmental conditions underground,* INSEMEX Study, 2008

[16.] Matei, I., Moraru, R, ş.a, *Environmental engineering and underground ventilation,* Bucharest Technical Publishing House, 2000

[17.] Patterson, A. M., *The Mine Ventilation Practitioner's DATA BOOCK*, M.V.S. of South Africa, 1992

https://doi.org/10.5593/sgem2024/1.1/s03.49

[18.] Le Roux, *Notes on Mine environmental control,* The MVS of South Africa 1990

[19.] CANMET, *Mining and Minerals Sciences Laboratories Underground Mine Environment and Ventilation - User manual* – 3D program – CANVENT – 2K

[20.] X X X, *The annual ventilation project of the Trotuș Salt Mine for the year 2023.*

THE CONTINUATION OF THE EXTRACTION OF USEFUL MINERAL SUBSTANCES IN THE CURRENT GEOPOLITICAL CONTEXT

PhD Eng. Adrian Matei[1]
PhD Eng. Doru Cioclea[1]
PhD Eng. Răzvan Drăgoescu[1]
PhD Eng. Alexandru Cămărășescu[1]
[1]National Institute for Research and Development in Mine Safety and Protection to Explosion – INSEMEX Petroşani, **Romania**

ABSTRACT

In the last decade, at the global level, most countries have emphasized the reduction of energy consumption produced with the help of solid fuels, trying to reduce the volume of greenhouse gases and polluting gases by identifying new sources and methods of energy production that have a low effect on the environment and people. Romania is preparing to ensure energy security by producing electricity from renewable sources. Romania's medium- and long-term strategy will be influenced by the European Green Pact, which has ambitious targets for the next period for reducing carbon emissions for each member state. These objectives may also include the recent turbulence in the energy markets in Europe as well as the effects of the conflict in Ukraine. If at the beginning of the implementation of the objectives to reduce the exploitation of useful mineral substances, the geopolitical situation of the world was stable and there were interconnections between the energy-producing states, in 2024 we were faced with a radical change in the global geopolitical context, a change that would require a rethinking of the strategy management of useful mineral resources.

The paper presents an analysis, in a global context, of the situation in Romania regarding the production of electricity from solid fuels.

Keywords: mineral, substance, development, production.

INTRODUCTION

On a global scale, mineral resources are an area where the theoretical and political stakes are closely linked. This is because the claims for their exploitation are based on new geopolitics, on a theoretical argument based on the limits of neoclassical analysis and its managerial failures and on the new forward-looking theories and methodologies of modern political economy. International conferences and conventions on the efficient use of natural resources have taken into account the effects of environmental degradation and the danger of depletion of natural resources. These conventions also took into account contemporary geopolitical circumstances. Currently, mineral resources are assessed on a global scale in terms of their diversity. The political redefinition of mineral resources as "geo-resources" was prompted by the reduction in the number of suppliers in the context of increased consumer demand. Instead, the list of strategic mineral resources has grown as a result of the demands of contemporary industries. They presented new resource requirements for new technologies such as

https://doi.org/10.5593/sgem2024/1.1/s03.50

microelectronics, telecommunications and the automotive industry. International meetings on the effects of mineral resource exploitation are accompanied by politicians' signatures. These signatures include enforcement measures such as reducing emissions, limiting the use of cyanide and highly polluting substances or sulfur dioxide, and regulations to reduce or eliminate hazardous practices. In the past, principles have been established, such as accepting the sovereign right of nations over natural resources within their borders and rejecting the concept of the common heritage of humanity as a principle for the exploitation of biodiversity, which was advocated at the 1992 Rio de Janeiro Conference In December 2015, an International Conference was held in Paris that reached agreements that will tighten the conditions for transportation, processing and exploitation of resources. Mineral resources are necessary for the development of civilization. The belief that they can be exploited in "other people's backyard" is extremely harmful. In recent decades, Europe and Romania have developed a philosophy that has imposed a series of limitations regarding the exploitation of resources. The idea that exploitation was limited to the third world was dismantled when the resource market changed significantly [1]. Through the understanding of the stake by some powers that have managed to control the potential of mineral resources, we have reached the situation where Europe risks losing the role it has. France, a nation that promoted freedom and environmentalism, was particularly affected by the coups in Africa. The coups in Africa especially affected France, the country that preached freedom and environmentalism. Imposing the expansion of protected areas without much discernment, environmental restrictions and the development of NGO concepts, which often "do not know where they come from", have led to a critical situation in the supply of resources, especially energy ones as well as metals from new technologies or steels and construction materials. The European Community developed on the need for coal and steel, having the original name of the Coal and Steel Community (CEEC), founded in 1951 by the Treaty of Paris, which included France, West Germany, Italy, Belgium, Luxembourg and the Netherlands. Lately, this community has believed that there is no need for the development of resource exploitation, but hastened with progress, without understanding its limits. Romania can become a source of mineral resources due to its potential and supply needs, both for itself and for Europe. Alarm signals have been sounded for a long time, but those responsible for managing these areas do not understand these needs, nor the dangers to which we are exposed. Despite the fact that there are still people, whether natural or legal, interested in participating in the exploitation of resources in Romania, the fragmentation of legislation and poor management of an institution is an effective barrier. Drawing up a logical scheme of the structure of the necessary documents to be approved (approval and authorizations) is a barrier that is becoming more and more difficult to overcome. These actions blatantly contradict the fundamental principle of the Mining Law, which specifies that the state stimulates the exploitation of mineral resources and encourages investments in the mining field through fiscal and administrative facilities. An analysis of the stages of obtaining approvals and authorizations shows those with a clear mind that a situation has been reached that is difficult to explain. The first victims are economic operators, followed by consumers shocked by the prices of materials, constructions, the poor quality of the products they need, or worse, their shortage. Wars consume enormous amounts of resources, as we see in Ukraine or Gaza. These resources need to be replenished in the future. All these needs will be accentuated even more. Failure to understand this context will accentuate the economic, social and environmental crisis.

All this leads us to be as involved as possible to avoid history repeating itself. The solution lies both in civil society and in politics [2].

WORLDWIDE

Even after the record increase in renewable energy in 2021, fossil fuels continue to dominate global energy use, with the global share of global energy consumption growing by just under eight percentage points over the past decade. In its annual overview of the renewable energy sector, the international policy network REN21 shows that the share of renewables in global energy consumption has stagnated despite increased investment. The renewables sector, which provided approximately 20% of the world's energy needs in 2011, represented a little over 28% in 2021 data presented in figure 1.

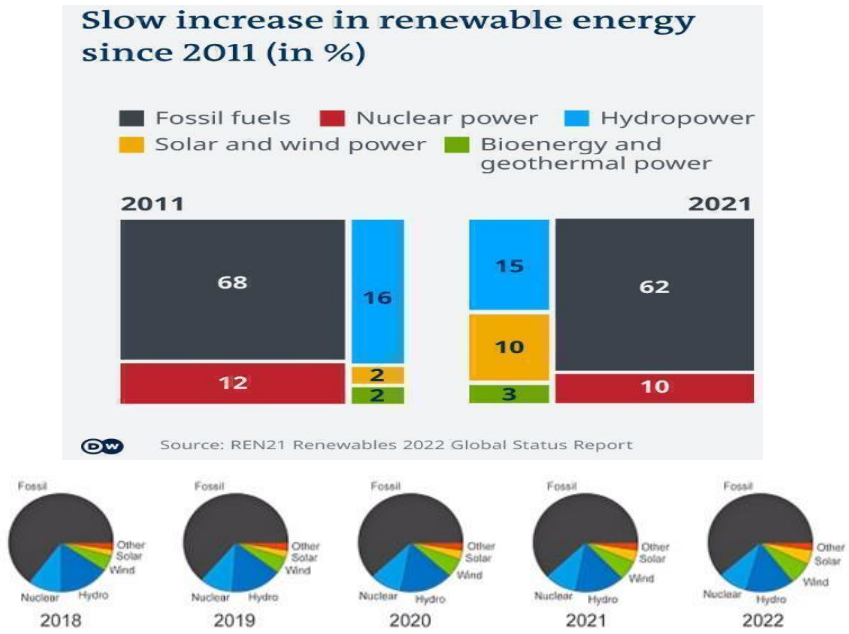


Fig. 1 REN21 Global Report

Evolution of world energy production

The gains in renewables in 2021 were on the back of a 4% increase in energy consumption as the world slowly began to recover from the COVID-19 lockdown, growth that was mainly covered by fossil fuels such as coal and natural gas [3]. Although many governments have committed to net zero greenhouse gas emissions by 2021, the reality is that in response to the energy crisis, most countries have returned to seeking new sources of fossil fuels and burning of even more coal, oil and gas. Despite expanding clean energy production capabilities, China is still "heavily dependent" on the polluting fossil fuels that power its energy-hungry economy. Coal produces about 60 percent of China's energy, according to government data. In fact, every year China burns more than half of the world's coal consumption, and it can only become a climate leader if it finds ways to overcome its dependence. Despite a goal to stabilize carbon emissions by 2030, Beijing has approved the construction of numerous new coal-fired

https://doi.org/10.5593/sgem2024/1.1/s03.50

power plants - up to two plants per week in 2022 and the first half of 2023. Chinese officials have justified the expansion of coal use as a guarantee amid the global energy crisis, given that the country has large coal reserves. "China Needs Coal for Green Energy Transition". China had previously promised to "reduce" coal consumption starting in 2026. But a few months ago, China's top climate official said a complete phase-out of fossil fuels was not realistic when the country had to maintain economic growth and provide backup power sources for when the wind doesn't blow and the sun doesn't shine. Paradoxically, China needs coal for its transition to green energy, says Lin Boqiang, a professor at the China Energy Policy Institute at Xiamen University. "Without coal, renewable energy simply cannot advance rapidly, because you cannot provide a stable energy source for the energy transition." A first starting point is the energy consumption data for the year 2020 figure 2 [4].

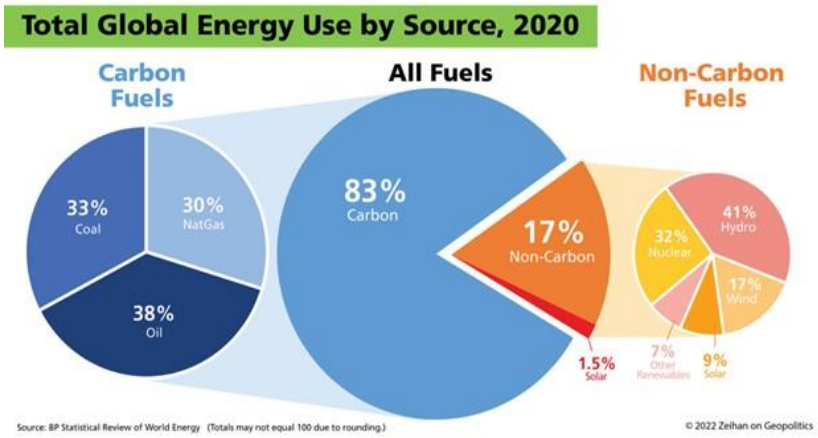


Fig. 2 Global energy consumption, by sources, in 2020.

The ratio between the consumption of carbon-based and non-carbon-based energies (83% vs. 17%) gives us an idea of how big the leverage we would need if we want to achieve a total de-carbonization (zero emissions) of the energy system. It should also be mentioned the extremely thin slice (1.5%) that the contribution of solar energy represents. Wind energy is also very low in the global mix - about 2.9%. The inconvenient reality for some is that carbon-based fuels work anytime, anywhere because they are physically concentrated energy in solid, liquid or gaseous form that we can easily store, for example in our means of transport. On the other hand, "green" energies are extremely location specific or very diluted or both. In conditions where more hydropower plants (due to lack of suitable locations) or more nuclear power plants (for political-economic reasons) cannot be built, it follows that the minuscule 4.4% of "green" energies will have to replace 83% of base energies of carbon. [5]

A second point of discussion is related to geology. Figure 3 shows what minerals and what quantities are needed to defeat the petro-dictators and execute the "green" energy transition?

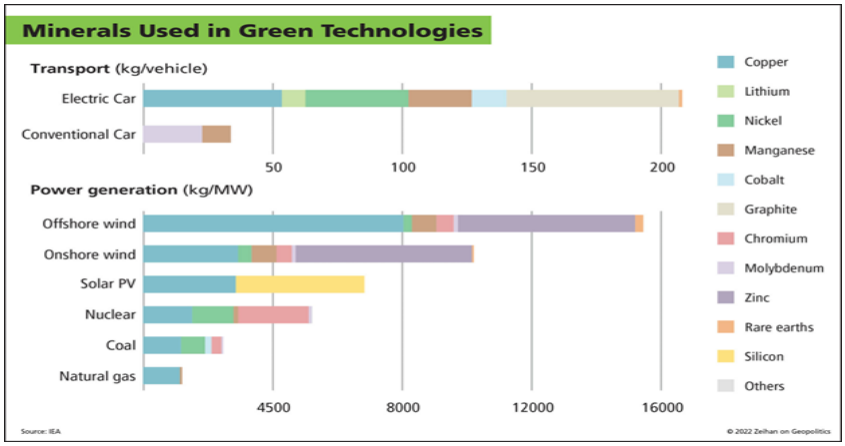


Fig. 3

Quantities of minerals used in "green" technologies: electric transport vs. conventional transport, respectively wind and solar energy vs. nuclear energy and those produced by coal and natural gas (aluminum and steel are not included).

If a conventional car (which will no longer be produced in the EU after 2035!) needs approx. 40 kg of minerals, an electric car will consume over 200 kg, i.e. five times more.

In the case of the energy transition, from gas and coal to "green" energies, solar and wind, the amount of minerals required for one megawatt of electricity is also clearly in favor of fossil fuels. While a gas-fired power plant needs about 1,000 kg of minerals per 1 MW, an offshore wind turbine uses almost 16,000 kg of minerals per 1 MW, over an order of magnitude more [6].

EUROPEAN UNION

Europe is 71% dependent on fossil fuels for energy production. Eurostat data for 2023 showed a slight increase compared to the previous year. In 2023, the European Union produced 70.9% of its energy from fossil fuels, and the rest from renewable or nuclear sources. It is an increase of one percent compared to the previous year, despite European policies regarding energy from renewable sources. But the pandemic also enters the equation, the one that changed consumption behavior in the two years. Moreover, in 2022 nuclear production was reduced due to the maintenance work of many European reactors, and several others were closed, in 2022 the German Government decided to restart 16 oil and coal-based power plants in a state of preservation and extension of operating authorizations for another 11. "The fact that due to Russia's brutal attack on Ukraine we now have to temporarily use some power plants that we had already taken out of operation is bitter", declared German Chancellor Olaf Scholz".

IN ROMANIA

In 2015, Romania had 5.7 GW installed in coal-based energy production, this year only 2 GW in coal-fired plants were still operating, and by 2030 they should completely exit the local energy system, a historic exit taking into account of the importance that coal had for Romania's energy [7].

https://doi.org/10.5593/sgem2024/1.1/s03.50

Furthermore, if in 2015 Romania had 4.5 GW installed in gas power plants, this year their capacity reached 2.4 GW, so that in 2030 gas will reach 4.4 GW again, according to the data from the new PNIESC (Integrated National Plan in the field of Energy and Climate Change) revised, this plan being in fact the true energy strategy of Romania. A good part of these gas plants should be powered by the new quantities extracted from the Black Sea. [8] However, Romania has a negative history regarding resource management, having rather unfavorable actions such as:

- sells raw material – resources of copper, gold, silver and other metals;

- introduces mining perimeters with important reserves into protected areas;

- destroys the millennial mining science and art;

- technical documentation on resources are in "mysterious" warehouses;

- uncertainties related to the validity and role of exploration licenses or exploitation;

- keeping some mining companies insolvent;

- vandalization/ alienation of mining, prospecting and exploration companies (IPEG), useful rock quarries, cement factories with related quarries, etc.

The reserves/resources of useful mineral substances belong exclusively to the Romanian state, the riches of the underground are the property of the state [9].

The management of mineral resources is the attribute/care of the state, through A.N.R.M - National Agency for Mineral Resources, from Bucharest.

Prospecting and exploration as well as mining operations are carried out by economic agents selected/approved by the Romanian state, through A.N.R.M, by granting licenses/exploitation premises in certain mining perimeters.

The land surfaces in private/private ownership, from the mining perimeters approved to be prospected, explored and/or exploited, are expropriated or occupied abusively in the community/national interest.

The prospecting, the explorations in order to appreciate the deposits of useful mineral substances are carried out by the decision of the state, the owner of the Romanian subsoil by specific law/laws.

Mining operations, the preparation and valorization of useful mineral substances, the opening of mines through mining works/investments, (made by the Romanian state and/or "strategic" investors), the preparation and extraction of mining products, are supported from production funds, resulting from the valorization/sale of production to the beneficiaries correct, who honor their assumed contracts, at the set deadline, pay the received production at the price agreed by the contract, (e.g. in mining: the mining operation/coal producer as well as the Mintia/Deva thermal power plant beneficiary being state enterprises, the difference between the cost of the delivered production and the price paid by the beneficiary was borne by the Romanian state through a subsidy). [10] The development of activity in the mining sector of the national economy and/or the continuation of exploitation, the cessation of mine activity, the conservation or closure and greening of mining areas are political decisions applied on the basis of specific technical documentation regulated by decisions of the Government of Romania followed by laws...etc. The decision-maker is the Romanian state, a political decision-maker.

CONCLUSIONS

After a brief analysis of the current situation of energy production worldwide, European and in Romania, its production method and the effects of the internal and external factors of each state, respectively the political situation and crisis situations (pandemics ,wars, financial crises, etc.) we can list some realistic conclusions on the subject touched on in this article such as:

Currently and in the current geopolitical context, according to some great researchers and decision-makers in the mining field, specialists and supporters of the coal industry from the United Kingdom of Great Britain and Northern Ireland (UK): "the time of coal will return, that's for sure".

Will decarbonisation eliminate all the world's evils, including petro-dictators? Probably not, especially since, according to Professor Vaclav Smil, the global transition that we have just begun, unevenly, is not the work of years, but of decades, if not centuries. The abandonment of fossil fuels should involve, in many cases, a forced development of "decarbonized" electricity production: renewable energy sources or nuclear energy, for the most part.

It is important that the reserves of useful mineral substances are preserved/secured in order to have access to them in the event of an international conflict, in this sense the researches and documents drawn up, existing, published and unpublished by some researchers must be taken into account in the global analysis of the situation.

In a more or less critical way, the energy transition promises to move from dependence on fossil fuels to dependence on a certain number of essential minerals and metals. The technical and organizational decisions to be made under the transition policies, which are largely unclear or contradictory in China, France, Germany and the United States.

The availability of future resources of cobalt, nickel, lithium, rare earths, copper: all are potential pitfalls on the perilous path of transition. The future ability to develop the production of these metals is largely uncertain and even unknown.

Romania and Europe need the development of the exploitation and exploitation sector of mineral resources, especially in the new geopolitical context. The war in Ukraine and the positioning of China and other states towards it radically changes the technology needs and the future supply of mineral resource markets. It must also be understood the current situation in which the progress in technology is so advanced that the production capacity is exceeded by the need for raw materials - mineral and energy resources. A new approach is needed in mineral resource strategies by supplementing the existing premises with armament needs, the increase in the consumption of mineral resources generated by war, earthquakes, climate change and the ratio between the production of goods and the need for raw materials. In the ethics of production, the origin of resources must also be taken into account, especially from areas of conflict, political instability, extraction with high environmental impact, etc.

ACKNOWLEDGEMENTS

This work was carried out through “Core program” of the National Research, Development and Innovation Plan 2022-2027, supported by MCID, project no. PN 23

https://doi.org/10.5593/sgem2024/1.1/s03.50

32 02 01 Developing the level of knowledge of the explosiveness parameters of hydrogen-based gaseous and hybrid mixtures, involved in the obtaining and storage processes in order to reduce the risk of explosion and IOSIN - PCDIEX.

REFERENCES

[1] https://gogreenresources.ro/despre-ong

[2] Reichl, M. Schatz - World Mining Data - Minerals Production, vol.38 Vienna 2023.

[3] Reichl, M. Schatz - World Mining Data - Minerals Production, Volume 37, Federal Ministry of Agriculture, Regions and Tourism Stubenring 1, 1010 Vienna, 2022.

[4] https://eurosunmining.com/ro/home/

[5] BP, 2022, Statistical Review of World Energy

[6] IEA, 2021, The Role of Critical Minerals in Clean Energy Transition

[7]Trembath, A., and Wang, S., 2022, Carbon Is Making Us Dependent on Dictators…but clean energy alone won't change that.

[8]https://www.dw.com/ro/china-erou-sau-r%C4%83uf%C4%83c%C4%83tor-climatic/a-67655734

[9] https://www.contributors.ro/combustibili-fosili-energii-verzi-dictatori/

[10] C.Sima – Opțiuni de exploatare a minereurilor din România ca țară membră a Uniunii Europene,2018

TRANSPORT CAPACITY OF MINING HOISTING EQUIPMENT - CALCULATION BASED ON SIMULATION

Assoc. prof. Janka Saderova, M.Sc., PhD.[1]
Prof. Andrea Rosova, M.Sc., PhD.[1]
Patricia Muchova, M.Sc.[1]
Marek Ondov, M.Sc.[1]

[1]Technical university of Košice, Faculty of mining, ecology, process control and geotechnologies, **Slovakia**

ABSTRACT

Transport by mine hoisting equipment is used to remove excavated materials, deliver materials, machinery, and equipment required for the mining process and related activities, as well as transport persons. These technological devices use transport containers to pull the load in the form of a skip, cage, or skip-cage from underground to the surface. Mining machines are intended for vertical and inclined pits. Scientific research discussed in the present article focuses on the transport capacity of the mine hoisting equipment in mining minerals. The article applies a mathematical calculation of transport capacity on the base simulation. A simulation model was created in the ExtendSim10 simulation system. ExtendSim10 combines discrete and continuous simulation possibilities and is used by researchers in various fields. The output from the simulation model (number of transport cycles) serves as the basis for the capacity determination. The simulation model can be used to verify the results obtained by calculation based on available mathematical relationships or measurements obtained during operation.

Keywords: capacity, hoisting equipment, simulation, experiment.

INTRODUCTION

The mining industry is still the only supplier of mineral resources, including metals, coal, and other useful mineral substances. Internal transport of mine companies plays a vital role in the industry. In underground operations, various transport systems are used for horizontal transport (mining rail transport, rake and belt conveyors, suspended transport, trackless mining transport, etc.). Vertical transport removes excavated materials, delivers materials, machinery, and equipment required for mining and related activities, and transports persons. This mode of transport is most frequently carried out in underground mines through hoisting equipment. Modern hoisting equipment must work reliably and safely for several decades during the daily operation of 16 to 22 hours. Hoisting equipment can be categorized from several systemic perspectives [1].

Hoisting equipment is divided according to the maximum rated speed into large hoisting equipment with a rated speed above 3 $m.s^{-1}$ and small hoisting equipment with a rated speed up to 3 $m.s^{-1}$.

The three principal types of hoists used in mining applications are friction hoists, drum hoists, and Blair multi-rope hoists. In drum hoists, the hoist rope is stored on the drum.

https://doi.org/10.5593/sgem2024/1.1/s03.52

They can be single drum hoists or double drum hoists. Drum hoists employ a drum, so the wire rope winds around it as the load/conveyance is hoisted to the surface.

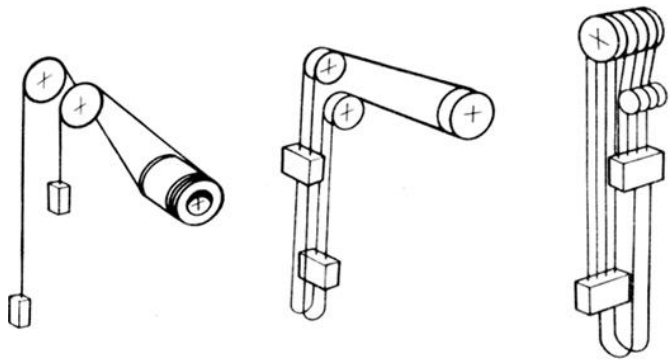
According to the method of transport, we differentiate:
A) Single-acting mine hoisting equipment is characterised by only one transport container being suspended from the rope. This hoisting equipment makes it possible to mine from any horizon without pushing the transport containers. Compared to double-acting mine hoists, they have half the performance capacity.
B) Double-acting mine hoisting equipment is used much more often than single-acting mine hoisting equipment. During transport, two transport containers are used, which can be hung on two hoisting ropes of a double drum hoisting machine to both ends of one rope or several hoisting ropes when using a hoisting machine with a friction disc. With this method, drum hoisting machines ensure transport from any horizon, allowing the hoisting rope to be lengthened or shortened. In the case of mining using a friction disc, dual-action transport can only be done from one horizon.

Sometimes, combined equipment is used, with different transport containers suspended on both ropes in drum equipment and on both ends of the rope in friction disc transport.

According to the number of hoisting ropes, the hoisting types of equipment are:
- one rope - the transport container is suspended on one rope,
- multiple ropes - the transport container is suspended on two or more ropes.

According to the location of the hoisting machine, we divide:

- ground hoisting machines that have an engine room near the shed on its level,
- tower hoisting machines are located directly at the head of the hoisting tower.



a b c

Figure 1 Types of hoisting equipment: a – drum hoist, b –two-rope friction hoist, c – tower hoisting machine with guide pulley [1]

Hoisting equipment has several structural components, such as drums, sheaves, steel wire ropes, skips, and others [2].

Simulation is a key technology for developing planning and exploratory models to optimize decision making as well as the design and operations of complex and smart production systems. In manufacturing and logistics systems, modeling and simulation denote a set of methods and technological tools that allows the experimentation and validation of products, processes, systems design and to predict system performance [3].

Simulation is widely used in various industries, including the mining industry. The articles summarise and present an overview of the digital technologies, including simulation, currently relevant to the mining company, as presented and discussed by mining magazines and media, and overview reports from leading consulting agencies across the mineral value chain [4,5].

The research discussed in this paper is focused on the transport capacity of double-acting equipment. The capacity of the hoisting equipment is the amount of mineral resources (material) transported for a specific unit of time. The theoretical hourly capacity Q_h, the real hourly capacity Q_R, and the daily capacity Q_d of the hoisting equipment are calculated based on the available mathematical relationships [1]. However, in this post, the capacity will be calculated based on the results of the simulation model of the hoisting equipment's transport cycle.

ExtendSim is used to create the simulation model. This simulation system combines discrete and continuous simulation capabilities and is a popular tool for PC_MS Windows and Macintosh computers. This tool was used by several authors in simulations in various areas: e.g., to simulate the container terminal handling system [6], for the simulation of homogeneous production processes [7], to create a simulation model of the intersection [8], for solving the bottleneck problem in a warehouse [9], to simulate the real ropeway system for transporting tourists in the High Tatra Mountains [10], for the simulation of process of bulk material loading [11].

METHODOLOGY

To develop and implement a simulation model of the transport cycle, components of the transport system must be analysed, Figure 2. In this case, the transport cycle of double-action hoisting equipment must be considered.

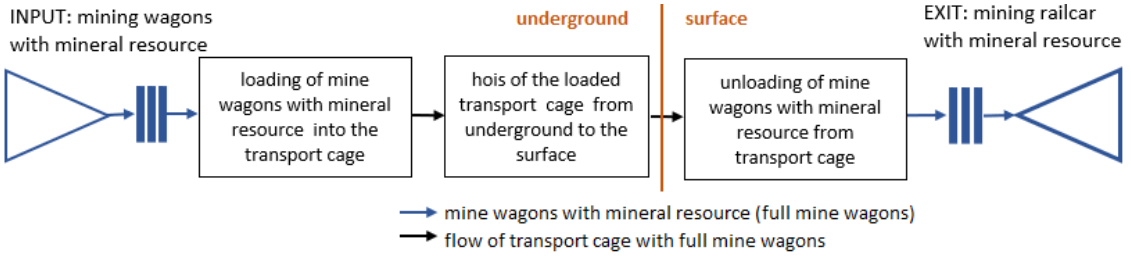


Figure 2 Formalised diagram of the transport cycle

The left part of the formalised diagram represents the loading of the transport cage underground (e.g., loading of mine wagons with raw materials into the cage), followed by its hoist movement. The last part is unloading the transport cage (e.g., unloading the mine wagons out of the transport cage).

Since the flow of a set of mine wagons is provided by a double-acting mine hoisting equipment (two transport cages), it is essential to point out that in that moment of loading the set into the cage (1) underground, the set is being unloaded from the cage (2) on the surface.

https://doi.org/10.5593/sgem2024/1.1/s03.52

The ExtendSim10 was chosen to simulate the transport cycle. Blocks from 2 libraries will be used to create simulation models. "Item" contains blocks for creating discrete simulation models, Figure 3. "Chart" - blocks that allow you to display the progress of the simulation. Figure 4 shows the Print Screen of the created simulation model.

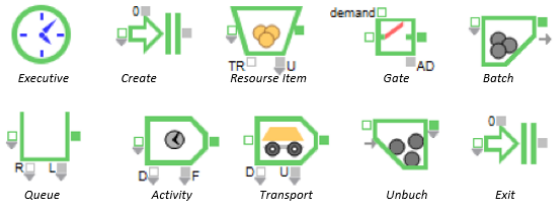


Figure 3 Blocks used for creating models

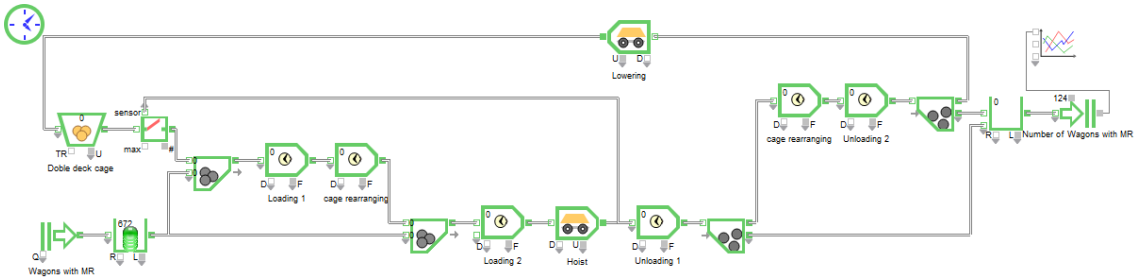


Figure. 4 Print Screen of the simulation model in ExtendSim10

The first step was to insert an *Executive* block for time management. The *Create* block will generate one unit. In this case, it generates mine wagons loaded into the transport cage. The mine wagons are generated into the *Queue* block—a buffer where the material is placed until it goes for processing. The following input to the model is the *Resource Item* block, representing a transport double-deck cage. The first *Batch* block connects two mine wagons with the first deck of the transport cage, Figure 5.

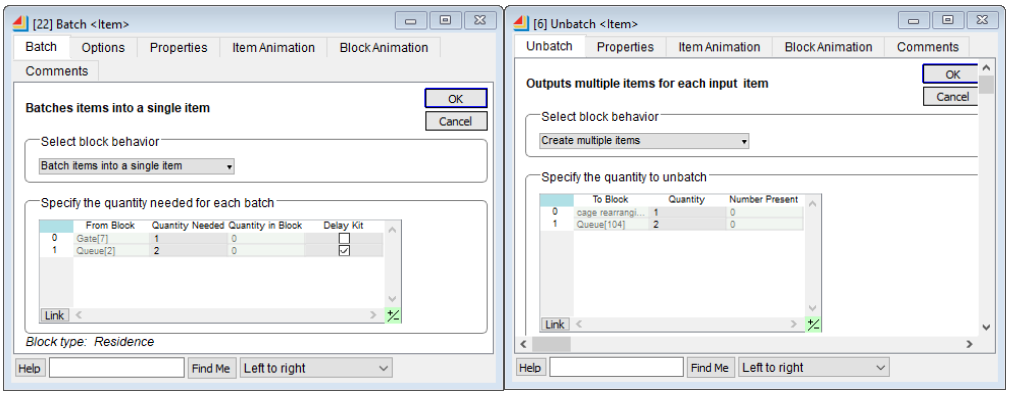


Figure 5 Batch and Unbatch blocks settings

Then, two activity blocks follow in the model. The first *Activity* block (Loading 1) represents the activity of loading wagons into the first deck of the transport cage. The

second *Activity* block is the cage rearranging activity. The second *Batch* block connects the two mine wagons with the second deck of the transport cage. Operations are followed again by the *Activity* block (Loading 2), the activity of loading two wagons into the second deck of the transport cage. By ending the activity in this block, the loading of wagons into the two-deck cage (1 cage = 4 wagons) is completed. The movement (hoist) of the transport cage from the underground to the surface is represented by the *Transport* (Hoist) block. Another part of the model represents unloading the wagons from the transport cage. The *Activity* (Unloading 1) block is included again, representing the unloading of wagons from the first deck of the cage.

Subsequently, the *Unbatch* block is included, separating the two wagons from the second deck of the cage. Wagons enter the *Queue* block and go to the *Exit* block - output, number of wagons. These operations are followed by the *Activity* block, which represents the rearranging of the cage, and the *Activity* block (Unloading 2), which represents the unloading of wagons from the 1st floor of the cage. The separate wagons from the cage deck enter the *Queue* block and go to the *Exit* block – output. The transport cage goes back (from the surface to the underground), again represented by *Transport (Lowering)* blocks.

Gate block - the task of the block is to ensure that the request enters the process at the moment the previous request completes the *Transport* block, i.e. that, in this case, ensures that both loading of the cage beneath the surface (1) and unloading of the cage (2) on the surface, occur within the one-time interval. This block in the model will ensure that the model works as a double-acting device.

Simulation inputs include work cycle time intervals of the activities. Model output is the parameter - number of wagons (block *Exit*). The daily capacity of the hoisting equipment can be calculated as the multiplication of the exported wagons and the amount of material in one wagon. Other outputs can be read from the Activities block. One of the outputs is the number of hoisted cages for the simulated time C_n. This parameter can be used for the calculation of daily capacity Q_d by the formula:

$$Q_d = C_n \cdot W_n \cdot M_w \cdot S_n \quad [t.day^{-1}] \quad (1)$$

where C_n - number of hoisted cages for the simulated time,
W_n is the number of wagons in the cage,
M_w is the mass of the useful load in one wagon in tones,
S_n is number of shifts.

The results section will present other outputs related to using individual blocks.

RESULTS AND DISCUSSION

Several experiments were performed on the simulation model, and the simulation results were used to calculate the daily capacity of the hoisting equipment. Hoisting equipment hoists mine wagons with mineral resources to the surface. One mine wagon weighs 500 kg, and the filling in the wagon weighs 2,300 kg.

The input values to the model, the times of individual activities, were obtained by observation directly in operation, as follows: loading (unloading) time of two wagons to one deck cage – 25 s, hoisting (lowering) time – 54 s, and time to rearrange the cage – 10 s.

https://doi.org/10.5593/sgem2024/1.1/s03.52

Experiment 1 was performed for a simulated time of 3,600 seconds. The results are shown in Figure 6 and Table 1. During the simulated time, 124 wagons were hoisted and unloaded from cages, corresponding to 31 cages. However, 32 cages were loaded.

Experiment 2 was performed for a simulated time of 6.3 hours (time reserved for mineral resources hoisting during one shift). The results of the experiment are shown in Figure 7. The results of the experiment are shown in Figure 7 and Table 1. During the simulated time, 792 wagons were hoisted and unloaded from cages, corresponding to 198 cages. However, 199 cages were loaded.

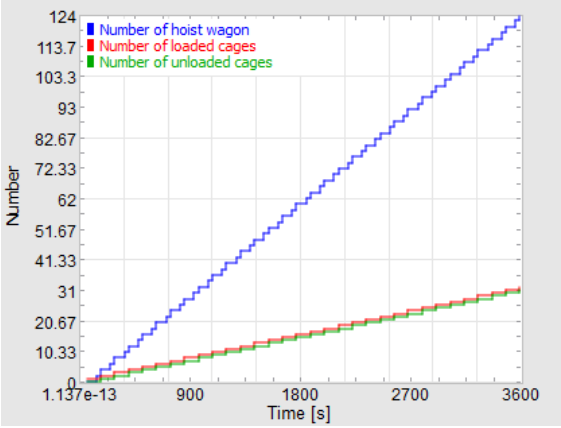


Figure 6 Experiment 1 results

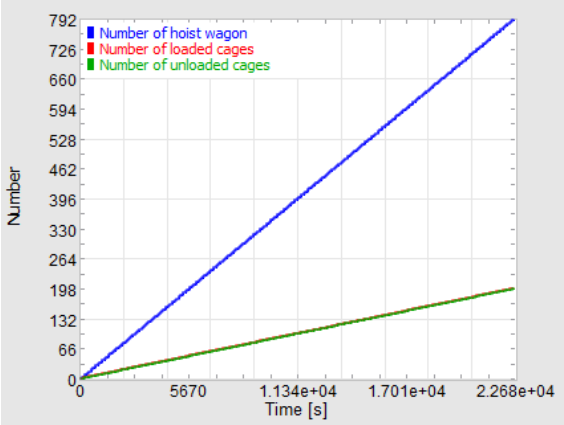


Figure 7 Experiment 2 results

Tab. 1 The results of the experiments

Experiment	**1**	**2**
Simulated time [hours]	1	6.3
Number of loaded cage	32	199
Number of the hoisted cage	31	198
Number of unloaded cages	31	198
Number of the hoisted mine wagons	124	792
Loading time of the transport cages (Loading1, cage rearranging, Loading 2) [min] /[%]	199 min / 52%	
Hoisting Time	179 min / 48%	

The transport cages' loading time accounted for more than 52% (199 minutes) of the total time for both simulation experiments. The cage unloading time was less than a per cent lower because when the first cage (underground) was loaded at the beginning of the simulation, the cage (on the surface) was empty. The hoisting of cages accounted for less than 48% (179 minutes) of the total time.

Daily capacity calculated based on relation (1) for simulated conditions, S_n = 1 is 1,821.35 tons.

CONCLUSION

The paper presents a simulation model of a double-acting hoisting equipment. The simulation model simulates the transport cycle of equipment that hoists mining wagons in a two-deck cage. The input to the model is the activity times of the transport cycle, the time of loading the wagons to the cage deck, the time of rearranging the cages, and the hoisting time. The main output of the model is the number of unloaded mine wagons. Another parameter can be read from the blocks of the simulation model. The daily capacity of this equipment was calculated based on the selected output parameter.

The mentioned model can also be modified for double-acting hoisting equipment with other operating parameters.

The presented simulation model can also be used for a single-deck cage. The input value is set to 0 for each block of Activities: Loading 2, Unloading 2, and both blocks of cage rearranging. If a skip is used against the cage, this also applies.

If a 3- or 4-deck cage is used, additional Activity blocks must be added - loading, cage rearranging, and unloading. The number of wagons per cage deck in the Batch and Unbatch blocks in the model can also be adjusted (see Figure 2).

We filled the above model with constant values, so further research will be devoted to creating an input generator so that the input data is not constant. The generator task will generate inputs so that the condition of the cage's underground loading and unloading on the surface must be realised simultaneously and for the same duration.

ACKNOWLEDGEMENTS

This work is supported by the Scientific Grant Agency of the Ministry of Education, Science, Research, and Sport of the Slovak Republic and the Slovak Academy Sciences as part of the research project VEGA 1/0430/22.

REFERENCES

[1] Marasová D., Husáková N., Boroška J., Strakoš V., Lukáč S., Intra-company transport in the mining industry, Košice, 2009. - 201 p.

[2] Popescu F.D., Radu S.M., Andraș A., Brînaș, I., Numerical Modeling of Mine Hoist Disc Brake Temperature for Safer Operation, Sustainability, vol.13/2874, 2021.

[3] Ferreira WD., Armellini F., De Santa-Eulalia LA., Simulation in industry 4.0: A state-of-the-art review, Computers & Industrial Engineering, vol. 149/November, 2020.

[4] Barnewold L., Lottermoser B., Identification of digital technologies and digitalisation trends in the mining industry, International Journal of Mining Science and Technology, vol. 30/issue 6, pp747–757, 2020.

[5] Quelopana A., Órdenes, J., Wilson R., Navarra A. Technology Upgrade Assessment for Open-Pit Mines through Mine Plan Optimization and Discrete Event Simulation, Minerals, vol.13/ 642, 2023.

[6] Du, D., Liu, T., & Guo, C. (2023). Analysis of Container Terminal Handling System Based on Petri Net and ExtendSim. *Promet - Traffic&Transportation*, vol*35*/1, pp 87–105, 2023.

https://doi.org/10.5593/sgem2024/1.1/s03.52

[7] Straka M., Sofranko M., Glova Vegsoova O., Kovalcik J., 2022. Simulation of homogeneous production processes, International Journal of Simulation Modelling, vol.21/issue 2, pp 214-225, 2022.

[8] Bindzar P., Macuga D., Brodny J., Tutak, M., Malindzakova M., Use of Universal Simulation Software Tools for Optimization of Signal Plans at Urban Intersections. Sustainabilit*y*, vol.*14*/2079, 2022.

[9] Jana Fabianova; Jaroslava Janekova; Jozef Horbulak: Solving the bottleneck problem in a warehouse using simulations. Acta logistica - International Scientific Journal about Logistics. vol. 8/ issue 2, pp 107-116, 2021.

[10] Fedorko G., Hana Neradilová H., Jackanin J., Discrete model simulation of a passenger cable car operation, Advances in Science and Technology - Research Journal, vol. 12/issue 2, pp 170–179, 2018.

[11] Šaderová, J, Ristovic, I. Application of the model approach for the process of bulk material loading. In: SGEM 2018 conference proceedings. 1.3. science and technologies in geology: exploration and mining: international multidisciplinary scientific geoconference. - Sofia (Bulharsko): STEF92 Technology s. 127-134 [print].

WIND BARRIERS AS A POSSIBLE SOLUTION TO PM_{10} EMISSIONS IN INDUSTRIAL PLANTS

PhD, Eng. S. Carbone[1]

Dr. V. De Brito[1]

[1] IC Engineering Consulting, HSE Division, **Italy**.

ABSTRACT

This paper refers on the outcomes of an experimental study developed in an industrial plant in the centre of Italy in which dust emission represents an important annoyance affecting the whole activity and so requiring to be managed in order to guarantee legal compliance but, above all, a safe workplace. This case study consists in the assessment of the efficacy of different reduction measures designed to avoid and, where not possible, to reduce dust emissions from stockpiles. According to a monitoring campaign based on field sampled data, these areas were identified as the most pollutant sources in the plant itself and many solutions were taken into consideration to reduce the emission due to wind erosion. Under these conditions wind fences represent a significant solution to be tested in addition to usual measures which are usually installed. In particular some simulations are performed in order to define the variation of wind velocity all around the stockpile and so to select and design the best solution and configuration to reduce the emission of fugitive dust from stockpiles when caused by wind erosion.

Keywords: fugitive dust sources, limestone quarry, $PM_{10,}$ solid fence

INTRODUCTION

Dust emissions are a significant source of industrial pollution caused by the wind action on exposed erodible materials. Industrial wind erosion represents an essential and sizeable fraction of the overall emission from industrial sites. Open storage piles of granular materials, such as raw materials, semi-finished, and finished products, present a typical example of industrial wind erosion sources. These stockpiles are usually uncovered due to frequent material transfers to and from stockyards. A lot of studies have investigated dust emissions from stockpiles of granular materials [1], [2], [3], [4], [5]. Dust emissions from these sources have been known to cause environmental problems, such as the degradation of air quality, as well as risks to human health and material losses for industries.

Numerous technical strategies and management measures have been implemented to mitigate fugitive dust emissions and particulate matter (PM) dispersion into the atmosphere. The storage of materials in enclosures and the erection of wind barriers, such as 3-sided enclosures around storage piles, are widely employed as control measures for reducing windblown fugitive dust from uncovered material stockpiles (WRAP, 2006). These wind barriers rapidly and significantly impact the shelter effect and reduce wind

https://doi.org/10.5593/sgem2024/1.1/s03.53

speed and momentum by obstructing the wind's path, preventing wind erosion and dust emission [6].

The efficacy of wind fences has been explored in detail by considering various parameters. For instance, recent studies [7] have introduced an innovative wind fence design that includes a curved deflector to further enhance the shelter effect of porous wind fences.

Although porous fences have been demonstrated to be highly effective in reducing dust emissions compared to solid ones, the latter continue to be widely used in industrial areas and ports as enclosures or windbreaks for open storage piles. Additionally, solid fences are frequently employed in arid regions to prevent sand deposition and drifting [8].

Compared to porous fences, solid fences are more efficient in reducing wind speed. However, the sheltered area behind a solid fence decreases rapidly [9], and the accumulation of sand and sedimentation at the windward side [10] can be considered problematic for solid fences.

It has been observed that the literature on the effectiveness of solid fences in preventing dust emissions from open storage may be improved when using porous fences. Furthermore the adoption of porous fences implies incurring significant expenses or necessitating the replacement of existing windbreak structures. Additionally, the economic aspect of the problem has been emphasized only occasionally.
On that account and considering the need to enhance the zero porosity fences efficiency, the present study aims to test the efficacy of solid fences to control and reduce dust emissions trying to define a best design approach to set the optimum geometry of fence itself.

Considering the impact of the issue on a global scale and the increasingly attention to the environmental impact assessment of industrial activities towards surrounding civil areas or workers' exposure to physical agents [11], the need for reliable reduction tools capable of reducing the contribution of quarrying activities to PM air pollution becomes apparent. After a sampling campaign aimed to focus the most pollutant sources all around the quarrying plant, stockpiles like those shown in the following figures were found to be the most annoying sources in the plant.

Table 1: dust sources and their classification

Source Type (space time characteristics)	**Quarrying activity**
Localized discontinuous	Blasting, Loading, unloading, stockpiling



Figure 1: stockpiles in the quarry area



Figure 2: Stockpiles for different materials

MATERIALS AND METHODS

The present study involves conducting three-dimensional (3D) simulations utilizing the commercial computational fluid dynamics (CFD) software ANSYS FLUENT. The objective of these simulations is to evaluate the effectiveness of solid fences when varying the geometry of the fence itelf installed behind an open storage pile to mitigate dust emissions.

https://doi.org/10.5593/sgem2024/1.1/s03.53

In this case study the flow field properties are taken into consideration with computing the impact of solid particles on turbulence. In addition all simulations were conducted under identical wind profiles with a reference velocity of 5 m s^{-1}.

This case study is focused on assessing the fence-deflector efficiency by taking into consideration the shear stress distribution over the surfaces of piles.

The following step was performed by estimating the emission factor (EF) using the USEPA model. Through this approach, the study aimed to provide insights into the potential for these deflectors to reduce the impact of emissions and mitigate environmental damage.

According to AP-42 Compilation of Air Pollutant Emission Factors, published by the United States Environmental Protection Agency (U.S. EPA, 2006), the emission factor due to wind erosion from a stockpile can be assessed as follows:

$$\mathrm{EF}=m\sum_{i=1}^{N}\sum_{j=1}^{M}P_{ij}\,S_{ii} \tag{1}$$

where m is a particle size multiplier (equal to 0.5 for PM_{10}), N is the total number of disturbances per year, M is the number of the subareas having a constant value of u_s/u_r, P_{ij} is the erosion potential (g m^{-2}), and S_{ij}(m^2) is the fraction of the subarea corresponding to a constant value of u_s/u_r.

The erosion potential is defined as:

$$P=58\,(u^*-u_t^*)^2+(u^*-u_t^*) \text{ for } u^*\geq u_t^* \tag{2}$$

$$P=0 \text{ for } u^*\leq u_t^* \tag{3}$$

where u_t^* is threshold velocity and u^* is given by the following equation,

$$u^*=0.1\,u_{10}+(u_s/u_r) \tag{4}$$

Where u_{10+} is the fastest mile of wind speed measured at 10 m height, u_s is the average wind speed at 25 cm from the pile surface and u_r is the average wind speed (reference value) at 10 m above terrain.
For this case study, it was assumed that the study had only one yearly disturbance (N=1). To ensure the most conservative estimation, the simulation adopted a reference value of u_t^* = 0 m/s. Consequently, eqn. 1 and 2 are defined as follows while retaining their original essence:

$$EF_0=0.5\,\Sigma P_{0j}\,S_j \tag{5}$$

$$P_0=58u*^2+25u* \tag{6}$$

In accordance with equation 5, the surface of the entire pile was partitioned into distinct subareas of uniform u_s/u_r values. Each of these subareas was treated as a single source, with u_s/u_r ratios being computed through CFD analysis and subsequently utilized in determining u* (as per Equation 4). It is worth noting that the upper bounds of the u_s/u_r intervals were employed in the computation.

FIELD STUDY

This section of the analysis aims to evaluate the impact of a solid fence with a varying height from 4.5 m to 5.5 m, positioned at 3 m from the pile, corresponding to 0.6 times the height of the stockpile. The assessment primarily focuses on the effects of this configuration on the velocity magnitude, flow pattern, and turbulence kinetic energy.

Additionally, the study intends to examine how these factors relate to dust emissions. The evaluation of these parameters will be crucial in understanding the impact of the solid fence on the environmental conditions and subsequent dust emissions.

The velocity contours and vector field around are shown in fig 3 and 4.

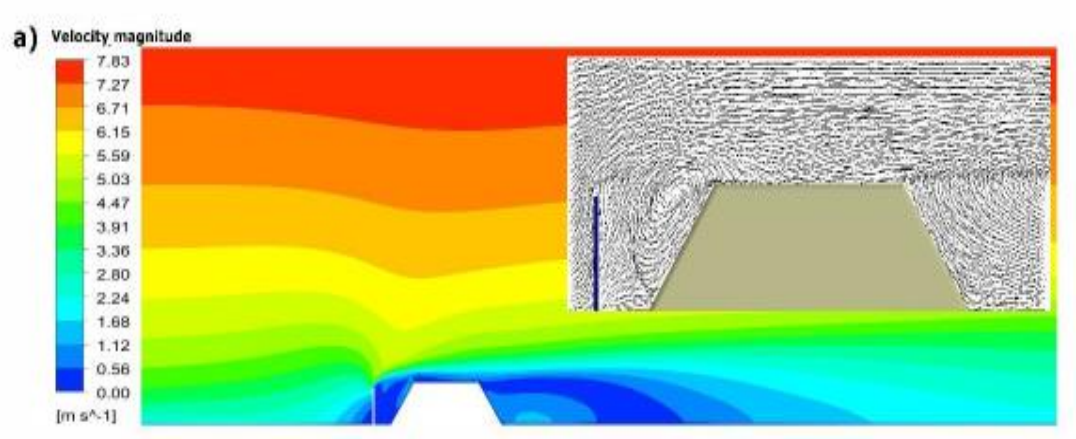


Fig. 3: Velocity contour map and vector field

In figure 3 may be noticed the presence of two recirculation zones, one between the fence and the pile and the other at the pile leeward due to the flow that separates from the crest.

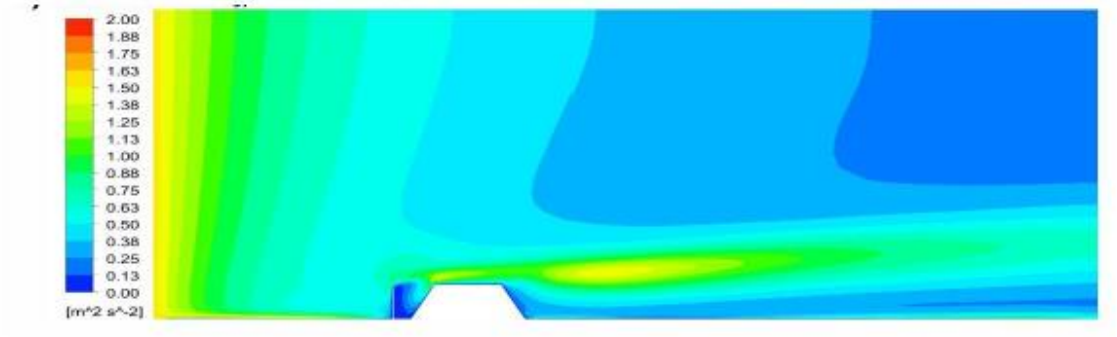


Fig. 4: Turbulent Kinetic Energy

https://doi.org/10.5593/sgem2024/1.1/s03.53

The region between the windbreak and the windward pile is also characterized by a critical TKE, as shown in Figure 4.

As a consequence the air flowing down the windward slope causes material particles to either fall to the ground or be carried upwards. These observations align with some findings in literature [12].

RESULTS

In the following table the results of four different simulations are summarized varying the high of the fence and taking into consideration mean shear stress. This last, as known, is defined as follows:

$$\tau=\rho\,(u^{*})^{2} \tag{7}$$

Where ρ is air density and $u*$ is defined according with eqn (4).

The dust emission data was obtained through the USEPA model. Contour maps of velocity were obtained through 3D numerical simulations for the solid fence of varying heights.

Data are ordered according with emission rate expressed as [mg $m^{-2}s^{-1}$] and carried out by means of equations (1), (2), (3), (4), (5) and (6).

Table 2: EF and mean shear stress comparison for each fence

Z [m]	Mean Shear stress [Pa]	EF [g/perturbation]
4.0	37.16	1215.86
4.5	35.81	1196.55
5.0	39.14	1365.21
5.5	32.86	1099.87

Comparing results according with varying configurations it is possible to assess the best set up design in terms of ratio between height of solid fence and pile itself also taking into consideration the horizontal distance between the fence and the pile.

In particular experimental data reveal substantial Turbulent Kinetic Energy (TKE) above the pile was generated in the cases of the single fence higher than the pile, which subsequently evolved in the leeward region behind the stockpile. The TKE increases as the height of the single solid fence increases. In particular when the fence height is raised from 4.0 m to 5.0 m, the TKE increases from 1.38 m^2s^{-2} to 2 m^2s^{-2} on the top of the surface pile. This phenomenon occurs because the shear flow separated from the fence hits the top of the windward pile surface, causing an increase in TKE in this region. However increasing the high of the fence, this effect is less affecting and the TKE tends to decrease. This phenomenon occurs when the ratio between the high of the pile and the fence one is set to 0.65

CONCLUSIONS

This study presents a design approach to solid fences for stockpiles in quarrying areas. The performance of the solid fence in reducing emissions from open storage piles and its impact on airflow structure were numerically investigated using 3D computational fluid dynamics (CFD) simulations. The research findings indicate that a solid fence significantly reduces flow velocity and TKE on the windward side of the pile. This, in turn, minimizes the recirculation flow on the leeward side or wake region. Furthermore, the results showed that the solid fence configuration with a height ratio (pile vs fence) of 0.6-0.7 reduced the shear stress on the surface of the open storage pile and dust emission better than the other tested configurations. This outcome was obtained with the pile positioned at a distance from the fence equal to its height. The comparisons between different configurations how a significant reduction in the shear stress and emission factor by 16% and 19%, respectively, compared to the best case. This result suggests that optimizing the design for changing operational or ambient conditions is not only possible but also useful.

REFERENCES

[1] Vella, J.A., Camilleri, R.,. Fine dust emissions from softstone quarrying in Malta. Xjenza. 10. pp. 47-54. 2005.

[2] Tartakovsky D. Stern E, Broday D.M, Dispersion of TSP and PM10 emissions from quarries in complex terrain, 2016, Science of the Total Environment, 542, pp. 946-954, 2016; doi: 10.1016/j.scitotenv.2015.10.133.

[3] Alfaro Degan, G., Di Bona, G., Lippiello D., Pinzari M. "PM10 dispersion model in quarrying activities, a comparison of an ISC3 approach to a mono/multivariate geostatistical estimation". WIT Transactions on Ecology and the Environment, Vol. 86, 2006, ISSN 1743-3541, pp. 111-120, doi: 10.2495/AIR06012.

[4] Alfaro Degan, G., Lippiello, D., Pinzari, M. Effectiveness of airborne dust control strategies in opencast quarrying activities: A case study near Rome. GEAM Geoingegneria Ambientale e Mineraria 139 (2), pp. 5 – 12, 2013, ISSN 1121-9041.

[5] Roney, J.A.; White, B.R. Estimating fugitive dust emission rates using an environmental boundary layer wind tunnel. Atmos. Environ. **2006**, 40, 7668–7685.

[6] Torshizi, M. R., Miri, A., Shahriari, A., Dong, Z., & Davidson-Arnott, R. The effectiveness of a multi-row Tamarix windbreak in reducing aeolian erosion and sediment flux, Niatak area, Iran. Journal of Environmental Management, 265, 110486. https://doi.org/10.1016/j.jenvman.2020.110486

[7] Qiu, Y., Yuan, Y., Yu, R., & Liu, J. (2022). Aerodynamic shape optimization of porous fences with curved deflectors using surrogate modelling. Optimization and Engineering. https://doi.org/10.1007/s11081-022-09777-6.

[8] Alghamdi, A. A., & Al-Kahtani, N. S. (2005). Sand Control Measures and Sand Drift Fences. Journal of Performance of Constructed Facilities, 19(4), 295–299. https://doi.org/10.1061/(ASCE)0887-3828(2005)19:4(295).

[9] Dong, Z., Qian, G., Luo, W., & Wang, H. (2006). Threshold velocity for wind erosion: The effects of porous fences. Environmental Geology, 51(3), 471–475. https://doi.org/10.1007/s00254-006-0343-9.

https://doi.org/10.5593/sgem2024/1.1/s03.53

[10] Bruno, L., Fransos, D., & Lo Giudice, A. (2018). Solid barriers for windblown sand mitigation: Aerodynamic behavior and conceptual design guidelines. Journal of Wind Engineering and Industrial Aerodynamics, 173, 79–90. https://doi.org/10.1016/j.jweia.2017.12.005

[11] Alfaro Degan G, Lippiello D, Pinzari M (2015). A comparison between methods for assessment of whole-body vibration exposure: A case study in a limestone quarry. International Journal of Safety and Security Engineering, 8 (1), p. 90-97, 2018. ISSN: 2041-904X, doi: 10.2495/SAFE-V8-N1-90-97.

[12] San, B., Zhao, Y., & Qiu, Y. (2019). Numerical simulation and optimization study of surface pressure and flow field around a triangular prism behind a porous fence. Environmental Fluid Mechanics, 19(4), 969–987. https://doi.org/10.1007/s10652-019-09695-9.

SECTION

MINERAL PROCESSING

ALUMINIUM SMELTER ANODE WASTE BOND INDEX DETERMINATION

Assoc. Prof. Dr. Surracco Marco

Prof. Tilocca Maria Caterina

Department of Civil-Environmental Engineering and Architecture, University of Cagliari, **Italy**

ABSTRACT

As part of the experimental studies carried out in the Department of Civil, Environmental Engineering and Architecture of the University of Cagliari, to identify the best techniques for recovering of combustible materials, contained in the waste resulting from the dismantling of the anodes of spent electrolytic cells used in the production of primary aluminium, to be concentrated by flotation, work was first carried out to reduce the size of the waste, in order to give it a particle size that would allow it to be fed to a flotation process and to improve the liberation degree of the carbon particles to be separated. Since the Bond's work index is an important factor in the design of the comminution circuits, in order to evaluate the grindability characteristics of the aluminium smelter anode scrap and, consequently optimize the grinding step, we proceeded to determine its Bond Index using the standard method. Bond's work index represents the energy required to reduce one short ton (907 kg) of a solid from an infinite size to 100 microns. Bond's energy law uses this index to predict the energy required to reduce the solid's size, which is the sum of the energy used to fracture the material and energy losses, such as mechanical losses occurring in comminution equipment or energy lost in the form of heat generated by attrition. A value of 11.07 kWh/sht was obtained for the Wi. This value is characteristic of rocks of medium hardness in terms of resistance to comminution. The Bond index obtained is valid for an industrial wet grinding process using a ball mill operating in a closed circuit with a mechanical classifier and a circulating charge of 250%.

Keywords: Bond work index, comminution, grindability, ball mill, carbon anode scrap.

INTRODUCTION

Finding new material or energy resources is becoming increasingly difficult. In addition, there are more and more obstacles to identifying potential areas where waste can be confined, and the cost of depositing them is constantly rising, partly because of increasingly stringent environmental regulations. All this requires, as a matter of priority, the pursuit of a reduction in the production of materials and consumer goods made from these materials, which are inevitably destined to become waste, and, as a cascade, the implementation of effective strategies for the reuse, recovery and recycling of the materials that compose the waste itself. [1]. Following this scale of priorities not only prevents the accumulation of waste, with its subsequent problems of damage to the environment and human and animal health, but also makes it possible to direct our development toward achieving the goal of a more circular economy in the use of materials and products. Therefore, even nations that do not have sufficient availability of specific natural resources for their industrial sector could have alternative access to

https://doi.org/10.5593/sgem2024/1.1/s04.54

these substances by replacing them, albeit not in their totality, with secondary materials, contained, in high concentrations, for example, in scrap, waste or end-of-life devices. Among the wastes generated by the electrolysis process for aluminum production are also the carbonaceous substances that constitute the anode electrodes. In fact, when spent anodes have to be replaced, unused portions of them inevitably remain. In addition, other wastes of the same kind may be generated due to damage during the transport stages of anodes [2]. Previous experimental trials conducted in the Department of Civil, Environmental Engineering and Architecture (DICAAR) of the University of Cagliari on anode waste have demonstrated the possibility of obtaining secondary materials suitable for use as fuel in blast furnaces and cement plants, in compliance with sector legislation, after undergoing appropriate treatment. The waste treatment operations comprised of two main stages: comminution and flotation. Comminution involved classical crushing and grinding stages to prepare different feeds for flotation, with d_{max} ranging from -1 mm to -0.3 mm. The flotation tests were conducted to obtain combustible material [3] [4]. For the flotation it is necessary to reach a grain size which ensures a good balance between cost-grinding levels and recoveries. Comminution operations, including grinding, are crucial in the treatment of solids. They are necessary to obtain raw materials that can be transformed industrially from underground resources. Mineral substances from mining processes must first undergo appropriate size reduction processes. The energy required for a comminution process is a significant factor in its overall economic evaluation. It can be particularly high in some cases. In addition, comminution processes are not limited to mineralurgical treatments but also extend to other industrial sectors such as cement production, road pavement aggregates, coal grinding for combustion in steam generators, cosmetics, pharmaceuticals, fillers for the plastics, rubber and paint industries, ceramic and paper industries. This also includes treatments carried out on waste to obtain secondary raw materials. In all cases, the energy required varies not only with the type of comminution but also, significantly, with the specific nature of the solid. In treatment plants, the size reduction section typically consumes the most treatment energy for any solid. Therefore, it is crucial to operate under optimized conditions to avoid unnecessary energy consumption in breaking down the material and producing undesirable ultrafine particle sizes [5]. To predict, as exactly as possible, the energy required for a comminution operation, various energy laws have been formulated over time. These theories include those of Rittinger (1867), Kick (1885), Bond (1951) [6], and Charles (1957) [7]. They can be used for plant design in the size reduction section. The most widely used energy law in industrial grinding operations with ball mills and rod mills is still the one proposed by Bond. According to Bond theory, the greater or lesser aptitude of a solid for grinding, or, in other words, its resistance to comminution, can be characterized through an index, normally denoted Wi, also referred to as the work index or Bond work index. The Wi represents the work required to reduce 1 sht (907 kg) of a given mineral from a theoretically infinite initial size to a final size of 100 microns (in practical terms, such that 80 percent of the comminution product is found to pass through the screen having a square mesh opening of 100 microns). Knowledge of the value of the Bond index, makes it possible to predict the energy that will be required, at the engine output, to subject a given solid (of finite initial size equal to D) to comminution in order to reduce it to a size smaller than a reference size, relative to which Wi has been determined. This is important in order to proceed with the sizing of industrial comminution circuits. The determined value of comminution energy is valid in relation to the solid being

considered and the fixed reference dimension. The reference size, used to determine Wi, must always be less than 28 Tyler mesh (0.589mm). Before testing, the solid must be crushed to less than 6 Tyler mesh (3.327mm) using a closed circuit jaw crusher. The determination of the working index is then carried out using a standard mill (size, weight and particle size distribution of the ball charge) under fixed operating conditions (mill rotational speed) on a sample of material whose weight must remain constant throughout a series of grinding tests. Specifically, the mill used for Wi determination is a cylindrical mill having equal diameter and length of 30.48cm (12"). The rotational speed is to be set at 70 rpm. The particle size distribution of the grinding charge as prescribed by Bond is shown in Table 1.

Table 1 - Ball grinding charge distribution.

Balls size	Balls number	Balls weight	Ball charge surface
[mm]		[Kg]	[mm^2]
36.830	43	8.803	
29.718	67	7.206	
25.400	10	0.672	
19.050	71	2.011	
15.494	94	1.433	
Total	285	20.125	543,227.246

The quantity of sample on which the determination is to be made is that which corresponds to the weight of an apparent volume of material equal to 700 cm^3. The value of Wi thus determined is to be used, according to Bond's theory, to predict the energy required for industrial wet grinding carried out with a ball mill of 8 ft internal diameter operating in closed circuit. Bond introduced a range of efficiency factors to address the differences in feed and operating conditions [8]. Bond formulated a similar procedure to determine Wi for grinding by rod mills. However, the dimensions of the standardized mill are different, and the grinding charge consists of rods of a predetermined size. Therefore, for minerals with a known Wi value, Bond's law (1) can be applied to predict the specific energy requirement at the drive pinions for a given comminution operation that provides a product with the desired grain size.

$$W = 10W_i \times \left(\frac{1}{\sqrt{d_{80}}} - \frac{1}{\sqrt{D_{80}}}\right) \qquad (1)$$

where: W is the specific energy, in kWh/sht; Wi is the Bond index, in kWh/sht; d_{80} is the sieve size, in μm, for which 80% of the product passes; D_{80} is the sieve size, in μm, for which 80% of the feed passes. The anodic electrodes utilized in electrolytic cells for aluminium production are composed of two phases: an aggregate resulting from petroleum coke, which is coarse-grained, and a binder consisting of coal tar pitch.

https://doi.org/10.5593/sgem2024/1.1/s04.54

Petroleum coke is produced through the carbonization of heavy oil fractions and oil residue. Coal tar pitch is a by-product of coal pyrolysis [2]. Since anode electrodes are subject to consumption during operation (to produce 1 tonne of primary aluminium, the smelting process consumes about 425 kg of carbon anode), after 20-30 days working in the cell the partially consumed anodes are taken out to be exchanged with a new anodes [9]. The anodes provided to our laboratories originated from spent electrolytic cells utilised in the aluminium metallurgy industry and were initially crushed. They were delivered in two pre-sorted particle size fractions: a coarse fraction larger than 10 mm and a fine fraction smaller than 10 mm. It is assumed that the above distribution is the result of a pre-crushing operation following the dismantling of the cells. The two-dimensional fractions had distinct characteristics because the coarse fraction appeared macroscopically richer in metal. Therefore, the two fractions were considered independently in an attempt to obtain end-products that could be reused as fuel after treatment. The fine fraction was studied to determine the possibility of enriching the contained carbon. The Bond index was determined for this fraction.

LABORATORY PROCEDURE AND EXPERIMENTAL DETERMINATION OF BOND INDEX

The Bond work index of the carbon-based material, which constitutes the -10mm fraction of the anode electrodes, was experimentally determined using the standard procedure described below. A representative sample of the material was collected and its particle size analysis is shown in Table 2.

Table 2 - Particle size analysis of source material (-10 mm).

Particle size class	Yield	Cumulative retained weight	Cumulative passing weight
[mm]	[%]	[%]	[%]
+ 5.0	9.30	9.30	-
-5.0 + 3.0	11.18	20.48	90.70
-3.0 + 2.0	10.64	31.12	79.52
-2.0 + 1.0	13.80	44.92	68.88
-1.0 + 0.7	6.49	51.42	55.08
-0.7 + 0.5	6.39	57.81	48.58
-0.5 +0.3	7.23	65.04	42.19
-0.3 +0.1	17.12	82.16	34.96
-0.1	17.84	-	17.84
	100.00		

This sample was reduced in the laboratory below the size of 3.327mm using a jaw crusher operating in closed circuit, following the procedure established by Bond. Approximately 10 kg of the dried crushed product was sampled [10], and dry particle size analysis was performed. The results are shown in Table 3.

Table 3 - Particle size analysis of the crushed product.

Particle size class	Yield	Cumulative retained weight	Cumulative passing weight
[mm]	[%]	[%]	[%]
+3.15	2.44	2.44	-
-3.15 +2.80	3.94	6.38	97.56
-2.80 +2.36	6.90	13.28	93.62
-2.36 +2.00	5.94	19.22	86.72
-2.00 +1.00	18.29	37.51	80.78
-1.00 +0.500	15.34	52.85	62.49
-0.500	47.16	-	47.15
	100.00		

For linear interpolation D_{80}=1.980 mm

Using a solids sampler, we extracted a representative sample from the -3.327mm product and compacted it inside a graduated cylinder with a volume of 1000 cm^3, as required by the procedure, up to the 700 cm^3 level.

The compacted material was weighed, resulting in a value of 1068.5g.

During the whole test, this weight must be kept constant by re-integrating the same sample during the grinding cycles performed to determine the working index.

The first grinding stage was made as long as 100 mill revolutions.

The reference screen size was set at 0.500 mm, which should not exceed 28 Tyler mesh. The choice of screen size depends on the particle size of the product to be obtained in the industrial comminution plant. It is important to note that Bond recommended choosing a screen with an opening that provides a final product with a d_{80} similar to that obtained in full scale for conducting the close circuit grinding test.

At the end of the first grinding cycle, the product was accurately collected and dry screened with a square-mesh screen equal to the chosen reference size. The undersize product was weighed and new feed was added to the retained product until the weight of 1068.5 g was reconstituted.

As previously mentioned, in order to simulate closed circuit grinding, the feed to the Bond mill was integrated, for all successive test cycles, with a quantity of material equal to that found to be passing through the reference dimension (0.500 mm).

The various grinding cycles were conducted with the objetive of identifying the number of mill revolutions for which there was a passing weight, at the opening screen of 0.500mm, of 28.6%. Under these conditions, a circulating charge of 250% is generated in the comminution circuit.

The weight value should be maintained at this level for at least three consecutive grinding cycles, even if the cycles are not performed with the same number of revolutions (refer to Table 4).

https://doi.org/10.5593/sgem2024/1.1/s04.54

Table 4 - Determination of the grindability index Im.

Cycle	Revolutions number	-0.500mm product	-0.500mm in feed	Net -0.500mm produced	Net -0.500mm produced per round	Circulating charge
		[g]	[g]	[g]	[g]	[%]
1	100	786.7	503.9	282.8	2.8	35.8
2	50	564.8	375.2	189.6	3.8	89.2
3	20	362.5	268.3	94.2	4.7	194.8
4	15	259.2	174.3	84.9	5.7	312.2
5	19	222.6	123.8	98.8	5.2	380.0
6	38	281.6	106.6	175.0	4.6	279.4
7	37	296.6	134.0	162.6	4.4	260.2
8	37	297.1	140.7	156.4	4.2	259.6
9	39	304.0	140.8	163.2	4.2	251.5
10	38	303.6	144.7	158.9	4.2	251.9
11	39	301.7	144.1	157.6	4.0	254.2

Im=4.13 g/revolution

When the throughput value stabilises at approximately 28.6%, a constant net product weight below the reference size per revolution will be achieved for several cycles.

The ore grindability index (referred to as Im) is expressed as the average of the last three values of passing product product, in net grams per mill revolution.

The Bond index is given by the following mathematical expression (2)

$$W_i = \frac{44.5}{(d_r)^{0.23} \cdot (Im)^{0.82} \cdot \left(\frac{10}{\sqrt{d_{80}}} - \frac{10}{\sqrt{D_{80}}}\right)} \qquad (2)$$

where:

Wi is the Bond index, in kWh/sht; d_r is the reference size, in μm; d_{80} is the sieve size opening, in μm, through which 80% of the feed to the last grinding cycle passes; D_{80} is the sieve size opening, in μm, through which 80% of the feed to the first grinding cycle passes.

Table 5 - Granulometric analysis of the product of the last cycle.

Particle size class [mm]		Yield [%]	Cumulative retained weight [%]	Cumulative passing weight [%]
+0.300		28.98	28.98	-
-0.300 +0.200		15.04	44.01	71.02
-0.200 +0.100		18.73	62.74	55.99
-0.100		37.26	-	37.26
		100.00		

For linear interpolation d_{80} = 0.362 mm

At this point experimental values found to be entered in relation (2) to calculate the Bond index of the material resulting from the demolition of the anodes of electrolytic cells used in aluminium metallurgy. The values were: d_r = 500 µm; d_{80} = 362 µm (refer to Table 5); D_{80} = 1,980 µm (refer to Table 3); Im = 4.13 g/revolution (which represents the average of the values of the net grams of -0.500 mm produced in the last three cycles, refer to Table 4). This results in Wi = 11.07 kWh/sht = 12.21 kWh/t.

Work index result ranks our solid, under the aspect of comminution resistance, in the field of rocks of medium hardness category [11].

The anodes must have good mechanical properties to avoid breakage and separation of individual parts into the electrolytic bath, when they are put into operation [2] [9].

As Wi is known, the energy required to reduce the spent anode electrodes under investigation from a size D to a size d in an industrial process can be predicted by applying Bond's energy law (1).

CONCLUSIONS

In this paper we report the results of laboratory tests carried out to determine the Bond Index value, using the standard method, for a material consisting of spent anode electrodes resulting from the demolition of electrolytic cells used in the production of primary aluminium.

The anodes delivered to our laboratories were first crushed after the dismantling of the electrolysis cells and they were delivered in a pre-sorted fraction of less than 10 mm.

For a reference screen size of 0.500mm, a Wi value of 11.07 kWh/sht was obtained, which ranks our sample, under the aspect of comminution resistance, in the medium hardness rock category.

The value obtained is valid for predicting, using Bond's law, the energy required to perform a given wet industrial grinding operation in a ball mill with an internal diameter of 2.44 m, in close circuit with a mechanical classifier and a circulating charge of 250%, starting from a feed of -3.350 mm.

To relate the value obtained to other conditions, such as dry grinding, open circuit grinding or mill diameters other than 8 ft, it is necessary to use Bond's empirical efficiency factors.

https://doi.org/10.5593/sgem2024/1.1/s04.54

REFERENCES

[1] Worrel Ernst, Reuter Markus A., Handbook of Recycling, 2014, Elsevier, ISBN: 978-0-12-39-64-59-5.

[2] Radenovic A., Properties of carbon anode components for aluminium production, NAFTA 63(3-4), pp 111-114, 2012.

[3] Ciccu R., Ghiani M., Mei G., Tilocca C. and Figus M., Recovery of Energetic Materials from Scrap Electrodes of Aluminium Smelter, Proceedings Sardinia 2009, Twelfth International Waste Management and Landfill Symposium S. Margherita di Pula, Cagliari, Italy; 5 - 9 October 2009, © 2009 by CISA Publisher, Italy.

[4] Ciccu R., Mei G., Tilocca C. and Figus M., Reuse of Products from Waste Anodes of Aluminium Smelter, Proceedings Sardinia 2011, Thirteenth International Waste Management and Landfill Symposium S. Margherita di Pula, Cagliari, Italy; 3 – 7 October 2011, © 2011 by CISA Publisher, Italy.

[5] M. Noaparast, S. Rahmati, G. Jozanikohan, S. Aslaniand A. Ghorbani, "A Methodology to Estimate Ores Work Index Values, Using Miduk Copper Mine Sample", Int. J. Min & Geo-Eng (IJMGE), Vol. 46, No. 2, Dec. 2012, pp. 133-140.

[6] Bond F.C., 1961, "Crushing and grinding calculations", British Chemical Engineering, Vol. 6, pp. 378-385 and 543-548.

[7] R. J. Charles, 1957, "Energy-Size Reduction Relationships in Comminution", Transactions on AIME Mining Engineering, Vol. 208, pp. 80-88.

[8] SME Mineral Processing & Extractive Metallurgy Handbook, Vol.1.

[9] D.H. Andersen, Z.L. Zhang, Fracture and physical properties of carbon anodes for the aluminum reduction cell, Engineering Fracture Mechanics, Volume 78, Issue 17, December 2011, Pages 2998-3016, ISSN 0013-7944.

[10] Determining the Bond Efficiency of Industrial Grinding Circuits. GMG01-MP-2021. Global Mining Guidelines Group (2021). https://gmggroup.org/wp-content/uploads/2021/12/GUIDELINE__Determining-the-Bond-Efficiency-of-Industrial-Grinding-Circuits_2021.pdf. Accessed May 2022.

[11] Shahani, N. M., Wan, Z., Qureshi, A. R., Ali, M., Ali, N., "Determination of Bond Work Index of Lucky Cement Limestone Pakistan", International Journal of Scientific & Engineering Research Volume 8, Issue 6, June-2017.

IMPROVEMENT OF MECHANICAL PROPERTIES OF AUSTEMPERED DUCTILE IRON (ADI) BY MAGNETIC FIELD

Assoc. Prof. Ing. Peter Futas, PhD.[1]

Prof. Ing. Alena Pribulova, PhD.[1]

Assoc. Prof. Ing. Jozef Petrik, PhD.[1]

Ing. Peter Peter Blasko, PhD.[1]

Dr hab. Inz. Marcin Brzezinski[2]

[1] Technical university of Kosice, Faculty of Materials, Metallurgy and Recycling, **Slovakia**
[2] Akademia Górniczo-Hutnicza w Krakowie, Wydział Odlewnictwa, **Poland**

ABSTRACT

Austempered Ductile Iron (ADI) is a promising material whose structure is obtained by isothermal processing, i.e. isothermal decomposition of austenite in the bainitic range. It is used in various industrial fields. It is characterized by an excellent combination of tensile strength and ductility, exceeding the properties of quenched and tempered steels in the strength range of 800 - 1500 MPa. Its production is problematic because the ferritic or ferritic-pearlitic ductile iron (SGI), which is the basis for the production of ADI cast iron, must meet demanding metallurgical properties. These are, above all, regular and uniformly distributed graphite spheres in the matrix. One of the ways to influence the metallurgical quality of ADI cast iron is the action of a magnetic field, which leads to the improvement of the metallurgical and mechanical properties of ADI cast iron. The article deals with the influence of a magnetic field on the mechanical properties of ADI in the process of isothermal hardening. In isothermal quenching, after austenitizing, the quench is first cooled to a lower temperature and then the temperature of the quenching medium is raised to a higher temperature. The entire process is carried out in the presence of a magnetic field. The mechanical properties and microstructure were compared with the conventional manufacturing process. In this way, an increase in the mechanical properties and a refinement of the cast iron structure was achieved.

Keywords: spheroidal graphite iron (SGI), austempered ductile iron (ADI), metallurgy, mechanical properties, magnetic field

INTRODUCTION

Austempered Ductile Iron (ADI) belongs to progressive high-quality materials. It isothermally hardened ductile iron, in which high mechanical properties are achieved by alloying with Ni, Cu, and especially by heat treatment, which creates a special austenitic-ferritic matrix in which graphite spheres are spaced.

https://doi.org/10.5593/sgem2024/1.1/s04.55

The temperature of the isothermal transformation and the holding time at this temperature determine the resulting structure and properties of the refined casting. At higher temperatures of 370 to 450 °C, ADI is obtained with lower strength properties and hardness, with higher ductility and toughness, and with better fatigue properties. Lower temperatures of 230 to 350 °C isothermal transformation of austenite are used when requirements for higher strength, hardness, and resistance to wear, ductility, and toughness decrease.

The structure of isothermally refined ADI cast iron consists of acicular to plate-like ferrite. The original graphite balls are stored in this base material. The structure should be free of pearlite, bainitic carbides, and martensite. A typical ADI microstructure is shown in **Fig. 1** [1].

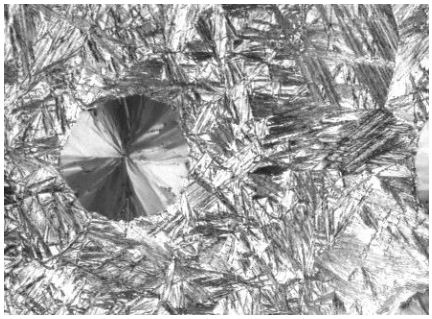


Fig. 1 Microstructure of ADI [1]

In its course, the bainitic transformation of ductile iron distinguishes two, respectively three stages.

At higher temperatures of the isothermal transformation of austenite, above 350 °C, the precipitation of bainitic lamellar ferrite (αB) takes place in the first stage. The remaining untransformed austenite is enriched with carbon (γC).

The process of transformation in the 1st stage can be described schematically $\gamma \rightarrow \alpha B + \gamma C$, i.e. austenite → bainitic ferrite + stabilized residual austenite.

In the 2nd stage, the reaction rate decreases and the transformation practically stops. The structure consists of bainitic ferrite and stabilized austenite-ausferite. Changes in the structure in the 3rd stage of isothermal endurance are characterized by the transformation of carbon-enriched austenite into a ferritic-carbide mixture according to the scheme $\gamma C \rightarrow \alpha + K$. The increase in its share during the 3rd stage is accompanied by a decrease in the plasticity and toughness of ADI and usually a slight increase in hardness.

The course of the isothermal transformation in the area of the lower bainite, below 350 °C, is closer to the bainitic transformation of steels.

In the 1st stage with the highest reaction rate, plates of bainitic ferrite are separated from the austenite. Its precipitation results in the enrichment of untransformed austenite with carbon. The course of the isothermal transformation in this stage can be written by the scheme $\gamma \rightarrow B + \gamma C$.

The 2nd stage is characterized by the concentration of carbon in untransformed austenite and the maximum amount of stabilized austenite (15 to 20%) in the structure.

The course of the 3rd stage can be expressed similarly to the upper bainite region by the scheme γC → α + K. However, the beginning and the end of this stage are shifted significantly to longer times [2, 3,4].

It has also been observed that the transformation of austenite to ferrite during the first reaction of ADI occurs by the nucleation and growth process [5, 6, 7]. Nucleation depends on the supercooling and it is possible to obtain higher carbon in austenite (γC) if the austempering temperature is higher. Thus, it was theorized here that by combining large super cooling and higher austempering temperature, it may be possible to increase the volume fraction of ferrite and at the same time we can have very fine ferrite and austenite in the matrix. This is expected to enhance the mechanical properties of ADI. Hence, a novel concept of a two-step austempering process was conceived by this investigator. This two-step process involves first quenching the alloy to a lower temperature after austenitizing and thus increasing the supercooling, and then immediately (once the nucleation is complete), raising the temperature of the quenching media to a higher temperature to facilitate faster enrichment of carbon content of the austenite.

A significant improvement in the mechanical properties of ADI is achieved by two-stage isothermal hardening [3, 8].

Some recent studies [9, 10, 11] have shown that in the case of steels, the transformation of austenite to ferrite is accelerated by a phase transformation induced by a high magnetic field due to an increase in the rate of ferrite nucleation. In ADI similar to γ→α during isothermal hardening, a transformation occurs. Therefore, it is quite likely that if the ADI is tempered in a sufficiently high magnetic field, there will be a significant increase in ferrite nucleation. As more ferrite is formed, the result should be a very fine-grain structure.

The main objective of this investigation was to verify these studies and to examine the effect of this magnetic treatment on the mechanical properties of ADI.

MATERIALS AND METHODS

The material used for the investigation was alloyed ductile iron EN-GJS-700-2. The chemical composition of the material is shown in **Tab. 1**.

Tab. 1 Chemical composition of the used material EN-GJS-700-2

Element	wt. [%]
C	3,70
Si	2,50
Mn	0,20
P	0,03
S	0,02
Ni	1,10
Mo	0,60
Mg	0,04

https://doi.org/10.5593/sgem2024/1.1/s04.55

The material was cast in the shape of circular cylindrical rods with a diameter of 30 mm. The microstructure of the cast material is shown in **Fig. 2**.

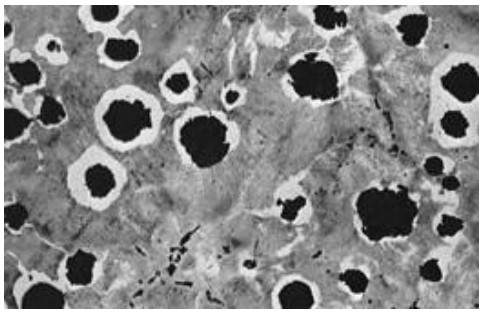


Fig. 2 Microstructure of the sample, 100×, etched Nital 2%.

The structure of cast material had a pearlitic structure with more than 80% pearlite. Cylindrical tensile samples for tensile tests and compact test samples for fracture toughness testing were prepared from these cast bars according to the STN 42 0315 standard.

Two samples were prepared and analyzed for comparison. Sample "A" was processed by a standard one-step isothermal quenching process. Sample "B" was processed by a two-stage isothermal hardening process in the presence of a magnetic field.

Sample "A" was subjected to austenitizing annealing at 927°C for 2 hours and then the austenitizing annealing temperature was reduced to 385°C for 2 hours.

Sample "B" was subjected to austenitizing annealing at 927°C for 2 hours and then the temperature was reduced to 270°C in the presence of a magnetic field. Immediately afterward, the temperature of the salt bath increased to 385°C. Subsequently, the sample was tempered at the given temperature for 2 hours in the presence of a 15 Tesla magnetic field. The testing was carried out in the research laboratory of STU Bratislava. This isothermal quenching was chosen so that the processing time corresponds to the processing of ADI cast iron.

The tensile test of all samples was performed according to the STN 42 0315 standard. Three identical samples were tested from each heat treatment. Average values from three test samples are shown here. Tests were performed on a Zwick/Roell Z600E machine under standard conditions in the laboratory of TUKE Kosice.

Microstructures of the heat-treated specimens were examined by optical microscopy after etching with 2% Nital. X-ray diffraction (XRD) analysis was performed to estimate the volume fraction of austenite and the carbon content of austenite with the use of an electron microscope Jeol 200kW (Germany) at the Institute of Materials TUKE Kosice.

The profiles were analyzed with Jade 6 software to obtain the peak positions and the integrated intensity of (1 1 1), (2 2 0), and (3 1 1) planes of FCC (face-centered cubic) austenite and (1 1 0) and (2 1 1) planes of BCC (body-centered cubic) ferrite. The volume fraction of ferrite ($X\alpha$) and austenite ($X\gamma$) were determined by the direct comparison method using the integrated intensities of (1 1 0) and (2 1 1) planes of ferrite and (1 1 1), (2 2 0) and (3 1 1) planes of austenite [12, 13].

The carbon content of austenite was determined by the Eq. 1 [13]:

$$a_\gamma = 0.3548 + 0.0044C_\gamma \qquad (1)$$

where: a_γ – lattice parameter of austenite in nm
C_γ – carbon content of austenite in wt. %

The {l 1 1}, {2 2 0}, and {3 1 1} planes of austenite were used to estimate the lattice parameter. The average from these three samples is presented here. The mean free path of dislocation (d) in ferrite (α) was determined (which represents the mean particle size of ferrite) from the XRD profile from the breadth of {2 1 1} diffraction peaks of ferrite using Eq. 2 [13]:

$$d = \frac{0.9\lambda}{\beta cos\,\theta} \qquad (2)$$

where: λ – wave length

β – breadth of (2 1 1) peak of ferrite at half height in radians

θ – Bragg angle

After heat treatment, the samples were prepared for the fracture toughness test under static load. Fracture toughness was measured following standard STN 42 0347:1990.

RESULTS AND DISCUSSION

The microstructure of the samples processed by the conventional one-step isothermal quenching process is shown in **Fig. 3**. Similarly, the microstructure of the samples processed by the two-step isothermal quenching process in the presence of a 15 Tesla magnetic field is shown in **Fig. 4**. The tempered microstructure of the "A" samples shows a matrix of dark acicular ferrite plus light-etched austenite with graphite nodules scattered in the matrix. Both austenite and ferrite had a coarse and feathery character, which is typical of the upper bainitic structure. No carbide precipitation was observed in any of the microstructures.

Austenite was found to exist in the form of pieces between the ferrite needles. Since the austempering temperature was in the upper bainitic region, a typical upper bainitic microstructure was observed.

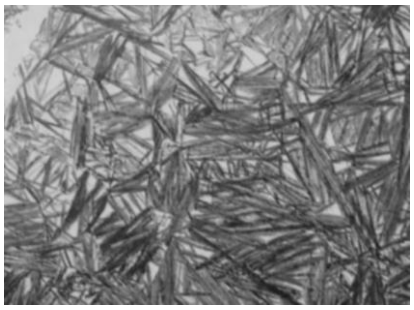


Fig. 3 The Microstructure of ADI (One-step austempering process)

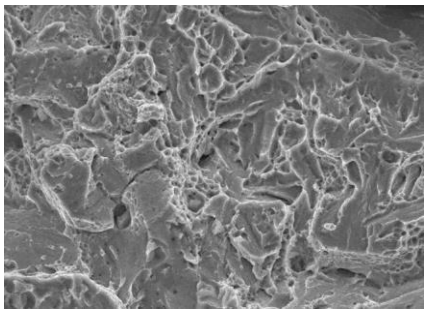


Fig. 4 The microstructure of ADI (Two-step austemp. – magnet. field 15 Tesla)

The volume fraction of ferrite and austenite, as well as its carbon content, were also determined using XRD. **Tab. 2** shows the volume fraction of ferrite and austenite, as

https://doi.org/10.5593/sgem2024/1.1/s04.55

well as the carbon content of austenite for all these samples. It is clear from this table that the magnetic isothermal quenching process led to a larger volume fraction of ferrite in the matrix.

The carbon content of the austenite is also shown in **Tab. 2**. From **Tab. 2**, it is clear that the magnetic isothermal quenching process resulted in a higher carbon content of the austenite than the conventional process. This is because, during the two-step isothermal quenching process, the samples were transferred to a second salt bath maintained at a high temperature (385°C). Since diffusion is a temperature-dependent process, the rate of diffusion of carbon atoms increased, leading to a greater distribution of carbon, and thus the carbon content of austenite was higher. In the presence of a magnetic field, carbon atoms spread much faster than in the absence of a magnetic field. Therefore, samples processed by a two-stage process in a magnetic field have a higher carbon content in austenite.

The effect of different thermal treatments on the mean free path (d) of dislocations in ferrite is shown in **Tab. 2**. The Scherrer equation gives this. This dislocation mean free path in the ferrite phase can be considered as a measure of the mean ferrite particle size (d) [14]. The values of this dislocation mean free path (d) in ferrite determined by XRD were considerably small (nm). The size of the ferritic cells was much smaller for the samples tempered in the magnetic field by the two-step process. These observations are consistent with the theory of the nucleation and growth process. The magnetically treated samples "B" were first cooled to a lower temperature of 260°C to create more supercooling. This was done to facilitate more ferrite nucleation. As the tempering temperature increased to the second tempering temperature level, the core ferrite grew at the expense of the austenite domains. Because more ferrite nucleation occurred, smaller ferritic cell sizes were obtained by this process.

Tab.2 Results of XRD analysis

Sample	Volume fraction of ferrite [%]	Volume fraction of austenite [%]	Ferritic cell size [nm]	Carbon content in austenite [%]
"A" one-step austemp. process	65,5	35,5	0,0552	1,90
"B" two-step austemp. process (magnetic field 15 Tesla)	94,6	8,1	0,0188	2,20

The mechanical properties of the samples are shown in **Tab. 3**. It is clear from this table that the magnetic hardness, yield strength, and tensile strength of the samples processed in the magnetic field were higher. The ductility of these samples processed in the presence of a magnetic field was lower than that of conventionally processed samples. This higher slip and tensile strength in the magnetically treated samples is due to the fact that finer scales of ferrite and austenite were produced in these samples. It is well known (Hall-Petch equation [15]) that finer grains result in higher slip and tensile strength. Moreover, the ferrite content in the magnetically processed samples was also high. This also contributed to the higher strength of these samples.

Tab. 3 Mechanical properties

Sample	Yield Strength [MPa]	Tensile strength [MPa]	Fracture Toughness [MPa.m$^{1/2}$]	Elongation [%]	Hardness HRC
"A"	670	1100	61,20	20,10	23,4
"B"	1280	1520	77,30	3,20	38,2

Tab. 3 shows that the magnetic isothermal quenching process resulted in higher fracture toughness than the conventional. The maximum fracture toughness obtained in ADI by the conventional one-step process is between 61 and 67 MPa.m$^{1/2}$. However, in the case of the two-step process in the magnetic field, the maximum fracture toughness of 77.30 MPa.m$^{1/2}$ was achieved, which is about 20% higher than in the conventional one-step process. Thus, the two-step magnetic field isothermal quenching process appears to be a viable process for improving the fracture toughness of materials.

The higher fracture toughness for magnetically processed samples is due to the fact that the ferrite content in these samples is higher than in conventionally processed samples. This corresponds to research published in the literature [3].

CONCLUSION

The concept of multi-stage isothermal hardening in a magnetic field, which was investigated in this paper, improves (increases) the mechanical properties of ADI compared to the conventional ADI production process. This fact is a consequence of the formation of a higher-quality microstructure of ADI cast iron. Very fine ferrite and austenite were obtained in the microstructure. The ferrite content was also significantly higher. The ADI cast iron samples were processed by a two-stage tempering process in a 15-Tesla magnetic field.
From this study follows:
1. The two-stage process of isothermal hardening in the presence of a magnetic field results in higher yield strength, tensile strength, and fracture toughness by approximately 20%.
2. The two-stage process of isothermal hardening in the presence of a magnetic field resulted in finer ferrite and austenite in the structure and a larger volume of ferrite in the structure.
3. The two-stage isothermal hardening process in the magnetic field improved the mechanical properties compared to the conventional isothermal hardening process.
These results correspond to the results published in the literature [13] where the magnetic field was 20-Tesla.

ACKNOWLEDGEMENTS

This work was supported by the Scientific Grant Agency of The Ministry of Education of the Slovak republic No. KEGA 018TUKE-4/2022, VEGA 1/0002/22 and APVV-22-0580, APVV-21-0142, Polish Ministry of Science and Higher Education Grant No. 16.16.170.7998

https://doi.org/10.5593/sgem2024/1.1/s04.55

REFERENCES

[1] Futas, P., Pribulova, A., Pokusova, M., Junakova, A.: Liatiny – vlastnosti, výroba, použitie, TUKE, Košice, 2020, ISBN 978-80-553-3644-2

[2] Putatunda, S. K. et. al.: Development of austenite free ADI (austempered ductile cast iron), Materials Science and Engineering: A, Vol. 435 – 436, pp. 112 – 122, 2006, DOI: 10.1016/j.msea.2006.07.051

[3] Putatunda, S. K.: Development of austempered ductile cast iron (ADI) with simultaneous high yield strength and fracture toughness by a novel two-step austempering process, Materials Science and Engineering: A, Vol. 315, pp. 70 – 80, 2001, DOI: 10.1016/S0921-5093(01)01210-2

[4] Futas, P., Pribulova, A., Pokusova, M., Junakova, A., Sabik, V.: Possibilities of Austempered Ductile Iron (ADI) Production, SGEM 2022, Vol. 22, pp. 483 – 490, 2022, DOI: 10.5593/sgem2022/1.1/s04.056

[5] Gundlach, R. B., and Janowak, J. F.: Development of a Ductile Iron for Commercial Austempering, AFS Transaction, Vol. 94, pp. 377-388 (1983)

[6] Johansson, M.: Austenitic Bainitic Ductile Iron, AFS Transaction, Vol.85, pp. 117 – 122, 1977

[7] Shanmugam, P. et. al.: Effect of Microstructure on the Fatigue Strength of an Austempered Ductile Iron, Journal of Materials Science, Vol. 29, pp. 4933 – 4940, 1994

[8] Yang, J., Putatunda, S. K.: Improvement in strength and toughness of austempered ductile cast iron by a novel two step austempering process, Material and Design, Vol. 25, pp 219 – 230, 2004.

[9] Xu, Y., Ohtsuka, H., Wada, H.: Transaction of the Materials Research Society of Japan, Vol 25, pp. 501 – 504, 2000.

[10] Ohtsuka, H. et. al.: Proceeding of the solid Phase Transformations, Japan Institute of Metals, pp. 393 – 396, 1999.

[11] Joo, H. D., Kim, S. U., Shin, N. S., Koo, Y. M.: An effect of magnetic field on phase transformation in Fe-C system, Materials Letter, Vol. 43, pp. 225 – 229, 2000.

[12] Cullity, B. D.: Elements of X-Ray Diffraction, Addison Wesley Publishing Company (1978), ISBN 0-201-01174-3

[13] Putatunda, S. K.: Influence of Magnetic Field on the Mechanical Properties of Austempered Ductile Iron (ADI), Materials Science Forum, Vol. 539 – 543, pp. 4657 – 4662, DOI: 10.4028/www.scientific.net/MSF.539-543.4657

[14] Monshi, A., Foroughi, M.R., Monshi, M.R.: Modified Scherrer Equation to Estimate More Accurately Nano-Crystallite Size Using XRD, World Journal of Nano Science and Engineering, Vol. 2, No. 3, Sept. 2012, DOI: 10.4236/wjnse.2012.23020

[15] Li, Y., Bushby, A. J., Dunstan, D.J.: The Hall–Petch effect as a manifestation of the general size effect, Proceedings of the Royal Society A, Mathematical, Physical and Engineering Sciences, June 2016, DOI: 10.1098/rspa.2015.0890

FLOTATION AND MAGNETIC SEPARATION PROCESSES FOR A MINERAL OF WOLLASTONITE

Assoc. Prof. Dr. Surracco Marco

Prof. Tilocca Maria Caterina

Department of Civil-Environmental Engineering and Architecture, University of Cagliari-via Marengo 2-09123 Cagliari – Sardinia – **Italy**

ABSTRACT

This paper presents the results of laboratory processing tests conducted to explore the potential for beneficiation of a wollastonite mineral (calcium metasilicate, $CaSiO_3$). The ore studied comes from a mineralized body located in the southern part of Sardinia (Italy), which has been studied in the past with geological surveys and sampling. In the investigated area the mineralization was very irregular. The encasing rocks consist of schist and the mineralized body is composed of wollastonite associated with limestone, garnets and silica. The sample used for treatment tests was taken from this area and underwent various tests, including grinding, froth flotation, and magnetic separation. Finally, we conducted an overall treatment test using the beneficiation techniques that yielded the best results in the previous experiments. The treatment scheme followed in the overall test utilized simple techniques such as grinding, calcite flotation and magnetic separation. As a result, the concentrate contained 80% wollastonite and met the pollutant element specifications. The final grinding stage was necessary to meet the market's required particle size specifications. The flotation tests were conducted in a Denver laboratory cell, while a Jones wet high-intensity magnetic laboratory scale separator was used for the magnetic separation tests. The effectiveness of the various steps of testing was verified by comparing the results obtained with the specifications required by the wollastonite market, which impose minimum quantities of contaminants, such as iron, titanium and magnesium, while being less severe with regard to SiO_2 and CaO contents.

Keywords: wollastonite, froth flotation, grinding, magnetic separation.

INTRODUCTION

The initial phase of studies conducted on a sample of Wollastonite ore (calcium metasilicate) from a mineralized body in the southwestern part of Sardinia aimed to assess the feasibility of beneficiation. The ultimate goal was to produce high-quality products that meet market requirements. The results showed that a concentrate with 81.31% Wollastonite content could be obtained through a reverse froth flotation process that removed, almost completely, the carbonate gangue present, with SiO_2 and CaO contents that are within market specifications [1].

The chemical and mineralogical compositions of the ore and concentrate obtained, represented by the flotation cell bottom, are summarised in Tables 1 and 2.

https://doi.org/10.5593/sgem2024/1.1/s04.56

Table 1 - Chemical analysis of the flotation feed and of the bottom cell flotation.

Product	SiO_2	CaO	Al_2O_3	Fe_2O_3	MgO	Na_2O	K_2O	TiO_2	MnO	L.O.I.
	%	%	%	%	%	%	%	%	%	%
Feed	48.88	41.48	1.50	0.99	0.41	0.10	0.27	0.07	0.11	5.63
Bottom cell	51.86	42.16	0.56	0.91	0.30	0.10	0.30	0.02	0.10	1.75

Table 2 - Mineralogical analysis of the flotation feed and of the bottom cell flotation.

Product		Wollastonite	CaCO3	Quartz	Other
		%	%	%	%
Feed		73.65	10.58	5.62	9.29
Bottom cell		81.31	2.02	9.68	6.97

The concentration of magnetic impurities, iron, still did not meet market specifications. Therefore, further study was deemed necessary to investigate the possibility of reducing the concentration of these pollutants in the Wollastonite concentrate to fully meet market demands. The mineralization from which the ore comes appears to be very irregular, with a lenticular appearance. The encasing rocks are schists and the mineralized body is composed of wollastonite associated with limestone, garnets, and silica. The sample used for investigation was taken from this area. Wollastonite deposits are not a geological rarity, but those with sufficient reserves to justify the development and use of innovative techniques to exploit them and obtain products with valuable specifications are rare [2]. As a result, the treatment techniques that are usually used are relatively simple and are already well known from the past [3]. Depending on the associated minerals (calcium carbonate, garnet, diopside, prehnite, quartz, etc.) and the size of the wollastonite crystals, magnetic separation, flotation, mechanical sorting are commonly used to produce high purity wollastonite concentrates to obtain marketable products [3] [4] [5] [6]. Paramagnetic minerals (garnet and diopside) normally associated with wollastonite are separated by high intensity magnetic separators. Calcite and feldspars can be removed by flotation. In practice, wollastonite mineral are generally beneficiated by flotation and magnetic separation after an initial comminution step [7] [8] [9] [10]. The experimental work reported has been carried out on wollastonite samples taken from a mineralized body located in the southern part of Sardinia (Italy), in the area called 'Gutturu is Abis', in order to identify the most suitable process scheme and the optimal tuning of the processing parameters for this specific mineral, using the common mineralogical processes applied worldwide to obtain commercial wollastonite concentrates.

MATERIALS & METHODS

Wollastonite is an inosilicate mineral with a theoretical composition of CaO=48.3% and SiO_2=51.7%. It may contain copper, magnesium or manganese as a replacement for calcium [11]. The properties of wollastonite in its pure form are summarised in Table 3 [12].

Table 3 - Characteristics of wollastonite.

Hardness (Moh's scale)	4.5/5
Density	2.80/3.09
Melting point [°C]	1,540
Moisture content	4% max
Index of refraction	1.616/1.631
Crystalline system	monoclinic
Form and habit	Sharp, fibrous, radiating mass of crystals with transparent or translucent appearance

When pure the mineral is white, however, it can take on gray and brown coloration, due to the presence of impurities [11], the nature of which determines the profitability in the use of the mineral.

Table 4 shows an example of the main requirements imposed by the market in Italy in order to limit the presence of elements that may affect the quality of the final product, giving problems regarding its use in industrial manufacturing.

Table 4 - Chemical and particle size characteristics required by the market for wollastonite.

Chemical specifications of wollastonite (technical data sheet provided by Cookson Mineraria S.p.A.)		
	[%]	Particle size less than [mm]
SiO2	49-50	0.075
CaO	45-50	0.045 (better)
Al2O3	0.30	0.038
Fe2O3	<0.30	
K2O	0.12	
MgO	1.30	
Na2O	0.05	
TiO2	0.02	
MnO	0.05	
L.O.I.	1-3	

To meet market specifications, wet high-intensity magnetic separation was used to obtain a concentrate with reduced magnetic impurities. The magnetic separator used is a Jones-type laboratory apparatus, suitable for treating suspensions with suspended solids smaller than 2mm. The magnetic field is generated by a pair of electromagnets. The installed power is 6.5 kW. A first series of magnetic separation tests was carried out on a wollastonite concentrate coming from a reverse flotation test performed in order to concentrate the calcite and quartz in the flotate, thereby reducing their presence in the cell bottom (wollastonite product) to levels within market specifications [1]. The magnetic field strengths applied were 19,000 Gauss, in the first passage, and 20,000 Gauss, in the repass, respectively.
Figure 1 illustrates the treatment scheme.

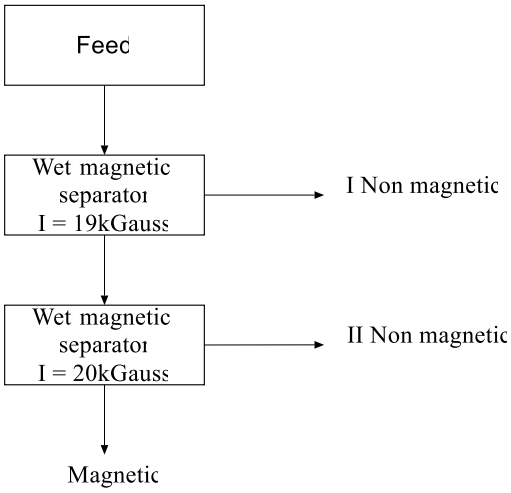


Figure 1 - Flowsheet of the first series of magnetic separator tests.

https://doi.org/10.5593/sgem2024/1.1/s04.56

Table 5 shows that the iron content in the non-magnetic product decreased by approximately 0.4%, specifically from 0.9% to around 0.5%. Additionally, the levels of other pollutants, such as TiO_2 and MgO, were also reduced.

Table 5 - Chemical analysis of the feed and products from the first series of magnetic separation tests.

Product	Yield	Fe2O3	MgO	TiO2
	%	%	%	%
Feed	100.00	0.90	0.36	0.04
I non magnetic	24.60	0.52	0.21	0.02
II non magnetic	70.19	0.58	0.22	0.02
Magnetic	5.21	6.80	2.60	0.41

To test the possibility of further reducing the magnetic contaminants, a second series of experiments were conducted using the magnetic separator with a field intensity of 20,000 Gauss. This second series of magnetic separation tests was conducted on a sample consisting of the mixture of the two nonmagnetic products obtained earlier. The sample was first reduced to a size below 0.044 mm by dry grinding using a porcelain ball mill operating in closed circuit. The control screening was performed by wet sieving. In this way, in addition to satisfying the requested particle size specifications for wollastonite (particle size less than 45μm), we also wanted to increase the degree of liberation of the contaminants to be separated. The figure 2 shows the scheme of the second series of tests carried out on the magnetic separator.

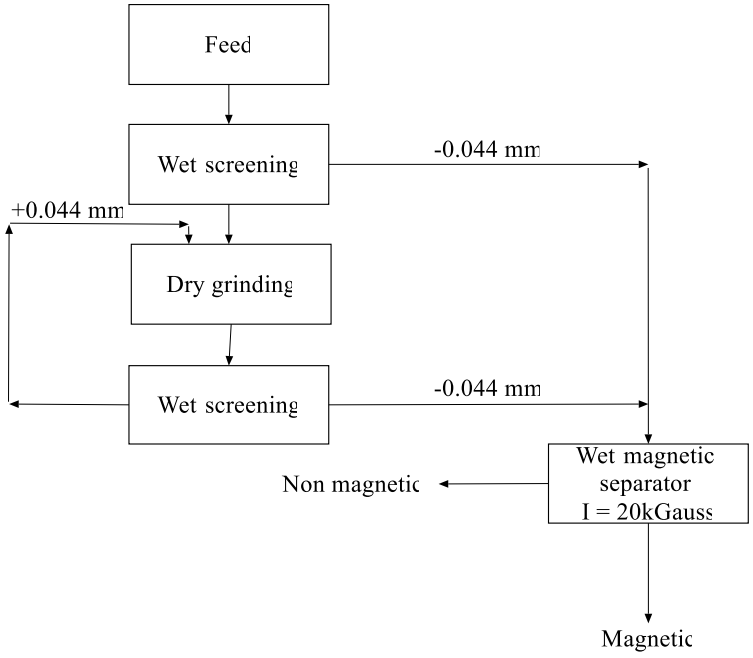


Figure 2 - Schematic diagram of the second series of tests carried out on the magnetic separator.

The results are positive: in the non-magnetic product, the Fe_2O_3 content has been reduced to 0.35%, as shown in Table 6.

Table 6 - Fe_2O_3 content in the in the feed and in the products obtained in the second series of magnetic separation tests.

Product	Yield	Fe2O3
	[%]	[%]
Feed	100.00	0.57
Magnetic	6.90	3.60
Non magnetic	93.10	0.35

Since, as has been verified previously [1], the beneficiation procedure that has provided the most interesting results is the one involving the flotation of calcite alone, it was decided to apply magnetic separation to the reject of this flotation. Therefore, both to further confirm the results obtained in the past and to define a possible treatment flowsheet, an overall test was carried out that starting from the ore would allow obtaining a good quality wollastonite concentrate. The process consisted of four steps: preparing the sample, removing calcite using flotation, grinding the cleaned wollastonite product to less than 0.045mm and finally magnetic separation. A significant amount of the ore was sampled, crushed, and then dry ground under 0.3mm using a porcelain ball mill operating in a closed circuit after removing the fraction smaller than 0.3mm. Both chemical and mineralogical analysis were carried out on the resulting sample, which represents the feed for the next flotation stage (see Table 7 and Table 8).

Table 7 - Chemical analysis of the flotation feed.

Sample	SiO2	CaO	Al2O3	Fe2O3	MgO	Na2O	K2O	TiO2	MnO	LOI
	%	%	%	%	%	%	%	%	%	%
Flotation feed	52.20	39.50	1.10	0.88	0.44	0.09	0.30	0.07	0.15	5.20

Table 8 - Mineralogical analysis of the flotation feed.

Sample	Wollastonite	Limestone	Quartz	Feldspars	Other
	%	%	%	%	%
Flotation feed	69	12	16	1	2

A carboxylate collector was used for calcite flotation, specifically an industrial olein (Pamak 4-Hercules/Pander Co.), in 2% aqueous emulsion. Sodium silicate in 2% aqueous solution was used as the depressant. Flotation was carried out in basic environment (pH = 9.5). A 1.2 litres Denver flotation cell, feed with 400 g of solid, was used to perform the tests. The impeller speed was set at 1,500 rpm. The conditioning time was 5 minutes. The following figure shows the flotation scheme adopted, with the quantities of reagents used in the various steps.

https://doi.org/10.5593/sgem2024/1.1/s04.56

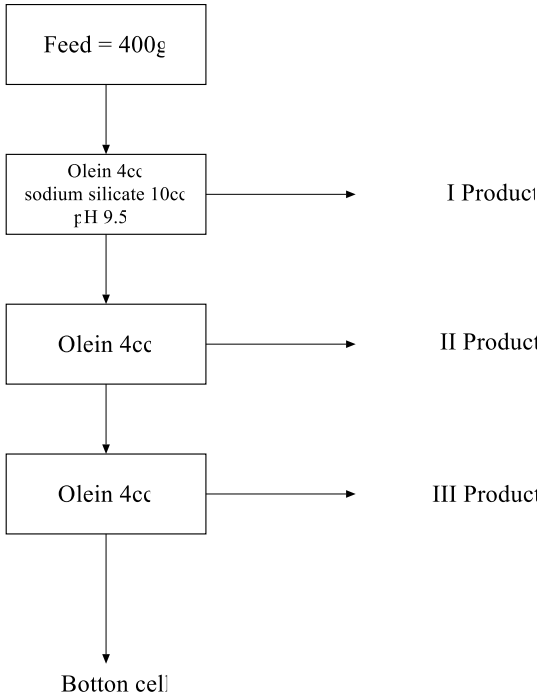


Figure 3 - Flotation scheme followed for calcite flotation.

In the final flotation stage, 3cc of 2% sulphuric acid is added to reduce the pH of the slurry to facilitate iron flotation. Table 9 presents the results of the chemical analysis of the products obtained from calcite flotation.

Table 9 - Chemical analysis of the flotation feed, of the floated products and of the bottom cell.

Product	Yield	SiO_2	CaO	Al_2O_3	Fe_2O_3	MgO	Na_2O	K_2O	TiO_2	MnO	LOI
	%	%	%	%	%	%	%	%	%	%	%
Feed	100.00	52.20	39.50	1.10	0.88	0.44	0.09	0.30	0.07	0.15	5.20
I Product	8.9	26.10	46.70	0.85	0.70	0.41	0.14	0.16	0.06	0.14	24.70
II Product	11.7	38.70	41.80	2.70	1.60	0.61	0.11	0.20	0.18	0.15	13.90
III Product	8.7	44.80	38.80	3.00	1.90	0.70	0.15	0.25	0.18	0.15	10.00
Bottom cell	70.7	58.62	38.30	0.63	0.66	0.38	0.07	0.34	0.04	0.15	0.72

The bottom of the cell from the previous flotation (Wollastonite concentrate) was wet ground under 45μm in closed circuit using a porcelain ball mill, with residence times of the Wollastonite concentrate inside the mill of 15 minutes. After grinding, the sample underwent magnetic separation in four steps. The first step was conducted at a field intensity of 20,000 Gauss, followed by three subsequent repasses at an intensity of 18,000 Gauss. Figure 4 shows the diagram of the multi-stage test at the magnetic separator.

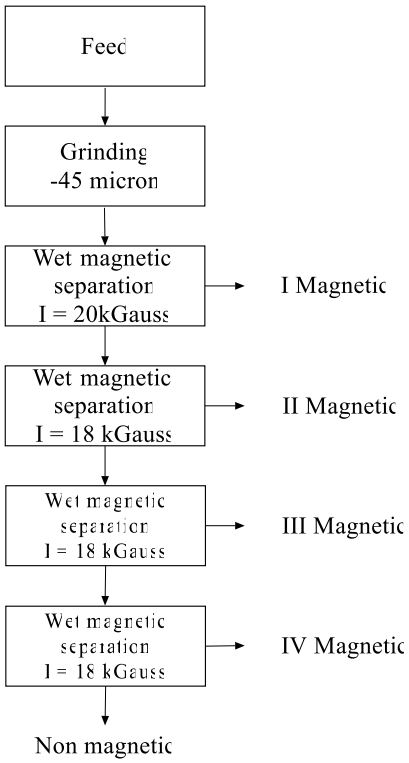


Figure 4 - Diagram of the magnetic separation test.

Table 10 shows the results of the chemical analysis of the magnetic separation product and Table 11 shows the results of the mineralogical analysis of the non-magnetic final product.

Table 10 - Chemical analysis of feed and magnetic separation products.

Product	Yield	SiO2	CaO	Al2O3	Fe2O3	MgO	Na2O	K2O	TiO2	MnO	LOI
	%	%	%	%	%	%	%	%	%	%	%
Feed	100.0	58.80	38.28	0.62	0.65	0.38	0.07	0.34	0.04	0.15	0.60
I Magnetic	7.6	53.10	37.60	2.30	2.90	1.20	0.15	0.16	0.11	0.20	2.20
II Magnetic	7.9	55.10	37.00	2.00	2.10	1.10	0.18	0.30	0.10	0.15	1.90
III Magnetic	1.7	51.20	33.30	4.30	4.40	2.40	0.42	0.33	0.28	0.20	3.10
IV Magnetic	2.8	53.20	37.60	2.30	1.70	1.00	0.45	0.28	0.14	0.14	3.10
Non magnetic	80.0	58.40	38.60	1.00	0.26	0.19	0.07	0.20	0.02	0.11	2.00

Table 11 - Mineralogical analysis of nonmagnetic product (Wollastonite concentrate).

Sample	wollastonite	Limestone	Quartz	Silicate various
	%	%	%	%
Non magnetic	80	5	5	10

CONCLUSIONS

The experimentation carried out verified the possibility of beneficiation of a wollastonite crude ore sample from a mineralized area in south-western Sardinia through an integrated process of reverse flotation and magnetic separation. Starting from a crude ore with a wollastonite grade of 69%, the treatment process applied resulted in a product with 80% wollastonite. Flotation, using carboxyl collectors,

https://doi.org/10.5593/sgem2024/1.1/s04.56

removed almost all the carbonate gangue. Magnetic separation, preceded by grinding and applied at a high field gradient, reduced the presence of magnetic particles. Grinding, performed prior to magnetic separation, not only increases the liberation degree of the contaminants, but also provides the final product with its marketable particle size specifications. It may be of some interest to verify the critical wollastonite content in the crude ore for which the beneficiation process may still be profitably, both technically and economically.

REFERENCES

[1] Surracco Marco, Tilocca Maria Caterina, "Beneficiation of a Wollastonite Mineral", in XXIInd International Multidisciplinary Scientific GeoConference Surveying, Geology and Mining, Ecology and Management, SGEM 2022, Conference proceedings, pp. 457-465, 2-11 July, Albena (Varna), Bulgaria.
[2] Development of Exploration and Industrial Technology to Exploit New Sources of Wollastonite in Europe. Brite-Euram II Project No. 5058-Syntesis Report. Project Funded by the European Community Under the Brite/Euram Programme.
[3] Kvyatkovskaya, K.K., Meitina, V.A., Enrichability of wollastonite rocks and the properties of wollastonitic wall tiles, Society for Mining Metallurgy and Exploration Inc. (ISSN 0361-7610), Glass and Ceramics #10, 25, pages 613-615, Springer, translated from Stekloi Keramika, No. 10, pp. 27-30, October 1968.
[4] Maxim L.D. and Mc Connell E.E., A Review of the Toxicology and Epidemiology of Wollastonite, Inhal. Toxicol., 2005, 17, pp. 451-466.
[5] V. V. Marchevskaya, S. V. Tereshchenko , A. F. Baranovsky, E. V. Beluzhenko , and E. D. Rukhlenko, Wollastonite Concentrate Production from Raw Material of Tyrnyauz Deposit, ISSN 1062-7391, Journal of Mining Science, 2017, Vol. 53, No. 3, pp. 585–590. © Pleiades Publishing, Ltd., 2017. Original Russian Text © V.V. Marchevskaya, S.V. Tereshchenko, A.F. Baranovsky, E.V. Beluzhenko, E.D. Rukhlenko, 2017, published in Fiziko-Tekhnicheskie Problemy Razrabotki Poleznykh Iskopaemykh, 2017, No. 3, pp. 175–181.
[6] Bulatovic S.M., Handbook of flotation reagents – Flotation of industrial minerals, Vol. III, Cap. 30 – Wollastonite, Elsevier, 2015.
[7] R. Sivamohan and F. Huang, Processing of the finely and complexly interlayered calcite rich wollastonite ore from northern Sweden, Minerals & Metallurgical Processing, May 1989, pp. 69-72.
[8] Robert L. Virta, U.S. Geological Survey, Industrial Minerals of the United States, Wollastonite – A Versatile Industrial Mineral, USGS Fact Sheet FS-002-01, February 2001.
[9] L. Daniel Maxim, Ron Niebo, Mark J. Utell, E. E. McConnell, Salvatore LaRosa and Alan M. Segrave, Wollastonite toxicity: an update, Inhal Toxicol, 2014; 26(2): 95–112.
[10] Gülay Bulut, Elif Suna Akçin, Murat Olgaç Kangal, Value added industrial minerals production from calcite-rich wollastonite, Gospodarka Surowcami Mineralnymi – Mineral Resources Management, 2019, 35(1), 43–58.
[11] Bauer, R.R., Copeland, J.R., and Santini, K., (1994), Wollastonite, in Carr, D.D., Ed. Industrial Minerals and Rocks, 6th Edition: Littleton, Colo., Society for Mining, Metallurgy, and Exploration, Inc., p. 1119–1128.
[12] La wollastonite: une substance minerale recherchee (gouv.qc.ca) at URL https://gq.mines.gouv.qc.ca/documents/examine/MB8812/MB8812.pdf

RECOVERY OF LITHIUM AND DESALTED WATER FROM OILFIELD BRINE

Dr. Ewa Knapik[1]

Dr. Grzegorz Rotko[1]

[1] AGH University of Krakow, Faculty of Drilling, Oil and Gas, al. A. Mickiewicza 30, 30-059 Krakow, **Poland**

ABSTRACT

Oilfield brine extracted with hydrocarbons is often considered as a problematic waste. The typical management option for this produced water is reinjection into the formation to maintain the reservoir pressure (or just for disposal). High salinity of produced water is on the one hand a drawback, but on the other hand an advantage because it can be used as a raw material for the production of valuable chemicals. In this paper a freezing-thawing desalination method was tested to obtain partially desalted water and concentrated brine from produced water. The obtained desalted water with conductivity lower than 10 mS/cm could be beneficially reuse for non-potable applications (crop irrigation, livestock watering). The concentrate with conductivity above 80 mS/cm is a suitable feed for salt/chemicals production. As the lithium content in the obtained concentrate was high, up to 20 mg/L, so the Mn-based sorbent was applied to recover it. The lithium-selective sorbent was prepared via solid state reaction and its morphological and textural parameters confirm its good chemical stability and high affinity towards lithium ions. The lithium recovery ration in static conditions was above 95 %. The obtained results prove that produced water may be beneficially reuse outside the energy sector.

Keywords: brine, oilfield, desalination, freezing-thawing, lithium recovery

INTRODUCTION

At mature oilfields the volume of produced water is 3-15 times higher than the volume of produced oil [1]. The management of this waste stream is crucial because may determine the profitability of the entire extraction process. There are several option of utilization/management of reservoir brine including reinjection into disposal wells, reinjection into formation to mantian reservoir pressure, surface discharge and beneficial reuse in oilfield operatation and outside the energy sector depending on water composition and local conditions [2]. Due to drinking water shortages, the use of these waters in agriculture is increasingly being advocated. Some reservoir brines show low salinity and low content of organic compounds which allow them to be considered as a potential feed for desalination installations. Some technical aspects support this concept and argue for its technical feasibility. The treatment of produced water requires a surface facility equipped with tanks, pumps, valves etc. This creates a possible opportunity for using existing pipeline and other infrastructures which are already in place. The reservoir conditions for each of the oilfield are well known and the production of reservoir fluids can be easily predicted. In desalination process, a large volume of produced water is treated to produce freshwater while a concentrated brine is

https://doi.org/10.5593/sgem2024/1.1/s04.57

a problematic waste stream. The concentrated brine contains a high concentration of salt and also chemicals used during desalination operations. In oilfields some wells may be used for underground reinjection of this brine into a non-productive formation. It is a common practice in exploitation to use both production and injection wells to reach different zones/locations.

The reuse of produced water for irrigation is not a new concept. Approximately 13% of the CBM water in Wyoming and 26% of the CBM water in Montana were used for irrigation in 2009 [1]. Kern County in California has been reusing its produced water for agriculture for decades [3]. In 1994, Chevron and the Cawelo Water District made a mutually beneficial deal to reuse produced water [4]. Chevron treats its produced water with walnut shell filters and sells the water to the water district for agricultural use. The food products (including citrus and nut crops) grown with this water have been distributed nationally for years. The task of treating produced water to agricultural standards may be technologically and economically feasible when comparing the cost of treatment to the cost of disposal in commercial wells as shown McCurdy et al. [5]. Other successful irrigation projects are reported in Australia [6]. In the Bowen Basin, up to 8 ML/day of reverse osmosis (RO) treated produced water was used to irrigate 234 ha of pasture crop and an 800,000 tree timber plantation. Also in Queensland, 300 ha of oilseed-bearing legume tree (Pongamia pinnata) plantation are irrigated with RO treated produced water. The Arabian Gulf region conducts an ambitious water management and agricultural development policies aiming to reinforce their food security through the reuse of marginal water resources [7]. It was calculated that the contribution of produced water to irrigation in the southeast Arabian Peninsula could be significant as the 365 million m^3/year. The above-described field experiences confirm the technical and economic feasibility of beneficial reuse of produced water.

Minerals present in brines can be a valuable chemical resource. There are reports in the literature about the possibility of recovering iodine, bromine, magnesium, boron, potassium or lithium from reservoir waters [8]. The combination of brine desalination with subsequent recovery of valuable elements from the resulting concentrate appears to be an excellent option for the use of waste reservoir water.

Beneficial uses of produced water outside the petroleum sector will require much more intensive water treatment than that required in oilfields operations. Treatment methods developed to deal with produced water for recycling include basic separation technologies, adsorption, ultrafiltration and desalination technologies. The choice of treatment methods depends largely on the composition of the reservoir brine. Shaffer et al. [9] suggested that mechanical vapor compression, membrane distillation and forward osmosis are suitable desalination technologies for high-salinity brine. The integration of two or more membrane-based and non-membrane-based technologies is a promising strategy to obtain water with required quality [10][11].

Among different desalination techniques the freezing/thawing (the FT) method offers some unique features. Comparing to the thermal desalination the FT requires much less energy: the latent heat of vaporization and freezing of water is 2256 kJ/kg and 330 kJ/kg, respectively [12]. The main obstacle for the development of this method is availability of cold energy. In the case of seawater the cold energy produced during the LNG regasification may be used [13]. Produced water may be freezed using cold energy generated during low temperature separation (LTS) process employed for natural gas

dehydration (stream of natural gas is rapidly decompressed via throttling expansion to cool and condense water and heavier hydrocarbons out of it). Our previous study shows that the the freezing desalination is an effective stratedy to obtain a partially desalted water [14]. This study is a continuation of previous research focusing on different type of brine (with relatively low salinity). The main novety of this research is a new methodology for freezing/thawing testing. We proposed a new construction of laboratory setup to precisely control the melting of obtained ice and separate desalted water from concentrate.

MATERIALS AND METHODS

The produced water from an oilfield located in the Carpathian Foredeep was used as a feedstock. All chemicals used in this study are the same as in our previous study [14]. The brine was pretreated via filtration: 5 L of brine was filtered through 10-µm filter bag filled with 1-cm layer of hydrophobic non-woven polypropylene. Physicochemical properties of raw and pretreated brine were determined as previously [14]. The obtained brine was freezed in a 800 mL cups at temperature of -20 ^{o}C for at least 12 hours. After this time, the entire volume of the cups froze, the cups were removed from the refrigerator and gently heated under a stream of warm water so as to bring out the lumps of ice. The ice was transferred to the same cups but with a perforated bottom, so that the melting ice could drain freely. The conductivity of the leaching filtrate was measured continuously so that the desalination process could be observed during thawing. The water obtained from the bottom of the cups (at the very beginning of the melting) was a brine concentrate, while the ice obtained at the top of the cups was virtually salt-free. Figure 1 shows the vessel for controlled thawing of ice.

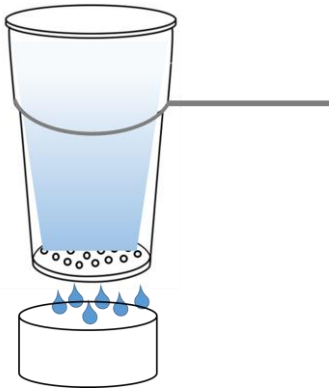


Figure 1. The laboratory vessel for thawing of the freezed brine.

The first 400 mL (the half of the freezed volume) from each cup was treated as a concentrate 1 and the second half was described as ice 1. Both fractions were frozen and thawed again to check how salinity of feed influences the spatial distribution of salt in cups.

The concentrate obtained after second FT stage was used as a raw material for lithium recovery. As a sorbent the previously reported [14] Mn-based material named LIS10 was applied. 0.5 g of the sorbent was contacted with brine concentrate for 24 hours and lithium concentration in the solution was measured by atomic absorption spectrometry using the AAnalyst 100 Atomic Absorption Spectrometer by PerkinElmer.

RESULTS

https://doi.org/10.5593/sgem2024/1.1/s04.57

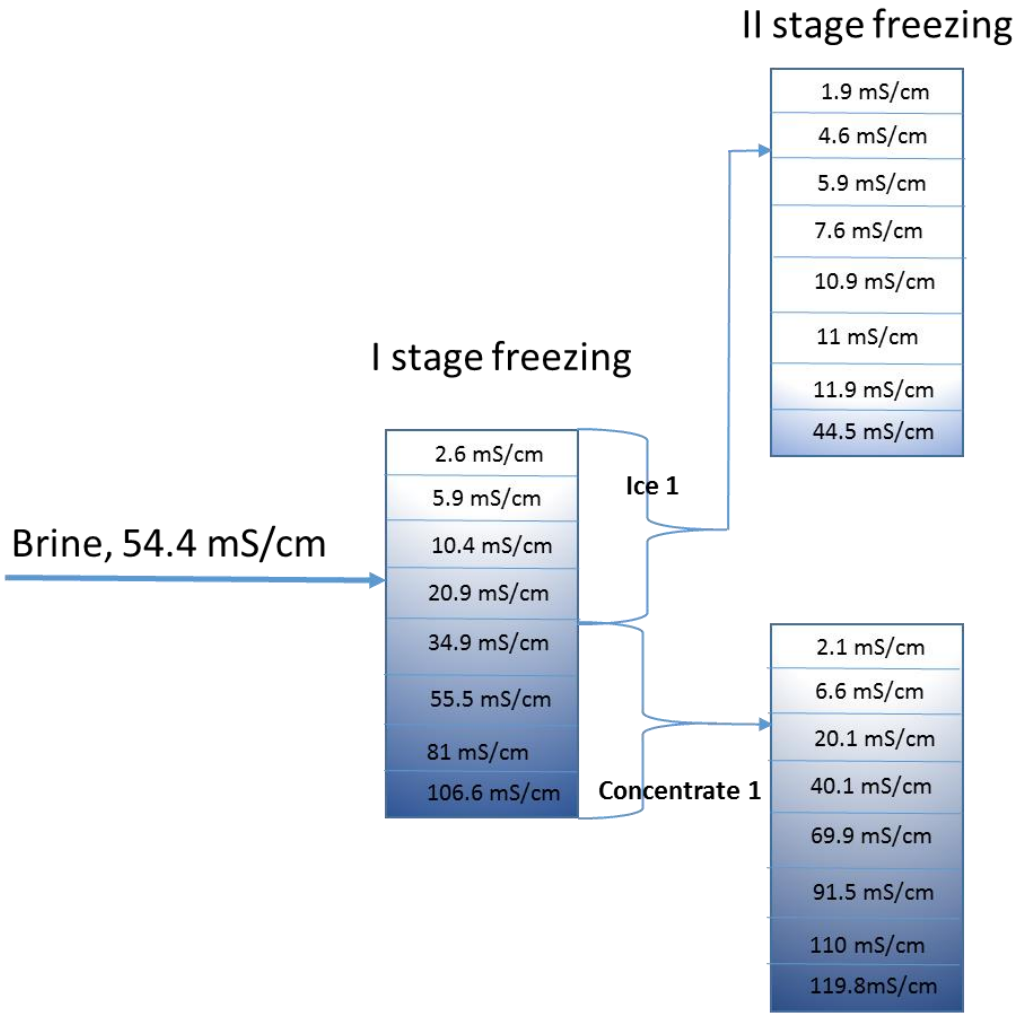
Physicochemical properties of tested brine before and after pretreatment are summarized in Table 1.

Table 1. Brine characteristics before and after pretreatment.

Parameter	Raw brine	Brine after filtration
Turbidity, FTU	31	7
pH	7.74	7.75
TDS, g/L	19.14	18.98
TSS, mg/L	439	6
Conductivity, mS/cm	54.5	54.4
Silica, mg/L	66.5	19.8

The applied pretreatment was succesfull in removing of suspended solids and silica.

Figure 3 shows the scheme of the FT desalination.



.

Figure 3. Changes in electric conductivity of water during controlled thawing of ice.

Figure 4 shows profiles of the FT desalination for initial brine (conductivity of 54.4 mS/cm), concentrate 1 (83.4 mS/cm) and ice 1 (14.03 mS/cm).

The LIS10 sorbent was effective in lithium recovery and 95.2 % of lithium was sorbed from brine concentrate.

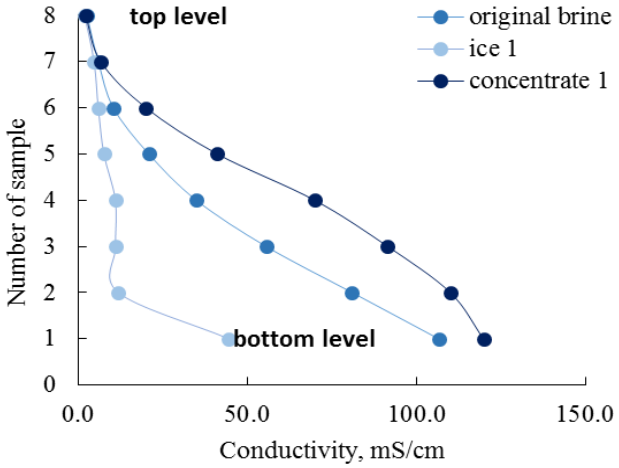


Figure 4. Profiles of conductivity changes during first and second stage of brine desalination.

DISCUSSION

The course of desalination is different for the initial brine and the obtained ice 1 and concentrate 1. In each case, the top layer of ice is desalted (conductivity of about 1 mS/cm). For fraction called ice 1 with conductivity of 14.03 mS/cm the freezing allows to quickly separate salty concentrate from partially desalted water (100 ml of brine concentrate with conductivity of 44.5 mS/cm per 700 ml of partially desalted water with conductivity of about 10 mS/cm). For concentrate 1 the desalination profile is wide and a large amount of intermediate fraction (water with conductivity similar to initial feed) is obtained. The proposed desalination was efficient and allowed to produce about 40% of water with conductivity lower than 10 mS/cm (suitable for irrigation of some crops). Table 2 shows conductivities of different types of water to assess the quality of the fractions received.

Table. 2. The typical conductivity ranges of different types of water [15].

Water type	Conductivity range (mS/cm)
Distilled water	0.0005-0.003
Snow (melted)	0.002-0.042
Tap water	0.05-0.800
Potable water (US standard)	0.03-1.5
Freshwater streams	0.1-2.0
Seawater	55

https://doi.org/10.5593/sgem2024/1.1/s04.57

CONCLUSION

Production of partially desalted water from saline brines for potable and non-potable uses gains more and more attention. When a waste cold stream is available in the facility the desalination of salty water can be realized by freezing/thawing method. The required operating temperature is about -20^{o}C which is easily achievable during LNG regasification or low-temperature natural gas purification. The obtained results show that brine with moderate salinity of about 20 g/L (comparable to seawater) may be desalted to produce irrigation water with 43% productivity. The initial brine salinity has a great impact on desalination efficiency. When the initial salt concentration is high, then during the freezing process a lot of salt accumulates at the bottom of the cup (the obtained concentrate has a high salinity) and at the top of the vessel a desalinated water is present. To achieve an acceptable water quality for drinking water it in necessary to apply a few stages (cycles) of freezing/thawing. The 2-stage FT in this study allowed to produce water suitbale only for irrigation or some industrial applications. Further research should focus upscaling of proposed technology (optimization of heat exchange and construction of FT equipment).

ACKNOWLEDGEMENTS

The research leading to these results has received funding from the National Centre for Research and Development (NCBR) in the frame of Project Contract No. LIDER/34/0174/L-12/20/NCBR/2021 under the LEADER Program.

REFERENCES

[1] Clark C. E., Veil J. A., Produced water volumes and management practices in the United States. Argonne National Laboratory (ANL), Oak Ridge, 2009.

[2] Jiang W., Lin L., Xu X., Wang H., Xu P., Analysis of regulatory framework for produced water management and reuse in major oil- and gas-producing regions in the United States, Water, vol. 14, no. 14. 2022, https://doi.org/10.3390/w14142162.

[3] Dolan F. C., Cath T. Y., Hogue T. S., Assessing the feasibility of using produced water for irrigation in Colorado, Science of the Total Environment, vol. 640–641, pp. 619–628, 2018, https://doi.org/10.1016/j.scitotenv.2018.05.200.

[4] Recycled oilfield produced water program, available online: https://www.cawelowd.org/recycled-produced-water (accessed on 24 Juni 2024).

[5] McCurdy, R., 2011, Underground injection wells for produced water disposal, Proceedings of the Technical Workshops for the Hydraulic Fracturing Study: Water Resources Management, available online: https://www.epa.gov/sites/default/files/documents/HF_Workshop_4_Proceedings_FINAL_508.pdf (accessed on 24 Juni 2024).

[6] Mallants D., Šimůnek J., Torkzaban S., Determining water quality requirements of coal seam gas produced water for sustainable irrigation," Agricultural Water Managment, vol. 189, pp. 52–69, 2017, https://doi.org/10.1016/j.agwat.2017.04.011

[7] Jaffar S., Khaliq A., Ahmed M., Al-Wardy M., Al-Busaidi A., Choudri B. S., Wastewater and sludge management and research in Oman: An overview, Journal of the Air & Waste Management Association, vol. 67, no. 3, pp. 267–278, 2017,

https://doi.org/10.1080/10962247.2016.1243595.

[8] Miranda M. A., Ghosh A., Mahmodi G., Xie, S., Shaw M., Kim S., Krzmarzick M .J., Lampert D. J., Aichelle C. P., Treatment and recovery of high-value elements from produced water, Water, vol. 14, no. 6. 2022, https://doi.org/10.3390/w14060880.

[9] Shaffer D. L., Arias Chavez L. H., Ben-Sasson M., Romero-Vargas Castrillón S., Yip N. Y., Elimelech M., Desalination and reuse of high-salinity shale gas produced water: drivers, technologies, and future directions, Environmental Science & Technology, vol. 47, no. 17, pp. 9569–9583, 2013, https://doi.org/10.1021/es401966e.

[10] Ricceri F., Giagnorio M., Farinelli G., Blandini G., Minella M., Vione D., Tiraferri A., Desalination of produced water by membrane distillation: effect of the feed components and of a pre- treatment by Fenton oxidation, Scientific Reports, vol. 9, pp. 1–12, 2019, https://doi.org/10.1038/s41598-019-51167-z.

[11] Ozgun H. *et al.*, Effects of the pre-treatment alternatives on the treatment of oil-gas field produced water by nanofiltration and reverse osmosis membranes, Journal of Chemical Technology and Biotechnology, vol. 88, no. 8, pp. 1576–1583, 2013, https://doi.org/10.1002/jctb.4007.

[12] Najim A., A review of advances in freeze desalination and future prospects, npj Clean Water, vol. 5, no. 1, p. 15, 2022, https://doi.org/10.1038/s41545-022-00158-1.

[13] Noor Akashah M. H., Mohammad Rozali N. E., Mahadzir S., Liew P. Y., Utilization of cold energy from LNG regasification process: a review of current trends, Processes, vol. 11, no. 2, 2023, https://doi.org/10.3390/pr11020517.

[14] Rotko G., Knapik E., Piotrowski M., Marszałek M., Oilfield brine as a source of water and valuable raw materials—proof of concept on a laboratory scale, Water, vol. 16, no. 11, 2024, https://doi.org/10.3390/w16111461.

[15] What is the typical water conductivity range?, 2022, available online: https://atlas-scientific.com/blog/water-conductivity-range/ (accessed on 24 Juni 2024).

https://doi.org/10.5593/sgem2024/1.1/s04.57

USE OF REGRESSION ANALYSIS AND SIMULATION TO OPTIMIZE THE COMPOSITION OF THE CAST IRON CHARGE

Assoc. Prof. Ing. Peter Futas, PhD.[1]

Prof. Ing. Alena Pribulová, PhD.[1]

Assoc. Prof. Ing. Jozef Petrik, PhD.[1]

Ing. Peter Peter Blasko, PhD.[1]

Assoc. Prof. Ing. Mária Mihaliková, PhD.[1]

[1] Technical University of Kosice, Faculty of Materials, Metallurgy and Recycling, **Slovakia**

ABSTRACT

Cast iron GG30 (EN-GJL-300C) has excellent mechanical properties and good machinability. It can be used in many industries such as hydraulics, engineering, automotive, oil and gas mining, and processing. It is suitable for the production of compressor and pump components. Return material, technological residue, iron scrap, fractional cast iron, liquid metal, and alloying components can be used as input raw materials in the production of cast iron, the first three were taken into account in the analysis. In practice, it is possible to choose their different ratio. At the same time, their chemical composition is somewhat variable. The aim of the paper is to compare two models, LINEST and DoE, which, with the help of regression analysis, determine the influence of these input raw materials (factors) on the mechanical properties: ultimate strength Rm, hardness HB of the final cast iron. The equations obtained will enable the calculation of the appropriate ratio of these three input raw materials to ensure the required mechanical properties of the final product. The equations obtained using DoE correspond more closely to the measured values than the equations obtained by LINEST, their calculation is more complex and requires the use of software. Based on these equations, taking into account the variability of the input data (for example, the fluctuation of the chemical composition of the iron scrap used), it is possible to estimate the proportion of castings with the required mechanical properties. For example, with a charge containing 40 % of technological residue, 22 % of returnable material, and 38 % of iron scrap with a variability of ± 10 %, it will meet the requirements of the standard for tensile strength Rm of 99.85 % of castings and hardness HB of 81.88 % of castings.

Keywords: cast iron, charge, mechanical properties, regression analysis, Monte Carlo

INTRODUCTION

Grey cast iron DIN 1691 GG30 [1] (or EN16482:2019 GJL-300-C; STN 42 2430) is a highly carbonaceous material with excellent characteristics. It is easy to process, absorbs sound, and is relatively inexpensive. This casting alloy is most widely used in engineering and street furniture but still has many other applications. It is suitable for applications where good wearing characteristics are required and when components

https://doi.org/10.5593/sgem2024/1.1/s04.58

need a combination of strength and wear resistance superior to those of other cast iron grades. It offers good compressive strength. Noise and vibration damping are excellent in this grade. It can be hardened by conventional methods typical applications include, dies, bearings, moulds, and machines for textile, and to the electric industry.

This cast iron contains 2.90-3.45 % carbon, 2.10-2.90 % silicon, 0.45-0.70 % manganese, max. 0.10 % sulphur, and max. 0.30 % phosphorous.

As for normal grey iron, the chemical composition is not important comparatively. The iron foundries could adjust the compositions according to their experience as long as they could meet the physical and mechanical requirements. Brinell hardness is above 260 HB and tensile strength Rm is above 300 MPa [2].

The contribution aims to design and test a simulation that will allow to design of the charge composition based on the required mechanical properties of the final CC30 cast iron casting. Based on experiments - real castings with different charge compositions, regression equations were created using the LINEST method using EXCEL software and the Design of Experiment (DoE) method. The results of the regression analysis were compared with the experimentally obtained results. Finally, the obtained regression equations were used in the Monte Carlo simulation, which made it possible to determine the proportion of castings that meet the requirements of the standard (or the customer) with the selected charge composition.

MATERIALS AND METHODS

The charge consisting of technological residue, return material, and iron scrap in a defined ratio was melted in an electric induction furnace (Otto Junker). The selected charge ratios are shown in Fig. 1, the composition of return material and iron scrap is in Table 1. After reaching a temperature of 1420°C, additives (ferrosilicon, pitch coke, and silicon carbide) were added. A total of 55 samples were cast, whose measured mechanical properties were used to calculate regression equations. Samples for chemical analysis of individual melts were taken from test bars intended for tensile strength testing. Chemical analysis was done using the classic titration and weighing method. The mechanical properties (tensile strength Rm and hardness HB) were determined on bars with a nominal diameter of d_0 = 20 mm taken from a pre-cast diameter of Ø 30 mm. The desired shape of the bars for the tensile test according to ČSN 42 0330 [3] was obtained by turning of cast bars.

Table 1. The composition of return material and iron scrap (in % wt.)

	C	Si	S	P	Mn
Return material	3.0-3.2	1.6-1.8	0.15	0.3	0.9-1.1
Iron scrap	0.66	0.95	0.014	0.055	0.633

The tensile test was performed on a ZDM 30 machine (fy. VEB Werkstoffprüfmaschinen – Leipzig) and hardness test according to Brinell hardness tester HPO 3000 (fy. VEB Werkstoffprüfmaschinen – Leipzig under conditions) 10/3000/10, i.e. ball diameter Ø10 mm, load force 30000 N and load time 10 seconds.

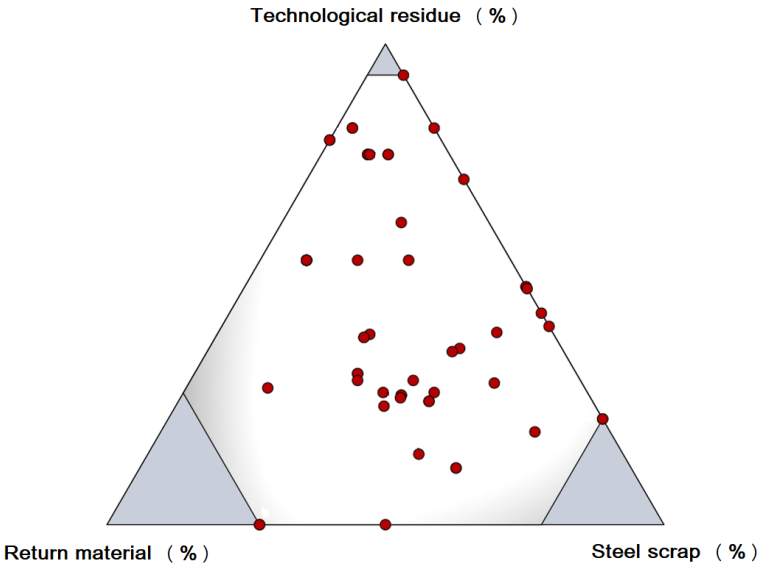


Fig. 1. Composition of charges used in the experiment

Technological residue is the residue left in the furnace after the previous melting. Return material is the cheapest and most available charge material. It is the foundry's technological waste and is the most valuable raw material that the foundry has. Before use, it must be thoroughly sorted (already when cleaning the castings) and cleaned (removed from the moulding material). A high proportion of returnable material in the charge is undesirable because it increases the viscosity of the slag, which causes problems during tapping - a maximum share of returnable material of 60 %. Steel scrap is used to reduce the carbon or silicon content in cast iron. It is usually 10-50 % of the charge. Contaminated steel waste, e.g. excessively rusted or contaminated with grease and organic impurities, increases the hydrogen content in the liquid metal, burns-out and the amount of slag. From an economic point of view, the use of steel waste in the charge is of great importance, as it is also reflected in the total costs of the charge of manufactured cast iron [4, 5, 6].

Linear regression

The multiple linear regression (EXCEL → LINEST program) was used for the study of the simultaneous effect of the charge on the tensile strength Rm and hardness HB of the castings [7, 8]. The results are equations (1) and (2).

Rm = 323.409+(0.00375*technological residue)-(0.0154*iron scrap) (1)

HB = 201.660+(0.08350 *technological residue)+(0.0268*iron scrap) (2)

The value of the determination coefficient R^2 indicates a relationship between considered input factors (composition of the charge) and output factors. It means that for example 32.2 of the variation of the output factor – the tensile strength can be explained by the effect of considered input factors. In the case of hardness, the value of the coefficient is 38.1. In both cases, the coefficient values are low. The reliability of the regression model is at best “medium”, which significantly limits its practical use. Both monitored parameters may be largely influenced by other factors such as melt temperature, and casting conditions.

https://doi.org/10.5593/sgem2024/1.1/s04.58

Design of experiments (DOE) is defined as a branch of applied statistics that deals with planning, conducting, analysing, and interpreting controlled tests to evaluate the factors that control the value of a parameter or group of parameters. DOE is a powerful data collection and analysis tool that can be used in a variety of experimental situations.

Many of the current statistical approaches to designed experiments originate from the work of R. A. Fisher in the early part of the 20th century. Fisher demonstrated how taking the time to seriously consider the design and execution of an experiment before trying it helped avoid frequently encountered problems in analysis. Key concepts in creating a designed experiment include blocking, randomization, and replication [9, 10, 11].

The DoE method using Design Expert software, was used to create a model to predict the tensile strength and hardness of the cast iron. Based on experimental data, was constructed the model, using the DoE mixture method. The matrix of the experiment consists of three factors with different levels: technological residue, return material, and iron scrap - the component of the charge (in wt. %) while two outputs, the same as in LINEST were monitored: tensile strength Rm and hardness HB. The result is triangular charts, with which we can visually evaluate the significance of the influence of individual input factors on the resultant investigated property of the cast iron and appropriate equations - equation (3) and Fig. 2 a) for tensile strength and equation (4) and Fig. 2 b) for hardness.

Rm = (3.3215*technological residue)+(3.47737*return material)+(3.25189* iron scrap)-(0.01275*technological residue*return material)-(0.003279* technological residue*iron scrap)-(0.008872*return material*iron scrap)-(0.000501*technological residue*return material*iron scrap) (3)

HB = (2.16606*technological residue)+(2.51082*return material)+(2.1898* iron scrap)-(0.00984*technological residue*return material)-(0.00448* technological residue*iron scrap)-(0.01471*return material *iron scrap)+(0.000239*technological residue*return material*iron scrap) (4)

Low values are observed in two cases - with a low content of scrap with an average content (approx. 50 % wt.) of technological residue and return material, as well as with a low content (up to 20 % wt.) of technological residue and average content (approx. 50 % wt.) of return material and iron scrap. The highest values of Rm are in the middle of the triangle - at contents of 30-40 % of each of the three components of the charge.

As for the hardness of HB, the low values are the same as for Rm in the area with a low content (up to 20 % wt.) of technological residue and average contents (approx. 50 % wt.) of return material and iron scrap. Towards the middle of the triangle, the hardness increases, and up to the top peak (the maximum value of the technological residue) it remains more or less constant. The highest values of hardness are in the area of the lower left peak (maximum value of returnable material and low value (up to 30 % wt.) of scrap and technological residue.

Capability of the DoE model serves to express the differences between predicted and measured values, thus expressing the quality of the model. The “Adequate precision“ measures the signal-to-noise ratio. It compares the range of the predicted values at the

design points to the average prediction error and it serves to express the differences between predicted and measured values, thus expressing the quality of the model. It can be calculated by equations (5) and (6). Ratios greater than 4 indicate adequate model discrimination and are desirable. The ratio of 5.29 for Rm and 4.98 for HB indicates an adequate signal. This model can be used to navigate the design space.

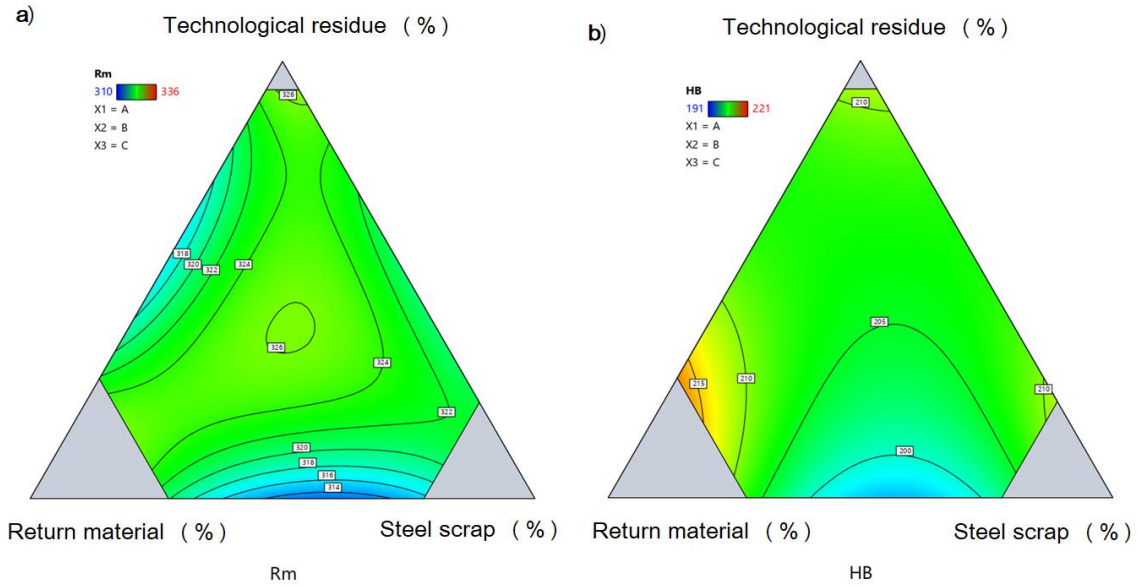


Fig. 2. DoE - tensile strength Rm a), hardness HB b)

Monte Carlo Method

The Monte Carlo method has a wide use of simulation of experiments, from counting some integrals, to solving differential equations. The basic idea of the method is very simple: we want to determine the mean value of a quantity that is the result of random action. Besides the mathematical problems, the Monte Carlo Method is used to solve economic problems, particularly in insurance and finance. The method helps to solve deterministic and probabilistic tasks by many times repeated random experiments on the input data sample. The method was dealt with by many authors, and the works [12, 13, 14] were used in the paper.

The Monte Carlo method was used to determine the probable proportion of castings with the required mechanical properties (Rm and HB) if a charge with a defined ratio of technological residue - return material - iron scrap is used with a certain tolerance (for example ± 10%).

We assumed that it corresponds to the triangular distribution. The calculation was performed using QUANTUM XL software with 10,000 simulations. Equations for DoE (3) and (4) were used as a mathematical model, which is more reliable than equations created using LINEST regression. The values according to the relevant standard [1] and specialist literature [2] were used as USL (upper standard limit) and LSL (lower standard limit). Based on equations, taking into account the variability of the input data (for example, the fluctuation of the chemical composition of the iron scrap used), it is possible to estimate the proportion of castings with the required mechanical properties. For example, with a charge containing 40 % of technological residue, 22 % of returnable material, and 38 % of iron scrap with a variability of ± 10 %, it will meet the

https://doi.org/10.5593/sgem2024/1.1/s04.58

requirements of the standard tensile strength Rm of 99.85 % of castings and for hardness HB of 81.88 % of castings.

As can be seen in Fig. 3, at composition of the charge is 40.3 % wt. technological residue, 22.1 % wt. return material and 37.6 % wt. of iron scrap with variability ± 2 % the hardness HB of 99,95 % of castings will meet the requirements of the standard.

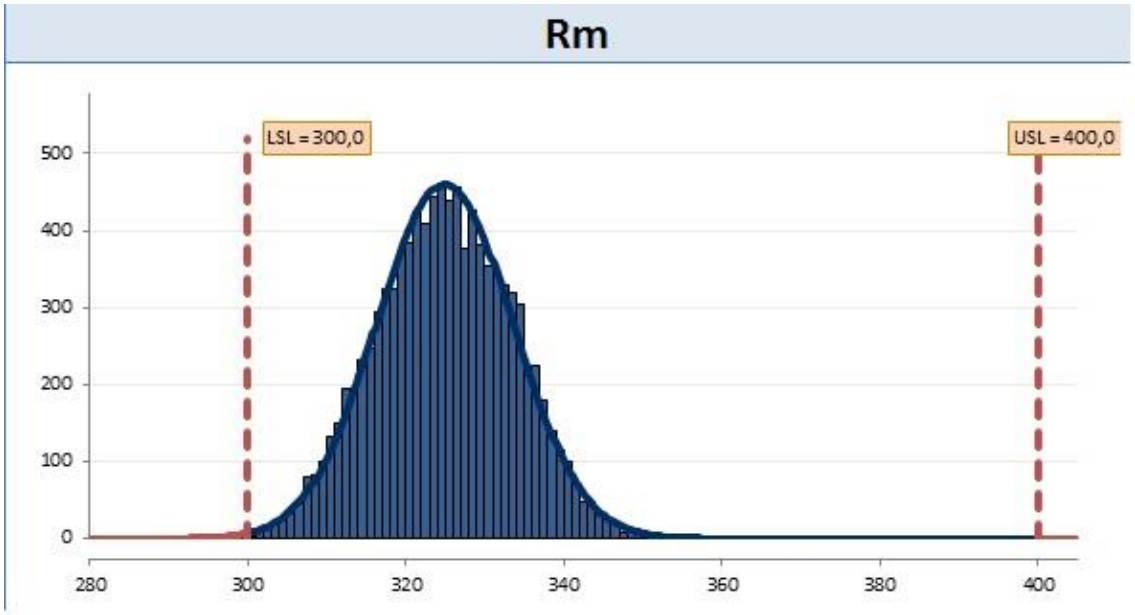


Fig. 3. Simulation Monte Carlo – Impact of a charge composition on the tensile strength

As can be seen in Fig. 4, at composition of the charge is 40.3 % wt. technological residue, 22.1 % wt. return material and 37.6 % wt. of iron scrap with variability ± 2 % the hardness HB of 89.28 % of castings will meet the requirements of the standard.

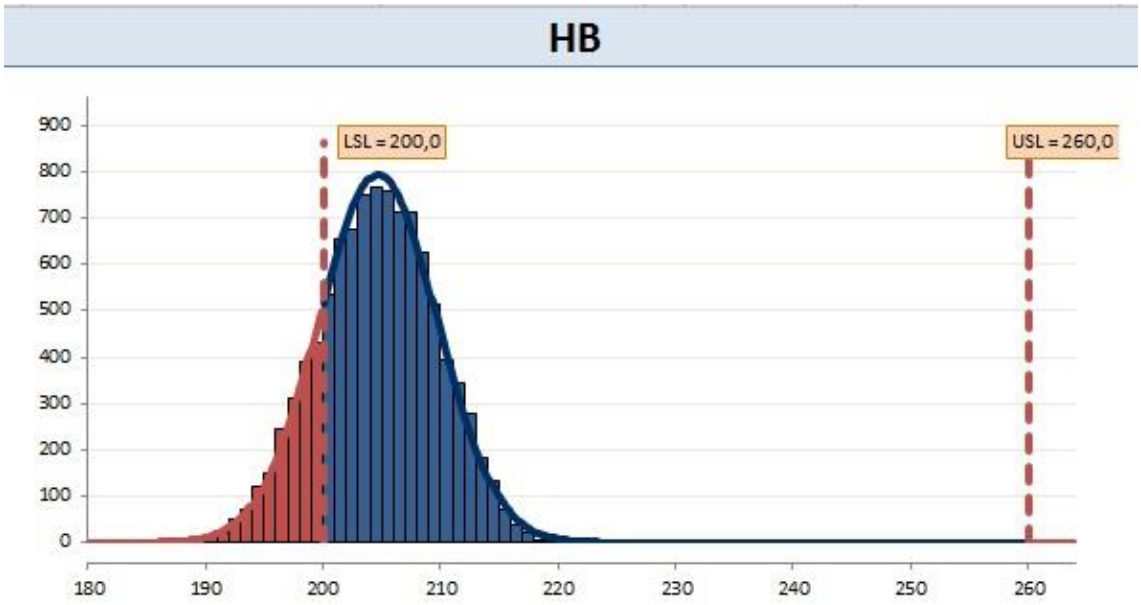


Fig. 4. Simulation Monte Carlo – Impact of a charge composition on the hardness

DISCUSSION

The use of regression equations for the approximate determination of mechanical properties of castings depending on the composition of the charge allows for savings of time and finance. It can use the results of already conducted practical tests to create a model. This with some probability makes it possible to determine the mechanical properties of the casting and also for the composition of a charge that has not been practically tested. It is suitable for a foundry that operates with a variable charge composition. It is the model that makes it easier to predict the impact of this variability on the quality of production. The use of the DoE method is more reliable, but it requires the use of the software and appraiser's skills. Only Excel, which is usually the basic PC software, is enough to use the LINEST method. With the use of simulations in modeling the composition, we also meet in the literature, such as the work of Saikaew and Harnsopa, 2023 [15]. Unlike the authors of the presented paper, they analysed a charge with four components and evaluated the hardness of the castings. They used the DOE method with a followed analysis of the dispersion of hardness with the Monte Carlo method to create regression. The authors used Monte Carlo to determine the share of identical castings. The methods mentioned in the paper can also be used for analyses based on the chemical composition of the charge (C, Si, Mn, S, P, Cr) and its variability due to variability of the charge This analysis will be the content of further research.

CONCLUSION

The paper deals with the issue of improving the quality of cast iron GG30, which is widely used in many branches of industry. Cast iron is prepared from a charge, the most important components of which are return material, technological residue, and iron scrap. One option to speed up and cheaper the process of prediction of mechanical properties of cast iron is the use of simple simulation methods. The simulations will provide a proposal for the ratio of the individual components of the charge so that the cast iron obtained in this way reached the required values of the tensile strength and hardness. The authors recommend the use of Design of Experiment (DoE), the results of which are reliable and produce outputs in the form of diagrams. These will allow the founder to quickly determine the composition of the charge that ensures the required mechanical properties of the casting. Equations that are an output of the methods allow being determined using the simulation method of casting compliance with requirements taking into account the possible variability of inputs, ie. the composition of the charge. The use of the described simulation methods will allow the owner or operator of the foundry to speed up work, improve the quality of castings and save time and costs. As shown in the paper, the equations can be used to simulate the proportion of castings with required mechanical values at a certain batch composition.

ACKNOWLEDGEMENTS

This work was supported by the Scientific Grant Agency of The Ministry of Education of the Slovak republic No. KEGA 018TUKE-4/2022, VEGA 1/0002/22 and APVV-22-0580, APVV-21-0142.

https://doi.org/10.5593/sgem2024/1.1/s04.58

REFERENCES

[1] DIN 1691:1985 Flake graphite cast iron (grey cast iron); properties.

[2] https://www.iron-foundry.com/DIN-1691-GG30-gray-cast-iron.html [online]. 2018 [viewed 2023-02-22].

[3] ČSN 42 0330:1983 Zkoušení kovů. Litina s lupínkovým grafitem. Stanovení pevnosti v tahu.

[4] Futáš, P., Pribulová, A., Vasková, I., Influence of steel scrap in a charge on cast iron properties, Archives of Foundry Engineering, Vol. 8, No. 2, pp. 71 – 74, 2008.

[5] Futáš, P., Pribulová, A., Malík, J., Vplyv vsádzkových surovín na vlastnosti liatiny EN-GJL 250 (Influence of raw materials on properties of cast iron EN-GJL 250), Acta Metalurgica Slovaca, Vol. 13, No. 4, pp. 67-71, 2007.

[6] Weiss, E. et al., Dependence of quality properties for grey iron on used raw materials, Metalurgija, Vol. 48, No. 1, pp. 43-45, 2009.

[7] Kelley, K., Maxwell, S. E., Sample Size for Multiple Regression: Obtaining Regression Coefficients That Are Accurate, Not Simply Significant. Psychological Methods Vol . 8, pp. 305–321, 2003, DOI:10.1037/1082-989X.8.3.305.

[8] Martín, J. et al., Multiple Linear Regression: An Overview with Analytical and Physico-Chemical Applications, International Journal of Advanced Research in Chemical Science (IJARCS), Volume 4, No. 11, pp. 32-60, 2017, DOI: 10.20431/2349-0403.0411005

[9] https://asq.org/quality-resources/design-of-experiments [online]. 2018 [viewed 2023-02-22].

[10] Sigma Zone. Quantum XL Software for Microsoft® Excel. [online] 2023 [viewed 2023-01-05], Available from: http://www.sigmazone.com/QuantumXL.htm.

[11] ASQ. Design of Experiments (DoE) Tutorial. [online]. 2018 [viewed 2023-02-22]. Retrieved from Design of Experiments: Available from: https://asqasktheexperts.com/2012/06/19/design-of-experiments-doe/.

[12] S. Raychaudhuri, S., Introduction to Monte Carlo simulation, in: Proceedings of the 2008 Winter Simulation Conference. [online]. 2008 [viewed 2014-03-14], Available from: http://www.informs-sim.org/wsc08papers/012.pdf

[13] Kuselman, F. Pennecchi, Epstein, M., Fajgelj, A., Monte Carlo simulation of expert judgments on human errors in chemical analysis. A case study of ICP-MS, Talanta, Vol. 1, 2014, No. 30, pp. 462-439, 2014, DOI: 10.1016/j.talanta.2014.07.036

[14] Sienkowski, S., Estimation of random variable distribution parameters by the Monte Carlo method, Metrology and Measurement Systems, Vol. 20, No. 2, pp. 249-262, 2013.

[15] Saikaew, C., Harnsopa, S., Influence of Component Proportions in Casting Process on Hardness and the Quality of Cast Iron. Archives of Foundry Engineering. Vol. 2023, No. 2, pp. 35 – 42, 2023, DOI: 10.24425/afe.2023.144293

SECTION

APPLIED AND ENVIRONMENTAL GEOPHYSICS

ASSESSMENT OF THE QUALITY FACTOR OF LITHOSPHERE FOR THE LENA DELTA (LAPTEV SEA REGION)

Dr. Artem A. Krylov[1]
Dr. Sergey A. Kovachev[1]

[1] Shirshov Institute of Oceanology, Russian Academy of Sciences, **Russia**

ABSTRACT

The parameters of strong ground motions necessary for seismic hazard assessing of construction sites have pronounced regional differences. In inaccessible and poorly studied areas, the development of a ground motion prediction equation (GMPE) requires determination of regional characteristics of the radiation and propagation of seismic waves, in particular, the quality factor of the lithosphere.

This work is devoted to determination of the quality factor and its frequency dependence for the Lena Delta, one of the key areas of the Laptev Sea region, the most seismically active of all Arctic marine regions of Russia. For this purpose, the coda normalization method was used in relation to signals from 5 microearthquakes with Ml > 2, recorded by a temporary local network of seismographs operating in the Lena Delta in 2016-2017.

Regional values of quality factor Q = 486±42 were obtained. The scatter of values is probably due to the anisotropy of the environment in the study area. The dependence of the quality factor on frequency is described by the found function $Q(f) = 84.328f^{0.8128}$. The exponent in this relationship is comparable to the values typical for regions of Mexico, Australia and Canada.

Keywords: quality factor of the lithosphere, Laptev Sea region, Lena Delta, seismic hazard assessment

INTRODUCTION

To assess seismic hazard and further earthquake-resistant construction, it is necessary to determine the parameters of ground motions during possible strong earthquakes. Typically, so-called ground motion prediction equations (GMPE) are developed using regression methods based on some strong motion database [1].

Strong motion databases are specific for different regions. The volume of strong motion records accumulated to date around the world has revealed significant (up to 10-15 times) regional differences in peak ground accelerations at a fixed magnitude and distance, due to regional differences in the properties of the sources and the propagation medium of seismic waves [2-3]. At the same time, in many seismically active regions of Russia, due to their remoteness, inaccessibility and harsh climatic conditions, there are practically no records of strong motions, which significantly complicates the correct assessment of seismic hazard. In this case, a different approach is used to develop GMPE – determination of the regional characteristics of radiation and propagation of seismic waves, primarily the quality factor of the lithosphere [1].

https://doi.org/10.5593/sgem2024/1.1/s05.59

One of such little-studied seismically active regions of Russia is the Laptev Sea region. In this work, to assess the quality factor of the crust and upper mantle Q of the Lena Delta region we have used the coda normalization method, developed and described in [3-7]. This method does not require assumptions about either the features of frequency dependence Q(f) or the focal spectrum.

MATERIALS AND METHODS

The quality factor Q is estimated independently in several frequency intervals. The spectral amplitudes of coda waves can be represented as:

$$A_i^c = E_i^c(f)G^c(f)D(f,t) \quad (1)$$

where D(f,t) characterizes the change in the intensity of coda waves over time and does not depend on both the source-receiver distance and direction, and the effects of the source $E_i^c(f)$ and the receiver $G^c(f)$ do not depend on the direction to the receiver [3]. This empirical conclusion can be explained by taking into account that coda waves are waves scattered by randomly distributed irregularities [6].

When estimating Q(f), it is necessary to make an assumption about the form of the geometric spreading function. These dependencies describe path effects by the formula [8]:

$$P(r,f) = Z(r)\exp[-\pi fr/Q(f)v] \quad (2)$$

where r is the epicentral distance, v is the velocity of transverse waves, Z(r) is a function describing the geometric spreading. Quite often it takes the form of a three-segment function [8-9]. For our calculations, we accepted the following geometric spreading function, shown in Figure 1: 1/r from 1 to 70 km, 1/70 from 70 to 130 km and $(130/r)^{0.5}/70$ at distances greater than 130 km [8].

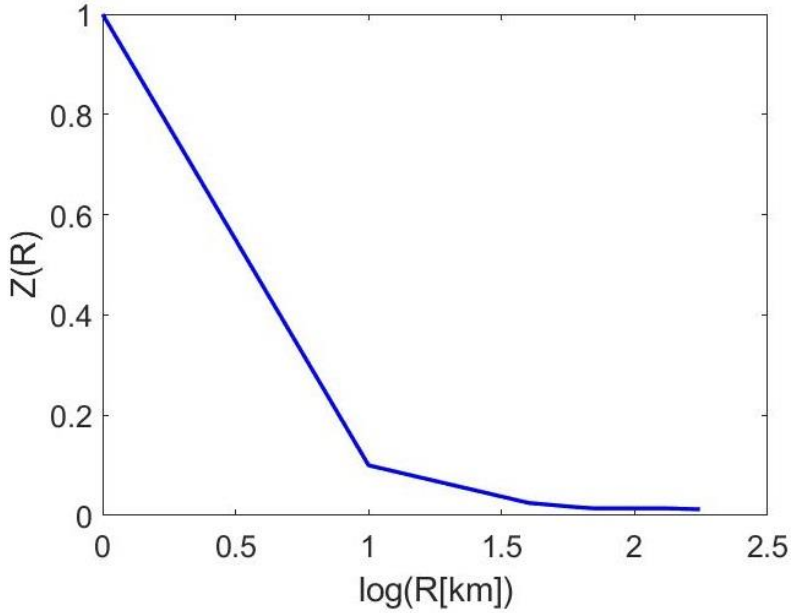


Figure 1. Geometric spreading function adopted for calculations when determining the quality factor of the lithosphere in the Lena Delta area.

To determine the quality factor of the environment, records of earthquakes with magnitude Ml > 2 that occurred in the vicinity of the Lena Delta were used (Figure 2). The records were obtained by a network of temporary autonomous seismic stations that operated in the Lena Delta in 2016-2017.

Recordings of earthquakes obtained by 13 seismographs were used, with a high signal-to-noise ratio on all instruments. The range of epicentral distances was 60-175 km. The recordings of the codas of these seismic events were not complicated by signals from other earthquakes following the main shock. This is very important when using the coda normalization method to determine the quality factor.

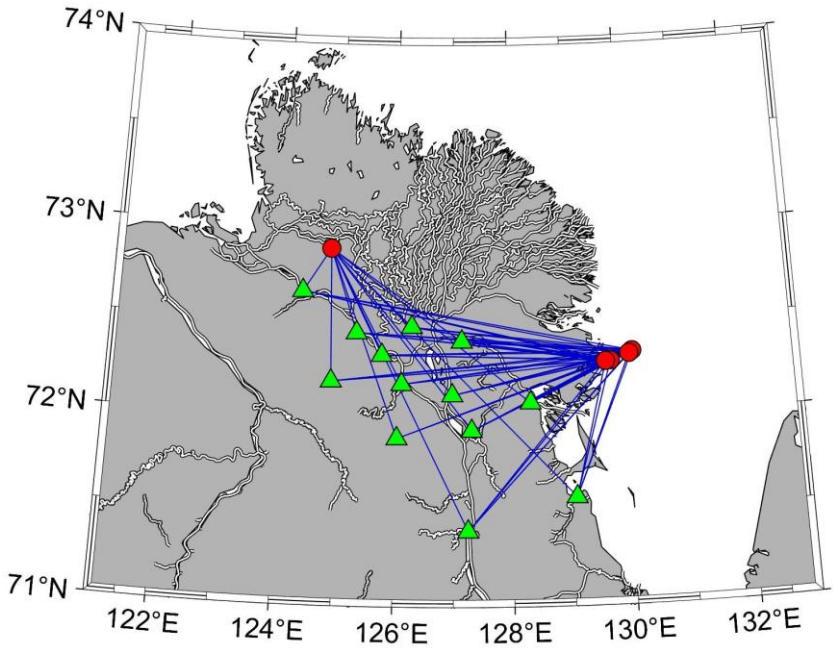


Figure 2. Positions of seismographs (green triangles) and earthquake sources (red circles), records of which were used to determine the quality factor of the crust in the Lena Delta vicinity. Blue lines are the traces of seismic rays from sources to seismographs.

At the first stage of processing, records of earthquakes were used without bandpass filtering. All of these earthquakes have a spectrum maximum at a frequency of about 8 Hz (Figure 3), so the quality factor of the crust in this case is determined for a frequency close to the dominant frequency of these seismic signals.

At the second stage, the quality factor Q was assessed independently in several frequency intervals. To obtain data on the frequency dependence of the quality factor, records of the earthquake were used that occurred on 2016-11-05 at 06:25 (UTC) with a source depth of 17 km and a magnitude of 2.4.

Seismograms of this earthquake obtained by seismograph 30 are shown in Figure 4. Here, the upper trace is the record of the west-east component of horizontal seismograph 30. Below are the traces obtained as a result of filtering using Butterworth bandpass filters with the central frequencies indicated in Figure 4 above each trace

https://doi.org/10.5593/sgem2024/1.1/s05.59

(2,4,8,12,16,20 Hz). The filter bandwidth was ±0.5 Hz for each center frequency, and the Butterworth filter order was 10.

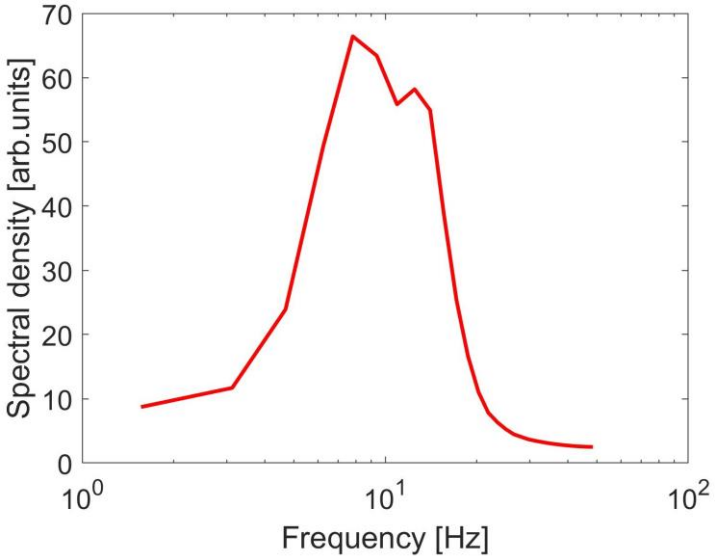


Figure 3. An example of a smoothed signal spectrum of the earthquake with magnitude M = 2.4 that occurred on 2016-11-05 at 6:25 (UTC).

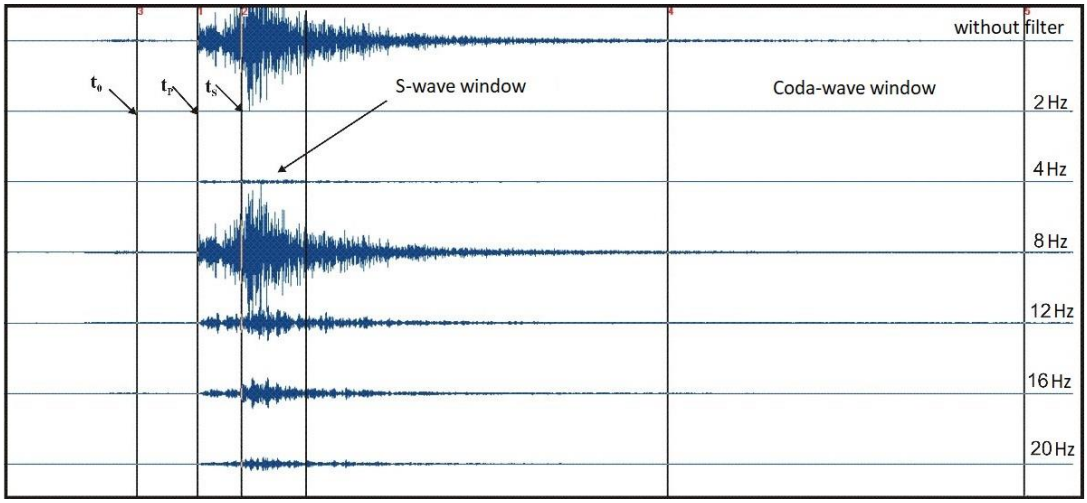


Figure 4. Seismograms of an earthquake with magnitude M = 2.4 that occurred on 2016-11-05 at 6:25 (UTC), obtained by seismograph 30 and filtered by different bandpass filters.

The dependences of the logarithms of the ratios of the spectral S-wave amplitudes, corrected for the geometric spreading function, to the spectral amplitudes of the coda waves on the source-receiver distance r were obtained for all seismic stations and all 5 earthquakes:

$$\ln\{A_i(f)/[Z(r)A_i^c(f,t_0)]\} \quad (3)$$

The spectra of S-waves were calculated in 10-second intervals starting at the moments of their arrival, then the root-mean-square value of their spectral density was determined. The coda spectra of the earthquake signal were determined in 60-second

time windows with the beginning after 90 seconds from the time at the source according to the recommendations from [10]. Then the spectra of the coda were determined in exactly the same way, and the root mean square values of the spectral density were calculated.

RESULTS AND DISCUSSION

As can be seen from Figure 5, the dependence described by formula (3) is approximated by a linear function determined by the least squares method with high coefficients of determination, which indicates the applicability of the coda normalization method for analyzing data from these stations. The slope of these linear dependencies b gives an estimate of the quality factor Q in the crust of the Lena Delta and in the southern Laptev Sea [11]. The following formula is used:

$$Q = \pi f / b V_S \quad (4)$$

where V_S is the speed of S-waves in km, f is the signal frequency in Hz, b is the slope.

The average quality factor obtained is Q=486±42. Perhaps the scatter of values is influenced by the anisotropy of the environment in the study area.

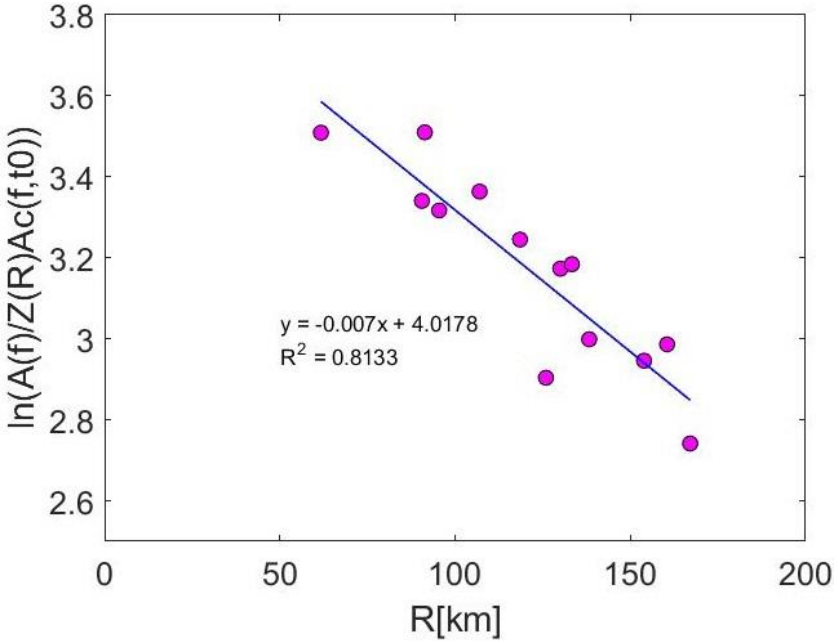


Figure 5. An example of the dependence of the logarithms of the ratios of S-wave amplitudes, corrected for the geometric spreading function, to the coda wave amplitudes on the source-receiver distance r for all seismic stations.

After this, graphs similar to those shown in Figure 5, were obtained for different stations and different frequency ranges using formula (3). For all frequencies, these dependences were approximated by linear functions determined using the least squares method. The quality factor for different frequencies was determined by formula (4). Figure 6 shows the dependence of the quality factor on frequency for the Lena Delta region, constructed on the basis of records of the earthquake occurred on 2016-11-05 at 6:25 (UTC) with its epicenter in the Buor-Khaya Gulf, Laptev Sea.

https://doi.org/10.5593/sgem2024/1.1/s05.59

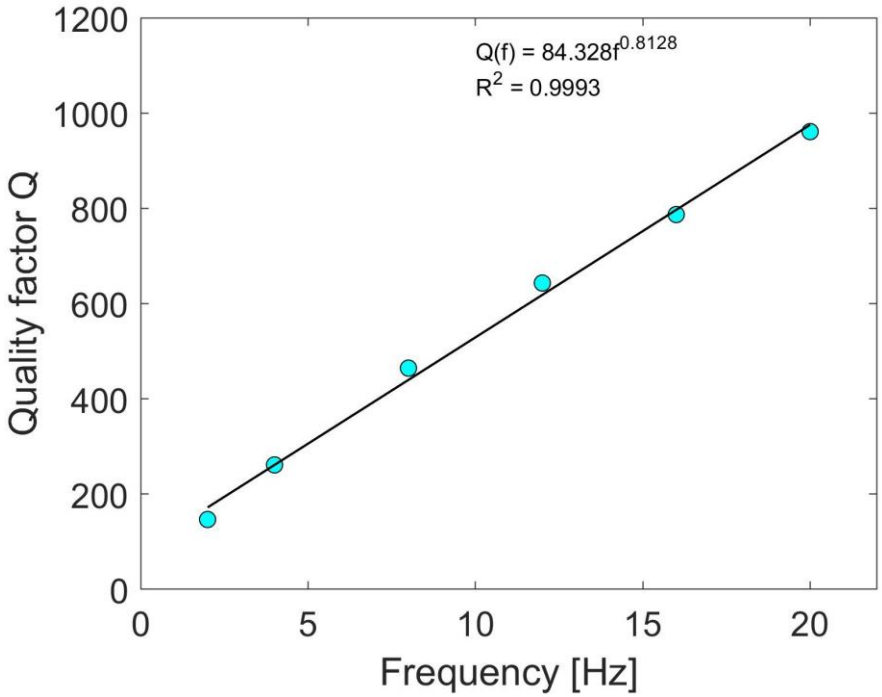


Figure 6. Dependence of the quality factor on frequency for the Lena Delta region with an approximating power function.

It should be noted that the quality factor obtained for a frequency of 8 Hz is close to the average quality factor obtained from records of several earthquakes. According to [10], the power depending on the quality factor varies from ~0.4 to ~1. In the crust of the Lena Delta, the quality factor depends on frequency to a power of the order of 0.81 (see Figure 6), which, according to [10], is close to this parameter in the regions of Mexico, Australia and Canada.

CONCLUSION

The Laptev Sea region, in general, and the Lena Delta, in particular, are seismically active, but little studied from the point of view of seismic hazard assessment. To develop regional GMPE, it is necessary to determine the regional value of the lithosphere quality factor and the features of its frequency dependence.

As a result of processing records of a temporary local network of seismographs in the Lena Delta, the 5 most powerful recorded microearthquakes with magnitude Ml > 2 were selected. By the coda normalization method using signals from these earthquakes, regional quality factor values Q = 486 ± 42 were obtained. The scatter of values is probably due to the anisotropy of the environment in the study area. The dependence of the quality factor on frequency is described by the found function $Q(f) = 84.328f^{0.8128}$. The exponent in this relationship is comparable to the values typical for regions of Mexico, Australia and Canada.

ACKNOWLEDGEMENTS

This work was financially supported by the Russian Science Foundation, project no. 23-17-00125 (determination of the quality factor of the lithosphere of the Lena Delta), the

Russian State Assignment, project no. FMWE-2024-0018 (routine processing of seismograms: earthquakes signals search, magnitude determination and localization).

REFERENCES

[1] Pavlenko V.A., Pavlenko O.V., Stochastic Simulation and Development of the Ground Motion Prediction Equation for the Baikal Rift Zone, Izv., Phys. Solid Earth, Vol. 59, pp. 29–40, 2023. DOI: 10.1134/S1069351323010032.

[2] Pavlenko O.V., Regional differences in the characteristics of seismic wave emission and propagation in Kamchatka and the Northern Caucasus, Dokl. Earth Sc., Vol. 438, pp. 846–852, 2011. DOI: 10.1134/S1028334X11060225.

[3] Pavlenko O.V., Seismic Wave Absorption in the Eastern Part of the North Caucasus Estimated from Records by Seismic Station “Makhachkala”, Izv., Phys. Solid Earth, Vol. 56, pp. 635–643, 2020. DOI: 10.1134/S1069351320050079.

[4] Aki K., Chouet B., Origin of codawaves: source, attenuation and scattering effects, Journ. Geophys. Res., Vol. 80, pp. 3322–3342, 1975.

[5] Rautian T.G., Khalturin V.I., Martynov V.G., Molnar P., Preliminary analysis of the spectral content of P and S waves from local earthquakes in the Garm, Tajikistan region, Bull. Seism. Soc. Am., Vol. 68, № 4, pp. 949–971, 1978.

[6] Aki K., Attenuation of shear waves in the lithosphere for frequencies from 0.05 to 25 Hz, Phys. Earth Planet. Interiors, Vol. 21, № 1, pp. 50–60, 1980a.

[7] Kromskii S.D., Pavlenko O.V., Gabsatarova I.P., Features of Radiation and Propagation of Seismic Waves in the Northern Caucasus: Manifestations in Regional Coda, Izv., Phys. Solid Earth, Vol. 54, pp. 222–232, 2018. DOI: 10.1134/S1069351318020106.

[8] Boore D.M., Simulation of Ground Motion Using the Stochastic Method, Pure Appl. Geoph., Vol. 160, pp. 635–676, 2003.

[9] Gusev A.A., Shumilina L.S., Modeling the intensity-magnitude-distance relation based on the concept of an incoherent extended earthquake source, Volc. Seis., Vol. 21, pp. 443-463, 2000.

[10] Havskov J., Ottemoller L., Routine data processing in earthquake seismology with sample data, exercises and software. Springer Science+Business Media B.V. 2010.

[11] Aki K., Scattering and attenuation of shear waves in the lithosphere, J. Geophys. Res., Vol. 85, pp. 6496–6504, 1980b.

https://doi.org/10.5593/sgem2024/1.1/s05.59

ASSESSMENT OF GEOPHYSICAL DATASET IN THE CENTRAL SEGMENT OF THE SOUTHERN CARPATHIANS ROMANIA

Dr. Natalia-Silvia Asimopolos[1]

Dr. Laurentiu Asimopolos[1]

Asist. Prof. Adrian-Aristide Asimopoos[2]

[1] Geological Institute of Romania, 1 Caransebes Str., 012271 - Bucharest, **Romania**
[2] National University for Science and Technology POLITEHNICA of Bucharest, Faculty of Transports, 313 Splaiul Independentei, 060042 - Bucharest, **Romania**.

ABSTRACT

In this work, I used the data from the geophysics portal of the Geological Institute of Romania (maps, sections), field measurements as well as the WGM 2012 model from the International Gravimetric Bureau. The measurements carried out in the south of the Southern Carpathians were represented by magnetometric measurements. Corroboration of geophysical information with geological and tectonic ones led to the confirmation of deep structures. The geological sources, which give geophysical samples specific to each geophysical method, are characterized differently depending on their size, depth, density contrast and magnetic properties. We filtered the geophysical data, using moving averaging and the calculation of trend surfaces, thus deciphering the depth of the geological sources, taking into account the depth of investigation of each geophysical method. Within these filters, we used moving windows of different linear (1D), rectangular (2D) and paralelipiped (3D) dimensions. I calculated the coefficients of the trend surfaces for different degrees of the polynomial, so that comparisons could be made between the results obtained through different types of filters and the analytical extensions in the upper half-space (with the Laplace equation) and the lower half-space (with the Poison equation). We also used the Pearson correlation coefficient, in moving windows of different sizes. The data obtained from the digitization of maps regarding the depth of the Conrad and Moho surfaces, as well as those of the geoid and quasi-geoid, represented valuable information in the study of deep tectonics in the study area.

Keywords: Geophysical data, Data smoothing and filtering, Deep geological structures, Southern Carpathians.

INTRODUCTION

In order to corroborate the geological information with the geophysical ones, it is important to use filtered data according to the depth of investigation of each geophysical method. Thus, gravimetric anomalies measure the density contrast from depths that exceed the Moho surface to the surface, and geological sources have different shapes and extents from local to regional. Magnetic anomalies measure the contrast of magnetic properties from sources located at the depth of the Curie surface (where the magnetic properties become zero) and up to the surface. So, the smoothing and filtering of these two types of anomalies is absolutely necessary, in order to separate the effects of deep geological sources from the effect of geological sources on the surface. Only by using the

https://doi.org/10.5593/sgem2024/1.1/s05.591

filtered data can we get the correct input data in the interactive modeling programs (for example: Geomodeler software).

METHODOLOGIES

Gravimetric anomalies sum up the effect of all sources, from depth to the surface, with different intensities and extents. For this reason, data filtering is a mandatory step in the interpretation of information.

Thus, the methods used in this work for which we developed the necessary calculation software (for moving averages and polynomial trend surfaces) have proven their usefulness, confirming and completing the information obtained through the analytical extension in the upper half-space and the lower half-space, presented in many works [1,3,4,5,10].

Polynomial trend surface analysis or regression analysis uses the least squares test. After calculating the coefficients of the polynomial we choose for different degrees, we establish the equation that establishes the trend of the measured values. The difference between the values calculated in the grid nodes and the measured values represents the residual values, which represent the geophysical effect given by the surface geological sources with local extension.

The calculation of the trend surface values, in the nodes of the interpolation grid, represents the geophysical effect of the deep and regional geological sources. Bandpass filtering was performed by subtracting the values of a lower-order trend surface from the values of the higher-order trend surface at each node of the grid.

If we use a mathematical function with one dependent variable (geophysical parameter) and two independent variables (latitude and longitude), we obtain the values of the geophysical parameter in the surface, which can be interpolated (using the Golden Surfer program). If we use a mathematical function with a dependent variable (geophysical parameter) and three independent variables (latitude, longitude and depth), we obtain the values of the geophysical parameter in 3D volume, which gives us the possibility of extracting many 2D sections that serve in the interpretation.

GEOLOGICAL AND GEOPHYSICAL SETTINGS

The relief of the Southern Carpathians has the highest altitudes in the Carpathian Mountains on the territory of Romania, exceeding 2500m (Moldoveanu 2541m, Negoiu 2535m, Omu 2509m), having an east-west orientation. The massive appearance of the relief is the result of the erosion of glaciers during the Ice Age, the main landforms being glacial cirques and glacial valleys.

A characteristic is the small number of depressions, and the main valleys that fragment the hard rocks are the rivers Olt and Jiu (Figure 1 and Figure 2).

The hydromineral deposits are mainly sulphurously and chloro-sodic, having the hydrogeological conditions of the Getic Depression. Mineral waters favored the development of spa resorts in the Oltului Valley (Govora, Căciulata, Călimănești, Olănești), [2, 6, 7, 8]. From a tectonic point of view, it is dominated by the IntraMoesic

fault, a seismically active fault, responsible for shallow / medium depth earthquakes and landslides in the Făgăraș Massif area.

Longitudinal faults affect the southern flanks of the Southern Carpathians and alternate with a series of NE-SW faults.

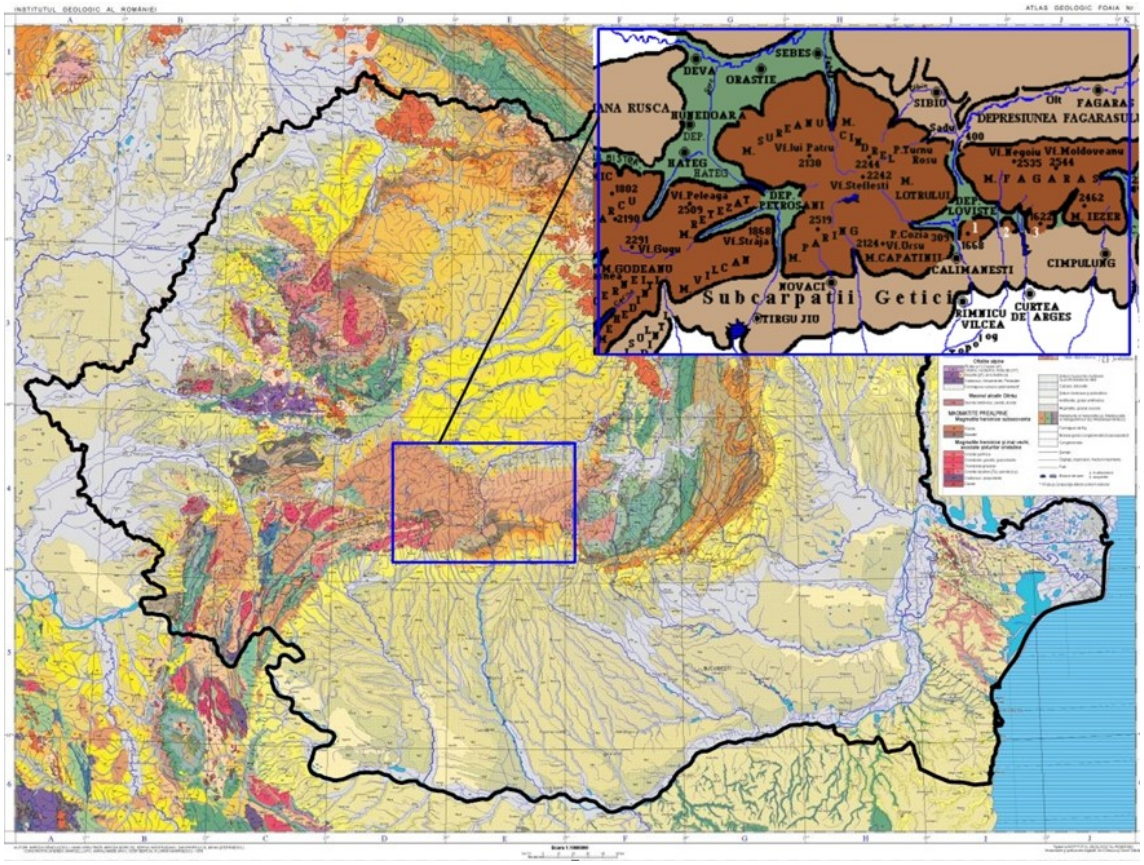


Figure 1 - Geological map of Romania, scale:1:1000000 (https://www.igr.ro) and central segment of the Southern Carpathians marked in a rectangle

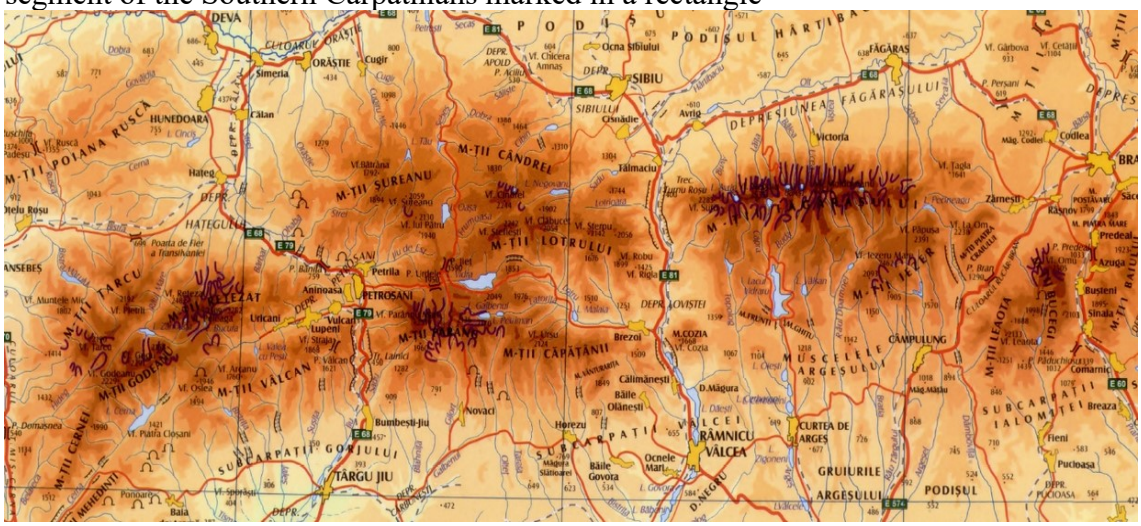


Figure 2 - Extracted from geological maps scale 1:200000, with mountains from the central segment of the Southern Carpathians. The four sectors of the Southern Carpathians: Bucegi, Făgăraş, Parâng and Retezat-Godeanu mountains.

https://doi.org/10.5593/sgem2024/1.1/s05.591

GEOPHYSICAL MAPS

Numerical developments about geophysical parameters provide us with information with different degrees of regionality and from different depths, which of course cannot be quantified until all the geological and geophysical information has been corroborated. These filters can bring both information about local and surface effects (residual maps, through "high pass" filters), mid-depth structures (through "band pass" filters), and deep structure (tendency maps, through "low pass" filter).

There are various methods for achieving separation of geophysical anomalies such as analytical expressions of the polynomial trends based on the least squares' method, highlighting the regional trend caused by the deep structures. Calculating the residual values resulting from the difference between the initial values and the trend values from the network nodes used, we can highlight the superficial local effects. Also, we can obtain information about the regional trend caused by geological structures at medium and large depths, by calculating the difference between geophysical parameters, obtained with different moving average windows or tendency surfaces with different degrees, interpolated in same network. The maps in Figures 1-4 were made using Surfer software, based on gravimetric data (Bouguer anomaly, Free Air anomaly, isostatic anomaly and gravity disturbance) available on the International Gravimetric Bureau website [10] and maps / data from the GIR geophysics portal [9].

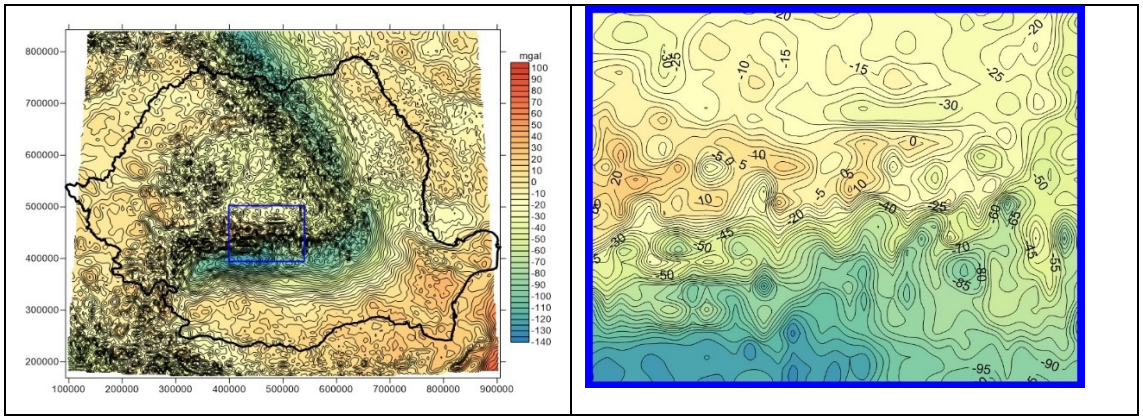


Figure 3 – Bouguer anomaly (left: in Romania, right: selected zone in Southern Carpathians) (after data from https://bgi.obs-mip.fr/)

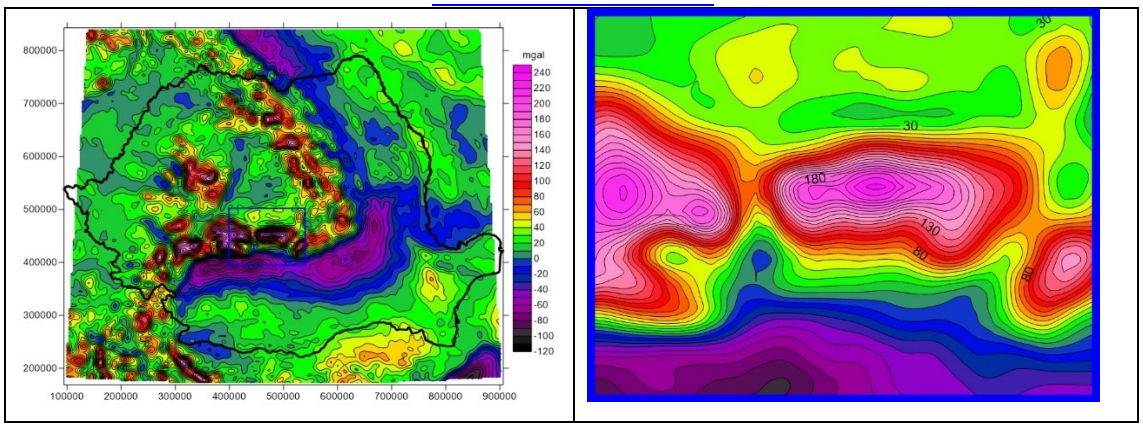


Figure 4 – Free Air anomaly (left: in Romania, right: selected zone in Southern Carpathians) (after data from https://bgi.obs-mip.fr/)

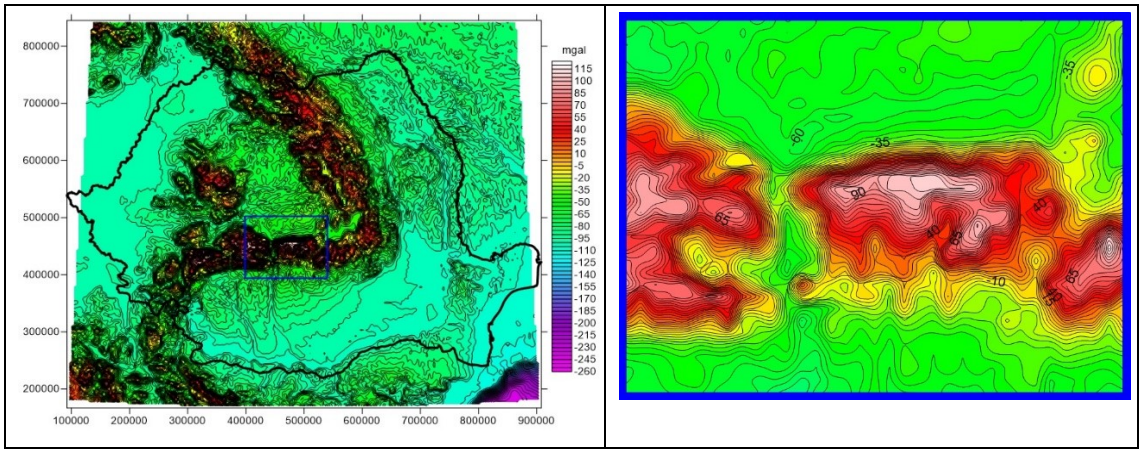


Figure 5 – Gravity disturbances anomaly (left: in Romania, right: selected zone in Southern Carpathians) (after data from https://bgi.obs-mip.fr/)

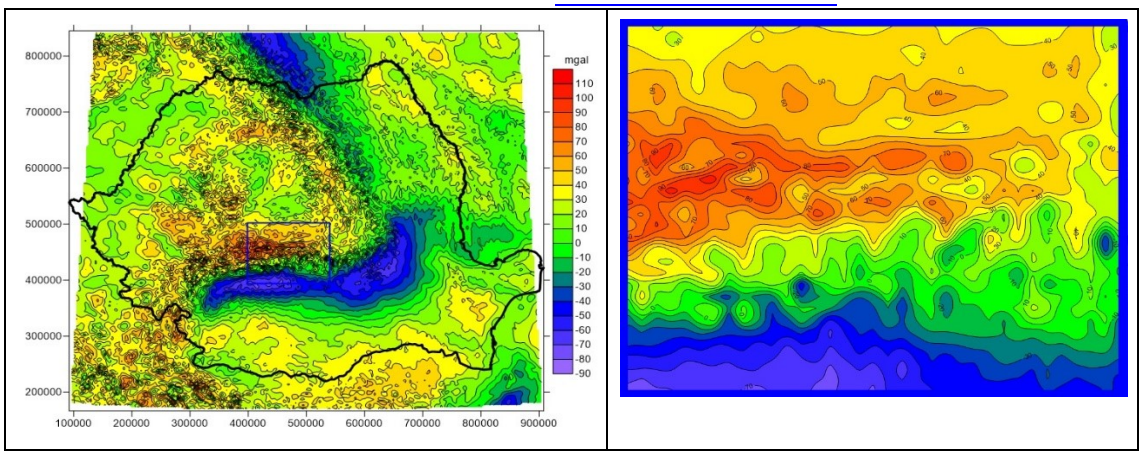


Figure 6 – Isostatic anomaly (left: in Romania, right: selected zone in Southern Carpathians) (after data from https://bgi.obs-mip.fr/)

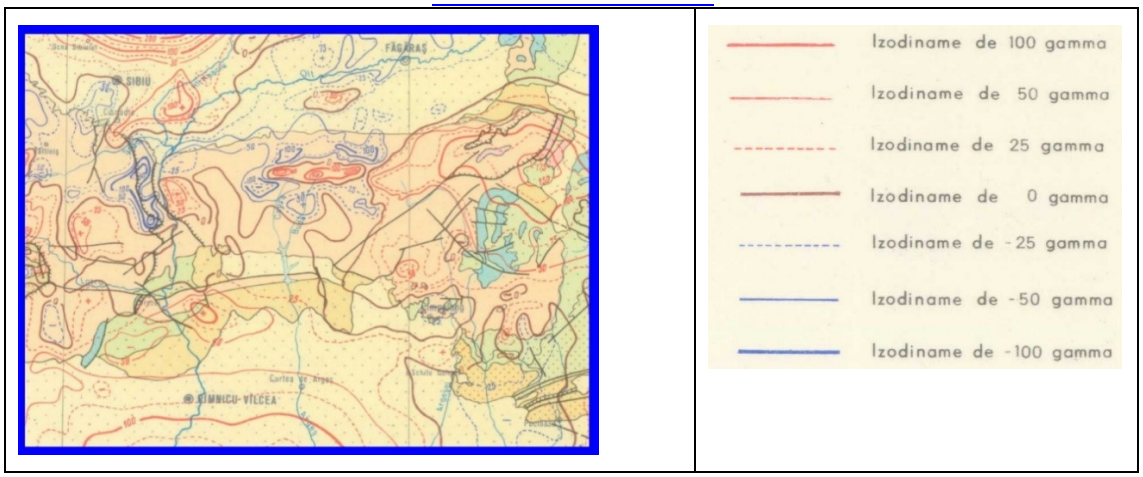


Figure 7 – Vertical magnetic field anomaly Δ Za (after data measured and magnetic map)

https://doi.org/10.5593/sgem2024/1.1/s05.591



Figure 8 – Vertical magnetic field Δ Z (after data measured and magnetic map)

The construction of the maps of the vertical component of the geomagnetic field (figure 5 and figure 6) was performed based on the data contained in the existing measurement summaries at Geological Institute of Romania [9]. These registers contain the geographical coordinates of the measuring points, the values of the vertical component recorded at the base stations of the network where the measurements were made, the values of the vertical component recorded at each point of the network and the corrected values of the reduced vertical component for 1967,5.

The calculated values of the ΔZ anomaly are also found in these registers. The values used in the variation maps of the vertical component of the magnetic field are those reduced at that time and those of the variation of the Z component uncorrected for the secular variation (transmitted Z). The value of the ΔZ anomaly is calculated by applying a normal field correction to the value of the vertical component of the geomagnetic field. The normal field correction represents the subtraction from the reduced value at a certain epoch at a certain point, of the normal value of the field at that epoch. The value of this correction corresponds to the variation with the latitude of the vertical component and represents the difference between the values recorded at a given time between the component recorded at Surlari and the one recorded at that station at that time, after both values were applied. secular.

It should be noted that the data contained in these summaries are not evenly distributed and the number of values is variable (between 600 and 1800 measurements on a 1: 200000 map sheet). There are areas with a high density of measurement points (in areas of interest at the time of prospecting, in valleys and in areas with accessible relief) but also areas with very poor coverage (in areas of low interest and in areas with heavy relief accessible. Such an inhomogeneous distribution can create problems in choosing the most appropriate form of interpolation network. The resulting data were interpolated by the kriging method using the Surfer program using a quadratic interpolation network.

The maps of magnetic anomalies (ΔZ and ΔZa) show that the bodies with high magnetic sensitivity that generate the anomalies are in the superficial geological environment, extending in depth. Positive anomalies coincide with fault zones.

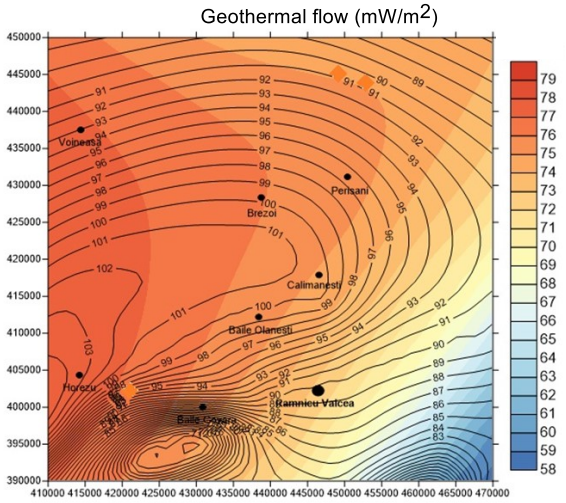


Figure 9 - Map with temperature isolines at a depth of 3000m, expressed in degrees Celsius superimposed over the geothermal flow map in mW/m2, expressed in color shades (in legend)

CONCLUSION

The necessary steps for filtering the geophysical data and entering them into the modeling programs are as follows:

- Bringing available geodetic and gravimetric data taken from various sources to the same format, coordinate system and grid network.

- Digitization of tectonic elements and inclusion of results in geodetic and gravimetric data files, function of coordinates and depths.

- Development of calculation procedures and their application in numerical applications regarding moving averaging with various windows, calculation of analytical expressions of trend surfaces and hypersurfaces, calculation of variation of correlation coefficient with various moving windows for multiparametric datasets.

- Realization of models, analytical continuations, filtering, correlations, spectral and wavelet analyses in case studies.

Geophysical data must be filtered according to the depth of the model we want to achieve. In the geological models after geophysical data, we need to use geophysical data appropriate to the depth we are calculating.

For a surface to small depth model, we need to enter the residual data (the difference between the data recorded at the surface and the data calculated as a trend for the cumulative effect of the anomaly). Trending surfaces with higher degree reflect a lower depth and trending surfaces with lower degree reflect a higher depth. As the depth of the model increases, the filtered data with different windows must be entered, going to the regional models and very deep to the trending surfaces and the limit case for the largest depth is given by the regional trend plan.

The Bouguer anomaly and its residual reflect the effect of geological structures extending from the surface to great depths, which corresponds to a low density of sedimentary deposits. These suggest thick geological bodies that extend from depth to the surface. The

https://doi.org/10.5593/sgem2024/1.1/s05.591

strong negative anomaly southwards correspond to the folded and thickened crust of the Carpathian Orogen, which reflects the low density of sedimentary deposits.

The strong positive anomalies of intra-mountain basins system reflect the presence of high-density geological structures extending close to the surface.

The map with temperature isolines at a depth of 3000m, expressed in degrees Celsius superimposed over the geothermal flow map in mW/m2, (figure 9) gradually indicates the areas with geothermal potential, by the correlation of the two parameters (temperature isolines at a depth of 3000m, geothermal flow).

ACKNOWLEDGEMENTS

We thanks to BGI [https://bgi.obs-mip.fr/] for possibility to use gravimetric data and UEFISCDI Romania for financing of projects: "The realization of 3D geological / geophysical models for the characterization of some areas of economic and scientific interest in Romania" and "Artificial Intelligence and Combined Survey Techniques for Stone Quarries- AI-COSTSQO", with contract no 305/2022.

REFERENCES

[1] N.S. Asimopolos., L. Asimopolos – 2017 - Separation of gravimetric anomalies with different degrees of regionality – "Oltenia. Studii si comunicari. Stiintele Naturii", Tom 33, vol.2, pag. 27-34

[2] L.M. Blaga, M. Florian – 1984 - Contribuţii la studiul hidrogeologic al zăcământului hidromineral Olăneşti cu ajutorul izotopilor stabili, St. tehn. econ. Inst. Geol. Geof., Seria E, 14, p. 63-84, Inst. Geol. Geof., Bucureşti.

[3] J.Y. Cruz, P. Laskowski – 1984 – Upward continuation of surface gravity anomalies – Reports of the Department of Geodetic Science and Surveying – Report No. 360 – The Ohio State University, 119pp.

[4] M. Kern – 2003 - An Analysis of the Combination and Downward Continuation of Satellite, Airborne and Terrestrial Gravity Data – UCGE Reports, No.20172 – Department of Geomatics Engineering, University of Calgary, 193pp.

[5] J. Huang, M. Sideris, P. Vaníček, I. Tziavos – 2003 - Numerical Investigation of Downward Continuation Techniques for Gravity Anomalies. Bollettino di Geodesia e Scienze Affini. 62., 18pp.

[6] A. Pricajan – 1972 - Mineral and thermal waters in Romania (in Romanian), Ed. Tehnică, Bucharest.

[7] A.M. Roanghes-Mureanu – 2012 - The Environmental Impact of Tourist Activities Performed in the Spa Resorts of Vâlcea Subcarpathians, Analele Univ. Buc., Geografie, LXI, 147-157.

[8] A.M. Roanghes-Mureanu – 2013 - The impact of tourism on the environment in the drainage Basin of the Olănești river, Riscuri şi catastrofe, nr. XII, vol.13, nr.2/2013.

[9] https://www.igr.ro

[10] https://bgi.obs-mip.fr/

DETERMINATION OF DEPTH PARAMETERS OF SUBSURFACE VOIDS USING GRAVIMETRIC AND GLOBAL NAVIGATION SATELITTE SYSTEMS MEASUREMENTS

PhD Eng. Severina Djorova[1]

Eng. Maria Nikolova[1]

[1] University of Architecture, Civil Engineering and Geodesy, Faculty of Geodesy, Sofia, **Bulgaria**

ABSTRACT

The main focus of the research is to investigate the application and effectiveness of gravimetry in cave detection, as well as in the determination the depth parameters of already localized subsurface voids. For this purpose, combined gravimetric and Global Navigation Satellite Systems (GNSS) measurements were used. Establishing the location of missing anomalous masses in the earth layers has always been of great interest to geologists, geomorphologists and speleologists. Over the years, geophysical methods, especially gravimetry, have gained significant prominence as powerful tools for identifying density variations and gravity anomalies associated with subsurface voids. A natural karst phenomenon on the territory of Bulgaria was chosen as the object of the study. The measurements performed and the processing of the results obtained are described in detail. The necessary corrections were applied, maps of the Bouguer anomalies and the local anomalies were drawn, and the data obtained were analyzed. The results are illustrated with appropriate graphs and tables.

Overall, the research has successfully proved the power of gravimetry as a tool for detection, cave exploration and determination of depth parameters, offering valuable applications in various subsurface features and geological phenomena. The applied technique could play a crucial role in identifying potential land hazards and instability, facilitating informed decisions and helping to take appropriate mitigation measures.

Keywords: gravimetry, gravity measurements, caves detection, Bouguer anomaly

INTRODUCTION

Over the past few decades, gravimetric measurements, among other geophysical methods, have proven highly effective in detecting subsurface anomalies, including cavities, salt deposits, chromite deposits, karst structures, etc.

In 1964, Raymundo Chico described the fundamental principle for detecting underground cavities based on gravimetric measurements. In his article [5], he noted that the key to interpretation lies in the density contrast between the underground cavity and its surrounding rocks. Air-filled cavities are known to have a density of 0 g/cm³, water-filled cavities have a density of 1 g/cm³, and the internationally accepted average density of the Earth's crust is 2.67 g/cm³. This density difference is clearly distinguishable on

https://doi.org/10.5593/sgem2024/1.1/s05.60

gravimetric maps, such as free-air anomaly maps and Bouguer anomaly maps, obtained from gravimetric measurements.

In 1984, Dwain Butler published his study on geophysical methodologies for detecting and delineating subsurface voids [2]. The research began in 1976 and was carried out in three phases:

- Assessment of geophysical methods for cavity detection at a man-made cavity test site;
- Assessment of geophysical methods for cavity detection at a shallow air-filled, natural cavity test site (~10m depth);
- Assessment of the most promising geophysical methods, identified in phase 2, at a deeper, waterfilled cavity test site(~30m depth);

The conclusion of the study indicated that for locating and determining the position of shallow cavities, gravimetric methods are the most promising field approach [2].

Since then, the accuracy of gravimetric instruments has improved, the influence of external factors has been reduced, and the topic remains highly relevant. In recent years, research has focused on combining gravimetric measurements with other geophysical methods to obtain the most comprehensive information about the location and characteristics of the study object.

In the article " Combined microgravity, electrical resistivity tomography and induced polarization to detect deeply buried caves: Algaidilla cave (Southern Spain)." [3], the feasibility of combining these methods for locating and characterizing karst caves deeper than 30 meters is discussed. It concludes that gravimetric measurements are a powerful tool for cave detecting, and applying Electrical Resistance Tomography (ERT) and Induced Polarization (IP) provides more accurate determination of the cave's geometry.

In 2006, the article "Using of gradient techniques for depth estimation of gravity source" [1] discusses a new method for determining the depth of a gravity source based on horizontal and vertical gradients. The horizontal and vertical gradients of each gravity anomaly profile intersect at three points. It is noted that the distance from the nearest point to the center of the gravity anomaly correlates with the depth of the anomalous body. Two relationships are presented for sources of anomalous fields approximated to spherical and horizontal cylindrical bodies. The proposed method was applied to determine the depth of the source in four cases with well-known depths of the disturbing body. The results showed errors ranging from 5% to 14% in depth estimation. The article highlights that the calculated depth value is always less than the actual depth, which may be due to considering the gravity anomaly before separating local from regional anomaly [1].

The current study examines methods for interpreting gravimetric data in combination with Global Navigation Satellite Systems (GNSS). The main focus of the research is on locating and determining the depth of the longest cave tunnel in Bulgaria – Prohodna Cave, located in Karlukovo village, Lukovit municipality.

METHODS

The study can be divided into several stages: measurements planning, field work, preliminary data processing, calculating the gravity acceleration at each point, graphical

presentation of the obtained results, determining the numerical characteristics of the considered object, and analyzing data and deriving conclusions.

- **Measurement planning**

During this phase, the essential initial data (such as maps and information on reference absolute gravimetric points) for the study area are collected. Subsequently, the scope of the investigation is delineated, and the position of the gravimetric stations is projected on the map.

A gravimetric point with a known value of gravitational acceleration located in the village of Yablanitsa, Yablanitsa municipality, approximately 20 kilometers from the Prohodna cave, was chosen as the starting point for the planned relative gravimetric measurements.

A total of 40 points were designed, distributed across four profiles, with an average distance of 20 meters between the points. The positioning of the points was strategized to align with the unique form of the cave tunnel, ensuring optimal adaptation to its shape and features.

- **Making the measurements**

The projected locations for gravimetric measurements were previously traced using GNSS measurements. An important focus in this case is the determination of the geodetic height, i.e. a method for its determination should be chosen to ensure a minimum relative accuracy of 5 centimeteres [6]. A quick and efficient method is to trace and capture the profile points using RTK method with own user station connected to the BGS2005 coordinate system (ETRS89, ETRF2000, epoch 2005 and DATUM GRS80).

For the gravimetric observation, classical wide-range "LaCoste & Romberg" model G gravimeter was used. Its precision of 0.04 mGal fully meets the objectives of the study. The measurements were realized in the current gravimetric reference system IGSN-71 by connecting to a starting point of the State Gravimetric Network of Bulgaria [4].

- **Preliminary data processing**

A series of corrections have been applied to the gravity observations to minimize the influence of external factors. The original gravimetric readings have been converted into milligals, and corrections for tidal effects, instrument height, and atmospheric conditions have been applied. Finally, the zero-point drift has been calculated to compensate for residual factors.

- **Determining the gravitational acceleration at the gravity stations**

The calculated adjusted readings were used to compute differences in gravity acceleration. The gravity acceleration value was determined for each of the gravity stations. Free - air and Bouguer anomalies were calculated.

- **Graphical presentation of the obtained results**

Gravimetric maps have been created, including a free-air anomalies map (Fig. 2) and another Bouguer anomalies map (Fig. 3). These maps serve for qualitative analysis and interpretation of the collected gravimetric data.

- **Depth estimation**

https://doi.org/10.5593/sgem2024/1.1/s05.60

To determine the depth, the so-called Half-Width Method of the anomaly has been applied, theoretically discussed in [7]. By definition, the half-width of the anomaly $x_{1/2}$ represents the horizontal distance from the maximum anomaly to the point where the anomaly reaches half of its maximum value. A graphs (Fig. 1) have been generated, depicting a vertical cross-sections of the acquired Bouguer anomaly values.

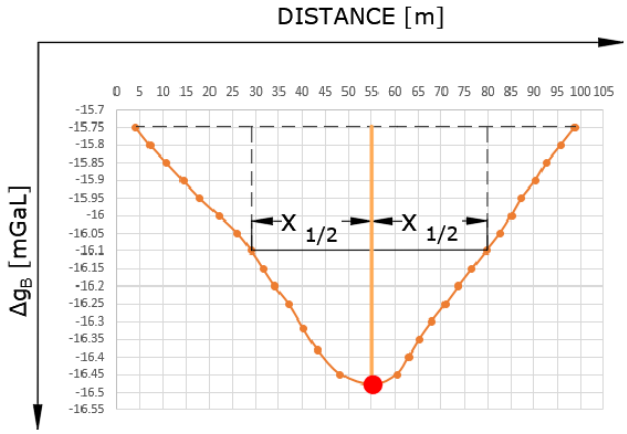


Fig.1 Results obtained from Applying the Half - Width Anomaly Method

The following formula for calculating depth in three-dimensional bodies [7] at different locations along the cave tunnel has been applied:

$$z < \frac{x_{1/2}}{(4^{1/3}-1)^{1/2}} \quad (1)$$

Attached are the results obtained.

RESULTS

As mentioned above, gravity acceleration anomalies and Bouguer anomalies are calculated using the gravimetric and GNSS measurements performed. Some of the obtained results are presented in Table 1.

Table 1 Part of Free - air and Bouguer anomalies calculation table

point №	Δg [mGal]	δgB [mGal]	ΔgB [mGal]
38	20.144	45.783	-25.638
pt500	11.548	27.056	-15.508
pt501	11.720	27.275	-15.555
pt502	11.524	27.168	-15.644
pt403	11.529	27.501	-15.972
pt303	11.251	27.552	-16.301
pt302	11.010	27.281	-16.271
pt202	11.039	27.308	-16.269
pt203	11.517	27.755	-16.238
pt102	11.272	27.284	-16.012

After the Free-air gravity and Bouguer anomalies are calculated, their corresponding models are created.

The Free-air gravity anomaly shows the difference between observed and expected gravity values, based only on the Earth's shape and rotation. It's important to note that these anomalies (Fig. 2) include all disruptions, whether on the Earth's surface or within it, without considering the influence of in-between masses on measured gravity.

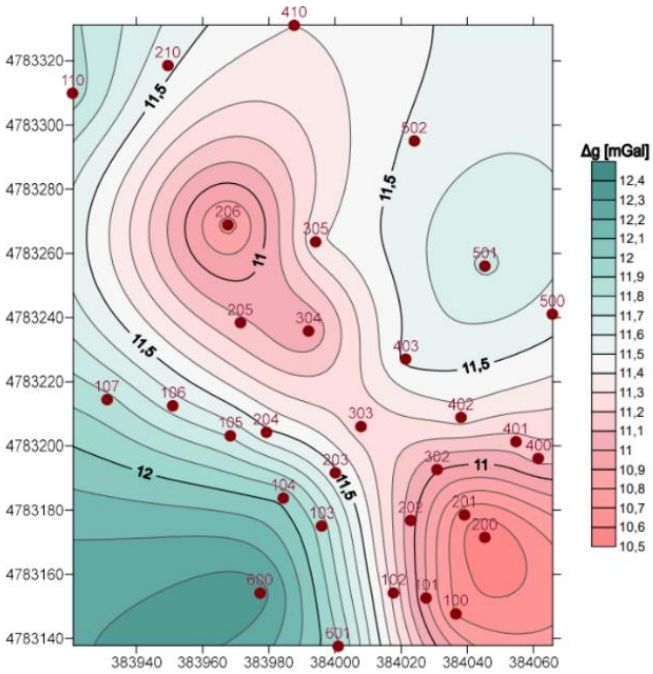


Fig.2 2D visualization of free-air gravity anomaly

Thus, these Free-air anomalies are not main focus the analyses, but they are needed for computing the Bouguer anomalies (Fig. 3) which consider elevation differences and subsurface density variations, offering a more accurate representation of subsurface anomalies.

DISCUSSION

The shape of the obtained isolines reveals the density contrast between the subsurface voids and their surrounding rocks. This clearly indicates the presence of an anomalous body beneath the study area. The created Bouguer anomaly map (Fig. 3) can be used in order to detect the void, as well as to determine the approximate size, and shape of the anomalous body.

The observed distinct negative values of the Bouguer anomalies are actually located above the small entrance of the cave tunnel (point 200) and above the second cave gallery (points 304 and 206), which confirms that the center of the anomalies is above the center of the anomalous body [7].

https://doi.org/10.5593/sgem2024/1.1/s05.60

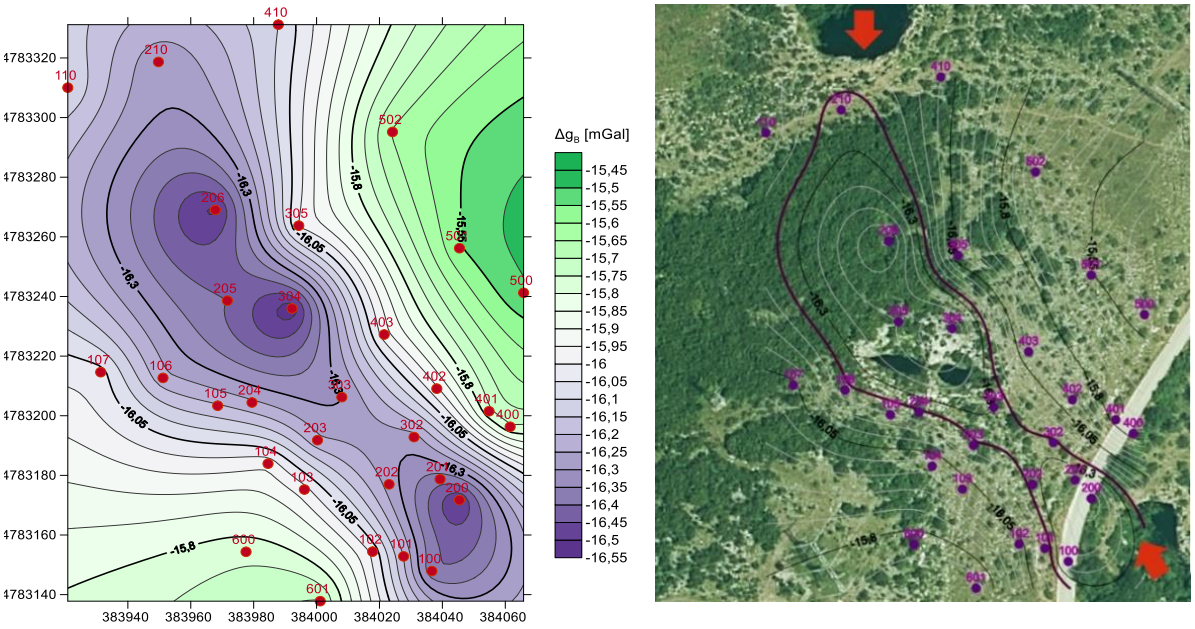


Fig.3 2D visualization of Bouguer gravity anomaly (left) and 2D visualization of Bouguer gravity anomaly with ortophoto below (right)

By applying the Half - Width Anomaly Method, an average depth value of approximately 39 meters was determined for the "Prohodna" cave tunnel. This value aligns well with the known height values of the two entrances: small entrance at 35 meters and large entrance at 45 meters (Fig. 4). The obtained average depth value is smaller than the actual depth [1].



Fig.4 Heights of the Prohodna's entrances

CONCLUSION

An analysis and interpretation of the obtained results were conducted, unequivocally proving the effectiveness and applicability of the proposed approach. The findings of this study clearly confirm the existence of an anomalous body, demonstrating the efficacy of combining gravimetric and GNSS methods to detect subsurface cavities, including caves and cave tunnels. This approach assists in locating and estimating the shape, size, and depth of subsurface voids.

The isoline maps distinctly highlight a zone of reduced anomaly values, confirming the presence of an anomalous body with a density lower than that of the surrounding rocks.

The pattern of the isolines on the Bouguer anomaly map (Fig. 3) also provides insights into the location and shape of the studied cave tunnel.

It is observed that outside the cave outline the values of Bouguer anomalies increase.

The quantitative analysis, using the Half-Width Anomaly Method, yielded a depth value z that closely matches the known heights of the cave tunnel openings. The applied method offers satisfactory accuracy and can be used as an alternative for determining the height from the base to the topographic surface of other similar cave tunnels and cavities when precise determination is not required.

In the case of surveys over larger areas, more sophisticated gravimetric measurement schemes would need to be applied. They have to allow the reliable determination and elimination of gravimeter zero-point drift. More sophisticated measurement schemes should also be applied where gravimeters with large zero drift are used.

For a more detailed and in-depth analysis it would be interesting to link the obtained gravimetric measurements with a three-dimensional model of the object. This information would also provide information on the spatial efficiency of the proposed method.

REFERENCES

[1] Al-Banna, Ahmed & Salih, Sabbar. (2006). Using of gradient techniques for depth estimation of gravity source. Tikrit journal of pure science. 11. 231-238.

[2] Butler Dwain K., Microgravimetric and gravity gradient techniques for detection of subsurface cavities, July 1984 Geophysics 49(7):1084-DOI:10.1190/1.1441723, https://www.researchgate.net/publication/260532892_Microgravimetric_and_gravity_gradient_techniques_for_detection_of_subsurface_cavities

[3] Martínez-Moreno, Francisco & Pedrera, Antonio & Ruano, Patricia & Galindo-Zaldivar, Jesus & Martos-Rosillo, Sergio & Gonzalez Castillo, Laura & Sánchez-Úbeda, Juan Pedro & Marín-Lechado, C.. (2013). Combined microgravity, electrical resistivity tomography and induced polarization to detect deeply buried caves: Algaidilla cave (Southern Spain). Engineering Geology. 162. 67–78. 10.1016/j.enggeo.2013.05.008

[4] Peneva, E., Patalov S., Research of the State Gravimetric Network for the territory of the republic of Bulgaria, 23rd International Multidisciplinary Scientific GeoConference SGEM 2023, DOI 10.5593/sgem2023/2.1/s09.31, DOI Issue 10.5593/sgem2023/2.1, ISSN, 1314-2704, ISBN 978-619-7603-57-6, Volume 23, Issue, 2.1

[5] Raymundo J. Chico, Detection of caves by Gravimetry, 1964, https://digitalcommons.usf.edu/cgi/viewcontent.cgi?article=1730&context=ijs

[6] Tsanovski, Yu., GNSS - Good Geodetic Practices, PaintBox Creative, 132 pages, 2023, ISBN: 978 619 92689-0-2

[7] Zidarov D., The inverse gravimetric problem in exploration and geodesy, 1984

https://doi.org/10.5593/sgem2024/1.1/s05.60

DETERMINISTIC EARTHQUAKE SCENARIO FOR THE CITY OF SOFIA

Prof. Dr. Dimcho Solakov[1]
Assoc. Prof. Dr. Stela Simeonova[1]
Assoc. Prof. Dr. Plamena Raykova[1]
[1] National Institute of Geophysic, Geodesy and Geography – Bulgarian Academy of Sciences, **Bulgaria**

ABSTRACT

In the present study a set of two deterministic earthquake scenarios (expressed in peak ground acceleration and macroseismic intensity MSK) are generated for the city of Sofia - the capital of Bulgaria. The study is guided by the perception that usable and realistic, based on both local seismic history and tectonic setting, ground motion maps to be produced for urban area.

The city is situated in the center of the Sofia area that is the most populated (the population is of more than 1.2 mil. inhabitants), industrial and cultural region of Bulgaria that faces considerable earthquake risk.

The contemporary tectonic activity of the Sofia area is predominantly associated with marginal faults of Sofia graben. In the study the local ground shaking levels are computed using the six ground-motion models selected (GMPE's) for tectonically active regions. The scenario maps account for soil amplification effects using the geotechnical zonation of the considered urban area. Two scenario earthquakes are considered: earthquake with magnitudes M_W6.5 occurred at the active fault located south of the city of Sofia (along the northern margin of the Vitosha Mountain) and M_W7.0 quake (occurred at the fault located northern of the city). The M_W6.5 event is the "true" historical 1858 earthquake with the strongest seismic impact on the city of Sofia.

The assessment of seismic hazard and generation of earthquake scenarios is the first link in the prevention chain and the first step in the evaluation of the seismic risk. The implementation of the earthquake scenarios into the policies for seismic risk reduction will allow focusing on the prevention of earthquake effects rather than on intervention following the disasters.

Keywords: deterministic scenario, Sofia seismogenic zone, the city of Sofia

INTRODUCTION

The city of Sofia is the capital and the largest city of Bulgaria (Fig.1). It is situated in the center of the Sofia area that is the most industrial and cultural region of Bulgaria, that faces considerable earthquake risk.

The history of Sofia, Bulgaria's capital and largest city, spans thousands of years from Antiquity to modern times, during which the city has been a commercial, industrial, cultural and economic center in its region and the Balkans.

The Sofia area has a history of nearly 7,000 years, with the great attraction of the hot water springs that still flow abundantly in the center of the city of Sofia. A Neolithic settlement discovered in Slatina, north-eastern Sofia, is dated to be from the 6th

https://doi.org/10.5593/sgem2024/1.1/s05.61

millennium BC. Another Neolithic settlement around the National Art Gallery is traced to the 3rd–4th millennium BC.

From the 12th to the 14th century, Sofia was a thriving center of trade and crafts. It was renamed Sofia in 1376 after the Church of St. Sophia.

From the 14th century till the 19th century Sofia was an important administrative center in the Ottoman Empire. It became the capital of the beylerbey of Rumelia (Rumelia Eyalet), the province that administered the Ottoman lands in Europe (the Balkans).

The city of Sofia was proposed as a capital by Marin Drinov and was accepted as such on 3 April 1879.

After World War II the city and its surrounding areas expanded and became the most industrialized region of the country. At present Sofia is the economic hub of Bulgaria and home to most major Bulgarian and international companies operating in the country. Sofia is home of many of the major local universities, cultural institutions and commercial companies.

The city is situated in western Bulgaria, at the northern foothills of the Vitosha mountain, in the Sofia Valley that is surrounded by the Balkan Mountains to the north and the mountains Vitosha and Lyulin to the south and west, respectively. Being in the center of the Balkans, it is midway between the Black Sea and the Adriatic Sea and closest to the Aegean Sea.



Fig. 1. The city of Sofia (https://balkannomad.com/30-zabelezhitelnosti-v-sofia/)

The city of Sofia is located in the Sofia seismogenic zone that encompasses the area around the NWW-SEE trending Sofia graben – the region that is characterized with medium-speed horizontal movements.

The present study is a comprehensive earthquake scenario study. In the study are presented deterministic scenarios for the city of Sofia (expressed in peak ground and macroseismic intensity MSK). Two scenario earthquakes are considered: earthquake with magnitudes M_W6.5 (that is the "true" historical 1858 earthquake with the strongest seismic impact on the city of Sofia) occurred at the active fault along the northern margin of the Vitosha Mountain and M_W7.0 quake that occurred at the fault located northern of the city.

The deterministic local ground-shaking representation for the city of Sofia is produced through a GIS, by combining: location of the scenario earthquakes with assigned magnitude with appropriate attenuation relations for the selected ground motion descriptor, and a seismically oriented geological/geotechnical zonation of the urban area.

The approach adopted in the Risk EU Project (2001-2004) funded by The European Economic Commission in the framework of the Fifth Research and Technological Development Program "Energy, Environment and Sustainable Development" (presented in [1] and [2]) was used to generate deterministic earthquake scenarios for the city of Sofia.

SEISMOTECTONICS

The tectonic situation in the Eastern Mediterranean and Balkans is dominated by the collision of the Arabian and African plates with the Eurasian (among others in [3]). The recent tectonics of Bulgaria is determined by the geotectonic of the region in which dominate the processes of extension with general direction north-south [4].

Analysis of the obtained horizontal velocities of the permanent GNSS stations and geodynamic networks shows that the horizontal velocities in Northern Bulgaria, are practically negligible which confirms that this region belongs to the Eurasian plate while Central Western and Southwestern Bulgaria belong to the so-called South Balkan Extensional Region – a transition zone between Eurasian continental plate and Aegean micro-plate [4].

The contemporary tectonic activity of the Sofia seismogenic zone is predominantly associated with the marginal faults of Sofia graben [5].

The available historical documents prove the occurrence of destructive earthquakes during the 15^{th}-18^{th} centuries in the Sofia zone. Prior to the 19^{th} century Sofia was a small town, deeply inside the Ottoman Empire and only few reports on earthquakes felt there in could be found. The first well-documented strong earthquake of magnitude M_S6.0 occurred in 1818 near the town of Sofia [6]. The strongest documented event that occurred in Sofia seismogenic zone was the earthquake on the 18/30th September 1858, with magnitude M_W6.5. The maximum epicentral intensity is I=9-10 MSK between Dragalevcy and Boyana. The earthquake was felt in south and south-west Bulgaria and northern Greece. From 28 mosques and 7 churches in the city of Sofia only 3 mosques and 2 churches, were not affected and could be used. The flow of water of the hot springs in the center of the town decreased before the earthquake and stopped for 24 hours after it. A new springs of water appeared near south-western part of Sofia [6].

During the 20^{th} century the strongest event occurred in the vicinity of the city of Sofia is the 1917 earthquake with M_S5.3 (I_0=7-8 MSK64). The earthquake caused a lot of damages in the town and changed the capacity of the thermal mineral springs in Sofia and surroundings. The earthquake was felt in an area of 50000 km^2 and followed by aftershocks, which lasted more than a year [5] (Fig.2).

Almost a century later an earthquake with M_W5.6 hit Sofia seismic zone, on May 22^{nd}, 2012. The earthquake is located at the vicinity of the city of Pernik and at about 25 km south west of the city of Sofia (Fig.3). Moderate to heavy damages were observed in the epicentral area - in the cities Pernik, Radomir and Sofia. The earthquake was largely felt on the territory of Bulgaria and neighboring countries: northern Greece, eastern Northern Macedonia, eastern Serbia and southern Romania [7].

https://doi.org/10.5593/sgem2024/1.1/s05.61



Fig. 2. Damages caused by the 1917 earthquake with M_S5.3



Fig. 3. Damages caused by the 2012 M_W5.6 earthquake

Regional seismicity pattern is illustrated in Figure 4. Figure represents epicentre map of historical and instrumental earthquakes occurred in the Sofia seismogenic zone. In the figure are presented the active faults [8]. The seismogenic potential of the active faults defined in [8] was considered in the deterministic scenarios generation.

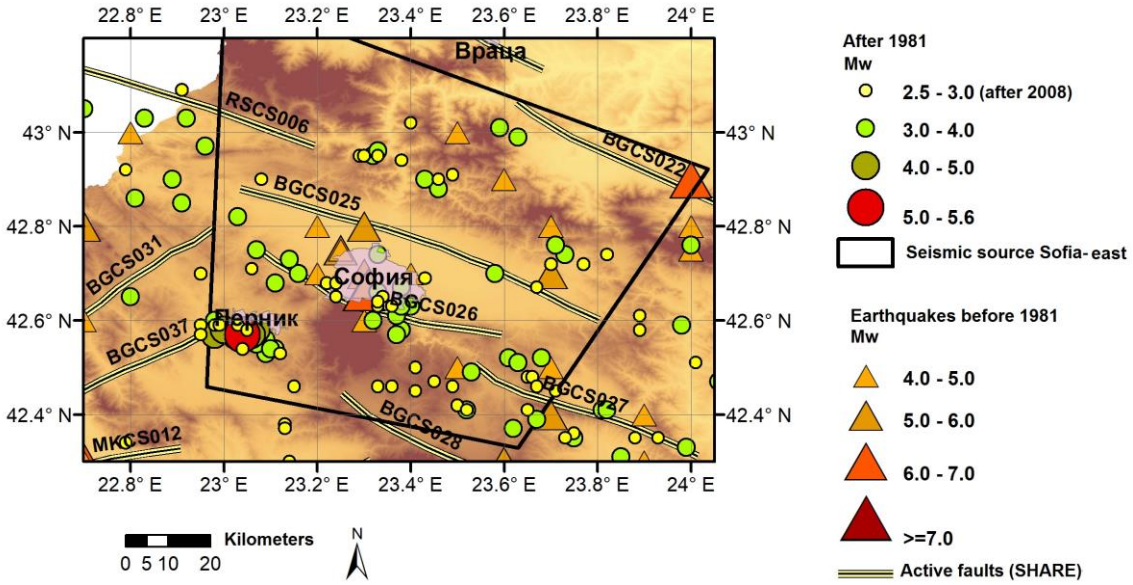


Fig. 4. Spatial pattern of seismicity (historical and instrumental earthquakes with M_W>3.0) and tectonic map for the city of Sofia and surroundings

SOIL PROPERTIES

The representation of the soil properties of the city was defined by the engineering parameter V_{s30} - average shear-wave velocity in the upper 30 m of the soil/rock profile. The V_{s30} values for the city of Sofia, (illustrated in Fig. 5) are based on the results presented in [4] and [9].

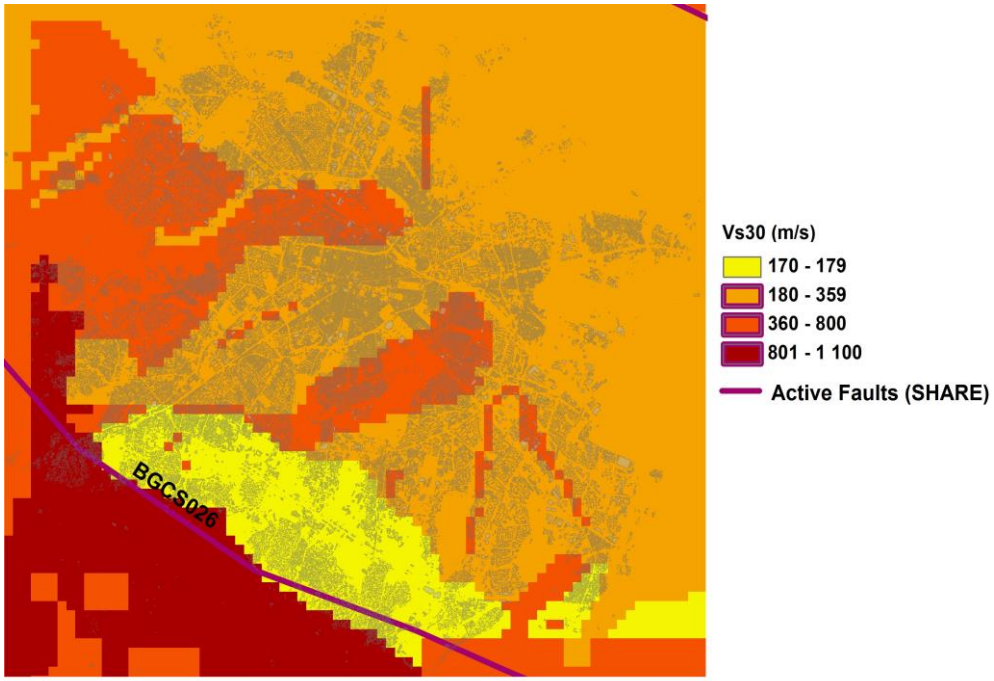


Fig. 5. Average shear-wave velocity in the upper 30 m of the soil/rock profile for the city of Sofia

GROUND MOTION ATTENUATION (GMPE' S)

The territory of Bulgaria is an active part of the Alpo-Himalayan seismic belt. Therefore, the selected six ground motion models for shallow earthquakes in tectonically active regions were selected and applied in our study.

The method presented in [10] is chosen for testing the selected 6 models against the actually recorded ground-motion data from the Balkan countries, Italy and the Middle East. The approach presented in [11] is used for ranking the selected six GMPE's.

Details for selection and justifications of the ground motion prediction equations are described in [4].

RESULTS

The deterministic scenarios were defined on the base of the seismogenic potential of the causative faults defined in the SHARE project [8]. Two scenario earthquakes are considered: earthquake with magnitudes M_W6.5 (that is the "true" historical 1858 earthquake with the strongest seismic impact on the city of Sofia) occurred at the active fault along the northern margin of the Vitosha Mountain and M_W7.0 quake that occurred at the fault located northern of the city.

https://doi.org/10.5593/sgem2024/1.1/s05.61

The epistemic uncertainty in the ground motion attenuation is represented by the application of the 6 GMPE's for active shallow crustal tectonic regime. The ground motions (in terms of macroseismic intensity I MSK and PGA in [g]) are calculated as follows:

$$GM(x,y) = \sum_{i=1}^{6} w_i \, g_i(x,y),$$

where *GM(x,y)* is the evaluated ground motion at point with coordinates *(x,y)*, $g_i(x,y)$ is the median ground motion predicted by i^{-th} GMPE and w_i is the corresponding weight, presented in [10].

The deterministic scenarios for M_W6.5 and M_W7.0 earthquakes (in terms of macroseismic intensity I MSK and PGA [g]) are mapped in Fig. 6 and Fig. 7, respectiv

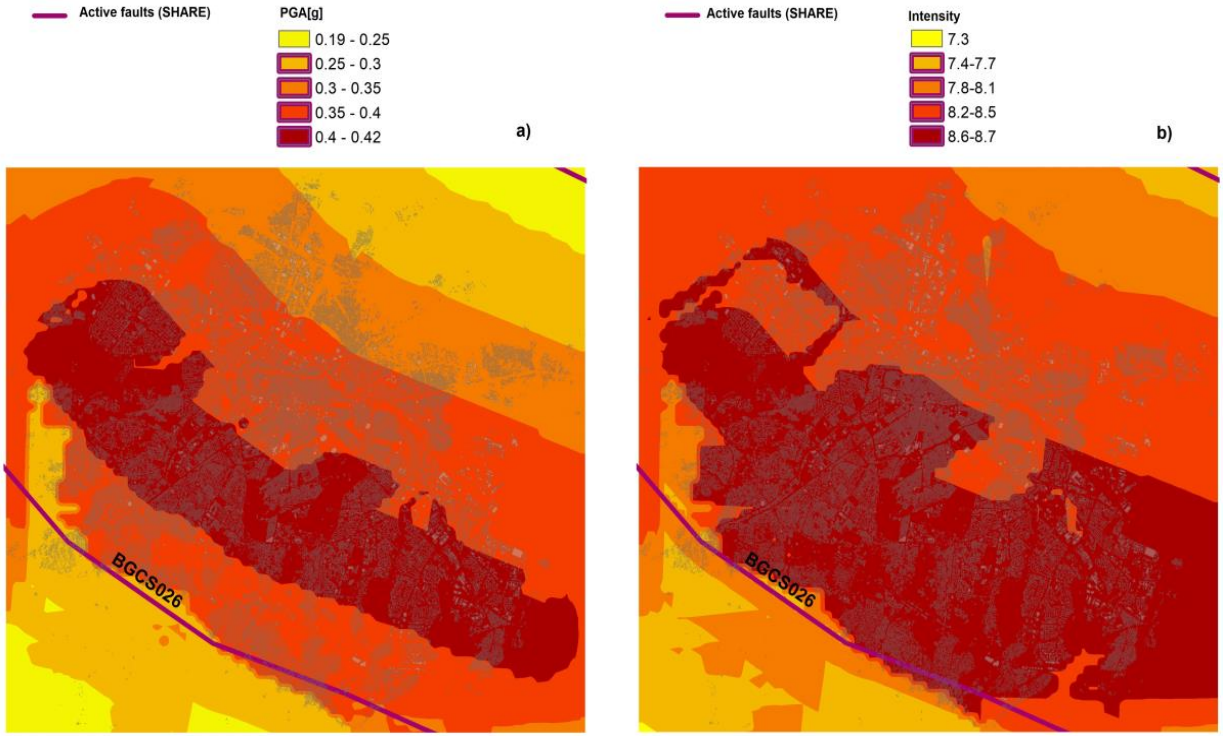


Fig. 6. The deterministic scenarios for M_W6.5 earthquake in terms of: a) PGA [g] and b) macroseismic intensity I MSK

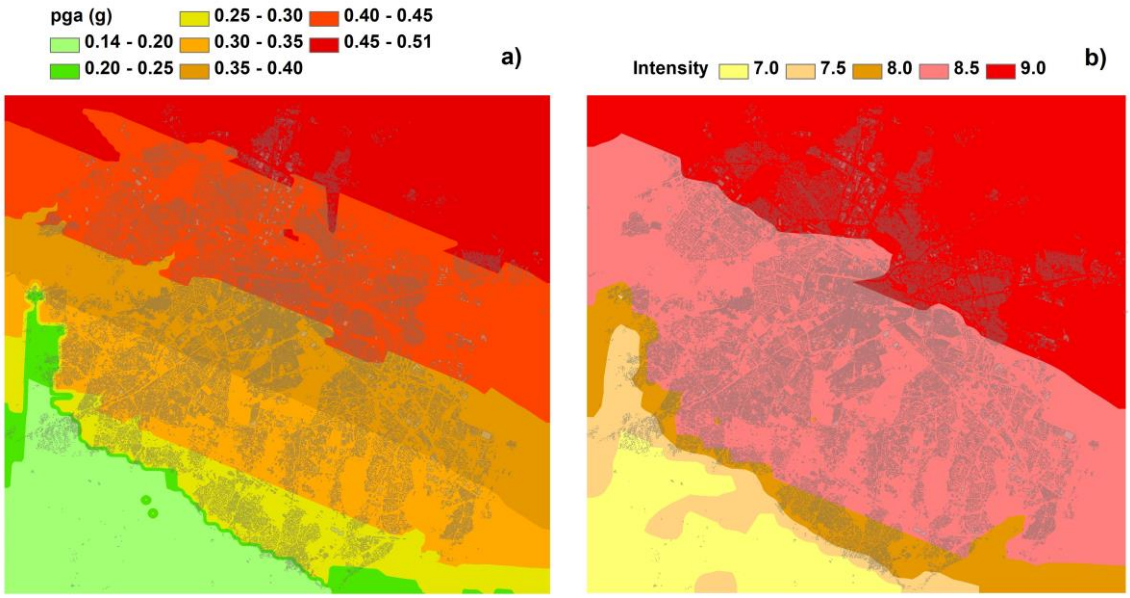


Fig. 7. The deterministic scenarios for M_W7.0 earthquake in terms of: a) PGA [g] and b) macroseismic intensity I MSK

CONCLUSION

The main conclusions from this study can be summarized as follows:

Deterministic earthquake scenarios (in term of peak ground acceleration PGA and Macroseismic intensity I MSK) are developed for the city of Sofia. The work on scenarios was guided by the perception that usable and realistic ground motion maps had at the end to be produced for the urban area;

Estimation of deterministic earthquake scenarios for a city is one of the most important challenges in the field of seismology. Moreover, it is a key step for the evaluation of seismic risk and loss estimation for a city. The generated scenario maps are reliable and can be used for developing risk scenario;

The generated scenarios may be efficiently used for the purpose of microzonation, urban planning, retrofitting or insurance of the built environment, etc.;

Finally, it is better to decrease the possible earthquake effects beforehand with implementation of earthquake scenarios into the policies rather than trying to cope with following the disasters.

ACKNOWLEDGEMENTS

This work has been carried out in the framework of the National Science Program "Environmental Protection and Reduction of Risks of Adverse Events and Natural Disasters" approved by the Resolution of the Council of Ministers № 577/17.08.2018 and supported by the Ministry of Education and Science (MES) of Bulgaria (Agreement № Д01-27/06.02.2024).

https://doi.org/10.5593/sgem2024/1.1/s05.61

REFERENCES

[1] Faccioli E. and Pessina V., WP2 Basis of a handbook of earthquake ground motions scenarios, RISK-UE, EVK4-CT-2000-00014, 2003.

[2] Faccioli, E., Seismic hazard assessment for derivation of earthquake scenarios in Risk-UE, Bulletin of Earthquake Engineering, 4, 4, 341-364, 2006.

[3] Jackson J., McKenzie D. The relationship between plate motions and seismic moment tensors, and the rates of active deformation in the Mediterranean and Middle East. Geophysical Journal 93, 45–73, 1988.

[4] Solakov D., Simeonova S., Trifonova P., Georgiev I., Raykova P., Metodiev M., Aleksandrova I., Building Seismic Risk Management, Part 2: Regional seismotectonic model and model of seismic sources. BAS Publ. House, S., 21-45, 2019 (in Bulgarian).

[5] Petkov, I. and Christoskov L., On seismicity in the region of the town of Sofia concerning the macroseismic zoning, *Annali Sofia Univ*., **58**, 163-179, 1965.

[6] Watzof, S., Earthquakes in Bulgaria during XIX century. Central Meteorological Station, Imprimerie de I′Etat, Sofia, pp 93, 1902 (in Bulgarian and French).

[7] Simeonova S., Solakov D., Aleksandrova I., Raykova P., Protopopova V., The 2012 Mw5.6 earthquake in Sofia seismic zone and some characteristics of the aftershock sequence**.** Bulgarian Chemical Communications, 47, Special Issue B, 398–405, 2015.

[8] Basili R., Kastelic V., Demircioglu M., Garcia Moreno D., Nemser E., et al., The European Database of Seismogenic Faults (EDSF) compiled in the framework of the Project SHARE. Available at http://diss.rm.ingv.it/share-edsf/, doi: 10.6092/INGV.IT-SHARE-EDSF, 2013.

[9] Worden, C.B., Wald D. J., Sanborn J., and Thompson E. M., Development of an open-source hybrid global Vs30 model, Seismological Society of America Annual Meeting, 21-23 April, Pasadena, California. 2015.

[10] Scherbaum, F., Delavaud E. and Riggelsen C., Model Selection in Seismic Hazard Analysis: An Information-Theoretic Perspective, BSSA, 99(6), pp. 3234–3247, 2009.

[11] Delavaud E, Scherbaum F., Kühn N., Allen T., Testing the Global Applicability of Ground-Motion Prediction Equations for Active Shallow Crustal Regions. Bull. Of the Seism Soc. of America, 102(2):707 http://dx.doi.org/10.1785/0120110113, 2012.

GEOPHYSICAL EXPLORATION IN ARGEMELA DISTRICT, FUNDÃO, PORTUGAL – VLF RESULTS

MSc Ricardo Ribeiro[1,2]
Assoc. Prof. Rui Moura[3,4]
MSc Ana Carvalho[1,2,3]
Assoc. Prof. Alexandre Lima[1,2]
Assoc. Prof. Charles Gumiaux[5]

[1]Department of Geosciences, Environment and Spatial Planning, Faculty of Sciences, University of Porto, **Portugal**

[2]Institute of Earth Sciences, Pole of University of Porto, **Portugal**

[3]CRAS INESCTEC - Centre of Robotics and Autonomous Systems, **Portugal**

[4]GEOBIOTEC – Geobiosciences, Geoengineering and Geotechnologies, Department of Geosciences, University of Aveiro, **Portugal**

[5]Université d'Orléans, CNRS, BRGM, ISTO, UMR 7327, F45071, **France**

ABSTRACT

Raw materials are essential for Europe's industrial base, as they are used to produce vital goods and technologies. The European Comission's assessment identifies lithium and tin as critical and strategic raw materials due to rising demand. A PhD thesis aims to create a 3D geological model of the Argemela District in Central Portugal to provide vital information about the genesis of the hydrothermal tin and lithium mineralizations founded in the region. The study places emphasis on the very-low-frequency (VLF) electromagnetic method as a tool to provide information about the mineralization, lithologic contacts, and structural features that can be related to the mineralizations. Argemela district has two main areas, the Argemela Tin and Lithium Mine and the Argemela Hill Top. VLF data was collected and analyzed, showing that low resistivity may be associated with mineralization in the Argemela Mine, while high resistivity may be linked to the Argemela microgranite in the Argemela Hill Top. This geophysical method is effective in non-invasively mapping subsurface features, assisting in the development of a comprehensive 3D geological model and enhancing resource evaluation.

Keywords: Lithium, Tin, VLF, Argemela

INTRODUCTION

Raw materials form a robust industrial base, producing a wide range of goods and applications used in modern technologies and everyday life. These raw materials can be crucial to Europe's economy. The European Commission conducted an assessment of

https://doi.org/10.5593/sgem2024/1.1/s05.62

critical raw materials with the main goal of identifying those with high economic importance and a high risk of supply shortage. The list of critical raw materials includes rare earth elements, Nb, Ta, Sb, Be, W, and others [1]. Although lithium and tin were not considered non-critical raw materials in the 2010s, their demand, especially for lithium, was increasing, leading to considering these two elements as critical and strategic for Europe [1]. Therefore, it is crucial to identify and assess lithium and tin resources and reserves to meet these growing demands.

The present work is part of a PhD thesis whose objective is to create a 3D geological model of the Argemela district. The district is characterized by the presence of a Rare Metal Granite and hydrothermal mineralization with Lithium (Li) and Tin (Sn).

The main objective of this work is to understand how the very-low-frequency (VLF) electromagnetic method responds to Sn and Li mineralizations and to map contact between lithologies and structural features.

The Argemela district is located ~ 13 km east of the Panasqueira world-class W mine and south of the Serra de Estrela and is part of the southern CIZ in Central Portugal. The area is dominated by rocks of the Schist-Greywacke Complex (SGC), mainly the Beira Group.

The Argemela Area (Figure 1) can be divided into two main areas: 1) Argemela Tin and Lithium Mine (ATLM) and 2) Argemela Hill Top (AHT).

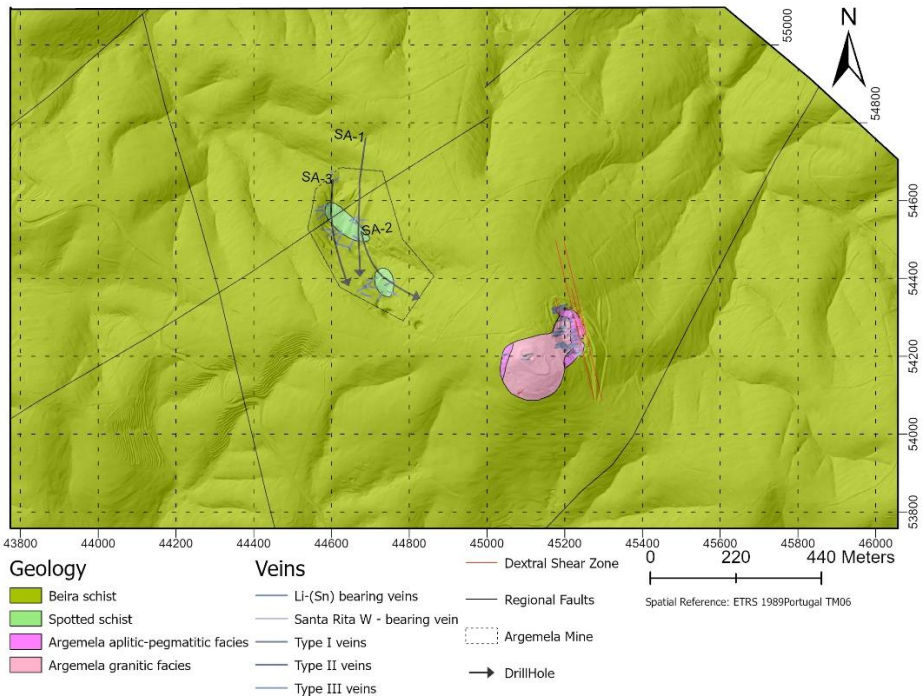


Figure 1 – Geological mapping of Argemela district. Argemela Mine is where the ATLM is located and the Argemela microgranite (Argemela aplitic-pegmatitic and granitic facies) is where the AHT is located. Adapted from [2-4].

In the Argemela Hill Top, we found the Argemela microgranite. It's considered a rare metal granite (RMG), being a leucocratic rock, and presents a porphyritic texture. It displays a small elliptical shape intrusion (300 m by 200 m), and the northeastern border is affected by a dextral shear zone [4]. This RMG has two facies. The first and main facies show a microgranitic texture with snowball quartz and white micas. The second facies appears in the border areas, and it presents a pegmatitic texture. All facies contain lithium phosphate minerals (amblygonite-montebrasite series), cassiterite, and columbite-tantalite minerals [3].

The ATLM is located less than 500 meters from the Argemela microgranite. It consists of a swarm of sub-vertical veins that cross-cut the schists of the SGC [2]. The sub-vertical veins are essentially composed of montebrasite, quartz, and turquoise [5]. Sometimes, cassiterite is found. This cassiterite occurs on the margin of the veins as an inclusion in the quartz. In the drill holes made in the 1970s, similar granitic rocks to the Argemela microgranite were found. These granitic rocks contain veins composed of quartz and lithium phosphate minerals and are intersected by some sulfide-bearing veins, with the presence of cassiterite being replaced by stannite.

MATERIALS AND METHODS

The very-low-frequency (VLF) electromagnetic method uses radio waves from radio transmission stations operating in the bandwidths of 15-30 kHz as a signal source. The instrument compares the primary magnetic field (transmitted) to the induced secondary magnetic field from the subsurface. When a conductor is crossed, the magnetic field becomes elliptically polarized and the major axis of the ellipse tilts with respect to the horizontal axis [6]. This electromagnetic system permits the measurement of the in-phase (real or tilt-angle) and the out-of-phase (imaginary, ellipticity, or quadrature) components.

The data from the VLF profiles were collected using the Scintrex OMNI-Plus VLF/Magnetometer System. This equipment permits the use of three different frequencies at the same time. After calibrating the equipment, it was decided to use the frequencies with the better signal: 22.1 kHz (GVT—Skelton, UK), 23.4 kHz (DHO38—Rhauderfenh, Germany), and 24.0 kHz (NAA—Cutler, USA). The use of these three frequencies allowed us to observe the responses of the conductive bodies and structures in almost every direction. In the VLF survey measurements were made in 940 stations with an average spacing of 5 meters, totalling 14 profiles around the Argemela district (Figure 2). The data, after being inverted, was represented in the 3D geological modeling software Leapfrog Geo from Seequent, as shown in Figure 3.

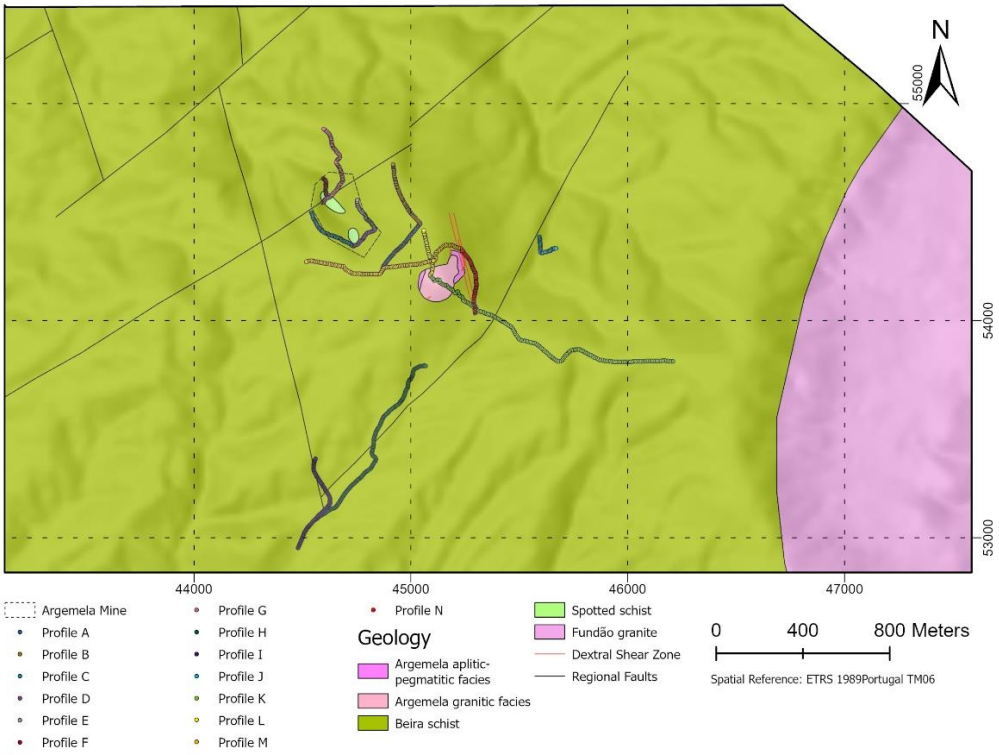


Figure 2 – Location of the VLF profiles in Argemela district. Most of the profiles were performed in the Argemela microgranite and in the Argemela tin and Lithium Mine.

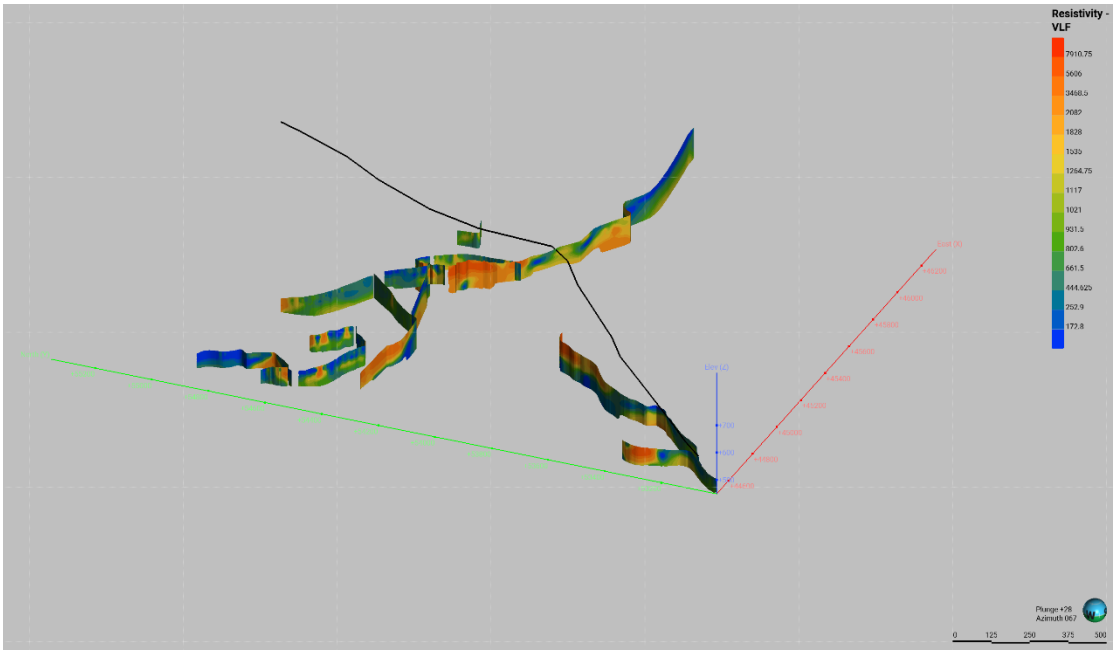


Figure 3 – Individual 2D VLF profiles projected in a 3D environment.

RESULTS AND DISCUSSION

Each profile had an interpolation done for every mentioned frequency. The frequency data that was most perpendicular to the profiles was chosen, taking into account each profile's overall direction. Subsequently, the profiles were organized in a 3D environment (Figure 3) to facilitate interpretation.
After that, the statistic for each profile was taken to make a logarithmic scale that could represent the overall resistivity in the area (Table 1).

Table 1 – Statistics of the chosen profiles considering the best frequency. All data is in ohm.m.

Name	Minimum	Mean	Maximum
Resistivity A	424.1	782.11	1798
Resistivity B	212.9	857.06	3671
Resistivity C	17.59	799.38	8050
Resistivity D	125.4	672.53	1953
Resistivity E	13.43	985.65	3871
Resistivity F	79.16	964.71	4141
Resistivity G	24.24	746.91	5329
Resistivity H	0.91	1315.75	12310
Resistivity I	98.66	1481.55	13330
Resistivity J	367.1	780.12	1442
Resistivity K	16.04	1816.50	18870
Resistivity L	105.8	797.92	4352
Resistivity M	16.61	1530.51	6013
Resistivity N	147.5	771.62	2127

Considering the data, a scale was utilized, where resistivities below 172 ohm.m are considered very low and those above 7910 ohm.m are considered very high.
Two profiles were chosen to show different characteristics in the Argemela district. Profile C (Figure 4) represents the area near the Argemela Tin and Lithium Mine. In this profile, we can see low resistivity in blue. These resistivities can be related to the hydrothermal veins that are mineralized in Sn and Li. Inverno [2] identified that the hydrothermal veins were emplaced in shear zones and fractures around the mine. The higher resistivities (in red) can be related to a more competent zone that is not affected by fractures or faults.
Near the Argemela microgranite, the profile K was done (Figure 5). This profile has the characteristic that was done with the intuition to obtain the contact between the microgranite and the country rock, as well as some regional faults that can be related to the emplacement of the Argemela Microgranite. In a black square, it represents the contact between the microgranite (right) and the country rock. The microgranite appears to have above 5000 ohm.m, and the country rock near it also has a more significant resistivity than the overall resistivity in the profile. In a black circle, we have the representation of a regional fault at the surface. This fault appears to incline NW as suggested by the region's mapping. On the left side of the profile (near A) it’s also possible to see a lower resistivity zone. This zone can be related to a fault that was mapped in the region.

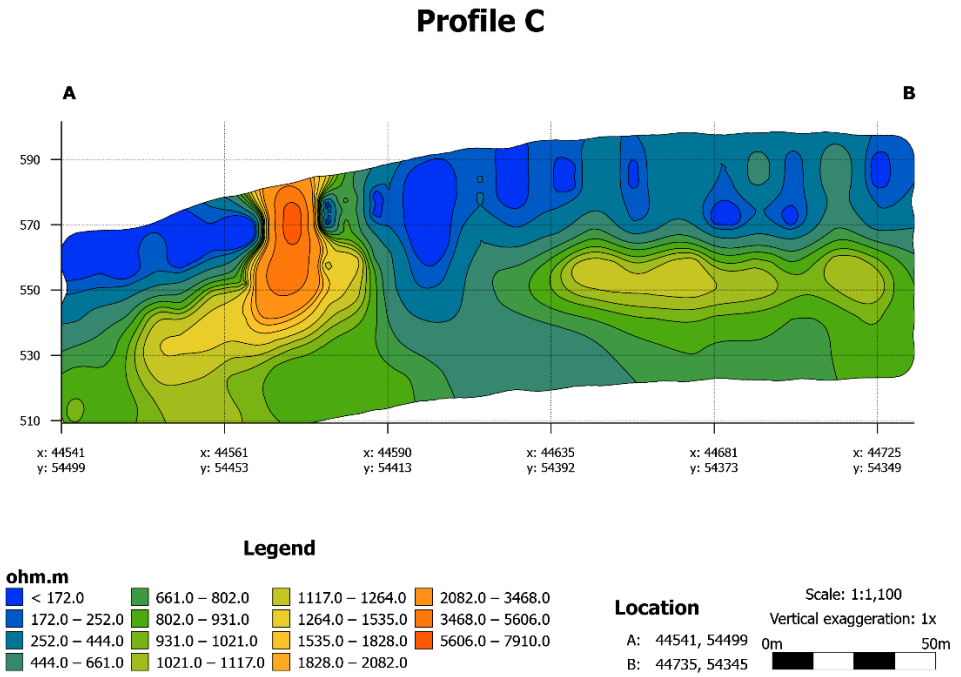


Figure 4 – VLF profile for the frequency of 22.1 kHz. ETRS89 Portugal tm-06 coordinate system.

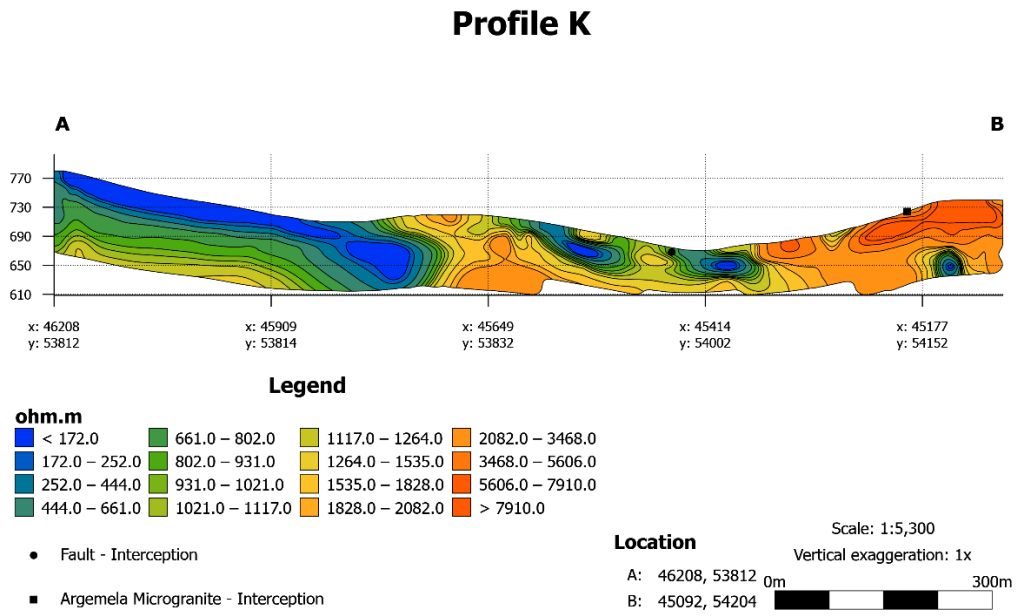


Figure 5 – VLF profile for the frequency of 23.4 kHz. The black square represents the contact between the Argemela microgranite (right) with the country rock (left). The black circle represents the regional fault at the surface. ETRS89 Portugal tm-06 coordinate system.

CONCLUSION

Our study was based on an assessment of the mineralizations in the Argemela district. The recent interest in lithium for battery production has raised the necessity of finding new lithium resources or better evaluating known resources. The use of geophysical methods is crucial because they are non-invasive and can provide essential information at depths that would otherwise require drilling.

The VLF method provided a way to obtain resistivity data more quickly and easily than other electromagnetic methods. Using this method, it was possible to map fractures and faults near the Argemela Tin and Lithium Mine that may be related to mineralization. It also allowed for mapping the contacts between different rock types, especially the Argemela microgranite and the country rock, as well as the faults associated with the emplacement of the microgranite.

These results will be very helpful in creating a 3D geological model for the Argemela District, raising knowledge of the region, and hopefully helping define its tin and lithium resources.

ACKNOWLEDGEMENTS

This work is supported by Portuguese National Funds through the FCT – Fundação para a Ciência e a Tecnologia, I.P. (Portugal), projects UIDB/04683/2020 (https://doi.org/10.54499/UIDB/04683/2020) and UIDP/04683/2020 (https://doi.org/10.54499/UIDP/04683/2020). Ricardo Ribeiro and Ana Carvalho were financially supported within the compass of their respective PhD thesis, SFRH/BD/140266/2018 and ref. 2022.10315.BD by national funds through FCT.

REFERENCES

[1] European Commission, Directorate-General for Internal Market, Industry, Entrepreneurship and SMEs, Grohol, M., Veeh, C. (2023). Study on the critical raw materials for the EU 2023: final report, Publications Office of the European Union. https://data.europa.eu/doi/10.2873/725585

[2] Inverno, C., & Ribeiro, M. L. (1980). Fracturação e cortejo filoneano nas Minas da Argemela (Fundão). Comun. Serv. Geolo. Portugal, 66, 185-193

[3] Charoy, B., & Noronha, F. (1996). Multistage Growth of a Rare-Element, Volatile-Rich Microgranite at Argemela (Portugal). Journal of Petrology, 37(1), 73-94. https://doi.org/10.1093/petrology/37.1.73

[4] Michaud, J. (2019). Rare Metal Granites - Origin, Emplacement and Mechanisms of the Magmatic-Hydrothermal Transition. University of Orlean. Orleans, France, p. 330.

[5] Ribeiro, R., Capela, D., Ferreira, M., Martins, R., Jorge, P., Guimarães, D., & Lima, A. (2021). X-ray Fluorescence and Laser-Induced Breakdown Spectroscopy Analysis of Li-Rich Minerals in Veins from Argemela Tin Mine, Central Portugal. Minerals, 11(11), 1169. https://www.mdpi.com/2075-163X/11/11/1169

[6] Milsom, J. (2003). Field geophysics (3rd ed.). Wiley.

PRELIMINARY ESTIMATION OF ELECTRICAL PROPERTIES OF THE LUNAR NEAR SURFACE FROM THE CHINESE YUTU-2 LUNAR PENETRATING RADAR (LPR)

Assoc. Prof. Rui Moura[1,2]
Assoc. Prof. Lucía Arévalo Lomas[3]
Assoc. Prof. Fernando Almeida[1]

[1] Centre GeoBioTec|UA, University of Aveiro, Santiago Campus, 3810-193 Aveiro, **Portugal**
[2] Centre for Robotics and Autonomous Systems CRAS|LSA, DEE, School of Engineering (ISEP), Polytechnic of Porto, Rua do Dr. António Bernardino de Almeida, 431, 4200-072 Porto, **Portugal**
[3] Department of Energy and Fuels, Universidad Politécnica de Madrid, C/ Ríos Rosas, 21, 28003, Madrid, **Spain**

ABSTRACT

Geophysical studies on the lunar surface have, in the past, used various methods that contribute not only towards the knowledge of the lunar subsurface but also contribute towards the design of future lunar missions, namely those that will, in the near future, take humans to the Moon's surface. This work analyzes a specific set of ground penetrating radar (GPR) data, collected during the Chang'E-4 mission of the Chinese Space Agency, using theYutu-2 rover within the von Kármán crater, on the far-side of the Moon. From this dataset two electrical parameters were estimated. The approach uses the backscatter of the electromagnetic wavefield in order to obtain estimates of the real component of the complex relative permittivity as well as the electrical resistivity.

Keywords: Ground Penetrating Radar (GPR), Lunar Penetrating Radar (LPR), geophysics, lunar geology

INTRODUCTION

The Yutu-2 rover (Figure 1), the mobile component of China's Chang'E-4 mission, has been exploring the Moon's far side since its historic landing on the 3rd of January 2019, specifically in the Von Kármán crater (Figure 2), where the lunar vehicle touched down [1]. This region is of particular interest due to its unique geological history and location within the South Pole-Aitken Basin, one of the largest and oldest impact basins in the solar system. One of the instruments onboard Yutu-2 is the Lunar Penetrating Radar (LPR) [2], also used on the Chang'E-3 mission [3] and capable of revealing the near-surface structure. This radar system has provided unprecedented insights into the Moon's geology. The LPR [1][2][3] is, in fact, a type of GPR, attached to the Yutu-2 rover for lunar subsurface profiling. The LPR is composed of two channels, each connected to a pair of antennas, a receiver and a transmitter, that operate in two different bands. The low-frequency channel (CH-1) operates at a center frequency of 60 MHz, with a 40 MHz bandwidth. The high-frequency channel (CH-2) operates at a center frequency of 500 MHz, with a 500 MHz bandwidth. The current work will perform an analysis of data

https://doi.org/10.5593/sgem2024/1.1/s05.63

collected with the high-frequency channel, CH-2. The LPR collects continuous data as the rover traverses the lunar surface. This data is then transmitted back to mission control for processing and analysis.

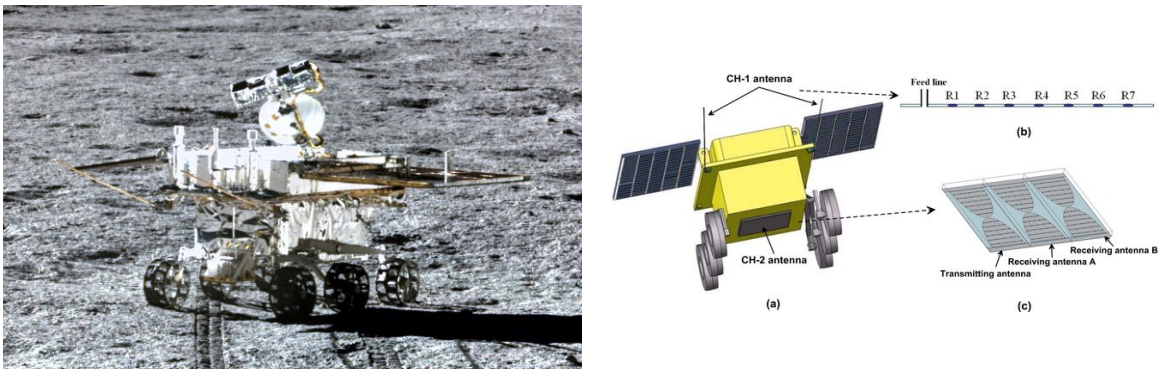


Figure 1. The Chang'E-4 lunar rover, Yutu-2 (left). The two types of LPR antennas on the Yutu Rovers (right): (a) Yutu rover model; (b) CH-1; (c) CH-2.. Credits: China National Space Administration (CNSA) and [2].

The CH-2 data was collected with an average trace separation of 3.6 cm and an acquisition time window of 640 nanoseconds (ns). The total distance of the collected profile was 1440.72 meters (Figure 2).

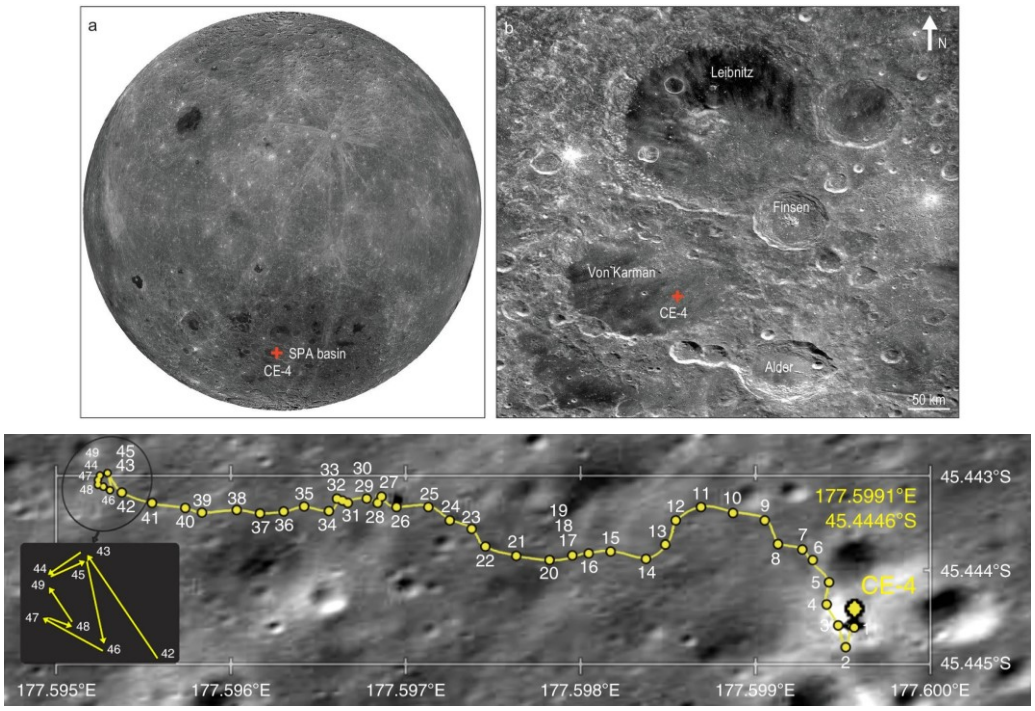


Figure 2. The Chang'E-4 mission landing site and Yutu-2 LPR profile in the von Kármán crater. Credits: [4][1] and base image: NASA/GSFC/Arizona State University.

So far a few researchers and research groups have processed the data, resulting in various published works [5][6][7] that have analyzed the results. Some of the main outcomes are:

- Layered Subsurface Structure: The LPR has revealed a complex, layered structure

beneath the Moon's surface. This includes multiple layers of regolith (loose, fragmented material) and buried rock formations. These layers suggest a history of volcanic activity and impact events that have shaped the lunar far side.

- Regolith Thickness: Analysis of the high-frequency data indicates that the regolith layer on the far side is much thicker than previously estimated, with variations in thickness across the traversed 1440 meter profile.
- Basaltic Rocks: The low-frequency data has identified extensive basaltic rock formations beneath the surface, indicating past volcanic activity. These findings help in understanding the Moon's thermal evolution and volcanic history.
- Impact Crater Insights: The LPR has also provided detailed views of the subsurface structures of impact craters. This includes information on the depth and distribution of ejecta materials, which are crucial for understanding the impact processes and crater formation.
- Water Ice Potential: Although not directly detected by the LPR, the data contributes to the broader search for water ice by identifying potential regions where subsurface ice might be present. This is based on the identification of regions with specific subsurface characteristics that might trap and preserve ice.

TECHNICAL BACKGROUND

Standard Ground Penetrating Radar data usually results in a set of collected signal traces that, when vertically laid side by side, provide a profile that can be interpreted in terms of geometrical relations, usually termed as a radar reflection section [8]. From these sections we can interpret the layering geometry as well as estimate their depths. In case hyperbolic diffraction events are present an estimate of the radio wave pulse velocity can also be measured.

However, the proposed data analysis will additionally use a method for an approximate solution, through inversion, for a continuous cross-sectional distribution of the electrical properties of the subsurface. This approach, known as backscatter of the electromagnetic wavefield (BSEF), analyzes the backscatter of the electromagnetic wavefield in order to obtain a stable solution and based on the construction of nonlinear spatial filters applied to a set of numerical values of the medium's dielectric constant. From the theoretical formulations it is known that the dielectric constant contributes towards the velocity of the electromagnetic wavefield [8]. The proposed approach [9] uses an automated algorithm for estimating the electrical properties of GPR sections and that effectively works in the presence of dispersive environments (Figure 3).

As a result of the first two steps of the algorithm, a set of points is obtained that have coordinates and attributes in the form of a velocity and frequency distribution. After these steps, some points are rejected, according to a velocity criterion, namely points with velocity values above 0.3 m/ns, the electromagnetic wave velocity in vacuum, as well as below 0.033 m/ns, the minimum electromagnetic wave velocity in water. Other constraining criteria may also be applied. As is known, the attenuation of GPR pulses depends on the frequency. High-frequency components of electromagnetic waves attenuate faster than the low-frequency components. On Earth, the subsurface moisture, of which the dielectric constant mainly depends on, also changes with depth and as a general rule increases with depth. If the values of the signal central frequency are determined

https://doi.org/10.5593/sgem2024/1.1/s05.63

during processing, along with the calculation of average values ε_{av} then the parameters can be plotted as point clouds. A regression equation can then be used as a correction function and the result increases the reliability of the section.

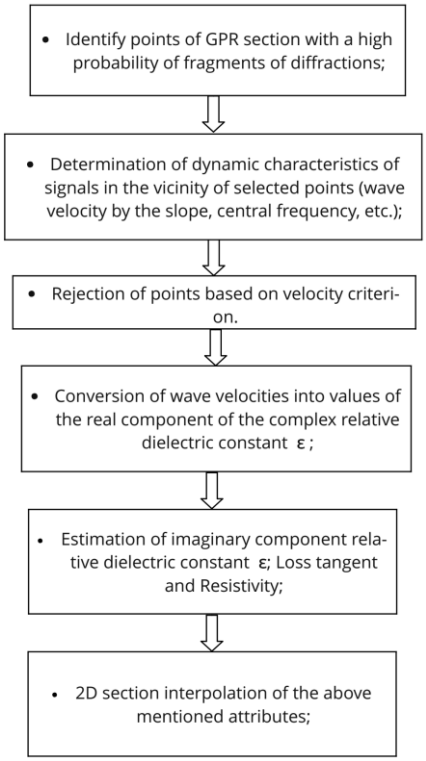


Figure 3. Processing flowchart of the backscatter of the electromagnetic wavefield analysis (BSEF). Adapted from [9].

Furthermore, the attributes, such as the imaginary component of relative permittivity, the loss tangent, resistivity, damping rate can be calculated from the following relationships:

$tg\delta = \varepsilon\,''/\,\varepsilon' = \sigma/(\omega\varepsilon'\varepsilon_o)$, where $tg\delta$ is loss tangent, where $\omega = 2\pi f$, complex permittivity is $\varepsilon = \varepsilon' + j\varepsilon''$ and $\varepsilon_o = 8.854 \times 10^{-12}$ (F/m):

σ – specific electric conductivity;

ε'' – imaginary component of the complex relative permittivity;

ε' – real part of the complex relative permittivity;

$\varepsilon\,''/\,\varepsilon' = 1/Q$;

$\rho = 1/\sigma$, where ρ is resistivity;

GEOLOGICAL SETTING OF THE VON KÁRMÁN CRATER

The Von Kármán crater, located on the far side of the Moon, has raised significant interest, especially since the successful landing of China's Chang'e-4 mission and its Yutu-2 rover [1]. This 180 km wide crater sits within the larger South Pole-Aitken Basin, one of the oldest and largest impact basins in the solar system. The geology of Von Kármán crater is relatively diverse with the floor largely covered by basaltic lava flows. These result from a set of volcanic events, where magma ascended through

fractures caused by an impact event that created the basin itself. These basaltic plains are similar to the Maria found on the near-side of the Moon. The region also seems to contain impact melt deposits that were melted during the formation of the crater, probably by a high-energy impact. Another group of rock formations, known as regolith and ejecta layers, consists of a fine, powdery sediment formed by the bombardment of meteorites and larger impacts. Beneath this surface regolith are layers of ejecta from the very impact that created the crater itself. These layers consist of fractured and mixed materials from different depths of the lunar crust. Bordering the basaltic plains we may also find highland materials. These are older, and mostly composed of anorthositic rocks, a calcium rich plagioclase feldspar dominated lithology. These rocks represent some of the Moon's original crust. Past geophysical measurements, conducted during the Apollo missions, confirm indications of thick non-consolidated, regolith and ejecta layers. These were obtained from the refraction data of the Active Seismic Experiments of Apollo 14 and 16 [11][12][13]. The Von Kármán crater also exhibits some tectonic features such as fractures and faults, which have formed due to stresses in the lunar crust.

PROCESSING AND RESULTS

The imported SEG-Y data (Figure 4.) was converted according a procedure described in [10]. The imported format was simply corrected in terms of low frequency content with a background removal routine and the application of bandpass filter, according to the specifications of the LPR's CH2 bandwidth, i.e. 250 to 750 MHz. The analysis of the section reveal various difraction hyperbola events that, when measured, indicate velocity values centered around 0.16 m/ns.

In order to extract and analyze the electrical parameters, that could in turn be relevant to characterizing the lunar near-surface, a workflow, as depicted in figure 3 was employed [9]. A relative permittivity search, guided by a preliminary velocity analysis of the hyperbolas that could be detected in the processed section of figure 5, was carried out. Constraining the automatic backscatter search procedure is important in order to assure it does not fall into other coherent events that could overestimate or underestimate the obtained electrical parameters, namely the real component of the complex relative permittivity. The results of the relative permittivity can be visualized in figure 6. The result, visible in Figure 7, uses the before mentioned procedure and formulas in order to obtain an estimate of a resistivity section. As we can observe from figure 6 the values of the real component of the complex relative permittivity vary between 2 and 4. These values are in close agreement to those published by various authors[5][6][7]. Figure 7 depicts the spatial subsurface estimate of the resistivity in Ohm·m. The estimated values fall between 5.5E+07 and 2.7E+08 Ohm·m (1.82E-08 and 3.7E-09 S/m) These values (between 1E-14 to 1E-09), when converted to conductivity are fairly close to those published by authors that have measured some of the Apollo lunar regolith and rock samples [14], although have a higher disagreement when compared to the permittivity values.

https://doi.org/10.5593/sgem2024/1.1/s05.63

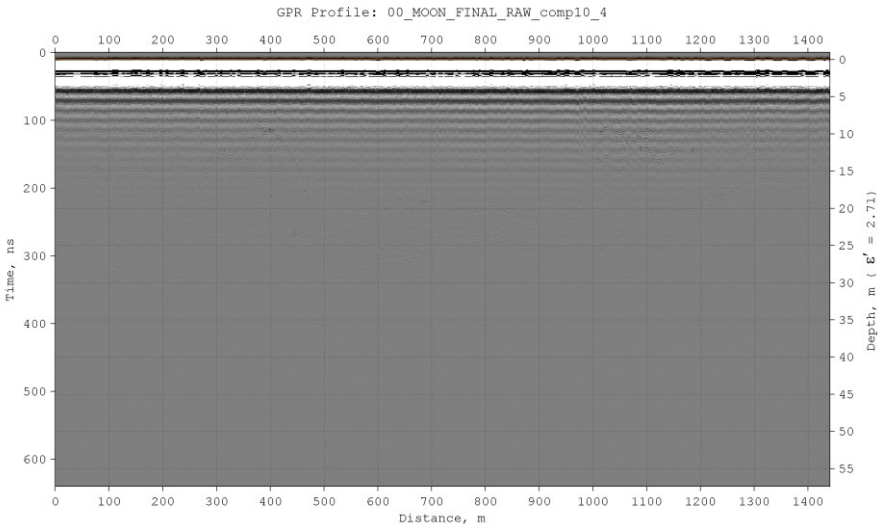


Figure 4. Original imported raw LPR data collected in the Von Kármán crater.

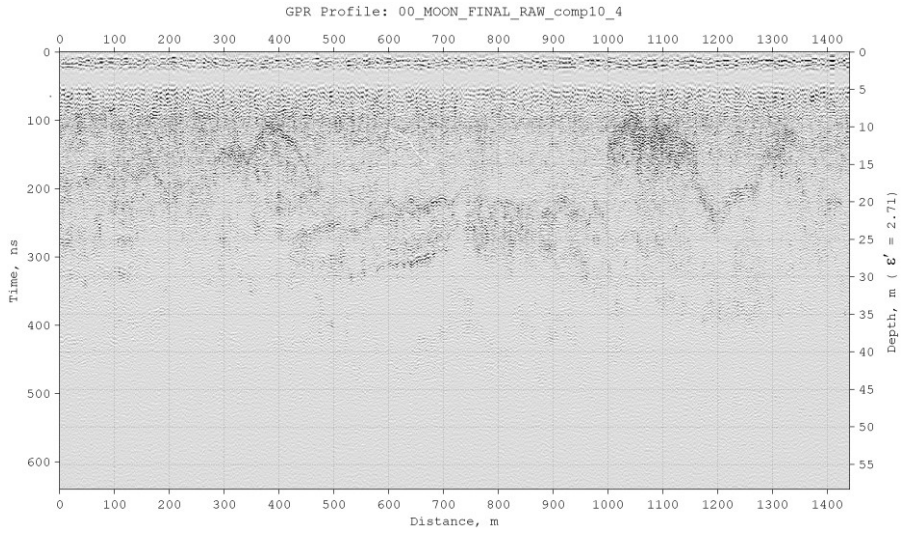


Figure 5. Results of the described basic processing of the LPR data.

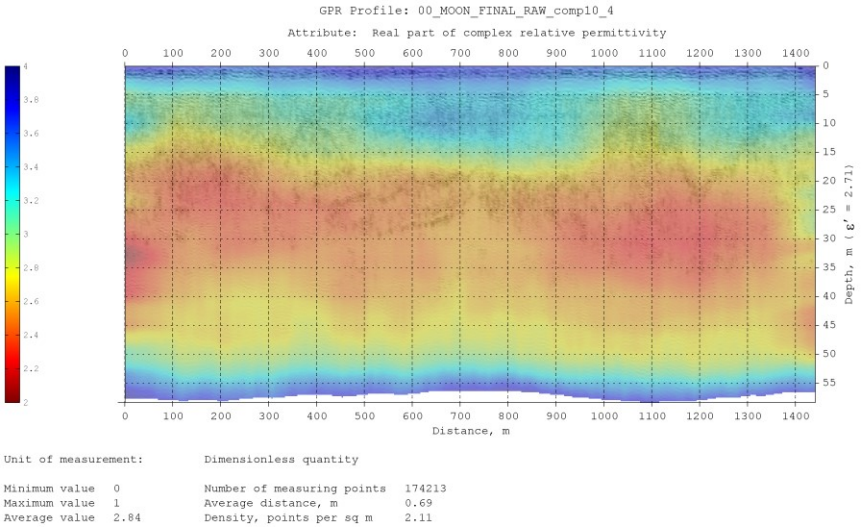


Figure 6. Results of the distribution of the permittivity, obtained by BSEF.

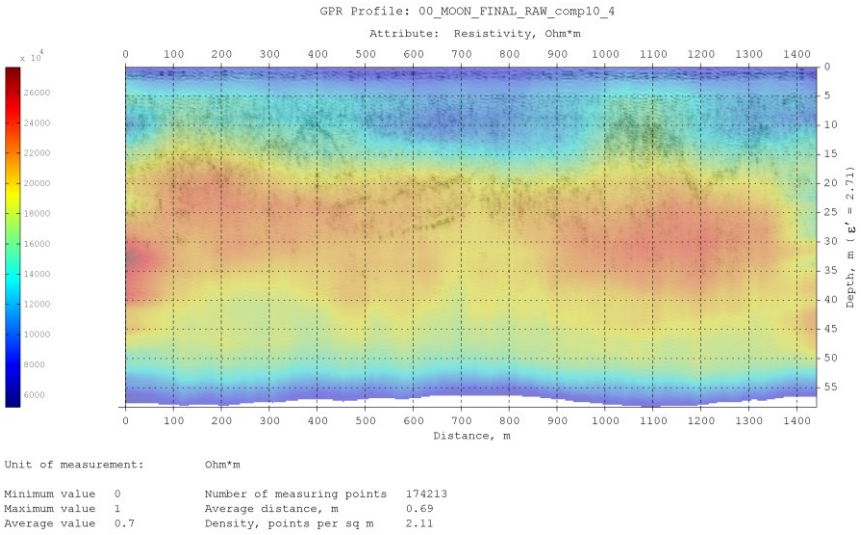


Figure 7. Results of the distribution of the electrical resistivity, obtained by the described procedure and formulas.

CONCLUSIONS

The Lunar Penetrating Radar on Yutu-2 has provided data with a fairly good resolution and reveals an excellent depth penetration for such a high central frequency. Our data processing and interpretation of the data reached depths of between 50 to 60 meters, whereas on Earth, due to the much higher conductivity, such an antenna, would only usually reach a depth of less than 5 meters. This fact and result provides some indication that the lunar near-surface structure is probably deprived of water and clay minerals, two key contributing factors towards increasing the electrical conductivity of the subsurface, that in turn decrease the penetration depth of the radar signal.

The estimated electrical values of relative permittivity and electrical resistivity fell, respectively, between 2 and 4 and 5.5E+07 and 2.7E+08 Ohm·m (1.82E-08 and 3.7E-09 S/m) and are in relative agreement with previous studies.

The Lunar Penetrating Radar on Yutu-2 has significantly advanced our knowledge of the Moon's subsurface. Its high-resolution imaging capabilities have uncovered some geometrically interesting geological features and processes that were previously unknown. This study, as well as those of other authors, also aims to contribute to provide a fairly consistent electrical model of the lunar subsurface. This tool has established a proof of concept and shown the utility of the technique towards the planning of future lunar missions. The success of the LPR highlights the importance of innovative instrumentation in space exploration and underscores China's growing capabilities in space science and technology.

ACKNOWLEDGEMENTS

Our acknowledgements for the financial support of our research group, Geobiotec (UIDB/04035/2020), Roman Denisov of *Georadar-Expert*, whose licensed software was used to process the data, the China National Space Administration (CNSA), for supplying the raw data and Giacomo Roncoroni, for the SEG-Y converted data.

https://doi.org/10.5593/sgem2024/1.1/s05.63

REFERENCES

[1] Lai, J., Xu, Y., Bugiolacchi, R. et al., First look by the Yutu-2 rover at the deep subsurface structure at the lunar farside. Nat Commun 11, 3426, (2020).
[2] Jia, Heming & Liu, & Zhang, Zhibin & Wu, Zhiwei, Weak Signal Extraction from Lunar Penetrating Radar Channel 1 Data Based on Local Correlation. Electronics 8, no. 5: 573, (2019).
[3] Zhang, Hongbo & Zheng, Lei & Su, Yan & Guangyou, Fang & Zhou, Bin & Feng, Jianqing & Shuguo, Xing & Dai, Shun & Li, Jun-Duo & Ji, Yi-Cai & Gao, Yun-Ze & Xiao, Yuan & Li, Chunlai, Performance evaluation of lunar penetrating radar onboard the rover of CE-3 probe based on results from ground experiments. Research in Astronomy and Astrophysics, (2014).
[4] Xiao Xiao, Shuoran Yu, Jun Huang, He Zhang, Youwei Zhang, Long Xiao, Thermophysical properties of the regolith on the lunar far side revealed by the in situ temperature probing of the Chang'E-4 mission, National Science Review, Volume 9, Issue 11, November, nwac175, (2022).
[5] Chen, Ruonan & Xu, Yi & Xie, Minggang & Zhang, Ling & Niu, Shengli & Bugiolacchi, R., Sub-surface stratification and dielectric permittivity distribution at the Chang'E-4 landing site revealed by the lunar penetrating radar. Astronomy & Astrophysics. 664, (2022).
[6] Li C, Su Y, Pettinelli E, Xing S, Ding C, Liu J, Ren X, . The Moon's farside shallow subsurface structure unveiled by chang'E-4 lunar penetrating radar. Science Advances; 6(9): eaay6898, (2020).

[7] Giannakis, I., Mcdonald, C., Feng, J., Zhou, F., Su, Y., Martin-Torres, J., Zorzano Mier, M.-P., Warren, C., Giannopoulos, A., & Leontidis, G., Automatic segmentation of radar data from the Chang'E-4 mission using unsupervised machine learning: A data-driven interpretation approach. *Icarus*, *417*, (2024).

[8] Davis, J., Annan, A., Ground Penetrating Radar for High Resolution Mapping of Soil and Rock Stratigraphy. Geophysical Prospecting, 37, 531-551, (1989).

[9] R. R. Denisov, V. V. Kapustin, Processing of georadar data in automatic mode, Geofizika No. 4, pp. 76-80, (in Russian) ISSN 1681-4568, (2010).

[10] Roncoroni, G., Forte, E., et al. High frequency Lunar Penetrating Radar quality control, editing and processing of Chang'E-4 lunar mission. Sci Data 11, 118, (2024).

[11] Moura, R., Almeida, F., & Teixeira, L., Seismic refraction traveltime tomography processing of Apollo 14 and 16 active seismic experiment data. International Multidisciplinary Scientific GeoConference Surveying Geology and Mining Ecology Management, SGEM, 19(1.1), 939-949, (2019).

[12] Dal Moro, G., Joint Analysis of Rayleigh-Wave Dispersion and HVSR of Lunar Seismic Data from the Apollo 14 and 16 Sites. Icarus. 254, (2015).

[13] Kovach, R., Watkins, J., and Talwani, P., Active Seismic Experiment; in Apollo 16, Preliminary Science Report NASA SP-315, p.10-1 – 10-14, (1972).

[14] Ping, J., Meng, Z., Lunar Surface Electrical Conductivity, Encyclopedia of Lunar Science, Springer International Publishing, pp. 1-3, (2017).

RECEIVER FUNCTIONS APPLICATION FOR STUDYING THE DEEP STRUCTURE OF THE LENA DELTA REGION

Mikhail Novikov[1]

Dr. Artem Krylov[1]

Dr. Konstantin Roginskiy[1]

[1] Shirshov Institute of Oceanology of Russian Academy of Sciences, **Russia**

ABSTRACT

Receiver function analysis is a critical tool in seismology, used to study the deep structure of the crust and upper mantle. Information about the deep structure of the crust and seismicity is important initial data for developing a source model and seismic hazard assessment.

The presence of sharp discontinuities beneath the monitoring station induces the generation of converted body waves, which propagate at slower velocities than those of the primary P-wave. Receiver function analysis utilizes the lag between the arrival times of converted waves to estimate the depths of interfaces. Furthermore, by using various inversion algorithms, including receiver function inversion and surface wave group velocity inversion, a shear wave velocity model under the station can be inferred.

This study seeks to examine the depth-velocity structure of the Lena Delta by analyzing receiver functions and surface-wave data. Receiver function analysis was performed using waveforms from the TIXI station, a component of the Yakutsk Regional Seismic Network of the Russian Federation. For the analysis, 245 large earthquakes (Ml > 7) occurring between 2000 and 2024, and located at distances ranging from 20° to 100° from the station, were initially selected. The iterative deconvolution was then used to obtain radial and transverse receiver functions. Three different inversion algorithms were used to attain the velocity model: receiver function inversion (rftn96), Rayleigh group wave velocity inversion (surf96), and joint inversion (joint96).

A wide peak lasting from 3 to 5 seconds after the initial P-wave arrival and a sharp peak at 7.5 seconds were observed on the radial receiver function. The presence of two distinct peaks complicates the application of conventional H-k stacking analysis, which assumes a single discontinuity. Rayleigh wave group velocity inversion only showed one sharp increase in shear wave velocity at 15 km, while both receiver function inversion and joint inversion showed step-like increases at 15, 30, and 40 km, which indicates the presence of layer boundaries at these depths. The obtained values are consistent with existing data on the region, including deep seismic sounding profiles and crustal models. Previous research, along with the findings of this study, indicates that 15 km is most likely the boundary between the upper and the lower crust, 30 km is a transition to the anomalous mantle, and 40 km is the Moho boundary.

Keywords: receiver function, Lena River Delta, surface wave inversion

https://doi.org/10.5593/sgem2024/1.1/s05.64

INTRODUCTION

Receiver function analysis is a common tool in seismology for investigating the structure of the Earth's crust and the upper mantle. This method is based on the idea that sharp discontinuities within the Earth produce converted waves, which can then be captured in recorded waveforms. Converted body waves travel more slowly than the initial P-wave, and by analyzing the lag in their arrival, the depth of the interface can be determined. Since the vertical component of the seismogram contains the source wavelet, it undergoes a deconvolution from the radial component to form a receiver function. Receiver function analysis technique requires at least a few dozen strong, distant earthquakes to be captured by three-component seismic sensor.

The study area, the Lena Delta, is located in the Laptev Sea region of the Russian Arctic. The Lena Delta has high levels of seismicity, most of which occur inside the crust, which is 30-40 km thick [1]. Most seismic events occur along the sublatitudinal faults and are part of the Lena-Taymyr earthquake zone [2]. The stressed state of the crust is characterized by compression in the center, transpression in the western part and transtention in the eastern part of the delta [3].

This region is located on the boundary of the Siberian Craton and the Laptev Sea rift system, in an area of relatively abrupt change in crustal thickness. This determines the interest in the complex tectonics and deep structure of this region. In addition, data on the deep structure of the crust are of practical importance for seismic hazard assessment.

Due to low accessibility and the absence of dense permanent seismological networks, the region is poorly studied in terms of seismicity and crustal structures. The primary objective of this study is to investigate the depth-velocity structure of the Lena Delta using receiver function analysis and surface-wave data.

MATERIALS AND METHODS

We used recordings from TIXI station, which is located approximately 50 km away from the Lena River's main channel and is part of the Yakutsk Regional Seismic Network. For the receiver function analysis, 245 large events (Ml>7) that occurred between January 2000 and January 2024 with epicentral distances from 30 to 100 degrees were selected. For surface wave group velocity inversion, smaller events (Ml >6) were also used, with a total of 525 earthquakes.

For receiver function analysis, the Funclab toolbox for Matlab [4] was used. Seismograms were first converted to a ZRT coordinate system, 0.02 to 2 Hz bandpass filter was applied, and then iterative deconvolution with Gaussian parameter 1.5 was performed [5]. Subsequently, 103 receiver functions were handpicked for further analysis.

For depth-velocity structure inversion, Computer Programs in Seismology (CPS) package was used [6]. We've carried out three different inversions: receiver function inversion (using rftn96 subroutine), surface wave group velocity inversion (using surf96s subroutine), and simultaneous receiver function and surface wave group velocity inversion (using joint96 subroutine). For all inversion methods, a simplified AK135 starting model without a near-surface low-velocity zone was utilized [7].

Velocity dispersion curves were created for a 2000 second-long period after the P-wave arrival using Multiple Filter Technique [8] with $\alpha = 50$, and fundamental modes for Rayleigh wave group velocity were picked. Based on 31 fundamental modes, surface

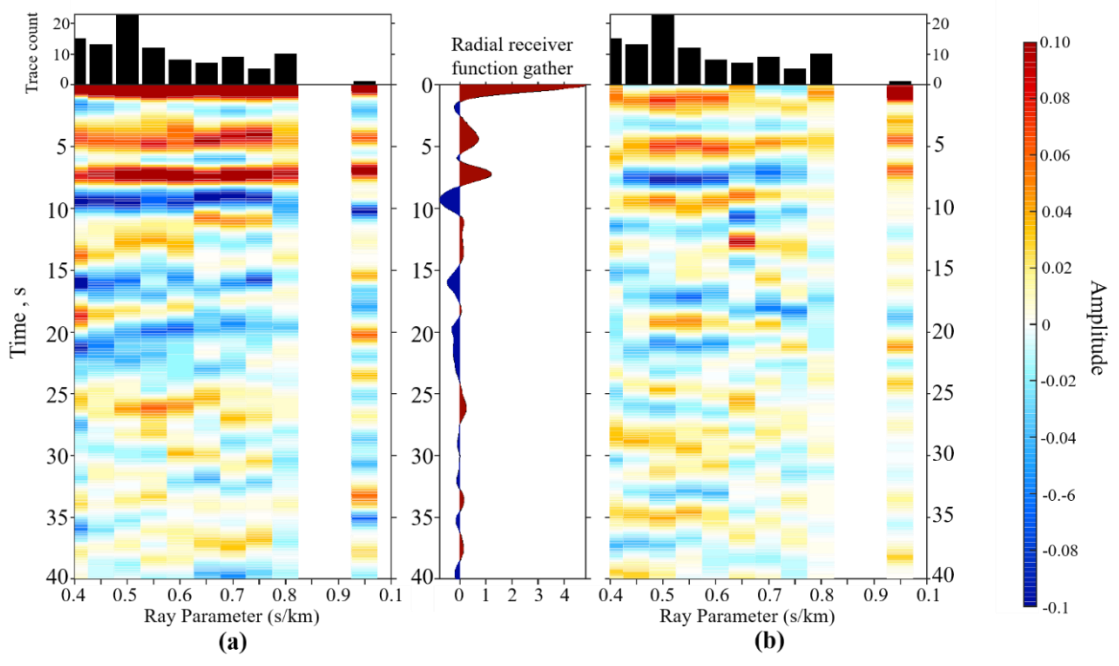
wave group velocity inversion was performed for 32 iterations of the algorithm. For both receiver function inversion and joint inversion, 90 traces were used for 18 iterations. The damping parameter was selected to be 10, 0.5, and 2 for rftn96, surf96, and joint96, respectively.

RESULTS

Receiver functions grouped by ray parameters with an interval of 0.05 s/km are shown in Figure 1. Radial receiver functions (Figure 1a) across the whole ray parameter range exhibit a wide peak 3-5 seconds after the initial P-wave arrival, as well as a sharp peak at about 7.5 seconds, followed by a decrease at around 10 seconds. Local maxima at approximately 13 and 18 seconds, followed by minima, are much more scattered in time and may indicate the Ppps and Psss phase arrivals. Transverse receiver functions (Figure 1b) have narrow peaks at 2, 5, and 10 seconds for all ray parameters.

Similarly, Figure 2 shows receiver functions grouped by backazimuths with an interval of 25°. The wide peak shifts from around 4.5 seconds for backazimuth intervals of 0-80° and 200-300° to approximately 3.5 seconds for backazimuths between 80-200°. The sharp 7.5 second peak can be clearly seen on receiver function from all events, except for a dozen earthquakes with backazimuths from 0 to 80°.

The results of receiver function inversion obtained by rftn96 package are shown in Figure 3a. Most of the observed receiver functions are well approximated by the model curves (Figure 3b). A near-surface low velocity zone is clearly visible from 0 to 15 kilometers, followed by a sharp increase in Vs. Notable sharp increases are also present at 30 and 40 km, followed by a stable 4.1 km/s velocity zone from 40 to 60 km.



.

Figure 1. Radial (a) and transverse (b) receiver functions grouped by ray parameter for TIXI station. Trace count is the number of traces in each of the ray parameter bins. Radial receiver function gather, shown in the middle, is created by stacking multiple receiver functions. The amplitude of receiver functions is shown in colour.

https://doi.org/10.5593/sgem2024/1.1/s05.64

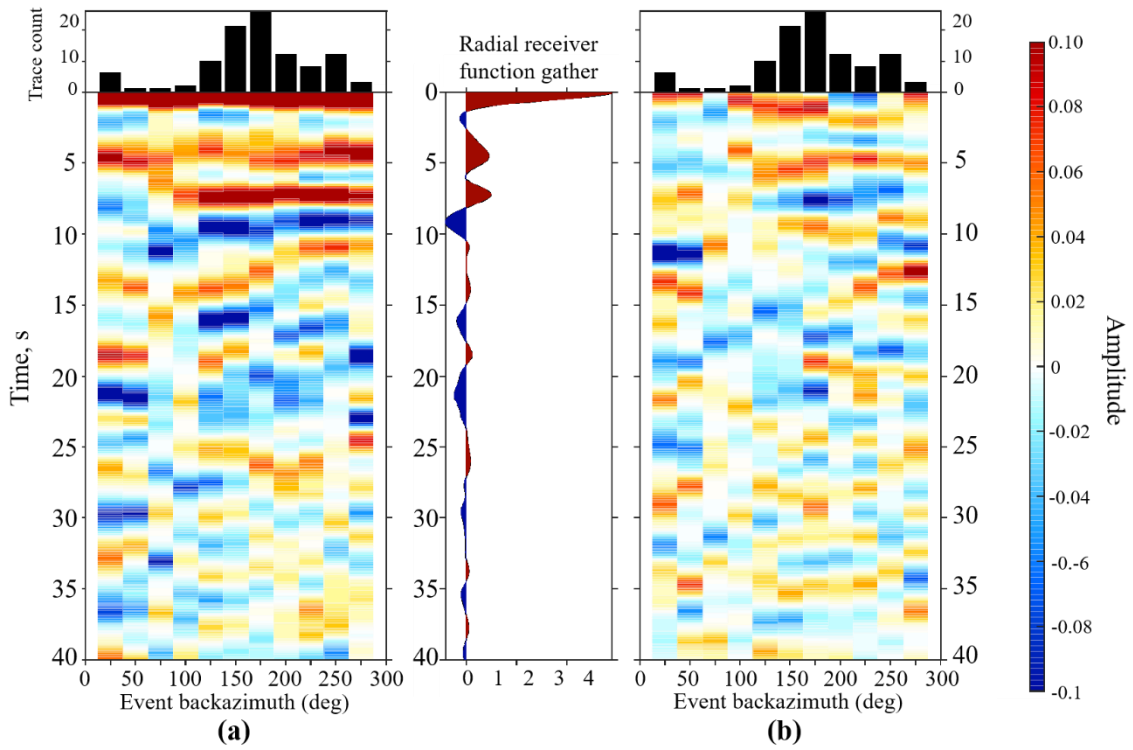


Figure 2. Radial (a) and transverse (b) receiver functions grouped by backazimuths for TIXI station. Trace count is the number of traces in each of the backazimuth bins. Radial receiver function gather, shown in the middle, is made by stacking multiple receiver functions. The amplitude of receiver functions is shown by colour.

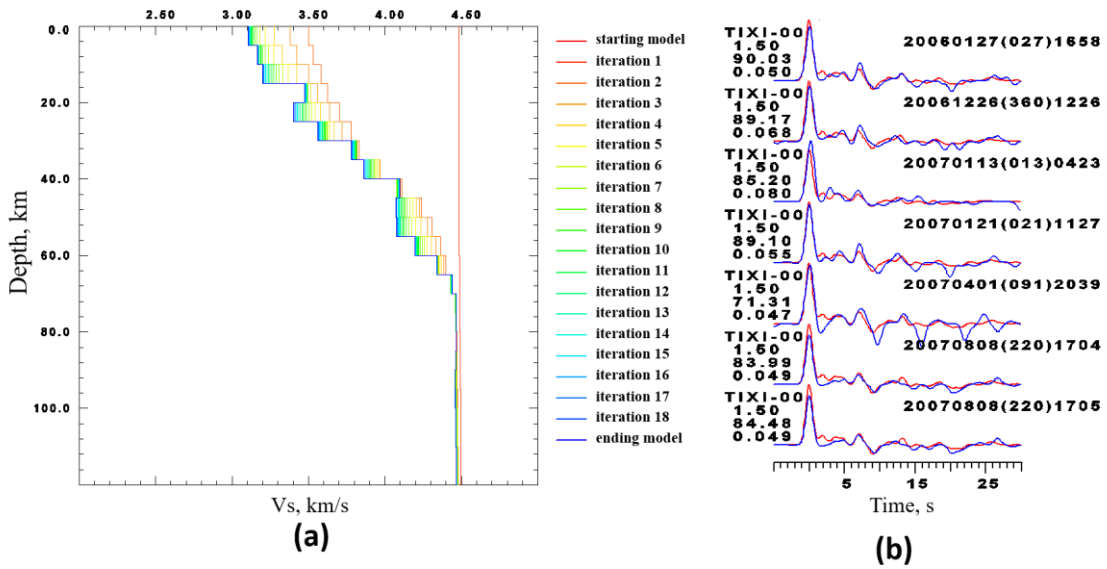


Figure 3. Vs depth distribution (a) and model fit to some observed receiver functions (b) obtained by rftn96. The lines of different colours on the left picture demonstrate the iterations of the model: the red line is the initial model, the blue line is the final model, and other colours are intermediate iterations. On the right picture, the red lines are observed receiver functions and the blue lines are model estimations.

The shear wave velocity distribution by depth obtained by surf96 is shown in Figure 4a, while Figure 4b presents the model curve fitted to the data. The low velocity zone is visible from 0 to 10-15 km, followed by a stable increase up to 4.5 km/s at 50 km.

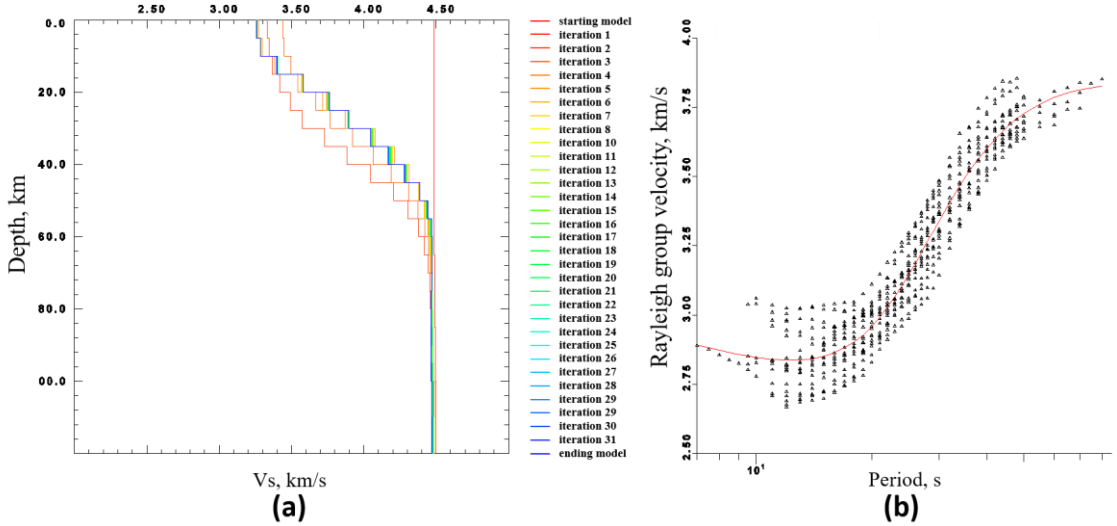


Figure 4. Vs depth distribution (a) and model fit to observed velocity curves (b) obtained by surf96. The lines of different colours on the left picture demonstrate the iterations of the model: the red line is the initial model, the blue line is the final model, and other colours are intermediate iterations. On the right picture, the red lines are observed receiver functions and the blue lines are model estimations

A comparison of the two velocity depth distributions obtained, as well as the one made by joint96 subroutine, are demonstrated in Figure 5. All models exhibit a distinct velocity increase at 15 km and 40 km, as well as a pronounced increase at 30 km.

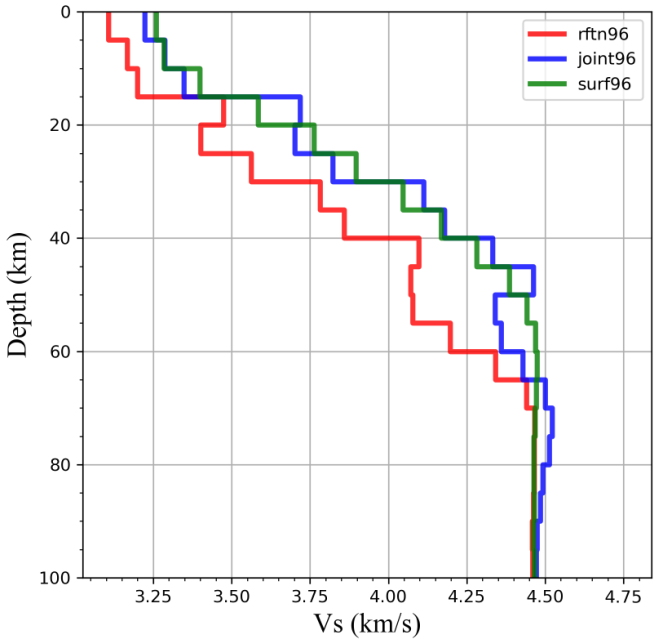


Figure 5. Comparison of Vs depth distributions obtained by rftn96 (red), surf96 (green), and joint96 (blue) subroutines.

https://doi.org/10.5593/sgem2024/1.1/s05.64

DISCUSSION

The presence of two distinct peaks (4-6 sec and 7.5 sec) on the receiver functions complicates the application of conventional H-k stacking analysis, which assumes a two-layer structure with a single discontinuity. The scattering of the Ppps and Psss phases is also expected in cases of more than one boundary.

Only the 15 km more or less clear boundary is visible on the surf96 velocity distribution, which shows limitations of this method using one station data. The velocity distribution, obtained both by rftn96 and joint96, showed noticeable velocity increases at 15, 30, and 40 km, which likely indicate boundaries at these depths. The results map well with existing data on the deep structure of the Ust-Lenskiy trough [2]: at depths of 18-20 km the upper boundary of the horizontal K1 layer is marked, at depths of 29-31 km a transition to the anomalous mantle (underplating) is noted, and at 39-40 km there is a transition to the normal mantle.

According to the composite seismogeologic section encompassing the Tiksi area, the boundary between the upper and lower crust is situated at 15-18 km depth, while the anomalous mantle lies beneath 30 km and the transition to the normal mantle occurs at 40-45 km [9]. The ending of the “Shpat 1983” deep seismic sounding profile lies near Tiksi and demonstrates the Moho boundary at 46 km with intermediate reflection horizons at 17 and 28 km [10].

The global crustal model CRUST 1.0 shows the Moho boundary to be 40 km deep for the area near Tiksi [11]. The refined velocity model of the Siberean Craton SibCrust [12] shows similar horizon depth values for the point near the edge of the Siberian platform (68.9N, 118E) —15 km for the upper to middle crust transition, 30 km for the middle to lower crust, and 40-42 km from the lower crust to the upper mantle. Furthermore, the boundaries obtained in the current study are consistent with different receiver function inversion method, which shows a sharp Vs increase at 18 and 40 km [13].

CONCLUSION

Examination of receiver functions revealed two prominent peaks, that consistently appear across various backazimuths and ray parameters, suggesting the potential existence of at least two major discontinuities in the near-surface area. To study the deep structure in more detail, we applied three different inversion methods: receiver function inversion, Rayleigh wave group velocity inversion, and joint inversion. Three incremental increases in shear wave velocity at 15, 30, and 40 km were found, which likely represent the boundaries of subsurface layers. These depth values align well with existing data obtained by different methods in previous studies of this region. The results of current and earlier studies suggest that 15 km is most likely the boundary between upper and lower crust (Conrad disconunity), 30 km is the transition to anomalous mantle (underplating), and 40 km is the Moho boundary. For a more comprehensive analysis of the subsurface structures beneath the TIXI station, it is necessary to take into account Vp and Vp/Vs distributions with depth. The current findings can be used in addition to multi-station receiver function analysis, surface wave tomography, and local earthquake tomography to form more advanced and informative insights into the deep structure beneath the Lena Delta, notable for being the boundary region between the platform and the rift system.

ACKNOWLEDGEMENTS

This work was financially supported by the Russian Science Foundation, project no. 23-17-00125 (routine processing of earthquakes signals from the TIXI station in the Lena Delta), the Russian State Assignment, project no. FMWE-2021-0011 (determination the deep structure of the crust).

REFERENCES

[1] Avetisov, G.P. Hypocentria and focal mechanisms of earthquakes of the Lena River delta and its surroundings. Volcanology and Seismology, Russia, vol. 6, pp. 59-69, 1991 (in Russian).

[2] Avetisov, G.P., Guseva, Y.B. Deep structure of the Lena delta area according to seismological data. Soviet Geology, Russia, vol. 4, pp. 73-80, 1991 (in Russian).

[3] Imaeva L.P., Gusev G.S., Imaev V.S., Dynamics of the relief and seismotectonic activity of the modern structures in the Lena River delta, Geotectonics, Russia, vol. 5, pp. 62-77, 2019 (in Russian).

[4] Porritt, R.W., Miller, M.S. Updates to FuncLab, a Matlab based GUI for handling receiver functions. Computers & Geosciences, vol. 111, pp. 260–271, 2018.

[5] Ligorría, J.P., Ammon, C.J. Iterative deconvolution and receiver-function estimation. Bulletin of the Seismological Society of America, vol. 89, no. 5, pp. 1395–1400, 1999.

[6] Herrmann, R.B. Computer programs in seismology: An evolving tool for instruction and research. Seismological Research Letters, vol. 84, pp. 1081-1088, 2013.

[7] Kennett, B.L.N. Engdahl, E.R., Buland R. Constraints on seismic velocities in the Earth from travel times. Geophysical Journal International, 122, pp. 108-124, 1995.

[8] Dziewonski, A., Bloch, S., Landisman, M. A technique for the analysis of transient seismic signals. Bulletin of the Seismological Society of America, vol. 59, no. 1, pp. 427–444, 1969.

[9] Avetisov, G.P. Seismicity and depth structure of the Laptev Sea and the Novosibirsk Islands. Structure of the Earth's crust of continents and oceans, Publishing House of the Leningrad State University, Proceedings of LOE 1983, vol. 77, pp. 117-124. 1983 (in Russian)

[10] Atlas "REFERENCE GEOLOGICAL AND GEOPHYSICAL PROFILES OF RUSSIA, Deep seismic sections along DSS profiles". Saint-Petersburg, 2013 (in Russian)

[11] Laske, G., Masters, G., Ma, Z., Pasyanos, M. Update on CRUST1.0 - A 1-degree Global Model of Earth’s Crust. Presented at the EGU General Assembly Conference Abstracts, EGU2013-2658, 2013.

[12] Cherepanova, Y., Artemieva, I.M., Thybo, H., Chemia, Z. Crustal structure of the Siberian craton and the West Siberian basin: An appraisal of existing seismic data. Tectonophysics, vol. 609, pp. 154–183, 2013.

[13] Vinnik, L., Oreshin, S., Makeyeva, L., Dündar, S. Fluid-filled porosity of magmatic underplates from joint inversion of P and S receiver functions. Geophysical Journal International, vol. 209, no. 2, pp. 961–968, 2017.

https://doi.org/10.5593/sgem2024/1.1/s05.64

SEISMIC RISK ASSESMENT FOR TRANSBOUNDARY AREA OF ROMANIA AND REPUBLIC OF MOLDOVA UNGHENI – UNGHENI-PRUT

Prof. Dr. hab. Vasile Alcaz[1]

Assoc. Prof. Dr. Igor Nicoara[1]

Assoc. Prof. Dr. Alina-Mihaela Precul[2]

Evgheni Isicico[1]

Lecturer Ioana Olteanu [2]

[1] Moldova State University, Institute of Geology and Seismology – **Republic of Moldova**

[2] Gheorghe Asachi" Technical University of Iași - **Romania**

ABSTRACT

Present paper objective is to assess the seismic hazard and seismic risk and provide an analyses of earthquake scenario for the transboundary area of Ungheni town in Republic of Moldova and Ungheni-Prut in Romania. For the present study as design seismic action (earthquake scenario) was selected the Vrancea earthquake with 475 years return period and magnitude M_w = 7.9. At first it was analyzed specified earthquake scenario using special macro seismic attenuation equation. This allowed the obtaining of probable distribution of the intensity in the study area. The estimation of seismic risk analyses and vulnerability of buildings in the study area was made based on statistical data and field evaluation in terms of MSK-64, especially for urban area of Ungheni, and transboundary villages.

Keywords: earthquake, hazard, risk, vulnerability, damages.

INTRODUCTION

The territory of Republic of Moldova is subject to the impact of earthquakes originating from Vrancea seismic zone, which is placed in Romania. Earthquakes of significant intensities can cause serious damage within both countries. The aim of this paper is to assess the seismic hazard and seismic risk for an area from Republic of Moldova, named Ungheni town in correlation with Border Village called also Ungheni, from Romania. Both residential areas have the particularity of being border cities. The main differences between them are area, population number, buildings number and type. Ungheni town from Republic of Moldova is larger in population number and area so that, in case of an earthquake, the probability of an increased number of casualties and loses is higher. It is known that human casualties are caused not by the seismic impacts themselves, no matter how strong they are, but by buildings that cannot withstand these impacts. Solving the problem of minimizing earthquake damage is only possible through the joint study of probable seismic impacts and the vulnerability of buildings in populated areas. Such tasks fall under the category of seismic risk assessment.

MATERIALS AND METHODS

Seismic risk is understood as the probability of socio-economic damage resulted from potential earthquakes in accordance with the calculated seismic hazard of the territory (H) and the vulnerability of the constructed and natural built environment (V):

$$R = H * V \quad (1)$$

The parameters characterizing the seismic hazard include the maximum seismic impacts that occur with a certain probability in a given area, over a specified period of time.

Seismic risk is a spatial-temporal category [1] and is usually calculated for specific areas and recurrence periods. According to Eurocode 8 [2] for a recurrence period equal to 475 years, events with a magnitude of M_w=7.9 correspond to Vrancea focal area of deep earthquakes. The intensity distribution of Vrancea earthquakes can be described as a function of earthquake magnitudes, the logarithm of the hypocentral distance, and the isoseismal ellipticity factor. The first two parameters traditionally participate in the description of any macroseismic field. The last parameter reflects the specific characteristics of Vrancea earthquakes, that have a pronounced isoseismal ellipticity, and establishes the location of the observation point relative to the average position of the ellipse axes.

The mathematical model of the intensity field, obtained from macroseismic data of the earthquakes on November 10, 1940, and August 30, 1986, which had the greatest macroseismic effect in the territory of the Republic of Moldova and eastern part of Romania, due to the northeast rupture direction, can be represented by the following equation:

$$I = 1.084\, M_w - 6.85 \lg R + 1.54 \cos\gamma + 13.7 \pm 0.35 \quad (2)$$

Where:

M_w - magnitude by seismic moment;

R – hypocentral distance;

γ – angle between the azimuth of the observation point and the azimuth of the major axis of the ellipse (θ_0 = 54 ± 2 [3]).

The equations of the macroseismic field were determined using the multiple regression method. Archived data on observed shaking intensity for a series of settlements in the territories of the Republic of Moldova, Romania and Ukraine, concentrated in the azimuth range of 0÷110˚ relative to the earthquake epicenter, were used as initial data for equation definition. A total of 279 data points were used in the correlation field: 211 for 1986 event and 68 for 1940 earthquake. Unlike several previous works that studied the general patterns of attenuation of intensity fields of Vrancea earthquakes [4, 5, 6, 7], equation (2) was derived for the best approximation of earthquake intensity fields with a northeast rupture direction. It allows obtaining the calculated value of earthquake intensity at any point within Republic of Moldova for a selected magnitude. Calculations indicate that during a scenario considering an earthquake with a magnitude of M_w=7.9 in the populated areas of Ungheni region, shaking intensities of 7 and 8 degrees will be observed and the average intensity of shaking will be 7.7 degrees. The expected acceleration for the populated areas will be 0.22 g.

The second fundamental element defining seismic risk is the seismic vulnerability of the built environment. An object vulnerability is understood as the property of a structure to lose its qualitative or quantitative reliability and safety due to any impact. Vulnerability varies between 0 and 1. The relationship between vulnerability and seismic impact is called the vulnerability function. The vulnerability function, linking the degree of damage to the level of seismic impact, expressed in degrees on the MSK scale is usually determined empirically for buildings with different structural systems. To create vulnerability functions, engineering consequences of strong local earthquakes are studied, global statistical data on damages for various classes of objects in similar seismo-geological situations are involved. Vulnerability functions primarily reflects the established construction practices in the region.

As an example, vulnerability functions for stone buildings (B type, MSK-64 scale), widely represented in the built environment of Ungheni region, are provided in Fig. 1.
According to the MSK-64 scale, there are six damage levels:
d_0 - no damage;
d_1 - slight damage; fine cracks in plaster, chipping of small pieces of plaster;
d_2 - moderate damage; small cracks in walls, chipping of fairly large pieces of plaster, roof tile falls, cracks in chimney stacks, parts of chimney stacks fall;
d_3 - heavy damage; large deep and through cracks in walls, chimney stack falls;
d_4 - destruction: collapse of internal walls and frame filling walls, breaches in walls, collapse of building parts, destruction of connections between building parts and
d_5 - collapses: complete destruction of buildings.

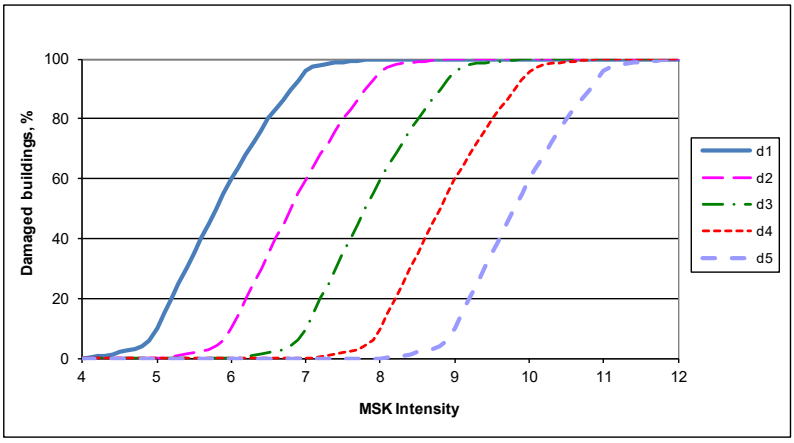


Fig. 1. Vulnerability function of stone buildings
(d_1- d_5 - degrees of damage according to the MSK-64 scale)

One of the most important stages in vulnerability assessment is the classification of buildings according to their response to a given seismic impact, i.e., determining their seismic resistance type. Such classification is carried out according to the MSK-64 seismic intensity scale, which provides for three types of structural systems:

A – buildings constructed of adobe, clay with straw (cob), clay cylinders, rubble stone, clay panels;

B – buildings made of wood, rubble and slag concrete, unreinforced foam concrete, brick, sawn limestone (boilers) without concrete reinforcement;

C – buildings of standard series and individual projects with seismic reinforcement, made of brick, stone, as well as concrete blocks and panels, reinforced monolithic concrete.

RESULTS

In the frameworks of this work, buildings in the region were classified according to types of their seismic resistance. Table 1 contains information about the infrastructure potential of the Ungheni cross-border region. It includes:

- on the Romanian side – the villages of Bosia, Ungheni, Coada Stâncii, Mânzăteşti (1712 households);
- on the Republic of Moldova side – the city of Ungheni (8225 households).

Table 1. Building stock and seismic resistance type of Ungheni district households according to EMS-98 scale

Name	State	No. of households	% of households by seismic resistance types		
			A	B	C, D, E *
Ungheni-Prut, Bosia, Coada Stâncii, Mânzăteşti	Romania	1712	46	30	24
Ungheni	RM	8225	27	39	34

* D, E – vulnerability classes according EMS-98.

All types of buildings are represented in the settlements. Unfortunately, the number of the most vulnerable buildings from a seismic point of view, type A, remains quite high.

Knowing the intensity of the seismic impact, the infrastructure exposed to the impact, and its vulnerability, it is possible to calculate the risk of damage. The probabilistic value of seismic risk, represented in the classic form by expression (1), is largely abstract and may be difficult for most users to comprehend. In everyday life, it is more convenient to use tangible indicators arising from a given seismic event, such as expected damage, volume of presumed destruction, number of affected residents, etc.

In this study, seismic risk was determined in the form of forecasts of average damage and the number of destroyed buildings within each populated area. The averaging of the calculation results and their mapping were carried out within the conventionally designated blocks. The averaging of the obtained results and their mapping was carried out within conventionally delineated blocks (quarters).

In first case within populated areas, the average degree of damage to objects was determined for the selected seismic event using vulnerability matrices constructed for this purpose.

$$\bar{d} = \sum_i d_i n_i \ / \ \sum_i n_i \qquad (3)$$

Where:

d_i – degree of building damage;

n_i – number of similar buildings with damages d_i.

The map of quarter-wise averaged damage degrees is shown in Fig. 2.

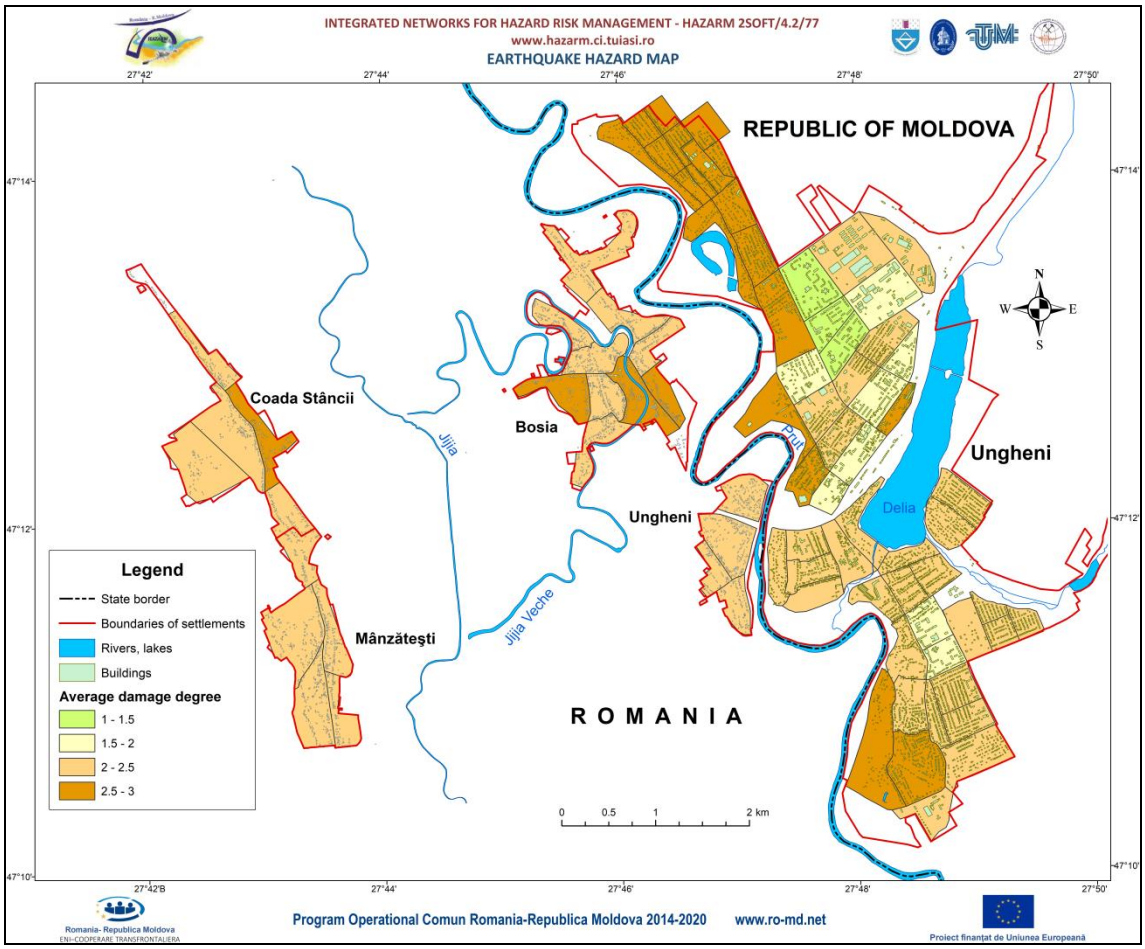


Fig. 2. Damage degree of buildings in Ungheni region in case of an earthquake with M_w=7.9

In second case the resulting indicator was the volume of presumed destruction within each populated cvartal of settlements. Destroyed buildings mean structures that are typically irreparable and have sustained damage of the fourth (d_4) and fifth (d_5) degrees. The map of potential damage volumes is presented in Fig. 3.

https://doi.org/10.5593/sgem2024/1.1/s05.65

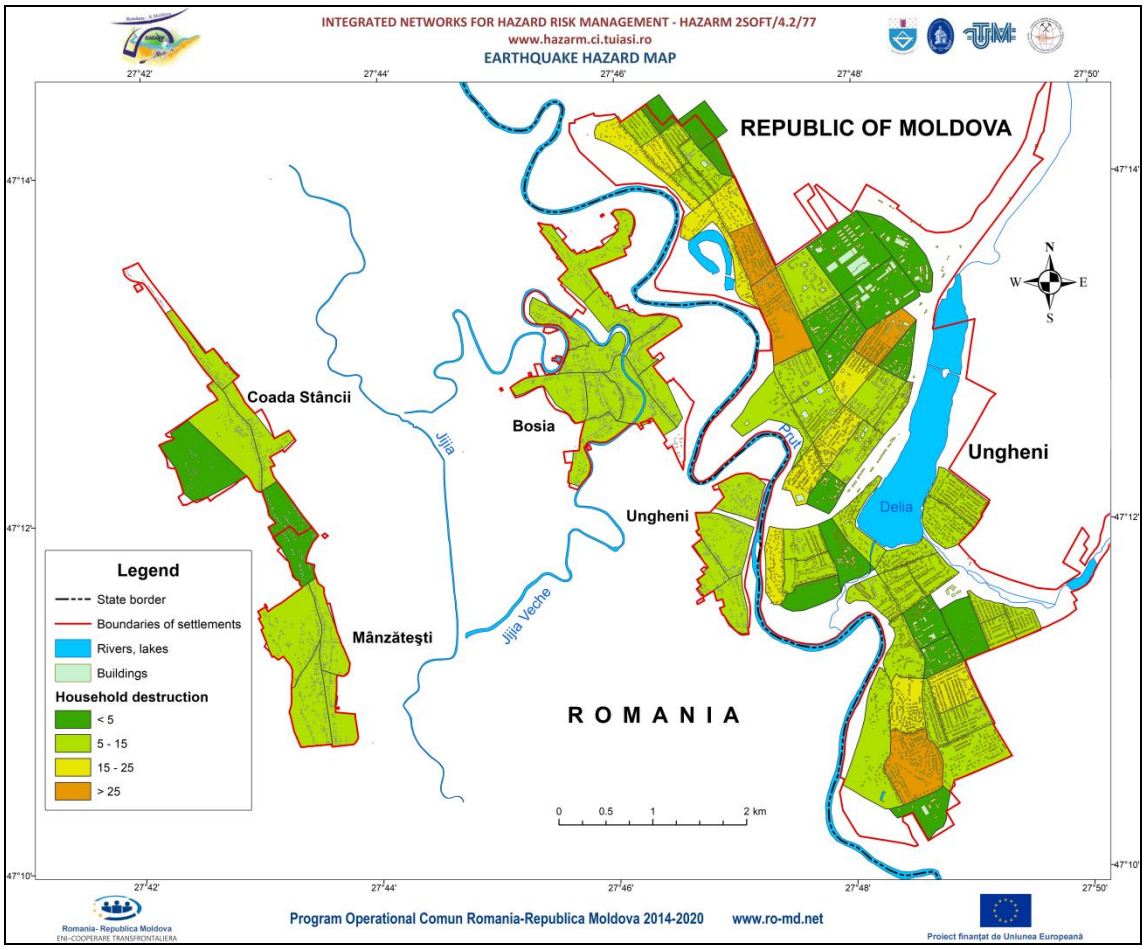


Fig. 3. Possible destruction of households in the Ungheni region in case of an earthquake with M_w=7.9

The expected statistics of damages to different types of buildings for Ungheni region during a scenario earthquake are shown in Fig. 4.

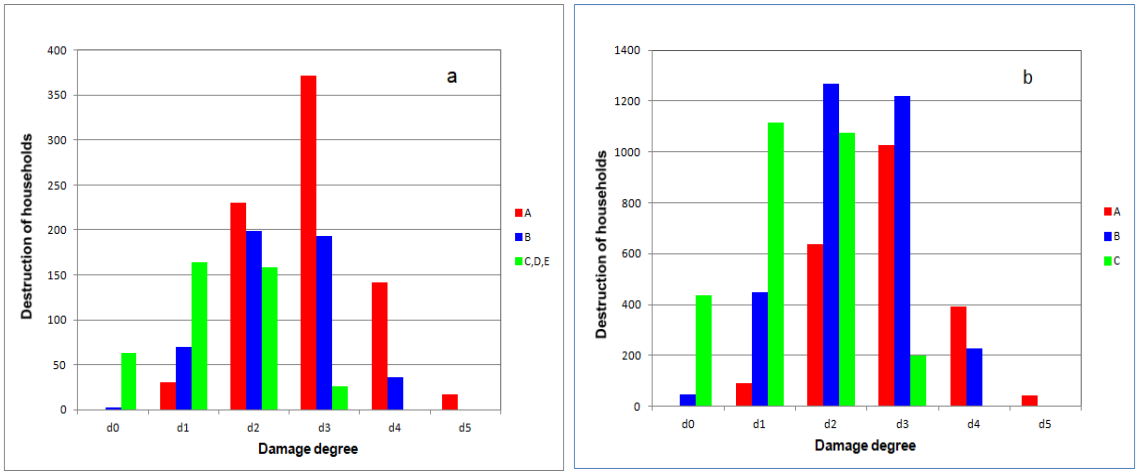


Fig. 4. Vulnerability and damageability of households in Romanian part (a) and Moldovian part (b) localities.

DISCUSSION

Must be understood that the presented results are probabilistic in nature. Thus, when specifying the initial seismic impact (scenario earthquake), were made a number of assumptions regarding the earthquake's strength, location of its focus, intensity attenuation function with distance and so forth. Moreover, the probabilistic nature of building vulnerability under the specified impact was accounted by vulnerability matrices.

Upon examining Fig. 2, 3, 4 several questions arise: how should one interpret the obtained results and what is their likelihood? Especially considering that both components of seismic risk in formula (1), the calculated seismic hazard and vulnerability, have a probabilistic nature. They should be approached as such - bearing in mind that once every five centuries Ungheni region, possessing the specified infrastructure and vulnerability of structures, if subjected to an earthquake with a magnitude of M_w=7.9, might experience the damages as shown on presented figures.

Regarding the accuracy of the absolute forecast of potential damage, the authors of this study see its value primarily in determining the mathematical order of magnitude of possible destruction and casualties. In other words, it can be asserted that during such a scenario earthquake, Ungheni transboundary region will face serious consequences in the form of hundreds of destroyed houses and, as a consequence, hundreds of affected residents. The forecast of the territorial distribution of possible material and social damage can provide invaluable assistance in planning and carrying out preventive and future recovery efforts following severe earthquakes in Vrancea region.

CONCLUSION

The major contributor to the economic prejudices inflicted by seismic hazard is the massive damage that could occur in urban and rural areas. The probable distribution of seismic risk in Ungheni region (transboundary area of Ungheni town în Republic of Moldova and Ungheni-Prut in Romania) from scenario earthquake was evaluated. Estimates were performed in terms of probably building damage for buildings of different types of seismic resistance.

Despite the apparent significant distance of Ungheni region from Vrancea earthquake zone, potential seismic impacts in this area pose one of the main threats to the residents of Romania and the Republic of Moldova. With a seismic event of magnitude Mw=7.9, as considered by Eurocode 8 for this focal point as the normative standard, the examined settlements will face serious threats of both infrastructure and social nature. Given the current vulnerability of structures, hundreds of houses in these settlements will be prone to destruction, resulting in hundreds of affected residents. To minimize potential damage, significant attention should be focused on enhancing the seismic resilience of residential buildings and social facilities.

So, the practical significance of seismic risk evaluation consists in identification of the most vulnerable to earthquake areas, thus providing the opportunity of elaboration of media- and long term strategic plans for minimizing material and human losses.

https://doi.org/10.5593/sgem2024/1.1/s05.65

ACKNOWLEDGEMENTS

Thanks to all team members of transboundary project HAZARM. The study was performed in the frame of EU Joint Operational Programme Romania-Republic of Moldova, project HAZARM 2SOFT/4.2.77/2020 and national research subprogramme of Republic of Moldova with cod 01.09.01.

REFERENCES

[1] Papadopouos G.A., Arvantides, A.. Earthquake Risk Assessment in Greece, in Schenk (ed.), Earthquake Hazard and Risk, Ser. "Advances in Nat. and Technol. Hazards Research", v.6, The Netherlands, Editorial Office Kluwer Acad.Publ., 1996, pp. 221-229.

[2] Eurocode 8: Design of structures for earthquake resistance. - European Committee for Standardization, May 2002. 213 p.

[3] Shumila V.I. Models of the seismic intensity field of transient Carpatian earthquakes in the Vrancea region. In. Carpatian earthquake 1986, Kishinev. “Shtiintsa”, 1990. pp.127-133. (in russian)

[4] Marza V. & Pantea A., Probabilistic Estimation of Seismic Intensity Attenuation for Vrancea Subcrustal Sourses, Proceedings of the XXIV General Assembly, V.III, Athens, Greece, 1994, pp. 1752-1761.

[5] Constantinescu L., Enescu D., Relatia Energie-Manitudine-Intensitate pentru cutremurele carpatiene. Parametrii regimului seismic pentru regiunea Vrancea. St. Cercetari. Geofizice, 1, 1963, p.239-268.

[6] Zaicenco A., Lungu D., Alkaz V. and Cornea T., Classification and Evaluation of Vrancea Earthquake Records from Republic of Moldova. In: Vrancea Earthquakes: Tectonics, Hazard and Risk Mitigation. Kluver Academic Publishers, Dordrecht/Boston/London, 1999, pp.67-76.

[7] Drumea A.V., Shebalin N.V. Earthquake: what, where, when? Kishinev, Shtiintsa, 1985, 196 p. (In russian)

PROBABILISTIC EARTHQUAKE SCENARIOS FOR THE CITY OF VARNA

Prof. Dimcho Solakov[1]

Assoc. Prof. Stela Simeonova[1]

Assoc. Prof. Plamena Raykova[1]

[1]National Institute of Geophysics, Geodesy and Geography, Bulgarian Academy of Sciences, Sofia 1113, **Bulgaria**

ABSTRACT

In the present study probabilistic earthquake, scenarios for the city of Varna the third-largest earthquake-prone city in Bulgaria are presented.
The probabilistic hazard for a city is obtained by integrating the effects of ground motion from earthquakes of different size occurring at different locations within different seismic source regions and with different frequencies of occurrence.
The ground motion maps for the city of Varna are generated combining via GIS, source geometry, earthquake occurrence model, maximum earthquake magnitude, and the appropriate attenuation relations. The probabilistic scenario maps are created in terms of MSK intensity, Peak Ground Acceleration (PGA) and response spectral accelerations for 95- and 475-year return periods. The estimated values of PGA for 95- and 475-year return periods vary along the city from 0.08 to 0.11 and from 0.15g to 0.23g) respectively. For the considered return periods the macroseismic intensity (MSK) vary from 6.4 to 6.8 and from 7.4 to 7.8 (for 95 and 475-year return period respectively).
The main objective of the study is to integrate basic geo-datasets and to assess the seismic hazard using GIS to provide a basis for disaster management of the city of Varna. Spatial distribution of the obtained results is available in GIS format and can be used not only for scientific purposes but also for practical measures to reduce the risk and limit the consequences of a future strong earthquake.

Keywords: earthquake, probabilistic earthquake scenario, GIS, the city of Varna

INTRODUCTION

The city of Varna (historically known as Odessos) is one of the oldest settlements in Bulgaria and has been a major economic, social and cultural centre for almost three millennia. Nowadays, the city of Varna is an important administrative, economic, educational, and cultural centre.
The present study focuses on the probabilistic seismic hazard for the third-largest earthquake-prone city in Bulgaria - the city of Varna. The city has experienced strong earthquake more than hundred years ago in 1901 [1].
The study on seismic hazard is performed applying the approach adopted for developing ground motion hazard maps (earthquake scenarios) in the Risk EU Project (2001-2004) funded by The European Economic Commission (presented in [2]) Two approach are adopted for developing ground motion hazard maps (earthquake scenarios) – deterministic and probabilistic

https://doi.org/10.5593/sgem2024/1.1/s05.651

The work on scenarios is guided by the perception that usable and realistic (also in the sense of being compatible with seismic histories of cities that are several centuries long) ground motion maps had to be produced for urban areas.
By deterministic scenario it is mean a representation of the severity of ground shaking over an urban area, using one or more hazard descriptors. The important feature of the approach is that the deterministic scenario must be consistent with the seismic history of the city and with known active faults close to the city. Ddeterministic earthquake scenarios for the city of Varna are generated in our previous work and presented in [3].
The Probabilistic seismic hazard is the probability that various levels of strong ground motion will be exceeded during a specified time period at a site (city, region, country etc.). The analysis methodology is based on the conception that the seismic hazard at a site is a function of three main components: the space geometry of seismic sources, the statistics of their seismicity and the characteristics of seismic wave propagation in the region.
Probabilistic approaches were developed to provide a more systematic method to deal with the "uncertainty in the number, sizes, and locations of future earthquakes" [4] than the arbitrary selections used previously [5]. PSHA was developed in the late 1960s and early 1970s at the Universidad National Autonoma de Mexico (UNAM) and the Massachusetts Institute of Technology (MIT) and it has now become the most widely used approach for estimating seismic-design loads. Modern techniques allow uncertainties in the seismic input to be included in the analysis. In the present study, the PSHA was performed by using a version of machine code EQRISK [6] that was developed and used in practice for hazard assessment in Bulgaria [among others in 7].
When both deterministic and probabilistic results are obtained, deterministic assessments can be used to check the probabilistic ones in terms of the reasonableness of the results while the probabilistic results allow deterministic values to be evaluated within a probabilistic framework.

MATERIALS AND METHODS

Seismic source model

A seismic source model, which demands translating seismotectonic information into a spatial approximation of earthquake location and recurrence, is a key component of seismic hazard assessment. Seismicity in the 200 km region surrounding the city of Varna is associated within 12 seismic sources. The regional seismic source model used in seismic hazard analysis for the city of Varna is illustrated in Fig. 1 and specified in Table 1. Each source is characterized by its own specific seismicity, and geological and tectonic development. The source model includes all seismic sources that substantially influence the seismic hazard of the city of Varna. For each seismic source, the geometry, active fault parameters, earthquake distribution within the source area, earthquake recurrence frequency and maximum potential earthquake magnitude are defined (details are presented in [7]).

Earthquake recurrence

The exponential magnitude model and average rate of occurrence are adequate to specified seismicity in a source. In the present study a truncated exponential distribution is assumed as seismicity model for each seismic source.

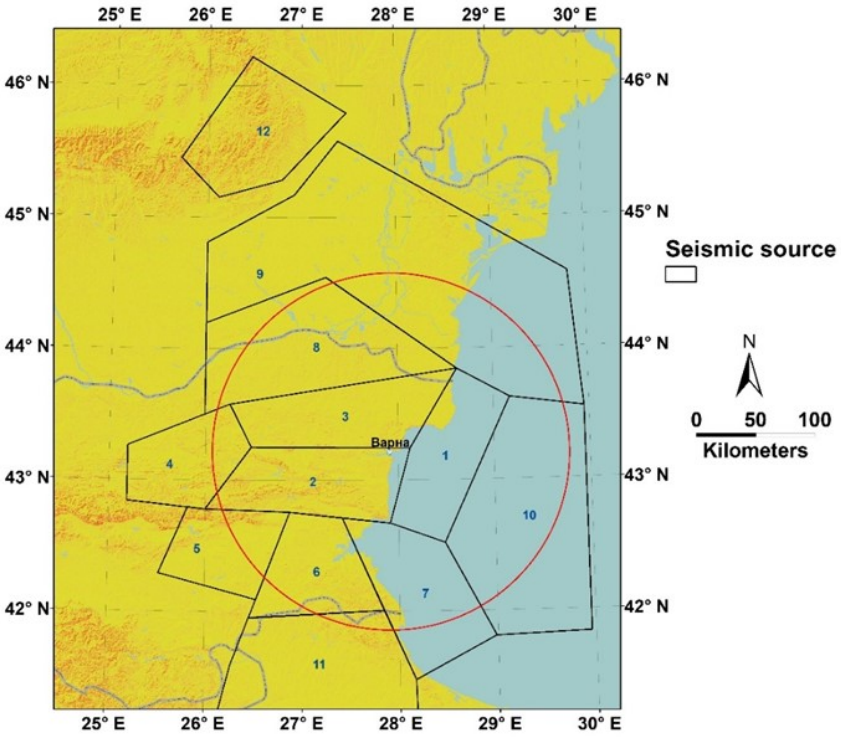


Figure 1. Seismic source model (modified from [7])

Table 1 Seismic source parameters used in the hazard analysis

Source number	Gr		M_{max} Observed	M_{max} Estimated
	a	*b*		
S1	1.79	0.68	7.1	7.7
S2	2.25	0.80	5.0	7.1
S3	1.84	0.80	5.7	6.2
S4	2.18	0.80	6.8	7.1
S5	2.52	0.80	6.0	6.9
S6	2.02	0.80	4.9	6.2
S7	1.74	0.80	4.7	6.9
S8	2.03	0.80	6.3	7.2
S9	2.90	0.94	5.4	6.5
S10	3.81	0.90	6.8	7.5
S11	2.68	0.90	7.1	7.7
S12	4.50	0.85	7.9	8.0

Gr — estimated parameters of the Gutenberg-Richter relationship
M_{max}—maximum magnitude

Consequently, the seismicity statistics are defined by specifying the magnitude-frequency relation with the annual seismic rate parameter, λ, the *b*-value of the Gutenberg-Richter exponential relation [8], the minimum magnitude, M_{min} and the maximum magnitude, M_{max}.

The rate of occurrence λ is calculated on the base of the parameters *a* and *b* in Gutenberg-Richter exponential relation (log N = a-bM). The seismicity parameters for

https://doi.org/10.5593/sgem2024/1.1/s05.651

each seismic source in the area within a radius of 200 km surrounding the city of Varna that are used in the PSHA are presented in Table 1.

Ground Motion Attenuation

The relations between some strong motion parameters and earthquake rupture parameters, wave propagation paths and local site conditions are represented with mathematical equations, such as ground motion prediction equations - GMPEs. Selection of the GMPEs (also referred to as attenuation relations or models) is an essential step in seismic hazard assessment.

To select the appropriate prediction equations, a set of criteria related to tectonic settings, the characteristics of basic data sets, the frequency ranges of prediction equations, and others are defined. Finally, six GMPE's models for shallow earthquakes in tectonically active regions and one for intermediate depth earthquakes generated in Vrancea, Romania [9] were selected and applied for seismic hazard assessment.

The method presented in [10] is chosen for testing the selected models against the actually recorded ground-motion data from the Balkan countries, Italy and the Middle East [11]. The approach describes in [12] is used for ranking the selected six GMPE's.

Details of the selection process and GMPE's justification can be found in [7].

Treatment of Uncertainties

The epistemic variability (uncertainties) comes from statistical or modelled variations. The large uncertainties in seismic hazard result from lack of knowledge about earthquake cause, characteristics, ground motions, i.e. from uncertainties in seismic input. Modern methods of seismic hazard analysis incorporate uncertainties into the analysis to assess their impact on the estimate of the expected level of seismic hazard as well as the uncertainty in that estimate.

In the present study for accounting the epistemic uncertainties in the seismic input, a logic tree approach ([13], [14]) is used.

For the PSHA analysis of the city of Varna, the 4 logic tree levels have been used (details are presented in [7]): Level 1 - Seismic source model- the seismic source model presented in Fig. 1 is considered; Level 2 - Seismic sources - a logical tree is generated for each seismic source; Level 3 - Ground Motion Prediction Equations (GMPE's) – the selected GMPE's for shallow and intermediate depth earthquakes; Level 4 - Soil properties - the V_{S30} map for the city presented in [3] is applied.

RESULTS

Probabilistic Earthquake Scenarios for the City of Varna

Using the model of seismic sources presented in Figure 1 and defined in Table 1, probabilistic seismic analysis (PSHA) for the city of Varna is performed. The ground motion PGA values (in terms of g) are calculated using the selected GMPEs (six for shallow and one for intermediate earthquakes). Four level logic trees for each seismic source are developed to account for uncertain-ties in seismic input. The soil properties of the urban area are incorporated in the scenario generation by using the map for average shear-wave velocity in the upper 30 m of the soil/rock profile for the city of Varna that is presented in [3]. The epistemic uncertainties are considered, with 4-level logic trees generated for each seismic source. Probabilistic scenario maps are created in terms of PGA and macroseismic intensity (MSK) for 95- 475- and 1000-year return

periods. The scenario maps for 95-and 475- year return periods are presented in figures 2 and 3.
The figures show that the maximum PGA and macroseismic intensity values are at the central part of the city of Varna.
The estimated PGA for the city of Varna varies from 0.08g to 0.11g and between 0.15g-0.23g, for 95- and 475-year return periods, respectively (as shown in Figures 2a and 2b). Figures 3a and 3b illustrate that macroseismic intensity (MSK) varies from 6.4 to 6.8 and between 7.4 and 7.8, for the 95- and 475- year return periods, respectively.

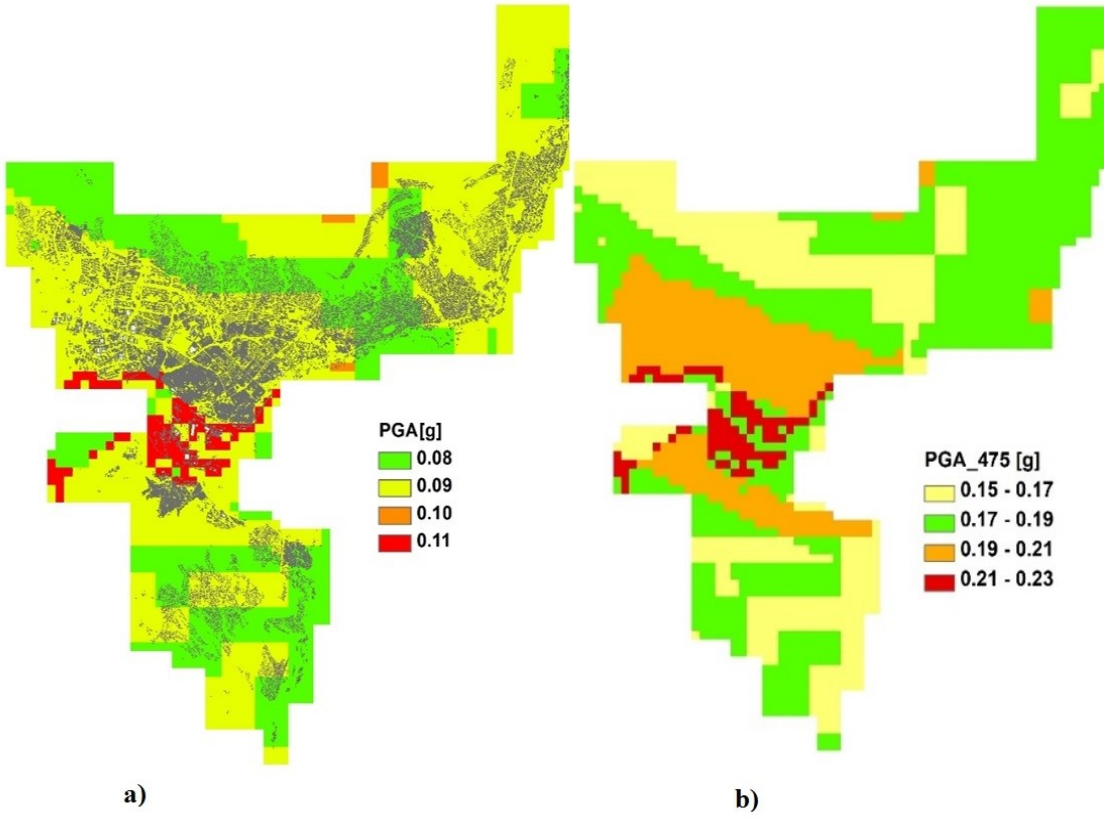


Figure 2. Probabilistic scenario maps in terms of PGA: a) for 95-year return period; b) for 475-year return period

https://doi.org/10.5593/sgem2024/1.1/s05.651

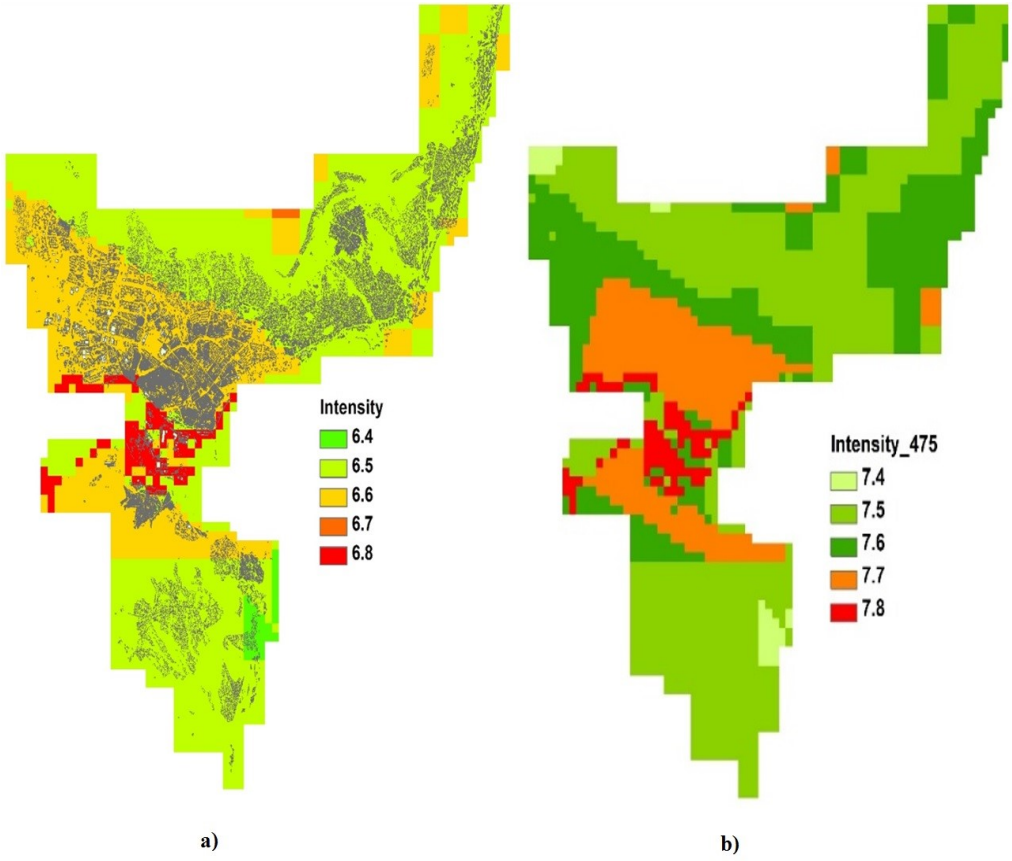


Figure 2. Probabilistic scenario maps in terms of macroseismic intensity (MSK): a) for 95-year return period; b) for 475-year return period

To compare the results of the deterministic and probabilistic analysis, the parameters (PGA and macroseismic intensity) evaluated using both methods (presented in Table 2) are considered.

Table 2 Deterministic and probabilistic estimates for the city of Varna

Earthquake scenario	**PGA [g]**	**Intensity (MSK)**
Deterministic scenario for Mw7.2 quake	0.07 - 0.14	6.2 - 7.2
Deterministic scenario for Mw6.5 quake	0.14 - 0.44	6.9 - 8.7
Probabilistic scenario for 95-year return period	0.08 - 0.11	6.4 - 6.8
Probabilistic scenario for 475-year return period	0.15 - 0.23	7.4 – 7.8

The data presented in Table 2 show a comparatively good agreement between deterministic estimates of PGA and macroseismic intensity (MSK) for M_W7.2 quake (occurred in Kaliakra strike slip fault - Shabla seismogenic zone) and the same strong motion parameters evaluated for the 95-year return period using the probabilistic approach.

The generated maps in terms of intensity (MSK) and PGA [g] for scenario earthquake with M_W=7.2 in Kaliakra fault zone are presented in the study.

In addition, the estimated impacts on the city of Varna of the 1901 M_W7.2 earthquake are of intensity between 7.0 and 7.5 MSK [3 and 15]. As shown in Table 2, the highest

deterministic estimates of macroseismic intensity (7.2 MSK) for M_W7.2 quake (occurred in Kaliakra strike slip fault) is very close to the lowest value of the same strong motion parameter evaluated for the 475-year return period (7.4 MSK). Both deterministic and probabilistic macroseismic intensity estimates are within the interval [7.0-7.5] that is defined by the observed impacts on the city.

CONCLUSION

In the present study, probabilistic earthquake scenarios in terms of PGA and macroseismic intensity (MSK) for 95 - and 475- year return periods are generated.
Two deterministic scenarios for earthquakes with different location and magnitudes (M_W6.5 earthquake in the nearest normal fault located northern from the city of Varna and M_W7.2 quake in Kaliakra strike slip fault) were presented in [3].
Finally, it should be stated that both deterministic and probabilistic earthquake scenarios are considered as a basic input for developing detailed earthquake damage scenarios for the cities and can be used in earthquake-safe town and infrastructure planning and mitigating disasters.
In conclusion, the consideration of the earthquake scenarios into the policies for seismic risk reduction will allow focusing on the prevention of earthquake effects rather than on the activities following the disasters.

ACKNOWLEDGEMENTS

This work has been carried out in the framework of the National Science Program "Environmental Protection and Reduction of Risks of Adverse Events and Natural Disasters", approved by the Resolution of the Council of Ministers № 577/17.08.2018 and supported by the Ministry of Education and Science (MES) of Bulgaria (Agreement № Д01-271/09.12.2022).

REFERENCES

[1] Watzof S., Earthquakes in Bulgaria. Report on the earthquakes felt in 1901. Central Meteor. Inst., S., pp.39 (in Bulgarian, abstract in French), 1902

[2] Faccioli F. and V. Pessina V., WP2 Basis of a handbook of earthquake ground motions scenarios, RISK-UE, EVK4-CT-2000-00014, 2003

[3] Solakov D., S. Simeonova. P. Raykova, Deterministic earthquake scenario for the city of Varna. In: 22 International Multidisciplinary Scientific GeoConference: Science and Technologies in Geology, Exploration and Mining, SGEM 2022, Albena August 2022

[4] Cornell, C., Engineering seismic risk analysis. BSSA 5, pp.1583, 1968

[5] Bommer, J., Abrahamson, N., Why Do Modern Probabilistic Seismic-Hazard Analyses Often Lead to Increased Hazard Estimates? Bulletin of the Seismological Society of America, Vol. 96, No. 6, pp. 1967–1977, 2006

[6] McGuire, R., FORTRAN Computer Program for Seismic Risk Analysis, U.S. Geol. Surv. 491 Open-File Rep. 76–67, U.S., Rep. 1–90, 1976

https://doi.org/10.5593/sgem2024/1.1/s05.651

[7] Solakov, D., Simeonova, S., Trifonova, P., Georgiev, I., Raykova, P., Metodiev, M., Aleksandrova, I., Building Seismic Risk Management, Part 1 Probabilistic Seismic Hazard Assessment BAS Publ. House, Sofia, pp. 13-110, 2019 (in Bulgarian).

[8] Gutenberg, B., Richter, C.F., Frequency of earthquakes in California. Bull. Seism. Soc. Am. 497, 34, pp. 185–188, 1944

[9] Vacareanu R., M. Radulian, M. Iancovici, F. Pavel, and C. Neagu.. Fore-arc and back-arc ground motion prediction model for Vrancea intermediate depth seismic source. Journal of Earthquake Engineering, 19(3): 535-562.

[10] Scherbaum, F., Delavaud E. and Riggelsen C., Model Selection in Seismic Hazard Analysis An Information-Theoretic Perspective, BSSA, 99(6), pp. 3234–3247, 2009

[11] Basili R., Kastelic V., Demircioglu M., Garcia Moreno D., Nemser E., Petricca P., Sboras S., Besana-Ostman G., Cabral J., Camelbeeck T., Caputo R., Danciu L., Domac H., Fonseca J., García-Mayordomo J., Giardini D., Glavatovic B., Gulen L., Ince Y., Pavlides S., Sesetyan K., Tarabusi G., Tiberti M., Utkucu M., Valensise G., Vanneste K., Vilanova S., Wössner J. The European Database of Seismogenic Faults (EDSF) compiled in the framework of the Project SHARE. http://diss.rm.ingv.it/share-edsf/, doi: 10.6092/INGV.IT-SHARE-EDSF, 2013

[12] Delavaud E, Scherbaum F., Kühn N., Allen T., Testing the Global Applicability of Ground-Motion Prediction Equations for Active Shallow Crustal Regions, Bull. of the Seism Soc. of America, 102(2):707 http://dx.doi.org/10.1785/0120110113, 2012

[13] Kulkarni, R., Youngs, R., Coppersmith, K., Assessment of confidence intervals for results of 501 seismic hazard analysis. In: Proceedings of the 8th World Conference on Earthquake Engineering, vol. 1, pp. 263, San Francisco, California, 1984

[14] Coppersmith, K., Youngs, R., Capturing uncertainty in probabilistic seismic hazard assessments 504 within intraplate environments. In: Proceedings of the 3rd National Conference on Earthquake Engineering, vol. I, pp, 301, Charleston, August 24–28, 1986

[15] Shebalin N.V. V. Karnik and D. Hadzievski (Editors), Catalogue of earthquakes of the Balkan Region. Part III, Atlas of Isoseismal maps. UNDP/UNESCO Survey of the seismicity of the Balkan region, UNESCO, Skopje, 275, 1974

SECTION

OIL AND GAS EXPLORATION

ANALYSIS AND ASSESSMENT OF SECURITY REQUIREMENTS FOR USE OF HYDROGEN AS A FUEL IN THE TRANSPORT SYSTEM

Danut Grecea[1]

Gabriela Pupazan[1]

Adriana Andris[1]

Alexandru Beldiman[1]

Aurelian Nicola[2]

[1] National Institute for Research and Development in Mine Safety and Protection to Explosion - INSEMEX, 32-34 G-ral Vasile Milea Street, Petrosani, **Romania**
[2] University of Petrosani, 20 University Street, 332006, Petrosani, **Romania**

ABSTRACT

The Growing concern about climate change and the actions that need to be taken to protect environment have begun to occupy the top places on global agenda in recent years.

Transport of the future will look different: ecological, economic and maximum efficiency. But it's not only car manufacturers who are making efforts to reduce as much as possible the climate impact of vehicles. One of solutions is and the major interest of using hydrogen as a viable answer for decarbonizing industrial processes and economic sectors where carbon reduction is both urgent and difficult to achieve. Thus, a new approach to climate policy is required, the development of storage technologies and charging infrastructure, in order to have a healthier way of life and a cleaner environment.

The paper presents an analysis of all aspects, from the point of view of explosion protection, for use hydrogen as an alternative fuel source, using simulation in MATLAB-Simulink of production, storage and use it. All these processes can generate critical situations, and the analysis of pressures, temperatures and other defining parameters are of major importance for the assessment of explosion risks in the context of safety and health and environmental protection, the minimum ignition energy of hydrogen being about 17 μJ.

Keywords: explosive hydrogen, explosive atmosphere; explosion protection; types of protection; electrical equipment.

INTRODUCTION

Transition to green technologies has brought hydrogen to the top of list of flammable substances. Other resources, such as methane, propane, other crude oil derivatives and coal, are the players preparing to hand over the baton, mainly for zero emissions in use.

Technological maturity allows the design of ecological solutions, but they do not yet meet the requirements of economic competitiveness. The current pressures exerted by new technologies, and especially efforts to reduce pollution, leave no room for pessimism.

Therefore, hydrogen-based technologies are imminent, but the problems they raise must also be anticipated. These challenges could include high-pressure storage solutions,

https://doi.org/10.5593/sgem2024/1.1/s06.66

structural stability of materials in contact with hydrogen, and last but not least, explosion risks. [1]

The field analyzed in this paper is that of transport, a branch of industry significantly affected by the explosion of prices for traditional fuels (gasoline and diesel) but also by the constraint adopted both in Europe and worldwide by drastic reduction of environmental pollution. In order to remain competitive, in a competitive market with restrictions and characteristic particularities, steps have been taken to use alternative fuels.

ANALYSIS OF PRODUCTION, STORAGE AND USE OF HYDROGEN

Hydrogen is a source of energy, but in order to take advantage of it, it must first be produced. In general, there are two ways to produce hydrogen: electrolysis or from fossil fuels. [2]

Electrolysis is the process that uses electricity and water to produce hydrogen. Electricity can be produced from renewable sources (e.g. wind or photovoltaic), in this way we can produce hydrogen in a sustainable way, green hydrogen (Green Hydrogen). [3]

The EU directives on alternative fuel infrastructure establish a common framework of measures for implementation of alternative fuel infrastructure in EU to minimize dependence on oil and to mitigate the impact of transport on the environment and, at the same time, establish minimum requirements for construction of infrastructure, for alternative fuels, including stations of hydrogen supply, figure 1.

A hydrogen-powered vehicle is a vehicle that uses hydrogen, stored in the vehicle, as fuel for its engines. Such vehicles convert the chemical energy of hydrogen to mechanical energy, either by burning hydrogen in an internal combustion engine, or by reacting hydrogen with oxygen in a fuel cell to power electric motors.

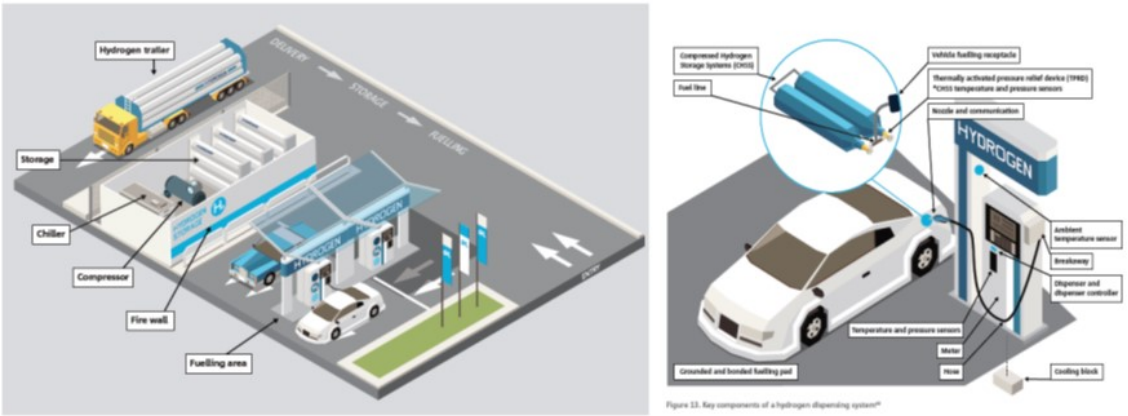


Fig. 1 Hydrogen fuel station

An example of a simulation model for determining the essential parameters (pressures, temperatures, etc.), analyzed in this paper is a hydrogen filling station, model for simulation is shown in figure 2. For simulation, the hydrogen is stored in storage tanks of low pressure at 200 bar at the station. A 3-stage intercooler compressor maintains required pressure in a cascaded buffer storage system so the station is ready to send hydrogen to any connected vehicle. The buffer is divided into high pressure tanks at 950 bar, medium

pressure tanks at 650 bar and low-pressure tanks at 450 bar. To avoid wasting compression energy, the lowest buffer pressure that is higher than the vehicle's tank pressure is used to ship hydrogen. Priority valves switch between the various buffer tanks to control which buffer tanks to fill and discharge from.

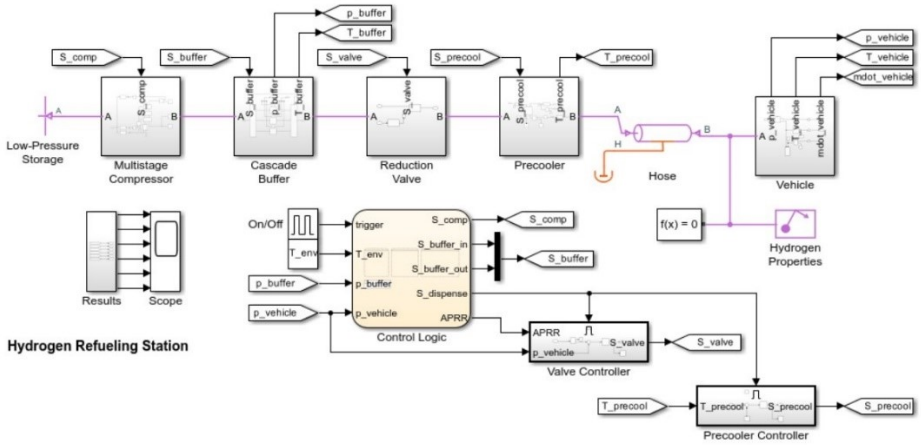


Fig. 2 Hydrogen refueling station model

When dispensing, a reducing valve controls the flow between the cascaded buffer storage and vehicle tank. A pre-cooler cools the hydrogen before it is shipped to vehicle to avoid excessive temperature rise in the vehicle's tank. This example is modeled after an existing refueling station type from the refueling protocols, meaning hydrogen is delivered at -40ºC and up to 700 bar.

A Stateflow®, [4], diagram is used to model the logic required to control station operations. It determines when to turn on the compressor to recharge the buffer, when to send hydrogen to the vehicle, and logic to switch buffer priority valves in the cascade. When dispensing, the Valve Controller and Precooler Controller subsystems are enabled. They contain PI controllers that maintain the flow rate and temperature of the hydrogen fuel being shipped.

The state of the hydrogen fuel in vehicle tank is shown in the left column of the graphs, figure 3. At t = 2400 s, the dispenser is triggered and filling begins. Pressure rise is maintained at a constant slope, called the Average Pressure Ramp Rate, by valve controller. Filling stops once the target pressure is reached. The APRR and target pressure come from the fueling protocols and depend on ambient temperature and the initial pressure in vehicle. In this example, they are 18.5 MPa/min and 74.5 Mpa respectively.

During filling, the temperature rises significantly due to amount of compression that occurs in vehicle's tank. This sets a maximum temperature limit of 85ºC. In this example, temperature reaches 68.6 °C when it is full. This is achieved by pre-cooling the hydrogen to -40ºC before entering vehicle, as shown in the lower right graph.

The lower left graphs show flow of hydrogen in vehicle tank. Since the controller maintains an APRR, the mass flow rate decreases as pressure increases. The two peaks of flow occur when it passes from the low-pressure buffer to medium-pressure buffer and from medium-pressure buffer to high-pressure buffer. Further valve timing adjustments during pad switching can reduce these peaks. However, the flow rate is below the maximum limit of 0.06 kg/s set by standards in force.

https://doi.org/10.5593/sgem2024/1.1/s06.66

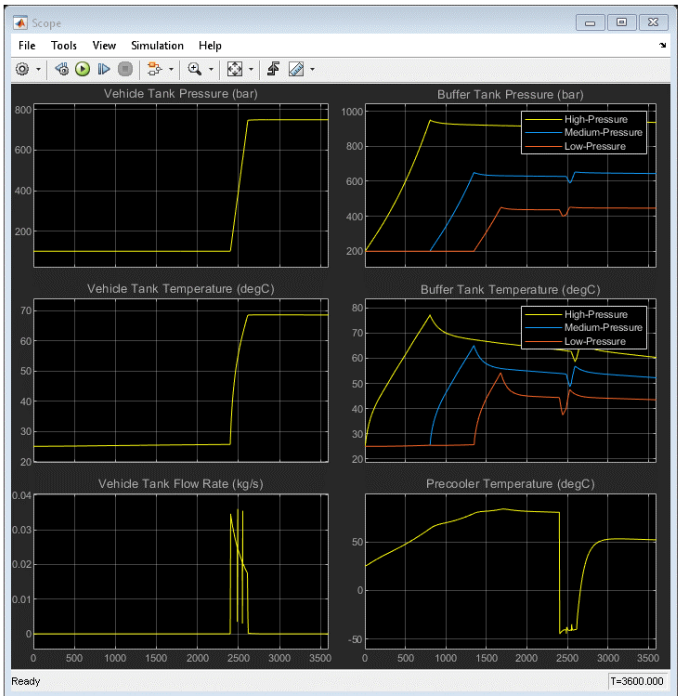


Fig. 3 Variation of parameters obtained after the simulation

The top two graphs in right column show the state of cascading buffer. At the beginning of simulation, compressor is started to fill the buffer in order from high pressure tank to low pressure tank. Sending hydrogen to vehicle causes a drop in buffer pressure. Therefore, compressor starts again to fill the buffer tanks and maintain buffer pressure.

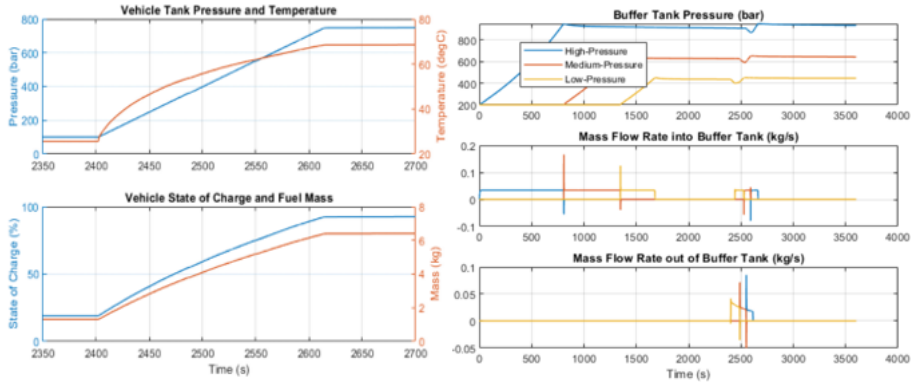


Fig. 4 Variation of the state of hydrogen in vehicle tank while it is being filled and the state of charge / total mass of hydrogen in vehicle and pressures and mass flow in the cascaded storage buffer tanks

Graph in figure 16, shows a closer view of the state of hydrogen in vehicle's tank while it is being filled. It also shows the state of charge and total mass of hydrogen in vehicle. State of charge is defined as density of hydrogen in vehicle divided by density of hydrogen at nominal working pressure and 15 °C. State of charge should never exceed 100%.

Density of hydrogen in storage tanks, correlated with certain pressures and temperatures, is shown in figure 5.

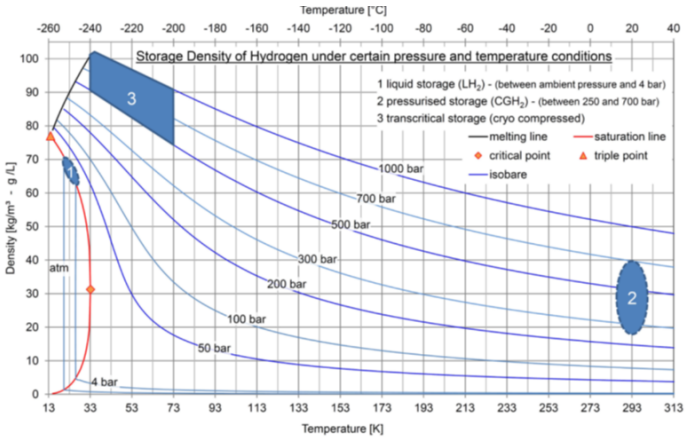


Fig. 5 Hydrogen density response to pressure and temperature

EXPLOSION HAZARD ASPECTS

Danger of explosion can occur in all activities involving flammable substances. Thus, almost all branches of industry are affected by this risk, as the hazards generated by explosive atmospheres occur in a wide range of processes and operations. The explosion hazard is found at confluence of three factors: the flammable substance, oxygen and ignition source. [5]

After classifying the area, a risk assessment can be performed to determine if consequences of igniting an explosive atmosphere require the use of equipment with a higher protection level (EPL). [6], [7]

Explosion protection has role of preventing ignition of explosive atmospheres, i.e. preventing potential sources of ignition. Regarding the explosion hazard assumed by zone classification, technical equipment used in these zones must be eligible. This results in equipment protection categories and levels, shown in figure 6.

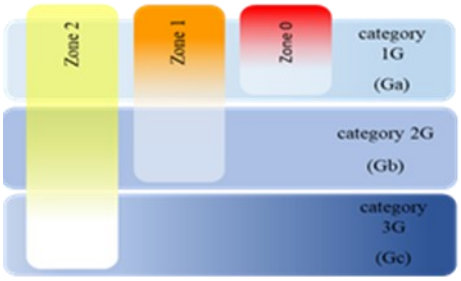


Fig. 6 Area correlation-protection category /level

In order to identify the effect on explosion risk, [8-10], induced by use of hydrogen, a comparative analysis was carried out with three other substances commonly used in transport system (methane, propane and butane).

Table 1 shows a selection of parameters: relative density to air, flammability limits (concentrations), auto-ignition temperature together with temperature class and subgroup of gases and vapours.

Following the analysis based on values in table 1, a comparative risk diagram of the four mentioned flammable gases was drawn up. This diagram is shown in figure 7.

https://doi.org/10.5593/sgem2024/1.1/s06.66

Table 1 Relative variation of the final instantaneous concentration

Substance	Density relative to air	LFL [% v/v]	UFL [% v/v]	Ignition temperature [°C]	Temperature class	Subgroup
Hydrogen	0,07	4,00	77,0	560	T1	IIC
Methane	0,53	4,40	17,0	537	T1	IIA
Propane	1,56	1,70	10,9	470	T1	IIA
Butane	2,05	1,40	9,3	372	T2	IIA

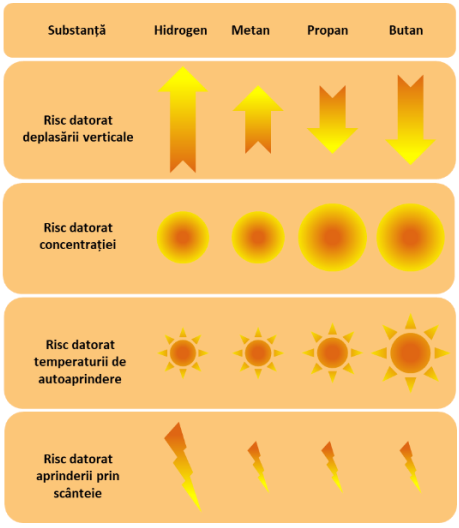


Fig. 7 Risk comparison chart

A comparison of various risks between hydrogen, methane, propane and butane showed that the shift to widespread use of hydrogen brings with it an increased risk of electrical ignition of hydrogen-air mixtures. Of all flammable substances, hydrogen has the greatest sensitivity to ignition.

Taking into account the parameters (pressures, temperatures, density, etc.) from the process of production, storage and use of hydrogen based on SR IEC 60079 - 10 – 1, [9] and risk analysis, the extent of dangerous areas can be determined.

Hypothesis 1: The dispenser is considered active from the time the connector is attached to the vehicle's filler (start of transaction) until *15 seconds* after the connector is removed (end of flow and dissipation delay for H_2).

Hypothesis 2: The flow rate is controlled by an automatic button or a dispenser assisted by trained personnel.

Hypothesis 3: Any H_2 leaking from the connector interface to the vehicle or to the fuel system through a hose break will enter the atmosphere and begin to rise at about 1 meter/second. The LEL is 4% for hydrogen.

Relative velocity of volume expelled through the interface surface (without considering gravity) is:

$$P_s = (\frac{Q}{1000})/(S_i) = (\frac{Q}{1000})/\pi \cdot R^2 \quad (1)$$

Taking into account gravity (and the 1 m/s migration velocity of H_2), concentration of H_2 at the top of the hydrogen-air interface is $C = P_S/1.0$, C must be less than the target LEL concentration for a such area.

$$C = \frac{P_S}{1.0} = \frac{\frac{Q}{1000}}{\pi R^2} \rightarrow R = \sqrt{Q/(1000 \cdot \pi \cdot C} \quad (2)$$

Application of the formula for hydrogen:

- Zone 0 assumes any potential concentration above the LEL, i.e. 4%
- Zone 1 assumes any potential concentration above 20% of the LEL, i.e. 0.8%
- Zone 2 assumes any potential concentration above 5% of the LEL, i.e. 0.2%

The results for all areas and standard and flow scenarios are recorded in figure 8.

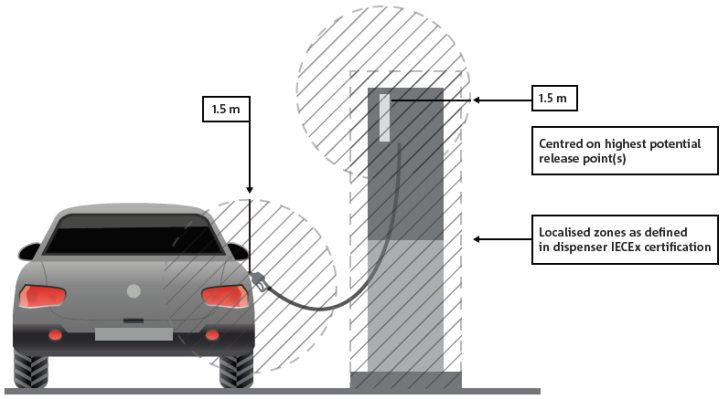


Fig. 8 Hazardous area zone classification for hydrogen dispenser refueling

CONCLUSIONS

Risk of ignition of an explosive atmosphere can be reduced by using equipment, components and protection systems designed in accordance with the provisions of the technical standards for protection against explosion in force. Also, evaluation of the explosion risk takes into account determinations and interpretations of combustible gas parameters. The main purpose of explosion risk assessment is to increase the level of safety in the place where an explosive atmosphere can occur.

Thus, this paper presents the simulation models to highlight the essential parameters in the design, optimization and, last but not least, the operation of hydrogen production, storage and utilization systems. Knowing that all these processes can generate critical situations, the minimum ignition energy being about *17 μJ*, the analysis of pressures, temperatures and other parameters present are of major importance for the evaluation of explosion risks in context of safety and health and environmental protection.

As can be seen in almost all developed countries, the issue of addressing the sustainable development of hydrogen-based technologies is raised at the governmental level. In this sense, social partners were created for consultations that include both economic agents and research entities or members of the academic community in order to find the optimal solutions for the implementation of a coherent program for the development of hydrogen-based technologies, as well as the need for legislation adequate to facilitate the development of the infrastructure that is needed in safe conditions.

https://doi.org/10.5593/sgem2024/1.1/s06.66

ACKNOWLEDGMENTS

This work was carried out through the "Nucleu" program of the National Research, Development and Innovation Plan 2022-2027, supported by MCID, project no. PN23320102 and use equipment from IOSIN-PCDIEX.

REFERENCES

[1] ATEX Directive, Directive 2014/34/EU of the European Parliament and the Council of 26 February 2014 on the harmonization of the laws of the Member States relating to equipment and protective systems intended for use in potentially explosive atmospheres, Official Journal of the European Union, L96/309, 29.03.2014;

[2] https://ec.europa.eu/commission/presscorner/detail/en/FS_20_1296, [Accessed 10.03.2024];

[3] Grecea, D. et al, "Hydrogen, the new green energy resource", MATEC Web of Conferences 389, 00027 (2024), https://doi.org/10.1051/matecconf/ 202438900027, 2024;

[4] MATLAB and Simulink Examples Available on https://www.mathworks.com/ academia/ examples.html;

[5] Government Decision no. 245 of April 6, 2016 on establishing the conditions for making equipment and protection systems intended for use in potentially explosive atmospheres available on the market the, 2016;

[6] SR EN (IEC) 60079-0:2018 - Explosive atmospheres - Part 0: Equipment – General requirements, ASRO, 2018;

[7] SR EN (IEC) 60079-17:2024, Explosive atmospheres - Part 17: Electrical installations inspection and maintenance, ASRO, 2024;

[8] Government Decision no. 1058 of August 9, 2006 on the minimum requirements for improving the safety and health protection of workers who may be exposed to a potential risk due to explosive atmospheres, 2006;

[9] SR EN (IEC) 60079-10-1:2021 - Explosive atmospheres. Part 1. Classification of areas. Explosive gas atmospheres, ASRO, 2021;

[10] Csaszar T., Pasculescu D., Darie M., Ionescu J., Burian S., (2012), Method for assessing energy limited supply sources, designed for use in potentially explosive atmospheres, Environmental Engineering and Management Journal, 11, 1281-1285. National Instruments, „NI modul Project Essentials Guide" – 2015.

APPLICATION OF CULTURE SUPERNATANTS CONTAINING SURFACTANTS TO ENHANCE OIL RECOVERY

Dr. Liliya Biktasheva[1]
Nikita Ezhkin[1,2]
Zlata Osmorskaya[1,2]
Alexander Gordeev[1]
Assoc. Prof. Dr. Polina Kuryntseva[1]

[1]Kazan (Volga Region) Federal University, 42008, Kazan, **Russian Federation**
[2]LLC Organic Park, 420095, Kazan, **Russian Federation**

ABSTRACT

Currently, a big problem is increasing the production of residual oil, for which so-called tertiary recovery methods are used. One common tertiary recovery method is the use of surfactants. The use of biological surfactants instead of synthetic ones can solve the problem of increasing oil production and reducing the toxic impact on the environment. To obtain biosurfactants, two strains of *Bacillus mojavensis* and *Bacillus amyloliquefaciens* were used. These strains are characterized by the ability to produce biosurfactants. Biosurfactants produced by these strains belonged to the group of lipopeptides, represented mainly by surfactin molecules. The qPCR method established that in strains *B. mojavensis* and *B. amyloliquefaciens* the number of *srfAA* and *ituC* genes responsible for the production of surfactin was $2.8x10^4$ and $1.9x10^3$ gene copies ml^{-1}, and iturin for $4.6x10^2$ gene copies ml^{-1} in strain *B amyloliquefaciens*. To evaluate the effectiveness of MEOR, culture supernatant containing biosurfactants was tested on sand cores simulating oil reservoir. The surface tension of the culture supernatants of the B. mojavensis and B. amyloliquefaciens strains was 29.79 ± 0.039 and 31.18 ± 0.065 mN m^{-1}. When culture supernatants were used, additional oil recovery was 11.1 and 11.8% for *B. mojavensis* and *B. amyloliquefaciens*, respectively.

Keywords: Biosurfactants, microbial enhanced oil recovery, MEOR

INTRODUCTION

Research interest in the use of biosurfactants to enhance oil recovery is caused by a steady increase in attention to these substances - highly effective and environmentally friendly surfactants [1,2]. They have many properties such as emulsifying ability, influencing adhesion and detergent activity. Microbiological enhanced oil recovery (MEOR) methods using biosurfactants as a replacement for chemical surfactants are considered effective and safe [3, 4]. This is also justified by environmental safety requirements, which require the abandonment of the use of highly toxic chemicals in industry, including surfactants, usually obtained as a result of petrochemical synthesis.
Biosurfactants, in purified form or contained in bacterial nutrient media, are one of the promising areas in the field of microbiological enhanced oil recovery [5, 6], since they remain active under various conditions: pressure, temperature, salt concentrations and of

varying acidity, in contrast to living microorganisms - their producers. However, the extraction and purification of biosurfactants, as well as their working concentrations and efficiency in real oil field conditions remain an unresolved problem.
Many authors focus on the fact that it is preferable to use cultures of indigenous microorganisms in the production of biosurfactants for specific oil wells. Native microorganisms, as a rule, are adapted to the unique conditions corresponding to the deposit from which they were isolated. These essential microorganisms can be found not only in crude oil, but also in oil-contaminated soils and wastes.
The study focuses on the potential use of biotechnology in the oil industry, in particular the use of biosurfactants obtained from the cultivation of *Bacillus mojavensis* and *Bacillus amyloliquefaciens*, as an alternative to traditional methods of enhanced oil recovery. This work involves in-depth study of the properties of biosurfactants and evaluation of their effectiveness in oil field conditions.

MATERIALS AND METHODS

For increased biosurfactant production, *Bacillus amyloliquefaciens* VKMA B-12464 and *Bacillus mojavensis* PS17 (provided by the ORGANIC PARK LLC, The Bionovatic) was cultivated in glycerol nitrate medium at 35 °C and 180 rpm for 6 days. The concentration of crude glycerol in the medium was 40 g L^{-1}. The medium except crude glycerol contained (g L^{-1}): $NaNO_3$ (4.0), $K_2HPO_4 \cdot 3H_2O$ (4.0), KH_2PO_4 (3.0), $MgSO_4 \cdot 7H_2O$ (0.5), KCl (0.5), NaCl (0.5), $CaCl_2 \cdot 2H_2O$ (0.2).
Three millilitres of biosurfactant containing culture supernatant and 3 mL of respective oils were added in test tubes followed by rapid vigorous vortexing for 2 min. By adopting the formula given below the E24% was calculated.
E24% = (Height of the emulsified layer/total height of liquid column) × 100.
Then, the mixture of crude biosurfactants produced by the strain was extracted using acid precipitation and purified as described at Hu et al (2022) [7]. As a result, the acid precipitated fraction was obtained and used for further analyses. To determine the type and structure of biosurfactant, were performed FTIR (Lumos I, Bruker, USA) and TLC (CAMAG, Switzerland).
In order to MEOR simulation and replicate the impact of a cell-free culture supernatant containing a biosurfactant on oil within an oil reservoir, vertically oriented cylindrical PVC columns, each with a volume of 200 mL, were employed. These columns were filled with river sand that had been pre-calcined at 800 °C and possessed a particle size ranging from 0.1 to 1.0 mm, following the design outlined in Suthar et al. (2008) [8]. Brine solution, an aqueous solution containing 20 g L^{-1} NaCl and 10 g L^{-1} $CaCl^2$, was injected for primary flooding of the column using a syringe through a silicone tube. Next, the columns were filled with oil from the Romashkinskoye field. Oil was introduced at a rate of 5 ml/min, which corresponds to two pore volumes. Oil displacement from the brine was monitored and the volume of brine displaced was measured using a graduated cylinder representing the original oil in place (OOIP). The ratio of OOIP to PV allowed the initial oil saturation (Soi) to be calculated, expressed as a percentage. After filling the columns with oil for 48 h at room temperature, they were washed again with brine at a rate of 10 ml/min until no more oil flowed from the column. The volume of oil recovered was measured using a graduated cylinder after centrifugation to separate the oil from the partially mixed water. This volume was considered to be oil recovered by brine flood (Sorbf). The percentage of oil recovered was determined by the ratio of Sorbf to OOIP, expressed as a percentage.

The remaining Sor oil was exposed to one pore volume (PV) of cell-free culture supernatant containing a biosurfactant and an aqueous solution of a commercial drug at concentrations of 0.3%, which corresponds to the working concentrations for anionic surfactants used in oil production. The columns were kept at room temperature for 24 hours, and the resulting water-oil emulsion was separated by centrifugation to determine the volume of oil obtained. The volume of oil recovered by flooding cell-free culture supernatant containing surfactants (Sorsf — oil recovered by surfactant flood) was used to calculate total oil recovery (TOR) and additional oil recovery (AOR). AOR represents the volume of oil recovered by the biosurfactant relative to the remaining oil after brine flooding, while TOR represents the volume of oil recovered by the biosurfactant relative to the original volume of oil initially injected into the pore space (OOIP). AOR is expressed as the fraction of oil recovered by flooding the cell-free culture supernatant relative to the volume of oil remaining after brine flooding, and TOR is expressed as the fraction of oil recovered by the cell-free culture. flooding of the supernatant relative to the original volume of oil that occupied the pore space.

RESULTS AND DISCUSSION

To conduct the study, the bacterial strains *Bacillus amyloliquefaciens* VKMA B-12464 and *Bacillus mojavensis* PS17 were used. To evaluate the emulsifying activity, the E24 test was used (Figure 1).

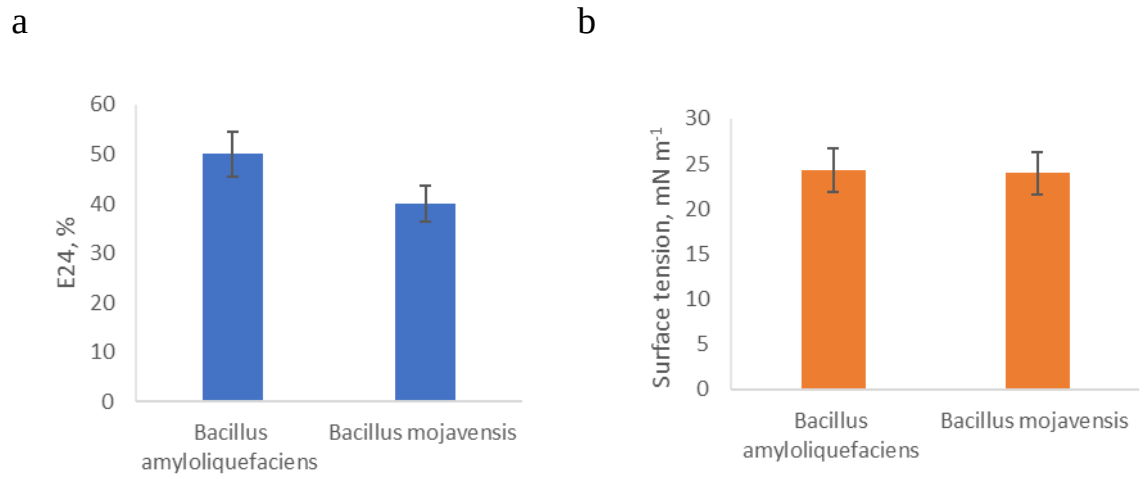


Figure 1. - Evaluation of emulsifying activity (a) and surface activity of *B. amiloliquofaciens* and *B. mojavensis* culture supernatants (b).

The emulsifying activity of the *B. amiloliquofaciens* E24 strain reached 50%, while for the *B. mojavensis* strain this figure was 40% (Fig. 1a). As a result of surface tension measurements, it was recorded that the biosurfactant produced by *B. amiloliquofaciens* was able to reduce the surface tension to 24.29 mN m^{-1} (1b). If we talk about *B. mojavensis*, it should be noted that the minimum surface tension was 23.96 mN m^{-1}. The obtained surface tension data are consistent with the data obtained by Al-Wahaibi et al. (2014) for *Bacillus subtilis* B30 [9].

To confirm the presence of biosurfactants in the supernatant of the strains, the isolated biosurfactants were analyzed by IR spectroscopy with ATR (Fig. 3) and TLC (Fig. 2).

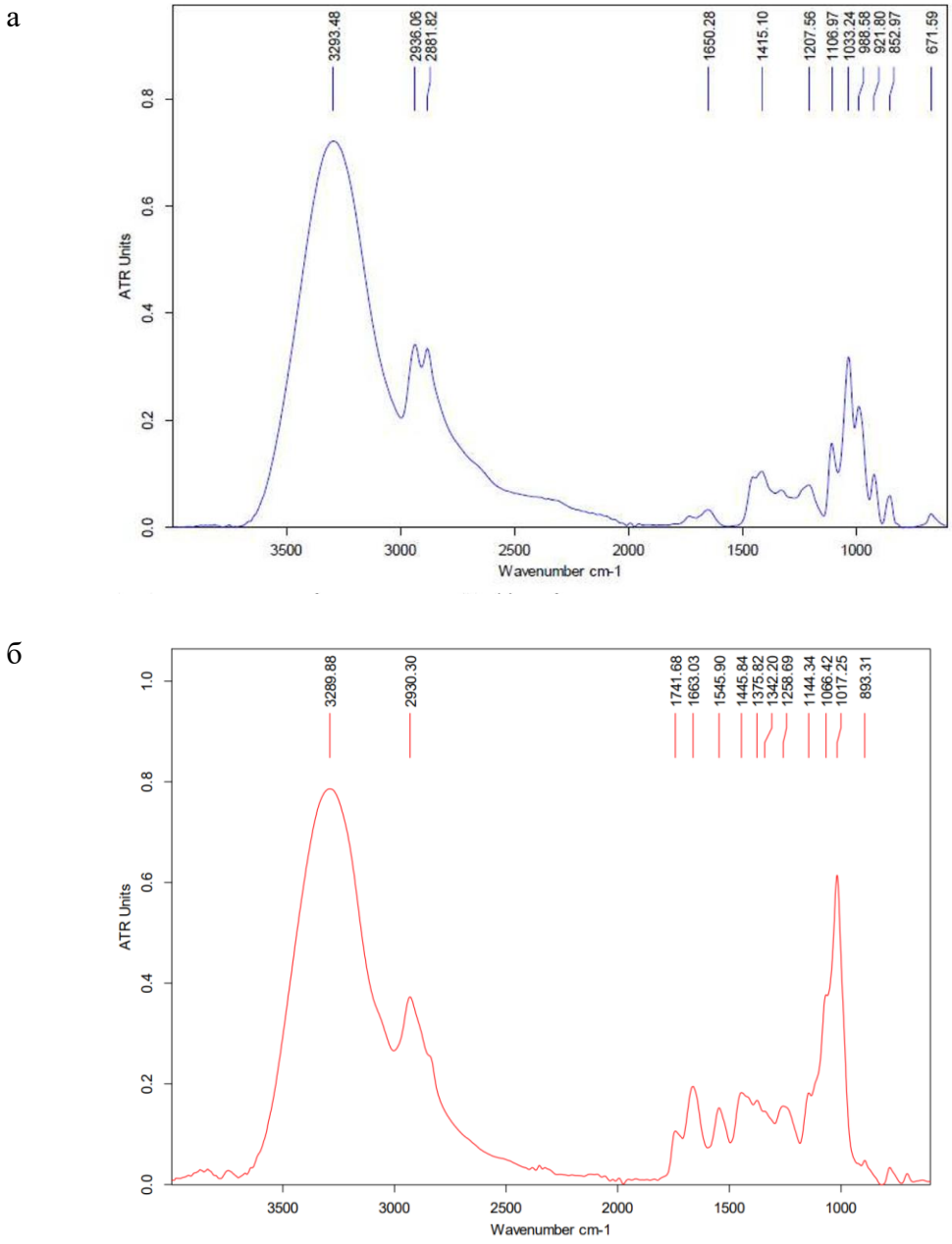


Figure 2. - Infrared spectrum of biosurfactant isolated from the culture liquid of *B. Mojavensis* (a) and *B. Amiloliquofaciens* (b).

Figure 3a shows the infrared absorption spectrum obtained for the biosurfactant isolated from the culture liquid of *B. mojavensis* on the third day of cultivation. The peak at 3293.48 cm^{-1} indicates the presence of absorption of infrared radiation by hydroxyl groups. The peak position in the range of 3000 - 3400 cm−1 is characteristic not only of the hydroxyl group, but also of the peptide bond, which is specific for amino acid fragments presented in the form -NH_2. Since it is known that microorganisms of the genus *Bacillus* are capable of producing predominantly lipopeptide biosurfactants, including surfactin, the obtained IR spectrum suggests that the isolated biosurfactants contain a peptide bond characteristic of the amino acid sequences that are part of the hydrophilic “head” of the surfactin molecule. The peak width of 3293.48 cm^{-1}

appearing in this range is the result of the contribution of the hydroxyl group -OH, which is a normal phenomenon for stretching vibrations. The peak at a depth of 1650.26 cm^{-1}, recorded in the range of 1600–1700 cm^{-1}, corresponds to bending vibrations of the peptide fragments $-NH^{3+}$ and the -CO-N bond, which are typical for biosurfactants produced by bacteria of the genus Bacillus. In addition, the peaks at 2936.06 cm^{-1} and 2881.82 cm^{-1} obtained as doublets in the range of 2800–3000 cm^{-1} correspond to asymmetric vibrations in the alkyl fragments (-CH3 and -CH2-). These vibrations also appear in the wavenumber range of 1200–1400 cm^{-1}. These segments of absorption spectra, as a rule, serve as landmarks in identifying the characteristic features of lipopeptide biosurfactants.

In addition, a low intensity peak at wavenumber 1033 cm^{-1} indicates molecular vibrations specific to the -COO- carboxyl group, a characteristic common to all amino acids. Intensity peaks at wavenumbers of 988.24 cm^{-1} and 921.80 cm^{-1} correspond to vibrations of ester bonds in aliphatic fragments with C-O-C bonds.

Analyzing the spectrum obtained for *B. amiloliquofaciens,* it can be noted that the spectra from Figure 2a and 2b are close in mutual signal intensity and peak positions, but some differences are noted. Thus, the peak at 3289.88 cm^{-1} in the region of 3100 - 3400 cm^{-1} also demonstrates the presence of hydroxyl and peptide groups. If we talk about the peak at 2930.30 cm^{-1} in the range of 2900-3000, it indicates the presence of a CH_n group. With all this, the peak is not sufficiently resolved due to possible impurities in the sample. As a result of the analysis, it can be judged that the biosurfactants produced by the strains of *B. mojavensis* and *B. amiloliquofaciens* belong to the group of lipopetides. Further analysis by thin layer chromatography will help to better understand the nature of the biosurfactants of the strains.

Confirmation of the biosurfactant class was performed using a UV detection method at 254 nm.

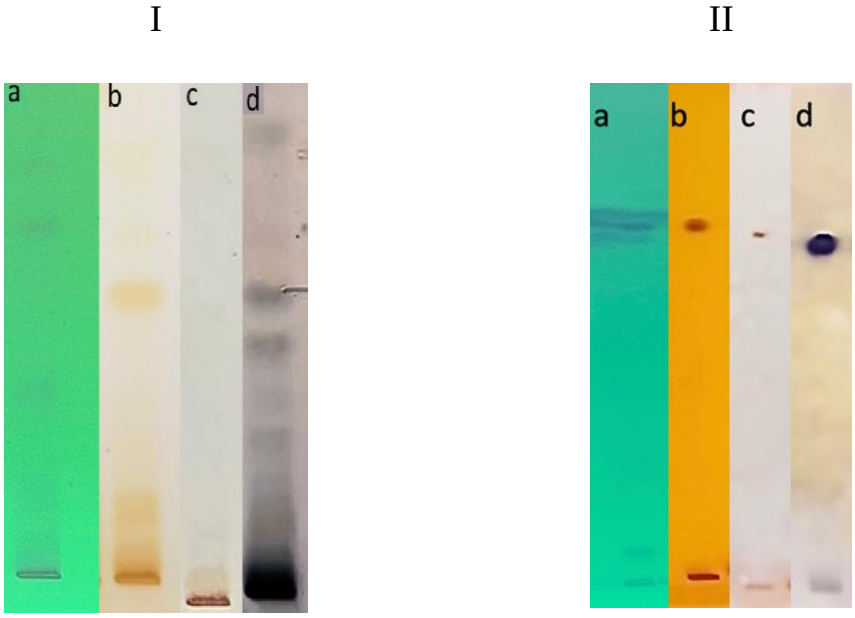


Figure 3. - TLC of biosurfactants isolated from the culture liquid of *B. amiloliquofaciens* (I) and *B. mojavensis* (II), visualized under UV radiation (a), iodine vapor (b), ninhydrin solution (c) and anisaldehyde solution (d).

https://doi.org/10.5593/sgem2024/1.1/s06.67

In the ultraviolet range, components of the sample were identified that did not fluoresce at a wavelength of 254 nm and appeared on the plate in the form of dark spots. Thus, the polycomponent nature of the sample was assessed and the fact that the solvent mixture was able to well separate the components on the plate. Subsequently, a qualitative assessment of the components of the samples was carried out by processing them with coloring reagents.

Samples isolated from the culture fluids of *B. amiloliquofaciens* (Figure 3a) and *B. mojavensis* (Figure 3b) demonstrated the presence of both hydrophobic fragments - "tails" of fatty acids, colored by iodine vapor, and hydrophilic groups - "heads" of peptide fragments, demonstrating a qualitative reaction with ninhydrin solution. The data obtained indicate the presence of biosurfactants in the samples, which can be identified as lipopeptides.

The effectiveness of using biosurfactants to increase oil production efficiency was assessed using models simulating oil production conditions in highly porous rocks. The models consisted of PVC pipes filled with quartz sand, into which a cell-free culture liquid containing a biosurfactant was poured.

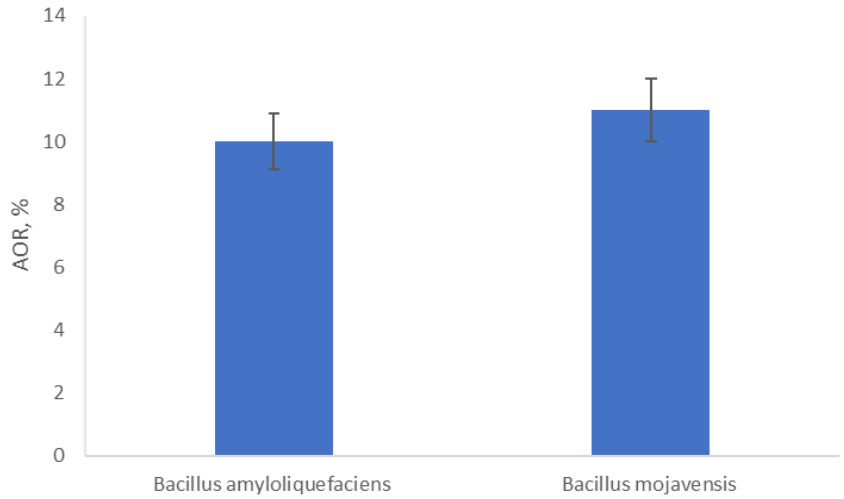


Figure 4. - MEOR simulation results

Analyzing the data obtained when adding cell-free culture liquid to the columns, we can say that when using cell-free culture liquid containing a dissolved biosurfactant, it was possible to improve the efficiency of the tertiary method of enhanced oil recovery by 10% AOR for *B. amiloliquofaciens* and 11% AOR for *B. mojavensis* (Figure 4). This result is quite high for environmentally friendly compounds that can be used for more efficient oil production. The data obtained for the microbiological enhanced oil recovery method are similar to the data obtained by Bryant et al. (1994) [10].

CONCLUSION

The work explored the possibility of using supernatants from cultures that produce biosurfactants for MEOR purposes. The effectiveness of using culture fluids of *Bacillus amyloliquefaciens* and *Bacillus mojavensis* strains containing biosurfactants to enhance oil recovery was assessed using the MEOR modeling method. The E24 emulsification index for the *B. amyloliquefaciens* supernatant was 50%, while for the Bacillus

mojavensis strain this figure was 40%. An assessment of the surface tension force showed that the supernatant of *B. amiloliquofaciens* reduced the surface tension to 24.29 mN m^{-1}, *B. mojavensis* - to 23.96 mN m^{-1}. The group affiliation of biosurfactants produced by the microorganisms *B. mojavensis* and *B. amyloliquefaciens* was determined. Data obtained using FTIR and thin layer chromatography techniques indicate the presence of biosurfactants in the samples, which are lipopeptides. Modeling of oil recovery using strain supernatants showed that their use can increase oil recovery by 11% with *Bacillus mojavensis* and by 10% with *Bacillus amyloliquefaciens*.

ACKNOWLEDGEMENTS

This work was supported by the Ministry of Science and Higher Education of the Russian Federation under agreement No. 075-15-2022-299 within the framework of the development program for a world-class research center “Efficient development of the global liquid hydrocarbon reserves”.

REFERENCES

[1]Bhardwaj G., Cameotra S. S., Chopra H. K. Biosurfactants from fungi: a review, J Pet Environ Biotechnol., vol. 4. (6), pp 1-6, 2013

[2]Campos J. M. et al. Microbial biosurfactants as additives for food industries, Biotechnology progress. Vol.5, pp 1097-1108, 2013

[3]Ahuja K., Singh S. Biosurfactants Market Trends 2020–2026. Growth Projections, Rep. GMI484, 564 p, 2020.

[4]De Almeida D.G., Soares Da Silva R.C.F., Luna J.M., Rufino R.D., Santos V.A., Banat I.M., Sarubbo L.A. Biosurfactants: Promising molecules for petroleum biotechnology advances. Front. Microbiol., vol. 7, art. 1718, pp. 1–14, 2016

[5]Lazar I., Petrisor I.G., Yen T.F. Microbial enhanced oil recovery (MEOR), Pet. Sci. Technol. vol. 25(11), pp 1353–1366, 2007.

[6]Brown L.R. Microbial enhanced oil recovery (MEOR), Curr. Opin. Microbiol. vol 13 (3), pp 316–320, 2010

[7]Meizhong Hu, Jiansheng Yu, Huaqi Zhang, Qingsong Xu, An efficient method for the recovery and separation of surfactin from fermentation broth by extraction-back extraction, Process Biochemistry, Vol. 114, pp 59-65, 2022

[8]Suthar, H., Hingurao, K., Desai, A., Nerurkar, A. Evaluation of Bioemulsifier Mediated Microbial Enhanced Oil Recovery Using Sand Pack Column, J Microbiol Methods, vol. 75, pp 225–230, 2008

[9]Al-Wahaibi Y. et al. Biosurfactant production by Bacillus subtilis B30 and its application in enhancing oil recovery //Colloids and Surfaces B: Biointerfaces. – 2014. – T. 114. – C. 324-333.

[10] Bryant R. S. et al. Microbial enhanced waterflooding field tests, SPE Improved Oil Recovery Conference. – SPE, pp SPE-27751-MS, 1994.

ASSESSING THE IGNITION SOURCES GENERATED BY THE MECHANICAL EQUIPMENT IN THE CONTEXT OF HYDROGEN EXPLOSIVE ATMOSPHERES

Sc. Res. I PhD Eng. Adrian Marius Jurca[1]
Sc. Res. I PhD Eng. Florin Adrian Păun[1]
Sc. Res. III PhD Eng. Mihai Cătălin Popa[1]
Sc.Res.PhD Eng.Mirela Radu[1]
[1] National Institute for Mine Safety and Protection to Explosion - NRDI INSEMEX Petroșani, **România**

ABSTRACT

A potentially explosive atmosphere exists when a mixture of air, gases, vapours, mists or dust combines in a way that can ignite under certain operating conditions. Hydrogen is the special gas in this context. Those who have knowledge of the properties and flammability of hydrogen will recognize that hazards due to explosive atmospheres must be assessed more and more frequently as the element is utilized, and, if necessary, appropriate protective measures must be taken. In this kind of atmosphere, special attention should be given to the mechanical equipment that are being used for operational purposes, as they might initiate an explosion. Mechanical equipment used in explosive atmospheres should be assessed through an ignition hazard assessment. They must fulfil the essential health and safety requirements, which implies that they shall be assessed according to their ability to prevent them from becoming ignition sources and their ability to protect against the consequences of an explosion.
This paper presents the issue of the ignition hazard assessment of mechanical equipment and points out some aspects that may be important to consider when assessing mechanical systems for use in potentially explosive atmospheres. Ignition of explosive atmospheres by mechanical equipment occurs when energy supplied by equipment is converted into heat, usually as the result of a mechanical failure of the equipment or associated systems. The ignition hazard assessment procedure also involves a series of specific laboratory tests. These tests demonstrate the non-sparking character of the materials used in the manufacture of mechanical equipment and the fact that the assessed equipment does not generate ignition sources able to initiate a potentially explosive atmosphere.

Keywords: non-electrical equipment, hydrogen, hazard assessment, potentially explosive atmospheres.

INTRODUCTION

Explosion prevention and protection has a major importance in preserving workers safety and health since explosions endanger human life and health as a result of uncontrolled effects of fires and explosions.

With the widespread introduction of hydrogen technologies in the chemical and energy industries, hazards due to explosive atmospheres must be assessed and if necessary, appropriate protective measures must be taken [5]. Hydrogen is the special gas in this

https://doi.org/10.5593/sgem2024/1.1/s06.68

context. Those who have knowledge of the properties and flammability of hydrogen will recognize that hazards due to explosive atmospheres must be assessed more and more frequently as the element is utilized, and, if necessary, appropriate protective measures must be taken.

Hydrogen is a substance that occurs in gaseous form at normal atmospheric temperature and pressure. Hydrogen is a lighter gas than air, which diffuses rapidly with a tendency to rise upwards. The flammability range of hydrogen in air is between 4% and 77% by volume. The flammability range is 5-10 times higher than for conventional hydrocarbons, the minimum ignition energy is 5-10 times lower – shown in table 1 and figure 1, comparison of explosion characteristics under atmospheric conditions. In other words, hydrogen explosions lead to much greater consequences [8].

Table 1. Comparison of explosion characteristics under atmospheric conditions

	Unit	Methane	Hydrogen	Gasoline
Lower explosion limit	vol-%	4,4	4,0	1,3
Upper explosion limit	vol-%	17,0	77,0	7,1
Minimum ignition energy	mJ	0,23	0,017	0,8
Ignition temperature	^{0}C	595	560	300
Maximum explosion pressure	bar	8,2	8,2	8,0

As an intrinsic property, hydrogen is very flammable requiring only a small amount of energy to ignite. As can be seen in figure 1, hydrogen has a wide flammability range compared to methane and gasoline.

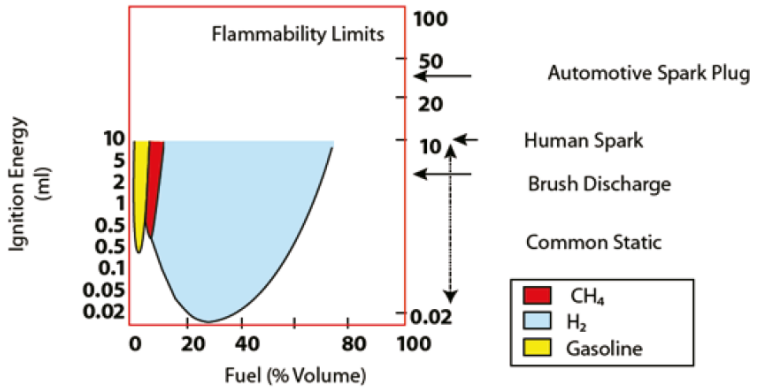


Figure 1 - Flammability limits and ignition energy of H2, CH4 (or NG) and gasoline

In this type of plants, special attention should be given to the mechanical equipment that are being used for technological purposes as they might cause an ignition sources. The types of ignition sources which occur include on the one hand hot surfaces due to longer duration friction or rubbing and on the other hand mechanical sparks from shorter but usually higher speed grinding or impact which consist of a few metal particles up to an extended cluster of heated particles which have a high temperature. Ignition of explosive atmospheres by mechanical equipment occurs when energy supplied by equipment is converted into heat, usually as the result of a mechanical failure of the equipment or associated systems. Friction between two solid bodies is a process through which

mechanical energy is transformed into heat. "Friction " and "grinding" might be understood as continuous mechanical solicitation where both heat and effort have reached a steady state and may more or less be analyzed by means of standard engineering approach [1], [2].

The ignition hazard assessment is a process that consists of a series of logical steps that enable designers and safety engineers to examine in a methodical manner the function of an equipment arising from its use in a potentially explosive atmosphere and to decide whether protective measures and/or types of protection are required. The ignition hazard assessment procedure also involves a series of specific laboratory tests.

The purpose of the paper is to verify the non-sparking character of some materials during tests in explosive hydrogen mixtures. In addition to these tests in explosive hydrogen mixtures, the temperature developed by the friction process between the pairs of materials will also be measured.

CLASSIFICATION OF MECHANICAL EQUIPMENT FOR USE IN POTENTIALLY EXPLOSIVE ATMOSPHERES

Classification of non-electrical equipment is done making a difference between different categories of equipment and protection levels as specified in Directive 2014/34/EU. These categories reflect the measures for different areas and conditions of hazard. The non-electrical equipment's for potentially explosive atmospheres are classified in groups and categories – table 2 [4],[9].

Table 2. Relation between Equipment protection levels (EPLs) and zones

SR EN ISO 80079-36		Directive 2014/34/UE (GD no. 245/2016)		SR EN 60079-10-1 SR EN 60079-10-2
EPL	Group	Equipment Group	Equipment Category	Zones
Ma	I	I	M1	Not Applicable
Mb			M2	
Ga	II	II	1G	0
Gb			2G	1
Gc			3G	2

Category 3G – no ignition sources under normal operation - for use in zone 2 (areas in which explosive atmospheres caused by gases, vapours, mists, or air/dust mixtures are unlikely to occur or, if they do occur, are likely to do so only infrequently and for a short period only) Are designed to be capable of functioning in conformity with the operating parameters established by the manufacturer and ensuring a normal level of protection.

Category 2G – avoidance of ignition sources during foreseeable malfunctions - for use in zone 1 (areas in which explosive atmospheres caused by gases are likely to occur occasionally). Additional precautions to prevent ignition sources produced as a result of foreseeable faults are also required. Are designed to be capable of functioning in conformity with the operational parameters established by the manufacturer and of ensuring a high level of protection.

Category 1G – avoidance of ignition sources even under rare malfunctions - category 1 equipment (for use in zone 0 - areas in which explosive atmospheres caused by mixtures

https://doi.org/10.5593/sgem2024/1.1/s06.68

of air and gases are present continuously, for long periods or frequently) is by far the most problematic. Equipment category 1 comprises equipment designed to be capable of functioning in conformity with the operational parameters established by the manufacturer and ensuring a very high level of protection.

HAZARD ASSESSMENT GENERATED BY MECHANICAL SPARK IGNITION SOURCES OF THE EQUIPMENT

As a result of friction, impact or abrasion processes, such as polishing, the particles can be separated from solids and become hot due to the energy generated in the separation process. If these particles consist of oxidized substances, for example iron or steel, they can be part of an oxidation process, thus reaching even higher temperatures. These sparks can ignite gas / air mixtures [3]. Light metals, titanium and zirconium can also generate sparks at the impact or friction of materials, sparks that are strong enough, even in the absence of rust. In special situations, light metals can generate by shock or friction mechanical sparks able to ignite the explosive gas/air mixtures. Mechanical sparks are metallic or other particles detached from one of the friction surfaces that are incandescent either from the initial phase of decomposition or from the oxidation process in contact with atmospheric air. Both the impact and the friction of the solid bodies are characterized by the friction phenomenon, so that this process can be considered as the main factor generating mechanical sparks and overheated surfaces.

For assessing the intrinsic safety to mechanical sparks, two dedicated methods are implemented in testing laboratories and they are used for the conformity assessment of products with regard to explosive atmospheres ignition, namely:

- impact test for the technical equipment whose predictable faults may generate single-impact interactions between components, and

- friction test for the technical equipment whose predictable faults may generate mixed contact impact friction interactions between components, for this case the interaction between elements generating mechanical sparks and hot surfaces.

Within the article the results obtained by using the friction test method are treated, results which shall be used in further research for comparison with the ones resulting from the impact test.

LABORATORY TEST METHOD FOR NON-SPARKING MATERIALS AND TESTED MATERIALS

Friction test is performed in laboratory conditions and is represented by simulations performed on special test setups (test stands), reproducing the process of mechanical sparks generation by friction. Ignition of explosive mixtures from mechanical sparks is a complex process influenced by physical-chemical parameters, mechanical parameters and by the nature of materials involved in mechanical interaction [6]. The theoretical study of the ignition is required to be continued with the experimental study which shall confirm, correct or even infirm the theoretical considerations and hypotheses, but especially to verify the technical solutions for explosion protection applicable to technical equipment and tools intended for use in potentially explosive atmosphere. Simulations are carried out on a special test stand used for generating the friction between test specimens (pairs of materials A and B) [7],[10].

In particular, the test stand consists of an explosion resistant chamber equipped with:

- pipelines for adding in chamber the explosive mixture made by means of the automated installation for making explosive mixtures;

-equipment for measuring the concentration of the explosive mixture inside the chamber;

-a mechanism generating mechanical sparks or overheated surfaces, on which the specimens to be tested are mounted;

- explosion pressure discharger (one wall of the chamber covered with a thin plastic film which does not resist the explosion pressure);

- a controlled ignition source (electrical spark) to confirm the existence of the explosive atmosphere and to ensure operator protection at the end of the tests. The stand used is shown in Figure 2.

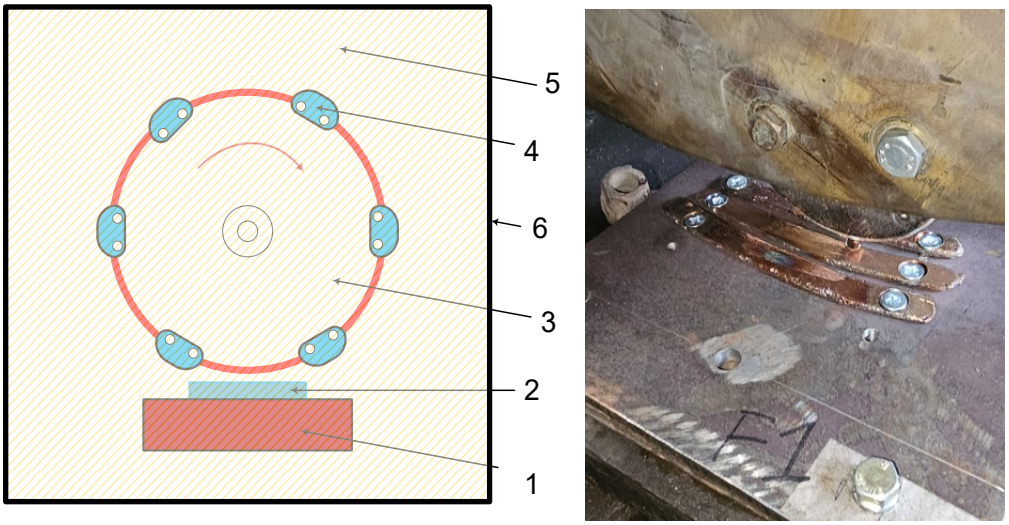


Figure 2 - Assembly for testing non-sparking materials at friction in explosive mixture

Legend:
1 – device for longitudinal / transverse movement on which the test samples are fixed;
2 - test sample/specimen -A;
3 - rotating disk on which the test samples are fixed;
4 - test sample/specimen-B;
5- explosive mixture;
6 - test chamber.

For modelling the ignition by mechanical sparks, the achievement and determination the concentrations which are ignited most easily, respectively the most susceptible to ignition mixtures, are of theoretical and practical interest. The crucial fact which can influence the test /assessment and acceptance process for non-sparking materials is represented by the manner in which the explosive mixture is achieved and on the accuracy of its concentration measurement. According to specific test requirements provided by the regulations in force, the explosive mixture is achieved according to the intended use of the material [6]. Considering the paper's topic, we performed the tests in an explosive mixture of air and 10% H2 with an accuracy of 0.02%.

https://doi.org/10.5593/sgem2024/1.1/s06.68

The friction test simulates the process of the formation of mechanical sparks, between two pairs of materials (two samples) in the case of accidental or technological friction. The shape of the tested samples, the type of friction (continuous or intermittent), the relative sliding speed, and the contact pressure between the samples involved in the friction process, determine the spark formation process. Formula 1 determines the relative sliding speed for the tests.

$$v = \frac{\pi dn}{60} \qquad (1)$$

Where:
n – is the rotation speed of the rotating disc [rot/min]

d - diameter of the circle described by the samples mounted on the rotating disc [m].

Generally, the relative sliding speed and the contact pressure between the samples involved in the friction process are established by agreement between the equipment manufacturer and the test laboratory. These tests were carried out at the following parameters: relative sliding speed was 17 rpm and the contact pressure was 6,1kg/cm^2. The tested materials are presented in table 3 for CuAlBe alloys and table 4 for CuTi alloys.

Table 3. Chemical composition of experimental CuAlBe alloys.

Chemical composition	**Cu %**	**Al %**	**Be %**
Alloy 1 – CuAlBe (F1)	90.7	8.5	0.8
Alloy 2 – CuAlBe (F2)	91.2	8.4	0.4

Table 4. Chemical composition of experimental CuTi alloys.

Chemical composition	**Cu %**	**Ti %**
Alloy 1- CuTi (F3)	97.26	2,74
Alloy 2 – CuTi (F4)	98.11	1.89

RESULTS

The results obtained for the pairs of materials tested in explosive mixture (10%H2) are presented in table 5.

Tabel 5 - Results

Nr. crt.	Sample type	Explosive mixture (10% H_2)	Pair of materials	Occurrence of ignition in explosive mixture (YES / NO)
1.	**Alloy 1 – CuAlBe (F1)**	10% H_2	F1- and steel	NO
2.	**Alloy 2 – CuAlBe (F2)**		F2- and steel	NO
3.	**Alloy 1- CuTi (F3)**		F3- and steel	NO
4.	**Alloy 2 – CuTi (F4)**		F4- and steel	NO

DISCUSSION

Pairs of materials tested in an explosive air-hydrogen mixture (10%H2), do not generate mechanical sparks. Analysing the samples after testing, due to the chemical composition of the alloys (see tables 3 and 4), significant wear can be observed on the surface of the alloy samples as well as oxidation of the material – see figure 3.

For each case, the ignition hazard assessment procedure must consider all potential ignition sources (in all operating modes, normal operation, expected and rare malfunction), taking into account the level of protection that all equipment must provide, depending on the category and implicitly the destination of use (see table 2). Friction processes between metallic materials, under certain conditions, can also generate hot surfaces and, by default, an ignition source. The fact that the explosive mixture was not initiated means that the temperature generated by the tested material pairs did not reach the value of 560 degrees C (hydrogen ignition temperature - see table 1). However, we measured the temperature resulting from the friction process between the tested material pairs to verify this temperature value. We used a FLIR thermal imaging camera. The measured values are presented in table 6.



Figure 3 - significant wear and oxidation on the sample surface

Tabel 6 - the measured values regarding the temperature generated by the friction process

Nr. crt.	Sample type	Pair of materials	Maximum temperature value [^{0}C]
1.	**Alloy 1 – CuAlBe (F1)**	F1- and steel	320
2.	**Alloy 2 – CuAlBe (F2)**	F2- and steel	335
3.	**Alloy 1- CuTi (F3)**	F3- and steel	360
4.	**Alloy 2 – CuTi (F4)**	F4- and steel	350

CONCLUSION

The equipment shall be subjected to a formally documented ignition hazard assessment to identify all potential ignition sources that could occur during normal operation, expected malfunctions and rare malfunctions. The friction process between the component parts of the equipment can be a technological or accidental phenomenon.

The tests in explosive mixtures as well as the determination of the temperature generated by the friction process represent an important step in the evaluation procedure of the

https://doi.org/10.5593/sgem2024/1.1/s06.68

ignition hazard generated by mechanical equipment. The obtained results provide relevant information both for equipment manufacturers and for the personnel involved in the conformity assessment procedure of mechanical equipment intended for use in potentially explosive atmospheres.

In other words, depending on the intended EPL of the equipment and the obtained results, mitigation can be applied to each of these potential ignition sources to minimize the likelihood that they could become effective ignition sources.

Further research will compare the obtained results with those from the impact test.

Technical equipment to be used in explosive atmospheres generated by hydrogen together with atmospheric air must comply with the essential safety and health requirements regulated by Directive 2014/34/EU (ATEX).

ACKNOWLEDGMENTS

This work was carried out through the "Nucleu" program of the National Research, Development and Innovation Plan 2022-2027, supported by MCID, project no. PN23320102.

REFERENCES

[1] Proust C. and Raveau D., "Towards Modelling of Frictional Ignition" 11 International Loss Prevention Symposium, 31 May–3 June 2004, Praha, Czech Republic;

[2] C. Proust, D. Raveau. Toward modelling of frictional ignition. 11. International Symposium on Loss Prevention and Safety Promotion in the Process Industry, May 2004, Praha, Czech Republic. pp.3348-3358. ffineris-00972452.

[3] Powell F (1986) "Can non sparking tools and materials prevent gas explosions",

Gas-Wasser-Abwasser 66, Jahrang 1986, Nr 6.

[4] EN ISO 80079-36 (2016), Explosive atmosphere – part 36 Non-electrical equipment for use in potentially explosive atmospheres -Basic method and requirements (2016)

[5] EN 1127-1 (2011), Explosive atmospheres. Explosion prevention and protection. Basic concepts and methodology.

[6] Prodan M., Mitu M., Razus D., Oancea D., Spark ignition and propagation properties of methane-air mixtures from early stages of pressure history, *Revue Romaine de Chimie*, 61, pp 299-305, 2016.

[7] STAS 10449-86, (1986), Electrical Equipment for Potentially Explosive Atmospheres Impact and Friction Testing, The Romanian Standardization Institute, Romania.

[8] ***, SR EN ISO/IEC 80079-20-1:2020, Explosive atmospheres — Part 20-1: Material characteristics for gas and vapour classification — Test methods and data, ASRO, 2020

[9] ***, Directive 2014/34/EU on the harmonisation of the laws of the Member States relating to equipment and protective systems intended for use in potentially explosive atmospheres (recast), Official Journal of the European Union, no.96, 2014

[10] Jurca A., Ghicioi E., Păun F., Gabor D., Lupu L., Modernization of the test method for non-sparking materials intended for use in explosive areas, Environmental Engineering and Management Journal, vol.18, no.4, pp847-852, 2019.

DETERMINATION OF EXPLOSION PARAMETERS FOR AIR-GASOLINE MIXTURES

PhD Chem. Eng. Irina Nălboc[1]

Ph.D Chem. Maria Prodan[1]

Ph.D Chem. Andrei Szolloşi-Moţa[1]

Ph.D Phys. Sonia Suvar[1]

[1]National Institute for Research and Development in Mine Safety and Protection to Explosion – INSEMEX Petroşani, **Romania**

ABSTRACT

The explosive atmosphere may be caused by flammable gases, vapors, or combustible dust. In the event that the material is combined with air in an adequate proportion, an ignition source is required to produce an explosion. Fuels and other liquids, as well as solvents from industrial items, release volatile vapors that can catch fire or explode when they come into contact with the air. At normal temperatures, flammable liquids can emit enough vapor to form combustible mixtures with air, heat, and often thick, black, and toxic clouds of smoke. The potential causes of explosions within work systems are represented by the intrinsic properties of flammable/combustible chemical substances and preparations used, dangerous chemical reactions, energy sources, or the ability of technical equipment, work methods, or techniques to cause human or material damage. Understanding the characteristic explosive parameters in regulated settings is essential to evaluating the risk of explosion and the evolution of explosion in such mixtures.

In this paper maximum explosion pressure p_{max} and maximum rate of pressure rise $(dp/dt)_{max}$ for gasoline-air mixtures were determined in a standard 20 dm^3 spherical explosion vessel in order to validate in the laboratory the method of determining the explosion parameters of air-vapor mixtures.

Keywords: explosion parameters, explosive atmosphere, gasoline sample, flammability, safety

INTRODUCTION

Oil-based materials are volatile, explosive, flammable, and dangerous. It is possible for the vapors produced by their evaporation to combine with air to create flammable gasoline-air mixes. When these combinations come into contact with open flames, hot surfaces, or static electricity, they have the potential to explode and cause serious fires once they reach a specific volume fraction. Gasoline-air combination fires and explosions have been regularly placed among the most costly and destructive mishaps during the oil manufacturing, transportation, storage, and filling processes [1]. Gasoline, one of the most commonly used fuels in industry, is volatile and its vapors can easily form a flammable gas mixture with air. Further, explosions of this mixture are the most frequent incidents occurring in the petrochemical industry, leading to equipment

https://doi.org/10.5593/sgem2024/1.1/s06.69

destruction and even casualties [2]. Explosions are defined as any chemical reaction that is followed by the abrupt release of a significant amount of heat. Systems that can sustain this process are referred to as explosive or flammable systems.

The probability that an explosion will occur depends on the coexistence of three factors:

- Combustible (flammable gaseous substance);
- Oxidizing (oxygen from air);
- Sources of ignition [3, 4].

Whether or whether they result in fire, explosions are catastrophic phenomena with significant societal and economic ramifications, particularly in light of modern technological advancements. Therefore, it is the responsibility of every employer to analyze the risk of explosions and safeguard employee safety and health by putting into practice the risk management guidelines outlined in regulations. authors. While several industrial risks have been resolved as a result of technological advancement, there are still many risks and hazards that need to be considered, such as the impressive risk of explosion that can have serious consequences, including material and human losses, which can have a significant impact on social relations and the indirect costs of the final product [5]. Such situation justifies the high interest to the problem of formation of explosive mixtures with air which takes the form of fine dispersion of gas, vapor, mist or dust. The requirement for finding solutions to three issues—prediction, prevention, and protection of events (accidents) involving explosions caused by chemical compounds justifies the need to justify the high oil explosivity problem, which is demonstrated by this situation as well as by studies addressing this research. Depending on the specific activities are being used different types of substances with flammable properties. Various explosive atmospheres can occur in both civilian and industrial areas. Flammable gases and vapors that may escape from an installation due to various causes (broken pipes, broken machinery, uncontrolled reactions, etc.) not ignited at the site of the leak may cause the occurrence of explosive mixtures. If flammable gases and vapors do not ignite at the source of escape, depending on the composition, physical characteristics, environmental conditions, they move in the form of a cloud, at various distances, until some source ignites it. In general, explosive atmospheres can be formed from gases that are lighter than air (e.g. hydrogen, methane, ammonia), but their explosion is less frequent, as they rise to the top of workspaces or disperse quickly. Liquefied or highly refrigerated gases, with a specific gravity close to that of air or higher, most frequently form explosive atmospheres.

Explosive atmospheres generated by flammable liquids can consist of: vapors - air, vapors and / or fog - air, fine liquid dispersed (sprayed) in the air. The biggest danger is the fog, which also contains the vapors of the flammable substance from which it comes, because it has a high susceptibility to ignition and a high concentration of fuel. The primary indicator for determining the explosion danger of air-gasoline mixtures is the explosion limit, which is a crucial parameter of flammable and explosive substances. It also serves as a foundation for defining pertinent standards and specifications. The explosive properties of combustible liquid vapors have been extensively discussed in the literature. Furthermore, vapor explosion in a closed vessel is a complex process involving fuel atomization, vaporization, mixing, ignition, and combustion. In order to experimentally ascertain the basic explosive properties of methanol-air mixtures using a closed vessel, Saeed, K. implemented a new multizone model and evaluated the

parameters of maximum explosion pressure and maximum pressure rise rate of methanol-air mixtures at various initial conditions of temperature, pressure, and equivalence ratio [6]. Zhenyi Liu studied the relationship between explosion limits and the critical oxygen content of petroleum vapor at various temperatures, and the results revealed that as temperature rose, the critical oxygen content decreased and the explosion limits became more varied [7]. Using an internal flammable liquid explosion-limit testing system, Ganbing Yao studied the explosion limits and inerting mechanisms of RP-5 and RP-3 oils [8].

The following are the primary characteristics of an explosion [9]:

- Lower explosive limit (LEL) which is the concentration of flammable gas, vapour or mist in air below which an explosive gas atmosphere will not be formed;

- Upper explosive limit (UEL) which is defined as the concentration of flammable gas, vapour or mist in air, above which an explosive gas atmosphere will not be formed.

- Maximum explosion pressure p_{max} is the highest pressure that occurs during of an explosion of a flammable mixture in a closed vessel;

- Maximum rate of pressure rise (dp / dt)max is the maximum value of the pressure rise per unit of time during explosion of any explosive atmosphere type within the explosiveness range of a flammable substance in a closed vessel, under specified test conditions;

- Explosion index K - the volume-dependent parameter of a given dust/gas/hybrid mixture, which is calculated using the cubic law equation:

$$K_{\max} = K_{st} = K_G = (dp/dt)_{\max} \cdot V^{1/3} \quad (1)$$

K_{st} – dust explosion index

K_G – gas explosion index

$(dp / dt)_{max}$ - maximum rate of pressure rise

V – explosion vessel volume

In this paper, an experimental study of the explosion characteristics of the gasoline-air mixture using the CA 20L explosion chamber was investigated. A commercial gasoline sample was used.

MATERIALS AND METHODS

This section will describe the substance tested, the equipment used and the operating procedures that were used to measure the explosion parameters.

There were performed explosivity tests for one commercial standard 95 gasoline sample to determine the maximum explosion pressure p_{max} and maximum rate of pressure rise $(dp/dt)_{max}$. Various distinct hydrocarbons are combined to create commercial gasoline. There are numerous engine performance requirements that gasoline must satisfy, and its composition can vary considerably.

The analysis was performed in accordance with EN 15967:2022 Determination of maximum explosion pressure and the maximum rate of pressure rise of gases and vapors [10]. The experimental equipment used for the measurements is explosion chamber CA 20L instrument presented in figure 1:

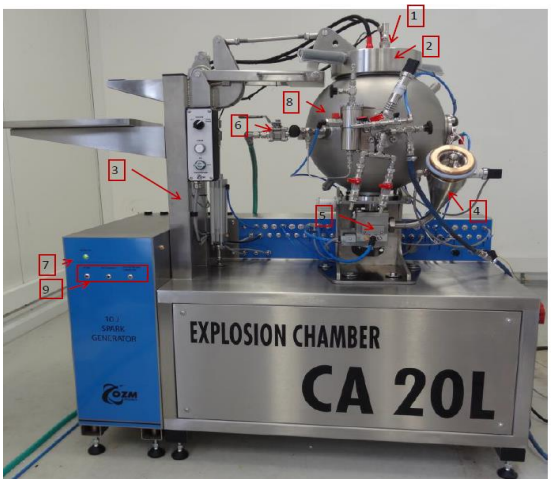


Figure 1 Explosion chamber CA 20L

1-lid with electrodes, 2-lock, 3-stand, 4-equipped dust reservoir, 5-outlet valve, 6-output ball valve, 7-LED power indication, 8-20L chamber, 9-LED power indication for ignition source

Spherical explosion chamber allows the measurement of parameters of flammable gas/vapor mixture with air explosion, hence the determination of the maximum explosion pressure and determination of the maximum explosion pressure rise $(dp/dt)_{max}$, determination of the explosion limits and the determination of the limiting oxygen concentration LOC. The chamber is a vessel of spherical shape with an inside diameter of 336 mm and a capacity of 20 l. The vessel is provided with an opening of inside diameter equal to 145 mm, which is provided with a flange and a lock for locking the lid closing. Lock is locked manually with safety position sensing "locked." Explosion chamber is made of stainless steel. The material and components comply with the use of equipment for experiments at atmospheric initial pressure and initial laboratory temperature (15-200°C). The system is sealed to the extent that the occurrence of an explosive atmosphere during normal operation outside the delivered system is not supposed [10].

At the beginning of the experiment, a vacuum was created with a vacuum pump. Then a certain amount of gasoline sample was introduced and stirring was started to accelerate the vaporization of the sample. Then air was introduced up to a pressure of 1 bar and permanent spark ignition was applied. After ignition, whether or not explosion occurred, the gas in the chamber was evacuated.

RESULTS AND DISCUSSION

After performing various experiments for several concentrations in the 20 L explosion vessel, were obtained the results presented in the table 1:

Table 1 Result

Concentration (% vol)	Pmax (bar)	(dP/dt)max (bar/s)
1.3	2.8	16
1.7	5.8	168
1.9	6.4	210
2.2	7.2	305
2.7	3.7	19

An essential factor in determining a gasoline-air mixture's explosive destructive potential is the maximum overpressure peak value. In the figure 2 it is displayed the overpressure versus time curve at a gasoline-air mixtures in various concentrations, respectively from 1.3% vol. to 2.7 % vol. This picture illustrates how the overpressure builds up quickly at first and then gradually diminishes as it approaches its max value, which occurs at approximatively 100 ms for the concentrations near the most reactive mixtures, while for the weaker mixtures to be approximatively 500 ms. After the gasoline-air mixture ignites, a lot of active chemical processes release a lot of heat by conduction and radiation, which is more heat than the heat loss from the tank wall. This is because of the chain reaction. As soon as the gasoline-air mixture ignites, the overpressure quickly rises (from 0 to 100 ms).

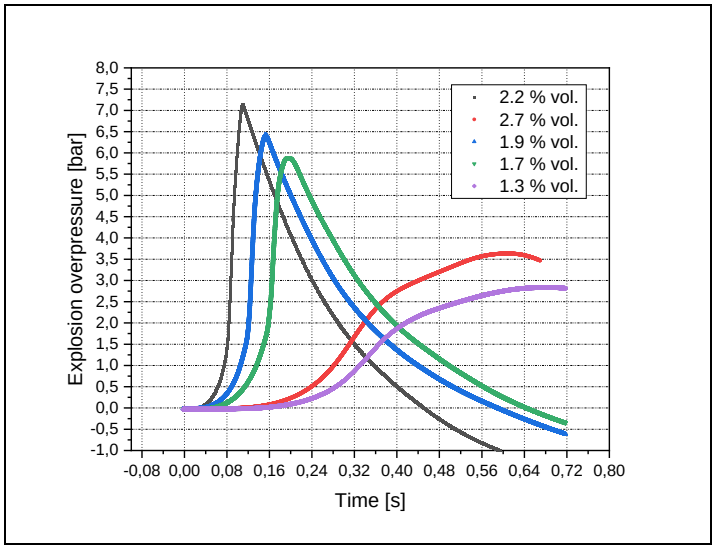


Figure 2 Explosion overpressure time series curves for gasoline concentration of 1.3% 1.7%, 1.9%, 2.2% and 2.7% vol

Figure 3 displays the gasoline-air mixture's overpressure versus concentration. This is a standard downward parabola curve. There is enough O2 present to carry out the combustion reaction when the concentration of the gasoline-air mixture is low.

https://doi.org/10.5593/sgem2024/1.1/s06.69

Consequently, when the concentration of the gasoline-air combination grows, so does the rate of heat release per unit mass, and this expansion is accompanied by an increase in explosive overpressure. Overpressure peaks when the concentration of gasoline-air mixture approaches the critical explosion concentration. After that, though, the overpressure lessens as the concentration of the gasoline-air mixture keeps increasing. To this work the peak explosion overpressure was obtained at a concentration of 2.2 % vol. The value obtained is in good accordance with the literature data [2,11] considering the fact that gasoline is a complex hydrocarbon with variable molecular mass.

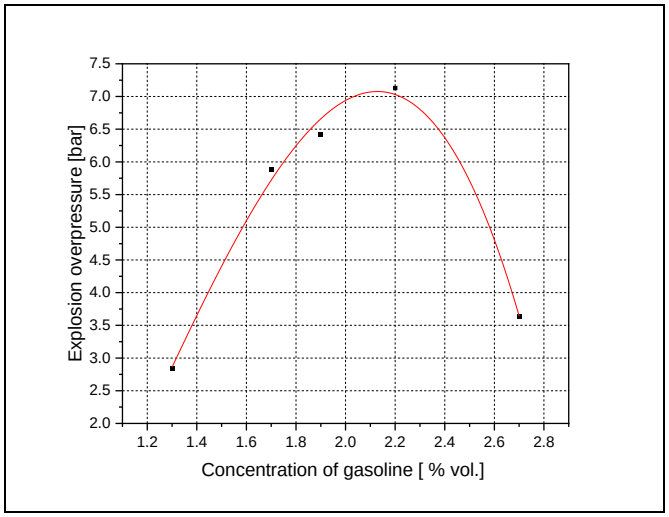


Figure 3 The explosion overpressure versus concentration curve

The maximum rate of pressure rise was calculated from the first derivative of the explosion pressure, with Savitzky–Golay method, the results obtained for the tested concentrations are also in good agreement with the literature [2].

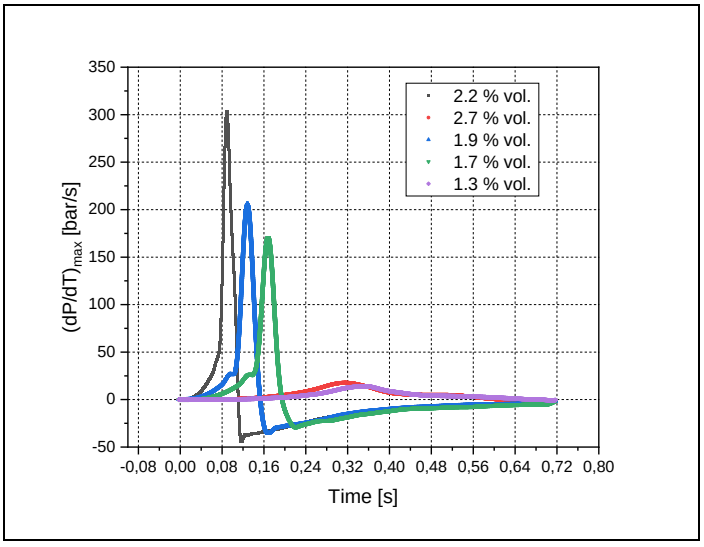


Figure 4 Maximum rate of pressure rise for gasoline concentration of 1.3% 1.7%, 1.9%, 2.2% and 2.7% vol

The experiments over gasoline sample were performed in order to verify the method for determining the explosion parameters of combustible liquids and to compare with the literature data. Taking into account that the gasoline does not have the same exact composition, the results obtained for this work are satisfactory. The comparison with the existing literature data confirmed that for the similar tested concentration range, similar values for the explosion pressure and maximum rate of pressure rise were obtained.

CONCLUSION

Materials based on oil are toxic, combustible, explosive and volatile. It's conceivable for the vapors released during their evaporation to interact with air and produce gasoline-air mixtures that catch fire. Once these combinations reach a certain volume fraction, they have the ability to explode and create serious fires when they come into touch with hot surfaces, open flames, or static electricity. Explosions and gasoline-air combination fires have consistently been ranked among the most expensive and catastrophic accidents that occur during the production, filling, and transportation of oil. This scenario and studies addressing this research show that the need to justify the high oil explosivity problem is justified by the need to find solutions for three issues: prediction, prevention, and protection of events (accidents) involving explosions caused by chemical compounds. Different kinds of chemicals with combustible qualities are utilized depending on the particular activity.

This report presents an experimental investigation of the gasoline-air mixture's explosion properties utilizing the CA 20L explosion chamber. A sample of commercial gasoline was utilized. At a concentration of 2.2% vol., the maximal explosive overpressure was obtained for this investigation. Given that gasoline is a complex hydrocarbon with a variable molecular mass, the value obtained is in good agreement with the data from the literature. Using the Savitzky–Golay method, the maximum rate of pressure rise was determined by taking the first derivative of the explosion pressure; the values obtained for the tested concentrations likewise show good agreement with the literature.

The experiments with the gasoline sample were conducted to confirm the procedure for figuring out combustible liquid explosion parameters and to compare the results with data from the literature. The findings acquired for this investigation are satisfactory, considering that the gasoline's exact composition varies. The comparison of the acquired values for the explosion pressure and maximum rate of pressure rise with the data from the literature revealed that equivalent values were obtained for the tested concentration range.

ACKNOWLEDGEMENTS

This work was carried out through “Core program” of the National Research, Development and Innovation Plan 2022-2027, supported by MCID, project no. PN 23 32 02 01 Developing the level of knowledge of the explosiveness parameters of hydrogen-based gaseous and hybrid mixtures, involved in the obtaining and storage processes in order to reduce the risk of explosion and IOSIN - PCDIEX.

REFERENCES

[1] Wang, S.M. Experimental Research and Numerical Simulation on the Evolution Characteristics of Oil and Gas Explosions in Confined Spaces with Weak Intensity Surface., Ph.D. Thesis, Army Logistics Academy, Chongqing, China, 2018

[2] Jiang, X.; Zhou, D.; Zhang, P.; Cai, Y.; Chen, R.; He, D.; Qin, X.; Lin, K.; Wang, S Explosive Characteristics Analysis of Gasoline–Air Mixtures within Horizontal Oil Tanks, Fire 2024, 24, China, vol. 7(1), 2024. https://doi.org/10.3390/fire7010024

[3] Bartknecht W., Springer Verlag, Explosions, Berlin Heidelberg New York, 1981

[4] C. Carloganu, Combustii rapide în gaze si pulberi, Ed. Tehnica, Bucuresti, 1986

[5] M. Prodan, E. Ghicioi, A. Szollosi-Mota, I. Nalboc, M. Paraian, Proceedings of the 6th International Conferince on Manufacturing Science and Education, pp 325-328, 2013

[6] K. Saeed, Determination of the explosion characteristics of methanol–air mixture in a constant volume vessel, Fuel, 210, pp 729-737, 2017

[7] Z.Y. Liu, H. Li, J. Xing, P. Huang, Y. Zhou, Explosion limits and critical oxygen content of crude oil vapor at different ambient temperatures, Ciesc J, 62, 2011

[8] G.B. Yao, L.F. Xie, J.C. Liu, X. Wang, Experimental study on explosion limits and suppression of combustible liquid, Chin. J. Energetic Mater, 18, pp 439-442, 2010

[9] Hattwing, H. Steen, Handbook of explosion prevention and protection, Cap. 3, Ed. Wiley-VCH, 2004

[10] Tehnical book Explosion chamber CA 20L, OZM research, 2023

[11] Yi Zhou, Y. Du, X. Zhao, P. Zhang, S. Qi, Experimental study on the explosion of gasoline-air mixture in reduced-scale storage tank, The Open Petroleum Engineering Journal, Vol 9, pp 150-158, 2016

DEVELOPMENT OF A COMBINED SPUD BIT FOR DRILLING TECHNOLOGICAL WELLS IN KAZAKHSTAN

Prof. Dr. Boranbay Ratov[1]

Prof. Dr. Boris Fedorov[1]

Assoc. Prof. Dr. Volodymyr Khomenko[2]

Assoc. Prof. Dr. Aidar Kuttybayev[1]

Assoc. Prof. Manshuk Sarbopeyeva[3]
[1] Satbayev University **– Republic of Kazakhstan**
[2] Dnipro University of Technology – **Ukraine**
[3]Yessenov University **– Republic of Kazakhstan**

ABSTRACT

The development of efficient drilling tools tailored to the unique geological conditions of Kazakhstan's drilling sites is paramount for optimizing well construction operations. This study focuses on the design, fabrication, and evaluation of a combined spud bit specifically engineered for drilling technological wells in Kazakhstan. The combined spud bit integrates both polycrystalline diamond compact (PDC) and carbide cutters within a single robust structure to enhance drilling performance across a diverse range of rock formations.

It is an annular housing with stepped weapons, and a pilot is attached to the lower end of the housing, at the end of which alternating weapons are placed: a carbide cutter-PDC cutter. Mixed stepped blades equipped with weapons are welded onto the side surface of the annular pilot with their transverse direction towards the face.

The main design solution is to raise the blades of carbide cutters above the edges of the blades of PDC cutters, i.e. the former are located closer to the face than the latter. This makes it possible to work out initially carbide cutters when the face is destroyed. In addition, the latter are located further from the axis of rotation of the tool and will have greater wear resistance. As drilling progresses, the height of the carbide cutter edges decreases and, finally, their height becomes equal to the height of the PDC cutter edges. As a result, the speed of deepening the well to the design depth increases sharply.

The findings of this study contribute valuable insights into the development of advanced drilling technologies tailored to Kazakhstan's geological challenges, with implications for improved well construction practices and resource extraction efficiency.

Keywords: spud bit, PDC drill bit, combined drill bit, annular pilot

INTRODUCTION

Drilling technological wells in Kazakhstan's diverse geological terrains presents a unique set of challenges necessitating innovative solutions in rock cutting tools design [1, 2]. These wells, crucial for the exploration and extraction of hydrocarbons, demand precision, efficiency, and durability in drilling operations. Central to the success of these endeavors is the design and optimization of blade drill bits, which play a pivotal role in the drilling process. Kazakhstan boasts a varied geological landscape, ranging from sedimentary basins to mountainous regions, each presenting distinct drilling conditions [3, 4, 5]. The effectiveness of drilling operations hinges on the adaptation of

https://doi.org/10.5593/sgem2024/1.1/s06.71

blade tools to these diverse environments, ensuring optimal performance and productivity. Moreover, with the increasing depths and complexities of wells being drilled, the demand for advanced blade tool designs that can withstand high temperatures, pressures, and abrasive formations is ever more pressing.

In recent years, significant strides have been made in the development of blade tool technologies, driven by advancements in materials science, engineering methodologies, and computational modeling [6, 7]. These advancements have facilitated the exploration of unconventional reserves and enhanced the efficiency of drilling operations in challenging environments. However, there remains ample scope for further research and innovation to address the specific requirements of drilling technological wells in Kazakhstan [3, 5].

MATERIALS AND METHODS

The assigned tasks were solved by a comprehensive research method, including a review and synthesis of literary sources, conducting patent research, conducting analytical studies of the scope of application, advantages and disadvantages of existing designs of cutting drill bits.

The development process of the combined spud bit for drilling technological wells in Kazakhstan commenced with comprehensive design considerations. The design phase involved analyzing the geological characteristics of the drilling sites in Kazakhstan, including rock types, formations, and drilling challenges. Based on this analysis, a conceptual design was formulated to integrate both PDC (polycrystalline diamond compact) and carbide cutters into a single bit structure. Upon finalizing the design, the fabrication process was initiated. High-quality materials suitable for drilling operations in diverse geological conditions were selected. The manufacturing process involved precision machining and assembly techniques to ensure the accurate integration of PDC and carbide cutters onto the bit's blades. Special attention was paid to the arrangement and orientation of the cutters to optimize cutting efficiency and drilling performance.

A series of laboratory tests will be conducted to assess the performance and efficacy of the developed combined spud bit. Testing protocols will be designed to simulate drilling conditions representative of those encountered in Kazakhstan's geological formations. Tests will include evaluating rate of penetration, cutting efficiency, and wear resistance of the PDC and carbide cutters under various drilling parameters.

RESULTS

Drilling wells involves the utilization of various rock cutting tools, each designed to address specific geological conditions and drilling requirements. Three commonly used types of rock cutting tools are roller cone bits, diamond bits, and PDC drill bits. Let's compare these tools based on key factors such as performance, durability, and suitability for different drilling environments.

Roller Cone Bits

– Design. Roller cone bits feature two or more cones with metal teeth or inserts that crush or gouge the rock as the bit rotates. These bits are versatile and can be designed with different cone configurations to optimize performance in various formations [8].

– Performance. Roller cone bits are well-suited for drilling in softer formations such as sandstone, shale, and clay. They offer good rate of penetration (ROP) in these formations due to their ability to crush and disintegrate the rock effectively.

– Durability. Roller cone bits may experience wear on the cone teeth or inserts during drilling, particularly in abrasive formations. However, they can often be refurbished or repaired, extending their operational life.
– Cost. Roller cone bits are typically more affordable compared to diamond bits and PDC drill bits, making them a cost-effective choice for certain drilling applications.

Diamond Bits

– Design. Diamond bits utilize industrial-grade diamonds embedded in the cutting face to grind through rock formations. They are available in two main types: natural diamond bits and synthetic diamond bits. Depending on the location of the diamond reinforcement, single-layer and impregnated bits are distinguished [9, 10, 11].
– Performance. Diamond bits excel in drilling through hard and abrasive formations such as granite, basalt, and quartzite. They offer relatively low ROP, which is however compensated by their other advantages.
– Durability. Diamond bits are highly durable and can withstand extreme heat and abrasion. They exhibit minimal wear compared to roller cone bits and PDC drill bits, providing longer operational life and reduced downtime. Therefore, their efficiency increases with increasing drilling depth.
– Cost. Diamond bits are typically more expensive than roller cone bits and PDC drill bits due to the cost of diamond materials and manufacturing processes. However, their superior performance and durability justify the investment in certain drilling applications.

PDC Drill Bits

– Design. PDC drill bits feature a fixed cutting structure with polycrystalline diamond cutters (PDCs) arranged on the bit's face. PDC cutters are manufactured using high-pressure, high-temperature processes to create a tough, wear-resistant cutting surface [12, 13, 14].
– Performance. PDC drill bits are versatile and perform well in a wide range of formations, including both soft and hard rocks. They offer high ROP and efficient cuttings removal, contributing to faster drilling progress.
– Durability. PDC drill bits are highly durable and exhibit minimal wear compared to roller cone bits. The PDC cutters maintain their sharpness over extended periods, resulting in longer run times and reduced maintenance requirements.
– Cost. PDC drill bits are usually more expensive than roller bits and cheaper than diamond bits. However, they provide greater durability than roller bits and greater rate of penetration than diamond bits. Therefore, these bits are usually more cost-effective in most geological and technical conditions. Their durability and performance make them the preferred choice for many drilling applications.

PDC drill bits have emerged as a preferred choice for many drilling applications due to several significant advantages over traditional roller cone and diamond drill bits. Here are some key reasons why PDC drill bits are considered significantly superior.

1. Higher Rate of Penetration (ROP). PDC drill bits are renowned for their exceptional drilling speed. The fixed cutting structure with polycrystalline diamond cutters (PDCs) on the bit's face provides continuous and efficient cutting action, resulting in faster penetration rates compared to roller cone and diamond bits. This increased ROP translates to reduced drilling time and lower overall costs.
2. Versatility. PDC drill bits exhibit versatility across a wide range of formations, from soft to hard rocks. Unlike roller cone bits, which may struggle in hard formations, and diamond bits, which can be less effective in softer formations, PDC drill bits offer

https://doi.org/10.5593/sgem2024/1.1/s06.71

consistent performance across various geological conditions. This versatility makes them suitable for a diverse range of drilling applications.
3. Durability. PDC drill bits are highly durable and resistant to wear and abrasion. The polycrystalline diamond cutters maintain their sharpness and cutting efficiency over extended periods, resulting in longer run times and reduced downtime for maintenance and replacement. In contrast, roller cone bits may experience wear on the cone teeth or inserts, and diamond bits may wear down their diamond cutting elements over time.
4. Improved Hydraulics and Cuttings Removal. The fixed cutting structure of PDC drill bits allows for efficient cuttings removal and improved hydraulics compared to roller cone bits. This enhances drilling performance by reducing the risk of bit balling and improving hole cleaning, particularly in challenging drilling environments [15].
5. Reduced Drilling Vibrations. PDC drill bits often produce smoother drilling operations with reduced vibrations compared to roller cone bits. This contributes to enhanced drilling efficiency, improved tool stability, and reduced wear and tear on drilling equipment.
6. Advanced Design and Engineering. PDC drill bits benefit from continuous advancements in design, engineering, and manufacturing technologies. Innovations such as optimized cutter geometries, enhanced cutter materials, and improved bit body designs further enhance their performance, durability, and reliability in demanding drilling applications [16, 17].
7. Cost-Effectiveness. While PDC drill bits may have a higher initial cost compared to roller cone bits, their superior performance, durability, and faster drilling speeds result in overall cost savings over the life of the bit. Reduced drilling time, extended run times, and lower maintenance requirements contribute to improved cost-effectiveness and higher returns on investment.
Overall, the combination of high drilling speeds, versatility, durability, and cost-effectiveness makes PDC drill bits significantly superior to roller cone and diamond drill bits in many drilling applications, leading to their widespread adoption in the oil and gas industry and other drilling sectors.
The Kazakh National Research Technical University (Satbayev University) located in Almaty has undertaken extensive research and development endeavors aimed at enhancing the efficiency of drilling operations in the construction of technological wells [18]. Specifically, comprehensive studies have been conducted to investigate the forces exerted on the cutters positioned along the blades of spud bits at various distances from the axis of rotation. The findings reveal a notable phenomenon occurring in the near-axial rotation zone, where zero rotational speeds induce a sharp increase in axial load, often reaching levels 8-10 times higher or more [19]. Consequently, this abrupt rise in axial load frequently leads to tool rotation cessation and a sluggish rock destruction process, posing significant complications to drilling procedures. Furthermore, such circumstances accelerate wear on the central part of the tool, resulting in diminished productivity even during drilling operations within the upper section interval.
Recent field tests of a spud bit model labeled as PK-2, conducted at the Budenovskoye field, have demonstrated its superior efficiency compared to previously utilized blade tools equipped with carbide cutters [20]. During drilling operations within the upper section, the drill's speed exhibited variance ranging from 18-20 m/hour to 10-12 m/hour, gradually decreasing to as low as 3 m/hour and even halting entirely. This reduction in drilling speed can be attributed to the bending of the lower stages of the blades, resulting in the formation of an annular cut in an effort to augment the axial load on the

tool. Remarkably, the PK-2 spud bit successfully covered an impressive interval spanning from 0 to 436 m, setting a record for the utilization of carbide blade tools.

Subsequent analysis of the operational results of spud bits revealed their ineffectiveness when drilling through the harder rocks found within the lower geological section: productivity plummeted to an average of 2-3 m/hour, with wear resistance dropping to a mere 50-80 m of penetration.

However, with the emergence of bladed bits equipped with PDC cutters, tangible opportunities arise to significantly elevate drilling productivity within the harder rocks of the lower geological section, thereby replacing the previously utilized carbide-tipped tools. Despite the relatively higher cost associated with PDC tools, their adoption is justified due to the substantial reduction in the construction time of technological wells.

A mixed well drilling technology is economically implemented at various sites:

– The initial geological unit, characterized by a thickness ranging from 0 to 350-400 m, consisting of easily penetrable rocks, is drilled using spud bits equipped with carbide cutters.

– The subsequent geological unit, spanning from 350-400 m to 700-800 m (reaching the design depth), comprising more challenging-to-drill rocks, is drilled using bladed bits equipped with PDC cutters.

This mixed technology allows for the maximization of the capabilities of bladed bits with carbide cutters to effectively penetrate soft rocks, while simultaneously providing a substantial increase in productivity and tool longevity in harder rocks. This effectively offsets the higher cost associated with bladed PDC bits. However, the primary drawback of this technology lies in the time required for hoisting operations, specifically the duration needed to replace spent carbide cutter-equipped spud bits and lower the bladed PDC bit to continue drilling the well to the designated depth.

In essence, there is a pressing need to devise a rock-cutting tool whose design encompasses the following parameters:

– A fusion of the positive attributes of carbide cutters (their cost-effectiveness) and PDC cutters (their high destructive capacity), with each type of cutter effectively utilized depending on the properties of the rock being drilled.

– The incorporation of calibrating elements to maintain the well diameter to the designated depth (ranging from 750-850 m).

– Ensuring the optimal balance of related technological parameters such as feed speed, axial load, and tool rotation speed.

A technical solution for the creation of such a tool tailored for the conditions of drilling technological wells in the Shu-Sarysu province has been identified and patented in the Republic of Kazakhstan [20]. Figure 1 provides a visual representation of the proposed combined tool.

https://doi.org/10.5593/sgem2024/1.1/s06.71

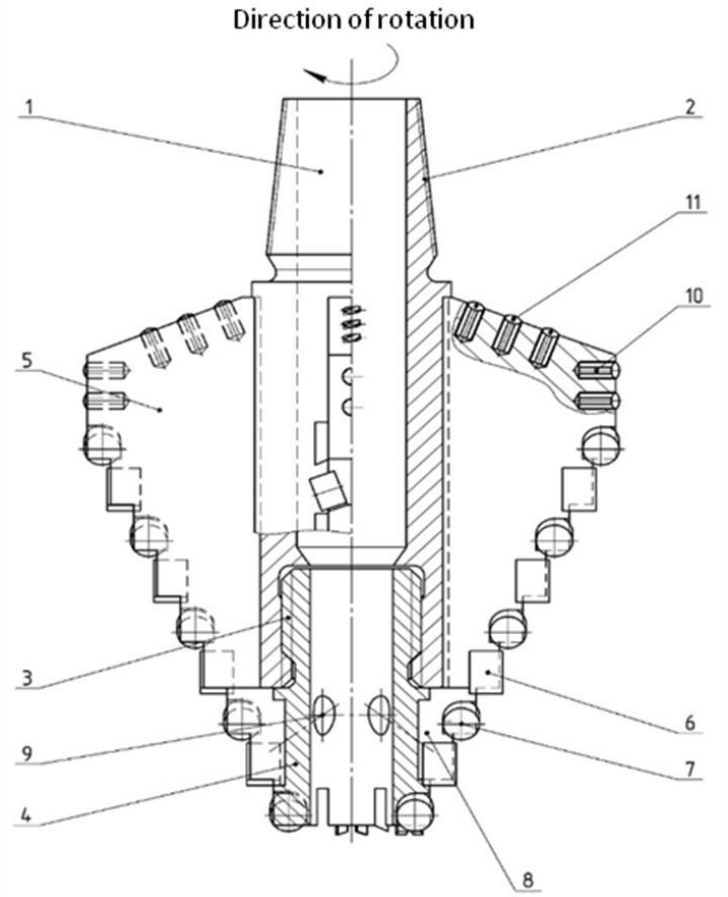


Fig. 1. Combined spud bit (according to RK patent No. 35606)

The tool comprises an annular housing 1 (referred to as the main body) and an annular blade pilot 4, both featuring threads 2 and 3 for connection with the drill string and each other, respectively. On the side surface of the annular housing 1, four stepped blades 5 are securely welded. These blades alternate in their configuration, each equipped with either carbide cutters or PDC cutters 7. Additionally, blades 8 are welded onto the side surface of the annular pilot 4, seamlessly continuing the pattern established by the main body blades 5. Notably, these annular pilot blades taper gradually, reducing their transverse size in a stepwise manner.

The annular pilot body integrates four inclined channels 9 designed to facilitate the passage of drilling fluid. Positioned at the end of the annular pilot body are four carbide cutters and an equal number of PDC cutters. To accommodate the geological variations encountered during drilling, the positioning of these cutters is adjusted accordingly. Specifically, when encountering softer rock formations within the upper interval of the geological section, drilling is performed using carbide cutters. Consequently, the edges of these carbide cutters are positioned closer to the bottom of the well, maintaining a distance 'h' relative to the edges of the PDC cutters (Fig. 2).

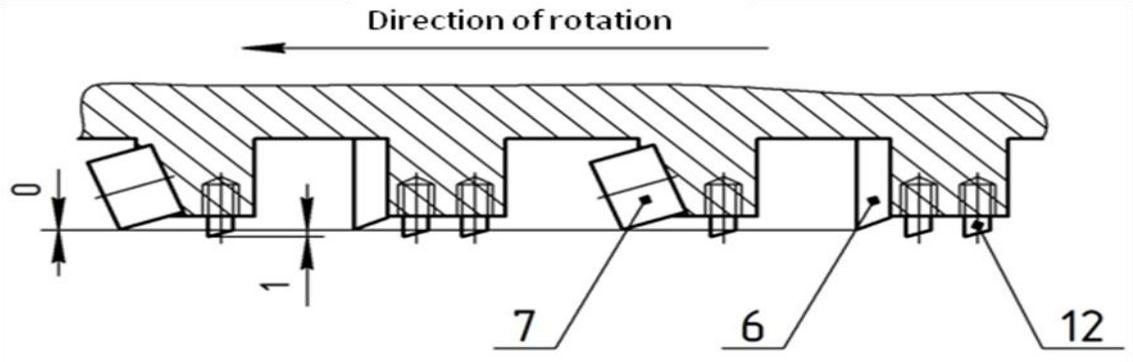


Fig. 2. Development along the middle circle of the end of the annular pilot
7 – PDC cutter; 6 – main carbide cutter; 12 – auxiliary carbide cutters

This design configuration ensures optimal drilling efficiency and adaptability to varying geological conditions. By seamlessly integrating both carbide and PDC cutters within the same tool, drilling operations can be efficiently executed across a spectrum of rock types and formations. Moreover, the tapered design of the annular pilot blades enables smooth transition and enhanced performance during drilling operations. Overall, the combined spud bit represents a significant advancement in drilling technology, promising improved productivity and versatility in well construction projects.

On the stepped blades, calibrating elements 10 are positioned at the location of their maximum transverse dimension. These elements serve a crucial role in preserving the diameter of the well throughout its entire depth. Furthermore, to mitigate complications encountered during drilling operations, such as rock falls onto the tool, the rear part of the blades is equipped with emergency carbide tools 11. Additionally, carbide cutters 12 are strategically placed to enhance the formation of the annular bottom.

DISCUSSION

Combination bits equipped with both PDC cutters and carbide cutters offer several advantages compared to bits equipped solely with PDC cutters:

1. Versatility. Combination bits can effectively drill through a wider range of formations due to the presence of both PDC and carbide cutters. Carbide cutters are particularly effective in softer formations, while PDC cutters excel in harder formations. This versatility allows for continuous drilling progress across varying geological conditions without the need for frequent bit changes.

2. Enhanced Performance. By combining the cutting capabilities of both PDC and carbide cutters, combination bits can achieve higher drilling speeds and increased efficiency. PDC cutters provide superior cutting performance in hard formations, while carbide cutters contribute to smoother drilling in softer formations. This results in overall improved drilling performance and reduced drilling time.

3. Improved Durability. The inclusion of carbide cutters in combination bits helps distribute the cutting workload, reducing wear and extending the operational life of the bit. Carbide cutters are more resistant to impact and abrasion compared to PDC cutters, making them suitable for handling challenging drilling conditions and increasing the overall durability of the bit.

https://doi.org/10.5593/sgem2024/1.1/s06.71

4. Cost-Effectiveness. While PDC cutters are known for their high performance, they are also associated with higher costs compared to carbide cutters. Combination bits offer a cost-effective solution by incorporating carbide cutters for drilling through softer formations where the performance benefits of PDC cutters may not be fully utilized. This helps optimize drilling costs while maintaining high performance across different rock types.

5. Reduced Risk of Stalling. In certain drilling scenarios, such as encountering sudden changes in formation hardness, bits equipped solely with PDC cutters may experience stalling or slowdowns in drilling progress. Combination bits mitigate this risk by incorporating carbide cutters, which can effectively handle softer formations without stalling, ensuring continuous drilling operations and improved overall efficiency.

CONCLUSION

In summary, combination bits equipped with both PDC and carbide cutters offer the advantages of versatility, enhanced performance, improved durability, cost-effectiveness, and reduced risk of stalling compared to bits equipped solely with PDC cutters. These benefits make combination bits a preferred choice for drilling operations across diverse geological formations and drilling conditions.

Technical solutions have been devised and patented to optimize the utilization of two distinct types of cutters within a single design of a rock-cutting tool. This innovative approach integrates cost-effective carbide cutters, ideal for the upper section of uranium deposits comprising soft, easily penetrable rocks, and high-performance PDC cutters, suitable for the lower section characterized by harder formations. Maximizing the potential of both types of cutters entails positioning the edges of the carbide cutters slightly below those of the PDC cutter blades, ensuring the former are closer to the well bottom during drilling of the softer rock interval. Additionally, the tool incorporates a detachable annular pilot equipped with the aforementioned mixed cutters at its end section, facilitating enhanced drilling efficiency across varying rock types and formations.

ACKNOWLEDGEMENTS

The study was supported by the Science Committee of the Ministry of Science and Higher Education of the Republic of Kazakhstan (grant No. AP14869271).

REFERENCES

[1] Akhundov F.A., Sarbopeeva M.D., Bayamirova R.U., Togasheva A.R., Zholbasarova A.T. On the issue of preparing the wellbore for its fastening. News of the National Academy of Sciences of the Republic of Kazakhstan, Series of Geology and Technical Sciences, 3(459), pp 22–35, 2023. https://doi.org/10.32014/2023.2518-170x.296

[2] Ismailova J., Abdukarimov A., Delikesheva D., Mombekov B., Ismailov A. Application of fusion property estimation within the multisolid wax prediction model on Kazakhstani crude. Heat Transfer, 53(2), pp 533–557, 2023. https://doi.org/10.1002/htj.22960

[3] Rakhmanova S.N., Umirova G.K., Ablessenova Z.N. Study of the greater Karatau's south-west by range of geophysical surveys in search of the crust-karst type polymetallic mineralization. News of the National Academy of Sciences of the Republic of Kazakhstan, Series of Geology and Technical Sciences, 1, pp 76–82, 2022 https://doi.org/10.32014/2518-170X.252

[4] Togasheva A.R., Bayamirova R.Y., Zholbassarova A.T., Sarbopeeva M.D., Arshidinova M.T. Pilot field tests of shock-wave treatment of wells at the fields of JSC «Ozenmunaigas». International Multidisciplinary Scientific GeoConference SGEM, 2023. https://doi.org/10.5593/sgem2023/1.1/s06.86

[5] Umirova G. K., Ahatkyzy D. Some features of structural interpretation of CDP 3D seismic data under conditions of the Bezymyannoye field. News of the National Academy of Sciences of the Republic of Kazakhstan, Series of Geology and Technical Sciences, 6(456), pp 233–246, 2022. https://doi.org/10.32014/2518-170X.252

[6] Dreus A., Kozhevnikov A., Lysenko K., Sudakov A. Investigation of heating of the drilling bits and definition of the energy efficient drilling modes. Eastern-European Journal of Enterprise Technologies, 3(7(81)), 41, 2016. https://doi.org/10.15587/1729-4061.2016.71995

[7] Mazen A.Z., Mujtaba I.M., Hassanpour A., Rahmanian N. Mathematical modelling of performance and wear prediction of PDC drill bits: Impact of bit profile, bit hydraulic, and rock strength. Journal of Petroleum Science and Engineering, 188, 106849, 2020. https://doi.org/10.1016/j.petrol.2019.106849.

[8] Koroviaka Ye.A., Ihnatov A.O., Pavlychenko A.V., Valouch K., Rastsvietaiev V.O., Matyash O.V., Mekshun M.R., Shypunov S.O. Studying the performance features of drilling rock destruction and technological tools. Journal of Superhard Materials, 45(6), pp 466-476, 2023. https://doi.org/10.3103/S1063457623060059

[9] He M., Li N., Zhu J., Chen Y. Advanced prediction for field strength parameters of rock using drilling operational data from impregnated diamond bit. Journal of Petroleum Science and Engineering, 187, 106847–106847, 2020. https://doi.org/10.1016/j.petrol.2019.106847

[10] Sun W., Gao H., Tan S., Wang Z., Duan L. Wear detection of WC-Cu based impregnated diamond bit matrix based on SEM image and deep learning. International Journal of Refractory Metals and Hard Materials, 98, 105530, 2021. https://doi.org/10.1016/j.ijrmhm.2021.105530

https://doi.org/10.5593/sgem2024/1.1/s06.71

[11] Vynohradova O.P., Zakora A.P., Shul'zhenko A.A., Gargin V.G., Sokolov A.N., Efrosinin D.V., Zakora I.A. Comparative evaluation of the performance of drill bits with a diamond-containing matrix and inserts made of diamond-containing composites. Journal of Superhard Materials, 44(1), pp 57–61, 2022. https://doi.org/10.3103/s1063457622010099

[12] Maystrenko A.L., Bondarenko M.O., Antonyuk V.S., Petasyuk G.A., Vinogradova O.P., Vasylchuk O.S., Zakora A.P., Zakutevsky O.I., Oleinyk N.O. Wear intensity of the functional components made of diamond-containing composite materials during the operation of tools in the process of Rock Destruction. Journal of Superhard Materials, 45(3), pp 208–216, 2023. https://doi.org/10.3103/s1063457623030164

[13] Ratov B.T., Fedorov B. V, Khomenko V. L, Baiboz A. R, Korgasbekov D. R. Some features of drilling technology with PDC bits. Naukovyi Visnyk Natsionalnoho Hirnychoho Universytetu, 3, pp 13–18, 2020. https://doi.org/10.33271/nvngu/2020-3/013

[14] Biletsky M.T., Kozhevnykov A.A., Ratov B.T., Khomenko V.L. Dependence of the drilling speed on the frictional forces on the cutters of the rock-cutting tool. Naukovyi Visnyk Natsionalnoho Hirnychoho Universytetu, 1, pp 21–27, 2019. https://doi.org/10.29202/nvngu/2019-1/22

[15] Ihnatov A.O., Koroviaka Y.A., Haddad J., Tershak B.A., Kaliuzhna T.M., Yavorska V.V. Experimental and theoretical studies on the operating parameters of hydromechanical drilling. Naukovyi Visnyk Natsionalnoho Hirnychoho Universytetu, (1), pp 20-27, 2022. https://doi.org/10.33271/nvngu/2022-1/020

[16] Maksymovych O., Lazorko A., Sudakov A., Hnatiuk O., Mazurak A., Dmitriiev O. Stress concentration in bounded compositeplates with carbon reinforcement. Actual Challenges in Materials Science and Processing Technologies II. Advanced Materials Research. 1045, pp 147-156, 2021. https://doi.org/10.4028/www.scientific.net/MSF.1045.147

[17] Dong G., Chen P., Wang X., Fu J., Yang, Y. Modelling and mechanical characteristics of PDC cutter-rock interaction by combining mixed fragmentation modes with dynamic rock strength. Petroleum, 2023. http://dx.doi.org/10.2118/205342-PA

[18] Borash A.R., Nurshakhanova L.K., Arshidinova M.T., Kenzhegaliyeva ZH.M., Zhanggirkhanova A.A. Improving the efficiency of PDC bits in oil and gas drilling. International Multidisciplinary Scientific GeoConference SGEM, 2023. https://doi.org/10.5593/sgem2023/1.1/s06.84

[19] Dong G., Yuan H., Chen Y., Fu J., Rong Z., Luo S., Han Q. The dynamic characteristics of PDC cutter-rock interaction considering mixed fragmentation mode and dynamic rock strength. In Rock Dynamics: Progress and Prospect, Volume 2: Proceedings of the Fourth International Conference on Rock Dynamics And Applications, p. 395, 2023. CRC Press. https://doi.org/10.1201/9781003359159-70

[20] Ratov B.T., Mechnik V.A., Rucki M., Gevorkyan E.S., Bondarenko N.A., Kolodnitskyi V.M., Chishkala V.A., Kudaikulova G.A., Muzaparova A.B., Korostyshevskyi D.L. $C_{diamond}$–(WC–Co)–ZrO_2 Composite materials with improved mechanical and adhesive properties. Journal of Superhard Materials, 45(2), pp 103–117, 2023. https://doi.org/10.3103/s1063457623020107

DEVELOPMENT OF METHODOLOGY FOR OPTIMAL CYCLIC INJECTION TECHNIQUES BASED ON MATHEMATICAL MODELING

Idrisov Kamil M.[1]
Shipaeva Maria S.[1]
Ziniukov Rustam A.[1]
Sudakov Vladislav A.[1]
[1]Kazan Federal University, **Russian Federation**

ABSTRACT

The study aims to identify the optimal operating conditions of wells to increase oil recovery without incurring additional costs for Enhanced Oil Recovery (EOR). The study analyzes various scenarios based on different properties of geological formations and wells.

This work was carried out using three-dimensional hydrodynamic modeling. These models represent a simplified hydrodynamic model of a real object, which was created for the purpose of analyzing the processes being studied, but does not claim to be a complete description of the geological structure. At the same time, when constructing synthetic hydrodynamic models, the geological and physical properties of the modeled formation were taken into account.

One of the most critical field and technological parameters determining the effectiveness of cyclic flooding technologies is the duration of the half-cycle. Calculations show a strong increase in accumulated oil in calculations during cyclic flooding with a half-cycle length of 3 days. However, this result strongly depends on the formation's piezoelectric conductivity and the distance between the injection and production wells.

The following two experiments were carried out to identify the influence of the direction of the well pattern on the relative increase in oil production. At the first stage, the grid was modified to position the wells at the center of the model's boundary area. At the second stage, the wells are located so that they are at a certain distance from the boundaries of the model. This experiment indicates that the orientation of the well pattern significantly affects the outcomes of cyclic waterflooding. The results remained consistent with a diagonal well arrangement irrespective of the model size.

To select models with different rock parameters in order to determine the possibility of working in further projects, an experiment was conducted to determine the effectiveness of cyclic flooding in hydrophobic rock. The simulation results indicate that cyclic flooding is ineffective in hydrophobic reservoirs. This is explained by the inability of the rock to retain water in its pores, as a result of which the oil remains practically motionless.

Keywords: enhanced oil recovery methods, cyclic waterflood, analysis, terrigenous reservoirs.

https://doi.org/10.5593/sgem2024/1.1/s06.72

INTRODUCTION

At present, the global energy consumption is exhibiting rapid growth. In light of this, the imperative to ensure the maximal production of hydrocarbon resources is ascending in significance for the oil industry.

Among the notable methods for enhancing oil recovery, the cyclic injection method stands out due to its efficiency and relatively low financial burden. This technique endeavours to enhance the elastic reserve within rock formations through the application of cyclic pressure via pressurized water. The variable pressures employed in the cyclic injection process foster dynamic changes in pressure and fluid flow between reservoir layers of differing permeability. An increase in water pressure promotes its penetration into layers with higher permeability, whereas reduced pressures enable the mobilization of oil from less permeable strata toward more permeable regions of the reservoir [1].

Principles of Cyclic Flooding

The physical essence of the cyclic impact is illustrated in Figure 1. It demonstrates a two-layer reservoir model, where the upper layer has higher permeability compared to the lower layer.

In the first part of Figure 1, the displacement process under conditions of stationary flooding is depicted. The upper layer exhibits a higher rate of formation development and consequently, a greater degree of water breakthrough in the production well. Conversely, the lower layer is less developed but contains oil reserves that are not engaged in the drainage process [1].

The second part of Figure 1 illustrates the change in the displacement process during the phase of increased injection pressure. As shown, a significant pressure gradient between the two layers induces the movement of water from the upper layer to the lower one. The final phase of the cycle, presented in the lower part of the figure, demonstrates a reduction in injection pressure. During this phase, the pressure in the upper layer decreases more rapidly than in the lower layer due to its greater piezoconductivity, leading to the extraction of additional oil reserves from the lower layer that remained untapped during stationary flooding [2].

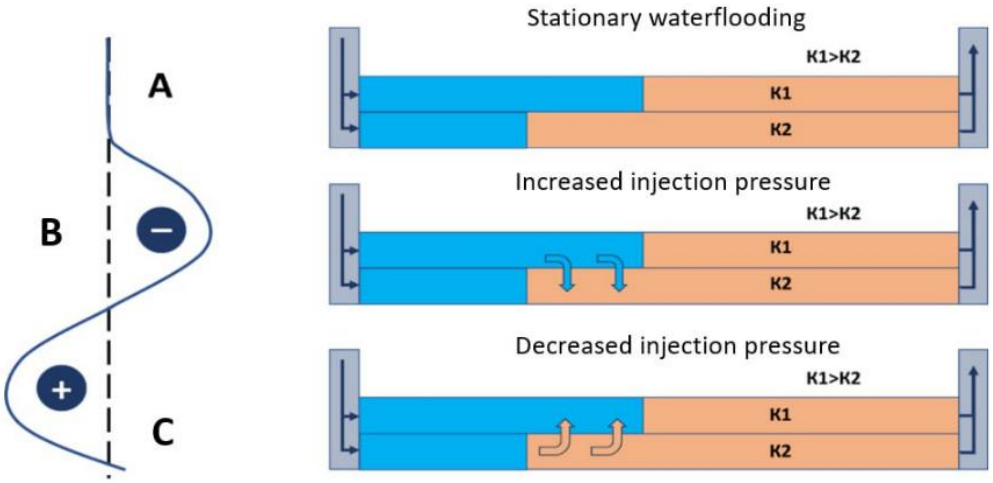


Figure 1- Displacement process during stationary flooding

MATERIALS AND METHODS

Based on the presented cyclic impact mechanism, the additional volume of oil not involved in intensive development during stationary waterflooding is displaced through cyclic injection.

This work was carried out using three-dimensional hydrodynamic modeling, during which a set of synthetic models of symmetry elements of well placement systems was created. These models represent a simplified hydrodynamic model of a real object, which was created for the purpose of analyzing the processes being studied, but does not claim to be a complete description of the geological structure. At the same time, when constructing synthetic hydrodynamic models, the geological and physical properties of the modeled formation were considered.

To create hydrodynamic synthetic ones, a variant of a two-phase three-dimensional isothermal model with two phases (water, oil) was chosen, which is a model of non-volatile oil BlackOil [3].

In this study, five computational models were evaluated, each distinguished by the following parameters:

1. Cyclic water injection into the reservoir with varying half-cycle periods. A complete cycle comprises an injection phase and a well shutdown phase, with analyses being performed more conveniently using half-cycle periods.

2. Variation in the thickness ratios of high and low permeability layers, maintaining the same half-cycle duration as in point 1.

3. Evaluation of the effectiveness of cyclic flooding on an oil-wet reservoir. The half-period is the same as in point 1.

4. Application of cyclic flooding on a conceptual model of a real field (using conclusions obtained in points 2, 3, and 4: water-wet reservoir, influence of formation thickness and injection half-cycle).

5. Variation in well injectivity and subsequent evaluation of oil recovery efficiency from the field described in point 5.

RESULTS

Simulation model parameters

To determine the dimensions of the simulation area, the distances between wells and their spatial arrangement were taken into consideration. The grid characteristics of the synthetic model are detailed in Table 1, while initial data on the physicochemical properties of formation hydrocarbons and water are presented in Table 2.

Table 1 - Characteristics of the synthetic model grid

Area size, m	Cell size, m	Number of cells
700*700*3	25*25*0.2	13456

The model incorporated the option of scaling the relative permeability curves (EndScale). Parameters such as associated water saturation (Swl), critical water saturation (Swcr), and residual oil saturation in the oil-water system (Sowcr) were

https://doi.org/10.5593/sgem2024/1.1/s06.72

derived from permeability based on the relationships shown in Figure 2. The initial saturation distribution is depicted in Figure 3.

Table 2 – Initial data on the physical and chemical properties of reservoir hydrocarbons and water

Oil density, kg/m^3	Water density, kg/m^3	Volumetric coefficient of oil	Initial gas content, m^3/t	Viscosity, mPa*s		Compressibility, MPa^{-1}		Saturation pressure, MPa	Reservoir pressure, MPa
				Oil	Water	Oil	Water		
868	1014	1.085	35	2.57	0.435	0.0012	0.000485	7.5	18.52

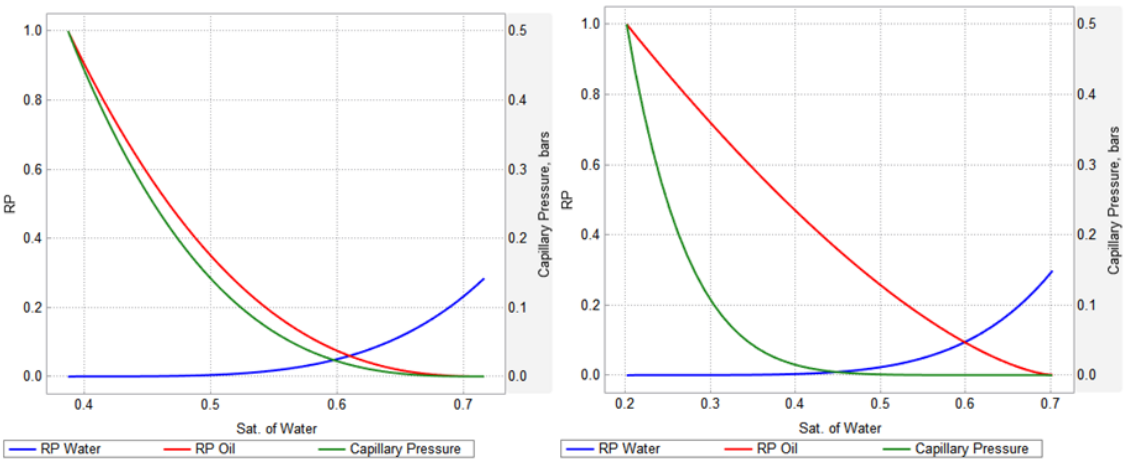


Figure 2 – Relationships of relative phase permeabilities for oil and water on water saturation

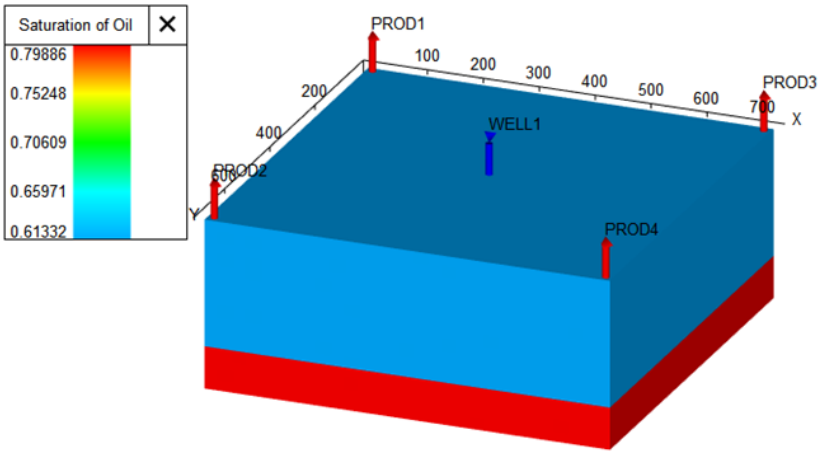


Figure 3 – Oil saturation cube

1. Assessing the limits of effective application of cyclic flooding

A critical field and technological parameter influencing the efficacy of cyclic flooding technologies is the duration of the half-cycle. To determine the optimal half-cycle duration, calculations were performed using the base model. The considered half-cycle durations included: 1, 3, 5, 15, 30, and 60 days. The results of these calculations are provided in Table 3.

Table 3 – Results of calculations of technological development indicators for various half-cycle durations.

Half-cycle duration, days	Water flooding technology	Cumulative oil production, thousand m^3	Relative increase in cumulative oil production, %
-	Stationary	82858.1	0
1	Cyclic	85265.2	2.91
3	Cyclic	85356.7	3.02
5	Cyclic	85259.3	2.90
15	Cyclic	84842.5	2.39
30	Cyclic	84320.2	1.76
60	Cyclic	83489.1	0.76

Calculations indicate a significant increase in cumulative oil production during cyclic flooding with a half-cycle duration of 3 days. However, this increase is heavily influenced by the piezoelectric conductivity of the formation and the distance between the injection and production wells [4]. This relationship is described by the following equation:

$$t = \frac{l}{2\chi}, \quad (1)$$

where t is the duration of the half-cycle, l is the distance from the injection well to the front of oil displacement by water, χ is the piezoelectric conductivity of the formation.

2. Study of the influence of the ratio of thicknesses of low-permeability and high-permeability layers on the efficiency of cyclic flooding

Another critical parameter that influences the effectiveness of cyclic flooding technologies is the ratio of the thicknesses of high-permeability and low-permeability interlayers. To determine the optimal ratio, calculations were performed using the basic model. The following thickness ratios were examined: 15/1, 3/1, 1/1, and 1/3. Given that the thickness ratio directly impacts reserves, and consequently oil production, it was decided to calculate the increase in oil production relative to stationary waterflooding for each ratio under identical conditions. The calculation results are presented in Table 4.

Table 4 – Results of calculations of technological development indicators for various ratios of thickness of high- and low-permeability layers

Relation of thickness of layers	Waterflooding technology	Cumulative oil production, thousand m^3	Relative increase in cumulative oil production, %
15/1	Stationary	85632.3	1.01
	Cyclic	86500.6	
3/1	Stationary	98463.6	3.39
	Cyclic	101804.7	
1/1	Stationary	130786.0	1.07
	Cyclic	132184.6	
1/3	Stationary	164544.7	-0.01
	Cyclic	164525.6	

The experiment results indicate that the most effective ratio for cyclic flooding is a thickness ratio of low- to high-permeability layers of 3/1 (or, equivalently, 12/4 in the

https://doi.org/10.5593/sgem2024/1.1/s06.72

experimental setup). To further validate the findings, an additional experiment was conducted with the reverse arrangement of interlayers [5]. This calculation demonstrated that under the given conditions, cyclic flooding exhibited minimal improvement.

3. Study of the influence of rock wettability on the efficiency of cyclic flooding.

To evaluate models with varying rock properties and assess their potential for future projects, an experiment was conducted to determine the efficiency of cyclic flooding in oil-wet reservoir.

The simulation results (Table 5) indicate that cyclic flooding is not suitable for oil-wet reservoirs. This limitation arises from the rock's inability to retain water in its pores, resulting in the oil remaining largely immobile.

Table 5 – Results of calculations of technological development indicators for an oil-wet reservoir.

Number of days	Waterflood type	Cumulative oil production, thousand m^3	Relative increase in cumulative oil production, %
0	Stationary	38745.8	0
1	Cyclic	38719.3	-0.07
3	Cyclic	38665.1	-0.21
5	Cyclic	38179.2	-1.46
30	Cyclic	36571.9	-5.61
60	Cyclic	34019.0	-12,20

The results obtained are depicted in Figure 4. Experimental findings suggest that cyclic flooding is most effective in:

- water-wet reservoirs;
- where the thickness ratio of low-permeability to high-permeability layers is 3:1;
- with an optimal half-cycle period that varies depending on reservoir properties.

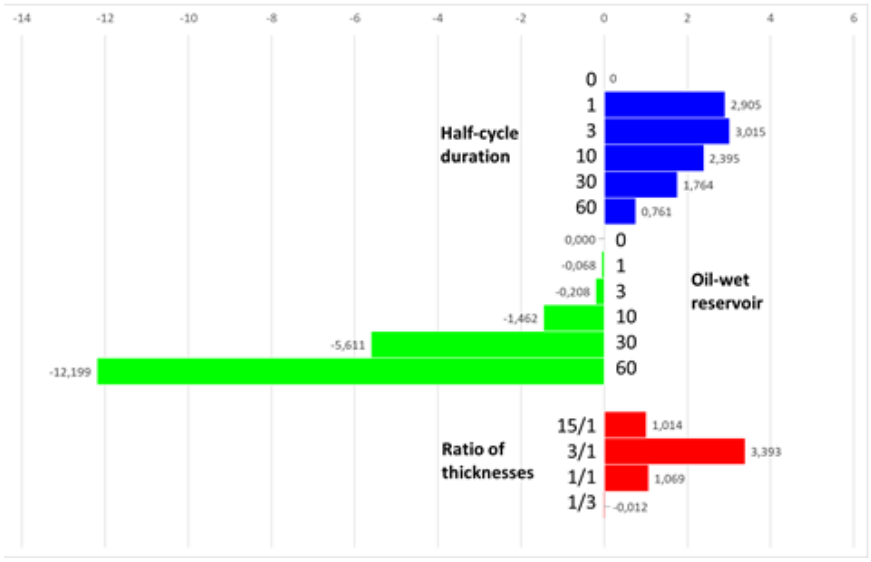


Figure 4 – Summary chart based on the results of the experiments

DISCUSSION

Based on the criterion values obtained during the sensitivity analysis, a section of one of the fields located in the Republic of Tatarstan was selected, whose parameters matched the optimal criteria. A conceptual model has been created for this section.

4. Selection of the optimal half-cycle period for the injection well on the conceptual model of field under study

Based on previous study results, a conceptual model was developed using data from a field in Tatarstan. Given that the formation parameters are well understood, further experiments were designed to alter the operational modes of wells. These alterations include modifying the well startup and shutdown periods as well as adjusting the injection volume.

The first series of experiments focused on varying the well operation cycle durations. The following half-cycle durations were considered: 1, 3, 10, and 30 days. The results of these calculations are shown in Table 6.

Table 6 – Results of production parameters calculation

Number of days	Waterflood type	Cumulative oil production, thousand m^3	Relative increase in cumulative oil production, %
0	Stationary	166178.3	0
1	Cyclic	167840.6	1.00
3	Cyclic	169642.4	2.08
10	Cyclic	171229.4	3.04
30	Cyclic	170486.7	2.59

The most substantial increase in oil production was observed with a half-cycle period of 10 days, demonstrating the effectiveness of cyclic waterflooding in this particular field.

5. Selection of the optimal injectivity for the injection well on the conceptual model of field under study

The second series of experiments examined the effect of different water injection volumes on the reservoir. The injection volumes tested were 100, 200, and 400 m^3/day, with the results presented in Table 7

Table 7 – Results of production parameters calculations for different injectivities

Water injectivity, m3/day	Waterflooding technology	Cumulative oil production, thousand m^3	Relative increase in cumulative oil production, %
100	Stationary	166178.3	2.73
	Cyclic	171229.4	
200	Stationary	180101	3.04
	Cyclic	184688.9	
400	Stationary	136569.1	2.55
	Cyclic	140294	

This experiment identified the optimal injection volume for cyclic flooding as 200 m^3/day.

https://doi.org/10.5593/sgem2024/1.1/s06.72

CONCLUSION

Thus, based on a comprehensive analysis of technological parameters on synthetic models, standardized dependencies for the computation of geological, petrophysical, and operational criteria for the cyclic flooding applicability were obtained. These models facilitate the evaluation of the method's viability according to each calculated criterion. A sensitivity analysis was performed to evaluate the impact of cyclic flooding on model parameters and well performance. The results of the study demonstrated that cyclic flooding is most effective in a hydrophilic reservoir, where the low-permeability layer's thickness is threefold compared to the high-permeability layer. The findings indicated that cyclic flooding is applicable to a terrigenous reservoir in one of the fields in Tatarstan. This hypothesis was validated through experiments detailed at the end of the work. Investigations involving cyclic flooding will be extended to include the examination of additional model parameters, as well as the evaluation of a modified enhanced oil recovery (EOR) technique—altering the direction of filtration dynamics.

ACKNOWLEDGEMENTS

This work was supported by the Ministry of Science and Higher Education of the Russian Federation under agreement No. 075-15-2022-299 within the framework of the development program for a world-class Research Center "Efficient development of the global liquid hydrocarbon reserves".

REFERENCES

[1] Safuanov, R.I., Ziniukov, R.A., Poryvaev, T., Petrov, T., & Farkhutdiniov, I.. Statistical and neural network methods for localizing residual oil reserves, SGEM International Multidisciplinary Scientific GeoConference EXPO Proceedings, 2021.

[2] Surguchev M.L. Cyclic (pulse) stimulation of the reservoir as a method for increasing oil recovery during waterflooding, Oil industry, No. 3, 1965.

[3] Surguchev M.L. Tsynkova O.E., Sharbatova I.N. Cyclic waterflooding of oil formations, M.: VNIIOENG, 1977.

[4] Sharbatova I.N., Surguchev M.L Cyclic impact on heterogeneous oil reservoirs, M: Subsoil., Russia, 1988, 121p.

[5] Aubakirov A.R. Design of optimal cyclic flooding technology based on hydrodynamic modeling, Exposition Oil Gas. No. 7, Russia, 2015, pp 40-44.

DETERMINATION OF EXPLOSION CHARACTERISTICS FOR COMBUSTIBLE POWDERS (STARCH – MAGNESIUM)

Ph.D Chem. Maria Prodan[1]

Ph.D Chem. Eng. Irina Nălboc[1]

Ph.D Chem. Andrei Szolloşi-Moţa[1]

Ph.D Phys. Sonia Suvar[1]

[1]National Institute for Research and Development in Mine Safety and Protection to Explosion – INSEMEX Petroşani, **Romania**

ABSTRACT

Accidental explosions and fires caused by combustible dust are some of the most significant threats in many industries where layers of combustible dust and clouds are formed as a result of technological processes. Combustible powders react with air oxygen in a process known as oxidation, which produces carbon dioxide, carbon oxide, water, and other gases whose contents depend on the temperature at which the oxidation occurs. The dust cloud is the main form of existence of combustible dust in the production area and together with the existence of effective ignition sources are the main causes of dust explosions in production processes. Dust explosions are mainly characterized by the minimum ignition temperature, explosion limits, the minimum ignition energy, maximum explosion pressure and the rate of pressure rise. The explosive behaviors which is represented by a mixture of air and flammable substances are influenced by many factors of which the most important parameters are the chemical composition and concentration of flammable and explosive mixture with air. In particular, for the combustible powders intervening additional factors related to the physic-chemical properties of combustible solids, the shape and size of dust particles, as well as the environmental conditions under which dust exist in suspension.

For this work flammability tests have been performed for powder mixture of starch and magnesium respectively minimum ignition temperature, lower explosion limit, explosion pressure, the maximum rate of pressure rise, minimum ignition temperature in the layer of the dust cloud.

Keywords: explosion parameters, explosive atmosphere, combustible powder, dust cloud safety

INTRODUCTION

Explosions of combustible dust or flammable gases/vapours with air are frequent and devastating phenomena in industry. Secondary explosions are the most serious and occur when the pressure wave of the first explosion involves the layers of dust already present in the plant, thus creating a dust cloud larger than that generated by the first explosion. As the pressure wave propagates inside the plant, the powder feeds the unfolding flame, resulting in greater damage due to the large amount of powder involved and the higher explosive pressure. The consequences of a secondary powder

explosion can be disastrous, so a minor explosion can turn into a major explosion if proper measures are not taken [1]. Although it is important to eliminate the risk of the first explosion, it is even more important to reduce the possibility that the first explosion will generate other explosions, in other words to prevent the "domino effect" - fig. no. 1, due to the fact that the secondary explosions are more violent than the primary one [2,3].

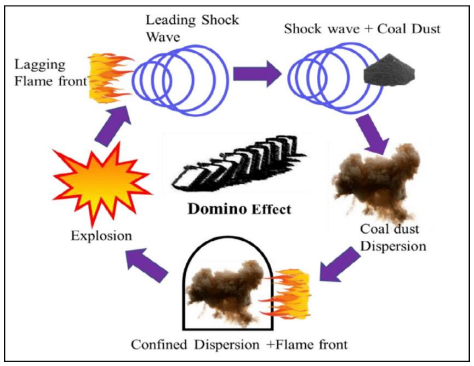


Figure 1 Domino effect of dust explosion

The most important and often reported in the literature of explosiveness parameters for combustible powders are, according to the series of standards SR EN 14034-1,2,3: Determination of the explosion characteristics of dust clouds, [4]: Maximum explosion pressure Pex; The maximum rate of pressure rise (dP/dt)max;Severity factor - Kmax, Kst; Minimum explosion concentration or lower explosion limit (CmEx, LIE or LEL); Minimum ignition energy MIE; Minimum ignition temperature of a dust cloud MIT; The minimum ignition temperature of the powder layer LIT. The values of these parameters can be found in the literature or in online databases, but these values should be considered as indications and not as a basis for the design of safety measures in the industry, which should be based on specific data for each powder in part. It is important to know that these parameters are not intrinsic properties of materials. They are strongly dependent on both material properties (moisture, particle size, shape, porosity) and experimental conditions (vessel volume, degree of powder cloud turbulence, applied initiation source and its energy) [5]. The parameter (dP/dt) max is dependent on the volume of the explosion chamber and cannot be used for vessels with different volumes. To scale to larger volumes, the maximum pressure rise rates are normalized by multiplying by the cube root of the blast chamber volume. Even this procedure does not have a well-founded theoretical justification and is disputed by some researchers. The maximum rate of pressure rise obtained in a dust-air explosion is not only a measure of the explosiveness of the powder but is a key property underlying explosion detection and protection systems. According to classical combustion theory, in the ideal case, the absolute pressure as a function of time, P(t), at a constant volume, in the spherical cell, is related to the volume V(t) of the sphere occupied by the reaction products, as follows [6,7]:

$$\frac{P(t) - P_0}{P_{max} - P_0} = k \frac{V(t)}{V_0} \qquad \text{(I.1.)}$$

where P0 is the absolute initial pressure, V0 the volume of the explosion chamber and k is a correction factor related to the density difference between the reacted products and the remaining unreacted reactants. For spherical propagation from a point source [6]:

$$\frac{V(t)}{V_0} = \left[\frac{r(t)}{r_0}\right]^3 = \left[\frac{S_b t}{r_0}\right]^3 \quad \text{(I.2.)}$$

where r(t) is the radius of the spherical volume occupied by the reacted products, r0 the radius of the explosion chamber and Sb is the flame speed, given by:

$$S_b = \frac{dr(t)}{dt} = \left(\frac{\rho_u}{\rho_b}\right) S_u \quad \text{(I.3.)}$$

Where, ρu/ρb is the ratio of unburned gas density to burned gas density. The normal burning speed, Su is the speed of flame propagation relative to the unreacted mixture in front of it. The flame speed Sb is relative to a fixed reference point. Both velocities refer to laminar conditions for explosions of combustible powders dispersed in air. For spherical propagation in a spherical explosion enclosure, the maximum explosion pressure is reached when the flame contacts the cell wall. At that time, k=1. Applying the first-order derivative of equation I.1 with respect to time and substituting eq. I.2 and I.3, we get:

$$\frac{dP(t)}{dt} = 3(Pmax - P_0)\left(\frac{\rho_u}{\rho_b}\right) S_u \frac{r(t)^2}{r_0^3} \quad \text{(I.4.)}$$

Considering:

$$r(t) = r_0 = \left(\frac{3V_0}{4\pi}\right)^{1/3} \quad \text{(I.5.)}$$

and:

$$\frac{\rho_u}{\rho_b} \approx \frac{T_b}{T_0} \approx \frac{P_{max}}{P_0} \quad \text{(I.1.)}$$

It is obtained [6]:

$$K_{St} = \left[\frac{dP(t)}{dt}\right]_{max} V_0^{1/3} = 4.84\left(\frac{P_{max}}{P_0} - 1\right) P_{max} S_u \quad \text{(I.2.)}$$

Kst is the maximum rate of pressure rise normalized to volume. Equation I.7 is called the cubic law, and Kst the powder constant (st comes from the German word powder – staub). Bartknecht [8] and Wiemann [9] who studied the effect of initial pressure on the maximum pressure Pmax and on Kst found that Pmax increases linearly with increasing initial pressure in the range from 1 bar to 4 bar. They also found that Kst increases with initial pressure. The cubic law with experimental results of the constant Kst was used to estimate the overpressure created in explosions in a closed space by Bartknecht in 1981. On the other hand, the method does not consider geometrical factors. This equation is

valid for nearly cubic enclosures and will not be valid for other enclosures, because the flame front reaches the walls faster than in spherical geometries and if there is no central initiation. The pressure generated in the closed explosion vessel has little relevance for explosions in open spaces (chambers). Windows, doors, walls yield at pressures that are 1% of the pressure increases obtained in closed blast cells. The maximum explosion pressure is in this case determined by the size and resistance pressures of these exhaust zones. In the case of buildings, the windows act as an outlet for the explosion. In industrial buildings there are pressure release systems to avoid destruction. For this paper the explosion parameters for cornstarch dust – air mixtures and minimum ignition temperature of dust cloud and layer were determined for magnesium and cornstarch dust.

MATERIALS AND METHODS

The experimental equipment used for the explosion parameters such as p_{max}, (dP/dt)max and Kst measurements is explosion chamber CA 20L instrument presented in figure 2.

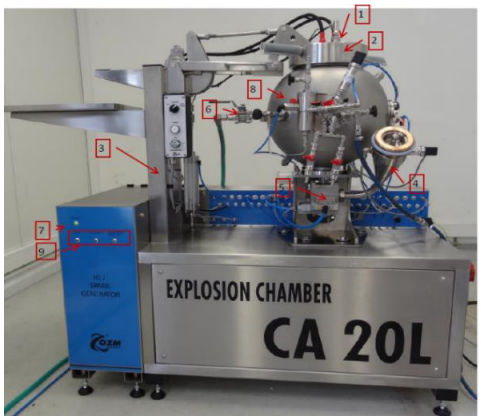


Figure 2 Explosion chamber CA 20L

1-lid with electrodes, 2-lock, 3-stand, 4-equipped dust reservoir, 5-outlet valve, 6-output ball valve, 7-LED power indication, 8-20L chamber, 9-LED power indication for ignition source

Spherical explosion chamber allows the measurement of parameters of flammable gas/vapor mixture with air explosion, hence the determination of the maximum explosion pressure and determination of the maximum explosion pressure rise (dp/dt)max, determination of the explosion limits and the determination of the limiting oxygen concentration LOC. The chamber is a vessel of spherical shape with an inside diameter of 336 mm and a capacity of 20 l. The vessel is provided with an opening of inside diameter equal to 145 mm, which is provided with a flange and a lock for locking the lid closing. Lock is locked manually with safety position sensing "locked." Explosion chamber is made of stainless steel. The material and components comply with the use of equipment for experiments at atmospheric initial pressure and initial laboratory temperature (15-200°C). The system is sealed to the extent that the occurrence of an explosive atmosphere during normal operation outside the delivered system is not supposed. [10]. To determine the ignition temperature of the dust, two experimental stands were used, namely the stand for determining the ignition temperature of the dust layer (Figure 3) and the stand for determining the ignition temperature of the combustible dust cloud (Figure 4).



Figure 3 Experimental stand for the determination of minimum ignition temperature of dust layer



Figure 4 Experimental stand for the determination of minimum ignition temperature of dust cloud

RESULTS AND DISCUSSION

In the figure 5 there are shown the results obtained from the determination of maximum explosion pressure at the cornstarch – air mixtures versus time. The measurements were carried out in a 20 L explosion chamber. The source of initiation for every test was two chemical igniters of 5 kJ (10 kJ in total) according to the specifications in the standard 14034 [4].

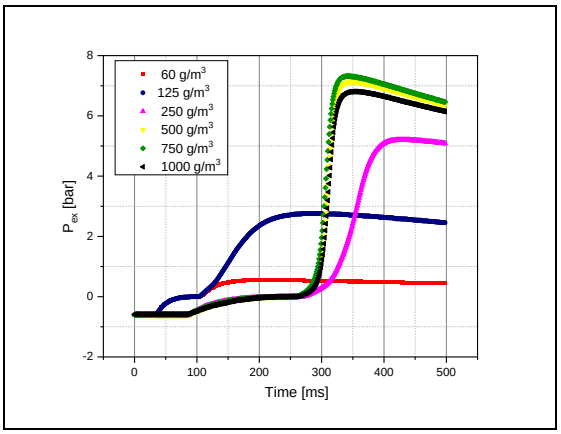


Figure 5 Explosion pressure versus time at different cornstarch concentrations

Table 1 shows the measured explosion parameters for cornstarch – air mixtures:

Table 1 Results

Concentration (g/m^3)	Pmax (bar)	(dP/dt)max (bar/s)	Kst (bar*m/s)
125	2.6	32	32
250	5.2	224	224
500	7.0	390	390
750	7.3	436	436
1000	7.1	466	466

https://doi.org/10.5593/sgem2024/1.1/s06.73

In the figure 6 and 7 there are shown the (dP/dt)max and Kst function of dust concentration.

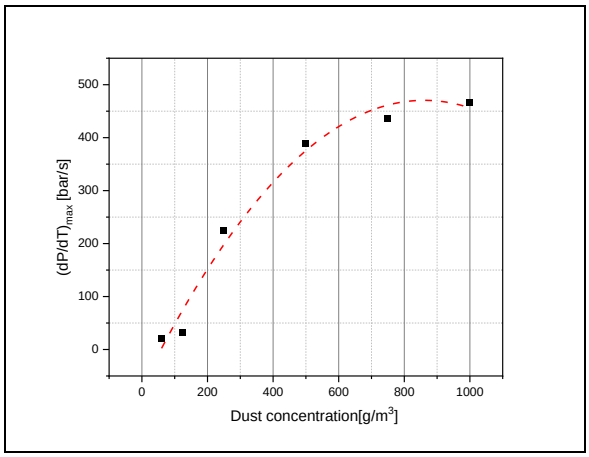


Figure 6 (dP/dt)max function of dust concentration.

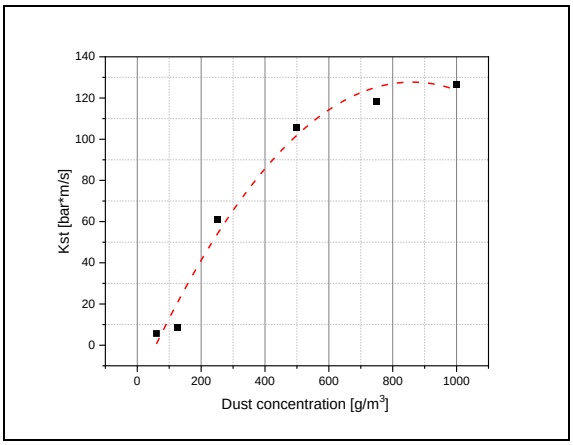


Figure 7 Kst function of dust concentration

In the figures 8 and 9 are presented frames from the determinations of minimum ignition temperature of dust cloud for magnesium and cornstarch. For the magnesium it was determined a minimum ignition temperature of 500 °C and for the cornstarch a minimum ignition temperature of 420 °C.

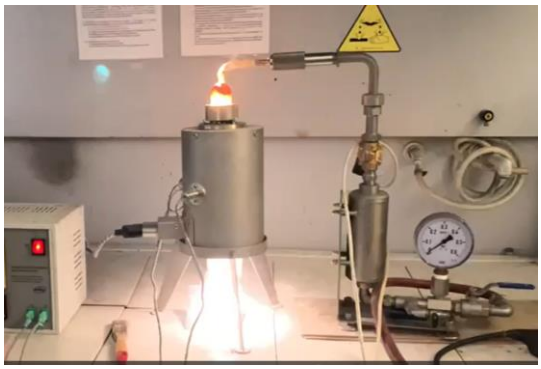


Figure 8 Magnesium cloud minimum ignition temperature determination



Figure 9 Cornstarch cloud minimum ignition temperature determination

In the figures 10, 11 there is presented images from the determination of the minimum ignition of dust layer for both magnesium and cornstarch dust. For both of them, because of the standard limits the determination at 400°C, the minimum ignition temperature was found to be higher than 400 °C.



Figure 10 Magnesium dust minimum ignition of dust layer temperature



Figure 11 Cornstarch dust minimum ignition of dust layer temperature

The results obtained for the maximum explosion parameters of cornstarch are well fitted in the literature data, for example maximum explosion pressure found by Helegda et al. in 2024, 7.8 bar [11], are very close to the one found in the present paper of 7.3 bar. The same values close to the ones reported in the literature was also found for the maximum rate pf pressure rise and for the severity factor. The comparisons with the literature data are very important due to the fact that one needs to continuously verify their methods in order to be able to study various dusts that does not have explosion properties well established.

CONCLUSION

In the industrial sector, explosions involving flammable gases or vapours, or combustible dust are common and catastrophic events. The most dangerous secondary explosions happen when the first explosion's pressure wave penetrates the plant's preexisting dust layers, producing a dust cloud that is greater than that of the initial explosion. Because there is a lot of powder and more explosive pressure, the powder feeds the flame as the pressure wave moves through the plant, causing more damage.

Reducing the likelihood that the initial explosion will set off additional explosions is more crucial than removing the risk of the first one altogether; this is known as the "domino effect" because secondary explosions are always more violent than the original. The literature and internet databases contain the explosion parameter values; however, these values should only be used as guidelines and not as the foundation for designing industry safety protocols, which ought to be based in part on unique data for each powder. It is crucial to understand that these characteristics are not inherent to the materials. They are highly reliant on the experimental parameters (vessel volume, degree of powder cloud turbulence, applied initiation source and its energy) as well as the material qualities (moisture, particle size, shape, and porosity).

https://doi.org/10.5593/sgem2024/1.1/s06.73

The results produced for the cornstarch maximum explosion parameters fit the existing data quite well; for instance, the maximum explosion pressure reported in this paper was 7.3 bar. For the severity factor and the maximal rate of pressure rise, similar values to those documented in the literature were also discovered. Because one must constantly validate their methodology in order to research different dusts that do not have well-established explosion properties, comparisons with published data are crucial.

ACKNOWLEDGEMENTS

This work was carried out through "Core program" of the National Research, Development and Innovation Plan 2022-2027, supported by MCID, project no. PN 23 32 02 01 Developing the level of knowledge of the explosiveness parameters of hydrogen-based gaseous and hybrid mixtures, involved in the obtaining and storage processes in order to reduce the risk of explosion and IOSIN- PCDIEX.

REFERENCES

[1] Taveau J., Secondary dust explosions: How to prevent the or mitigate their effects?, Process Safety Progress, vol. 2011, pp. 36-50, 2011

[2] Abbasi T., Abbasi S., Dust explosions–Cases, causes, consequences, and control, Journal of Hazardous Materials, vol. 140, pp. 7-44, 2007

[3] Mannan S., Lees' loss prevention in the process industries, 3rd ed., Amsterdam: Elsevier, 2012

[4] SR EN 14034-1:3, Determinarea caracteristicilor de explozie a norilor de praf. Determinarea presiunii de explozie. Determinarea valorii maxime de creștere a presiunii de explozi și determinarea limitei inferioare a norilor de praf," EN Standard, 2011

[5] Călămar A.N., Alexandru, S., Toth, L., Simion S., Nicolescu, C., Improving the method of calculating the ecological footprint generated by road traffic – Case study, Environmental Engineering and Management Journal, 18, No. 4, 781-789, 2019

[6] Amyotte P., Eckhoff R., Dust explosion causation, prevention and mitigation: An overview, Journal of Chemical Health and Safety, vol. 17, nr. 1, pp. 15-28, 2010

[7] Hertzberg M., Cashdollar K.L., Introduction to dust explosions, in Proceedings of the Industrial Dust Explosions STP 958, American Society for Testing and Materials, West Conshohocken, PA, pp. 5–32, 1987

[8] Bartknecht W., Dust Explosions: Course, Prevention, Protection, Berlin: Springer, 1989

[9] Wiemann W., Influence of temperature and pressure on the explosion characteristics of dust-air and dust air inert gas mixtures, West Conshohocken, 1987

[10] CA 20 L manual, OZM

HYDROGEOCHEMICAL CHARACTERIZATION OF CARBONATE OIL DEPOSITS: INSIGHTS INTO IONIC COMPOSITION, FRACTURING AND CONNECTIVITY

Maria Shipaeva[1]
Kamilya Talipova[1]
Nil Fakhriev[1]
Vladislav Sudakov
[1] Kazan Federal University, **Russia**

ABSTRACT

In this work, the ionic composition of formation water of three oil deposits (C_2vr, C_2b, C_1pr) was studied. The study of these deposits holds both practical and scientific interest. Due to their complex geological structure, they are difficult to develop. Productive deposits are characterized by the presence of widespread unconsolidated zones with high vertical and horizontal fracturing, high layered heterogeneity, the absence of significant regional reservoir-seal rock, and difficulties in cross-well section correlation. The close position of the Oil-Water Contact (OWC) and the high degree of fracturing contribute to the rapid watering of production wells.

Reservoir brines are characterized by an unusual hydrogeological composition: this is a significantly lower mineralization (30 g/l) of C_2b and C_1pr deposits instead of 250 g/l in comparison with brines of the same age in neighboring areas. We found the different ratio of the main ions, a lower position of the upper boundary of the zone of distribution of calcium chloride-type brines, lower content microcomponents.

In the work, the ionic composition of about 200 brine samples of the deposits was studied. Mass concentrations of six macrocomponents: HCO_3^-, SO_4^{2-}, Cl^-, Ca^{2+}, Mg^{2+}, $Na+K^+$—were determined, along with measurements of TDS, acidity, and density of formation waters. Based on the results of the analysis, the features of the hydrogeochemical properties within the carbonate deposits were established. Zones of hydrodynamic connectivity of the deposits with each other have been identified. New fractures were found. The results obtained are recommended to be used for identifying the water source in case of well interventions.

Keywords: watercut, ionic composition, carbonate reservoirs, fracturing, connectivity.

INTRODUCTION

The carbonate deposits of the **C_2vr, C_2b, C_1pr** sediments contain significant oil reserves. They are characterized by a complex geological structure:

- presence of multidirectional faults,
- a high degree of fracturing of reservoirs [2,10],
- the presence of extensive zones of decompaction,
- secondary alteration (dolomitization, sulfatization, calcitization, desalination),
- the absence of cap rock between reservoirs,
- closeness oil-water contact,
- hydrodynamic connectivity [3,13].

https://doi.org/10.5593/sgem2024/1.1/s06.74

All these characteristics complicate reservoirs development. Almost 70% of the oil wells is producing with water cut more than 40% at the beginning. Increasing water cut is always the reason of hydrodynamic connectivity between watered lower layers [9].
To find the source and reason of high water cut geochemical studies were held [11]. Based on the ionic composition of formation waters we determine their source for carbonate reservoirs: C_2vr, C_2b, C_1pr (figure 1). C2vr-C1p deposits within the Volga-Ural oil-bearing region contain calcium chloride waters with a TDS 180-240 g/l and a density 1.11-1.17 g/cm^3 [5].

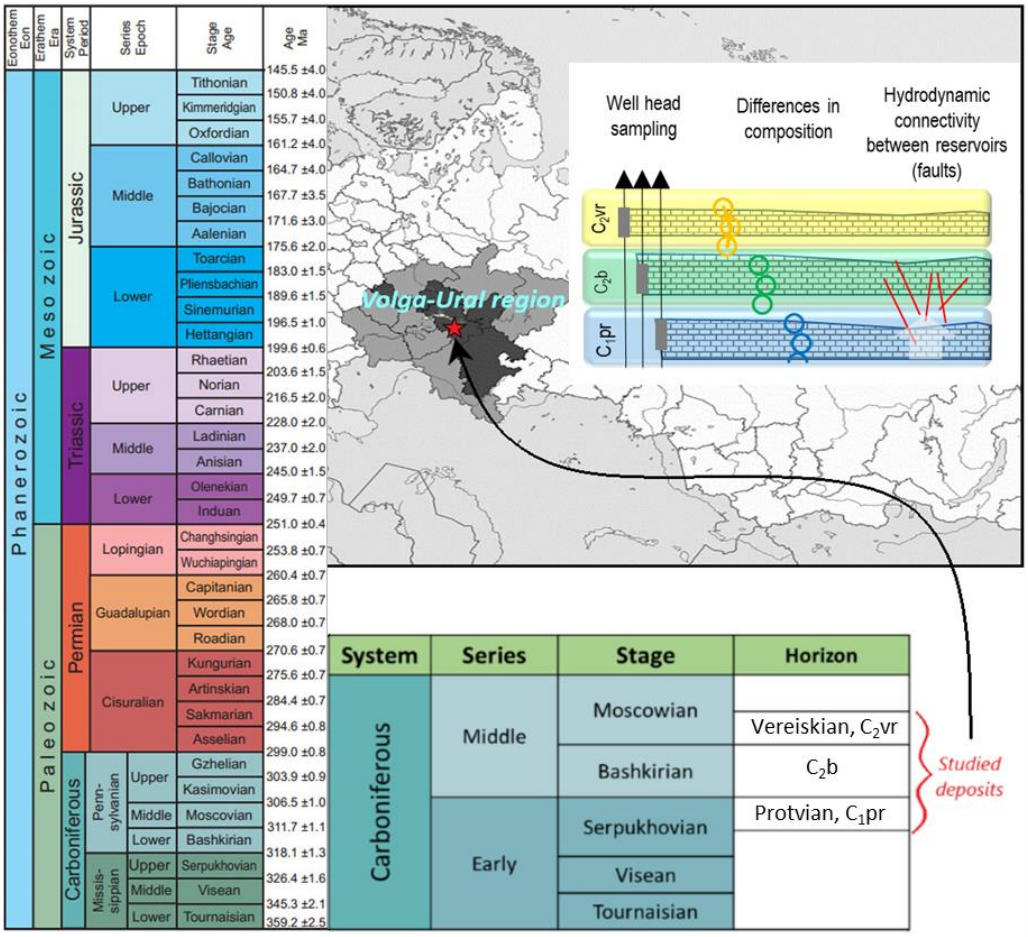


Figure 1 – Studied area

MATERIALS AND METHODS

The ionic composition of 213 samples of formation waters was analyzed. The mass concentrations of six main ions were determined: carbonates, sulfates, chlorides, calcium, magnesium, sodium + potassium. The salinity, density, acidity and hardness of formation waters were measured.

The obtained primary data was processed in several stages:

1. First, graphs of density, mineralization and ion content in the waters of the studied sediments were constructed. The main characteristics of the ion composition for each horizon were described using these graphs.

2. Based on the ratios of the main ions, the types of water were determined according to the classification of V.A. Sulin [12]. The type of water is determined by the following coefficients: rNa/rCl, r(Cl-(Na+K))/rMg, r((Na+K)-Cl)/rSO4 (Table 1).

Table 1 – Classification of formation waters according to V.A. Sulin [12]

Type of water	r Na^+/ r Cl^-	(r Na^+- r Cl^-)/ r SO^{2-}_4	(r Cl^- - r Na^+)/ r Mg^{2+}
Sodium bicarbonate (Na-HCO_3)	>1	>1	-
Sodium sulfate (Na_2-SO_4)	>1	<1	-
Magnesium chloride (Mg-Cl_2)	<1	-	<1
Calcium chloride (Ca-Cl_2)	<1	-	>1

3. Geochemical maps of ion content in waters were constructed for **C_2b** and **C_1pr** reservoirs. Maps were not built for the **C_2vr** reservoir due to the low content of studied wells (5 wells). Zones of hydrodynamic connectivity have been established.

RESULTS

1. The collected samples have density ranges from 1,01 to 1,07 with an average 1.04 g/cm^3. The ionic composition of formation waters is presented in the Table 2, Figure 2. Formation waters of the studied sediments are characterized by the following features:

- C_2vr – calcium chloride (Ca-Cl_2) waters with the highest mineralization (53-105 g/l) and density (1.041-1.072 g/cm^3), as well as the content of chlorine ions (29-62.5 g/l), calcium (1.5 -5 g/l), sodium + potassium (17-33 g/l).
- C_2b – predominantly sodium sulfate waters (Na_2-SO_4), but also magnesium chloride ($MgCl_2$), calcium chloride (Ca-Cl_2), and transitional types. The waters are characterized by the largest range of ion content values (Table 2), due to their intermediate position in the section and interaction with both the C_2vr and C_1pr sediments.
- C_1pr – sulfate-sodium (Na_2-SO_4) waters with the lowest mineralization (19.5-71.5 g/l) and density (1.01-1.05 g/cm^3), but the highest content of sulfates (3.5-6 g/l) and bicarbonates (0.41-1.57 g/l).

The composition of formation waters changes with depth. Widely viewed as in hydrogeological sections of oil fields, the TDS of formation waters increases with depth, and the type of water changes from hydrocarbonate and sulfate to the chloride type. With geological time, during interaction with rocks, groundwater undergoes metamorphosis, changes its composition and becomes highly mineralized brines [1, 4]. In the studied area water mineralization does not increase with depth, but decreases. It is called an inversion of the groundwater (Figure 2). This feature was discovered and examined by researchers earlier. In articles [3,7], the lower position of the upper limit of distribution of calcium chloride brines is explained by deep infiltration of surface water due to a system of multidirectional cracks and strong decompaction of carbonate rocks.

https://doi.org/10.5593/sgem2024/1.1/s06.74

Table 2 – Chemical compositions of the collected groundwater samples

Reservoir	**C2vr**			**C2bsh**			**C1pr**		
Number of samples	**5**			**101**			**107**		
Values	**max**	**min**	**mean**	**max**	**min**	**mean**	**max**	**min**	**mean**
Density, g/cm^3	1,073	1,041	1,057	1,069	1,010	1,030	1,050	1,010	1,020
TDS, g/l	104,8	53,3	79,2	100,2	12,8	35,8	71,5	19,5	30,3
HCO_3^-, g/l	1,1	0,1	0,7	1,4	0,2	0,9	1,6	0,4	1,0
SO_4^-, g/l	5,1	2,3	3,1	7,4	1,3	5,0	6,4	3,4	5,9
Cl^-, g/l	62,5	29,4	45,7	59,5	3,3	16,7	38,2	6,4	12,6
Ca^{2+}, g/l	5,1	1,6	3,6	4,5	0,6	1,1	2,4	0,5	0,8
Mg^{2+}, g/l	1,8	0,7	1,3	2,8	0,2	0,5	1,0	0,3	0,4
Na+K, g/l	33,4	16,8	24,9	32,1	3,1	11,4	23,2	5,7	9,8
Type	Calcium chloride: 5			Sulfate-sodium: 71			Sulfate-sodium: 105		
				Magnesium chloride: 19			Magnesium chloride: 2		
				Calcium chloride: 11					

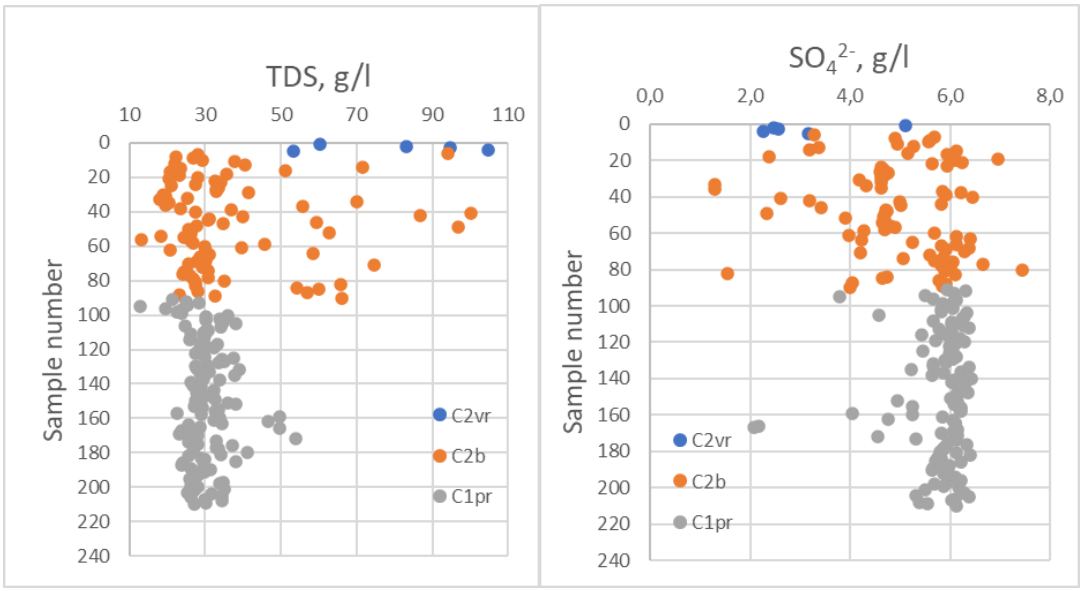


Figure 2 – Graphs of TDS and sulfate ion content

The studied structure is located in a zone of increased tectonic activity and borders a regional fault. Geodynamic activity of the fault is greatest in the strike area of the structure under study [8, 10]. This may be the reason for anomalies water composition.

2. A graph of water genetic types (Figure 3) shows:

- brines of the C_2vr deposit are located in the area of chloride-calcium waters (blue dots),
- brines of the C_1pr deposits are located in the area of sulfate-sodium waters (green color),
- and water samples from the C_2b reservoir are distributed over two areas - the zone of sulfate-sodium waters, similar to the C_1pr, and the zone of chloride waters, similar to C_2vr.

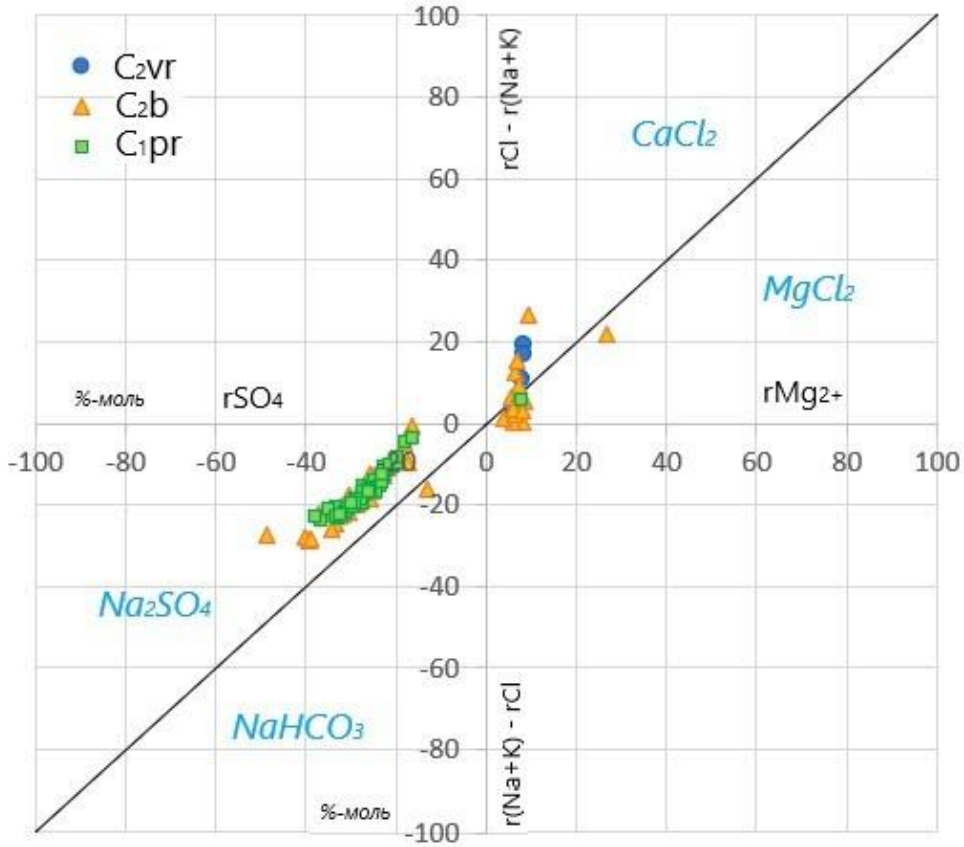


Figure 3 – Genetic types of groundwater by applying Sulin's diagram

3. Spatial distribution of different ions for the C_2b and C_1pr deposits were constructed in the ArcGIS ArcMap program using IDW tool (Inverse Distance Weighted). The IDW (Inverse Distance Weighted) tool uses a method of interpolation that estimates cell values by averaging the values of sample data points in the neighborhood of each processing cell. The closer a point is to the center of the cell being estimated, the more influence, or weight, it has in the averaging process.

On the maps, red color areas show content maximum, green areas indicate minimum content (Fig.4,5):

- C_1pr horizon, the lowest one, on the entire area is characterized by stable composition (Fig.4,5): high sulfate content (5-7 g/l) and low magnesium content (0.2-0.5 g/l).
- On the maps of the C_2b we see multi-colored areas with different ion contents, because waters are characterized by a wide range of components.
- Most important areas on the maps are eastern part of the deposits: on the maps of the C_2b, an area of high sulfate content (6-7 g/l) and at the same time a minimum content of magnesium ion (0.2-0.45 g/l) in the east is clearly visible. Such contents characterize the waters of the C_1pr horizon throughout the entire study area. We interpreted this area in the east as a zone of hydrodynamic connectivity of C_1pr and C_2b.

https://doi.org/10.5593/sgem2024/1.1/s06.74

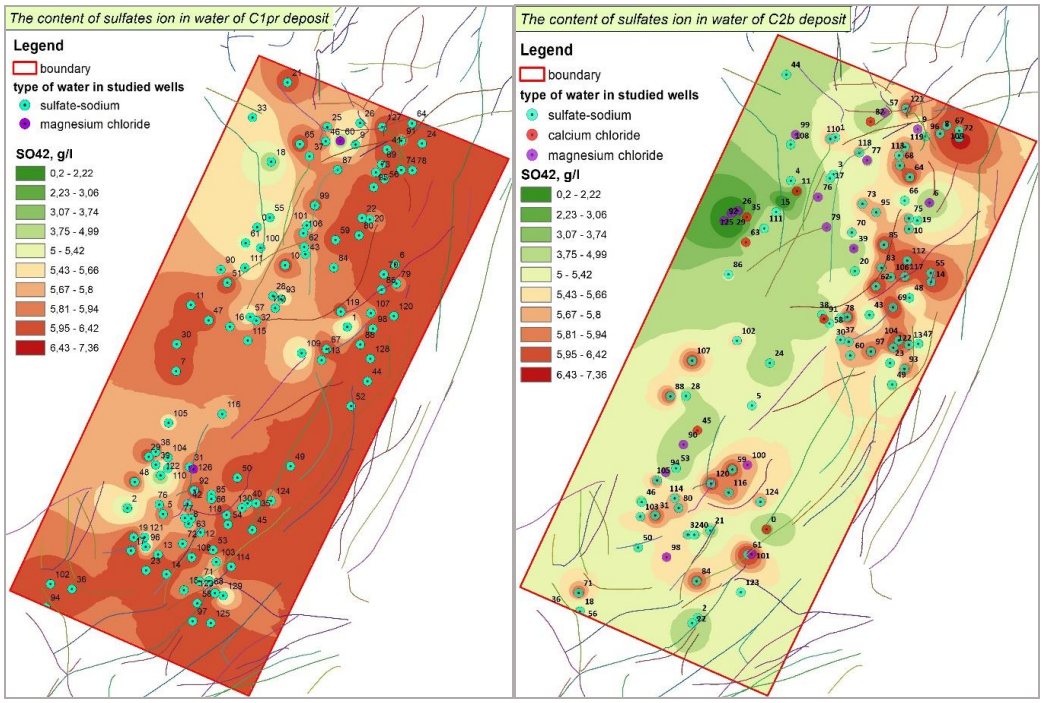


Figure 4 – Spatial distribution of sulfate ion in the waters of the C_1pr and C_2b

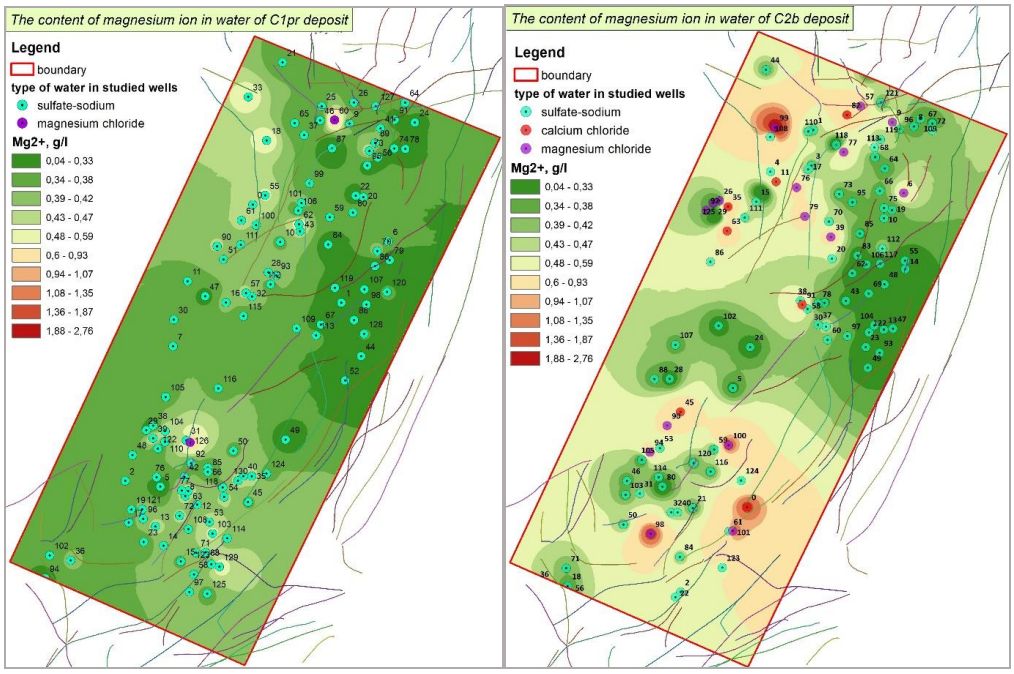


Figure 5 - Spatial distribution of magnesium ion in the waters of the C_1pr and C_2b

DISCUSSION

Differences in the composition of formation waters are associated with different lithological composition of reservoir rocks: C_2b - consists of carbonate rocks, C_1pr - consists of sulfate-carbonate rocks, with the presence of gypsum and dolomite.

Waters of the sulfate-sodium type are formed in the presence of gypsum or anhydrite of both primary and secondary origin in the section. Dissolution of gypsum by

groundwater, i.e. the transition of $CaSO_4$ into solution causes exchange adsorption reactions, since calcium has high absorption energy and displaces magnesium and sodium adsorbed by the rocks. The reactions proceed according to the following scheme:

$$CaSO_4\,(fluid) + Mg\,(rock) \rightarrow Ca\,(rock) + MgSO_4\,(fluid)$$
$$CaSO_4\,(fluid) + 2Na\,(rock) \rightarrow Ca\,(rock) + Na_2SO_4\,(fluid)$$

In basins where there is no gypsum, waters of the sulfate-sodium subtype are not widespread. They form only where suitable conditions exist for the formation of secondary gypsum and the preservation of sulfates in solution.

Differences in Mg^{2+} contents may be explained by dolomitization processes. The C_1pr horizon is composed of limestones and dolomites, while the C_2b is homogeneous in its lithological composition and is composed mainly of limestones [6]. Magnesium in the waters of the C_2b was preserved in the liquid phase and shows high concentrations in the waters. In the section of the C_1pr, magnesium passed from the liquid phase to the solid phase due to the metasomatic replacement of rock calcium by magnesium solution with the transformation of limestone into dolomite:

$$2CaCO_3+MgSO_4=CaMg(CO_3)_2+CaSO_4$$

Therefore, there is less magnesium in the water of the C_1pr horizon than in the C_2b horizon. Thus, the existence of sulfate waters in the C_2b carbonate reservoir is not possible. Their appearance is possible only due to a developed network of multidirectional cracks. In this case, water is drawn up from the water-saturated C_1pr into the reservoirs of the C_2b.

CONCLUSION

The hydrogeochemical conditions within the carbonate reservoirs were studied. Based on the results, the following conclusions were drawn:

- within the field, an inversion of the hydrogeological section is observed: with depth, mineralization and the density of formation waters does not increase, but decreases; in addition, the content of sulfates increases down the section of carbonate sediments;
- the studied deposits are characterized by different compositions of the formation waters: the C_2vr deposit contains waters of calcium chloride type, their TDS averages 80 g/l; deposit C_2b includes sulfate-sodium, chloride-calcium and chloride-magnesium waters, as well as waters of transition types, the average TDS is 36 g/l; the C_1pr deposit includes exclusively sulfate-sodium waters with an average TDS of 30 g/l;
- in the east of the studied area there is a zone of hydrodynamic connectivity of the deposits: on the maps of C_2b deposit, an area with a water composition different from the general background and similar to the composition of the waters of the C_1pr deposit is noted. All wells in this area produce water from C_1pr, regardless of perforation C2b, C1pr or both.

This territory is characterized by complex geological and non-standard hydrogeological conditions, and therefore requires further more detailed comprehensive study to identify the reasons for the formation of these conditions. This knowledge will allow us to fully take into account the characteristics of the field and increase the efficiency of its development.

https://doi.org/10.5593/sgem2024/1.1/s06.74

ACKNOWLEDGEMENTS

This work was supported by the Ministry of Science and Higher Education of the Russian Federation under agreement No. 075-15-2022-299 within the framework of the development program for a world-class Research Center “Efficient development of the global liquid hydrocarbon reserves”.

REFERENCES

[1] Alexeev, S.V., Alexeeva, L.P., Vakhromeev, A.G. Brines of the Siberian platform (Russia): Geochemistry and processing prospects, Applied Geochemistry, 2020. DOI: 10.1016/j.apgeochem.2020.104588.

[2] Bazarevskaya, V.G., Dulaeva, E.N., Lykov, G.A., Martynov, A.N., Galimov, I.F., Akhmetshina, A.S., Determination of fracturing of Bashkirian and Serpukhovian sediments in Romashkinskoye field deposits 301-303. Methods analysis and integration, 2015. ISSN: 0028-2448.

[3] Guskov, D.V., Galimov, I.F. Features of oil-bearing carbonate reservoirs of Kuakbash swell (belonging to the Romashkino field) related with flooding process of producing wells. *Petroleum Geology - Theoretical and Applied Studies,* 2012, vol.7, no.4, pp. 9-28.

[4] Karcev, A. A., Vagin, S. B., Matusevich, V. M. Hydrogeology of Oil- and Gas-Bearing Basins. Moscow, *Nedra Publ*., 1986, 224 p.

[5] Khisamov R.S., Gatiyatullin N.S., Ibragimov R.L., Pokrovsky V.A. Hydrogeological conditions of oil fields of Tatarstan. *«Fan». Kazan,* 2009.

[6] Kolchugin, A., Morozov, V.P., Korolev, E., Eskin, A., Gazeeva, F.M., Typical sections of Bashkirian carbonate rocks and structure of oil deposits in southeast part of the Republic of Tatarstan. 2013, Neftyanoe khozyaystvo - Oil Industry, pp. 84-86.

[7] Kovalev, V. S. Determination of fracturing of carbonate reservoir A4, Kuleshov field, *Tr. Giprovostokneft’*, 1965, vol. 9, p. 95-52.

[8] Mingazov, M.N., Ibragimov, R.L., Karimov, M.Z., Khvoronova, T.N., Strizhenok, A.A., Anoshina, M.M. Specification of geological structure of Kuakbashskiy bank on the basis of a complex of searches. 2007, Neftyanoe khozyaystvo, pp. 25-29.

[9] Renpu Wan, Advanced Well Completion Engineering (Third Edition) 2011, pp. 1-74. DOI: 10.1016/B978-0-12-385868-9.00001-4

[10] Shajdullin, R. G., Gus'kov, D. V. Model of fracture formation in carbonate massive of 302, 303 oil deposits of Romashkin field, *Georesursy*, 2007, no.4, pp. 4-17.

[11] Shipaeva, M. S., Nurgaliev, D. K., Sudakov, V. A., Shakirov, A. A., Ganiev, B. G., and A. A. Lutfullin, Flow Profile Evaluation in Producer Wells by Geochemical Studies of Oil and Water and Analysis of Anomalies Associated with Deep Fault Zones, 2023. DOI: 10.2118/216170-MS

[12] Sulin, V. A. Waters of petroleum formations in the system of natural water. 1946. Gostoptekhiz-dat, Moscow (in Russian), *3596*.

[13] Zinina, I.A., Andronov, S.N., Kurochkin, B.M. Opening of a productive formation with zones of high-intensity circulation loss in wells of 301-303 deposits of Romashkinsky field. *Construction of oil and gas wells on land and sea,* 2013, no.4, pp. 29-32.

IDENTIFICATION OF INPUT-OUTPUT PARAMETERS OF THE COMMAND AND CONTROL SYSTEM FOR TESTING FLAMEPROOF PROTECTED ELECTRIC MOTORS USED IN HYDROGEN ATMOSPHERE

PhD.eng. Marcel Daniel Rad
PhD.eng. Mihai Magyari
PhD.eng. Dragos Fotau
Eng. Attila Sorin Zsido
Eng. Constantin Valentin Sirbu
National Institute for Research and Development in Mine Safety and Protection to Explosion – INSEMEX PETROSANI, **Romania**

ABSTRACT

The certification requirements for electrical equipment used in potentially explosive environments are outlined in EU Directive 2014/34.

In order to certify electrical equipment used in potentially explosive environments, the EU has set requirements. Certification and compliance requirements are outlined in EU Directive 2014/34. All electrical equipment used in potentially explosive environments must abide by this guideline. Electrical equipment makers and their authorized representatives are subject to the directive. The regulation lays forth the safety standards that electrical equipment needs to fulfill in order to be approved for use in potentially explosive environments. According to the directive, there are three categories of potentially explosive atmospheres: Zone 0, Zone 1, and Zone 2. The rule also specifies how electrical equipment that has been approved for use in potentially explosive environments must be marked.

Testing to make sure the equipment satisfies safety regulations is a necessary step in the certification process for electrical equipment. Testing is carried out by accredited testing facilities. The appropriate national accrediting agencies have granted testing laboratories their accreditation. The testing labs adhere to the guidelines provided in the electrical equipment testing directive. Equipment for electrical, mechanical, and thermal safety is tested as part of the testing process. The equipment's capacity to stop potentially explosive environments from igniting is also being tested.

Keywords: electrical equipment, explosive atmosphere, certification

INTRODUCTION

In order to obtain certification, the equipment that makes up an explosion-proof system must be evaluated and tested. This is crucial because the current explosion risk must be reduced in order to protect people's health and safety, avoid damage to property, and, last but not least, preserve the environment.

Electric motors protected with flameproof enclosure type of protection are essential in dangerous environments, such as the atmosphere in which the environment with a risk of explosion is hydrogen, where the risk of explosion is high. To ensure the safe and efficient operation of these electric motors, it is important to identify and understand the

https://doi.org/10.5593/sgem2024/1.1/s06.75

input-output parameters of the command and control system. This paper focuses on investigating these parameters and their importance in testing and operating electric motors in explosive hydrogen environments.

Protected electric motors are designed to prevent the ignition of flammable atmospheres by using specific protection mechanisms. In the case of engines used in the hydrogen atmosphere, flameproof enclosure protection is crucial to avoid explosions.

The command and control system is responsible for managing and monitoring the operation of the protected electric motors. Correct identification of the parameters of this system is essential to ensure safe and efficient operation of engines in hazardous environments. Input parameters such as supply voltage and current, ambient temperature and pressure, and output parameters such as motor speed and torque must be precisely monitored and controlled to prevent any dangerous situation.

ACTUAL METHODES TO TEST EQUIPMENTS WITH FLAMEPROOF ENCLOSURE TYPE OF PROTECTION, USED IN EXPLOSIVE AREAS

Type tests are required in order to certify electrical equipment with flameproof enclosure type of protection "d." The tests conducted in hydrogen atmospheres are also included in the type test category. This kind of equipment needs to be put through the following kinds of tests in hydrogen atmospheres:

a) determination of explosion pressure (reference pressure);

b) overpressure test;

c) non-transmission of an internal ignition test. [2]

The group-specific test gases or subgroup-specific test gases associated with the equipment must be used for each of these tests.

The tests comprises the following steps:

- Start the air compressor and air dryer.

- After half-our necessary for the air in the gas circuit to dry, the calibration of oxygen analyzer is made;

- Power-on the test rig and computers

Function of product group and subgroup, the ventils for the required gases are opened:

- group I: methane ;

- group IIA: propane;

- group IIB: ethylene;

- group IIC: acetylene and hydrogen. [1]

The two computers that controls the testing process have two softwares installed on them, called “Ventil” and “Druckmess”, one on each computer. The first one commands the test rig (operating system IBM OS/2), and the second one gathers the information obtained during tests and issues the test report (operating system Windows NT). After these programs are launched in execution, the job that has to be done is picked-up in “Druckmess”. [3]

The remaining test types that must be performed are as follows: internal ignition test non-transmission, overpressure test, and explosion pressure determination.

Measuring points and the working range are chosen from program menu.

With the help of „Ventil" program, the air is circulated inside of equipment and testing chamber until the humidity is reduced under a certain value required by the standards. [2]

Also in the „Ventil" program is established the concentration of hydrogen atmospheres through Bronkhorst flow controllers. The necessary concentration required by standards to be obtained is surveilled and validated in the „Druckmess" program. When the concentration of testing mixture is the required one the data regarding necessary parameters are saved. [3]

The pressure (atmospheric pressure or overpressure) inside the equipment and testing chamber is established function of the test required to be done;

- set the range of charge amplifiers;
- all the control valves are closed from the "Ventil" program;
- the hydrogen atmospheres inside of equipment under test is ignited from the control desk, the obtained data is recorded first in oscilloscopes memory (HP54645A) and saved further in the computer memory; and the test program goes on with the next test, until the end; [3]

After each test and at the end of tests, the inside of equipment and (if necessary) the testing chamber is circulated with fresh air. [4]

After completing all tests the testing report is edited. Further, a photo of the equipment is placed in the test report together with other necessary images.

FLOWCHART FOR TEST ANALYSIS AND CONTROL

The flowchart diagram provided in Figure 1(a,b,c) depicts the sequential procedures required to conduct testing in hydrogen atmospheres.

This flowchart represents a new possibility to run the tests in hydrogen atmospheres, and in the same time has the support offered by standards in respecting the necessary requirements provided by them.

https://doi.org/10.5593/sgem2024/1.1/s06.75

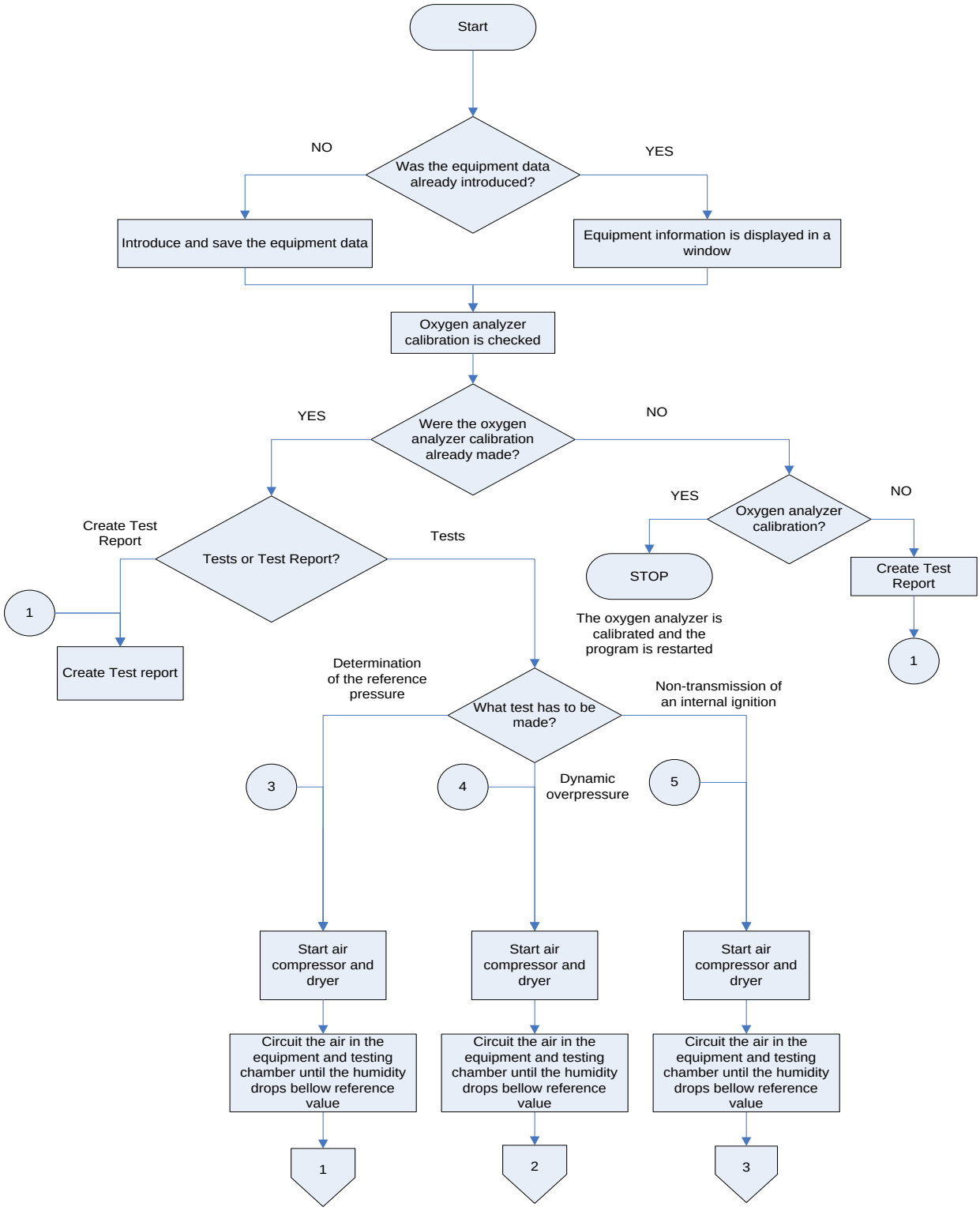


Figure 1a. A flowchart illustrating the process of analyzing and controlling tests conducted in hydrogen atmospheres for flameproof enclosure type protective systems.
(continues in next page)

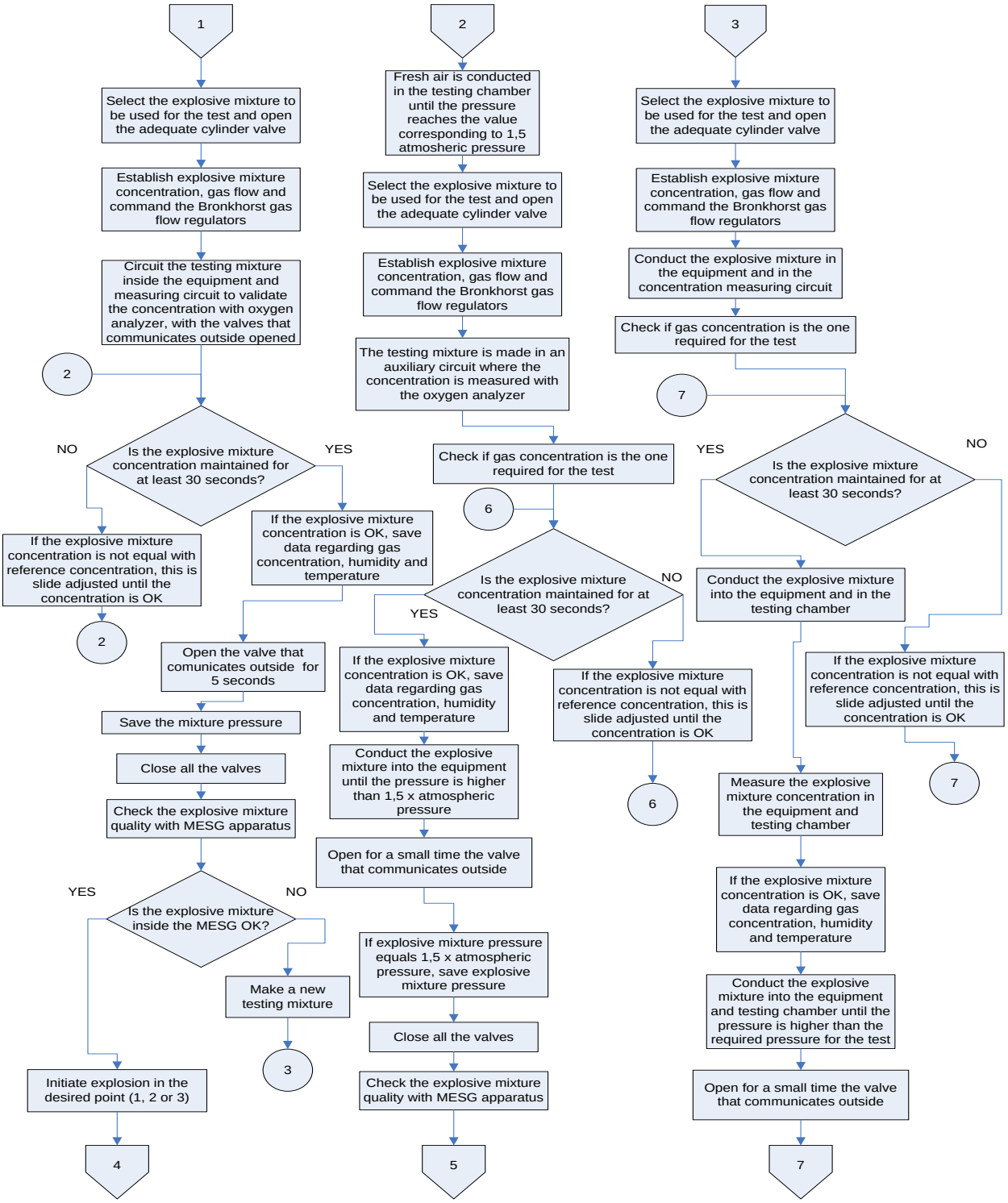


Figure 1b. A flowchart illustrating the process of analyzing and controlling tests conducted in hydrogen atmospheres for flameproof enclosure type protective systems. (continues in next page)

https://doi.org/10.5593/sgem2024/1.1/s06.75

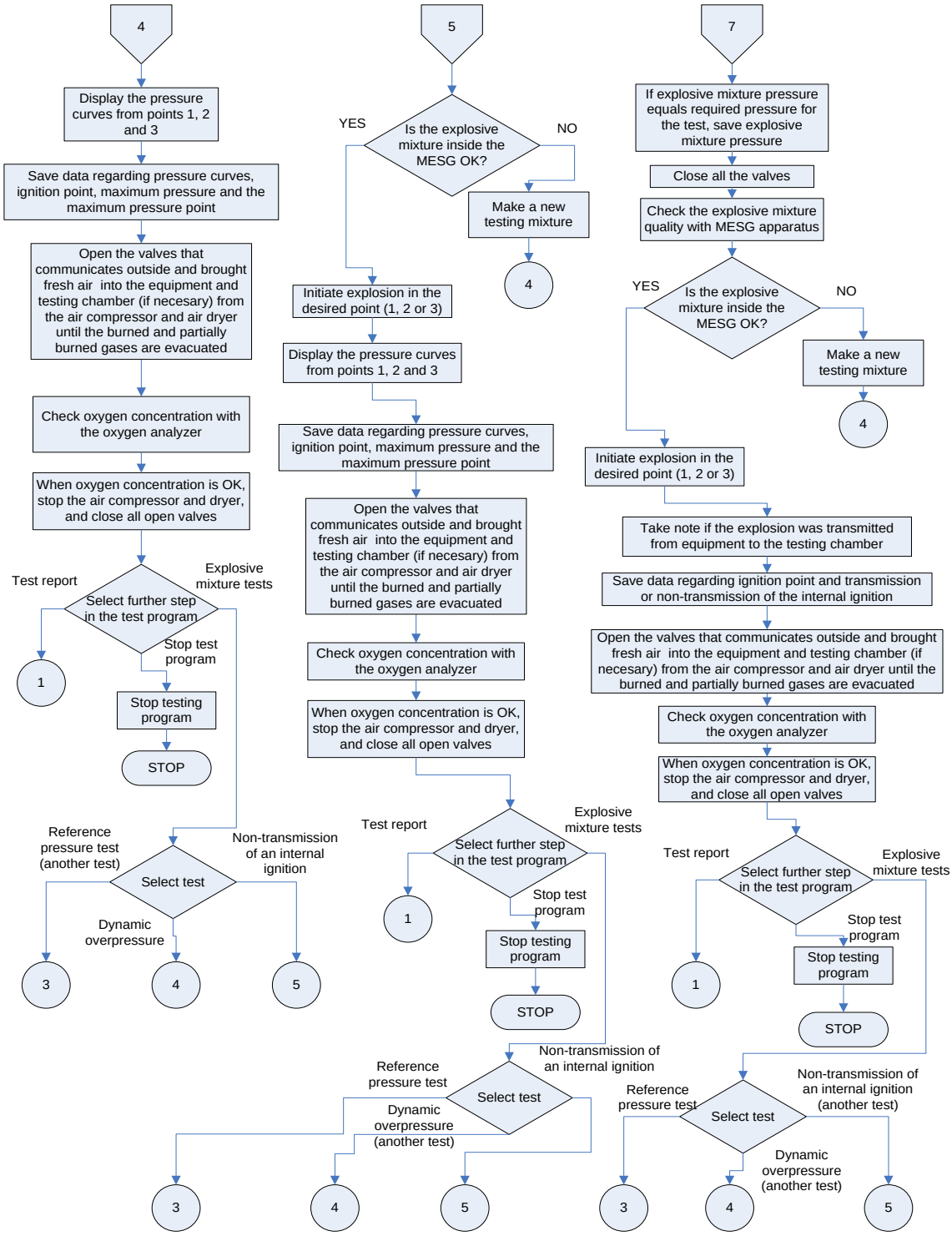


Figure 1c. A flowchart illustrating the process of analyzing and controlling tests conducted in hydrogen atmospheres for flameproof enclosure type protective systems.

IDENTIFICATION OF INPUT-OUTPUT VARIABLES

The Specific Inputs and Outputs are graphically presented further into an I/O block diagram of the command and control system according the test procedure for flameproof protected equipments designed for use in hydrogen atmospheres

Figure 2. I/O block diagram of the command and control system according the test procedure for flameproof protected equipments designed for use in hydrogen atmospheres

From the flowchart of analyzed process result specific inputs and outputs which are presented in Table 1.

Table 1. Specific Inputs and Outputs for the command and control system according the test procedure for flameproof protected equipments designed for use in hydrogen atmosphere

No.	Logical variables Input [X_i] Output [Y_i]	Analogue variables	Reference	Label
1.	i	-	-	Start test rig apparatus
2.	o	-	-	Stop test rig apparatus
3.	X_1, Y_1	-	-	Oxygen analyzer calibrations
4.	X_2, Y_2	-	-	Test selection
5.	X_3, Y_3	Δt	-	Ventilation time
6.	X_4	-	-	Equipment data
7.	Y4			Save equipment data
8.	X_5	-	-	Select the explosive gas for tests
9.	Y_5	-	-	Drive electro-valves for the test required gases
10.	X_6, Y_6	-	-	Test Report
11.	X_7	rH	rH_{ref}	Humidity
12.	Y_7	-	-	Drive air compressor and air dryer
13.	X_8, Y_8	% O_2	O_2 conc	O_2 concentration
14.	X_9, Y_9	% gas(H)	Gas(H) conc	Explosive gas (hydrogen) concentration
15.	X_{10}, Y_{10}	T	-	Temperature
16.	X_{11}, Y_{11}	P_a	P_{atm}	Atmospheric pressure
17.	X_{12}, Y_{12}	P	P_{ref}	Test mixture pressure
18.	X_{13}, Y_{13}	-	-	Bronkhorst flow controller drive
19.	X_{14}, Y_{14}	l/min	Air ref	Air flow
20.	X_{15}, Y_{15}	l/min	Gas ref	Explosive gas flow
21.	X_{16}, Y_{16}	sec	T_{O2ct}	Time of constant oxygen concentration
22.	X_{17}, Y_{17}	-	-	Drive electro-valves to introduce hydrogen atmospheres into equipment and measuring circuit
23.	X_{18}, Y_{18}	-	-	Save hydrogen atmospheres parameters (O_2 and hydrogen atmospheres concentration, temperature, humidity)
24.	X_{19}, Y_{19}	-	-	Drive electro-valve that communicates outside
25.	X_{20}, Y_{20}			Save explosive's mixture pressure
26.	X_{21}, Y_{21}			Ignition of test mixture (point 1, 2 or 3)
27.	X_{22}, Y_{22}	P_{expl}	-	Explosion pressure
28.	X_{23}, Y_{23}	-	-	Save explosion parameters (ignition point, maximum pressure, maximum pressure point)
29.	X_{24}, Y_{24}	-	-	Drive electro-valves to conduct air in the testing chamber
30.	X_{25}, Y_{25}	-	-	Drive electro-valves to introduce explosive gas in the testing chamber
31.	X_{26}, Y_{26}	-	-	Drive electro-valves for the testing chamber to communicate outside

https://doi.org/10.5593/sgem2024/1.1/s06.75

No.	Logical variables Input [X_i] Output [Y_i]	Analogue variables	Reference	Label
32.	X_{27}, Y_{27}			Drive electro-valves to conduct hydrogen atmospheres in an auxiliary circuit and into the measuring circuit
33.	X_{28}, Y_{28}			Drive electro-valve to measure the hydrogen atmospheres pressure from the equipment
34.	X_{29}, Y_{29}			Drive electro-valve to measure testing chamber pressure
35.	X_{30}, Y_{30}	-	-	Drive electro-valves to measure oxygen concentration for the mixture in the testing chamber and equipment
36.	X_{31}, Y_{31}			Close all open electro-valves
37.	X_{32}, Y_{32}			Adjust MESG apparatus gap
38.	X_{33}			Ignite hydrogen atmospheres inside MESG apparatus
39.	Y_{33}			MESG ignition result
40.	X_{34}, Y_{34}	-	-	Transmission or non-transmission of an internal ignition

CONCLUSIONS

The purpose of this paper is to identify the input-output variables of the command and control system for testing flameproof protected equipments designed for use in hydrogen atmospheres.

By identifying the input-output variables the possibilities to design a new testing system may arise. This desiderate may be done by using also new equipments connected in new configurations.

The correct identification and understanding of the input-output parameters of the command and control system for testing electric motors protected by the type of explosion-proof capsular protection are essential to ensure the safe and efficient operation of these motors in hazardous environments, namely the explosive atmosphere of hydrogen.

Constant monitoring of relevant parameters and implementation of appropriate corrective measures can significantly contribute to the prevention of accidents and equipment damage. It is important that the engineers and technicians responsible for testing and maintaining these engines are well trained and have adequate equipment to properly handle emergency situations and ensure safe and reliable operation of the equipment.

REFERENCES

[1] SR EN 60079-0:2020 – Electrical apparatus for explosive gas atmospheres. Part 0: General requirements

[2] SR EN 60079-1:2015 - Electrical apparatus for explosive gas atmospheres. Part 1: Flameproof enclosure “d”

[3] INSEMEX-LIEx, PI-Ex-01.1 Test procedure to verify flameproof equipments – Tests in explosive mixtures, Edition 6, 2008

[4] M. Schönhoff, M. Oppermann – Ventilsteuerung für OS/2, Benutzerhandbuch, PTB Braunschweig, 1999

IMPEDANCE SPECTROSCOPY ANALYSIS OF INTRINSIC SAFETY CIRCUITS

Sc. Res. I Ph.D Eng. Marius DARIE[1]

Sc. Res. I Ph.D Eng. Sorin BURIAN[1]

Sc. Res. I Ph.D Eng. Tiberiu CSASZAR[1]

Sc. Res. I Ph.D Eng. Cosmin COLDA[1]

Assoc. Profesor. Ph.D Chem. Clementina MOLDOVAN[2]

[1] National Institute for Research and Development in Mine Safety and Protection to Explosion - INSEMEX, 32-34 G-ral Vasile Milea Street, Petrosani, **ROMANIA**

[2]University of Petroșani, 20 Universității Street, Petrosani, **ROMANIA**

ABSTRACT

The paper presents issues regarding impedance spectroscopy analysis for the identification of intrinsically safe circuits.

The first part of the paperwork presents the explosion risk. In industrial applications, the presence of flammable substances leads to additional requirements for technical equipment used in such spaces.

On the other hand, technical equipment used in such spaces must remain in working order even when the risk of explosion is high. For this purpose, equipment used in such spaces should be assessed, tested, and certified so that it functions safely related to explosion hazard aspects.

The second part presents the theoretical model employed for the identification of intrinsically safe circuits.

In the third part are presented the results and discussion of the intrinsically safe circuit identification based on the impedance spectroscopy analysis and use.

An important conclusion of the approach is that the identification of intrinsically safe circuits using impedance spectroscopy can be a useful tool.

Keywords: uncertainty, small component ignition tests, intrinsic safety, explosion risk.

INTRODUCTION

Current trends make the emergence of new technologies and integrated systems an easy process, making the time from concept to implementation relatively short.

On the other hand, by adapting these technologies and integrated systems to the specific characteristics of their use in potentially explosive atmospheres, the process mentioned above is significantly slowed down. This is mainly due to the need for experience with standardized requirements for the construction and use of electrical equipment in potentially explosive atmospheres.

Also noteworthy is the increased pace of introduction and implementation of new editions of standards and even new standards in this area. This is explained in particular by the process of homogenization and globalization initiated and maintained by the IEC.

https://doi.org/10.5593/sgem2024/1.1/s06.76

The increasing complexity of the circuits of low-current equipment often makes it difficult to carry out the process of assessing explosion protection by type of intrinsically safe protection.

In addition, the application of intrinsically safe explosion protection requires the circuit to be classified into certain circuit types, resistive, capacitive, inductive, linear, or non-linear sources.

Thus, without resorting to oversimplification, the question arises as to whether the circuits to be evaluated should be classified into one of these types.

Considering the aspects mentioned above, the present paper proposes a method for classifying circuits to be evaluated in one of the types mentioned above.

According to the ATEX Directive 0, electrical equipment intended for operation in potentially explosive atmospheres is divided into two groups: group I - electrical equipment for underground grey mines and group II - electrical equipment for places with potentially explosive atmospheres other than grey mines.

The vast majority of standards used in Europe in the field of equipment and installations for explosive atmospheres are maintained by the International Commission on Electrotechnics. Thus, the standard 0, which sets out general requirements for electrical equipment used in explosive atmospheres 0, 0 is taken from the IEC standardization system. In the general requirements standard, explosive atmospheres are divided into three groups (the third group is reserved for flammable dust clouds, which have been taken over from group II).

Also in the general requirements standard, the distribution of Group II equipment into three sub-groups is shown in IIA, IIB, and IIC, depending on the nature of the potentially explosive atmosphere for which it is intended. Equipment marked for subgroup IIB also corresponds to applications requiring equipment in subgroup IIA. Similarly, equipment marked for sub-group IIC is also suitable for applications requiring equipment in sub-groups IIA or IIB.

Technical equipment in general and electrical equipment, in particular, are tested against a specific explosive atmosphere subgroup 0.

An important aspect to be considered is the danger of ignition of explosive atmospheres from hot surfaces. Thus, it is important to take into account the correlation between the maximum surface temperature and the ignition temperature of the flammable substance that determines the presence of the explosive atmosphere.

The main "beneficiary" of the ignition test from small components is the "intrinsically safe" type of protection 0, which is used by low-current equipment.

An important aspect for characterizing the risk of explosion is the consideration of the frequency of occurrence of explosive atmosphere in the reference space. Taking this factor into account, when classifying hazardous areas, three types of zones are distinguished: zone 0 is the space in which an explosive atmosphere exists permanently or for long periods; zone 1 is the space in which a gaseous explosive atmosphere is likely to occur during normal operation of technological installations which may have flammable gas emissions; and zone 2 is the space in which a gaseous explosive atmosphere is not likely to occur during normal operation of technological installations.

In these locations, explosive atmospheres may occur infrequently and for a short period due to foreseeable malfunctions 0.

In the manufacture of equipment intended for use in potentially explosive atmospheres, compliance with the provisions of the ATEX Directive is achieved through the use of harmonized standards. In general, explosion protection for machinery for use in potentially explosive atmospheres is covered by standards in the EN 60079 series. Depending on the design features, operating conditions, and characteristics of the explosive atmosphere, protection types are chosen according to the EN 60079 series of standards.
A type of protection represents specific measures consisting of particular constructive measures, which are applied to the equipment to prevent the ignition of an explosive atmosphere in the surroundings.
Different sets of requirements have led to different types of protection for equipment. Thus, there are several types of protection suitable for electrical equipment for gases and dust, or non-electrical equipment.

MATERIALS & METHODS

In the case of low-current equipment protected by the intrinsically safe type of protection, both the energy flowing through the circuits and the energy stored in them are limited by the type of protection so that, in the event of a fault, the atmosphere cannot be ignited by electrical effects (sparking).

It is also known that the storage of electrical energy is carried out in inductors and capacitors. Thus, limitations are imposed on inductance and capacitance values.

The results of the preliminary tests carried out have been included in the specific standard 0.

The use of these standards requires prior knowledge of the electrical parameters including inductance and capacitance to deduce from the ignition diagrams the compliance of the circuit with the spark ignition protection requirements.

On the other hand, in the case of complex circuits, it is difficult to assess these parameters without resorting to cover approximations. This approach, however, will not reflect the factual situation.

To solve this difficulty, it is proposed to use the methods proposed by impedance spectroscopy.

Thus, for a given circuit, using impedance spectroscopy, the values of resistance, inductance, and equivalent internal capacitance can be obtained.

From the point of view of intrinsically safe explosion protection, the series R, L, C circuit is particularly relevant. For this case, the circuit shown in the diagram in Figure 1 is considered.

Considering the circuit diagram shown in Figure 1, the equivalent impedance expression of the circuit is shown in Equation 1 and the logarithm diagram of the decimal impedance expressed as a plotted contour versus angular frequency and external resistance is shown in Figure 2.

For the approach of the paper, the values of R, L, and C are taken as unknown. Specific values for the parameters R, L, and C were used to create a candidate system for the application and verification of the identification algorithm.

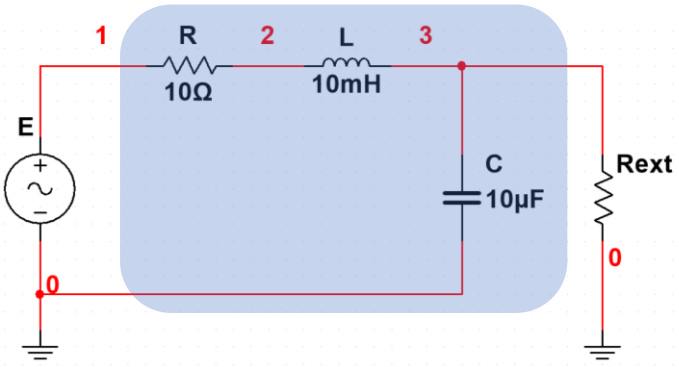


Figure 1 Employed circuit for the analysis

$$log_{10}(|Z(\omega, Rext)|) = log_{10}(|R + j\omega L + (j\omega C + Rext^{-1})^{-1}|) \quad (1)$$

To determine the equivalent R, L, C parameters characterizing a series circuit having the impedance with the values shown in the contour diagram in Figure 2, an objective function defining the distance between a variable area defined by equation (1) and the parameters Rx, Lx and Cx has been implemented.

$$D(Rx, Lx, Cx) = log_{10}(\sum_{Rext=0}^{6} \sum_{\omega=0}^{9} (Z_x - Z_0)^2) \quad (2)$$

where:

$$Z_x = |Z(10^{\omega}, R_x, L_x, C_x, 10^{Rext})| \quad (3)$$

$$Z_0 = |Z(10^{\omega}, 10^{Rext})| \quad (4)$$

Z0 represents the experimental impedance diagram obtained by impedance spectroscopy and Zx represents the theoretical impedance defined by equation (2).

The effective determination of the parameters that define the model closest to the experimental values is based on an optimization approach that involves minimizing the distance defined by equation (2).

The generation of the various configurations is based on a random process according to equation (5), where A and B are uniformly distributed values in intervals whose limits are shown in Table 1. Where [B] is a whole part of B.

RESULTS

By considering the circuit in Figure 1, the experimental diagram obtained by simulation and shown by the contour diagram in Figure 2 was obtained.

Table 1 Ranges of variation for electrical parameters

Parameter	Min	Max
R	1	$9 \cdot 10^{3}$
L	$1 \cdot 10^{-6}$	$9 \cdot 10^{-2}$
C	$1 \cdot 10^{-9}$	$9 \cdot 10^{-5}$

Preliminary tests carried out showed that the initial values of the unknown parameters are better to be positive and as small as possible. For about 10% of the cases, it was necessary to successively choose random initial configurations.

For this configuration, a circuit with parameters having the values: $R=10^{-10}\Omega$, $L=10^{-10}$mH, and $C=10^{-10}\mu$F was considered. This circuit is characterized by the diagram shown in Figure 3.

Following the optimization process the circuit under consideration was correctly identified. The optimization aimed at minimizing the residual value calculated according to equations (2) to (4).

Considering the initial parameters, the resulting impedance values are shown in the diagram in Figure 3.

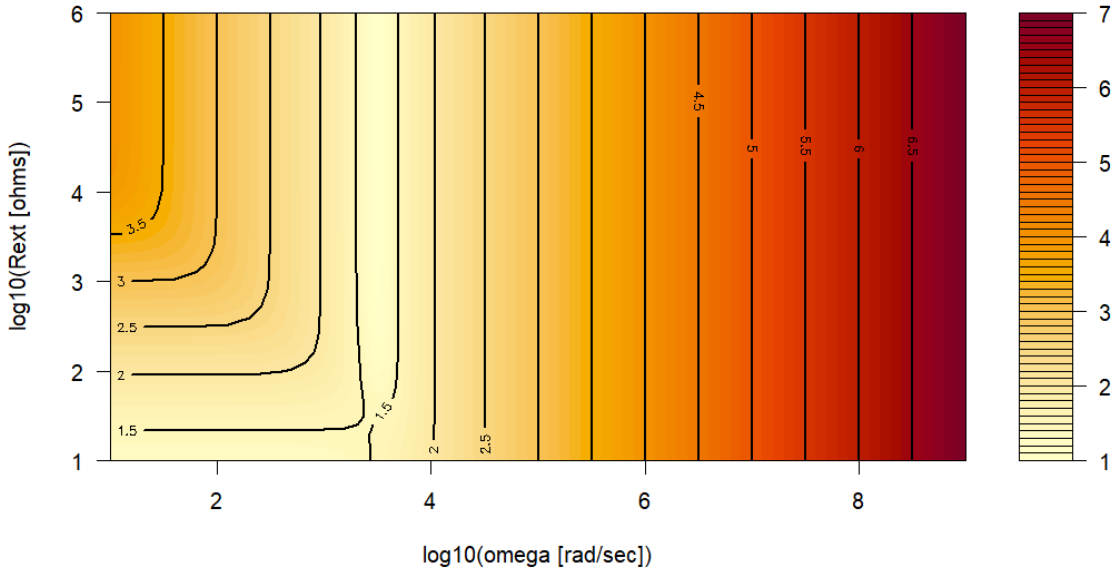


Figure 2 Equivalent impedance of unknown R, L, and C series circuit as a function of angular frequency and external resistance.

Next, the process presented above was applied to 10^5 impedance spectroscopy plots obtained by simulation.

The correctly identified parameters characterizing these configurations are shown by the density plots presented in Figures 3 and 4.

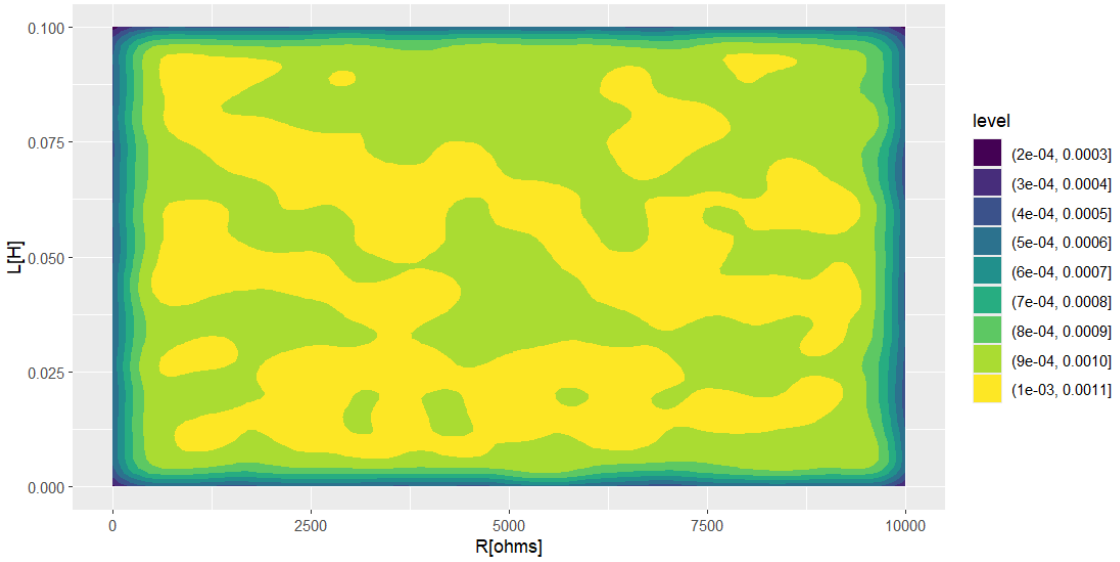


Figure 4 Density plot of pairs R[ohms] and L[H] for all configurations.

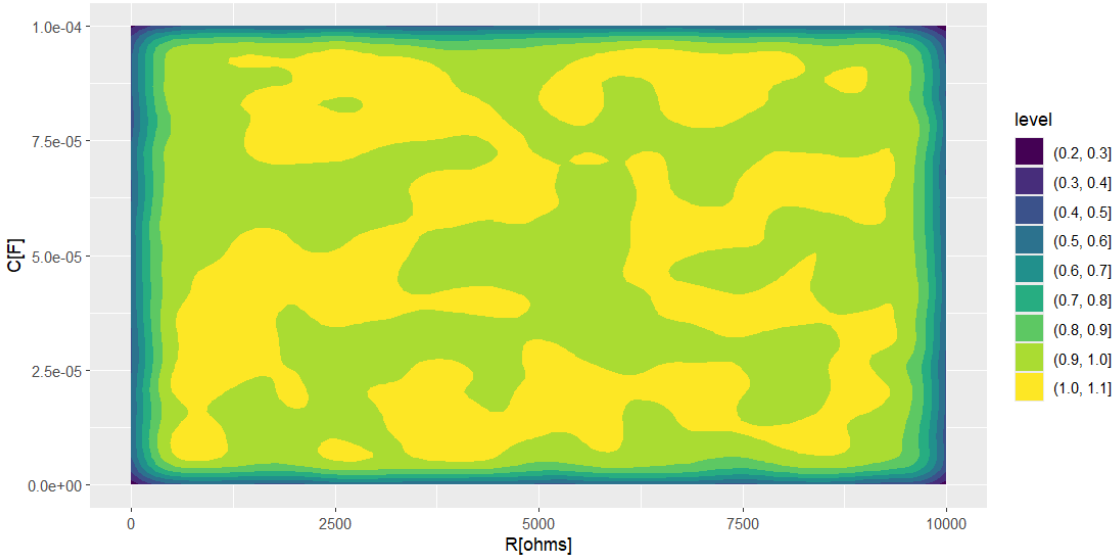


Figure 5 Density plot of pairs R[ohms] and C[F] for all configurations.

The characterization of the entire experimental set with 10^5 configurations is summarized in Table 2.

Table 2 Summary of experimental circuits set

	log10(R[ohms])	log10(L[H])	log10(C[F])
Min.	0.004321	-5.704	-8.826
1st Qu.	3.396.294	-1.605	-4.602
Median	3.697.477	-1.303	-4.301
Mean	3.564.378	-1.436	-4.433
3rd Qu.	3.874.459	-1.126	-4.124
Max.	3.999.997	-1.000	-4.000

Applying the optimization process to the whole set of 10^5 configurations resulted in a set of residual values according to equation (2). The set of residual values was characterized by the density distribution shown in Figure 6.

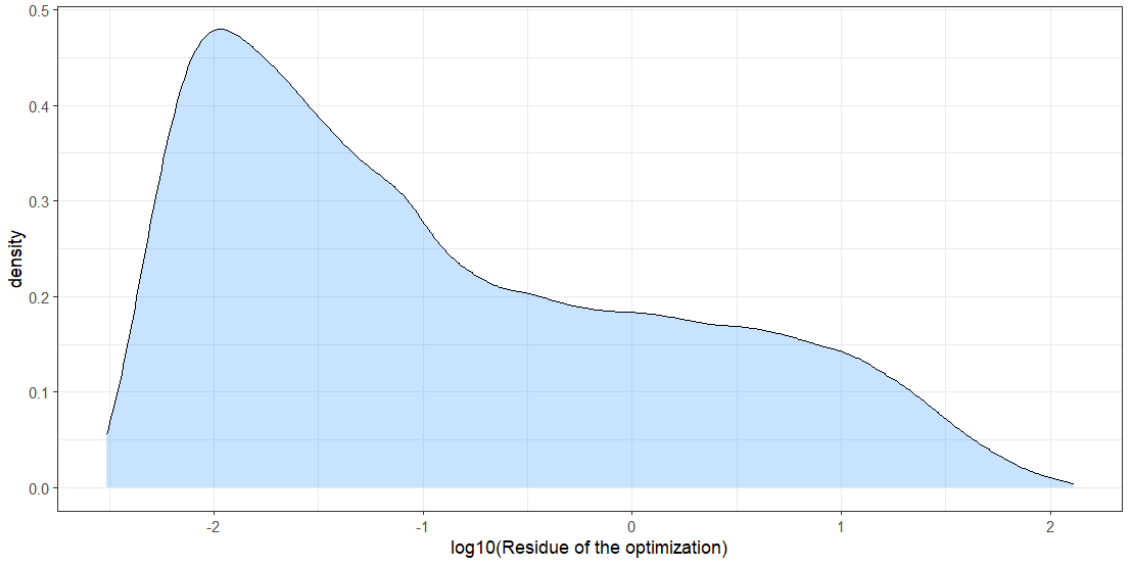


Figure 6 Density plot optimization residuals for the entire set of simulated configurations.

DISCUSSION

The simulation space with boundaries chosen according to Table 1 was investigated by 10^5 simulated configurations.

For each impedance plot as a function of angular frequency and generated external resistance it was possible, with the help of the proposed model, to identify a circuit R, L, and C whose behavior was very close to each generated impedance plot. The residual values are less than 10^2.

Although the generated random values were based on the uniform distribution, in the density plots in Figures 4 and 5 some accumulation due to the adopted generation model can be observed. However, the space of possible configurations was covered.

The theoretical model used is based on an R, L, and C circuit without nonlinear components. Their presence may cause deviations from the expected values.

CONCLUSION

To identify the parameters characterizing the R, L, and C series circuits, a theoretical model was used together with an optimization process.

The range of variation of the parameters was explored by choosing 10^5 experimental impedance plots obtained by randomly generated impedance spectroscopy.

For all experimental impedance spectroscopy impedance plots, the associated R, L, and C series circuits were identified with good accuracy.

Even though for some scenarios the optimization process was very slow or required re-initialization the optimization process had convergence.

https://doi.org/10.5593/sgem2024/1.1/s06.76

ACKNOWLEDGEMENTS

This work was carried out through the "Nucleu" program of the National Research, Development and Innovation Plan 2022-2027, supported by MCID, project no. PN23320102 and facility of national interest - IOSIN-PCDIEX.

Preliminary simulations were performed with Multisim version 14.3 and PTC Mathcad Prime 9.0.

The calculation and plotting were used by R and R Studio 0 and 0.

REFERENCES

[1] ATEX Directive, Equipment for potentially explosive atmospheres (ATEX), available https://ec.europa.eu/growth/sectors/mechanical-engineering/atexen, 2014.

[2] Pasculescu V.M., Vlasin N.I., Florea D., Suvar M.C., Improving the quality of the process for selecting electrical equipment intended to be used in potentially explosive atmospheres, Quality - Access to Success, Romania, vol. 18/issue S1, pp 97-102, 2017.

[3] Prodan, M., Ghicioi E., LupuC., Nălboc., Szollosi-Mota A., Flammability characterization of a petroleum derivative for increasing the safety of personnel and environmental protection, International Multidisciplinary Scientific GeoConference: SGEM; Sofia, Vol. 4, 2016.

[4] Călămar A., Gaman G. A., Pupazan, D., Toth L., Kovacs I., (2017) Analysis of environmental components by monitoring gas concentrations in the environment, Environmental Engineering and Management Journal, March, 16, No.6, pag. 1249-1257, ISSN 1582-9596

[5] R Core Team, R: A language and environment for statistical computing. R Foundation for Statistical Computing, Vienna, Austria. URL http://www.R-project.org/, 2015.

[6] R Development Core Team, R: A language and environment for statistical computing. R Foundation for Statistical Computing, Vienna, Austria. ISBN 3-900051-07-0, URL http://www.R-project.org, 2008.

[7] Standard EN IEC 60079-0: 2018 - Explosive atmospheres - Part 0: Equipment - General requirements 2018.

[8] Standard ISO/IEC 80079-20-1, Explosive atmospheres - Part 20-1: Material characteristics for gas and vapour classification – Test methods and data, 2020.

[9] Standard EN 60079-11, Explosive atmospheres -- Part 11: Equipment protection by intrinsic safety "i", 2012.

[10] Bottrill G., Cheyne D., Vijayaraghavan G., Practical electrical equipment and Installations in Hazardous Areas, Elsevier Newness, Oxford, 2007

INVESTIGATION OF THE PROCESS OF INTRODUCING THE CENTRALIZER SLATS INTO THE WALLS OF THE TRUNK WHEN DRILLING INCLINED WELLS

Prof. Dr. Akshyryn Zholbassarova[1]
Prof. Dr. Danabek Saduakassov[1]
Prof. Dr. Aliya Togasheva[1]
Prof. Dr. Maxat Tabylganov[1]
Prof. Dr. Aigul Gusmanova[1]
[1]Caspian state university of technologies and engineering named after S.Yessenov, **Republic of Kazakhstan**

ABSTRACT

In this article, a theoretical and experimental study of the processes of embedding the centralizer bars on the walls of the well during drilling is carried out. For this purpose, a mathematical model has been created that describes the dynamics of the process, taking into account the axial load on the bit and the own weight of the drilling column. The formation of a compacted core in front of the centralizer, as well as the stress-strain state of the medium, is considered. The proposed approach allows us to take into account the possibility of introducing a centralizer on the walls of the well and adjust the curvature parameters of the trunk of inclined wells. The results of this study can be useful for optimizing the drilling process and improving the efficiency of wells. The study is aimed at analyzing the technical and economic aspects of the installation of inclined wells, based on the state of spatial curvature of the trunk. It was found that stabilization of the design azimuth of the curvature is a difficult task in deep inclined wells due to the lack of continuous information about the course of the curvature parameters. Technological problems such as measurement inaccuracy and selection of equipment parameters are described. Special attention is paid to the use of a magnetic translator and a downhole inclinometer to accurately orient the deflector at the bottom of the well, which is the most accurate and cost-effective method in modern drilling operations.

Keywords: centralizer, inclined well, mathematical model, stress-strain state, deflector.

INTRODUCTION

Directional and horizontal drilling of deep oil and gas wells plays a key role in the modern oil and gas industry. These mining methods can significantly increase the efficiency and cost-effectiveness of the process, providing access to resources that were previously unavailable or economically impractical for development [1-3].
The large-scale growth of horizontal drilling from 10,8% in 2010 to 46,4% in 2018, projected to reach a level of 74% by 2030, has a significant impact on the oilfield

https://doi.org/10.5593/sgem2024/1.1/s06.77

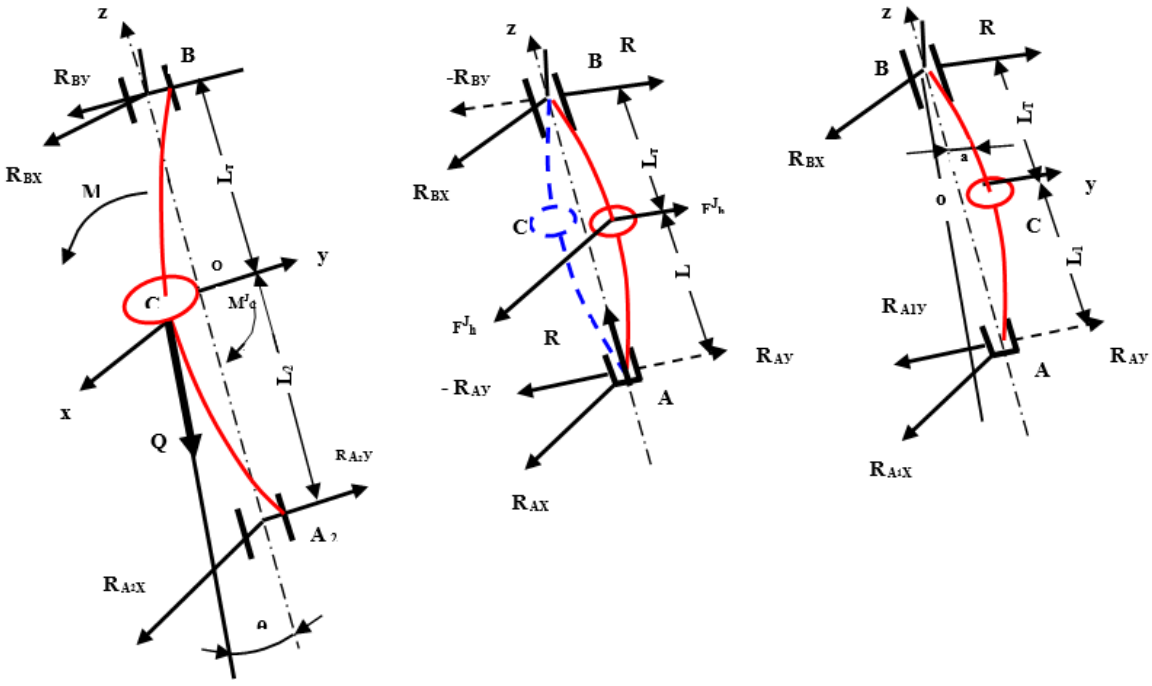
services market, both in terms of volume and structure. Increase in horizontal drilling penetration by 19% in 2018 (up to 13,4 million m), with a parallel decrease in penetration in vertical drilling by 13%, is a reflection of this trend.

Statistical data indicate a significant decrease in drilling efficiency from 26,6 t/m in 2014 to 20,1 t/m in 2023, and this negative trend continues. Vibrations caused by the eccentric rotation of the bit on the face are one of the main reasons for this decrease in efficiency. Drilling wells with rotation is often accompanied by torque fluctuations caused by the jamming of the bit due to high friction in the open trunk and subsequent failure, which leads to an increase in the rotation of the bit and damage to the cutters. These problems are also associated with transverse and axial vibrations of the drill string and an increase in accidents [4,5].

MATERIALS AND METHODS OF RESEARCH

The scientific work is devoted to a detailed study of the processes associated with the installation of centralizers in the walls of the well during drilling. As part of the research, a mathematical model was developed, shown in Figure 1, which is a symmetrical stamp. This method allows for a deeper understanding and description of the mechanisms of the introduction of centralizers and their impact on the drilling process. The results obtained are of significant importance for optimizing the drilling process and improving the efficiency of downhole equipment.

The introduction of this centralizer into the walls of the well is being investigated under the influence of axial load on the bit and the own weight of the BHA. When the centralizer is inserted into the walls of the well, regardless of its shape, a compacted core is formed in front of it. This core takes on a shape close to parabolic. This process, described by the mathematical model shown in Figure 1, is analyzed in detail within the framework of this study. The results obtained allow us to better understand the interaction of the centralizer with the walls of the well and optimize the drilling process to achieve maximum efficiency. Therefore, when considering the process of implementing the centralizer, we take the core in the form of a parabola of the form $y = x^{2n}$.



а) unscrewing the borehole (a set of zenith angle); б) well stabilization; в) twisting (decrease in curvature)

Figure 1 - Diagram of the dynamic forces acting on the "well-rotating arrangement of the bottom of the drill string" system (ABDS)

The stress-strain state of the medium is described by a number of partial differential equations [4]. Unlike a plastic medium, the following sign rule for stresses is accepted for a connected medium.

$$\frac{2\tau}{\delta_x - \delta_y} = \frac{\left(\frac{\partial V_x}{\partial y} + \frac{\partial V_y}{\partial x}\right) \pm \left(\frac{\partial V_x}{\partial x} + \frac{\partial V_y}{\partial y}\right) tg\varphi}{\left(\frac{\partial V_x}{\partial x} - \frac{\partial V_y}{\partial y}\right) \pm \left(\frac{\partial V_y}{\partial x} + \frac{\partial V_x}{\partial y}\right) tg\varphi}; \quad (1)$$

where X, У - projections of mass forces whose positive directions coincide with the positive directions of the coordinate axes; ρ_o- density; t - time; V_x, V_y - velocity projections; φ - the angle of internal friction; τ - tangential stress; k - coefficient of adhesion; δ_x, δ_y - normal voltages.

Equation (1) is a condition of ultimate equilibrium. It consists in the fact that at each point of the medium, the maximum difference between the tangential stress and the corresponding normal stress multiplied by the tangent of the angle of internal friction is equal to the limiting coupling stress k. These equations and conditions play an important role in describing the behavior of a material under the influence of mechanical forces and provide an understanding of the processes of deformation and fracture in materials. Their use makes it possible to more accurately model and analyze the behavior of materials under various loading conditions. It is performed at each point on two sites that make up sharp angles with the direction of the maximum main normal stress ±y:

https://doi.org/10.5593/sgem2024/1.1/s06.77

where $y = \frac{\pi}{4} - \frac{\varphi}{2};$ (2)

Two families of lines that coincide at each point with the directions of these sites are called slip lines.

For a loose medium, condition (2) determines the mismatch of the main stress axes and the main axes of strain velocities, since the sliding lines form angles other than δ, equal to $\frac{\pi}{4}$, with the direction of the maximum main normal stress $\frac{\pi}{4} - \frac{\varphi}{2}$. Thus, the angle of mutual rotation of the main axes is equal to half the angle of internal friction.

The choice of the sign in equation (2) is determined by which of the families of sliding lines, the first or the second, is the active family. The upper characters are selected when the first family is active. The lower ones are in the opposite case.

When the centralizer is installed on the walls of the borehole, a bulge phenomenon is observed, in which an elevation, or slide, is formed near the centralizer. Thus, understanding and modeling the centralizer implementation process requires taking into account a variety of factors and complex mathematical models to achieve accurate results.

The curve describing the shape of the released material with sufficient accuracy was described using the Rayleigh distribution density equation known from probability theory:

$$y = \frac{x \cdot e^{-\left(\frac{x^2}{2 \cdot \delta^2}\right)}}{\delta^2}, \quad x \geq 0; \tag{3}$$

The equation of the curve of the boundary of the moving medium AD separating the rigid and plastic regions is found from the condition that the equation of such a curve will be the equation of one of the sliding curves. As the literature review has shown, the processes occurring around the walls of the borehole have not been sufficiently investigated. Therefore, our proposed study allows us to take into account the possibility of introducing centralizer slats on the walls of the borehole, and adjust the curvature parameters of the trunk of inclined wells with great accuracy and intensity. So, if the trunk of an inclined well is curved strictly in accordance with the design profile, the selection of drilling mode parameters is not particularly difficult, the danger of tool seizure and other complications is much less than in comparable conditions in a well with a sharp change in curvature and azimuth.

However, it should be noted that in conditions of deep inclined drilling, achieving stability of the design azimuth of curvature is a rather difficult problem. In addition, certain technological techniques for choosing the angle of installation of the deflector and its orientation, tool build-up, as well as inaccuracies in measurements with some control and measuring devices have not been perfected. The specific drilling conditions of deep and ultra-deep inclined wells also require very high qualifications and experience, accuracy and accuracy in work on the part of sighting technicians, drillers and all members of the drilling team. Of course, achieving the set values of the curvature and azimuth of the wellbore largely depends on the correct choice of stiffness and geometric parameters and dimensions of the deflector, WDP, turbobur, bit, taking

into account the geological conditions of drilling, the azimuth of the deflector installation.

Of these factors, a special place is occupied by the influence of the angle between the direction of action of the deflecting force on the bit during drilling and the direction of curvature of the well bore $У_{sl}$, on the intensity of changes in curvature and azimuth i_y. In essence, this issue is one of the most difficult issues of inclined well wiring technology. A number of works are devoted to the study of the choice of the angle of installation of the deflector, among which the well-known study by M.P.Gulizade should be highlighted [5-7].

Figure 2 shows some results of this theoretical solution, where the azimuth increments along the ordinate axis Y_a, the angle of drilling of the diverter is postponed along the abscissa axis Y and the angle α of the downhole reaction (curvature) at different angles of curvature of wells α_0.

The graph shows the azimuth changes with solid lines and the curvature angles with dotted lines. Specific calculations have been performed for the chisel layout ∅ 269 mm, T12M3B-9″, curved pipe ∅168 mm, with a bending angle of 3^0 with an axial load on the chisel 10 tons.

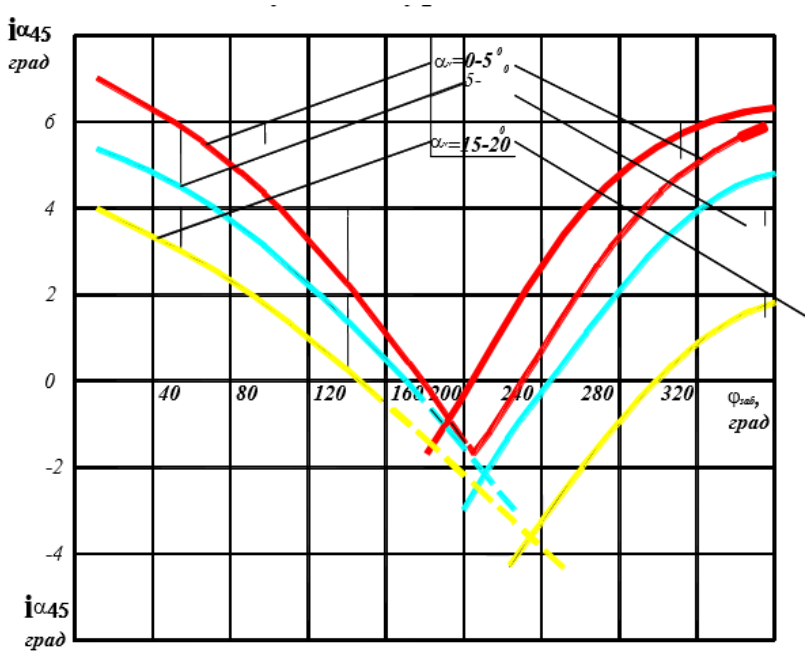


Figure 2 - Dependence of the intensity
of the curvature set on the angle of installation of the deflector

Note that, despite the fact that the above dependences of the increment of the angle and azimuth of the well on the angle of installation of the diverter are made for the case of using a curved pipe as a diverter, the revealed patterns are widely used in practice such when using a curved translator [5,8,9].

https://doi.org/10.5593/sgem2024/1.1/s06.77

RESULTS

The study, taking into account the specific geological and technical conditions of drilling, was carried out according to the wiring of inclined wells at the Uzen field, Zhetybai of the chisel layout ∅ 269 mm**,** T12M3B-9″, 3° curved translator, WDP ∅203 mm, length 10 m, 140 mm drill pipes. Drilling with a diverter was carried out in the range from 1600 m to 2000 m in Zhetybayskaya square with axial loads on the chisel of 10÷12 tons, the productivity of drilling pumps of 40÷42 l/sec.

Data processing and the establishment of the desired dependence was carried out according to the following methodology. According to the data of inclinometric measurements of the intervals of the trunk drilled using a deflector, the intensity of changes in curvature $i\alpha_{45}$ and azimuth iy_{45} for 45 penetrations for each inclined well separately was calculated. Then these data were systematized by the magnitude of the initial angle of curvature, the azimuth of the deflector installation, the purpose of the deflector descent, and the correlation dependences $i\alpha_{45}$ and iy_{45} on the Y_{sl} were found [7,8].

A similar data processing was performed for all chisels with a deflector for each inclined well separately and for all 86 analyzed wells. Due to the complexity of the process and the influence of a variety of factors, a number of values of the rate of change of curvature and azimuth correspond to the same value of Y_{sl}.

The results of data processing are presented in Figure 2 in the form of theoretical regression lines. Moreover, empirical regression lines were first constructed, where the arithmetic mean of $i\alpha_{45}$ and $i\alpha_{45}$ corresponds to each value of the Y_{sl}, and then correlation coefficients and correlation relations were determined to assess the strength of the relationship between the indicators and the factors influencing them.It is established that the relationship between the intensity of the change in curvature and azimuth from the drilling angle is curved.

A distinctive feature of the revealed patterns is that the given rates of change while changing the azimuth, in other words, these values more accurately reflect the efficiency of the deflector and the layout as a whole [6,9-20]. This method provides the necessary accuracy and efficiency in monitoring the parameters of downhole drilling, which significantly affects the success and economic profitability of the entire project.

DISCUSSION

The results of the study are directly correlated with the initial question of optimizing the well drilling process using deflectors. The data confirm the hypothesis that the effective use of deflectors can be achieved by taking into account factors such as drilling angle, azimuth and other geological and technical conditions. Thus, the results of the study are consistent with the proposed hypothesis and confirm them with the help of data collected and analyzed during the research work.

CONCLUSION

In the course of the study, a data processing technique was developed based on the analysis of inclinometric measurements and the establishment of dependencies between the intensity of changes in the curvature and azimuth of the well from various factors such as the drilling angle and the layout parameters with a deflector. The results obtained make it possible to optimize the drilling process and increase the efficiency of the diverter and layout.

The study, conducted taking into account the specific geological and technical conditions of drilling at the Uzen and Zhetybai fields, allowed us to obtain significant results that have important practical applications. Thus, the results of the study represent an important contribution to the development of well drilling technologies and can be used in planning and conducting geological and technical work on oil and gas fields.
The work was implemented with support of the Science Committee of the Ministry of Science and Higher Education of the Republic of Kazakhstan (grant no. AP19679430).

REFERENCES

[1] Shlyun N.V., Gulyayev V.I. Buckling of a drill-string in two-sectional bore-holes. Int. J. Mech. Sci. 2020, 172, 105427.https://doi.org/10.1016/j.ijmecsci.2020.105427
[2] El Sabeh K., Gaurina-Medimurec N., Mijic P., Medved I., Pašic B. Extended-Reach Drilling (ERD)—The Main Problems and Current Achievements. Appl. Sci. 2023, 13, 4112. https://doi.org/10.3390/app13074112
[3] Tong H., Shao Y. Mechanical Analysis of DS in Horizontal Directional Drilling. Appl. Sci. 2022, 12, 3145. https://doi.org/10.3390/app12063145
[4] Lashari S., Takbiri-Borujeni A., Fathi E. Drilling performance monitoring and optimization: A data-driven approach. J. Petrol. Explor. Prod. Technol. 2019, 9, 2747–2756. https://doi.org/10.1007/s13202-019-0657-2
[5] Epelle E.I., Gerogiorgis D.I. A review of technological advances and open challenges for oil and gas drilling systems engineering. 2020 AIChE Journal 66(4),e16842. https://doi.org/10.1002/aic.16842
[6] Khajiyeva L.A., Andrianov I.V., Sabirova Y.F., Kudaibergenov A.K. Analysis of Drill-String Nonlinear Dynamics Using the Lumped-Parameter Method. Symmetry 2022, 14, 1495. https://doi.org/10.3390/sym14071495
[7] Erge O. Modeling Cuttings Transport and Annular Pack-Off Using Local Fluid Velocities with the Effects of Drillstring Rotation and Eccentricity/ Oney Erge, Eric van Oort // Paper SPE 199587. – 2020. – 18 p. https://doi.org/10.2118/199587-MS
[8] Shirangi M.G.Digital Twins for Drilling Fluids: Advances and Opportunities / M. G.Shirangi// Paper SPE 199681. – 2020. – 18 p. https://doi.org/10.2118/199681-MS
[9] D.M. Lobo, T.G. Ritto, D.A.Castello, M.L.M. de Souza. On the calibration of drill-string models based on hysteresis cycles data. International Journal of Mechanical Sciences Volume 177, 1 July 2020, 105578. https://doi.org/10.1016/j.ijmecsci.2020.105578
[10] Togasheva A., Bayamirova R., Sarbopeyeva M., Bisengaliev M., Khomenko V.L. Measures to prevent and combat complications in the operation of high-viscosity oils of western Kazakhstan. News of the National Academy of Sciences of the Republic of Kazakhstan, Series of Geology and Technical Sciences. Volume 1. Number 463 (2024), Pp.257–270. https://doi.org/10.32014/2024.2518-170X.379
[11] Togasheva A.R., Bayamirova R.Y., Zholbassarova A.T., Sarbopeeva, M.D., Arshidinova M.T. (2023). Pilot field tests of shock-wave treatment of wells at the fields of JSC Ozenmunaigas. International Multidisciplinary Scientific GeoConference Surveying Geology and Mining Ecology Management, SGEM. – 23(1.1). Pp.719–727. doi 10.5593/sgem2023/1.1/s06.86.
[12] Ratov B.T., Fedorov B.V. (2013) Hydroimpulsive development of fluid-containing recovery. Life Science Journal, 10(SPL.ISSUE11), pp. 302–305. ISSN 10978135
[13] Ratov, B. T., Mechnik, V. A., Gevorkyan, E. S., Matijosius, J., Kolodnitskyi, V. M., Chishkala, V. A., Kuzin, N. O., Siemiatkowski, Z., & Rucki, M. (2022a). Influence

https://doi.org/10.5593/sgem2024/1.1/s06.77

of CRB2 additive on the morphology, structure, microhardness and fracture resistance of Diamond Composites based on WC–Co Matrix. Materialia, *25*, 101546. https://doi.org/10.1016/j.mtla.2022.101546
[14] Chernova, M., Kuntsyak, Y., Ratov, B., Sudakov, A., & Nuranbayeva, B. (2022). Substantiation of the use of polymer-composite materials, which reduce the influence of dynamic friction forces of macrostructural surfaces, when drilling wells. SGEM International Multidisciplinary Scientific GeoConference. EXPO Proceedings. https://doi.org/10.5593/sgem2022/1.1/s03.049
[15] Mamalis, A., Mechnik, V., Morozow, D., Ratov, B., Kolodnitskyi, V., Samociuk, W., & Bondarenko, N. (2022). Properties of cutting tool composite material diamond–(fe–ni–cu–sn) reinforced with nano-VN. Machines, 10(6), 410. https://doi.org/10.3390/machines10060410
[16] Ratov, B. T., Mechnik, V. A., Bondarenko, N. A., Kolodnitskyi, V. M., Kuzin, N. O., Gevorkyan, E. S., & Chishkala, V. A. (2021). Effect of vanadium nitride additive on the structure and strength characteristics of diamond-containing composites based on the fe–cu–ni–SN matrix, formed by cold pressing followed by Vacuum Hot Pressing. Journal of Superhard Materials, 43(6), 423–434. https://doi.org/10.3103/s1063457621060095
[17] Ratov, B. T., Fedorov, B. V., Khomenko, V. L., Baiboz, A. R., & Korgasbekov, D. R. (2020). Some features of drilling technology with PDC bits. Naukovyi Visnyk Natsionalnoho Hirnychoho Universytetu, (3), 13–18. https://doi.org/10.33271/nvngu/2020-3/013
[18] Biletsky M.T., Ratov B.T., Kozhevnykov A.A., Baiboz A.R., Delikesheva D.N. (2018) Updating the theoretic model of rock destruction in the course of drilling. News of the National Academy of Sciences of the Republic of Kazakhstan, Series of Geology and Technical Sciences, 2018, 2(428), pp. 63–71. ISSN 22245278
[19] Ratov, B. T., Fedorov, B. V., Omirzakova, E. J., & Korgasbekov, D. R. (2019a). Development and improvement of design factors for PDC Cutter Bits. Mining Informational and Analytical Bulletin, 11, 73–80. https://doi.org/10.25018/0236-1493-2019-11-0-73-80
[20] Kasenov, A. K., Biletskiy, M. T., Ratov, B. T., & Korotchenko, T. V. (2015a). Problem analysis of geotechnical well drilling in complex environment. IOP Conference Series: Earth and Environmental Science, 24, 012026. https://doi.org/10.1088/1755-1315/24/1/012026

METHODOLOGY FOR OPTIMIZING DRILL BIT PERFORMANCE

Assoc. Prof. Dr. Oleksandr Pashchenko[1]
Prof. Dr. Boranbay Ratov[2]
Assoc. Prof. Dr. Volodymyr Khomenko[1]
Assoc. Prof. Aigul Gusmanova[3]
Assoc. Prof. Elmira Omirzakova[1]

[1]Dnipro University of Technology – Dnipro, **Ukraine**
[2]Satbayev University - Almaty, **Republic of Kazakhstan**
[3]Yessenov University – **Republic of Kazakhstan**

ABSTRACT

The optimization of technological processes is vital for advancing scientific and technical progress in exploration activities, particularly in drilling operations. The integration of operating microprocessor equipment and automated management systems has opened up new opportunities for theoretical research in optimization processes and drillings. Control systems for drilling exploration wells on solid minerals enable real-time operation and data collection, processing, and diagnosis of equipment functionality. Optimization of technological processes using modern equipment aims to enhance production efficiency, improve quality, and reduce costs. Despite advancements in equipment, tools, and drilling technology, there are still significant opportunities for increasing productivity and improving technical and economic indicators in prospecting drilling. Optimization criteria vary depending on the objectives, with the maximum productivity often achieved by minimizing drilling time. The task of finding the maximum drilling speed per run involves optimizing parameters such as weight on bit, tool speed, and mud flow rate. A novel technique proposed in this study involves cyclic intra-run changes in speed per minute as the optimization criterion, rather than mechanical speed. The developed method is applicable to any rock cutting instrument and drilling method, with the optimization of drilling speed per run as a function of drilling time. The use of time and speed coefficients simplifies calculations and reveals regularities in the drilling process, contributing to the optimization of drilling operations.

Keywords: borehole drilling, rocks destruction, rate of penetration, weight on bit, rotation speed

INTRODUCTION

Optimization technological process makes an important part of scientific and technical progress when conducting exploration works. Theoretical researches in the field of optimization process and drillings had new opportunities of implementation with the advent of the operating microprocessor equipment and creation on its basis of systems of automated management [1, 2, 3].
Various samples of control systems of process of drilling of exploratory wells on solid minerals allow not only to operate process of drilling in real time on any of the known algorithms, but also to collect, to accumulate and process information on drilling

https://doi.org/10.5593/sgem2024/1.1/s06.78

process and also to diagnose operability of separate knots and mechanisms [4, 5, 6].
Optimization technological processes on the basis of the modern equipment has to provide a production intensification, improvement of quality and decrease in product cost.
Need of it follows from the analysis of production activity of the prospecting organizations for performance of plan targets. In spite of the fact that introduction of the modern equipment, tools, progressive technology of drilling, means of mechanization and automation of separate operations, improvement of the organization of work in general provided performance of these tasks, in prospecting drilling there are considerable reserves of increase in labor productivity and improvement of its technical and economic indicators. These reserves consist first of all in optimization process and well-drillings and in improvement of the organization of works [7, 8, 9].
Depending on the optimization purposes process and drillings it is possible to optimize by various criteria. For achievement of the maximum productivity it is necessary to minimize time for a well driving including time of drilling and time for the hoisting and accompanying run other operations. In this case for non-stationary process of drilling of criterion optimization will be run speed of drilling. And will be interested to the maximum of run speed reached at a certain combination of parameters of the mode of drilling. It is known that key parameters, having significant effect on efficiency of process of drilling, are weight on bit (*F*), tool speed (*n*) and amount of the mud supplied at the borehole bottom (*Q*). A problem of search of an extremum of run speed as functions of several variables – *F*, *n* and *Q* and time *t* – it is difficult. For simplification of a task for these conditions we accept the best *F* and *Q*. Thus, the task comes down to search of the maximum drilling speed per run *V_p* as functions *n* and *t* [10, 11, 12].
In the offered technique search of a maximum of drilling speed per run is made at cyclic intra run change of speed per minute. The first main difference of the offered technique from known in which speed in run also cyclically changes is use as optimization criterion of run speed in drilling, but not mechanical speed. The following difference is the research of optimization criterion of drilling speed per run as functions in time, but not single determination of numerical value of criterion – average mechanical speed as it takes place in the known techniques. Further drilling time on each mode variable, depending on speed per minute, but not constant is offered [13, 14, 15].

RESEARCH METHODS

General scheme of the choice n_e and t_e.

Choice n_e and t_e for these conditions: the rocks, well depth, type of the rock cutting tool - is carried out on experimental data with use of the necessary information obtained directly on boring and definitely processed. For certain geological specifications. These works carry out one-time, but not in each run [16, 17].
The technique includes the works which are carried out according to the following scheme:

1) Skilled drilling – with change of speed per minute in run.
2) Drilling process timing – with registration of necessary information.
3) Calculation and creation of dependences *L=f(t)* and $V_p = f(t)$ for various *n*. It is not obligatory to build dependences, data can be submitted tables.
4) The analysis of the received dependences and issue of recommendations.

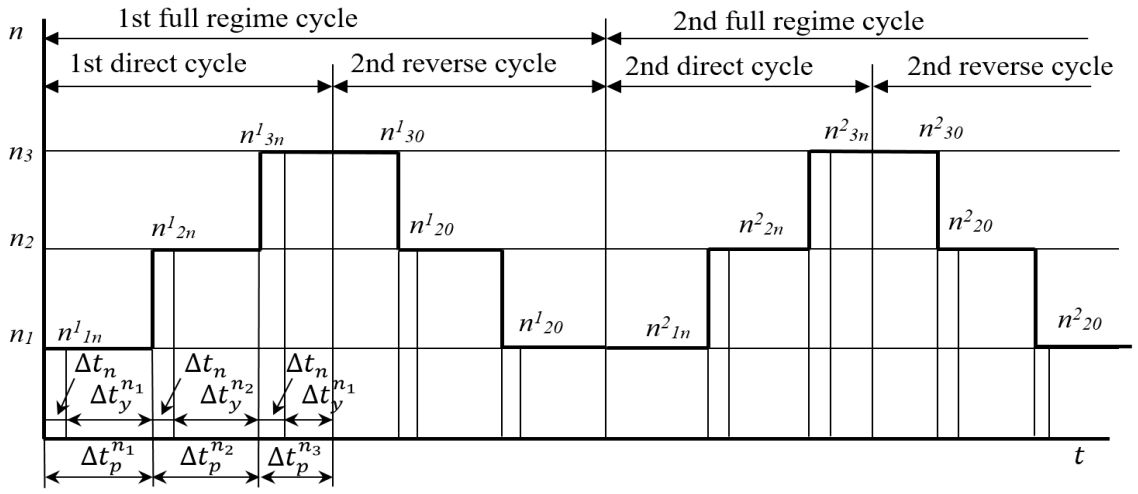


Figure 1. Change of rotation speed (*n*) in unit of time (*t*) in run

Drilling time in each elementary mode Δt_p^{ni} constantly at identical value of speed. At various values *n* Δt_p^{ni} variously. Δt_p^{ni} consists from Δt_n and Δt_y^{ni}, where Δt_n - time of drilling at which there is a transition process caused by change of speed.

According to literary data Δt_n for different conditions of drilling makes several minutes, 1-3 min. Δt_y^{ni}, - drilling time on established the drilling mode. It depends on tool speed in a minute and is selected it that work of friction forces ΔA_{ni} on the elementary modes during drilling Δt_y^{ni} it was constant, i.e. at constant *F* it is necessary, it is necessary that the work n_i Δt_y^{ni} was constant.

Therefore,

$$\Delta t_y^i = \frac{a}{n_i}, \tag{1}$$

where *a* – constant.

Size Δt_y^{ni}, has to be selected for receiving bigger number of full regime cycles. If $\Delta t_y^{ni} >> \Delta t_n$ to allocate separately Δt_n it is not recommended; it is possible to include size Δt_n in size Δt_y^{ni}, what will simplify maintaining timing. When drilling few abrasive rocks will be a special case of a technique – cycles only straight lines and Δt_y =*const* [18, 19, 20].

Calculation and creation of dependences *L=f(t)* and $V_p = f(t)$

On the basis of data drillings it is possible make calculation and creation of graphs *L=f(t)* for various *n* (Fig. 2).

In each full regime cycle the average driving penetration off $\Delta L_y^{n_i^j}$ for everyone *n* taking into account direct and return cycles

$$\Delta \bar{L}_y^{ni} = \frac{\Delta L_y^{n_{in}^j} + \Delta L_y^{n_{i0}^j}}{2}. \tag{2}$$

To a driving and time of the previous full regime cycle the driving and time of the subsequent cycle, etc. increases.

$$\overline{\Delta L_y^{n_i^1}} + \overline{\Delta L_y^{n_i^2}} + \cdots + \overline{\Delta L_y^{n_i^j}}, \tag{3}$$

$$\Delta t_y^{n_i^1} + \Delta t_y^{n_i^2} + \cdots + \Delta t_y^{n_i^j}. \tag{4}$$

https://doi.org/10.5593/sgem2024/1.1/s06.78

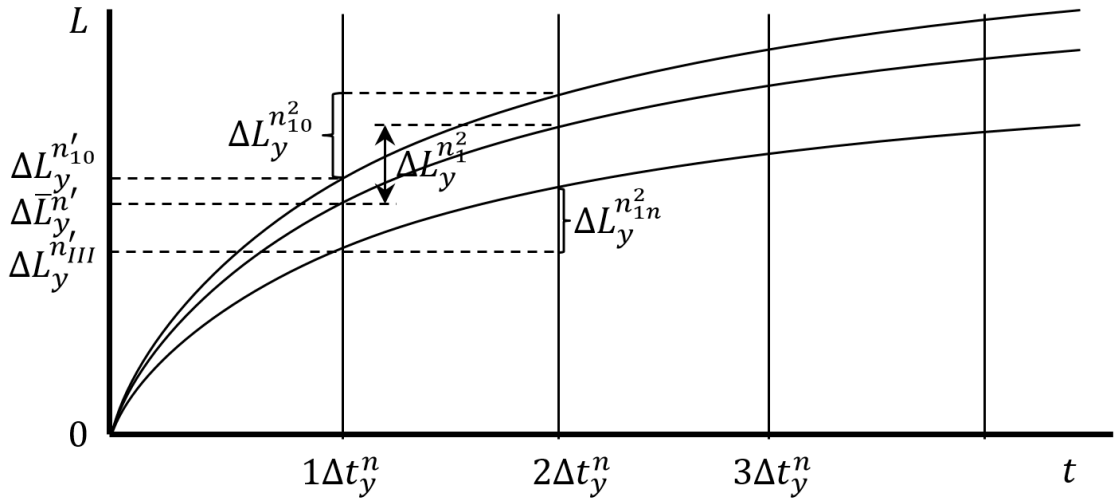


Figure 2. Dependence *L=f(t)* for rotation speed *n*.

According to these data build dependences *L=f(t)* for equal *n*.
In order that data were reliable, it is necessary to carry out several runs.
By data *L*, *t* and t_{ud} it is possible calculate and to construct dependences $V_p = f_1(t)$ for different *n*.

The analysis of the received dependences and issue of recommendations

It is necessary for carrying out the analysis that *k-1* curves $V_p = f_1(t)$ reached V_{pe}, where *k* – number of values *n*. If V_{pe} it is not reached in bigger number of curves, it is necessary to complete these curves, having determined the equation of regression of drilling speed per run by skilled data.
As a result can various arrangement of curves will turn out $V_p = f_1(t)$ and various combination V_{pe} and t_e for different *n*; options of such arrangement and a combination are presented on fig. 3.

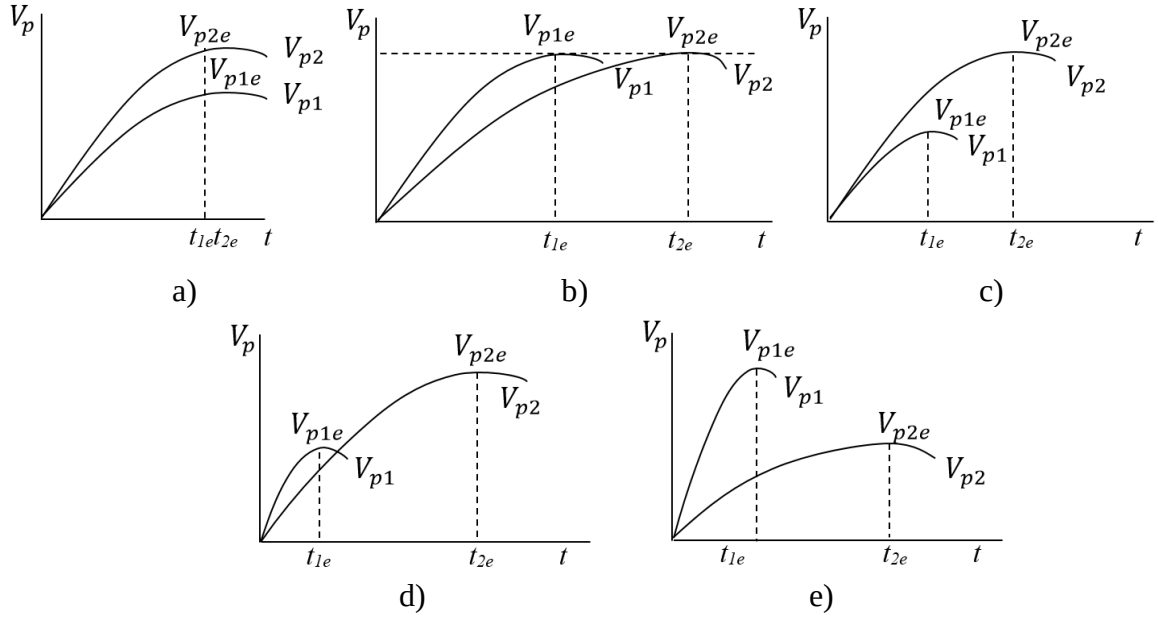


Figure 3. Dependence $V_p = f_1(t)$ for different rotation frequencies *n*.

Proceeding from the drilling process optimization purpose – increase in productivity – the best *n* and *t* will be such which provide a maximum V_{pe}. It is fair for dependences *a, b, c, d* at fig. 3.

In case of equality V_{pe} (Fig. 3, *b*) for the compared modes, the mode for drilling can be chosen as any of compared; here it is obviously possible to consider a condition of the equipment and tool at the choice of the mode.

In case of the choice of the mode with number n_1, the driving for run will be smaller, than at n_2.

$$|L|_{1e} = V_{p_{1e}} t_{1e} + V_{p_{1e}} t_{ud}, \quad (5)$$

$$|L|_{2e} = V_{p_{2e}} t_{2e} + V_{p_{2e}} t_{ud}, \quad (6)$$

$$|L|_{2e} > |L|_{1e}, t_{ud}, \text{ etc. } V_{p_{1e}} \approx V_{p_{2e}}. \quad (7)$$

It will bring at n_1 to increase in time of all hoisting operations and bigger loading of the winch. At n_2 the winch will be loaded less, and the rotator is more.

Similarly, the choice of the best value F_{oc} for given n, Q can be done. Then the change in F_{oc} will look as shown in fig. 4 cyclogram *F*.

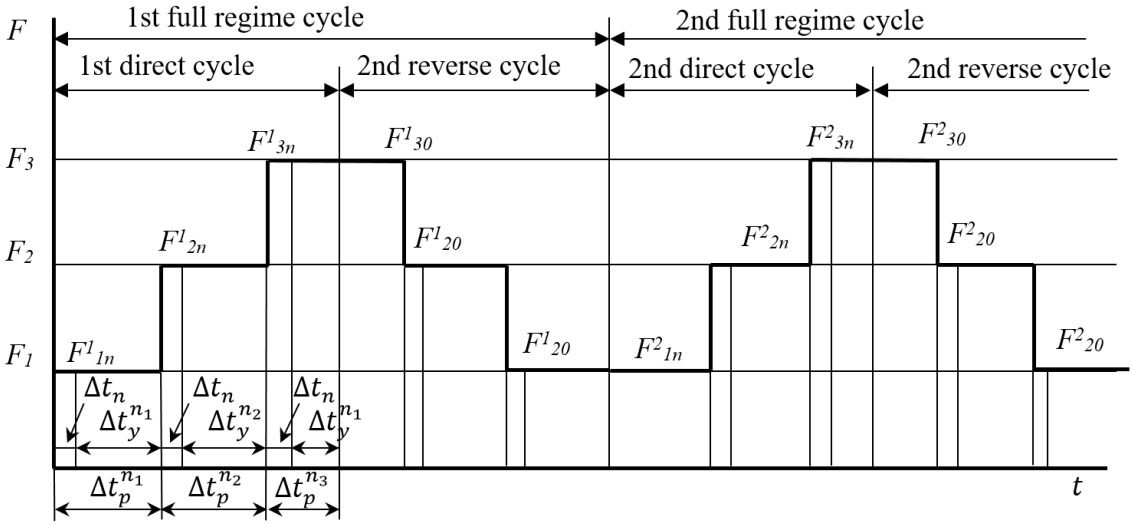


Figure 4. Dependence $V_p = f_1(F)$ for different rotation frequencies *n*.

Similarly, when a joint change in nF, a sequence diagram of a change in this pair of parameters will look like fig. 5.

It is known that the drilling parameters of the weight on bit F_{oc} affect the borehole bottom power N when drilling a well according to the following dependence:

$$N_{bh} = kF_{oc}D_{cp}. \quad (8)$$

k - depends on the method of drilling, so whatever parameter of the drilling mode does not change F_{oc}, n or their combination of nF_{oc} in each case, this leads to a change in N_{bh}. Consequently, N_{bh} acts as an integral indicator of the drilling process and the N_{bh} cyclical schedule during a run is presented in fig.6.

Thus, the N_{bh} process indicator is an integral optimization parameter.

https://doi.org/10.5593/sgem2024/1.1/s06.78

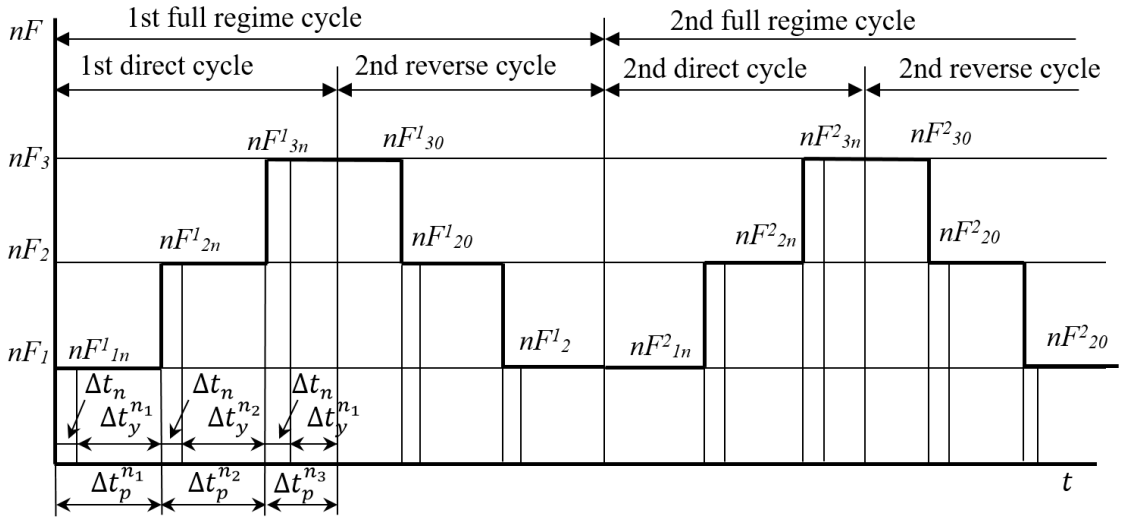


Figure 5. Dependence $V_p = f_1(nF)$ for different rotation frequencies *n*.

Analysis of components of drilling speed per run

Generally the drilling speed per run it is possible will express a formula:

$$V_p = \frac{L}{t_b + t_{ud}}, \tag{9}$$

where L – drilling interval; t_b – drilling time; t_{ud} – time of hoisting operations.

Having divided numerator and a denominator for the period of pure drilling we will receive:

$$V_p = \frac{\frac{L}{t_b}}{\frac{t_b}{t_b} + \frac{t_{ud}}{t_b}},$$

at the same time $\frac{L}{t_b} = V_m$,

Let's enter dimensionless time coefficient (the relation of time for hoisting operations to time of pure drilling) $K_t = \frac{t_{ud}}{t_b}$.

Then run speed

$$V_p = \frac{V_m}{1 + K_t}. \tag{10}$$

Let's conduct researches of influence of dimensionless time coefficient on time drillings (table 1).

Table 1. Influence of time coefficient for the period of drilling

K_t	10	5	2	1	0,5	0,2	0,1
t_b	$0{,}1t_{ud}$	$0{,}2t_{ud}$	$0{,}5t_{ud}$	t_{ud}	$2t_{ud}$	$5t_{ud}$	$10t_{ud}$

Thus it is visible (Fig. 6), that the time coefficient exponential influences on time of pure drilling.

Function of run speed from drilling time - $V_p = \frac{\frac{L}{t_b}}{1 + K_t}$

$$t_b = \frac{L/V_p}{1+K_t} = \frac{L}{V_p} + \frac{LK_t}{V_p} \quad (11)$$

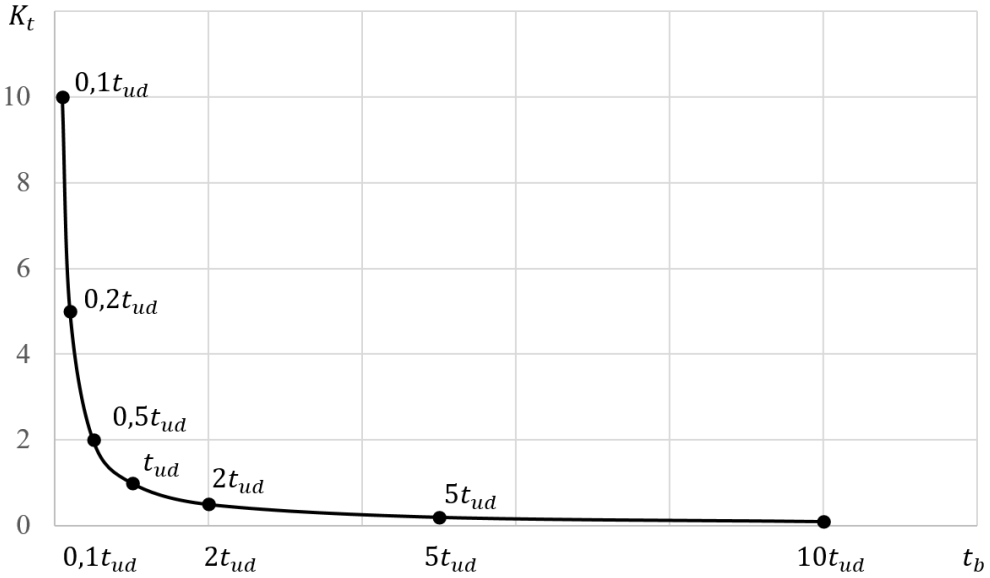


Fig. 6. Influence of time coefficient for the period of drilling

Thus, having entered a new argument (N_{bh}) and new function (h_{ob} – penetration for a turn), offer a new technique of optimization of process of drilling.
From this dependence it is possible to make conclusions on step expenses of power on a borehole bottom in the generalized case in the process of drilling.

CONCLUSIONS

The developed methodology for optimizing drilling operations is applicable to various rock cutting instruments and drilling methods, provided that the drilling speed as a function of drilling time exhibits a maximum value. By utilizing time and speed coefficients, the process of calculation is simplified, and underlying regularities can be revealed more effectively. Theoretical analysis of the functional relationship between drilling mode parameters suggests a parameter N_{bh} for optimizing drilling operations when drilling a well. This parameter serves as a key factor in determining the most efficient drilling approach, contributing to enhanced productivity and cost-effectiveness in exploration activities. So main keys of these methodic are:

- Thus, the developed methodic of the optimization mode of drilling is suitable for any rock cutting instrument and a way of drilling at which the run speed as function of time of drilling has a maximum.
- Use of time and speed coefficients allows to simplify and reveal considerably regularities when calculating.
- Theoretical consideration of the functional relationship of the parameters of the drilling mode suggests a parameter for optimizing N_{bh} when drilling a well.

ACKNOWLEDGEMENTS

The study was supported by the Science Committee of the Ministry of Science and Higher Education of the Republic of Kazakhstan (grant No. AP14869271).

https://doi.org/10.5593/sgem2024/1.1/s06.78

REFERENCES

[1] Kale A., Zhang D., David A., Heuermann-Kuehn L., Fanini O. Methodology for Optimizing Operational Performance and Life Management of Drilling Systems Using Real Time-Data and Predictive Analytics. Paper presented at the SPE Digital Energy Conference and Exhibition, The Woodlands, Texas, USA, 2015. https://doi.org/SPE-173419-MS

[2] Khomenko V., Ratov B., Pashchenko O., Davydenko O., Borash B. Justification of drilling parameters of a typical well in the conditions of the Samskoye field. IOP Conference Series: Earth and Environmental Science, Vol. 1254, p. 012052, 2023. https://doi.org/10.1088/1755-1315/1254/1/012052

[3] Kozhevnykov A., Khomenko V., Liu B., Kamyshatskyi O., Pashchenko O. The History of Gas Hydrates Studies: From Laboratory Curiosity to a New Fuel Alternative. Key Engineering Materials, 844, pp 49–64, 2020. https://doi.org/10.4028/www.scientific.net/kem.844.49

[4] Asgharzadeh S.R., Hubbell. C., Perez H., Hedengren J., Pixton D. Combined rate of penetration and pressure regulation for drilling optimization by use of high-speed telemetry. SPE Drill Complet 30(01), pp 17–26, 2015.

[5] Hossein Yavari, Mohammad Fazaelizadeh, Bernt Sigve Aadnoy, Rasool Khosravanian, Jafar Qajar, Mostafa Sedaghatzadeh, Masoud Riazi. An approach for optimization of controllable drilling parameters for motorized bottom hole assembly in a specific formation, Results in Engineering, Volume 20, 101548, 2023. ISSN 2590-1230, https://doi.org/10.1016/j.rineng.2023.101548

[6] Hankins D., Salehi S., Karbalaei S. F. An integrated approach for drilling optimization using advanced drilling optimizer. J Pet Eng 2015:281276, 2015.

[7] Ratov, B., Borash, A., Biletskiy, M., Khomenko, V., Koroviaka, Y., Gusmanova, A., Pashchenko, O., Rastsvietaiev, V., & Matyash O. Identifying the operating features of a device for creating implosion impact on the water bearing formation. Eastern-European Journal of Enterprise Technologies, 5(1 (125), pp 35–44. 2023. https://doi.org/10.15587/1729-4061.2023.287447

[8] Eren Tuna, Ozbayoglu, Evren. Real Time Optimization of Drilling Parameters During Drilling Operations. 10.2118/129126-MS, 2010. https://doi.org/10.1016/j.petrol.2015.07.027

[9] Yang Zhiyuan Liu, Yongsheng Qin, Xing Dou, Zijun Yang, Gansheng Lv, Jianguo Hu, Yuanbiao. Optimization of drilling parameters of target wells based on machine learning and data analysis. Arabian Journal for Science and Engineering. 48, 2022. https://doi.org/10.1007/s13369-022-07103-x

[10] Riazi M., Mehrjoo H., Nakhaei R., Jalalifar H., Shateri M., Riazi M., Ostadhassan M., Hemmati-Sarapardeh A. Modelling rate of penetration in drilling operations using RBF, MLP, LSSVM, and DT models. Scientific Reports, 12, 2022. https://doi.org/10.1038/s41598-022-14710-z

[11] Said, Mohammed & Pilgrim, Rick & Rideout, D. & Butt, Stephen. (2022). Theoretical Development of a Digital-Twin Based Automation System for Oil Well Drilling Rigs. https://doi.org/10.2118/208902-MS

[12] Ashena, Rahman & Rabiei, M. & Rasouli, Vamegh & Mohammadi, Amir & Mishani, Siamak. Drilling parameters optimization using an innovative artificial intelligence model. Journal of Energy Resources Technology. 143. 050902-1, 2021. https://doi.org/10.1115/1.4050050

[13] Bataee, Mahmood & Saleh, Mohseni. (2011). Application of Artificial Intelligent Systems in ROP Optimization: a Case Study. https://doi.org/10.2118/140029-MS

[14] Darwesh, Ali & Rasmussen, Thorkild & Al-Ansari, Nadhir. (2019). Controllable drilling parameter optimization for roller cone and polycrystalline diamond bits. Journal of Petroleum Exploration and Production Technology. https://doi.org/10. 10.1007/s13202-019-00823-1

[15] Andrade, Caetano & Saavedra, Luis & Tunkiel, Andrzej & Sui, Dan. (2021). Rotary steerable systems: mathematical modeling and their case study. Journal of Petroleum Exploration and Production Technology. 11. 2743-2761. https://doi.org/10.1007/s13202-021-01182-6

[16] Abbas, Ahmed & Alqatrani, Ghassan & Saba, Mortadha & Mohammed, Haider & Al-Bazzaz, Waleed. (2020). Application of Statistical Analysis to Optimize Rate of Penetration. https://doi.org/10.2523/IPTC-19825-MS

[17] Roohi A., Ashena R., Thonhauser G., Finkbeiner T., Gerbaud L., Rasouli V. An experimental investigation of drilling performance improvement using reaming while drilling. Journal of Energy Resources Technology, 144, pp 1-17, 2021. https://doi.org/10.1115/1.4052611

[18] Hadian M., Etesami D., Zhang W. A formation-based approach for modeling of rate of penetration for an offshore gas field using artificial neural networks. Journal of Natural Gas Science and Engineering. 95, 2021. https://doi.org/10.1016/j.jngse.2021.104104

[19] Zhang Qi-Zhi & LI, Wei-Xiao & SHA, Lin-Xiu. (2017). Drilling Parameters Optimization Based on Chaotic Multi-Objective Particle Swarm Optimization Algorithm. DEStech Transactions on Engineering and Technology Research. https://doi.org/10.12783/dtetr/iceeac2017/10730

[20] Mahasneh M. 2017. Optimization of weight on bit during drilling operation based on rate of penetration. International Journal of Oil, Gas and Coal Engineering. 5. 13-18, 2017. https://doi.org/10.11648/j.ogce.20170502.11

https://doi.org/10.5593/sgem2024/1.1/s06.78

PHYSICAL EXPERIMENTS REGARDING THE LINEAR PROPAGATION OF HYDROGEN EXPLOSIONS IN ENCLOSED SPACES

Phd. Ress. Eng. Gheorghe Daniel Florea[1]

Phd. Eng. Nicolae Ioan Vlasin[1]

Phd. Ress. Eng. Adrian Bogdan Simon-Marinica[1]

Phd. Ress. Eng. Cristian Raul Cioara[1]

Eng. Laurentiu Munteanu[1]

[1] National Institute for Research and Development in Mine Safety and Protection to Explosion, INSEMEX Petroşani, **Romania**

ABSTRACT

Hydrogen, known for its high flammability and potential explosive characteristics, presents significant challenges in safety engineering, particularly in enclosed spaces where explosions can lead to catastrophic consequences. This paper presents the results of physical experiments conducted to investigate the linear propagation of hydrogen explosions within confined environments. The experiments were designed to simulate real-world scenarios and assess the factors influencing the extent and characteristics of explosion propagation. Various parameters including initial pressure, hydrogen concentration, confinement geometry, and ignition source location were systematically varied to analyze their effects on explosion dynamics. The experimental setup involved controlled release of hydrogen into enclosed spaces followed by ignition under controlled conditions, utilizing a series of friable obstacles. High-speed imaging with use of Schlieren techniques, pressure measurements, and post-explosion analysis techniques were employed to characterize the explosion phenomena. The findings provide valuable insights into the mechanisms governing hydrogen explosion propagation in confined spaces and offer implications for enhancing safety measures and designing mitigation strategies in hydrogen-related applications. This research contributes to the advancement of knowledge in the field of explosion dynamics and provides a basis for further studies aimed at improving safety standards in hydrogen storage, transportation, and utilization systems.

Keywords: explosions, hydrogen, ignition, experimental stand, Schlieren techniques

https://doi.org/10.5593/sgem2024/1.1/s06.79

INTRODUCTION

In an era marked by growing concerns about climate change and energy security, hydrogen has emerged as a promising alternative to fossil fuels[1], offering significant prospects in the field of sustainable energy.

This work focuses on investigating how hydrogen explosions occur in enclosed spaces, aiming to better understand the associated phenomena and their implications. We expect the results of these experiments to make significant contributions to areas such as industrial safety, the development of hydrogen-based energy technologies, and the formulation of safety regulations.

By analyzing the results of the experiments and interpreting them in the context of existing theory, we aim to shed light on how hydrogen interacts with its surrounding environment in scenarios of explosion in enclosed spaces. Understanding these interactions is essential for the development of safer and more efficient technologies that utilize hydrogen as a clean and sustainable energy source.

Therefore, this work represents an important step in researching and understanding the behavior of hydrogen in enclosed environments, with the potential to contribute to advancing knowledge and developing practical applications in the field of sustainable energy.

Through rigorous experiments, meticulous analysis, and interdisciplinary collaboration, "Physical Experiments Regarding the Linear Propagation of Hydrogen Explosions in Enclosed Spaces" aims to push the boundaries of our understanding, paving the way for safer, more efficient, and more sustainable hydrogen-based technologies. As we embark on this journey of discovery, let us not only unlock the secrets of hydrogen's explosive nature, but also harness its immense potential to bring about positive change for future generations.

HYDROGEN EXPLOSIVE PROPERTIES

Hydrogen is considered an important new energy carrier, meaning it can store and deliver energy in a usable form. At a standard temperature and pressure (0°C and 1013 hPa), we can discover hydrogen in a gaseous form. It is odorless, colorless, tasteless, non-toxic and lighter than air. The stoichiometric fraction of the mixture air and hydrogen is 70.4 % volume fractions of air and 29.6 % volume fractions of hydrogen, and for the mixture of oxygen and hydrogen, the stoichiometric fraction is 66.66 % volume fractions of air and 33.33 % volume fractions of oxygen. Abundant on Earth as an element, hydrogen is present everywhere, representing 75 % mass fractions of 90 % volume of al matter. Being an energy carrier, hydrogen is not an energy source itself, it can only be produced from other energy sources such as fossil fuels, renewable sources or nuclear energy through various energy conversions processes. The exothermic combustion reaction with oxygen forms water (combustion heat 1.4 x 108 J/kg-1) and no carbon greenhouse gases are emitted into the atmosphere during the combustion [2].

The energy content of hydrogen is 33.3 kWh/kg-1 corresponding to 120 MJ/ kg-1 (the lower thermal power value) and 39.4 kWh/kg-1 corresponding to 142 MJ/kg-1 (the higher thermal power value). The difference between the lower and higher calorific value is the molar enthalpy of the vaporization of water, which is 44.01 KJ/mol-1. We can obtain a higher thermal power as a result of burning hydrogen in the process of

steam production, while the lower thermal power is obtained when the produced water is condensed back into liquid [3], [4], [5].

Compared to other fuels such as methanol, gasoline, diesel or kerosene, it is obvious that hydrogen produces much more energy per weight unit than any other fuel (about three times that of gasoline, diesel or kerosene) and can be dangerous to handle. The flammability range is the highest for hydrogen, but as long as it remains in an area that is properly ventilated there will be no risk of reaching this flammability range.

Furthermore, hydrogen has an ignition temperature of 560° C, unlike gasoline, which has an ignition temperature of 280° C. Hydrogen ignites very easily and burns with a wide range of mixtures with oxygen or air, compared to any other fuel [3]. Compared to most hydrocarbons, we find that hydrogen has a large flammability range, from 4 % volume fractions (lower flammability limit) up to 75 % volume fractions (upper flammability limit) in air, from 4 to 95 % volume fractions in oxygen and the detonation from 11 to 59 % volume fractions in air. These flammability limits increasing with temperature, for example the lower limit decreases from 4 % volume fractions at normal temperature and pressure (20°C and 1 atmosphere) to 3 % volume fractions at 100° C. Referring to these values, hydrogen has a very low minimum ignition energy of 0.017 MJ in air and 0.0012 MJ in oxygen at 25°C and 1 bar pressure. Regarding a comparison, the minimum ignition energy for most fuels is the range of 0.1 – 0.3 MJ, and for the oxygen they are at least an order of magnitude smaller [6].

As a brief reminder regarding hydrogen's explosive properties, we note that hydrogen can be easily ignited in the presence of an ignition source, such as a spark, flame, or even a surface with high temperature [7], [8]. Once ignited, hydrogen burns with an invisible flame, producing ultraviolet light. Additionally, hydrogen burns extremely rapidly and has rapid flame expansion.

MATERIALS AND METHODS

- **Experimental configuration**

The experimental configuration used in this study was designed to analyze the linear propagation of explosions resulting from mixtures of air and hydrogen. It consisted of a precise and robust measurement system that allowed for the accurate monitoring and recording of parameters [9].

In order to achieve the intended purpose, the experimental setup had to meet the following conditions:

- be of adequate size for laboratory work;
- provide safety for workers and the work environment;
- include a system for initiating explosive atmospheres, powered by a direct current source;
- the explosion chamber had to be transparent for video recording of the rapid oxidation phenomenon;
- include a system for highlighting the Schlieren effect;
- include a high-speed camera for video recording;
- allow for adjustment of distances between stand components to maximize the efficiency of the Schlieren effect.

https://doi.org/10.5593/sgem2024/1.1/s06.79

Schlieren techniques are optical methods used to observe refractive index gradients in gases, especially air, or in other transparent media. These gradients can be generated by differences in temperature, pressure, and density; a gas medium at high temperature has a lower density (and therefore a lower refractive index) than the same medium at normal temperature.

Figure 1 shows a simple Schlieren configuration, where a light beam is projected from a source onto a parabolic mirror, and the reflected light is recorded by the video camera. A knife edge placed at the focal point of the mirror acts as a filter for light intensity, with any ray refracted by a medium with different density (A-B) illuminating the camera sensor with a different intensity, resulting in increased contrast.

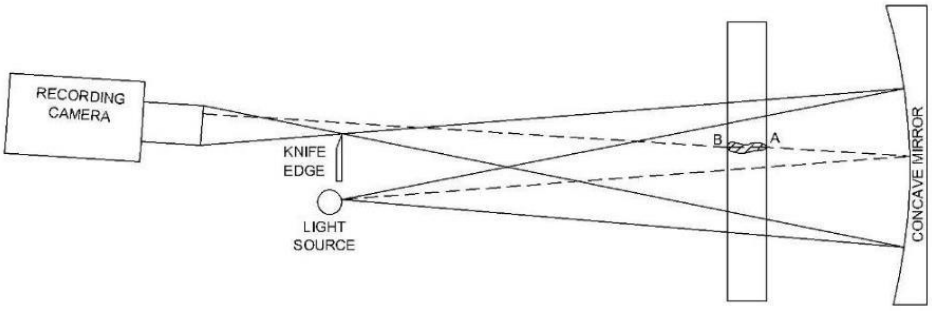


Fig. 1. The layout of a basic Schlieren setup

- **Development and instrumentation of the experimental model for analyzing the linear propagation of explosions caused by air-hydrogen mixtures**

The structural material of the experimental model for analyzing the linear propagation of explosions was selected as 20 mm thick polycarbonate sheet, due to its transparency and superior resistance to shocks and high pressures (Fig. 2.).

Keeping in mind the safety of conducting experiments, the interior section of the explosion tunnel was set at dimensions of 50 x 30 mm, with the length of the stand being 1040 mm and resulted in an internal volume of 1,56 liter.



Fig. 2. Progress during the construction and finalization of the linear model

For sealing, gaskets were crafted on the upper and lower closing plates of the model. Additionally, at various intervals along the median line, three rectangular shutters were constructed and mounted, each consisting of two plates with two 12 mm diameter holes.

Transparent plastic film was inserted between the plates to separate the tunnel into distinct chambers (Fig. 3). The first chamber, designated for initiating the air-hydrogen mixture, was outfitted with electrodes for generating electric sparks, a cap device for introducing hydrogen, and a pressure sensor. Chambers 2 and 3 were equipped with a cap device for hydrogen introduction and a pressure sensor each, while the fourth chamber only housed a pressure sensor.



Fig. 3. Arrangement of the construction between parabolic mirrors and the transparent frame for high speed video recordings

The linear stand construction was positioned between two parabolic mirrors, with the Schlieren technique adopted. This technique involved the projection of a light beam in the shape of the letter Z, with the parallel light beam passing vertically through the interior of the construction. Eventually, it was focused by the upper mirror onto the objective of the high-speed camera for video recordings.

RESULTS

The physical experiments conducted on the previously described setup aimed, in the first stage, at testing the image recording and pressure measuring equipment during the explosion process. Attention was also paid to the structural integrity of the linear construction under the developed overpressures inside it, the occurrence of leaks, and the resolution of these deficiencies. Adjusting the parabolic mirrors and the equipment necessary for video recordings was also an important step in setting up the entire stand to achieve quality results.

Concentrations of 20% volume hydrogen in air [10] were used to charge the three separate chambers with the previously described foil-covered orifice shutters. The volumes of the three chambers were 157.5 ml (chamber 1), 138 ml (chamber 2), and 193.5 ml (chamber 3), with the remainder of the explosion path left open to clean air (fig. 4).

https://doi.org/10.5593/sgem2024/1.1/s06.79

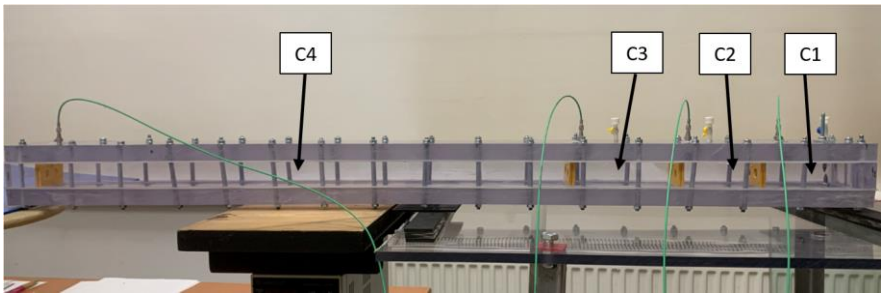


Fig. 4. Experimental model for analyzing the linear propagation of explosions

Video recordings were made using a high-speed Phantom camera, at a frequency of 30,000 frames per second. Images of the flame front behavior were recorded at a speed of 30,000 frames per second with the high-speed camera.

During this experiment, the flame front traversed all three chambers, breaking the foil shutters and extinguishing upon the fuel gas depletion (Figure 5-9).



Fig. 5. Initiation of the explosive mixture air-hydrogen



Fig. 6. The flame front at the beginning of the explosion process in the first chamber

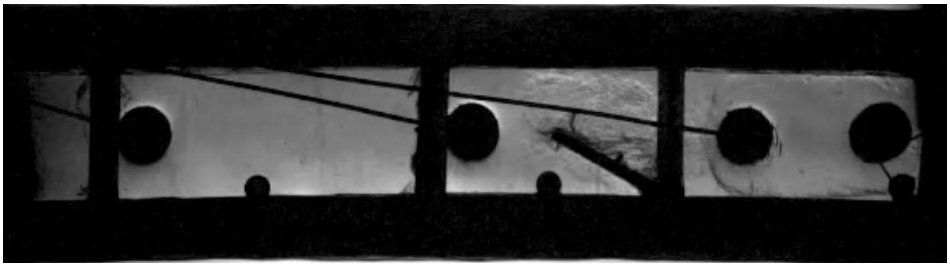


Fig. 7. The advance of the flame front into the second chamber.



Fig. 8. Propagation of the flame front in chamber 3



Fig. 9. Expansion of the explosion into chamber 4

The recorded pressure values can be found in the graph in Figure 7. An increase in pressures can be observed as we advance along the linear tube trajectory. A detailed investigation of the behavior of the pressure waves generated inside the experimental setup may be the subject of future research.

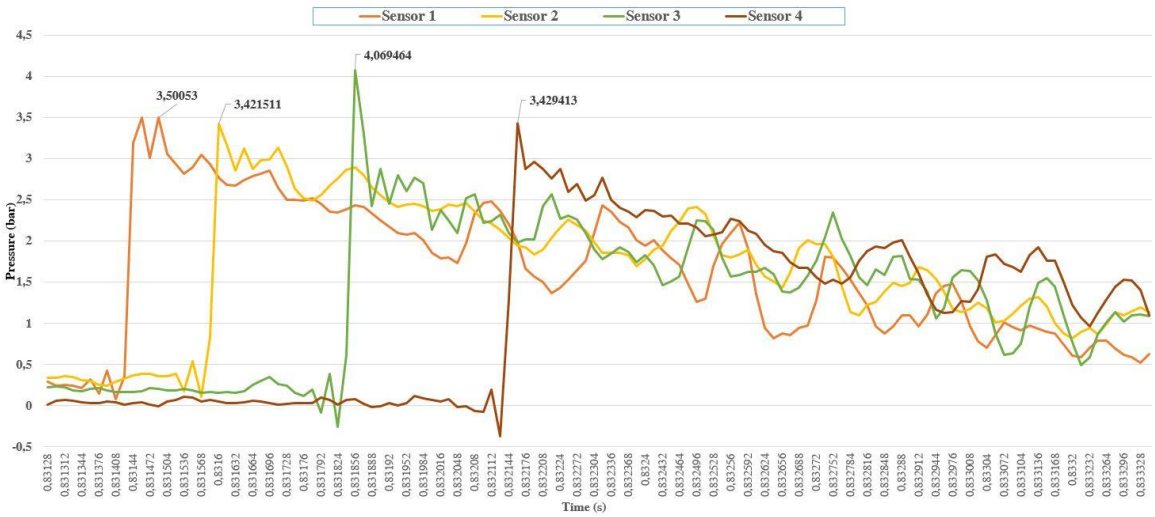


Fig. 10. Graphic display of the pressures recorded

CONCLUSION

Following the physical experiment of the air-hydrogen explosion, it was observed that the selection of construction materials and the assembly method of the elements were appropriate decisions, as the experiments proceeded safely. No cracks, fractures, or displacements were detected in the structural integrity of the models. The movements of the shutters are anticipated dynamic effects, typically generated by explosion overpressures.

https://doi.org/10.5593/sgem2024/1.1/s06.79

Thus, the conducted experiment demonstrates the functionality of the experimental model, both in terms of recording explosion pressures and visualizing and recording the behavior of the flame front, as well as ensuring safety in operation.

From the graph obtained with the recorded pressures, it can be observed that the maximum pressure recorded was in chamber number 3. The movement of pressure in the linear stand can be compared to the movement of a piston causing a variation in volume inside a chamber (the piston principle). Due to the lack of combustible support, towards the last chamber, the explosion extinguishes and the pressure decreases.

The experimental setup and the use of Schlieren techniques represent valuable tools for researching and understanding hydrogen explosions. Not only do they help us observe and record the behavior of the flame front in real time, but they also allow us to evaluate and improve theoretical models, which significantly impacts the development of more effective safety strategies in various industrial and scientific fields.

ACKNOWLEDGEMENTS

This work was carried out through the ”Nucleu” Program within the National Plan for Research, Development and Innovation 2022-2027, with the support of the Romanian Ministry of Research, Innovation and Digitalisation, project no. 23 32 02 02, title: Numerical modelling on the ignition and propagation of explosions generated by air-hydrogen mixtures – H2Model.

REFERENCES

[1] Calamar A.N., Gaman G.A., Kovacs M., Pupazan D., Lorand T. Analysis of polluant imissions generated by bone meal production, Quality-access to succes, 18, pag. 178-183, ISSN 1582-2559, 2017

[2] Xing, HD; Yu, RZ; Xu, GA; Li, XD; Qiu, YY; Wang, DR; Li, B; Xie, LF, Theoretical and experimental investigation of explosion characteristics of hydrogen explosion in a closed vessel, Energies, Vol. 15, Issue 22, 2022

[3] Petrilean D.C., Irimie S.I., Operational influence on the energetic efficiency of a gas cogenerated operated electricity generator, Journal of environmental protection and ecology. 1,17(4):1464-71, 2016

[4] Pasculescu V.M., Vlasin N.I., Ghicioi E., Florea G.D., Suvar M.C., New tools for estimating the extent of hazardous areas generated by gas leak explosions, Environmental Engineering and Management Journal, Vol. 18, Issue 4, ISSN 1582-9596, 2019

[5] Shi, JH; Chang, B; Khan, F; Chang, YJ; Zhu, Y; Chen, GM; Zhang, CJ, Stochastic explosion risk analysis of hydrogen production facilities, International Journal of Hydrogen Energy, Vol. 45, Issue 24, ISSN 0360-3199, 2020

[6] Simon A. B., Arad S., Samoila L., Monitoring systems in explosive and potentially toxic environments for reducing risk factors, 5th International Symposium on Electrical and Electronics Engineering (ISEEE), Galati, Romania, pp. 1-5, 2017

[7] Păsculescu D, Romănescu A, Pasculescu V, Tătar A, Fotău I, Vajai G. „*Presentation and simulation of a modern distance protection from the national energy system”*,

In10th International Conference of Environment and Electrical Engineering, Rome, Italy, pp. 6-11, 2011

[8] Florea, G. D., #Petrilean, D. C., Computational Simulation of Methane Ignition in Enclosed Spaces, Mining Revue, 30(1), 58-67, 2024

[9] Prodan, M., Szolloşi-Moţa, A., Nalboc, I., Suvar, S., Ghicioi, E., Explosion limits experimental determination for gasoline, diesel fuel and acetone vapors, International Multidisciplinary Scientific GeoConference: SGEM 23, Albena, Bulgary (1.1), 333-340, 2023.

[10] Jurca, A.M., Păun, F.A., Popa, M.C., 2024. Ignition risk assessment to the non-electrical equipment from hydrogen production, storage, transport and use facilities. In MATEC Web of Conferences (Vol. 389, p. 00035). EDP Sciences.

https://doi.org/10.5593/sgem2024/1.1/s06.79

PRACTICAL ASPECTS OF IMPROPER INSTALLATION AND MAINTENANCE OF EQUIPMENT INTENDED TO BE USED IN POTENTIALLY EXPLOSIVE AREAS AND RECOMMENDED MEASURES

Sc. Res. I Ph.D Eng. Tiberiu Csaszar[1]

Sc. Res. I Ph.D Eng. Cosmin Colda[1]

Sc. Res. III Ph.D Eng. Danut Grecea[1]

Sc. Res. III Ph.D Eng. Gabriela Pupăzan[1]

Eng. Alexandru Beldiman[1]

[1]National Institute for Mine Safety and Protection to Explosion -INSEMEX, Petroşani - **Romania**

ABSTRACT

In the evaluation activity of technical equipment intended to be used in potentially explosive atmospheres, by national and international legislation, non-compliant aspects were often reported regarding the choice, installation and maintenance of this explosion-proof equipment. The following main aspects were pointed out: the equipment that was initially chosen and installed appropriately for the specific application but later, over time, improperly maintained; respectively, the situation in which they were inappropriately selected from the beginning for the intended application, by ignoring the existing hazard due to the presence of potentially explosive atmospheres. Both reported situations could induce major hazards in the short or long-term operating conditions of the respective equipment, which can become an effective source of ignition of the atmospheres endangered by the presence of explosive mixtures within the flammability limits.
The work is intended to be a warning signal regarding the negative aspects detected during the evaluation activity and also provides solutions for their remedy.

Keywords: installation, maintenance, evaluation activity, explosion-proof equipment

INTRODUCTION

An explosive atmosphere [1] is defined as a mixture with air, under atmospheric conditions, of a flammable material mixed with air in which, after ignition, the combustion propagates throughout the whole unconsumed mixture. In situations where an explosive atmosphere may occur, the following measures should be provided:

- eliminate the probability of an explosive atmosphere occurring near the ignition source, or
- eliminate sources of ignition.

Installations where flammable materials are handled or stored must be designed, operated and maintained in such a way that all releases of flammable materials, and consequently

https://doi.org/10.5593/sgem2024/1.1/s06.80

the extent of hazardous areas, are kept to a minimum, in terms of frequency, duration and quantity.

If these measures cannot be applied, preventive measures must be chosen and applied, so that the probability of the simultaneous occurrence of the two elements listed above is brought to a sufficiently low level to be accepted.

For an explosive atmosphere to exist, the flammable substance must be present in certain concentrations. If the concentration is too low (poor mixture) or too high (rich mixture) no explosion can occur a weak combustion reaction may occur but not a reaction in the whole mixture. Thus, the explosion can occur only in the presence of an ignition source and when the concentration is in the explosive range of the substance, respectively between the lower flammability limit (LFL) and the upper flammability limit (UFL) [1].

Hazardous areas are classified into three zones, according to the frequency of occurrence and duration of the presence of explosive gas mixture generated as follows [2]:

- Zone 0 - an area where the explosive atmosphere is present permanently, or for long periods.
- Zone 1 - an area in which the explosive atmosphere is likely to occur in normal operation.
- Zone 2 - an area in which an explosive atmosphere is not likely to occur during normal operation and in which, if it does occur, it is likely to occur only rarely and only for a short period.

In determining where a release of flammable gas or vapour may occur, the likelihood and duration of the release should be assessed by the definitions of continuous, primary and secondary grades of release. Once the grade of release, the release rate, concentration, velocity, ventilation and other factors are assessed there is then a firm basis on which to assess the likely presence of an explosive gas atmosphere in the surrounding areas and determine the type and/or extent of the hazardous zones.

The source of the release approach can be summarized as follows:

- identify sources of release;
- determine the release rate and grade of release for each source, based on likely frequency and duration of release;
- assess ventilation or dilution conditions and effectiveness;
- determine zone type based on the grade of release and ventilation or dilution effectiveness;
- determine the extent of the zone.

Hazardous area classification is a method of analysis and classification of the environment in which gaseous explosive atmospheres may occur, to facilitate the correct choice and installation of usable equipment without generating a hazard in this environment. This is done by taking into account the gas groups gas temperature classes and ignition temperature [3].

Starting from the explosion protection principles stated above, Table 1 summarises the requirements for technical equipment, electrical and non-electrical, depending on the intended use [4], [5].

Table 1 - Requirements for technical equipment depending on the intended use

ZONE	The presence of an explosive atmosphere	Avoiding sources of ignition	Required level of protection
0	Continuous, frequent or for long periods	Also, during rare failures (two independent faults)	VERY HIGH
1	Likely to occur	Also, during predictable failures	HIGH
2	Unlikely or only for a short period	During normal operation	NORMAL
Requirements for users		Requirements for manufacturers	
Directive 1999/92/EC approved by HG 1058/2006		**Directive 2014/34/EU approved by HG 245/2016**	

In particular, the following categories of equipment must be used in the zones indicated, provided they are suitable for gases, and vapours as appropriate [2]:

- in zone 0, category 1 equipment is permitted, and equipment protection level (EPL): Ga;
- in zone 1, category 1 or 2 equipment is permitted, and equipment protection level (EPL): Ga or Gb;
- in zone 2 categories 1, 2 or 3 equipment is permitted, and equipment protection level (EPL): Ga, Gb or Gc

The probability of ignition is higher in zone 0 than in zone 1 or zone 2. The technical equipment used in these zones must therefore ensure an adequate level of safety.

On the other hand, the performance of the types of protection, indicated by the Equipment Protection Level (EPL), allows equipment protected with these types of protection to be used only in certain zones. The EPL levels provided are summarised in the diagram in Figure 1.

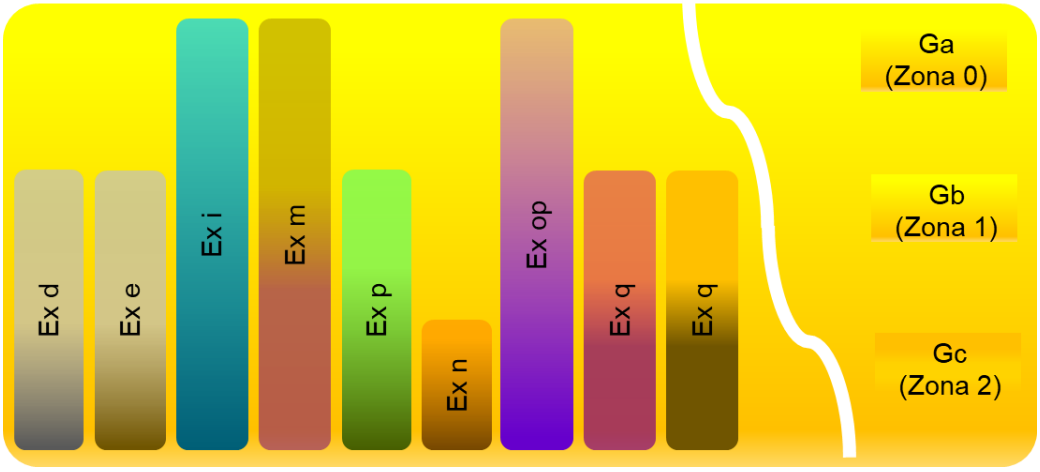


Figure 1. Explosion protection performance - protection level (Ex zone).

https://doi.org/10.5593/sgem2024/1.1/s06.80

REQUIREMENTS FOR ELECTRICAL EQUIPMENT

Electrical equipment for potentially explosive atmospheres must comply with the requirements of the general specific standard and the specific standards to the type or types of protection that were used for the construction of that device. The types of protection for electrical equipment intended for use in explosive atmospheres generated by gases and vapours can be grouped into three categories, depending on the presence of the ignition source and the potentially explosive atmospheres [2]:

- types of protection that allow direct contact between the ignition source and the hazardous atmosphere (eg. flameproof enclosure “d”, intrinsic safety “i”).

- types of protection that do not allow direct contact between the ignition source and the hazardous atmosphere (eg. oil immersion ”o”; pressurized enclosure ”p”, powder filling ”q”, encapsulation “m”).

- types of protection which by construction try to eliminate the ignition source under specified conditions (eg. increased safety "e").

This classification is in fact, a ranking of the level of safety offered by each type of protection.

A very important aspect that must be taken into account when installing electrical equipment intended to be used in potentially explosive atmospheres is the choice of cable entry systems and sealing elements, in order not to endanger the type of protection (e.g. flameproof enclosure “d”) [6].

Cable entries, adapters and blanking elements must follow the specific standard requirement and must be chosen to maintain the requirements of the method of protection in accordance with the type of protection [2], [6], according to Table 2.

Table 2. Selection of cable entries, adapters and blanking elements

Protection method for equipment	**Protection method for cable entries, adapters and blanking elements**		
	Ex „d”	Ex „e”	Ex „n”
Ex „d”	X		
Ex „e”	X	X	
Ex „i”	X	X	X
Ex „m”	Ex "m" would not normally apply to connections. The protection method for the connections must correspond to the cable system used		
Ex „n”	X	X	X
Ex „o”	Ex "o" would not normally apply to connections. The protection method for the connections must correspond to the cable system used		
Ex „p”	X	X	X
Ex „q”	Ex "q" would not normally apply to connections. The protection method for the connections must correspond to the cable system used		

Cable entries must be installed in such a way that, after installation, they can only be loosened or removed using a tool. If additional fastening is required to prevent cable pulling and twisting from transmitting forces to the conductor ends inside the housing. A clamp should be provided with the cable as close as possible to the cable entry.

The connection of cables to electrical equipment must be made through cable entries appropriate to the type of cable used and must maintain the integrity of the relevant explosion protection type. Where the threaded entry or hole size is different from the cable entry, a threaded adapter must be provided in accordance with Table 2.

The assessment of technical installations operating in potentially explosive atmospheres is of high importance considering the existing explosion risk [4], [7]. The assessment applies to all installations operating in potentially explosive atmospheres for example: installations for oil and gas extraction, transport, storage and processing, or gas stations, etc. When performing the assessment, the provisions of applicable standards and regulations in force are used. Some common issues that were found during the assessment are:

1. Location of electrical equipment in normal construction in Ex classified areas



Image 1. - Non-Ex equipment found in Ex classified areas: electronic cash register near of fuel dispenser.

2. Modifications to the certified Ex equipment compromise the Ex certifications and invalidate the Ex “d” type to explosion protection [8].

...  

Image 2, 3 - Example of the improper choosing Ex “m” protection type cable entry for Ex “d” type to explosion protection equipment

https://doi.org/10.5593/sgem2024/1.1/s06.80

3. Lack of mandatory maintenance preventive operations in case of failure or damage on Ex equipment [7], [9]




Image 4, 5 - Example of improper mandatory maintenance applied to Ex equipment.

4. Not allowed drilling, in the explosion-proof encapsulation, of the holes for the cable glands and incorrectly chosen of them, for the type of protection of the stripped housing [8]

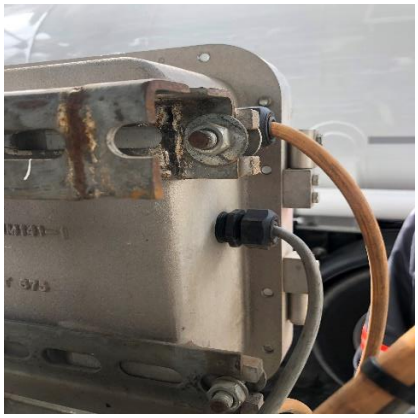


Image 6 - Unauthorised modification of Ex construction equipment

5. Non-compliance with electrical separation requirements distances [10], between circuits with intrinsic safety “i” and those without intrinsic safety [11].

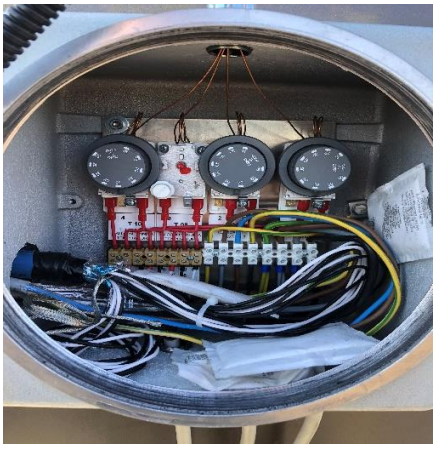


Image 7 - Non-compliance with electrical isolation and circuit distances.

RECOMMENDED MEASURES TO MAINTAIN THE SECURITY LEVEL OF TECHNICAL EQUIPMENT OPERATING IN POTENTIALLY EXPLOSIVE ATMOSPHERES

Any equipment designed for use in potentially explosive atmospheres placed on the market after the conformity assessment procedures of the ATEX Directive were applied, the explosion protection characteristics can be altered due to multiple factors [1]:

- an incorrect selection of the equipment according to the final destination;
- an incorrect design of the installation in which the product is going to be incorporated;
- not performing mandatory periodic inspections for the certified Ex equipment;
- inadequate performance of inspection operations and maintenance of equipment;
- unauthorised modifications to Ex certified equipment;
- inadequate repairs applied to the certified Ex equipment.

For the above-mentioned operations that can compromise the explosion protection characteristics, only the manufacturer instructions and the requirements of the ATEX Directive are not enough. In these conditions, the member states adopted their legislation regarding those issues. In Romania, in 2007 after the adhesion to the EU, the normative document was adopted [9]. According to this norm at the commissioning of a technical installation operating in potentially explosive atmospheres, a verification of the technical documentation and an on-site assessment must be performed. This is to assess the technical installation to check if all the measures required to ensure protection against explosion are adopted, especially those regarding the equipment/protective systems used in Ex classified areas [7].

ACKNOWLEDGEMENTS

This work was carried out through the “Nucleu” program of the National Research, Development and Innovation Plan 2022-2027, supported by MCID, project no. PN23320102.

This paper is the result of the author's field research and "in-site" evaluation work, on the assessment of equipment and installations operating in potentially explosive atmospheres.

CONCLUSION

Even if a product designed for use in potentially explosive atmospheres is placed on the market considering the conformity assessment procedures of the ATEX Directive 2014/34/EU, the explosion protection characteristics can be altered due to multiple factors such as incorrect selection of the equipment, incorrect installation of the product, inadequate maintenance of equipment, or unauthorised modifications to Ex certified equipment.

Assessing the risk of an explosion due to the operation of electrical and non-electrical equipment in hazardous areas is a complex task that must be carried out by qualified and experienced personnel.

Some examples of non-conformities identified during the assessment were shown in this paper. Also, information was presented regarding how to improve the activities: design, mounting, inspection, and maintenance, carried out about installations operating in

https://doi.org/10.5593/sgem2024/1.1/s06.80

potentially explosive atmospheres to preserve explosion protection characteristics for ATEx dedicated equipment.

In Romania, the NEx 01-06 regulation is in force and it was adopted in 2007. At the commissioning of a technical installation operating in potentially explosive atmospheres, a verification of the technical documentation and an on-site assessment must be performed by ATEX experts within INSEMEX - Petroşani.

REFERENCES

[1] SR EN IEC 60079-10-1- Explosive atmospheres - Part 10-1: Classification of areas - Explosive gas atmospheres, ASRO, 2021

[2] Standard EN 60079-0: Explosive atmospheres - Part 0: Equipment - General requirements, 2018

[3] Prodan, M., Ghicioi E., Lupu C., Nălboc., Szollosi-Mota A.,- Flammability characterization of a petroleum derivative for increasing the safety of personnel and environmental protection, International Multidisciplinary Scientific GeoConference: SGEM; Sofia, Vol. 4, 2016.

[4] Directive 2014/34/EU of the European Parliament and of the Council of 26 February 2014 on the harmonisation of the laws of the Member States relating to equipment and protective systems intended for use in potentially explosive atmospheres

[5] Directive 1999/92/EC of the European Parliament and of the Council of 16 December 1999 on minimum requirements for improving the safety and health protection of workers potentially at risk from explosive atmospheres, 1999

[6] SR SR EN 60079-14 - Explosive atmospheres - Part 14: Electrical installations design, selection and erection, ASRO, 2014

[7] Normative NEx 01-06 - Normative on explosion prevention for design, erection, commissioning, use, repair and maintenance of technical installations operating in atmospheres potentially explosive atmospheres, 2007

[8] Fotau D., Colda C., Burian S., Friedmann M., Magyari M, Moldovan L., Aspects Regarding the Use and Maintenance of Electric Equipments to Be Used in Explosive Atmospheres Protected by Flameproof Enclosures, Proc. 1st International Conference on Electronics and Electrical Engineering, Valencia, Spain, 113-116, 2013.

[9] SR EN 60079-17 - Explosive atmospheres - Part 17: Electrical installations inspection and maintenance, ASRO, 2014

[10] SR EN 60079-11 - Explosive atmospheres - Part 11: Equipment protection by intrinsic safety "i", ASRO, 2012.

[11] Darie M., Burian C., Csaszar T., Colda C., Grecea D., - Separation fault scenarios in intrinsic safety circuits, Environmental Engineering and Management Journal, Romania, 18 (4), pp 797-802, 2019

PREVENTING PIPE STICKING IN OIL AND GAS WELLS USING AN IMPROVED TORQUE AND DRAG MODEL, ALONG WITH ANALYTICAL AND MACHINE LEARNING METHODS

Assistant Professor, PhD, Dr. Aizada B. Sharaouva[2] / Machine Learning Engineer, Bs of Computer Science, Myrzanov Beket Senior lecturer, Dinara N. Delikesheva[1]

[1] Atyrau University of Oil and Gas, Atyrau, **Kazakhstan**

[2] Satbayev University, Almaty, **Kazakhstan**

ABSTRACT

Effectively preventing pipe sticking in oil and gas wells is a key aspect of safety and productivity in the oil and gas industry. This paper presents a new torque and drag model developed using machine learning techniques to improve accuracy and predictive capabilities. The model is based on a comprehensive analysis of many factors, including geological characteristics of the well, drilling parameters, fluid parameters, hydraulic conditions, and production equipment parameters. This research explores the application of a chained regression model combining Multilayer Perceptron (MLP) and XGBoost for predicting multiple physical properties in the oil and gas industry. The study aims to enhance prediction accuracy in hydraulics, torque, and drag by leveraging the strengths of both models. The model will help improve the monitoring and interpretation of drilling data streams. Besides the model will help detect signs of other interfering problems in the downhole wellbore conditions and take the necessary measures in advance to prevent them. As a result, it will help optimize costs, minimize non-productive time, and improve safety.

Keywords: torque and drag, machine learning, drilling, pipe sticking, regression model.

INTRODUCTION

With the increasing availability of data, machine learning has become an active field of research over recent decades. It has been widely used in various fields such as finance, healthcare, entertainment, and the oil and gas industry. Machine learning's ability to learn and approximate almost any function has led to its exploration in classification and regression tasks [1]. Historically, the oil and gas industry, requiring high precision, has been slow to adopt automation and replace manual human labor. However, with innovative algorithms in artificial intelligence and machine learning, this trend is changing [2-3]. This paper focuses on using stacked regression models, specifically Multilayer Perceptron (MLP) and XGBoost, to predict multiple physical properties in hydraulics, torque, and drag.

Data from a variety of sources was used to develop the model, including historical stuck data, geological surveys and well test results. Using machine learning techniques such as neural networks, deep learning algorithms and regression analysis to generate features to identify deep connections, Ridge and Xgboost models were trained on this data,

https://doi.org/10.5593/sgem2024/1.1/s06.81

identifying complex relationships and patterns, including sinusoidal and spiral bends, that can lead to tacks. The greatest advantage of this model, based on historical data, is the automatic self-improvement and addition of the database.

This model is used to determine measured weights and moments in special operations, on-bottom rotation, above-bottom rotation, steered drilling, and reverse drilling. Such information can be used to determine whether a well can be drilled or to evaluate the condition of the wellbore during drilling.

After the model was trained, validation was carried out using the internationally recognized WellPlann software. The results showed that the model has a high accuracy in predicting sticking, with an error of no more than 8% (standard scaler) compared to the predictions and calculations made by the WellPlann software. This approach allows oil and gas well operators to make more informed decisions and take precautions to prevent sticking, which significantly improves the safety and efficiency of well operations.

MATERIALS AND METHODS

The stacking model consists of two state-of-the-art models: Multilayer Perceptron and XGBoost regressor. An MLP is a type of neural network that includes an input layer, one or more hidden layers, and an output layer [4]. It is suitable for classification and regression prediction problems and handles tabular datasets effectively. The XGBoost regressor is a powerful machine learning algorithm known for its efficiency and accuracy in handling regression tasks, excelling in capturing complex relationships between input features and target variables, and providing high predictive performance.

The first training phase involves training and obtaining cross-validated predictions from the MLP. In the second phase, MLP predictions are appended to the input data, and the XGBoost Regressor is trained on this augmented input data. Figure 1 illustrates the basic principle of chained regression. The rationale for using two models is that MLP can be sensitive to noisy data and produce incorrect outputs; therefore, XGBoost is used as the final estimator due to its robustness and resistance to overfitting. The MLP has 2 layers with 64 and 42 nodes, respectively. The XGBoost regressor consists of 100 trees with a depth of 5 and a subcolumn rate of 0.9. All the input and target data was normalized using normal distribution.

The model was trained on data from two oil wells (moldabek2737 and aktobe120) and evaluated on an unseen well dataset (balgimbayev245). The primary metric used was the Weighted Mean Absolute Percentage Error (WMAPE), which measures forecast accuracy by accounting for the size of the actual values, providing a more balanced error metric compared to the traditional Mean Absolute Percentage Error (MAPE).

Chained regression model of forecast accuracy that accounts for the size of the actual values, providing a more balanced error metric compared to traditional MAPE (Mean Absolute Percentage Error):

$$wMAPE = \frac{\sum_{i=1}^{n}|A_i - F_i|}{\sum_{i=1}^{n}|A_i|}$$

where A_i - is actual value, F_i - is forecast value, n - is total number of observations.

RESULTS

Table 1. wMAPE scores in evaluation dataset

index	wmape	type
Lifting	0.06	ves_na_kru
Derrick load capacity	0.48	ves_na_kru
Drilling with a hydraulic downhole motor	0.18	ves_na_kru
Rotary drilling	0.14	ves_na_kru
Minimum weight before helical buckling (descent)	0.29	ves_na_kru
Maximum weight to yield limit (lifting)	0.31	ves_na_kru
Descent	0.11	ves_na_kru
Lifting	3.94	effect_na
Derrick load capacity	0.00	effect_na
Drilling with a hydraulic downhole motor	3.40	effect_na
Rotary drilling	6.62	effect_na
Helical buckling (with rotation)	0.47	effect_na
Sinusoidal buckling (all operations)	0.47	effect_na
True vertical depth	0.85	effect_na
Descent	7.21	effect_na
Tension limit	0.38	effect_na
Helical buckling (without rotation)	0.47	effect_na
Lifting	0.00	moment
Make-up Torque	0.13	moment
Rotary drilling	0.16	moment
Torque	0.13	moment
Descent	0.00	moment
Minimum weight on bit before sinusoidal bending (rotary drilling)	0.51	min_ves
Minimum weight on bit before sinusoidal buckling (drilling with a hydraulic downhole motor)	0.26	min_ves
Minimum weight on bit before helical buckling (rotary drilling)	0.45	min_ves
Minimum weight on bit before helical buckling (drilling with a hydraulic downhole motor)	0.17	min_ves

The wMAPE across different domains are not homogeneous.

To identify key drilling parameters to create a model, the following work was done:

The first and very important part in completing the task is processing and analyzing data using mathematical statistics methods [5]:

High-quality data sampling (filtering - filtering out “extra” data and sorting data; calculation of variation, which is characterized by the range of variation (R=xmax - xmin), the average linear deviation, dispersion and standard deviation are calculated.

The Pearson correlation (r) coefficient was calculated, according to which the key parameters (input data) were selected.

After training the model on historical data, it built a model for a new, previously unseen well, the drilling parameters of which were identified satisfactorily in comparison with

https://doi.org/10.5593/sgem2024/1.1/s06.81

the results of WellPlan software from Haliburton. Below we present graphs for visual comparison and analysis of the model. Comparison of Hook load values (Fig.1-2).

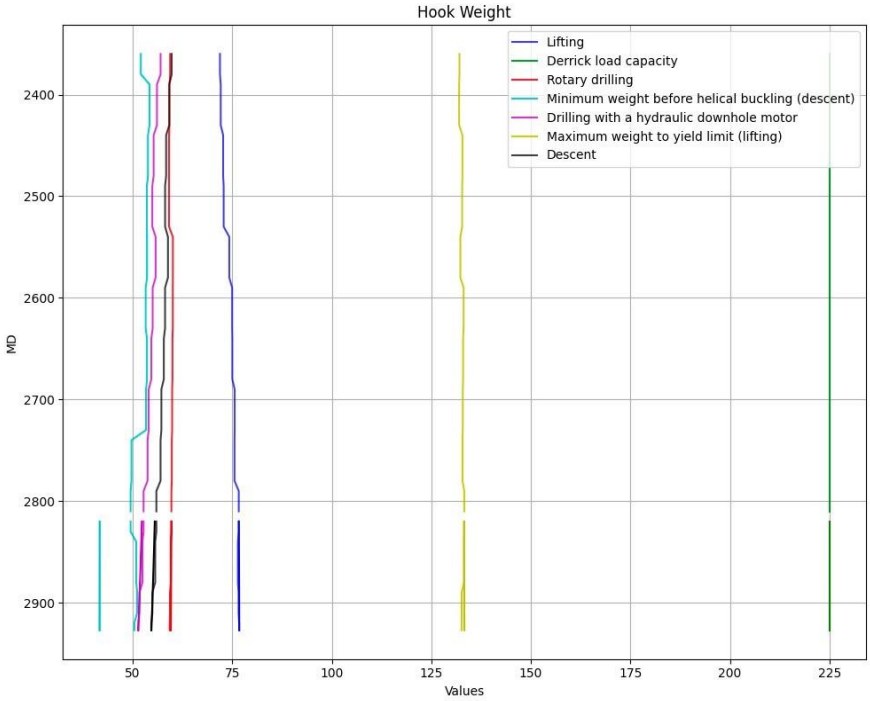


Figure 1. Hook load vs MD from ML (aktobe120).

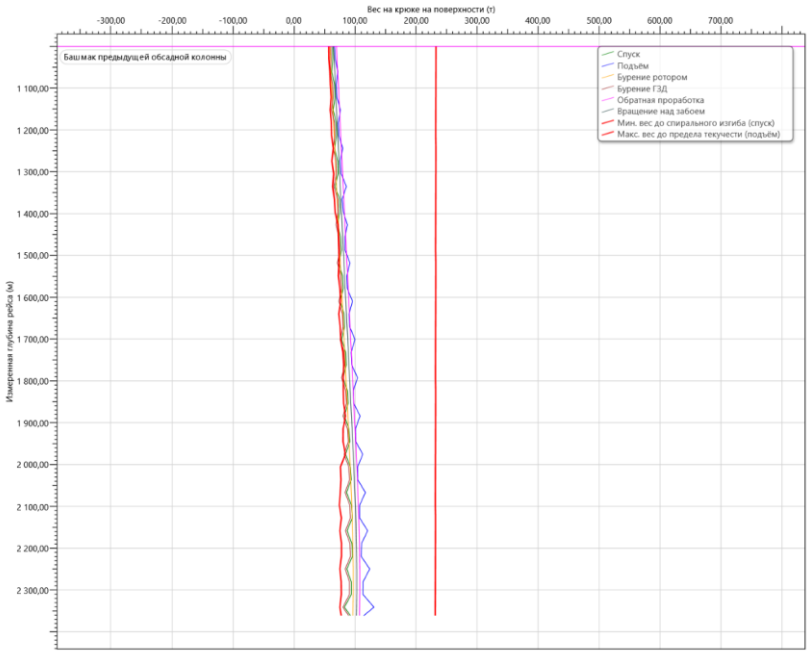


Figure 2. Hook load vs MD Wellplan results (aktobe120).

As we can see, the values of all parameters, including critical ones according to the constructed model, agree very well with the values from WellPlan. The maximum weight up to the yield point according to machine learning was 134.2 tons, and according to the

calculation results it was 131.92 tons, that is, the error is 1.7%. Comparison of Torque results (Fig. 3 - 4).

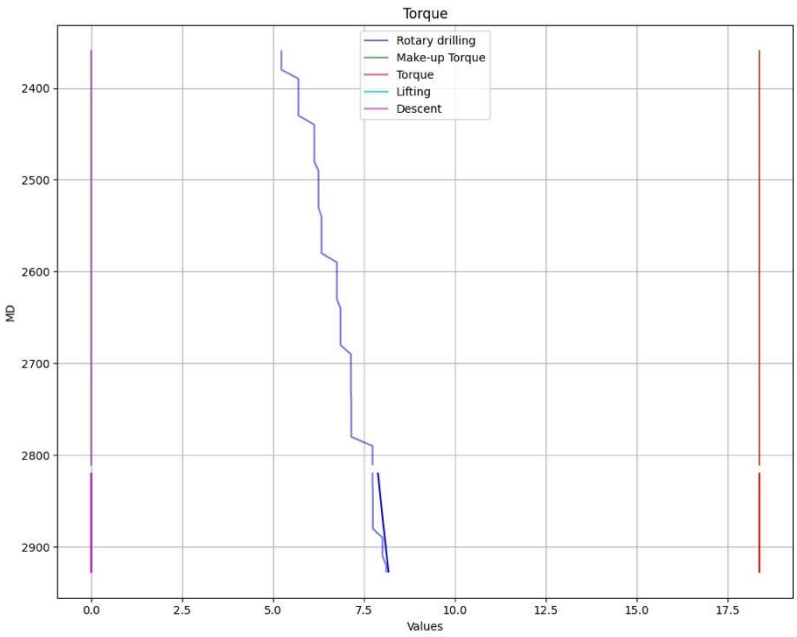


Figure 3. Torque vs MD from ML (aktobe120).

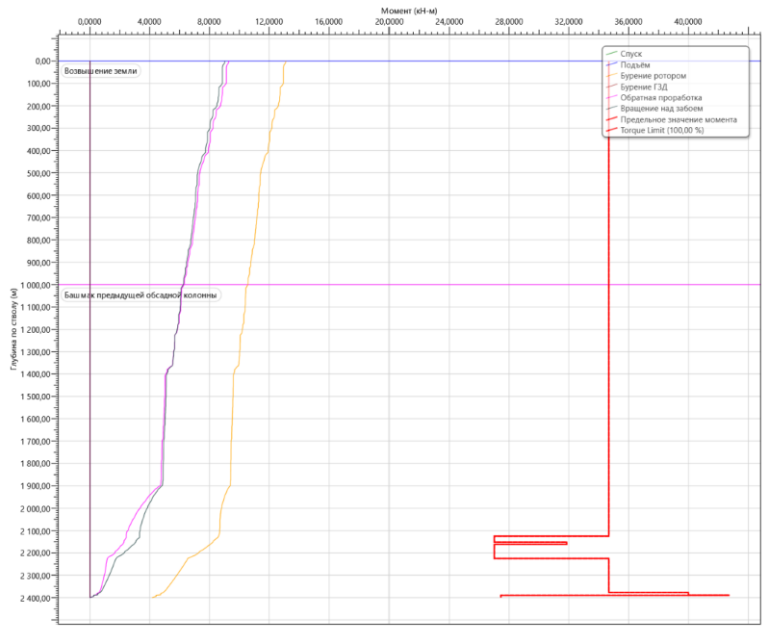


Figure 4. Torque vs MD Wellplan results (aktobe120).

We also see excellent convergence in the initial values; if the make-up torque according to machine learning is 18.67kN*m, then according to WellPlan calculations it is 18.39kN*m. That is, the error is 1.5%, which is within acceptable limits.

Comparison of Weight on Bit results (Fig. 5- 6).

https://doi.org/10.5593/sgem2024/1.1/s06.81

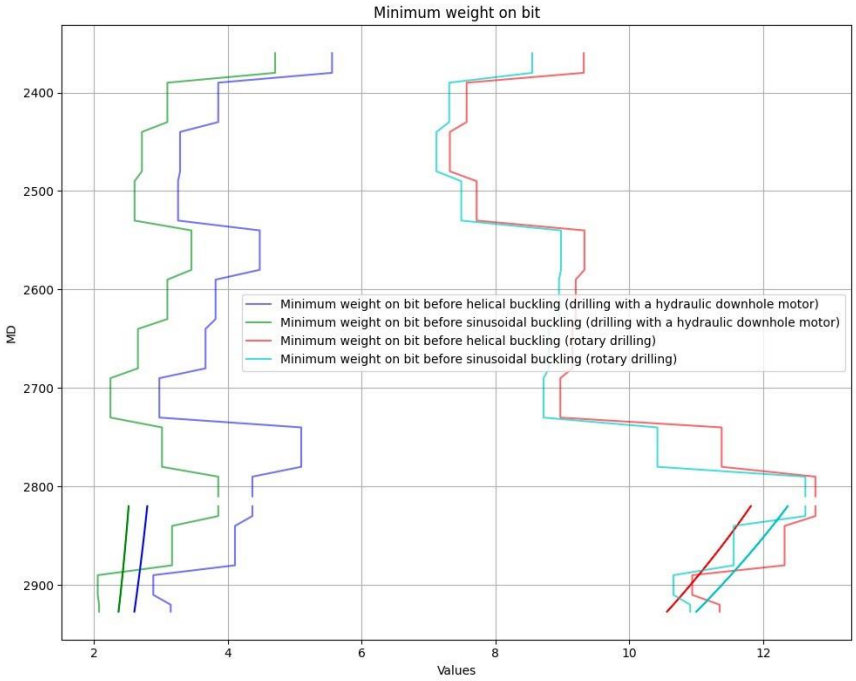


Figure 5. Weight on Bit vs MD from ML (aktobe120).

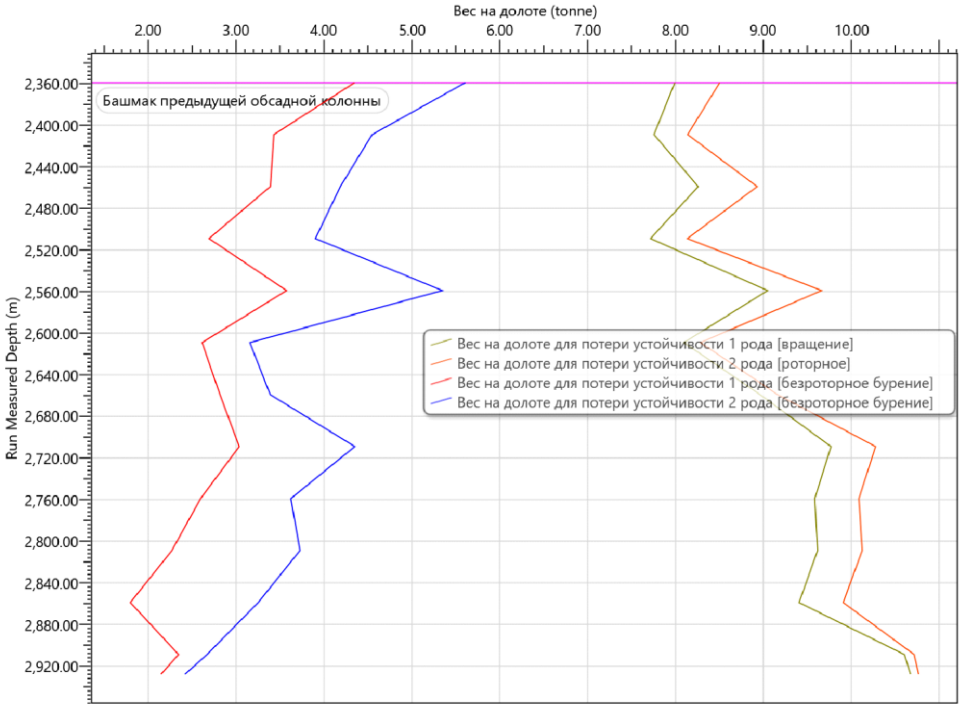


Figure 6. Weight on Bit vs MD from Wellplan (aktobe120).

According to these graphs, we also see an almost perfect correspondence between the output data of the trained model and the results of calculations by the world-renowned Wellplan software. According to the model, the minimum weight on the bit before the

sinusoidal bend (MSD drilling) is 3.09 tons, while Wellplan gives a value of 3.32 tons. The error is 6.6%, which is within acceptable limits.

DISCUSSION

The results demonstrated by the implementation of a chained regression model combining Multilayer Perceptron (MLP) and XGBoost for predicting torque and drag in oil wells are encouraging. The model's high accuracy is illustrated through its comparison with the widely recognized WellPlann software, affirming its capability to predict sticking events with minimal error.

Specifically, the model performed exceptionally in predicting the Hook load with a notable accuracy, where the error margin was as low as 1.7% compared to WellPlann results (Figures 1 and 2). Similarly, torque predictions exhibited excellent agreement with WellPlann, where the make-up torque recorded a minimal error of 1.5% (Figures 3 and 4). Moreover, the Weight on Bit comparison showed a near-perfect match with an error of only 6.6%, demonstrating the model’s effective calibration (Figure 5).

However, the presence of substantial error values in some instances, as indicated by wMAPE scores exceeding 600%, suggests that the model's performance can vary significantly with different data characteristics. This variability highlights the challenges in dealing with complex geological datasets and emphasizes the need for enhanced model robustness.

The model's success in several cases, outperforming established software, highlights its utility not just in routine predictions but also in its ability to foresee and mitigate potential problems before they escalate. This proactive capability is crucial for enhancing safety and reducing non-productive time in drilling operations.

Nonetheless, the model’s reliance on geological similarities among the training wells points to its limited generalizability. Future work should aim at broadening the training dataset to include a more diverse range of geological conditions. This expansion could potentially improve the model’s versatility and reliability across different drilling environments.

Additionally, integrating real-time data analytics into the model could provide dynamic adaptability, allowing it to adjust predictions based on live data from the drilling site. Such a feature would be invaluable in continuously challenging drilling conditions, ensuring that the model remains accurate and relevant.

Future research should also explore the inclusion of other machine learning techniques, such as deep learning or reinforcement learning, to enhance feature detection and predictive accuracy. These methodologies could uncover new patterns and relationships that are not immediately apparent with current modeling techniques.

CONCLUSIONS

The chained model architecture combining Multilayer Perceptron (MLP) and XGBoost regressors has shown promising results, with an average wMAPE score of 0.29, excluding outlier values higher than 1. This performance indicates a strong potential for

https://doi.org/10.5593/sgem2024/1.1/s06.81

the model to enhance the predictability and management of torque and drag in oil wells, significantly improving operational safety and efficiency.

Despite these strengths, our results also highlight areas needing improvement. The variation in error metrics across different datasets suggests that further research is necessary to test the model's robustness and accuracy more comprehensively. Recommendations for future research include expanding the dimensions and diversity of the dataset, experimenting with different regression models, implementing L1 feature elimination, and performing rigorous hyperparameter tuning using Bayesian Optimization.

Such improvements are expected to refine the model's predictive capabilities further, allowing it to adapt to a broader range of geological conditions and operational scenarios. Continuing to enhance the dataset's quality and the model's analytical techniques will likely lead to more reliable and robust applications, thus providing critical support in the challenging environments typical of oil and gas extraction.

ACKNOWLEDGEMENTS

The article was prepared within the framework of project No. AP13068658 “Developing torque and drag, hydraulic models to prevent stuck pipe by monitoring drilling parameters in real time” as part of the ongoing competition for grant funding for fundamental and applied research of young scientists in scientific and (or) scientific technical projects for 2022–2024 Ministry of Science and Higher Education of the Republic of Kazakhstan.

REFERENCES

[1] Chamkalani, A., Shahri, M. P., and Poordad, S. 2013. Support Vector Machine Model: A New Methodology for Stuck Pipe Prediction. Presented at the SPE Unconventional Gas Conference and Exhibition, Muscat, Oman, 28–30 January. SPE-164003-MS. https://doi.org/10.2118/164003-MS.

[2] Salminen, K., Cheatham, C., Smith, M., et al. 2017. Stuck-Pipe Prediction by Use of Automated Real-Time Modeling and Data Analysis. SPE Drilling & Completion 32 (03): 184–193. https://doi.org/10.2118/178888-PA.

[3] Belaskie, J. P., McCann, D. P., & Leshikar, J. F. (1994, January 1). A Practical Method To Minimize Stuck Pipe Integrating Surface and MWD Measurements. Society of Petroleum Engineers. doi:10.2118/27494-MS

[4] Johancsik, C.A., Friesen, D.B. and Dawson, R., 1984. Torque and drag in directional wells-prediction and measurement [J]. Journal of Petroleum Technology: 36(06), pp.987– 992.

[5] Weakley, R. R. (1990, January 1). Use of Stuck Pipe Statistics To Reduce the Occurrence of Stuck Pipe. Society of Petroleum Engineers. doi:10.2118/20410-MS

SPECIFIC ASPECTS REGARDING THE TESTING OF FLAMEPROOF ENCLOSURE EQUIPMENT INTENDED FOR USE IN HAZARDOUS AREAS ENDANGERED BY THE PRESENCE OF HYDROGEN

Sc.res. I PhD Eng. Lucian Moldovan[1]
Sc.res. I PhD Eng. Adrian Jurca[1]
Sc.res. I PhD Eng. Mihai Magyari[1]
Sc.res. III PhD Eng. Marcel Rad[1]
Sc.res. assist. Eng. Valentin Sîrbu[1]
[1] National Institute for Research and Development INSEMEX Petrosani, **Romania**

ABSTRACT

The type of protection flameproof enclosure consists in placing the parts that can ignite an explosive atmosphere into an enclosure that can withstand an internal explosion and it prevents the transmission of the explosion effects (hot gases, flames, incandescent particles etc.) capable of ignition to the external explosive atmosphere in which the equipment is placed.

The purpose of the paper is to underline some specific situations that can occur during the tests in explosive mixtures needed to verify the characteristics ensuring explosion protection in case of flameproof enclosure "d" type of protection. When speaking of enclosures having regular geometrical shapes and normal internal distribution of components the pressures and pressure curves exhibit a normal behavior. But, when the enclosure has an internal distribution of components that leads to pressure peaks and pre-compression phenomena during an internal explosion the results will present a different behavior. The tests in explosive mixture will be performed to a specific flameproof enclosure according to the testing methodology presented in the standard EN 60079-1 with explosive mixtures of hydrogen-air and acetylene-air. The obtained results of the tests, will be compared to show some specific particular aspects related to the tests in explosive mixtures, especially regarding the maximum explosion pressure.

Keywords: Flameproof enclosure, hydrogen, tests, internal explosion, explosion pressure

INTRODUCTION

Equipment protected to explosion by the type of protection flameproof enclosure "d" are considered, generally, equipment that can produce electrical arcs and sparks in normal operation and the parts considered to be an ignition source are placed inside of an enclosure, constructed so as to resist the explosion pressure (developed during an internal explosion) of an explosive mixture, also preventing the transmission of the explosion effects to the explosive atmosphere surrounding the enclosure [6], [10]. The requirements for assessing flameproof enclosure equipment are described in SR EN IEC 60079-0 and SR EN 60079-1 [1], [8], [10].

The flameproof enclosure "d" type of protection presents specific elements called flameproof joints [3], [6], [10]. The flameproof joints can be threaded, non-treaded or

https://doi.org/10.5593/sgem2024/1.1/s06.82

special. Non-threaded joints (flanged, spigot, conical) (Fig. 1) are characterized by specific parameters: width of joint (L) and the gap of joint (i) [3], [6], [10].

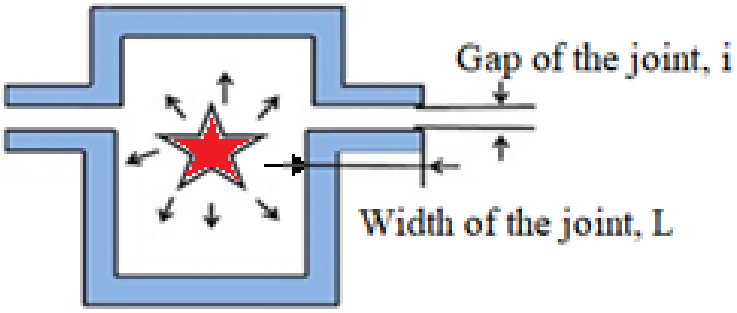


Fig. 1 - Flameproof joint characteristics

The specific standards [8], [10], under Directive 2014/34/EU [12], indicate also the required tests to be performed in order to assess equipment with type of protection flameproof enclosure. In the specific tests category, indicated in the standard [10] are also included the tests in explosive mixtures. The tests to be performed in explosive mixtures, in case of a flameproof equipment are: determination of explosion pressure, overpressure test and the test for non-transmission of an internal ignition [10].

Hydrogen represents a highly flammable substance and is included in group IIC, with an autoignition temperature of 560˚C [13]. In order to use an equipment in explosive atmospheres endangered by the presence of hydrogen, the equipment must be suitable for those conditions. For equipment designed for use in explosive atmospheres endangered by the presence of hydrogen, group IIC equipment can be used and, also, equipment in group IIB + H_2 [8], [9], [11]. When performing the tests in explosive mixtures, in case of group IIC equipment with type of protection flameproof enclosures air-hydrogen and air-acetylene explosive mixtures are used [10]. Usually, when performing the tests with acetylene-air explosive mixtures, the explosion pressures will be higher than in case of hydrogen-air explosive mixtures [6].

MATERIALS AND METHODS

Determination of reference pressure (explosion pressure) is one of the tests in explosive mixtures that needs to be performed in order to assess the explosion characteristics of equipment with type of protection “d” - flameproof enclosure. The reference pressure is considered as the highest value of the explosion pressure (considering the maximum smoothed pressure – using a 5 kHz ± 0.5 kHz with a 3 dB point low-pass filter) [10].

For this test, the explosive mixture is placed inside the enclosure (at ambient pressure and temperature) and ignited. The explosion pressure is then determined and recorded. The ignition sources are placed so as to give the highest explosion pressure (the pressure sensors are placed so as to be able to measure the explosion pressure). Gaskets must be fitted to the enclosure when the equipment is designed and provided with gaskets. The electrical equipment enclosure, under test, is designed for use in ambient temperature between –20 °C and +40 °C and the reference pressure shall be determined at ambient

temperature and pressure. The explosive mixture inside the enclosure is ignited and the explosion pressure is measured by the help of dynamic pressure transducers [10].

The pressure transducers used for the tests are Kistler, type 603 CAB. The output of the pressure transducers is connected to charge amplifiers (Kistler, type 5011) and the electrical charge is transformed to voltage. The charge amplifiers are connected to oscilloscopes (HP 54645A) and then to a computer. In order to operate the test rig (Fig. 2) and to record the specific parameters during the tests in explosive mixtures 2 computers are used (one to control the test rig and one to record the specific parameters).



Fig. 2 - Test rig to perform the tests in explosive mixtures

In case of electrical equipment in group IIC, five tests with (14 ± 1) % acetylene and five tests with (31 ± 1) % hydrogen have to be performed [4], [10].

The test sample used consisted of a cast aluminium enclosure with the external dimensions (L x W x H) 155 mm x 155 mm x 132 mm [4]; together with a screw cover (fig. 3). Inside, a fixed solid obstruction (baffle plate) was placed and fixed with screws [4] in order to simulate the internal equipment (fig. 4).



Fig. 3 - Test sample connected to gas inlet and outlet



Fig. 4 - Baffle plate mounted inside the test sample

Under the baffle plate silicone adhesive was used to create a small compartment (fig. 5).

https://doi.org/10.5593/sgem2024/1.1/s06.82



Fig. 5 - Silicone adhesive inside the test sample

The explosion pressure was measured using two testing configurations.

In case of the first testing configuration (Configuration 1) only one pressure transducer was used to measure the explosion pressure and the baffle plate was removed. The pressure transducer was placed in the middle of the screwed cover of the testing enclosure (fig. 3). The ignition source was placed on the front side of the enclosure [4].

In case of the second configuration (Configuration 2) the baffle plate was placed on position. In this configuration two pressure transducers were used to measure the explosion pressure, one of them being placed in the middle of the screwed cover, and the second one in the point where the maximum explosion pressure was expected to occur (under the baffle plate, in the middle of silicone free area) (fig. 6).



Fig. 6 - Test sample prepared for Configuration 2

RESULTS

When performing the tests in explosive mixtures, to determine the reference pressure (explosion pressure) in case of Configuration 1 (without the baffle plate) – tests performed with hydrogen-air mixture, the maximum recorded pressure was between 5,74 ÷ 5,86 bar. The pressure diagram was normal (smooth) showing that no pressure pilling has occurred (fig. 7).

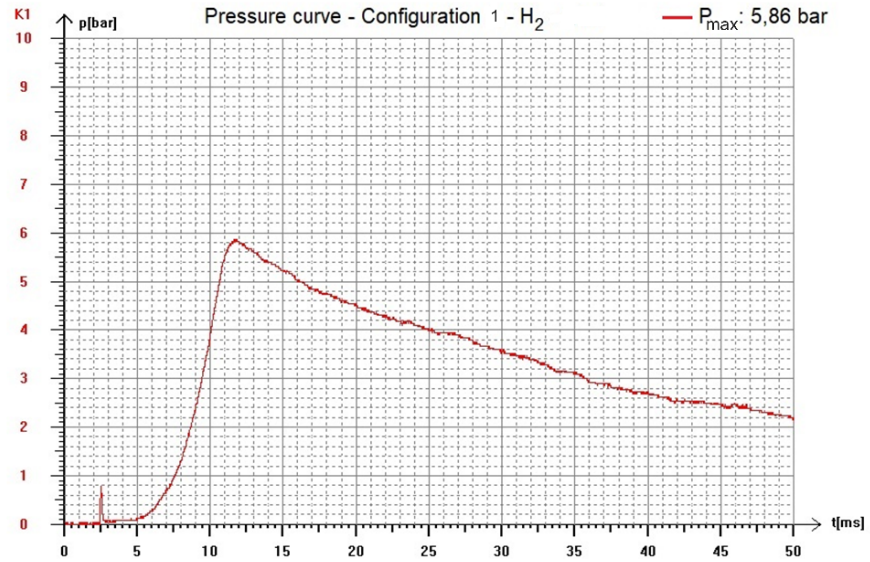


Fig. 7 - Pressure curve resulted when testing with explosive mixture of hydrogen – air – Configuration 1

The same situation (normal pressure diagram showing no pressure pilling) was identified when performing the tests with acetylene-air mixture – Configuration 1, with maximum recorded pressures between 7,54 ÷ 7,62 bar (fig. 7).

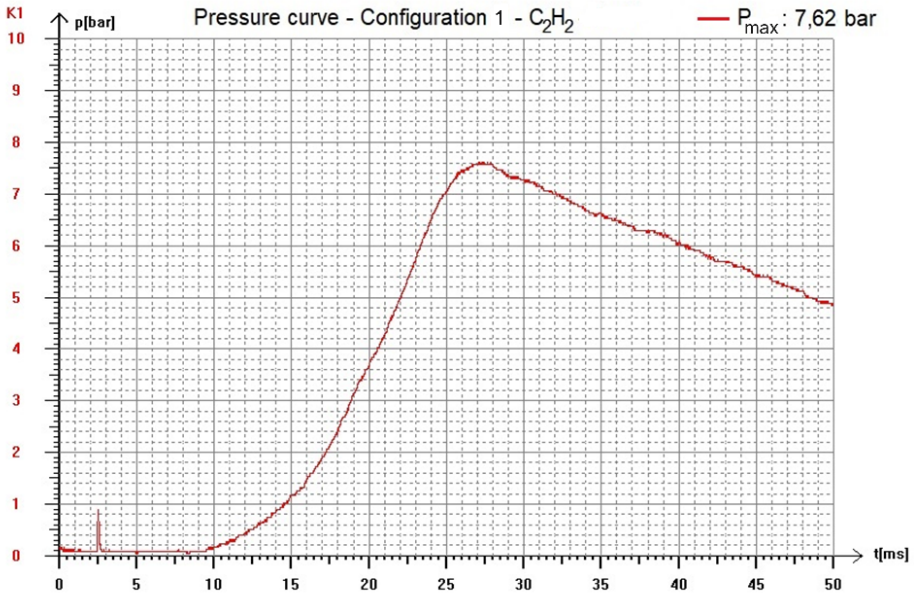


Fig. 8 - Pressure curve resulted when testing with explosive mixture of acetylene – air – Configuration 1

When performing the tests in explosive mixtures using Configuration 2 (with the baffle plate installed), the results were different and the pressure pilling phenomena was present. At first, the tests were performed with a mixture of hydrogen-air and the maximum recorded pressures were in the range of 6,02 ÷ 6,72 bar in case of the first pressure transducer (located in the middle of the screwed cover) and 10,16 ÷ 12,03 bar

https://doi.org/10.5593/sgem2024/1.1/s06.82

in case of the second pressure transducer (located under the baffle plate). A specific pressure diagram is presented in fig. 9.

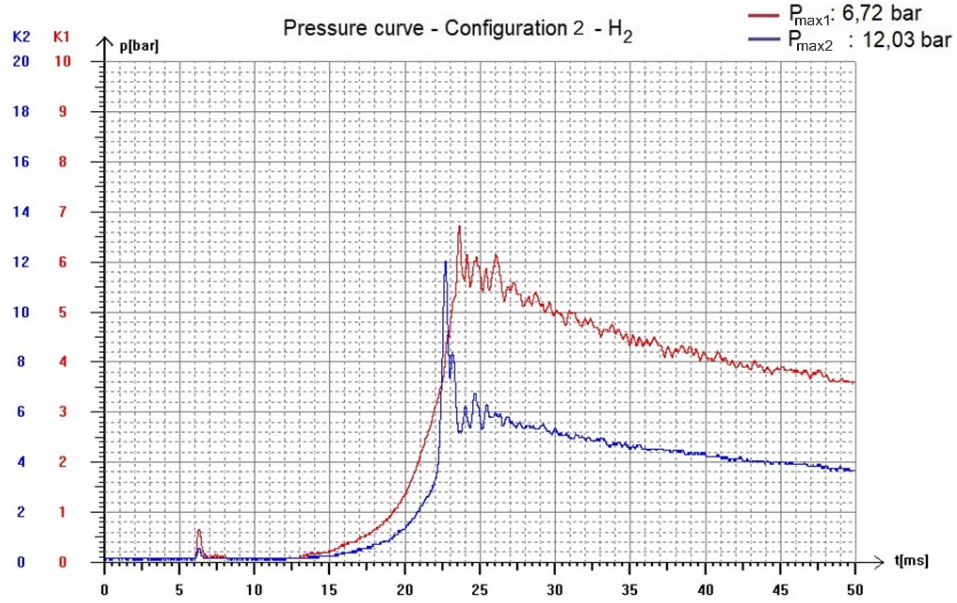


Fig. 9 - Pressure curve resulted when testing with explosive mixture of hydrogen – air – Configuration 2

The same situation (pressure diagram showing pressure pilling) was identified when performing the tests with acetylene-air mixture – Configuration 2. The maximum recorded pressures were between 7,77 ÷ 7,85 bar in case of the first pressure transducer and between 8,16 ÷ 9,18 bar in case of the second pressure transducer. A specific pressure diagram is presented in fig. 10.

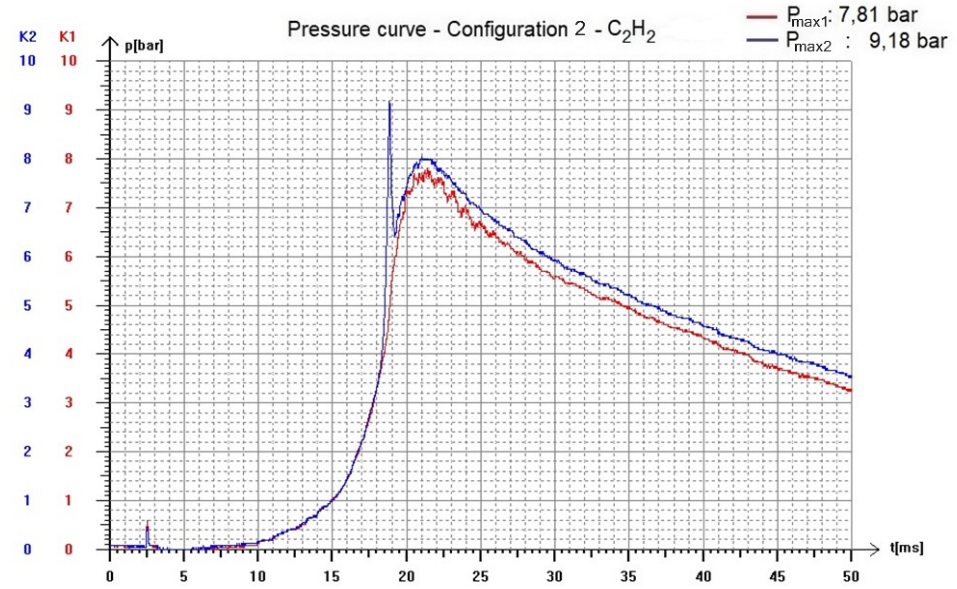


Fig. 10 - Pressure curve resulted when testing with explosive mixture of acetylene – air – Configuration 2

DISCUSSION

The results obtained when performing the tests in explosive mixtures according Configuration 1 showed that the explosion pressure exhibit a normal diagram (smooth) with no pressure pilling, both for hydrogen-air mixtures and acetylene-air mixtures. Also, the explosion pressures (considering that the tests were performed in the same testing conditions related to pressure and temperature) are, as expected, higher in case of explosive mixtures of acetylene-air than in case of explosive mixtures of hydrogen-air.

When performing the tests in explosive mixtures in case of Configuration 2 (with the baffle plate mounted inside the enclosure) one can see that the pressure diagrams did not have the same normal behaviour as in Configuration 1. The pressure diagrams show that the pressure pilling phenomena is present. Also, an interesting fact is represented by the explosion pressure values recorded during the tests in Configuration 2. The maximum explosion pressure recorded by the first pressure transducer exhibit a normal behaviour (the explosion pressures in case of hydrogen-air mixtures are lower than in case of acetylene-air mixtures), even if pressure pilling occurs. But, the maximum explosion pressures recorded by the second pressure transducer (placed under the baffle plate) are higher for the specific tests made with hydrogen-air explosive mixtures (values of 10,16 ÷ 12,03 bar) than in case of tests performed with acetylene-air explosive mixtures (values of 8,16 ÷ 9,18 bar).

One explanation of the explosion pressure values recorded in case of Configuration 2, for the second pressure transducer, is the position of the baffle plate that influences the explosion pressure by creating a small compartment under the baffle plate. This small compartment communicates with the main compartment by a small orifice. The ignition of the explosive mixture in the main compartment will lead to an explosion. During the burning of the explosive mixture in the main compartment, a part of the unburnt explosive mixture from the main compartment will migrate in the small compartment (created under the baffle plate) and will increase the pressure of the explosive mixture in this small compartment [6]. When the flame will reach the small compartment (under the baffle plate) it will meet a pre-compressed explosive mixture, resulting in higher explosion pressures.

One reason for the higher values of explosion pressure in case of tests performed in Configuration 2 with hydrogen-air explosive mixtures than with acetylene-air explosive mixtures could be the smaller size of hydrogen molecules [2], [7] compared to acetylene molecules [5]. Thus, hydrogen can easily diffuse and enter the small compartment through the small orifice that makes the communication of the two compartments. In this case, a higher quantity of hydrogen-air is pre-compressed in the small compartment, resulting in higher explosion pressures compared to acetylene-air mixtures.

CONCLUSION

The tests in explosive mixtures represents the specific tests to be carried out in order to assess explosion protection in case of equipment with type of protection flameproof enclosure “d”. One of these specific tests is represented by determination of explosion pressure.

In case of flameproof equipment of Group IIC, the tests in explosive mixtures are performed both with hydrogen-air and acetylene-air explosive mixtures.

https://doi.org/10.5593/sgem2024/1.1/s06.82

Even if in many cases the tests in explosive mixtures performed with acetylene-air result in higher explosion pressures than the tests performed with hydrogen-air, there are some specific cases when the situation can be different. In these specific cases, when the enclosure has more compartments that communicates between them through small orifices, the pressure pilling phenomena can occur and the explosion pressures can reach higher values for hydrogen-air explosive mixtures compared to acetylene-air explosive mixtures.

The testing laboratories performing the tests in explosive mixtures for flameproof enclosure equipment of Group IIC shall not rely only on the tests performed with acetylene-air mixtures; they have to perform, as required by the standards, also the tests with hydrogen-air explosive mixtures in order to provide a full and correct assessment of the equipment.

ACKNOWLEDGEMENTS

This work was carried out through the “Nucleu” program of the National Research, Development and Innovation Plan 2022-2027, supported by MCID, project no. PN23320102.

REFERENCES

[1] Burian S., Grecea D., Pupazan G., Evaluation of equipment used in Ex atmospheres - interdisciplinary field, Proceedings of the 10th International Symposium on Occupational Health and Safety SESAM 2021, Matec Web of Conferences, Vol 354, Art. No.00038, 2022

[2] Jolly, William Lee. "hydrogen". Encyclopedia Britannica, 19 Apr. 2024, https://www.britannica.com/science/hydrogen. Accessed 25 April 2024.

[3] McMillan A., Electrical Installations in Hazardous Areas, Butterworth-Heinemann Publishing House, Great Britain, 1998

[4] Krause T., Ostermann L, Wu J., Procedure Instruction Explosion Pressure (“EP”) Test Round 2023, Physikalisch-Technische Bundesanstalt, Document-ID: PI-EP2023-01

[5] Lin RB, Li L, Wu H, Arman H, Li B, Lin RG, Zhou W, Chen B, Optimized Separation of Acetylene from Carbon Dioxide and Ethylene in a Microporous Material, Journal of the American Chemical Society, Issue 139(23), pp 8022-8028, 2017

[6] Moldovan L., Burian S., Magyari M., Fotău D., Rad M., Aspects on testing electrical equipment with type of protection flameproof enclosure “d”, Proceedings of the 19th International Multidisciplinary Scientific Geoconference (SGEM), Science and Technology in Geology, Oil and Gas Exploration, Bulgaria, Issue 1.2, Vol 19, pp 663-670, 2019

[7] Sabo D, Varma S, Martin MG, Rempe SB. Studies of the thermodynamic properties of hydrogen gas in bulk water, The Journal of Physical Chemistry B, Issue 112(3), pp 867-876, 2008

[8] ***, SR EN IEC 60079-0, Explosive atmospheres - Part 0: Equipment – General requirements, ASRO, 2018

[9] ***, SR EN 1127-1, Explosive atmospheres. Explosion prevention and protection Basic concepts and methodology, ASRO, 2019

[10] ***, SR EN 60079-1, Explosive atmospheres - Part 1: Equipment protection by flameproof enclosures "d", ASRO, 2015

[11] ***, SR EN 60079-14, Explosive atmospheres - Part 14: Electrical installations design, selection and erection, ASRO, 2014

[12] ***, Directive 2014/34/EU on the harmonisation of the laws of the Member States relating to equipment and protective systems intended for use in potentially explosive atmospheres (recast), Official Journal of the European Union, no.96, 2014

[13] ***, SR EN ISO/IEC 80079-20-1:2020, Explosive atmospheres — Part 20-1: Material characteristics for gas and vapour classification — Test methods and data, ASRO, 2020

https://doi.org/10.5593/sgem2024/1.1/s06.82

THE PARTICULARITIES OF ELECTRICAL EQUIPMENT WITH TYPE OF PROTECTION FLAMEPROOF ENCLOSURE USED IN POTENTIALLY EXPLOSIVE ATMOSPHERES GENERATED BY HYDROGEN

PhD. Eng. Dragoş Fotău[1]

PhD. Eng. Lucian Moldovan[1]

Eng. Râsnoveanu Sorin[1]

Eng. Sîrbu Valentin[1]

PhD. Eng. Diana Sălăşan [1]

[1]National Institute for Research and Development in Mine Safety and Protection to Explosion – INSEMEX Petroşani, 32-34 G-ral Vasile Milea Street, Petroşani 332047, **Romania**

ABSTRACT

Electrical equipment that operates in a potentially explosive atmosphere, have characteristics specially designed for operation in this area. For security reasons, it is essential that the integrity of these special features be preserved in these areas throughout the life of the installation.

Using electric equipment in potentially explosive atmospheres brings forward several particularities therefore the problems that appear during the design, construction and operation of electrical devices and installations brings forward numerous difficulties, their approach requiring special attention considering all the technical, economical and labor safety aspects.

The purpose of the paper is to reveal the particularities of electrical equipment with type of protection flameproof enclosure design to be used in potentially explosive atmospheres generated by hydrogen.

Evaluation of explosion-proof protected electrical equipment in scope of certification is extremely important considering the risk of explosion that has to be minimized in order to ensure life safety and health of workers and to prevent damaging of property and the environment, as well as free movement of goods when they meet the essential safety requirements at European level.

Keywords: electrical equipment, explosive atmosphere, hydrogen.

INTRODUCTION

Explosive atmospheres can occur in various industrial fields, in installations in which flammable substances are processed, transferred or stored.

Using electric energy in potentially explosive atmospheres brings forward several particularities therefore the problems that appear during the design, construction and operation of electrical devices and installations brings forward numerous difficulties, their approach requiring special attention considering all the technical, economical and labour safety aspects.[1] [5]

The risk of explosion may appear in all the fields of activity in which flammable substances are involved, such as gases, vapours, dusts, mists, which mixed with air may result in potentially explosive atmospheres. [1] [5]

To prevent the ignition of explosive atmospheres, the electrical equipment used in such areas must be made with different types of protection so that it cannot ignite the explosive mixture surrounding the electrical equipment. [5]

Types of protection represent all the specific measures that are applied to electrical equipment in order to avoid the ignition of the explosive atmosphere surrounding the equipment [2]

For each type of protection applied to electrical equipment used in potentially explosive atmosphere, a wide range of type tests have been developed so that they can be used safely [2].

The evaluation of explosion-protected electrical equipment with type of protection increased safety is carried out by means of tests and verifications performed on the basis of the reference standards (SR EN 60079-0 - which includes the general requirements for all explosion-protected electrical equipment and the standards specific to the types of protection involved in the manufacture of the equipment). In the case of flameproof enclosure protection type, the specific standard is SR EN 60079-1 [1,2].

In order to verify explosion protection, the representative samples made available by explosion-protected equipment manufacturers are tested under the most unfavourable conditions that may occur in operation.

CLASIFICATION OF EXPLOSIVE ATMOSPHERES

Explosive atmospheres are defined as a mixture of air, under atmospheric conditions, of flammable substances in the form of flammable gases, mist vapors or combustible dusts, in which, after ignition, combustion is spread throughout the unburned mixture. To generate an explosive atmosphere, the flammable substance must be present in certain concentrations, between the Lower Explosive Limit and Upper Explosive Limit. Explosion limits of the substance may depend on pressure, oxygen concentration in the air and temperature. [1] [6]

The mechanism of an explosion generated by a mixture of flammable gas, vapor or mist with air can be expressed by the well-known explosion triangle shown in Figure 1. The occurrence of an explosion is conditioned by the simultaneous presence of the following three factors: fuel (flammable gases, vapours, mists), oxygen (oxygen, oxidizing substances) and efficient ignition source (hot surfaces, sparks, short circuit, static energy, electric arcs) for ensuring the activation of molecules in order to ignite and propagate the fast combustion reaction. [5]

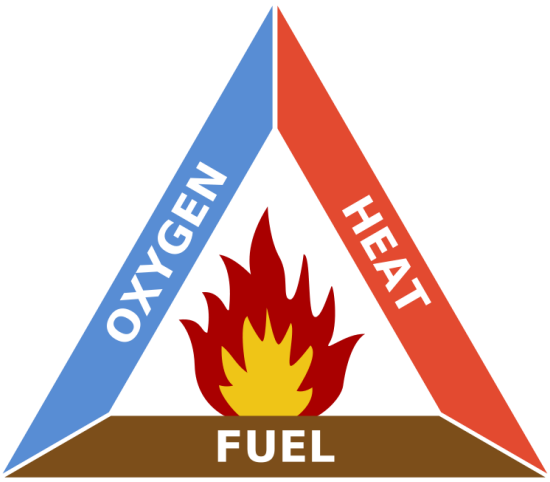


Fig. 1– The explosion triangle

According to ATEx Directive 2014/34/EU are defined several types of groups and categories of electrical equipment:

Equipment Group I: equipment used for underground mines and for parts of the installations located at the surface of these mines, susceptible to firedamp and/or combustible powders.

Equipment Group II: equipment intended to be used in explosive atmospheres, other than the ones in Group I.

The specific standards for electrical equipment used in potentially explosive atmosphere (EN 60079 series) divided Group II of electrical equipment into Group II for gases, vapours and mists and Group III for flammable powders. These standards have also introduced the Equipment Protection Level concept: Ga, Gb, Gc for gases and Da, Db, Dc for equipment intended to be used in potentially explosive atmospheres generated by flammable dusts in air.

Therefore, a new classification in groups and categories arises:

Gr I mining

Gr II (A, B, C) surface gases

Gr III (A, B, C) dusts

A very important component on which the explosion protection depends is the surface temperature of the equipment. This is the highest temperature reached in operation under the most unfavorable conditions (but within the tolerances set), by any part or surface of the electrical equipment (in the case of gaseous explosive atmospheres which may occur in technical installations operating in oil and gas industry, this temperature may appear on an internal component or on the outer surface of the case , depending on the type of protection used). [2]

https://doi.org/10.5593/sgem2024/1.1/s06.83

The ignition temperature of potentially explosive substances is an important aspect in the choice of equipment in the installation. The temperature classes for equipment (maximum temperature), given in table 1, must be below the ignition temperature of the substance in which it operates. [6]

Table. 1– The correspondence between ignition temperature and the temperature class of the equipment

Temperature class of the equipment	Ignition temperature of gas or vapor (°C)	Allowed temperature classes for the equipment
T1	450	T1 – T6
T2	300	T2 – T6
T3	200	T3 – T6
T4	135	T4 – T6
T5	100	T5 – T6
T6	85	T6

ELECTRICAL EQUIPMENT WITH TYPE OF PROTECTION FLAMEPROOF ENCLOSURE USED IN POTENTIALLY EXPLOSIVE ATMOSPHERES GENERATED BY HYDROGEN

Like any flammable fuel, hydrogen can combust. But hydrogen's buoyancy, diffusivity and small molecular size make it difficult to contain and create a combustible situation. In order for a hydrogen fire to occur, an adequate concentration of hydrogen, the presence of an ignition source and the right amount of oxidizer (like oxygen) must be present at the same time. Hydrogen has a wide flammability range (4- 74% in air) and the energy required to ignite hydrogen (0.02mJ) can be very low. However, at low concentrations (below 10%) the energy required to ignite hydrogen is high--similar to the energy required to ignite natural gas and gasoline in their respective flammability ranges-making hydrogen realistically more difficult to ignite near the lower flammability limit. On the other hand, if conditions exist where the hydrogen concentration increased toward the stoichiometric (most easily ignited) mixture of 29% hydrogen (in air), the ignition energy drops to about one fifteenth of that required to ignite natural gas (or one tenth for gasoline). [5] [8]

Hydrogen is a gas of the IIC group and belongs to the temperature class T1, which makes it one of the hottest and most dangerous gases.

The most used electrical equipment in potentially explosive atmosphere is made with type of protection flameproof enclosure. [2]

Flameproof enclosure "d" is an enclosure in which the parts which can ignite an explosive gas atmosphere are placed and which can withstand the pressure developed during an internal explosion of an explosive mixture, and which prevents the transmission of the explosion to the explosive gas atmosphere surrounding the enclosure. [4], [5]

According to specific standards for electrical equipment with flameproof enclosure type of protection, for each group of explosions there is minimum width of joint and maximum gap for enclosures as shown in table 3.

Table. 3– Minimum width of joint and maximum gap for Group IIC enclosures

Type of joint		Minimum width of joint L mm	Maximum gap mm			
			For a volume cm³ $V \leq 100$	For a volume cm³ $100 < V \leq 500$	For a volume cm³ $500 < V \leq 2\,000$	For a volume cm³ $V > 2\,000$
Flanged joints[a]		6	0,10	–	–	–
		9,5	0,10	0,10	–	–
		15,8	0,10	0,10	0,04	–
		25	0,10	0,10	0,04	0,04
Spigot joints (Figure 2a)	$c \geq 6$ mm	12,5	0,15	0,15	0,15	–
	$d \geq 0,5\ L$	25	0,18[b]	0,18[b]	0,18[b]	0,18[b]
	$L = c + d$	40	0,20[c]	0,20[c]	0,20[c]	0,20[c]
	$f \leq 1$ mm					
Cylindrical joints Spigot joints (Figure 2b)		6	0,10	–	–	–
		9,5	0,10	0,10	–	–
		12,5	0,15	0,15	0,15	–
		25	0,15	0,15	0,15	0,15
		40	0,20	0,20	0,20	0,20
Cylindrical joints for shaft glands of rotating electrical machines with rolling element bearings		6	0,15	–	–	–
		9,5	0,15	0,15	–	–
		12,5	0,25	0,25	0,25	–
		25	0,25	0,25	0,25	0,25
		40	0,30	0,30	0,30	0,30

One of the most important components of electrical equipment with type of protection flameproof enclosure is the flameproof join, that's why it is necessary to be properly maintained.

The maintenance of the integrity of the type of protection foreseen for the equipment has to be especially considered. Spare parts need to be according to the documentation for safety protection and assurance. [4] [7]

If the case or one of the components if severely corroded, the part affected needs to be treated by covering it accordingly against corrosion, the frequency and the nature of such a treatment being determined by the nature of the environmental conditions. [4]

If the flameproof enclosures are reassembled, all the joints need to be thoroughly cleaned and lubricated easily with a sort of Vaseline for the prevention of corrosion and to increase their weatherproofing. In order to clean the flanges a nonmetallic grater and noncorrosive cleaning products need to be used. The bolds and tenons and similar parts on which the type of protection depends need to be replaced only with similar parts according to the design and recommendations of the producer. The deteriorated sealing gaskets need to be replaced. The condensation proof devices shall be verified to see if they work accordingly. [4]

https://doi.org/10.5593/sgem2024/1.1/s06.83

RESULTS

Since a good part of the electrical equipment that works in potentially explosive atmospheres is made with flameproof enclosure type of protection, it is very important that they are chosen appropriately so that they can be used safely in the areas with a risk of explosion where they are located.

In the laboratory at INSEMEX and in other laboratories in the world, numerous tests in explosive mixtures have been carried out over the years on electrical equipment with flameproof enclosure type of protection. These tests have shown that it is very important to respect the maximum gap allowed for each individual equipment group. If the electrical equipment does not have the joint length long enough and the joint gap small enough to be used in the explosive atmosphere generated by hydrogen, a possible internal explosion can easily be transmitted from the inside to the outside of the case, and thus the potentially explosive atmosphere surrounding the equipment could be ignited.

Over the years, research conducted at INSEMEX has shown that the maximum period of three years between two detailed inspections is often too long. Because of this, the equipment may suffer damage that may invalidate the type of protection, or high repair costs.

CONCLUSION

The process of selecting electrical equipment for use in areas with potentially explosive atmospheres, generated by mixtures of air and oil, flammable gases or vapours, requires in-depth knowledge in this field.

This paper aims to increase safety in the choice of equipment used in potentially explosive environments, helping users who have no knowledge in this field but are determining factors in their purchase or use.

Hydrogen mixed with air gives rise to one of the most dangerous explosive mixtures, because it has a very low ignition energy and a very high explosion pressure. At the global level, there is a great emphasis on the use of hydrogen as a fuel, both in the automotive industry and in other industries, and that is why it is important that the users of electrical installations that produce, store and use hydrogen, know very well the dangers generated by this gas.

Electrical equipment that operates in potentially explosive environments generated by hydrogen must be certified to be used in potentially explosive atmospheres included in subgroup IIC of gases or be certified for subgroup IIB+H_2. If the equipment is included in other gas subgroups, they cannot be used in potentially explosive atmospheres generated by hydrogen.

Flameproof enclosure electrical equipment has features specifically designed for operating in hazardous areas. For these reasons it is essential that equipment with type of protection flameproof enclosure throughout their lifetime, need to be properly maintained so that the type of protection is not canceled.

For the proper functioning of electrical equipment used in potentially explosive atmosphere, the inspection, maintenance and proper repair of these is of great

importance. These things must be done by personnel who know the principles of the types of protection, and also to have the necessary infrastructure for a proper repair.

The inspection and maintenance of the equipment is done according to the requirements of standard EN 60079-17, and the revision and repair of the equipment is done according to the requirements specified in the standard EN 60079-19.

This process takes time and to increase its quality and to facilitate the correct selection of electrical equipment intended for use in such atmospheres, an application has been developed to be a useful tool for personnel working in the industries that process, store or carries flammable substances.

The application presented in the paper provides technical staff with an easy-to-use, intuitive, fast and reliable tool for selecting explosion-proof electrical equipment. The equipment is selected in accordance with the safety and explosion protection in force and brings with it an increase in the level of health and safety at work in industries with potentially explosive atmospheres.

ACKNOWLEDGEMENTS

This paper was carried out through the “Nucleu” program of the National Research, Development and Innovation Plan 2022-2027, supported by MCID, project no. PN23320102.

REFERENCES

[1] Directive 2014/34/EU of the European Parliament and of the Council of 26 February 2014 on the harmonization of the laws of the Member States relating to equipment and protective systems intended for use in potentially explosive atmospheres (recast) Text with EEA relevance, 2014.

[2] Standard IEC 60079-0 - Explosive atmospheres - Part 0: General requirements, 2013.

[3] Standard IEC 60079-1 - Explosive atmospheres - Part 1: Equipment protection by flameproof enclosure "d", 2015.

[4] Standard IEC 60079-19 - Explosive atmospheres – Part19: Equipment repair, overhaul and reclamation, 2011

[5] Niculescu T, Pasculescu D, Pasculescu VM, Stoica IO., *„Evaluation of electrical parameters of intrinsic safety barriers of the electrical equipment intended to be used in atmospheres with explosion hazard*”, International Multidisciplinary Scientific GeoConference Surveying Geology and Mining Ecology Management. 2014; 1(2):169-176.

[6] Burian S., Ionescu J., Darie M., Csaszar T., Andriş A., (2007), *Requirements for Installations in Areas with Explosive Atmosphere, Other than Mines, (in Romanian)*, INSEMEX – Petrosani Publishing House, Romania.

[7] Niculescu T, Pasculescu D., *„Use of numerical simulation to study capacitive loads which is connecting to an AC power source*”, In15th International Multidisciplinary Scientific Geoconference SGEM 2015 2015 (pp. 391-398).

[8] Pana L, Grabara J, Pasculescu D, Pasculescu VM, Moraru RI., *„Optimal quality management algorithm for assessing the usage capacity level of mining transformers”,* Polish Journal of Management Studies. 2018;18(2):233-44.

USING MACHINE LEARNING TECHNIQUES TO FORECAST CUTTINGS REMOVAL IN HOLE CLEANING

Senior lecturer, Dinara N. Delikesheva[1]

Assistant Professor, PhD, Dr. Aizada B. Sharaouva[2]

[1] Satbayev University, Almaty, **Kazakhstan**

[2] Atyrau University of Oil and Gas, Atyrau, **Kazakhstan**

ABSTRACT

This study addresses the significant challenge of hole cleaning in drilling operations, which is essential for preventing stuck pipe incidents—a major cause of non-productive time and additional costs in drilling. This research aims to develop and validate machine learning models that enhance the prediction and optimization of cuttings removal during drilling. Utilizing a dataset derived from historical drilling operations, we employed regression analysis and neural network models to forecast the presence and height of slurry beds. The models were trained on variables such as borehole dimensions, drilling fluid characteristics, and operational parameters. Our results demonstrate that these models effectively predict conditions that could lead to stuck pipes, allowing for preemptive adjustments to drilling operations. This capability could significantly reduce unplanned downtime and associated costs. The primary contribution of this study lies in its innovative use of machine learning to transform predictive maintenance in drilling operations, offering substantial improvements in efficiency and safety. These advancements represent a crucial step forward in drilling technology, with the potential to mitigate risks and enhance operational decision-making across the industry.

Keywords: hole cleaning, cuttings removal, regression analysis, machine learning, pipe sticking

INTRODUCTION

Stuck pipe is a significant unplanned event during drilling operations, accounting for at least 25% of non-production time (NPT), equivalent to the annual cost of two drilling years [1]. The duration of the stuck pipe and recovery process can vary significantly, often extending from a few days to over a month for remediation [2].

In addition to the lost time and daily rig rates, incidents of stuck pipe often incur repair-related costs, including lost tooling, fishing costs, and sidetracking expenses [3]. One primary cause of pipe sticking is the ineffective removal of drill cuttings from the wellbore, which can occur at various stages of the drilling process [4,5].

https://doi.org/10.5593/sgem2024/1.1/s06.84

Effective cuttings transportation and hole cleaning are crucial for optimizing drilling operations. During inclined and horizontal drilling, cleaning challenges intensify as the well's inclination angle increases, leading to the formation of a “cushion” of solid particles. This occurs due to the settling of cuttings along the bottom and low side of the well [5,6].

Cuttings transport is influenced by several variables, including borehole and drill pipe diameters, borehole inclination, drill pipe rotation speed, drill pipe eccentricity, rate of penetration, cuttings characteristics (such as size and formation porosity), and drilling fluid characteristics (such as flow rate, fluid velocity, flow regime, type of drilling fluid, and the non-Newtonian rheology of the drilling fluid). Optimizing well cleanup involves a well-considered plan, appropriate drilling fluid properties, and extensive drilling experience [6-8].

To mitigate hole cleaning issues, machine learning-based algorithms can be utilized. These algorithms can learn from data derived from past drilling operations to identify patterns and relationships that help predict optimal drilling parameters for specific wells. Therefore, the primary aim of this study is to develop and validate machine learning models that can predict and optimize the cleaning of wellbores from drill cuttings, enhancing the efficiency and safety of drilling operations. This paper explores various machine learning algorithms and approaches, including supervised learning, and discusses the challenges and limitations associated with using machine learning to estimate the height of the slurry bed, along with potential solutions.

Initially, the data was analysed and assessed for potential issues. Subsequently, the outcomes of various machine learning methods were evaluated, and conclusions were drawn regarding the practical implications of these findings.

MATERIALS AND METHODS

The data used in this work was obtained using WellPlan software. The process begins with the collection of data related to geologic reservoir properties, well geometry, drilling parameters, and other factors influencing cutting bed heights and presence. This initial dataset was sourced primarily from the WellPlan™ software, which provided comprehensive drilling records from multiple wells within the same field.

After entering all the necessary data, which consists of lithology, characteristics of machinery and equipment and casing. An appropriate machine learning model or neural network was selected to predict the cutting bed height. This choice was based on the dataset's characteristics and the specific predictive requirements of the task, evaluating various models for their suitability.

The continuous variable we are trying to predict is the height of the slurry bed. Therefore, in this study, regression algorithms are used to model the problem. Methods included include linear regression, principal component analysis, decision trees, and deep learning [8].

To predict the presence of cuttings in the wellbore, a machine learning task was used - classification.

Post-training, the model was validated using a set of pending data that was not included during the training phase. This crucial step tested the model's accuracy and its ability to generalize to new, unseen data.

The development of the model encountered notable challenges, particularly in data collection and expansion. The initial dataset included basic parameters like "Distance along string," "Vertical depth," and "Min. flow," which needed enhancement with additional critical variables such as "drilling fluid rheological properties," "drilling fluid temperature," and "cuttings characteristics." Complications arose from the data's imperfections and its limited applicability to the wells sampled. Efforts to extend dynamic parameters like "ROP" (Rate of Penetration) and "RPM" (Revolutions Per Minute) across different well depths were crucial, as these variations impact the model's ability to generalize across various drilling conditions.

Regression model for bed height prediction.

Regression is a supervised machine learning technique used to predict continuous values. It involves training a neural network to map input features to a numerical target. The network learns this mapping by adjusting its weights and biases to minimize errors in predictions, using optimization algorithms like stochastic gradient descent or Adam. Commonly used loss functions include mean squared error (MSE) or mean absolute error (MAE). Our experiments showed that using NAdam—an optimizer that combines Adam with Nesterov momentum—and MSE as the loss function yielded the best results. [9].

The Mean Squared Error (MSE) is an invaluable metric for regression models as it quantifies the average of the squares of the errors—that is, the average squared difference between the estimated values and the actual value. Here's the mathematical expression of MSE [11]:

$$MSE = \frac{1}{n}\sum\left(y_{actual} - y_{predicted}\right)^2 \quad (1)$$

Where: y_{actual} is the actual value, $y_{predicted}$ is the predicted value from the model, n is the number of observations. Basically, the lower value of MSE the better.

Classification is a machine learning task whose goal is to determine which of several classes an observation belongs to. In its most basic form, it involves identifying whether an observation belongs to one of two classes, also known as binary classification. In this work, using binary classification, we can train a neural network to segment the drilling interval into areas at risk of forming a mud cake and those without [10].

RESULTS

Collected data underwent several pre-processing steps. These included cleaning outliers, scaling numerical data to a standard range, and transforming variables to meet the specific requirements of the analytical models.

And after extracting the data, we get the data that is shown in Table 1.

https://doi.org/10.5593/sgem2024/1.1/s06.84

Table 1 – Classification report

Min. consumption	Distance along the column	Vertical Depth	Temp	Pressure	Density	Plastic visc	Rate of penetration	Cutting particle parameter	Cutting pad porosity	Rotor speed	Cutting particle density	Calculation interval by well bore depth	Feed pumps
15.539	120	119.35	30	1	1120	14	15	3	36	40	2.5	10	30
-	-	-	-	-	-	-	-	-	-	-	-	-	-
11.875	230	230	21	1	1200	20	15	3	36	40	2.5	10	32

Prediction of Slurry Bed Presence. We trained a multilayer neural network on it. During several experiments we find following configuration to be optimal in computation speed and performance, which consist of 14 input units, 2 hidden layers consists of 12 and 8 relu units and the last output sigmoid unit, that we use for classification (Figure 1).

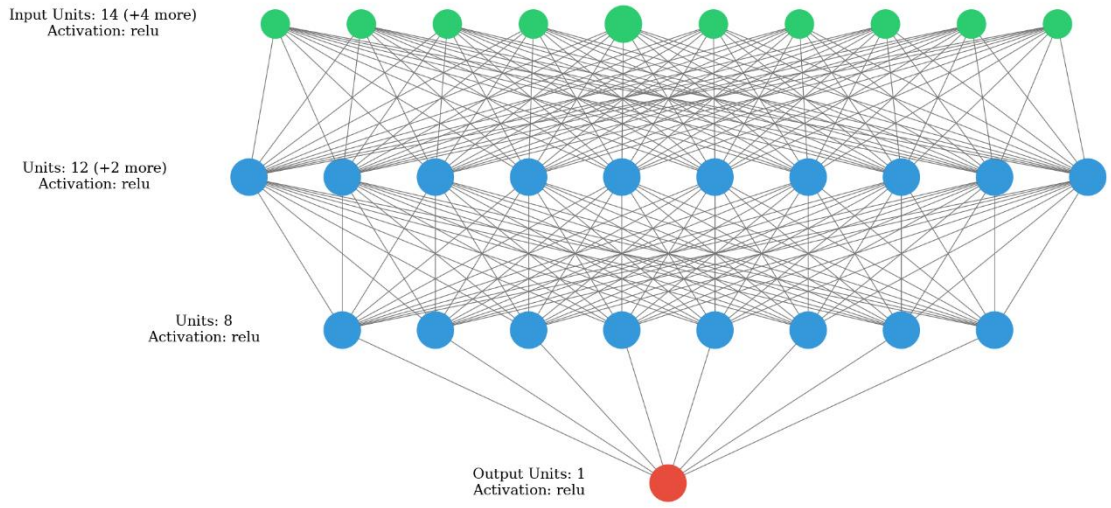


Figure 1. Classification neural network structure

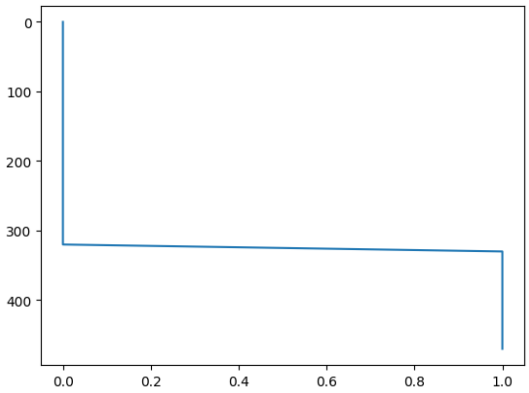
When using neural networks, there are problems of underfitting and overfitting, both leading to poor prediction results. Underfitting often occurs due to insufficient data or suboptimal network architecture. This can be corrected by increasing the amount of data and modifying the network structure. Overfitting occurs when a model performs perfectly on the training data but poorly on the new data. To avoid this, they use data division into training, test and validation. The validation set simulates new data, which helps train the model to generalize the results.

After training, our model shows the following results on validation data:

	precision	recall	f1-score	support
0	0.90	1.00	0.95	106
1	1.00	0.61	0.76	31
accuracy			0.91	137
macro avg	0.95	0.81	0.85	137
weighted avg	0.92	0.91	0.90	137

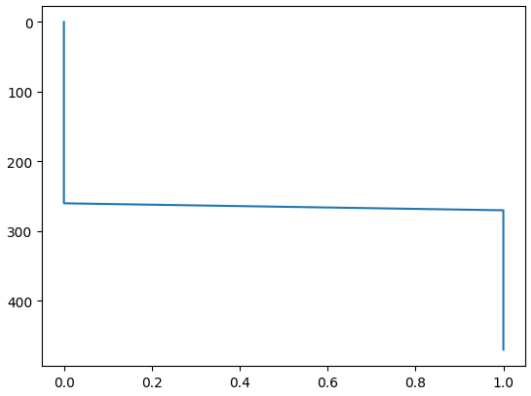
Precision, recall, F1-score, and support are key metrics for evaluating a model's performance. For class 0, precision is high at 0.90, and recall is perfect at 1.00, resulting in an F1-score of 0.95. Class 1 has a perfect precision of 1.00 but lower recall at 0.61, leading to an F1-score of 0.76. The support counts are 106 for class 0 and 31 for class 1. Overall, the model has an accuracy of 91%. The macro averages for precision, recall, and F1-score are 0.95, 0.81, and 0.85 respectively, while the weighted averages are 0.92 for precision, 0.91 for accuracy, and 0.90 for F1-score. These metrics indicate the model's strengths and areas for improvement, particularly in managing imbalances between classes.

When tested on new data not previously used in the training process, our model delivered promising results, as detailed in Figures 2 and 3. Figure 2 presents the actual observed outcomes regarding the presence of cutting beds, while Figure 3 illustrates the model's predictions.



1 – presence of a cutting bed; 0 – indicates no cutting bed

Figure 2. Real results on the presence of a cutting bed



1 – presence of a cutting bed; 0 – indicates no cutting bed

Figure 3. Prediction of the presence of a cutting bed

Our model demonstrates strong performance with new data, effectively predicting the formation of cuttings earlier than it occurs. This proactive prediction minimizes the need for additional interventions, as it helps to prevent the accumulation of a cuttings layer that could potentially cause the drillstring to become stuck. This preemptive approach enhances drilling efficiency and reduces the risk of operational delays.

https://doi.org/10.5593/sgem2024/1.1/s06.84

Predicting the height of the cutting bed. In our case, through experiments with various optimizers and metrics, we came to the optimal configuration, which looks like this: NAdam (Adam with Nesterov momentum) as an optimizer and MSE evaluation metric.

Our neural network consists of 14 input units (Min.q, Measured Depth, Vertical Depth, Temperature, Pressure, Density, Plastic Viscosity, Penetration Velocity, Mud function with 12, 8 and 16 units and one. output relu. ‘Diameter '', 'Mud porosity', 'Revolutions per minute', 'Mud density', 'Wellbore depth calculation interval', 'Injection capacity'), 3 hidden layers with relu activation. You can see a visualization of our model in Figure 4. After training and evaluating on the test set, our MSE is 0.00648.

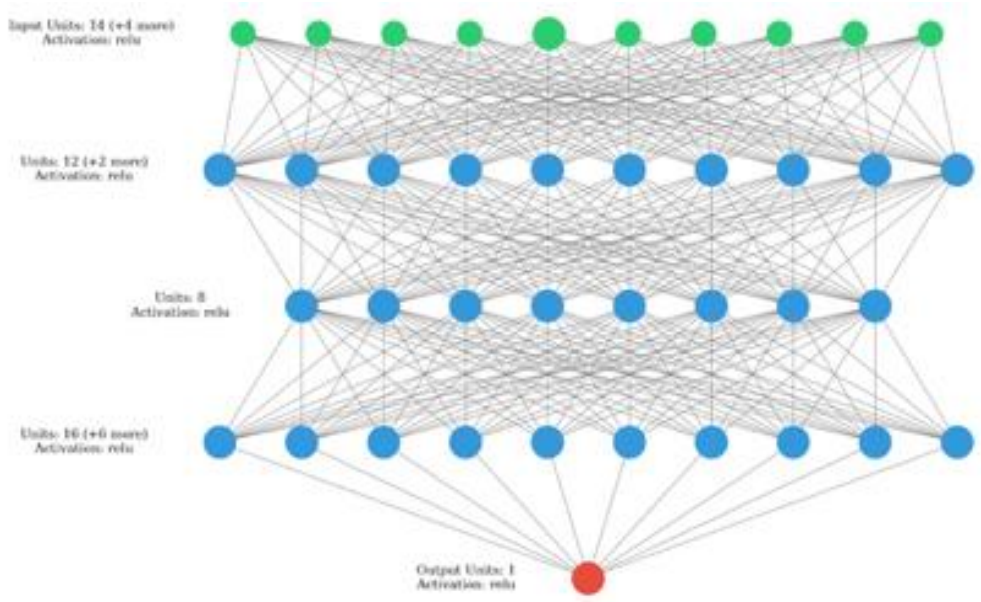


Figure 4. Regression neural network configuration

After forecasting new data, we received the following results (Figures 5 and 6):

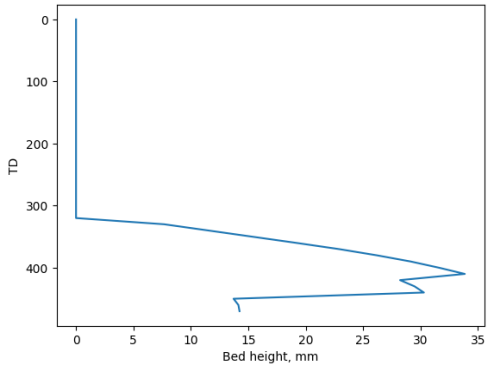


Figure 5. Results of the height of the sludge cushion based on real data

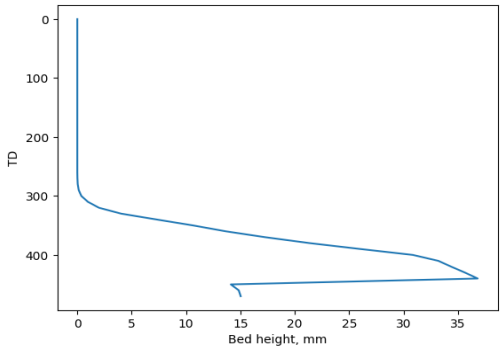


Figure 6. Results of the height of the cutting bed according to predicted data

DISCUSSION

The results of this study underscore the potential of machine learning models to revolutionize wellbore cleaning practices by providing real-time predictive insights that

enhance drilling efficiency and safety. The deployment of two distinct machine learning models has demonstrated significant capabilities in forecasting the presence and severity of slurry beds within the wellbore.

The first model, which effectively predicts the onset and presence of slurry beds during the drilling process, utilizes real-time field data to offer timely predictions (as illustrated in Figure 2 and Figure 3). Specifically, the neural network model achieved a precision of 90% and a recall of 100% for the non-presence of slurry beds (class 0), which translated into an F1-score of 0.95. For predicting the presence of slurry beds (class 1), the model achieved a precision of 100% and a recall of 61%, resulting in an F1-score of 0.76, as shown in our results (Table 1). These metrics underscore the model's high reliability in conditions typical of drilling scenarios where preventing pipe sticking is crucial.

The regression model used for estimating the height of the slurry bed provides a quantitative assessment of potential severity at the wellbore's bottom (Figure 5 and Figure 6) and delivered an MSE (Mean Squared Error) of 0.00648 on the test set. This low error rate demonstrates the model's accuracy but also raises concerns about potential overfitting, highlighted by subsequent tests on new, unseen data (Figures 5 and 6).

A recurring challenge in the application of these models is their ability to generalize effectively to new, unseen data sets. While the models performed well on the training data, extensive validation was required to ensure accuracy when confronted with new geological and operational conditions (as discussed in the results section). Data quality significantly impacted the study's outcomes.

Addressing these limitations, future work should aim to enhance data collection processes, perhaps by integrating real-time data acquisition systems that can provide a more comprehensive dataset. Furthermore, the use of advanced machine learning techniques, such as ensemble methods or hybrid models that combine machine learning with physics-based models, could potentially increase the robustness and accuracy of predictions. The implications of our findings are profound, suggesting that while machine learning presents a powerful tool for enhancing drilling operations, its deployment must be carefully managed to maximize benefits while mitigating risks associated with data quality and model overfitting. Continued advancements in machine learning and drilling technology will likely pave the way for even more refined models, potentially transforming drilling operations in terms of efficiency, safety, and cost-effectiveness.

CONCLUSION

In conclusion, the research presented in this paper successfully demonstrates the application of machine learning techniques to improve the predictability and efficiency of hole cleaning in drilling operations. By employing regression and neural network models, we have achieved significant advancements in forecasting the presence and dimensions of slurry beds, which are crucial for preventing stuck pipe incidents. The machine learning models, developed through rigorous data analysis and validation, not only enhance operational decision-making but also minimize non-productive time and associated costs in drilling.

Despite these promising outcomes, challenges such as model overfitting and the need for extensive data validation highlight the complexities of applying machine learning in real-world settings. Future work will focus on refining data collection methods, enhancing model robustness, and exploring advanced machine learning strategies to further improve

https://doi.org/10.5593/sgem2024/1.1/s06.84

the reliability and accuracy of predictive models in drilling operations. This ongoing research continues to support the broader goal of enhancing operational efficiency and safety in the oil and gas industry, making a significant contribution to the field of drilling technology.

ACKNOWLEDGEMENTS

The article was prepared within the framework of project No. AP13068658 “Developing torque and drag, hydraulic models to prevent stuck pipe by monitoring drilling parameters in real time” as part of the ongoing competition for grant funding for fundamental and applied research of young scientists in scientific and (or) scientific technical projects for 2022–2024 Ministry of Science and Higher Education of the Republic of Kazakhstan.

REFERENCES

[1] Muqeem M.A, Weekse A.E, Al-Hajji A.A. Stuck pipe best practices: a challenging approach to reducing stuck pipe costs // Saudi Arabia section technical symposium and exhibition. – Al-Khobar, Saudi Arabia, 2012. https://doi.org/10.2118/160845-MS

[2] Abdelhalim Kh., Al Zaabi M., Al Ali S., Abdel Karim I., Jadallah H., Al Beshr A., Shigeru E. A Challenging Drilling Campaign Unleashed a Unique Fast Drill String Recovery Methodology Eliminating Utilizing Wireline, CT and Overcome Highly Deviated String Accessibility // Middle East Drilling Technology Conference and Exhibition. – Abu Dhabi, UAE, 2021. doi: https://doi.org/10.2118/202153-MS

[3] Aljubran M. J., Looni Q. D., Ramadhan, A. A., Neacsu M., Mora C. T., Emam A. A., Alomoush J., Ali A. M. Completion Planning and Execution of the World's Longest ICD Partially Cemented Production System in an Offshore Horizontal Well // Abu Dhabi International Petroleum Exhibition & Conference. – Abu Dhabi, UAE, 2016. doi: https://doi.org/10.2118/182937-MS

[4] Mitchell J. Trouble-Free Drilling, third edition. – Houston: Drillbert Engineering, 2004. – P. 230.

[5] Egenti N.B. Understanding Drill-cuttings Transportation in Deviated and Horizontal Wells // Nigeria Annual International Conference and Exhibition. – Lagos, Nigeria, 2014.

[6] Malekzadeh N., Mohammadsalehi M. Hole Cleaning Optimization in Horizontal Wells: A New Method to Compensate Negative Hole Inclination Effects // Brasil Offshore. – Macae´, Brazil, 2011. https://doi.org/10.2118/143676MS.

[7] Busahmin B., Saed N.H, Alusta G. Analysis of Hole Cleaning for a Vertical Well // Open Access Library Journal, 2017. – Vol. 4. – P.1-10. https://doi.org/oalib.1103579.

[8] Biletskiy, M.T.; Ratov, B.T.; Syzdykov, A.K.; Delikesheva, D.N. Express method for measuring the drilling muds rheological parameters // International Multidisciplinary Scientific GeoConference Surveying Geology and Mining Ecology Management, SGEM 2019 | Conference paper. DOI: 10.5593/sgem2019/1.2/S06.109

[9] Mendez, Michael, Ahmed, Ramadan, Karami, Hamidreza, Nasser, Mustafa, Hussein, Ibnelwaleed A., Garcia, Sergio, and Andres Gonzalez. "Applications of Machine Learning Methods to Predict Hole Cleaning in Horizontal and Highly Deviated Wells." SPE Drill & Compl 38 (2023): 606–617. doi: https://doi.org/10.2118/212912-PA

[10] Soofi A. A., Awan A. Classification techniques in machine learning: applications and issues // J. Basic Appl. Sci, 2017. – Vol. 13. – P. 459-465. https://doi.org/10.6000/1927-5129.2017.13.76.

[11] Kalyan Das. Jiming Jiang. J. N. K. Rao. "Mean squared error of empirical predictor." Ann. Statist. 32 (2) 818 - 840, April 2004. https://doi.org/10.1214/009053604000000201